HIGH FIDELITY MEASUREMENT OF BIOELECTRICAL SIGNALS

by

Michael Alan McLain Jr.

A dissertation submitted to the faculty of
The University of North Carolina at Charlotte
in partial fulfillment of the requirements
for the degree of Doctor of Philosophy in
Electrical Engineering

Charlotte

2014

Approved by:

_____
Dr. S. Mehdi Miri

_____
Dr. Ryan Adams

_____
Dr. Yogendra Kakad

_____
Dr. Joanna Krueger

©2014
Michael Alan McLain Jr.
ALL RIGHTS RESERVED

ABSTRACT

MICHAEL ALAN MCLAIN JR. High fidelity measurement of bioelectrical signals (Under the direction of DR. S. MEHDI MIRI.)

Previous research regarding the acquisition and electrical characterization of bioelectrical signals of both noninvasive "*oriundis in vivo*", generally associated with electromyography (EMG), electrocardiography (EKG), or electroencephalography (EEG), and active "*oriundis ex vivo et vitro*" material characterization, generally associated with bioimpedance spectroscopy (BIS); while successfully providing beneficial results, was ultimately plagued with a variety of intrinsic electrical distortions [1] [2]. Conversely, the frequent manifestation of such distortions resulted in an investigation into the nature of their occurrence, which subsequently resulted in my research into the nature of such distortions, the conditions in which they occur, useful techniques to model and minimize their impact, and the underlying methodology needed to obtain the highest fidelity possible when acquiring such measurements. Furthermore, the techniques developed are then applied to both noninvasively obtained "*oriundis in vivo*" and active "*oriundis ex vivo et vitro*" applied bioelectrical signals, and the compensated measurements are compared with the uncompensated measurements obtained within the previously mentioned research.

DEDICATION

Because this dissertation, in its current form, is the byproduct of years of hard work and life experiences — some of which were good, while others not so good —, this dissertation is dedicated to a number of people within my life who I feel deserves a moment of sincere pause and my personal recognition.

Thus, with this being said, this dissertation is dedicated to my beloved Andrea for her active encouragement in the pursuits of my studies, her patience over the years of my studies, and her desire for me to achieve my dreams, to my mother and father who, in all their wisdom, supported my endeavor to obtain knowledge to my mamaw, for her willingness to endure life's unfortunate frailties to see this documents completion, to my family who supported and believed in me over the years, to my friends and colleagues who encouraged me to complete the challenges set before me, to my great aunts, Laurestine, Alice, and Carolyn, who unfortunately left this world to explore the realm beyond sea and star, but who would, nonetheless, be proud, and last, though far from ever being least, this dissertation is dedicated to my papaw, who while eagerly awaiting this documents completion; unfortunately had to put on his hat, saddle up his horse, and ride off into the sunset, but whom I know would be proud of my accomplishments, no matter what range he now roams.

ACKNOWLEDGMENTS

Throughout The writing of this dissertation there have been many people who have willingly come to my aid with their guidance and thus, I would like to acknowledge the following people: My academic adviser, Dr. S. Mehdi Miri, who was not only part of the foundation upon which my research was built but has been there with insightful information every step of the way. Dr. Ryan Adams, who has always been willing to lend a helping hand and happily endure my RF related questions time and time again. Dr. Stephen M. Bobbio, who is always open to discussion about the various topics I have encountered throughout my research. Dr. Yogendra Kakad, who is also always been open to discussion about the various topics I have encountered throughout my research. Dr. Frederick D. Esenwein, who so graciously allowed me access to his collection of books. Eddie Hill, for helping me obtain measuring equipment and accessories needed throughout my research. Yawo Amengonu, for always lending me his ear and intellectual insight. Lastly, I would like to thank anybody else who has helped me out in the pursuit of my dreams and while your name is not written here today you are not forgotten in my thoughts.

TABLE OF CONTENTS

CHAPTER 1: PREFACE

The act of investigating observations pertinent to the advancement of the biomedical research area, or more specifically, investigating the occurrence of bioelectrical phenomena, is a task that is, for the most part, best summarized as being both intellectually challenging — primarily because of the large number of interdisciplinary concepts required to effectively research such subjects, an attribute that requires a highly diverse academic background that few researchers generally possess — and, on a humanistic level, can be emotionally gratifying since the knowledge obtained can potentially be utilized to enhance or develop medical applications that can, in turn, improve the overall quality of medical care provided.

Conversely, because one of the underlying objectives of the biomedical and, to some extent, the bioelectrical research area, is the creation and advancement of medical applications — although, admittedly the occasional theoretical tangent arises out of necessity —; thus, in retrospect, the attempt to reach such underlying objectives, along with the enriched historical heritage in which the area was metaphorically forged, has seemingly instilled a number of principles found within the medical profession into this research area, while, at the same time, creating a unique and somewhat diverse research atmosphere. Yet, despite such observations being generally considered moderately abstract, a notion that will be addressed and clarified to some degree within this dissertation; however, the study of bioelectrical phenomenon, like any isolatable research area, has its own unique, though somewhat nomadic, research culture, regardless of the conceptual theories utilized, and while some theoretical overlap might exist between the disciplines — in this case a

reference is being made to the electrical engineering discipline — it is important to recognize that the possession of similar theoretical knowledge does not necessarily equate to comparable research objectives nor motivations.

With this in mind, while some of the notions, previously presented, might seem somewhat vague — a impression that will soon be addressed within the coming chapters; however, before beginning any in-depth discussion on the subject, it is important to first briefly discuss the organizational structure utilized within this dissertation to help negate possible confusion. To begin, it is important to recognize that the subjects addressed, within this dissertation, though admittedly being researched from an electrical engineering perspective, are inherently interdisciplinary in nature. Likewise, because interdisciplinary concepts were utilized, within this dissertation, an attempt was made to present theoretical concepts without a disciplinary bias or, in other words, additional explanation was provided that, in some instances, might seem somewhat superficial in order to better accommodate an interdisciplinary reader. Conversely, this dissertation can arguably be divided into two conceptual sections; the first section attempts to address the abstract and philosophical attributes that are fundamentally associated with both the interdisciplinary research and the biomedical research area, while the second section addresses the more academically palatable physical research that is generally expected within a scientific dissertation. While the separation of such concepts — or more precisely the inclusion of philosophical concepts within a scientific dissertation — might, at first, seem strange; however, the interdisciplinary nature of the research area, the extensive history from which the area arises, and the number of ways miscommunications can occur between disciplines — within an interdisciplinary environment —, makes such discussion, in many ways, as important, if not more so, than the physical concepts being presented.

On that note, the general progression of the chapters presented, within this dissertation, is as follows: First, the physical research objectives will be discussed along with a more detailed discussion regarding the theoretical background needed to understand those concepts. Second, the subject of biomedical and bioelectrical research will be discussed from an organizational and philosophical perspective, while a number of metaphysical concepts pertaining to these subjects will be presented along with a number of unique interdisciplinary attributes. Third, the historical development of the research area will be discussed and, to some extent, will be related to the metaphysical development from the previous chapter. Forth, a number of theoretical concepts that are utilized by the physical research being presented will be discussed, primarily from an electrical and pseudo-chemistry perspective, while a number of biomedical specifics, like biomaterials and some safety considerations, will also be addressed. Fifth, the physical research conducted will be presented and the subjects discussed are outlined in more detail by the next chapter. Sixth, concluding remarks, research summaries, and future research topics will be discussed.

Additionally, it is worth mentioning that, while the organization of this dissertation was intended for linear reading, it is understandable that certain information, within particular chapters, is more important than other information, and if the quick acquisition of research specifics becomes extremely important, primarily because of time restrictions, the historical and philosophical chapters, although beneficial to interdisciplinary research, can be skipped, the theoretical fundamental section can be skimmed, the experimentation and research section reviewed as needed, and the summary read.

CHAPTER 2: INTRODUCTION

The high fidelity acquisition of a bioelectrical signal, or more specifically, the high fidelity acquisition of a bioelectrical signal obtained through noninvasive active or passive acquisition techniques — like bioimpedance spectroscopy (BIS) and electromyography (EMG) — is an extremely important attribute within contemporary biomedical research, especially since — within the biomedical research area — the fidelity of a signal obtained oftentimes determines the type of medical treatment that a patient receives or the inherent assumptions made by biomedical researchers surrounding a particular biomedical process observed. Conversely, given the overall — high stakes nature — that is increasingly dependent upon the fidelity of the bioelectrical acquisition obtained, the ability to obtain the highest fidelity possible is of paramount importance; yet, despite the underlying importance of acquisition fidelity, because the biomedical research community is an extremely diverse interdisciplinary area — including, but not limited to, chemistry, electrical engineering, medicine, and biology —, often times the expertise needed to obtain the required signal fidelity is unfortunately lacking — possibly because of the amount of faith being placed within commercially available acquisition solutions without a complete understanding of the actual fidelity obtained.

Likewise, to provide some examples of the subjects overall importance, because the acquisition of a high fidelity bioelectrical signal — like the acquisition of a non-invasive surface electromyogram (sEMG) — can play a substantial role in the creation of a prosthetic hand with the ability to control individual finger movements based upon remaining myoelectrical

stimulus, or the quantitative analysis — in this particular case — of sEMG signals could aid in the diagnosis of more than 100 neuromuscular disorders [3] [4]. Conversely, because myoelectric signals are becoming more prevalent within modern human-computer interfaces — implying the everyday usage of such acquisitions is not far away —, and because the utilization of classical filtering techniques — like Butterworth filtering — generally distorts and delays an acquired signal — which implies a degradation of the signals overall acquisition fidelity — the ability to acquire a raw high fidelity bioelectrical signal — like an sEMG — is highly desirable attribute [5].

Conversely, with this being said, it is the intent of this dissertation to examine: First, the interdisciplinary nature of the biomedical research area in order to obtain an understanding of the researchers who work within this area, such that the information presented — within this dissertation — can be provided in a form easily metaphorically palatable by all. Second, examine what a high fidelity acquisition actually entails relative to the requirements of the biomedical discipline. Third, identify the fundamental causes of fidelity degradation from a theoretical perspective. Forth, provide an experimental methodology for determining the amount of fidelity available from an existing commercial acquisition device at both AC and DC conditions. Fifth, demonstrate how the experimental apparatus can define the amount of fidelity obtained and provide techniques to improve this fidelity — including how to manage hi frequency unbalanced transmission line scenarios —. Sixth, examine how the fidelity processes — previously described — ultimately come together within a actual BIS modeling application. Seventh, examine how the experimental BIS examination of biomaterials can ultimately limit the amount of fidelity obtained, and provide some solutions to this particular problem. Eighth, examine how passive measuring techniques can be improved using the, previously discussed, fidelity methods provided. Ninth, examine

how the, previously discussed, material distortions play a substantial role in the bioelectrical signals commonly encountered, And lastly, provide some concluding remarks regarding the implementation of these techniques within a number of biomedical applications.

CHAPTER 3: PHILOSOPHY AND FOUNDATIONS

Few perceptible events have enthralled the mind, cultivated social growth, and promoted technological innovation as the observation of naturally occurring phenomena has, and starting from humanities cognitive birth — an important period of time in which humanity developed the ability to perceive, observe, and comprehend corporeal things — an intrinsic desire has existed (to) "*ad notitiam pervenire*" [†1] all unexplained naturally observable phenomena [6, p.826] [7, pp.259–270, pp.376–378] [8, pp.283–286]. Conversely, in terms of the physical manifestation of such attributes, such inborn inquisitiveness has, on more than one occasion, resulted in humanity appearing to be possessed by an almost zealous curiosity that, in turn, has yielded a number of profound intellectual advancements over the years regarding an assortment of unexplained natural occurrences [9, p.84] [10, pp.xx-xxii] [8, pp.283–286]. Nevertheless, while such notable intellectual accomplishments might best be attributed to the creation and application of procedural methodologies — like the organization and classification of corporeal characteristics — or, by some classical scholars, strictly associated as the product of philosophical thought; however, regardless of the assumed method of formulation, it is worth mentioning that humanity has been able (to) "*certam rei notitiam habere*" [†2] a significant number of these unknown natural occurrences since its humble beginnings and such accomplishments are the metaphoric steel upon which scientific understanding was forged [6, p.826] [11, pp.1–9] [12, pp.vii–51] [8, pp.283–286] [13, p.79].

[†1] Latin phrase for: to understand, perceive, or to discover.

[†2] Latin phrase for: to understand perfectly.

Furthermore, while humanities zealous curiosity and prolific intellectual growth over its cognitive existence is quite impressive — although such sentiments are unavoidably biased —, nature still remains a vast and wondrous entity that, despite all of humanities greatest intellectual efforts, appears completely unwilling to divulge its secrets and, if metaphorically associated with a living entity, seems determined to remain shrouded in an unperceivable veil of eternal mystery [14, pp.9–10, pp.221–225] [15, pp.57–59]. While such grim descriptions, at least upon considering the intrinsic flexibility that accompanies its metaphoric status, can be applied freely to describe a variety of currently unknown natural occurrences and the extensive frustration scholars have endured upon attempting to unravel such mysteries; however, out of all of the contemporary unknown natural occurrences currently being studied within the scientific community, there are few occurrences that can truly exemplify such, previously mentioned, metaphoric descriptions as the study of biomedical phenomena can [14, pp.9–10, pp.221–225] [15, pp.57–59].

3.1.1 Preliminary Observations

Conversely, to provide some rationale to justify this sentiment, while, at the same time, attempting to preserve some sense of scientific objectivity; it is important to recognize that — such sentiments — primarily arise because biomedical phenomena, at least upon being observed, tends to manifest itself in an inherently enigmatic and intellectually strenuous way [16, p.71,p.318] [17, p.201] [18] [19, p.138]. Likewise, such descriptions — insofar as how they pertain to the relationship between biomedical research versus other natural scientific research — seems to differ from their counterparts, based upon the observation that humanities ability to completely comprehend a particular biomedical phenomenon always seems to be slightly beyond humanities current cognitive capacity to rationalize

that occurrence [20, p.111] [21, p.72] [22] [14, p.9, pp.35–36, p.48–49]. Furthermore, to complicate such attributes further, such innate — though internally perceived — cognitive inhibitions, seem to have imparted the preconception that attempting to obtain intellectual gratification on a particular biomedical subject is, not only unlikely, but futile, at least when compared in relative terms to the underlying certainty that seemingly radiates from researchers within other scientific research areas [14, pp.9–10, pp.221–225] [15, pp.57–59].

Yet, while such sentiments might appear to be rather harsh — if not dubious —, it is important to recognize that — such sentiments — were never intended to imply that humanity is either intellectually incapable of understanding the fundamental mechanisms behind biomedical phenomena or to trivialize and demean the intellectual discoveries of non-biomedical researchers [19, pp.31–33] [14, pp.221–225] [23] [24] [25] [26]. After all, a brief walk through a modern hospital would clearly indicate that humanity has some level of understanding regarding biomedical phenomena, while clearly the study of quantum mechanics or, for that matter, power distribution — to provide some examples of non-biomedical research subjects — are far from being either simplistic or trivial [19, pp.31–33] [14, pp.221–225] [23] [24] [25] [26]. Nevertheless, regardless of the observable similarities, non-biomedical research subjects tend to follow a rigid philosophy of scientific analysis that is focused upon a particular and readily measurable series of corporeal attributes, in which assumptions are made regarding the methodological processes used to define those attributes, whereas, biomedical research subjects, generally possess a seemingly innate methodological flexibility — as opposed to the, previously mentioned, procedural simplicity — that, in turn, creates the associated obscurities [19, pp.31–33] [14, pp.221–225] [23] [24] [25] [26]. Conversely, based upon such observations, it is the occurrence of methodological flexibility, at least within the biomedical research area, — since such

flexibility is rarely encountered outside of this particular research area — that appears to metaphorically shroud this already perplexing subject in an additional veil of mystery and, as chance would have it, the abundance of such mystery is what makes, the previously mentioned description, an accurate metaphor to describe the overall extent of nature's mystique [19, pp.31–33] [14, pp.221–225] [23] [24] [25] [26].

Thus, in an attempt to reiterate such sentiments in less abstract terms, it is easy to categorize a physical attribute — such as labeling water falling from the sky as rain —, more difficult to understand a corporeal composition — such as rain is comprised of water molecules —, but nearly impossible to define why something occurs — such as why does rain exist —, and while the question of why has likely been asked within every research subject, the close association of the biomedical research area with life tends to increase the frequency in which this question is asked and, as a result, has inadvertently introduced methodological flexibility in the seemingly inflexible scientific methodology [9, pp.193–287] [27, p.235] [28, pp.107–133] [29, pp.66–69] [10, pp.2–8] [8, pp.1–6] [14, pp.40–43] [11, pp.1–9]. Yet, while it should be pointed out that some scholars — particularly those scholars unaccustomed to biomedical research, though some outliers lie within the research area — might proclaim that the question of why, at least in this particular example, can be defined as a relatively straightforward problem that can be answered through the utilization of environmental modeling — thus demonstrating one possible way in which other research areas are easily able to obtain intellectual certainty —; however, a minor caveat does exist here since such conclusions can never completely satisfy all possible interpretations [30, §§.16.1–16.7] [14, p.9, pp.35–36, p.48–49] [31] [12]. Nevertheless, despite the validity of such observations, this particular counterpoint tends to be somewhat moot within external research areas — primarily because of the contemporary academic trend that, even if

such observations were actively considered, most scientific researchers would generally be unwilling to implement such alternative interpretations, at least within their own scientific research —, since the inclusion of such possibilities would seem to only further complicate a previously rationalized and relatively straightforward explanation, and in many respects, such a stance is not without merit since, after all, science tends to pride itself on providing intellectual clarity and clockwork precision within its explanations [9, pp.193–287] [27, p.235] [28, pp.107–133] [29, pp.66–69] [10, pp.2–8] [8, pp.1–6] [14, pp.40–43] [11, pp.1–9].

Still, despite this unfortunate set of circumstances, it is important to recognize that such abstract interpretations do, in fact, play a significant role within academic research — particularly biomedical research —, insofar as, such ambiguous interpretations, while by in large being ignored, do inadvertently have profound scientific and social methodological ramifications because of the, previously mentioned, methodological flexibility that is inadvertently created by the questions inherent existence [9, pp.193–287] [27, p.235] [28, pp.107–133] [29, pp.66–69] [10, pp.2–8] [8, pp.1–6] [14, pp.40–43] [11, pp.1–9]. Yet, regardless of such observations, the fact remains that when such methodological flexibility is inevitably encountered, such flexibility is generally attributed to life being a inherently complicated process, primarily because a living entity is made up of many independent physical attributes that seemingly come together to create something unique, that is fundamentally difficult to observe and theoretically predict, thus making it an ideal scapegoat to rationalize the occurrence of such methodological flexibility [9, pp.193–287] [27, p.235] [28, pp.107–133] [29, pp.66–69] [10, pp.2–8] [8, pp.1–6] [14, pp.40–43] [11, pp.1–9].

Conversely, to clarify this point further, consider the methodological flexibility observed within theoretical models found within mainstream biomedical publications, and although some of the theoretical models currently circulating, particularly those models that were

experimentally fitted to predict a particular biomedical process, have had varying degrees of success; however, the underlying attribute that implies the existence of methodological flexibility, at least within this particular case, is the fact that the theoretical utilization of such models appears to actively invoke apprehension within fellow researchers — as the endorsement of a particular model, within this research area, is an extremely rare occurrence —, thus implying the existence of some uncertainty surrounding the intent of the original research objective [32] [33] [34] [35] [36] [11] [14] [29]. While it is possible that such consequences are, simply the result of the overall complexity of life, yet it could also be argued that such apprehension arises from personal preconceptions surrounding these, previously mentioned, alternative interpretations, as such preconceptions tend to be strongly associated with the assumptions made by the researcher since, after all, the context in which a piece of research was interpreted tends to effect its appearance of validity, regardless of its underlying theoretical accuracy, as such attributes seemingly go hand and hand in defining a researchers ability, at least in this particular case, to accept and effectively utilize a particular theoretical model [11, pp.1–4] [19, pp.31–33] [14] [29].

Yet, while this notion of a philosophically oriented methodological flexibility, at least to a scientifically indoctrinated mind, might seem, at first, unlikely given that the overall complexity and number of theoretical models utilized in biomedical research is staggering, as such depictions tends to provide a scientifically sound alternative to the philosophical explanation for the, previously mentioned, methodological flexibility found in the area based upon the classical alternative approach argument [11, pp.1–4] [19, pp.31–33] [14] [29] [37] [38] [39] [40, pp.5–10]. After all, as long as a theoretical model can provide accurate predictions of a given occurrence it is generally considered to be a legitimate explanation until it is proven otherwise, and likewise concurrent explanations of a given

occurrence are also perfectly valid as long as both explanations are accurate — at least as long as Ockham's razor produces equivalent ambiguity; a notion that is elegantly depicted by the contemporary theory regarding the wave particle duality of light [11] [41, §§.1–2] [42, §.1.1] [35] [31] [8] [43] [44] [45]. Nevertheless, while such traditional explanations are indeed acceptable origins for the occurrence of methodological flexibility, it should not be forgotten that the biomedical research area has also had a lengthy historical heritage that is abundant with years of abstract inquiry, as some of the earliest biomedical discussions have attempted to define life and its meaning, and although it will be conceded that such inquiry — while being very similar to the, previously mentioned, philosophical question of why, insofar as, having more than one possible interpretation — is, once again, typically perceived by many contemporary scientist as being an interesting but irrelevant aside within modern scientific research [46] [47] [48] [12] [8] [43] [11] [14] [49] [50] [51] [36].

Furthermore, such philosophical inquiry, at least upon further examination, tends to vindicate the notion that the, previously mentioned, philosophical origins are, at the minimum a secondary source, if not a primary source, of methodological flexibility within the biomedical research area, insofar as, an assortment of social and cultural beliefs, once again naturally developing over humanities cognitive existence, have definitively played a role in defining the research methodologies utilized by the area, for better or worse [14, pp.221–225] [52]. Although some skepticism might arise regarding this source of methodological flexibility; however, a skeptical scholar need only consider how social and cultural beliefs have swayed scientific research methodologies in years past, and if such thoughts are not enough to drive away all doubt, further proof can be found upon examination of the historical conflicts between theology and science throughout the dark ages [53] [12] [48] [54]. While evoking evidence that theological conflict has changed research methodologies —

even if such conflict does still occur, on occasion, in contemporary times — is generally considered, at least by most scholars, as an ominous subject within a scientific dissertation, yet fortunately the methodological flexibility that arises from such theological conflicts is only a metaphoric minor cord amongst a greater metaphysical symphony, as the more scientifically palatable subject of biomedical ethics tends to examine the social acceptability of biomedical research methodologies in a more scholarly acceptable light [31] [19] [55] [43] [11] [14] [18, p.31, p.366] [56] [12] [57]. Yet, while an overly critical scholar might make it a point to emphasize the fact that the methodological subjects addressed within biomedical ethics do have underlying theological connections and that such metaphysical connections are oftentimes exchanged with more corporeal concepts to manage such associations; however, in the sake of preserving forward momentum, such overly critical observations, while duly noted, should be set aside and the subject of biomedical ethics accepted — for the time — as a reasonable academic alternative to the, previously mentioned, theological connections [58] [19, p.260, p.310] [56] [57] [52] [9] [10]. Likewise, while such substitution might seem rather, peculiar given that the discussion regarding theological sources of methodological flexibility is, in fact, an very interesting aside; however, regardless of the inherent interest, such discussion was not directly intended primarily because theological discussion is best handled with significant care, and such care a little far beyond the scope of this discussion, such concepts will not be explored in any further detail [19, pp.31–33] [8, pp.418–420] [43] [53, pp.47–48] [31].

Nevertheless, because the investigation of such abstract interpretations does inevitably bring up metaphysical concepts, it is worth mentioning that the subjects of science and philosophy, while both being thoroughly studied and once deemed equally important, at least in the eyes of classical academia, is rarely applied simultaneously within the

confines of the biomedical discipline and, as previously mentioned, is seldom directly considered by the majority of scientists despite its effect on methodological flexibility [11] [43] [14] [29] [15] [31] [19]. Yet, to be fair, it is important to recognize that such depictions primarily arise because few scientific researchers are extensively versed on metaphysical subjects, and sadly this lack of metaphysical versatility has left most contemporary scientific researchers with an inherent mistrust of metaphysical ideologies: a sentiment that is ironically starting to permeate throughout contemporary society and is changing current research methodologies in itself [11, pp.vii-x,pp.1–4] [43] [14] [29] [15] [31] [19] [50] [9] [10]. Thus, while discussion regarding the sources of methodological flexibility, or for that matter the acknowledgement of the subject in itself, almost never arises within non-biomedical research, primarily because such research is narrowly focused on a particular physical attribute, such as what is electrical conduction rather than why does electrical conduction exist; however, such metaphysical mistrust, in turn, can have significant consequences once a theory is applied that has methodological prerequisites extending beyond the scope of a particular discipline, as such mistrust tends to prevent the realization that a methodological problem has occurred [43] [14] [29] [15] [31] [19] [50] [9] [10] [11] [8] [59].

Yet the acknowledgment and resolution of such methodological problems is particularly important within an interdisciplinary research environment, especially a culturally diverse one, like the biomedical research area, and while such discussion might appear counterintuitive, after all the clarification of ambiguity within scientific study is generally considered to be a step in the right direction, as opposed to introducing new and abstract metaphysical concepts; however, in order to vindicate such a notion one need only consider the ways in which a strong mistrust of metaphysical concepts could make it particularly difficult, at least for a new researcher, to begin working within the biomedical research area

[19, pp.31–33] [11, pp.vii-x,pp.1–4] [15] [31] [19] [50] [9] [10]. After all, a new metaphysically limited researcher, naturally being limited to knowledge from a particular discipline, is generally unbeknownst to that researcher, indoctrinated with a particular methodological background, and upon acquiring new theoretical concepts from other disciplines, a task that is required in interdisciplinary research, will eventually encounter a theoretical concept that is based upon methodological assumptions that diverge from their own background [49] [19] [60] [14] [31] [40] [20] [61]. Although it will be conceded that the scientific language is inherently designed to convey information across disciplinary boundaries, thus the new interdisciplinary researcher should be able to both acquire and use the new theoretical knowledge obtained [35, pp.114–117] [62, pp.793–795] [63] [20] [64]. Yet the methodological context in which the information was obtained is seldom ever conveyed across such boundaries without an active effort and, as it was previously mentioned, without an understanding of the methodological context in which a theory was developed the ability to accept that theory wholeheartedly becomes questionable, regardless of the theories accuracy, and this lack of contextual understanding generally creates one or more of the following scenarios [20] [64] [65] [66] [11] [43] [14].

The first possible scenario involves a new interdisciplinary researcher who, while formally acknowledging the existence of an interdisciplinary theory that can predict a particular biomedical phenomenon, will be unwilling to utilize this theory based upon their personal mistrust of its derivation and opt instead to devote resources into developing an alternative approach that conforms to their own methodological background [20] [64] [65] [66] [11] [43] [14] [67, pp.v-vii, §.1] [51] [50]. While such a depiction tends to surmise the repetitive nature of the scientific methodology, along with the inherent mistrust of the cynical scholar, as any scenario that introduces alternative scientifically

acceptable theory is, once again, generally viewed by the scientific community in a positive light [20] [64] [65] [66] [11] [43] [14] [67, pp.v-vii, §.1] [51] [50]. Yet it is important to point out that the original objective was to research a topic based upon a given theory rather than metaphorically reinvent the wheel in a color that is appeasing to a particular discipline, and while the introduction of complementary theory in the grand scheme of things is generally beneficial; however, the time spent redeveloping this theory could have been focused upon theoretical extension rather than theoretical reintegration [20] [64] [65] [66] [11] [43] [14] [67, pp.v-vii, §.1] [51] [50]. Likewise, the presentation of an alternative theory back into an interdisciplinary research community can create strife between contributing disciplines, as an alternative approach could be equated with incorrectness, and such strife typically will only deepen methodological mistrust and can dissuade further collaboration [20] [64] [65] [66] [11] [43] [14] [67, pp.v-vii, §.1] [51] [50] [35] [31] [68].

Alternatively, the second possible scenario involves a new interdisciplinary researcher who, unlike the researcher first depicted, will not only acknowledge the interdisciplinary theory that can, once again, predict a particular biomedical phenomenon, but will also utilize that theory without understanding the methodological nuances associated with its derivation [20] [64] [65] [66] [11] [43] [14] [67, §.1] [51] [50] [35] [31] [68] [61] [69, pp.103–105]. Conversely, because the theory in question was strictly defined using the scientific language of mathematics, the new researcher, in this particular example, would be able to correctly obtain a solution to their problem, yet because the methodological nuances associated with the, previously mentioned, theories derivation were not fully understood, the presentation of this research back into the interdisciplinary research community could, more than likely, result in a different methodological perspective being utilized to describe that research [20] [64] [65] [66] [11] [43] [14] [67, pp.v-vii, §.1] [51] [50] [35] [31] [68] [61] [69, pp.103–105].

In turn, such alternative descriptions does have a tendency to create confusion, as one discipline might interpret a methodological concept very literally while another discipline might interpret the same methodological concept symbolically, and such confusion can, once again, be equated with incorrectness, regardless of accuracy, which can also dissuade collaboration between diverging disciplines [20] [64] [65] [66] [11] [43] [14] [67, pp.v-vii, §.1] [51] [50] [35] [31] [68] [61] [69, pp.103–105] [70] [71].

Thus, such scenarios, although other cases do exist, tends to reinforce the observation that the ability to effectively research a particular interdisciplinary research topic, at least for a metaphysically limited researcher, becomes increasingly problematic the more decentralized the subject is from a singular discipline [29] [15]. While such observations primarily arise from the methodological differences between historically separated scientific disciplines, which happens to be both a consequence and possible instigator of methodological flexibility in itself, and probably occurs because of the lack of a standardized, "*de facto*" [†1] , philosophically equivalent methodological approach across all of these historically separated scientific disciplines [72, p.127] [73, p.vi-vii] [74] [19] [31] [11] [43] [14]. Yet, in this respect, the lack of a philosophically equivalent methodological approach is what makes the biomedical research area, a new and unique research frontier that in many ways is metaphorically analogous to the American Wild West of the nineteenth century, insofar as, the number of historically separated scientific disciplines involved, at least within this particular research area, makes obtaining methodological standardization across all involved disciplines currently a distant dream [75] [35] [19] [31] [8, pp.1–6] [14, pp.40–43] [11, pp.1–9] [43]. Although it is worth mentioning that methodological standardization and the unification of these disciplines into a singular entity, should in theory, alleviate

[†1] Latin phrase for: being such in effect though not formally recognized.

such metaphysical problems in time [73, p.307–308] [75] [35] [19] [31] [8, pp.1–6] [14, pp.40–43] [11, pp.1–9] [43].

3.1.2 Identifiable Concepts and Scope

Even so, because the formal methodological standardization of the area has not yet occurred, it is prudent to address some of these underlying metaphysical and mostly philosophical attributes prior to addressing any particular research concepts, especially since the research being presented, within this dissertation, relies heavily upon the accumulative interdisciplinary knowledge of the biomedical research area [31, pp.1–10] [11, pp.1–9] [20] [43] [14]. Thus, in order to avoid the, previously mentioned, interdisciplinary communication problems that can originate, once again, from methodological flexibility and the lack of a standardized research methodology, a number of metaphysical concepts will be discussed in substantial detail [31, pp.1–10] [11, pp.1–9] [20] [43] [14]. Likewise, to provide a general outline of the subjects that will be covered, within this introductory chapter, the following concepts will be discussed: Firstly, a brief discussion regarding the philosophical foundations of the subject will be briefly provided. Secondly, the objectives of the research presented within this dissertation will be discussed. Thirdly, the structure of the information presented, within this dissertation, will be outlined. Lastly, an attempt will be made to summarize all the concepts presented, within this introduction, into a — hopefully — easily understandable and logical form.

3.1.3 Methodologies and Metaphysical Foundations

Thus, to begin understanding the metaphysical and philosophical foundations that have naturally developed and defined biomedical research methodologies, the concept that humanity has come a long way, cognitively, at least since its humble beginnings, needs to be examined further [7, pp.259–270, pp.376–378] [29] [15] [76]. Likewise, upon further exam-

ination of this concept, it is revealed that humanities cognitive capabilities have, in fact, significantly advanced, so much so, that to some extent humanity appears to take solace in its current level of conceptual understanding despite the vast number of natural occurrences that currently remain unexplained [7, pp.259–270, pp.376–378] [77] [20] [43] [8] [14] [11] [31]. Although it is worth mentioning that such solace, if it ever became the social norm — neglecting for the moment, the abhorrent number of intellectual presumptions humanity would need to make in order to achieve such a unwholesome state — could be potentially disastrous since intellectual stagnation would, logically seem to result in humanities overall cognitive degeneration after a period of time [54, p.176] [52, pp.70–75] [19] [52] [77] [43]. Yet it could also be argued, at least based upon the intrinsic characteristics of humanity psyche, that the likelihood of such an occurrence, despite the contemporary tendency of migrating towards intellectual solace, is simply speculative, at worst, as humanities inherently zealous curiosity and the inevitable manifestation of intellectual discontent with the "*status quo*" †[1] should prevent cognitive degeneration from occurring [54, p.176] [52, pp.70–75] [78, p.204] [43] [8] [14] [11] [31].

While the validity of either hypothetical argument is debatable, since both arguments have a scientifically based foundation that can call upon the theory of evolution and adaptation for support, yet the corporeal definitiveness of such questions, at least as it pertains to the objective of this discussion, is not as important as the observation of the positions taken by each proponent [79] [52] [9] [10] [61] [80] [8] [14] [11] [31]. After all, one position tends to view intellectual complacency thru the lens of engineering cynicism, while the other position, in contrast, views the same information thru the eyes of humanities natural optimism [79] [52] [9] [10] [61] [80] [8] [14] [11] [31] [81] [82] [83]. Nevertheless,

†[1] Latin phrase for: situation existing before (an event).

because there is much wisdom in planning for the worst, a concept that is practically mandated — and for good reason — within the engineering discipline, such optimistic notions generally require far more evidence for a scientific mind to accept than its metaphorically jaded counterpart does [79] [52] [9] [10] [61] [80] [8] [14] [11] [31] [81] [82] [83]. Thus, in an attempt to prevent such optimistic notions from being inherently discredited, it will be amended that the previously mentioned intellectual discontent, arising, once again, from humanities seemingly compulsive inquisitive nature, ideally prevents cognitive degeneration from occurring by promoting a progressive, though not necessarily constant, desire to obtain intellectual knowledge, and such desires are speculatively driven and reinforced thru the continual observation of unexplained natural occurrences [54, p.176] [52, pp.70–75] [79] [9] [10] [61] [80] [8] [14] [11] [31] [81] [82] [83]. Yet, it is important to reiterate that the introduction of such an amendment is neither an endorsement nor an interest in the overall validity of the argument in itself, as the rationale behind each stance, rather than the argument presented, is the concept of paramount importance; nevertheless, it is apparent that such discussion can seem definitively out of place and can appear unrelated to the biomedical communities' metaphysical nature [79] [52] [9] [10] [61] [80] [8] [14] [11] [31] [81] [82] [83]. Conversely, the examination of such metaphysical concepts, in themselves, also tends to fall under equal suspicion, at least within a scientific publication such as this one; however, it is important to recognize that such divergence in perspective is, in fact, the foundation upon which metaphysical events occur, and that such metaphysical concepts symbolize, at least on a fundamental level — regardless of whether science gives such ideas credence or not — the basic rationale behind humanities desire for intellectual understanding and its need for intellectual advancement [79] [52] [9] [10] [61] [80] [8] [14] [11] [31] [81] [82] [83].

Yet in order to rationalize such conclusions, further amendment of the, previ-

ously mentioned, optimistic dialog is required and such amendment reveals that because nature is, at least from humanities perspective, seemingly vast, it would seem unlikely, even after considering humanities collective knowledge and current rate of intellectual growth, that every natural occurrence has been, or for that matter, ever truly can be, observed and fundamentally understood [84, pp.215–216] [50, pp.22–26] [79] [52] [9] [10] [61] [80] [8] [14] [11] [31] [81] [82] [83]. Likewise, this vastness, in turn, appears to make it possible for the continual enrichment and progression of humanities intellect and allows for the continuation of its intellectual advancement beyond humanities perceivable future [84, pp.215–216] [50, pp.22–26] [79] [52] [9] [10] [61] [80] [8] [14] [11] [31] [81] [82] [83] [40]. Conversely, such intellectual discontent, particularly for those born with the disposition of a scholar — as those frequently found within contemporary academia — generally would find it difficult, at best, to obtain an intellectual state of solace no matter the amount of knowledge acquired [84, pp.215–216] [50, pp.22–26] [9, p.84] [10, p.420, p.453] [85, p.166] [8, pp.283–286] [13, pp.114–117] [43] [14] [11] [31] [40]. After all, to a scholar a world in which everything is already known, simply stated, is no world worth living in, since, for a scholar, it is the thrill of obtaining that brief moment of illuminated clarity amongst the metaphoric abysmal sea of uncertainty that best surmises a scholars existence [10, p.420, p.453] [8, pp.283–286] [13, p.79] [14] [11] [31] [40] [79] [52] [9] [10] [61] [80] [81] [82] [83]. Yet, while the amount of intellectual discontent does categorically tend to separate the scholar from the layman, after all there is no denying that a scholar has a ferocious curiosity that is fortunately complemented by a world abundant with natural uncertainty, yet it is questionable as to whether such intellectual discontent, no matter the knowledge obtained, could ever be appeased, even temporarily [9, p.84] [10, p.420, p.453] [8, pp.283–

286] [14] [11] [31] [40] [79] [52] [9] [10] [61] [80] [81] [82] [83]. Furthermore, in the unlikely event that such discontent could reach a state of appeasement — making the path towards cognitive degeneration once again viable — it would still be questionable as to whether such appeasement was acquired through the acquisition of knowledge, in itself, or rather by the act of creating and applying methodological approaches during the attempt [9, p.84] [10, p.420, p.453] [8, pp.283–286] [14] [11] [31] [40] [79] [52] [9] [10] [61] [80] [81] [82] [83]. While differentiation between the two might seem to be a moot point, especially upon including the cynical alternative of cognitive degeneration, yet one of these metaphoric paths implies the mastery of nature, while the other metaphoric path implies the mastery of mind, and although both paths result in a similar end; yet it is the underlying purpose of the metaphysical to impart upon humanity that the journey down such a metaphoric path and the meaning obtained from that journey is definitively different in each case [14] [11] [31] [40] [79] [52] [9] [10] [61] [80] [8] [14] [11] [31] [81] [82] [83] [40].

Still, such statements, despite being mostly presented in anecdotal and metaphoric form, does have a tendency to make humanities overall cognitive degeneration seem unlikely, even upon considering the conservatism found within the veil of cynicism, and while it will be, once again, conceded that such questions do, in fact, feel out of place within a contemporary scientific dissertation [14] [11] [31] [40] [79] [52] [9] [10] [61] [80] [8] [14] [11] [31] [81] [82] [83] [40]. Particularly within a dissertation that is focused upon addressing the electrical attributes of bioelectrical materials since, after all, the contemporary approach to such a problem would mandate that the information presented be limited to only concepts related to the subject of electrical engineering [50, pp.21–22] [86] [87] [88] [89] [8] [14] [11] [31] [43] [59]. Nevertheless, as it was previously mentioned, the study of biomedical phenomenon is neither strictly confined within the electrical engi-

neering discipline nor, as it will soon be shown, can it effectively be studied by adhering to such restrictions; in fact, in order to obtain a comprehensive understanding of the biomedical research area, the previously mentioned and seemingly tangent dialogue regarding humanities cognitive future, is actually an important milestone towards understanding and dealing with complex interdisciplinary dynamics that naturally occur within this research area [19, pp.3–5] [8] [14] [11] [31] [43] [59]. While such a statement might seem bodacious and definitively "*obscurum per obscurius*" [†1] , yet it is the intent of this discussion to clarify such obscurities, show that such questions are, in fact, relevant, and cast the bioelectrical research presented in a, hopefully refreshing light, particularly upon comparison with traditional intra-disciplinary approaches [78, p.156] [8] [14] [11] [31] [43] [59].

Thus based upon the objectives provided, it would seem to be a reasonable course of action to continue the discussion regarding these two, previously mentioned, metaphoric paths, as there introduction symbolizes a definitive point of contention between both constituents within the cognitive degeneration argument and, interestingly enough, such discussion ultimately reveals how a seemingly small difference in perspective, despite both perspectives having the same inevitable end, is what ultimately fragments the scientific methodological unanimity of the biomedical research area as a whole [8] [14] [11] [31] [43] [59] [71] [35] [61] [82] [56] [52]. Nevertheless, it shall be conceded, once again, that the academically palatable proof needed to vindicate such a bold statement is unfortunately, metaphorically buried deeply within the metaphysical domain and requires a lengthy amount of abstract discussion to figuratively exhume; however, because such knowledge is ultimately beneficial and relevant, such discussion is not completely without merit despite any inherent misgivings that might arise from its inclusion

[†1] Latin phrase for: the obscure by the obscure.

[8] [14] [11] [31] [43] [59] [71] [35] [61] [82] [56] [52]. Thus based upon the previous discussion, once again regarding humanities current migration towards intellectual complacency and the effects such complacency has upon humanities future cognitive development, it can be observed how such discussion, while being inherently subjective, can have definitively classifiable characteristics [8] [14] [11] [31] [43] [59] [71] [35] [61] [82] [56] [52]. Likewise, such classifiable characteristics, like the inclusion of humanities curiosity and the road taken to reach intellectual complacency, despite such discussion being based upon the views of a particular characteristic, in this particular case the optimistic perspective, interestingly enough, results in a categorizable conclusion that is very similar to the previously discussed characteristics [8] [14] [11] [31] [43] [59] [71] [35] [61] [82] [56] [52].

While such observations do raise some interesting questions regarding the nature of abstract thought and the ability to categorize it; However, the critical question, at least in this particular case, is how such observations create interdisciplinary communication problems, since this question in particular has not been directly addressed as of yet [8] [14] [11] [31] [43] [59] [71] [35] [61] [82] [56] [52] [20]. Thus to investigate this particular question further, while possibly shedding some light upon the origination of abstract categorization, consider for the moment a possible interaction between two people who, for the sake of simplification, shall have contradictory answers to the previously mentioned question regarding the path of knowledge vs. the path of methodological creation [19, p.xiii, pp.3–5] [8] [14] [11] [31] [43] [59] [71] [35] [61] [82] [56] [52] [20]. Additionally, it should also be assumed that one of these people shall believe that methodology alone is the driving force behind intellectual advancement, while the other person shall believe, in contrast, that the acquisition of knowledge is the only important factor in promoting such intellectual advancement [8] [14] [11] [31] [43] [59] [71] [35] [61] [82] [56] [52] [20]. Likewise, it

should also be assumed, although, admittedly it was inherently implied, that both people believe there is a strong correlation between intellectual advancement and humanities curiosity of natural phenomena, and that a dialog shall occur between them regarding their conflicting beliefs [8] [14] [11] [31] [43] [59] [71] [35] [61] [82] [56] [52] [20]. Thus to initiate such a dialogue, it is necessary to assume that one person shall begin, in this particular case, by proposing that there are an infinite number of methodological approaches for every natural unknown [8] [14] [11] [31] [43] [59] [71] [35] [61] [82] [56] [52] [20] [85]. Additionally, this argument, upon considering the limitations imposed by the human perspective, which is arguably the only perspective humans are capable of perceiving, implies that nature has a finite number of humanly perceivable natural uncertainties that can be discovered [90, p.125] [91, pp.147–149] [60, pp.340–347]. Likewise, neglecting for the moment the possible re-occurrence of cognitive degeneration, although such degeneration should be prevented, in this particular case, by the introduction of new methodological forces, this argument is generally expressed, at least within contemporary American culture, by the idiom "*There's more than one way to skin a cat*" [92, p.693] [84, pp.215–216] [50, pp.22–26] [9, p.84] [10, p.420, p.453] [85, p.166] [8, pp.283–286] [13, pp.114–117]. Furthermore, this argument, as it pertains to the metaphoric path taken, definitively supports the idea that the utilization of methodology alone is the primary catalyst in promoting intellectual advancement [90, p.125] [91, pp.147–149] [60, pp.340–347]. Conversely, in contrast to the previous argument provided, the counter argument presented, once again by the second person, would intuitively propose that there are a finite number of methodological approaches for an infinite number of natural unknowns [93, p.43, p.94] [14, pp.47–59] [8, pp.8–27]. Such an argument, in turn, is generally expressed within contemporary American culture, thru the idioms "*knowledge is power*" and "*the ends justify the means*", and such idioms,

in turn, convey the idea that the act of acquiring knowledge is the primary catalyst in promoting intellectual advancement [92, p.382] [94] [8, pp.8–27] [70, pp.9–19].

At this point, it is important to mention that both arguments were intentionally presented in extreme terms, as a more realistic Rogerian argument between the two could have been equally presented [8] [14] [11] [31] [43] [59] [71] [35] [61] [82] [56] [52]. Yet the examination of extremes does, from time to time, have a tendency to provide beneficial conceptual insight, particularly under linear conditions, and, in this particular case, such extremes aid in depicting the interdisciplinary problems encountered within this research area [95] [96, pp.237–241] [85, pp.49–58] [91, pp.xi-xii] [19, pp.x-xvi]. Thus, upon exploring this interaction further, it is important to considered that support for the first argument can be found upon reviewing the metaphysical concepts generally associated by the term bundle theory [29, pp.1–25] [28, p.73] [15, pp.96–116] [8] [14] [11] [31] [43] [59]. As such concepts embrace the notion that reality is defined through perception and because only perceptible occurrences can exist, referring in this case to the limits imposed by the human perception, thus, the number of natural unknowns are limited, once again, by the number of perceptible human experiences available [29, pp.1–25] [28, p.73] [15, pp.96–116] [8] [14] [11] [31] [43] [59]. Likewise, because the human mind is capable of abstracting perceptible experiences in an arbitrary number of ways this, in turn, results in an infinite number of methodological derivations for a finite number of perceivable occurrences [29, pp.1–25] [28, p.39, p.73] [15, pp.96–116] [8] [14] [11] [31] [43] [59].

Conversely, similar support can be found for the second argument and such support, once again originating from metaphysical concepts, is generally found upon review of the concepts commonly associated with the philosophical term substance theory [29, pp.1–25] [28, p.73] [15, pp.96–116] [8] [14] [11] [31] [43] [59]. While such arguments, though gen-

erally acknowledging the limits of humanities perspective, significantly differs from bundle theory by allowing the inclusion of additional perspectives, such as the inclusion of a natural perspective, that can occur concurrently and independently from humanities perspective [29, pp.1–25] [28, p.73] [15, pp.96–116] [8] [14] [11] [31] [43] [59]. Additionally, such natural perspectives can be governed by there own set of dynamics, and, in turn, it would appear that humanities dynamics are seemingly dependent upon the dynamics of this newly created natural perspective [9, p.173] [85, p.60] [28, p.90–105] [8] [14] [11] [31] [43] [59]. Furthermore, based upon the assumptions presented above, it can be concluded that the human perspective ultimately is the limiting factor, thus this fact, in turn, results in limits being placed upon the number of methodological approaches humanity can utilize to study the, previously mentioned, boundless number of natural unknowns that exist independently from humanities perspective [28, p.90–105] [8] [14] [11] [31] [43] [59].

While such dialog, at least to some scholars, is considered intellectually stimulating, yet it quickly diverges deeply into the philosophical and metaphysical domain and such a deviation was again not the objective of this discussion as the focus was upon the origin of interdisciplinary communication problems [28, p.90–105] [8] [14] [11] [31] [43] [59]. Thus, in an attempt to focus the concepts previously mentioned in order to achieve the required objective, the accompanying philosophical and metaphysical attributes will now be abridged into a more simplistic form, and while it shall be conceded that scholars who are — better versed — in such theory might protest such an oversimplification; However, it is interesting to observe that all of the concepts previously presented can best be explained thru the analysis of the classical philosophical phrase "*When a tree falls in a lonely forest, and no animal is* (nearby) *to hear it, does it make a sound?*" [29] [9, pp.193–287] [27, p.235]. Although it will be conceded that such a simplification does appear to be just as complicated, if not

more so, than the information presented within the previous discussion, yet this phrase, while being ambiguous, is not inherently complicated and, in fact, does have a relatively straightforward metaphysical answer, though it shall be conceded that this answer is dependent upon the interpretation of the question [28, pp.107–133] [29, pp.66–69] [10, pp.2–8]. Therefore, in order to clarify this point further, while, at the same time, relating it to the previously presented dialog, it can be found upon careful consideration of this subject that the solution to the question proposed in the previous phrase, at least based upon the perspective of the first person from the prior discussion, would be —no— the falling tree does not make a sound [28, pp.107–133] [29, pp.66–69] [10, pp.2–8]. Likewise, the rationale in this particular case is that the limitations imposed, once again by humanities limited perspective, mandates that if a person is not around to perceive the sound then the experience of sound cannot be perceived [28, pp.107–133] [29, pp.66–69] [10, pp.2–8]. In contrast the second person, once again referring to the prior dialog, would say — yes — to the previous question, because of their belief that nature can exist independently and concurrently from humanities ability to perceive it, thus, physically the event would occur regardless of whether the event was perceived or not [28, pp.107–133] [29, pp.66–69] [10, pp.2–8]. Yet, to articulate a minor caveat here, it is important to realize that the first person, while answering the question with no, is not necessarily implying that, within this particular example, sound waves cannot physically occur without the presence of human observation [28, pp.107–133] [29, pp.66–69] [10, pp.2–8] [8, pp.1–6] [14, pp.40–43] [11, pp.1–9]. After all, it is both reasonable and scientifically sound to assume physical events are not dependent upon humanities perception of there occurrence. Therefore, the message being conveyed by the first person is not that the human perspective defines natural occurrences, but rather humanity is only capable of mentally and emotionally experiencing events that produce

perceptible stimulation [28, pp.107–133] [29, pp.66–69] [10, pp.2–8] [8, pp.1–6] [14, pp.40–43] [11, pp.1–9].

Although such concepts might seem foreign and strange, particularly to an academic within a scientific discipline, yet this example conceptually illustrates how a question that might appear, at first, reasonably straightforward can, in turn, result in a metaphoric apples to oranges comparison when different assumptions are made regarding the perspective in which the question was interpreted [28, pp.107–133] [29, pp.66–69] [10, pp.2–8] [8, pp.1–6] [14, pp.40–43] [11, pp.1–9]. Similarly, it should now be apparent that the question "*When a tree falls in a lonely forest, and no animal is* (nearby) *to hear it, does it make a sound?*" can be interpreted differently depending upon the perspective utilize to answer the question, and to illustrate this point further, in the case of this particular phrase, the first person assumed the question was referring to the internal human experience of hearing while the second person made the assumption that the question was referring to the physical stimulus that propagates through air [9, pp.193–287] [27, p.235] [28, pp.107–133] [29, pp.66–69] [10, pp.2–8] [8, pp.1–6] [14, pp.40–43] [11, pp.1–9]. Additionally, if such observations are applied to the analysis of the previously presented dialog, a parallel appears to exist, insofar as, the solutions provided are the result of two fundamentally different interpretations of a singular question [28, pp.107–133] [29, pp.66–69] [10, pp.2–8] [8, pp.1–6] [14, pp.40–43] [11, pp.1–9]. Likewise, after reflecting upon the previous dialog further, it becomes apparent that the first person answered the question based upon humanities ability to experience perceptible phenomenon, whereas, the second person answered the same question based upon the perspective that events can occur without humanities involvement [28, pp.107–133] [29, pp.66–69] [10, pp.2–8] [8, pp.1–6] [14, pp.40–43] [11, pp.1–9]. Yet it is important to clarified that, although there are many parallels to the previously discussed philosophical

phrase, it is important to recognize that such comparisons are not necessarily equivalent, as other philosophical attributes are present that were not directly addressed by this analysis [28, pp.107–133] [29, pp.66–69] [10, pp.2–8] [8, pp.1–6] [14, pp.40–43] [11, pp.1–9]. Such attributes include, though are not limited to, questions regarding how indirectly perceptible physical quantities are defined, like electricity for example. Conversely, such indirectly perceptible quantities can, typically, only be defined through the concession that , if an assumption works, like a mathematical model that predicts the flow of electrons, then the indirectly observable physical system, until proven otherwise, must physically exist in the manner defined by the models assumptions [8, pp.1–6] [14, pp.40–43] [11, pp.1–9] [43] [59].

Yet If such discrepancies are set aside for the moment, it is interesting to observe how both answers, previously mentioned, can be considered equally correct based upon the context of interpretation, and such equality summarizes the origin of almost all interdisciplinary communication problems [28, pp.107–133] [29, pp.66–69] [10, pp.2–8] [8, pp.1–6] [14, pp.40–43] [11, pp.1–9] [19]. While this particular portrayal might seem somewhat distorted, primarily because scientists are trained to analyze problems from the physical perspective, which is analogously summarized by the second person's argument, thus creating a strong belief in the uniformity of a scientific solution, yet it is such assumptions that truly are at the foundation of most interdisciplinary problems encountered [28, pp.107–133] [29, pp.66–69] [10, pp.2–8] [8, pp.1–6] [14, pp.40–43] [11, pp.1–9] [19]. Although it will be conceded that extreme deviations in perspective are generally easy to identify, or at least are quickly discovered after a few heated moments of contention, yet extreme cases are not the primary problem, but rather, it is the Rogerian blending of these, previously mentioned, extreme perspectives that ultimately cause almost all interdisciplinary problems encountered [28, pp.107–133] [29, pp.66–69] [10, pp.2–8] [8, pp.1–6] [14, pp.40–43] [11, pp.1–

9] [19] [95]. After all, some scientific disciplines, particularly those disciplines that deal with human research topics, like those found within the biomedical research area, despite great efforts by researchers within the area to maintain, the previously mentioned, scientific uniformity, do have a tendency to inadvertently incorporate alternative perspectives into their research that, for the most part, goes unnoticed [28, pp.107–133] [29, pp.66–69] [10, pp.2–8] [8, pp.1–6] [14, pp.40–43] [11, pp.1–9] [19]. Yet, it is important to point out that such deviations in perspective, even minor ones, are not necessarily the result of an arbitrary decision to present a subject differently, but rather, generally occur because of the extensive historical heritage that has diverged and incorporated an assortment of philosophical concepts into its research methodology since humanities cognitive beginnings [28, pp.107–133] [29, pp.66–69] [10, pp.2–8] [8, pp.1–6] [14, pp.40–43] [11, pp.1–9] [19].

Although there are numerous rationales to describe such phenomena, and some of these reasons will be discussed later in more detail within this dissertation [28, pp.107–133] [29, pp.66–69] [10, pp.2–8] [8, pp.1–6] [14, pp.40–43] [11, pp.1–9] [19]. Nevertheless, upon returning to the original question of choosing between methodological diversity versus intellectual acquisition, it becomes apparent, upon taking into account the information previously presented, that not only are both conclusions definitively possible but both are equally probable depending upon the discipline being discussed and the question being asked [28, pp.107–133] [29, pp.66–69] [10, pp.2–8] [8, pp.1–6] [14, pp.40–43] [11, pp.1–9] [19]. Thus, in the wake of such a conclusion, which arguably produced more questions than answers, the next logical step would be to observe the occurrence of such phenomena as it naturally arises within academic research [28, pp.107–133] [29, pp.66–69] [10, pp.2–8] [8, pp.1–6] [14, pp.40–43] [11, pp.1–9] [19]. Likewise, towards this end, as research is presented, within this dissertation, an effort will be made to highlight such philosophical

ambiguity, when it arises, and further discussion will be made regarding how such ambiguity relates to the information provided above [28, p.90–105] [8] [14] [11] [31] [43] [59].

3.2 Bioelectrical Philosophy and Foundations

On that note, it is now time to consolidate the scope of the previous discussion from the term biomedical towards a particular subset that, within this dissertation, will be identified by the term bioelectrical [16, pp.1–2] [97, pp.ix-x, pp.1–2]. While such consolidation might seem to be a purely linguistic change; however, it is important to note that the term biomedical is generally considered a generic, umbrella term, which identifies sciences working towards life-oriented objectives [38, pp.ix-x] [98, pp.xv-xvii]. Whereas, the term bioelectrical, while also working towards life-oriented objectives, is focused specifically upon the electrical research attributes found within biomedical research [16, pp.1–2] [97, pp.ix-x, pp.1–2]. Although such linguistic terms and there meaning can be extremely confusing, especially to those unfamiliar with this research area, a simple analogy can help alleviate such confusion [16, pp.1–2] [97, pp.ix-x, pp.1–2] [31].

Towards this end, the term biomedical can best be symbolized as a country, such as the United States, while the term bioelectrical can best be symbolized as a state within that country, such as North Carolina [38] [36] [31]. Similarly, the electrical engineering discipline could be symbolized as a county within that state, such as Mecklenburg, and in the same manner that a state consists of many counties and a country consists of many states, the same can be said for the biomedical and bioelectrical research area [38] [36] [31]. Likewise, the parallels found within such analogies are ultimately the reason why the biomedical and bioelectrical research area were surmised by the ancient Latin idiom "*obscurum per obscurius*" [†1] or in English "*one obscure thing* (is defined) *by something* ... (even) *more*

[†1] Latin phrase for: the obscure by the obscure.

obscure" [78, p.156] [38] [36] [31]. Nevertheless, while it might be jestingly surmised that the journey towards understanding the bioelectrical research area is a metaphorically long and perilous one; however, the sincerity of the subjects studied within this area compels the remark that the nature of this area, or to be more specific, the study of bioelectrical phenomena, is a subject of paramount importance to both the humanities and the sciences alike as the practical application of such theory, once again cultivated from humanities observation of natural occurrences, has resulted in the profound creation of many modern concepts [36, pp.vii-viii] [38] [36] [31]. Conversely, Such concepts include, but are not strictly limited to, electronic devices that are able to detect the presence of harmful biological pathogens and literary classics, like Mary Shelley's Frankenstein, as both of these examples elegantly illustrate the long term consequences bioelectrical research can have upon society and how such applications can change humanity for better or worse [99] [100, pp.122–123] [36, pp.5–7] [101] [102] [103].

3.2.1 Defining Bioelectrical Research

Yet, while such applications are undisputedly paramount, they only depict the result of a complicated and involved process that, under certain circumstances, can be enlightening; however, in this particular case, such displays do not provide much insight regarding the fundamental nature of bioelectrical research [38] [36] [31]. Towards that end, the best way to obtain such insight is by starting with electrical engineering fundamentals and slowly adding attributes that genuinely make the term bioelectrical research unique [38] [36] [31]. Thus, to begin defining the term bioelectrical research, the electrical engineering ability to accurately produce, acquire, and analyze electrical signals should be considered, and despite such capabilities being a relatively recent circa 1900's achievement, such capabilities frequently go unnoticed within contemporary society [59] [104, pp.ix-xii] [105, pp.1–

17] [106, pp.1–18] [107, pp.1–21]. Additionally, these capabilities, despite going unnoticed, are a necessity for the proper operation and daily usage of nearly every consumer application currently found throughout contemporary society [108] [97, p.388] [109, p.37, p.739]. Likewise, to illustrate this point, without having to discuss a diverse number of common consumer applications, consider for the moment a modern digital voice recorder that might be utilized to record a lengthy office meeting or a short grocery list [105, pp.1–17] [106, pp.1–18] [107, pp.1–21] [108]. Such a device would naturally utilize a microphone in order to convert spoken words into an analog electrical signal, and such a conversion is a common example of electrical signal acquisition [105, pp.1–17] [106, pp.1–18] [107, pp.1–21] [108]. Likewise, this analog signal, in turn, can be digitized into a binary value using an analog to digital converter, and such a conversion depicts signal analysis and signal production [105, pp.1–17] [106, pp.1–18] [107, pp.1–21] [108]. Similarly, this digital quantity can be processed by a microcontroller, in order to enhance sound clarity, and stored on a physical medium, such as a SD card, and these steps further depict signal analysis and signal production [105, pp.1–17] [106, pp.1–18] [107, pp.1–21] [108].

While the example application, described above, is definitively a product of electrical engineering, applications developed by the bioelectrical research area are fundamentally similar, insofar as, such applications utilize the fundamental electrical engineering techniques of signal production, signal acquisition, and signal analysis [110, pp.1–28]. Yet, one fundamental difference between the two research areas is, while electrical engineering is generally only concerned with electrical conduction in metals and semiconductors; the bioelectrical research area is primarily focused upon the electrical propagation through atypically conductive materials [110, pp.1–28] [38] [36] [31]. Additionally, such atypically conductive materials, at least within the biomedical and bioelectrical research commu-

nity, are generally classified by the term biomaterials and such materials include both organic and inorganic nonmetal mediums, some of which are sub classified as being liquids [109] [16] [111, p.103–127]. Although such descriptions might seem, at least to an electrical engineer, minor, primarily because of the belief in a unified electrical conduction theory; however, upon further analysis it is discovered that modern electrical propagation theory can seldom be directly applied to such mediums without a significant amount of error being introduced [112] [113] [114] [33]. Yet, this is not to say that such theory is necessarily incorrect, but rather, promotes the possibility that either the theory can only be accurately applied in an impractical manner, or is missing parameters, which are generally unremarkable upon the analysis of a traditional medium, but become remarkable within a biomaterial [38] [36] [31].

While, the analysis of such electrical anomalies does play an important role in differentiating the bioelectrical research area from the electrical engineering research area; although it should be noted that an electrical engineer would find such electrical anomalies intriguing, mostly from a theoretical perspective [14] [8] [11]. Yet, in contrast with the electrical engineering discipline, the biomedical community is generally less concerned with theory and more concerned with benefiting humanity through the utilization of such theory; however, this is not to say that the electrical engineering discipline is without heart [19] [70] [55]. After all, only the cruel would willingly wish harm upon another, but rather, society tends to assign jobs based upon familiarity, which implies that society expects life-related applications from the biomedical researcher and consumer applications from the electrical engineer [70] [38] [36] [31] [8] [14] [11] [43]. Although such a depiction could be considered stereotypical, as diversification does occur, yet other attributes also help distinguish the engineer from the bioelectrical engineer and such attributes include minor procedural

differences during the development process [115, pp.160–215] [38] [36] [31] [8] [14] [11] [43]. Such procedural differences, although subtle, can be observed upon comparing how an electrical engineer and a bioelectrical engineer would go about designing a power generation system [38] [36] [31] [8] [14] [11] [43]. To elaborate further, an electrical engineer, during the design process, would be primarily concerned with maximizing the power generated and minimizing the power lost, primarily because these parameters are valued, within the electrical engineering discipline, as being extremely important in power generation design [116, pp.1–12] [117, pp.xi–37] [118, pp.26:1–26:21]. Conversely, a bioelectrical engineer, while hopefully understanding the importance of such parameters, would also make human safety a priority in the design by, for example, making the transmission system less likely to cause cardiac arrest upon accidental contact, despite such safety considerations reducing the designs overall efficiency or increasing the designs overall cost [19] [70] [55] [119] [120] [121] [122] [123] [124] [125, p.58–61] [126].

This example, in particular, is rather peculiar because it illustrates a possible metaphysical conflict that can occur when different disciplines value different perspectives, and although both disciplines might possess similar theoretical knowledge, the knowledge and methodological approach is definitively valued differently between the two [28, pp.107–133] [29, pp.66–69] [10, pp.2–8] [8, pp.1–6] [14, pp.40–43] [11, pp.1–9] [19]. Yet questions might remain as to how such differences can exist when, ideally a bioelectrical engineer was, at one point in time, an electrical engineer who became involved with biomedical research [38] [36] [31] [8] [14] [11] [43]. Although, such a linear progression might seem logical, particularly to an electrical engineer; however, the term bioelectrical engineer is, once again, like a metaphoric state with many counties and it is equally possible for someone with a chemical or biological background to be identified by such a term [36, pp.1–12] [100, pp.iv-

x] [127] [73] [97, pp.411–418]. Likewise, as implied previously, such an all-encompassing classification tends to make generalization, regarding the bioelectrical discipline, a risky proposition, since usage of the term cannot definitively convey the background knowledge a person working in the area has [128] [129, pp.19–49]. In fact, within some disciplines, particularly biology and biochemistry, the term bioelectrical implies the exclusive study of electrical phenomenon found within living cells, whereas electrical engineering and physics tend to view bioelectrical engineering in a broader light by the inclusion of material spectroscopy and magnetic resonance imaging [129, pp.19–49] [38] [36] [31].

Yet, this ambiguity in a bioelectrical researchers theoretical background, in itself, is just another unique distinction between a bioelectrical engineer and an electrical engineer; however, setting such ambiguity aside for the moment, a common purpose does exist, within the bioelectrical research area, insofar as, the ultimate objective of bioelectrical research, even if the results seem insignificant, is to improve the overall well-being of humanity [19] [70] [55] [129, pp.19–49]. Likewise, based upon such remarks, it is easy to see, even if the theoretical background requirements are ambiguous, how a point of comradely can be found, amongst fellow members, when the subject of human longevity arises [17, pp.v-vi]. Additionally, further comparison seems to reveal the presence of a natural bias, within the subject, towards the selection of topics that arise from such comradely, like improvements to medical diagnostic equipment, as opposed to sole theoretical improvements regarding electrical propagation theory [11, pp.7–9]. Yet, while there is a natural tendency for researchers, within this area, to pick topics beneficial to the overall well-being of humanity; however, such a preference tends to be a moot point when it comes to receiving interdisciplinary aid, as traditional research areas, primarily because of the ambiguous nature of the bioelectrical research area, are reluctant to become involved unless motivated to do

so [19] [70] [55] [129, pp.19–49] [65]. Likewise, such interdisciplinary stigmas are yet just another unique attribute of the bioelectrical research area, although admittedly, similar parallels do exist amongst other disciplines, such as the contention that exist between electrical engineering and physics to provide an example [65] [38] [36] [31] [8] [14] [11] [43]. Nevertheless, such contention is not limited to interdisciplinary aid, as social comradely can only go so far, thus, it should come as no surprise that internal contentions does exist within the bioelectrical research area, and, based upon the previous metaphysical discussion, a unilateral agreement for any given research topic is rarely obtained without some initial reluctance or rejection [65] [38] [36] [31] [8] [14] [11] [43].

3.2.2 Outlining the Disciplines Involved

Be that if it may, the study of bioelectrical phenomena has progressed significantly, almost seemingly parallel with humanities cognitive development, and over this lengthy history a number of fundamental sciences have emerged that have greatly contributed to the subject success despite the, previously mentioned, contentions [7, pp.259–270, pp.376–378] [129, pp.19–49]. Likewise, to illustrate such contributions, consider for the moment the research being conducted within the health sciences that is attempting to analyze the electrical nature of synapses in the brain [23, pp.391–404] [39, pp.319–332]. Equally, the life sciences are currently researching the use of bioelectrical signal theory to analyze both DNA and the electrical signals emitted by plant roots [130] [131]. Additionally the natural science of chemistry has contributed significantly to the conceptual understanding of bioelectrical conductivity [132, pp.812–818]. Moreover, the natural science of physics has developed a number of fundamental electrical principles that are frequently applied to the research area of bioimpedance spectroscopy and bioelectrical signal analysis [133]. While the examples, previously mentioned, cannot fully convey the significance of the bioelectri-

cal research area, yet such examples do effectively portray the immensity of bioelectrical research topics and highlights the areas interdisciplinary nature [65]. Nevertheless, as it was previously mentioned, the bioelectrical research area, being the metaphoric state that contains many counties, frequently utilizes knowledge from a variety of disciplines, and although the definition of the term disciplines can vary, depending upon the terminology used, its usage will be limited to identifying traditionally categorized academic subjects [38] [36] [31]. Likewise, based upon such a definition, it is frequently stated, predominantly throughout numerous bioelectrical texts, that the disciplines of medicine, biology, physics, electronics, and engineering are fundamental to bioelectrical research [129, pp.19–49]. Yet, it would also be prudent to include the disciplines of chemistry, physical chemistry, mathematics, and even the humanities, since such disciplines are also fundamental to bioelectrical research but seemingly go unmentioned within the few educational texts available on the subject [129, pp.19–49] [16] [97] [134] [127] [135].

Although such lists can provide a brief glimpse of the type of knowledge needed to effectively perform bioelectrical research; however, there is no doubt that, such lists, are neither fully comprehensive nor specific enough to provide in-depth insight regarding a particular research subject and admittedly such problems are twofold [38] [36] [31] [8] [14] [11] [43]. Firstly, as it was previously mentioned, the term bioelectrical is currently rather ambiguous, as there is no "*de facto*" [†1] definition [72, p.127]. Likewise, because the term is generally applied within a research community, the definitions meaning typically reflects the knowledge being applied to a topic being actively researched rather than the research area as a whole [65]. Secondly, because such definitions are ambiguous and are generally redefined by individual researchers, such definitions tend to emphasize particular subsets,

[†1] Latin phrase for: being such in effect though not formally recognized.

without effectively considering the context in which that subset exists [65]. Conversely, such contextualization is analogous to summarizing the electrical engineering discipline as the study of power transmission, when in reality electrical engineering encompasses a diverse number of electrical topics [116] [136] [104] [137] [107]. While attempts were made to avoid conceptual stereotyping within this dissertation, it will be conceded that the disciplines mentioned were — inevitably — based upon prior research experiences, and despite an effort to make this list unambiguous, it is possible that an involved discipline could have been either overlooked or understated [38] [36] [31] [8] [14] [11] [43]. Keeping this in mind, in order to convey how the knowledge categorized by the disciplines, previously mentioned, is applied to bioelectrical research, it would be prudent to briefly discuss each discipline mentioned and highlight a few interesting and important attributes that each discipline brings to the bioelectrical research area [38] [36] [31] [8] [14] [11] [43].

To begin such a dialogue, firstly, the discipline of medicine will be considered and, as it might be expected, the usage of this term, does little to accurately surmise a vast and time honored traditional research area that mostly pertains to the preservation and study of life [55] [12] [70] [138]. Likewise, the discipline of medicine, is in fact, analogous to the state verses county metaphor, previously mentioned, insofar as, there are numerous subsets found within the term that are generally surmise through its usage [139, p.3] [140] [141] [142] [143] [144] [145] [146] [147] [148] [149] [150] [151]. Such subsets include, though are not limited to, the sub disciplines of emergency medicine, sports medicine, psychiatric, cardiology, dermatology, surgery, and obstetrics [139, p.3] [140] [141] [142] [143] [144] [145] [146] [147] [148] [149] [150] [151]. While the actual definition of the medical discipline seems to be more of an umbrella term than a definitive identifier, as it pertains to the bioelectrical research area, this term generally refers to the

electrical processes found in cardiology, neurology, and physiology along with the material effects defined by anatomy and pharmacology [146] [147] [148] [152] [25] [23] [26] [153]. In order to clarify any misconceptions that might have arisen because of the diversity of the medical discipline, consider for the moment the bioelectrical cardiovascular specific application, in which the electrical signals produced by the heart are noninvasively measured, and this application is commonly referred to as an electrocardiogram or EKG for short [16] [154] [155] [156]. Likewise, a similar neurological application, in which the electrical signals produced by the brain are measured, is referred to as an electroencephalogram or EEG for short [16] [157]. Similarly, a physiological application, in which the electrical signals produced by the movement of muscles within the body are measured, is referred to as an electromyogram or EMG for short [16] [1] [25] [158]. Furthermore, all of these biomedical measurements utilize knowledge of anatomy, in order to put the measurements in the proper physical context and pharmacology to contextualize the electrochemical processes measured within the body [16] [109] [153] [1] [23].

Secondly, the discipline of biology, while not as all-inclusive as the umbrella term medical discipline, does include some topics that are frequently utilized within the medical discipline but are primarily studied from a theoretical perspective rather than an applied perspective [115, p.23] [39] [19, p.6, pp. 32–36] [20, pp.43–49] [11] [18] [159]. In many respects, an analogy between the disciplines of physics and electrical engineering can be applied here, insofar as, biology represents the theoretical study of life, which is analogous to physics, while the medical discipline represents the application of that knowledge, which is analogous to electrical engineering [115, pp.62–72] [18] [159] [160] [161] [162] [79] [61]. While admittedly, such comparisons are abstract and assume a certain amount of familiarity with the electrical engineering discipline; however, such comparisons, despite being

presumptuous and somewhat inaccurate, help to build a mental picture of disciplinary causality [38] [36] [31] [8] [14] [11] [43]. With this in mind, biology, while studying a vast assortment of life related phenomena, some of which will, unfortunately, go unmentioned, is best known for its study of living processes, cells, evolution, genetics, reproduction, and environmental effects [39, pp.xi-xxviii] [18, pp. v-vi]. Likewise, such knowledge generally manifest itself, within the bioelectrical research area, through the development of electrophoresis devices used in DNA analysis, electric cellular understanding, which is used to put EKG, EMG, and EEG measurements into proper context, and a general understanding of biomaterials in which electrical signals propagate through [163] [164] [165] [109].

Thirdly, the discipline of physics, as it was previously surmised, is primarily focused upon the study of the mechanics of nature and can be generally separated into two separate categories. The first category is commonly expressed by the term classical mechanics and, most notably, studies natural forces, energy, momentum, gravity, sound and collision [166, pp.63–65] [27] [167]. Likewise, the second category is usually expressed by the term modern physics and, most notably, studies electromagnetic phenomena, optics, nuclear phenomena, and quantum mechanics [168] [169] [167] [166, pp.63–65] [170] [171]. In general, physics can metaphorically be conceptualized as the — great scientific bridge — that embodies the, previously discussed, natural perspective that humanity is dependent on [35, pp.129–144] [9, p.173] [85, p.60] [28, p.90–105] [65]. Conversely, because physics is, in essence, humanities metaphoric translation of the language of nature, it should come as no surprise that practically every scientific discipline utilizes numerous concepts developed within the discipline of physics [35, pp.129–144] [65] [172] [173]. Yet, this should not imply that a physicist is necessarily versed on all scientific knowledge, since after all, just because a person can speak a language does not necessarily mean they intuitively understand every

word within that language [35, pp.129–144] [65] [172] [173]. Likewise, there is a subtle difference between theorizing what is likely to happen versus using personal experience to intuitively predict what will happen [160] [15]. After all, when something is translated from one language to another often times a part of the message is lost during the translation and the same thing can be said when comparing theoretical models with natural events [66] [160] [15]. Nevertheless, the theoretical foundations provided by physics does play a critical role within the bioelectrical research area, particularly in the utilization of classical mechanics to model physical biological phenomenon and modern physics to model bioelectrical phenomena [16] [174, pp.3–29] [37] [175].

Fourthly, the engineering discipline, which within the bioelectrical research area generally includes electrical engineering, mechanical engineering, chemical engineering and truthfully any related subset that develops biomedical applications from theoretical knowledge, is yet another ambiguous umbrella term [61, pp.365–366] [157, pp.ix-x] [35, pp.129–131]. Although the development of applications, which ultimately takes an intellectual idea and turns it into a physical object, is very important; however, discussion beyond this basic engineering observation is difficult without specifying a particular theoretical attribute [176] [177]. While such theoretical attributes could be provided and discussed, such an approach would become redundant in time. Thus, for this reason, let it just be stated that electrical engineers mostly develop applications derived from the physical theory of electromagnetics, mechanical engineers mostly develop applications related to the physical theory of classical mechanics, and chemical engineers mostly develop applications related to chemical theory [178] [179] [180] [27] [181]. While mechanical, chemical, and other unspecified engineering disciplines have played an important part in the bioelectrical research area, most notably by modeling biological mechanics and developing corrosive resistant

materials for biological devices [182] [183] [109] [102] [127] [16]. Yet the most pertinent attributes are found within the discipline of electrical engineering, as the electrical engineering discipline utilizes the, previously mentioned, methods of signal acquisition, signal production, and signal processing in practically every bioelectrical application, including EKG, EEG, and EMG devices [73] [16] [102] [127] [155] [157].

Fifthly, the discipline of chemistry, while going unmentioned within some bioelectrical texts, primarily studies the physical properties of atomic elements and the interactions that occur between them [129] [16] [97] [135] [184] [132, pp.1–28] [185] [186]. In many respects, it could be argued that a parallel exists between the methodological differences, previously mentioned, and the differences observed upon comparing physics to chemistry [68] [35, pp.129–144] [9, p.173] [85, p.60] [28, p.90–105] [65] [184] [132, pp.1–28] [185] [186]. Such points of comparison generally manifest themselves through the realization that physics, while predominantly focusing upon understanding the language of nature, chemistry on the other hand attempts to metaphorically perceive events from the atomic perspective [184] [132, pp.1–28] [185] [186] [68] [28]. Likewise, such a perspective tends to define nature based upon elemental interactions, rather than attempting to define nature thru the usage of quantum mechanics [184] [132, pp.1–28] [185] [186]. Yet, as the philosophical example previously mentioned depicted, just because a difference in perspective happens to exist does not necessarily imply that either answer is inherently incorrect or that either perspective must discredit the other [28, pp.107–133] [29, pp.66–69] [10, pp.2–8] [8, pp.1–6] [14, pp.40–43] [11, pp.1–9] [19]. In fact, chemistry, like any other discipline, has benefited from physics and physics, in turn, has benefited just as much from chemistry [68] [28] [187] [46]. Nevertheless, such observations are interesting to observe, insofar as, they reiterate a, previously mentioned, fundamental philosophical difference that

can create contention amongst interdisciplinary collaborators [20] [65] [115]. With that in mind, the primary role of chemistry, within the bioelectrical research area, is to provide information that will allow the electrical characterization of a biomaterial based upon its atomic composition [73] [16] [115] [134] [188].

Sixthly, the discipline of physical chemistry, while also unmentioned within some bioelectrical texts, will for the sake of simplicity, be summarized as the blending of chemistry with physics to create a new discipline that, might humorously be referred to as — glorified electrochemistry [73] [16] [189] [190]. Setting such jest aside for the moment, physical chemistry primarily deals with modeling molecular forces, such as ion implantation forces, deposition rates, thermodynamic properties, and numerous electrochemical principles [189] [190] [191] [192] [134] [188] [193]. In terms of its application, within the bioelectrical research area, like chemistry, the physical related chemical property studied within this research area are frequently applied when modeling biomaterials [73] [16] [189] [190] [134] [188].

Seventhly, the discipline of mathematics, although generally never directly mentioned within biomedical texts, cannot be ignored as mathematics is like physics, insofar as, if physics is attempting to translate the properties of nature into a scientific language then mathematics, ultimately, is the language in which physicists speak [28] [71] [194] [195] [69]. Likewise, because all models fundamentally utilize mathematics to represent physical phenomena, thus, it is understood that mathematics is a necessary part of bioelectrical research and without it, there would be no bioelectrical models [28] [71] [194] [195] [69] [73] [16] [134] [188].

Lastly, the humanities, as previously mentioned in the discussion regarding philosophical concepts, while generally surmised, at least by some scientists, as an ambiguous aca-

demic catchall, commonly used to categorize a number of academic disciplines generally considered to exist outside of the influence of modern scientific philosophy, is important to the bioelectrical research area for a variety of reasons [196] [28, pp.107–133] [29, pp.66–69] [10, pp.2–8] [8, pp.1–6] [14, pp.40–43] [11, pp.1–9] [19]. Some of these reasons, as previously discussed, were inherently philosophical, while other reasons, some of which were not discussed, simply provide a metaphoric window into the mechanics of the human perspective [49] [196] [172] [28, pp.107–133] [29, pp.66–69] [10, pp.2–8] [8, pp.1–6] [14, pp.40–43] [11, pp.1–9] [19]. While such disciplines are generally overlooked, especially within the sciences, a basic understanding of such disciplines, or at least the acknowledgment of there presence, can help prevent interdisciplinary communication problems along with possibly increase research productivity [49] [196] [172] [28, pp.107–133] [29, pp.66–69] [10, pp.2–8] [8, pp.1–6] [14, pp.40–43] [11, pp.1–9] [19]. Likewise, such knowledge tends to put research into its proper perspective and gives research meaning on a supreme scale [49] [196] [172] [28, pp.107–133] [29, pp.66–69] [10, pp.2–8] [8, pp.1–6] [14, pp.40–43] [11, pp.1–9] [19]. Although such discussion is fascinating and profound, yet, for the sake of clarity, it should be surmised that the humanities, although frequently unacknowledged within the bioelectrical research area, have played a significant role within this area based upon the information provided in the previous discussion [49] [196] [172] [28, pp.107–133] [29, pp.66–69] [10, pp.2–8] [8, pp.1–6] [14, pp.40–43] [11, pp.1–9] [19].

3.3 Interdisciplinary Research

At this point, a brief introduction to the biomedical research area has been provided, a number of pertinent philosophical concepts were discussed, the term bioelectrical research was defined, and the principal disciplines associated with the research area were listed [31] [8] [14] [11] [43]. Yet, although such information does help to convey the overall im-

mensity of the area by outlining a number of fundamental research objectives; however, such information, at least based upon the previous discussion, does little to convey neither the natural manifestation of interdisciplinary communication problems nor the ramifications of such occurrences [31] [8] [14] [11] [43]. Thus, with this in mind, it would now seem prudent to clarify some of these ambiguities by examining how all of these individual attributes come together and ultimately function as a whole, or more precisely, function on a macroscopic interdisciplinary level [31] [8] [14] [11] [43] [20]. Likewise, to begin this process, it is prudent to point out that, although some interdisciplinary attributes have been mentioned and a few possible consequences discussed, such examples are best metaphorically surmised as being "just a drop of water in an endless sea" †[1] because of there narrow focus upon specific interdisciplinary events rather than on the macroscopic system as a whole [31] [8] [14] [11] [43] [20] [197].

3.3.1 Interdisciplinary Research and Scientific Cultures

Conversely it should also be pointed out that, until now, it has been inadvertently implied that intellectual background and methodological differences are the singular source of all interdisciplinary communication problems encountered, and while such singular attributes are, in fact, a foundation upon which communication problems can occur, such occurrences are generally the result of something more complicated than a singular event and such complexity is best surmised by the term interdisciplinary culture [31] [8] [14] [11] [43] [20]. Yet, while the usage of the term interdisciplinary culture does seem to imply the existence of some great metaphysical complexity or, at least, imparts that some type of abstract rhetoric is currently at work, primarily because of the number of parallels between social culture and interdisciplinary culture; however, usage of

†[1] Phrase from the Song "Dust in the Wind", written by Kerry Livgren of the band Kansas.

this term, at least upon limiting the term to the metaphysical attributes previously discussed, is best surmised as being predominantly focused upon a singular discipline's, such as electrical engineering, tendency to define intellectual commonalities in terms that are based upon a specific methodological approach utilized within that particular discipline [20] [19, p.xiv] [162] [62, pp.845–846] [31] [8] [14] [11] [43]. Likewise, such commonalities, once again manifesting from a commonly accepted metaphysical and theoretical background, create something that is best described by the phrase common knowledge, and while the assumption of a common intellectual background is extremely beneficial in some cases, especially when researchers are conveying new ideas within their own discipline [31] [8] [14] [11] [43] [49, pp.47–48] [84] [198] [57]. Yet, despite it being conceptually possible that some commonalities are, in fact, ingrained throughout corresponding disciplines, more so if the correspondence is a frequent occurrence and the disciplines are historically related; however, such assumptions are, once again, generally a risky proposition given the number of ways information can be misinterpreted, and while it shall be admitted that such discussion might seem to imply that interdisciplinary correspondence should be avoided at all cost [31] [8] [14] [11] [43] [49, pp.47–48] [84] [198] [57]. Nevertheless, even if such academic isolation was feasible, such implications were neither intended nor supported, especially given the number of successful interdisciplinary research efforts currently found within contemporary academia [31] [8] [14] [11] [43] [49, pp.47–48] [84] [198] [57]. A notable example of such occurrences being, the theories that have been developed after the collaboration of the physical chemistry discipline and the electrochemical impedance spectroscopy research area; in which their sharing of conceptual theory and frequent scientific collaboration has yielded a number of theoretical models that are able to predict an assortment of chemical phenomena ranging from electrode health analysis to material

deposition rates [189] [188] [31] [8] [14] [11] [43] [49, pp.47–48] [84] [198] [57].

Yet such success stories are not without their share of scientifically oriented cultural problems, after all, as the practice of interdisciplinary collaboration becomes more frequent, the number of cultural problems encountered is bound to increase [196, pp.49–59] [56] [31] [8] [14] [11] [43] [49, pp.47–48] [84] [198] [57]. Likewise, such problems, particularly within the bioelectrical research area — since such research exist at the forefront of contemporary interdisciplinary research efforts, tends to encounter these problems at a more frequent interval because of the considerable number of historically diverse disciplines required to effectively research this particular subject and the number of deferring definitions of common knowledge found within each collaborating discipline [196, pp.49–59] [56] [31] [8] [14] [11] [43] [49, pp.47–48] [84] [198] [57] [35] [19]. Conversely, to demonstrate the existence of such problems, consider for the moment the difference between the electrical engineering notations of voltage (V) and current density (J) verses the electrochemical impedance spectroscopy notations of voltage (Φ) and current density (i) [106] [133] [188]. Likewise, because notational differences can exist, arguably because of the previously mentioned scientific culture, great care must be taken to ensure that an idea communicated within one discipline is correctly conveyed within the other, or alternatively, that a discipline attempting to apply information obtained from another discipline is aware of the notational context in which the information was originally presented [196, pp.49–59] [56] [31] [8] [14] [11] [43] [49, pp.47–48] [84] [198] [57] [35] [19] [199] [200]. While such occurrences might, at least at first, seem like an isolated event; however, such notational differences are rather frequent, especially within the bioelectrical research area, because of the limited number of mathematical variables available and the overwhelming number of theoretical concepts that need to be conveyed thru the usage of those variables

[199] [97] [68] [177] [195] [106] [133] [188] [129] [200].

Yet, while such notational conflicts tend to make interdisciplinary communication challenging but possible, problems that originate from assumptions based upon disciplinary common knowledge tends to yield far greater consequences than the surmised temporary confusion notational disorientation can bring [20] [200] [49] [69, pp.136–138] [11, pp.3–5]. Likewise the problems that arise from such assumptions, which can only be surmised as an overall miscommunication between two or more disciplines, typically occurs when research done within one discipline is presented within an interdisciplinary forum without taking into account the fundamental metaphysical and theoretical differences between participating disciplines [200, p.44]. While some of these consequences were previously mentioned in the sections above, to expand such notions further, typically such miscommunications, at best, result in some of the subtle nuances of one discipline, which are generally considered to be common knowledge, thus trivial, being misinterpreted in a way that a false since of conceptual understanding is obtained by the other discipline. While, once again, these types of misconceptions are oftentimes correct on a theoretical level, they are typically not technically accurate in every aspect, thus there application usually results in a rigid theory being applied rather abnormally to a problem that, more often than not, will generally produce a theoretically sound answer that is embedded with sporadic points of ambiguity [200, p.44] [49, ch.iv] [8] [14] [11] [201].

Conversely, to further illustrate this point, consider for the moment an electrical impedance spectroscopy publication that describes how an electrochemical model can be synthesize from measured data. Likewise, within this particular publication, a flowchart was provided that depicts each step of a chemical identification process, in which a symbolic operational amplifier was metaphorically used because the information obtained, at least

upon review of electrical engineering publications, seem to indicate that because an operational amplifiers inputs are always equal such a component would make an ideal symbolic descriptor for one of the steps within there identification process [202]. Furthermore, this, previously mentioned, flowchart also depicts a generic feedback component being applied to this symbolic operational amplifier, because it is stated that such feedback will inherently reduce the error measured within the identification process being depicted [202]. While, at least from a metaphoric perspective, such an analogy might make perfect sense to someone within the electrical impedance spectroscopy research area; however, someone within the electrical engineering discipline would, for the most part, highly disagree with this metaphoric usage, as the electrical engineer would know, based upon their common knowledge, that an operational amplifier only has equal input voltages when the amplifier has a high internal gain and uses a negative feedback configuration [203, p.69–93].

Similarly, a control systems engineer would find the liberal usage of the term feedback, within the process depicted, rather offensive since there is more than one type of feedback to select from and not all feedback will reduce error [204]. Thus, based upon this example, it becomes clear that disciplinary common knowledge can, at the very least, cause unintentional attributes to be applied to an interdisciplinary topic, like the identification process previously mentioned, and such unintentional attributes can quickly result in the misinterpretation of critical concepts within an interdisciplinary research forum [200, p.44] [49, ch.iv] [8] [14] [11] [201]. Yet, it is important to recognize that such misinterpretations do not necessarily imply that the concepts being presented were inherently incorrect; rather, it is important to recognize that when common disciplinary knowledge is assumed, especially within an interdisciplinary forum, good ideas can quickly have unintentional attributes attached to them that will make them seem incorrect, thus great care is required when apply-

ing or interpreting concepts that have common disciplinary knowledge associated with them [200, p.44] [49, ch.iv] [8] [14] [11] [201]. While most technical publications — fortunately — tend to avoid the liberal usage of such metaphoric comparisons when presenting their theoretical ideas; however, a similar type of problem can also occur when measured data is presented within the same interdisciplinary forum, as the commonly accepted units of measurement typically vary between disciplines [200, p.44] [49, ch.iv] [8] [14] [11] [201] [65]. Conversely, to provide an example of such differences, the subject of bioimpedance spectroscopy typically provides measured data in terms of permittivity and conductivity, both of which require some type of assumed circuit topology, while the electrical engineering discipline tends to present measured data in terms of voltage and current in order to avoid such assumptions [16, p.62–69] [136, p.259–262]. Yet, once again, both methods, in this particular case, while having sound scientific merit, will probably result in an electrical engineer making a few cynical comments regarding the units used to depict the data measured [200, p.44] [49, ch.iv] [8] [14] [11] [201] [65].

Equally, another example can be found upon comparing the electrical engineering disciplines tendency to refer to the complex verses frequency graphical representation of measured data as a Nyquist plot, the bioimpedance spectroscopy fields tendency to refer to them as a Wessel diagram, and the electrochemical impedance spectroscopy fields tendency to refer to them as a complex-plane impedance plot [204, p.585–586] [16, p.68–69] [205]. While it is important to recognize that the subtleties being assumed in each plot are not necessarily the same; however, all of these plots do depict the same physical attributes, real numbers verses imaginary numbers as they change over frequency, and such assumptions, once again, open the door for possible criticism upon interdisciplinary review [200, p.44] [49, ch.iv] [8] [14] [11] [201] [65] [204, p.585–586] [16, p.68–69] [205].

Yet, while such cultural problems are naturally prevalent within interdisciplinary research, more so within the bioelectrical research area than any other area, yet it should be noted that an effort has been made, at least within the bioelectrical research area, to reduce such contentions thru the migration towards a singular research discipline; however, such contentions are , once again, at best difficult, if not impossible to completely resolve since the task of unifying every piece of known knowledge into a single discipline would be, rather challenging, in itself, and upon inclusion of the fact that a fair amount of centuries old scientific traditions would also have to be modified in order to achieve such a task only compounds the problem further [200, p.44] [49, ch.iv] [8] [14] [11] [201] [65] [204, p.585–586] [16, p.68–69] [205] [177] [18] [86]. Thus, as it might be expected, such cultural problems are, for the most part, simply a fact of life when working within an interdisciplinary research environment, particularly within the bioelectrical research area.

Yet, while such cultural observations are, for the most part, more superficially abstract than inherently metaphysical; however, the natural progression of such observations, thus far, seems to merit discussing a more metaphysically oriented derivative — the metaphysical duality of common knowledge [200, p.44] [49, ch.iv] [8] [14] [11] [201] [65] [177] [18] [86]. Likewise, such discussion — once again arising primarily from the previous dialog regarding humanities ability to describe a perceived occurrence differently based upon the metaphysical philosophy of the observer — begins by considering how the existence of deferring methodological research sequences, which is a notion very similar to the metaphysical concepts previously discussed, can naturally and frequently occur despite such occurrences seaming like a scientifically illogical possibility [200, p.44] [49, ch.iv] [8] [14] [11] [201] [65] [177] [18] [86] [85] [90]. Yet, as it might be expected, the rationale behind such notions stems from the definition of understanding and its meaning within each

scientific discipline, while further examination of this attribute seems to reveal the presence of two accepted definitions of the term understanding [200] [49, ch.iv] [8] [14] [11] [85] [90]. Likewise, the first definition seems to allow for the inclusion of averages, a notion that seems to be attributed to the philosophy of applied science, while the second definition, being more rigid, appears to only allow for the inclusion of quantifiable certainty, a concept best attributed to the philosophy of pure science, and both of these definitions, upon being contextualized together, seem to be at the foundation of most common knowledge problems encountered during interdisciplinary research [200] [49, ch.iv] [43] [8] [14] [11] [85] [90] [35, pp.129–144] [65] [172] [173].

While the examination of such metaphysical notions, as previously observed, does have a tendency to result in more questions than answers, yet because analyzing a real world example can oftentimes help clarify such ambiguities, it is found, at least upon the examination of the electrical engineering discipline, that this discipline makes use of applied science, thru its usage of electron averages within the Ohm's law equation, and pure science, thru its usage of theoretical force equations when modeling individual particle velocities [200] [49, ch.iv] [8] [14] [11] [85] [90] [35, pp.129–144] [65] [172] [173] [177] [203] [106]. Yet such examples seem to raise more questions than answers, after all, it would have been logical to assume that each discipline would have adhered to one philosophy or the other, but alas, the dreaded Rogerian case, as previously mentioned, seems to best describe this particular scenario, and because engineering is traditionally considered to be the discipline in which scientific theory is transformed into a real world application, such Rogerian blending of methodological philosophy should, in retrospect, come as no surprise [200] [49, ch.iv] [8] [14] [11] [85] [90] [35, pp.129–144] [65] [172] [173] [56] [206]. While the Rogerian blending of methodological philosophy might now be considered a common oc-

currence; however, this is not to say that all scientific disciplines are without some type of philosophical bias, after all, if some type of bias did not exist then interdisciplinary research problems would be a rather trivial occurrence and clearly they are not [200] [49, ch.iv] [8] [14] [11] [85] [90] [35, pp.129–144] [65] [172] [173] [56] [206] [31] [43] [8]. Likewise, while some blending of methodological philosophy, in retrospect, does logically appear to make sense, yet the notion that one methodological philosophy is more dominant then the other, at least within a particular discipline, would seem to require further investigation and consequently, within the electrical engineering discipline, it has been observed that most of the concepts utilized do tend to make assumptions that are based upon averages rather than theoretical specifics, and such assumptions seem to imply that the methodological philosophy of applied science is, in fact, the conceptual norm within this area [200] [49, ch.iv] [8] [14] [11] [85] [90] [35, pp.129–144] [65] [172] [173] [56] [206] [31] [43] [8].

Although, many academic disciplines do inherently migrate towards a common definition of conceptual understanding, some biased towards averages while others biased towards quantitative certainty; yet such philosophical inconsistencies, as one might imagine, can become very problematic within an interdisciplinary research forum like the bioelectrical research area, and to illustrate this point further, consider for the moment the electrical engineering discipline versus the physical chemistry discipline usage of scientific methodology to solve the same biomaterial modeling problem [200] [49, ch.iv] [8] [14] [11] [85] [90] [35, pp.129–144] [65] [172] [173] [56] [206] [31] [43] [8]. To begin such a comparison, because the electrical engineering discipline tends to be biased towards the philosophy of applied science, upon being given such a problem an electrical engineer, speculatively speaking, might propose that any discrepancies found between contemporary theory, or a pure science prediction, can be accounted for through an applied

science process known as network synthesis [200] [49, ch.iv] [8] [14] [11] [85] [90] [35, pp.129–144] [65] [172] [173] [56] [206] [31] [43] [8] [207]. While network synthesis can be — loosely — defined as a series of procedural steps that attempts to represent any observed electrical signal thru the concatenation of passive electrical components; however, despite such approaches being interesting and useful, the important point to take away from this example is the circuit structure produced, at least by this particular method, generally will have no real world physical correlation to the physical system observed, and such abstract representation depicts how the application of the methodological philosophy of applied science will typically manifest itself along with the limitations that generally result from its usage [200] [49, ch.iv] [8] [14] [11] [85] [90] [35, pp.129–144] [65] [172] [173] [56] [206] [31] [43] [8] [207].

Conversely, the physical chemistry approach towards this problem, once again speculatively speaking, will more than likely be significantly different from the electrical engineering approach, particularly because of this disciplines better acquaintance with the fundamental elements that biomaterials are comprised of along with the deeply rooted historical connection to the discipline of physics [200] [49, ch.iv] [8] [14] [11] [85] [90] [35, pp.129–144] [65] [172] [173] [56] [206] [31] [43] [8] [115] [189]. Likewise, because the discipline of physics is more theoretically based, or generally considered to have more of a pure science methodological bias, it should come as no surprise that some of the methods utilized within the physical chemistry discipline will possess a similar bias, and such a bias makes the physical chemistry disciplines usage of electrohydrodynamics modeling, or EHD modeling for short, a natural possibility to the problem previously given [200] [49, ch.iv] [8] [14] [11] [85] [90] [35, pp.129–144] [65] [172] [173] [56] [206] [31] [43] [8] [208] [209]. On that note, EHD modeling can be — loosely — summarized as a process in which various fundamental principles, such as basic fluid mechanics or thermodynamics, are cou-

pled with fundamental electromagnetic principles in order to create a series of equations that attempt to predict the electromechanical propagation of a signal, within a biomaterial, at the molecular level [208] [209]. While such an approach, at least upon considering the implied level of theoretical complexity, is admittedly impressive; however, the important concept to take away from this example is the fact that such theoretical complexity is generally also accompanied by computational complexity, as this particular example would probably require a super computer to mathematically converge, which makes this approach impractical and furthermore, such approaches — inevitably— have some type of natural assumption built into them that tends to invalidate the ideal pure scientific methodological principal [200] [49, ch.iv] [8] [14] [11] [85] [90] [35, pp.129–144] [65] [172] [173] [56] [206] [31] [43] [8] [208] [209] [210].

Yet, because both approaches, the electrical engineering approach versus the physical chemistry approach, are capable of producing accurate biomaterial models, so long as certain initial conditions exist and the limitations of each approach are known; however, a comparison between the two techniques, despite being interesting, was not intended, as the concept that differences in methodological research perspective could, once again speculatively speaking, result in radically different approaches to a similar problem [200] [49, ch.iv] [8] [14] [11] [85] [90] [35, pp.129–144] [65] [172] [173] [56] [206] [31] [43] [8] [208] [209] [115] [189] [207] [210]. While such differences in methodological origin generally only manifest themselves upon comparison of the macroscopic versus microscopic metaphysical perspective of interdisciplinary research, a notion that would seem to inherently imply that one perspective is better suited to accurately predict observable averages than singular occurrences or singular occurrences over observable averages; yet, to complicate matters further, it could also

be argued, as it was previously pointed out, that because the physical chemistry example did utilize equations with some amount of averages intrinsically embedded within them that either the methodological categorization was incorrect or the methodological category used is simply flawed and everything is truly based upon the methodological philosophy of averages [200] [49, ch.iv] [8] [14] [11] [85] [90] [35, pp.129–144] [65] [172] [173] [56] [206] [31] [43] [8] [208] [209] [115] [189] [207] [210].

Yet such cynical observations can only occur, primarily because the definition of conceptual understanding is a relatively abstract term, and such abstraction inherently implies that metaphoric shades of gray can and, in fact, do exist [29, pp.11–13] [9] [31] [19] [201]. Likewise, the scientific utilization of such abstraction mandates that a definitive benchmark is defined prior to conducting any assessment, and to illustrate this point further by using the previous example as a guide, If, for the sake of argument, the electrical engineering methodological approach utilized was selected as the conceptual understanding benchmark and compared to the physical chemistry modeling approach then the conclusion would be — relatively speaking — that the physical chemistry approach is more quantitatively certain than the electrical engineering approach because it utilizes a greater amount of theoretical detail, at least regarding the physical structure of the biomaterial under observation, within its prediction than the electrical engineering approach [211] [212] [14] [172] [49] [8] [43]. Conversely, as it has already been discussed, it is easy to recognize that this argument, regarding the definition of conceptual understanding, extends deeply into the metaphysical domain and although such discussion can be rather enlightening, the only attribute of current concern is the metaphysical duality, previously discussed, that arises from the metaphysical differences interpreting natural events based upon the limitations of the human perspective [29] [15] [9] [10] [14] [49] [8] [43].

Nevertheless, despite encountering some minor philosophical ambiguities, both disciplines depicted, speculatively, did in fact utilize the same scientifically accepted methodology; however, both disciplines, at least upon application of the same scientific research methodology, once again, naturally interpreted and limited by disciplinary conceptual understanding, produced different approaches to solve the same problem that, under applicable circumstances, can provide similar results [200] [213] [214] [31] [65] [14] [49] [8] [43] [210]. While such results tend to articulate the existence of a seemingly illogical possibility, as the mind has a tendency to believe that both methods cannot yield a correct answer while being fundamentally different, yet, as previously discussed, such an occurrence is neither illogical nor impossible and such occurrences are, once again, a fundamental reminder that all scientific research is fundamentally limited by humanities interpretation and such limitations are the metaphoric highway that all interdisciplinary interactions inevitably travel upon [15] [29] [206] [12, pp.32–37] [215, pp.75–79] [173] [14] [49] [8] [43]. Although this point could be rearticulated further, a notable seventeenth century mathematician by the name of Blaise Pascal best surmised this particular scenario by writing

> "*The world is a good judge of things, for it is in natural ignorance, which is man's true state. The sciences have two extremes which meet. The first is the pure natural ignorance in which all men find themselves at birth. The other extreme is that reached by great intellects, who, having run through all that men can know, find they know nothing, and come back again to that same ignorance from which they set out; but this is a learned ignorance which is conscious of itself. Those between the two, who have departed from natural ignorance and not been able to reach the other, have some smattering of this vain knowledge, and pretend to be wise. These trouble the world, and are bad judges of everything.*

The people and the wise constitute the world; these despise it, and are despised. They judge badly of everything, and the world judges rightly of them" [216, p.66].

While Pascal's acrid tone could be attributed to his age and declining health, as Pensees [†1] was written near the end of his life, yet his message, despite being acrid, does embody the true spirit of scientific research by elaborating its close connection with the metaphysics of nature [217, p.621] [14] [49] [8] [43] [218] [219] [220] [221]. Likewise, Pascal, at least within this particular passage, seems to be articulating the accumulated wisdom obtained thru many years of intellectual inquiry and seems to be imparting the message that proclaiming scientific wisdom by denying the existence of humanities metaphysical uncertainty simply blinds a person to the reality of the natural world; as doing so would be as silly as proclaiming natural events cannot occur without a human perceiving those events [14] [49] [8] [43] [218] [219] [220] [221]. Although Pascal's words are dated, his message has survived times scrutiny and has been modernized and refined; a notion that is elegantly depicted by the twentieth century philosophical works of Lecomte du Nouy who wrote

"*Scientific learning is composed of two opposites which nonetheless meet each other. The first is the natural ignorance that is man's lot at birth. The second is represented by those great minds that have investigated all knowledge accumulated by man only to discover at the end that in fact they know nothing. Thus they return to the same fundamental ignorance they had thought to leave. Yet this ignorance they have now discovered is an intellectual achievement. It is those who have departed from their original condition of ignorance but have been incapable of completing the full cycle of learning who offer us a smattering*

[†1] French phrase for: That which the mind thinks

of scientific knowledge and pass sweeping judgments. These are the mischief makers, the false prophets" [14, p.13]

[49] [8] [43] [218] [219] [220] [221].

While Nouy tends to be a touch more zealous, but a shade brighter than Pascal's acrid scorn, the message being conveyed is the same, if not a touch more illuminating than Pascal's original statement, and such philosophical sentiments are — in many respects — an interesting paradigm to live by, as such notions are very applicable to both intra-disciplinary research and interdisciplinary research alike, at least based upon the discussion provided above [14] [49] [8] [43] [218] [219] [220] [221] [20] [200] [65] [222] [210]. Thus, with this being said, it becomes obvious that effective interdisciplinary research begins with understanding scientific culture, and this understanding can only be obtained by not only recognizing the obvious differences, like notational differences, but also the unspoken metaphysically oriented differences that exist, which requires keeping an open mind along with a willingness to immerse oneself into a foreign research culture [14] [49] [8] [43] [20] [200] [65] [223] [224] [222] [222] [210]. Although, interdisciplinary research is possible without taking such attributes under advisement; nevertheless, based upon the wisdom of Nouy's and Pascal's sentiments, the occurrence of "*sweeping judgments*" within interdisciplinary research, at least under such conditions, would seem to to be an inevitability — if such considerations are not taken under advisement — and the occurrence of such judgments — as a result — would be seemingly destined to hinder further research, if not completely discourage such research entirely [14] [49] [8] [43] [20] [200] [65] [223] [224] [216] [210].

3.3.2 Interdisciplinary Research and Contemporary Society

Although such discussion, at least regarding the effects scientific culture has had on in-

terdisciplinary research, despite being interesting and intellectually stimulating, did suggest that a similar parallel could be found upon comparison of the subject with contemporary society and such notions merit further examination, though not necessarily to the same extent the previous section received [20] [200] [9] [10] [65] [87]. Likewise, to begin such an examination, it should be mentioned, once again, that most modern consumer electrical applications are, in principle, very electrically similar to the digital voice recorder example previously provided, yet despite such fundamental similarities, at least based upon the varying amounts of social popularity that such applications have received, it would appear that society, in general, seems to have a tendency to prioritize the importance of such applications using a rather arbitrary and somewhat irrational scale, as opposed to categorizing them using a more systematic process, for example, such as prioritizing such applications based upon there overall function or there overall intellectual complexity [136] [203] [225] [226, pp.1–2] [176] [227] [7] [206] [228] [229] [230] [231]. Yet while such prioritization might appear arbitrary; however, such prioritization does seem to be — loosely — dependent upon the overall perceived social benefit of the application within contemporary society, and although science tends to rigorously abhor such ambiguity, particularly social ambiguity, some clarity can be obtained from the observation, at least within the bioelectrical research area, that a somewhat less arbitrary connection does exist between the socially perceived benefit of an application and the ability of that application to positively affect human health or extend human longevity, more so under circumstances in which life would have otherwise been previously discontinued [176] [227] [7] [206] [229] [230] [231] [31] [19]. Conversely, an interesting consequence that arises, at least from such social consensus, is the substantial amount of economic resources that are frequently being invested in to the development and improvement of applications that are perceived beneficial, a task that is

primarily observed — at least within the biomedical research community — through targeted funding of specific research subjects [232] [233] [234] [235] [236] [237] [238]. Similarly, further investigation reveals both an overall positive social opinion of biomedical research and also an underlying desire to contribute to the advancement of the subject in some way, shape, or form; a notion that is generally made manifest by the organization of community events, such as walks or awareness campaigns, that are — more often than not — geared towards the acquisition of additional research funding [239] [240] [241] [20] [242] [243] [244].

Nevertheless, despite societies desire to positively contribute to the understanding of such applications, at least upon confinement of the discussion within the boundaries of the biomedical research area, it is interesting to observe the overall social tendency to summarize significant research contributions through the usage of generic categories like: cancer research, Parkinson's disease research, human immunodeficiency virus (HIV) research, cosmetic research, or deoxyribonucleic acid (DNA) research [245] [246] [234] [240] [100, p.284] [159] [200] [244] [232]. Yet, such summarization, while defining an end application or research objective, tends to overlook the significance of individual disciplinary research contributions and fails to specify the disciplines needed to research that particular objective [200] [20] [176] [247] [248] [249] [250] [251]. Likewise, while it is tempting to attribute societies overall summarization of complex biomedical research based solely upon its general ignorance of scientific subjects; however, such blame would be misplaced, especially given the number of disciplines required to effectively research such topics and the metaphoric interdisciplinary quagmire created that some veteran interdisciplinary researchers, at times, have difficulty navigating [252] [253] [254] [255] [256] [10] [9] [115]. Thus, it should come as no surprise that if a veteran interdisciplinary researcher can have difficulties keeping interdisciplinary concepts straight that the average layman would natu-

rally find such concepts far more confusing, hence why such concepts are typically socially communicated thru the usage of generic summarization regardless of how scientifically inaccurate that summarization is [20] [200] [115] [65] [244] [239] [19] [198] [257] [70, pp.80–85] [90, pp.39–40] [258] [259] [260]. Conversely, to better illustrate why and how such summarization generally occurs, consider for the moment one common socially perceived biomedical application called the electrocardiogram, a common medical diagnostic device found in hospitals around the world, that is capable of providing information regarding the movement of the heart based upon noninvasive measured electrical activity, and examine the fundamental concepts that were used to develop this particular application [129, p.18–19] [155] [154] [157] [148] [261] [165].

Thus, without having to provide a substantial amount of technical detail, although such technical detail will be discussed in later chapters, it can be said that, at least upon reviewing the knowledge needed to develop and utilize this particular application, an electrocardiogram (ECG or EKG) system would need to utilize electrical engineering theory, which is naturally based upon a number of theoretical principles from the discipline of physics, in the acquisition and analysis of electrical signals produced by the heart [129, p.18–19] [155] [154] [157] [148] [261] [165] [110]. Similarly, a basic knowledge of medical physiology is also required to correlate the measured electrical signals with the physical movement of the heart, and some knowledge of both biology and chemistry would be needed to determine optimal electrode placement for accurate detection of electrical signals along with some understanding surrounding the chemical gradients in the heart that created those signals [129, p.18–19] [155] [154] [157] [148] [261] [165] [110]. Furthermore, additional scientific disciplines would be needed to determine how the device would be commercially manufactured along with how to make the device electrically safe for hu-

man usage [129, p.18–19] [155] [154] [157] [148] [261] [165] [110] [176] [125] [119]. Yet despite the significant number of disciplines needed to develop this particular application, society in general will mentally summarize the electrocardiogram by its end usage within the medical discipline rather than recognizing the other disciplines involved with the devices development [255] [256] [254] [252]. Similarly, other medical devices, including the electromyogram (EMG), used to observe electrical signals produced by muscle movements, along with the electroencephalogram (EEG), used to observe electrical signals produced by the brain, fall into a similar social classification that is, once again, based upon their end usage rather than the interdisciplinary knowledge utilized during there development [129, p.18–19] [155] [154] [157] [148] [261] [165] [110] [176] [125] [119] [255] [256] [254] [252]. Likewise, another medical device called a nuclear magnetic resonance imager (MRI), which applies electromagnetic theory to observe nuclear magnetic resonance, within the human body, makes use of a similar amount of disciplinary knowledge as the previous examples, although requiring a slightly different theoretical distribution of such knowledge, is yet another example of a device that is categorized socially in a similar manner as the EKG, EMG, and EEG [261] [262] [129, p.18–19] [155] [154] [157] [148] [261] [165] [110] [176] [125] [119] [255] [256] [254] [252]. Furthermore, a medical device called a biological impedance analyzer (BIA), which utilizes low-voltage alternating current signals to analyze skin impedance, is yet another example of a medical device that requires an assortment of interdisciplinary concepts that are, once again, surmised, at least within contemporary society, by its consumer application [263] [97] [16] [1] [261] [255] [256] [254] [252].

Using these previous examples as a guide, it is interesting to observe the number of diverse disciplinary concepts required to develop even the most rudimentary biomedical ap-

plication and the amount of time that would be required to individually understand every pertinent theoretical concept used by such applications [58] [115] [19] [31] [102] [36] [97] [16]. While such examples do tend to vindicate societies usage of generic social summarization when it comes to discussing scientific research, and — at the very least — does offer some insight behind its occurrence since, after all, the years of intellectual inquiry needed to understand every theoretical attribute associated with a particular application is simply a luxury that a layman seldom has — or, for that matter, would be willing to endure [58] [115] [19] [31] [102] [36] [97] [16] [255] [256] [254] [252]. Yet such summarization would almost seem inevitably destined to have future consequences and likewise, problems can arise, as it might be expected, that can have profound consequences, particularly within the bioelectrical engineering research area [255] [256] [254] [252]. To elaborate this point further, consider for the moment the social distribution of research funding, at least as it pertains to its distribution within the biomedical research area, as there seems to be a strong correlation between the amount of funding received verses the amount of overall positive social attention a research topic has received, and such observations tend to metaphorically pave the way for some interesting discussion regarding societies fundamental role within the sciences [255] [256] [254] [252] [18] [257] [232] [234] [239] [240] [235]. While, it is important to recognize that such observations are not necessarily absolute for every circumstance, after all there are always unique exceptions to such generalizations, a notable example being the number of socially oriented government programs that have provided research funding based upon academic merit, like America's NSF or DARPA programs to provide some examples — though the previously discussed effects of scientific culture seem to play a significant role in determining funding distribution for this particular case; however, regardless of the method utilized, even if funding was directly

distributed based upon the subjects overall intellectual merit, such funding does ultimately originate from society in one way, shape, or form, and thus, on some level, will inevitably be distributed based upon a criteria that originates from or is biased by social expectations [255] [256] [254] [252] [18] [257] [232] [234] [239] [240] [235] [264] [265]. Conversely, a common consequence of this type of scientific funding generally results in either perceived socially beneficial research topics, that were fortunate enough to fall under this classification, receiving an overwhelming amount of support or socially unacknowledged research areas, like particular bioelectrical research topics, modifying the scope of their research to include perceived socially beneficial objectives, since such modification would increase the likelihood of such research being socially perceived and thus increase the odds of receiving future funding [255] [256] [254] [252] [18] [257] [232] [234] [239] [240] [235] [264] [265] [266].

While such descriptions might appear to be somewhat intellectually grim — although there typically is some type of natural "pro" [†1] for every mentioned "contra" [†2] under such circumstances— yet the critical concept to take away from this observation is the fact that, regardless of whether academia admits it or not, societies perception of science and even its metaphysical beliefs, ultimately effect what subjects are researched in some way, shape, or form [267, p.1462,p.432] [255] [256] [254] [252] [18] [257] [232] [234] [239] [240] [235] [264] [265] [266] [20] [259] [28] [52] [14] [8] [43]. Nevertheless, while such attributes might appear somewhat grim to an intellectually driven mind; however, societies scientific expectations, as previously mentioned, while having a tendency to focus scientific research towards a specific issue or onto a particular consumer application, is not necessarily without some merit or benefit; after all, there is a metaphoric idiom that states that "*a chain is only as strong as its weakest link*" and the same can

[†1] Latin for: on behalf of.
[†2] Latin for: against.

be said for society, since to quote Arthur C. Clarke "*Any sufficiently advanced technology is indistinguishable from magic*", thus based upon such a depiction, it should come as no surprise that society would naturally seem to fear, or for that matter hate, anything that is beyond its current ability to intellectually comprehend; a notion that would seem to make societies involvement within the sciences a good thing [92, p.93] [267, p.1462,p.432] [268, p.13–36] [255] [256] [254] [252] [18] [257] [232] [234] [239] [240] [235] [264] [265] [266] [20] [259] [28] [52] [14] [8] [43]. Yet it is important to point out that such observations do not necessarily imply that the social dictation of scientific research is a good thing; after all there is a definitive difference between social involvement and social dictation, and one need only consider the events that occurred during the dark ages to show that the social dictation of scientific objectives generally yields horrible results [255] [256] [254] [252] [18] [257] [232] [234] [239] [240] [235] [264] [265] [266] [20] [259] [28] [52] [14] [8] [43] [53] [177] [159] [54].

While such observations are beginning to extend beyond the intended scope of this discussion, the important concept to take away from all of this is the fact that connections do exist between scientific research and societies overall cultural perception of that research [255] [256] [254] [252] [18] [257] [232] [234] [239] [240] [235] [264] [265] [266] [20] [259] [28] [52] [14] [8] [43]. Likewise, it is also important to recognize that such connections play a significant role, though a frequently unacknowledged role, in determining the subjects that scientific disciplines end up researching and such social connections, at least as they pertain to the biomedical and bioelectrical research area, tend to result in a significant amount of importance being placed upon particular medical applications, like cancer research for example, since funding for such research is more available and the positive metaphysical attributes, such as social prestige and the likelihood of scien-

tific martyrdom, are also greater [255] [256] [254] [252] [18] [257] [232] [234] [239] [240] [235] [264] [265] [266] [20] [259] [28] [52] [14] [8] [43] [213] [269] [11] [224] [234] [214]. Yet, while research funding and positive metaphysical attributes are a significant enticement in determining scientific research topics; however, social opinion is inherently volatile and is always changing, an observation that is easily observed upon analyzing how social opinion changes political opinion and political opinion changes social opinion, so much so that any scientific research selected based solely upon social funding becomes a metaphoric tree in the wind that will have to continually bend and sway with the current social perspective to keep from breaking [255] [256] [254] [252] [18] [257] [232] [234] [239] [240] [235] [264] [265] [266] [20] [259] [28] [52] [14] [8] [43] [213] [269] [11] [224] [234] [214]. While it could be argued that political opinion is simply an aggregate social opinion with a lengthy time delay, and that the oscillatory effects observed appear to imply that a marginal instability exists within the structure of contemporary society; however, setting such observations aside, it would appear that social volatility is yet, just another fact of life and that such volatility has shaped biomedical research topic selection for better or worse, a fact that is generally made manifest by particular research topics becoming metaphorically taboo [255] [256] [254] [252] [18] [257] [232] [234] [239] [240] [235] [264] [265] [266] [20] [259] [28] [52] [14] [8] [43] [213] [269] [11] [224] [234] [214].

Although, to imply that the scientific community would actively discourage any legitimate scientific research based solely upon its desire for further social funding would clearly be an overstatement, yet there definitively is a political attribute within the scientific community, particularly within academia, and such connections, from time to time, tend to be rather persuasive when it comes to the subject of topic selection [255] [256] [254] [252] [18] [257] [232] [234] [239] [240] [235] [264] [265] [266] [20] [259]

[28] [52] [14] [8] [43] [213] [269] [11] [224] [234] [214]. Nevertheless, while such social issues can directly affect the intended objectives of scientific research or at least govern the rate at which that research is done thru financial regulation; however, the metaphysical principles that merge together to create the pillars of social ethics have had a more prominent effect in defining the limitations placed upon scientific research and its derivative applications, as anything that attempts to go beyond the boundaries defined by contemporary social ethics will — rightfully — induce public outcry, if not a riot [255] [256] [254] [252] [18] [257] [232] [234] [239] [240] [235] [264] [265] [266] [20] [259] [28] [52] [14] [8] [43] [213] [269] [11] [224] [234] [214]. While such boundaries present a metaphoric doubled edged sword, since on one hand, if the intended research is inherently beneficial and, for the most part truly ethically benign, but society is not sufficiently intellectually advanced enough to understand that research, an example exemplified by the correlation between Mary Shelly's book Frankenstein and — Luigi Galvani's nephew — Giovanni Aldini's public electrical experimentation with human cadavers that resulted in the development of a profound social stigma of bioelectrical research in the eighteenth century, then such socially imposed ethical boundaries are more of a hindrance to the progression of intellectual advancement than beneficial; However, on the other hand, if the intended research, even if it promises to provide beneficial results, is considered to be socially unethical over a lengthy period of time and heavily diverges from the sentiment do no harm, an example exemplified by some of the world war two scientific atrocities conducted by the Nazi doctor Josef Mengele — atrocities so horrible that, after the war, his actions were, in part, responsible for the creation of a code of scientific ethics, outlined within the Nuremberg code, that paved the way for modern biomedical ethical guidelines — then such research, regardless of any possible benefit, should be neither conducted nor aca-

demically condoned [255] [256] [254] [252] [18] [257] [232] [234] [239] [240] [235] [264] [265] [266] [20] [259] [28] [52] [14] [8] [43] [213] [269] [11] [224] [234] [214] [99] [270] [271] [272] [273].

3.3.3 Interdisciplinary Research and Intra-disciplinary Opinion

While such attributes — referring to, once again, the previous discussion regarding the metaphysical nature of the biomedical research area, the social problems encountered, and the scientific cultures that have developed as a result — have provided a solid real-world depiction of the many interdisciplinary challenges faced by contemporary researchers working within this area [29] [15] [49] [14] [8] [43] [227]. Nevertheless, while a number of different interdisciplinary perspectives and considerations were provided — along with the occasional intra-disciplinary concern —, yet, for the most part, the topic of intra-disciplinary relations was, by and large, generally ignored [227] [257] [31] [162] [200] [115]. Therefore, with this being said, it now seems prudent to examine the effects intra-disciplinary interactions can have within interdisciplinary research in order to provide a metaphoric complete picture of the numerous metaphysical challenges being faced by researchers who choose to work within an interdisciplinary environment [227] [257] [31] [162] [200] [115].

To begin such a discussion, it is important to reiterate that, for the most part, researchers who have chosen to work within an interdisciplinary research area — like the biomedical and bioelectrical research area — were not explicitly trained — as in possessing a degree explicitly stating, for example, bioelectrical engineer — to work within this particular area and, as a result, these researchers ultimately have a metaphoric point of academic origin — for example, a bioelectrical researcher might possess a degree in electrical engineering and, at least amongst other electrical engineers, still be considered, first and foremost, as an electrical engineer rather than a bioelectrical engineer [227] [257] [31] [162] [200] [115] [213] [222] [65] [229] [173] [231] [257]. Likewise, the in-

herent existence of this metaphoric point of academic origin has a tendency to create some interesting interdisciplinary dynamics upon the introduction of intra-disciplinary interactions — as in the introduction of interactions between an interdisciplinary researcher and the researchers discipline of academic origin — and such interactions, like the many interdisciplinary problems previously discussed, can be extremely problematic if left unaddressed [227] [257] [31] [162] [200] [115] [213] [222] [65] [229] [173] [231] [257]. Conversely, to explore such attributes further, consider for the moment the, previously discussed, concept of scientific cultures and the discussion that arose regarding the manifestation of something best described as being disciplinary common knowledge found within each isolatable scientific culture [239] [254] [252] [13] [49] [14] [8] [43] [227].

While the problems associated with the occurrence of scientific common knowledge were addressed within the scientific cultures section, at least from the perspective of interactions between unrelated disciplines; however, this particular discussion did not incorporate interactions between an interdisciplinary researcher — well-versed in such differences — and an intra-disciplinary researcher who is not [227] [257] [31] [162] [200] [115] [213] [222] [65] [229] [173] [231] [239] [254] [252] [13] [49] [14] [8] [43]. Thus, upon considering such scenarios, it is possible to presumed that, because a well-versed interdisciplinary researcher is involved, no significant interdisciplinary communication problems would — or for that matter could — arise since, after all, a well-versed interdisciplinary researcher would have both the ability to foresee and compensate for any problems that might naturally arise [227] [257] [31] [162] [200] [115] [213] [222] [65] [229] [173] [231] [239] [254] [252] [13] [49] [14] [8] [43]. Yet such assumptions, while being both fundamentally sound and seemingly correct, fail to incorporate the intellectual and emo-

tional burden being placed upon the interdisciplinary researcher — as the responsibility of cultural translation is being extensively placed upon the interdisciplinary researcher — and such burdens, particularly after significant repetition over an extended period of time, tend to metaphorically brew malcontent — if not full-blown resentment — of such interactions, and such tendencies can manifest themselves negatively in a number of observable ways [20] [7] [206] [229] [244] [241] [274] [227] [257] [70] [162] [19] [14] [8] [43].

For starters, because the initial manifestation of malcontent — and the progressive path towards resentment — is, at least at its initial onset, typically a reasonably slow process — although other factors can modify the rate of manifestation —, thus making it extremely difficult to provide a definitive step-by-step prognosis and systematic depiction of every individual manifestation; nevertheless, one possible manifestation of this particular occurrence — although variations and deviations are expected — begins initially with the presentation of an interdisciplinary concept in a highly contextualized manner — specifically geared towards the discipline of origin — that is ultimately conveyed in more or less contextualized detail depending upon the effectiveness of the communication as time progresses [275] [276] [277] [20] [7] [206] [229] [244] [241] [274] [227] [257] [70] [162] [19] [14] [8] [43]. While such attributes, at least at first, appear relatively reasonable and straightforward; however, during this process a communicational bias is being innately created — based upon the contextualization level necessitated to provide effective communication — and such biases, consequently, tend to set the precedent — or tone — for future intra-disciplinary interactions [19] [256] [255] [70] [14] [8] [43] [276] [173]. Now, with this being said, one might be tempted to proposed that the manifestation of a communication bias is both natural and beneficial, as repetition has a tendency to promote efficiency, yet such efficiency comes at the price of assumption and the frequent utiliza-

tion of such assumptions can become problematic if rigidly adhered and overly applied [275] [276] [277] [20] [7] [206] [229] [244] [241] [274] [227] [257] [70] [162] [19] [14] [8] [43]. For example, the rigid utilization of such assumptions does not account for — or for that matter permit — contextual advancement — or the intra-disciplinary researcher expanding their contextual understanding of the interdisciplinary perspective — and although the ideas being communicated between the two could be presented in a more interdisciplinary context as time progresses — as opposed to the previously assumed context — such changes never occur and such contextual stagnation results in the interdisciplinary researcher becoming irritated at having to constantly contextualize — or metaphorically down-sample — information while the intra-disciplinary researcher becomes irritated at being consistently demeaned — by the consistent contextualization — whether such demeaning was intentional or not [275] [276] [277] [20] [7] [206] [229] [244] [241] [274] [227] [257] [70] [162] [19] [14] [8] [43] [278].

Conversely, while this particular example articulates the notion of intra-disciplinary contextual advancement, such scenarios are neither strictly explicit nor are always expected since — although ideally, progressive intellectual advancement should be at the heart of an academic researchers internal core — often times such advancements never occur, either because of a lack of motivation that originates from the, previously mentioned contextual demeaning — so much so, that any concern for the subject is eventually negated, thus avoided —, or simply a lack of general interest in the subject — an attribute that is both perfectly acceptable and completely human [227] [257] [31] [162] [200] [115] [213] [222] [65] [229] [173] [231] [239] [254] [252] [13] [49] [14] [8] [43]. While the occurrence of either scenario is extremely detrimental to future interdisciplinary communication, although the former rationale — if identified quickly —

can be compensated for — through adjustment of the method of contextualization —, but the latter rationale is generally beyond improvement since, after all, it is one thing to lead a scientist to a metaphoric pool of knowledge, but quite another to make that scientist drink from that pool; nevertheless, either scenario can result in the development of a negative opinion of the interdisciplinary research being conveyed and alternatively, taint any future interactions with a particular intra-disciplinary discipline by the interdisciplinary researcher [227] [257] [31] [162] [200] [115] [213] [222] [65] [229] [173] [231] [239] [254] [252] [13] [49] [14] [8] [43] [92, p.776]. Consequently, as it might be expected, the manifestation of such characteristics — although, once again, such manifestations were based upon a particular sequence of events that can manifest differently — can not only provide the necessary catalyst to promote malcontent that — over a period of time — can also yield the, previously mentioned, intra-disciplinary resentment, but also such occurrences, — particularly when future contextual advancement is hampered by a lack of overall interest — can invoke feelings of either superiority — in cases where the lack of interest, by the intra-disciplinary researcher, is assumed to be because of an inability to understand the presented interdisciplinary concepts — or feelings of inferiority — in cases where the lack of interest, by the intra-disciplinary researcher, is assumed to be because of conceptual triviality of the concepts being presented [227] [257] [31] [162] [200] [115] [213] [222] [65] [229] [173] [231] [239] [254] [252] [13] [49] [14] [8] [43].

Likewise, while the opinionated development of such attributes — superiority or inferiority —, at least by textbook standards, should have no significant effect upon the application of the scientific methodology, and thus should play no role in the overall development of interdisciplinary research, — or for that matter, hinder

intra-disciplinary communications —; however, in all actuality, scientific communication and the scientific methodology — while generally striving to remove all metaphysical obscurities — can never completely manifest itself within reality without some ingrained metaphysical attributes present, and such ingrained metaphysical attributes ultimately play a role in defining a researchers ability to both develop and convey research effectively [227] [257] [31] [162] [200] [115] [213] [222] [65] [229] [173] [231] [239] [254] [252] [13] [49] [14] [8] [43] [11]. While such notions, like many of the concepts presented within this chapter, are, to some extent, difficult for a scientifically indoctrinated mind to accept at face value and rightfully so, yet such attribute should not be discredited outright without some thought since, after all, the outright exclusion of such notions supports the notion of intra-disciplinary pretenses and further demonstrates a possible effect of malcontent and resentment. Conversely, with this being said, because interdisciplinary interactions are far from being ideal, it seems natural to speculate that any intra-disciplinary developed predispositions — like superiority or inferiority for example — can in turn, not only hinder intra-disciplinary communication but also hinder the development of interdisciplinary research, since the effective collaboration of ideas amongst disciplines is critical to further scientific advancement [227] [257] [31] [162] [200] [115] [213] [222] [65] [229] [173] [231] [239] [254] [252] [13] [49] [14] [8] [43] [11].

Conversely, To elaborate on this attribute further, in the case of presumed superiority, interdisciplinary interactions and research alike are overlooked because they are viewed to be trivial and irrelevant; while, in the case of presumed inferiority, such interactions are also avoided — not because they are viewed as being trivial or irrelevant — but because such interactions generally result in the development of internal feelings of losing personal prestige or a desire to place no inconvenience upon a fellow researcher through

the perceived conveyance of trivial interdisciplinary concepts — that are, more often than not, not trivial [227] [257] [31] [162] [200] [115] [213] [222] [65] [229] [173] [231] [239] [254] [252] [13] [49] [14] [8] [43] [11]. Nevertheless, while either scenario — superiority or inferiority — are generally considered to be extreme consequences of such contextualization, as both scenarios can only potentially develop after a significant amount of time has passed in relation to a substantial number of negative interactions since, after all, the inescapable dynamics of humanity are clearly dominant; yet, while such occurrences are ultimately the product of intra-disciplinary or peer interactions — for better or worse —, it is important to recognize that such interactions are generally inevitable, especially within scientific research, and thus such occurrences are to be expected [227] [257] [31] [162] [200] [115] [213] [222] [65] [229] [173] [231] [239] [254] [252] [13] [49] [14] [8] [43] [269].

Likewise, with this being said, while there are a number of metaphysical dynamics — some of which were previously discussed within this chapter — that should be taken under advisement prior to attempting to become involved with interdisciplinary research topics; however — the concept best conveyed within this particular section is — before beginning such an in-depth undertaking it is important to, first and foremost, "nosce te ipsum" [†1] followed closely by learning the nature of scientific humility — depicted within Pascal's writings — since the process of knowing oneself should help aid in the identification — and possible correction — of any personally ingrained contextual irrationalities, while, at the same time, nurturing scientific humility within can, not only aid in the identification of contextual biases but also help overcome – or at the very least help mend — other researchers contextual biases — once again, in this particular case, developed

[†1] Latin for: Know thyself

as a result of intra-disciplinary interactions — since, humility — with a touch of rigid stability — can go a long way in changing contextual perceptions, if given enough time [279, p.576] [227] [257] [31] [162] [200] [115] [213] [222] [65] [229] [173] [231] [239] [254] [252] [13] [49] [14] [8] [43] [269] [216].

CHAPTER 4: HISTORICAL HERITAGE

The historical development of the bioelectrical research area is — to put it mildly — a substantially vast subject, and depending upon the historical boundaries selected, will likely begin with the presentation of circa 1900 "*Anno Domini*" [†1] or circa 600's "*Ante Christum*" [†2] material — although the occasional circa 1800's, 1700's, and 1600's starting points are utilized depending upon what historical events the presenter deems relevant [78, pp.24–25, p.127]. Nevertheless, while the existence of such a lengthy scientific heritage is, in itself, an extremely profound observation — in fact, it could be argued that all scientific disciplines fundamentally arise from the study of bioelectrical and biomedical phenomena —; however, given the amount of philosophical discussion already provided and the isolation of core background concepts into a unique chapter, it seems appropriate to briefly discuss the subjects ancient heritage, followed shortly by a minor summary of the biomedical related events that occurred within the circa 1600's to 1800's — implying that a slight gap in the historical discussion provided will exist between the fall of Rome and the circa 1600's — prior to concluding with an overview of the current state of bioelectrical affairs.

Likewise, with this being said, while much of the information surrounding the beginnings of the bioelectrical research area has been — as it might be expected — metaphorically lost in the ebb of time; however, based upon the information that did survive, it appears that the fundamental theories that sparked this particular subject seem to have originated

[†1] Latin phrase for: in the year of our Lord — commonly abbreviated as A.D. or interculturally defined as C.E.

[†2] Latin phrase for: Before Christ — commonly abbreviated as B.C. or interculturally defined as B.C.E.

— in part — from the ancient Greek philosopher Thales who lived somewhere between 625 to 547 Ante Christum [78, pp.24–25] [129, p.11]. While it is worth mentioning that this particular piece of information is only known because it was written within the writings of another Greek philosopher — Diogenes Laertius — who lived around 200 Anno Domini — note the substantial general gap between the two philosophers — Laertius' writings seem to indicate that Thales wrote two books — sadly neither survived the test of time — that, by some accounts, seem to have contained Thales' written observations regarding electrostatic and magnetic phenomena [78, pp.24–25] [280, p.121] [281, p.14].

While, all that remains of Thales' observations —- regarding, once again, electrical phenomena — seems to primarily arise from secondhand accounts — likely obtained by reading his now defunct book — were predominately reiterated within the writings of Aristotle — yet another Greek philosopher who lived around 384 Ante Christum —; however, based upon the frequent reference to Thales's work by Aristotle, Laertius, and a few other Greek philosophers of the era, it seems likely that Thales' observations were some of the first ever written on the subject — excluding for the moment the possible Egyptian electric catfish hieroglyphic [78, pp.24–25] [280, p.55] [281, p.15] [48].

Nevertheless, Diogenes wrote — in his written historical accounts — that Thales seem to enjoy speculating about the underlying nature of the electrical phenomena he observed upon rubbing animal skin against amber, and the phenomena he observed when a magnet was placed near iron — now called electrostatic and electromagnetic phenomena respectively [281, p.15]. Likewise, while Diogenes' historical accounts — again regarding Thales — are also somewhat substantiated within Aristotle's — who was the ancient equivalent of a modern day blogger — writings, in which Aristotle recounts Thales proposing that magnets

might have an "anima" [†1] because of the phenomenas ability to attract iron — movement was equated with life within this era — [281, p.15] [47, p.405a–15]. While it should be noted that Thales did seem to believe — based upon the writing's of Diogenes and Aristotle — that a "anima", soul, or life force, had the ability to produce a motive force, thus making it logical for him to conclude that a magnet was alive and had a soul because of its ability to attract iron [47, p.405a–15]; yet, based upon such documented observations, it could be proposed that Thales would have also held a similar belief surrounding his observations of electrostatically charged amber; although, the translated works of Aristotle, upon further consultation, neglect to make any mention of this particular attribute [47, p.405a–15]. While the lack of written discussion by Aristotle on this topic is unfortunate, since it would help strengthen Diogenes historical recount; however, it is also quite possible that Aristotle did in fact mention Thales views — on this subject — but such details were simply lost over the years or during the translation of his works [281, p.15] [47, p405a–15] [282].

Nevertheless, while it might be somewhat unclear as to why Thales is important enough to mention in an historical discussion regarding bioelectrical signal acquisition — other than to illustrate the subjective view that Thales might have been the first person to openly discuss observing magnetic and electrostatic phenomena — especially since — from a modern scientific perspective — it could have been equally augured that it would have been far more efficient to casually state that Thales may have discovered electricity, though no direct evidence exist to affirm such a statement, and simply move to the next historical milestone; however, Thales' electromagnetic observations, while important, are not necessarily critical when compared to the philosophical questions he proposed and there ramifications upon the historical development of electromagnetic research that occurred after his time. To

[†1] Latin for: Soul

explain this point further, it is first necessary to neglect any theological attributes that Thales might have invoked and consider how his statement regarding the origin of the soul directed scientific research during his time. Conversely, because It is clear within Aristotle's writings that the philosophers of the day had a fundamental desire to understand what life was and why it existed, hence their desire to define the soul, this in turn resulted in their investigation of subjects related to these fundamental questions [47, p.405a–15]. Likewise, it is clear throughout Aristotle's De Anima that the various philosophers of the day explored these fundamental questions thru an iterative process of proposition, discussion and rebuttal which resulted in the creation of a lengthy list of what the soul was not but never what the soul was [47, 402b–435b] [78, pp.24–25, p.66].

While philosophers, even in this day in age still debate these topics, primarily because the answers to such questions are inherently open-ended, it is important to observe that it is not the answer to such questions that is important but it is the act of trying to answer such questions which paved the way for the development of bioelectrical signal acquisition theory. To illustrate this point, consider how Aristotle's desire to understand the true nature of the soul, one such account is documented in his book Historia Animalium, resulted in Aristotle studying various animals from a scientific perspective and creating a detail list of his observations [283] [78, pp.24–25, p.107]. Although Aristotle was never able to definitively define what the soul was, his writings recollecting the attempt were beneficial to the advancement of many scientific subjects and were important to the topic of bioelectrical signal acquisition thru his recollection regarding the torpedo fish in Historia Animalium [283, p.620b].

The torpedo fish, as Aristotle recounts in Historia Animalium, is able to narcotize prey using the power of electric shock, though it should be noted that while the Greeks did have

some knowledge surrounding electrical phenomena there is no evidence to suggest that they either comprehended the phenomena or made the connection between the torpedo's shock and the electromagnetic phenomena observed during their day [283, p.620b] [47, pp.402b–435b]. While it is very interesting to see Aristotle mention the torpedo during his exploration of the soul, he was not the only philosopher from ancient times to take note of the unusual electrical properties of the torpedo as observed by its usage in Plato's dialogue Meno which was written around 390 Ante Christum [284, p.12] [78, pp.24–25]. Upon examining the metaphoric usage of the torpedo within Plato's Meno seems to imply that a common knowledge about the torpedo's unusual numbing properties was well established long before Aristotle's writings on the subject [284, pp.12–13]. Additional supporting evidence of this statement is found within Hippocrates' Hippocratis Corpus which discusses the dietary value of the torpedo's soft skin for the treatment of internal diseases yet neglects to mention any numbing properties of the torpedo's shock [285, p.124] [286] [287, pp.151–178].

While Hippocrates lack of description about the electrical nature of the torpedo is somewhat peculiar, it is reasonable to assume that the ancient Greeks did eat the torpedo on occasion and thus fishermen during this time had to have known about the numbing properties of the fish upon catching them [285, p.124] [286] [287, pp.151–178]. One possible explanation for Hippocrates silence on the electrical nature of the torpedo could have been because this numbing property was so widely known it was not worth mentioning within his writings though there is no definitive evidence to support this theory [285, p.124] [286] [287, pp.151–178]. While it is clear that the ancient Greeks did have knowledge of the electric fish, it is speculated that they were not the first ancient culture to have possessed such knowledge and this speculation is supported by Egyptian hieroglyphs that date back to

approximately 3000 Ante Christum that are assumed to depict the electric catfish of the Nile [78, pp.24–25] [48, pp.19–28] [129, p.11]. However, this evidence is somewhat unclear because of the unknown nature of old Egyptian hieroglyphs which differ from middle and late Egyptian hieroglyphs because of linguistic revisions to the language that occurred around 2100 Ante Christum [78, pp.24–25] [48, pp.19–28] [288, p.1]. What is known for sure is that an old Egyptian hieroglyph was used to represent the name of the Egyptian pharaoh Narmer and within this hieroglyph there is a picture of a fish that closely resembles the electric catfish of the Nile thus yielding the source of scholarly speculation on the subject [48, pp.19–28] [288, p.1, p.9–11]. Although Narmer's hieroglyph could potentially be the first written word depicting the Egyptian electric catfish additional depictions of the fish are found on the walls of Egyptian tombs that have been verified to have been created before the writings of the Greek philosophers but after the time of Narmer [48, pp.19–28] [288, p.1, pp.9–11] [129, p.11] [286].

Even though the historical importance of both the torpedo fish and the electric catfish is not yet visible to the development of bioelectrical signal acquisition, a few morsels of modern history must be introduced in order to fully understand why the discovery of the electric fish was so important to the overall advancement of the subject. To elaborate further, it is known from the historical information provided above that the philosophers of the day had no formal knowledge of electrical phenomena, thus it is relatively straight forward to come to the conclusion that those philosophers were completely unaware of the electrical nature of these fish beyond their firsthand experience with the fish's power to numb [283, p.620b] [47, pp.402b–435b]. While those philosophers could not understand the nature of the electric fish, modern electrical theory has illuminated the subject and has revealed that the torpedo fish, depending upon the species, is capable of producing

an electrical potential between 45V to 220V while the electric catfish, depending upon the species, is capable of producing an electrical potential of around 350V [289] [286] [290, p.814]. Furthermore, research into this subject has also revealed that the torpedo fish, which is native to salt water, can produce an average short circuit current on the order of 4A while the electric catfish, which is native to fresh water, has not been studied in enough detail to provide a definitive value for their average short circuit current [291, pp.1025–1038] [292] [293] [294] [295].

While it is unfortunate that a value cannot be given to illustrate the average short circuit current capabilities of the electric catfish, it should not be assumed that no research has been done on the subject since there are many scientific publications available that have researched the catfish's, along with the torpedo's, physiological structure, electrical response to external stimulation, and ability to communicate with electrical impulses [290, pp.813–831] [296] [297] [298] [299]. While definitive values of the average short circuit current are unavailable for the electric catfish it has been found that the electric catfish along with the electric eel are very similar in both there electrical organ structure and in their ability to supply a constant voltage independent of loading because of their higher internal resistance [289] [300] [301] [302]. Based upon the electric eels ability to produce a 600V at 1A pulse it can be reasonably assumed that the electric catfish is capable of sourcing a similar amount of current despite the lack of definitive information on the subject [293]. With this in mind, a critical concept to take away from this modern analysis is the potentially hazardous electrical conditions that an electric fish can possibly induce upon contact, such injuries include minor to severe skin burns and the possibility of ventricular fibrillation of the heart [123] [124] [121] [303]. While the occurrence of a fish induced electrical injury is, for the most part, uncommon yet rationally understood in modern times; however, the

occurrence of such an injury during ancient times, though rare, was oftentimes attributed to be the work of divine intervention as illustrated by a Greek passage, written by Diodorus Siculus, which describes the death of a young man swimming in a Babylonia lake who drown as the result of a torpedo sting [285, p.122].

Taking a moment to reflect upon all of the information presented above, it becomes clear that early observations of electromagnetic and bioelectrical phenomenon resulted in the minds of ancient scholars being filled with numerous unanswered questions. Such questions, like those addressed throughout Aristotle's writings, set the foundation upon which all electrical theory is built and more importantly set the environment for the philosophical exploration of what it means to be alive [283, 620b] [47, pp.402b–435b]. These questions, at face value, might appear to be inconsequential to the development of bioelectrical signal acquisition theory, yet upon deeper exploration are found to be essential to the overall development of the subject. It is reasonable to assume that observations of birth and death during ancient times most likely caused some initial inquiry into the nature of life, similarly, it can also be reasoned based upon topics that arise in our own time, that when the unexpected is experienced it causes profound confusion as well as the desire for immediate rationalization of the experienced event [304, pp.17–61]. Thus it could be reasoned that the ancient's initial encounter with the electric fish, especially fish related deaths, resulted in many questions regarding the fundamental nature behind both the fishes' electrical abilities along with its purpose in nature. Furthermore, the ancients' interaction with magnetic and electrostatic phenomenon also resulted in the formulation of similar questions regarding the phenomenon's purpose and nature [285, p.122]. These questions, in turn, resulted in debate amongst ancient scholars who, attempted to rationalize such observations, though it should be noted that they were unable to do so. However, the ancient scholars' inability

to explain such phenomena did not diminish their desire to gain understanding of the subject, which is seen throughout their writings, and ultimately it was this unyielding desire that inspired future scientists to correctly answer such underlying questions surrounding electricity [129, pp.11–27].

With the introduction of an unyielding desire to obtain understanding, complements of the ancient philosophers of the early Ante Christum era, resulted in an unfortunate misadventure into the depths of superstition caused by the development of new philosophical ideologies that resulted in the cementation of Hippocrates' views along with ideological changes that occurred as a result of the volatile political climate that notably features the conquests of Alexander the Great and the Rise of the Roman Empire [51, pp.182–188] [78, pp.24–25] [285, p.127] [138, pp.13–26] [53, pp.1–4]. One critical concept to observe throughout this time is the migration away from the selective intellectual conglomeration to the dissemination of conglomerated ideologies. Furthermore the broad scope of philosophical enquiries, which was the norm throughout early Greek times, was distorted by refinements in dialog towards topics that have practical importance to the inner workings of Roman society [51, pp.183–185] [53, pp.3–6]. Despite this progressive decline of intellectual diversification within the sciences during this time, Lucretius, a poet that lived between 95 Ante Christum to 55 Ante Christum, stands out amongst this period as a reviving dabble of early Greek ideologies thru discussions regarding the finite nature of matter, also called atomic conception, which can be summarized by the concept that matter is inherently finite thus the atom is the smallest quantity of all matter [305, p.1] [78, pp.24–25] [53, pp.5–7] . While the notion of a fundamental unit, such as the atom, was a concept that had been taught as far back as 450 Ante Christum by Leucippus, an ideology that was opposed by Aristotle's belief in the continuity of matter, Lucretius so profoundly wrote that "*Nothing*

is ever gotten out of nothing by divine power", everything occurs in "*determinate units*", and "*Things cannot then ever be turned to naught*" [306, p.3] [53, pp.5–7] [78, pp.24–25].

Lucretius' writings, which at first appear to predict modern atomic theory along with the laws of conservation, are obviously premature in their development because, while the early Greeks did have a knowledgeable insight into the fundamental nature of the world, they had no definitive ability to validate such insight nor the scientific expertise to understand the result of such validation [306, p.3] [53, pp.5–7]. Thus this early atomic conception diverges from modern atomic theory by the ancients belief in variations in size and shape of atoms along with the fact that the Aristotle ideology was dominantly promoted by the intellectual dissemination that had begun within this time period [53, pp.5–7]. It is unfortunate that the ideologies of Leucippus or Lucretius were buried amongst the chaos of the resulting intellectual paradigm change that resulted in Aristotle's philosophy, regarding the continuity of matter, becoming the dominate ideology for centuries [53, pp.5–7]. It is doubly unfortunate that Lucretius writings regarding pestilence, water-spouts, volcanos, thunderbolts, suffocating vapors along with thunder and lightning also got buried because of the intellectual change that occurred within this time period [53, pp.7–10] [306, pp.84–85]. Such misfortunate events raise the question as to whether or not the embracement of Lucretius ideologies, at this period in time, would have brought about the understanding of the electrical nature of both electrostatic and bioelectrical phenomena sooner. However, putting such fixations aside for the moment, while it is unfortunate that the suppression of Lucretius ideologies did occur, it only delayed the inevitable since their ultimate rediscovery helped to put some spark into the formalization of electrostatic phenomena and might have helped in the development of modern atomic theory [53, pp.7–10].

While Lucretius' philosophical writings were, in many ways, some of the last that ad-

hered to the old Greek paradigm, this paradigm shifted progressively towards Roman practicality and such paradigm changes are accented by the 46 Anno Domini writings of Scribonius Largus who was both a Roman physician along with an avid follower of the unscientific method [53, p.22] [78, pp.23–24] [285, p.127] [48, pp.45–46]. Largus' critical contributions, within the context of this discussion, are his writings which describe the usage of the torpedo fish as a medical cure for the treatment of headaches and gout [285, p.127] [48, pp.45–46] [287, p.153] [129, p.11]. Largus' treatment represents a significant change in the medical usage of the torpedo, upon comparison to the treatments prescribed by Hippocrates for troubles in the digestion track, because of the utilization of the torpedo's numbing power that gracefully illustrates a classic hallmark of the Roman paradigm to implement rather than to understand [285, p.127] [48, p.45–46] [53, p.22]. While Largus' medical usage of the torpedo is quite notable, not all prescribed remedies applied during this time were based upon scientific reasoning as illustrated throughout the various folk medicines which are best highlighted by the usage of a torpedo's gall as a aphrodisiac and the electric catfish charm that supposedly would induce inseparable desire between newlyweds [285, pp.128–129].

While the transition away from the mysticism that developed during this period of time was a profound step forward, such philosophical changes did not occur quickly, which implies that various folk medicines were still being commonly prescribed and such remedies, within the scope of electric fishes, included using the torpedo's gall as a aphrodisiac along with the catfish as a ritualistic charm to induce inseparable desire [285, pp.128–129]. While mysticism remained dominant throughout this time, a medical doctor born in 130 Anno Domini by the name of Galen helped to further impart physical reason, within the medical discipline, thru the documentation of various remedies in order to determine what remedies

cured their prescribed ailment [78, pp.24–25] [138, p.41] [285, pp.131–133] [307, pp.118–122] [286]. During Galen's research Galen discovered that some confusion surrounding Largus' treatment, in particular the detail that the torpedo had to be alive was forgotten over the years, and Galen, upon discovering this thru experimentation, formally documented Largus' treatment as being valid along with the necessary conditions required in its usage [138, p.41] [285, pp.131–133] [307, pp.118–122] [286]. While Galen's contribution helped to reduce the hold that mysticism had upon the medical discipline, some of his underlying theories behind the torpedo's numbing powers were incorrect, mostly because of Galen's belief in the four humours, which resulted in Galen deducing that application of the frigorific principle would make it possible to extract the power of the torpedo and store it for later use [138, pp.39–51] [285, pp.131–133] [307, pp.118–122, pp.142–144] [286] [308, p.716]. Likewise, as it might be expected, the collapse of the Roman Empire — around this period of time — signified the beginning of the Dark Ages and resulted in a lengthy period of time in which the preservation of past traditions was status quo and resulted in a long period of scientific stagnation as illustrated by the upholding of Galen's ideas for more than a thousand years [78, p.205] [286] [307, pp.187–191] [48, pp.64–84].

Conversely, while this particular period of time — the dark ages until around circa 1600 — is, for the most part, historically moot in terms of the development of bioelectrical theory, the historical heritage of the subject seems to loosely begin again with William Gilberts book — within the circa 1600's — De Magnete, regarding lodestone and magnetic effects, and progresses further — within the circa 1700's — with the development of the electrostatic generator and the leyden jar, along with a number of publicized electrostatic experiments — the most interesting of which, arguably being, Benjamin Franklin attempting to shock a turkey using electrostatic phenomena [16]. Likewise, further advancements were made by

Luigi Galvani and Alessandro Volta — somewhere between the late 1700's and early 1800's — surrounding electrochemical phenomenon, while the work of Michael Faraday — in the 1800's — in many respects, paved the way for the majority of the bioelectrical research done within contemporary times [16].

Similarly, in terms of contemporary biomedical milestones — from a highly selective perspective — some notable contemporary achievements are: Du Bois-Raymond was able to measure the electrical currents produced by frog nerves in circa 1843. Richard Caton was able to acquire — though with low fidelity — currents produced by the brain in circa 1875. August Waller was able to obtain a human EKG in circa 1887. Rudolf Hoeber was able to determine that a frequency dependency existed within the conductivity of blood and postulated that cell membranes existed in circa 1911. The Cole brothers developed methods of modeling tissue impedance beginning in circa 1928. Debye begun developing is polar relaxation models around circa 1929. Schwan — considered by some as a founder of the biomedical engineering discipline — began developing an assortment of material characterization techniques, starting around circa 1950, that ultimately led to the development of contemporary BIS characterization techniques [16].

Likewise, while, there are a substantial number of historically relevant events — notably the work of legendary names like Hertz, Orsted, Maxwell, Einstein, Tesla, Webber, and Ohm, to name a few —, along with an overwhelming amount of contemporary research regarding EMG, EKG, EEG, and BIS that could be discussed within this chapter; however, it was decided to address each of these attributes within there research related context as needed, rather than simply listing the achievement in a chronological order, since such theory is still actively utilized — and in some cases improved — rather than simply serving as a notable historical reference [16].

CHAPTER 5: FUNDAMENTAL BACKGROUND THEORY

5.1 Electrical Engineering Fundamentals

In order to effectively analyze and create an accurate equivalent circuit model, particularly for a given atypically conductive biomaterial, an understanding of a number of fundamental electrical concepts is required, of which, an in-depth understanding of electrical impedance analysis is generally considered to be at the forefront of such discussion. Conversely, with this being said, it is the underlying purpose of this particular chapter to examine and present significant concepts, within this substantial pool of electrical knowledge, that is required to effectively model a biomaterial and to explain the results obtain throughout the research presented within this dissertation.

5.1.1 Overview of Electrical Fundamentals

Towards this end, because impedance analysis is, in fact, one of the most frequently utilized electrical engineering concepts that is generally applied upon performing transient analysis within an electrical circuit; this chapter makes the assumption that the reader is either fluent in such techniques or, at the very least, is somewhat familiar with the underlying fundamentals utilized within impedance analysis and, as such, only provides a quick and limited review of the theoretical basics needed to accomplish this particular task. Thus, with this being said, it should be noted that the original intent of this particular chapter was to simply provide a reader, whose specialization might be inside the field of electrical engineering, a place of theoretical reference, while at the same time, providing a reader, who specialization might lie outside of the electrical engineering discipline, a brief

introduction to the theory utilized while, at the same time, providing an assortment of critical keywords to aid in future inquiry, if such inquiry is necessitated. Conversely, it is also worth mentioning that this particular subsection within this chapter focuses primarily upon the theoretical aspects of impedance analysis — a theoretical concept that is frequently utilized within the confines of this dissertation.

5.1.2 Introduction to Electrical Analysis

To begin such a discussion, bioimpedances — excluding for the moment the nonlinear properties that neither adhere to Ohm's law, Kirchhoff's current law (KCL), or Kirchhoff's voltage law (KVL) — are, from a theoretical perspective, analogous to a traditional electrical impedance, insofar as, such impedances have a number of fundamental electrical characteristics that, when observed within a laboratory, can generally be mathematically represented — to varying degrees of success — through the utilization of traditional electrical engineering impedance modeling techniques. Thus, based upon this particular attribute, it seems prevalent to begin examining such attributes by first examining the underlying concepts found within impedance analysis [p.1][Grimnes2000]. Likewise, with this being said, because a electrical impedance is generally formally defined as being the "*ratio of the phasor voltage V to the phasor current I*", a concept that can be expressed mathematically by Equation: (1), the examination of this particular definition would seem to be a solid starting point [136, p.273].

$$Z = \frac{V\angle\theta_V^\circ}{I\angle\theta_I^\circ} \tag{1}$$

Conversely, when the term impedance is utilized within a given application, it generally

implies that there is some type of electrical storage element, within the material being examined, that will inevitably manifest itself as a reactive element within the theoretical model developed. Thus, loosely speaking, the introduction of a storage element or reactive component — within the model — is generally associated with a temporal shift between the observed voltage and the observed current — within the system being examined —, and the test to determine if this particular attribute exist — within the material being examined — typically utilizes an active source comparison between an appropriately selected alternating current (AC) input signal versus the observed phase shift within the material. Likewise, with this being said, the term impedance is oftentimes interchanged — if not confused — with the term resistance, as both impedance and resistance are based upon Ohm's law — which states that "*the voltage across a resistance is directly proportional to the current flowing through it*", or expressed mathematically by Equation: (2); however, while there are cases in which such substitution is merited, the fundamental difference, between a resistance and a impedance, is the numbers found within there mathematical representation [136, p.15].

$$V = IR \tag{2}$$

For example, impedances generally possess both a real and a imaginary numerical component ($\jmath$) — although the imaginary component could, in theory, be zero —, while a resistance is assumed to possess only a real numerical component and — based upon this definition — can never have an imaginary component. Thus, from a mathematical perspective, a resistance could, in theory, be written as an impedance without losing any mathematical information; however, an impedance cannot be written as a resistance without the

loss of the imaginary part that represents the phase shift observed. Therefore, with this being said, the term resistance is generally utilized to represent quasi-static or direct current (DC) electrical measurements that possess no phase shift, while the term impedance, is generally utilized to represent quasi-transient or steady-state alternating current (AC) electrical measurements. Conversely, now that the terms resistance and impedance have been defined, the mathematical expression for this term, found through the mathematical manipulation of Equation: (2), can be obtained by simply dividing both sides of the equation by the current I, as shown by Equation: (3) — in the case of a resistance — and by Equation: (1) — in the case of an impedance.

$$R = \frac{V}{I} \tag{3}$$

5.1.3 Introduction to Impedances by Measuring Phase

Because an impedance can be thought of as a resistive value with a phase angle θ° attached to it in order to preserve this imaginary component conceptually this attached phase angle is defined as the angular difference between the voltage and the current which is illustrated by Figure: (1) [263]. Generally measurements taken in the laboratory by a oscilloscope are in this graphical form which makes understanding how to find phase information graphically very important for analyzing experimental data throughout this thesis.

The time difference (Δ_Z) which is illustrated by Figure: (1) needs to be converted into a phase angle (θ°) in order to obtain any meaningful impedance information and this can be done easily if the applied signal is sinusoidal by the mathematical expression depicted

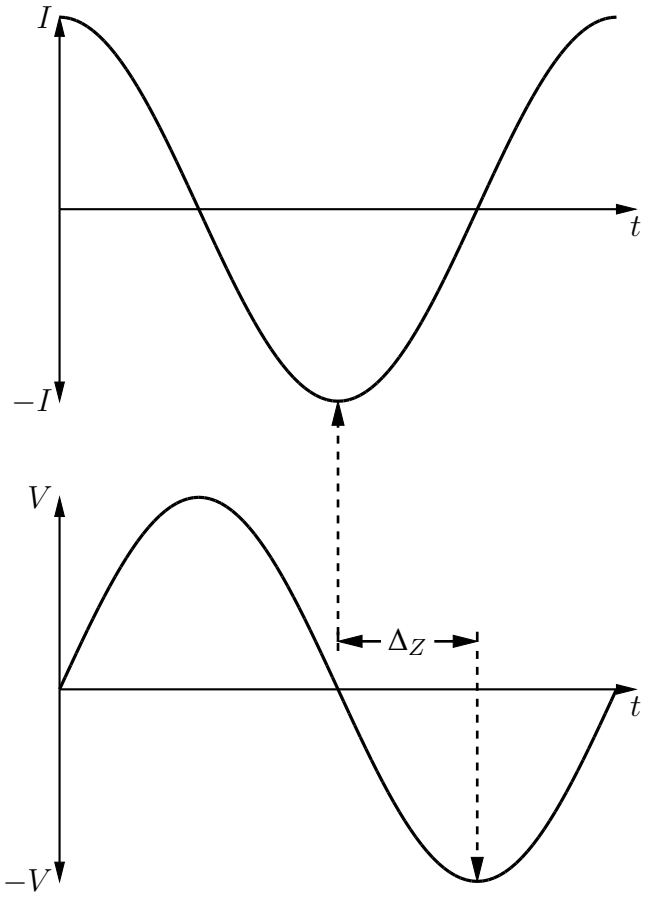

Figure 1: visual representation of θ_Z°

by Equation: (4) in which frequency f is the frequency of the applied sinusoidal signal.

$$\theta_Z^\circ = \frac{2\pi\Delta_Z f 180}{\pi} \tag{4}$$

The mathematical conversion expressed by Equation: (4) can be derived by using the following methodology. First, the measured signals are assumed to be of a sinusoidal form, which can be represented mathematically by Equation: (5) in which angular frequency ω defines the period of oscillation while time (t) represents a voltage or current location being measured in the signal. A change to either angular frequency or period of oscillation is illustrated by Figure: (2) and an additional parameter called phase shift θ_s^r describes how much the sinusoidal waves will be shifted to the left or right while such changes in

phase values are illustrated by Figure: (3) [136, pp.266–267].

$$g\,(t) = \sin\left(\omega t + \theta_s^r\right) \tag{5}$$

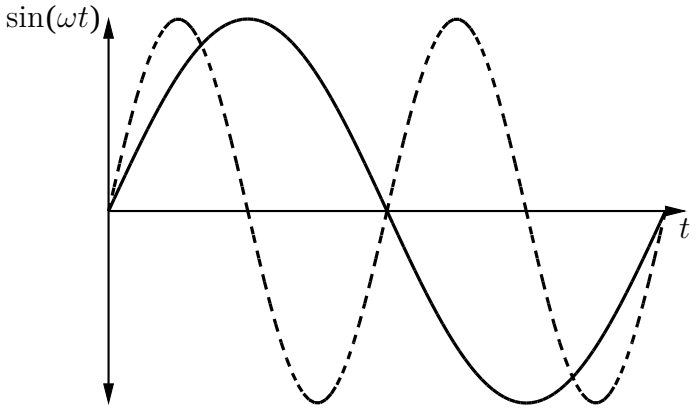

Figure 2: graphical depiction of sine with ω changed

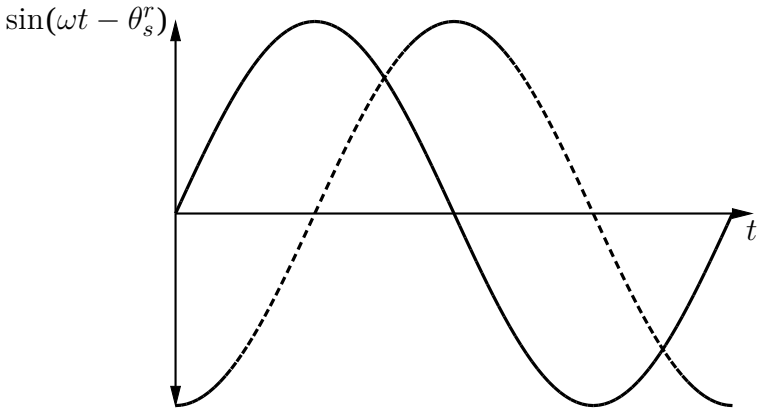

Figure 3: graphical depiction of sine with θ_s^r changed

Secondly, since it is assumed that the experimentally measured waveforms have a sinusoidal shape they can be equated to each other by the mathematical expression shown in Equation: (6). Because both signals are periodic yet shifted in phase this implies that at two points in time equal normalized amplitude values will occur such that the time difference between these values will corresponds to a phase shift between the two signals which allows the signals to be equated each other.

$$\sin\left(\omega_1 t_1 + \theta_{s1}^r\right) = \sin\left(\omega_2 t_2 + \theta_{s2}^r\right) \tag{6}$$

Thirdly, it can be assumed that because most passive impedance systems cannot change either their input or output frequency the values of ω_1 and ω_2 can be assumed to be identical which is expressed mathematically by Equation: (7). Applying this assumption to Equation: (6) results in the creation of Equation: (8).

$$\omega_1 = \omega_2 \tag{7}$$

$$\sin\left(\omega t_1 + \theta_{s1}^r\right) = \sin\left(\omega t_2 + \theta_{s2}^r\right) \tag{8}$$

At this point algebraic simplification can be applied and the inverse sine function can be used on both sides of Equation: (8) shown by Equation: (9). This simplification will result in the creation of Equation: (10).

$$\sin^{-1}\left[\sin\left(\omega t_1 + \theta_{s1}^r\right) = \sin\left(\omega t_2 + \theta_{s2}^r\right)\right] \tag{9}$$

$$\omega t_1 + \theta_{s1}^r = \omega t_2 + \theta_{s2}^r \tag{10}$$

Fourthly, typically when experimental measurements are taken the mathematical sinusoidal equation is generally unknown thus another assumption must be made about the input phase angle of the applied signal. In order to keep the mathematics simple the starting phase angle will be assumed to be zero which will allow the output phase angle

to represent the angular phase difference between the two signals. This assumption is expressed mathematically by Equation: (11) and its application to Equation: (10) results in the creation of Equation: (12).

$$\theta_{s1}^{r} = 0 \tag{11}$$

$$\omega t_1 = \omega t_2 + \theta_{s2}^{r} \tag{12}$$

Solving Equation: (12) for θ_{s2}^{r} produces Equation: (14) and factoring ω results in Equation: (15). Since t_1 and t_2 represent the time difference between the two normalized amplitude values illustrated graphically by Figure: (1) this notation can be simplified by the substitution of Δ_Z found in Equation: (13) into Equation: (15) which results in Equation: (16).

$$t_1 - t_2 = \Delta_Z \tag{13}$$

$$\omega t_1 - \omega t_2 = \theta_{s2}^{r} \tag{14}$$

$$\omega \left(t_1 - t_2\right) = \theta_{s2}^{r} \tag{15}$$

$$\omega \Delta_Z = \theta_{s2}^{r} \tag{16}$$

Because ω is expressed as angular frequency which has a base unit of radians per second while most measurements taken experimentally are done in frequency whose base unit is in Hertz a conversion from angular frequency to frequency will be required. This conversion is mathematically expressed by Equation: (17) and once applied to Equation: (16) results in the manifestation of Equation: (18) [136, pp.259–260].

$$\omega = 2\pi f \tag{17}$$

$$2\pi f \Delta_Z = \theta_{s2}^{r} \tag{18}$$

At this point θ_{s2}^{r} represents a radian phase angle however, traditionally phase angles are represented in degrees since it is conceptually easier for most people to visualize an angle in degrees thus another conversion will have to be applied to Equation: (18). This conversion is mathematically expressed by Equation: (19) and once applied to Equation: (18) results in the formation of Equation: (12) [309, pp.186–187].

$$\theta^{\circ} = \frac{180}{\pi}\theta^{r} \tag{19}$$

$$\frac{2\pi f \Delta_Z 180}{\pi} = \theta_{s2}^{\circ} \tag{20}$$

Lastly, because it was assumed early on that θ_{s1}° was equal to zero this in turn means that θ_{s2}° represents the phase difference between θ_{s1}° and θ_{s2}° thus θ_{s2}° can be written as θ_{Z}°. Substituting this change in notation into Equation: (20) produces Equation: (21) which is the same expression shown in Equation: (4) and thus concludes the derivation of this equation.

$$\frac{2\pi f \Delta_Z 180}{\pi} = \theta_{Z}^{\circ} \tag{21}$$

5.1.4 Explanation of Phase by Phasor Notation

When mathematically working with an impedance, two methods of representing the impedance value exist. One such method is formally called phasor notation and represents the impedance value in terms of a resistive magnitude and a phase angle. Phasor notation is based off of the polar coordinate system in which there is a fixed point called a pole that is located at the origin and a fixed ray called the polar axis. The origin is located at the center of the real and imaginary axis while the ray starts at the origin and continues outwards along the real positive axis. In the polar coordinate system points are defined by a coordinate pair that consists of a directed distance r from the origin to a point and an angle that starts at the polar axis and ends at the same point [309, pp.362–363]. This polar coordinate system is depicted by Figure: (4) and an impedance phasor shown by Equation: (22) is illustrated in Figure: (5) [309, pp.362–363] [136, pp.270–271].

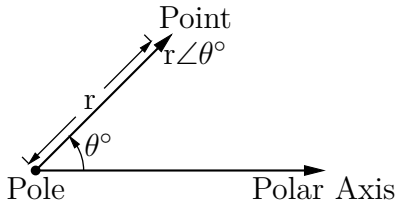

Figure 4: visual depiction of polar coordinates

$$\begin{aligned} Z &= R\angle\theta_Z^\circ \\ &= \frac{V\angle\theta_V^\circ}{I\angle\theta_I^\circ} \end{aligned} \tag{22}$$

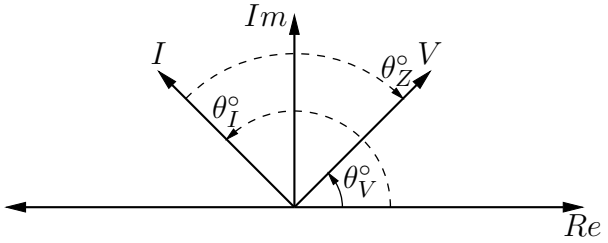

Figure 5: example of a impedance phasor depicted graphically

5.1.5 Representation by Rectangular Notation

Again, because two methods of representing an impedance value exist, the second method is formally called rectangular notation and it represents numbers in terms of a real and an imaginary component. Rectangular notation is based off the Cartesian coordinate system in which two numbered lines, also called axes, are drawn perpendicular to each other and intersect at a central point called the origin. The vertical axis is referred to as the imaginary axis, while the horizontal axis is called the real axis. A point in the rectangular system is defined by a set of real and imaginary numbers [309, pp.22–23]. While this rectangular notation concept is depicted in Figure: (6). The generalized form of an impedance in rectangular notation can be mathematically represented byEquation: (23) in which rectangular resistance R' and reactance X represent the notational parameters [136, pp.273–274].

$$Z = R^{'} + \jmath X \tag{23}$$

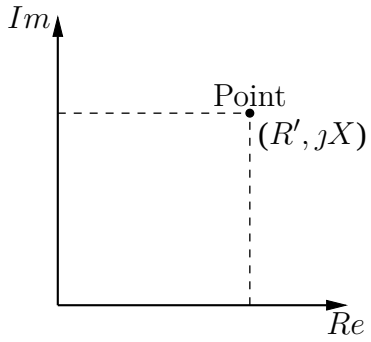

Figure 6: example of a rectangular notation depicted graphically

5.1.6 Rectangular to Phasor and Phasor to Rectangular Conversion

Because each impedance notation has its own advantages, depending upon the mathematical operations being performed, transformations between notations are often times required in mathematical computations. Typically phasor notation is used in mathematical computations that require division or multiplication, while rectangular notation is used in computations that require addition or subtraction. In order to convert a impedance from phasor notation to rectangular notation Equation: (24) and Equation: (25) can be substituted into Equation: (23) which will result in the creation of the phasor to rectangular transformation that can be expressed formally by Equation: (26) [136, pp.273–274].

$$R' = R\cos(\theta_Z^\circ) \tag{24}$$

$$X = R\sin(\theta_Z^\circ) \tag{25}$$

$$Z = R\cos(\theta_Z^\circ) + \jmath R\sin(\theta_Z^\circ) \tag{26}$$

Likewise, an impedance in rectangular notation can be converted to phasor notation by substituting Equation: (27) and Equation: (28) into $R\angle\theta_Z^\circ$ which will result in the creation of the rectangular to phasor transformation that can be expressed formally by Equation:

(29) [136, pp.273–274].

$$R = \sqrt{[R']^2 + [X]^2} \tag{27}$$

$$\theta_Z^\circ = \tan^{-1}\left(\frac{X}{R'}\right) \tag{28}$$

$$Z_{\angle\theta_Z^\circ} = \sqrt{[R']^2 + [X]^2}\angle \tan^{-1}\left(\frac{X}{R'}\right) \tag{29}$$

5.1.7 Interdisciplinary Research and Intra-disciplinary Opinion

One important concept that is embedded in impedance analysis is the ability to represent and model an impedance by passive components. This concept is important because it allows the creation of equivalent circuit models for a given impedance based upon phase and magnitude information obtained from experimental measurements. Typically impedances can be modeled thru a combination of one or more of three available passive components which include resistors R, capacitors C and, inductors L.

5.1.8 Overview of Laplace Transformation

Since impedance analysis makes use of the Laplace transformation, some brief background needs to be discussed before reactive components can be examined. The definition of the Laplace transformation, shown in Equation: (30), in which the complex frequency s is defined by Equation: (31) allows for the transformation of a signal from the time domain to the complex frequency domain in order to solve a problem using algebra rather than with differential equations. Typically, if a time domain result is required all of the mathematics are performed in the Laplace domain and the inverse Laplace transformation, shown in Equation: (32), is used to convert the result back to the time domain [136, p.497, pp.500–502, p.520].

$$\begin{aligned}\mathcal{L}\left[f\left(t\right)\right] &= F\left(s\right)\\ &= \int_0^\infty f\left(t\right)e^{-st}dt \qquad (30)\end{aligned}$$

$$s = \sigma_r + \jmath\omega \qquad (31)$$

$$\begin{aligned}\mathcal{L}^{-1}\left[F\left(s\right)\right] &= f\left(t\right)\\ &= \frac{1}{2\pi j}\int_{\sigma_{r_1}-j\infty}^{\sigma_{r_1}+j\infty} F\left(s\right)e^{st}ds \qquad (32)\end{aligned}$$

For most applications in impedance analysis the definition of both the Laplace transformation shown by Equation: (30) and the inverse Laplace transformation shown by Equation: (32) are generally never used to solve circuit problems because a lengthy table of common Laplace and inverse Laplace transformations has been created which makes taking a Laplace or inverse Laplace transformation a simple matter of looking at the table for most circuit problems.

5.1.9 Impedance Theory of Resistors

As discussed earlier in this chapter a resistor is a device that has no phase shift associated with it which in the case of a uniform conductor follows Ohms law expressed by Equation: (2) or in a non-uniform conductor is found by the application of the potential difference expressed by Equation: (33) divided by the current through the resistors surface expressed by Equation: (34) which creates Equation: (35) [136, pp.15–16] [310, p.134, pp.163–164, p.223]. Substituting current density J for electric field E shown by Equation: (36) will produce Equation: (37) which is the resistance of a non-uniform conductor [136, pp.15–16] [310, p.134, pp.163–164, p.223]. Resistors are symbolized in a circuit model by the symbol shown in Figure: (7) and are thought of as a device that passively dissipate power

by transforming it into heat [136, pp.16–17].

$$V = -\int E \cdot d\mathbb{L} \tag{33}$$

$$I = \oint J \cdot d\mathbb{A} \tag{34}$$

$$R = \frac{\int E \cdot d\mathbb{L}}{\oint J \cdot d\mathbb{A}} \tag{35}$$

$$J = \sigma E \tag{36}$$

$$R = \frac{\int E \cdot d\mathbb{L}}{\oint \sigma E \cdot d\mathbb{A}} \tag{37}$$

Figure 7: symbol for a resistor

Resistors exhibit two distinctive properties depending upon the topology they are used in for a given circuit model. Resistors in series depicted by Figure: (8) can be combined together to create a equivalent resistance thru the application of Equation: (38) while resistors in parallel depicted by Figure: (9) can be combined together to create an equivalent resistance thru the application of Figure: (39) [136, pp.28–31, p.35].

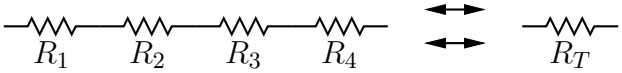

Figure 8: equivalent series resistance

$$R_T = R_1 + R_2 + \cdots + R_N \tag{38}$$

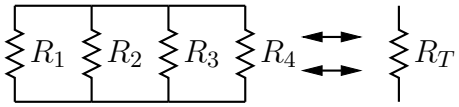

Figure 9: equivalent parallel resistance

$$R_T = \frac{1}{\frac{1}{R_1} + \frac{1}{R_2} + \cdots + \frac{1}{R_N}} \tag{39}$$

Assuming for the moment a uniform conductor, a resistor from a DC steady state perspective can be modeled directly by Ohms law which creates a linear relationship between current, voltage, and, resistance. A resistors from a DC transient or AC steady state perspective retain this same linear characteristic found at DC steady state and this fact is clearly visible by observing the resistor's Laplace transformation shown in Equation: (40) as it implies that a resistor is functioning as a linear scalar [136, pp.28–31, p.35, p.497, pp.500–502, p.520].

$$RF(t) \xrightarrow{\mathcal{L}} RF(s) \tag{40}$$

5.1.10 Impedance Theory of Capacitors

A reactive component found in impedance analysis is a capacitor, which is symbolized in a circuit model by the symbol shown in Figure: (10) [136, pp.159–162] [311, p.61, pp.64–66]. Capacitance is defined as the measure of how easy it is for electrical flux Ψ to propagate between conductive plates and can be described as the ability for the conductive plates to hold an electrical charge Q at a particular voltage [136, pp.159–162] [311, p.61, pp.64–66].

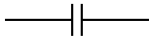

Figure 10: symbol for a capacitor

Generally speaking, in order to create a capacitor two or more conductive plates must

exist and they must carry equal yet opposite charges. Such conditions implicitly imply that all the electrical flux will leave the surface of one conducting plate of a capacitor and terminate at the surface of another conducting plate [310, pp.124–125, pp.223–226]. Since electric flux can be defined as the electric flux density D times the dot product of the surface area $\mathbb{A}_s$ which is mathematically expressed by Equation: (41) or correlated to the electric field E thru a scaling value of the permittivity ε by the substitution of Equation: (42) into Equation: (41) results in electric flux being related to electric charge Q thru the application of Gauss's Law [310, pp.122–125] [133, pp.51–57]. Gauss's Law which is expressed mathematically by Equation: (43) requires the surface to be a closed surface and equates the total flux from the system to the total enclosed charge [310, pp.122–125] [133, pp.51–57].

$$\Psi = \int D \cdot d\mathbb{A}_s \tag{41}$$

$$D = \varepsilon E \tag{42}$$

$$\begin{aligned} Q &= \Psi \\ &= \oint_{\mathbb{A}_s} \varepsilon E \cdot d\mathbb{A}_s \end{aligned} \tag{43}$$

Since capacitance can be defined as the ratio of the magnitude of the charge on the conductive plates to the potential difference between the plates this is expressed mathematically by Equation: (44) or more formally by substituting elements from Equation: (43) and Equation: (33) into Equation: (44) produces Equation: (45) [310, pp.223–226].

$$C = \frac{Q}{V} \tag{44}$$

$$C = \frac{\varepsilon \oint_{\mathbb{A}_s} E \cdot d\mathbb{A}_s}{\int E \cdot d\mathbb{L}} \tag{45}$$

Most capacitors that are model in impedance analysis are parallel plate capacitors, which consist of two conducting plates that have some defined area $\mathbb{W} \times \mathbb{L}$ that is separated electrically by a dielectric medium with a thickness $\mathbb{T}$ and permittivity ε illustrated by Figure: (11) [136, pp.159–162] [311, pp.74–78]. The structure of a parallel plate capacitor simplifies Equation: (45) to Equation: (46) by making the assumption that electric field is uniformed because the distance between the plates is very small [310, pp.223–226].

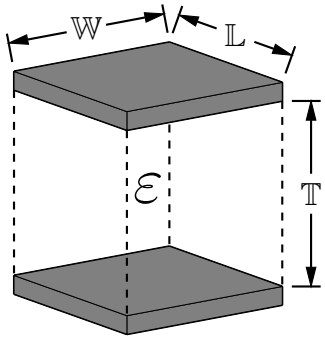

Figure 11: physical structure of a parallel capacitor

$$C = \frac{\varepsilon \mathbb{A}_s}{\mathbb{T}} \tag{46}$$

Often tines when taking experimental bioimpedance measurements the value of capacitance for a biomaterial can be measured but generally the relative permittivity ε_r is unknown. However, a relationship to solve for relative permittivity can be developed thru the application of Equation: (45) since permittivity is defined by Equation: (47) substi-

tution into Equation: (45) will produce Equation: (48) [310, pp.223–226]. Because the permittivity of free space ε_0 is known the capacitance of the biomaterial when the dielectric permittivity is that of free space C_0 can be calculated and this is expressed mathematically by Equation: (49) [310, pp.223–226]. Division of Equation: (48) by Equation: (49) will result in the creation of Equation: (50) which allows for a unknown relative permittivity of a biomaterial to be found if its capacitance is known along with the area and the thickness of the used parallel plate capacitor parameters [310, pp.223–226].

$$\varepsilon = \varepsilon_r \varepsilon_0 \tag{47}$$

$$C = \frac{\varepsilon_r \varepsilon_0 \mathbb{A}_s}{\mathbb{T}} \tag{48}$$

$$C_0 = \frac{\varepsilon_0 \mathbb{A}_s}{\mathbb{T}} \tag{49}$$

$$\frac{C}{C_0} = \varepsilon_r \tag{50}$$

Capacitors from an impedance analysis perspective exhibit two properties depending upon the topology they are used in for a given circuit model. Capacitors in series depicted by Figure: (12) can be combined together to create a equivalent capacitance thru the application of Equation: (51) while capacitors in parallel depicted by Figure: (13) can be combined together to create a equivalent capacitance thru the application of Equation: (52) [136, pp.159–162, pp.172–174] [311, pp.74–78].

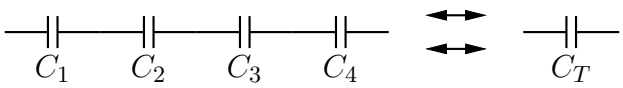

Figure 12: equivalent series capacitance

$$C_T = \frac{1}{\frac{1}{C_1} + \frac{1}{C_2} + \cdots + \frac{1}{C_N}} \tag{51}$$

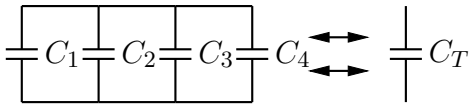

Figure 13: equivalent parallel capacitance

$$C_T = C_1 + C_2 + \cdots + C_N \tag{52}$$

Capacitors from a DC steady state perspective function as an electrical open circuit because after long periods of time the capacitor charges up to the applied DC potential. Capacitors from a DC transient perspective exhibit a different behavior that is described for current flowing thru the capacitor by Equation: (53) and for the voltage across the capacitor by Equation: (54) [136, pp.159–162].

$$I = C\frac{dv}{dt} \tag{53}$$

$$V = \frac{1}{C}\int_{t_0}^{t_1} i(t)dt + V_c(t_0) \tag{54}$$

Capacitors from a AC steady state perspective are best analyze from the Laplace domain and applying the Laplace transformation shown by Equation: (55) to Equation: (54) results in the creation of Equation: (56). Mathematical manipulation can be applied to Equation: (56) and will result in the creation of Equation: (57) which is commonly used in impedance calculations [136, pp.159–162] [312, pp.453–454]. Comparing the voltage

to current relationship for a capacitor illustrated by Figure: (14) it can be said that the current leads the voltage or the voltage lags the current by 90° [136, pp.270–271].

$$\int F(t)dt \xrightarrow{\mathcal{L}} \frac{F(s)}{s} \tag{55}$$

$$V(s) = \frac{I(s)}{sC} \tag{56}$$

$$\frac{V(s)}{I(s)} = \frac{1}{sC} \tag{57}$$

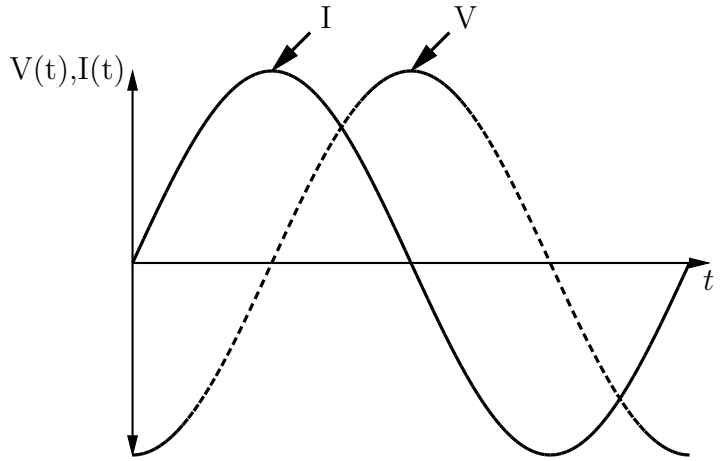

Figure 14: phase between current and voltage in a capacitor

5.1.11 Impedance Theory of Inductors

The last reactive component used in impedance analysis is an inductor, which is symbolized in a circuit model by the symbol shown in Figure: (15) [136, pp.166–167].

Figure 15: symbol for a inductor

When current flowing thru a conductor produces a magnetic field B it also produces a magnetic flux Φ defined by Equation: (58) to occur at each turn of the conductor [310, pp.336–337]. If more than one identical turn exists flux linkage λ between the turns will occur which can be expressed mathematically by Equation: (59) and in the event that the medium surrounding the conductor is linear then this flux linkage produced will be propor-

tional to the current that produced it which is expressed mathematically by Equation: (60) [310, pp.336–337]. The proportionality consonant mathematically expressed by Equation: (61) represents the inductance L of the conductor with N turns and the term inductor is used to categorize any element that contains inductance [310, pp.336–337].

$$\Phi = \int B \cdot d\mathbb{A} \tag{58}$$

$$\lambda = N\Phi \tag{59}$$

$$\lambda = LI \tag{60}$$

$$\begin{aligned} L &= \frac{\lambda}{I} \\ &= \frac{N\Phi}{I} \end{aligned} \tag{61}$$

From a bioimpedance standpoint inductance is an impedance analysis element that is not observed when modeling a biomaterial but inductance is used in the modeling of experimental apparatus such as electrodes and amplification circuitry that is attached to the biomaterial.

Inductors from a DC steady state perspective function as an electrical short circuit because after long periods of time the current stabilize and remains the same while inductors from a DC transient perspective exhibit a different behavior that is described for current flow thru the inductor by Equation: (62) and for voltage across the inductor by Equation: (63) [136, pp.166–167].

$$I(t) = I(t_0) + \frac{1}{L}\int_{t_0}^{t_1} V(t)dt \tag{62}$$

$$V(t) = L\frac{di(t)}{dt} \tag{63}$$

Inductors from a AC steady state perspective are best analyzed from the Laplace domain and applying the Laplace transformation shown by Equation: (64) to Equation: (63) results in the creation of Equation: (65). Mathematical manipulation can be applied to Equation: (65) and will result in the creation of Equation: (66) if $I(0) = 0$ which is commonly used in impedance calculations [312, pp.446–448] [136, pp.166–167]. Comparing the voltage to current relationship for a capacitor illustrated by Figure: (16) it can be said that the current lags the voltage or the voltage leads the current by 90° [136, pp.270–271].

$$\frac{df(t)}{dt} \xrightarrow{\mathcal{L}} sF(s) - f(0) \tag{64}$$

$$V(s) = LsI(s) - I(0) \tag{65}$$

$$\frac{V(s)}{I(s)} = Ls \tag{66}$$

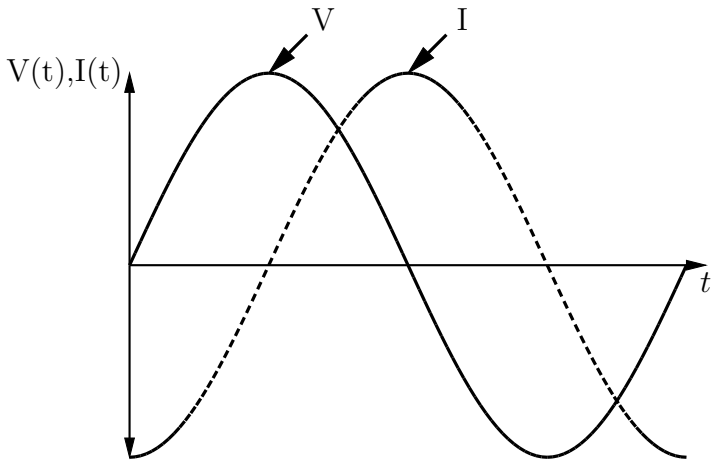

Figure 16: phase between current and voltage in a inductor

Inductors from an impedance analysis perspective exhibit two properties depending upon the topology they are used in for a given circuit model. Inductors in series depicted

by Figure: (17) can be combined together to create an equivalent inductance thru the application of Equation: (67) while inductors in parallel depicted by Figure: (18) can be combined together to create an equivalent inductance thru the application of Equation: (68) [136, pp.166–167, pp.175–176].

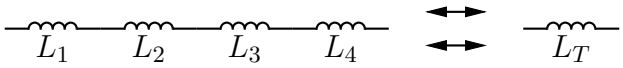

Figure 17: equivalent series inductance

$$L_T = L_1 + L_2 + \cdots + L_N \tag{67}$$

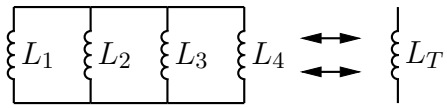

Figure 18: equivalent parallel inductance

$$L_T = \frac{1}{\frac{1}{L_1} + \frac{1}{L_2} + \cdots + \frac{1}{L_N}} \tag{68}$$

5.1.12 RLC Combination Impedance Theory

Because impedance analysis is traditionally performed by using steady state AC analysis in which all circuit components are converted into the frequency domain by the Laplace transformation this allows for two common circuit topology operations to occur when simplifying a circuit's impedance. When resistors, capacitors and inductors are represented in frequency domain representation they can expressed symbolically as a impedance which is symbolized in a circuit model by Figure: (19). Impedances in series depicted by Figure: (20) can be combined together to create an equivalent Impedance thru the application

of Equation: (69) while Impedances in parallel depicted by Figure: (21) can be combined together to create an equivalent Impedances thru the application of Equation: (70) [136, p.274]. This aspect of impedance analysis is important because all of the impedance elements can be mathematically manipulated using a common methodology rather than an array of different series and parallel combination rules shown earlier in the element analysis.

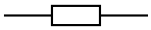

Figure 19: symbol for a impedance

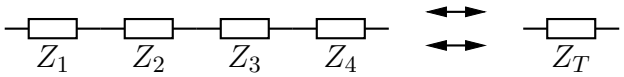

Figure 20: equivalent series impedance

$$Z_T = Z_1 + Z_2 + \cdots + Z_N \tag{69}$$

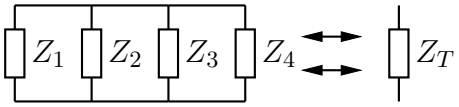

Figure 21: equivalent parallel impedance

$$Z_T = \frac{1}{\frac{1}{Z_1} + \frac{1}{Z_2} + \cdots + \frac{1}{Z_N}} \tag{70}$$

5.1.13 RLC Resonance

One interesting phenomena that appears as a result of combination RLC theory is the concept of circuit resonance. Resonance circuits in their most generic form come in both series and parallel topologies both of which are illustrated by Figure: (22) and Figure: (23) [136, p.439].

In both topologies the underlying elements that make up a resonance circuit are resis-

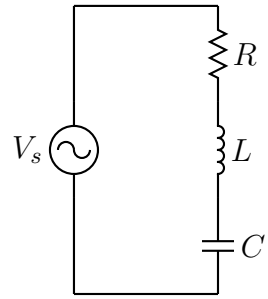

Figure 22: series resonance circuit

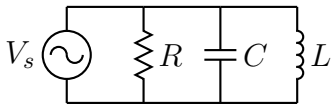

Figure 23: parallel resonance circuit

tive, capacitive, and inductive elements that are combined together to create a purely real component at some resonance frequency ω_0 which when this case occurs the circuit is said to be in resonance [136, p.440]. When a circuit is in resonance the voltage and current are in phase with each other which implies that the phase angle observed is zero which fundamentally means the inductive and capacitive elements have canceled each other out leaving only the resistive component of the impedance at the resonance frequency [136, p.440]. This cancellation effect is very attractive from a muscle stimulation perspective because thru the introduction of an inductor in the stimulation circuit the capacitive impedance of the bioimpedance can be removed which reduces the overall attenuation of the body and allows for lower voltage stimulation.

To illustrate the concept of resonance mathematically if the series resonance circuit shown in Figure: (22) is expressed by steady state AC impedance analysis shown by Equation: (71) then resonance will occur at Equation: (72) [136, pp.439–440].

$$Z(\jmath\omega) = R + \jmath\omega L + \frac{1}{\jmath\omega C} \tag{71}$$

$$\jmath\omega L = \frac{1}{\jmath\omega C} \tag{72}$$

Since ω in both equations has to be the same input frequency it can be solved for which produces Equation: (73) and because this point is when the resonance frequency will occur it can be rewritten as Equation: (74) [136, pp.440].

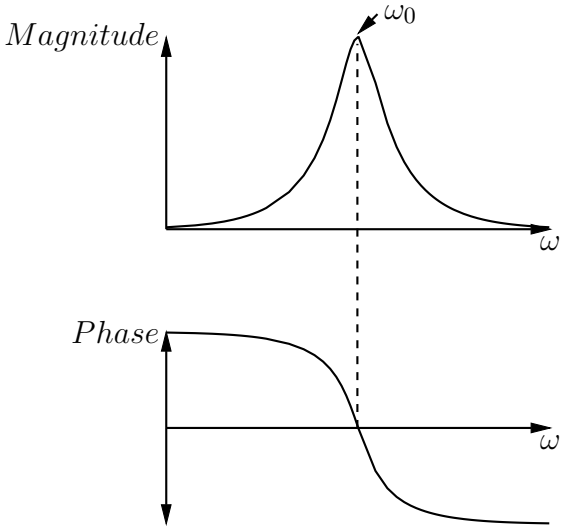

Figure 24: series resonance plot

$$\omega = \frac{1}{\sqrt{LC}} \tag{73}$$

$$\omega_0 = \frac{1}{\sqrt{LC}} \tag{74}$$

The importance of this resonance frequency which can be clearly observed by Figure: (24) in which the voltage across the capacitor or in real life the bioimpedance is shown over frequency and ω_0 represents the maximum voltage point that will be across the bioimpedance when the phase angle is zero because of cancellation of the capacitive element by the introduction of an inductive element [136, pp.445].

5.2 Overview of Bioimpedances

A biological impedance or bioimpedance for short is simply an impedance measurement of some type of biological or organic material that is often times called a biomaterial

for short [16, pp.1–2]. Some common examples of biomaterials include plants, animals, skin, blood, muscle, and an assortment of other materials related to organic life whether it be living or dead [16, pp.1–2]. Bioimpedances have unique and diverse properties because of their electrolytic and electrochemical nature, which allow them to exhibit both linear and nonlinear characteristics depending upon the voltage the biomaterial is subjected to [16, pp.1–2]. Since bioimpedance analysis, is based upon impedance analysis along with biological and chemical theory it is important to understand the concepts of these fundamental subjects before attempting to model a biomaterial.

5.3 Chemistry and Bioimpedances

The information discussed in impedance analysis is part of the fundamental knowledge required to understand common circuit problems found in electrical engineering; however, in the world of bioimpedance analysis this knowledge by itself in its current context is not enough to make much headway when working with biomaterials alone. The reason behind this lack of understanding that impedance analysis provides to the world of bioimpedance analysis can be contributed to the fact that most systems found in electrical engineering are assumed to have a certain set of electrical properties because a common set of materials such as metals for example are traditionally used while biomaterials on the other hand have a wide assortment of chemical compositions which as a result of this mixture of compounds creates metaphoric foreign ground when trying to apply traditional impedance analysis to the subject. It should be noted that this observation does not invalidate impedance analysis but implies that special considerations from a chemical understanding of biomaterials needs to be examined prior to applying impedance analysis theory which is why the fundamentals of chemistry needs to be explored in detail before attempting to model the electrical characteristics of a biomaterial.

5.4 A Review of Basic Chemistry

The world upon which we live in can be thought of as being a collection of matter, energy, and, empty space [313, p.3]. Chemistry is the science that deals with the study of matter and how it interacts with its surrounding environment [313, p.3]. Such interactions studied in chemistry can be classified into two possible categories one of which being a chemical interaction in which matter is transformed into a chemically different substance and the other type of classification being a physical change in which the physical appearance changes but the composition remains the same [313, p.3] [132, p.10].

Matter in the general since can be define as a object of some size that is made up of an assortment of atoms in which the atom is the smallest possible size matter can have and still retain all of its chemical properties [313, p.3, pp.27–28, p.31]. Matter can be classified further into two classifications the first classification being an element which is defined as a substance that cannot be decomposed into a simpler substance and the second classification being an chemical compound which is defined as a piece of matter that is made up of two or more different types of elements that retain a unique chemical identity [313, p.3, pp.27–28] [132, p.6]. In the event that elements or compounds are combined together but the resulting combination causes no change in the chemical identity of any of the components then the resulting substance is called an mixture which can be classified as either being homogeneous meaning all parts of the mixture are uniformly distributed throughout the substance or if the resulting mixture is randomly distributed then it is called a heterogeneous mixture [313, pp.27–31] [132, p.6].

The fundamental difference between a chemical compound and a mixture is in the case of a mixture physical separation can be used to separate the components of a mixture into their individual elements or compounds while in a chemical compound the change is

irreversible as it cannot be separated back into its individual elements by physical means [313, p.28]. The process of organizing matter into different classifications can be illustrated by the creation of a flowchart shown in Figure: (25).

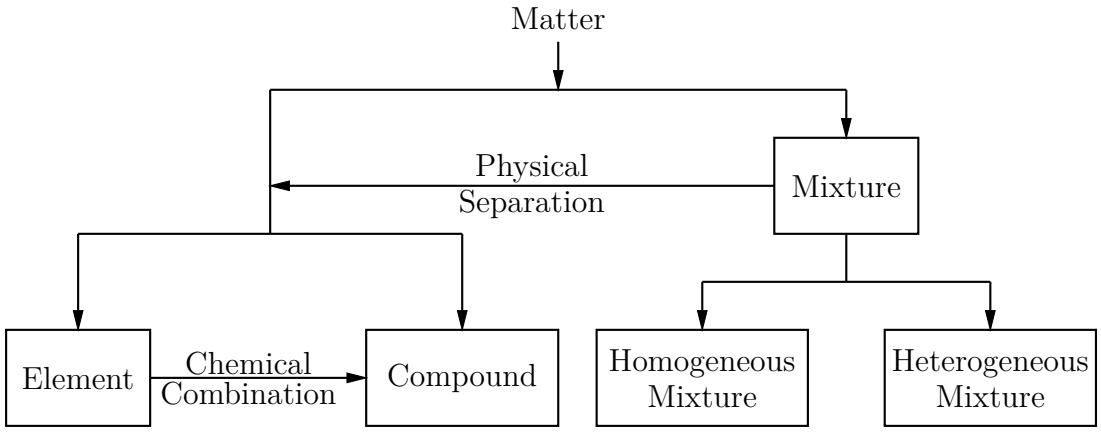

Figure 25: matter classification flowchart

The fundamental unit of matter which is called an atom is generally considered to be made up of three main subatomic particles that consist of protons, electrons, and neutrons [313, p.34]. Protons have a positive charge, electrons have a negative charge, and neutrons have no charge at all [313, p.34]. Protons and neutrons are found bound together in a tight cluster at the center of an atom which is also called the nucleus while electrons are found some distance away from the nucleus in confined regions called principle energy levels that are also referred to as electron shells or electron orbitals depending upon the atomic model being used [313, p.34, p.44]. The conceptual structure of an atom can be illustrated by Figure: (26).

The number of protons that an element has defines its chemical identity which is also referred to as the atomic number which is how the periodic table of elements is organized [132, p.43]. In order for an atom to have no net charge an equal number of electrons and protons must exist in an electrically neutral atom [132, p.43]. However, this need for electrical neutrality does not appear to be a primary factor when it comes to chemical interactions between elements because energy levels appear to have a metaphoric desire to

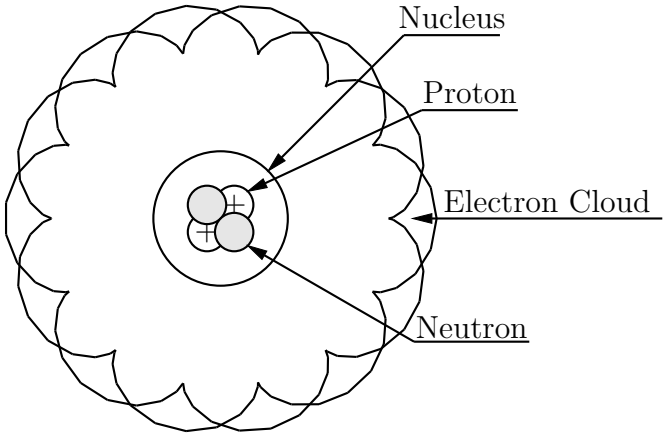

Figure 26: conceptual structure of an atom

obtain or lose a defined number of electrons in there valance electron shell in order to achieve electrical stability which is more important than electrical neutrality from the perspective of a single atom otherwise chemical reactions would not occur if electrical neutrality was preferred [313, p.59].

5.4.1 Ionization and Bonding

The elemental ideology upon which chemistry is based upon is the concept of ionization which fundamentally implies that the reactions that make up the world are the end result of the need for charge to be transferred. When an atom gains or loses an electron and is no longer electrically neutral it becomes a charged particle that is referred to as an ion [313, p.59] [132, p.52]. If an atom loses an electron which results in the atom becoming positively charged this result is referred to as a cation and likewise when an atom gains an additional electron the result becomes a negatively charged atom that is referred to an anion [313, p.59]. Chemical equations can be used to represent the ionization process for example Equation: (75) represents the element sodium losing an electron while Equation: (76) represents the element chlorine gaining an electron [313, p.59].

$$Na \longrightarrow Na^{+} + e^{-} \tag{75}$$

$$Cl + e^{-} \longrightarrow Cl^{-} \tag{76}$$

Despite all of these concepts it is oftentimes necessary to determine how two elements will chemically interact with each other in terms of electron transference and several tables have been developed thru years of research and experimentation that make predictions easier to obtain. One method of prediction is based upon examining an atoms ionization energy which measures how easy it is for an atom to lose valance electrons, another predictive method looks at an atoms electronegative in order to determine how tightly the valance electrons are bound to the atom, and the last method that should be discussed is electron affinity which examines the energy needed for an atom to lose a electron [313, p.59, p.64] [16, p.6]. A visual representation of the energy required to ionize an electron from a element is shown in Figure: (27) while a visual representation of the electronegative of some of the periodic elements is shown by Figure: (28) along with a visual representation of electron affinities for some of the periodic elements shown by Figure: (29) [313, p.64] [314, p.9:74, pp.10:147–10:148, pp.10:175–10:176] [315, p.345].

H 13.5																	He 24.5
Li 5.3	Be 9.3											B 8.2	C 11.2	N 14.5	O 13.6	F 17.4	Ne 21.5
Na 5.1	Mg 7.6											Al 5.9	Si 8.1	P 10.4	S 10.3	Cl 12.9	Ar 15.7
K 4.3	Ca 6.1	Sc 6.5	Ti 6.8	V 6.7	Cr 6.8	Mn 7.4	Fe 7.9	Co 7.8	Ni 7.6	Cu 7.2	Zn 9.3	Ga 5.9	Ge 7.8	As 9.8	Se 9.7	Br 11.8	Kr 13.9
Rb 4.1	Sr 5.6	Y 6.2	Zr 6.6	Nb 6.7	Mo 7.0	Tc 7.2	Ru 7.3	Rh 7.4	Pd 8.3	Ag 7.5	Cd 8.9	In 5.7	Sn 7.3	Sb 8.6	Te 9.0	I 10.4	Xe 12.1
Cs 3.8	Ba 5.2	La 5.5	Hf 6.8	Ta 7.5	W 7.9	Re 7.8	Os 8.4	Ir 9.0	Pt 8.9	Au 9.2	Hg 10.4	Ti 6.1	Pb 7.4	Bi 7.2	Po 8.4	At 9.5	Rn 10.7

Figure 27: first ionization energy (data from [314, pp.10:175-10:176] and [315, p.345])

H 2.1																	He -
Li 1.0	Be 1.5											B 2.0	C 2.5	N 3.0	O 3.5	F 4.0	Ne -
Na 0.9	Mg 1.2											Al 1.5	Si 1.8	P 2.1	S 2.5	Cl 3.0	Ar -
K 0.8	Ca 1.0	Sc 1.3	Ti 1.5	V 1.6	Cr 1.6	Mn 1.5	Fe 1.8	Co 1.8	Ni 1.8	Cu 1.9	Zn 1.6	Ga 1.6	Ge 1.8	As 2.0	Se 2.4	Br 2.8	Kr -
Rb 0.8	Sr 1.0	Y 1.2	Zr 1.4	Nb 1.6	Mo 1.8	Tc 1.9	Ru 2.2	Rh 2.2	Pd 2.2	Ag 1.9	Cd 1.7	In 1.7	Sn 1.8	Sb 1.9	Te 2.1	I 2.5	Xe -
Cs 0.7	Ba 0.9	La 1.1	Hf 1.3	Ta 1.5	W 1.7	Re 1.9	Os 2.2	Ir 2.2	Pt 2.2	Au 2.4	Hg 1.9	Ti 1.8	Pb 1.8	Bi 1.9	Po 2.0	At 2.2	Rn -

Figure 28: electronegative (data from [314, p.9:74])

H 0.7																	He -
Li 0.6	Be -											B 0.2	C 1.2	N -	O 1.4	F 3.4	Ne -
Na 0.5	Mg -											Al 0.4	Si 1.3	P 0.7	S 2.0	Cl 3.6	Ar -
K 0.5	Ca 0.2	Sc 0.1	Ti 0.1	V 0.5	Cr 0.6	Mn -	Fe 0.1	Co 0.6	Ni 1.1	Cu 1.2	Zn -	Ga 0.3	Ge 1.2	As 0.8	Se 2.0	Br 3.3	Kr -
Rb 0.4	Sr 0.1	Y 0.3	Zr 0.4	Nb 0.8	Mo 0.7	Tc 0.5	Ru 1.0	Rh 1.1	Pd 0.5	Ag 1.3	Cd -	In 0.3	Sn 1.1	Sb 1.0	Te 1.9	I 3.0	Xe -
Cs 0.4	Ba 0.1	La 0.5	Hf 0.0	Ta 0.3	W 0.8	Re 0.1	Os 1.1	Ir 1.5	Pt 2.1	Au 2.3	Hg -	Ti 0.2	Pb 0.3	Bi 0.9	Po 1.9	At 2.8	Rn -

Figure 29: electron affinities (data from [314, pp.10:147-10:148])

When elements chemically interact with each other and ionization is a result of this interaction then this interaction can be described as chemical bonding [313, pp.63–64]. A chemical bond is defined as the force that is acting between atoms and can be generalized into one of four classifications [16, p.6]. The first chemical bond classification is an ionic bond in which a highly electronegative atom interacts with a low electronegative atom such that valance electrons are transferred from the low electronegative atom to the high electronegative atom that results in the formation of an anion and a cation which because of columbic forces the ions stay together in a solid state under most circumstances [313, pp.65–67] [16, pp.6–7]. This ionic bond can be illustrated thru the application of a Lewis dot structure in which the valance shell electrons for a given element are depicted before and after a chemical reaction [313, pp.49–50]. An example of an ionic bond illustrated as a Lewis structure is shown by Figure: (30) [313, p.66].

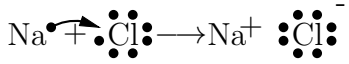

Figure 30: ionic bond between sodium and chloride

The second chemical bond classification is a covalent bond in which two elements of similar electronegative values share valance electrons such that the electrons that are being shared fill both bonded atoms valence shells at the same time [313, pp.70–71] [16, pp.6–7]. Since atoms in a covalent bond share electrons the extent of how evenly these valance electrons are shared amongst the bonded elements varies depending upon the electronegative of the elements involved which results in the sub classification of covalent bonds into two cases one of which is a non-polar covalent bond where atoms share their valance electrons equally and the second case being a polar covalent bond where atoms share their valance electrons unequally [313, pp.70–71]. A Lewis dot structure can be used to illustrate a non-polar covalent bond shown by Figure: (31) in which the solid line in the Lewis dot structure represents an electron pair being shared [313, p.70].

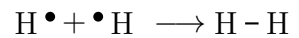

Figure 31: nonpolar covalent bond between hydrogen and hydrogen

The polar covalent bond because of its unequal electron sharing causes a separation of charge between the bonded elements to occur and this charge separation is referred to as a dipole while the measure of the strength of this dipole is referred to as a dipole moment [313, pp.70–71] [132, p.228]. A Lewis dot structure can be used to illustrate a polar covalent bond shown by Figure: (32) in which because a dipole exist in water the physical structure of the water molecule gets bent downwards [313, p.73].

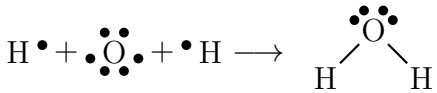

Figure 32: polar covalent bond of water

The third chemical bond classification is a metallic bond that occurs between metals which is similar to that of a covalent bond however rather than the electrons being shared

between two atoms they are highly mobile belonging to no particular atom in general [16, pp.6–7]. This high electron mobility occurs because the valence electron orbitals overlap with other valence electron orbitals in metals which results in the formation of additional orbital energy levels per each new addition of a metal atom to the overall molecule [132, p.931] [316, p.16]. After numerous metal atom additions the valence electron energy bands become continuous which allows the free movement of electrons in the metal and this concept is illustrated by Figure: (33) [132, p.931]. This high electron mobility found in metallic bonds generally yields properties of high electrical conductivity and luster [132, p.276].

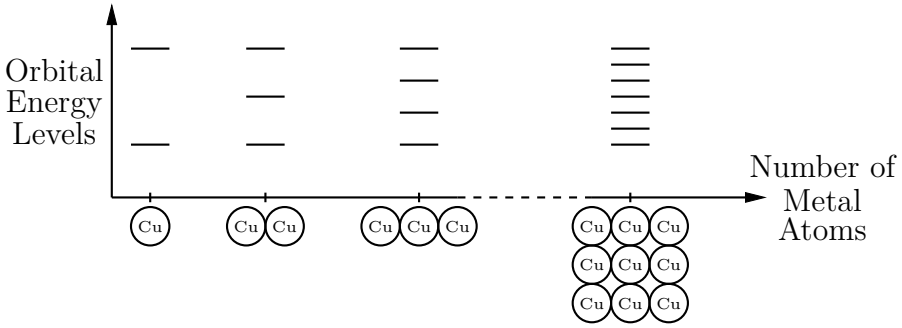

Figure 33: metallic bonding and energy levels

The last chemical bond classification worth mentioning is a Van der Waals bond in which an electron that is revolving around its nucleus is considered to be an electric dipole because of the London dispersion force [132, p.411] [16, pp.6–7]. The London dispersion force states that an atoms electrons can create an instantaneous dipole moment because if the location of a atoms electrons could be known for a given instant of time then it is possible that all of the electrons would be located in a particular region of the electron cloud that would result in the creation of a dipole [132, p.411] [316, p.16].

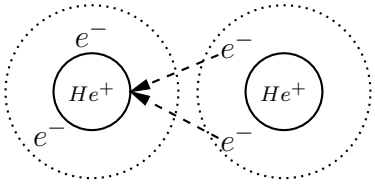

Figure 34: van der waals bond between two helium atoms

This instantaneous dipole moment would result in the attraction between molecules that are close together and such a dipole would be extremely weak meaning that it could only occur when other forces such as polarization or any other strong force that would overpower the Van der Waal force does not exists [132, p.411] [316, p.16]. The Van der Waals bond is generally found between organic heterogeneous masses and the overall cohesion from this force is considered to be relatively weak when compared to the other types of bonds also Figure: (34) illustrates conceptually what Van der Waal forces look like.

5.4.2 Solutions and Solubility

Now that a brief overview of chemistry along with a short introduction on chemical bonds has been discussed an important gateway topic can be introduced that will eventually lead into the impedance aspects of biomaterials such that the theoretical properties of bioimpedance modeling can be explained.

One of the concepts that was discussed in A Review of Basic Chemistry was the concept of mixtures which could be categorized as either being heterogeneous or homogeneous in nature [313, p.153]. However, there also exists an additional classification were the substance is not quite heterogeneously or homogeneously distributed and this type of distribution is referred to as a colloidal dispersion which is the classification that numerous biomaterials fall into [313, p.153]. Despite the addition of this new colloidal classification in order to make the explanation of solutions and the concept of solubility simplistic colloidal dispersions will be neglected for the moment and only homogeneously distributed substances which are often times referred to as solutions will be examined [313, p.153].

A solution can exist as any state of matter whether it be solid, liquid or gas and should a solution in the state of a gas or solid be dissolved into a solution of a liquid then the solution of gas or solid is referred to as a solute while the liquid solution is referred to

as a solvent [313, p.154]. In the event that two liquid solutions are dissolved into each other questions about which one is the solvent and which one is the solute can arise and in most cases the one with the larger concentration is considered to be the solvent while the lesser concentration is considered to be the solute yet this method of identification does not rigidly apply in all instances as there is no formal method of identification for this case [313, p.154].

With the terms solvent and solute defined the term solubility is simply the measure of how easy it is for a solute to dissolve into a solvent at a defined temperature [313, p.156]. Solubility is a physical property of the solvent that has a defined constant for a given temperature and when the temperature of the solvent increases the solubility of the solvent increases as a result [313, pp.156–157]. When a solute does not easily dissolve into a solvent that solute is said to have a low solubility for that particular solvent and is oftentimes referred to as the solute being insoluble while when a solute can easily dissolve into a solvent the solute is referred to as being soluble for a that particular solvent [313, p.154]. Once a solvent has dissolved its solubility constant of a solute at a particular temperature it is said to be saturated and any additional solute added to the solvent will not be dissolved into the solvent while if a solvent has not reached this saturation constant for a particular temperature it is said to be unsaturated meaning that additional solute will be dissolved into the solvent [313, p.154]. The concepts of insoluble, soluble, and saturated are depicted in Figure: (34) [313, p.66].

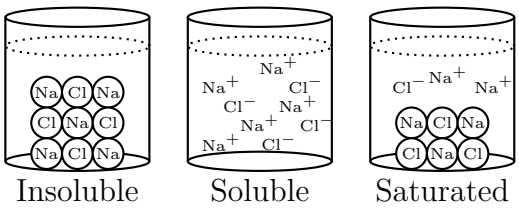

Figure 35: visual difference between insoluble, soluble, and saturated solubility.

One interesting aspect about the nature of the solubility of a solvent and solute is the fact that similar compounds are more likely to be soluble with each other and this is believed to be a result of molecular polarity since polar molecules tend to dissolve other polar molecules while nonpolar molecules tend to dissolve other nonpolar molecules however polar molecules generally do not dissolve other nonpolar molecules [313, pp.156–157].

5.4.3 Aqueous Solutions

Now that the definition of solubility has been given a problem arises from the rather lengthy list of elements this definition can apply to thus in order to reduce the overall complexity of the concept of solubility in general further restrictions will be applied thru limiting the elements discussed to those elements commonly found in a biomaterial.

Because the earth is covered by an abundance of a substance known as water this substance for very logical reasons is a common substance found in most biomaterials and water is also considered to be the most important polar solvent when it comes to solubility [313, p.157] [132, p.113]. With the introduction of water as a solvent comes a new terminology called aqueous that is used to indicate that a solution uses water as a solvent and because water is so commonly found as a solvent typically when the term solubility is used it is often times assumed that water is the involved solvent [132, p.113].

When water dissolves an ionic compound it does so by surrounding each ionic molecule in a way that the negative dipole of water attracts the anions of the ionic compound along with the positive dipole of water attracts the cations of the ionic compound and as a result of the introduction of this dipole attraction the ionic bonds dislocate which causes the ionic compound to dissolve into ions that are surrounded by water molecules [313, p.165]. The ions that form as a result of this dissolving process are said to be hydrated when water is the solvent or solvated when water is not the solvent and this salvation layer which is

more simply stated as the surrounding of solute ions by solvent functions as a cushion by preventing the solute ions from interacting with each other because the solvent shields the solute which naturally prevents the ions from recombining [313, p.167]. The concept of a substance being dissolved into water can be easily illustrated by observing the reaction between water and sodium chloride depicted by Figure: (36) in which the water molecules strong dipole causes the bond holding the sodium and chloride atoms together to break after which the lone ions get surrounded by water dipoles preventing them from returning to their former state [313, pp.166–167].

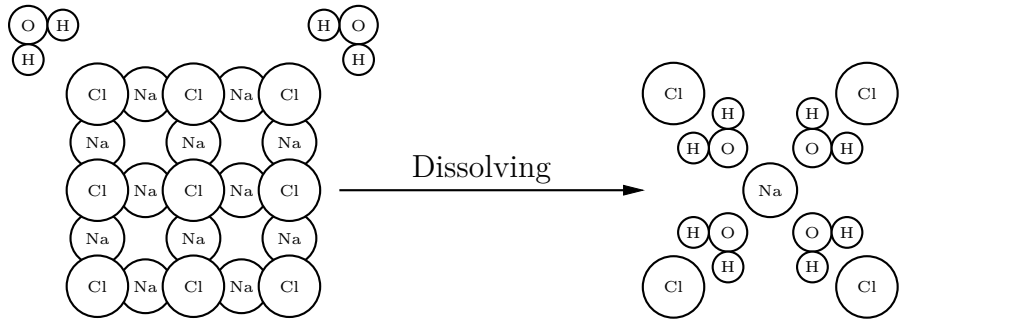

Figure 36: sodium chloride dissolved in water

Water can not only can dissolve most ionic compounds but it can also dissolve numerous covalent compounds by either chemically reacting with the compound to create a new aqueous substance or by surrounding the covalent compound and solvating it [313, p.169]. An example of water chemically reacting with a covalent compound can be seen in Equation: (77) which shows a reaction between hydrochloric acid and water which the result in the formation of an aqueous solution with ions [313, p.169].

$$HCl_{Gas} + H_2O_{Liquid} \longrightarrow Cl^-_{Aqueous} + H_3O^+_{Aqueous} \tag{77}$$

5.5 Electrochemistry

5.5.1 Interdisciplinary Research and Intra-disciplinary Opinion

Despite waters intrinsic ability to solvate a very diverse range of chemical substances the most interesting aspect that results from a substance being solvated in water results when it has the ability to conduct electricity and if a solvated substance can conduct electricity it is referred to as an electrolyte [132, p.114] [16, p.3]. Electrical conduction in an electrolyte is quite different than electrical conduction in a metal because the movement of charge in a metal is done thru the propagation of a near massless particle called an electron while the movement of charge in an electrolyte is performed by the propagation of both positive cations and negative anions that are massive in size when compared to an electron and not equal in charge which results in chemical concentration gradient developing in the aqueous solution [16, p.3] [189, pp.711–729]. This concept of charge propagation thru ions can be illustrated by Figure: (37) in which sodium cations are attracted to the negatively charged plate while chlorine anions are attracted to the positively charged plate and the net movement of these ions produces a current allows electrical conduction to occur [313, pp. 167–168].

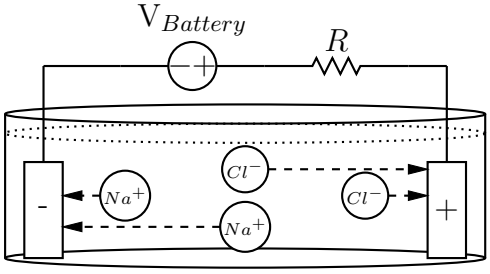

Figure 37: illustration of electrolytic conduction

Electrolytes come in two classifications; the first classification is a strong electrolyte in which solutes dissolve completely into ions which generally occurs in ionic compounds while the second classification is a weak electrolyte in which solutes only partially dissolve into ions which generally occurs in covalent compounds [313, pp. 167–168]. Because electrical

conduction in an electrolyte is dependent upon the number of ions available to propagate charge this strong verses weak electrolyte assignment directly reflects upon how well a substance will conduct electricity [313, pp. 167–168].

5.5.2 Electrolysis

One interesting phenomena of electrolytic conduction occurs when charge that is flowing from a metal conductor propagates into an electrolyte. This change in medium causes a chemical reaction called electrolysis to occur at the metal electrolyte boundary. Since bioimpedance spectroscopy uses metal electrodes to directly connect to a biomaterial the effects of electrolysis are always a concern when trying to model a bioimpedance especially when a direct current is used as the applied signal [189, pp.711–729].

The most fundamental case of electrolysis occurs when a DC signal is applied to a set of electrodes that are in contact with a electrolyte and the resulting reaction can be described by two laws called Faraday's laws of electrolysis [189, pp.711–729]. Faraday's first law states "*that the amount of a chemical reaction which occurs at any electrode is proportional to the quantity of electricity passed*" shown in Equation: (78) in which $M_{\mathfrak{F}}$ is defined as the mass of the resulting product, I is the electrical current applied, t is the duration the current was applied, and $\mathcal{Z}_{\mathfrak{F}}$ is the electrochemical equivalent of the product [189, pp.711–729].

$$M_{\mathfrak{F}} = \mathcal{Z}_{\mathfrak{F}} I t \tag{78}$$

Since electrical charge Q can be defined by Equation: (79) this equation can be substituted into Equation: (78) resulting inEquation: (80) [189, pp.711–729].

$$Q = It \tag{79}$$

$$M_{\mathfrak{F}} = \mathcal{Z}_{\mathfrak{F}} Q \tag{80}$$

Faraday's second law states that "*the passage of a fixed quantity of electricity produces amounts of two different substances in proportion to their chemical equivalent weights*" this law is shown by Equation: (81) in which $E_{\mathfrak{F}}$ represents the chemical equivalent weights [317, pp.485–493].

$$\frac{M_{\mathfrak{F}A}}{M_{\mathfrak{F}B}} = \frac{E_{\mathfrak{F}A}}{E_{\mathfrak{F}B}} \tag{81}$$

Faraday's two laws of electrolysis can be combined together to produce an equation that incorporates both quantity of electricity passed and number of electrolytic substances available. To accomplish this task two electrolytes will be assumed to exist and Equation: (78) can be used to defined the chemical reaction occurring from the DC current being applied to both electrolytes shown by Equation: (82) and Equation: (83) [189, pp.711–729] [317, pp.485–493].

$$M_{\mathfrak{F}A} = \mathcal{Z}_{\mathfrak{F}A} It \tag{82}$$

$$M_{\mathfrak{F}B} = \mathcal{Z}_{\mathfrak{F}B} It \tag{83}$$

If Equation: (82) is divided by Equation: (83) it yields Equation: (100) [317, pp.485–

493].

$$F_{ion} = \mathscr{M}_{ion}\mathscr{A}_{ion} \tag{84}$$

$$\mathscr{A}_{ion} = \frac{\mathscr{V}_{ion}}{\mathscr{T}_{ion}} \tag{85}$$

$$F_{ion} = \frac{\mathscr{M}_{ion}\mathscr{V}_{ion}}{\mathscr{T}_{ion}} \tag{86}$$

From Faraday's second law shown in Equation: (81), Equation: (100) $\mathcal{Z}_{\mathfrak{F}}$ can be equated to the chemical equivalents $E_{\mathfrak{F}}$ shown by Equation: (87) [317, pp.485–493].

$$\frac{\mathcal{Z}_{\mathfrak{F}A}}{\mathcal{Z}_{\mathfrak{F}B}} = \frac{E_{\mathfrak{F}A}}{E_{\mathfrak{F}B}} \tag{87}$$

Equation: (87) can then be rewritten into the form shown in Equation: (88) [317, pp.485–493].

$$\frac{E_{\mathfrak{F}A}}{\mathcal{Z}_{\mathfrak{F}A}} = \frac{E_{\mathfrak{F}B}}{\mathcal{Z}_{\mathfrak{F}B}} \tag{88}$$

Generally speaking Equation: (78) can be defined in a singular case shown by Equation: (78) and this is the starting point for the general expression of Faraday's constant $\mathfrak{F}$ [317, pp.485–493].

$$\frac{E_{\mathfrak{F}}}{\mathcal{Z}_{\mathfrak{F}}} = \mathfrak{F} \tag{89}$$

$$= Constant$$

If Equation: (78) is solved for $\mathcal{Z}_{\mathfrak{F}}$ shown in Equation: (90) and substituted into Equation: (89) the result is Equation: (91) [317, pp.485–493].

$$\mathcal{Z}_{\mathfrak{F}} = \frac{M_{\mathfrak{F}}}{Q} \tag{90}$$

$$\mathfrak{F} = \frac{E_{\mathfrak{F}} Q}{M_{\mathfrak{F}}} \tag{91}$$

If the condition shown in Equation: (92) Occurs and substituted into Equation: (91) then Equation: (93) is produced [317, pp.485–493].

$$E_{\mathfrak{F}} = M_{\mathfrak{F}} \tag{92}$$

$$\mathfrak{F} = Q \tag{93}$$

Since Faraday's constant defines the amount of charge required to move one gram of equivalent substance during electrolysis and since there is one gram per one mol this allows for Avogadro's number N_A to be multiplied by the charge of a electron in order to obtain the total charge of one gram of electrons. The total charge of a gram of electrons is equal to Faraday's constant shown in Equation: (95) by Equation: (93) since $E_{\mathfrak{F}} = 1$ and $M_{\mathfrak{F}} = 1$ are equal to each other [317, pp.485–493]. In summery the Faraday constant fundamentally represents the magnitude of charge on an Avogadro number of electrons [189, p.712].

$$Q = N_A e \tag{94}$$

$$\begin{aligned} \mathfrak{F} &= Q \\ &= N_A e \\ &= 96,490 \frac{C}{mol} \end{aligned} \tag{95}$$

5.5.3 Ion Conductivity by an Induced Potential

So far only the basic theories behind how electrolytes are formed and the interesting phenomena of electrolysis has been presented leaving the conduction equations in the bulk of the electrolyte a topic that needs to be discussed in more detail.

In order to obtain the amount of charge that is being moved through an electrolytic volume a current density J must be obtained for a cross sectional area that is perpendicular to the ion propagation [189, p.707]. Current density can be found by taking the ion charge density ρ_{ion} an multiplying it by its velocity $\mathscr{V}_{ion}$ shown by Equation: (96) where charge density is defined as the number $\mathscr{N}_{ion}$ of ions multiplied by their charge Q_{ion} per unit volume shown by Equation: (97) [310, p.164].

$$J = \rho_{ion} \mathscr{V}_{ion} \tag{96}$$

$$\rho_{ion} = \mathscr{N}_{ion} Q_{ion} \tag{97}$$

While this approach to finding current density is valid generally charge density is not known nor is a charges velocity however, the electric field E is typically known and when

an electric field is applied to a ion of a defined charge by definition from Coulomb's law shown by Equation: (98) it will produce a force which can be defined as the charge times the electric field shown by Equation: (99) [310, p.164] [133, p.30].

$$F_t = Q_t E \tag{98}$$

$$F_{ion} = Q_{ion} E \tag{99}$$

When a ion is moving in a electric field that ion because it has both mass $\mathscr{M}_{ion}$ and acceleration $\mathscr{A}_{ion}$ also has a force which can be described by Newton's second law of motion shown by Equation: (100) where acceleration can be written as velocity per average time between ion collisions $\mathscr{T}_{ion}$ shown by Equation: (101) and substitution of Equation: (101) into Equation: (100) will result in the creation of Equation: (102) [310, p.164] [167, p.77].

$$F_{ion} = \mathscr{M}_{ion} \mathscr{A}_{ion} \tag{100}$$

$$\mathscr{A}_{ion} = \frac{\mathscr{V}_{ion}}{\mathscr{T}_{ion}} \tag{101}$$

$$F_{ion} = \frac{\mathscr{M}_{ion} \mathscr{V}_{ion}}{\mathscr{T}_{ion}} \tag{102}$$

From this point Equation: (102) and Equation: (99) can be equated to each other shown by Equation: (103) allowing the velocity to be solved as shown by Equation: (104) [310, p.164]. This velocity equation shown by Equation: (104) can then be substituted into the current density equation shown by Equation: (96) and the result of this substitution is the creation of Equation: (105) [310, p.164].

$$Q_{ion}E = \frac{\mathscr{M}_{ion}\mathscr{V}_{ion}}{\mathscr{T}_{ion}} \tag{103}$$

$$\mathscr{V}_{ion} = \frac{Q_{ion}\mathscr{T}_{ion}}{\mathscr{M}_{ion}} \tag{104}$$

$$J = \rho_{ion}\frac{Q_{ion}\mathscr{T}_{ion}}{\mathscr{M}_{ion}}E \tag{105}$$

Next the charge density shown by Equation: (97) can be substituted into Equation: (105) and the result of this substitution is the creation of Equation: (106) [310, p.164].

$$J = \mathscr{N}_{ion}Q_{ion}\frac{Q_{ion}\mathscr{T}_{ion}}{\mathscr{M}_{ion}}E \tag{106}$$

Simplification of Equation: (106) produces Equation: (107).

$$J = \frac{\mathscr{N}_{ion}Q_{ion}^2\mathscr{T}_{ion}}{\mathscr{M}_{ion}}E \tag{107}$$

At this point the term before the electric field in Equation: (107) can be defined as the ion conductivity σ_{ion} shown by Equation: (108) and substituting this ion conductivity into Equation: (105) results in the creation of Equation: (109) which is very similar to the current density discussed earlier in the basic review of impedance analysis [310, p.164].

$$\sigma_{ion} = \frac{\mathscr{N}_{ion}Q_{ion}^2\mathscr{T}_{ion}}{\mathscr{M}_{ion}} \tag{108}$$

$$J = \sigma_{ion}E \tag{109}$$

A problem now exist with this definition of current density as shown by Equation: (109) because electrolytes are neutral meaning that both anions and cations exist in a solvated state and Equation: (109) only considers the current density of the movement of one type of ion [189, p.713] [16, p.12].

Faced with the electrolyte current density problem a physicist by the name of Friedrich Kohlrausch discovered that electrolytes obeyed Ohm's law accurately after the effects of electrolysis were removed from the system by the introduction of an AC source and more importantly Kohlrausch developed by experimental means Kohlrausch's law of independent migration of ions which can be summarized as the total ionic current density of an electrolyte by the summation of each ions current density [189, p.713] [318, pp.92–93].

Going back to the current density equation shown in Equation: (96) and the ion charge density equation shown in Equation: (97). Kohlrausch calculated the total current density of an electrolyte by summing together the individual current densities of both anions and cations which is expressed mathematically by Equation: (110) [189, p.713] [16, p.12].

$$J = \rho_{ion_-} \mathscr{V}_{ion_-} + \rho_{ion_+} \mathscr{V}_{ion_+} \tag{110}$$

Substitution into Equation: (110) produces Equation: (111),

$$J = \mathscr{N}_{ion_-} \mathscr{V}_{ion_-} Q_{ion_-} + \mathscr{N}_{ion_+} \mathscr{V}_{ion_+} Q_{ion_+} \tag{111}$$

Again, because an electrolyte must remain electrically neutral the charge produced by the anions must equal the charge produced by the cations and this can be expressed

mathematically by Equation: (112) [189, p.713] [16, p.13].

$$\mathscr{N}_{ion_-} Q_{ion_-} = \mathscr{N}_{ion_+} Q_{ion_+} \tag{112}$$

Earlier in the discussion on electrolysis it was shown that the Faraday constant is equal to the amount of equivalent substance moved as a result of a applied charge and this constant can be multiplied by the concentration $\mathcal{C}_{ion}$ of the electrolyte to determine the charge that exist for a given electrolyte as shown by Equation: (113) [189, pp.712–713] [16, p.12].

$$Q_{ion} = \mathfrak{F}\mathcal{C}_{ion} \tag{113}$$

One issue that arises from Equation: (113) is the assumption that the concentration is dissociated meaning this equation neglects the effects that real world dynamics such as temperature or pressure for example would have on a solution. Because real world concentrations are not dissociated a so called effective concentration or chemical activity $\mathcal{A}_{ion}$ was developed to account for these effects and its application to Equation: (113) produces Equation: (114) [16, p.12] [319, p.11] [320, p.6] [321, p.578].

$$Q_{ion} = \mathfrak{F}\mathcal{A}_{ion} \tag{114}$$

A chemist by the name of Gilbert Lewis defined an relation which related chemical

activity in terms of chemical potential along with incorporating thermodynamic properties of pressure and temperature into a equation shown by Equation: (115) in which $\mathscr{P}_{ion}$ represents chemical potential of the desired entity, $\mathscr{K}_{ion}$ represents the standard chemical potential of the desired entity, $\mathcal{R}$ represents the universal gas constant, $\mathcal{T}$ represents the absolute temperature, and $\mathcal{A}_{ion}$ represents the chemical activity [322] [320, pp.5–6] [321, p.578] [319, p.11].

$$\mathscr{P}_{ion} = \mathscr{K}_{ion} + \mathcal{R}\mathcal{T}\ln(\mathcal{A}_{ion}) \tag{115}$$

Solving Equation: (115) for chemical activity produces Equation: (116) [319, p.11].

$$\mathcal{A}_{ion} = e^{\frac{\mathscr{P}_{ion}-\mathscr{K}_{ion}}{\mathcal{R}\mathcal{T}}} \tag{116}$$

While Equation: (115) and Equation: (116) are valid means of finding chemical activity some more issues on this subject need to be addressed [320, pp.6–7]. First of all standard chemical potentials can vary depending on exactly how activity is defined and how the units of concentration are expressed [320, pp.6–7]. Secondly measuring an individual ion's chemical potential or its absolute activity is an example of one of the classical unsolved problems in this particular field making it necessary to examine comparative changes in activities with changing conditions [320, pp.6–7]. Such necessities force the measurement of chemical activity to be taken using an arbitrary standard chemical potential at some static temperature and pressure [320, pp.6–7]. Generally, the standard state is limited to the reference behavior of the system either when the limiting behavior of the substance

approaches zero or when the limiting behavior of the substance approaches unity which loosely translates into the concentration of the system-approaching zero or unity [320, pp.6–7].

Such assumptions discussed above allow for simplification of the Lewis equation into a good low concentration approximation defined by Equation: (117) in which chemical activity is equal to the concentration multiplied by the activity coefficient γ_{ion} [320, pp.5–9].

$$\mathcal{A}_{ion} = \mathscr{C}_{ion}\gamma_{ion} \tag{117}$$

Since chemical activity is generally not known but chemical concentration and activity coefficient tables are both easily found it is logical that Equation: (117) should be substituted into Equation: (114) which results in the creation of Equation: (118) [16, pp.12–13].

$$Q_{ion} = \mathfrak{F}\mathscr{C}_{ion}\gamma_{ion} \tag{118}$$

Application of Equation: (118) to Equation: (112) produces Equation: (119)

$$\begin{aligned} \mathscr{N}_{ion_-}Q_{ion_-} &= \mathscr{N}_{ion_+}Q_{ion_+} \\ &= \mathfrak{F}\mathscr{C}_{ion}\gamma_{ion} \end{aligned} \tag{119}$$

This electric neutrality concept from Equation: (119) can then be applied to Equation:

(111) which results in the creation of Equation: (120) [189, p.713].

$$J = \mathfrak{F}\mathscr{C}_{ion}\gamma_{ion}\mathscr{V}_{ion_-} + \mathfrak{F}\mathscr{C}_{ion}\gamma_{ion}\mathscr{V}_{ion_+} \tag{120}$$

Factoring Equation: (120) results in the creation of Equation: (121).

$$J = \mathfrak{F}\mathscr{C}_{ion}\gamma_{ion}(\mathscr{V}_{ion_-} + \mathscr{V}_{ion_+}) \tag{121}$$

At this point an equation that relates drift velocity to electric field intensity thru the ion mobility shown by Equation: (122) can be applied to Equation: (121) which results in the creation of Equation: (123) [189, p.708, p.714] [133, p.120].

$$\mathscr{V}_{ion} = \mu_{ion}E \tag{122}$$

$$J = \mathfrak{F}\mathscr{C}_{ion}\gamma_{ion}(\mu_{ion_-}E + \mu_{ion_+}E) \tag{123}$$

Factoring Equation: (123) results in the creation of Equation: (121).

$$J = \mathfrak{F}\mathscr{C}_{ion}\gamma_{ion}(\mu_{ion_-} + \mu_{ion_+})E \tag{124}$$

Upon comparing Equation: (124) to Equation: (109) commonalities appear and the term before the E in Equation: (124) becomes analogous to the term before the E in Equation: (109) which upon equating the two to each other creates Equation: (125) [189,

p.708, p.714] [16, p.13].

$$\sigma_{ion} = \mathfrak{F}\mathscr{C}_{ion}\gamma_{ion}(\mu_{ion_-} + \mu_{ion_+}) \tag{125}$$

Kohlrausch then normalized Equation: (125) to bring the conductivity to a consistent basis and called the result of this normalization the equivalent conductivity (Λ_{ion}) shown by Equation: (126) [189, p.714] [16, p.13].

$$\Lambda_{ion} = \frac{\mathfrak{F}\mathscr{C}_{ion}\gamma_{ion}(\mu_{ion_-} + \mu_{ion_+})}{\mathscr{C}_{ion}} \tag{126}$$

Simplification of Equation: (126) results in the creation of Equation: (127)

$$\Lambda_{ion} = \mathfrak{F}\gamma_{ion}(\mu_{ion_-} + \mu_{ion_+}) \tag{127}$$

Since the equivalent conductivity is the sum of the conductivity of both the anions and cations the equivalent conductivity of the individual ions $\mathfrak{X}_{ion}$ can be defined by expanding Equation: (127) which is shown by Equation: (128) and extracting each individual equivalent ion conductivity as shown by Equation: (129) and Equation: (130) [189, p.714].

$$\Lambda_{ion} = \mathfrak{F}\gamma_{ion}\mu_{ion_-} + \mathfrak{F}\gamma_{ion}\mu_{ion_+} \tag{128}$$

$$\mathfrak{X}_{ion_+} = \mathfrak{F}\gamma_{ion}\mu_{ion_+} \tag{129}$$

$$\text{Ϫ}_{ion_-} = \text{ϑ}\gamma_{ion}\mu_{ion_-} \tag{130}$$

The equivalent conductivity can be written as the sum of Equation: (129) and Equation: (130) which results in the creation of Equation: (131) [189, p.714].

$$\Lambda_{ion} = \text{Ϫ}_{ion_-} + \text{Ϫ}_{ion_+} \tag{131}$$

The equation shown in Equation: (131) is strictly correct when the electrolyte is infinitely dilute because of internal forces between ions in close proximity to each other. Kohlrausch discovered that this proximity effect could be compensated for in diluted strong electrolytes by finding the equivalent conductivity at an infinite dilution Λ^0_{ion} shown by Equation: (132) and offsetting the equivalent conductivity by a dependency factor $\mathscr{B}_{ion}$ that can vary based on temperature, viscosity, and other worldly effects which is shown by Equation: (133) [189, p.714].

$$\Lambda^0_{ion} = \text{Ϫ}^0_{ion_-} + \text{Ϫ}^0_{ion_+} \tag{132}$$

$$\Lambda_{ion} = \Lambda^0_{ion} - \mathscr{B}_{ion}\sqrt{\mathscr{C}_{ion}} \tag{133}$$

While Equation: (133) worked well for the equivalent conductivity of dilute strong electrolytic solutions the equivalent conductivity of weak electrolytes was found to decrease more rapidly than Equation: (126) predicts and a physicist by the name of Svante Arrhenius upon examining this particular problem suggested molecular dissociation α_{ion} in a electrolyte was related to its equivalent conductivity by Equation: (134) [189, p.715] [76,

pp.66–67].

$$\alpha_{ion} = \frac{\Lambda_{ion}}{\Lambda^{0}_{ion}} \tag{134}$$

A physical chemist by the name of Wilhelm Ostwald found Arrhenius ideas on dissociation intriguing and decided to use the relation shown in Equation: (134) in conjunction with the law of mass action to attempt to describe the equivalent conductivity of weak electrolytes with an undiluted concentration [189, p.715] [323].

The Guldberg-Waage law or law of mass action stems from the concept of chemical equilibrium in which when reacting substances are combined together and produce a chemical reaction the conversion between reactants to products as shown by Equation: (135) is often times incomplete no matter how long the reaction is allowed to continue [16, p.17] [324, p.269].

$$A_{reactant} + B_{reactant} \longrightarrow C_{product} + D_{product} \tag{135}$$

For further illustration of this concept of chemical equilibrium if reactant A reacts with reactant B to produce products C and D then by taking measurements over a period of time it can be shown that the amount of reactants will decrease while the amount of products will increase until a point in time occurs where both the reactants and products stay at a constant level which is defined as the equilibrium time t_{eq} [324, pp.269–270]. This point of equilibrium can be expressed by Equation: (136) or Equation: (137) [324, p.270].

$$A_{reactant} + B_{reactant} \rightleftharpoons C_{product} + D_{product} \tag{136}$$

$$A_{reactant} + B_{reactant} = C_{product} + D_{product} \tag{137}$$

The law of mass action takes the concept of equilibrium discussed above and defines a relationship between the ratios of the product of the chemical products to the product of the chemical reactants such that a balanced general equation shown by Equation: (138) can be substituted in to the law of mass action shown by Equation: (139) to find an equilibrium constant $\mathscr{K}_{eq}$ [324, p.271].

$$W_{coef}(A_{react}) + X_{coef}(B_{react}) + \cdots \rightleftharpoons Y_{coef}(C_{prod}) + Z_{coef}(D_{prod}) + \ldots \tag{138}$$

$$\mathscr{K}_{eq} = \frac{[A_{react}]^{W_{coef}}[B_{react}]^{X_{coef}} \ldots}{[C_{prod}]^{Y_{coef}}[D_{prod}]^{Z_{coef}} \ldots} \tag{139}$$

Ostwald considered the dissociation of acetic acid shown by Equation: (140) and defined the concentration of the reactants by Equation: (141) and the products by Equation: (142) [189, p.715].

$$HAc \rightleftharpoons H^{+} + Ac^{-} \tag{140}$$

$$\mathscr{C}_{HAc} = (1 - \alpha_{ion})\mathscr{C}_{ion} \tag{141}$$

$$\mathscr{C}_{H^{+}} = \mathscr{C}_{Ac^{-}} = \alpha_{ion}\mathscr{C}_{ion} \tag{142}$$

Ostwald then used the law of mass action to produce Equation: (143) which can be

simplified to Equation: (144) [189, p.715].

$$\mathscr{K}_{eq} = \frac{(\alpha_{ion}\mathscr{C}_{ion})(\alpha_{ion}\mathscr{C}_{ion})}{(1-\alpha_{ion})\mathscr{C}_{ion}} \tag{143}$$

$$\mathscr{K}_{eq} = \frac{\alpha_{ion}^2\mathscr{C}_{ion}}{1-\alpha_{ion}} \tag{144}$$

Substituting Equation: (134) into Equation: (144) results in the creation of Equation: (145) and further simplification results in the creation of Equation: (146) [189, p.715].

$$\mathscr{K}_{eq} = \frac{(\frac{\Lambda_{ion}}{\Lambda_{ion}^0})^2\mathscr{C}_{ion}}{1-(\frac{\Lambda_{ion}}{\Lambda_{ion}^0})} \tag{145}$$

$$\mathscr{K}_{eq} = \frac{\mathscr{C}_{ion}\Lambda_{ion}^2}{\Lambda_{ion}^0(\Lambda_{ion}^0-\Lambda_{ion})} \tag{146}$$

The equation shown in Equation: (146) is referred to as the Ostwald dilution law and it relates equivalent conductivity to concentration [189, pp.715–716]. Upon comparison of the Ostwald dilution law to the conductivity of weak electrolytes it was concluded that this law was a reasonable way to determine the dissociation constant of weak electrolytes but it was also found that this law was not very good at predicting strong electrolytes [189, pp.715–716].

Further developments on this subject was made by chemist Lars Onsager who applied Debye's and Huckel's theories about mean activity coefficients of strong electrolytes to the problem along with Walden's theories of electrolyte frictional forces [189, pp.715–716] [320, p.9] [325].

Debye-Huckel theories on the activity coefficients of individual ions along with the mean

activity coefficients of strong electrolytes stem from considering the interactions between ions from both a thermal forces and charge repulsion perspective [320, p.9]. Since charge repulsion is described by Coulomb's law while thermal counter effects to charge repulsion is described by the Boltzmann distribution law shown by Equation: (147) in which ψ_{ion} represents electrical potential of a point with respect to an electrically neutral point, $\mathscr{Z}_{ion}$ represents the number of ions involved, Q_{ion} represents the charge per each ion, $\mathscr{C}_{\psi}^{0}$ represents an electrically neutral concentration, $\mathscr{C}_{\psi}$ represents a concentration at a defined electric potential, k represents the Boltzmann constant, and $\mathcal{T}$ represents the absolute temperature of the solution such that these two laws were used by Debye-Huckel in the creation of their activity theories [320, p.9].

$$\mathscr{C}_{\psi} = \mathscr{C}_{\psi}^{0} e^{\frac{-\mathscr{Z}_{ion} Q_{ion} \psi_{ion}}{k\mathcal{T}}} \tag{147}$$

According to the Boltzmann distribution law concentrations of similar ions are diminished by being near other similar charged ions while at the same time dissimilar ions attract causing an increase in concentration which causes the formation of an ion atmosphere [320, pp.9–10]. Because an electrolyte is electrically neutral the charged ion atmosphere that forms between dissimilar ions has to be equal to the charge of the central ion responsible for the atmospheres formation [320, pp.9–10]. Furthermore, the attractive nature of this atmosphere will fall off exponentially over distance and is dependent upon temperature since thermal agitation works to counteract this atmospheric attraction [320, pp.9–10].

Debye and Huckel considered at first a simplistic case in which all the ions are assumed to be point charges to avoid complexity [320, pp.9–10]. Debye and Huckel then applied their theories to Equation: (147) which produced Equation: (148) in which κ_{ion} repre-

sents the reciprocal radius of the ionic atmosphere which is also called the Debye length [320, p10] [189, p.717]. This reciprocal radius is proportional to the square root of the concentration as shown by Equation: (149) in which $\mathscr{I}_{ion}$ represents the ionic strength of the electrolyte that is defined by Equation: (150) [320, p.10].

$$\ln(\gamma_{ion}) = \frac{-\mathscr{Z}_{ion}^2 Q_{ion}^2 \kappa_{ion}}{2\varepsilon_0 \varepsilon_r k \mathcal{T}} \tag{148}$$

$$\kappa_{ion} = \sqrt{\frac{8\pi Q_{ion}^2 N_A}{1000\varepsilon_0 \varepsilon_r k \mathcal{T}}} \sqrt{\mathscr{I}_{ion}} \tag{149}$$

$$\mathscr{I}_{ion} = \frac{\sum \mathscr{C}_{i_{ion}} \mathscr{Z}_{i_{ion}}^2}{2} \tag{150}$$

Next Equation: (148) and Equation: (149) can be combined together along with further simplification that results in the creation of the Debye-Huckel limiting law (DHLL) which is shown by Equation: (151) in which $\mathscr{O}_{ion}$ is a constant that is proportional to the $-\frac{3}{2}$ power of both the dielectric constant and the absolute temperature and also contains a conversion factor of $\frac{1}{2.303}$ to convert natural logarithms to base 10 logarithms [320, p.11].

$$-\log(\gamma_{i_{ion}}) = \mathscr{O}_{ion} \mathscr{Z}_{i_{ion}}^2 \sqrt{\mathscr{I}_{ion}} \tag{151}$$

Because The Debye-Huckel limiting law does not take into account the finite sizes of ions (DHLL) tends to produce results that overcompensate for ionic attraction and repulsion [320, pp.12–13]. Debye and Huckel later revised there derivation which is called the extended Debye-Huckel equation (EDHE) which resulted in the creation of Equation: (152) in which the additional parameter $\mathscr{D}_{ion}$ represents the mean distance of approach between ions [320, pp.12–13].

$$-\log(\gamma_{i_{ion}}) = \frac{\mathscr{O}_{ion}\mathscr{Z}_{i_{ion}}^{2}\sqrt{\mathscr{I}_{ion}}}{1+\kappa_{ion}\mathscr{D}_{ion}} \tag{152}$$

Onsager took the concepts that Debye and Huckel developed in their theory and applied Walden's theory that considered the notion that ions that are immersed in a fluid will experience retardation as a result of frictional forces that are described by Stokes' law shown by Equation: (153) in which η_{ion} is the viscosity of the solvent and $\mathfrak{R}_{ion}$ is the radius of ion [189, p.716].

$$F_{ion} = 6\pi\eta_{ion}\mathfrak{R}_{ion}\mathscr{V}_{ion} \tag{153}$$

In Walden's equations the frictional force opposing the ions motion shown by Equation: (153) are equated to the applied electrical force on the ion shown by Equation: (154) which when combined together creates a relationship between the two as shown by Equation: (155) [189, p.716].

$$F_{ion} = \mathscr{Z}_{ion}Q_{ion}E \tag{154}$$

$$\mathscr{Z}_{ion}Q_{ion}E = 6\pi\eta_{ion}\mathfrak{R}_{ion}\mathscr{V}_{ion} \tag{155}$$

Walden's equations shown by Equation: (155) can then be solved in terms that can be substituted for mobility as shown by Equation: (156) [189, p.716].

$$\mu_{ion} = \frac{\mathscr{V}_{ion}}{E} = \frac{\mathscr{Z}_{ion} Q_{ion}}{6\pi\eta_{ion}\mathfrak{R}_{ion}(300)} \tag{156}$$

Next the theory of equivalent conductivity shown by Equation: (127) can be applied to Walden's equations shown by Equation: (156) which results in the creation of Equation: (157) [189, pp.716–717].

$$\Lambda^{0}_{ion} = \frac{\mathfrak{F}\gamma_{ion} Q_{ion}}{6\pi\eta_{ion}(300)} \left(\frac{\mathscr{Z}_{ion+}}{\mathfrak{R}_{ion+}} + \frac{\mathscr{Z}_{ion-}}{\mathfrak{R}_{ion-}} \right) \tag{157}$$

Because the only medium dependency in Equation: (157) is the viscosity and equivalent conductivity multiplication of the viscosity can be performed such that viscosity is moved next to the equivalent conductivity [189, p.717]. This operation produces a viscosity equivalent conductivity comparison that is equal to a constant value as shown by Equation: (158) which is referred to as Walden's rule and produces results that are not very accurate when working with large ions [189, p.717].

$$\Lambda^{0}_{ion}\eta_{ion} = C_{onstant} \tag{158}$$

Onsager in the development of the Onsager equation combined both the viscosity and ionic atmospheric effects on conductivity by substituting the Debye radius $\mathfrak{R}_{debye}$ shown by Equation: (159) into the Walden equation shown by Equation: (158) which results in the creation of Equation: (160) [189, p.718].

$$\mathfrak{K}_{debye} = \frac{1}{\kappa_{ion}} \tag{159}$$

$$\Lambda^{0}_{ion} = \frac{\mathfrak{F}\gamma_{ion}Q_{ion}(\mathscr{Z}_{ion+} + \mathscr{Z}_{ion-})\kappa_{ion}}{6\pi\eta_{ion}(300)} \tag{160}$$

Applying theory found in Equation: (133) to Equation: (160) equivalent conductivity can be found by subtracting the equivalent conductivity at an infinite dilution shown by Equation: (161) [189, p.718].

$$\Lambda_{ion} = \frac{\mathfrak{F}\gamma_{ion}Q_{ion}}{6\pi\eta_{ion}(300)}\left(\frac{\mathscr{Z}_{ion+}}{\mathfrak{K}_{ion+}} - \frac{\mathscr{Z}_{ion+}}{\mathfrak{K}_{debye}} + \frac{\mathscr{Z}_{ion-}}{\mathfrak{K}_{ion-}} - \frac{\mathscr{Z}_{ion-}}{\mathfrak{K}_{debye}}\right) \tag{161}$$

The equation shown by Equation: (161) upon substitution and simplification of variables results in the creation of the Onsager equation which is shown by Equation: (162) [189, p.718].

$$\Lambda_{ion} = \Lambda^{0}_{ion} - \left[\frac{82.4}{\sqrt{\varepsilon_0\varepsilon_r\mathcal{T}}\eta_{ion}} + \frac{8.20\times10^{5}\Lambda^{0}_{ion}}{\sqrt{(\varepsilon_0\varepsilon_r\mathcal{T})^{3}}}\right]\sqrt{\mathscr{C}_{ion}} \tag{162}$$

This equation is usually abbreviated as shown by Equation: (163) in which A_{abb} is defined by Equation: (164) and B_{abb} is defined by Equation: (165) [189, p. 718].

$$\Lambda_{ion} = \Lambda^{0}_{ion} - \left(A_{abb} + B_{abb}\Lambda^{0}_{ion}\right)\sqrt{\mathscr{C}_{ion}} \tag{163}$$

$$A_{abb} = \frac{82.4}{\sqrt{\varepsilon_0\varepsilon_r\mathcal{T}}\eta_{ion}} \tag{164}$$

$$B_{abb} = \frac{8.20 \times 10^5}{\sqrt{(\varepsilon_0 \varepsilon_r \mathcal{T})^3}} \tag{165}$$

Comparison of the Onsager equation to experimental data produces the conclusion that the Onsager method works extremely well for very dilute solutions but underestimates the conductivity when electrolyte concentrations increase [189, pp.718–719].

High concentrations of electrolytes in a solvent are somewhat problematic to model since the interactions between each of the ions are more frequent and chaotic resulting in a reduction of their overall mobility. Furthermore, as the value of concentration increases a point in which the solvent become saturated will occur and this point will prevent further ionization from occurring which forces the un-ionized molecules to coexist with aqueous ions in a very tightly packed solution that slows overall ion mobility [16, p.14]. Generally speaking electrolytes exist in low to moderate concentrations because as concentrations increase the line that separates a solvent from a solute becomes blurred since both of the definitions are based upon the amount of quantity of each component [16, p.14].

Another point of interest that should be noted is on the subject of additional research conducted by Wien and Debye-Falkenhagen that produced results that are nonlinear when electrolytes are exposed to high electric fields $E > 100000\frac{V}{cm}$ or high frequencies $f > 3000000\frac{c}{s}$ and these nonlinearities occur because the ions are moving so fast that the ionic atmosphere around the ion never forms which increases the electrolyte mobility [189, p.719]. Additional nonlinearities can occur if the viscosity of the electrolyte changes or if the number of ions per volume changes and while in some particular cases the effects of these nonlinearities are negligible nonlinearities as a whole should always be considered when modeling a biomaterial [16, p.48].

5.5.4 Ion Conductivity by Diffusion

Another phenomenon seen in electrolytic solutions is the concept of ion migration thru diffusion [16, p.23]. The general idea behind ionic migration thru diffusion can best be illustrated by an example in which a solute is dissolved into a neutral solvent at some particular region such that this region will initially have a high concentration of solute that will gradually decrease over a period of time until the solute gets distributed equally over the solvent [16, pp.23–25].

Diffusion is defined as the process that occurs as the result of the random motion of molecules in which a net flow of matter occurs from regions of high concentration to regions of lower concentration and this process is governed by the concepts of Brownian motion, molecular collisions and the mean free path between collisions [16, p.23]. Molecular diffusion can be mathematically described thru the application of Fick's first law as shown by Equation: (166) in which $\mathfrak{F}_{fick}$ represents the molar flux, $\mathfrak{D}_{fick}$ represents the diffusion coefficient, x represents the current position, and $\mathscr{C}$ represents the concentration [16, p.23]. While values of molar flux is of interest in some applications it is oftentimes more desirable to know how concentration will change over a period of time and this can be found thru the application of Fick's second law as shown by Equation: (167) in which t represents the time that has passed [16, p.24].

$$\mathfrak{F}_{fick} = -\mathfrak{D}_{fick}\frac{\partial \mathscr{C}}{\partial x} \tag{166}$$

$$\left(\frac{\partial \mathscr{C}}{\partial t}\right) = \mathfrak{D}_{fick}\frac{\partial^2 \mathscr{C}}{\partial x^2} \tag{167}$$

The overall effects of diffusion from a bioimpedance perspective is somewhat variant depending upon the vantage point taken on the subject because in one perspective elec-

trolytes in a biomaterial could be considered initially diffused when measured since the measurements that are taken generally happen long after the original concentration of the solute was dissolved which allows the diffusion effect to be neglected [16, p.23–25]. Another possible perspective on the subject is since living biomaterials are constantly undergoing chemical processes and forming concentration gradients diffusion would always be an active and somewhat unpredictable part of a bioimpedance measurement that would have to be considered [16, p.23–25]. Yet another possible perspective on this subject comes from the electrode electrolyte boundary in which new solutes are created thru electrolysis and oxidation reduction effects that will diffuse from the electrodes out into the solvent over a period of time which could potentially change the concentration of the electrolyte such that diffusion would have to be considered [16, p.23–25]. Lastly several theories exist in which diffusion plays a central role in the inner workings of internal cellular conduction meaning it would have to be considered [16, p.23–25]. All and all diffusion is an effect that needs to be thought about carefully and possibly accounted for depending upon the type of bioimpedance being measured [16, p.23–25].

5.5.5 Ion Potential And Oxidation Reduction Effects

An interesting property that typically arises as a result of the introduction of a metal electrode into an electrolyte is the concept of oxidation reduction which is often referred to as redox for short [132, pp.128–129] [16, p.36]. Looking at the individual components of oxidation reduction for a moment conceptually oxidation is the process of an element losing free electrons to another element while reduction is the process of an element gaining additional electrons from another element [132, pp.128–129]. The combined term oxidation reduction indicates that both oxidation and reduction is occurring at the same time in a given chemical reaction or in other words one element is losing electrons while another one

is gaining electrons during a chemical reaction [132, pp.128–129].

Elements typically can be classified into oxidizing agents or reducing agents by their oxidation number which is equal to the number of electrons that a element wants to gain or lose from valance electron theory in there neutral state or equal to their current charge when ionized [132, pp.128–129]. From a chemical equation perspective an example of a redox reaction can be seen thru the introduction of zinc into an aqueous hydrogen solution such as a hydrogen based acid for example as shown by Equation: (168) in which the zinc as a result of the redox reaction becomes aqueous in the solution and the hydrogen bubbles out of the solution as a gas [132, pp.128–129, p.777]. It should be noted that total charge must remain zero during a redox reaction therefore balancing coefficients are used to maintain this zero net charge [132, pp.128–129, p.777].

$$Zn_{Solid} + 2H^{+}_{Aqueous} \longrightarrow Zn^{2+}_{Aqueous} + H_{2_{Gas}} \tag{168}$$

While there are several different types of redox reactions only the ones that are prevalent to bioimpedance analysis are of interest and such reactions as could be imagined involve electrochemistry which is generally summarized as the study of the relationship between chemical reactions and electricity [132, p.777]. One point of interest that arises from redox reactions is spontaneous redox reactions from which voltaic and galvanic cells originate [132, p.784]. Voltaic and galvanic effects are important because the transfer of electrons from the chemical reaction can be channeled thru an external pathway such as a metal conductor for example which depending upon the amount of electrons being channeled could in theory be used to power an electrical device [132, pp.784–785].

While the fundamentals of what could be loosely referred to as battery theory which

voltaic-galvanic cells are best known for there are a few effects that these phenomena impose upon a bioimpedance model thus meriting an introduction to the subject [132, pp.784–785] [16, pp.36–37]. In order to illustrate how a voltaic cell operates an example of a spontaneous redox reaction shown by Equation: (169) needs to be discussed in some detail [132, p.784].

$$Zn_{Solid} + Cu^{2+}_{Aqueous} \longrightarrow Zn^{2+}_{Aqueous} + Cu_{Solid} \tag{169}$$

In the spontaneous redox reaction shown by Equation: (169) a piece of zinc metal is placed into a aqueous solution of ionized copper which as an result of this combination the zinc metal is oxidized into a aqueous state while the copper becomes reduced returning to a solid state [132, pp.784–785]. This reaction by itself is not inherently useful however the oxidation and reduction components can be separated into what is formally called a half-reaction shown in this particular case by Equation: (170) and Equation: (171) [132, p.785].

$$Zn_{Solid} \longrightarrow Zn^{2+}_{Aqueous} - 2e^{-} \tag{170}$$

$$Cu^{2+}_{Aqueous} + 2e^{-} \longrightarrow Cu_{Solid} \tag{171}$$

A voltaic system takes both redox components defined by their half-reactions and places each chemical component into separate containers referred to as half-cells with the addition of a common nonreactive aqueous electrolyte in both of the cells [132, pp.784–785]. Additionally solid bars of the un-ionized metal are added to the appropriate half-cell which in the case of this example a solid zinc bar will be submerged into the zinc half-cell while

a solid copper bar will be submerged into the copper half-cell [132, pp.784–785].

If an electrical connection is made from the zinc bar to the copper bar with some load impedance between the two electrical connections, theoretically electrons should flow from the zinc bar to the copper bar because an electrical potential exist as a result of the redox reaction that will occur at the onset of additional electrons in the copper solution [132, pp.784–789]; however, upon connecting a voltaic cell in this particular configuration no electrical current will occur because electrical neutrality of the solution is required thus no redox reaction can occur in order to preserve this chemical neutrality [132, pp.784–789].

Because chemical neutrality must be maintained in a solution one way to overcome this problem is by the introduction of an additional common nonreactive aqueous electrolyte in both of the half-cells that can create an electrical return path which allows additional charge to migrate back to the zinc solution from the copper solution via an ion bridge which allows the redox reaction to occur and the flow of electrical current [132, pp.784–785]. Typically this electrical bridge is created using a "U" shaped tube that is inserted between the two cells that contains some type of aqueous salt that ionizes in solvent but does not react chemically with the redox salute allowing charge to be transfer back to the zinc half-cell from the copper half-cell [132, pp.784–785].

While this example highlights a particular redox reaction other materials can exhibit a similar galvanic behavior when subjected to similar conditions [132, p.799]. Studies were conducted on this subject by a German chemist by the name of Walther Nernst on different redox materials and Nernst developed a relationship between galvanic potential and concentration called the Nernst equation as shown by Equation: (172) in which V_0 is the standard electrode potential of the redox system, $\mathcal{A}_{ox}$ is the chemical activity of the oxidization ion, and $\mathcal{A}_{red}$ is the chemical activity of the reduction ion [132, p.799] [16, p.37].

$$V = V_0 + \frac{\mathcal{RT}}{\mathscr{N}_{ion}\mathfrak{F}} \ln\left(\frac{\mathcal{A}_{ox}}{\mathcal{A}_{red}}\right) \tag{172}$$

Another interesting phenomenon that can occur in a voltaic cell is the formation of a potential difference between two identical half-cells with different ionic concentrations which is commonly referred to as a concentration cell [132, p.801]. In the example given above the copper half-cell would be replaced by another zinc half-cell with a different concentration of zinc ions. Because a difference in concentration of ions exists between the two zinc half-cells a potential difference also exists and electricity will flow around a closed loop as discussed earlier until the charge concentration is equalized and equilibrium occurs [132, pp.784–785, p.801].

Yet Another phenomenon that is related to the concentration cell phenomenon is called the liquid junction potential in which a potential voltage is created between dissimilar electrolytic solutions as a result of Brownian motion [132, p.801] [16, p. 39]. The liquid junction phenomenon is described mathematically by a variation of the Nernst equation and is referred to as the Henderson equation, which is shown by Equation: (173) in which V_{LJ} is the liquid junction potential [132, p.801] [16, p.39].

$$V_{LJ} = \frac{\mu_{ion_+} - \mu_{ion_-}}{\mu_{ion_+} + \mu_{ion_-}} \frac{\mathcal{RT}}{\mathscr{N}_{ion}\mathfrak{F}} \ln\left(\frac{\mathscr{C}_{ion_1}}{\mathscr{C}_{ion_2}}\right) \tag{173}$$

The equation shown in Equation: (173) makes the assumption that the two liquids are in contact with each other However, in biomaterials there is oftentimes a porous membrane that separates the involved electrolytes which will result in a slightly different potential

difference which can be modeled by the application of the Donnan equation as shown by Equation: (174) in which V_D is the Donnan potential difference [16, p.39].

$$V_D = \frac{\mathcal{RT}}{\mathfrak{F}} \ln\left(\frac{\mathcal{A}_{ion_1}}{\mathcal{A}_{ion_2}}\right) \tag{174}$$

5.5.6 Ion Conductivity and the Double Layer

Another interesting phenomena that occurs at the electrode to electrolyte boundary is the concept of an double layer that is formed as a result of the surface charge of the electrode attracting molecules of opposite polarity which creates a molecular charge screening layer that looks very capacitive [16, pp.25–26].

Because the double layer can be thought of as a molecular capacitor a scientist by the name of Helmholtz theorized that when an electrolyte concentration is very high the capacitive value of the double layer will be very large because the size of the double layer becomes small and tightly packed near the electrode [16, pp.25–26].

Helmholtz theory is only valid for high concentrated electrolytes and as the electrolyte concentration decreases the size of the double layer will increase causing the effective capacitance in the double layer to decrease [16, pp.25–26]. Additionally, as the double layer increases the screening effect will also decrease and this decrease in screening will allow ions to migrate thru the double layer which is why the double layer is sometimes referred to as the diffuse electric layer to indicate the occurrence of ion migration in the double layer [16, pp.25–26].

Several mathematical models have been proposed after the development of the Helmholtz theory which takes into consideration the effects that occur from lower con-

centrations found in the diffused electric layer [16, pp.25–26]. These models include the Gouy-Chapman theory which takes into account the effects of thermal motion in the diffused electric layer, the Debye-Huckel model proposes approximations that can be used when working with a spherical or a flat diffused electric layer, the Stern theory expands upon the Gouy-Chapman model, and the Schwartz theory takes into consideration the effects of lateral movement in the diffused electric layer [16, pp.25–29].

While double layer effects as a whole are important in a physical liquid electrode boundary their overall importance when it comes to modeling a biomaterial is somewhat dubious at least from a macroscopic vantage point since on the macroscopic level capacitances are oftentimes lumped together and compensated for depending upon the models impedance topology [16, pp.25–29]. The key concept to take away from the double layer is the concept that a capacitance will exist as the result of a liquid electrode boundary [16, pp.25–29].

5.5.7 Introduction to Dielectrics and Polarization

When most people hear the term dielectric typically a mental image of some type of electrical insulator comes to mind and many electrical products utilize dielectrics like a capacitor for example that uses a dielectric material to separate its electrical plates from an applied electric field [16, p.51]. While this imagery is accurate to some degree a general description describes a dielectric as a material in which an electric field can fully penetrate the material which differs from a conductor since in the case of the conductor a static electric field cannot fully penetrate a conductive material [16, p.51]. With mental imagery and general definitions aside formally a material is only classified as a dielectric if the material has a capacitive displacement current that is larger than its phase current which can be mathematically defined by Equation: (175) in which G_{di} is defined as the conductance of the material or in a more generalized from by Equation: (176) [16, p.51].

$$\omega C_{di} > G_{di} \tag{175}$$

$$f > \frac{\sigma}{2\pi\varepsilon} \tag{176}$$

The equations shown above suggest that the classification of a material as a dielectric is dependent upon the frequency being used for the observation which means that a particular material can act like a conductor for a given frequency range while acting like a dielectric in another frequency range [16, p.51]. This conductor dielectric duality makes absolute material classification somewhat problematic but it also implies that a biomaterial could be examined as a conductor or as a dielectric depending upon the analysis being performed [16, p.51]. Furthermore, because this duality exist both conductors and dielectrics have intrinsic properties which consider the occurrence of the counter phenomena , for example conductors are classified by impedance parameters which has a variable to account for a dielectric phenomena while a dielectric is classified by a complex permittivity which has a variable to account for conductance phenomena [16, p.51]. While the concept of impedances and permittivities are not foreign to the electrical engineering profession these concepts becomes somewhat abstract when being measured by a profession outside of the electrical engineering community which makes finding common ground for measurement comparison between disciplines difficult [16, p.51]. Additionally some of the information needed to understand the properties of dielectrics has already been discussed in the impedance analysis section under the topic of impedance theory of a capacitor.

One topic that arises upon investigating the properties of dielectrics is the concept of polarization which for a uniform dielectric can be defined as a disturbance of the charge distribution for a particular region of the dielectric as the result of a field induced dis-

turbance [16, p.52]. Nonpolar materials require the application of an external energy in order to be polarized while polar materials have an intrinsic dipole that is polarized with a random orientation which requires the application of an external energy in order to obtain a common direction [16, pp.52–53] [310, pp.171–172].

Polarization is measured by first finding the dipole moment which is a quantitative measurement of the magnitude of the distortion of the molecules electron cloud which can be found thru the application of coulombs law that results in the creation of Equation: (177) in which $p_{\uparrow}$ is the dipole moment, and $\ell_{\uparrow}$ is the dipole distance [16, p.54] [310, p.171] [132, p.288].

$$p_{\uparrow} = Q\ell_{\uparrow} \tag{177}$$

Next the total dipole moment over a given volume can be found thru the summation of the individual dipoles over a defined region as shown by Equation: (178) in which $p_{\uparrow_{total}}$ is the total dipole moment, n is the number of dipoles per unit volume, and Δ_v is the defined volume [132, p.288] [133, p.138].

$$p_{\uparrow_{total}} = \sum_{i=1}^{n\Delta_v} p_{\uparrow_i} \tag{178}$$

Polarization can then be found by taking the limit of the volume as it approaches zero as shown by Equation: (179) in which $P_{\uparrow}$ is the polarization [133, p.138].

$$\begin{aligned} P_{\uparrow} &= \lim_{\Delta V \to 0} \frac{1}{\Delta_v} p_{\uparrow_{total}} \\ &= \lim_{\Delta V \to 0} \frac{1}{\Delta_v} \sum_{i=1}^{n\Delta_v} p_{\uparrow_i} \end{aligned} \tag{179}$$

The electrical potential that is created as a result of polarization can be found thru the application of electromagnetic and divergence theory shown by Equation: (180) in which Θ_n is the outward unit normal to the selected surface, and ℓ_R is the length between a volume element and a point [310, pp.172–173].

$$V_{\uparrow} = \int_{\mathbb{S}} \frac{P_{\uparrow} \cdot \Theta_n}{4\pi\varepsilon_0 \ell_R} d\mathbb{S} + \int_{\mathbb{V}} \frac{-\nabla \cdot P_{\uparrow}}{4\pi\varepsilon_0 \ell_R} d\mathbb{V} \tag{180}$$

Simplification and transformation of surface and volume potentials to charge densities results in the creation of Equation: (181) and Equation: (182) in which $\rho_{\uparrow_{\mathbb{S}}}$ is the surface charge density, and $\rho_{\uparrow_{\mathbb{V}}}$ is the volume charge density [310, p.173].

$$\rho_{\uparrow_{\mathbb{S}}} = P_{\uparrow} \cdot \Theta_n \tag{181}$$

$$\rho_{\uparrow_{\mathbb{V}}} = -\nabla \cdot P_{\uparrow} \tag{182}$$

Converting the charge densities to enclosed charges can be accomplished by application of Equation: (183) and Equation: (184) in which $Q_{\mathbb{S}}$ is the surface charge and $Q_{\mathbb{V}}$ is the volume charge [133, p.140].

$$Q_{\mathbb{S}} = \int_{\mathbb{V}} \rho_{\uparrow_{\mathbb{S}}} d\mathbb{V} \tag{183}$$

$$Q_{\mathbb{V}} = \int_{\mathbb{V}} \rho_{\uparrow_{\mathbb{V}}} d\mathbb{V} \tag{184}$$

The enclosed charge equations shown by Equation: (183) and Equation: (184) can also be written in terms of polarization and electric flux density as shown by Equation: (185) and Equation: (186) [133, pp.139–140].

$$Q_{\mathbb{S}} = \oint_{\mathbb{S}} D \cdot d\mathbb{S} \tag{185}$$

$$Q_{\mathbb{V}} = -\oint_{\mathbb{S}} P_{\uparrow} \cdot d\mathbb{S} \tag{186}$$

The total enclosed charged $Q_{\mathbb{T}}$ can be found by summing the surface charge and the volume charge together as shown by Equation: (187) [133, p.139].

$$Q_{\mathbb{T}} = Q_{\mathbb{V}} + Q_{\mathbb{S}} \tag{187}$$

The total enclosed charge can also be found thru the application of gauss's law which results in the creation of Equation: (188) [133, p.139].

$$Q_{\mathbb{T}} = \oint_{\mathbb{S}} \varepsilon_0 E \cdot d\mathbb{S} \tag{188}$$

Substitution of Equation: (185), Equation: (186), and Equation: (188) into Equation: (187) results in the creation of Equation: (189) [133, pp.139–140].

$$\oint_{\mathbb{S}} \varepsilon_0 E \cdot d\mathbb{S} = -\oint_{\mathbb{S}} P_{\uparrow} \cdot d\mathbb{S} + \oint_{\mathbb{S}} D \cdot d\mathbb{S} \tag{189}$$

Applying assumptions and solving for D in Equation: (189) results in the creation of Equation: (190) [133, p.140].

$$D = \varepsilon_0 E + P_{\uparrow} \tag{190}$$

If the dielectric under examination is not ferroelectric and has a linear relationship between the materials electrical polarization to its applied electric field a scaling factor called the electric susceptibility χ_e can be used to create a linear relationship between the two as shown by Equation: (191) [133, pp.140–141].

$$P_{\uparrow} = \chi_e \varepsilon_0 E \tag{191}$$

Substitution of the linear relationship provided by Equation: (191) into Equation: (190) results in the creation of Equation: (192) which upon factoring common terms results in the creation of Equation: (193) [133, p.141].

$$D = \varepsilon_0 E + \chi_e \varepsilon_0 E \tag{192}$$

$$D = \varepsilon_0 E \left(1 + \chi_e\right) \tag{193}$$

The factored term $\left(1 + \chi_e\right)$ can be defined as the relative permittivity or dielectric constant for the material under observation as shown by Equation: (194) which results in the abbreviated permittivity term shown by Equation: (195) that is oftentimes used in the application of dielectric theory [133, pp.141].

$$\varepsilon_r = 1 + \chi_e \tag{194}$$

$$\varepsilon = \varepsilon_r \varepsilon_0 \tag{195}$$

The key concept that should be taken away from this derivation is the concept that polarization can result from the application of an electric field also it should be noted that this induced polarization can modify the applied electric field inside of the material by a value known as the permittivity [133, pp.141–142].

Additionally it is often times useful to look at how the permittivity will affect the dipole moment and this can be accomplished by utilizing a concept called the polarizability $\alpha_\uparrow$ as shown by Equation: (196) in which E_ℓ is the local electric field strength [16, p.55].

$$p_\uparrow = \alpha_\uparrow E_\ell \tag{196}$$

This polarizability concept extends to molecular polarization as shown by Equation: (197) in which $N_{\uparrow}$ is the volume density of the material, also a relationship exist between the polarizability and permittivity which is easily identified upon comparing Equation: (197) to Equation: (191) [16, p.55].

$$P_{\uparrow} = N_{\uparrow}\alpha_{\uparrow}E \tag{197}$$

This polarizability relationship can be extended further in the case of non-polar materials and results in the creation of the Clausius-Mossotti relationship as shown by Equation: (198) which relates polarization to molecular structure [16, pp.55–56].

$$\frac{\varepsilon_r - 1}{\varepsilon_r + 2} = \frac{N_{\uparrow}\alpha_{\uparrow}}{3\varepsilon_0} \tag{198}$$

The nonpolar Clausius-Mossotti relationship can be expanded to include the effects of polar materials which results in the creation of the Debye equation shown by Equation: (199) in which $v_{\uparrow}$ is the molar volume [16, p.56].

$$\frac{\varepsilon_r - 1}{\varepsilon_r + 2} = \frac{N_A\left(\alpha_{\uparrow} + \frac{p_{\uparrow}^2}{3k\mathcal{T}}\right)}{3v_{\uparrow}} \tag{199}$$

5.5.8 Discussion on Dielectric Parameters

As mentioned earlier in this chapter an impedance can account for the presence of a dielectric thru the introduction of a complex variable and similarly a permittivity can

account for the presence of a conductor thru the introduction of a complex variable [16, p.59]. Conceptually a complex permittivity will take on the form shown by Equation: (200) in which $\varepsilon_r^{\Re}$ denotes the real relative permittivity part and $\varepsilon_r^{\Im}$ denotes the imagery relative permittivity part [16, pp.59–60].

$$\begin{aligned} \varepsilon &= \varepsilon_r \varepsilon_0 \\ \varepsilon &= \varepsilon_r^{\Re} \varepsilon_0 - \jmath \varepsilon_r^{\Im} \varepsilon_0 \\ \varepsilon &= \left(\varepsilon_r^{\Re} - \jmath \varepsilon_r^{\Im} \right) \varepsilon_0 \end{aligned} \tag{200}$$

Similarly, a complex conductance will take on the form shown by Equation: (201) in which $\sigma^{\Re}$ denotes the real conductivity part and $\sigma^{\Im}$ denotes the imagery conductivity part [16, pp.59–60].

$$\sigma = \sigma^{\Re} + \jmath \sigma^{\Im} \tag{201}$$

As discussed in the impedance analysis section of this chapter the impedance of a capacitor is defined as shown by Equation: (202) however, it is oftentimes easier mathematically to convert an impedance into a admittance Y as shown by Equation: (203) which upon application of the admittance operation to the impedance of a capacitor results in the creation of the admittance of a capacitor shown by Equation: (204) [16, p.59].

$$Z = \frac{1}{\jmath \omega C} \tag{202}$$

$$Y = \frac{1}{Z} \tag{203}$$

$$= \frac{1}{\frac{1}{\jmath\omega C}}$$

$$= \jmath\omega C \tag{204}$$

Again from the impedance analyses section the definition of a parallel plate capacitor shown by Equation: (49) can be substituted into the admittance of a capacitor shown by Equation: (204) which results in the creation of Equation: (205) [16, pp.59–60].

$$Y = \jmath\omega\frac{\mathbb{A}_s\varepsilon}{\mathbb{T}} \tag{205}$$

Substitution of a complex permittivity shown in Equation: (200) into Equation: (205) results in the creation of Equation: (206) which effectively describes a capacitance as a complex permittivity [16, p.60].

$$Y = \jmath\omega\frac{\mathbb{A}_s}{\mathbb{T}}\left(\varepsilon_r^{\Re} - \jmath\varepsilon_r^{\Im}\right)\varepsilon_0 \tag{206}$$

In order to reduce the number of terms substitution for real and complex permittivity shown by Equation: (207) and Equation: (208) will be performed on Equation: (206) which results in the creation of Equation: (209) [16, pp.59–60].

$$\varepsilon^{\Re} = \varepsilon_r^{\Re}\varepsilon_0 \tag{207}$$

$$\varepsilon^{\Im} = \varepsilon_r^{\Im}\varepsilon_0 \tag{208}$$

$$Y = \jmath\omega\frac{\mathbb{A}_s}{\mathbb{T}}\left(\varepsilon^{\Re} - \jmath\varepsilon^{\Im}\right) \tag{209}$$

A relationship exists between the real part of the conductivity and the imaginary part of the permittivity as shown by Equation: (210) which is to be expected since the goal of introducing complex variables in to the equation was to account for conductance effects in a dielectric material [16, p.60].

$$\varepsilon^{\Im} = \frac{\sigma^{\Re}}{\omega} \tag{210}$$

Application of Equation: (210) to Equation: (209) results in the creation of a mixed permittivity and conductivity representation of the admittance of a capacitor as shown by Equation: (211) [16, pp.59–61].

$$\begin{aligned} Y &= \jmath\omega\frac{\mathbb{A}_s}{\mathbb{T}}\left(\varepsilon^{\Re} - \jmath\varepsilon^{\Im}\right) \\ &= \frac{\mathbb{A}_s}{\mathbb{T}}\left(\jmath\omega\varepsilon^{\Re} - \jmath\omega\jmath\varepsilon^{\Im}\right) \\ &= \frac{\mathbb{A}_s}{\mathbb{T}}\left(\jmath\omega\varepsilon^{\Re} + \omega\varepsilon^{\Im}\right) \\ &= \frac{\mathbb{A}_s}{\mathbb{T}}\left(\jmath\omega\varepsilon^{\Re} + \omega\frac{\sigma^{\Re}}{\omega}\right) \\ &= \frac{\mathbb{A}_s}{\mathbb{T}}\left(\jmath\omega\varepsilon^{\Re} + \sigma^{\Re}\right) \end{aligned} \tag{211}$$

Additionally another relationship between the real part of the permittivity and the complex part of the conductivity exist as shown by Equation: (212) [16, p.61].

$$\sigma^{\Im} = \omega\varepsilon^{\Re} \tag{212}$$

Application of Equation: (212) to Equation: (211) results in the creation of Equation: (213) which is the admittance of a capacitor in terms of conductivity parameters [16, p.61].

$$\begin{aligned} Y &= \frac{\mathbb{A}_s}{\mathbb{T}} \left(\jmath\omega\varepsilon^{\Re} + \sigma^{\Re} \right) \\ &= \frac{\mathbb{A}_s}{\mathbb{T}} \left(\jmath\sigma^{\Im} + \sigma^{\Re} \right) \\ &= \frac{\mathbb{A}_s}{\mathbb{T}} \left(\sigma^{\Re} + \jmath\sigma^{\Im} \right) \end{aligned} \tag{213}$$

Another complex parameter called resistivity ρ shown by Equation: (214) is defined as the inverse of the conductivity as shown by Equation: (215) and represents another way in which a dielectric material can be mathematically described [16, p.61].

$$\rho = \rho^{\Re} - \jmath\rho^{\Im} \tag{214}$$

$$\rho = \frac{1}{\sigma} \tag{215}$$

Similarly another complex parameter called the modulus (M) shown by Equation: (216) is defined as the inverse of the permittivity as shown by Equation: (217) and represents yet another way in which a dielectric material can be mathematically described [16, p.61].

$$M = M^{\Re} + \jmath M^{\Im} \tag{216}$$

$$M = \frac{1}{\varepsilon} \tag{217}$$

The last method of dielectric representation which needs to be mentioned is the concept of loss factor φ and loss tangent δ which look at dielectric losses in terms of a phase angle as shown by Equation: (218) and Equation: (219) [16, p.61].

$$\varphi = \tan^{-1}\left(\frac{\varepsilon^{\Re}}{\varepsilon^{\Im}}\right) \tag{218}$$

$$\delta = \cot^{-1}\left(\frac{\varepsilon^{\Re}}{\varepsilon^{\Im}}\right) \tag{219}$$

While all of the mathematical representations discussed above might appear somewhat redundant and trivial one of the major problems that occurs as a result of all of these different notations is a very confusing communication barrier that exists between different bioimpedance related disciplines because each discipline utilizes a different dielectric representation for their given application [16, p.61]. Not only does a barrier exist between different disciplines but the notations have also changed over time which can cause confusion when examining older research documents [16, p.61]. Because of this broad representation that the bioimpedance subject as a whole brings to the table it is very important to be familiar with the common dielectric representations that are available and commonly used in different disciplines research documents [16, p.61].

5.5.9 Relaxation and Dispersion

No introduction of dielectrics would be complete without briefly discussing the concepts of relaxation and dispersion [16, p.63]. Because polarization and the displacement of charge are processes that cannot occur instantaneously the period of time required for these phenomena to occur is the starting point for the concepts of relaxation [16, p.63].

The concept of relaxation was first used by Maxwell when looking at the elastic forces in gaseous substances and it was later utilized by Debye to define the amount of time it takes a dipolar molecule to orient itself in a given direction [16, p.63]. Relaxation is generally measured thru the application of a step function in which after the step function has disturbed the material under examination the material is allowed to relax back to some equilibrium point and the time it takes the material to return to this equilibrium point is called the relaxation time [16, p.63]. This relaxation time is dependent upon the size of the dipole meaning that smaller dipoles will rotate back to an equilibrium point quicker than large molecular dipoles which take longer to rotate back to an equilibrium point [16, pp.63–64].

Since relaxation is a time domain concept it is only natural to assume that some frequency domain equivalent also exists and such a frequency domain equivalent is called dispersion which fundamentally relates the permittivity as a function of frequency [16, p.64]. A simple dispersion is generally characterized by a defined permittivity at two different frequencies and a transition region near the relaxation frequency [16, p.64].

5.6 Biomaterials and Electrical Properties

5.6.1 General Properties

As discussed in the section on a review of basic chemistry water plays an important role in biomaterials because of its unique ability to hydrated a wide assortment of chemical

compounds and the unique electrical properties that occur as a result of this ability. Because water is made up of a combination of two hydrogen atoms to one oxygen atom it can be concluded that a large majority of the atoms found inside a biomaterial such as the human body for example will consist mostly of hydrogen and oxygen [16, p.87].

It is predicted that hydrogen is the most abundant element in the human body with an estimated sixty-three percent of total body composition while oxygen is the second most abundant element at an estimated twenty-five percent of total body composition [16, p.87]. Additional elements that are found throughout the body are carbon at an estimated nine percent total body composition and nitrogen at an estimated one point four percent total body composition which rounds out the top four elements that are found abundantly throughout the human body [16, p.87].

While other elements are present in the human body there quantity is not large enough to be of substantial value however, while these trace elements are insignificant in quantity this is not to say there contribution to a bioimpedance system as a whole is not important since elements that produce ions such as sodium are very important for electrical conduction in a living biomaterial [16, p.87].

To elaborate further on the fundamental composition of an biomaterial the elements hydrogen and oxygen are the fundamental elements that combine together to create water and since water as discussed earlier plays a critical role in the biological functionality of an living biomaterial it becomes very obvious as to why these two elements dominate a biomaterials composition [16, p.87].

Carbons role in a biomaterial is a very interesting one as a result of carbons very versatile bonding nature because carbon in some cases will either gain or lose an electron as a result of its middle of the road valance electron number while nitrogen on the other hand is

an element that prefers to accept electrons thru the creation of mildly strong covalent bonds which tends to allow for chemical interaction between many different biomaterial compounds [16, p.87].

All of these elements as it might be imagined are found throughout most organic compounds such as proteins, carbohydrates, and lipids to name a few examples [16, p.87]. It should also be noted that the explanation provided above behind a biomaterials composition is a generalized simplification based upon basic chemical analysis meaning that there is advanced organic chemical theory in existence that explains why these particular chemicals are found throughout organic materials which will not be discussed in more detail [16, p.87]. This lack of discussion is not to say that this information is not important since there are many theories about the existence and nature of life which are based upon this information but overall this information is not needed to grasp the basic understanding needed to model a biomaterial hence why it is not disused in any further detail [16, p.87].

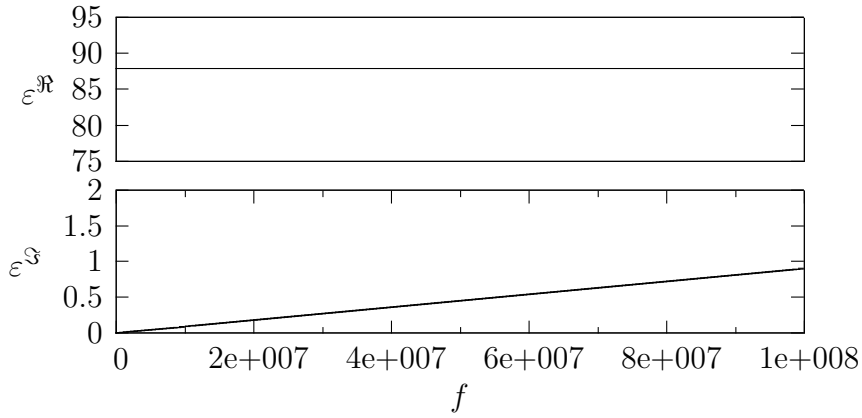

Figure 38: permittivity of water vs frequency at 0°C ([314, pp.6-13])

Looking at some of the inherent properties of water for a moment, water in a liquid form at room temperature has a relative permittivity in the neighborhood of 80 which will vary inversely to a change in temperature which means that as the temperature increases the rel-

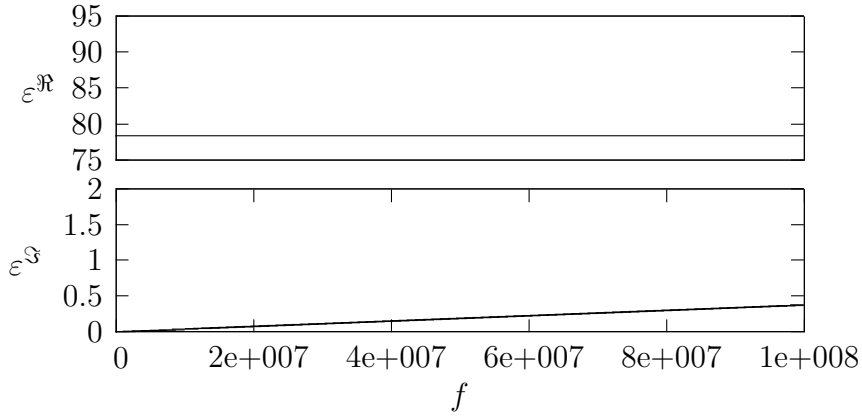

Figure 39: permittivity of water vs frequency at 25°C ([314, pp.6-13])

ative permittivity will decrease or when the temperature decreases the relative permittivity will increase [16, p.87].

This change in relative permittivity can be visually observed over frequency by Figure: (38), Figure: (39), and Figure: (40) [314, pp.6–13]. These figures conceptually illustrate how the permittivity of water changes as a result of changes in waters physical structure which can be easily seen by Figure: (41) in which water at an applied frequency of 100 MHz changes over temperature [314, pp.6–13].

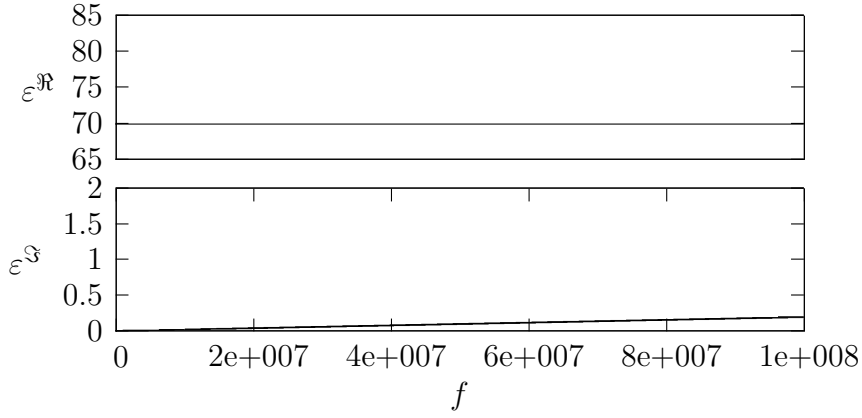

Figure 40: permittivity of water vs frequency at 50°C ([314, pp.6-13])

The addition of electrolytes to water will as might be expected lower the relative per-

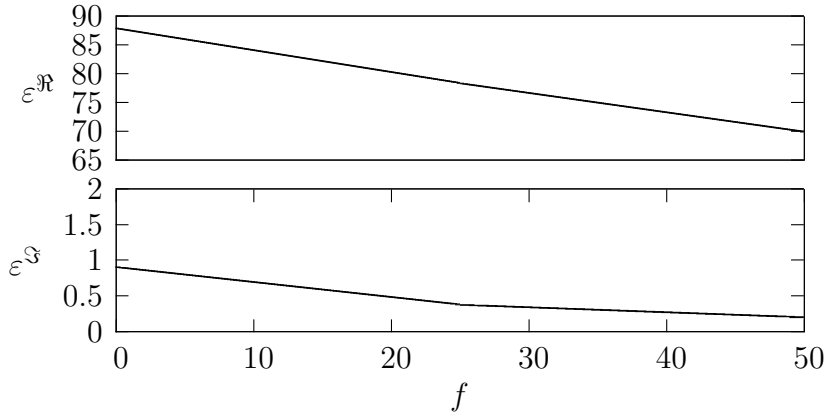

Figure 41: ε_r water vs temperature at 100 mhz ([314, pp.6-13])

mittivity proportionally to the concentration of the electrolyte dissolved in water so for example when potassium chloride (KCL) is dissolved by water the relative permittivity of the water on average will decrease by four for every 250 mmoles per liter of KCL added to the water [16, p.87]. Pure water will exhibit a Debye dispersion characteristic frequency in the area of 17 GHz at room temperature which is well above the frequencies under investigation throughout this thesis meaning that the effects of dispersion for pure water can be neglected [16, pp.87–88].

Because pure water has a high Debye dispersion frequency all of the interesting phenomena found in a biomaterial with a high water concentration must involve either substances which are dissolved into water as discussed in the KCL example which shows how a change in the relative permittivity occurs as a result of concentration and composition or the biomaterial must be chemically bonded to water which would cause a similar effect seen by a reduction in the temperature of pure water [16, pp.87–88].

Since the effects of aqueous electrolytes modify waters relative permittivity a list of the common ions found in the human body are hydrogen H^+, sodium Na^+, potassium K^+, calcium Ca^{+2}, magnesium Mg^{+2}, sulfate SO_4^{-2}, hydrogen phosphate HPO_4^{-2}, Chlorine

Cl^-, Bicarbonate HCO_3^-, and an assortment of different types of proteins in blood can be researched further in order to obtain a relative idea about what changes to waters relative permittivity should be expected from their addition to water [16, p.88].

Under most cases the addition of these common ions causes an electrolytic conductivity increase on the order of 1 Siemen per meter for every percent increase in ion concentration assuming that total ion concentration is relatively low and the applied frequency is lower than 10 MHz which is a valid assumption since 10 MHz is well above the frequencies used throughout this thesis for bioimpedance testing [16, p.21, p.88].

While proteins that ionize in water increase the overall conductivity as discussed above, not all proteins found throughout a biomaterial are in an aqueous state and since proteins make up about sixty-five percent of intracellular mass there relative permittivity should be considered just on the basis of their large volume in percent composition [16, pp.88–89].

The overall physical classification of a protein is based upon covalent bonds between amino acids and it should be noted that any protein can be created thru the combination of one or more of twenty different types of amino acids [16, pp.88–89]. One interesting phenomena that surrounds a proteins relative permittivity is in the fact that eight of the amino acids are non-polar meaning that they have no substantial dipole, seven of the amino acids tend to ionize which results in electrolytic properties, two of the amino acids have an inherent negative charge, three of the amino acids have a inherent positive charge, and because of so many different chemical characteristics that a protein could potentially have makes identifying the relative permittivity quite interesting [16, p.89].

Additionally to make matters more complicated the net charge of a protein is dependent upon the concentration of the protein and while some proteins such as glycine have no net electrical charge other proteins could be acidic or basic depending upon their concentration.

Attempts to apply polar dielectric theory such as Equation: (198) to a isoelectric substance such as glycine will produce inaccurate results which can be quite problematic when the exact composition of a substance is unknown as to what equations are valid for a given set of conditions [16, pp.55–56, p.89].

For this reason total protein composition of the FDI region are both relative to the person and to the moment at which the measurements were taken as a result of the structural differences between individual biomaterials along with continuous changes which occur inside a living biomaterial [16, pp.88–94].

Another material found throughout the FDI region is tissue which because of its inhomogeneous composition possesses a wide assortment of possible permittivity values [16, p.99]. Muscle tissue tends to exhibit a higher dielectric loss at low frequencies in the direction of the muscles conductive channel while at the same time also exhibiting a lower dielectric loss when measured perpendicular to the conductive channel making the electrode orientation an important factor when measuring a bioimpedance [16, p.101].

Adipose and bone tissue as would be expected also have a wide assortment of possible permittivity values that vary depending upon the amount of biological liquids perfused by the tissue and is typically consider to have a high permittivity at lower frequencies [16, p.101, p.104]. Blood which is a substance that can be perfused by both adipose and bone also exhibit capacitive properties at lower frequencies so its introduction or removal thru perfusion will modify the overall permittivity [16, pp.104–105].

At lower frequencies the stratum corneum has a high permittivity and will dominate the overall permittivity of the skin unless hydrated or a conductive gel applied between the electrode stratum corneum boundary because dead biomaterials are generally dehydrated thus ionic effects that promote conductivity are limited which make permittivity values

high [16, pp.105–106].

At higher frequencies as the permittivity of the stratum corneum declines and the viable skin beneath the stratum corneum which is living and hydrated becomes the dominant permittivity thus because hydrated living tissues can promote ionic movement much better than dehydrated tissues a steady resistivity at higher frequencies is typically observed [16, pp.105–106].

It should also be mentioned that additional tissues such as nerve tissue for example can exhibit non linear behavior because of its inherent ability to be self excitable however because this biomaterial is only found in high concentrations in the brain this implies that this biomaterial can be neglected for all intents and purposes in the FDI region [16, p.101].

5.6.2 Interdisciplinary Research and Intra-disciplinary Opinion

The FDI region where all of the bioimpedance measurements were taken is located between the radio-carpal and the metacarpo bones of the hand as illustrated by Figure: (42) [26, p.323, p.328] [326].

Upon taking a side profile of this region as shown by Figure: (43) it can be clearly seen that the FDI region under investigation consist primarily of the muscles of the thumb, anterior and posterior ligaments, along with additional substances such as nerves, fat, skin, and blood vessels [26, p.323, p.328, p.377] [326].

While the physical depictions shown by Figure: (42) and Figure: (43) are anatomically correct a rather large simplification thru the lump sum classification of several physical structures of the FDI region was made in order to reduce the overall complexity of the model created [26, p.323, p.328, p.377] [326]. Thus this approximation should be noted and in the event that some additional phenomena occurs that is not predicted by the approximated structure additional structural items for the FDI region would need to be

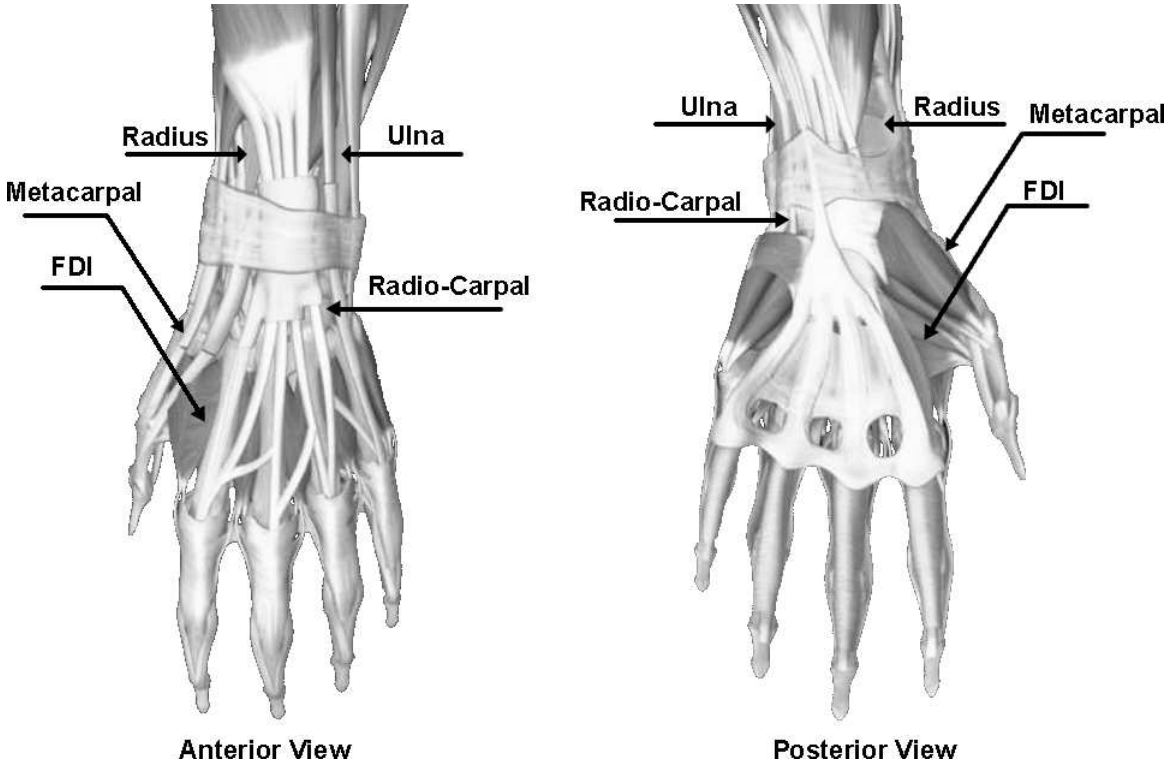

Figure 42: the human hand ([26, p.323, p.328] [326])

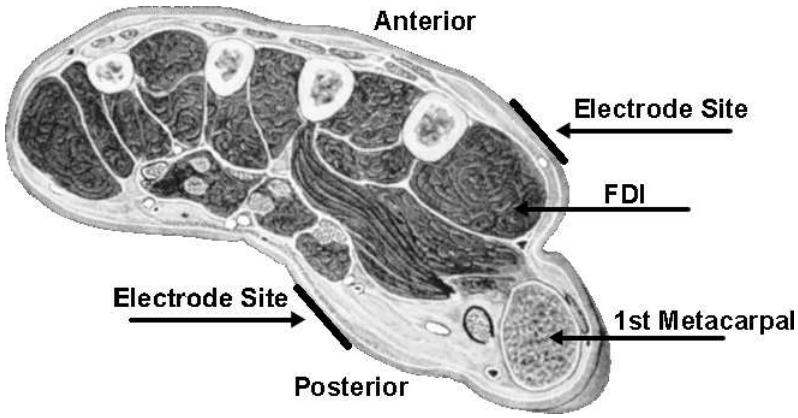

Figure 43: side profile of fdi ([26, p.323, p.328] [326])

and could be added to improve the approximation.

Based upon the conceptual impedance path shown by Figure: (43) it could be summarized that the bioimpedance model created of the FDI region would have to take into account the effects of skin tissues, adipose, muscle tissue, possibly bone tissue, blood, proteins, and various other electrolytes heterogeneously distributed throughout the FDI region [26, p.323, p.328, p.377] [326] [16, pp.87–125].

As discussed throughout this chapter many of these materials within the electrode path

cannot simply be defined as a constant permittivity value even if the frequency remains constant because of the inherent chemical properties that dynamically change a chemicals permittivity based upon many factors discussed in the chapter on bioimpedances from a chemical perspective such as temperature, pressure and diffusion to provide a few examples. Additionally complex biological processes in the body which could arguably be classified as an extremely complex chemical process by definition such as perfusion to give a example also add yet another way upon which permittivity can change even for a relatively small electrode path in the FDI region shown by Figure: (43) [26, p.323, p.328, p.377] [326] [16, pp.87–125].

Because noninvasive methods of measurement are being used to obtain bioimpedance measurements these material considerations along with the noninvasive limitations of not being able to perform in vitro experiments to determine internal impedance parameters makes absolute modeling all but impossible [16, p.115]. However, a total bioimpedance approximation of the FDI region can be made by using bioimpedance spectroscopy along with some predictions about some of the internal biomaterial components can be made thru the careful selection of input signal, frequency, and electrode conditions. Many techniques mentioned above were utilized throughout the experimental modeling process with rather effective results and the chemical dynamics of the materials in the FDI region were also considered since if a substance is known to be highly capacitive then conceptually it should not be model as a resistance nor should a resistance be model as a capacitance to provide a example.

5.7 Medical Applications

5.7.1 Bioimpedance Spectroscopy

Bioimpedance spectroscopy has a rather lengthy history and one of the first docu-

mented bioimpedance spectroscopy experiments was performed in 1913 by a researcher named Galler who measured the resistance across the body of a frog [327, p.1]. Galler during his research observed significant differences in the resistance between living and dead biomaterials and such observations paved the way for future bioimpedance spectroscopy research [327, p.1]. A lot of research has been done in the bioimpedance spectroscopy field since Gallers time and bioimpedance spectroscopy is now commonly found in various medical applications to quickly and noninvasively estimate body composition [328].

The bioimpedance spectroscopy systems that are currently used in the medical field today came about as the result of bioimpedance spectroscopy research that was performed in the twentieth century [16, p.316]. Examples of these early twentieth century bioimpedance spectroscopy systems can be seen by the apparatus created to measure human specific resistance in 1943 and the apparatus created to measure the impedance of dog tissue in 1956 [329] [330] [331].

These pioneering systems utilized either a two electrode or four electrode configuration and either injected a direct current or alternating current signal into the medium in order to obtain impedance information [331]. From early research in this area it was discovered that two electrode systems were very problematic in performing direct current measurements since material polarization effects would occur and skew results [188, pp.97–105] [331]. Four electrode systems alleviate this problem by compensating for polarization effects and have the added advantage of canceling out some of the errors that are associated with impedance imbalances between leads connected to the measurement electrodes thru crossed rod compensation theory [332, p.587] [333, pp.42–44] [331] [188, pp.97–105].

Despite the improvements to accuracy that multiple electrode systems provide other issues surrounding electrode placement arose as a result of the coulombic forces between

the spectroscopy electrodes and the resulting formation of electric flux that occurs from those coulombic forces [311, pp.57–64]. These forces cause the measured impedance to be a function of both the physical structure of the electrode and of the flux path created by the electrode placement on the biomaterials surface [16, pp.126–152].

An illustration of the differences between two and four electrode systems can be seen from experimental data collected in which a electrode was randomly orientated on a segment of horse tissue and the bioimpedance measured was discovered to be almost two times higher in the two electrode system than was measured in the four electrode system [331]. Further investigation also revealed that as the four electrode placement was changed variations of nearly fifty-seven percent were observed between the highest measured impedance value and the lowest [331].

These measurements neglected ionic electrochemical phenomena and assumed that the biomaterial under observation responded as a dielectric medium and thus could be modeled using dielectric theory which employs formulas for known geometric structures of electric flux thru a material [331] [311, pp.57–64].

Such formulas typically assume certain dielectric properties along with a defined physical state, typically solid, in order to derive an impedance value [311, pp.57–64] [334, pp.1–74]. However, most biomaterials do not behave strictly as static dielectric since the medium is typical polarized in nature meaning that additional theory about polar molecules is needed to account for polarization [335, p.67] [16, pp.86–125]. Such additional theories include the study of polarized dielectrics in a gaseous state by Debye and expansion of Debye's work to handle liquid dielectrics by Cole [336] [337] [338]. Cole later expanded his research to incorporate observable effects of alternating and direct current by modeling absorption phenomenon found in polarized dielectrics [339] [340].

This dielectric research paved the way for component level dielectric modeling techniques which include the Dow method, the Cole parameter method, as well as the fractional impedance pole method and many of these modeling techniques are commonly used in bioimpedance characterization with varying degrees of success [341] [327, pp.28–29] [338]. While electrode placement, as discussed earlier, is a decisive factor in synthesizing a dielectric component model, similar effects can occur as a function of the electrodes shape as clearly illustrated by a experiment which modeled the characteristic impedance of fractal shaped electrodes [342] [134, pp.79–80].

Additionally, there are significant differences between in vivo and ex vivo electrode placement that also modify dielectric modeling techniques as observed in various skin depth characterization experiments that range from surface skin electrode placement to varied amounts of electrode penetration into the skin [343] [344] [345, pp.62–63].

While ex vivo measurements tend to follow dielectric modeling theory, in vivo measurements are problematic and typically fluctuate rapidly upon electrode insertion [344] [345, pp.62–63]. From these in vivo experiments it has been discovered that an electrodes composition can significantly change the measured impedance value as a result of chemical phenomena such as electrochemical oxidation along with galvanic effects [327, pp.5–12] [132, pp.784–820] [188, pp.73–105]. To complicate things further, an applied signal will be characterized differently depending upon the electrode composition, thus some types of electrodes are only usable under well defined conditions based upon the signal that will be applied to the electrode [345, pp.56–62] [327, pp.5–12].

Some of the dielectric models discussed above can, in some cases, produce reasonable approximation to simplistic bioelectrical phenomena [16, pp.260–261]. However, most of these models make assumptions regarding a linear relationship between a materials polar-

ization and the electrical field thru the material and such assumptions are not intrinsically true since nonlinear attributes are prevalent throughout most biomaterials [133, p.141] [134, p.28].

Additionally, dielectric modeling theory makes the assumption that the material is not conductive and the only current propagating thru the material is a conceptual displacement current [311, pp.60–63]. This assumption is somewhat valid in some ex vivo bioimpedance measurements such as dehydrated skin measurements for example, since dehydrated skin is electrically similar to a lossy dielectric [345, pp.56–62] [343] [346]. However ex vivo measurements of hydrated skin and deep in vivo biomaterial measurements allow other types of chemical conductive mechanisms to occur in addition to dielectric related displacement currents because of the electrodes contact with an electrolyte [134, p.30] [16, pp.86–125].

As a result of the addition of this electrochemical phenomena dielectric modeling theory alone become inadequate and electrochemical effects must be introduced in the characterization model [134, p.42]. Such electrochemical effects include accounting for the transport of ions thru the electrolyte, metal to ionic interfaces that are formed at the electrode boundaries, and potential gradients that exist or are created as a result of an applied signal [134, pp.42–72] [188, pp.73–95] [184, pp.1–25].

The process of modeling electrochemical phenomena is extremely difficult and even under the most simplistic assumptions modeling the mass transport of ions thru an electrolyte requires the application of advanced mathematics [134, p.42]. While the application of advanced mathematics to model simplistic problems is not a new concept, especially so in the electrochemical impedance spectroscopy field, biomaterials, while requiring electrochemical models under certain conditions, are typically modeled using lossy dielectric theory [16, pp.86–125] [327, pp.28–29]. This strict application of dielectric theory is partly because

most bioimpedance measurements are taken noninvasively ex vivo, since it is speculated that most people prefer noninvasive ex vivo measurements to invasive in vivo measurements and because most bioimpedance spectroscopy models are limited in length which allows for linearization of nonlinear time varying phenomenon into something that can be represented by a component level model [347] [348] [202] [349].

Most commercial bioimpedance analyzers utilize a four terminal measuring apparatus that applies a fixed 50kHz signal to the biomaterial under investigation [263]. A single frequency restriction of 50kHz was applied because of safety concerns that additional frequencies could stimulate electrically excitable tissue and to attempt to create a standardized region of operation that was independent of electrochemical effects [350]. These commercial devices typically display impedance information in either complex or phasor notation and depending upon the features offered by the manufacture might display values of permittivity or resistivity depending upon an assumed dielectric structure [350] [263] [351].

Commercial devices that display structurally dependent parameters typically expand the single frequency restriction to include multiple frequencies in order to obtain more information to aid in model parameter synthesization [263]. As it would be expected, the addition of multiple frequencies opens the possibility that electrochemical phenomenon can occur, as discussed earlier, which can distort model parameters along with safety concerns arising regarding the effects of additional frequencies on electrically excitable tissue [350] [134, pp.42–72] [188, pp.73–95] [184, pp.1–25].

While there are many design considerations that are taken into account during the development of a commercial spectroscopy systems, the fundamental objective of these systems is to estimate a number of different biometric parameters including, but not limited to, whole body impedance, total body water, fat-free mass, adiposity, body cell mass

and tissue impedance [33] [351] [350] [114] [352] [353] [354]. These biometric estimations are made by application of logical assumptions regarding the geometric structure of the biomaterial under observation based upon electrode placement and applied signal characteristics [114] [351]. Many of these biometric estimations make the assumption that because bioimpedance's are a function of electrolytic concentration thus some correlation must exists between a bioimpedance and a particular biometric parameter [114] [351].

While there are a substantial number of studies which illustrate that such correlations exist, there is no definitive bioimpedance spectroscopy to biometric formulation because of the number of factors that can significantly change results in a bioimpedance measurement [341] [355] [350]. Some of the problems that prevent definitive formulation were mentioned earlier, however, additional sources of correlation error can occur as a result of patient studies that do not correctly account for parameters such as age, gender, height, body structure, race, and overall health [112] [356] [357] [358] [359] [360] [361]. Furthermore, apparatus distortion can bias measurements if not taken into account and the effects of stray capacitance from electrode leads not only presents a potential safety hazard from leakage current in microshock friendly patients, but can skew measured results [112] [113] [123].

However, bioimpedance spectroscopy biometric correlation has proven that accurate results can be obtained provided that consistency exists in measurement procedure, conditions that induce electrochemical dependent phenomena are avoided, safety procedure are followed, and that biometric correlations are only applied based upon a matching reference population [362] [363] [364]. With this in mind, there has been a growing initiative to create a public domain bioelectrical impedance database in order to improve the accuracy of biometric correlations from bioimpedance measurements [364]. While the cataloging of large scale bioimpedance measurements is one method to improve biometric correlations

alternative techniques which attempt to characterize individual component of the body are currently being explored along with statistical estimation methods to predict biometric correlation factors [365] [32] [366] [367] [368] [369] [370].

Considering all of the topics discussed above it can clearly be seen that bioimpedance spectroscopy is a subject that started out because of a fundamental curiosity about how electricity interacts with living things [16, p.i-p]. Such curiosities were further enthralled by scientific discoveries that resulted in both additional research being conducted along with the development of commercial devices that attempt to characterize human health by making predictions about biometric parameters [16, p.i-p] [263]. While it is true that biometric predictions are very volatile by their inherent nature, this in turn implies that there is a lot of room for growth within this subject thru additional research that will hopefully reduce the volatile nature of measurements obtained and thus increase the accuracy of biometric predictions [370] [112]. It is this underlying reason that makes application of the research conducted throughout this dissertation in relation to bioimpedance spectroscopy a point of particular interest since any improvement in this subject, even very small improvements, has the potential to result in the improvement of the quality of a person's life.

5.7.2 Bioelectrical Signal Acquisition

The term bioelectrical signal acquisition is a somewhat ambiguous definition that is used throughout this dissertation to describe all passively measured bioelectrical phenomena. While ambiguity in general is typically frowned upon throughout the scientific community it is a necessary evil in this particular case because other disciplinary definitions tend to encompass more than just the act of measuring bioelectrical phenomena or fall short of being an accurately descriptive term.

An illustration of this point can be found in the term biophysical measurement in which

the keyword biophysical is the adjective form of the word biophysics that is used to describe a sub discipline of biology that primarily studies biological structures along with related biological processes [371, p.122] [308, p.205]. While it is very probable that an electrical signal will be recorded during a biophysical measurement, biophysical measurements are not limited to electrical measurements and the definition of the word inherently implies that the information collected will be correlated to some type of biological structure or process which results in the term having implications that makes it ill-suited to be used throughout this dissertation as a accurately descriptive term [371, p.122] [308, p.205].

Another illustration of this point can be found in the disciplinary term electrophysiological measurement in which the keyword electrophysiological is the adjective form of the word electrophysiology that is used to describe a sub discipline of medical sciences that studies the correlation of electrical phenomena to an observable physiological process [308, p.577]. While a very strong similarity exists between the passive measurements taken throughout this dissertation and the method in which most electrophysiological measurements are taken. Dissimilarities arise because of the assortment of electrophysiological measurement techniques in practice along with the various types of physiological correlations performed on collected data that goes beyond the scope of measurements taken throughout this dissertation [372] [308, p.577].

A final illustration of this point can be found in the generic term electrogram where by its early definition is described as any electrical measurement that is physically recorded or by its more modern electrophysiology definition represents any bioelectrical signal that is recorded [308, p.575] [373, p.266] [371, p.387]. While the term electrogram, which at first does appear to accurately describe the process of performing a passively measured bioelectrical signal, presents a weakness upon further examination because this definition

lacks a stringent implication about how the data will be used [308, p.575]. While one might argue that based upon the vague introductory description initially provided that the term electrogram matches perfectly, however, as it will soon be discussed, the goal of bioelectrical signal acquisition extends beyond the scope of only performing a bioelectrical recording thus making the term ill-suited to be used throughout this dissertation as an accurately descriptive term.

Upon taking into consideration all of the hidden implications discussed above results in the conclusion that it is absolutely imperative that a formal definition be selected that is capable of both accurately representing the types of measurements taken and describes the overall purpose for taking such measurements without the introduction of any disciplinary bias. Thus it was decided that rather than trying to amend an existing disciplinary biased definition, such as the definitions discussed above, that a somewhat abstract term bioelectrical signal acquisition would be used to describe the measurements performed throughout this dissertation and formally defined in a way that would significantly reduce the occurrence of disciplinary bias while clearly articulating the goals of the measurements taken.

To this end, before formally defining bioelectrical signal acquisition the intrinsic definition of the word should first be examined. The term bioelectrical is formally defined as the integration of biological and electrical theory into a unified subject while the term signal is defined as a transitory electrical change that is typically used to exchange information between electrical devices [374, p.83, p.838]. The last term acquisition is defined as the act of obtaining electrical data and assessing this obtained data in a way that implies something more than data collection occurred but something less than data analysis occurred [374, p.8]. Based upon the linguistic definitions discussed above, bioelectrical signal acquisition, in its intrinsic context, implies that biological theory along with electrical theory was

applied to an observable bioelectrical phenomenon such that any bioelectrical phenomenon detected is recorded and preliminary assessed [374, p.8, p.83, p.838].

The intrinsic definition of bioelectrical signal acquisition can be refined by restricting the signals being observed to only bioelectrical phenomena that is observable via ex vivo skin contact and to measurements taken by laboratory apparatus designed to emulate observable ex vivo bioelectrical conditions. To further refine this term, bioelectrical signal acquisition only occurs if the source of the signal under observation is isolated by a bioelectrical medium such that the process of observing the originating signal can be represented by the addition of an infinite parallel impedance to the original signal model.

Fundamentally, this bioelectrical isolation implies that the electrical grounds between the originating signal and the point of observation are different. Such differences between grounds are easily illustrated by considering how bioelectrical phenomena produced within the body can be measured from the surface of the skin without the physical existence of a common ground between the in vivo signal and the ex vivo measurement [375] [376] [377, p.79–91]. While assumptions regarding isolated grounds are typically valid throughout bioelectrical signal acquisition, there are cases in which such assumptions are invalid. To illustrate this point, consider the case in which bioimpedance spectroscopy is used to inject a signal via ex vivo skin contact and bioelectrical signal acquisition is used to observe the effect. Under these conditions it is possible that the bioimpedance spectroscopy apparatus ground can be connected to the bioelectrical signal acquisition apparatus such that no grounding differential exists between the two devices. It is important to note that while electrical isolation is a requirement for the occurrence of bioelectrical signal acquisition a formal definition of ground is not required thus careful consideration about what potential is being observed by the bioelectrical signal acquisition apparatus must be taken into account

prior to signal analysis.

While the refinements discussed above help clarify what bioelectrical signal acquisition is, at this point one obvious ambiguity remains regarding the preliminary assessment stage of bioelectrical signal acquisition since by its inherent definition it was implied that some type of basic signal processing was performed on the measured signal yet no details have thus far been discussed [374, p.8]. To clarify this ambiguity within this dissertation, it can be assumed that signals obtained using bioelectrical signal acquisition have been discretized, scaled, and smoothed in order to reduce noise. Furthermore it is to be expected that measured data will be processed such that either an electrical model of the isolated bioelectrical medium is synthesized or predictions about the original signal source are created based upon an existing isolated bioelectrical model.

One minor caveat should be noted regarding the declaration of the term acquisition in respect to any topic related to commercial implementations of bioelectrical signal acquisition devices. Under these circumstances it should not be assumed that discretization, scaling, and smoothing of the signal under observation by the commercial device was performed. However, It is important to note, that under these particular circumstances, the term bioelectrical signal acquisition still implies that an ex vivo bioelectrical isolated signal is being measured just no assumptions should be made regarding what processing steps are performed after this measurements is taken.

5.7.3 Safety Considerations

Because electrical safety in the medical field is a subject of significant concern, commercial systems are inherently designed to limit applied current to avoid causing macroshocks and microshocks [350] [123]. Such designed constraints significantly reduce the risk that ventricular fibrillation will occur as it should be noted that ventricular fibrillation is the

most common cause of death from electrical shock [123] [378]. Ex vivo along with some in vivo electrode configurations only have to consider macroshock conditions since the amount of current that could conceivability flow thru the body and its numerous inhomogeneous conductive paths would be unable to cause electrical excitation of the heart tissue [119] [123] [378] [124].

However, internal body impedances tend to remain somewhat constant at a given frequency when compared to skin impedances which fluctuate significantly depending upon the skins electrolytic hydration, whether it be natural hydration such as sweat or artificially applied electrolyte, and the fact that in vivo measurements bypass the skins impedance, lower macroshock thresholds have to be considered when such circumstances exist [379] [123] [124].

Guidelines for generic ex vivo safety conditions are set near 500μA while in vivo and high risk ex vivo safety conditions reduce this number to around 100μA [123] [124]. While a 100μA safety limitation is sufficient for most medical circumstances it is not enough protection for patients that have an intracardiac catheter which bypasses both skin and body impedance by touching heart tissue directly via in vivo catheter [123] [120] [380]. When conditions exist, such that an electrical shock can be received as a result of electrical contact with heart tissue, this condition is classified as a microshock condition [123] [120]. Guidelines for microshock safety conditions are set near 10μA in order to prevent ventricular fibrillation from occurring from a electrical shock as a result of direct contact with heart tissue [123] [122].

The safety guidelines discussed above are defined primarily for 60Hz transmission line signals and while a few investigative studies have been done to observe the effects of frequency on the occurrence of ventricular fibrillation a complete broad-spectrum study is not

a subject that is fully discussed [123] [124]. However, some research into the effects of broad-spectrum frequencies on human body impedance has been done in relation to their electrical hazard and the general consensus from these studies is since body impedance changes as a function of frequency that some frequencies are statistically less likely to be electrically hazardous than others [381] [123] [120] [378]. Conceptual justification of this finding is inherently apparent based upon common observation from linear Impedance analysis and thus it would intuitively be expected, but not inherently known, that it is easier to experience an electrical hazard at some frequencies but not others [136, pp.284–294] [123] [120] [378].

As mentioned earlier, averages of the body impedances at 50kHz has revealed higher impedance values than those measured at 60Hz which is one reason why a commercial bioimpedance spectroscopy system designer would choose to operate the device at 50kHz rather 60Hz [350] [381]. However, bioimpedance spectroscopy systems that operate at multiple frequencies have to take into account how the body's impedance changes as a function of frequency in order to maintain safety standards and as it might be expected, the design process required to implement a single frequency current limiting system is less involved than the implementation of a multi-frequency current limiting system [382, pp.1.56–1.112] [377, pp.499–558] [123].

While design considerations effectively nullify macroshock possibilities in commercial implementations of bioimpedance spectroscopy systems microshock protection is a subject that remains somewhat unknown since there are no formal safety standards for these devices [350] [123] [124]. Because microshock can be caused by exposure to leakage current and the amount of leakage current that bioimpedance spectroscopy systems emit has not been characterized in sufficient detail, some reservations remain about whether or not

bioimpedance spectroscopy systems can safely be used in a microshock friendly environment [350] [123]. Despite these concerns, there is a general consensus amongst the bioimpedance spectroscopy community that bioimpedance spectroscopy systems are safe to use as long as careful thought is given to macroshock and microshock conditions in both apparatus design and electrode placement [350] [123].

CHAPTER 6: EXPERIMENTATION AND RESEARCH RESULTS

The acquisition of high fidelity bioelectrical measurements, at its most rudimentary level, begins with the selection of a specific research objective, such as measuring the electrical signals produced by the human heart, after which some type of scientific instrumentation is then utilized to acquire pertinent information regarding this objective, and — assuming that the information obtained is both metaphorically good and beneficial — can then be analyzed, mathematically modeled, and — hopefully — utilized in a way that allows for the intellectual advancement of the intended subject. Nevertheless, while such descriptions could effectively summarize the majority of most contemporary scientific research methodologies currently being implemented; however, to be fair in such assessments, because the scientific method — a methodological research procedure that appears within most academic text in six or more concise steps as: formulating the problem, constructing the model, testing the model, deriving a solution from the model, testing and controlling the solution, implementing the solution —, is the metaphoric "*cooking 101*" recipe that most academic researchers are trained to follow — and for very good reason too! —, such reoccurring methods would appear to be both theoretically sound and expected within any scientific publication [11, p.26] [16] [97].

Yet, while it is true that the vast majority of scientific research begins with the utilization of such intellectual methods and should inevitably apply the, previously listed, methodological procedures; however, it is also important to recognize that the methodological order actually implemented — or metaphoric methodological path taken — upon

application of such procedures is seldom ever the same between implementations, in so far as, methodological iteration — of the steps previously listed — is a common occurrence and such iteration can make the — cumulative procedural methodology followed — a touch more complicated than the simplistic application of six — seemingly straightforward — methodological steps in a chronological order [49] [11]. Likewise, while such information typically falls under the purview of academic common knowledge, insofar as, these iterations are seldom ever openly discussed beyond a rudimentary acknowledgment that the scientific method was, in fact, implemented — and even then, such concepts are seldom considered beyond a subconscious, or intuitive level [49] [11]. Nevertheless, because such information is fundamentally important — though admittedly not substantially intrusive —, and given the interdisciplinary foundations of the subjects being examined, it is worth mentioning that the original foundations upon which this dissertation was begun was to: expand upon the previous noninvasive investigation into the electrical properties of the FDI region of the human hand, attempt to determine the feasibility of detecting the point of origin of a FDI muscle movement, and attempt to determine the viability of artificial FDI muscle stimulation [1] [2] [16] [97].

Yet, to highlight the hidden role that methodological iteration can play within scientific research, as the objectives — listed above — were studied, the inevitable — but highly unconsidered — process of scientific methodological iteration occurred, and refinements to these — previously listed — objectives were made — such refinements typically resulted in examining unincorporated real world considerations that were inherently overlooked —, and — as a result — these, previously listed, objectives were periodically modified, reduced, or expanded in order to aid in obtaining an overall, metaphorically better understanding of the subject as a whole. Thus, to elaborate upon such occurrences further, consider for the

moment how an investigation into the noninvasive electrical properties of the FDI region of the human hand might result in additional inquiry regarding the conductive properties of aqueous sodium chloride — since normal saline is a dominant material within the human body [383] [1] [16] [97]. Likewise, how an investigation into measuring passive FDI muscle movements might result in the inclusion of high fidelity electrical instrumentation research, while prompting an investigation into the electrical properties of the FDI region of the human hand, thus diverting the topic of observation from predominately EMG measurements to passive EKG measurements that — ironically — spawned a in depth investigation into radio frequency (RF) convection currents, because of a perceived correlation between human interactions and the electrical distortions encountered. Similarly, how the process of determining the viability of FDI muscle stimulation might result in additional investigation into the usage of a pseudo-modulated resistive loading technique, a brief examination of the usage of a Wein bridge oscillator as a material characterization device, and possible discovery of, what can only be loosely surmised as being, a low frequency liquid diode effect.

While this particular progression tends to overly exemplify the definition of the term, methodological iteration; yet it is important to take note of how a few seemingly straightforward scientific objectives can substantially expand — particularly upon researching a subject that requires prerequisite interdisciplinary knowledge — into a unique and complex methodological structure that is far from being intuitive. Yet while such complexities, at least upon reflecting on the underlying interdisciplinary nature that is inherently associated with such topics; while, at first appearing somewhat arbitrary, are in retrospect, actually a highly logical and straightforward progression that has simply been obfuscated by the introduction of interdisciplinary concepts and the rigors of iterative research methodology

[49] [11].

6.1 Overview, Objectives, and Contributions

The fundamental rationale behind the experimentation and research results section was to develop a methodology — as shown by Figure: (44) and Figure: (45) — to obtain the highest fidelity bioelectrical acquisition possible. Likewise, during the development of this methodology a number of obstacles were discovered that had to be investigated in order to create a solid theoretical foundation to build upon. Conversely, the discovery of such problems during the development of this high fidelity acquisition methodology was part of the unique contributions presented within this dissertation, while the solving of some of these problems discovered constituted another part of the contributions presented. Similarly, during this investigation process, it was discovered that classical transmission line theory is not applicable to many of today's common transmission line structures such as striplines, microstrips, and instrumentation probes because they are unbalanced. Likewise, based upon such assessments the classical transmission line theory was expanded into a new fundamental theory that is applicable to all two-conductor transmission lines, by the inclusion of theory that describes the generation of nonlinear convection currents — the mysterious common-mode current — and includes its radiation parameters in the transmission line equations developed. Additionally, during this investigation process, it was also discovered that both aqueous sodium chloride solutions and human biomaterials exhibit unique nonlinear electrical properties and a number of methods were developed to examine, describe, and account for such effects.

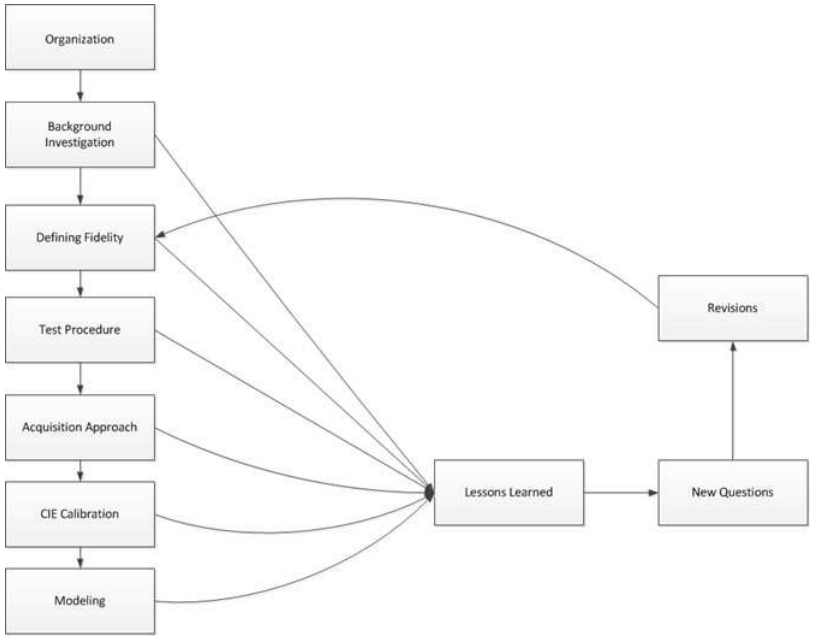

Figure 44: conceptual research organization flowchart

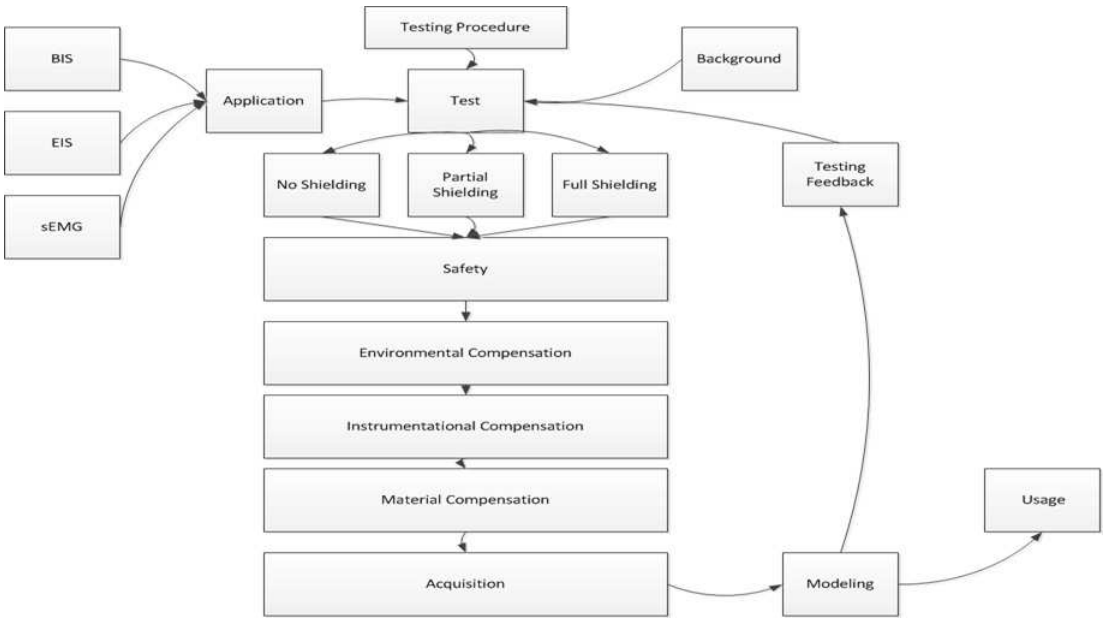

Figure 45: conceptual high fidelity testing methodology flowchart

6.2 Defining the Term High Fidelity

Nevertheless, upon setting such notions aside for personal reflection, it would seem both natural and logical to begin presenting the information obtained, from investigating the, previously mentioned, objectives — and there iterative consequences —, by first examining the fundamental terminology applied to describe those objectives, and while there are a

number of research related terms that need to be addressed, the implications associated with the term high fidelity (HI-FI) is a reasonably, metaphorically good, starting point. Likewise, while the term high fidelity, despite being frequently utilized to describe audio devices, is in fact, a rather ambiguous term that seems to impart the preconceived notion that — perhaps thru means of marketing black-magic and supernatural business invocations — a high fidelity device is fundamentally better than a device that is not categorized as such, and despite their being some merit in accepting such assumptions at face value — on some rare occasions —, the existence of such ambiguity, particularly within scientific research, is oftentimes more harmful than good [384, p.391] [385] [30] [165]. Yet, while describing the term high fidelity as ambiguous might feel somewhat unnatural, after all, generally when the term high fidelity is utilized, particularly within the sciences, metaphoric good results or profound improvements seem to shortly follow; however, further inquiry into the actual standard behind the term reveals that there is, in fact, no definitive standard, "*per se*" [†1] , at least by contemporary IEEE standards, nor does any consistent criteria to the terms usage seem to arise — although there is a presumptuous claim by a English man, named Henry Alexander Hartley, who in circa 1927 supposedly invented the term to promote the creation of a audio reproduction standard — [384, p.391] [385] [30] [165] [386]. Likewise, based upon such observations it can be concluded that — at best — the only attribute that seems to remain consistent — when it comes to the usage of the term — is that the terms seems to appear within the title of a multitude of academic publications year after year [384, p.391] [385] [30] [165].

Thus while the usage of this term, at least within this particular context, would seem to be more of a positive adjective for a scientific improvement rather than any specific and

[†1] Latin phrase for: by itself.

measurable quality; yet an unspoken social connection also seems to be attached to the terms usage, in so far as, the term seems to invoke the feeling that something far superior has occurred rather than simply a meager improvement [384, p.391] [385] [30] [165]. After all, it would be hard to rationalize, at least based upon the terminology utilized — especially within the contemporary American consumer marketplace — that a consumer, at least after being given the choice to select between an improved device or a high fidelity device — naturally assuming the prices are the same —, would select the improved device — without some prior inquiry into the term high fidelity —; since the term high fidelity tends to impart that some type of standard does in fact exist [230] [198] [253]. Yet, while such observations tend to invoke some metaphysical inquiry, a point that was rationalized and explained in previous chapters; however, the frequent appearance of the term, despite its inherent ambiguity, does seem to impart the existence of some commonality in the terms usage: First, because when the term appears, particularly within a scientific publication, it seems to correspond with the introduction of a potential methodological standard, hence one possible explanation for the terms frequent association with some type of quantitative attribute. Second, because such associations are frequently made, the term would seem to be more accurately surmised as being a contemporary technological benchmark rather than simply a quantitative improvement. Third, because the term is typically associated with the existence of some type of implied standard, such implications also tend to impart the existence of technological maturity, since a standard can only typically arise after a period of lengthy testing, and such implications also tend to impart contemporary practicality and stability over cutting-edge novelty and possible uncertainty.

While such observations are predominantly considered, at least by most academics, to be inherently anecdotal — although there is some empirical support for such descriptions

and a few qualitative studies that attempt to address such metaphysical attributes — however, because such notions do tend to extend well beyond the intended scope of discussion, as the acknowledgment that such ambiguity does exist is far more relevant than attempting to clarify the why and the how [385] [30] [165] [386] [230] [198] [253]. Thus, upon taking such attributes under advisement, it would now seem prudent to carefully articulate the quantitative attributes, or standards, along with any assumed implications that are attached to the usage of the term, high fidelity, within the confines of this dissertation.

Likewise, to begin clarifying such attributes, it should be noted that the usage of the term, high fidelity measurement, once again within the confines of this dissertation, was not intended to be a descriptive standardized term, "*per se*" [†1] , insofar as, associating a set of attributes with signal acquisition parameters, but rather, its usage was intended to associate the information being presented — within this dissertation — as a viable contemporary review of the current standards being implemented and there applicability — or inapplicability — within the bioelectrical research area, while also attempting to provide a contemporary framework for the acquisition of bioelectrical signals — which also includes some processing and reproductive elements. Conversely, while the inherent implications that are associated with the introduction of such attributes represents, as it was previously mentioned, a possible, feasible, and logical — metaphoric next step — to creating a bioelectrical high fidelity standard that could become commercially viable, although the inclusion of more — fundamentally mature — interdisciplinary concepts would be inherently necessitated. Yet, while such attributes are more of a musing than being anything remotely of future relevance; however, it is important to recognize that the predominate invocation of the consumer term — high fidelity —, while being visually stimulating, does

[†1] Latin phrase for: by itself.

not inherently imply the restriction of research topics to just progressive improvements nor to mature theoretical applications — as some cutting-edge and commercially immature processes will be examined — within this dissertation — that the term — high fidelity — would — indeed —- not inherently included by its most common utilization.

Thus, upon taking such attributes under advisement, it is reasonable to begin defining the term, high fidelity, at least within the confines of this dissertation, based upon its application to the process of signal acquisition and signal reproduction. Likewise, such beginnings, because they are predominantly described using electrical engineering terminology, are typically best defined by the following parameters: bandwidth, direct current (DC) offset, dynamic range, quiescent or bias conditions, and other electrical and physical limitations. Furthermore, such quantitative parameters are typically governed by conditional circumstances, such as: environmental effects, instrumentational effects, and material effects, and while, under most circumstances, such quantitative parameters, are typically presented within a — worst case scenario — surmised singular value — that is naturally based upon some in-depth analysis of these conditional circumstances; however, the process of defining a new — high fidelity — specification tends to require that such conditional circumstances are both isolated and examined prior to parameter summarization, thus making it necessary to examine each of these listed effects in further — individual — detail.

6.2.1 Overview, Objectives, and Contributions

The fundamental rationale behind the defining the term high fidelity section was to define and provide information regarding a — generally unavoidable and innately existent — electrical phenomenon that routinely diminishes the overall electrical fidelity of nearly all commercial and experimental bioelectrical devices utilized for both passive and active biomedical applications, define and demonstrate information regarding the commonly

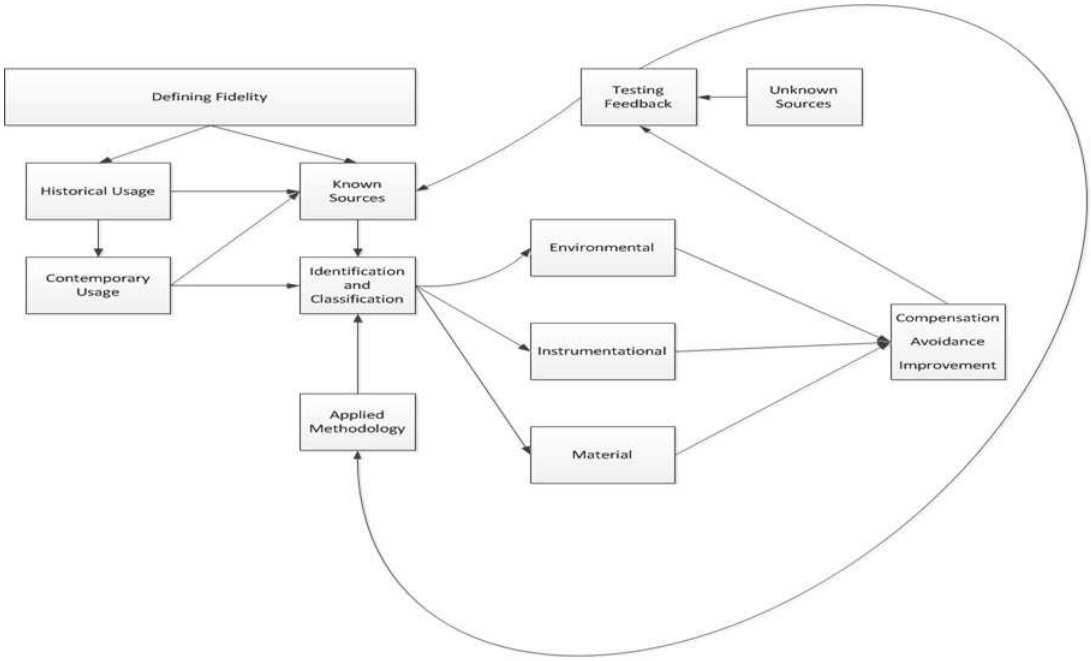

Figure 46: conceptual high fidelity testing definition flowchart

identifiable — within contemporary literature — sources of distortions within biomedical devices — like quantization error, sampling, inadvertent filtering, bandwidth, phase inversion, clipping, clamping, truncation, parasitic and feedback problems, and define and demonstrate information regarding the commonly identifiable sources of distortion within bioelectrical acquisitions that — while arguably could be categorizable as being instrumentational in origin, at least depending upon the categorizing criteria utilized — were classified by the term material effects — within this dissertation — because of their intrinsic association — in terms of manifestation — with the objective being examined — as depicted by Figure: (46). Furthermore, the problems discovered within this section — predominantly concerning reduction in acquisition fidelity — were examined, methods developed to compensate or resolve such problems, and the foundation setup for further — in depth— development of the previously discussed high fidelity bioelectrical acquisition methodology.

6.2.2 Environmental Effects

One of the fundamental rationales behind the environmental effects section was to de-

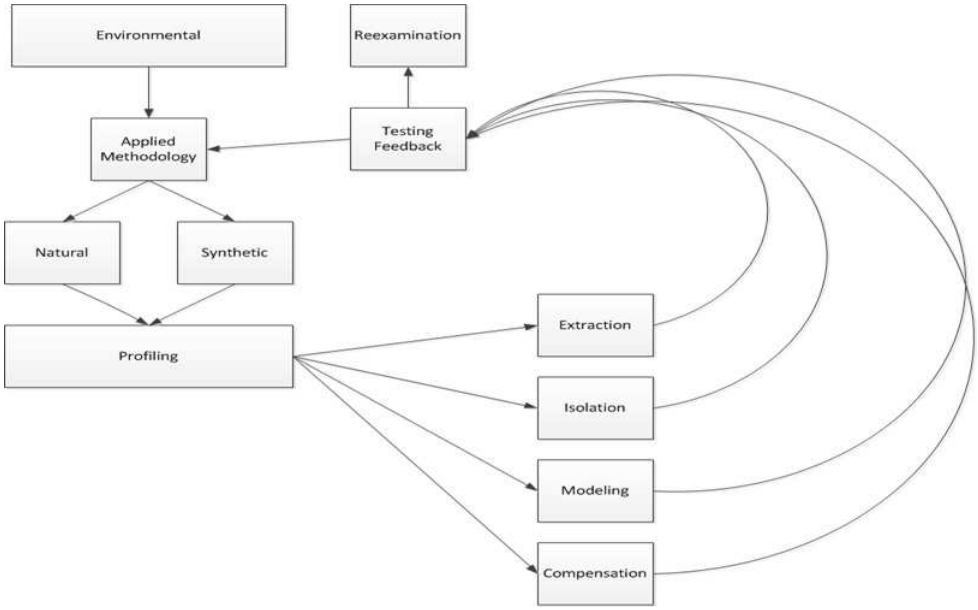

Figure 47: conceptual environmental effects flowchart

fine and provide information regarding a — generally unavoidable and innately existent — electrical phenomenon that routinely diminishes the overall electrical fidelity of nearly all commercial and experimental bioelectrical devices utilized for both passive and active biomedical applications. Additionally, this section endeavors to collectively present such information in a manner that is both unique and directly applicable to the advancement of bioelectrical instrumentational research while, at the same time, providing the environmental conditions that existed within the research laboratory utilized upon acquiring the bioelectrical measurements presented within this dissertation. Likewise, this section — after defining formal definitions — provides examples of actual — real world — operational environmental conditions that are inherently present within the majority of all bioelectrical devices currently utilized — including both contemporary consumer and experimentally created devices — and then isolates the environmental effects observed into categorizable quantities — either synthetic or natural in origin. Conversely, the methodology developed — as outlined within Figure: (47), Figure: (48), Figure: (49), and Figure: (50) — to perform this isolation and separation task is both profound and unique for a multitude of

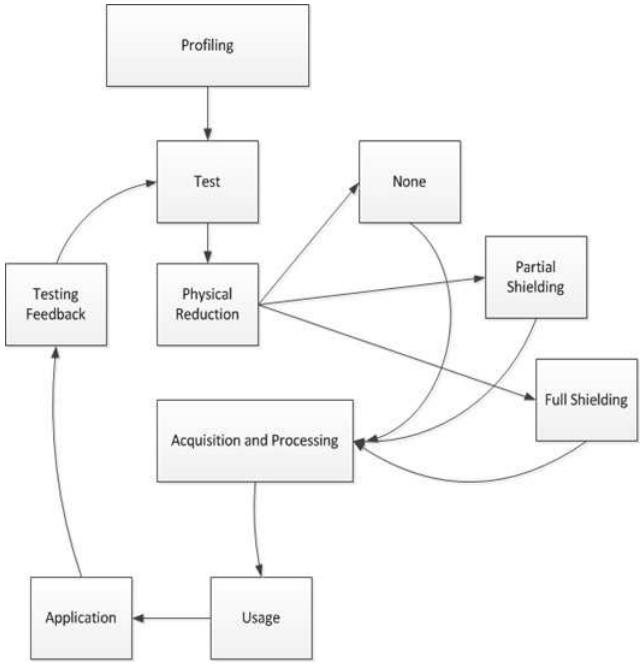

Figure 48: conceptual environmental effects profiling flowchart

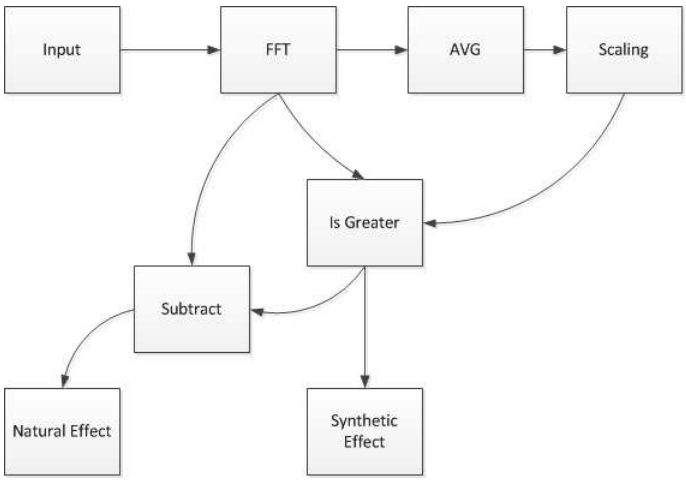

Figure 49: conceptual environmental effects acquisition flowchart

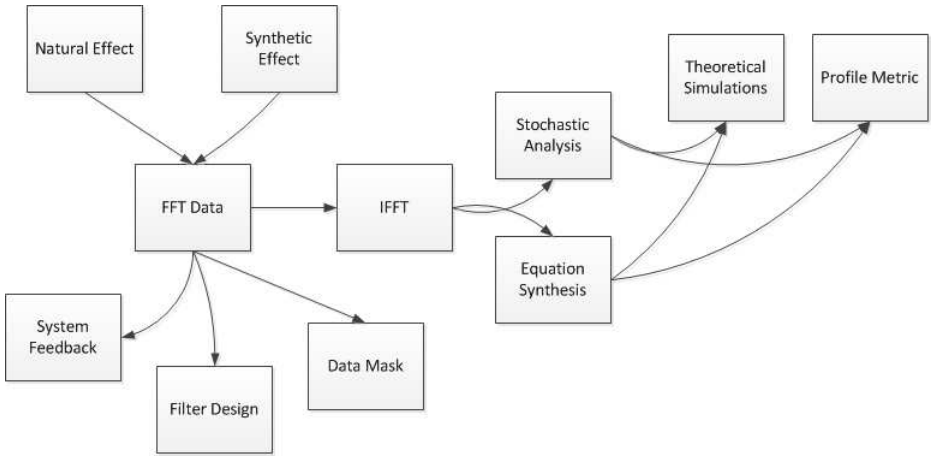

Figure 50: onceptual environmental effects usages flowchart

reasons.

First, this method's overall ease of implementation within contemporary microprocessor architectures — an attribute deliberately considered during its development —, allows for this methods implementation without a substantial amount of hardware modification or additional cost to most contemporary biomedical devices currently in production. Second, unlike contemporary reductive methods that either removes environmental effects through the usage of a somewhat arbitrarily selected static signal processing filter — like physical Butterworth or Chebyshev filtering or DSP techniques like FIR — or through the implementation of predictive feedback techniques — like Kalman or Wiener filtering —, this method was designed to permit easy access to information regarding the current environmental effects encountered by the biomedical device — as this information is an extremely good metric of measuring the environmental distortions encountered — and, upon incorporating this information into spectral filtering techniques, the environmental effects encountered can be attenuated in a less intrusive manner than those traditionally obtained through the utilization of static signal processing techniques or without the inherent difficulties found within feedback reductive techniques — like coefficient selection for all operational environments or dampening problems. Third, because this method is extremely effective at providing an accurate description of the current environmental effects encountered by the biomedical device being utilized for any given operational environment — in the case of biomedical acquisition devices — the inclusion of this information alongside acquired biometric data would go a long way in reducing the contemporary ambiguity between biometric data comparisons within the biomedical research community, and help increase the confidence in biomedical correlations — particularly within the bioimpedance spectroscopy research area — between observed biometric data and a observed medical

or material characteristic. Fourth, because biomedical applications have an assortment of diverse end user applications — some of these applications focus on signal recognition than the overall signal fidelity, as is the case within normal EKG applications — this method can also be easily incorporated into existing static filtering implementations — although notable differences in the environmental effect profile obtained will be noted at filtered frequencies — or into more advanced reductive feedback techniques — noting that control coefficients can be dynamically adjusted based upon the results obtained from the usage of this method — in cases where classical reduction techniques are mandated by the application but the descriptive capabilities provided by this particular method is desired. Lastly, in cases where physical black box input testing is required to validate a biomedical devices overall susceptibility to environmental effects — an attribute that can help ensure operational stability of any feedback techniques implemented —, this method allows for the synthesization — thru mathematical formulation and later function generation — of signals that can accurately represent actual environmental conditions acquired by an operating biomedical device, and such capabilities are particularly beneficial when attempting to duplicate an observed biomedical acquisition — an attribute that further endorses the proposed concept of including the results obtained from the usage of this method in conjunction with acquired biometric data, especially within characterization applications were fidelity is of paramount importance. Likewise, after the in-depth examination of both the — previously discussed — extraction method developed and the environmental conditions routinely encountered by contemporary biomedical devices in common commercial usages, the importance that physical shielding has upon the — previously observed — environmental effects encountered was examined in order to obtain quantifiable metrics regarding the amount of reduction generally obtained upon the implementation of these physical reduc-

tion techniques — like the usage of a biomedical device within an RF shielded enclosure; noting that this particular attribute has not been thoroughly examined within contemporary bioelectrical research beyond the simplistic operation within a RF shielding enclosure. Conversely, the metrics obtained during this inquiry into physical shielding — of both the partially shielded and fully shielded scenario — reveals that substantial reduction in the environmental effects encountered can be obtained through the usage of physical shielding techniques — an attribute that was expected — and such observations quantitatively reveal that biomedical devices operating within a physically shielded environment will encounter — depending upon the amount of physical shielding utilized — between 20 to 50 percent less environmental distortions through the utilization of such techniques, and while it is difficult to translate this reduction into a metric of overall device improvement — as such metrics are application specific —; however, within biomedical signal acquisition applications, such reductions were found to be substantially profound and in some instances — particularly within sEMG acquisitions — arguably constitutes a one-to-one improvement after instrumentational CMRR reduction was considered — an attribute that was not expected. Furthermore, the methodology developed was then utilized to profile and mathematically represent the physical shielded cases selected — partially and fully shielded —, and an overall analysis was conducted in order to both profile the fidelity of the bioelectrical measurements taken — within this dissertation — and to provide an example of how the methodology developed can be utilized in conjunction with existing biometric collection methods.

Thus, with this being said, environmental effects, while in some instances possessing highly localized and conditional characteristics, are predominantly considered stochastic and continual. Likewise, such effects typically fall into one of the following categories:

synthetic environmental effects, or natural environmental effects, in which synthetic environmental effects are best described as being an artificial source of electromagnetic (EM) radiation that generally permeates everything that interacts with it, such as the 60Hz EM radiation produced by power lines [387] [226]. Conversely, natural environmental effects, while theoretically similar to synthetic environmental sources of EM radiation, generally fall into one of two additional sub environmental classifications: macro-natural environmental effects, or Micro-natural environmental effects, in which macro-natural environmental effects are generally described as being natural large-scale sources of EM radiation, such as atmospheric impulses — like lightning — or other space related EM sources, while micro-natural environmental effects, in contrast, are generally described as being small-scale sources of EM radiation, such as thermal emission [388] [387] [226] [389].

Yet, while the isolation and categorization of individual environmental effects has its place within certain academic research areas — after all the industrial electronics research area has utilized synthetic environmental modeling for load identification, while the research area of material science has frequently utilized natural environmental modeling during the development of an assortment of applications; however, such characterization, at least beyond a basic level, or more precisely beyond the collective categorization of obvious synthetic versus natural sources of EM radiation, becomes more of a theoretical exercise, if not an anecdotal exercise, since such classification is generally not beneficial, at least beyond this basic level, because of the collective nature of EM environmental effects that tends to prevent the accurate isolation and direct identification of individual sources of EM radiation upon broad spectrum acquisition [388] [387] [226] [389] [36] [203]. Thus, upon considering such attributes, to begin a basic characterization of such environmental parameters, while also, for the moment, neglecting the undiscussed topic of instrumen-

tational effects, considered the following unshielded high impedance (High-Z) laboratory measurement taken within a typical small commercial structure (SCS) as shown by Figure: (51).

Likewise, visual inspection of Figure: (51), appears to depict a relatively small amplitude pseudo-periodic and partly stochastic signal that provides a reasonable representation of how environmental effects collectively manifest themselves upon experimental or commercial measurement instrumentation, and such observations also represent the laboratory environmental conditions that existed when unshielded measurements were taken by laboratory signal acquisition equipment within this dissertation. Thus, to begin analyzing and characterizing the unshielded environmental conditions, as shown by Figure: (51), a histogram with a discrete bin interval of five, as shown by Figure: (52), was created. Although histograms are seldom ever used within the electrical engineering discipline; however, because environmental effects have a pseudo-stochastic nature, the examination of a histogram can be useful in determining the probability distribution of the stochastic component of the signal, should such a component exist, while, at the same time, also providing some insight into the electrical symmetry of the signal — although time domain analysis is frequently

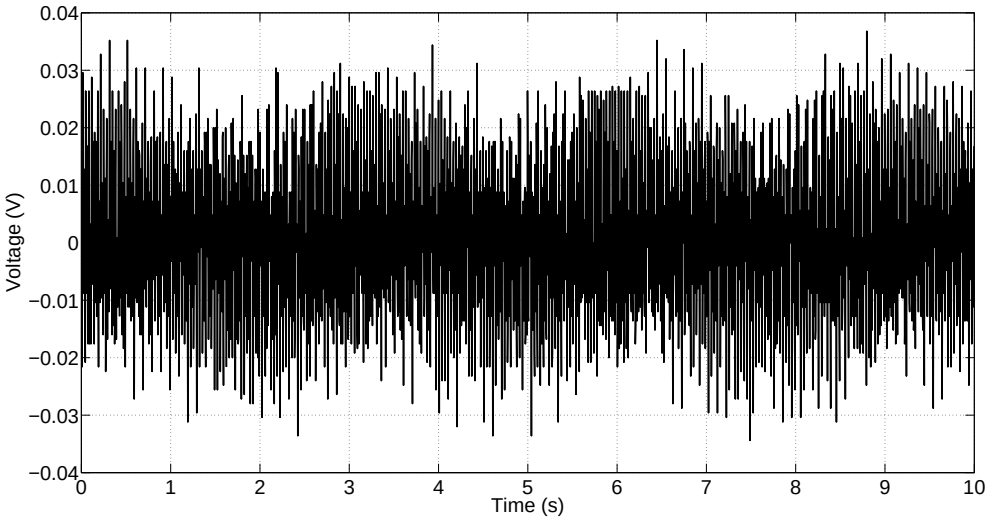

Figure 51: high-z unshielded scs environmental measurement

used to accomplish this particular task.

Likewise, visual inspection of Figure: (52) reveals a shape similar to a Gaussian probability distribution and a somewhat symmetric voltage swing between ±40mV. Similarly, decreasing the discrete bin interval of the X-axis to 15, as shown by Figure: (53), and to 50, as shown by Figure: (54), produces a similar but higher resolution diagram of Figure: (52) that, with the exception of a few outliers, tends to indicate the same probability

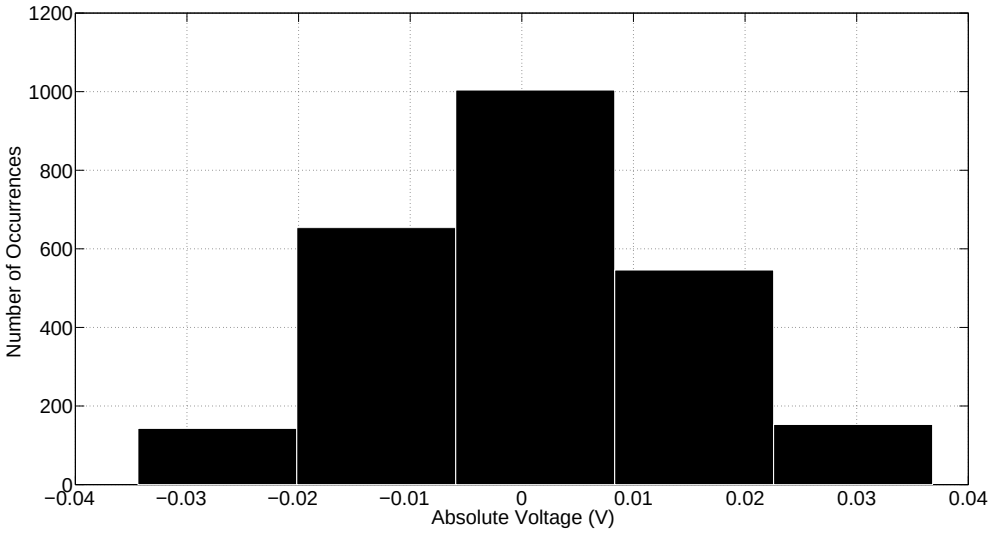

Figure 52: high-z unshielded scs environmental histogram with discrete interval at 5

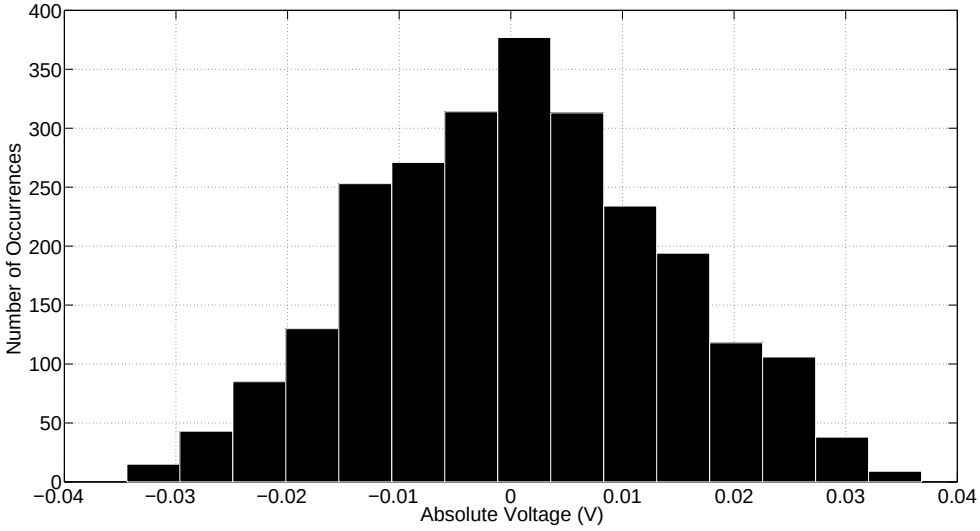

Figure 53: high-z unshielded scs environmental histogram with discrete interval at 15

distribution observed in Figure: (52).

Conversely, traditional frequency domain analysis of Figure: (52) — accomplish primarily through the Discrete Fourier Transform (DFT), or more specifically through the utilization of the MATLAB Fast Fourier Transform (FFT) algorithm — yields a periodogram, as shown by Figure: (55), that indicates the existence of both synthetic EM sources — predominantly 60Hz EM radiation and its harmonics — along with other natural stochastic EM sources.

Likewise, the real and imaginary coefficients obtained from the FFT operation, at least upon limiting the viewing area to a single side, can be manipulated into the following form,

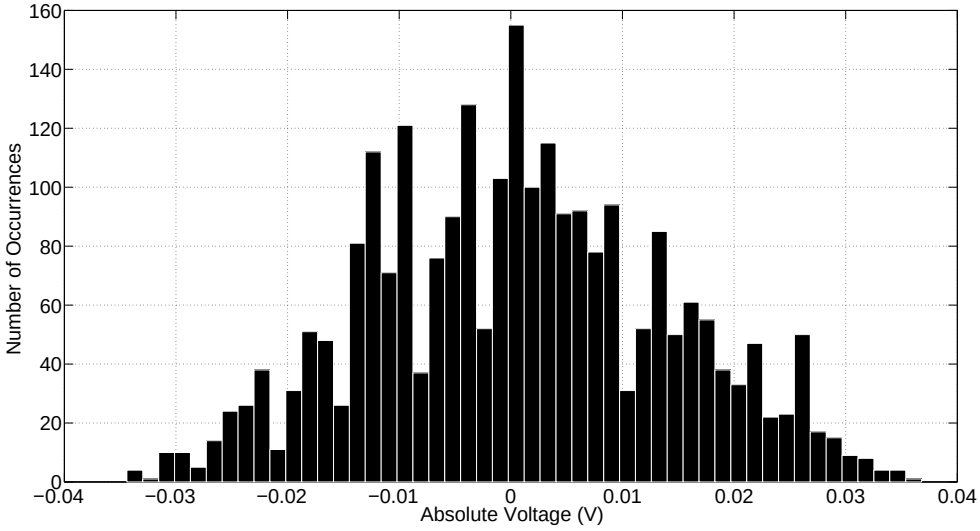

Figure 54: high-z unshielded scs environmental histogram with discrete interval at 50

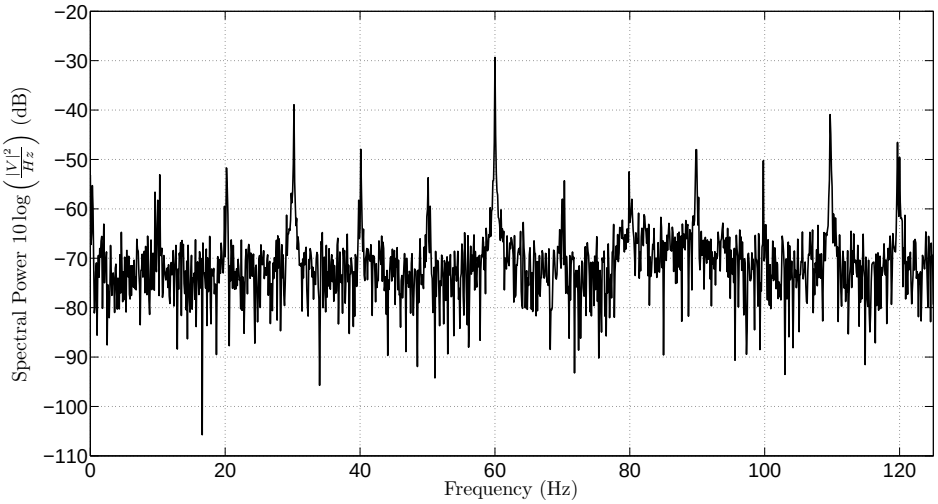

Figure 55: high-z unshielded scs environmental periodogram

as shown by Equation: (220), in which A_{V} represents the amplitude coefficients, as shown by Figure: (56), f represents the frequency, t represents the time, and θ_{Rad} represents the phase coefficients, as shown by Figure: (57).

$$F(t) = A_{\mathrm{V}} \cos\left(2\pi f t + \theta_{\mathrm{Rad}}\right) \tag{220}$$

Upon reviewing the periodogram, as shown by Figure: (51), the amplitude coefficients, as shown by Figure: (56), and based upon the observation that periodic synthetic EM sources

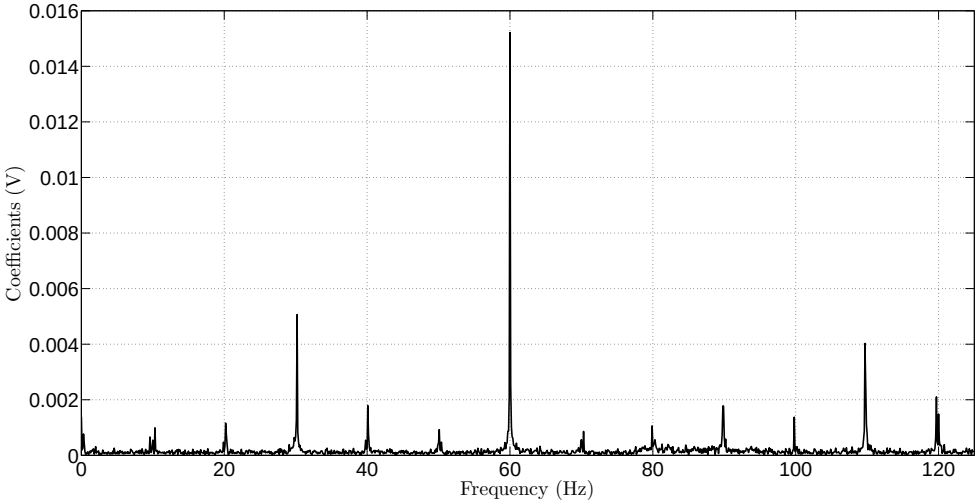

Figure 56: high-z unshielded scs environmental fft magnitude coefficients

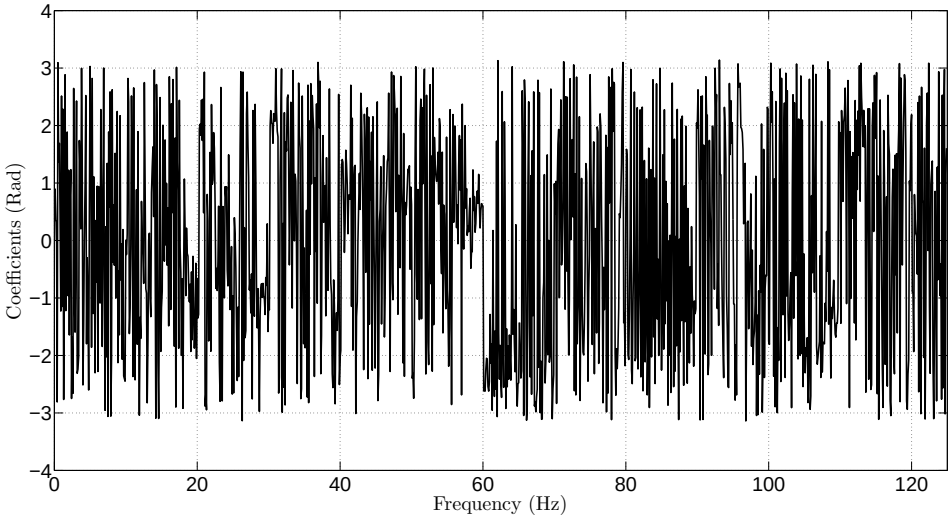

Figure 57: high-z unshielded scs environmental fft phase coefficients

tend to be stronger than natural EM sources, at least within a unshielded SCS environment, it can be assumed that synthetic EM sources can be separated from natural EM sources through the isolation and manipulation of the calculated FFT coefficients. While there are a number of digital signal processing (DSP) paradigms available to accomplish this specific task, the methodology selected attempted to isolate the synthetic EM sources from the natural EM sources, as previously mentioned, by selecting pertinent coefficients above or below the average natural EM signal floor depending upon the desired environmental model needed [390] [107].

Thus, to begin utilizing this process to separate definitively synthetic EM sources from presumed natural EM sources a separation point, or signal floor, must first be established and a visual inspection of Figure: (51) seems to indicate that the selection of a separation point that is around three times the mean value of the amplitude coefficients, as shown by Figure: (58), is a reasonable separation boundary.

Likewise, based upon the separation boundary selected, as shown by Figure: (58), the unshaded area represents amplitude coefficients that were extracted in order to synthesize a

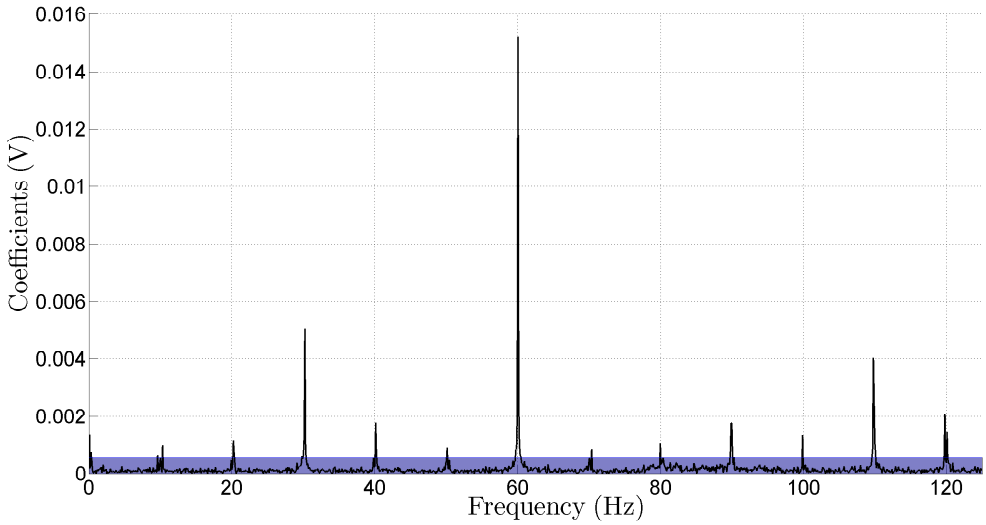

Figure 58: high-z unshielded scs environmental fft magnitude coefficients with synthetic separation boundary shaded

model that represents the synthetic environmental effects observed, while the shaded amplitude coefficients were used in determining a stochastic process that models the presumed natural environmental effects observed. Conversely, this process can be achieved programmatically using the MATLAB code shown within Appendix E script 1 and Appendix E script 2.

$$F(t) = \sum_{k=1}^{n} A_{\mathrm{V}}(k) \cos\left(2\pi f(k)t + \theta_{\mathrm{Rad}}(k)\right) \tag{221}$$

and upon modifying Equation: (220) to incorporate multiple coefficients, as shown by Equation: (221), the MATLAB code shown within Appendix E script 3 is obtained and can be utilized to calculate a mathematical model that predicts unshielded SCS synthetic environmental effects, as shown by Figure: (59). Equally, a formal mathematical expression can be obtained for the unshielded SCS synthetic environmental effects previously discussed, as shown by Equation: (222); however usage of such an equation, because of its significant length, is rather tedious to calculate by hand and is generally calculated using

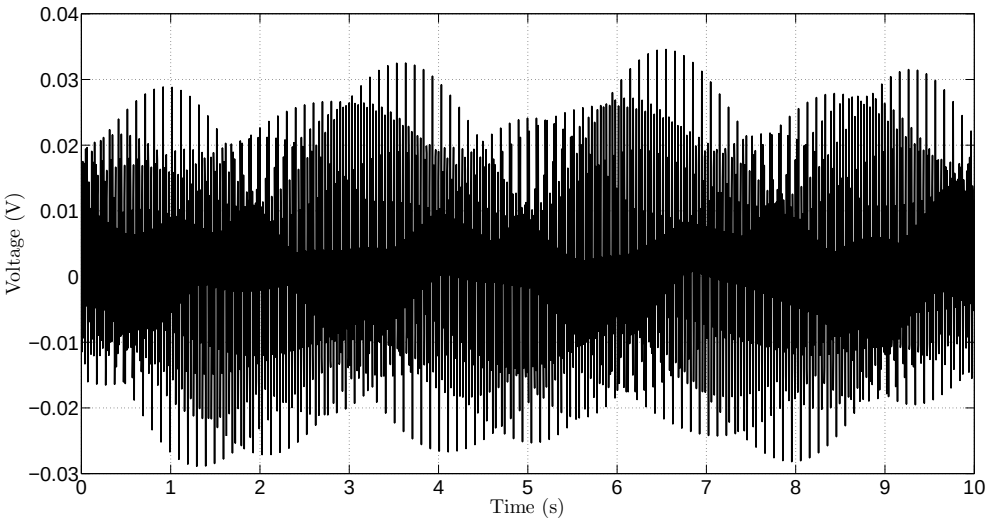

Figure 59: simulated unshielded scs synthetic environmental effects

the computational method previously discussed.

$$
\begin{aligned}
S_u(t) = {} & 0.00139136\cos(2\pi 0 + 0) + 0.000768739\cos(2\pi 0.3 + 0.333263) \\
& + 0.000660634\cos(2\pi 9.6 + 0.189944) + 0.000990404\cos(2\pi 10.3 + 2.81991) \\
& + 0.00115992\cos(2\pi 20.2 - 1.2841) + 0.000739955\cos(2\pi 20.3 + 1.94705) \\
& + 0.000643065\cos(2\pi 29.8 + 0.290192) + 0.000673467\cos(2\pi 30 - 1.13684) \\
& + 0.00127599\cos(2\pi 30.1 - 1.20601) + 0.00506458\cos(2\pi 30.2 + 1.9924) \\
& + 0.000843514\cos(2\pi 30.3 + 2.26047) + 0.00179242\cos(2\pi 40.1 - 1.91432) \\
& + 0.00073617\cos(2\pi 40.2 + 1.29648) + 0.000924165\cos(2\pi 50.1 - 2.39735) \\
& + 0.000860016\cos(2\pi 59.7 + 0.522888) + 0.000869306\cos(2\pi 59.8 + 0.641643) \\
& + 0.00209666\cos(2\pi 59.9 + 0.59827) + 0.0152153\cos(2\pi 60 + 0.601839) \\
& + 0.00250203\cos(2\pi 60.1 - 2.61755) + 0.00102477\cos(2\pi 60.2 - 2.60346) \\
& + 0.000674847\cos(2\pi 60.3 - 2.62121) + 0.00061831\cos(2\pi 60.4 - 2.24491) \\
& + 0.000561792\cos(2\pi 70 + 0.987552) + 0.000861259\cos(2\pi 70.3 - 2.8343) \\
& + 0.00106032\cos(2\pi 79.9 - 2.17911) + 0.000559896\cos(2\pi 80.3 - 1.97532) \\
& + 0.000735553\cos(2\pi 89.7 - 1.27288) + 0.00177789\cos(2\pi 89.8 - 1.18985) \\
& + 0.00177437\cos(2\pi 89.9 + 2.0447) + 0.000656547\cos(2\pi 90 + 1.95337) \\
& + 0.000584816\cos(2\pi 90.2 + 1.80375) + 0.00137311\cos(2\pi 99.8 + 2.3178) \\
& + 0.000580476\cos(2\pi 109.5 - 1.43858) + 0.000876143\cos(2\pi 109.6 - 1.43795) \\
& + 0.0040253\cos(2\pi 109.7 - 1.18166) + 0.00255694\cos(2\pi 109.8 + 2.06472) \\
& + 0.00110232\cos(2\pi 109.9 + 1.74666) + 0.000747692\cos(2\pi 110 + 1.87743) \\
& + 0.000657407\cos(2\pi 119.6 - 2.07662) + 0.00210412\cos(2\pi 119.7 + 1.03554) \\
& + 0.00148479\cos(2\pi 120 + 2.18964)
\end{aligned} \tag{222}
$$

Similarly, the coefficients that were previously obtained can be used to create a digital

mask, or digital notch filter, by using the MATLAB code shown within Appendix E script 4, and the separation mask obtained, as shown by Figure: (60), at least upon visual inspection, indicates that the coefficients selected are reasonable separation points between synthetic environmental effects and natural environmental effects, such that the MATLAB code shown within Appendix E script 5 can be utilized to remove the synthetic effects from the natural effects, as shown by Figure: (61) and Figure: (62).

Likewise, a histogram of Figure: (63), as shown by Figure: (62), seems to indicate that a Gaussian distribution could be utilized to model the natural effects observed in Figure:

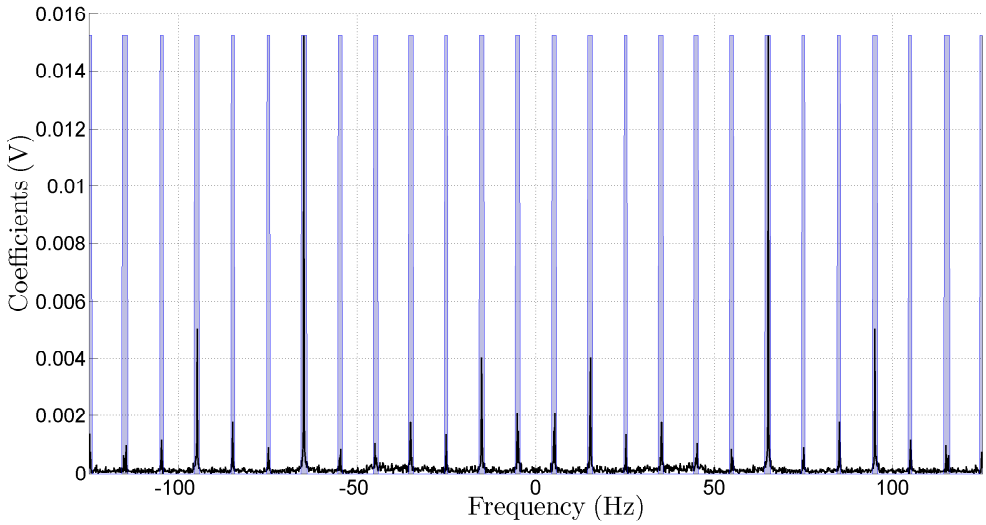

Figure 60: scs unshielded synthetic inverted filter mask versus magnitude fft coefficients

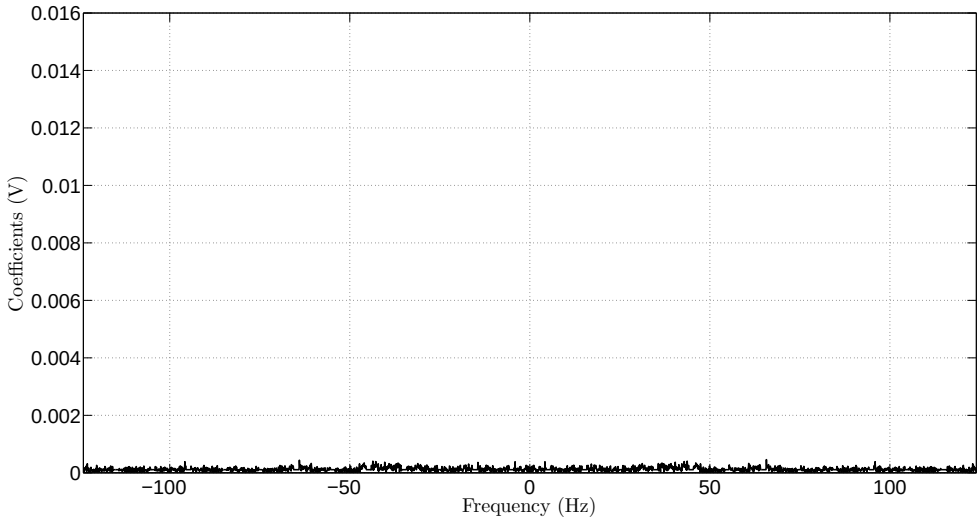

Figure 61: scs unshielded filtered fft magnitude coefficients of natural effects

(62) — although the observed process is not strictly Gaussian distributed — and upon estimating the Gaussian distribution mean (μ) and variance (σ) of Figure: (62), a task accomplished by the MATLAB code shown within Appendix E script 6, and the following parameters were obtained, as shown by Equation: (223) and Equation: (224).

Conversely, the parameters obtained can be used to model the natural environmental effects through the utilization of a Gaussian weighted random number generation algorithm, a task accomplished by the MATLAB code shown within Appendix E script 7, and results in random data being created resembling Figure: (64), with a histogram resembling Figure:

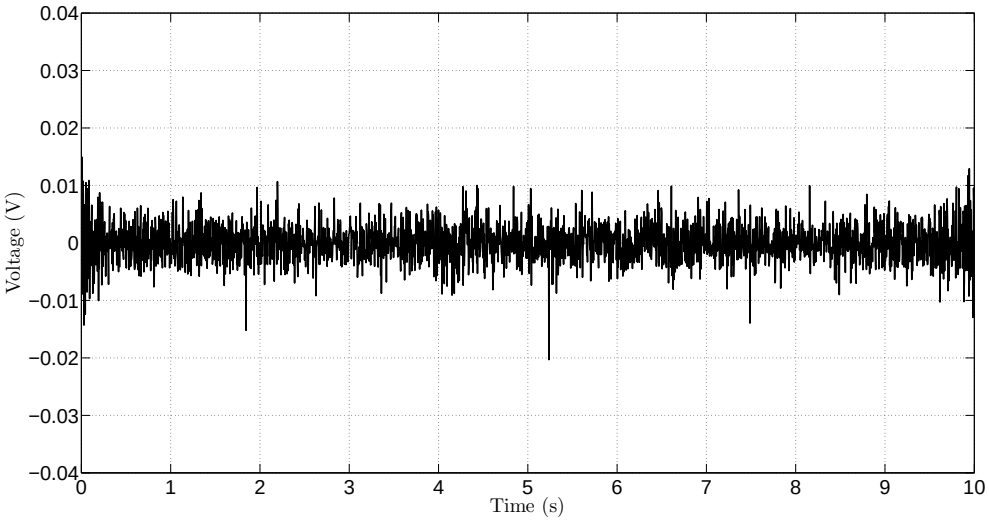

Figure 62: scs unshielded filtered natural effects in time domain

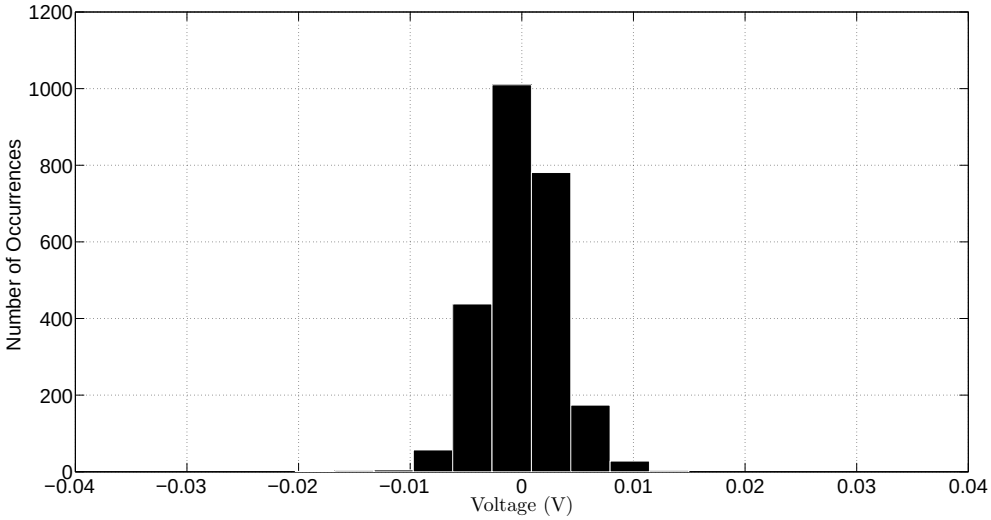

Figure 63: scs unshielded filtered natural effects histogram

(65).

$$\mu_u = 4.3465 \times 10^{-8} \tag{223}$$

$$\sigma_u = 0.0033 \tag{224}$$

Likewise, visual comparison between Figure: (65) versus Figure: (63) and Figure: (62) versus Figure: (64), while possessing some expected dissimilarities since the natural function is not strictly a Gaussian distribution, appears to be a acceptable approximation of the natural environmental processes observed within the laboratory.

Conversely, the combination of the synthetic model with the natural model, as shown by Equation: (226), results in data being created that resembles Figure: (66) with a histogram resembling Figure: (67), a periodogram resembling Figure: (68), and a comparison between the original signal and the synthetic model resembling Figure: (69).

$$N_u(t) = S_u(t) + \text{NormRnd}(\mu_u, \sigma_u) \tag{225}$$

$$N_u(t) = S_u(t) + \text{NormRnd}(4.3465 \times 10^{-8}, 0.0033) \tag{226}$$

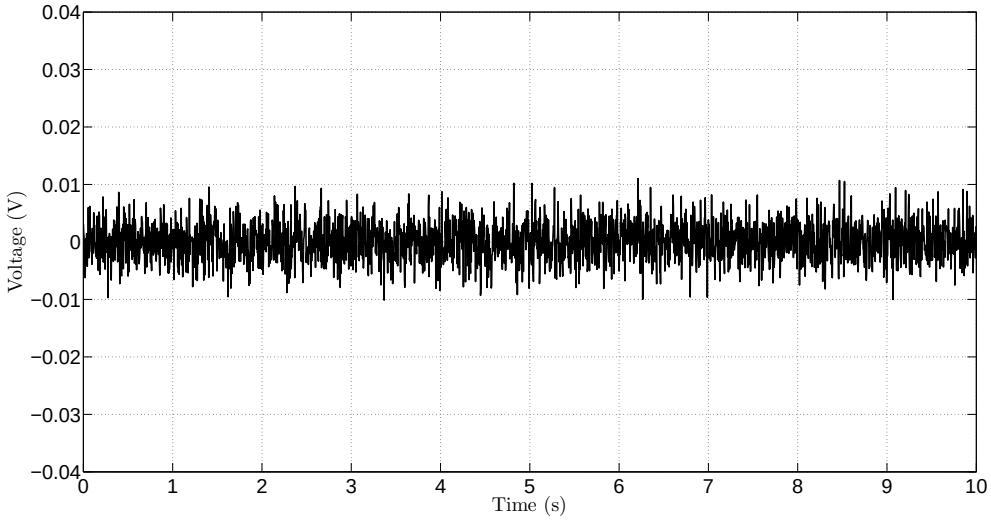

Figure 64: simulated scs unshielded natural effects

Likewise, visual comparison of the observed unshielded environmental effects with the simulated environmental effects, seems to indicate that the simulated high-z unshielded environmental effects can effectively approximate the observed unshielded environmental effects and that the environmental modeling methodology, previously described, appears to be an effective environmental modeling method. Nevertheless, it is important to mention that the parameters obtained above, at least for the unshielded SCS environmental model, are — strictly speaking — only providing an accurate representation of the environmental conditions that existed within the unshielded laboratory when measurements were taken and

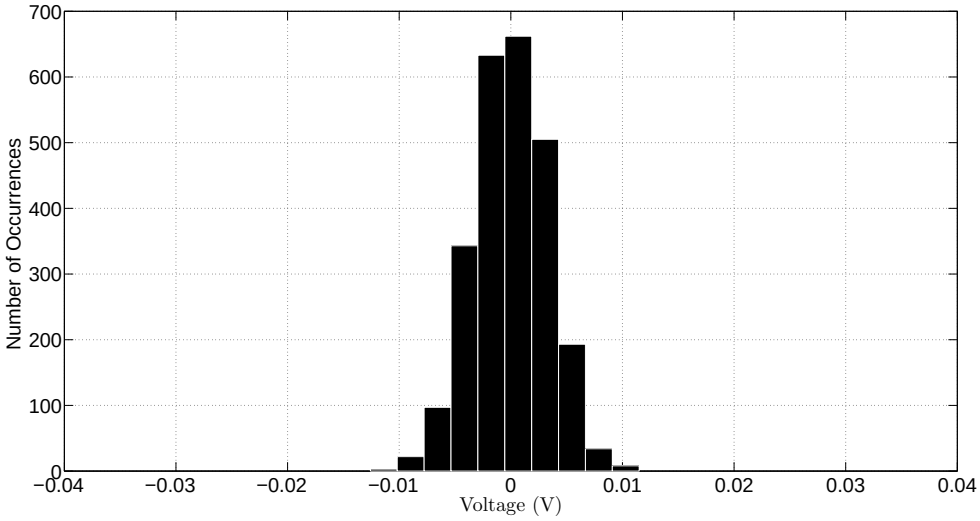

Figure 65: simulated scs unshielded natural effects histogram

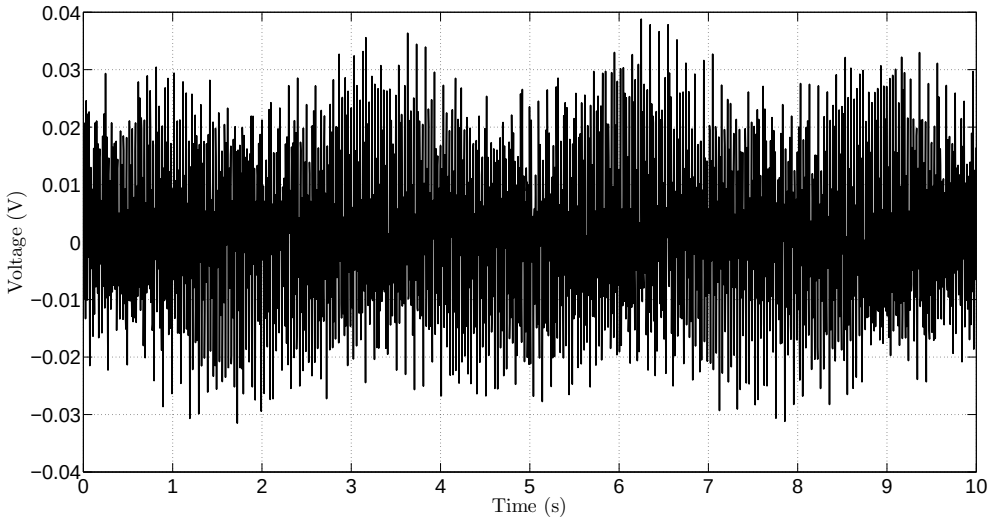

Figure 66: high-z simulated scs unshielded environmental effects

are not necessarily directly applicable to other unshielded SCS environments. Yet, despite this fact, the unshielded SCS environmental model, previously described, is a reasonable starting point for the preliminary modeling of such environments and, in cases where unshielded SCS environmental conditions exist without any prior environmental knowledge, application of this model will likely provide a better approximation than simply neglecting environmental effects.

Thus, while unshielded SCS environmental conditions are the commercial norm that most bioelectrical devices typically operate in; however, the study of such conditions is

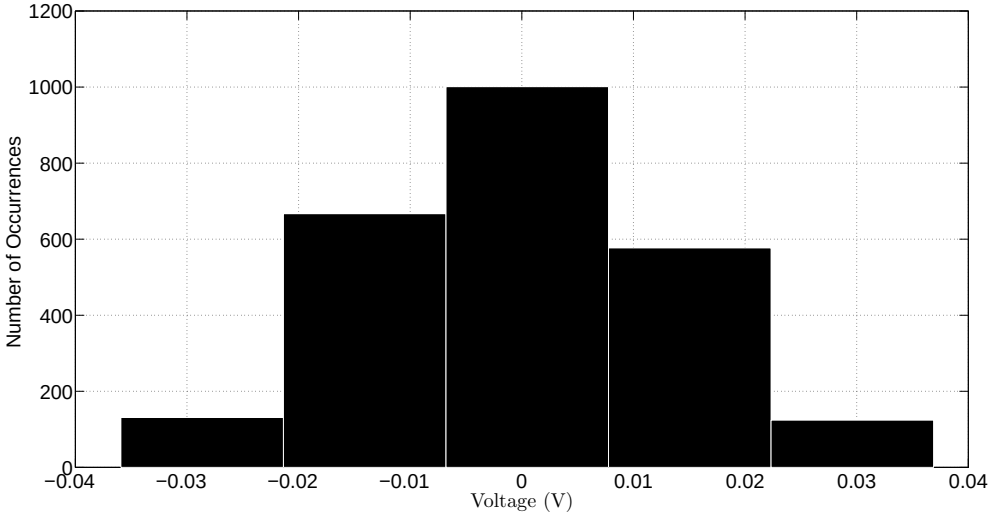

Figure 67: high-z simulated scs unshielded environmental effects histogram

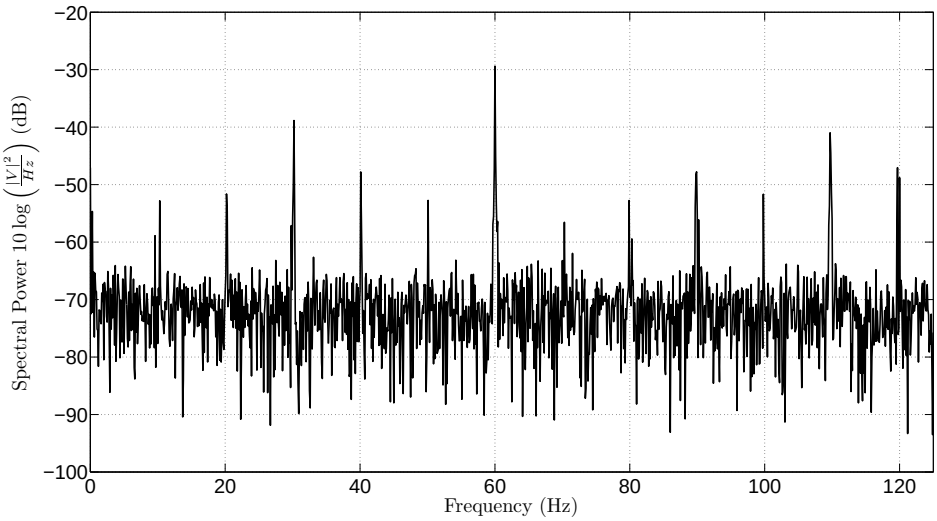

Figure 68: high-z simulated scs unshielded environmental effects periodogram

not strictly limited within the bioelectrical research area, and has been heavily researched within the electrical engineering discipline, particularly within the signals and systems research area. Likewise, because the subject of environmental effects, or ambient noise, has been frequently examined, it should come as no surprise that a number of techniques, both physical and virtual, have been developed to combat such effects and are frequently employed within most contemporary commercial biomedical devices. Yet, while such techniques are extremely important, especially when creating a commercial biomedical device, such compensation techniques typically do have some type of problem that is associated with their usage and such methods, at least within this dissertation, were avoided, particularly virtual methods, since the basic idea behind modeling is mathematical simulation rather than active real time compensation. Although, it is worth mentioning that once such conditions have been successfully modeled, the ability to actively compensate for their occurrence does generally become easier. Nevertheless, while some compensation methods were applied, within this dissertation, in order to isolate a particular effect within a laboratory measurement, for the most part, the information presented within this dissertation will primarily address mathematical modeling, rather than active compensation methods;

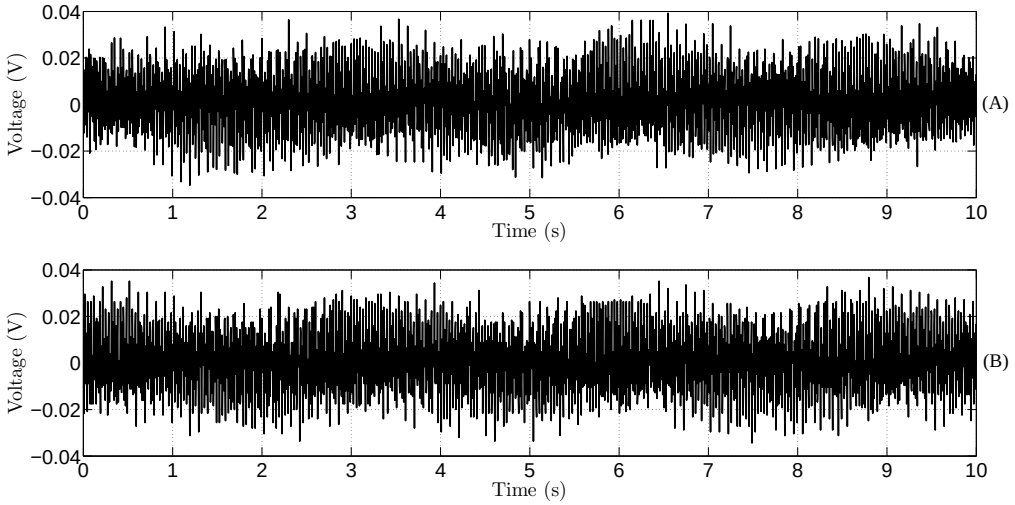

Figure 69: (plot a) high-z simulated scs unshielded environmental effects versus (plot b) high-z measured scs unshielded environmental effects

however, it is important to note that developing a compensation method, at least from the models presented within this dissertation, — particularly if the compensation method utilized is a virtual method, such as a finite impulse response (FIR) filter — is a relatively straightforward process and a natural extension of the research being presented.

With this being stated, it is important to also recognize that unshielded SCS environmental conditions, while representing typical commercial operating conditions, are far from being ideal, particularly when trying to develop a new contemporary high fidelity research standard. Thus, while virtual compensation techniques were avoided, physical compensation techniques were utilized, as the majority of the laboratory measurements taken, at least within this dissertation, utilized either a partially shielded or a fully shielded measurement environment, as shown by Figure: (70), in which the term partially shielded implies the usage of a partially or fully sealed Faraday cage without electrical isolation, as shown by Figure: (71) right, while the term fully shielded implies the usage of a completely sealed Faraday cage with electrical isolation, as shown by Figure: (71) left.

Likewise, high-z SCS environmental measurements were taken for each case and the methodology, previously discussed, was applied to each measurement. Conversely, based upon the methods previously described, the partially shielded and fully shielded SCS environmental measurements, as shown by Figure: (72) and Figure: (73), were observed to have a $\pm$25mV and $\pm$1mV pseudo-periodic component respectively. Likewise, visual inspection of each measurements histogram, as shown by Figure: (74) and Figure: (75), while depicting the obvious difference in signal amplitude, reveals the existence of a attenuated synthetic pseudo-periodic component along with the expected Gaussian distribution that was previously modeled.

Similarly, the periodogram of Figure: (72) and Figure: (73), as shown by Figure: (76) and

Figure: (77) respectively, while visually possessing a similar spectral frequency content, as previously discussed, does impart, at least upon visual inspection, a notable difference in spectral power density upon comparison of the unshielded environmental measurements to the partially shielded environmental measurements to the fully shielded environmental measurements. Yet, such differences in spectral power density were, in many ways, intuitively expected given the significant amount of synthetic environmental effects previously

Figure 70: lindgren rf enclosure: model number 26-5/5-i

Figure 71: (left) partially shielded rf enclosure with external power, (right) fully shielded rf enclosure without external power

observed, insofar as, a progressive decline in the spectral power density of such frequencies as the level of physical environmental shielding was increased would be expected because the Faraday cage utilized, within this dissertation, was predominantly designed to minimize such synthetic effects — particularly the effects of 60Hz EM radiation.

Nevertheless, comparison of the unshielded periodogram, as shown by Figure: (55), with the partially shielded periodogram, as shown by Figure: (76), while visually appearing numerically similar, does reveal an approximate 4 dB drop in most frequencies that were previously presumed to be synthetic and, curiously enough, shows that no substantial drop

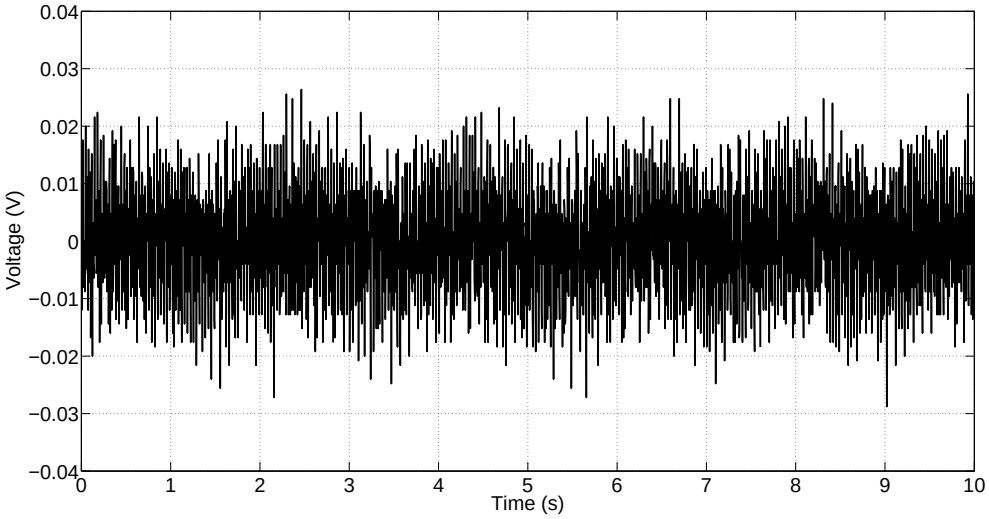

Figure 72: high-z scs partly shielded environmental measurement

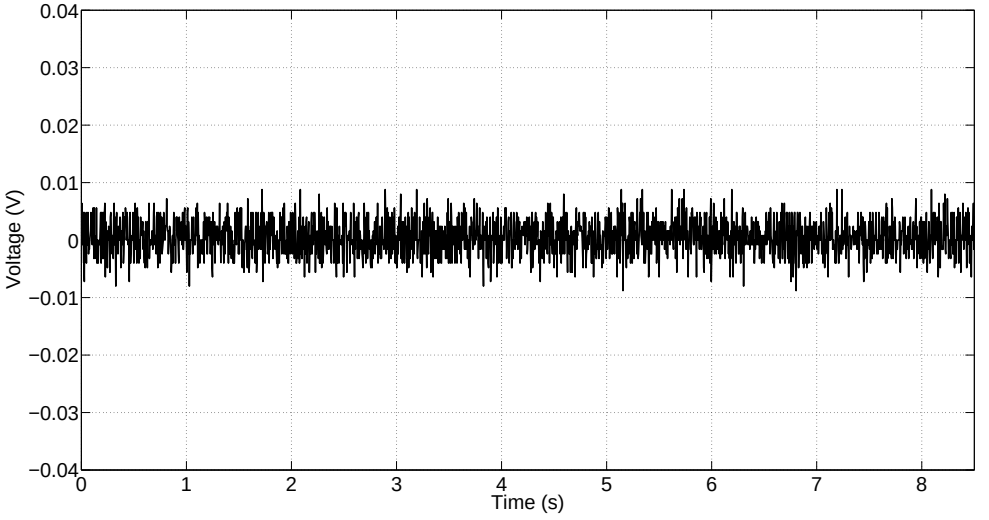

Figure 73: high-z scs fully shielded environmental measurement

in spectral power occurred for the frequency of approximately 110 Hz upon the application of increased physical shielding. Similarly, a slight increase in spectral power between the frequencies of 40 Hz to 50 Hz was also noted, while notable fluctuations of spectral power were observed across the previously presumed natural environmental frequencies. Conversely, the 4 dB power drop across the presumed synthetic frequencies observed, upon the application of partial physical shielding, while possibly sounding somewhat insignificant given that the natural environmental floor is 40 dB lower than the measured synthetic values, represents an approximate half power reduction of extremely prominent and im-

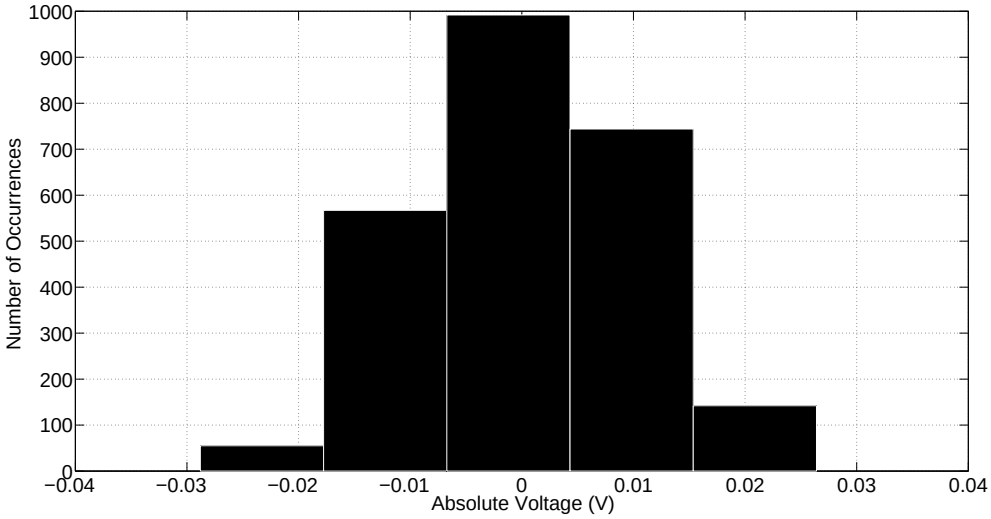

Figure 74: high-z scs partly shielded histogram with bin size of 5

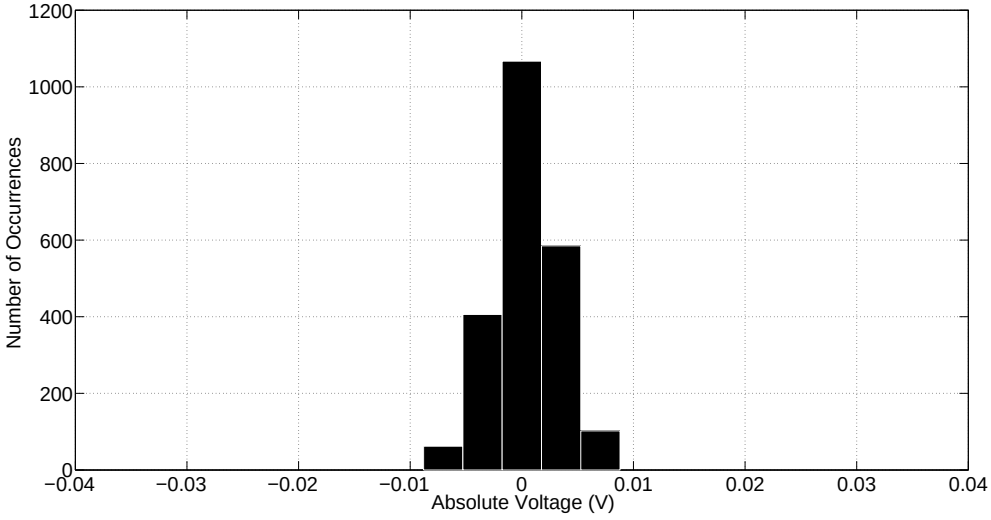

Figure 75: high-z scs fully shielded histogram with bin size of 5

posing synthetic EM sources and such a reduction should not be taken lightly. Likewise, the observed lack of reduction in spectral power at approximately 110 Hz would seem to imply the existence of a synthetic source that was independent of the applied environmental shielding, and given the fact that the oscilloscope used to obtain these measurements was connected to the electrical power grid in both cases, it is reasonable to assume that the synthetic source observed is predominantly a instrumentation effect, a concept that will be discussed in another section, rather than simply being simply a synthetic environmental effect. Additionally, the slight increase in spectral power between the frequencies of 40 Hz

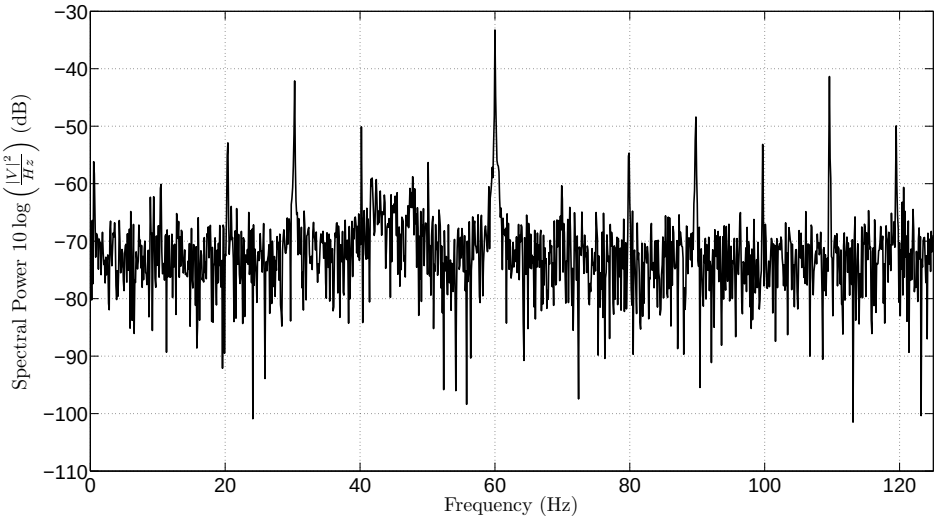

Figure 76: high-z partially shielded scs environmental periodogram

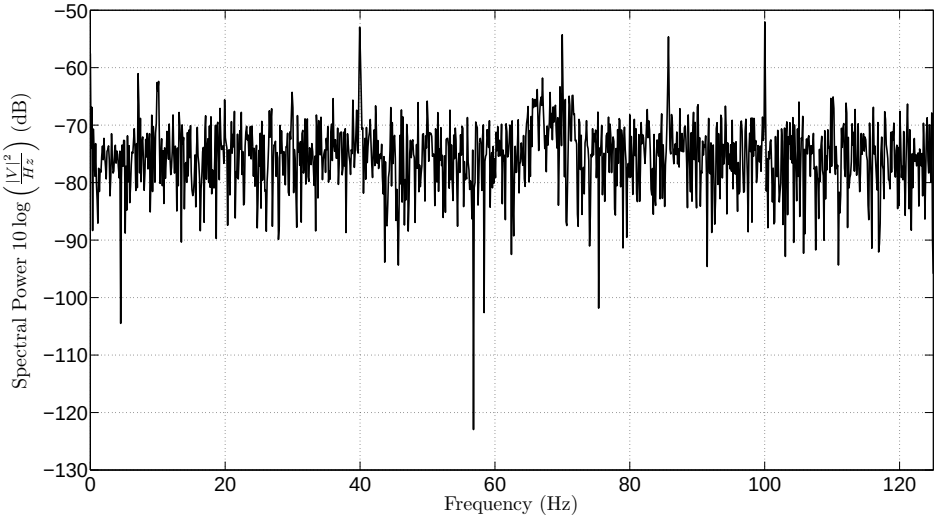

Figure 77: high-z fully shielded scs environmental periodogram

to 50 Hz and the natural fluctuations observed, might be attributed to instrumentational effects since, any EM emissions created by the measuring instrumentation inside the Faraday cage would, in anecdotal fashion, have a tendency to bounce around the enclosure — in a manner that might be metaphorically depicted by a rubber ball bouncing around a small room — that could effectively change the observed EM radiation pattern measured significantly. Alternatively, such increases could just as easily have been attributed to the power filtering system that was incorporated into the Faraday cage or to a temporary load that was briefly attached to the SCS power grid when the partially shielded measurements were taken, and the existence of such possibilities is a prime example of why the identification of unique environmental sources is an extremely difficult task that, for the most part, was generally avoided whenever possible in favor of surmised predictive models.

Conversely, a comparison between the unshielded periodogram as shown by Figure: (55), and partially shielded periodogram, as shown by Figure: (76), versus the shielded periodogram, as shown by Figure: (77), indicates an approximate 40 dB drop in all presumed synthetic environmental effects. While such a reduction in the observed synthetic environmental effects is, in fact, very profound, it is important to note that such reductions were primarily obtained thru decoupling the Faraday cage from the SCS power grid and operating the laboratory measuring instrumentation within the fully shielded measuring environment using an isolated DC power source. Likewise, while the fully shielded measuring environment does effectively minimize most environmental sources, to the point that the presumed natural effects observed are more likely to be the result of instrumentational effects rather than natural effects; however, regardless of the origin, such measuring conditions are inherently problematic because of the required isolation from the SCS power grid that forces the usage of battery-operated laboratory apparatus. Nevertheless, while the

nuances of instrumentational effects and decoupled SCS shielded measuring protocols will be addressed in more detail in a later section, it is important to recognize that a number of environmental and instrumentation factors must be considered prior to conducting laboratory measurements, since the trade-offs between logistical complexity and the amount of environmental effects encountered varies significantly depending upon the measuring protocol utilized.

Yet, while such questions are very important, particularly from a designers perspective; however, these types of questions, at least when it comes to modeling such effects, are not

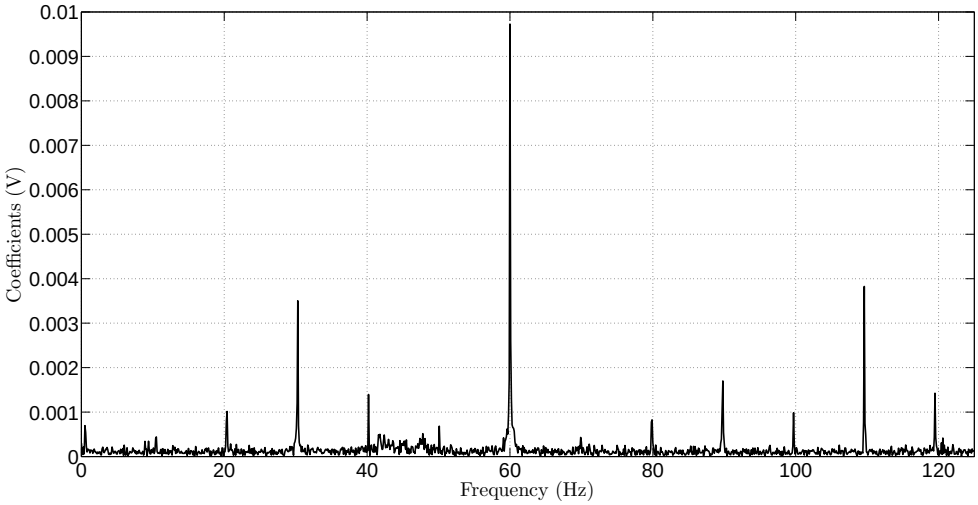

Figure 78: high-z partially shielded scs environmental magnitude coefficients

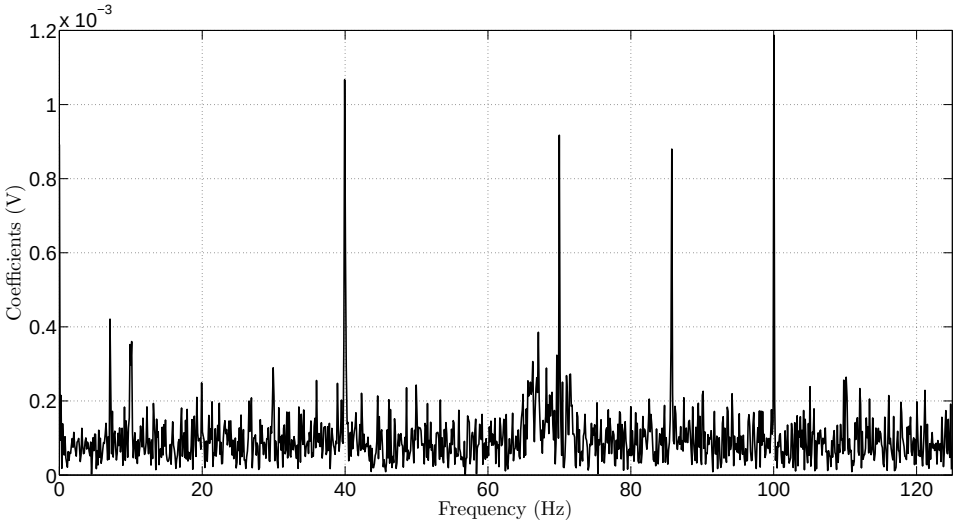

Figure 79: high-z fully shielded scs environmental magnitude coefficients

necessarily as profound especially since the modeling method, previously discussed, is directly applicable without possessing such knowledge. Thus because the method, previously applied, is still valid, application of this method, at least upon utilizing the MATLAB code previously provided, yields a FFT magnitude coefficient plot, as shown by Figure: (78) and Figure: (79), and a FFT phase coefficient plot, as shown by Figure: (80) and Figure: (81), for the partially shielded and fully shielded measurements taken. Likewise, calculation of three times the mean of the magnitude coefficients, once again in order to obtain the environmental effect floor, yields Figure: (82) and Figure: (83) that depicts the partially

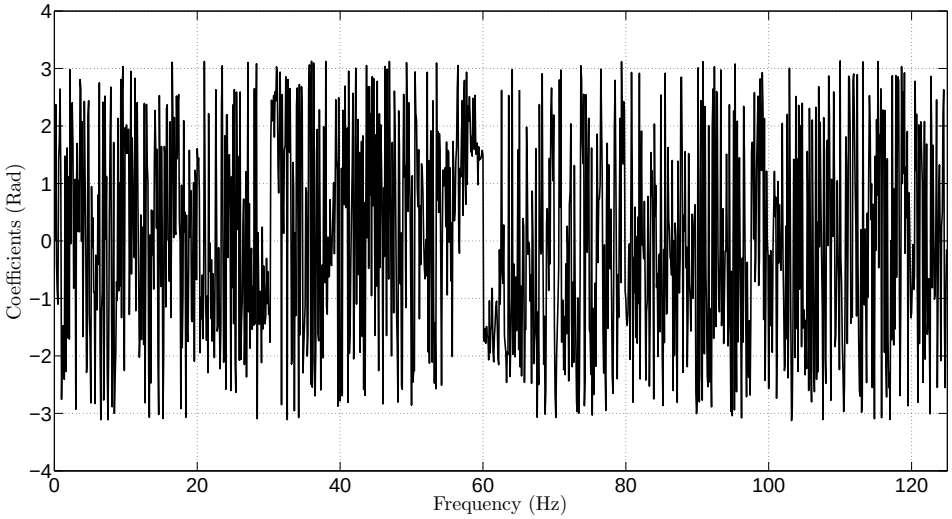

Figure 80: high-z partially shielded scs environmental phase coefficients

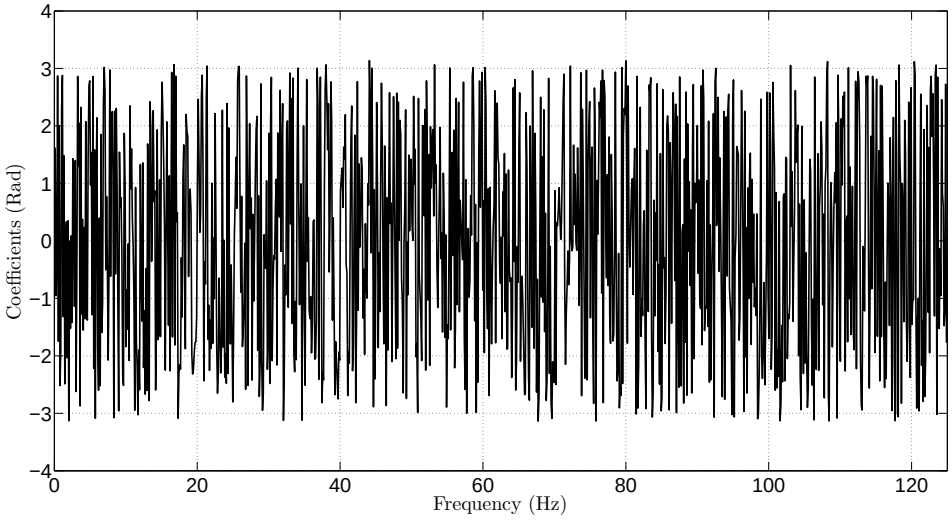

Figure 81: high-z fully shielded scs environmental phase coefficients

shielded and fully shielded natural environmental regions — which are shaded — and the synthetic environmental regions — which are not shaded.

While the region depicted by Figure: (82) appears to be fundamentally similar to the region depicted by Figure: (58), with the exception that the number of synthetic coefficients selected and the mean environmental floor has decreased; however, while this statement is also fundamentally true for the region depicted by Figure: (83), at least upon comparison with the region depicted by Figure: (82) or Figure: (58), yet, as it was previously men-

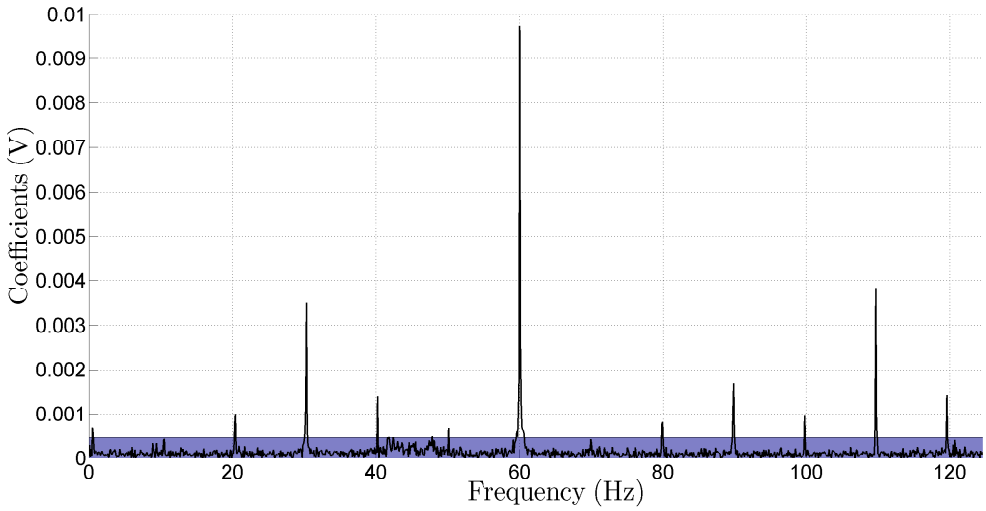

Figure 82: high-z partly shielded scs environmental fft magnitude coefficients with synthetic separation boundary shaded

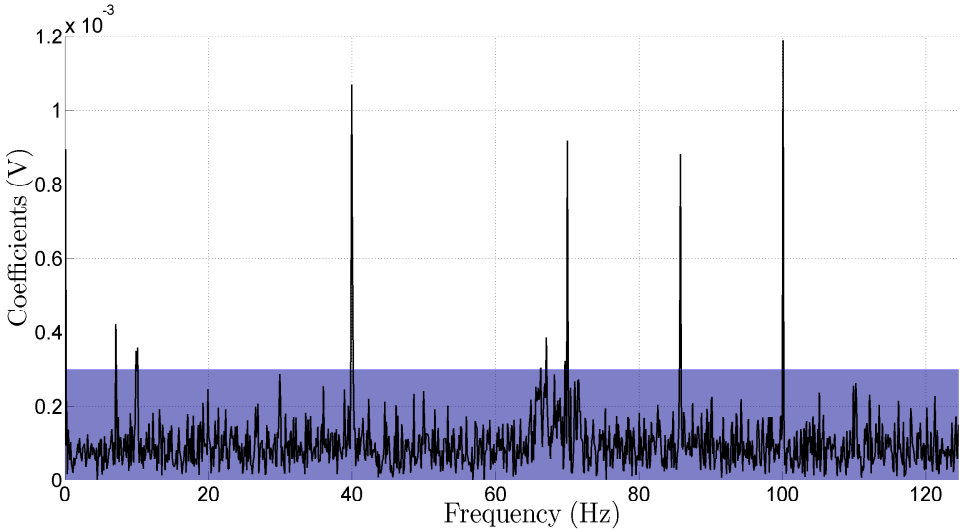

Figure 83: high-z fully shielded scs environmental fft magnitude coefficients with synthetic separation boundary shaded

tioned, the boundary depicted within Figure: (83), while possibly isolating a few synthetic parameters, is in truth, more than likely depicting the separation between instrumentation effects versus natural effects or primary instrumentation effects versus secondary instrumentation effects. Although some discussion will be provided within the instrumentation section pertaining to this particular issue, it is important to recognize that such attributes ultimately reveal a fundamental problem with attempting to categorize such effects into a singular model, since the collective manifestation of such phenomena makes the complete isolation and separation of individual effects extremely difficult if not fundamentally impossible. Thus, while the isolation and separation of individual effects might be truly an unrealistic expectation, the collective representation of such manifestations is definitively possible, as previously shown, so long as care is taken not to represent the same phenomenon more than once while modeling a particular system.

Likewise, the calculated mean environmental floor for the partially shielded environment, as shown by Figure: (82), and the fully shielded environment, as shown by Figure: (83), at least upon application of the synthetic isolation MATLAB code previously presented, will yield a model for the partially shielded synthetic effects, as shown by Equation: (227), and the fully shielded synthetic effects, as shown by Equation: (228).

$$\begin{aligned} S_p(t) = {} & 0.000695534\cos\left(2\pi 0.5 - 1.10166\right) + 0.000542707\cos\left(2\pi 0.6 + 1.41164\right) \\ & + 0.000792954\cos\left(2\pi 20.3 + 0.858045\right) + 0.00101268\cos\left(2\pi 20.4 - 1.94404\right) \\ & + 0.000634165\cos\left(2\pi 30.1 - 1.16347\right) + 0.00120324\cos\left(2\pi 30.2 - 1.76342\right) \\ & + 0.00350308\cos\left(2\pi 30.3 + 1.73047\right) + 0.000699292\cos\left(2\pi 30.4 + 2.44924\right) \\ & + 0.00139526\cos\left(2\pi 40.2 + 1.26337\right) + 0.000490092\cos\left(2\pi 41.6 + 0.530732\right) \\ & + 0.000500878\cos\left(2\pi 41.8 + 2.56996\right) + 0.00048563\cos\left(2\pi 42.4 + 0.829374\right) \\ & + 0.000514546\cos\left(2\pi 47.8 + 0.302018\right) + 0.000682808\cos\left(2\pi 50.1 + 1.13332\right) \end{aligned}$$

$$
\begin{aligned}
&+ 0.000620205\cos\left(2\pi 59.6 + 1.43713\right) + 0.000504158\cos\left(2\pi 59.7 + 1.43209\right) \\
&+ 0.000967445\cos\left(2\pi 59.8 + 1.49618\right) + 0.00173836\cos\left(2\pi 59.9 + 1.5754\right) \\
&+ 0.00972806\cos\left(2\pi 60 + 1.49055\right) + 0.00259792\cos\left(2\pi 60.1 - 1.68996\right) \\
&+ 0.0012803\cos\left(2\pi 60.2 - 1.75237\right) + 0.000711629\cos\left(2\pi 60.3 - 1.52459\right) \\
&+ 0.000652824\cos\left(2\pi 60.4 - 1.77968\right) + 0.00063628\cos\left(2\pi 60.5 - 1.48746\right) \\
&+ 0.000568952\cos\left(2\pi 60.6 - 1.65704\right) + 0.000777536\cos\left(2\pi 79.8 + 2.26991\right) \\
&+ 0.000825244\cos\left(2\pi 79.9 - 0.866926\right) + 0.00106407\cos\left(2\pi 89.7 + 0.62963\right) \\
&+ 0.00170042\cos\left(2\pi 89.8 - 2.65373\right) + 0.000540165\cos\left(2\pi 89.9 - 3.00559\right) \\
&+ 0.000982834\cos\left(2\pi 99.7 + 1.2165\right) + 0.00077689\cos\left(2\pi 109.5 - 0.779948\right) \\
&+ 0.00382605\cos\left(2\pi 109.6 + 1.0486\right) + 0.000744262\cos\left(2\pi 109.7 - 0.217239\right) \\
&+ 0.000499302\cos\left(2\pi 109.8 - 0.65514\right) + 0.00142433\cos\left(2\pi 119.5 - 2.86773\right)
\end{aligned} \tag{227}
$$

$$
\begin{aligned}
S_f(t) = {} & 0.000892169\cos\left(2\pi 0 + 0\right) + 0.000420896\cos\left(2\pi 7.08821 + 2.59781\right) \\
&+ 0.000352315\cos\left(2\pi 9.90099 + 0.991342\right) + 0.000360353\cos\left(2\pi 10.126 - 0.853383\right) \\
&+ 0.000359435\cos\left(2\pi 39.829 - 1.93504\right) + 0.00106691\cos\left(2\pi 39.9415 - 2.07584\right) \\
&+ 0.000603601\cos\left(2\pi 40.054 + 0.855575\right) + 0.000306393\cos\left(2\pi 66.2691 - 0.871087\right) \\
&+ 0.000385384\cos\left(2\pi 67.0567 + 0.666659\right) + 0.000323526\cos\left(2\pi 69.6445 - 3.08924\right) \\
&+ 0.000917324\cos\left(2\pi 69.982 - 2.46616\right) + 0.000345281\cos\left(2\pi 85.6211 - 0.891654\right) \\
&+ 0.000879891\cos\left(2\pi 85.7336 + 2.00976\right) + 0.00118705\cos\left(2\pi 100.023 - 1.69832\right)
\end{aligned} \tag{228}
$$

Conversely, Equation: (227) and Equation: (228), upon visual analysis in the time domain, yields plots for both the partially shielded synthetic effects, as shown by Figure: (84), and for the fully shielded synthetic effects, as shown by Figure: (85). Similarly, the synthetic

coefficients obtained through the utilization of the MATLAB code previously presented, can be utilized to create a digital mask or digital notch filter, using the techniques described earlier, in order to isolate the synthetic effects from the natural effects for both the partially shielded scenario, as shown by Figure: (86), and the fully shielded scenario, as shown by Figure: (87).

Likewise, application of the synthetic isolation filters, as depicted by Figure: (86) and Figure: (87), once again upon the utilization of the MATLAB code previously presented, results in the presumed separation of the synthetic effects from the natural effects for

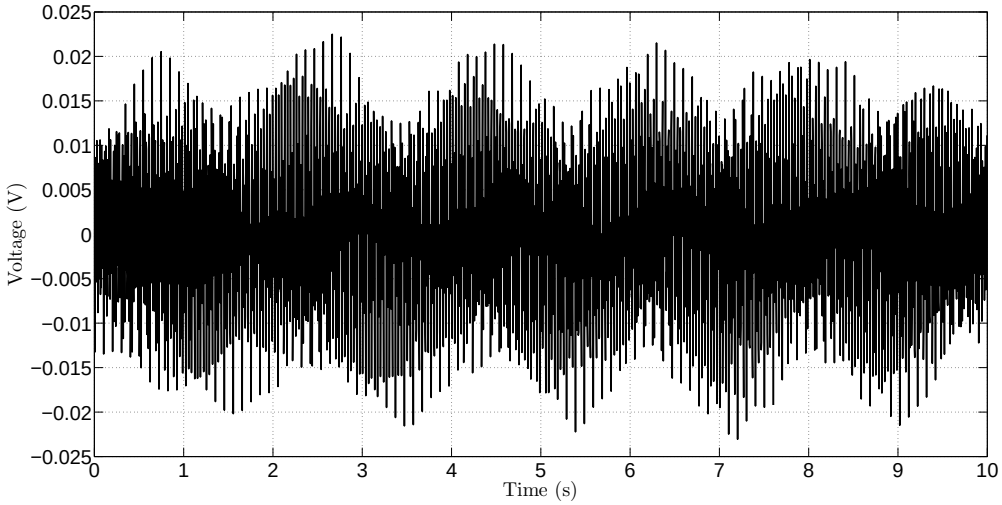

Figure 84: simulated partially shielded scs synthetic environmental effects

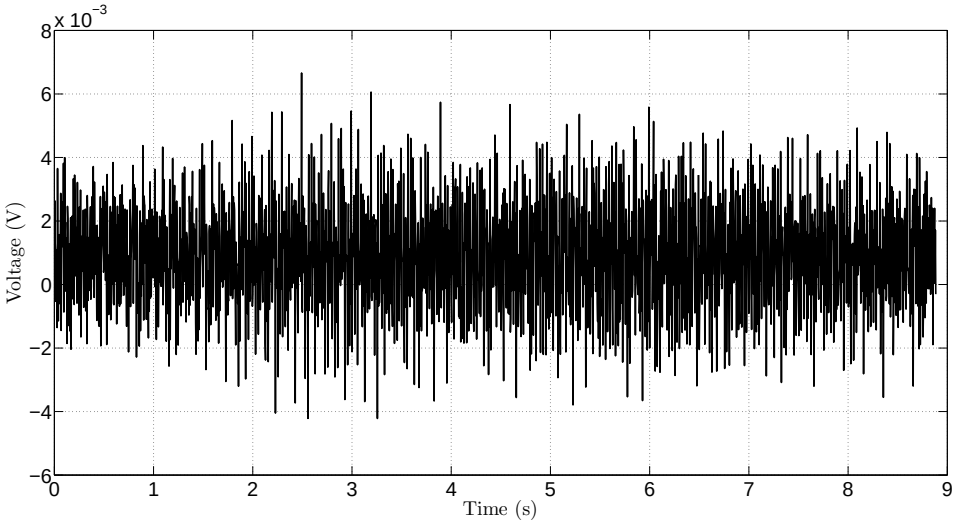

Figure 85: simulated fully shielded scs synthetic environmental effects

both the partially shielded and fully shielded environmental scenarios, as depicted by the magnitude coefficient plots Figure: (88) and Figure: (89) respectively.

Conversely, application of the inverse fast Fourier transform (IFFT) to the FFT coefficients, previously mentioned, results in the acquisition of time domain information regarding the partially shielded and fully shielded presumed natural effects, as shown by Figure: (90) and Figure: (91) respectively.

Similarly, a histogram of the partially shielded and fully shielded presumed natural effects, as shown by Figure: (92) and Figure: (93) respectively, reveals the existence of an

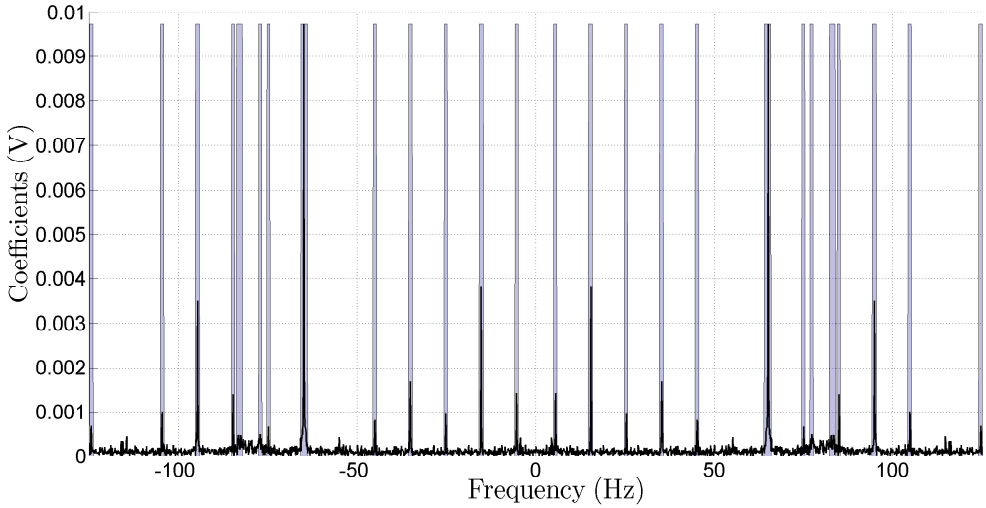

Figure 86: scs partially shielded synthetic inverted filter mask

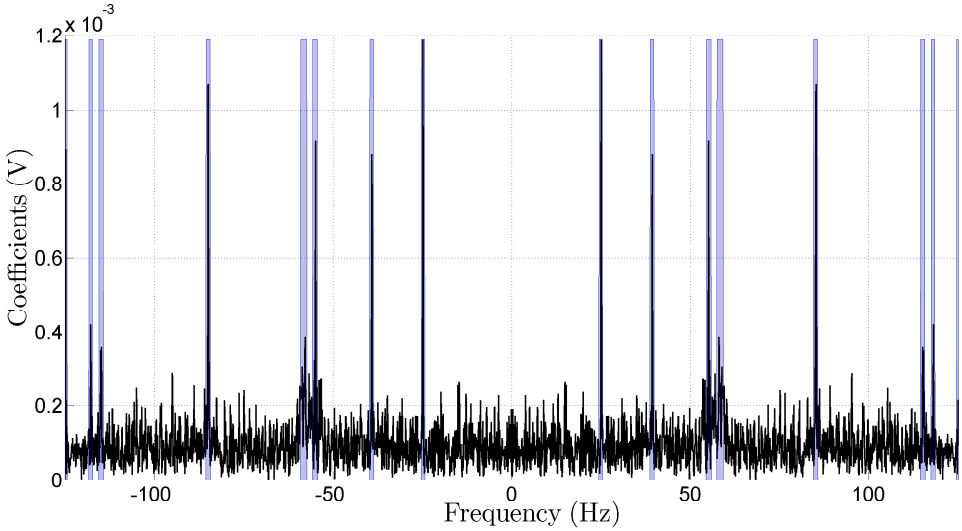

Figure 87: scs fully shielded synthetic inverted filter mask

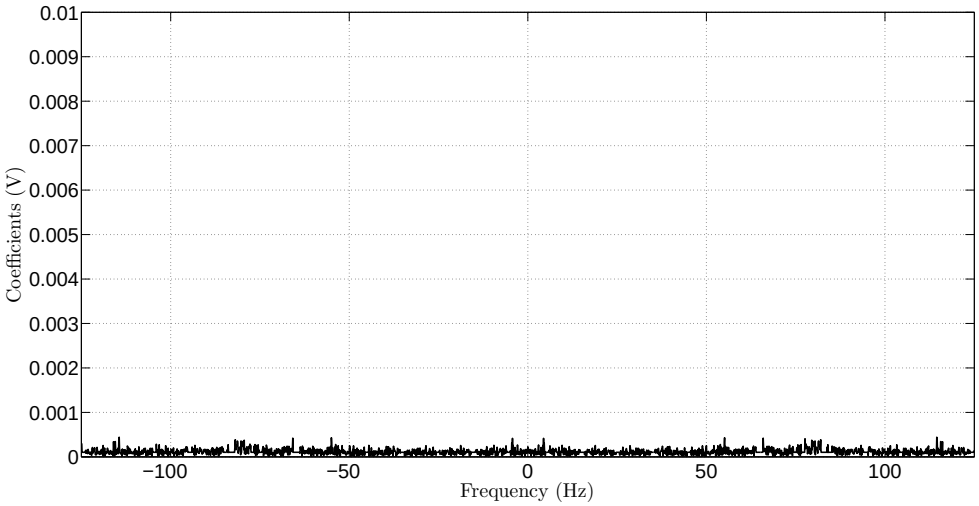

Figure 88: scs partially shielded filtered fft magnitude coefficients of natural effects

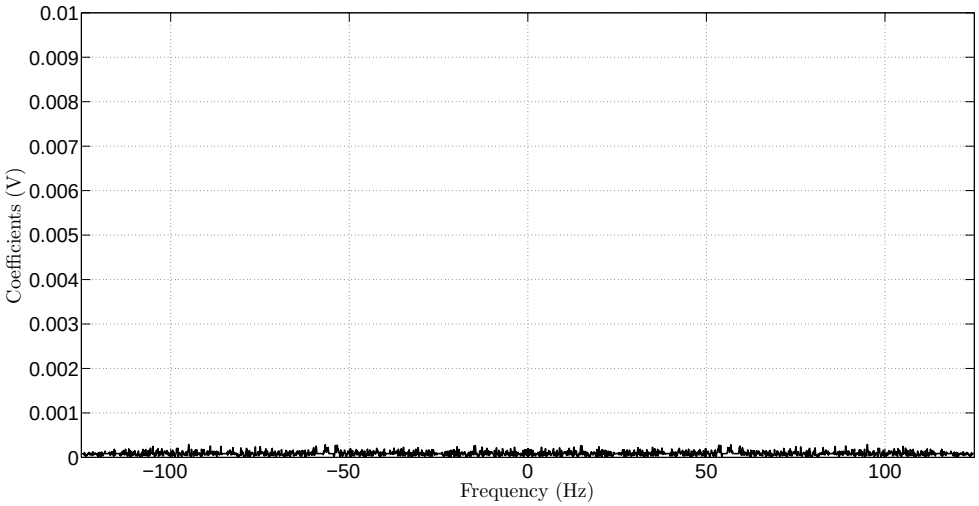

Figure 89: scs fully shielded filtered fft magnitude coefficients of natural effects

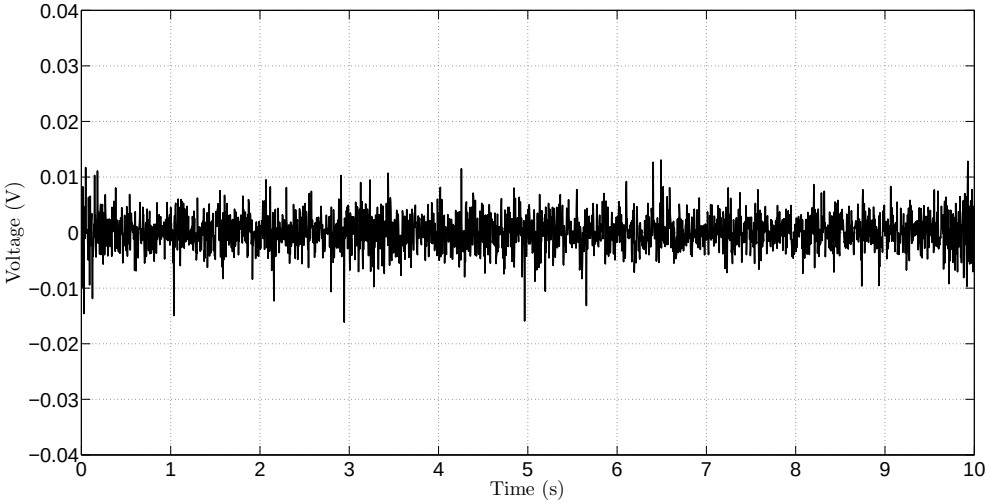

Figure 90: scs partially shielded filtered natural effects in time domain

expected Gaussian distribution, such that estimation of the Gaussian parameters can be accomplished, once again, through the utilization of the previously discussed MATLAB code, such that the partially shielded natural effects can be simulated by the utilization of those estimated parameters, as shown by Equation: (229) and Equation: (230), while the fully shielded natural effects can be simulated using those estimated parameters, as shown by Equation: (231) and Equation: (232).

$$\mu_p = 1.520 \times 10^{-4} \tag{229}$$

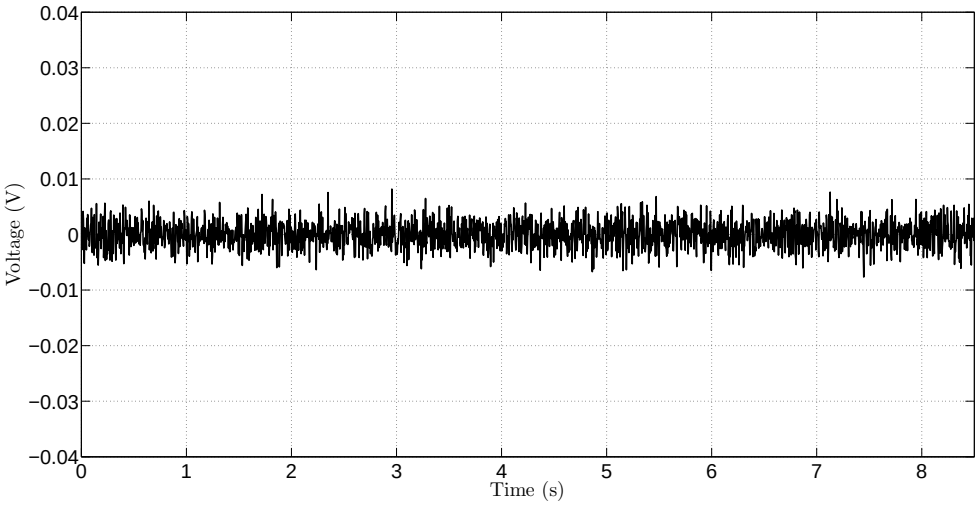

Figure 91: scs fully shielded filtered natural effects in time domain

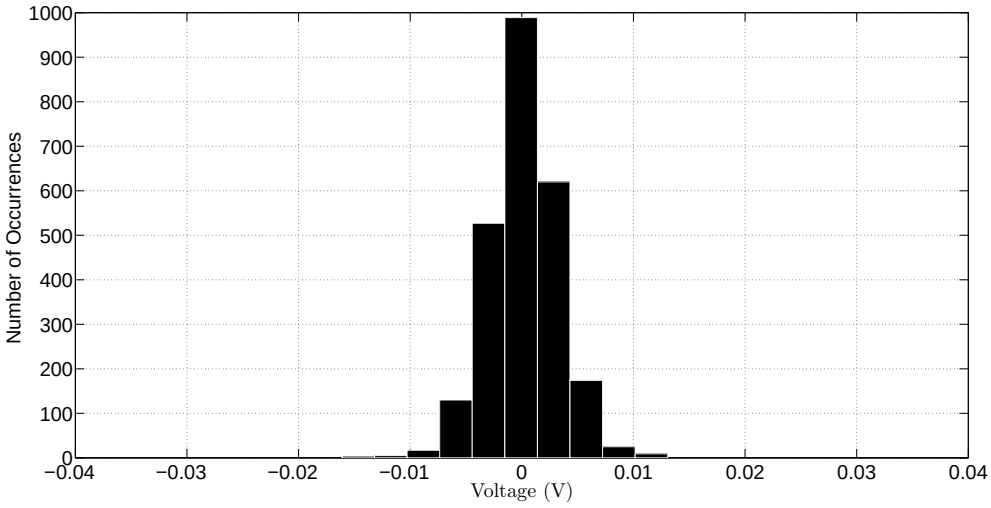

Figure 92: scs partially shielded filtered natural effects histogram

$$\sigma_p = 0.0031 \tag{230}$$

$$\mu_f = 3.7914 \times 10^{-8} \tag{231}$$

$$\sigma_f = 0.0024 \tag{232}$$

Likewise, the utilization of a random number generator with a Gaussian distribution, like the one depicted in the MATLAB code previously provided, yields, at least upon utilizing the partially shielded estimated parameters, as shown by Equation: (229) and Equation: (230), a time domain plot resembling Figure: (94) and a histogram resembling Figure: (95). Conversely, the utilization of the fully shielded estimated parameters, as shown by Equation: (231) and Equation: (232), into the, previously discussed, MATLAB Gaussian distributed random number generator, yields a time domain plot resembling Figure: (96) and a histogram resembling Figure: (97).

Similarly, the process of combining the synthetic model created, as shown by Equation: (227) and Equation: (228), with the MATLAB Gaussian distributed random number gen-

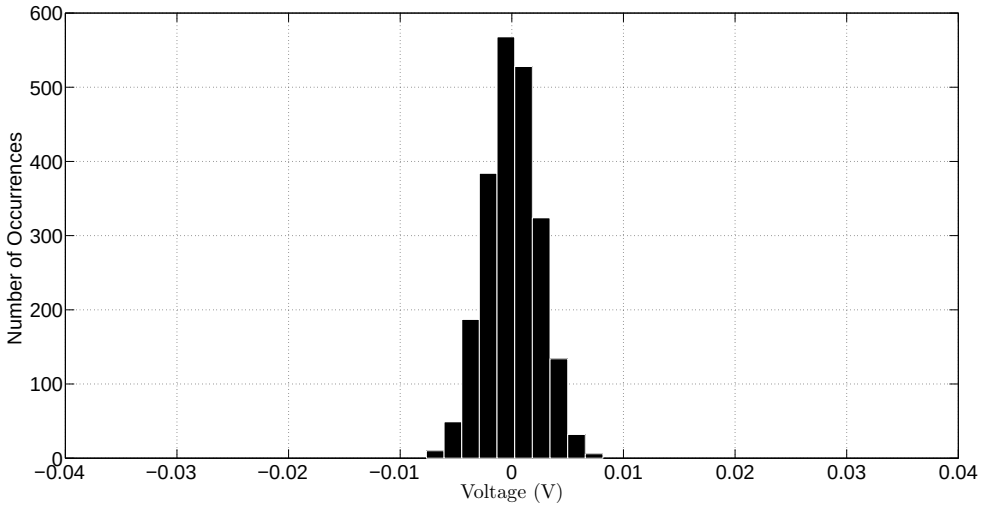

Figure 93: scs fully shielded filtered natural effects histogram

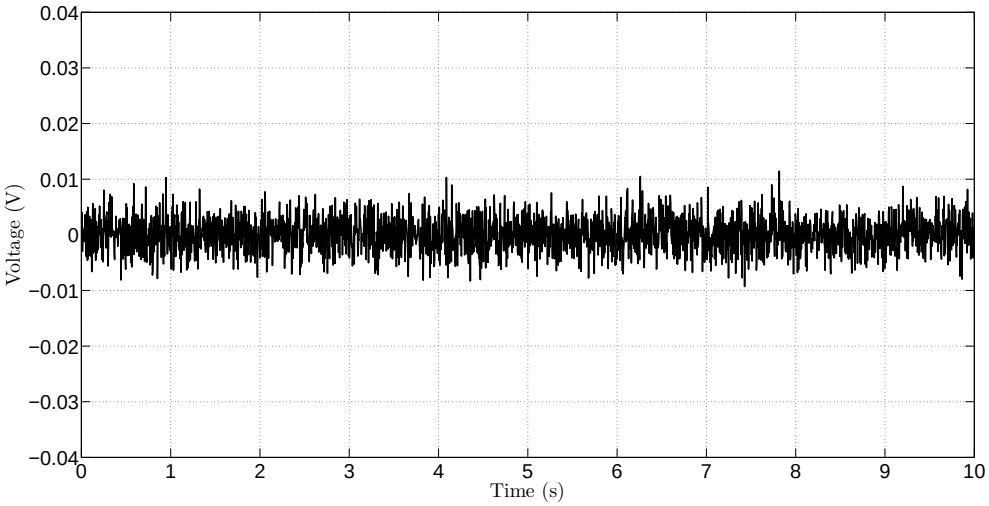

Figure 94: simulated scs partially shielded natural effects

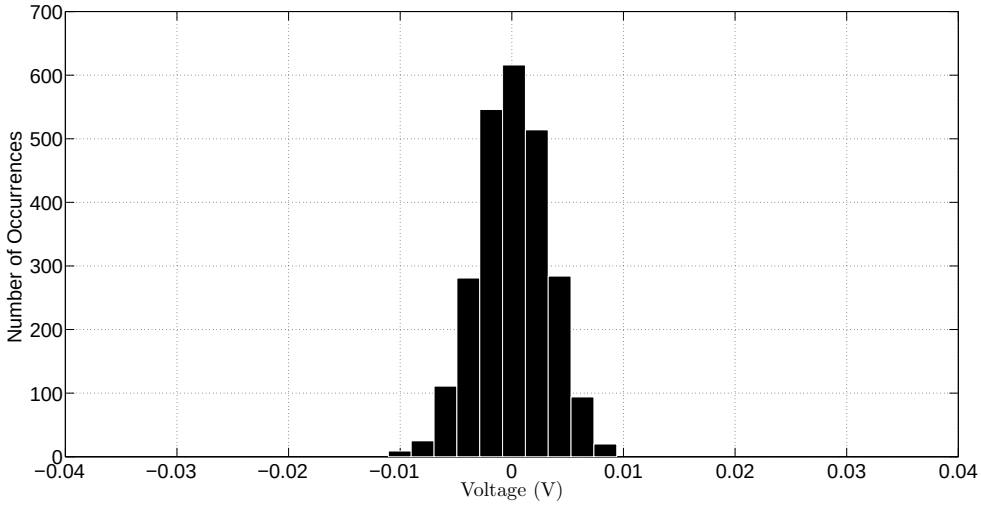

Figure 95: simulated partially shielded natural effects histogram

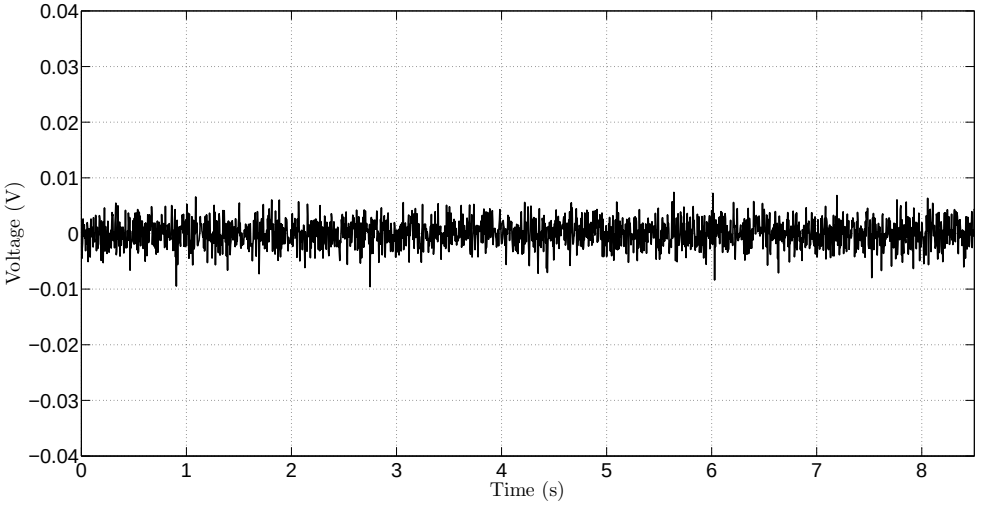

Figure 96: simulated scs fully shielded natural effects

erator, previously discussed, results in the creation of, in the case of the partially shielded scenario, Equation: (234), or, in the case of the fully shielded scenario, Equation: (236).

$$N_p(t) = S_p(t) + \text{NormRnd}(\mu_p, \sigma_p) \tag{233}$$

$$N_p(t) = S_p(t) + \text{NormRnd}(1.520 \times 10^{-4}, 0.0031) \tag{234}$$

$$N_f(t) = S_f(t) + \text{NormRnd}(\mu_f, \sigma_F) \tag{235}$$

$$N_f(t) = S_f(t) + \text{NormRnd}(3.7914 \times 10^{-8}, 0.0024) \tag{236}$$

Likewise, graphical inspection of the partially shielded environmental equation, as shown by Equation: (234), over the time span previously measured, results in the creation of a simulated partially shielded time domain plot, as shown by Figure: (98), and corresponding amplitude histogram, as shown by Figure: (99). Conversely, a similar inspection of the fully shielded environmental equation, as shown by Equation: (236), once again over the time span previously measured, results in the creation of a simulated fully shielded time domain

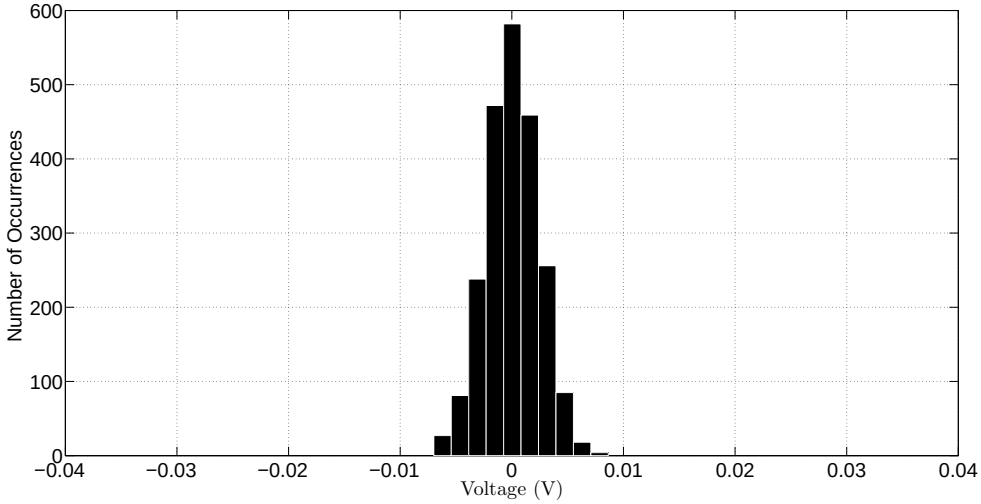

Figure 97: simulated fully shielded natural effects histogram

plot, as shown by Figure: (100), and a corresponding amplitude histogram, as shown by Figure: (101).

Similarly, a periodogram of the partially shielded time domain simulations, as shown by Figure: (102), indicates the existence of a visually similar spectral power density as the previously depicted laboratory periodogram, and a similar analysis between the fully shielded simulated periodogram, obtained using the methods previously described, as shown by Figure: (103), also produced a visually similar spectral power density upon comparison with prior to laboratory observations. Yet, despite such observable similarities inevitably re-

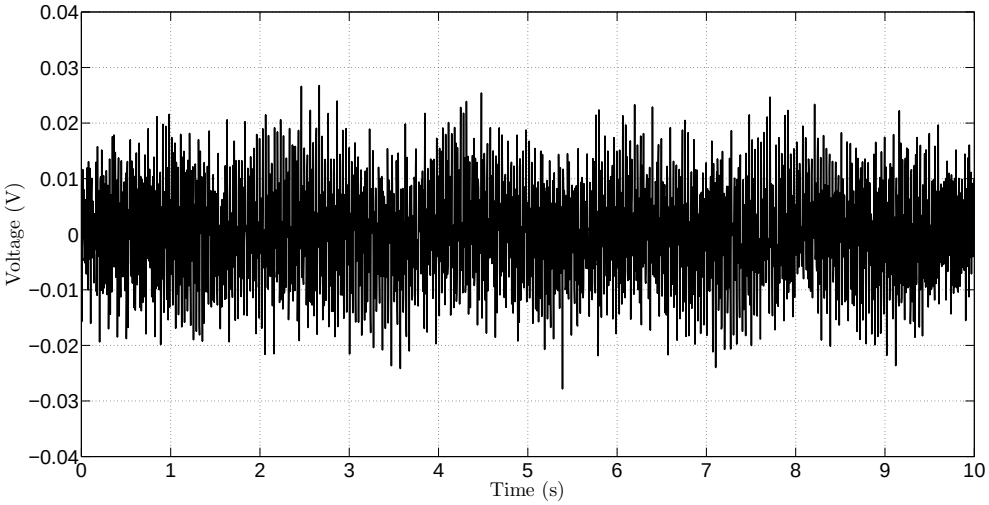

Figure 98: high-z simulated scs partially shielded environmental effects

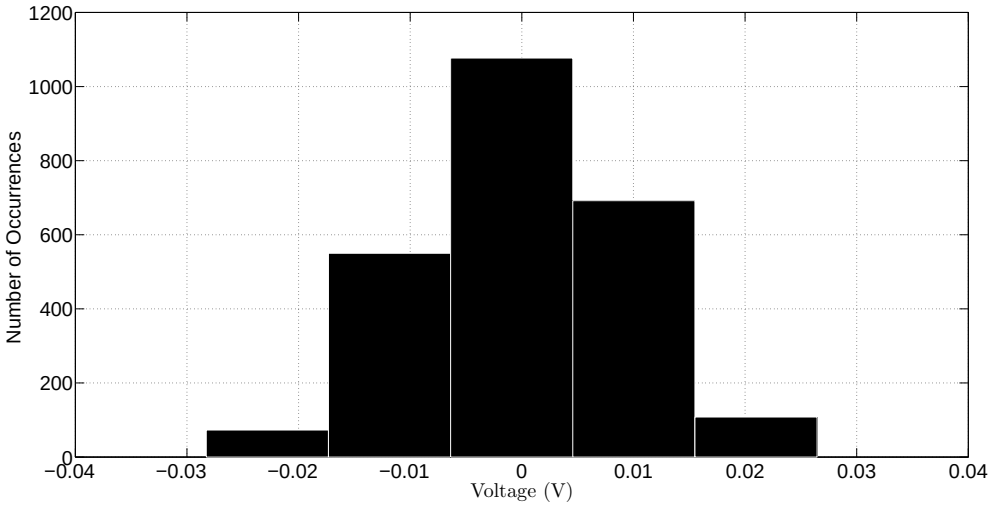

Figure 99: high-z simulated scs partially shielded environmental effects histogram

quiring further analysis to quantify; however, the existence of such visual similarities, while not necessarily providing quantitative information regarding the overall models accuracy, is still fundamentally a good metaphoric omen that the techniques being utilized are, at the very least, appearing to be somewhat applicable.

Nevertheless, side-by-side comparison of the partially shielded time domain measurements with the simulated model, as shown by Figure: (104), does help support the previously presented visual observation — once again referring to the partially shielded scenario — while a similar comparison of the fully shielded time domain measurements with the simu-

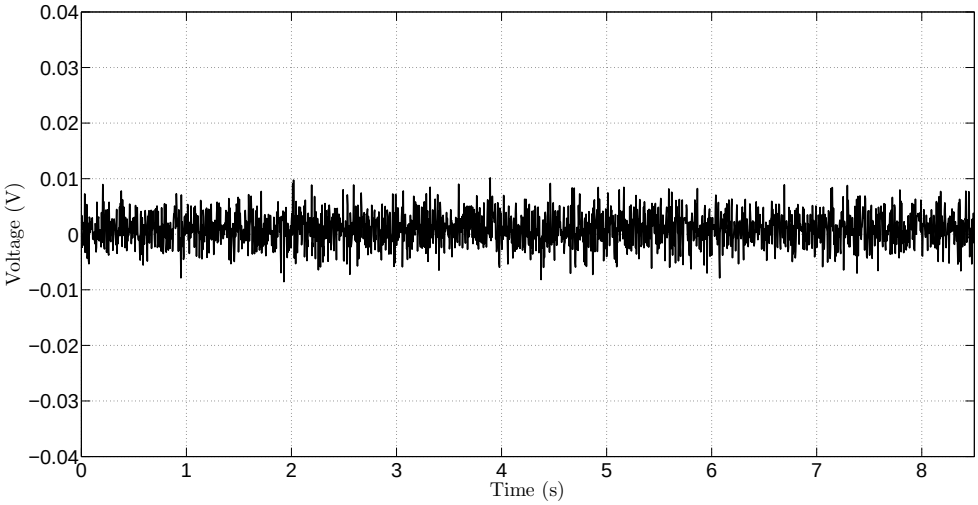

Figure 100: high-z simulated scs fully shielded environmental effects

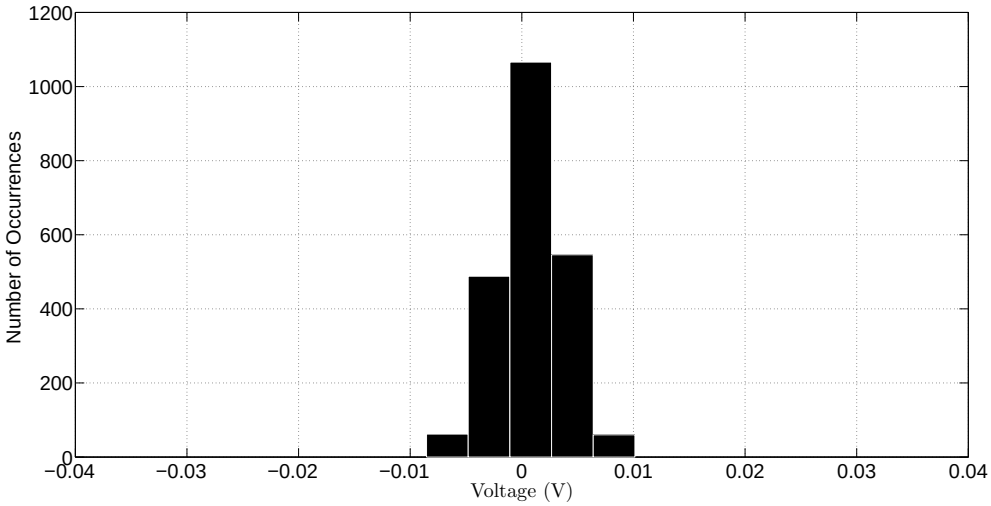

Figure 101: high-z simulated scs fully shielded environmental effects histogram

lated model, as shown by Figure: (105), also helps vindicate the previous visual assessment. Yet, although the incorporation of a stochastic component into the environmental model, previously expressed, does make a traditional time domain point-by-point comparison between a synthetic model and a laboratory measurement, at any given time, rather dubious; however, upon visual review of the power spectral density plot or time domain amplitude histogram, such models, as those previously expressed, do appear to provide a reasonable approximation of the environmental effects encountered. Likewise, while the comparison between the measured and simulated environmental effects, as shown by Figure: (69), Fig-

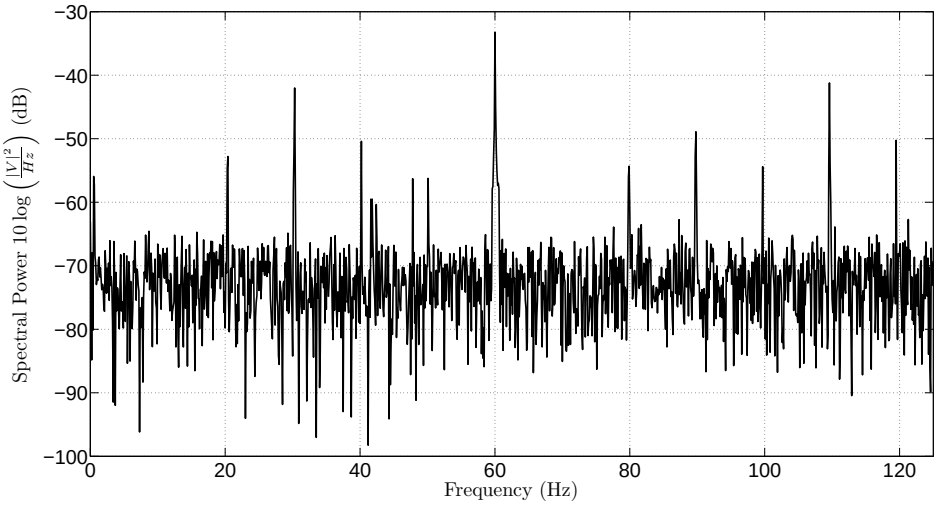

Figure 102: high-z simulated scs partially shielded environmental effects periodogram

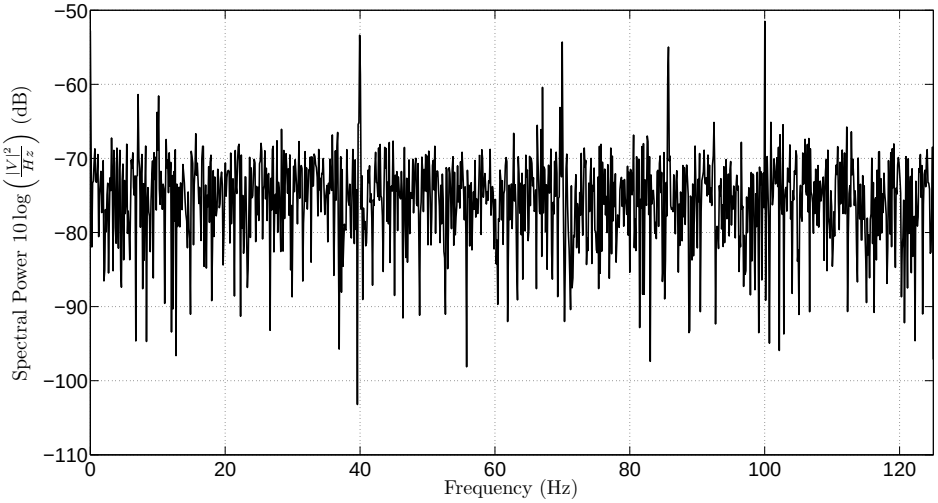

Figure 103: high-z simulated scs fully shielded environmental effects periodogram

ure: (104), and Figure: (105), does provide some reassurance that the models developed, at least for each SCS environmental scenario previously discussed, is capable of providing a reasonable visual approximation of the signals measured; however, a more quantifiable comparison that is based upon percent error and percent difference, as shown by Equation: (237) and Equation: (238), can be utilized to obtain a numerical quantity that describes

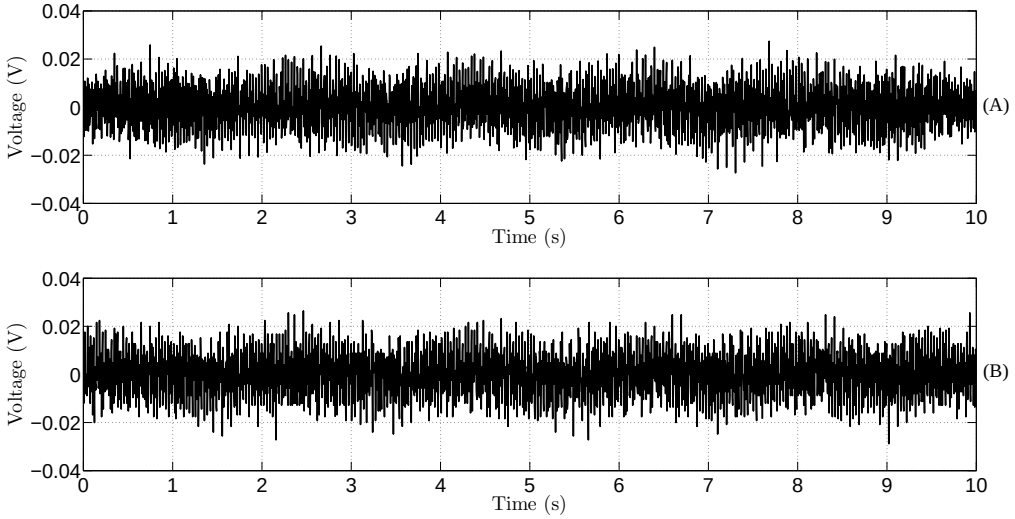

Figure 104: (plot a) high-z simulated scs partially shielded environmental effects versus (plot b) high-z measured scs partially shielded environmental effects

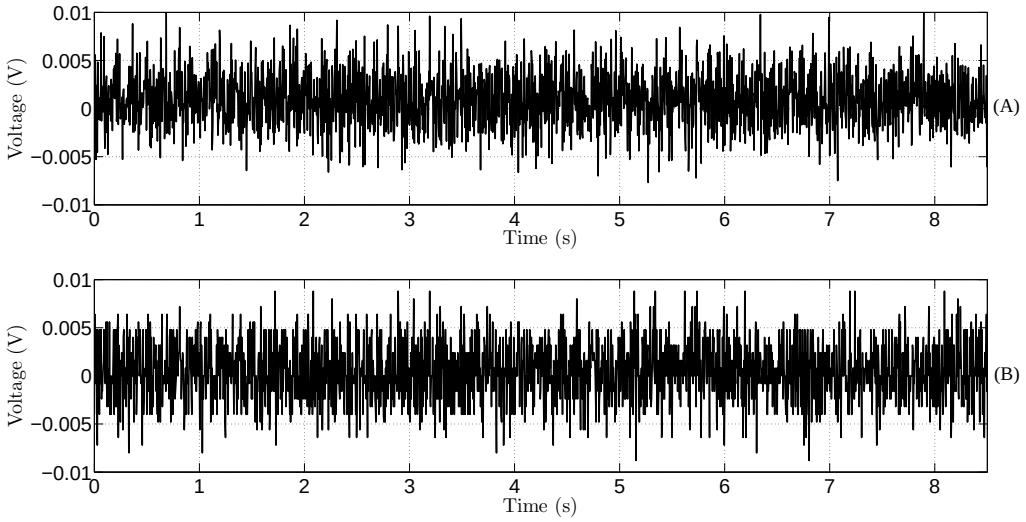

Figure 105: (plot a) high-z simulated scs fully shielded environmental effects versus (plot b) high-z measured scs fully shielded environmental effects

the overall dissimilarities between the models developed versus the measurements obtained.

$$E_{\%}(k) = \left(\frac{M(k) - S(k)}{M(k)} \right) 100\% \tag{237}$$

$$E_{\Delta\%}(k) = \left(\frac{|M(k) - S(k)|}{\frac{|M(k)+S(k)|}{2}} \right) 100\% \tag{238}$$

Conversely, quantifiable error analysis of the unshielded environmental conditions, at least upon comparison of the relative difference between the measured power spectrum density and the simulated power spectrum density, as shown by Figure: (106), indicates that enough similarity between the two signals existed, at least upon subtracting the simulated results from the measurements obtained, that an approximate signal with a delta of 50 dB in value was created that remained relatively constant across the frequency window selected. Yet, while the signal created, upon application of the difference operation, is generally considered to have a relatively small value; however, it is important to note that the value of the signal created also has the same order of magnitude as the natural environmental effects observed, and that such graphical depictions, while showing that the model created approximated the synthetic effects observed reasonably well, does not, in its current form, inherently convey the same level of accuracy for the natural effects observed.

Thus, in order to better examine the accuracy of the unshielded synthetic model versus the measured observations, a point by point percent error and percent difference comparison between the two periodograms, previously provided, was calculated, as shown by Figure: (108) and Figure: (107) respectively. Likewise, visual inspection of Figure: (107) indicates that the simulated model, at lease at any particular frequency, will conservatively vary from the measured power spectral density value by approximately ± 20 percent, while a visual

inspection of Figure: (108), appears to also convey the same overall percentage. Yet, while both Figure: (107) and Figure: (108) have a number of frequencies that differ between the simulated and measured value by an amount above 40 percent; however, the majority of variations observed are, in fact, visually below 20 percent and half of those below 20 percent are visually below 10 percent.

Conversely, while such variations between the simulated model and the measured labo-

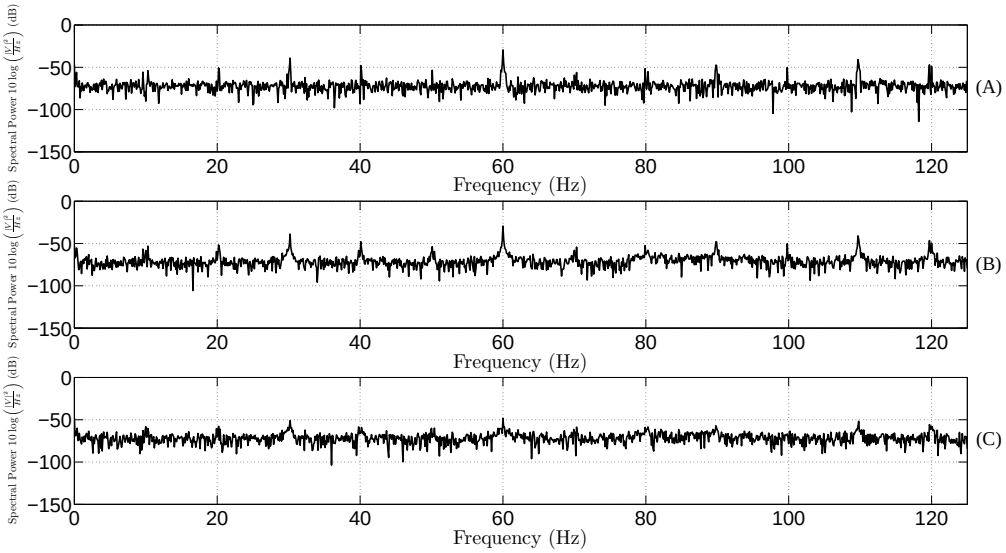

Figure 106: (plot a) high-z simulated scs unshielded environmental effects versus (plot b) high-z measured scs unshielded environmental effects versus (plot c) the difference between plot b and plot a

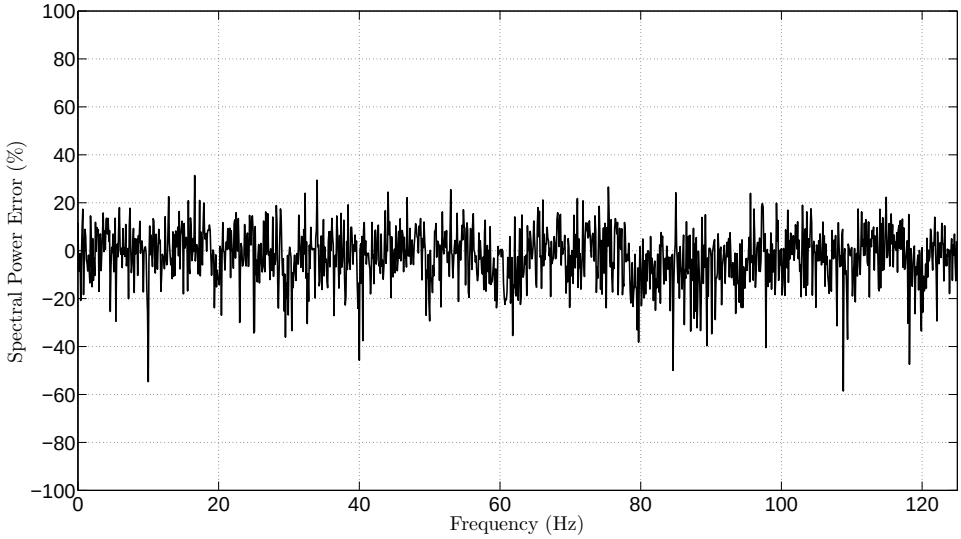

Figure 107: high-z simulated versus measured scs unshielded environmental effects percent error periodogram

ratory observations might, at first, appear somewhat substantial; however, because the numbers being compared are, in themselves relatively small, the actual variation observed is, in fact, not as substantial as it might at first appear. Similarly, because the units previously compared — although used with some frequency when working within the electromagnetics research area — are not regularly utilized within the electrical engineering discipline, thus the rationalization behind such percentile comparisons, like those previously presented, is something that tends to be inherently difficult for most electrical engineers to conceptualize, at least based upon given the overall lack of familiarity with the power spectral density unit and the associated percentile comparisons. Conversely, to help clarify such uncertainties, while also presenting the error analysis using an alternative method, the previously examined amplitude histograms, as shown by Figure: (52) and Figure: (67), between the SCS High-Z unshielded simulated and measured signals can be compared in terms of percent error and percent difference, as shown by Figure: (109) and Figure: (110). Likewise, while the periodogram based analysis, previously discussed, fundamentally examines the frequencies needed to re-create a particular signal, alternatively the amplitude

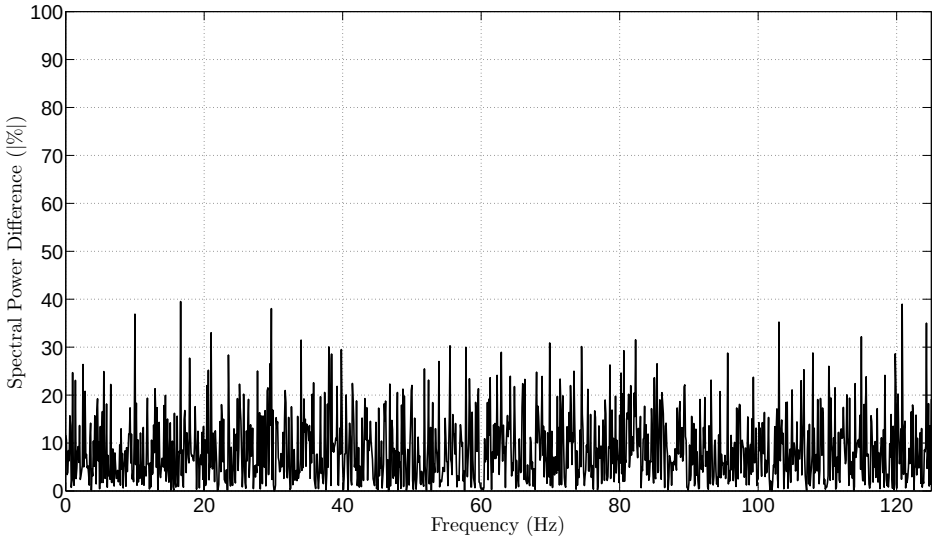

Figure 108: high-z simulated versus measured scs unshielded environmental effects percent difference periodogram

histogram, as shown by Figure: (52) and Figure: (67), counts the number of times a particular amplitude occurred, and such a method is particularly useful when the amplitude being measured is based upon a pseudo-stochastic process, like the one previously provided, since it allows for the estimation of the likelihood that a given amplitude will occur. Conversely, the percent error and percent difference calculation of an amplitude histogram, as shown by Figure: (109) and Figure: (110), is fundamentally comparing the effectiveness

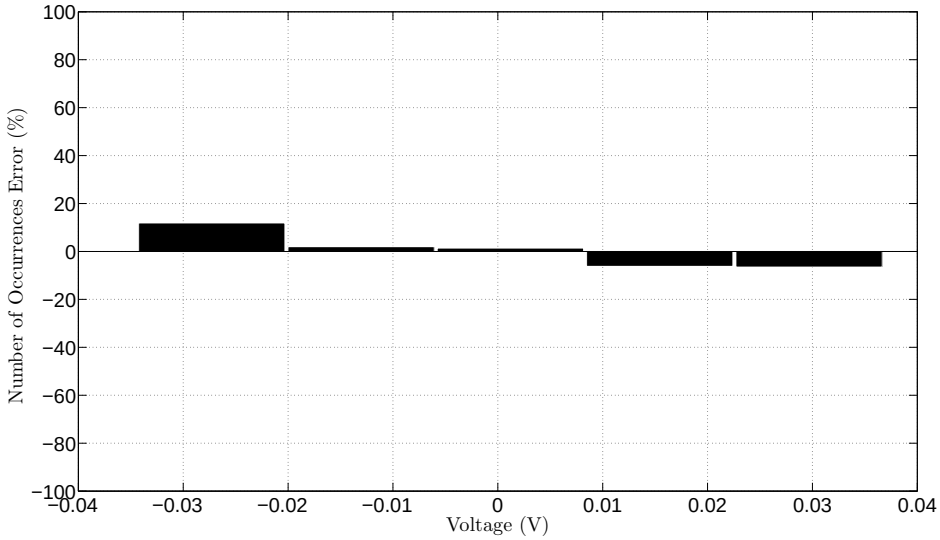

Figure 109: high-z simulated versus measured scs unshielded environmental effects percent error histogram

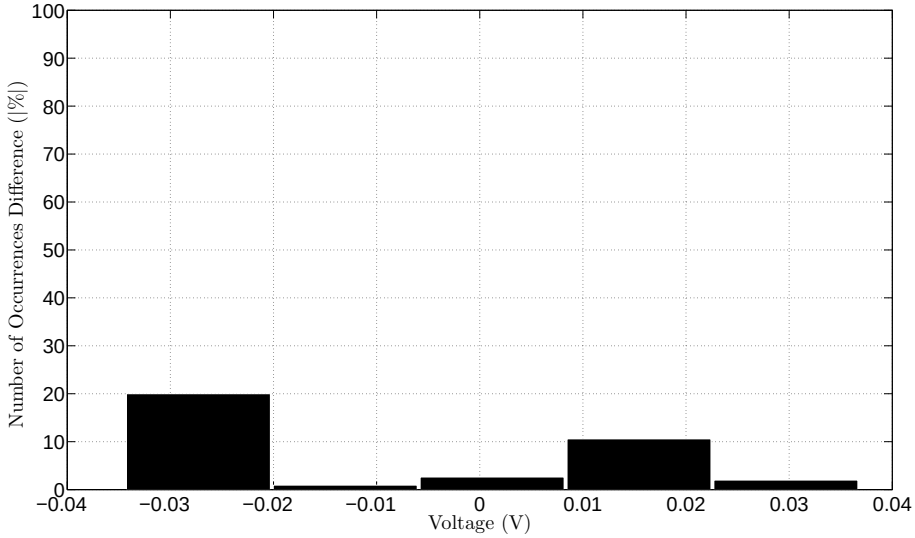

Figure 110: high-z simulated versus measured scs unshielded environmental effects percent difference histogram

of the pseudo-stochastic process utilized by the model to the pseudo-stochastic process observed in the unshielded SCS environment. Likewise, based upon the information depicted within Figure: (109) and Figure: (110), it is clearly visible that the amplitude occurrence rate, upon comparison to the simulated model, is below the ±20 percent error rate, and is actually lower than the ±10 percent error rate between the ±20 mV signal boundary. Conversely, the small percent error and percent difference, previously discussed, implies that the pseudo-stochastic model developed is reasonably approximating the pseudo-stochastic process measured in the unshielded SCS environment, while the slightly higher percent error and percent difference observed in the — previously examined — periodogram, indicates that certain frequency estimations of the unshielded SCS model are slightly incorrect; however, such errors appear, at least upon consideration of the overall accuracy of the model, relatively minor, especially given the pseudo-stochastic properties of the environment being modeled.

Similarly, examination between the partially shielded SCS simulated versus measured periodogram, as shown by Figure: (111), reveals a signal that is slightly lower than 50 dB

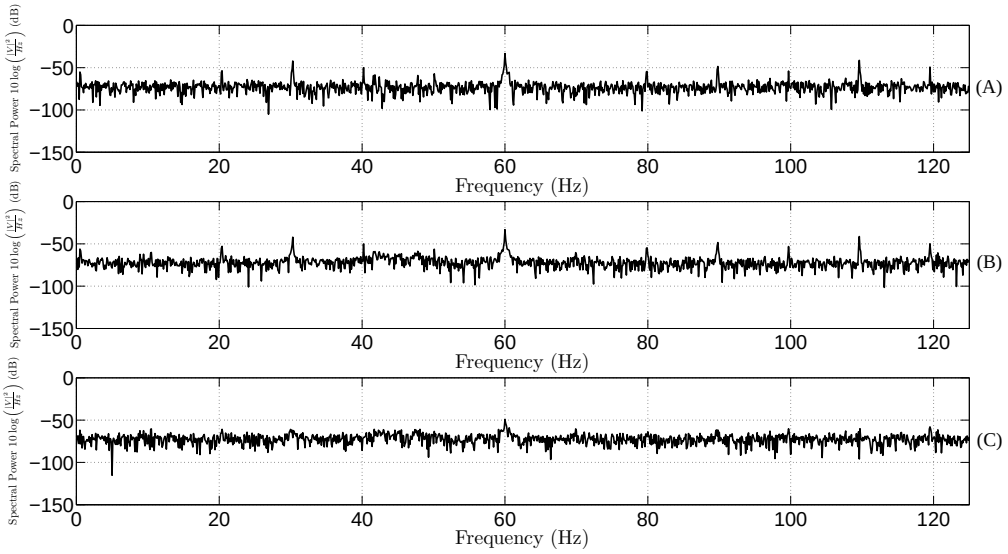

Figure 111: (plot a) high-z simulated scs partially shielded environmental effects versus (plot b) high-z measured scs partially shielded environmental effects versus (plot c) the difference between plot b and plot a

— created upon subtracting the simulated signal from the measured signal — that not only resembles the unshielded case, as shown by Figure: (106), but also possesses similar attributes, once again previously discussed, that rationalize why the signal is approximately the same order of magnitude as the identified natural environmental effects. Conversely, examination of the percent error and percent difference between the simulated versus measured periodograms, as shown by Figure: (112) and Figure: (113), reveals a slightly lower number of peak errors — which is defined as particular frequencies where the error briefly jumps to around 40 percent and then falls below the visual average error rate rapidly at near frequencies — and a similar 20 percent error range, in which half of those errors are below 10 percent, that resembles the unshielded case previously discussed.

Likewise, examination of the amplitude histograms, as shown by Figure: (114) and Figure: (115), reveal a similar percent error rate, as previously discussed upon examining the unshielded amplitude histogram, between the ±20 mV signal boundary, but a slightly higher error rate outside of the boundary. Conversely, such consistency between error rates in the unshielded and partially shielded scenario seems to imply that the natural and

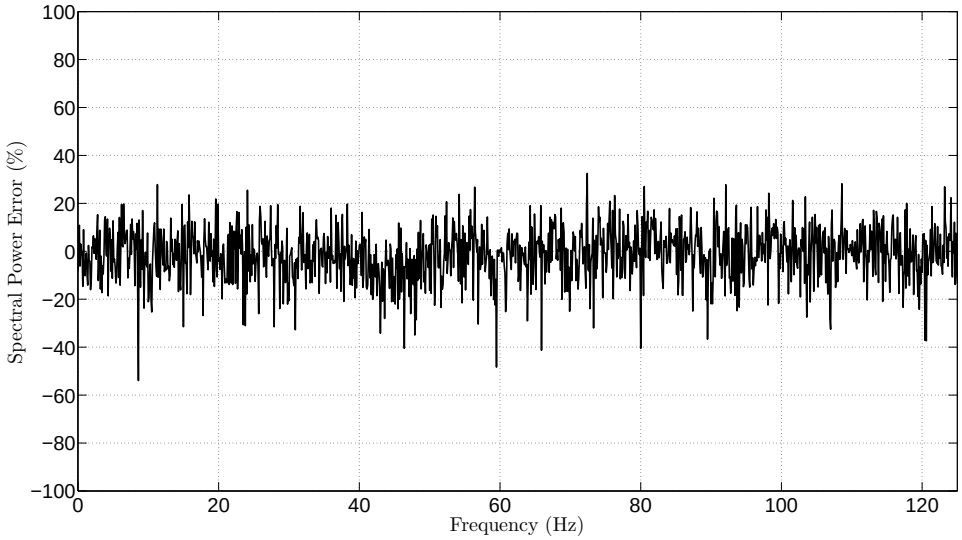

Figure 112: high-z simulated versus measured scs partially shielded environmental effects percent error periodogram

synthetic environmental effects encountered, while being reduced in magnitude upon the introduction of partial shielding, are fundamentally similar, insofar as, the methodology, previously developed, to model both the synthetic and natural effects appears to remain relatively consistent in its overall effectiveness. Similarly, the existence of such consistency between the unshielded and partially shielded scenario, tends to imply that minor improvements to the, previously mentioned, methodology would improve the overall accuracy of the unshielded and partially shielded model, and given the techniques applied, within the methodology utilized, the most obvious improvements would be to change the Gaussian distribution utilized to something that better fits the observed amplitude and spectral histograms. Yet, while such changes might improve the overall accuracy of the unshielded and partially shielded models created; however, such changes would also require increasing the models overall complexity, since simulating a custom numerical distribution would also require creating a random number generator that would produce the desired distribution, and although this task is not necessarily difficult, such improvements, at least upon considering the fundamental pseudo-stochastic nature of environmental effects, are hard to justify

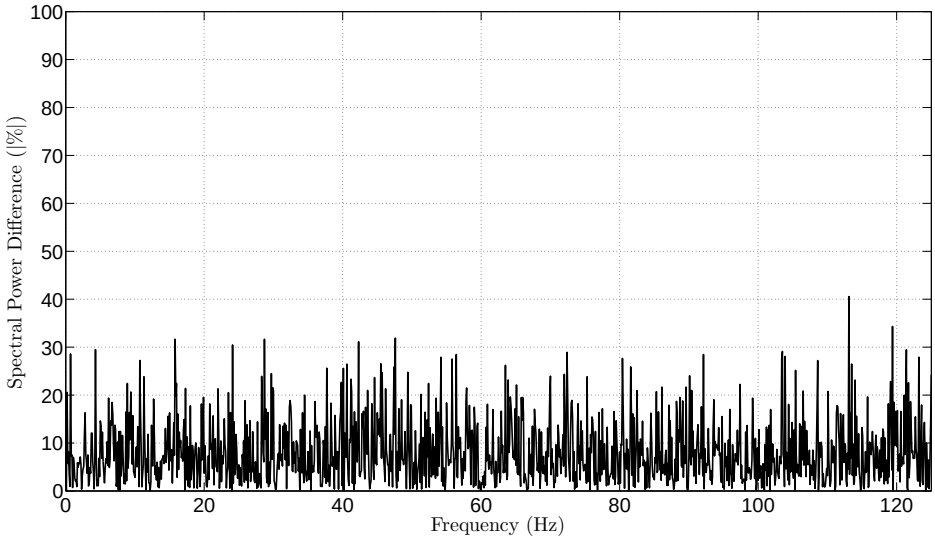

Figure 113: high-z simulated versus measured scs partially shielded environmental effects percent difference periodogram

given the current level of accuracy already obtained.

Thus, while these improvements in accuracy are definitively possible, should the need for additional accuracy of SCS environmental conditions arise; however, such improvements were not incorporated into the, previously discussed, unshielded and partially shielded models since the level of accuracy already obtained is more than sufficient for most applications. Likewise, examination between the fully shielded SCS simulated versus measured

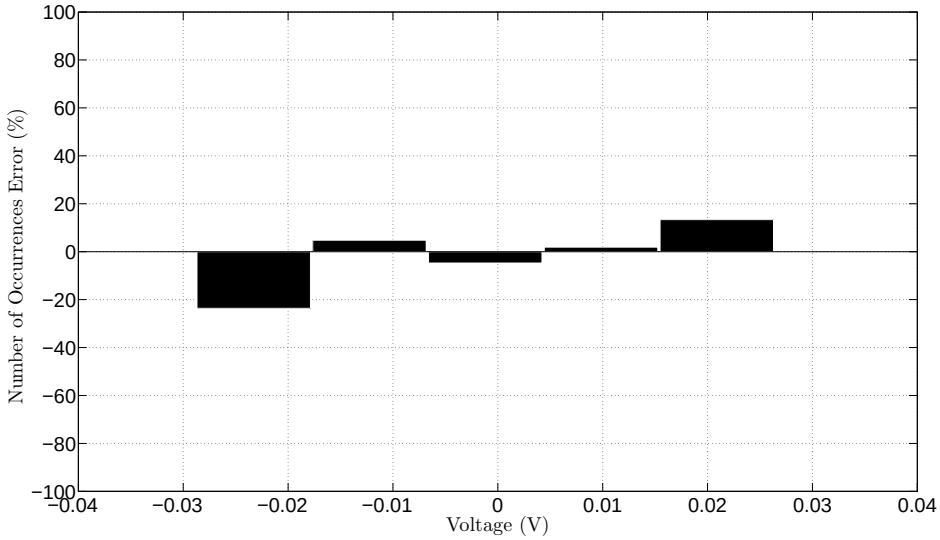

Figure 114: high-z simulated versus measured scs partially shielded environmental effects percent error histogram

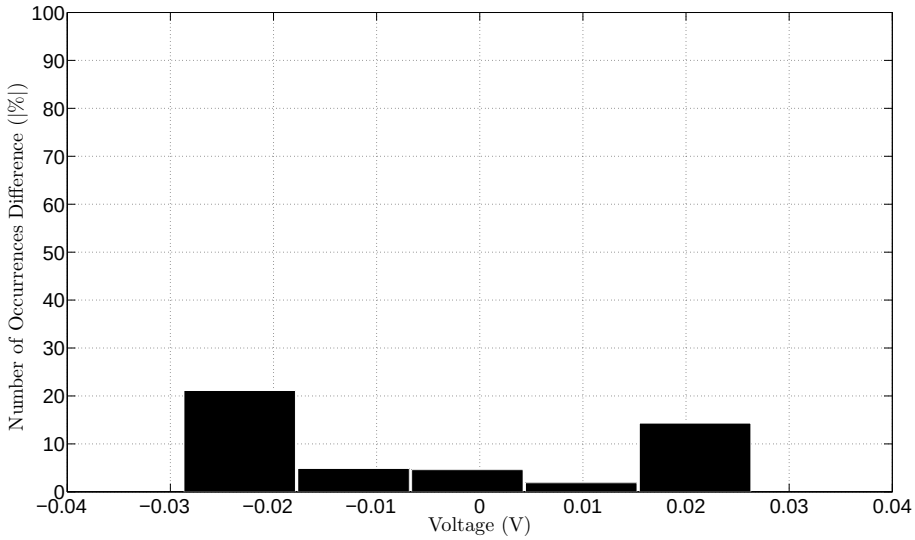

Figure 115: high-z simulated versus measured scs partially shielded environmental effects percent difference histogram

periodogram, as shown by Figure: (116), once again reveals a signal that is slightly lower than 50 dB — created upon subtracting the simulated signal from the measured signal — that not only resembles the unshielded case and the partially shielded case, but also possesses similar attributes, as previously discussed, that further rationalizes why the signal is approximately the same order of magnitude as the previously identified natural environmental effects. Conversely, examination of the percent error and percent difference between the simulated versus measured fully shielded periodograms, as shown by Figure: (117) and Figure: (118), reveals a slightly higher number of peak errors — which is defined as particular frequencies where the error briefly jumps to around 40 to 50 percent and then falls below the visual average error rate rapidly at near frequencies — and a similar 20 percent error range, in which half of those errors are around 10 percent, that resembles the unshielded and partially shielded cases previously discussed.

Likewise, examination of the amplitude histograms, as shown by Figure: (119) and Figure: (120), reveal a similar percent error rate, as previously discussed upon examining the unshielded and partially shielded amplitude histogram, between the ±5 mV signal boundary,

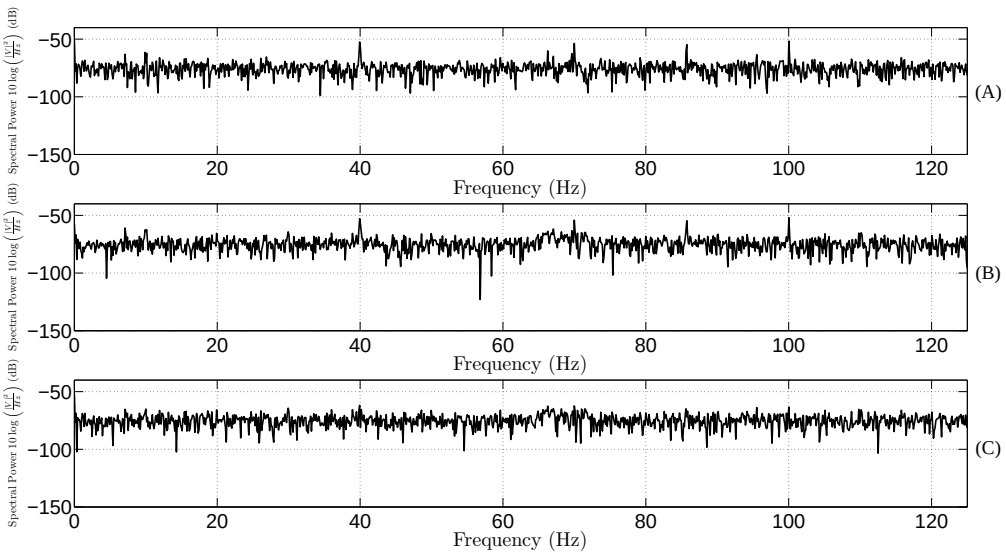

Figure 116: (plot a) high-z simulated scs fully shielded environmental effects versus (plot b) high-z measured scs fully shielded environmental effects versus (plot c) the difference between plot b and plot a

but a significantly higher error rate, on the order of 30 to 80 percent, beyond this boundary. Conversely, while such sizable values of percent error and percent difference do appear extremely large; however, given the small amplitude of the fully shielded signal being observed and the pseudo-stochastic nature of the model, a number of possible explanations exist for the occurrence of such sizable values. Likewise, out of those explanations, while not necessarily being at the forefront of the list, it was previously — though briefly —

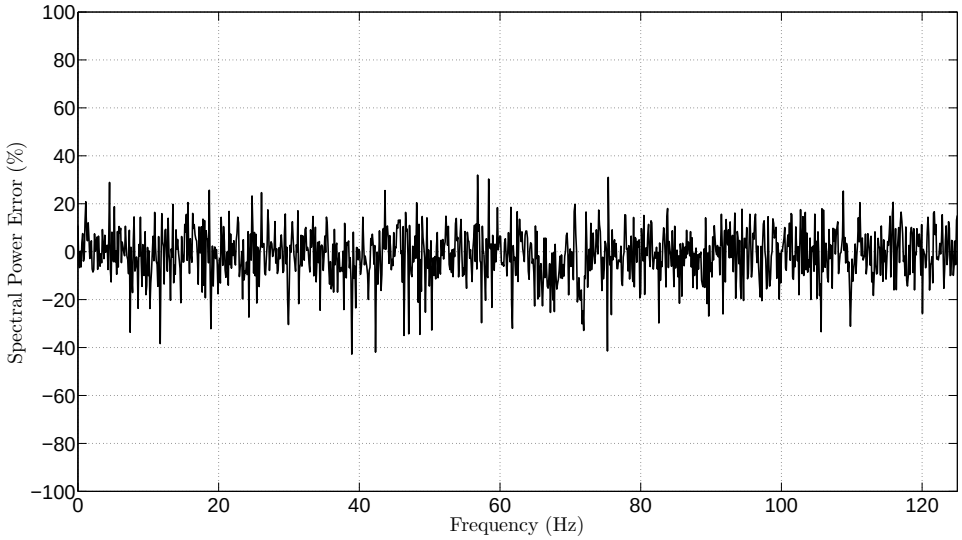

Figure 117: high-z simulated versus measured scs fully shielded environmental effects percent error periodogram

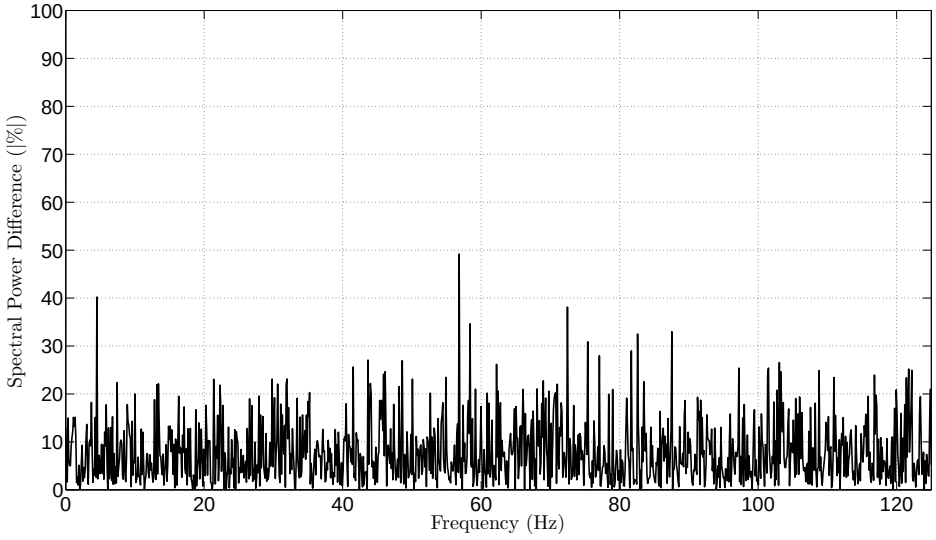

Figure 118: high-z simulated versus measured scs fully shielded environmental effects percent difference periodogram

mentioned, that some of these observed errors could be attributed to the undiscussed topic of instrumentational effects, since, after all, the signals being observed were approaching the acquisition limits of the laboratory measuring apparatus. Conversely, such errors could also be, just as easily, attributed to the physical changes that occurred upon changing the shielding environment, since the fully shielded environment is radically different from the unshielded and partially shielded environment, insofar as, the fully shielded environment

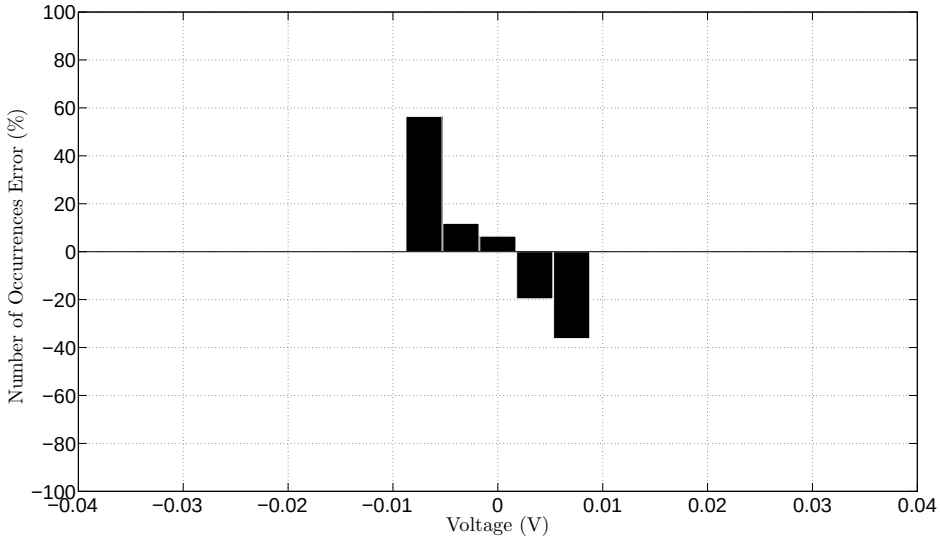

Figure 119: high-z simulated versus measured scs fully shielded environmental effects percent error periodogram

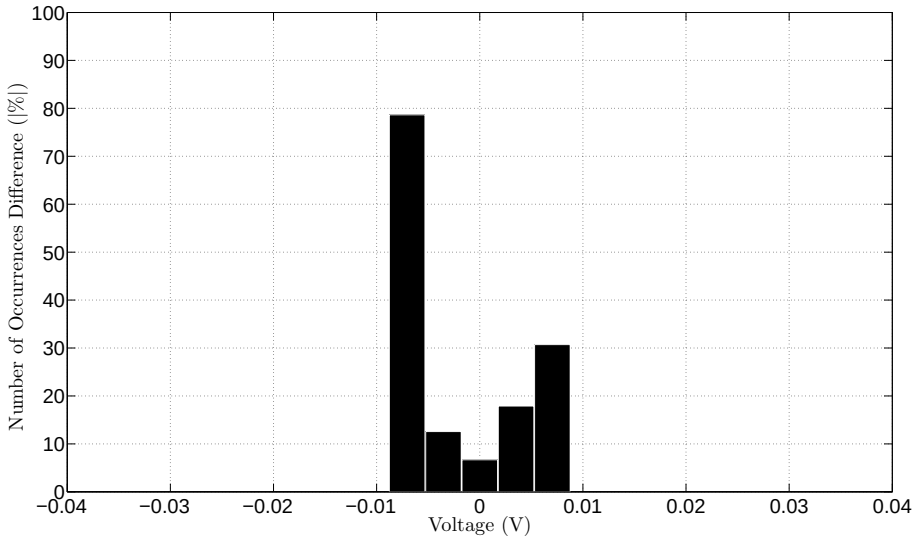

Figure 120: high-z simulated versus measured scs fully shielded environmental effects percent difference periodogram

utilized electrical isolation from the SCS internal electrical distribution network and, as a result, the significant drop in synthetic effects observed could have made the assumed, three times the mean signal separation boundary, previously discussed, an insufficient or inaccurate point of separation to isolate the remaining synthetic effects from the, now predominant, natural effects. Thus, based upon this particular scenario, it would seem only natural that some of the errors encountered might be attributed to incorrect mathematical modeling since, after all, if a particular frequency was modeled using an assumed periodic synthetic model when, in fact, that particular frequency was either governed by stochastic or aperiodic processes then observing such errors would not only be logical but would also be expected. Yet, despite such observations, it is interesting to note that the percent error and percent difference calculated, at least upon examining the periodograms, appears to remain reasonably consistent, unlike the error observed upon examining the amplitude histograms, and such consistency tends to imply that, for the most part, the spectral component of the model created appears to be a reasonably accurate estimation, even if the error observed within the amplitude histograms seems somewhat dubious.

Nevertheless, while a discrete point-by-point (k) percent error and percent difference comparison can be useful, it is important to recognize that the pseudo-stochastic nature of the model makes the analysis of a singular simulation, like the ones previously presented, somewhat of a moot point, since such pseudo-stochastic processes, found within the model utilized, requires the error analysis of a sizable number of simulations in order to determine a realistic estimation of the models overall accuracy; although, it is also worth mentioning that a complete estimation of the current models overall effectiveness would require an extensive amount of measured laboratory data of the, previously mentioned, environmental shielding conditions that existed and such an in-depth analysis, because it was well beyond

the intended depth of study, was not conducted. Furthermore, because the minimum, mean, and maximum percent error and percent difference, once again for each shielding scenario, is typically considered more beneficial, especially when it comes to real world implementation and possible environmental compensation, the calculated positive and negative minimum and maximum percent error values obtained, along with the average percent error, between the simulated and measured environmental models for the unshielded, partially shielded, and fully shielded scenario was tabulated from twenty thousand computational executions of the techniques utilized to calculate the, previously provided, percent error and percent difference periodograms and histograms. Conversely, the twenty thousand simulations of environmental effects, once again calculated utilizing the simulated environmental models previously discussed, yielded a periodogram percent error table, as shown by Table: (1), that contains information regarding the minimum, mean, and maximum percent error encountered for each shielding scenario previously discussed. Likewise, to better clarify the error encountered, the minimum and maximum values obtained was separated into two categories: the first category isolated positive values of percent error encountered, while the second category isolated negative values of percent error encountered. Similarly, each of the categories, previously mentioned, were separated into two subcategories: the first subcategory examines the largest, or sub-maximum, occurrence of percent error observed, based upon the criteria defined by the prior category — or to better clarify this point, the number found under the minimum positive sub-maximum section of the table would represent the smallest positive percent error encountered out of twenty thousand simulations — while the second subcategory examines the sub-average occurrence of percent error observed — or the number found under the minimum positive sub-average section of the table would represent the average smallest positive percent error encountered out of twenty

thousand simulations.

Table 1: twenty thousand test comparisons between the simulated versus measured periodogram percent error for each scs environmental model presented

Periodogram Percent Error									
Model	Min				Mean	Max			
	+		-			+		-	
	Max	Mean	Max	Mean		Max	Mean	Max	Mean
Unshielded	1.1443	0.0202	-5.4921	-0.0239	-1.8822	41.7843	31.9177	-123.277	-60.6869
Partly Shielded	2.49	0.0522	-1.389	-0.0242	-1.472	39.78	31.86	-132.42	-49.55
Fully Shielded	2.2013	0.023	-4.083	-0.033	-0.8926	48.87	41.13	-97.52	-46.66

Likewise, to clarify this particular point further, based upon the values shown within Table: (1), or more specifically, the maximum negative sub-maximum percent error of approximately –123 percent implies that, out of twenty thousand simulations, the largest negative error found after a K point-by-point comparison was –123 percent, while the average negative maximum error encountered, or maximum negative sub-average, after twenty thousand K point-by-point comparisons, was approximately –61 percent. Conversely, while such numbers might seem rather large, it is important to recognize that the maximum and minimum values tabulated do, in fact, represent the worst values obtained, within its general category, after twenty thousand K point-by-point comparisons, and such comparisons are not directly representative of the overall models accuracy, but rather represent the generally more conservative designer guidelines for possible model deviation. Thus, keeping such concepts under advisement, based upon the information presented within Table: (1), it can be concluded that the average accuracy of the models, previously presented, at least from a periodogram perspective, is approximately 98 percent, or alternatively that these models, on average, have less than 2 percent error relative to the laboratory events measured.

Likewise, a similar analysis of the amplitude histogram percent error, as shown by Table: (2), reveals a slightly higher average percent error that yields an approximate 97 percent model accuracy, or alternatively, that these models, on average, have less than 3 percent

Table 2: twenty thousand test comparisons between the simulated versus measured amplitude histogram percent error for each scs environmental model presented

Histogram Percent Error									
Model	Min				Mean	Max			
	+		-			+		-	
	Max	Mean	Max	Mean		Max	Mean	Max	Mean
Unshielded	0.0996	1.6009	-0.0996	-3.7876	1.8547	34.96	18.734	-19.6	-8.416
Partly Shielded	0.1344	1.9498	-0.1344	-4.276	-2.4855	28.8732	6.4232	-56.3636	-21.8411
Fully Shielded	0.093	9.207	-0.246	-23.37	0.4585	74.19	40.559	-91.17	-36.52

error, once again, relative to the measurements observed within the laboratory.

Table 3: twenty thousand test comparisons between the simulated versus measured average periodogram and amplitude histogram percent difference for each scs environmental model presented

Average Percent Error									
Model	Min				Mean	Max			
	+		-			+		-	
	Max	Mean	Max	Mean		Max	Mean	Max	Mean
Unshielded	0.6220	0.8106	-2.7959	-1.9058	-0.0137	38.3722	25.3259	-71.4385	-34.5515
Partly Shielded	1.3122	1.0010	-0.7617	-2.1501	-1.9788	34.3266	19.1416	-94.3918	-35.6956
Fully Shielded	1.1472	4.6150	-2.1645	-11.7015	-0.2171	61.5300	40.8445	-94.3450	-41.5900

Table 4: twenty thousand test comparisons between the simulated versus measured periodogram percent difference for each scs environmental model presented

Periodogram Percent Difference					
Model	Min		Mean	Max	
	Max	Mean		Max	Mean
Unshielded	5.4921	0.01517	8.3867	76.267	47.712
Partly Shielded	1.3895	0.0238	8.215	79.6734	40.652
Fully Shielded	0.0000004	0.02006	7.787	65.55	51.8618

Conversely, averaging the values depicted within Table: (1) and Table: (2) yields the overall average model error, as shown by Table: (6), that is, once again, found to be approximately 98 percent accurate, or that these models are, on average, have less than 2 percent error, once again, relative to the measurements observed within the laboratory. Similarly, the percent difference of the periodogram and amplitude histogram was calculated in a similar manner, as shown by Table: (4) and Table: (5), along with the average of the two, as shown by Table: (3), was also tabulated for the sake of completeness. Likewise, based upon the average error calculated, it is reasonable to conclude, at least based upon the relatively low value observed, that the models developed are capable of providing relatively reasonable approximations of the synthetic and natural environmental effects encountered within a

Table 5: twenty thousand test comparisons between the simulated versus measured amplitude histogram percent difference for each scs environmental model presented

Histogram Percent Difference					
Model	Min		Mean	Max	
	Max	Mean		Max	Mean
Unshielded	0.0995	0.786	7.1189	42.3728	20.69
Partly Shielded	0.134	1.9728	7.374	43.971	19.859
Fully Shielded	0.09376	9.656	25.254	117.94	51.6261

Table 6: twenty thousand test comparisons between the simulated versus measured average periodogram and amplitude histogram percent error for each scs environmental model presented

Average Percent Difference					
Model	Min		Mean	Max	
	Max	Mean		Max	Mean
Unshielded	2.7958	0.400585	7.7528	59.3199	34.201
Partly Shielded	0.76175	0.9983	7.7945	61.8222	30.2555
Fully Shielded	0.0468802	4.83803	16.5205	91.745	51.74395

SCS laboratory conditions. Although, once again, it is worth mentioning that a better, or more accurate, comparison between the simulated model and the measured laboratory conditions can be obtained through the utilization of more SCS laboratory measurements; however, despite this fact, it is also worth mentioning that the level of analysis currently obtained is, in truth, more than sufficient to both depict the effectiveness of this particular modeling methodology, while, at the same time, also providing a sufficient amount of mathematical environmental representation as well as demonstrating the effects of different levels of physical shielding.

6.2.3 Instrumentational Effects

The fundamental rationale behind the instrumentational effects section was to define and demonstrate information regarding the commonly identifiable — within contemporary literature — sources of distortions within biomedical devices — like quantization error, sampling, inadvertent filtering, bandwidth, phase inversion, clipping, clamping, truncation, parasitic and feedback problems. Likewise, this broad background information was then narrowed to address the attributes that directly affect biomedical devices — particularly biomedical acquisition devices, like bioimpedance spectroscopy, EMG, and EKG acquisi-

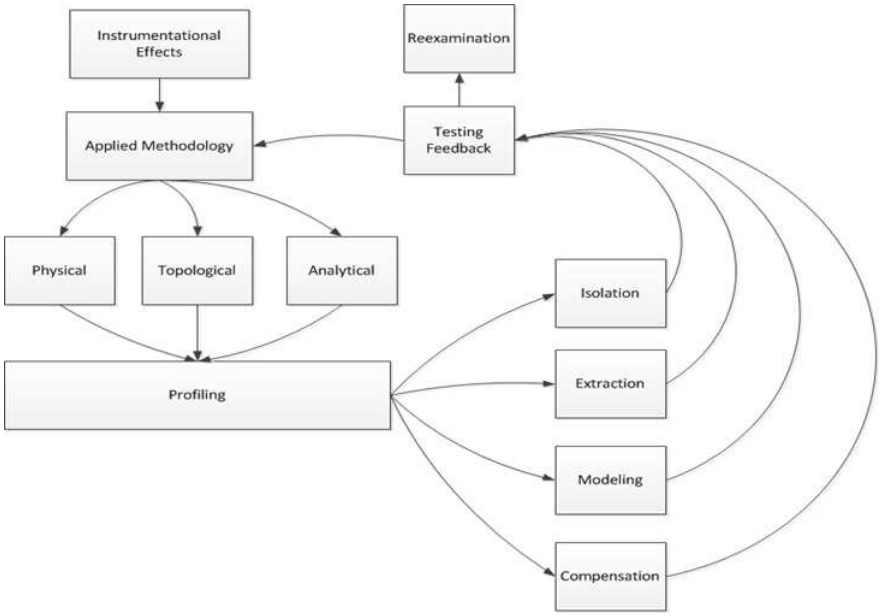

Figure 121: conceptual instrumentational effects flowchart

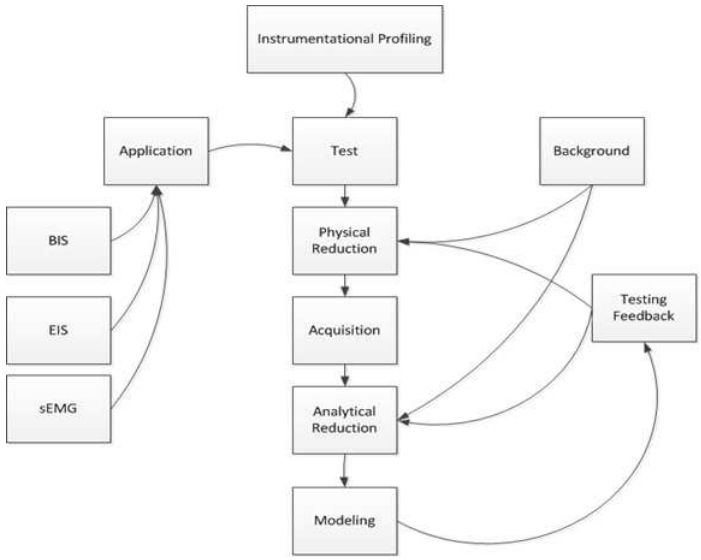

Figure 122: conceptual research organization flowchart

tion devices, — and these attributes were utilized to develop a unique equivalent circuit synthesization methodology — conceptually illustrated within Figure: (121) and Figure: (122) —, that was developed through years of experimental observation and experience synthesizing such systems — that can represent and help negate these distortions within the biometric acquisition process.

Likewise, because — in some instances — the utilization of such equivalent circuit modeling techniques — once again, to fully describe the inherent instrumentational distortions

found within a biomedical device — can yield an extremely complex and computationally unwieldy equivalent circuit model — an attribute that was demonstrated within the equivalent circuit model of a non-ideal instrumentational amplifier — additional considerations were also incorporated within the modeling methodology developed in order to account for the intended application of the model since, in the case where parameter estimation was required, complex equivalent representations — like those observed within the non-ideal instrumentational amplifier — were found to be not only more difficult to work with mathematically but generally resulted in a substantial disassociation between the mathematically estimated parameters obtained and the actual physical parameters within the device. Furthermore, a number of other synthesization techniques were examined — notably those based upon Laplace analysis — in order to further strengthen the rationale behind the utilization of the developed methodology since these alternative techniques — while being applicable to some extent — were generally difficult to utilize given the underlying topological uncertainty that is inherent within most biomedical applications — as researchers, especially within the biomedical research area , seldom have complete unimpeded access to the inner workings of the electrical instrumentation utilized nor is predicting the collective interaction between multiple instrumentational devices operating as a singular apparatus easily described — outright — , even if such topological knowledge was definitively known.

Thus, with this being said, instrumentational effects — while being briefly mentioned within the environmental effects section — is best surmised as being the corporeal limitations that defines humanities basic senses along with the scientific tools that were developed to enhance those senses. Yet, while such terminology might seem more applicable to constructs that are inherently metaphysical, such descriptions are neither incorrect nor are without descriptive merit. After all, the scientific method, previously discussed, and hu-

manities ability to observe natural phenomenon using its perceptive senses, is the common denominator amongst the six methodological steps, previously mentioned, within the scientific method. For example, in true semi-rhetorical form: First, if humanity did not possess any senses, thus making it incapable of sensing the existence of a particular problem, how, in turn, would it be possible to formulate the existence of such a problem? Second, if it were not possible to formulate a problem, based upon the previous question, how then would it be possible to describe such a problem? Third, in turn, if no model could be developed, because of the previous rationale, how would it then be possible to test such a seemingly nonexistent model? Forth, if the ability to test a model becomes questionable, because of the third question, then so would the ability to derive a solution from that model. Fifth, if no solution can be obtained, based upon the fourth question, then the possibility of testing and controlling a solution becomes questionable as well. Sixth, if no ability to test and control a solution could exist, based upon the fifth question, how then would it be possible to implement a solution?

While some scientists might find questions of this nature to be either senseless or possibly, to some degree, even juvenile; however, such pseudo-rhetorical questions do effectively articulate the importance of humanities perceptible senses since, at least within the sciences — a notion that was previously discussed, to some degree, within the earlier philosophical chapter — humanities perspective is ultimately defined by its ability to perceive the world in which it exists. Conversely, although such comparisons might seem out of place, yet such descriptions are also applicable to discussion regarding the effects of scientific instrumentation. For example, scientific instrumentation, at its fundamental level, has a finite resolution, has an accuracy that will vary with design, and is capable of introducing unwanted distortion. Likewise, such attributes can also be connected to the concepts, previ-

ously listed, insofar as, humanities intrinsic senses also have a finite perceptible range, their accuracy can vary based upon internal perception, and such perceptions can be distorted; however, while such observations do help provide some inherent insight into the fundamental foundations upon which all scientific theory is based, it is also important to correlate these fundamental notions directly to the subject of high fidelity instrumentational effects.

Thus, to begin such correlation, it is important to recognize that the scientific instrumentation utilized within this dissertation and, for that matter, the majority of scientific measuring apparatus, can be categorized into three surmised categories — some of which have already been mentioned within previous chapters — as follows: acquisition instrumentation, process and storage instrumentation, production or generation instrumentation. Similarly, the term acquisition instrumentation is typically utilized to describe devices that are capable of measuring physical events — in this particular case, such events are generally referring to electrical phenomenon —, the term process and storage instrumentation is utilized to describe devices that are capable of analyzing, filtering, and possibly storing previously acquired physical events. While the term production or generation instrumentation is utilized to describe devices that are either capable of re-creating measured physical events or creating user specified physical events — and in both cases, such events are referring to the creation of electrical phenomenon. Conversely, as it might be expected and will soon be discussed, each type of instrumentation has some type of effect associated with its usage that, once again, arises from the natural limitations of the, previously discussed, sensory perceptions.

Likewise, to begin discussing the acquisition instrumentational effects encountered — insofar as, how such effects directly relate to the observation of electrical phenomenon — such effects originate from the inherent attribute that arises when a pseudo-continuous

natural signal — pseudo in this particular case because a signal could have a finite bandwidth or duration yet arguably be classified as locally continuous within the boundary of its existence — is observed through finite observation, or more traditionally surmised, within the electrical engineering discipline, as being sampled, discretized, or bandwidth limited [390] [107]. Conversely, the necessary application of such acquisition methods results in the, previously mentioned, pseudo-continuous signal being measured in an discontinuous manner, such that some information about the signal is inherently lost [390] [107]. To demonstrate this effect, a symbolic pseudo-continuous signal that is described by Equation: (239), as shown by Figure: (123), is acquired through the process of innate discretization, as shown by Figure: (124), and, upon visual inspection, the acquired signal clearly appears to be distorted, or more formally described, within the electrical engineering discipline, by the term aliased [390] [107].

$$F(t) = cos(2\pi 40t) + cos(2\pi 50t) + cos(2\pi 60t) \tag{239}$$

Similarly, while the information presented, within Figure: (124), does clearly indicate that

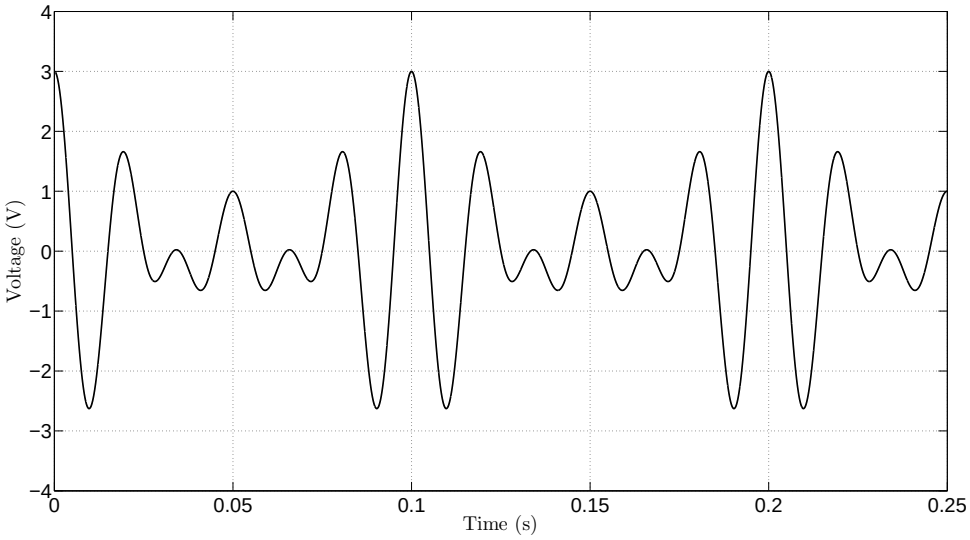

Figure 123: a three frequency symbolic pseudo-continuous signal

some of the information, shown within Figure: (123), was lost upon the utilization of simulated signal acquisition; however, it is important to recognize that the information presented, within Figure: (124), is only demonstrating a specific kind of acquisition loss called undersampling — a phenomenon that occurs when a signal is sampled below the Nyquist-Shannon sampling criteria, as generally surmise by Equation: (240) and typically stated as a signal ($S_{\mathrm{BW}}(t)$) must be sampled at a sample rate (F_s), with a minimum of, twice the signal bandwidth (S_{BW}) to avoid the effects of aliasing.

$$F_s \geq 2S_{\mathrm{BW}} \tag{240}$$

Likewise, as an aside, it is important to recognize that the signal bandwidth, as shown within Equation: (240), is oftentimes confused with the maximum signal frequency, since the most commonly encountered signals do, in fact, have a bandwidth that is centered around the origin, an attribute that allows the highest frequency component of the signal to be equal to the signal bandwidth; however, bandwidth shifting techniques, like AM

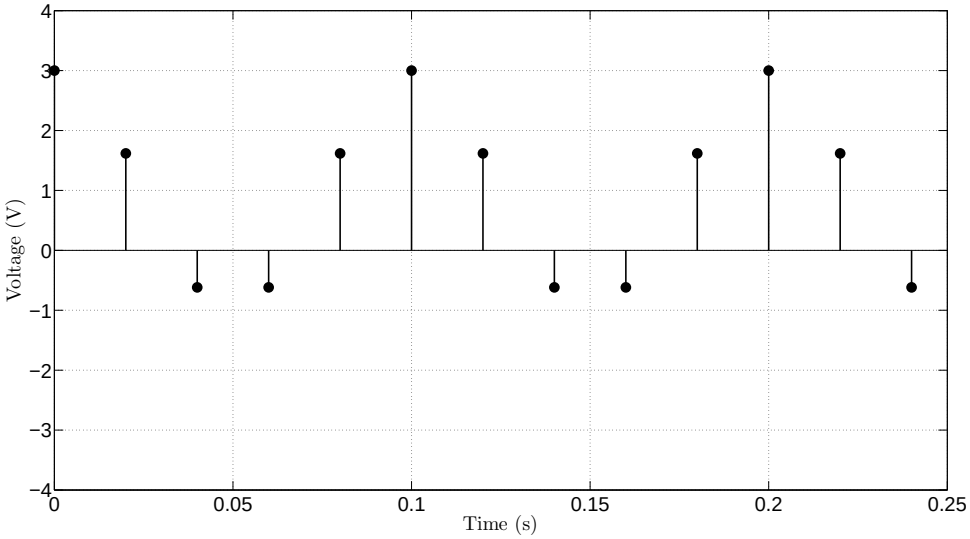

Figure 124: the result of undersampling (f_s = 50hz) a three frequency symbolic pseudo-continuous signal

modulation, as shown by Equation: (241), can offset the signal bandwidth center by a carrier frequency (F_c) and can be accurately acquired by utilizing a sampling rate that is significantly lower than the carrier frequency but greater than or equal to twice the signals bandwidth if digital signal processing (DSP) spectral reflection rules are carefully followed. A process that is depicted by the signal, as defined by Equation: (239) and illustrated by Figure: (123), being shifted in frequency, by application of Equation: (241) and illustrated by Figure: (125), and sampled, as shown by Figure: (127) and Figure: (126).

$$F(t) = S_{\mathrm{BW}}(t)\cos(2\pi F_c t) \tag{241}$$

Conversely, visual comparison of the original signal, as shown by Figure: (123), to the sampled signal, as shown by Figure: (126), appears to indicate that the acquisition techniques, previously described, are able to successfully provide reasonably accurate information about the desired pseudo-continuous signal without a significant amount of appreciable signal spectral loss. Nevertheless, while it is important to recognize that the acquisition losses

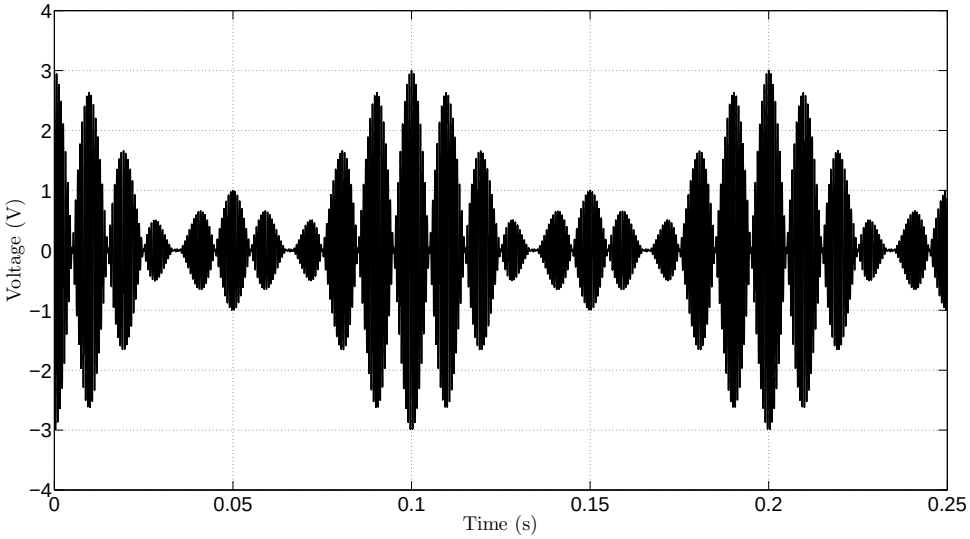

Figure 125: a modulated (f_c = 1600 hz) three frequency symbolic pseudo-continuous signal

incurred, when a signal is sampled, can be quite profound if the bandwidth of the signal is not considered prior to sampling; however, other sources of instrumentational acquisition errors, such as discretization error and physical bandwidth limitations, do concurrently exist and need to be considered as well.

$$0 \geq \ N \ \geq \ 2^{N_{\text{bits}}} - 1 \tag{242}$$

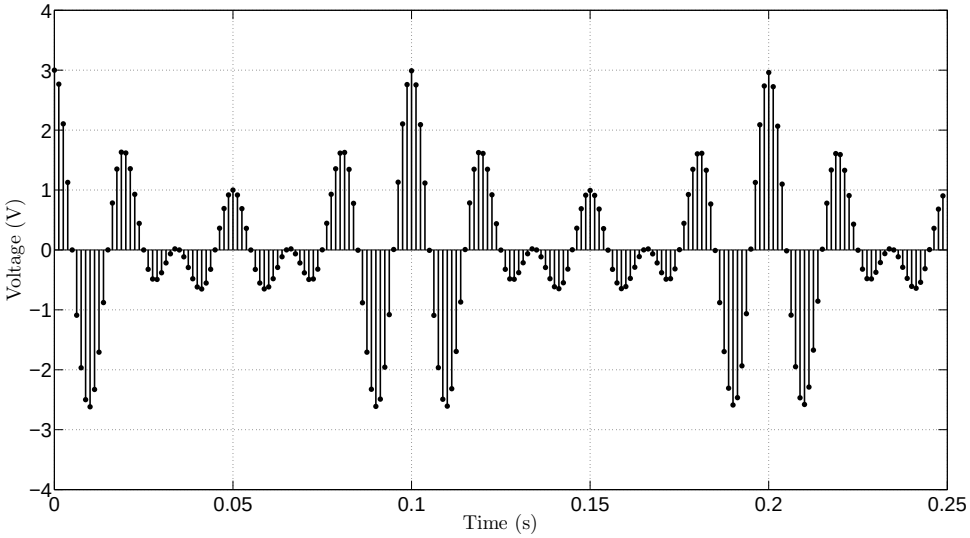

Figure 126: a sampled (f_s = 800 hz) modulated (f_c = 1600 hz) three frequency symbolic pseudo-continuous signal as a stem plot

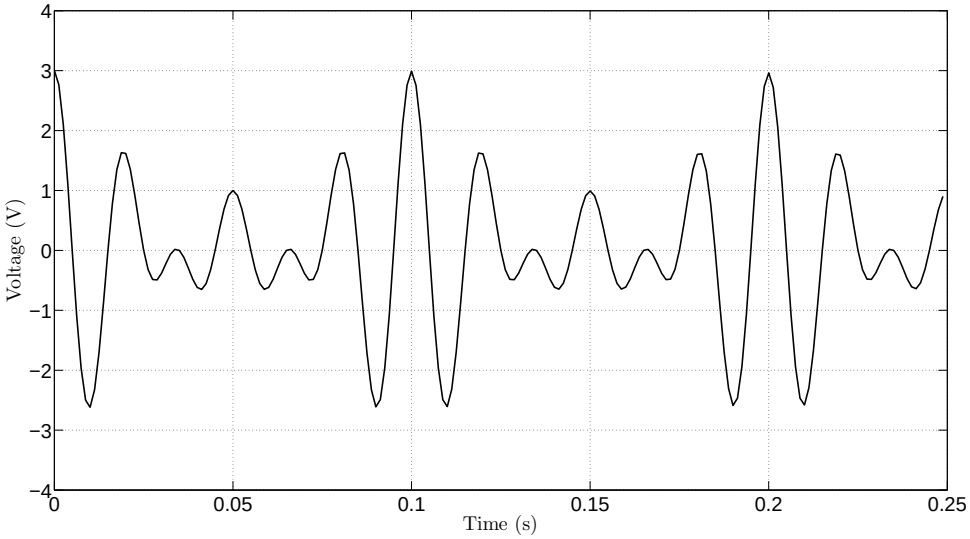

Figure 127: a sampled (f_s = 800 hz) modulated (f_c = 1600 hz) three frequency symbolic pseudo-continuous signal

Likewise, the occurrence of instrumentational acquisition discretization error primarily arises from the usage of an, inherently finite, analog-to-digital converter (ADC) — a digital devise designed to take a pseudo-continuous signal and quantize it into a finite number (N) of representative values that typically vary between zero to a device specified (N_{bits}) power of two, as described by Equation: (242), in which each value digitally represents a specific range of possible pseudo-continuous amplitude values. Conversely, quantization error differs from sampling error, insofar as, — referring to the traditional Cartesian plot of a voltage versus time pseudo-continuous signal — the occurrence of signal quantization implies that the possible values of the Y axis, or signal amplitude axis, are limited to discrete numerical values, whereas the occurrence of sampling, or aliasing error, implies the discretization of the X-axis, or the time axis, at some specified interval.

Although an assortment of quantization methods utilized by contemporary ADC devices — ranging from simplistic window comparison to successive approximation — along with an assortment of ADC encoding schemes — such as linear, a-law, and μ-law —; however, as it might be expected, each quantization method utilized also has some type of unique instrumentational acquisition effect associated with its usage. Conversely, to briefly demonstrate the occurrence of such effects, consider for the moment what happens when the, previously provided, pseudo-continuous signal, as shown by Figure: (123), is discretized through the utilization of a simplistic and linearly encoded four bit ADC, as shown by Figure: (128), and the values obtained from this conversion are translated back into their respective voltage values, as shown by Figure: (129).

Likewise, visual comparison of both Figure: (128) and Figure: (129) to Figure: (123) reveals a substantial amount of signal distortion from the quantization process, and upon comparing the magnitude coefficients, obtained by utilizing the FFT operation, of the

signals previously shown, as shown by Figure: (130) and Figure: (131), it becomes evident that the ADC quantization process does introduce new spectral components that were not prevalent within the original signal. Yet before discussing such distortions further, a few ADC attributes, some of which were previously mentioned, need to be clarified to better explain the figures provided; since, after all, the process of quantization that is typically utilized by most contemporary ADC devices, makes use of an assortment of

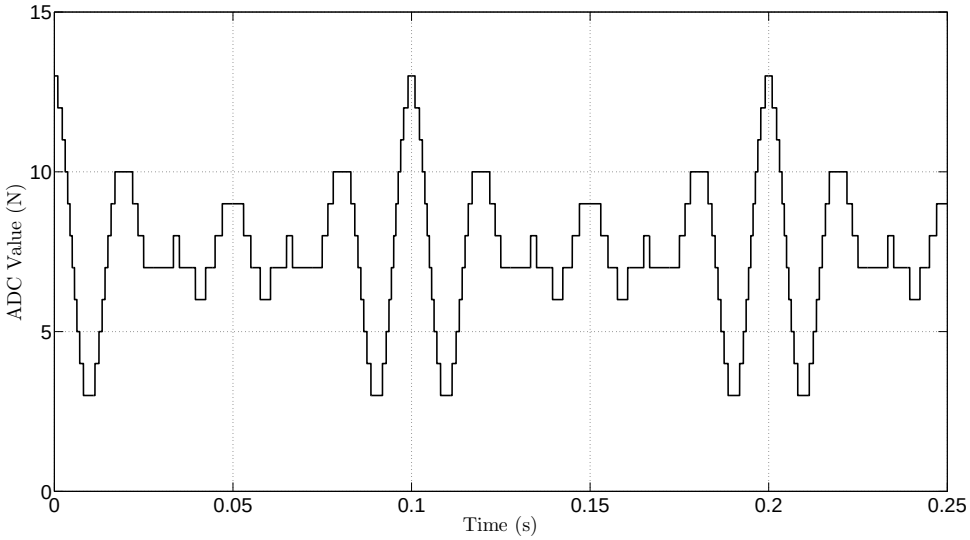

Figure 128: a $n_{\text{bit}} = 4$ discretize linearly encoded three frequency symbolic pseudo-continuous signal in adc values

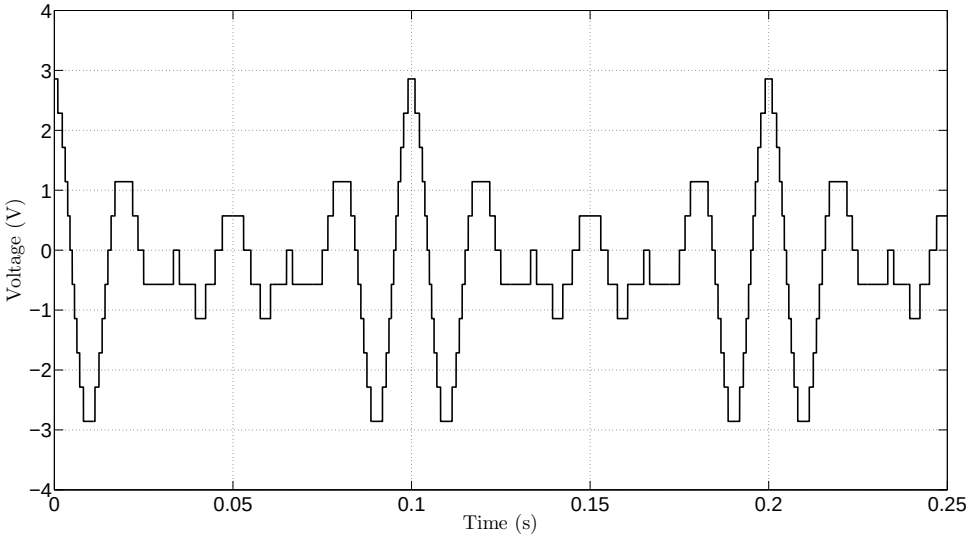

Figure 129: a $n_{\text{bit}} = 4$ discretize linearly encoded three frequency symbolic pseudo-continuous signal in adc voltage values

physical parameters that can radically change the quantization process. For example, most contemporary ADCs are typically controlled by a sampling clock in order to alleviate internal transient effects and to allow associated devices time to obtain the quantized result.

Naturally, as it was previously mentioned, if a signal is sampled at an insufficient or incorrectly augmented sample rate, distortion, or aliasing, will occur, yet despite such contemporary ADC operational attributes being, in fact, very important; however, such characteristics, as it was previously mentioned, have already been examined and were

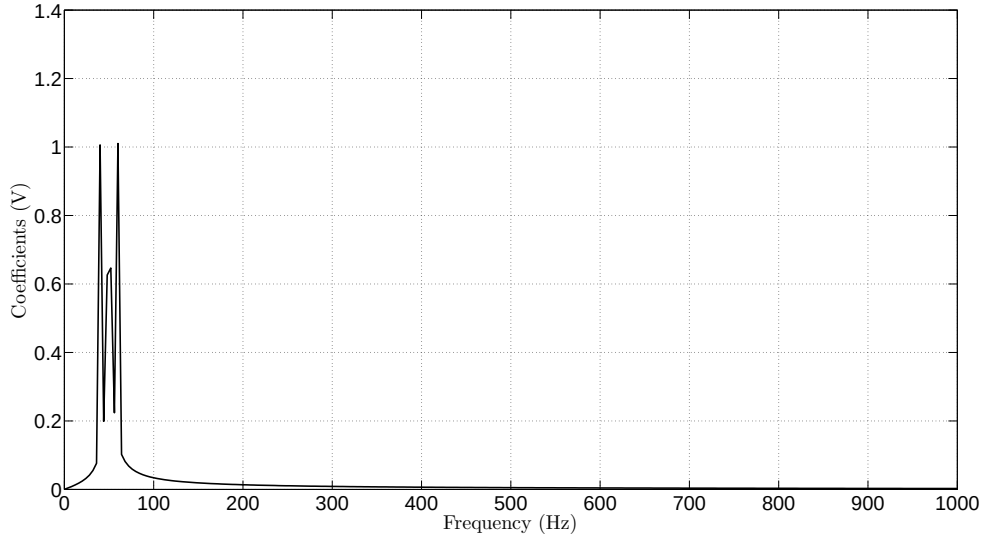

Figure 130: magnitude coefficients of a three frequency symbolic pseudo-continuous signal

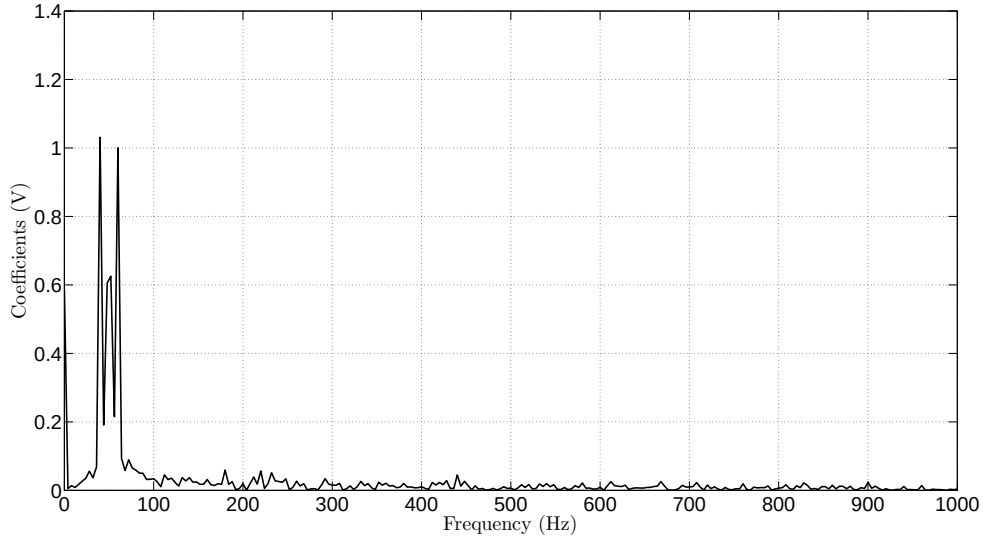

Figure 131: magnitude coefficients of a quantized three frequency symbolic pseudo-continuous signal

only mentioned again as an operational reference. Conversely, contemporary ADCs are generally defined in terms of numerical resolution — a term that is commonly expressed by the exponent of a power of two, also called bits — and the method utilized to convert a pseudo-continuous signal into a quantize value is typically referred to as the encoding scheme. Similarly, the encoding scheme utilized to perform such a conversion, is inherently based upon the physical minimum and maximum voltage connected to the ADC and a segmentation scheme that divides the applied voltage into a discrete number of comparison points that are ultimately utilized to determine how a pseudo-continuous signal will be discreetly represented. Likewise, it is important to recognize that physical limitations — also known as real world considerations — also play a significant role in defining such characteristics, since electronic devices — like the ADC — will only function correctly over a finite range of operational conditions, of which, environmental effects have been found to play a substantial role in defining.

Thus, with this information as a guide, it is reasonable to conclude the following: First, if the ADC sample rate is incorrectly defined relative to the bandwidth of the pseudo-continuous signal then the acquired signal will be distorted. Second, if the environmental effects encountered are substantial in magnitude and are actively producing interference on the ADC power supply rails then the encoding scheme utilized — which once again, is based upon the ADC voltage rails — will result in the quantized output varying as a function of the environmental noise encountered and will inevitably yield distortions. Third, the numerical resolution of the ADC — typically expressed in bits — will ultimately determine the overall resolution of the encoding scheme utilized; similarly, the higher the numerical resolution of the ADC is the more accurate the discretized signal will be, at least upon comparison with the original pseudo-continuous signal.

Conversely, now that some background information behind the most common sources of digital ADC acquisition effects has been provided, it is important to recognize that the specific quantization effects, physically depicted within Figure: (129) and spectrally depicted within Figure: (131), are primarily the result of the digital — one or zero — nature of contemporary ADC acquisition devices, since such acquisition devices are notorious for approximating a pseudo-continuous signal as a mathematical some of unit step functions. Likewise, while environmental effects were not incorporated within the demonstration, depicted by Figure: (129), it is important to recognize that these, previously discussed, environmental effects are, when actually implemented, inherently embedded into the quantization process and are extremely difficult, if not nearly impossible, to completely isolate into individual effect models. Thus, when such effects are typically modeled, the quantization effects are oftentimes represented within the environmental model — in the case of a large numerical resolution with small signal estimation discontinuities — or by the environmental model with an added quantization model incorporated into the derivation — in the case of a small numerical resolution with large signal estimation discontinuities.

Nevertheless, while it is true that a majority of contemporary acquisition devices, once again, used to obtain measurements of electrical phenomenon, frequently utilize digital methods of acquisition, previously discussed; however, analog acquisition systems — while being frequently integrated, in part, into contemporary digital acquisition systems — are, on occasion, solely utilized to perform signal acquisition, and despite the term analog being oftentimes associated with signal continuity, it is important to recognize that even analog methods of acquisition do, in fact, have physical limitations that are not continuous. Likewise, to demonstrate this point, consider for the moment a possible, though relatively simplistic, single stage operational amplifier (OP-AMP) analog acquisition device, in this

particular case an un-ideal inverting band pass filter, as shown by Figure: (132), in which a band pass device was selected to simplistically symbolize some of the most basic physical limitations that are inherently found within real-world analog devices.

While the circuit, shown by Figure: (132), is typically designed with the aid of the ideal high band cut off point (F_{HPF}) equation — as shown by Equation: (243) —, low band cut off point (F_{LPF}) equation — as shown by Equation: (244) —, and pass band gain (A_{PB}) equation — as shown by Equation: (245) — and is typically simulated within the frequency domain; however, because non-ideal transient time domain effects were of significant interest within this dissertation, — an attribute that will be rationalized within this chapter — such design methods, including Laplace analysis, were not utilized within this example.

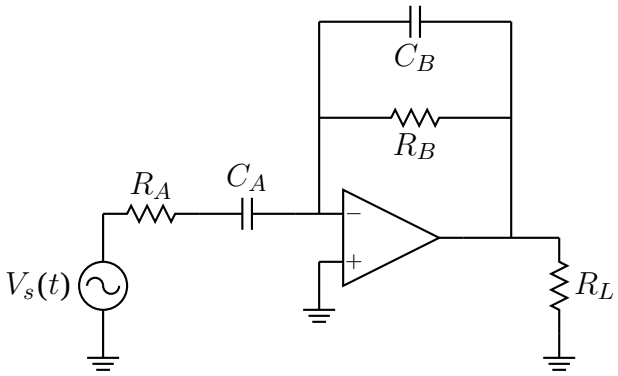

Figure 132: a simplistic inverting band pass filter

$$F_{\mathrm{HPF}} = \frac{1}{2\pi R_A C_A} \tag{243}$$

$$F_{\mathrm{LPF}} = \frac{1}{2\pi R_B C_B} \tag{244}$$

$$A_{\mathrm{PB}} = \frac{-R_B}{R_A} \tag{245}$$

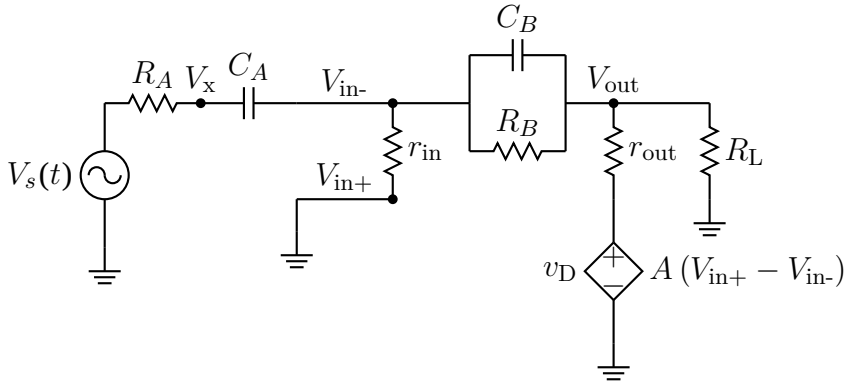

Figure 133: a simplistic inverting band pass filter un-ideal circuit model

Conversely, upon converting the simplified OP-AMP model, depicted within Figure: (132), into its equivalent un-ideal circuit model, as shown by Figure: (133), a number of innate mathematical characteristics are known based upon the circuit components utilized, as shown by Equation: (249) through Equation: (252).

$$V'_{\mathrm{x}}(k) = \frac{\mathrm{V_x(k)}}{\Delta \mathrm{t}} - \frac{\mathrm{V_x(k-1)}}{\Delta \mathrm{t}} \tag{246}$$

$$V'_{\mathrm{in\_}}(k) = \frac{\mathrm{V_{in\_}(k)}}{\Delta \mathrm{t}} - \frac{\mathrm{V_{in\_}(k-1)}}{\Delta \mathrm{t}} \tag{247}$$

$$V'_{\mathrm{out}}(k) = \frac{\mathrm{V_{out}(k)}}{\Delta \mathrm{t}} - \frac{\mathrm{V_{out}(k-1)}}{\Delta \mathrm{t}} \tag{248}$$

$$I_{C_A}(t) = C_A \frac{d}{dt}\left[V_{C_A}(t)\right] \tag{249}$$

$$I_{C_B}(t) = C_B \frac{d}{dt}\left[V_{C_B}(t)\right] \tag{250}$$

$$V_{C_A}(t) = \frac{1}{C_A}\int \left[I_{C_A}(t)\right] dt \tag{251}$$

$$V_{C_B}(t) = \frac{1}{C_B}\int \left[I_{C_B}(t)\right] dt \tag{252}$$

Likewise, because a numerical simulation was utilized to perform the analysis, the numerical approximation of a derivative — in this particular case, the backward difference formula, as shown by Equation: (246) through Equation: (248) — can be utilized to approximate any required derivatives, while values of continuous time (t) can be expressed in terms of discretized steps (k).

$$I_{R_A}(k) = \frac{\mathrm{V_s(k)}}{\mathrm{R_A}} - \frac{\mathrm{V_x(k)}}{\mathrm{R_A}} \tag{253}$$

$$KVL_1 : \ 0 = \frac{\mathrm{V_{in_-}(k)}}{\Delta \mathrm{t}} - \frac{\mathrm{V_{in_-}(k-1)}}{\Delta \mathrm{t}} - \frac{\mathrm{V_x(k)}}{\Delta \mathrm{t}} + \frac{\mathrm{V_x(k-1)}}{\Delta \mathrm{t}} + \frac{\mathrm{V_s(k)}}{\mathrm{C_A\,R_A}} - \frac{\mathrm{V_x(k)}}{\mathrm{C_A\,R_A}} \tag{254}$$

$$I_{C_A}(k) = \frac{\mathrm{C_A\,V_{in_-}(k-1)}}{\Delta \mathrm{t}} - \frac{\mathrm{C_A\,V_{in_-}(k)}}{\Delta \mathrm{t}} + \frac{\mathrm{C_A\,V_x(k)}}{\Delta \mathrm{t}} - \frac{\mathrm{C_A\,V_x(k-1)}}{\Delta \mathrm{t}} \tag{255}$$

$$I_{r_{\mathrm{in}}}(k) = \frac{\mathrm{V_{in_-}(k)}}{\mathrm{r_{in}}} - \frac{\mathrm{V_{in_+}(k)}}{\mathrm{r_{in}}} \tag{256}$$

$$I_{R_B}(k) = \frac{\mathrm{V_{in_-}(k)}}{\mathrm{R_B}} - \frac{\mathrm{V_{out}(k)}}{\mathrm{R_B}} \tag{257}$$

$$I_{C_B}(k) = \frac{\mathrm{C_B\,V_{in_-}(k)}}{\Delta \mathrm{t}} - \frac{\mathrm{C_B\,V_{in_-}(k-1)}}{\Delta \mathrm{t}} - \frac{\mathrm{C_B\,V_{out}(k)}}{\Delta \mathrm{t}} + \frac{\mathrm{C_B\,V_{out}(k-1)}}{\Delta \mathrm{t}} \tag{258}$$

$$\begin{aligned} KCL_1 : \ 0 = {} & \frac{\mathrm{V_{out}(k)}}{\mathrm{R_B}} - \frac{\mathrm{V_{in_-}(k)}}{\mathrm{R_B}} - \frac{\mathrm{V_{in_-}(k)}}{\mathrm{r_{in}}} + \frac{\mathrm{V_{in_+}(k)}}{\mathrm{r_{in}}} - \frac{\mathrm{C_A\,V_{in_-}(k)}}{\Delta \mathrm{t}} \\ & + \frac{\mathrm{C_A\,V_{in_-}(k-1)}}{\Delta \mathrm{t}} - \frac{\mathrm{C_B\,V_{in_-}(k)}}{\Delta \mathrm{t}} + \frac{\mathrm{C_B\,V_{in_-}(k-1)}}{\Delta \mathrm{t}} + \frac{\mathrm{C_B\,V_{out}(k)}}{\Delta \mathrm{t}} \\ & - \frac{\mathrm{C_B\,V_{out}(k-1)}}{\Delta \mathrm{t}} + \frac{\mathrm{C_A\,V_x(k)}}{\Delta \mathrm{t}} - \frac{\mathrm{C_A\,V_x(k-1)}}{\Delta \mathrm{t}} \end{aligned} \tag{259}$$

$$V_d(k) = \mathrm{A\,V_{in_+}(k)} - \mathrm{A\,V_{in_-}(k)} \tag{260}$$

$$I_{r_{\mathrm{out}}}(k) = \frac{\mathrm{A\,V_{in_+}(k)}}{\mathrm{r_{out}}} - \frac{\mathrm{A\,V_{in_-}(k)}}{\mathrm{r_{out}}} - \frac{\mathrm{V_{out}(k)}}{\mathrm{r_{out}}} \tag{261}$$

$$I_{R_L}(k) = \frac{\mathrm{V_{out}(k)}}{\mathrm{R_L}} \tag{262}$$

$$I_{R_B}(k) = \frac{\mathrm{V_{out}(k)}}{\mathrm{R_B}} - \frac{\mathrm{V_{in_-}(k)}}{\mathrm{R_B}} \tag{263}$$

$$I_{C_B}(k) = \frac{\mathrm{C_B\,V_{in_-}(k-1)}}{\Delta \mathrm{t}} - \frac{\mathrm{C_B\,V_{in_-}(k)}}{\Delta \mathrm{t}} + \frac{\mathrm{C_B\,V_{out}(k)}}{\Delta \mathrm{t}} - \frac{\mathrm{C_B\,V_{out}(k-1)}}{\Delta \mathrm{t}} \tag{264}$$

$$\begin{aligned} KCL_2: \; 0 = {} & \frac{\mathrm{V_{in_-}(k)}}{\mathrm{R_B}} - \frac{\mathrm{V_{out}(k)}}{\mathrm{R_B}} - \frac{\mathrm{V_{out}(k)}}{\mathrm{R_L}} - \frac{\mathrm{V_{out}(k)}}{\mathrm{r_{out}}} - \frac{\mathrm{A\,V_{in_-}(k)}}{\mathrm{r_{out}}} + \frac{\mathrm{A\,V_{in_+}(k)}}{\mathrm{r_{out}}} \\ & + \frac{\mathrm{C_B\,V_{in_-}(k)}}{\Delta \mathrm{t}} - \frac{\mathrm{C_B\,V_{in_-}(k-1)}}{\Delta \mathrm{t}} - \frac{\mathrm{C_B\,V_{out}(k)}}{\Delta \mathrm{t}} + \frac{\mathrm{C_B\,V_{out}(k-1)}}{\Delta \mathrm{t}} \end{aligned} \tag{265}$$

Similarly, application of fundamental circuit principles, such as Kirchhoff's current law (KCL) and Kirchhoff's voltage law (KVL) — as shown by Equation: (254), Equation: (259), and Equation: (265) — can be utilized to obtain simulation circuit Equation: (267), Equation: (266), and Equation: (270).

$$\begin{aligned} V_{\mathrm{x}}(k) = {} & \frac{\Delta \mathrm{t\,V_s(k)}}{\Delta \mathrm{t} + \mathrm{C_A\,R_A}} + \frac{\mathrm{C_A\,R_A\,V_{in_-}(k)}}{\Delta \mathrm{t} + \mathrm{C_A\,R_A}} - \frac{\mathrm{C_A\,R_A\,V_{in_-}(k-1)}}{\Delta \mathrm{t} + \mathrm{C_A\,R_A}} \\ & + \frac{\mathrm{C_A\,R_A\,V_x(k-1)}}{\Delta \mathrm{t} + \mathrm{C_A\,R_A}} \end{aligned} \tag{266}$$

$$V_{\mathrm{in_-}}(k) = \frac{\alpha_1}{\beta_1} \tag{267}$$

$$\begin{aligned} \alpha_1 = {} & \Delta \mathrm{t}^4\,\mathrm{R_B}^2\,\mathrm{r_{in}}\,\mathrm{V_{in_+}(k)} + \Delta \mathrm{t}^4\,\mathrm{R_B}\,\mathrm{r_{in}}^2\,\mathrm{V_{out}(k)} + \mathrm{C_A}\,\Delta \mathrm{t}^3\,\mathrm{R_B}^2\,\mathrm{r_{in}}^2\,\mathrm{V_{in_-}(k-1)} \\ & + \mathrm{C_B}\,\Delta \mathrm{t}^3\,\mathrm{R_B}^2\,\mathrm{r_{in}}^2\,\mathrm{V_{in_-}(k-1)} + \mathrm{C_B}\,\Delta \mathrm{t}^3\,\mathrm{R_B}^2\,\mathrm{r_{in}}^2\,\mathrm{V_{out}(k)} \\ & - \mathrm{C_B}\,\Delta \mathrm{t}^3\,\mathrm{R_B}^2\,\mathrm{r_{in}}^2\,\mathrm{V_{out}(k-1)} + \mathrm{C_A}\,\Delta \mathrm{t}^3\,\mathrm{R_B}^2\,\mathrm{r_{in}}^2\,\mathrm{V_s(k)} \\ & - \mathrm{C_A}\,\Delta \mathrm{t}^3\,\mathrm{R_B}^2\,\mathrm{r_{in}}^2\,\mathrm{V_x(k-1)} + \mathrm{C_A}^2\,\Delta \mathrm{t}^2\,\mathrm{R_A}^2\,\mathrm{R_B}^2\,\mathrm{r_{in}}\,\mathrm{V_{in_+}(k)} \\ & + \mathrm{C_A}^2\,\Delta \mathrm{t}^2\,\mathrm{R_A}^2\,\mathrm{R_B}\,\mathrm{r_{in}}^2\,\mathrm{V_{out}(k)} + \mathrm{C_A}^2\,\Delta \mathrm{t}^2\,\mathrm{R_A}\,\mathrm{R_B}^2\,\mathrm{r_{in}}^2\,\mathrm{V_s(k)} \\ & - \mathrm{C_A}^2\,\Delta \mathrm{t}^2\,\mathrm{R_A}\,\mathrm{R_B}^2\,\mathrm{r_{in}}^2\,\mathrm{V_x(k-1)} + 2\,\mathrm{C_A}\,\Delta \mathrm{t}^3\,\mathrm{R_A}\,\mathrm{R_B}^2\,\mathrm{r_{in}}\,\mathrm{V_{in_+}(k)} \\ & + 2\,\mathrm{C_A}\,\Delta \mathrm{t}^3\,\mathrm{R_A}\,\mathrm{R_B}\,\mathrm{r_{in}}^2\,\mathrm{V_{out}(k)} + 2\,\mathrm{C_A}\,\mathrm{C_B}\,\Delta \mathrm{t}^2\,\mathrm{R_A}\,\mathrm{R_B}^2\,\mathrm{r_{in}}^2\,\mathrm{V_{in_-}(k-1)} \\ & + 2\,\mathrm{C_A}\,\mathrm{C_B}\,\Delta \mathrm{t}^2\,\mathrm{R_A}\,\mathrm{R_B}^2\,\mathrm{r_{in}}^2\,\mathrm{V_{out}(k)} - 2\,\mathrm{C_A}\,\mathrm{C_B}\,\Delta \mathrm{t}^2\,\mathrm{R_A}\,\mathrm{R_B}^2\,\mathrm{r_{in}}^2\,\mathrm{V_{out}(k-1)} \\ & + \mathrm{C_A}^2\,\mathrm{C_B}\,\Delta \mathrm{t}\,\mathrm{R_A}^2\,\mathrm{R_B}^2\,\mathrm{r_{in}}^2\,\mathrm{V_{in_-}(k-1)} + \mathrm{C_A}^2\,\mathrm{C_B}\,\Delta \mathrm{t}\,\mathrm{R_A}^2\,\mathrm{R_B}^2\,\mathrm{r_{in}}^2\,\mathrm{V_{out}(k)} \\ & - \mathrm{C_A}^2\,\mathrm{C_B}\,\Delta \mathrm{t}\,\mathrm{R_A}^2\,\mathrm{R_B}^2\,\mathrm{r_{in}}^2\,\mathrm{V_{out}(k-1)} \end{aligned}$$

$$+ {C_A}^2\,\Delta t^2\,R_A\,{R_B}^2\,{r_{in}}^2\,V_{in_-}(k-1) \tag{268}$$

$$\begin{aligned}\beta_1 = {}& {C_A}^2\,\Delta t^2\,{R_A}^2\,{R_B}^2\,r_{in} + {C_A}^2\,\Delta t^2\,{R_A}^2\,R_B\,{r_{in}}^2 + {C_A}^2\,\Delta t^2\,R_A\,{R_B}^2\,{r_{in}}^2 \\ & + C_B\,{C_A}^2\,\Delta t\,{R_A}^2\,{R_B}^2\,{r_{in}}^2 + 2\,C_A\,\Delta t^3\,R_A\,{R_B}^2\,r_{in} + 2\,C_A\,\Delta t^3\,R_A\,R_B\,{r_{in}}^2 \\ & + C_A\,\Delta t^3\,{R_B}^2\,{r_{in}}^2 + 2\,C_B\,C_A\,\Delta t^2\,R_A\,{R_B}^2\,{r_{in}}^2 + \Delta t^4\,{R_B}^2\,r_{in} \\ & + \Delta t^4\,R_B\,{r_{in}}^2 + C_B\,\Delta t^3\,{R_B}^2\,{r_{in}}^2\end{aligned} \tag{269}$$

$$V_{out}(k) = \frac{\alpha_2}{\beta_2} \tag{270}$$

$$\begin{aligned}\alpha_2 = {}& \Delta t^2\,R_L\,r_{out}\,V_{in_+}(k) + A\,\Delta t^2\,r_{in}\,R_L\,V_{in_+}(k) + C_A\,\Delta t\,R_A\,R_L\,r_{out}\,V_{in_+}(k) \\ & + C_B\,\Delta t\,R_B\,R_L\,r_{out}\,V_{in_+}(k) - C_B\,\Delta t\,R_B\,R_L\,r_{out}\,V_{in_-}(k-1) \\ & + C_B\,\Delta t\,R_B\,R_L\,r_{out}\,V_{out}(k-1) + C_A\,\Delta t\,r_{in}\,R_L\,r_{out}\,V_{in_-}(k-1) \\ & + C_A\,\Delta t\,r_{in}\,R_L\,r_{out}\,V_s(k) - C_A\,\Delta t\,r_{in}\,R_L\,r_{out}\,V_x(k-1) \\ & + A\,C_A\,\Delta t\,R_A\,r_{in}\,R_L\,V_{in_+}(k) + A\,C_A\,\Delta t\,R_B\,r_{in}\,R_L\,V_{in_+}(k) \\ & - A\,C_A\,\Delta t\,R_B\,r_{in}\,R_L\,V_{in_-}(k-1) + A\,C_B\,\Delta t\,R_B\,r_{in}\,R_L\,V_{in_+}(k) \\ & - A\,C_B\,\Delta t\,R_B\,r_{in}\,R_L\,V_{in_-}(k-1) + A\,C_B\,\Delta t\,R_B\,r_{in}\,R_L\,V_{out}(k-1) \\ & - A\,C_A\,\Delta t\,R_B\,r_{in}\,R_L\,V_s(k) + A\,C_A\,\Delta t\,R_B\,r_{in}\,R_L\,V_x(k-1) \\ & + C_A\,C_B\,R_A\,R_B\,R_L\,r_{out}\,V_{in_+}(k) - C_A\,C_B\,R_A\,R_B\,R_L\,r_{out}\,V_{in_-}(k-1) \\ & + C_A\,C_B\,R_A\,R_B\,R_L\,r_{out}\,V_{out}(k-1) + C_A\,C_B\,R_B\,r_{in}\,R_L\,r_{out}\,V_{out}(k-1) \\ & + C_A\,C_B\,R_B\,r_{in}\,R_L\,r_{out}\,V_s(k) - C_A\,C_B\,R_B\,r_{in}\,R_L\,r_{out}\,V_x(k-1) \\ & + A\,C_A\,C_B\,R_A\,R_B\,r_{in}\,R_L\,V_{in_+}(k) - A\,C_A\,C_B\,R_A\,R_B\,r_{in}\,R_L\,V_{in_-}(k-1) \\ & + A\,C_A\,C_B\,R_A\,R_B\,r_{in}\,R_L\,V_{out}(k-1)\end{aligned} \tag{271}$$

$$\begin{aligned}\beta_2 = {}& \Delta t^2\,R_B\,R_L + \Delta t^2\,R_B\,r_{out} + \Delta t^2\,r_{in}\,R_L + \Delta t^2\,r_{in}\,r_{out} + \Delta t^2\,R_L\,r_{out} \\ & + A\,\Delta t^2\,r_{in}\,R_L + C_A\,\Delta t\,R_A\,R_B\,R_L + C_A\,\Delta t\,R_A\,R_B\,r_{out} \\ & + C_A\,\Delta t\,R_A\,r_{in}\,R_L + C_A\,\Delta t\,R_B\,r_{in}\,R_L + C_B\,\Delta t\,R_B\,r_{in}\,R_L\end{aligned}$$

$$+ C_A \Delta t R_A r_{in} r_{out} + C_A \Delta t R_B r_{in} r_{out} + C_B \Delta t R_B r_{in} r_{out}$$

$$+ C_A \Delta t R_A R_L r_{out} + C_B \Delta t R_B R_L r_{out} + C_A \Delta t r_{in} R_L r_{out}$$

$$+ A C_A \Delta t R_A r_{in} R_L + A C_B \Delta t R_B r_{in} R_L + C_A C_B R_A R_B r_{in} R_L$$

$$+ C_A C_B R_A R_B r_{in} r_{out} + C_A C_B R_A R_B R_L r_{out}$$

$$+ C_A C_B R_B r_{in} R_L r_{out} + A C_A C_B R_A R_B r_{in} R_L \tag{272}$$

Conversely, the numerical simulation of Equation: (267), Equation: (266), and Equation: (270), upon selection of component parameters, as shown by Table: (7), and application of an input pulse of width (Δt) — or pseudo approximate delta function — as the input signal, yields a frequency spectrum plot, as shown by Figure: (134), that demonstrates the bandwidth characteristics of the circuit depicted within Figure: (132) and Figure: (133). While the band pass spectral response, between the frequencies of (F_{LPF} = 159.1549Hz) and (F_{HPF} = 2652.6Hz), was expected — primarily because of having prior knowledge of both the component values and the circuit topology utilized —; however, this spectral response — once again, referring to the observed band pass response — is, for the most part, known to occur within essentially every manufactured analog device in some way, shape, or form. Conversely, such innate analog band pass characteristics inevitably result in signal attenuation for frequencies beyond the devices specified operational range, and the occurrence of such attenuation can prevent the accurate acquisition of an observed signal, especially if that signal exceeds the devices operational specifications. While such bandwidth considerations are fundamentally different from the discretization effects previously discussed, insofar as, discretization distortions generally introduce additional spectral components, whereas bandwidth limitations generally tend to remove or reduce such components; however, both types of distortions can be equally problematic when attempting

to acquire an electrical phenomenon.

Table 7: circuit parameters utilized within numerical simulation

Variable	Value	Units	Description
Δt	0.00001	s	Simulation Step Size
A	10000000	$\frac{V}{V}$	OP-AMP Internal Gain
r_{out}	1	Ω	OP-AMP Internal Output Resistance
r_{in}	10000000	Ω	OP-AMP Internal Input Resistance
R_L	10000	Ω	Output Loading Resistor
R_A	1	Ω	HPF Resistor
R_B	1	Ω	LPF Resistor
C_A	0.001	F	HPF Capacitor
C_B	0.00006	F	LPF Capacitor

Nevertheless, while the bandwidth limitations previously observed, within analog acquisition systems, are yet another attribute that must be considered prior to attempting to acquire a natural signal; however, such attributes only address the analog time domain — or Cartesian X-axis — continuity limitations previously discussed. Similarly, because the majority of analog circuitry — excluding for the moment power production devices like solar cells — require an external source of power to function correctly, the voltage axis — or Cartesian Y-axis — previously discussed, also possesses similar continuity limitations — or boundaries — that are generally defined by the external power source applied. Conversely, because such attributes are common amongst almost all analog devices, it would

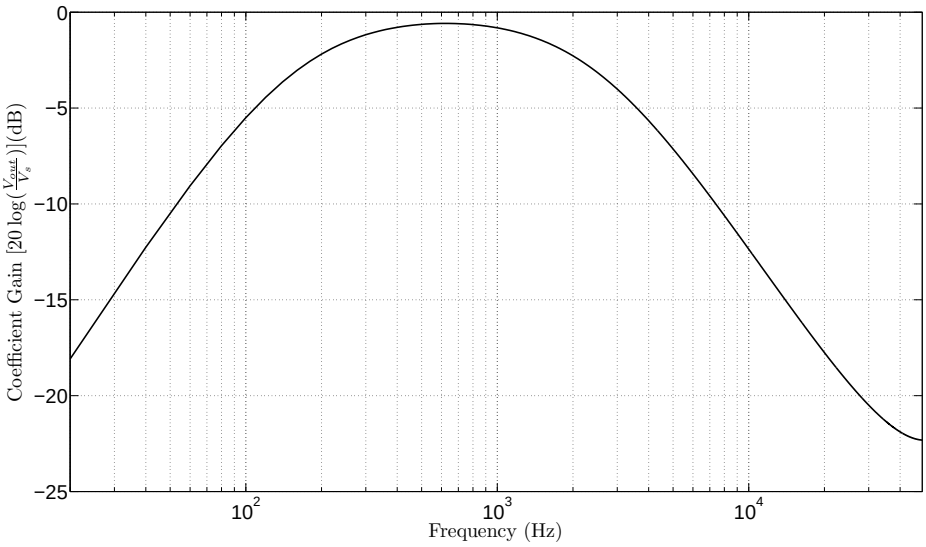

Figure 134: voltage gain plot of the band pass circuit frequency response obtained using fft magnitude coefficients

seem prudent to present such effects through the utilization of a relatively simplistic analog device, like a un-ideal inverting OP-AMP, as depicted by Figure: (135) and Figure: (136), with the following component parameters, as shown by Table: (8), and formulated using Equation: (276) and Equation: (280) and simulated using Equation: (281) and Equation: (282).

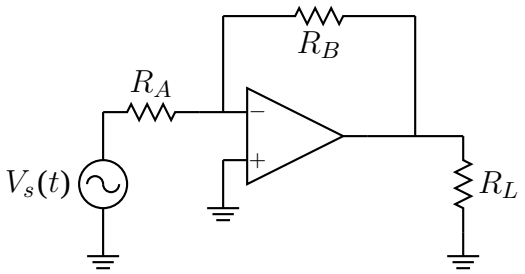

Figure 135: inverting operational amplifier

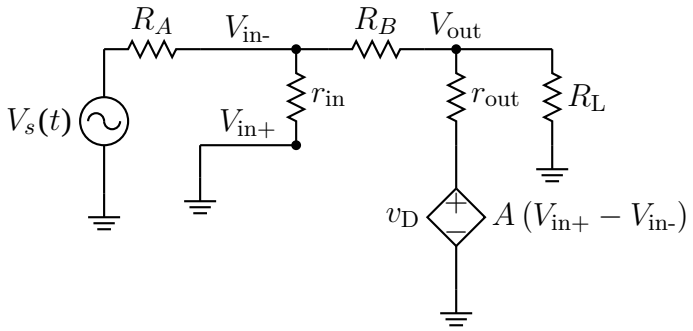

Figure 136: un-ideal inverting operational amplifier equivalent model

Table 8: circuit parameters utilized within numerical simulation

Variable	Value	Units	Description
A	1000000	$\frac{V}{V}$	OP-AMP Internal Gain
r_{out}	1	Ω	OP-AMP Internal Output Resistance
r_{in}	100000000	Ω	OP-AMP Internal Input Resistance
R_L	10000	Ω	Output Loading Resistor
R_A	1000	Ω	Input Resistor
R_B	2000	Ω	Feedback Resistor
V_{dd}	10	V	Positive Power Supply
V_{ss}	-10	V	Negative Power Supply

$$I_{R_A}(k) = \frac{\mathrm{V_s(k)}}{\mathrm{R_A}} - \frac{\mathrm{V_{in_-}(k)}}{\mathrm{R_A}} \tag{273}$$

$$I_{R_B}(k) = \frac{\mathrm{V_{in_-}(k)}}{\mathrm{R_B}} - \frac{\mathrm{V_{out}(k)}}{\mathrm{R_B}} \tag{274}$$

$$I_{r_{\mathrm{in}}}(k) = \frac{\mathrm{V_{in_-}(k)}}{\mathrm{r_{in}}} - \frac{\mathrm{V_{in_+}(k)}}{\mathrm{r_{in}}} \tag{275}$$

$$KCL_1: \quad = \frac{\mathrm{V_{out}(k)}}{\mathrm{R_B}} - \frac{\mathrm{V_{in_-}(k)}}{\mathrm{R_B}} - \frac{\mathrm{V_{in_-}(k)}}{\mathrm{R_A}} - \frac{\mathrm{V_{in_-}(k)}}{\mathrm{r_{in}}} + \frac{\mathrm{V_{in_+}(k)}}{\mathrm{r_{in}}} + \frac{\mathrm{V_s(k)}}{\mathrm{R_A}} \tag{276}$$

$$V_d(k) = \mathrm{A\,V_{in_+}(k)} - \mathrm{A\,V_{in_-}(k)} \tag{277}$$

$$V_{\mathrm{rout}}(k) = \frac{\mathrm{A\,V_{in_+}(k)}}{\mathrm{r_{out}}} - \frac{\mathrm{A\,V_{in_-}(k)}}{\mathrm{r_{out}}} - \frac{\mathrm{V_{out}(k)}}{\mathrm{r_{out}}} \tag{278}$$

$$V_{R_B}(k) = \frac{\mathrm{V_{out}(k)}}{\mathrm{R_B}} - \frac{\mathrm{V_{in_-}(k)}}{\mathrm{R_B}} \tag{279}$$

$$KVL_1: \quad = \mathrm{A\,V_{in_+}(k)} - \mathrm{V_{out}(k)} - \mathrm{A\,V_{in_-}(k)} - \mathrm{V_{in_-}(k)} \tag{280}$$

$$\begin{aligned} V_{\mathrm{in_-}}(k) = {} & \frac{\mathrm{R_A\,R_B\,V_{in_+}(k)}}{\mathrm{R_A\,R_B + R_A\,r_{in} + R_B\,r_{in}}} + \frac{\mathrm{R_A\,r_{in}\,V_{out}(k)}}{\mathrm{R_A\,R_B + R_A\,r_{in} + R_B\,r_{in}}} \\ & + \frac{\mathrm{R_B\,r_{in}\,V_s(k)}}{\mathrm{R_A\,R_B + R_A\,r_{in} + R_B\,r_{in}}} \end{aligned} \tag{281}$$

$$\begin{aligned} V_{\mathrm{out}}(k) = {} & \frac{\mathrm{A\,R_A\,r_{in}\,V_{in_+}(k)}}{\mathrm{R_A\,R_B + 2\,R_A\,r_{in} + R_B\,r_{in} + A\,R_A\,r_{in}}} \\ & - \frac{\mathrm{R_B\,r_{in}\,V_s(k)}}{\mathrm{R_A\,R_B + 2\,R_A\,r_{in} + R_B\,r_{in} + A\,R_A\,r_{in}}} \\ & - \frac{\mathrm{R_A\,R_B\,V_{in_+}(k)}}{\mathrm{R_A\,R_B + 2\,R_A\,r_{in} + R_B\,r_{in} + A\,R_A\,r_{in}}} \\ & + \frac{\mathrm{A\,R_B\,r_{in}\,V_{in_+}(k)}}{\mathrm{R_A\,R_B + 2\,R_A\,r_{in} + R_B\,r_{in} + A\,R_A\,r_{in}}} \\ & - \frac{\mathrm{A\,R_B\,r_{in}\,V_s(k)}}{\mathrm{R_A\,R_B + 2\,R_A\,r_{in} + R_B\,r_{in} + A\,R_A\,r_{in}}} \end{aligned} \tag{282}$$

Likewise, such analog external power supply boundaries — or power rails —, previously

discussed, typically manifest themselves in one of two ways. The first way involves the input signal, as shown by Figure: (137), being significantly larger in voltage magnitude than the voltage supplied by the external power supply, while the second way involves the operational pass band gain being set to amplified the acquired signal beyond the maximum output magnitude supplied by the external power supply, as shown by Figure: (138). Additionally, because both of the voltage limitations, previously discussed, results in signal distortion through voltage amplitude clipping, as shown by Figure: (139) and Figure: (140), a parallel between the discretization effects observed within Figure: (129) can be made. Conversely, the occurrence of analog amplitude clipping — in a manner similar to the discretization instrumentational effects previously discussed — will, upon utilization of FFT analysis, result in plots depicting the addition of new spectral frequencies, as shown by Figure: (141) and Figure: (142), that did not previously exist within the FFT analysis of the input signal, as shown by Figure: (143) and Figure: (144).

Similarly, to provide further explanation for each of the cases depicted, first, it is important to recognize that although the input signals, depicted by Figure: (137) and Figure: (138), are only mathematically different in terms of voltage amplitude; however, such math-

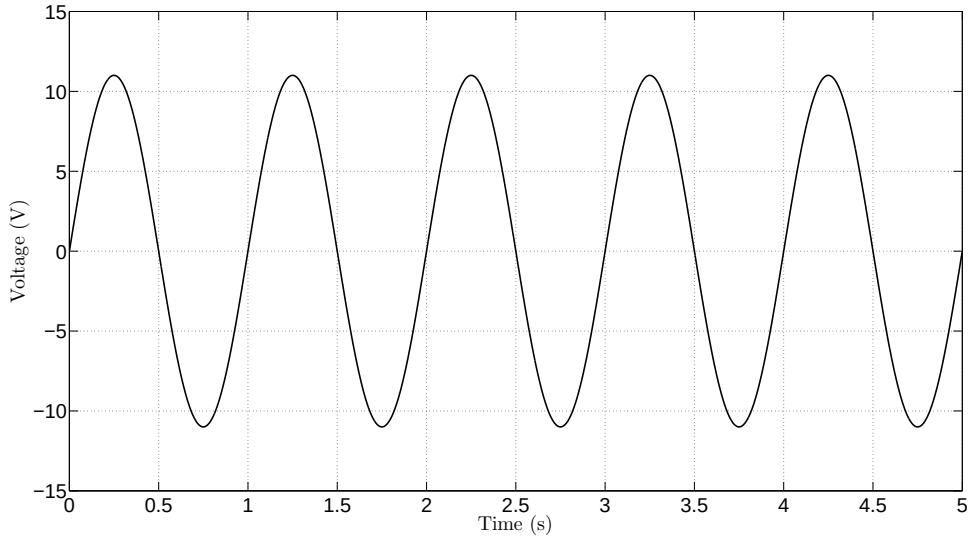

Figure 137: a 1 hz input signal with a amplitude greater than the op-amp's supply rails

ematical differences are not of significant concern relative to the knowledge that the natural circumstances in which each signal was symbolically applied was radically different. For example, in the case of Figure: (137), it is assumed that the natural signal being observed can exceed the operational voltage limitations of the device attempting to measure this signal; conversely, when these operational voltage boundaries are exceeded, not only will acquisition distortion occur, as shown by Figure: (139), since the acquisition device is incapable of acquiring parts of the signal that exceed these boundaries, but the acquisition

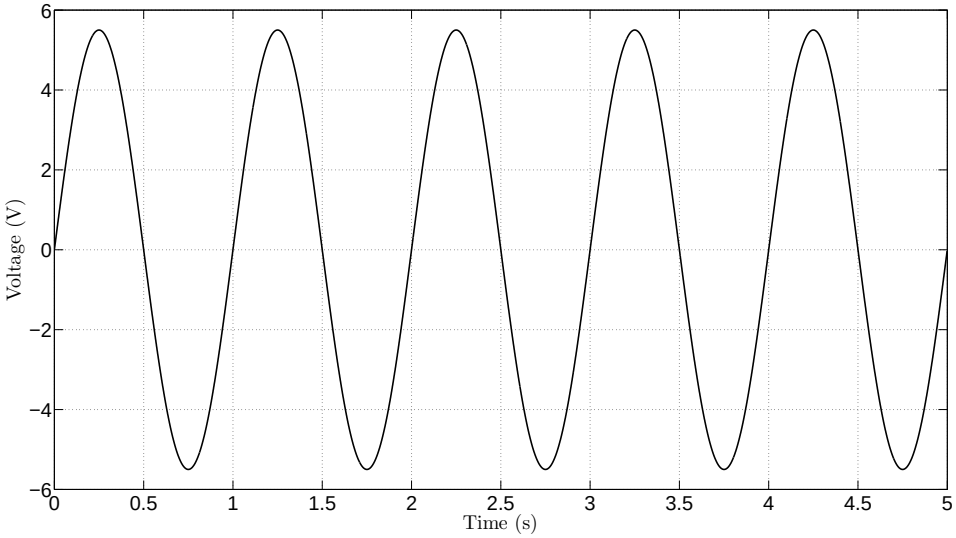

Figure 138: a 1 hz input signal with a amplitude less than the op-amp supply rails

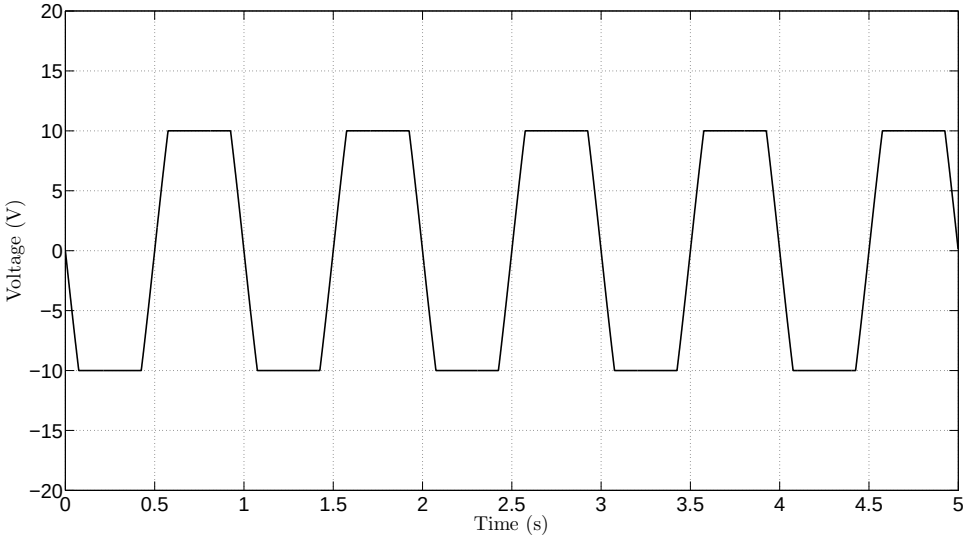

Figure 139: the output signal of un-ideal inverting op-amp upon application of a input signal greater than the op-amp's supply rails

device can, in itself, be damaged or destroyed while, at the same time, the natural signal being observed can, in some cases, be directly modified by the voltage boundaries of the measuring apparatus — primarily through the addition of a sudden change in input loading impedance. Alternatively, the input signal depicted within Figure: (138), represents a natural signal that will not exceed the operational voltage limitations of a device attempting to measure that signal; however, this input signal does embody the characteristic of a

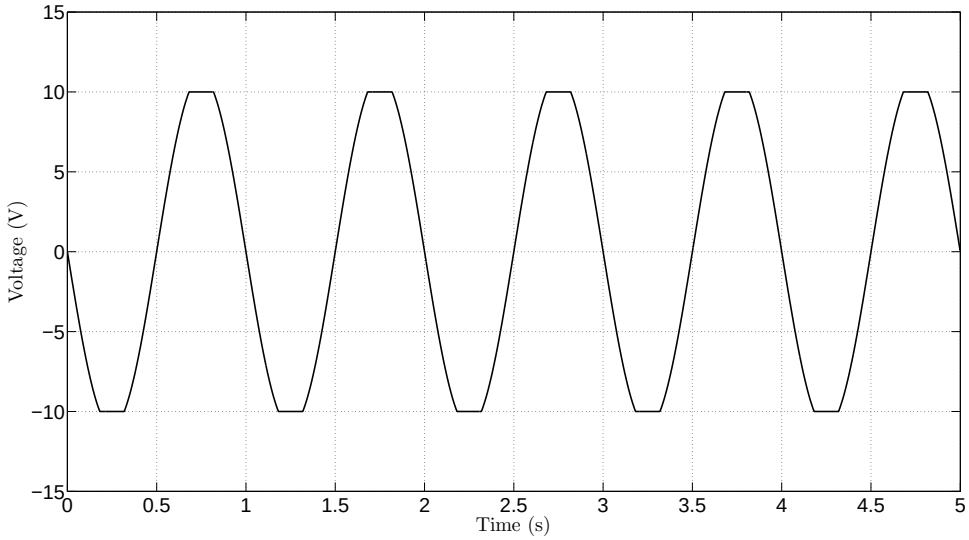

Figure 140: the output signal of un-ideal inverting op-amp upon application of a input signal less than the op-amp's supply rails but above the op-amp voltage gain limitations

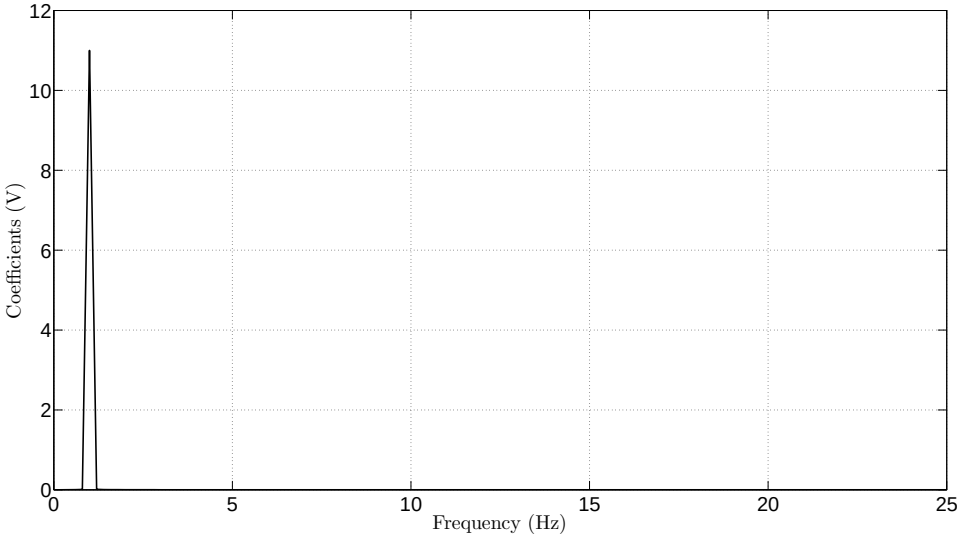

Figure 141: a plot of the fft input voltage magnitude coefficients of a 1 hz input signal with a amplitude greater than the op-amp's supply rails

natural system with a large dynamic range, or in less technical terms, represents a natural system that is capable of rapidly varying its voltage amplitude between a relatively small voltage value and a relatively large voltage value.

Conversely, such variations in input signal voltage can make the acquisition of such a signal extremely difficult, primarily because smaller amplitude signals generally require more amplification to accurately obtain than larger amplitude signals and such attributes

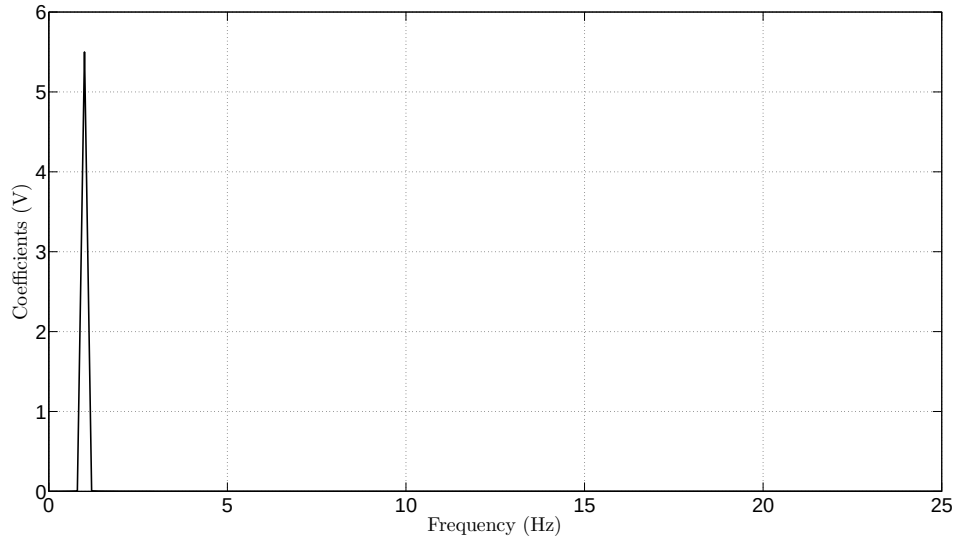

Figure 142: a plot of the fft input voltage magnitude coefficients of a 1 hz input signal with a amplitude less than the op-amp's supply rails

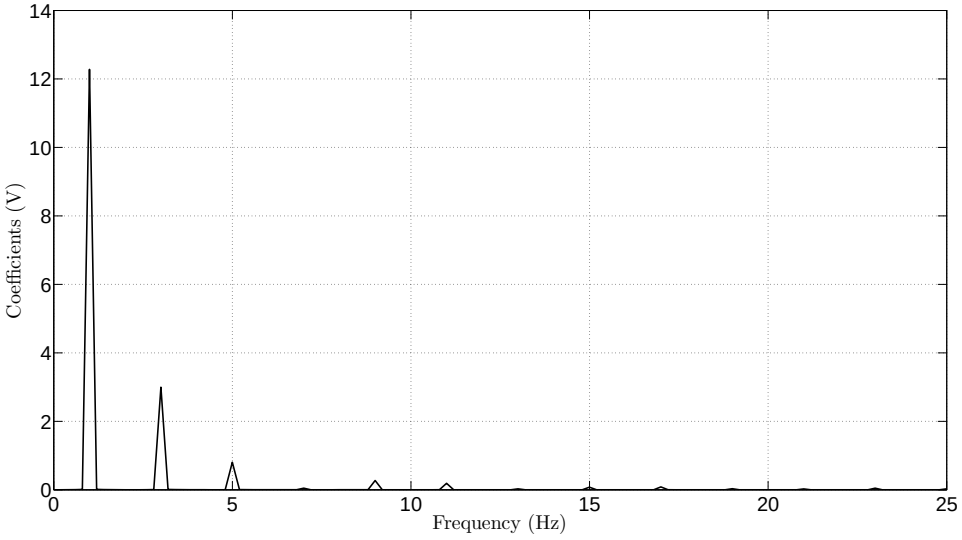

Figure 143: a plot of the fft output voltage magnitude coefficients of a 1 hz input signal with a amplitude greater than the op-amp's supply rails

limit the amount of amplification that an acquisition device can constantly apply. Thus, the distortions observed within Figure: (140), occur primarily because of the inability of the acquisition device to linearly accept the dynamic range of the natural system being observed; however, unlike the previous example, such distortions, while appearing on the output signal, neither directly harm the acquisition device nor modify the natural system beyond the innate effects introduced upon attaching the acquisition apparatus to the natural system. While the acquisition distortions depicted within Figure: (139) and Figure: (140), at least within these particular simulations, appear to be very similar because the effects of a changing input impedance or device damage were not considered, thus making any differences between the FFT spectral analysis depicted within Figure: (143) and Figure: (144) simply the result of when the amplitude exceeded the voltage rails of the acquisition device; however, such distortions will not necessarily manifest themselves in a similar spectral manner, especially since acquisition device damage or dynamic input loading, can yield erratic results relative to the reasonably simplistic spectral additions of improper acquisition dynamic range.

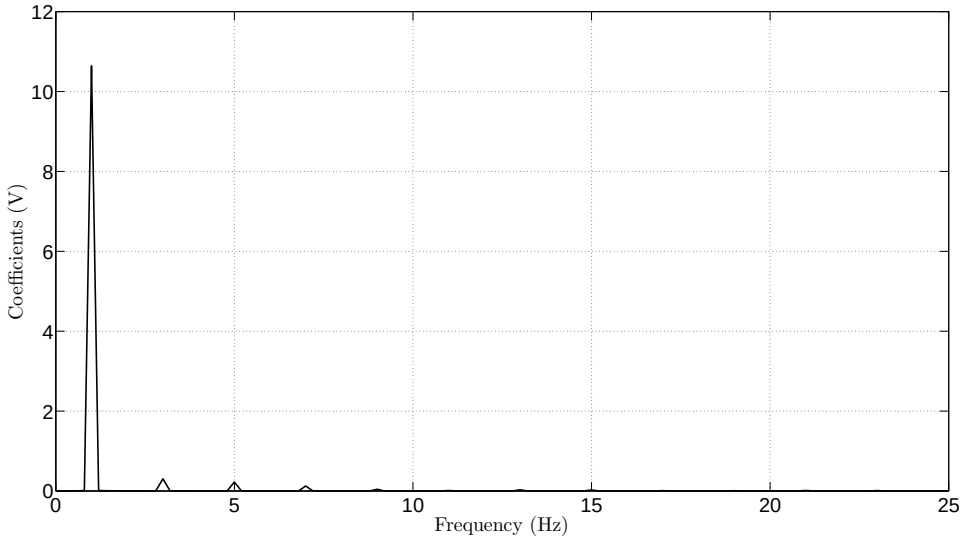

Figure 144: a plot of the fft output voltage magnitude coefficients of a 1 hz input signal with a amplitude less than the op-amp's supply rails but above the op-amp voltage gain limitations

Conversely, while an in-depth understanding of an input signals dynamic range, as previously provided, is extremely important in avoiding both acquisition distortion and possible instrumentational damage; however, another type of distortion that should also be considered is the effects of instrumentational phase shifting or amplitude inversion. Although it is worth mentioning that trying to categorize such effects as either being an X-axis amplitude distortion or a Y-axis time distortion can be somewhat convoluted,

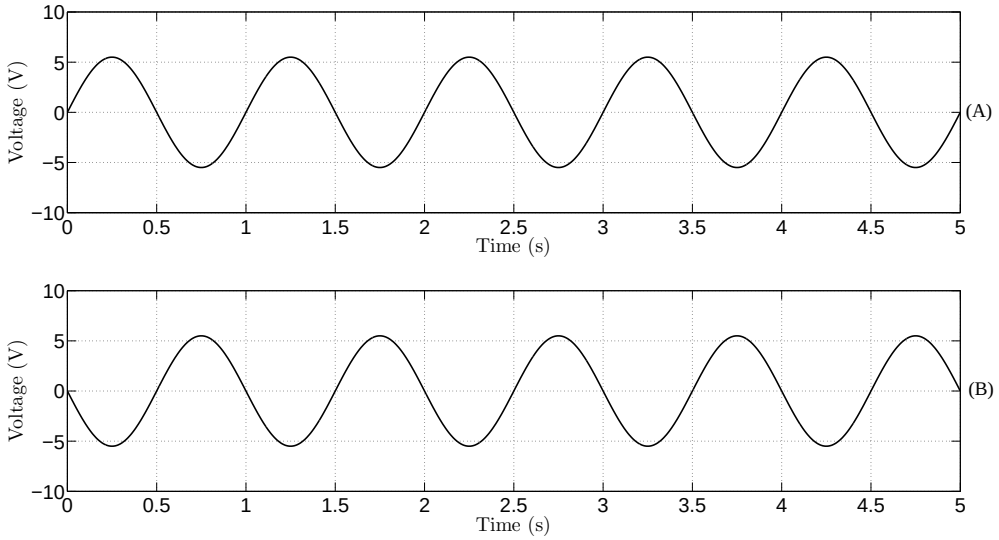

Figure 145: plots comparing (a) input voltage to (b) output voltage for a un-ideal inverting operational amplifier with a unity gain

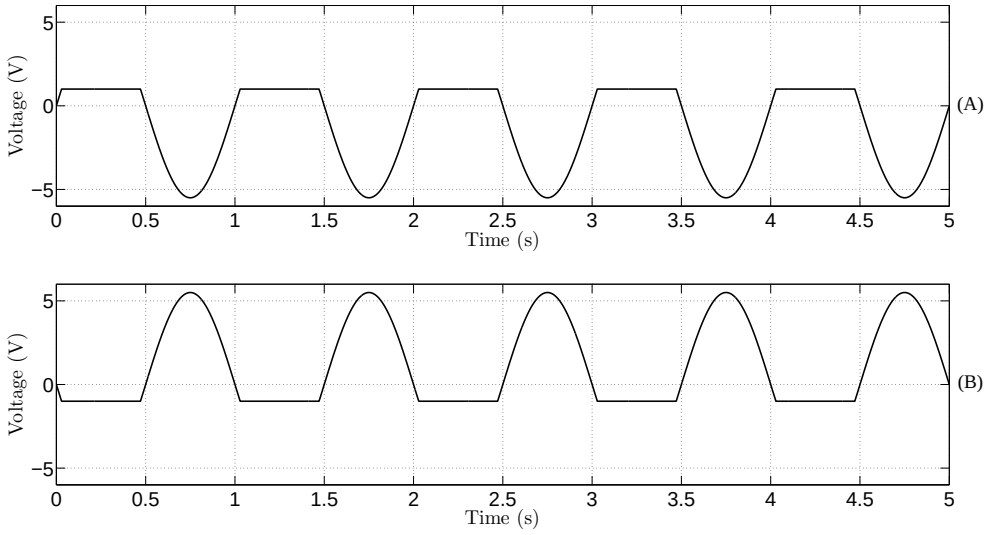

Figure 146: plots comparing a asymmetric (a) input voltage to (b) output voltage for a un-ideal inverting operational amplifier with a unity gain

primarily because the type of signal applied, along with the observational perspective taken, can make such determinations somewhat arbitrary. Nevertheless, as a general rule, an input signal that falls within the spectral pass band boundaries of an analog acquisition device — assuming for the moment the previously provided inverting operational amplifier topology — will be categorized as a amplitude distortion, while a input signal that is near or at the spectral pass band boundaries will be categorized as a time distortion. Likewise, to further clarify such attributes, consider for the moment the relationship between the input signal and the output signal, as shown by Figure: (145), in which the output signal is equal to the input signal multiplied by negative one. While, for this particular case, it could be argued that the inversion of the input signal is also equivalent to a phase shift — or time delay — of 180 degrees, at least based upon the periodic nature of the input signal to the output signal; however, from a device perspective, because there is no temporal delaying mechanism nor a prior state dependency, it is hard to physically quantify such similarities beyond simple happenstance, since, after all, the inversion of an asymmetric periodic waveform will not inherently yield a delayed or phase shifted signal, as shown by Figure: (146).

Similarly, an input signal that has a spectral content near or at the LPF or HPF ana-

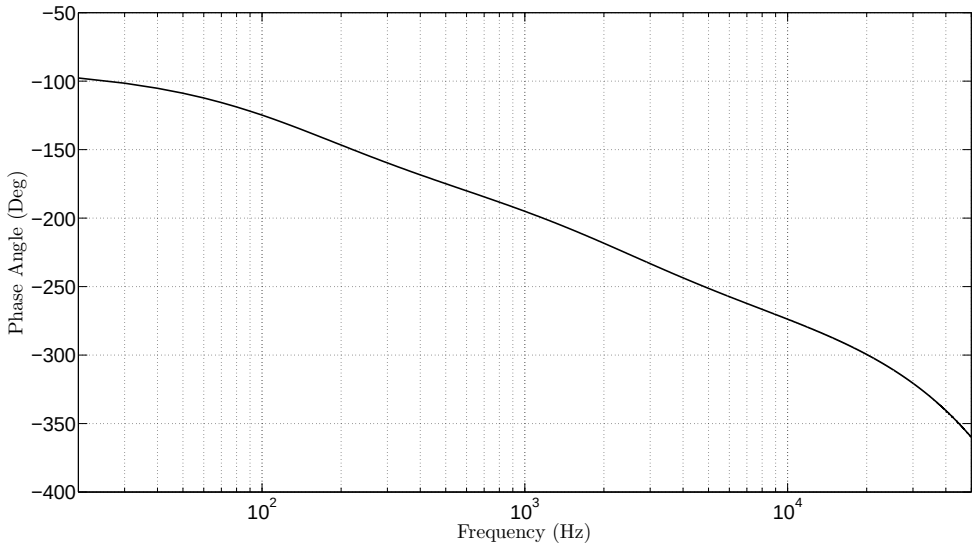

Figure 147: a phase plot of an operational amplifier band pass filter topology

log boundary will, unlike the previous example, encounter a physically produced temporal delay, or physical state dependency, that will shift or delay the applied effected spectral content by a specific amount, a notion that is illustrated by the FFT spectral phase diagram plotted within Figure: (147) of the previously described analog band pass filter that, once again, symbolizes the common types of analog operational limitations encountered. Although, it is worth mentioning that most analog devices, unlike the demonstrated band pass response previously presented, typically do have an operational region that has no phase shift associated with its usage rather than the, previously depicted, constant phase shift that arises upon the utilization of the band pass filter topology. Yet, while phase shifts or amplitude inversions are generally not considered extremely problematic or, for that matter, are seldom ever classified as being a distortion; however, such effects, if not consciously considered, can result in an acquired signal being interpreted incorrectly and can cause possible signal processing errors upon careless utilization of phase dependent mathematical operations.

$$A(t) = 52 + \text{Randi}\,(-50, 50) \tag{283}$$

$$A(t) = 52 + 50\sin\,(2\pi 2t) \tag{284}$$

Nevertheless, while the effects of analog phase distortions must be considered, especially prior to performing phase dependent mathematical operations, such device and topology-oriented effects are not the only analog specific acquisition effects that should be considered. After all, another acquisition effect — although, in some cases, this effect could arguably be classified as an environmental effect rather than an instrumentational effect — is the occurrence of time dependent component fluctuations, or more specifically, the effects of

internal gain fluctuations. Likewise, to better explain the classification ambiguity and the fundamental nature of such effects, it is important to recognize that such fluctuations have been known to occur because of changes in ambient temperature and because of physical human interaction with the acquisition system. Conversely, to elaborate further, changes in ambient temperature can cause external circuit parameters and internal gains to vary from their room temperature value, while physical human interaction can create loose

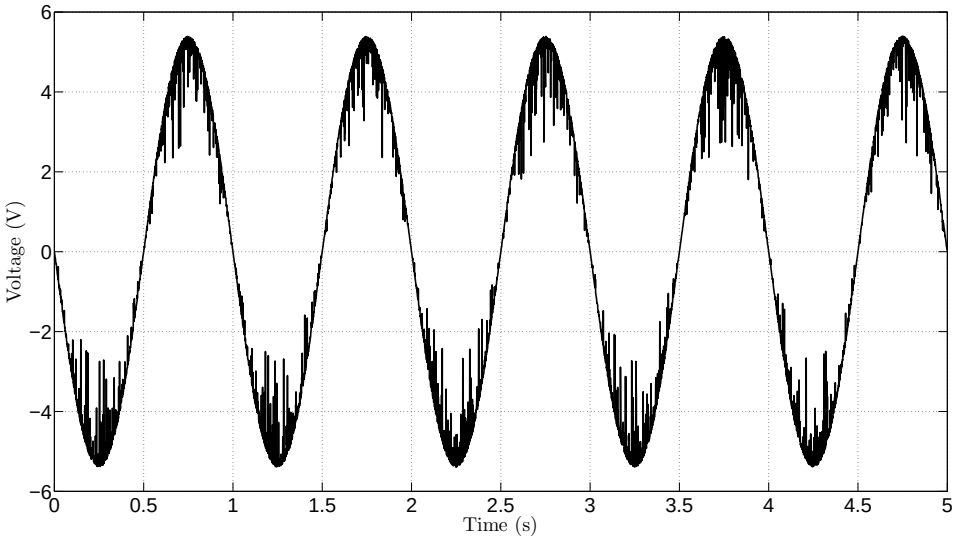

Figure 148: plot of un-ideal inverting operational amplifier output with a randomly varying internal gain

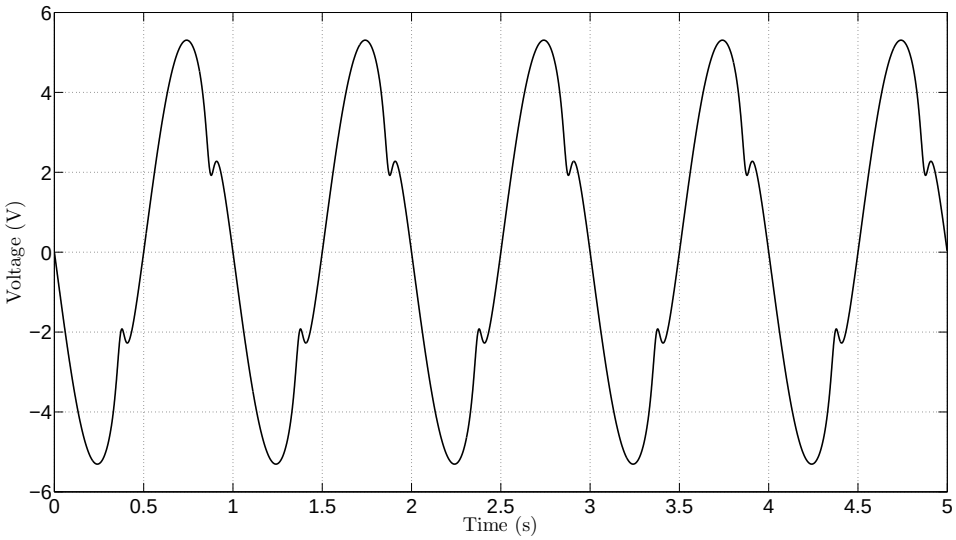

Figure 149: plot of un-ideal inverting operational amplifier output with a periodically varying internal gain

connections — especially within a prototyping environment — along with, under certain circumstances, inadvertently change circuit parameters through a process loosely surmised by the term parasitic coupling. Similarly, To illustrate this point, consider for the moment an un-ideal inverting operational amplifier with a unity pass band gain, as previously described, and an internal device gain defined by Equation: (283). Conversely, simulation of this particular scenario, using the input signal depicted within plot (A) of Figure: (145), yields an output signal, as shown by Figure: (148), that, interestingly enough, resembles some of the previously presented environmental effects. Yet, despite such visual similarities, it is important to recognize that the Gaussian properties that were previously associated with the environmental model and the Gaussian fluctuations utilized to modify the models internal gain are, in fact, the predominant rationale behind why Figure: (148) visually resembles the environmental characteristics previously presented, and furthermore, it is important to also recognize that a periodic variation, like the internal device gain defined by Equation: (284), or an arbitrary variation, could have been just as easily been utilized and would have produced visually different output characteristics — relative to the observed environmental effects —, such as those depicted within Figure: (149).

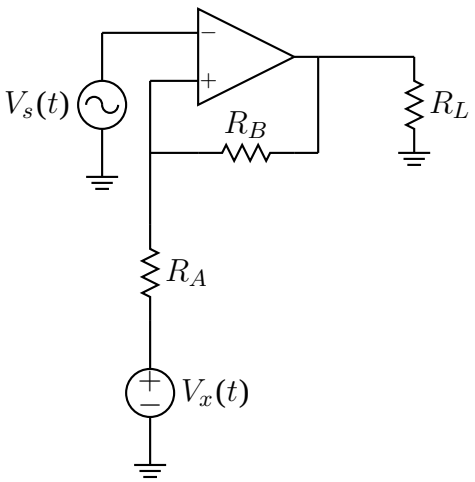

Figure 150: an operational amplifier in a schmitt trigger configuration

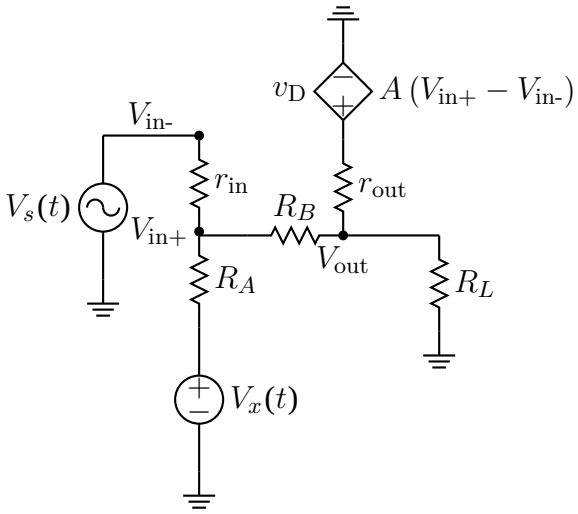

Figure 151: a un-ideal model of an operational amplifier in a schmitt trigger configuration

Likewise, while such fluctuations in instrumentational parameters — particularly fluctuations that can be associated with human interaction — are of paramount importance — a notion that will be justified through additional discussion within this chapter —; nevertheless, another instrumentational acquisition effect that should also be considered — though interestingly enough, this effect might potentially be considered a possible consequence of the, previously mentioned, concept of parasitic coupling — is the effects of temporal state dependency or previous state dependency that originates from the control system theory concept of positive feedback. While the theoretical foundations associated with positive feedback are rigorously studied and frequently applied within the electrical engineering sub discipline of control system theory, and, for the most part, such concepts, at least as they pertain to the research being presented within this dissertation, tend to promote more tangential discussion than additional clarity of pertinent concepts. Nevertheless, because control system theory concepts do occasionally manifest themselves — often times when least expected — particularly within instrumentational devices, a brief discussion on relevant concepts is merited. Conversely, to provide a brief — and heavily abridged — summarization of important control system concepts, it is important to rec-

ognize that the existence of positive feedback, at least within a given system, is typically associated with a decrease in system stability, while alternatively, the existence of negative feedback is typically associated with an increase in system stability.

Likewise, although such summarizations are far from being either theoretically explicit or complete; however, despite the inherent level of abstraction utilized, the term stability does tend to be easily correlated with device functionality and it could be rationalized that the more stable something is the better — although this is not explicitly true based upon the criteria selected and the undiscussed concept of system optimization. Nevertheless, based upon such rationalizations, a connection between why real world acquisition devices, like those previously depicted, generally utilize negative feedback within their design, and furthermore helps, to some degree, explain why oscillatory or state dependent circuit topologies — both of these topologies require some instability to function correctly — utilize some positive feedback within their design. Conversely, to begin expanding and correlating the manifestation of positive feedback topologies, particularly with possible acquisition distortions encountered, consider for the moment the visual effects of a state or temporal dependency through examination of a circuit topology commonly referred to as a Schmitt trigger, as shown by Figure: (150) and Figure: (151).

$$I_{r_{\mathrm{in}}}(k) = \frac{\mathrm{V_s(k)}}{\mathrm{r_{in}}} - \frac{\mathrm{V_{in_+}(k)}}{\mathrm{r_{in}}} \tag{285}$$

$$I_{R_B}(k) = \frac{\mathrm{V_{in_+}(k)}}{\mathrm{R_B}} - \frac{\mathrm{V_{out}(k)}}{\mathrm{R_B}} \tag{286}$$

$$I_{R_A}(k) = \frac{\mathrm{V_{in_+}(k)}}{\mathrm{R_A}} - \frac{\mathrm{V_x(k)}}{\mathrm{R_A}} \tag{287}$$

$$KCL_1 : \ 0 = \frac{\mathrm{V_{out}(k)}}{\mathrm{R_B}} - \frac{\mathrm{V_{in_+}(k)}}{\mathrm{R_B}} - \frac{\mathrm{V_{in_+}(k)}}{\mathrm{R_A}} - \frac{\mathrm{V_{in_+}(k)}}{\mathrm{r_{in}}} + \frac{\mathrm{V_x(k)}}{\mathrm{R_A}} + \frac{\mathrm{V_s(k)}}{\mathrm{r_{in}}} \tag{288}$$

$$V_d(k) = \mathrm{A}\,\mathrm{V_{in_+}(k-1)} - \mathrm{A}\,\mathrm{V_s(k)} \tag{289}$$

$$I_{r_{\mathrm{out}}}(k) = \frac{\mathrm{A}\,\mathrm{V_{in_+}(k-1)}}{\mathrm{r_{out}}} - \frac{\mathrm{V_{out}(k)}}{\mathrm{r_{out}}} - \frac{\mathrm{A}\,\mathrm{V_s(k)}}{\mathrm{r_{out}}} \tag{290}$$

$$I_{R_L}(k) = \frac{\mathrm{V_{out}(k)}}{\mathrm{R_L}} \tag{291}$$

$$I_{R_B}(k) = \frac{\mathrm{V_{out}(k)}}{\mathrm{R_B}} - \frac{\mathrm{V_{in_+}(k)}}{\mathrm{R_B}} \tag{292}$$

$$KCL_2: \; 0 = \frac{\mathrm{V_{in_+}(k)}}{\mathrm{R_B}} - \frac{\mathrm{V_{out}(k)}}{\mathrm{R_B}} - \frac{\mathrm{V_{out}(k)}}{\mathrm{R_L}} - \frac{\mathrm{V_{out}(k)}}{\mathrm{r_{out}}} + \frac{\mathrm{A}\,\mathrm{V_{in_+}(k-1)}}{\mathrm{r_{out}}} - \frac{\mathrm{A}\,\mathrm{V_s(k)}}{\mathrm{r_{out}}} \tag{293}$$

$$V_{\mathrm{in_+}}(k) = \frac{\mathrm{R_A}\,\mathrm{R_B}\,\mathrm{V_s(k)}}{\mathrm{R_A}\,\mathrm{R_B} + \mathrm{R_A}\,\mathrm{r_{in}} + \mathrm{R_B}\,\mathrm{r_{in}}} + \frac{\mathrm{R_A}\,\mathrm{r_{in}}\,\mathrm{V_{out}(k)}}{\mathrm{R_A}\,\mathrm{R_B} + \mathrm{R_A}\,\mathrm{r_{in}} + \mathrm{R_B}\,\mathrm{r_{in}}} + \frac{\mathrm{R_B}\,\mathrm{r_{in}}\,\mathrm{V_x(k)}}{\mathrm{R_A}\,\mathrm{R_B} + \mathrm{R_A}\,\mathrm{r_{in}} + \mathrm{R_B}\,\mathrm{r_{in}}} \tag{294}$$

$$V_{\mathrm{out}}(k) = \frac{\alpha_1}{\beta_1} \tag{295}$$

$$\begin{aligned}
\alpha_1 = {} & \mathrm{R_A}^2\,\mathrm{R_B}\,\mathrm{R_L}\,\mathrm{r_{out}}^2\,\mathrm{V_s(k)} + \mathrm{R_A}^2\,\mathrm{r_{in}}\,\mathrm{R_L}\,\mathrm{r_{out}}^2\,\mathrm{V_s(k)} \\
& + \mathrm{R_A}\,\mathrm{r_{in}}^2\,\mathrm{R_L}\,\mathrm{r_{out}}^2\,\mathrm{V_x(k)} + \mathrm{R_B}\,\mathrm{r_{in}}^2\,\mathrm{R_L}\,\mathrm{r_{out}}^2\,\mathrm{V_x(k)} \\
& + \mathrm{R_A}\,\mathrm{R_B}\,\mathrm{r_{in}}\,\mathrm{R_L}\,\mathrm{r_{out}}^2\,\mathrm{V_s(k)} + \mathrm{R_A}\,\mathrm{R_B}\,\mathrm{r_{in}}\,\mathrm{R_L}\,\mathrm{r_{out}}^2\,\mathrm{V_x(k)} \\
& + \mathrm{A}\,\mathrm{R_A}^2\,\mathrm{R_B}^2\,\mathrm{R_L}\,\mathrm{r_{out}}\,\mathrm{V_{in_+}(k-1)} + \mathrm{A}\,\mathrm{R_A}^2\,\mathrm{r_{in}}^2\,\mathrm{R_L}\,\mathrm{r_{out}}\,\mathrm{V_{in_+}(k-1)} \\
& + \mathrm{A}\,\mathrm{R_B}^2\,\mathrm{r_{in}}^2\,\mathrm{R_L}\,\mathrm{r_{out}}\,\mathrm{V_{in_+}(k-1)} - \mathrm{A}\,\mathrm{R_A}^2\,\mathrm{R_B}^2\,\mathrm{R_L}\,\mathrm{r_{out}}\,\mathrm{V_s(k)} \\
& - \mathrm{A}\,\mathrm{R_A}^2\,\mathrm{r_{in}}^2\,\mathrm{R_L}\,\mathrm{r_{out}}\,\mathrm{V_s(k)} - \mathrm{A}\,\mathrm{R_B}^2\,\mathrm{r_{in}}^2\,\mathrm{R_L}\,\mathrm{r_{out}}\,\mathrm{V_s(k)} \\
& + 2\,\mathrm{A}\,\mathrm{R_A}\,\mathrm{R_B}\,\mathrm{r_{in}}^2\,\mathrm{R_L}\,\mathrm{r_{out}}\,\mathrm{V_{in_+}(k-1)} + 2\,\mathrm{A}\,\mathrm{R_A}\,\mathrm{R_B}^2\,\mathrm{r_{in}}\,\mathrm{R_L}\,\mathrm{r_{out}}\,\mathrm{V_{in_+}(k-1)} \\
& + 2\,\mathrm{A}\,\mathrm{R_A}^2\,\mathrm{R_B}\,\mathrm{r_{in}}\,\mathrm{R_L}\,\mathrm{r_{out}}\,\mathrm{V_{in_+}(k-1)} - 2\,\mathrm{A}\,\mathrm{R_A}\,\mathrm{R_B}\,\mathrm{r_{in}}^2\,\mathrm{R_L}\,\mathrm{r_{out}}\,\mathrm{V_s(k)} \\
& - 2\,\mathrm{A}\,\mathrm{R_A}\,\mathrm{R_B}^2\,\mathrm{r_{in}}\,\mathrm{R_L}\,\mathrm{r_{out}}\,\mathrm{V_s(k)} - 2\,\mathrm{A}\,\mathrm{R_A}^2\,\mathrm{R_B}\,\mathrm{r_{in}}\,\mathrm{R_L}\,\mathrm{r_{out}}\,\mathrm{V_s(k)}
\end{aligned} \tag{296}$$

$$\beta_1 = \mathrm{R_A}^2\,\mathrm{R_B}^2\,\mathrm{r_{out}}^2 + \mathrm{R_L}\,\mathrm{R_A}^2\,\mathrm{R_B}^2\,\mathrm{r_{out}} + 2\,\mathrm{R_A}^2\,\mathrm{R_B}\,\mathrm{r_{in}}\,\mathrm{r_{out}}^2$$

$$+ 2\,\mathrm{R_L}\,{\mathrm{R_A}}^2\,\mathrm{R_B}\,\mathrm{r_{in}}\,\mathrm{r_{out}} + \mathrm{R_L}\,{\mathrm{R_A}}^2\,\mathrm{R_B}\,{\mathrm{r_{out}}}^2{\mathrm{R_A}}^2\,{\mathrm{r_{in}}}^2\,{\mathrm{r_{out}}}^2$$

$$+ \mathrm{R_L}\,{\mathrm{R_A}}^2\,{\mathrm{r_{in}}}^2\,\mathrm{r_{out}} + \mathrm{R_L}\,{\mathrm{R_A}}^2\,\mathrm{r_{in}}\,{\mathrm{r_{out}}}^2 + 2\,\mathrm{R_A}\,{\mathrm{R_B}}^2\,\mathrm{r_{in}}\,{\mathrm{r_{out}}}^2$$

$$+ 2\,\mathrm{R_L}\,\mathrm{R_A}\,{\mathrm{R_B}}^2\,\mathrm{r_{in}}\,\mathrm{r_{out}} + 2\,\mathrm{R_A}\,\mathrm{R_B}\,{\mathrm{r_{in}}}^2\,{\mathrm{r_{out}}}^2 + 2\,\mathrm{R_L}\,\mathrm{R_A}\,\mathrm{R_B}\,{\mathrm{r_{in}}}^2\,\mathrm{r_{out}}$$

$$+ 2\,\mathrm{R_L}\,\mathrm{R_A}\,\mathrm{R_B}\,\mathrm{r_{in}}\,{\mathrm{r_{out}}}^2 + \mathrm{R_L}\,\mathrm{R_A}\,{\mathrm{r_{in}}}^2\,{\mathrm{r_{out}}}^2 + {\mathrm{R_B}}^2\,{\mathrm{r_{in}}}^2\,{\mathrm{r_{out}}}^2$$

$$+ \mathrm{R_L}\,{\mathrm{R_B}}^2\,{\mathrm{r_{in}}}^2\,\mathrm{r_{out}} + \mathrm{R_L}\,\mathrm{R_B}\,{\mathrm{r_{in}}}^2\,{\mathrm{r_{out}}}^2 \tag{297}$$

Table 9: circuit parameters utilized within numerical simulation

Variable	Value	Units	Description
A	1000000	$\frac{V}{V}$	OP-AMP Internal Gain
r_{out}	1	$\mathbf{\Omega}$	OP-AMP Internal Output Resistance
r_{in}	10000000	$\mathbf{\Omega}$	OP-AMP Internal Input Resistance
R_L	10000	$\mathbf{\Omega}$	Output Loading Resistor
R_A	1000	$\mathbf{\Omega}$	Input Resistor
R_B	1000	$\mathbf{\Omega}$	Feedback Resistor
V_{dd}	15	V	Positive Power Supply
V_{ss}	-15	V	Negative Power Supply
V_x	-3	V	Hysteresis Offset

Likewise, the model provided within Figure: (151) can be described mathematically through the utilization of Equation: (288) and Equation: (293) — note the delayed

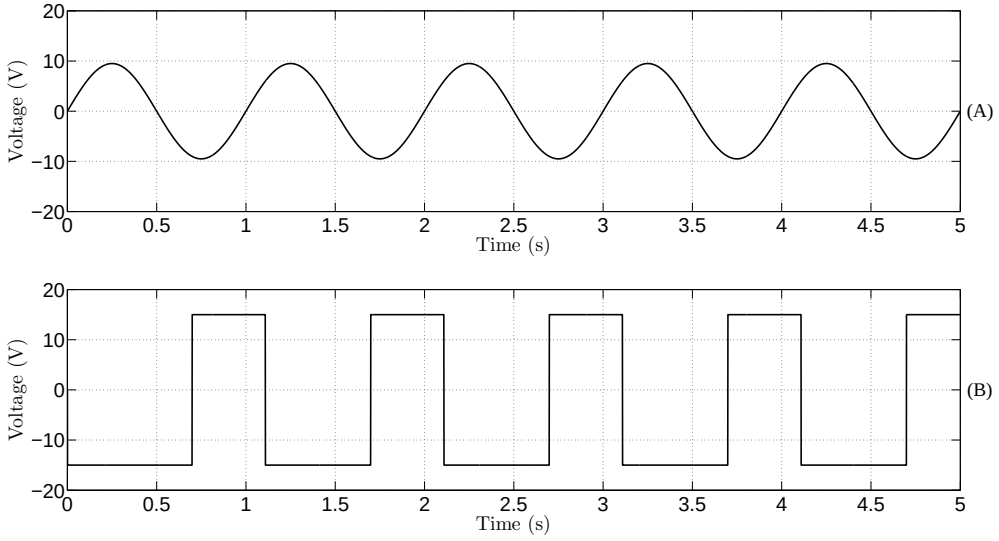

Figure 152: plot of an un-ideal schmitt trigger (a) input voltage versus (b) output voltage

$V_{\text{in}_+}(k-1)$ term was added to (A) in order to add an innate state dependency, or temporal delay, to make the equations simulate correctly — and then simulated using Equation: (294) and Equation: (295) that were substituted with component values listed within Table: (9), as shown by Figure: (152). Similarly, upon plotting the input voltage versus the output voltage, as shown by Figure: (153), a noticeable difference in the output characteristics between a forward input voltage path and a reverse input voltage path is observed upon exceeding a particular topology defined threshold. Conversely, this observable difference between forward and reverse output voltage, once again based upon the input path taken, is commonly referred to as a hysteresis response, and the presence of such a visual characteristic is indicative of a system with some type of state or temporal dependency.

Similarly, such visual characteristics, although within this particular case created through the careful selection of circuit topology, can occur naturally within electrically conductive materials, like inductors or ionic solutions, and such materials can be extremely difficult to theoretically predict depending upon the type of hysteresis observed — since not all materials have a singular state dependency that is easy to model. Still, while most

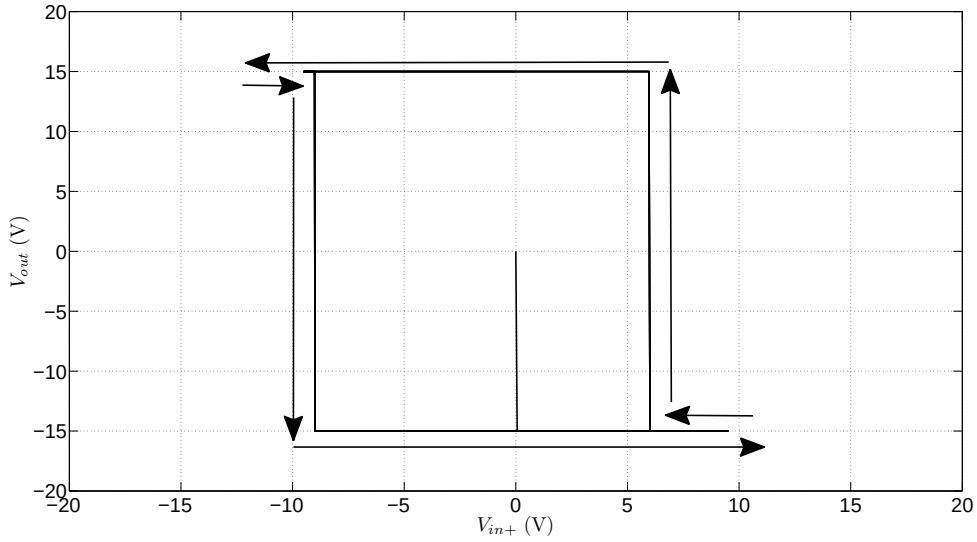

Figure 153: plot of an un-ideal schmitt trigger input voltage versus output voltage with arrows depicting the direction the input voltage is changing

acquisition topologies typically do not inherently incorporate such state or temporal dependencies within their internal design, — although apparatus wires and wire interconnections do inherently have some inductive properties associated with their usage, though such attributes are usually considered negligible —, it is possible that the improper connection of a measuring apparatus could accidentally introduce such dependencies if a positive feedback path was achieved from such a connection. Nevertheless, although encountering or accidentally introducing such dependencies, particularly within commercial instrumentation, is considered to be an extremely rare occurrence; however, the ability to recognize and isolate such occurrences is an extremely beneficial skill, especially when trying to determine if an observed hysteresis resulted from a instrumentational effect or a natural occurrence.

Conversely, while a hysteresis response is a possible consequence of positive feedback; however, such consequences are not necessarily the norm since, more often than not, the haphazard introduction of positive feedback, at least within an electrical system, generally results in system instability and produces observable oscillatory characteristics; although it is worth mentioning that, such oscillatory characteristics, are not — necessarily — always the result of system instability, since the manifestation of such characteristics, particularly within a mechanical system, can result in the physical destruction of the system rather than a steady-state oscillatory response. Yet, because electrical systems are generally bounded by the power that is supplied to them, such boundaries do tend to prevent such instabilities from destroying an unstable electrical system, hence why oscillatory characteristics are frequently associated with electrical instability rather than with the devices destruction. Likewise, while there are a number of disciplinary caveats associated with the terms oscillatory and instability — generally the term marginal instability is associated with stable oscillatory phenomena — yet, such levels of theoretical understanding, while being very

important for the successful analysis and implementation of a actual control system, is not strictly necessary for the visual identification and classification of positive feedback.

Conversely, because the current focus of discussion is primarily oriented on the visual identification and localization of instrumentational distortions — as opposed to the theoretical analysis and implementation of control system theory —, consider for the moment the Wein bridge oscillator circuit topology — a topology that, at least when configured correctly, is best surmised as being a marginally stable circuit that is created through the careful application of both positive and negative feedback —, as shown by Figure: (154) and Figure: (155), that is mathematically modeled by Equation: (300), Equation: (305), Equation: (309), and Equation: (314).

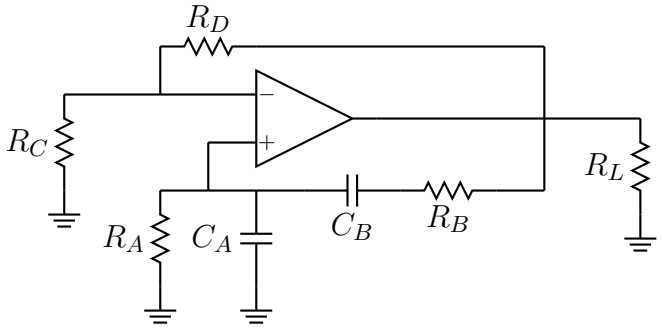

Figure 154: an operational amplifier in a wein bridge oscillator configuration

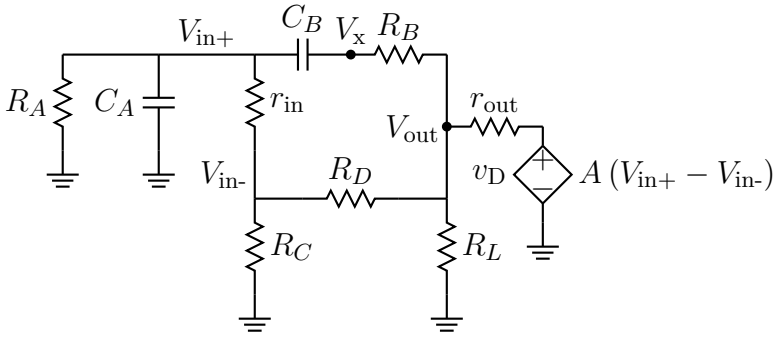

Figure 155: a un-ideal model of an operational amplifier in a wein bridge oscillator configuration

$$V'_{\mathrm{in}_+}(k) = \frac{\mathrm{V_{in_+}(k)}}{\Delta \mathrm{t}} - \frac{\mathrm{V_{in_+}(k-1)}}{\Delta \mathrm{t}} \tag{298}$$

$$V'_{\mathrm{x}}(k) = \frac{\mathrm{V_x(k)}}{\Delta \mathrm{t}} - \frac{\mathrm{V_x(k-1)}}{\Delta \mathrm{t}} \tag{299}$$

$$KVL_1: \ 0 = \mathrm{V_{in_+}(k)} - \frac{\mathrm{V_x(k)}}{\Delta \mathrm{t}} + \frac{\mathrm{V_x(k-1)}}{\Delta \mathrm{t}} + \frac{\mathrm{V_{out}(k)}}{\mathrm{C_B\,R_B}} - \frac{\mathrm{V_x(k)}}{\mathrm{C_B\,R_B}} \tag{300}$$

$$I_{C_B}(k) = \frac{\mathrm{C_B\,V_{in_+}(k-1)}}{\Delta \mathrm{t}} - \frac{\mathrm{C_B\,V_{in_+}(k)}}{\Delta \mathrm{t}} + \frac{\mathrm{C_B\,V_x(k)}}{\Delta \mathrm{t}} - \frac{\mathrm{C_B\,V_x(k-1)}}{\Delta \mathrm{t}} \tag{301}$$

$$I_{r_{\mathrm{in}}}(k) = \frac{\mathrm{V_{in_+}(k)}}{\mathrm{r_{in}}} - \frac{\mathrm{V_{in_-}(k)}}{\mathrm{r_{in}}} \tag{302}$$

$$I_{C_A}(k) = \frac{\mathrm{C_A\,V_{in_+}(k)}}{\Delta \mathrm{t}} - \frac{\mathrm{C_A\,V_{in_+}(k-1)}}{\Delta \mathrm{t}} \tag{303}$$

$$I_{R_A}(k) = \frac{\mathrm{V_{in_+}(k)}}{\mathrm{R_A}} \tag{304}$$

$$\begin{aligned} KCL_1: \ 0 = {} & \frac{\mathrm{V_{in_-}(k)}}{\mathrm{r_{in}}} - \frac{\mathrm{V_{in_+}(k)}}{\mathrm{R_A}} - \frac{\mathrm{V_{in_+}(k)}}{\mathrm{r_{in}}} - \frac{\mathrm{C_A\,V_{in_+}(k)}}{\Delta \mathrm{t}} + \frac{\mathrm{C_A\,V_{in_+}(k-1)}}{\Delta \mathrm{t}} \\ & - \frac{\mathrm{C_B\,V_{in_+}(k)}}{\Delta \mathrm{t}} + \frac{\mathrm{C_B\,V_{in_+}(k-1)}}{\Delta \mathrm{t}} + \frac{\mathrm{C_B\,V_x(k)}}{\Delta \mathrm{t}} - \frac{\mathrm{C_B\,V_x(k-1)}}{\Delta \mathrm{t}} \end{aligned} \tag{305}$$

$$I_{R_D}(k) = \frac{\mathrm{V_{out}(k)}}{\mathrm{R_D}} - \frac{\mathrm{V_{in_-}(k)}}{\mathrm{R_D}} \tag{306}$$

$$I_{R_C}(k) = \frac{\mathrm{V_{in_-}(k)}}{\mathrm{R_C}} \tag{307}$$

$$I_{r_{\mathrm{in}}}(k) = \frac{\mathrm{V_{in_-}(k)}}{\mathrm{r_{in}}} - \frac{\mathrm{V_{in_+}(k)}}{\mathrm{r_{in}}} \tag{308}$$

$$KCL_2: \ 0 = \frac{\mathrm{V_{in_+}(k)}}{\mathrm{r_{in}}} - \frac{\mathrm{V_{in_-}(k)}}{\mathrm{R_D}} - \frac{\mathrm{V_{in_-}(k)}}{\mathrm{r_{in}}} - \frac{\mathrm{V_{in_-}(k)}}{\mathrm{R_C}} + \frac{\mathrm{V_{out}(k)}}{\mathrm{R_D}} \tag{309}$$

$$V_d(k) = \mathrm{A\,V_{in_+}(k)} - \mathrm{A\,V_{in_-}(k)} \tag{310}$$

$$I_{r_{\mathrm{out}}}(k) = \frac{\mathrm{A\,V_{in_+}(k)}}{\mathrm{r_{out}}} - \frac{\mathrm{A\,V_{in_-}(k)}}{\mathrm{r_{out}}} - \frac{\mathrm{V_{out}(k)}}{\mathrm{r_{out}}} \tag{311}$$

$$I_{R_D}(k) = \frac{\mathrm{V_{out}(k)}}{\mathrm{R_D}} - \frac{\mathrm{V_{in_-}(k)}}{\mathrm{R_D}} \tag{312}$$

$$I_{R_B}(k) = \frac{\mathrm{V_{out}(k)}}{\mathrm{R_B}} - \frac{\mathrm{V_x(k)}}{\mathrm{R_B}} \tag{313}$$

$$\begin{aligned} KCL_3: \ 0 = & \frac{\mathrm{V_{in_-}(k)}}{\mathrm{R_D}} - \frac{\mathrm{V_{out}(k)}}{\mathrm{R_B}} - \frac{\mathrm{V_{out}(k)}}{\mathrm{R_D}} + \frac{\mathrm{V_x(k)}}{\mathrm{R_B}} - \frac{\mathrm{V_{out}(k)}}{\mathrm{r_{out}}} \\ & - \frac{\mathrm{A\,V_{in_-}(k)}}{\mathrm{r_{out}}} + \frac{\mathrm{A\,V_{in_+}(k)}}{\mathrm{r_{out}}} \end{aligned} \tag{314}$$

Table 10: circuit parameters utilized within numerical simulation

Variable	Value	Units	Description
A	1000000	$\frac{V}{V}$	OP-AMP Internal Gain
r_{out}	1	Ω	OP-AMP Internal Output Resistance
r_{in}	1000000	Ω	OP-AMP Internal Input Resistance
R_L	100000	Ω	Output Loading Resistor
R_A	10000	Ω	Tank Resistor 1
R_B	10000	Ω	Tank Resistor 2
R_C	1000	Ω	Input Resistor
R_D	2100	Ω	Feedback Resistor
C_A	0.00000001	Ω	Tank Capacitor 1
C_B	0.00000001	Ω	Tank Capacitor 2
V_{dd}	15	V	Positive Power Supply
V_{ss}	-15	V	Negative Power Supply

Similarly, upon substituting the values found within Table: (10) into the solved system equations — as shown by Equation: (315), Equation: (316), Equation: (317), and Equation: (318) — and plotting the output signal, as shown by Figure: (156), yields an expected oscillatory response. Likewise, minor variations of the negative feedback gain ratio, as shown by Equation: (323), and re-simulation of the previous equations, produce plots, as shown by Figure: (157) and Figure: (158), that depict how system stability can be obtained through the variation of negative feedback — despite the presence of positive feedback within the system — and how bounded system instability generally will visually

manifest itself within an electrical system.

$$V_{\mathrm{x}}(k) = \frac{\Delta \mathrm{t}\, \mathrm{V_{out}(k)}}{\Delta \mathrm{t} + \mathrm{C_B}\, \mathrm{R_B}} + \frac{\mathrm{C_B}\, \mathrm{R_B}\, \mathrm{V_x(k-1)}}{\Delta \mathrm{t} + \mathrm{C_B}\, \mathrm{R_B}} + \frac{\mathrm{C_B}\, \Delta \mathrm{t}\, \mathrm{R_B}\, \mathrm{V_{in_+}(k)}}{\Delta \mathrm{t} + \mathrm{C_B}\, \mathrm{R_B}} \tag{315}$$

$$V_{\mathrm{in_-}}(k) = \frac{\mathrm{R_C}\, \mathrm{R_D}\, \mathrm{V_{in_+}(k)}}{\mathrm{R_C}\, \mathrm{R_D} + \mathrm{R_C}\, \mathrm{r_{in}} + \mathrm{R_D}\, \mathrm{r_{in}}} + \frac{\mathrm{R_C}\, \mathrm{r_{in}}\, \mathrm{V_{out}(k)}}{\mathrm{R_C}\, \mathrm{R_D} + \mathrm{R_C}\, \mathrm{r_{in}} + \mathrm{R_D}\, \mathrm{r_{in}}} \tag{316}$$

$$V_{\mathrm{in_+}}(k) = \frac{\alpha_1}{\beta_1} \tag{317}$$

$$V_{\mathrm{out}}(k) = \frac{\alpha_2}{\beta_2} \tag{318}$$

$$\begin{aligned}
\alpha_1 = {} & \Delta \mathrm{t}^4\, \mathrm{R_A}\, \mathrm{R_C}^2\, \mathrm{R_D}\, \mathrm{V_{out}(k)} + \Delta \mathrm{t}^4\, \mathrm{R_A}\, \mathrm{R_C}^2\, \mathrm{r_{in}}\, \mathrm{V_{out}(k)} + \mathrm{C_A}\, \Delta \mathrm{t}^3\, \mathrm{R_A}\, \mathrm{R_C}^2\, \mathrm{R_D}^2\, \mathrm{V_{in_+}(k-1)} \\
& + \mathrm{C_A}\, \Delta \mathrm{t}^3\, \mathrm{R_A}\, \mathrm{R_C}^2\, \mathrm{r_{in}}^2\, \mathrm{V_{in_+}(k-1)} + \mathrm{C_A}\, \Delta \mathrm{t}^3\, \mathrm{R_A}\, \mathrm{R_D}^2\, \mathrm{r_{in}}^2\, \mathrm{V_{in_+}(k-1)} \\
& + \mathrm{C_B}\, \Delta \mathrm{t}^3\, \mathrm{R_A}\, \mathrm{R_C}^2\, \mathrm{R_D}^2\, \mathrm{V_{out}(k)} + \mathrm{C_B}\, \Delta \mathrm{t}^3\, \mathrm{R_A}\, \mathrm{R_D}^2\, \mathrm{r_{in}}^2\, \mathrm{V_{in_+}(k-1)} \\
& + \mathrm{C_B}\, \Delta \mathrm{t}^3\, \mathrm{R_A}\, \mathrm{R_D}^2\, \mathrm{r_{in}}^2\, \mathrm{V_{out}(k)} - \mathrm{C_B}\, \Delta \mathrm{t}^3\, \mathrm{R_A}\, \mathrm{R_C}^2\, \mathrm{R_D}^2\, \mathrm{V_x(k-1)} \\
& - \mathrm{C_B}\, \Delta \mathrm{t}^3\, \mathrm{R_A}\, \mathrm{R_D}^2\, \mathrm{r_{in}}^2\, \mathrm{V_x(k-1)} + \Delta \mathrm{t}^4\, \mathrm{R_A}\, \mathrm{R_C}\, \mathrm{R_D}\, \mathrm{r_{in}}\, \mathrm{V_{out}(k)} \\
& + 2\, \mathrm{C_A}\, \Delta \mathrm{t}^3\, \mathrm{R_A}\, \mathrm{R_C}\, \mathrm{R_D}\, \mathrm{r_{in}}^2\, \mathrm{V_{in_+}(k-1)} + 2\, \mathrm{C_A}\, \Delta \mathrm{t}^3\, \mathrm{R_A}\, \mathrm{R_C}\, \mathrm{R_D}^2\, \mathrm{r_{in}}\, \mathrm{V_{in_+}(k-1)} \\
& + 2\, \mathrm{C_B}\, \Delta \mathrm{t}^3\, \mathrm{R_A}\, \mathrm{R_C}\, \mathrm{R_D}\, \mathrm{r_{in}}^2\, \mathrm{V_{in_+}(k-1)} + 2\, \mathrm{C_B}\, \Delta \mathrm{t}^3\, \mathrm{R_A}\, \mathrm{R_C}\, \mathrm{R_D}^2\, \mathrm{r_{in}}\, \mathrm{V_{in_+}(k-1)} \\
& + 2\, \mathrm{C_B}\, \Delta \mathrm{t}^3\, \mathrm{R_A}\, \mathrm{R_B}\, \mathrm{R_C}^2\, \mathrm{r_{in}}\, \mathrm{V_{out}(k)} + 2\, \mathrm{C_B}\, \Delta \mathrm{t}^3\, \mathrm{R_A}\, \mathrm{R_C}\, \mathrm{R_D}\, \mathrm{r_{in}}^2\, \mathrm{V_{out}(k)} \\
& + 2\, \mathrm{C_B}\, \Delta \mathrm{t}^3\, \mathrm{R_A}\, \mathrm{R_C}^2\, \mathrm{R_D}\, \mathrm{r_{in}}\, \mathrm{V_{out}(k)} - 2\, \mathrm{C_B}\, \Delta \mathrm{t}^3\, \mathrm{R_A}\, \mathrm{R_C}\, \mathrm{R_D}\, \mathrm{r_{in}}^2\, \mathrm{V_x(k-1)} \\
& - 2\, \mathrm{C_B}\, \Delta \mathrm{t}^3\, \mathrm{R_A}\, \mathrm{R_C}^2\, \mathrm{R_D}\, \mathrm{r_{in}}\, \mathrm{V_x(k-1)} + 2\, \mathrm{C_B}^2\, \Delta \mathrm{t}^2\, \mathrm{R_A}\, \mathrm{R_B}\, \mathrm{R_C}^2\, \mathrm{R_D}^2\, \mathrm{V_{in_+}(k-1)} \\
& + 2\, \mathrm{C_B}^2\, \Delta \mathrm{t}^2\, \mathrm{R_A}\, \mathrm{R_B}\, \mathrm{R_C}^2\, \mathrm{r_{in}}^2\, \mathrm{V_{in_+}(k-1)} + \mathrm{C_B}^3\, \Delta \mathrm{t}\, \mathrm{R_A}\, \mathrm{R_B}^2\, \mathrm{R_C}^2\, \mathrm{r_{in}}^2\, \mathrm{V_{in_+}(k-1)} \\
& + \mathrm{C_B}^2\, \Delta \mathrm{t}^2\, \mathrm{R_A}\, \mathrm{R_B}^2\, \mathrm{R_C}^2\, \mathrm{R_D}\, \mathrm{V_{out}(k)} + 2\, \mathrm{C_B}^2\, \Delta \mathrm{t}^2\, \mathrm{R_A}\, \mathrm{R_B}\, \mathrm{R_D}^2\, \mathrm{r_{in}}^2\, \mathrm{V_{in_+}(k-1)} \\
& + \mathrm{C_B}^2\, \Delta \mathrm{t}^2\, \mathrm{R_A}\, \mathrm{R_B}\, \mathrm{R_C}^2\, \mathrm{r_{in}}^2\, \mathrm{V_{out}(k)} + \mathrm{C_B}^2\, \Delta \mathrm{t}^2\, \mathrm{R_A}\, \mathrm{R_B}^2\, \mathrm{R_C}^2\, \mathrm{r_{in}}\, \mathrm{V_{out}(k)} \\
& - \mathrm{C_B}^2\, \Delta \mathrm{t}^2\, \mathrm{R_A}\, \mathrm{R_B}\, \mathrm{R_C}^2\, \mathrm{R_D}^2\, \mathrm{V_x(k-1)} - \mathrm{C_B}^2\, \Delta \mathrm{t}^2\, \mathrm{R_A}\, \mathrm{R_B}\, \mathrm{R_C}^2\, \mathrm{r_{in}}^2\, \mathrm{V_x(k-1)} \\
& + 2\, \mathrm{C_B}\, \Delta \mathrm{t}^3\, \mathrm{R_A}\, \mathrm{R_B}\, \mathrm{R_C}\, \mathrm{R_D}\, \mathrm{r_{in}}\, \mathrm{V_{out}(k)} + \mathrm{C_A}\, \mathrm{C_B}^2\, \Delta \mathrm{t}\, \mathrm{R_A}\, \mathrm{R_B}^2\, \mathrm{R_C}^2\, \mathrm{R_D}^2\, \mathrm{V_{in_+}(k-1)} \\
& + \mathrm{C_A}\, \mathrm{C_B}^2\, \Delta \mathrm{t}\, \mathrm{R_A}\, \mathrm{R_B}^2\, \mathrm{R_D}^2\, \mathrm{r_{in}}^2\, \mathrm{V_{in_+}(k-1)} + 2\, \mathrm{C_A}\, \mathrm{C_B}\, \Delta \mathrm{t}^2\, \mathrm{R_A}\, \mathrm{R_B}\, \mathrm{R_C}^2\, \mathrm{R_D}^2\, \mathrm{V_{in_+}(k-1)} \\
& + 2\, \mathrm{C_A}\, \mathrm{C_B}\, \Delta \mathrm{t}^2\, \mathrm{R_A}\, \mathrm{R_B}\, \mathrm{R_D}^2\, \mathrm{r_{in}}^2\, \mathrm{V_{in_+}(k-1)} + 4\, \mathrm{C_B}^2\, \Delta \mathrm{t}^2\, \mathrm{R_A}\, \mathrm{R_B}\, \mathrm{R_C}\, \mathrm{R_D}\, \mathrm{r_{in}}^2\, \mathrm{V_{in_+}(k-1)}
\end{aligned}$$

$$
\begin{aligned}
&+ 4\,C_B{}^2\,\Delta t^2\,R_A\,R_B\,R_C{}^2\,R_D\,r_{in}\,V_{in_+}(k-1) + 2\,C_B{}^3\,\Delta t\,R_A\,R_B{}^2\,R_C\,R_D\,r_{in}{}^2\,V_{in_+}(k-1)\\
&+ 2\,C_B{}^3\,\Delta t\,R_A\,R_B{}^2\,R_C{}^2\,R_D\,r_{in}\,V_{in_+}(k-1) + 2\,C_B{}^2\,\Delta t^2\,R_A\,R_B\,R_C\,R_D\,r_{in}{}^2\,V_{out}(k)\\
&+ 2\,C_B{}^2\,\Delta t^2\,R_A\,R_B\,R_C{}^2\,R_D\,r_{in}\,V_{out}(k) + C_B{}^2\,\Delta t^2\,R_A\,R_B{}^2\,R_C\,R_D\,r_{in}\,V_{out}(k)\\
&- 2\,C_B{}^2\,\Delta t^2\,R_A\,R_B\,R_C\,R_D{}^2\,r_{in}\,V_x(k-1) - 2\,C_B{}^2\,\Delta t^2\,R_A\,R_B\,R_C{}^2\,R_D\,r_{in}\,V_x(k-1)\\
&+ 2\,C_A\,C_B{}^2\,\Delta t\,R_A\,R_B{}^2\,R_C\,R_D{}^2\,r_{in}\,V_{in_+}(k-1)\\
&+ 4\,C_A\,C_B\,\Delta t^2\,R_A\,R_B\,R_C{}^2\,R_D\,r_{in}\,V_{in_+}(k-1)
\end{aligned}
\tag{319}
$$

$$
\begin{aligned}
\beta_1 = \; &- R_A\,C_B{}^3\,\Delta t^2\,R_B{}^2\,R_C{}^2\,R_D{}^2 - 2\,R_A\,C_B{}^3\,\Delta t^2\,R_B{}^2\,R_C{}^2\,R_D\,r_{in}\\
&- 2\,R_A\,C_B{}^3\,\Delta t^2\,R_B{}^2\,R_C\,R_D{}^2\,r_{in} - 2\,R_A\,C_B{}^3\,\Delta t^2\,R_B{}^2\,R_C\,R_D\,r_{in}{}^2 - R_A\,C_B{}^3\,\Delta t^2\,R_B{}^2\,R_D{}^2\,r_{in}{}^2\\
&+ 2\,R_A\,C_B{}^3\,\Delta t\,R_B{}^2\,R_C{}^2\,R_D\,r_{in} + R_A\,C_B{}^3\,\Delta t\,R_B{}^2\,R_C{}^2\,r_{in}{}^2 + 2\,R_A\,C_B{}^3\,\Delta t\,R_B{}^2\,R_C\,R_D{}^2\,r_{in}\\
&+ R_A\,C_B{}^3\,\Delta t\,R_B{}^2\,R_D{}^2\,r_{in}{}^2 - R_A\,C_B{}^2\,\Delta t^3\,R_B\,R_C{}^2\,R_D{}^2 - 2\,R_A\,C_B{}^2\,\Delta t^3\,R_B\,R_C{}^2\,R_D\,r_{in}\\
&- 2\,R_A\,C_B{}^2\,\Delta t^3\,R_B\,R_C\,R_D{}^2\,r_{in} - 2\,R_A\,C_B{}^2\,\Delta t^3\,R_B\,R_C\,R_D\,r_{in}{}^2 - R_A\,C_B{}^2\,\Delta t^3\,R_B\,R_D{}^2\,r_{in}{}^2\\
&+ 2\,C_B{}^2\,\Delta t^2\,R_B{}^2\,R_C{}^2\,R_D\,r_{in} + R_A\,C_B{}^2\,\Delta t^2\,R_B{}^2\,R_C{}^2\,R_D + C_B{}^2\,\Delta t^2\,R_B{}^2\,R_C{}^2\,r_{in}{}^2\\
&+ 2\,C_B{}^2\,\Delta t^2\,R_B{}^2\,R_C\,R_D{}^2\,r_{in} + R_A\,C_B{}^2\,\Delta t^2\,R_B{}^2\,R_C\,R_D{}^2 + 2\,C_B{}^2\,\Delta t^2\,R_B{}^2\,R_C\,R_D\,r_{in}{}^2\\
&+ C_B{}^2\,\Delta t^2\,R_B{}^2\,R_D{}^2\,r_{in}{}^2 + R_A\,C_B{}^2\,\Delta t^2\,R_B{}^2\,R_D{}^2\,r_{in} + 2\,R_A\,C_B{}^2\,\Delta t^2\,R_B\,R_C{}^2\,R_D{}^2\\
&+ 2\,R_A\,C_B{}^2\,\Delta t^2\,R_B\,R_C{}^2\,r_{in}{}^2 + 4\,R_A\,C_B{}^2\,\Delta t^2\,R_B\,R_C\,R_D{}^2\,r_{in} + 4\,R_A\,C_B{}^2\,\Delta t^2\,R_B\,R_C\,R_D\,r_{in}{}^2\\
&+ C_A\,R_A\,C_B{}^2\,\Delta t\,R_B{}^2\,R_C{}^2\,R_D{}^2 + 2\,C_A\,R_A\,C_B{}^2\,\Delta t\,R_B{}^2\,R_C{}^2\,R_D\,r_{in}\\
&+ 2\,C_A\,R_A\,C_B{}^2\,\Delta t\,R_B{}^2\,R_C\,R_D{}^2\,r_{in} + 2\,C_A\,R_A\,C_B{}^2\,\Delta t\,R_B{}^2\,R_C\,R_D\,r_{in}{}^2\\
&+ 2\,C_B\,\Delta t^3\,R_B\,R_C{}^2\,R_D{}^2 + 4\,C_B\,\Delta t^3\,R_B\,R_C{}^2\,R_D\,r_{in} + 2\,R_A\,C_B\,\Delta t^3\,R_B\,R_C{}^2\,R_D\\
&+ 2\,R_A\,C_B\,\Delta t^3\,R_B\,R_C{}^2\,r_{in} + 4\,C_B\,\Delta t^3\,R_B\,R_C\,R_D{}^2\,r_{in} + 2\,R_A\,C_B\,\Delta t^3\,R_B\,R_C\,R_D{}^2\\
&+ 4\,R_A\,C_B\,\Delta t^3\,R_B\,R_C\,R_D\,r_{in} + 2\,C_B\,\Delta t^3\,R_B\,R_D{}^2\,r_{in}{}^2 + 2\,R_A\,C_B\,\Delta t^3\,R_B\,R_D{}^2\,r_{in}\\
&+ 2\,R_A\,C_B\,\Delta t^3\,R_C{}^2\,R_D\,r_{in} + R_A\,C_B\,\Delta t^3\,R_C{}^2\,r_{in}{}^2 + 2\,R_A\,C_B\,\Delta t^3\,R_C\,R_D{}^2\,r_{in}\\
&+ R_A\,C_B\,\Delta t^3\,R_D{}^2\,r_{in}{}^2 + 2\,C_A\,R_A\,C_B\,\Delta t^2\,R_B\,R_C{}^2\,R_D{}^2 + 4\,C_A\,R_A\,C_B\,\Delta t^2\,R_B\,R_C{}^2\,R_D\,r_{in}\\
&+ 4\,C_A\,R_A\,C_B\,\Delta t^2\,R_B\,R_C\,R_D{}^2\,r_{in} + 4\,C_A\,R_A\,C_B\,\Delta t^2\,R_B\,R_C\,R_D\,r_{in}{}^2\\
&+ \Delta t^4\,R_C{}^2\,R_D{}^2 + 2\,\Delta t^4\,R_C{}^2\,R_D\,r_{in} + R_A\,\Delta t^4\,R_C{}^2\,R_D + \Delta t^4\,R_C{}^2\,r_{in}{}^2 + R_A\,\Delta t^4\,R_C{}^2\,r_{in}\\
&+ R_A\,\Delta t^4\,R_C\,R_D{}^2 + 2\,\Delta t^4\,R_C\,R_D\,r_{in}{}^2 + 2\,R_A\,\Delta t^4\,R_C\,R_D\,r_{in} + \Delta t^4\,R_D{}^2\,r_{in}{}^2 + R_A\,\Delta t^4\,R_D{}^2\,r_{in}\\
&+ 2\,C_A\,R_A\,\Delta t^3\,R_C{}^2\,R_D\,r_{in} + C_A\,R_A\,\Delta t^3\,R_C{}^2\,r_{in}{}^2 + 2\,C_A\,R_A\,\Delta t^3\,R_C\,R_D{}^2\,r_{in}
\end{aligned}
$$

$$+ C_A\, R_A\, \Delta t^3\, {R_D}^2\, {r_{in}}^2 \tag{320}$$

$$\begin{aligned}
\alpha_2 = {} & {C_B}^2\, R_A\, R_B\, R_C\, r_{out}\, V_{in_+}(k-1) + {C_B}^2\, R_A\, R_C\, R_D\, r_{out}\, V_x(k-1) \\
& + {C_B}^2\, R_A\, R_D\, r_{in}\, r_{out}\, V_x(k-1) + C_A\, \Delta t\, R_A\, R_C\, r_{out}\, V_{in_+}(k-1) \\
& + C_B\, \Delta t\, R_A\, R_D\, r_{out}\, V_x(k-1) + C_B\, \Delta t\, R_C\, R_D\, r_{out}\, V_x(k-1) + C_B\, \Delta t\, R_C\, r_{in}\, r_{out}\, V_x(k-1) \\
& + A\, C_A\, \Delta t\, R_A\, R_C\, r_{in}\, V_{in_+}(k-1) + A\, C_A\, \Delta t\, R_A\, R_D\, r_{in}\, V_{in_+}(k-1) \\
& + A\, C_B\, \Delta t\, R_A\, R_D\, r_{in}\, V_{in_+}(k-1) - A\, C_B\, \Delta t\, R_A\, R_C\, r_{in}\, V_x(k-1) \\
& + C_A\, C_B\, R_A\, R_B\, R_C\, r_{out}\, V_{in_+}(k-1) + C_A\, C_B\, R_A\, R_C\, R_D\, r_{out}\, V_x(k-1) \\
& + C_A\, C_B\, R_A\, R_D\, r_{in}\, r_{out}\, V_x(k-1) + A\, {C_B}^2\, R_A\, R_B\, R_C\, r_{in}\, V_{in_+}(k-1) \\
& + {C_B}^2\, \Delta t\, R_A\, R_C\, R_D\, r_{out}\, V_{in_+}(k-1) + {C_B}^2\, \Delta t\, R_A\, R_C\, r_{in}\, r_{out}\, V_{in_+}(k-1) \\
& - {C_B}^2\, \Delta t\, R_A\, R_C\, R_D\, r_{out}\, V_x(k-1) - {C_B}^2\, \Delta t\, R_A\, R_C\, r_{in}\, r_{out}\, V_x(k-1) \\
& + A\, C_A\, C_B\, R_A\, R_B\, R_C\, r_{in}\, V_{in_+}(k-1) + A\, C_A\, C_B\, R_A\, R_B\, R_D\, r_{in}\, V_{in_+}(k-1) \\
& + C_A\, C_B\, \Delta t\, R_A\, R_D\, r_{in}\, r_{out}\, V_{in_+}(k-1)
\end{aligned} \tag{321}$$

$$\begin{aligned}
\beta_2 = {} & \Delta t^2\, R_A\, R_C + \Delta t^2\, R_A\, R_D + \Delta t^2\, R_C\, R_D + \Delta t^2\, R_C\, r_{in} + \Delta t^2\, R_D\, r_{in} + \Delta t^2\, R_A\, r_{out} \\
& + \Delta t^2\, r_{in}\, r_{out} + A\, \Delta t^2\, R_C\, r_{in} + C_B\, \Delta t\, R_A\, R_B\, R_C + C_A\, \Delta t\, R_A\, R_C\, R_D + C_B\, \Delta t\, R_A\, R_B\, R_D \\
& + C_B\, \Delta t\, R_B\, R_C\, R_D + C_A\, \Delta t\, R_A\, R_C\, r_{in} + C_A\, \Delta t\, R_A\, R_D\, r_{in} + C_B\, \Delta t\, R_A\, R_C\, r_{in} \\
& + C_B\, \Delta t\, R_B\, R_C\, r_{in} + C_B\, \Delta t\, R_B\, R_D\, r_{in} + C_A\, \Delta t\, R_A\, R_C\, r_{out} + C_B\, \Delta t\, R_A\, R_B\, r_{out} \\
& + C_B\, \Delta t\, R_A\, R_D\, r_{out} + C_B\, \Delta t\, R_B\, R_C\, r_{out} + C_B\, \Delta t\, R_C\, R_D\, r_{out} + C_A\, \Delta t\, R_A\, r_{in}\, r_{out} \\
& + C_B\, \Delta t\, R_B\, r_{in}\, r_{out} + C_B\, \Delta t\, R_C\, r_{in}\, r_{out} + C_B\, \Delta t\, R_D\, r_{in}\, r_{out} - C_B\, \Delta t^2\, R_A\, R_C\, r_{out} \\
& + {C_B}^2\, R_A\, R_B\, R_C\, r_{in} + {C_B}^2\, R_A\, R_B\, R_D\, r_{in} + {C_B}^2\, R_A\, R_B\, R_C\, r_{out} + {C_B}^2\, R_A\, R_C\, R_D\, r_{out} \\
& + {C_B}^2\, R_A\, R_C\, r_{in}\, r_{out} + {C_B}^2\, R_A\, R_D\, r_{in}\, r_{out} + A\, {C_B}^2\, R_A\, R_B\, R_C\, r_{in} - {C_B}^2\, \Delta t\, R_A\, R_B\, R_C\, R_D \\
& - {C_B}^2\, \Delta t\, R_A\, R_B\, R_D\, r_{in} - {C_B}^2\, \Delta t\, R_A\, R_B\, R_C\, r_{out} - {C_B}^2\, \Delta t\, R_A\, R_C\, R_D\, r_{out} \\
& - {C_B}^2\, \Delta t\, R_A\, R_C\, r_{in}\, r_{out} - {C_B}^2\, \Delta t\, R_A\, R_D\, r_{in}\, r_{out} + A\, C_A\, \Delta t\, R_A\, R_C\, r_{in} - A\, C_B\, \Delta t\, R_A\, R_D\, r_{in} \\
& + C_A\, C_B\, R_A\, R_B\, R_C\, R_D + C_A\, C_B\, R_A\, R_B\, R_C\, r_{in} + C_A\, C_B\, R_A\, R_B\, R_D\, r_{in} \\
& + C_A\, C_B\, R_A\, R_C\, R_D\, r_{out} + C_A\, C_B\, R_A\, R_B\, r_{in}\, r_{out} + C_A\, C_B\, R_A\, R_C\, r_{in}\, r_{out} \\
& - A\, {C_B}^2\, \Delta t\, R_A\, R_B\, R_C\, r_{in}
\end{aligned} \tag{322}$$

$$A_{\text{NFBR}} = \frac{R_D}{R_C} \tag{323}$$

While it is important to recognize that the circuit topology selected was inherently designed to produce an oscillatory response, yet such oscillatory characteristics — at least

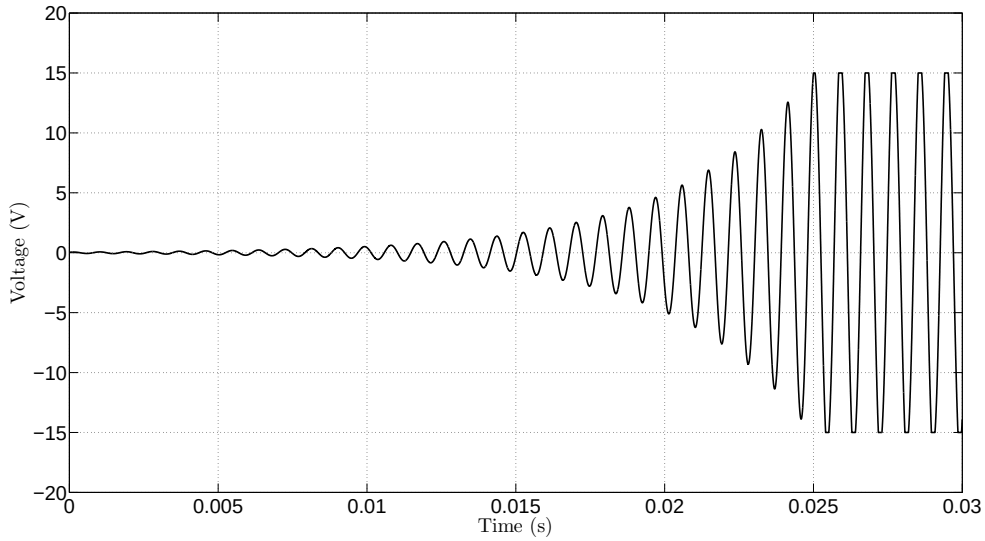

Figure 156: plot of the output of a unstable un-ideal wein bridge oscillator with a negative feedback gain of 2.1

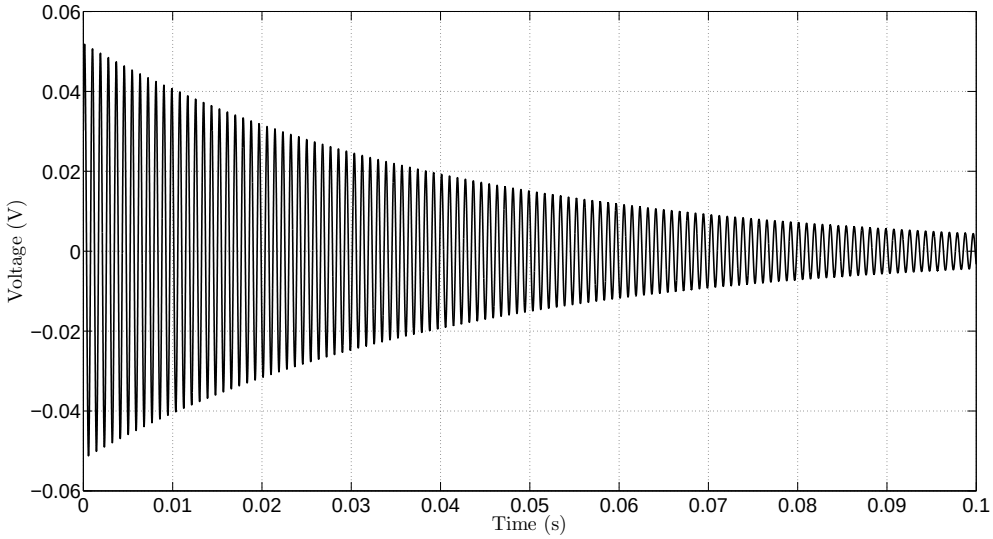

Figure 157: plot of the output of a stable un-ideal wein bridge oscillator with a negative feedback gain of 2

within an electrical system — are visually indicative of the existence of positive feedback, and although such attributes are seldom ever consciously implemented into acquisition instrumentation — excluding for the moment the commonly utilized digital clock or other subsidiary oscillatory sources —, yet such effects can possibly be inadvertently introduced, once again depending upon the acquisition topology utilized, through the improper selection and connection of measuring apparatus — especially if a unity gain unstable amplifier is utilized within the acquisition design or the applied test signal is dependent upon the acquisition instrumentation. Thus, while it is important to recognize that such occurrences are generally associated with real-time adaptive acquisition systems, and are seldom observed within most commercial laboratory measuring apparatus; however, such sources of distortion should be kept in mind and frequently considered, especially if oscillatory effects are observed during preliminary apparatus calibration.

Nevertheless, while the unexpected manifestation of positive feedback can be extremely detrimental to accurate signal acquisition, yet such occurrences are — by in large — extremely rare, especially given the unique and highly specific prerequisites required for its

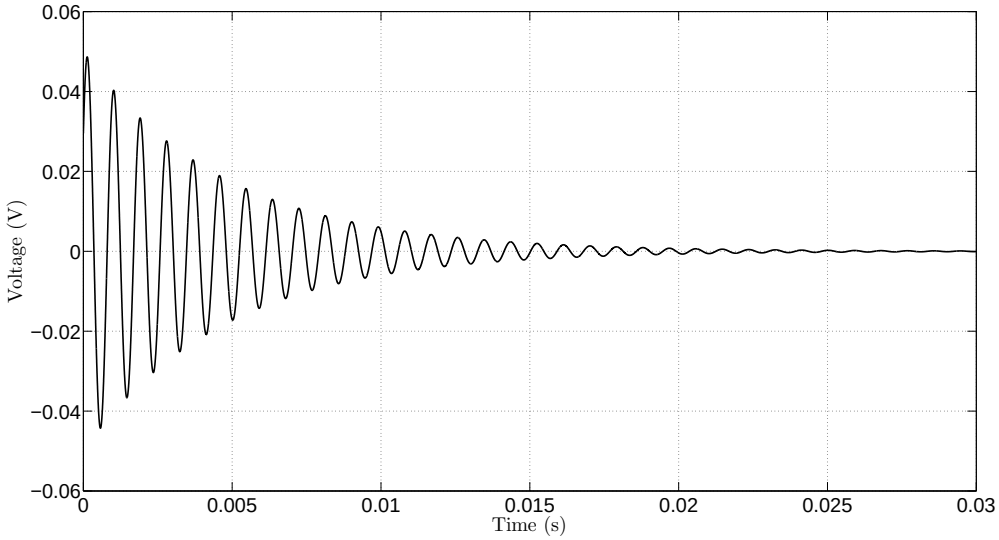

Figure 158: plot of the output of a stable un-ideal wein bridge oscillator with a negative feedback gain of 1.925

occurrence relative to the common acquisition topologies commercially implemented; thus, while such sources of distortion are necessary to review, especially when developing new acquisition circuitry, such attributes do have a tendency to become less concerning when working with an existing acquisition system. Conversely, because the majority of most laboratory measurements taken, at least within this dissertation, were done using commercially designed and sold instrumentation, and since the majority of these commercial acquisition devices typically do utilize a potential difference measurement — a measurement that is typically obtained through the utilization of an instrumentational amplifier stage, as shown by Figure: (159) and Figure: (160) — such effects do merit further investigation.

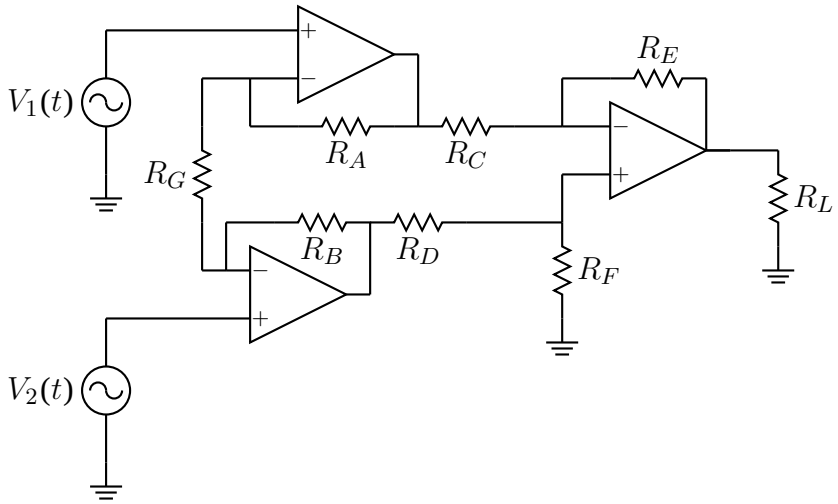

Figure 159: an operational amplifier in a instrumentational amplifier configuration

$$V_{1_{\text{in}_+}}(k) = \mathrm{V_1(k)} \tag{324}$$

$$I_{1_{\text{rin}}}(k) = \frac{\mathrm{V_1(k)} - \mathrm{V_{1_{in\_}}(k)}}{\mathrm{r_{1_{in}}}} \tag{325}$$

$$I_{R_G}(k) = \frac{\mathrm{V_{1_{in\_}}(k)} - \mathrm{V_{2_{in\_}}(k)}}{\mathrm{R_G}} \tag{326}$$

$$I_{R_A}(k) = \frac{\mathrm{V_{1_{in\_}}(k)} - \mathrm{V_{1_{out}}(k)}}{\mathrm{R_A}} \tag{327}$$

$$KCL_1 : \ 0 = \frac{\mathrm{V_1(k)} - \mathrm{V_{1_{in\_}}(k)}}{\mathrm{r_{1_{in}}}} - \frac{\mathrm{V_{1_{in\_}}(k)} - \mathrm{V_{2_{in\_}}(k)}}{\mathrm{R_G}} - \frac{\mathrm{V_{1_{in\_}}(k)} - \mathrm{V_{1_{out}}(k)}}{\mathrm{R_A}} \tag{328}$$

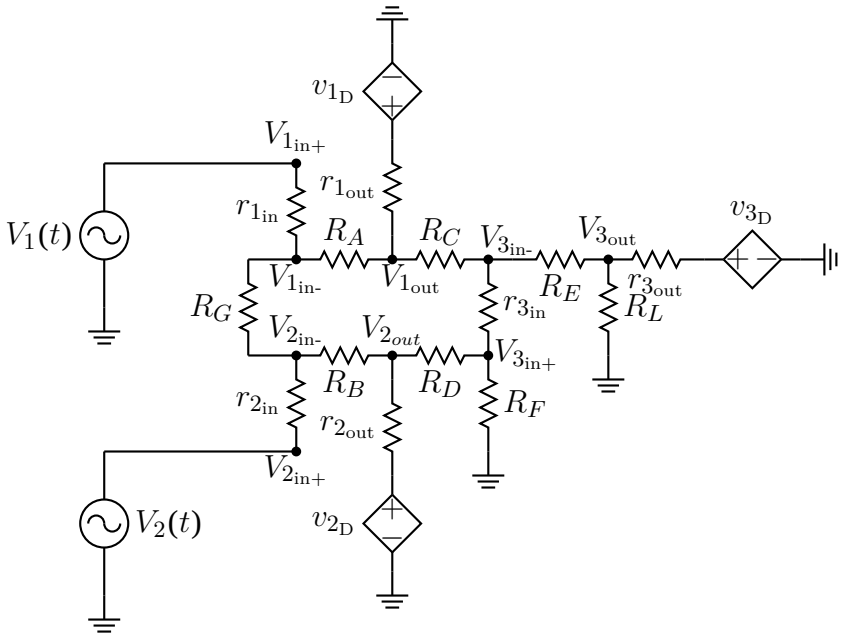

Figure 160: a un-ideal operational amplifier in a instrumentational amplifier configuration

$$V_{2_{in_+}}(k) = \mathrm{V_2(k)} \tag{329}$$

$$I_{2_{rin}}(k) = \frac{\mathrm{V_2(k)} - \mathrm{V_{2_{in\_}}(k)}}{\mathrm{r_{2_{in}}}} \tag{330}$$

$$I_{R_G}(k) = -\frac{\mathrm{V_{1_{in\_}}(k)} - \mathrm{V_{2_{in\_}}(k)}}{\mathrm{R_G}} \tag{331}$$

$$I_{R_B}(k) = \frac{\mathrm{V_{2_{in\_}}(k)} - \mathrm{V_{2_{out}}(k)}}{\mathrm{R_B}} \tag{332}$$

$$KCL_2: \ 0 = \frac{\mathrm{V_2(k)} - \mathrm{V_{2_{in\_}}(k)}}{\mathrm{r_{2_{in}}}} + \frac{\mathrm{V_{1_{in\_}}(k)} - \mathrm{V_{2_{in\_}}(k)}}{\mathrm{R_G}} - \frac{\mathrm{V_{2_{in\_}}(k)} - \mathrm{V_{2_{out}}(k)}}{\mathrm{R_B}} \tag{333}$$

$$V_{1_a}(k) = \mathrm{A_1}\ \Big(\mathrm{V_1(k)} - \mathrm{V_{1_{in\_}}(k)}\Big) \tag{334}$$

$$I_{1_{rout}}(k) = -\frac{\mathrm{V_{1_{out}}(k)} - \mathrm{A_1}\ \Big(\mathrm{V_1(k)} - \mathrm{V_{1_{in\_}}(k)}\Big)}{\mathrm{r_{1_{out}}}} \tag{335}$$

$$I_{R_A}(k) = -\frac{\mathrm{V_{1_{in\_}}(k)} - \mathrm{V_{1_{out}}(k)}}{\mathrm{R_A}} \tag{336}$$

$$I_{R_C}(k) = -\frac{\mathrm{V_{3_{in\_}}(k)} - \mathrm{V_{1_{out}}(k)}}{\mathrm{R_C}} \tag{337}$$

$$KCL_3: \ 0 = \frac{\mathrm{V}_{1_{\mathrm{in}\_}}(\mathrm{k}) - \mathrm{V}_{1_{\mathrm{out}}}(\mathrm{k})}{\mathrm{R_A}} - \frac{\mathrm{V}_{1_{\mathrm{out}}}(\mathrm{k}) - \mathrm{A}_1 \left(\mathrm{V}_1(\mathrm{k}) - \mathrm{V}_{1_{\mathrm{in}\_}}(\mathrm{k})\right)}{\mathrm{r}_{1_{\mathrm{out}}}} + \frac{\mathrm{V}_{3_{\mathrm{in}\_}}(\mathrm{k}) - \mathrm{V}_{1_{\mathrm{out}}}(\mathrm{k})}{\mathrm{R_C}} \tag{338}$$

$$V_{2_d}(k) = \mathrm{A}_2 \left(\mathrm{V}_2(\mathrm{k}) - \mathrm{V}_{2_{\mathrm{in}\_}}(\mathrm{k})\right) \tag{339}$$

$$I_{2_{\mathrm{rout}}}(k) = -\frac{\mathrm{V}_{2_{\mathrm{out}}}(\mathrm{k}) - \mathrm{A}_2 \left(\mathrm{V}_2(\mathrm{k}) - \mathrm{V}_{2_{\mathrm{in}\_}}(\mathrm{k})\right)}{\mathrm{r}_{2_{\mathrm{out}}}} \tag{340}$$

$$I_{R_B}(k) = -\frac{\mathrm{V}_{2_{\mathrm{in}\_}}(\mathrm{k}) - \mathrm{V}_{2_{\mathrm{out}}}(\mathrm{k})}{\mathrm{R_B}} \tag{341}$$

$$I_{R_D}(k) = -\frac{\mathrm{V}_{3_{\mathrm{in}_+}}(\mathrm{k}) - \mathrm{V}_{2_{\mathrm{out}}}(\mathrm{k})}{\mathrm{R_D}} \tag{342}$$

$$KCL_4: \ 0 = \frac{\mathrm{V}_{2_{\mathrm{in}\_}}(\mathrm{k}) - \mathrm{V}_{2_{\mathrm{out}}}(\mathrm{k})}{\mathrm{R_B}} - \frac{\mathrm{V}_{2_{\mathrm{out}}}(\mathrm{k}) - \mathrm{A}_2 \left(\mathrm{V}_2(\mathrm{k}) - \mathrm{V}_{2_{\mathrm{in}\_}}(\mathrm{k})\right)}{\mathrm{r}_{2_{\mathrm{out}}}} + \frac{\mathrm{V}_{3_{\mathrm{in}_+}}(\mathrm{k}) - \mathrm{V}_{2_{\mathrm{out}}}(\mathrm{k})}{\mathrm{R_D}} \tag{343}$$

$$I_{R_C}(k) = -\frac{\mathrm{V}_{3_{\mathrm{in}\_}}(\mathrm{k}) - \mathrm{V}_{1_{\mathrm{out}}}(\mathrm{k})}{\mathrm{R_C}} \tag{344}$$

$$I_{3_{\mathrm{rin}}}(k) = \frac{\mathrm{V}_{3_{\mathrm{in}\_}}(\mathrm{k}) - \mathrm{V}_{3_{\mathrm{in}_+}}(\mathrm{k})}{\mathrm{r}_{3_{\mathrm{in}}}} \tag{345}$$

$$I_{R_E}(k) = \frac{\mathrm{V}_{3_{\mathrm{in}\_}}(\mathrm{k}) - \mathrm{V}_{3_{\mathrm{out}}}(\mathrm{k})}{\mathrm{R_E}} \tag{346}$$

$$KCL_5: \ 0 = -\frac{\mathrm{V}_{3_{\mathrm{in}\_}}(\mathrm{k}) - \mathrm{V}_{1_{\mathrm{out}}}(\mathrm{k})}{\mathrm{R_C}} - \frac{\mathrm{V}_{3_{\mathrm{in}\_}}(\mathrm{k}) - \mathrm{V}_{3_{\mathrm{in}_+}}(\mathrm{k})}{\mathrm{r}_{3_{\mathrm{in}}}} - \frac{\mathrm{V}_{3_{\mathrm{in}\_}}(\mathrm{k}) - \mathrm{V}_{3_{\mathrm{out}}}(\mathrm{k})}{\mathrm{R_E}} \tag{347}$$

$$I_{R_D}(k) = -\frac{\mathrm{V}_{3_{\mathrm{in}_+}}(\mathrm{k}) - \mathrm{V}_{2_{\mathrm{out}}}(\mathrm{k})}{\mathrm{R_D}} \tag{348}$$

$$I_{R_F}(k) = \frac{\mathrm{V}_{3_{\mathrm{in}_+}}(\mathrm{k})}{\mathrm{R_F}} \tag{349}$$

$$I_{3_{\mathrm{rin}}}(k) = -\frac{\mathrm{V}_{3_{\mathrm{in}\_}}(\mathrm{k}) - \mathrm{V}_{3_{\mathrm{in}_+}}(\mathrm{k})}{\mathrm{r}_{3_{\mathrm{in}}}} \tag{350}$$

$$KCL_6: \ 0 = \frac{\mathrm{V}_{3_{\mathrm{in}_-}}(\mathrm{k}) - \mathrm{V}_{3_{\mathrm{in}_+}}(\mathrm{k})}{\mathrm{r}_{3_{\mathrm{in}}}} - \frac{\mathrm{V}_{3_{\mathrm{in}_+}}(\mathrm{k})}{\mathrm{R_F}} - \frac{\mathrm{V}_{3_{\mathrm{in}_+}}(\mathrm{k}) - \mathrm{V}_{2_{\mathrm{out}}}(\mathrm{k})}{\mathrm{R_D}} \tag{351}$$

$$V_{3_d}(k) = \ -\mathrm{A}_3 \ \left(\mathrm{V}_{3_{\mathrm{in}_-}}(\mathrm{k}) - \mathrm{V}_{3_{\mathrm{in}_+}}(\mathrm{k})\right) \tag{352}$$

$$I_{3_{\mathrm{rout}}}(k) = \ -\frac{\mathrm{V}_{3_{\mathrm{out}}}(\mathrm{k}) + \mathrm{A}_3 \ \left(\mathrm{V}_{3_{\mathrm{in}_-}}(\mathrm{k}) - \mathrm{V}_{3_{\mathrm{in}_+}}(\mathrm{k})\right)}{\mathrm{r}_{3_{\mathrm{out}}}} \tag{353}$$

$$I_{R_E}(k) = \ -\frac{\mathrm{V}_{3_{\mathrm{in}_-}}(\mathrm{k}) - \mathrm{V}_{3_{\mathrm{out}}}(\mathrm{k})}{\mathrm{R_E}} \tag{354}$$

$$I_{R_L}(k) = \frac{\mathrm{V}_{3_{\mathrm{out}}}(\mathrm{k})}{\mathrm{R_L}} \tag{355}$$

$$\begin{aligned} KCL_7: \ 0 = & \frac{\mathrm{V}_{3_{\mathrm{in}_-}}(\mathrm{k}) - \mathrm{V}_{3_{\mathrm{out}}}(\mathrm{k})}{\mathrm{R_E}} - \frac{\mathrm{V}_{3_{\mathrm{out}}}(\mathrm{k})}{\mathrm{R_L}} \\ & - \frac{\mathrm{V}_{3_{\mathrm{out}}}(\mathrm{k}) + \mathrm{A}_3 \ \left(\mathrm{V}_{3_{\mathrm{in}_-}}(\mathrm{k}) - \mathrm{V}_{3_{\mathrm{in}_+}}(\mathrm{k})\right)}{\mathrm{r}_{3_{\mathrm{out}}}} \end{aligned} \tag{356}$$

$$V_{1_{\mathrm{in}_-}}(k) = \frac{\mathrm{R_A\,R_G\,V_1(k)} + \mathrm{R_A\,r_{1_{in}}\,V_{2_{in_-}}(k)} + \mathrm{R_G\,r_{1_{in}}\,V_{1_{out}}(k)}}{\mathrm{R_A\,R_G} + \mathrm{R_A\,r_{1_{in}}} + \mathrm{R_G\,r_{1_{in}}}} \tag{357}$$

$$V_{2_{\mathrm{in}_-}}(k) = \frac{\alpha_1}{\beta_1} \tag{358}$$

$$V_{3_{\mathrm{in}_-}}(k) = \frac{\alpha_2}{\beta_2} \tag{359}$$

$$V_{3_{\mathrm{in}_+}}(k) = \frac{\alpha_3}{\beta_3} \tag{360}$$

$$V_{1_{\mathrm{out}}}(k) = \frac{\alpha_4}{\beta_4} \tag{361}$$

$$V_{2_{\mathrm{out}}}(k) = \frac{\alpha_5}{\beta_5} \tag{362}$$

$$V_{3_{\mathrm{out}}}(k) = \frac{\alpha_6}{\beta_6} \tag{363}$$

$$\begin{aligned} \alpha_1 = & \ \mathrm{R_A\,R_B\,R_G\,V_2(k)} + \mathrm{R_A\,R_B\,r_{2_{in}}\,V_1(k)} + \mathrm{R_A\,R_B\,r_{1_{in}}\,V_2(k)} + \mathrm{R_B\,R_G\,r_{1_{in}}\,V_2(k)} \\ & + \mathrm{R_G\,r_{1_{in}}\,r_{2_{in}}\,V_{2_{out}}(k)} \end{aligned} \tag{364}$$

$$\beta_1 = \mathrm{R_A\,R_B\,R_G} + \mathrm{R_A\,R_B\,r_{1_{in}}} + \mathrm{R_A\,R_B\,r_{2_{in}}} + \mathrm{R_A\,R_G\,r_{2_{in}}} + \mathrm{R_B\,R_G\,r_{1_{in}}} + \mathrm{R_A\,r_{1_{in}}\,r_{2_{in}}}$$

$$+ \mathrm{R_G}\,\mathrm{r}_{1_{\mathrm{in}}}\,\mathrm{r}_{2_{\mathrm{in}}} \tag{365}$$

$$\begin{aligned}
\alpha_2 = {} & \mathrm{R_B}\,\mathrm{R_D}\,\mathrm{R_E}\,\mathrm{R_G}\,\mathrm{r}_{3_{\mathrm{in}}}\,\mathrm{r}_{1_{\mathrm{out}}}\,\mathrm{V}_1(\mathrm{k}) + \mathrm{R_B}\,\mathrm{R_D}\,\mathrm{R_E}\,\mathrm{r}_{2_{\mathrm{in}}}\,\mathrm{r}_{3_{\mathrm{in}}}\,\mathrm{r}_{1_{\mathrm{out}}}\,\mathrm{V}_1(\mathrm{k}) \\
& + \mathrm{R_D}\,\mathrm{R_E}\,\mathrm{R_G}\,\mathrm{r}_{2_{\mathrm{in}}}\,\mathrm{r}_{3_{\mathrm{in}}}\,\mathrm{r}_{1_{\mathrm{out}}}\,\mathrm{V}_1(\mathrm{k}) + \mathrm{R_B}\,\mathrm{R_E}\,\mathrm{R_G}\,\mathrm{r}_{3_{\mathrm{in}}}\,\mathrm{r}_{1_{\mathrm{out}}}\,\mathrm{r}_{2_{\mathrm{out}}}\,\mathrm{V}_1(\mathrm{k}) \\
& + \mathrm{R_B}\,\mathrm{R_E}\,\mathrm{r}_{2_{\mathrm{in}}}\,\mathrm{r}_{3_{\mathrm{in}}}\,\mathrm{r}_{1_{\mathrm{out}}}\,\mathrm{r}_{2_{\mathrm{out}}}\,\mathrm{V}_1(\mathrm{k}) + \mathrm{R_B}\,\mathrm{R_E}\,\mathrm{r}_{1_{\mathrm{in}}}\,\mathrm{r}_{3_{\mathrm{in}}}\,\mathrm{r}_{1_{\mathrm{out}}}\,\mathrm{r}_{2_{\mathrm{out}}}\,\mathrm{V}_2(\mathrm{k}) \\
& + \mathrm{R_D}\,\mathrm{R_E}\,\mathrm{r}_{1_{\mathrm{in}}}\,\mathrm{r}_{3_{\mathrm{in}}}\,\mathrm{r}_{1_{\mathrm{out}}}\,\mathrm{r}_{2_{\mathrm{out}}}\,\mathrm{V}_2(\mathrm{k}) + \mathrm{R_E}\,\mathrm{R_G}\,\mathrm{r}_{2_{\mathrm{in}}}\,\mathrm{r}_{3_{\mathrm{in}}}\,\mathrm{r}_{1_{\mathrm{out}}}\,\mathrm{r}_{2_{\mathrm{out}}}\,\mathrm{V}_1(\mathrm{k}) \\
& + \mathrm{R_A}\,\mathrm{R_B}\,\mathrm{R_C}\,\mathrm{R_D}\,\mathrm{R_E}\,\mathrm{r}_{1_{\mathrm{in}}}\,\mathrm{V}_{3_{\mathrm{in}_+}}(\mathrm{k}) + \mathrm{R_A}\,\mathrm{R_B}\,\mathrm{R_C}\,\mathrm{R_D}\,\mathrm{R_E}\,\mathrm{r}_{2_{\mathrm{in}}}\,\mathrm{V}_{3_{\mathrm{in}_+}}(\mathrm{k}) \\
& + \mathrm{R_B}\,\mathrm{R_C}\,\mathrm{R_D}\,\mathrm{R_E}\,\mathrm{R_G}\,\mathrm{r}_{1_{\mathrm{in}}}\,\mathrm{V}_{3_{\mathrm{in}_+}}(\mathrm{k}) + \mathrm{R_A}\,\mathrm{R_C}\,\mathrm{R_D}\,\mathrm{R_E}\,\mathrm{r}_{1_{\mathrm{in}}}\,\mathrm{r}_{2_{\mathrm{in}}}\,\mathrm{V}_{3_{\mathrm{in}_+}}(\mathrm{k}) \\
& + \mathrm{R_B}\,\mathrm{R_C}\,\mathrm{R_D}\,\mathrm{R_E}\,\mathrm{r}_{1_{\mathrm{in}}}\,\mathrm{r}_{2_{\mathrm{in}}}\,\mathrm{V}_{3_{\mathrm{in}_+}}(\mathrm{k}) + \mathrm{R_A}\,\mathrm{R_B}\,\mathrm{R_C}\,\mathrm{R_E}\,\mathrm{R_G}\,\mathrm{r}_{2_{\mathrm{out}}}\,\mathrm{V}_{3_{\mathrm{in}_+}}(\mathrm{k}) \\
& + \mathrm{R_A}\,\mathrm{R_B}\,\mathrm{R_C}\,\mathrm{R_D}\,\mathrm{r}_{1_{\mathrm{in}}}\,\mathrm{r}_{3_{\mathrm{in}}}\,\mathrm{V}_{3_{\mathrm{out}}}(\mathrm{k}) + \mathrm{R_A}\,\mathrm{R_B}\,\mathrm{R_C}\,\mathrm{R_D}\,\mathrm{r}_{2_{\mathrm{in}}}\,\mathrm{r}_{3_{\mathrm{in}}}\,\mathrm{V}_{3_{\mathrm{out}}}(\mathrm{k}) \\
& + \mathrm{R_A}\,\mathrm{R_B}\,\mathrm{R_C}\,\mathrm{R_E}\,\mathrm{r}_{1_{\mathrm{in}}}\,\mathrm{r}_{2_{\mathrm{out}}}\,\mathrm{V}_{3_{\mathrm{in}_+}}(\mathrm{k}) + \mathrm{R_A}\,\mathrm{R_B}\,\mathrm{R_C}\,\mathrm{R_E}\,\mathrm{r}_{2_{\mathrm{in}}}\,\mathrm{r}_{2_{\mathrm{out}}}\,\mathrm{V}_{3_{\mathrm{in}_+}}(\mathrm{k}) \\
& + \mathrm{R_A}\,\mathrm{R_B}\,\mathrm{R_D}\,\mathrm{R_E}\,\mathrm{r}_{1_{\mathrm{in}}}\,\mathrm{r}_{1_{\mathrm{out}}}\,\mathrm{V}_{3_{\mathrm{in}_+}}(\mathrm{k}) + \mathrm{R_A}\,\mathrm{R_B}\,\mathrm{R_D}\,\mathrm{R_E}\,\mathrm{r}_{2_{\mathrm{in}}}\,\mathrm{r}_{1_{\mathrm{out}}}\,\mathrm{V}_{3_{\mathrm{in}_+}}(\mathrm{k}) \\
& + \mathrm{R_A}\,\mathrm{R_C}\,\mathrm{R_D}\,\mathrm{R_E}\,\mathrm{r}_{1_{\mathrm{in}}}\,\mathrm{r}_{2_{\mathrm{out}}}\,\mathrm{V}_{3_{\mathrm{in}_+}}(\mathrm{k}) + \mathrm{R_A}\,\mathrm{R_C}\,\mathrm{R_D}\,\mathrm{R_E}\,\mathrm{r}_{2_{\mathrm{in}}}\,\mathrm{r}_{2_{\mathrm{out}}}\,\mathrm{V}_{3_{\mathrm{in}_+}}(\mathrm{k}) \\
& + \mathrm{R_B}\,\mathrm{R_C}\,\mathrm{R_D}\,\mathrm{R_E}\,\mathrm{r}_{2_{\mathrm{in}}}\,\mathrm{r}_{1_{\mathrm{out}}}\,\mathrm{V}_{3_{\mathrm{in}_+}}(\mathrm{k}) + \mathrm{R_A}\,\mathrm{R_C}\,\mathrm{R_D}\,\mathrm{R_G}\,\mathrm{r}_{2_{\mathrm{in}}}\,\mathrm{r}_{3_{\mathrm{in}}}\,\mathrm{V}_{3_{\mathrm{out}}}(\mathrm{k}) \\
& + \mathrm{R_A}\,\mathrm{R_C}\,\mathrm{R_E}\,\mathrm{R_G}\,\mathrm{r}_{2_{\mathrm{in}}}\,\mathrm{r}_{2_{\mathrm{out}}}\,\mathrm{V}_{3_{\mathrm{in}_+}}(\mathrm{k}) + \mathrm{R_A}\,\mathrm{R_D}\,\mathrm{R_E}\,\mathrm{R_G}\,\mathrm{r}_{2_{\mathrm{in}}}\,\mathrm{r}_{1_{\mathrm{out}}}\,\mathrm{V}_{3_{\mathrm{in}_+}}(\mathrm{k}) \\
& + \mathrm{R_A}\,\mathrm{R_C}\,\mathrm{R_D}\,\mathrm{r}_{1_{\mathrm{in}}}\,\mathrm{r}_{2_{\mathrm{in}}}\,\mathrm{r}_{3_{\mathrm{in}}}\,\mathrm{V}_{3_{\mathrm{out}}}(\mathrm{k}) + \mathrm{R_B}\,\mathrm{R_D}\,\mathrm{R_E}\,\mathrm{R_G}\,\mathrm{r}_{1_{\mathrm{in}}}\,\mathrm{r}_{1_{\mathrm{out}}}\,\mathrm{V}_{3_{\mathrm{in}_+}}(\mathrm{k}) \\
& + \mathrm{R_A}\,\mathrm{R_C}\,\mathrm{R_E}\,\mathrm{r}_{1_{\mathrm{in}}}\,\mathrm{r}_{2_{\mathrm{in}}}\,\mathrm{r}_{2_{\mathrm{out}}}\,\mathrm{V}_{3_{\mathrm{in}_+}}(\mathrm{k}) + \mathrm{R_C}\,\mathrm{R_D}\,\mathrm{R_E}\,\mathrm{R_G}\,\mathrm{r}_{1_{\mathrm{in}}}\,\mathrm{r}_{2_{\mathrm{out}}}\,\mathrm{V}_{3_{\mathrm{in}_+}}(\mathrm{k}) \\
& + \mathrm{R_A}\,\mathrm{R_B}\,\mathrm{R_C}\,\mathrm{R_G}\,\mathrm{r}_{3_{\mathrm{in}}}\,\mathrm{r}_{2_{\mathrm{out}}}\,\mathrm{V}_{3_{\mathrm{out}}}(\mathrm{k}) + \mathrm{R_A}\,\mathrm{R_D}\,\mathrm{R_E}\,\mathrm{r}_{1_{\mathrm{in}}}\,\mathrm{r}_{2_{\mathrm{in}}}\,\mathrm{r}_{1_{\mathrm{out}}}\,\mathrm{V}_{3_{\mathrm{in}_+}}(\mathrm{k}) \\
& + \mathrm{R_A}\,\mathrm{R_B}\,\mathrm{R_D}\,\mathrm{R_G}\,\mathrm{r}_{3_{\mathrm{in}}}\,\mathrm{r}_{1_{\mathrm{out}}}\,\mathrm{V}_{3_{\mathrm{out}}}(\mathrm{k}) + \mathrm{R_B}\,\mathrm{R_D}\,\mathrm{R_E}\,\mathrm{r}_{1_{\mathrm{in}}}\,\mathrm{r}_{2_{\mathrm{in}}}\,\mathrm{r}_{1_{\mathrm{out}}}\,\mathrm{V}_{3_{\mathrm{in}_+}}(\mathrm{k}) \\
& + \mathrm{R_A}\,\mathrm{R_B}\,\mathrm{R_E}\,\mathrm{R_G}\,\mathrm{r}_{1_{\mathrm{out}}}\,\mathrm{r}_{2_{\mathrm{out}}}\,\mathrm{V}_{3_{\mathrm{in}_+}}(\mathrm{k}) + \mathrm{R_C}\,\mathrm{R_D}\,\mathrm{R_E}\,\mathrm{r}_{1_{\mathrm{in}}}\,\mathrm{r}_{2_{\mathrm{in}}}\,\mathrm{r}_{1_{\mathrm{out}}}\,\mathrm{V}_{3_{\mathrm{in}_+}}(\mathrm{k}) \\
& + \mathrm{R_A}\,\mathrm{R_B}\,\mathrm{R_C}\,\mathrm{r}_{1_{\mathrm{in}}}\,\mathrm{r}_{3_{\mathrm{in}}}\,\mathrm{r}_{2_{\mathrm{out}}}\,\mathrm{V}_{3_{\mathrm{out}}}(\mathrm{k}) + \mathrm{R_A}\,\mathrm{R_B}\,\mathrm{R_C}\,\mathrm{r}_{2_{\mathrm{in}}}\,\mathrm{r}_{3_{\mathrm{in}}}\,\mathrm{r}_{2_{\mathrm{out}}}\,\mathrm{V}_{3_{\mathrm{out}}}(\mathrm{k}) \\
& + \mathrm{R_A}\,\mathrm{R_B}\,\mathrm{R_D}\,\mathrm{r}_{1_{\mathrm{in}}}\,\mathrm{r}_{3_{\mathrm{in}}}\,\mathrm{r}_{1_{\mathrm{out}}}\,\mathrm{V}_{3_{\mathrm{out}}}(\mathrm{k}) + \mathrm{R_A}\,\mathrm{R_B}\,\mathrm{R_D}\,\mathrm{r}_{2_{\mathrm{in}}}\,\mathrm{r}_{3_{\mathrm{in}}}\,\mathrm{r}_{1_{\mathrm{out}}}\,\mathrm{V}_{3_{\mathrm{out}}}(\mathrm{k}) \\
& + \mathrm{R_B}\,\mathrm{R_C}\,\mathrm{R_E}\,\mathrm{R_G}\,\mathrm{r}_{1_{\mathrm{out}}}\,\mathrm{r}_{2_{\mathrm{out}}}\,\mathrm{V}_{3_{\mathrm{in}_+}}(\mathrm{k}) + \mathrm{R_C}\,\mathrm{R_D}\,\mathrm{R_G}\,\mathrm{r}_{1_{\mathrm{in}}}\,\mathrm{r}_{2_{\mathrm{in}}}\,\mathrm{r}_{3_{\mathrm{in}}}\,\mathrm{V}_{3_{\mathrm{out}}}(\mathrm{k}) \\
& + \mathrm{R_A}\,\mathrm{R_C}\,\mathrm{R_D}\,\mathrm{r}_{2_{\mathrm{in}}}\,\mathrm{r}_{3_{\mathrm{in}}}\,\mathrm{r}_{2_{\mathrm{out}}}\,\mathrm{V}_{3_{\mathrm{out}}}(\mathrm{k}) + \mathrm{R_A}\,\mathrm{R_B}\,\mathrm{R_E}\,\mathrm{r}_{1_{\mathrm{in}}}\,\mathrm{r}_{1_{\mathrm{out}}}\,\mathrm{r}_{2_{\mathrm{out}}}\,\mathrm{V}_{3_{\mathrm{in}_+}}(\mathrm{k}) \\
& + \mathrm{R_C}\,\mathrm{R_E}\,\mathrm{R_G}\,\mathrm{r}_{1_{\mathrm{in}}}\,\mathrm{r}_{2_{\mathrm{in}}}\,\mathrm{r}_{2_{\mathrm{out}}}\,\mathrm{V}_{3_{\mathrm{in}_+}}(\mathrm{k}) + \mathrm{R_B}\,\mathrm{R_C}\,\mathrm{R_D}\,\mathrm{r}_{1_{\mathrm{in}}}\,\mathrm{r}_{3_{\mathrm{in}}}\,\mathrm{r}_{1_{\mathrm{out}}}\,\mathrm{V}_{3_{\mathrm{out}}}(\mathrm{k}) \\
& + \mathrm{R_C}\,\mathrm{R_D}\,\mathrm{R_E}\,\mathrm{R_G}\,\mathrm{r}_{1_{\mathrm{out}}}\,\mathrm{r}_{2_{\mathrm{out}}}\,\mathrm{V}_{3_{\mathrm{in}_+}}(\mathrm{k}) + \mathrm{R_D}\,\mathrm{R_E}\,\mathrm{R_G}\,\mathrm{r}_{1_{\mathrm{in}}}\,\mathrm{r}_{2_{\mathrm{in}}}\,\mathrm{r}_{1_{\mathrm{out}}}\,\mathrm{V}_{3_{\mathrm{in}_+}}(\mathrm{k}) \\
& + \mathrm{R_B}\,\mathrm{R_C}\,\mathrm{R_E}\,\mathrm{r}_{1_{\mathrm{in}}}\,\mathrm{r}_{1_{\mathrm{out}}}\,\mathrm{r}_{2_{\mathrm{out}}}\,\mathrm{V}_{3_{\mathrm{in}_+}}(\mathrm{k}) + \mathrm{R_A}\,\mathrm{R_D}\,\mathrm{R_E}\,\mathrm{r}_{2_{\mathrm{in}}}\,\mathrm{r}_{1_{\mathrm{out}}}\,\mathrm{r}_{2_{\mathrm{out}}}\,\mathrm{V}_{3_{\mathrm{in}_+}}(\mathrm{k})
\end{aligned}$$

$$+ R_A\,R_C\,R_G\,r_{2_{in}}\,r_{3_{in}}\,r_{2_{out}}\,V_{3_{out}}(k) + R_A\,R_D\,R_G\,r_{2_{in}}\,r_{3_{in}}\,r_{1_{out}}\,V_{3_{out}}(k)$$

$$+ R_C\,R_D\,R_E\,r_{1_{in}}\,r_{1_{out}}\,r_{2_{out}}\,V_{3_{in_+}}(k) + R_C\,R_D\,R_E\,r_{2_{in}}\,r_{1_{out}}\,r_{2_{out}}\,V_{3_{in_+}}(k)$$

$$+ R_A\,R_E\,R_G\,r_{2_{in}}\,r_{1_{out}}\,r_{2_{out}}\,V_{3_{in_+}}(k) + R_A\,R_C\,r_{1_{in}}\,r_{2_{in}}\,r_{3_{in}}\,r_{2_{out}}\,V_{3_{out}}(k)$$

$$+ R_C\,R_D\,R_G\,r_{2_{in}}\,r_{3_{in}}\,r_{1_{out}}\,V_{3_{out}}(k) + R_B\,R_E\,R_G\,r_{1_{in}}\,r_{1_{out}}\,r_{2_{out}}\,V_{3_{in_+}}(k)$$

$$+ R_B\,R_C\,r_{1_{in}}\,r_{2_{in}}\,r_{3_{in}}\,r_{2_{out}}\,V_{3_{out}}(k) + R_C\,R_E\,R_G\,r_{2_{in}}\,r_{1_{out}}\,r_{2_{out}}\,V_{3_{in_+}}(k)$$

$$+ R_A\,R_E\,r_{1_{in}}\,r_{2_{in}}\,r_{1_{out}}\,r_{2_{out}}\,V_{3_{in_+}}(k) + R_D\,R_E\,R_G\,r_{1_{in}}\,r_{1_{out}}\,r_{2_{out}}\,V_{3_{in_+}}(k)$$

$$+ R_C\,R_D\,r_{1_{in}}\,r_{2_{in}}\,r_{3_{in}}\,r_{1_{out}}\,V_{3_{out}}(k) + R_C\,R_D\,r_{1_{in}}\,r_{2_{in}}\,r_{3_{in}}\,r_{2_{out}}\,V_{3_{out}}(k)$$

$$+ R_C\,R_E\,r_{1_{in}}\,r_{2_{in}}\,r_{1_{out}}\,r_{2_{out}}\,V_{3_{in_+}}(k) + R_A\,R_D\,R_G\,r_{3_{in}}\,r_{1_{out}}\,r_{2_{out}}\,V_{3_{out}}(k)$$

$$+ R_D\,R_E\,r_{1_{in}}\,r_{2_{in}}\,r_{1_{out}}\,r_{2_{out}}\,V_{3_{in_+}}(k) + R_A\,R_B\,r_{1_{in}}\,r_{3_{in}}\,r_{1_{out}}\,r_{2_{out}}\,V_{3_{out}}(k)$$

$$+ R_C\,R_G\,r_{1_{in}}\,r_{2_{in}}\,r_{3_{in}}\,r_{2_{out}}\,V_{3_{out}}(k) + R_C\,R_D\,R_G\,r_{3_{in}}\,r_{1_{out}}\,r_{2_{out}}\,V_{3_{out}}(k)$$

$$+ R_A\,R_D\,r_{1_{in}}\,r_{3_{in}}\,r_{1_{out}}\,r_{2_{out}}\,V_{3_{out}}(k) + R_B\,R_C\,r_{1_{in}}\,r_{3_{in}}\,r_{1_{out}}\,r_{2_{out}}\,V_{3_{out}}(k)$$

$$+ R_B\,R_C\,r_{2_{in}}\,r_{3_{in}}\,r_{1_{out}}\,r_{2_{out}}\,V_{3_{out}}(k) + R_E\,R_G\,r_{1_{in}}\,r_{2_{in}}\,r_{1_{out}}\,r_{2_{out}}\,V_{3_{in_+}}(k)$$

$$+ R_C\,R_D\,r_{2_{in}}\,r_{3_{in}}\,r_{1_{out}}\,r_{2_{out}}\,V_{3_{out}}(k) + R_A\,R_G\,r_{2_{in}}\,r_{3_{in}}\,r_{1_{out}}\,r_{2_{out}}\,V_{3_{out}}(k)$$

$$+ R_B\,R_G\,r_{1_{in}}\,r_{3_{in}}\,r_{1_{out}}\,r_{2_{out}}\,V_{3_{out}}(k) + R_C\,R_G\,r_{2_{in}}\,r_{3_{in}}\,r_{1_{out}}\,r_{2_{out}}\,V_{3_{out}}(k)$$

$$+ R_D\,R_G\,r_{1_{in}}\,r_{3_{in}}\,r_{1_{out}}\,r_{2_{out}}\,V_{3_{out}}(k) + R_B\,r_{1_{in}}\,r_{2_{in}}\,r_{3_{in}}\,r_{1_{out}}\,r_{2_{out}}\,V_{3_{out}}(k)$$

$$+ R_D\,r_{1_{in}}\,r_{2_{in}}\,r_{3_{in}}\,r_{1_{out}}\,r_{2_{out}}\,V_{3_{out}}(k) + R_G\,r_{1_{in}}\,r_{2_{in}}\,r_{3_{in}}\,r_{1_{out}}\,r_{2_{out}}\,V_{3_{out}}(k)$$

$$- A_1\,R_A\,R_B\,R_D\,R_E\,r_{1_{in}}\,r_{3_{in}}\,V_2(k) + A_1\,R_B\,R_D\,R_E\,R_G\,r_{1_{in}}\,r_{3_{in}}\,V_1(k)$$

$$+ A_1\,R_B\,R_D\,R_E\,r_{1_{in}}\,r_{2_{in}}\,r_{3_{in}}\,V_1(k) + A_1\,R_A\,R_B\,R_E\,r_{1_{in}}\,r_{3_{in}}\,r_{2_{out}}\,V_1(k)$$

$$+ A_1\,R_D\,R_E\,R_G\,r_{1_{in}}\,r_{2_{in}}\,r_{3_{in}}\,V_1(k) + A_1\,R_A\,R_D\,R_E\,r_{1_{in}}\,r_{3_{in}}\,r_{2_{out}}\,V_1(k)$$

$$+ A_1\,R_B\,R_E\,R_G\,r_{1_{in}}\,r_{3_{in}}\,r_{2_{out}}\,V_1(k) + A_1\,R_A\,R_E\,r_{1_{in}}\,r_{2_{in}}\,r_{3_{in}}\,r_{2_{out}}\,V_1(k)$$

$$+ A_2\,R_D\,R_E\,R_G\,r_{2_{in}}\,r_{3_{in}}\,r_{1_{out}}\,V_1(k) + A_1\,R_B\,R_E\,r_{1_{in}}\,r_{2_{in}}\,r_{3_{in}}\,r_{2_{out}}\,V_1(k)$$

$$+ A_2\,R_D\,R_E\,r_{1_{in}}\,r_{2_{in}}\,r_{3_{in}}\,r_{1_{out}}\,V_2(k) + A_1\,R_E\,R_G\,r_{1_{in}}\,r_{2_{in}}\,r_{3_{in}}\,r_{2_{out}}\,V_1(k)$$

$$+ A_1\,R_B\,R_C\,R_D\,R_E\,R_G\,r_{1_{in}}\,V_{3_{in_+}}(k) + A_2\,R_A\,R_C\,R_D\,R_E\,r_{1_{in}}\,r_{2_{in}}\,V_{3_{in_+}}(k)$$

$$+ A_1\,R_C\,R_D\,R_E\,R_G\,r_{1_{in}}\,r_{2_{in}}\,V_{3_{in_+}}(k) + A_2\,R_C\,R_D\,R_E\,R_G\,r_{1_{in}}\,r_{2_{in}}\,V_{3_{in_+}}(k)$$

$$+ A_1\,R_B\,R_C\,R_D\,R_G\,r_{1_{in}}\,r_{3_{in}}\,V_{3_{out}}(k) + A_1\,R_B\,R_C\,R_E\,R_G\,r_{1_{in}}\,r_{2_{out}}\,V_{3_{in_+}}(k)$$

$$+ A_2\,R_A\,R_C\,R_D\,r_{1_{in}}\,r_{2_{in}}\,r_{3_{in}}\,V_{3_{out}}(k) + A_1\,R_B\,R_C\,R_D\,r_{1_{in}}\,r_{2_{in}}\,r_{3_{in}}\,V_{3_{out}}(k)$$

$$
\begin{aligned}
&+ A_2\, R_C\, R_D\, R_E\, R_G\, r_{2_{in}}\, r_{1_{out}}\, V_{3_{in_+}}(k) + A_1\, R_B\, R_C\, R_E\, r_{1_{in}}\, r_{2_{in}}\, r_{2_{out}}\, V_{3_{in_+}}(k) \\
&+ A_1\, R_C\, R_D\, R_E\, r_{1_{in}}\, r_{2_{in}}\, r_{2_{out}}\, V_{3_{in_+}}(k) + A_2\, R_C\, R_D\, R_E\, r_{1_{in}}\, r_{2_{in}}\, r_{1_{out}}\, V_{3_{in_+}}(k) \\
&+ A_2\, R_C\, R_D\, R_G\, r_{1_{in}}\, r_{2_{in}}\, r_{3_{in}}\, V_{3_{out}}(k) + A_1\, R_C\, R_E\, R_G\, r_{1_{in}}\, r_{2_{in}}\, r_{2_{out}}\, V_{3_{in_+}}(k) \\
&+ A_2\, R_D\, R_E\, R_G\, r_{1_{in}}\, r_{2_{in}}\, r_{1_{out}}\, V_{3_{in_+}}(k) + A_1\, R_B\, R_C\, R_G\, r_{1_{in}}\, r_{3_{in}}\, r_{2_{out}}\, V_{3_{out}}(k) \\
&+ A_1\, R_C\, R_D\, R_G\, r_{1_{in}}\, r_{3_{in}}\, r_{2_{out}}\, V_{3_{out}}(k) + A_2\, R_C\, R_D\, R_G\, r_{2_{in}}\, r_{3_{in}}\, r_{1_{out}}\, V_{3_{out}}(k) \\
&+ A_2\, R_A\, R_D\, r_{1_{in}}\, r_{2_{in}}\, r_{3_{in}}\, r_{1_{out}}\, V_{3_{out}}(k) + A_1\, R_C\, R_D\, r_{1_{in}}\, r_{2_{in}}\, r_{3_{in}}\, r_{2_{out}}\, V_{3_{out}}(k) \\
&+ A_1\, R_C\, R_G\, r_{1_{in}}\, r_{2_{in}}\, r_{3_{in}}\, r_{2_{out}}\, V_{3_{out}}(k) + A_2\, R_D\, R_G\, r_{1_{in}}\, r_{2_{in}}\, r_{3_{in}}\, r_{1_{out}}\, V_{3_{out}}(k) \\
&- A_1\, A_2\, R_A\, R_D\, R_E\, r_{1_{in}}\, r_{2_{in}}\, r_{3_{in}}\, V_2(k) + A_1\, A_2\, R_D\, R_E\, R_G\, r_{1_{in}}\, r_{2_{in}}\, r_{3_{in}}\, V_1(k) \\
&+ A_1\, A_2\, R_C\, R_D\, R_G\, r_{1_{in}}\, r_{2_{in}}\, r_{3_{in}}\, V_{3_{out}}(k)
\end{aligned} \tag{366}
$$

$$
\begin{aligned}
\beta_2 = {} & R_A\, R_B\, R_C\, R_D\, R_E\, R_G + R_A\, R_B\, R_C\, R_D\, R_E\, r_{1_{in}} + R_A\, R_B\, R_C\, R_D\, R_E\, r_{2_{in}} \\
&+ R_A\, R_B\, R_D\, R_E\, R_G\, r_{3_{in}} + R_A\, R_B\, R_C\, R_D\, r_{1_{in}}\, r_{3_{in}} + R_A\, R_B\, R_C\, R_D\, r_{2_{in}}\, r_{3_{in}} \\
&+ R_B\, R_C\, R_D\, R_E\, R_G\, r_{1_{in}} + R_A\, R_B\, R_D\, R_E\, r_{1_{in}}\, r_{3_{in}} + R_A\, R_B\, R_D\, R_E\, r_{2_{in}}\, r_{3_{in}} \\
&+ R_B\, R_C\, R_D\, R_E\, r_{1_{in}}\, r_{2_{in}} + R_A\, R_B\, R_C\, R_E\, R_G\, r_{2_{out}} + R_A\, R_C\, R_D\, R_G\, r_{2_{in}}\, r_{3_{in}} \\
&+ R_B\, R_C\, R_D\, R_G\, r_{1_{in}}\, r_{3_{in}} + R_A\, R_C\, R_D\, R_E\, R_G\, r_{2_{out}} + R_A\, R_D\, R_E\, R_G\, r_{2_{in}}\, r_{3_{in}} \\
&+ R_A\, R_B\, R_C\, R_E\, r_{2_{in}}\, r_{2_{out}} + R_A\, R_C\, R_D\, r_{1_{in}}\, r_{2_{in}}\, r_{3_{in}} + R_B\, R_C\, R_D\, R_E\, R_G\, r_{1_{out}} \\
&+ R_A\, R_B\, R_D\, R_E\, r_{1_{in}}\, r_{1_{out}} + R_A\, R_B\, R_D\, R_E\, r_{2_{in}}\, r_{1_{out}} + R_B\, R_C\, R_D\, r_{1_{in}}\, r_{2_{in}}\, r_{3_{in}} \\
&+ R_A\, R_C\, R_D\, R_E\, r_{1_{in}}\, r_{2_{out}} + R_A\, R_C\, R_D\, R_E\, r_{2_{in}}\, r_{2_{out}} + R_A\, R_B\, R_C\, R_G\, r_{3_{in}}\, r_{2_{out}} \\
&+ R_B\, R_C\, R_D\, R_E\, r_{1_{in}}\, r_{1_{out}} + R_B\, R_C\, R_D\, R_E\, r_{2_{in}}\, r_{1_{out}} + R_A\, R_B\, R_D\, R_G\, r_{3_{in}}\, r_{1_{out}} \\
&+ R_A\, R_B\, R_E\, R_G\, r_{3_{in}}\, r_{2_{out}} + R_A\, R_C\, R_D\, R_G\, r_{3_{in}}\, r_{2_{out}} + R_A\, R_B\, R_C\, r_{1_{in}}\, r_{3_{in}}\, r_{2_{out}} \\
&+ R_A\, R_C\, R_E\, R_G\, r_{2_{in}}\, r_{2_{out}} + R_B\, R_C\, R_D\, R_G\, r_{3_{in}}\, r_{1_{out}} + R_A\, R_B\, R_D\, r_{1_{in}}\, r_{3_{in}}\, r_{1_{out}} \\
&+ R_A\, R_D\, R_E\, R_G\, r_{2_{in}}\, r_{1_{out}} + R_B\, R_C\, R_E\, R_G\, r_{1_{in}}\, r_{2_{out}} + R_A\, R_D\, R_E\, R_G\, r_{3_{in}}\, r_{2_{out}} \\
&+ R_A\, R_B\, R_E\, r_{1_{in}}\, r_{3_{in}}\, r_{2_{out}} + R_A\, R_C\, R_D\, r_{1_{in}}\, r_{3_{in}}\, r_{2_{out}} + R_A\, R_B\, R_E\, r_{2_{in}}\, r_{3_{in}}\, r_{2_{out}} \\
&+ R_B\, R_D\, R_E\, R_G\, r_{1_{in}}\, r_{1_{out}} + R_B\, R_D\, R_E\, R_G\, r_{3_{in}}\, r_{1_{out}} + R_A\, R_C\, R_E\, r_{1_{in}}\, r_{2_{in}}\, r_{2_{out}} \\
&+ R_B\, R_C\, R_D\, r_{2_{in}}\, r_{3_{in}}\, r_{1_{out}} + R_C\, R_D\, R_E\, R_G\, r_{1_{in}}\, r_{2_{out}} + R_C\, R_D\, R_E\, R_G\, r_{2_{in}}\, r_{1_{out}} \\
&+ R_A\, R_D\, R_E\, r_{1_{in}}\, r_{2_{in}}\, r_{1_{out}} + R_B\, R_C\, R_E\, r_{1_{in}}\, r_{2_{in}}\, r_{2_{out}} + R_A\, R_D\, R_E\, r_{1_{in}}\, r_{3_{in}}\, r_{2_{out}} \\
&+ R_B\, R_D\, R_E\, r_{1_{in}}\, r_{2_{in}}\, r_{1_{out}} + R_B\, R_D\, R_E\, r_{1_{in}}\, r_{3_{in}}\, r_{1_{out}} + R_B\, R_D\, R_E\, r_{2_{in}}\, r_{3_{in}}\, r_{1_{out}}
\end{aligned}
$$

$$+ \mathrm{R_A\,R_B\,R_E\,R_G\,r_{1_{out}}\,r_{2_{out}}} + \mathrm{R_C\,R_D\,R_E\,r_{1_{in}}\,r_{2_{in}}\,r_{1_{out}}} + \mathrm{R_C\,R_D\,R_E\,r_{1_{in}}\,r_{2_{in}}\,r_{2_{out}}}$$

$$+ \mathrm{R_B\,R_C\,R_G\,r_{1_{in}}\,r_{3_{in}}\,r_{2_{out}}} + \mathrm{R_B\,R_D\,R_G\,r_{1_{in}}\,r_{3_{in}}\,r_{1_{out}}} + \mathrm{R_A\,R_E\,R_G\,r_{2_{in}}\,r_{3_{in}}\,r_{2_{out}}}$$

$$+ \mathrm{R_A\,R_D\,R_E\,R_G\,r_{1_{out}}\,r_{2_{out}}} + \mathrm{R_B\,R_C\,R_E\,R_G\,r_{1_{out}}\,r_{2_{out}}} + \mathrm{R_B\,R_E\,R_G\,r_{1_{in}}\,r_{3_{in}}\,r_{2_{out}}}$$

$$+ \mathrm{R_C\,R_D\,R_G\,r_{2_{in}}\,r_{3_{in}}\,r_{1_{out}}} + \mathrm{R_A\,R_B\,R_E\,r_{1_{in}}\,r_{1_{out}}\,r_{2_{out}}} + \mathrm{R_A\,R_B\,R_E\,r_{2_{in}}\,r_{1_{out}}\,r_{2_{out}}}$$

$$+ \mathrm{R_B\,R_C\,r_{1_{in}}\,r_{2_{in}}\,r_{3_{in}}\,r_{2_{out}}} + \mathrm{R_C\,R_E\,R_G\,r_{1_{in}}\,r_{2_{in}}\,r_{2_{out}}} + \mathrm{R_B\,R_D\,r_{1_{in}}\,r_{2_{in}}\,r_{3_{in}}\,r_{1_{out}}}$$

$$+ \mathrm{R_C\,R_D\,R_E\,R_G\,r_{1_{out}}\,r_{2_{out}}} + \mathrm{R_D\,R_E\,R_G\,r_{1_{in}}\,r_{2_{in}}\,r_{1_{out}}} + \mathrm{R_D\,R_E\,R_G\,r_{1_{in}}\,r_{3_{in}}\,r_{2_{out}}}$$

$$+ \mathrm{R_A\,R_D\,R_E\,r_{1_{in}}\,r_{1_{out}}\,r_{2_{out}}} + \mathrm{R_B\,R_C\,R_E\,r_{1_{in}}\,r_{1_{out}}\,r_{2_{out}}} + \mathrm{R_A\,R_D\,R_E\,r_{2_{in}}\,r_{1_{out}}\,r_{2_{out}}}$$

$$+ \mathrm{R_A\,R_B\,R_G\,r_{3_{in}}\,r_{1_{out}}\,r_{2_{out}}} + \mathrm{R_C\,R_D\,r_{1_{in}}\,r_{2_{in}}\,r_{3_{in}}\,r_{1_{out}}} + \mathrm{R_B\,R_E\,r_{1_{in}}\,r_{2_{in}}\,r_{3_{in}}\,r_{2_{out}}}$$

$$+ \mathrm{R_C\,R_D\,R_E\,r_{1_{in}}\,r_{1_{out}}\,r_{2_{out}}} + \mathrm{R_C\,R_D\,R_E\,r_{2_{in}}\,r_{1_{out}}\,r_{2_{out}}} + \mathrm{R_A\,R_D\,R_G\,r_{3_{in}}\,r_{1_{out}}\,r_{2_{out}}}$$

$$+ \mathrm{R_D\,R_E\,r_{1_{in}}\,r_{2_{in}}\,r_{3_{in}}\,r_{1_{out}}} + \mathrm{R_D\,R_E\,r_{1_{in}}\,r_{2_{in}}\,r_{3_{in}}\,r_{2_{out}}} + \mathrm{R_A\,R_B\,r_{1_{in}}\,r_{3_{in}}\,r_{1_{out}}\,r_{2_{out}}}$$

$$+ \mathrm{R_A\,R_E\,R_G\,r_{2_{in}}\,r_{1_{out}}\,r_{2_{out}}} + \mathrm{R_C\,R_G\,r_{1_{in}}\,r_{2_{in}}\,r_{3_{in}}\,r_{2_{out}}} + \mathrm{R_B\,R_E\,R_G\,r_{1_{in}}\,r_{1_{out}}\,r_{2_{out}}}$$

$$+ \mathrm{R_C\,R_D\,R_G\,r_{3_{in}}\,r_{1_{out}}\,r_{2_{out}}} + \mathrm{R_D\,R_G\,r_{1_{in}}\,r_{2_{in}}\,r_{3_{in}}\,r_{1_{out}}} + \mathrm{R_A\,R_D\,r_{1_{in}}\,r_{3_{in}}\,r_{1_{out}}\,r_{2_{out}}}$$

$$+ \mathrm{R_A\,R_D\,r_{2_{in}}\,r_{3_{in}}\,r_{1_{out}}\,r_{2_{out}}} + \mathrm{R_B\,R_C\,r_{2_{in}}\,r_{3_{in}}\,r_{1_{out}}\,r_{2_{out}}} + \mathrm{R_C\,R_E\,R_G\,r_{2_{in}}\,r_{1_{out}}\,r_{2_{out}}}$$

$$+ \mathrm{R_A\,R_E\,r_{1_{in}}\,r_{2_{in}}\,r_{1_{out}}\,r_{2_{out}}} + \mathrm{R_D\,R_E\,R_G\,r_{1_{in}}\,r_{1_{out}}\,r_{2_{out}}} + \mathrm{R_D\,R_E\,R_G\,r_{3_{in}}\,r_{1_{out}}\,r_{2_{out}}}$$

$$+ \mathrm{R_B\,R_E\,r_{1_{in}}\,r_{3_{in}}\,r_{1_{out}}\,r_{2_{out}}} + \mathrm{R_C\,R_D\,r_{1_{in}}\,r_{3_{in}}\,r_{1_{out}}\,r_{2_{out}}} + \mathrm{R_B\,R_E\,r_{2_{in}}\,r_{3_{in}}\,r_{1_{out}}\,r_{2_{out}}}$$

$$+ \mathrm{R_C\,R_E\,r_{1_{in}}\,r_{2_{in}}\,r_{1_{out}}\,r_{2_{out}}} + \mathrm{R_A\,R_G\,r_{2_{in}}\,r_{3_{in}}\,r_{1_{out}}\,r_{2_{out}}} + \mathrm{R_D\,R_E\,r_{1_{in}}\,r_{2_{in}}\,r_{1_{out}}\,r_{2_{out}}}$$

$$+ \mathrm{R_D\,R_E\,r_{1_{in}}\,r_{3_{in}}\,r_{1_{out}}\,r_{2_{out}}} + \mathrm{R_D\,R_E\,r_{2_{in}}\,r_{3_{in}}\,r_{1_{out}}\,r_{2_{out}}} + \mathrm{R_C\,R_G\,r_{2_{in}}\,r_{3_{in}}\,r_{1_{out}}\,r_{2_{out}}}$$

$$+ \mathrm{R_D\,R_G\,r_{1_{in}}\,r_{3_{in}}\,r_{1_{out}}\,r_{2_{out}}} + \mathrm{R_B\,r_{1_{in}}\,r_{2_{in}}\,r_{3_{in}}\,r_{1_{out}}\,r_{2_{out}}} + \mathrm{R_E\,R_G\,r_{1_{in}}\,r_{2_{in}}\,r_{1_{out}}\,r_{2_{out}}}$$

$$+ \mathrm{R_C\,r_{1_{in}}\,r_{2_{in}}\,r_{3_{in}}\,r_{1_{out}}\,r_{2_{out}}} + \mathrm{R_D\,r_{1_{in}}\,r_{2_{in}}\,r_{3_{in}}\,r_{1_{out}}\,r_{2_{out}}} + \mathrm{R_E\,r_{1_{in}}\,r_{2_{in}}\,r_{3_{in}}\,r_{1_{out}}\,r_{2_{out}}}$$

$$+ \mathrm{A_2\,R_A\,R_C\,R_D\,R_E\,R_G\,r_{2_{in}}} + \mathrm{A_1\,R_B\,R_C\,R_D\,R_E\,R_G\,r_{1_{in}}} + \mathrm{A_2\,R_A\,R_C\,R_D\,R_E\,r_{1_{in}}\,r_{2_{in}}}$$

$$+ \mathrm{A_2\,R_A\,R_C\,R_D\,R_G\,r_{2_{in}}\,r_{3_{in}}} + \mathrm{A_1\,R_B\,R_C\,R_D\,R_G\,r_{1_{in}}\,r_{3_{in}}} + \mathrm{A_2\,R_A\,R_D\,R_E\,R_G\,r_{2_{in}}\,r_{3_{in}}}$$

$$+ \mathrm{A_1\,R_B\,R_D\,R_E\,R_G\,r_{1_{in}}\,r_{3_{in}}} + \mathrm{A_1\,R_B\,R_C\,R_D\,r_{1_{in}}\,r_{2_{in}}\,r_{3_{in}}} + \mathrm{A_1\,R_C\,R_D\,R_E\,R_G\,r_{1_{in}}\,r_{2_{in}}}$$

$$+ \mathrm{A_2\,R_A\,R_D\,R_E\,r_{1_{in}}\,r_{2_{in}}\,r_{3_{in}}} + \mathrm{A_1\,R_B\,R_D\,R_E\,r_{1_{in}}\,r_{2_{in}}\,r_{3_{in}}} + \mathrm{A_1\,R_B\,R_C\,R_E\,R_G\,r_{1_{in}}\,r_{2_{out}}}$$

$$+ \mathrm{A_1\,R_C\,R_D\,R_G\,r_{1_{in}}\,r_{2_{in}}\,r_{3_{in}}} + \mathrm{A_2\,R_C\,R_D\,R_G\,r_{1_{in}}\,r_{2_{in}}\,r_{3_{in}}} + \mathrm{A_1\,R_C\,R_D\,R_E\,R_G\,r_{1_{in}}\,r_{2_{out}}}$$

$$+ \mathrm{A_1\,R_D\,R_E\,R_G\,r_{1_{in}}\,r_{2_{in}}\,r_{3_{in}}} + \mathrm{A_2\,R_D\,R_E\,R_G\,r_{1_{in}}\,r_{2_{in}}\,r_{3_{in}}} + \mathrm{A_1\,R_B\,R_C\,R_E\,r_{1_{in}}\,r_{2_{in}}\,r_{2_{out}}}$$

$$+ \mathrm{A_1\,R_C\,R_D\,R_E\,r_{1_{in}}\,r_{2_{in}}\,r_{2_{out}}} + \mathrm{A_1\,R_B\,R_C\,R_G\,r_{1_{in}}\,r_{3_{in}}\,r_{2_{out}}} + \mathrm{A_2\,R_C\,R_D\,R_E\,r_{1_{in}}\,r_{2_{in}}\,r_{1_{out}}}$$

$$+ A_1\, R_B\, R_E\, R_G\, r_{1_{in}}\, r_{3_{in}}\, r_{2_{out}} + A_1\, R_C\, R_D\, R_G\, r_{1_{in}}\, r_{3_{in}}\, r_{2_{out}} + A_2\, R_C\, R_D\, R_G\, r_{2_{in}}\, r_{3_{in}}\, r_{1_{out}}$$

$$+ A_2\, R_A\, R_D\, r_{1_{in}}\, r_{2_{in}}\, r_{3_{in}}\, r_{1_{out}} + A_1\, R_C\, R_E\, R_G\, r_{1_{in}}\, r_{2_{in}}\, r_{2_{out}} + A_1\, R_D\, R_E\, R_G\, r_{1_{in}}\, r_{3_{in}}\, r_{2_{out}}$$

$$+ A_2\, R_D\, R_E\, R_G\, r_{2_{in}}\, r_{3_{in}}\, r_{1_{out}} + A_1\, R_B\, R_E\, r_{1_{in}}\, r_{2_{in}}\, r_{3_{in}}\, r_{2_{out}} + A_1\, R_C\, R_D\, r_{1_{in}}\, r_{2_{in}}\, r_{3_{in}}\, r_{2_{out}}$$

$$+ A_1\, R_D\, R_E\, r_{1_{in}}\, r_{2_{in}}\, r_{3_{in}}\, r_{2_{out}} + A_2\, R_D\, R_E\, r_{1_{in}}\, r_{2_{in}}\, r_{3_{in}}\, r_{1_{out}} + A_1\, R_C\, R_G\, r_{1_{in}}\, r_{2_{in}}\, r_{3_{in}}\, r_{2_{out}}$$

$$+ A_1\, A_2\, R_D\, R_E\, R_G\, r_{1_{in}}\, r_{2_{in}}\, r_{3_{in}} \tag{367}$$

$$\alpha_3 = R_A\, R_C\, R_E\, R_F\, R_G\, r_{2_{out}}\, V_2(k) + R_B\, R_D\, R_E\, R_F\, R_G\, r_{1_{out}}\, V_1(k)$$

$$+ R_A\, R_C\, R_E\, R_F\, r_{1_{in}}\, r_{2_{out}}\, V_2(k) + R_B\, R_D\, R_E\, R_F\, r_{2_{in}}\, r_{1_{out}}\, V_1(k)$$

$$+ R_A\, R_C\, R_F\, R_G\, r_{3_{in}}\, r_{2_{out}}\, V_2(k) + R_A\, R_C\, R_F\, r_{2_{in}}\, r_{3_{in}}\, r_{2_{out}}\, V_1(k)$$

$$+ R_A\, R_C\, R_F\, r_{1_{in}}\, r_{3_{in}}\, r_{2_{out}}\, V_2(k) + R_A\, R_E\, R_F\, r_{2_{in}}\, r_{3_{in}}\, r_{2_{out}}\, V_1(k)$$

$$+ R_D\, R_E\, R_F\, R_G\, r_{2_{in}}\, r_{1_{out}}\, V_1(k) + R_A\, R_E\, R_F\, r_{1_{in}}\, r_{3_{in}}\, r_{2_{out}}\, V_2(k)$$

$$+ R_B\, R_E\, R_F\, R_G\, r_{1_{out}}\, r_{2_{out}}\, V_1(k) + R_C\, R_F\, R_G\, r_{1_{in}}\, r_{3_{in}}\, r_{2_{out}}\, V_2(k)$$

$$+ R_C\, R_E\, R_F\, R_G\, r_{1_{out}}\, r_{2_{out}}\, V_2(k) + R_D\, R_E\, R_F\, R_G\, r_{1_{out}}\, r_{2_{out}}\, V_1(k)$$

$$+ R_A\, R_E\, R_F\, r_{1_{in}}\, r_{1_{out}}\, r_{2_{out}}\, V_2(k) + R_B\, R_E\, R_F\, r_{2_{in}}\, r_{1_{out}}\, r_{2_{out}}\, V_1(k)$$

$$+ R_C\, R_E\, R_F\, r_{2_{in}}\, r_{1_{out}}\, r_{2_{out}}\, V_1(k) + R_C\, R_E\, R_F\, r_{1_{in}}\, r_{1_{out}}\, r_{2_{out}}\, V_2(k)$$

$$+ R_A\, R_F\, R_G\, r_{3_{in}}\, r_{1_{out}}\, r_{2_{out}}\, V_2(k) + R_D\, R_E\, R_F\, r_{1_{in}}\, r_{1_{out}}\, r_{2_{out}}\, V_2(k)$$

$$+ R_C\, R_F\, R_G\, r_{3_{in}}\, r_{1_{out}}\, r_{2_{out}}\, V_2(k) + R_A\, R_F\, r_{1_{in}}\, r_{3_{in}}\, r_{1_{out}}\, r_{2_{out}}\, V_2(k)$$

$$+ R_C\, R_F\, r_{2_{in}}\, r_{3_{in}}\, r_{1_{out}}\, r_{2_{out}}\, V_1(k) + R_E\, R_F\, R_G\, r_{1_{in}}\, r_{1_{out}}\, r_{2_{out}}\, V_2(k)$$

$$+ R_C\, R_F\, r_{1_{in}}\, r_{3_{in}}\, r_{1_{out}}\, r_{2_{out}}\, V_2(k) + R_E\, R_F\, r_{2_{in}}\, r_{3_{in}}\, r_{1_{out}}\, r_{2_{out}}\, V_1(k)$$

$$+ R_F\, R_G\, r_{1_{in}}\, r_{3_{in}}\, r_{1_{out}}\, r_{2_{out}}\, V_2(k) + R_A\, R_B\, R_C\, R_D\, R_F\, R_G\, V_{3_{out}}(k)$$

$$+ R_A\, R_B\, R_C\, R_D\, R_F\, r_{2_{in}}\, V_{3_{out}}(k) + R_A\, R_C\, R_D\, R_F\, R_G\, r_{2_{in}}\, V_{3_{out}}(k)$$

$$+ R_A\, R_C\, R_D\, R_F\, r_{1_{in}}\, r_{2_{in}}\, V_{3_{out}}(k) + R_B\, R_C\, R_D\, R_F\, r_{1_{in}}\, r_{2_{in}}\, V_{3_{out}}(k)$$

$$+ R_A\, R_B\, R_D\, R_F\, R_G\, r_{1_{out}}\, V_{3_{out}}(k) + R_A\, R_C\, R_D\, R_F\, R_G\, r_{2_{out}}\, V_{3_{out}}(k)$$

$$+ R_A\, R_B\, R_C\, R_F\, r_{2_{in}}\, r_{2_{out}}\, V_{3_{out}}(k) + R_B\, R_C\, R_D\, R_F\, R_G\, r_{1_{out}}\, V_{3_{out}}(k)$$

$$+ R_A\, R_B\, R_D\, R_F\, r_{2_{in}}\, r_{1_{out}}\, V_{3_{out}}(k) + R_C\, R_D\, R_F\, R_G\, r_{1_{in}}\, r_{2_{in}}\, V_{3_{out}}(k)$$

$$+ R_A\, R_C\, R_D\, R_F\, r_{2_{in}}\, r_{2_{out}}\, V_{3_{out}}(k) + R_B\, R_C\, R_D\, R_F\, r_{1_{in}}\, r_{1_{out}}\, V_{3_{out}}(k)$$

$$+ R_A\, R_C\, R_F\, R_G\, r_{2_{in}}\, r_{2_{out}}\, V_{3_{out}}(k) + R_A\, R_D\, R_F\, R_G\, r_{2_{in}}\, r_{1_{out}}\, V_{3_{out}}(k)$$

$$+ R_B\,R_D\,R_F\,R_G\,r_{1_{in}}\,r_{1_{out}}\,V_{3_{out}}(k) + R_A\,R_C\,R_F\,r_{1_{in}}\,r_{2_{in}}\,r_{2_{out}}\,V_{3_{out}}(k)$$

$$+ R_C\,R_D\,R_F\,R_G\,r_{2_{in}}\,r_{1_{out}}\,V_{3_{out}}(k) + R_A\,R_D\,R_F\,r_{1_{in}}\,r_{2_{in}}\,r_{1_{out}}\,V_{3_{out}}(k)$$

$$+ R_B\,R_D\,R_F\,r_{1_{in}}\,r_{2_{in}}\,r_{1_{out}}\,V_{3_{out}}(k) + R_A\,R_B\,R_F\,R_G\,r_{1_{out}}\,r_{2_{out}}\,V_{3_{out}}(k)$$

$$+ R_C\,R_D\,R_F\,r_{1_{in}}\,r_{2_{in}}\,r_{2_{out}}\,V_{3_{out}}(k) + R_A\,R_D\,R_F\,R_G\,r_{1_{out}}\,r_{2_{out}}\,V_{3_{out}}(k)$$

$$+ R_A\,R_B\,R_F\,r_{1_{in}}\,r_{1_{out}}\,r_{2_{out}}\,V_{3_{out}}(k) + R_A\,R_B\,R_F\,r_{2_{in}}\,r_{1_{out}}\,r_{2_{out}}\,V_{3_{out}}(k)$$

$$+ R_C\,R_D\,R_F\,R_G\,r_{1_{out}}\,r_{2_{out}}\,V_{3_{out}}(k) + R_D\,R_F\,R_G\,r_{1_{in}}\,r_{2_{in}}\,r_{1_{out}}\,V_{3_{out}}(k)$$

$$+ R_B\,R_C\,R_F\,r_{1_{in}}\,r_{1_{out}}\,r_{2_{out}}\,V_{3_{out}}(k) + R_A\,R_D\,R_F\,r_{2_{in}}\,r_{1_{out}}\,r_{2_{out}}\,V_{3_{out}}(k)$$

$$+ R_C\,R_D\,R_F\,r_{1_{in}}\,r_{1_{out}}\,r_{2_{out}}\,V_{3_{out}}(k) + R_C\,R_D\,R_F\,r_{2_{in}}\,r_{1_{out}}\,r_{2_{out}}\,V_{3_{out}}(k)$$

$$+ R_B\,R_F\,R_G\,r_{1_{in}}\,r_{1_{out}}\,r_{2_{out}}\,V_{3_{out}}(k) + R_C\,R_F\,R_G\,r_{2_{in}}\,r_{1_{out}}\,r_{2_{out}}\,V_{3_{out}}(k)$$

$$+ R_D\,R_F\,R_G\,r_{1_{in}}\,r_{1_{out}}\,r_{2_{out}}\,V_{3_{out}}(k) + R_B\,R_F\,r_{1_{in}}\,r_{2_{in}}\,r_{1_{out}}\,r_{2_{out}}\,V_{3_{out}}(k)$$

$$+ R_D\,R_F\,r_{1_{in}}\,r_{2_{in}}\,r_{1_{out}}\,r_{2_{out}}\,V_{3_{out}}(k) + R_F\,R_G\,r_{1_{in}}\,r_{2_{in}}\,r_{1_{out}}\,r_{2_{out}}\,V_{3_{out}}(k)$$

$$- A_2\,R_A\,R_B\,R_C\,R_E\,R_F\,r_{2_{in}}\,V_1(k) + A_1\,R_A\,R_B\,R_D\,R_E\,R_F\,r_{1_{in}}\,V_1(k)$$

$$- A_1\,R_A\,R_B\,R_D\,R_E\,R_F\,r_{1_{in}}\,V_2(k) - A_2\,R_A\,R_B\,R_C\,R_F\,r_{2_{in}}\,r_{3_{in}}\,V_1(k)$$

$$+ A_2\,R_A\,R_C\,R_E\,R_F\,R_G\,r_{2_{in}}\,V_2(k) - A_2\,R_A\,R_B\,R_E\,R_F\,r_{2_{in}}\,r_{3_{in}}\,V_1(k)$$

$$+ A_2\,R_A\,R_B\,R_E\,R_F\,r_{2_{in}}\,r_{3_{in}}\,V_2(k) + A_1\,R_A\,R_D\,R_E\,R_F\,r_{1_{in}}\,r_{2_{in}}\,V_1(k)$$

$$+ A_1\,R_B\,R_D\,R_E\,R_F\,r_{1_{in}}\,r_{2_{in}}\,V_1(k) + A_2\,R_B\,R_C\,R_E\,R_F\,r_{1_{in}}\,r_{2_{in}}\,V_2(k)$$

$$+ A_2\,R_A\,R_E\,R_F\,R_G\,r_{2_{in}}\,r_{3_{in}}\,V_2(k) + A_1\,R_A\,R_B\,R_E\,R_F\,r_{1_{in}}\,r_{2_{out}}\,V_1(k)$$

$$+ A_2\,R_A\,R_C\,R_F\,r_{1_{in}}\,r_{2_{in}}\,r_{3_{in}}\,V_2(k) - A_1\,R_A\,R_B\,R_E\,R_F\,r_{1_{in}}\,r_{2_{out}}\,V_2(k)$$

$$+ A_2\,R_B\,R_C\,R_F\,r_{1_{in}}\,r_{2_{in}}\,r_{3_{in}}\,V_2(k) + A_1\,R_D\,R_E\,R_F\,R_G\,r_{1_{in}}\,r_{2_{in}}\,V_1(k)$$

$$+ A_1\,R_A\,R_D\,R_E\,R_F\,r_{1_{in}}\,r_{2_{out}}\,V_1(k) - A_2\,R_B\,R_C\,R_E\,R_F\,r_{2_{in}}\,r_{1_{out}}\,V_1(k)$$

$$- A_1\,R_A\,R_D\,R_E\,R_F\,r_{1_{in}}\,r_{2_{out}}\,V_2(k) + A_2\,R_B\,R_C\,R_E\,R_F\,r_{2_{in}}\,r_{1_{out}}\,V_2(k)$$

$$- A_2\,R_A\,R_B\,R_F\,r_{2_{in}}\,r_{3_{in}}\,r_{1_{out}}\,V_1(k) + A_2\,R_A\,R_B\,R_F\,r_{2_{in}}\,r_{3_{in}}\,r_{1_{out}}\,V_2(k)$$

$$+ A_2\,R_A\,R_E\,R_F\,R_G\,r_{2_{in}}\,r_{1_{out}}\,V_2(k) + A_2\,R_C\,R_F\,R_G\,r_{1_{in}}\,r_{2_{in}}\,r_{3_{in}}\,V_2(k)$$

$$+ A_1\,R_A\,R_E\,R_F\,r_{1_{in}}\,r_{2_{in}}\,r_{2_{out}}\,V_1(k) + A_2\,R_B\,R_C\,R_F\,r_{2_{in}}\,r_{3_{in}}\,r_{1_{out}}\,V_2(k)$$

$$+ A_1\,R_D\,R_E\,R_F\,R_G\,r_{1_{in}}\,r_{2_{out}}\,V_1(k) + A_2\,R_C\,R_E\,R_F\,R_G\,r_{2_{in}}\,r_{1_{out}}\,V_2(k)$$

$$+ A_2\,R_E\,R_F\,R_G\,r_{1_{in}}\,r_{2_{in}}\,r_{3_{in}}\,V_2(k) + A_1\,R_B\,R_E\,R_F\,r_{1_{in}}\,r_{2_{in}}\,r_{2_{out}}\,V_1(k)$$

$$
\begin{aligned}
&- A_2\,R_B\,R_E\,R_F\,r_{2_{in}}\,r_{3_{in}}\,r_{1_{out}}\,V_1(k) + A_1\,R_C\,R_E\,R_F\,r_{1_{in}}\,r_{2_{in}}\,r_{2_{out}}\,V_1(k)\\
&+ A_2\,R_B\,R_E\,R_F\,r_{2_{in}}\,r_{3_{in}}\,r_{1_{out}}\,V_2(k) + A_1\,R_D\,R_E\,R_F\,r_{1_{in}}\,r_{2_{in}}\,r_{2_{out}}\,V_1(k)\\
&+ A_2\,R_A\,R_F\,R_G\,r_{2_{in}}\,r_{3_{in}}\,r_{1_{out}}\,V_2(k) + A_2\,R_D\,R_E\,R_F\,r_{1_{in}}\,r_{2_{in}}\,r_{1_{out}}\,V_2(k)\\
&+ A_2\,R_C\,R_F\,R_G\,r_{2_{in}}\,r_{3_{in}}\,r_{1_{out}}\,V_2(k) + A_2\,R_A\,R_F\,r_{1_{in}}\,r_{2_{in}}\,r_{3_{in}}\,r_{1_{out}}\,V_2(k)\\
&+ A_1\,R_C\,R_F\,r_{1_{in}}\,r_{2_{in}}\,r_{3_{in}}\,r_{2_{out}}\,V_1(k) + A_2\,R_B\,R_F\,r_{1_{in}}\,r_{2_{in}}\,r_{3_{in}}\,r_{1_{out}}\,V_2(k)\\
&+ A_2\,R_E\,R_F\,R_G\,r_{1_{in}}\,r_{2_{in}}\,r_{1_{out}}\,V_2(k) + A_2\,R_E\,R_F\,R_G\,r_{2_{in}}\,r_{3_{in}}\,r_{1_{out}}\,V_2(k)\\
&+ A_1\,R_E\,R_F\,r_{1_{in}}\,r_{2_{in}}\,r_{3_{in}}\,r_{2_{out}}\,V_1(k) + A_2\,R_E\,R_F\,r_{1_{in}}\,r_{2_{in}}\,r_{3_{in}}\,r_{1_{out}}\,V_2(k)\\
&+ A_2\,R_A\,R_C\,R_D\,R_F\,R_G\,r_{2_{in}}\,V_{3_{out}}(k) + A_1\,R_B\,R_C\,R_D\,R_F\,R_G\,r_{1_{in}}\,V_{3_{out}}(k)\\
&+ A_1\,R_B\,R_C\,R_D\,R_F\,r_{1_{in}}\,r_{2_{in}}\,V_{3_{out}}(k) + A_1\,R_C\,R_D\,R_F\,R_G\,r_{1_{in}}\,r_{2_{in}}\,V_{3_{out}}(k)\\
&+ A_1\,R_B\,R_C\,R_F\,R_G\,r_{1_{in}}\,r_{2_{out}}\,V_{3_{out}}(k) + A_2\,R_A\,R_D\,R_F\,R_G\,r_{2_{in}}\,r_{1_{out}}\,V_{3_{out}}(k)\\
&+ A_2\,R_C\,R_D\,R_F\,R_G\,r_{2_{in}}\,r_{1_{out}}\,V_{3_{out}}(k) + A_1\,R_B\,R_C\,R_F\,r_{1_{in}}\,r_{2_{in}}\,r_{2_{out}}\,V_{3_{out}}(k)\\
&+ A_1\,R_C\,R_D\,R_F\,r_{1_{in}}\,r_{2_{in}}\,r_{2_{out}}\,V_{3_{out}}(k) + A_2\,R_C\,R_D\,R_F\,r_{1_{in}}\,r_{2_{in}}\,r_{1_{out}}\,V_{3_{out}}(k)\\
&+ A_2\,R_D\,R_F\,R_G\,r_{1_{in}}\,r_{2_{in}}\,r_{1_{out}}\,V_{3_{out}}(k) - A_2\,R_B\,R_F\,r_{1_{in}}\,r_{2_{in}}\,r_{3_{in}}\,r_{1_{out}}\,V_{3_{out}}(k)\\
&- A_1\,A_2\,R_B\,R_C\,R_E\,R_F\,r_{1_{in}}\,r_{2_{in}}\,V_1(k) - A_1\,A_2\,R_A\,R_D\,R_E\,R_F\,r_{1_{in}}\,r_{2_{in}}\,V_2(k)\\
&- A_1\,A_2\,R_B\,R_C\,R_F\,r_{1_{in}}\,r_{2_{in}}\,r_{3_{in}}\,V_1(k) + A_1\,A_2\,R_B\,R_C\,R_F\,r_{1_{in}}\,r_{2_{in}}\,r_{3_{in}}\,V_2(k)\\
&+ A_1\,A_2\,R_D\,R_E\,R_F\,R_G\,r_{1_{in}}\,r_{2_{in}}\,V_1(k) - A_1\,A_2\,R_B\,R_E\,R_F\,r_{1_{in}}\,r_{2_{in}}\,r_{3_{in}}\,V_1(k)\\
&+ A_1\,A_2\,R_C\,R_D\,R_F\,R_G\,r_{1_{in}}\,r_{2_{in}}\,V_{3_{out}}(k)
\end{aligned}
\tag{368}
$$

$$
\begin{aligned}
\beta_3 = {} & R_A\,R_B\,R_C\,R_D\,R_E\,R_G + R_A\,R_B\,R_C\,R_D\,R_F\,R_G + R_A\,R_B\,R_C\,R_E\,R_F\,R_G\\
&+ R_A\,R_B\,R_C\,R_D\,R_E\,r_{2_{in}} + R_A\,R_B\,R_D\,R_E\,R_F\,R_G + R_A\,R_B\,R_C\,R_D\,R_F\,r_{1_{in}}\\
&+ R_A\,R_B\,R_C\,R_E\,R_F\,r_{1_{in}} + R_A\,R_B\,R_C\,R_E\,R_F\,r_{2_{in}} + R_A\,R_B\,R_C\,R_D\,R_G\,r_{3_{in}}\\
&+ R_A\,R_B\,R_D\,R_E\,R_F\,r_{2_{in}} + R_A\,R_B\,R_C\,R_F\,R_G\,r_{3_{in}} + R_A\,R_B\,R_D\,R_E\,R_G\,r_{3_{in}}\\
&+ R_A\,R_B\,R_C\,R_D\,r_{2_{in}}\,r_{3_{in}} + R_A\,R_C\,R_D\,R_E\,R_G\,r_{2_{in}} + R_B\,R_C\,R_D\,R_E\,R_G\,r_{1_{in}}\\
&+ R_A\,R_B\,R_E\,R_F\,R_G\,r_{3_{in}} + R_A\,R_B\,R_C\,R_F\,r_{1_{in}}\,r_{3_{in}} + R_A\,R_B\,R_D\,R_E\,r_{1_{in}}\,r_{3_{in}}\\
&+ R_A\,R_B\,R_D\,R_E\,r_{2_{in}}\,r_{3_{in}} + R_B\,R_C\,R_D\,R_F\,R_G\,r_{1_{in}} + R_A\,R_C\,R_E\,R_F\,R_G\,r_{2_{in}}\\
&+ R_B\,R_C\,R_E\,R_F\,R_G\,r_{1_{in}} + R_A\,R_D\,R_E\,R_F\,R_G\,r_{2_{in}} + R_A\,R_C\,R_D\,R_F\,r_{1_{in}}\,r_{2_{in}}\\
&+ R_A\,R_B\,R_E\,R_F\,r_{1_{in}}\,r_{3_{in}} + R_A\,R_B\,R_E\,R_F\,r_{2_{in}}\,r_{3_{in}} + R_B\,R_D\,R_E\,R_F\,R_G\,r_{1_{in}}
\end{aligned}
$$

$$+ R_A\,R_C\,R_E\,R_F\,r_{1_{in}}\,r_{2_{in}} + R_B\,R_C\,R_D\,R_F\,r_{1_{in}}\,r_{2_{in}} + R_A\,R_C\,R_D\,R_G\,r_{2_{in}}\,r_{3_{in}}$$

$$+ R_A\,R_B\,R_C\,R_F\,R_G\,r_{2_{out}} + R_A\,R_D\,R_E\,R_F\,r_{1_{in}}\,r_{2_{in}} + R_B\,R_C\,R_E\,R_F\,r_{1_{in}}\,r_{2_{in}}$$

$$+ R_A\,R_B\,R_D\,R_F\,R_G\,r_{1_{out}} + R_A\,R_C\,R_D\,R_E\,R_G\,r_{2_{out}} + R_B\,R_D\,R_E\,R_F\,r_{1_{in}}\,r_{2_{in}}$$

$$+ R_A\,R_D\,R_E\,R_G\,r_{2_{in}}\,r_{3_{in}} + R_A\,R_B\,R_C\,R_E\,r_{1_{in}}\,r_{2_{out}} + R_A\,R_B\,R_C\,R_E\,r_{2_{in}}\,r_{2_{out}}$$

$$+ R_A\,R_B\,R_E\,R_F\,R_G\,r_{1_{out}} + R_B\,R_C\,R_D\,R_E\,R_G\,r_{1_{out}} + R_A\,R_B\,R_E\,R_F\,R_G\,r_{2_{out}}$$

$$+ R_B\,R_C\,R_F\,R_G\,r_{1_{in}}\,r_{3_{in}} + R_B\,R_D\,R_E\,R_G\,r_{1_{in}}\,r_{3_{in}} + R_A\,R_B\,R_D\,R_E\,r_{1_{in}}\,r_{1_{out}}$$

$$+ R_A\,R_B\,R_D\,R_E\,r_{2_{in}}\,r_{1_{out}} + R_A\,R_B\,R_C\,R_F\,r_{2_{in}}\,r_{2_{out}} + R_B\,R_C\,R_D\,r_{1_{in}}\,r_{2_{in}}\,r_{3_{in}}$$

$$+ R_A\,R_C\,R_E\,R_F\,R_G\,r_{2_{out}} + R_C\,R_D\,R_E\,R_G\,r_{1_{in}}\,r_{2_{in}} + R_A\,R_E\,R_F\,R_G\,r_{2_{in}}\,r_{3_{in}}$$

$$+ R_A\,R_B\,R_D\,R_F\,r_{2_{in}}\,r_{1_{out}} + R_A\,R_C\,R_D\,R_E\,r_{1_{in}}\,r_{2_{out}} + R_A\,R_C\,R_D\,R_E\,r_{2_{in}}\,r_{2_{out}}$$

$$+ R_A\,R_C\,R_F\,r_{1_{in}}\,r_{2_{in}}\,r_{3_{in}} + R_A\,R_D\,R_E\,r_{1_{in}}\,r_{2_{in}}\,r_{3_{in}} + R_B\,R_C\,R_E\,R_F\,R_G\,r_{1_{out}}$$

$$+ R_C\,R_D\,R_F\,R_G\,r_{1_{in}}\,r_{2_{in}} + R_B\,R_E\,R_F\,R_G\,r_{1_{in}}\,r_{3_{in}} + R_A\,R_B\,R_E\,R_F\,r_{1_{in}}\,r_{1_{out}}$$

$$+ R_A\,R_B\,R_E\,R_F\,r_{1_{in}}\,r_{2_{out}} + R_A\,R_B\,R_E\,R_F\,r_{2_{in}}\,r_{1_{out}} + R_A\,R_C\,R_D\,R_F\,r_{1_{in}}\,r_{2_{out}}$$

$$+ R_A\,R_B\,R_D\,R_G\,r_{3_{in}}\,r_{1_{out}} + R_A\,R_B\,R_E\,R_F\,r_{2_{in}}\,r_{2_{out}} + R_A\,R_C\,R_D\,R_F\,r_{2_{in}}\,r_{2_{out}}$$

$$+ R_B\,R_D\,R_E\,r_{1_{in}}\,r_{2_{in}}\,r_{3_{in}} + R_B\,R_D\,R_E\,R_F\,R_G\,r_{1_{out}} + R_C\,R_E\,R_F\,R_G\,r_{1_{in}}\,r_{2_{in}}$$

$$+ R_A\,R_C\,R_E\,R_F\,r_{1_{in}}\,r_{2_{out}} + R_B\,R_C\,R_D\,R_F\,r_{2_{in}}\,r_{1_{out}} + R_A\,R_C\,R_E\,R_F\,r_{2_{in}}\,r_{2_{out}}$$

$$+ R_A\,R_C\,R_D\,R_G\,r_{3_{in}}\,r_{2_{out}} + R_A\,R_E\,R_F\,r_{1_{in}}\,r_{2_{in}}\,r_{3_{in}} + R_A\,R_B\,R_C\,r_{1_{in}}\,r_{3_{in}}\,r_{2_{out}}$$

$$+ R_D\,R_E\,R_F\,R_G\,r_{1_{in}}\,r_{2_{in}} + R_B\,R_C\,R_E\,R_F\,r_{1_{in}}\,r_{1_{out}} + R_A\,R_D\,R_E\,R_F\,r_{1_{in}}\,r_{2_{out}}$$

$$+ R_A\,R_B\,R_F\,R_G\,r_{3_{in}}\,r_{1_{out}} + R_A\,R_C\,R_E\,R_G\,r_{2_{in}}\,r_{2_{out}} + R_A\,R_D\,R_E\,R_F\,r_{2_{in}}\,r_{2_{out}}$$

$$+ R_B\,R_E\,R_F\,r_{1_{in}}\,r_{2_{in}}\,r_{3_{in}} + R_A\,R_B\,R_D\,r_{1_{in}}\,r_{3_{in}}\,r_{1_{out}} + R_A\,R_B\,R_D\,r_{2_{in}}\,r_{3_{in}}\,r_{1_{out}}$$

$$+ R_A\,R_D\,R_E\,R_G\,r_{2_{in}}\,r_{1_{out}} + R_B\,R_C\,R_E\,R_G\,r_{1_{in}}\,r_{2_{out}} + R_B\,R_D\,R_E\,R_F\,r_{2_{in}}\,r_{1_{out}}$$

$$+ R_A\,R_C\,R_F\,R_G\,r_{3_{in}}\,r_{2_{out}} + R_A\,R_D\,R_E\,R_G\,r_{3_{in}}\,r_{2_{out}} + R_C\,R_D\,R_G\,r_{1_{in}}\,r_{2_{in}}\,r_{3_{in}}$$

$$+ R_A\,R_C\,R_D\,r_{1_{in}}\,r_{3_{in}}\,r_{2_{out}} + R_A\,R_B\,R_E\,r_{2_{in}}\,r_{3_{in}}\,r_{2_{out}} + R_A\,R_C\,R_D\,r_{2_{in}}\,r_{3_{in}}\,r_{2_{out}}$$

$$+ R_A\,R_D\,R_F\,R_G\,r_{2_{in}}\,r_{1_{out}} + R_B\,R_C\,R_F\,R_G\,r_{1_{in}}\,r_{2_{out}} + R_B\,R_C\,R_F\,R_G\,r_{3_{in}}\,r_{1_{out}}$$

$$+ R_A\,R_B\,R_F\,r_{1_{in}}\,r_{3_{in}}\,r_{1_{out}} + R_A\,R_C\,R_E\,r_{1_{in}}\,r_{2_{in}}\,r_{2_{out}} + R_B\,R_C\,R_D\,r_{1_{in}}\,r_{3_{in}}\,r_{1_{out}}$$

$$+ R_B\,R_C\,R_D\,r_{2_{in}}\,r_{3_{in}}\,r_{1_{out}} + R_B\,R_D\,R_F\,R_G\,r_{1_{in}}\,r_{1_{out}} + R_A\,R_E\,R_F\,R_G\,r_{2_{in}}\,r_{1_{out}}$$

$$+ R_C\,R_D\,R_E\,R_G\,r_{2_{in}}\,r_{1_{out}} + R_A\,R_E\,R_F\,R_G\,r_{2_{in}}\,r_{2_{out}} + R_A\,R_E\,R_F\,R_G\,r_{3_{in}}\,r_{2_{out}}$$

$$+ \mathrm{R_D\,R_E\,R_G\,r_{1_{in}}\,r_{2_{in}}\,r_{3_{in}}} + \mathrm{R_A\,R_D\,R_E\,r_{1_{in}}\,r_{2_{in}}\,r_{1_{out}}} + \mathrm{R_A\,R_C\,R_F\,r_{1_{in}}\,r_{2_{in}}\,r_{2_{out}}}$$

$$+ \mathrm{R_A\,R_C\,R_F\,r_{1_{in}}\,r_{3_{in}}\,r_{2_{out}}} + \mathrm{R_A\,R_D\,R_E\,r_{1_{in}}\,r_{3_{in}}\,r_{2_{out}}} + \mathrm{R_A\,R_C\,R_F\,r_{2_{in}}\,r_{3_{in}}\,r_{2_{out}}}$$

$$+ \mathrm{R_B\,R_E\,R_F\,R_G\,r_{1_{in}}\,r_{1_{out}}} + \mathrm{R_B\,R_E\,R_F\,R_G\,r_{1_{in}}\,r_{2_{out}}} + \mathrm{R_C\,R_D\,R_F\,R_G\,r_{1_{in}}\,r_{2_{out}}}$$

$$+ \mathrm{R_B\,R_E\,R_F\,R_G\,r_{3_{in}}\,r_{1_{out}}} + \mathrm{R_A\,R_D\,R_F\,r_{1_{in}}\,r_{2_{in}}\,r_{1_{out}}} + \mathrm{R_B\,R_D\,R_E\,r_{1_{in}}\,r_{2_{in}}\,r_{1_{out}}}$$

$$+ \mathrm{R_B\,R_C\,R_F\,r_{1_{in}}\,r_{3_{in}}\,r_{1_{out}}} + \mathrm{R_B\,R_D\,R_E\,r_{1_{in}}\,r_{3_{in}}\,r_{1_{out}}} + \mathrm{R_B\,R_C\,R_F\,r_{2_{in}}\,r_{3_{in}}\,r_{1_{out}}}$$

$$+ \mathrm{R_A\,R_C\,R_G\,r_{2_{in}}\,r_{3_{in}}\,r_{2_{out}}} + \mathrm{R_C\,R_E\,R_F\,R_G\,r_{1_{in}}\,r_{2_{out}}} + \mathrm{R_C\,R_E\,R_F\,R_G\,r_{2_{in}}\,r_{1_{out}}}$$

$$+ \mathrm{R_E\,R_F\,R_G\,r_{1_{in}}\,r_{2_{in}}\,r_{3_{in}}} + \mathrm{R_A\,R_E\,R_F\,r_{1_{in}}\,r_{2_{in}}\,r_{1_{out}}} + \mathrm{R_B\,R_D\,R_F\,r_{1_{in}}\,r_{2_{in}}\,r_{1_{out}}}$$

$$+ \mathrm{R_A\,R_E\,R_F\,r_{1_{in}}\,r_{2_{in}}\,r_{2_{out}}} + \mathrm{R_C\,R_D\,R_E\,r_{1_{in}}\,r_{2_{in}}\,r_{2_{out}}} + \mathrm{R_A\,R_D\,R_G\,r_{2_{in}}\,r_{3_{in}}\,r_{1_{out}}}$$

$$+ \mathrm{R_B\,R_C\,R_G\,r_{1_{in}}\,r_{3_{in}}\,r_{2_{out}}} + \mathrm{R_A\,R_E\,R_F\,r_{2_{in}}\,r_{3_{in}}\,r_{2_{out}}} + \mathrm{R_D\,R_E\,R_F\,R_G\,r_{1_{in}}\,r_{2_{out}}}$$

$$+ \mathrm{R_A\,R_B\,R_F\,R_G\,r_{1_{out}}\,r_{2_{out}}} + \mathrm{R_B\,R_E\,R_F\,r_{1_{in}}\,r_{2_{in}}\,r_{1_{out}}} + \mathrm{R_C\,R_D\,R_F\,r_{1_{in}}\,r_{2_{in}}\,r_{1_{out}}}$$

$$+ \mathrm{R_B\,R_E\,R_F\,r_{1_{in}}\,r_{2_{in}}\,r_{2_{out}}} + \mathrm{R_B\,R_E\,R_F\,r_{1_{in}}\,r_{3_{in}}\,r_{1_{out}}} + \mathrm{R_C\,R_D\,R_F\,r_{1_{in}}\,r_{2_{in}}\,r_{2_{out}}}$$

$$+ \mathrm{R_A\,R_E\,R_G\,r_{2_{in}}\,r_{3_{in}}\,r_{2_{out}}} + \mathrm{R_A\,R_C\,r_{1_{in}}\,r_{2_{in}}\,r_{3_{in}}\,r_{2_{out}}} + \mathrm{R_A\,R_D\,R_E\,R_G\,r_{1_{out}}\,r_{2_{out}}}$$

$$+ \mathrm{R_C\,R_E\,R_F\,r_{1_{in}}\,r_{2_{in}}\,r_{1_{out}}} + \mathrm{R_C\,R_E\,R_F\,r_{1_{in}}\,r_{2_{in}}\,r_{2_{out}}} + \mathrm{R_A\,R_F\,R_G\,r_{2_{in}}\,r_{3_{in}}\,r_{1_{out}}}$$

$$+ \mathrm{R_C\,R_D\,R_G\,r_{1_{in}}\,r_{3_{in}}\,r_{2_{out}}} + \mathrm{R_C\,R_D\,R_G\,r_{2_{in}}\,r_{3_{in}}\,r_{1_{out}}} + \mathrm{R_A\,R_B\,R_E\,r_{1_{in}}\,r_{1_{out}}\,r_{2_{out}}}$$

$$+ \mathrm{R_A\,R_D\,r_{1_{in}}\,r_{2_{in}}\,r_{3_{in}}\,r_{1_{out}}} + \mathrm{R_B\,R_C\,r_{1_{in}}\,r_{2_{in}}\,r_{3_{in}}\,r_{2_{out}}} + \mathrm{R_A\,R_D\,R_F\,R_G\,r_{1_{out}}\,r_{2_{out}}}$$

$$+ \mathrm{R_D\,R_E\,R_F\,r_{1_{in}}\,r_{2_{in}}\,r_{1_{out}}} + \mathrm{R_B\,R_F\,R_G\,r_{1_{in}}\,r_{3_{in}}\,r_{1_{out}}} + \mathrm{R_C\,R_E\,R_G\,r_{1_{in}}\,r_{2_{in}}\,r_{2_{out}}}$$

$$+ \mathrm{R_A\,R_B\,R_F\,r_{1_{in}}\,r_{1_{out}}\,r_{2_{out}}} + \mathrm{R_A\,R_B\,R_F\,r_{2_{in}}\,r_{1_{out}}\,r_{2_{out}}} + \mathrm{R_B\,R_D\,r_{1_{in}}\,r_{2_{in}}\,r_{3_{in}}\,r_{1_{out}}}$$

$$+ \mathrm{R_A\,R_E\,R_F\,R_G\,r_{1_{out}}\,r_{2_{out}}} + \mathrm{R_C\,R_D\,R_E\,R_G\,r_{1_{out}}\,r_{2_{out}}} + \mathrm{R_D\,R_E\,R_G\,r_{1_{in}}\,r_{2_{in}}\,r_{1_{out}}}$$

$$+ \mathrm{R_C\,R_F\,R_G\,r_{1_{in}}\,r_{3_{in}}\,r_{2_{out}}} + \mathrm{R_C\,R_F\,R_G\,r_{2_{in}}\,r_{3_{in}}\,r_{1_{out}}} + \mathrm{R_D\,R_E\,R_G\,r_{1_{in}}\,r_{3_{in}}\,r_{2_{out}}}$$

$$+ \mathrm{R_A\,R_D\,R_E\,r_{1_{in}}\,r_{1_{out}}\,r_{2_{out}}} + \mathrm{R_B\,R_C\,R_E\,r_{1_{in}}\,r_{1_{out}}\,r_{2_{out}}} + \mathrm{R_A\,R_D\,R_E\,r_{2_{in}}\,r_{1_{out}}\,r_{2_{out}}}$$

$$+ \mathrm{R_A\,R_B\,R_G\,r_{3_{in}}\,r_{1_{out}}\,r_{2_{out}}} + \mathrm{R_A\,R_F\,r_{1_{in}}\,r_{2_{in}}\,r_{3_{in}}\,r_{1_{out}}} + \mathrm{R_C\,R_D\,r_{1_{in}}\,r_{2_{in}}\,r_{3_{in}}\,r_{1_{out}}}$$

$$+ \mathrm{R_C\,R_D\,r_{1_{in}}\,r_{2_{in}}\,r_{3_{in}}\,r_{2_{out}}} + \mathrm{R_B\,R_E\,R_F\,R_G\,r_{1_{out}}\,r_{2_{out}}} + \mathrm{R_C\,R_D\,R_F\,R_G\,r_{1_{out}}\,r_{2_{out}}}$$

$$+ \mathrm{R_A\,R_D\,R_F\,r_{1_{in}}\,r_{1_{out}}\,r_{2_{out}}} + \mathrm{R_B\,R_C\,R_F\,r_{1_{in}}\,r_{1_{out}}\,r_{2_{out}}} + \mathrm{R_A\,R_D\,R_F\,r_{2_{in}}\,r_{1_{out}}\,r_{2_{out}}}$$

$$+ \mathrm{R_B\,R_F\,r_{1_{in}}\,r_{2_{in}}\,r_{3_{in}}\,r_{1_{out}}} + \mathrm{R_C\,R_E\,R_F\,R_G\,r_{1_{out}}\,r_{2_{out}}} + \mathrm{R_E\,R_F\,R_G\,r_{1_{in}}\,r_{2_{in}}\,r_{1_{out}}}$$

$$+ \mathrm{R_E\,R_F\,R_G\,r_{1_{in}}\,r_{3_{in}}\,r_{2_{out}}} + \mathrm{R_E\,R_F\,R_G\,r_{2_{in}}\,r_{3_{in}}\,r_{1_{out}}} + \mathrm{R_A\,R_E\,R_F\,r_{1_{in}}\,r_{1_{out}}\,r_{2_{out}}}$$

$$+ \mathrm{R_A\,R_E\,R_F\,r_{2_{in}}\,r_{1_{out}}\,r_{2_{out}}} + \mathrm{R_C\,R_D\,R_E\,r_{2_{in}}\,r_{1_{out}}\,r_{2_{out}}} + \mathrm{R_A\,R_D\,R_G\,r_{3_{in}}\,r_{1_{out}}\,r_{2_{out}}}$$

$$+ \mathrm{R_C\,R_F\,r_{1_{in}}\,r_{2_{in}}\,r_{3_{in}}\,r_{1_{out}}} + \mathrm{R_D\,R_E\,r_{1_{in}}\,r_{2_{in}}\,r_{3_{in}}\,r_{1_{out}}} + \mathrm{R_C\,R_F\,r_{1_{in}}\,r_{2_{in}}\,r_{3_{in}}\,r_{2_{out}}}$$

$$+ \mathrm{R_A\,R_B\,r_{1_{in}}\,r_{3_{in}}\,r_{1_{out}}\,r_{2_{out}}} + \mathrm{R_A\,R_B\,r_{2_{in}}\,r_{3_{in}}\,r_{1_{out}}\,r_{2_{out}}} + \mathrm{R_D\,R_E\,R_F\,R_G\,r_{1_{out}}\,r_{2_{out}}}$$

$$+ \mathrm{R_C\,R_D\,R_F\,r_{1_{in}}\,r_{1_{out}}\,r_{2_{out}}} + \mathrm{R_A\,R_E\,R_G\,r_{2_{in}}\,r_{1_{out}}\,r_{2_{out}}} + \mathrm{R_B\,R_E\,R_F\,r_{2_{in}}\,r_{1_{out}}\,r_{2_{out}}}$$

$$+ \mathrm{R_C\,R_G\,r_{1_{in}}\,r_{2_{in}}\,r_{3_{in}}\,r_{2_{out}}} + \mathrm{R_B\,R_E\,R_G\,r_{1_{in}}\,r_{1_{out}}\,r_{2_{out}}} + \mathrm{R_C\,R_E\,R_F\,r_{1_{in}}\,r_{1_{out}}\,r_{2_{out}}}$$

$$+ \mathrm{R_C\,R_E\,R_F\,r_{2_{in}}\,r_{1_{out}}\,r_{2_{out}}} + \mathrm{R_A\,R_F\,R_G\,r_{3_{in}}\,r_{1_{out}}\,r_{2_{out}}} + \mathrm{R_B\,R_E\,R_G\,r_{3_{in}}\,r_{1_{out}}\,r_{2_{out}}}$$

$$+ \mathrm{R_D\,R_G\,r_{1_{in}}\,r_{2_{in}}\,r_{3_{in}}\,r_{1_{out}}} + \mathrm{R_E\,R_F\,r_{1_{in}}\,r_{2_{in}}\,r_{3_{in}}\,r_{1_{out}}} + \mathrm{R_E\,R_F\,r_{1_{in}}\,r_{2_{in}}\,r_{3_{in}}\,r_{2_{out}}}$$

$$+ \mathrm{R_B\,R_C\,r_{1_{in}}\,r_{3_{in}}\,r_{1_{out}}\,r_{2_{out}}} + \mathrm{R_A\,R_D\,r_{2_{in}}\,r_{3_{in}}\,r_{1_{out}}\,r_{2_{out}}} + \mathrm{R_B\,R_C\,r_{2_{in}}\,r_{3_{in}}\,r_{1_{out}}\,r_{2_{out}}}$$

$$+ \mathrm{R_D\,R_E\,R_F\,r_{1_{in}}\,r_{1_{out}}\,r_{2_{out}}} + \mathrm{R_C\,R_E\,R_G\,r_{2_{in}}\,r_{1_{out}}\,r_{2_{out}}} + \mathrm{R_D\,R_E\,R_F\,r_{2_{in}}\,r_{1_{out}}\,r_{2_{out}}}$$

$$+ \mathrm{R_A\,R_E\,r_{1_{in}}\,r_{2_{in}}\,r_{1_{out}}\,r_{2_{out}}} + \mathrm{R_D\,R_E\,R_G\,r_{1_{in}}\,r_{1_{out}}\,r_{2_{out}}} + \mathrm{R_C\,R_F\,R_G\,r_{2_{in}}\,r_{1_{out}}\,r_{2_{out}}}$$

$$+ \mathrm{R_D\,R_E\,R_G\,r_{3_{in}}\,r_{1_{out}}\,r_{2_{out}}} + \mathrm{R_F\,R_G\,r_{1_{in}}\,r_{2_{in}}\,r_{3_{in}}\,r_{1_{out}}} + \mathrm{R_A\,R_F\,r_{1_{in}}\,r_{2_{in}}\,r_{1_{out}}\,r_{2_{out}}}$$

$$+ \mathrm{R_A\,R_F\,r_{1_{in}}\,r_{3_{in}}\,r_{1_{out}}\,r_{2_{out}}} + \mathrm{R_B\,R_E\,r_{1_{in}}\,r_{3_{in}}\,r_{1_{out}}\,r_{2_{out}}} + \mathrm{R_C\,R_D\,r_{1_{in}}\,r_{3_{in}}\,r_{1_{out}}\,r_{2_{out}}}$$

$$+ \mathrm{R_B\,R_E\,r_{2_{in}}\,r_{3_{in}}\,r_{1_{out}}\,r_{2_{out}}} + \mathrm{R_C\,R_D\,r_{2_{in}}\,r_{3_{in}}\,r_{1_{out}}\,r_{2_{out}}} + \mathrm{R_D\,R_F\,R_G\,r_{1_{in}}\,r_{1_{out}}\,r_{2_{out}}}$$

$$+ \mathrm{R_C\,R_E\,r_{1_{in}}\,r_{2_{in}}\,r_{1_{out}}\,r_{2_{out}}} + \mathrm{R_A\,R_G\,r_{2_{in}}\,r_{3_{in}}\,r_{1_{out}}\,r_{2_{out}}} + \mathrm{R_E\,R_F\,R_G\,r_{1_{in}}\,r_{1_{out}}\,r_{2_{out}}}$$

$$+ \mathrm{R_E\,R_F\,R_G\,r_{3_{in}}\,r_{1_{out}}\,r_{2_{out}}} + \mathrm{R_C\,R_F\,r_{1_{in}}\,r_{2_{in}}\,r_{1_{out}}\,r_{2_{out}}} + \mathrm{R_D\,R_E\,r_{1_{in}}\,r_{2_{in}}\,r_{1_{out}}\,r_{2_{out}}}$$

$$+ \mathrm{R_C\,R_F\,r_{1_{in}}\,r_{3_{in}}\,r_{1_{out}}\,r_{2_{out}}} + \mathrm{R_D\,R_E\,r_{1_{in}}\,r_{3_{in}}\,r_{1_{out}}\,r_{2_{out}}} + \mathrm{R_C\,R_F\,r_{2_{in}}\,r_{3_{in}}\,r_{1_{out}}\,r_{2_{out}}}$$

$$+ \mathrm{R_D\,R_F\,r_{1_{in}}\,r_{2_{in}}\,r_{1_{out}}\,r_{2_{out}}} + \mathrm{R_C\,R_G\,r_{2_{in}}\,r_{3_{in}}\,r_{1_{out}}\,r_{2_{out}}} + \mathrm{R_A\,r_{1_{in}}\,r_{2_{in}}\,r_{3_{in}}\,r_{1_{out}}\,r_{2_{out}}}$$

$$+ \mathrm{R_E\,R_F\,r_{1_{in}}\,r_{3_{in}}\,r_{1_{out}}\,r_{2_{out}}} + \mathrm{R_E\,R_F\,r_{2_{in}}\,r_{3_{in}}\,r_{1_{out}}\,r_{2_{out}}} + \mathrm{R_B\,r_{1_{in}}\,r_{2_{in}}\,r_{3_{in}}\,r_{1_{out}}\,r_{2_{out}}}$$

$$+ \mathrm{R_E\,R_G\,r_{2_{in}}\,r_{3_{in}}\,r_{1_{out}}\,r_{2_{out}}} + \mathrm{R_C\,r_{1_{in}}\,r_{2_{in}}\,r_{3_{in}}\,r_{1_{out}}\,r_{2_{out}}} + \mathrm{R_F\,R_G\,r_{1_{in}}\,r_{2_{in}}\,r_{1_{out}}\,r_{2_{out}}}$$

$$+ \mathrm{R_D\,r_{1_{in}}\,r_{2_{in}}\,r_{3_{in}}\,r_{1_{out}}\,r_{2_{out}}} + \mathrm{R_E\,r_{1_{in}}\,r_{2_{in}}\,r_{3_{in}}\,r_{1_{out}}\,r_{2_{out}}} + \mathrm{R_F\,r_{1_{in}}\,r_{2_{in}}\,r_{3_{in}}\,r_{1_{out}}\,r_{2_{out}}}$$

$$+ \mathrm{A_2\,R_A\,R_C\,R_D\,R_E\,R_G\,r_{2_{in}}} + \mathrm{A_1\,R_B\,R_C\,R_D\,R_E\,R_G\,r_{1_{in}}} + \mathrm{A_2\,R_A\,R_C\,R_D\,R_F\,R_G\,r_{2_{in}}}$$

$$+ \mathrm{A_2\,R_A\,R_C\,R_E\,R_F\,R_G\,r_{2_{in}}} + \mathrm{A_2\,R_A\,R_C\,R_D\,R_E\,r_{1_{in}}\,r_{2_{in}}} + \mathrm{A_1\,R_B\,R_C\,R_E\,R_F\,R_G\,r_{1_{in}}}$$

$$+ \mathrm{A_1\,R_B\,R_C\,R_D\,R_E\,r_{1_{in}}\,r_{2_{in}}} + \mathrm{A_2\,R_A\,R_C\,R_D\,R_F\,r_{1_{in}}\,r_{2_{in}}} + \mathrm{A_1\,R_B\,R_D\,R_E\,R_F\,R_G\,r_{1_{in}}}$$

$$+ \mathrm{A_2\,R_A\,R_C\,R_E\,R_F\,r_{1_{in}}\,r_{2_{in}}} + \mathrm{A_2\,R_A\,R_C\,R_D\,R_G\,r_{2_{in}}\,r_{3_{in}}} + \mathrm{A_1\,R_B\,R_C\,R_E\,R_F\,r_{1_{in}}\,r_{2_{in}}}$$

$$+ \mathrm{A_2\,R_A\,R_D\,R_E\,R_F\,r_{1_{in}}\,r_{2_{in}}} + \mathrm{A_1\,R_B\,R_D\,R_E\,R_F\,r_{1_{in}}\,r_{2_{in}}} + \mathrm{A_2\,R_A\,R_C\,R_F\,R_G\,r_{2_{in}}\,r_{3_{in}}}$$

$$+ \mathrm{A_2\,R_A\,R_C\,R_D\,r_{1_{in}}\,r_{2_{in}}\,r_{3_{in}}} + \mathrm{A_1\,R_B\,R_C\,R_F\,R_G\,r_{1_{in}}\,r_{3_{in}}} + \mathrm{A_1\,R_B\,R_D\,R_E\,R_G\,r_{1_{in}}\,r_{3_{in}}}$$

$$+ \mathrm{A_1\,R_C\,R_D\,R_E\,R_G\,r_{1_{in}}\,r_{2_{in}}} + \mathrm{A_2\,R_C\,R_D\,R_E\,R_G\,r_{1_{in}}\,r_{2_{in}}} + \mathrm{A_2\,R_A\,R_E\,R_F\,R_G\,r_{2_{in}}\,r_{3_{in}}}$$

$$
\begin{aligned}
&+ A_2\, R_A\, R_D\, R_E\, r_{1_{in}}\, r_{2_{in}}\, r_{3_{in}} + A_1\, R_C\, R_D\, R_F\, R_G\, r_{1_{in}}\, r_{2_{in}} + A_1\, R_B\, R_E\, R_F\, R_G\, r_{1_{in}}\, r_{3_{in}} \\
&+ A_1\, R_B\, R_C\, R_F\, r_{1_{in}}\, r_{2_{in}}\, r_{3_{in}} + A_1\, R_B\, R_D\, R_E\, r_{1_{in}}\, r_{2_{in}}\, r_{3_{in}} + A_1\, R_C\, R_E\, R_F\, R_G\, r_{1_{in}}\, r_{2_{in}} \\
&+ A_2\, R_A\, R_E\, R_F\, r_{1_{in}}\, r_{2_{in}}\, r_{3_{in}} + A_1\, R_D\, R_E\, R_F\, R_G\, r_{1_{in}}\, r_{2_{in}} + A_2\, R_D\, R_E\, R_F\, R_G\, r_{1_{in}}\, r_{2_{in}} \\
&+ A_1\, R_B\, R_C\, R_E\, R_G\, r_{1_{in}}\, r_{2_{out}} + A_2\, R_A\, R_D\, R_E\, R_G\, r_{2_{in}}\, r_{1_{out}} + A_1\, R_C\, R_D\, R_G\, r_{1_{in}}\, r_{2_{in}}\, r_{3_{in}} \\
&+ A_1\, R_B\, R_C\, R_F\, R_G\, r_{1_{in}}\, r_{2_{out}} + A_2\, R_A\, R_D\, R_F\, R_G\, r_{2_{in}}\, r_{1_{out}} + A_1\, R_C\, R_D\, R_E\, R_G\, r_{1_{in}}\, r_{2_{out}} \\
&+ A_2\, R_C\, R_D\, R_E\, R_G\, r_{2_{in}}\, r_{1_{out}} + A_1\, R_C\, R_F\, R_G\, r_{1_{in}}\, r_{2_{in}}\, r_{3_{in}} + A_1\, R_D\, R_E\, R_G\, r_{1_{in}}\, r_{2_{in}}\, r_{3_{in}} \\
&+ A_2\, R_D\, R_E\, R_G\, r_{1_{in}}\, r_{2_{in}}\, r_{3_{in}} + A_1\, R_B\, R_C\, R_E\, r_{1_{in}}\, r_{2_{in}}\, r_{2_{out}} + A_2\, R_A\, R_D\, R_E\, r_{1_{in}}\, r_{2_{in}}\, r_{1_{out}} \\
&+ A_1\, R_C\, R_D\, R_F\, R_G\, r_{1_{in}}\, r_{2_{out}} + A_2\, R_C\, R_D\, R_F\, R_G\, r_{2_{in}}\, r_{1_{out}} + A_1\, R_B\, R_C\, R_F\, r_{1_{in}}\, r_{2_{in}}\, r_{2_{out}} \\
&+ A_1\, R_C\, R_E\, R_F\, R_G\, r_{1_{in}}\, r_{2_{out}} + A_2\, R_C\, R_E\, R_F\, R_G\, r_{2_{in}}\, r_{1_{out}} + A_1\, R_E\, R_F\, R_G\, r_{1_{in}}\, r_{2_{in}}\, r_{3_{in}} \\
&+ A_1\, R_A\, R_E\, R_F\, r_{1_{in}}\, r_{2_{in}}\, r_{2_{out}} + A_1\, R_C\, R_D\, R_E\, r_{1_{in}}\, r_{2_{in}}\, r_{2_{out}} + A_1\, R_B\, R_C\, R_G\, r_{1_{in}}\, r_{3_{in}}\, r_{2_{out}} \\
&+ A_2\, R_C\, R_D\, R_E\, r_{1_{in}}\, r_{2_{in}}\, r_{1_{out}} + A_2\, R_A\, R_D\, R_G\, r_{2_{in}}\, r_{3_{in}}\, r_{1_{out}} + A_1\, R_D\, R_E\, R_F\, R_G\, r_{1_{in}}\, r_{2_{out}} \\
&+ A_1\, R_B\, R_E\, R_F\, r_{1_{in}}\, r_{2_{in}}\, r_{2_{out}} + A_1\, R_C\, R_D\, R_F\, r_{1_{in}}\, r_{2_{in}}\, r_{2_{out}} + A_2\, R_B\, R_E\, R_F\, r_{1_{in}}\, r_{2_{in}}\, r_{1_{out}} \\
&+ A_1\, R_C\, R_E\, R_F\, r_{1_{in}}\, r_{2_{in}}\, r_{2_{out}} + A_1\, R_B\, R_E\, R_G\, r_{1_{in}}\, r_{3_{in}}\, r_{2_{out}} + A_1\, R_C\, R_D\, R_G\, r_{1_{in}}\, r_{3_{in}}\, r_{2_{out}} \\
&+ A_2\, R_A\, R_F\, R_G\, r_{2_{in}}\, r_{3_{in}}\, r_{1_{out}} + A_2\, R_C\, R_D\, R_G\, r_{2_{in}}\, r_{3_{in}}\, r_{1_{out}} + A_1\, R_B\, R_C\, r_{1_{in}}\, r_{2_{in}}\, r_{3_{in}}\, r_{2_{out}} \\
&+ A_1\, R_C\, R_E\, R_G\, r_{1_{in}}\, r_{2_{in}}\, r_{2_{out}} + A_1\, R_D\, R_E\, R_F\, r_{1_{in}}\, r_{2_{in}}\, r_{2_{out}} + A_2\, R_D\, R_E\, R_F\, r_{1_{in}}\, r_{2_{in}}\, r_{1_{out}} \\
&+ A_1\, R_C\, R_F\, R_G\, r_{1_{in}}\, r_{3_{in}}\, r_{2_{out}} + A_1\, R_D\, R_E\, R_G\, r_{1_{in}}\, r_{3_{in}}\, r_{2_{out}} + A_2\, R_D\, R_E\, R_G\, r_{1_{in}}\, r_{2_{in}}\, r_{1_{out}} \\
&+ A_2\, R_D\, R_E\, R_G\, r_{2_{in}}\, r_{3_{in}}\, r_{1_{out}} + A_1\, R_B\, R_E\, r_{1_{in}}\, r_{2_{in}}\, r_{3_{in}}\, r_{2_{out}} + A_1\, R_C\, R_D\, r_{1_{in}}\, r_{2_{in}}\, r_{3_{in}}\, r_{2_{out}} \\
&+ A_2\, R_C\, R_D\, r_{1_{in}}\, r_{2_{in}}\, r_{3_{in}}\, r_{1_{out}} + A_2\, R_D\, R_F\, R_G\, r_{1_{in}}\, r_{2_{in}}\, r_{1_{out}} + A_1\, R_E\, R_F\, R_G\, r_{1_{in}}\, r_{2_{in}}\, r_{2_{out}} \\
&+ A_2\, R_E\, R_F\, R_G\, r_{1_{in}}\, r_{2_{in}}\, r_{1_{out}} + A_2\, R_E\, R_F\, R_G\, r_{2_{in}}\, r_{3_{in}}\, r_{1_{out}} + A_1\, R_C\, R_F\, r_{1_{in}}\, r_{2_{in}}\, r_{3_{in}}\, r_{2_{out}} \\
&+ A_2\, R_C\, R_F\, r_{1_{in}}\, r_{2_{in}}\, r_{3_{in}}\, r_{1_{out}} + A_2\, R_D\, R_E\, r_{1_{in}}\, r_{2_{in}}\, r_{3_{in}}\, r_{1_{out}} + A_1\, R_C\, R_G\, r_{1_{in}}\, r_{2_{in}}\, r_{3_{in}}\, r_{2_{out}} \\
&+ A_2\, R_D\, R_G\, r_{1_{in}}\, r_{2_{in}}\, r_{3_{in}}\, r_{1_{out}} + A_2\, R_E\, R_F\, r_{1_{in}}\, r_{2_{in}}\, r_{3_{in}}\, r_{1_{out}} + A_1\, R_E\, R_G\, r_{1_{in}}\, r_{2_{in}}\, r_{3_{in}}\, r_{2_{out}} \\
&+ A_1\, A_2\, R_C\, R_D\, R_E\, R_G\, r_{1_{in}}\, r_{2_{in}} + A_1\, A_2\, R_C\, R_D\, R_F\, R_G\, r_{1_{in}}\, r_{2_{in}} + A_1\, A_2\, R_C\, R_E\, R_F\, R_G\, r_{1_{in}}\, r_{2_{in}} \\
&+ A_1\, A_2\, R_E\, R_F\, R_G\, r_{1_{in}}\, r_{2_{in}}\, r_{3_{in}} \qquad (369)
\end{aligned}
$$

$$
\begin{aligned}
\alpha_4 = {} & R_B\, R_C\, R_G\, r_{1_{out}}\, V_1(k) + R_B\, R_C\, r_{2_{in}}\, r_{1_{out}}\, V_1(k) + R_B\, R_C\, r_{1_{in}}\, r_{1_{out}}\, V_2(k) \\
&+ R_A\, R_B\, R_G\, r_{1_{out}}\, V_{3_{in\_}}(k) + R_A\, R_B\, r_{1_{in}}\, r_{1_{out}}\, V_{3_{in\_}}(k) + R_A\, R_B\, r_{2_{in}}\, r_{1_{out}}\, V_{3_{in\_}}(k) \\
&+ R_B\, R_G\, r_{1_{in}}\, r_{1_{out}}\, V_{3_{in\_}}(k) + R_A\, r_{1_{in}}\, r_{2_{in}}\, r_{1_{out}}\, V_{3_{in\_}}(k) + R_B\, r_{1_{in}}\, r_{2_{in}}\, r_{1_{out}}\, V_{3_{in\_}}(k)
\end{aligned}
$$

$$+ R_C\, r1_{in}\, r2_{in}\, r1_{out}\, V2_{out}(k) + A_1\, R_A\, R_B\, R_C\, r1_{in}\, V1(k) - A_1\, R_A\, R_B\, R_C\, r1_{in}\, V2(k)$$

$$- A_1\, R_A\, R_C\, r1_{in}\, r2_{in}\, V2_{out}(k) \tag{370}$$

$$\beta_4 = R_A\, R_B\, R_C\, R_G + R_A\, R_B\, R_C\, r1_{in} + R_A\, R_B\, R_C\, r2_{in} + R_A\, R_C\, R_G\, r2_{in} + R_B\, R_C\, R_G\, r1_{in}$$

$$+ R_B\, R_C\, r1_{in}\, r2_{in} + R_A\, R_B\, R_G\, r1_{out} + R_B\, R_C\, R_G\, r1_{out} + R_A\, R_B\, r1_{in}\, r1_{out} + R_A\, R_B\, r2_{in}\, r1_{out}$$

$$+ R_B\, R_C\, r1_{in}\, r1_{out} + R_B\, R_C\, r2_{in}\, r1_{out} + R_A\, R_G\, r2_{in}\, r1_{out} + R_B\, R_G\, r1_{in}\, r1_{out} + R_C\, R_G\, r2_{in}\, r1_{out}$$

$$+ R_B\, r1_{in}\, r2_{in}\, r1_{out} + R_C\, r1_{in}\, r2_{in}\, r1_{out} + R_G\, r1_{in}\, r2_{in}\, r1_{out} + A_1\, R_B\, R_C\, R_G\, r1_{in}$$

$$+ A_1\, R_C\, R_G\, r1_{in}\, r2_{in} \tag{371}$$

$$\alpha_5 = R_A\, R_C\, R_D\, R_G\, r2_{out}\, V2(k) + R_A\, R_C\, R_D\, r2_{in}\, r2_{out}\, V1(k) + R_A\, R_C\, R_D\, r1_{in}\, r2_{out}\, V2(k)$$

$$+ R_A\, R_D\, R_G\, r1_{out}\, r2_{out}\, V2(k) + R_A\, R_D\, r2_{in}\, r1_{out}\, r2_{out}\, V1(k) + R_C\, R_D\, R_G\, r1_{out}\, r2_{out}\, V2(k)$$

$$+ R_C\, R_D\, r2_{in}\, r1_{out}\, r2_{out}\, V1(k) + R_C\, R_D\, r1_{in}\, r1_{out}\, r2_{out}\, V2(k) + R_D\, R_G\, r1_{in}\, r1_{out}\, r2_{out}\, V2(k)$$

$$+ R_A\, R_B\, R_C\, r1_{in}\, r2_{out}\, V3_{in_+}(k) + R_A\, R_B\, R_C\, r2_{in}\, r2_{out}\, V3_{in_+}(k) + R_A\, R_C\, R_G\, r2_{in}\, r2_{out}\, V3_{in_+}(k)$$

$$+ R_A\, R_C\, r1_{in}\, r2_{in}\, r2_{out}\, V3_{in_+}(k) + R_B\, R_C\, r1_{in}\, r2_{in}\, r2_{out}\, V3_{in_+}(k) + R_A\, R_B\, R_G\, r1_{out}\, r2_{out}\, V3_{in_+}(k)$$

$$+ R_A\, R_B\, r1_{in}\, r1_{out}\, r2_{out}\, V3_{in_+}(k) + R_A\, R_B\, r2_{in}\, r1_{out}\, r2_{out}\, V3_{in_+}(k)$$

$$+ R_B\, R_C\, r1_{in}\, r1_{out}\, r2_{out}\, V3_{in_+}(k) + R_B\, R_C\, r2_{in}\, r1_{out}\, r2_{out}\, V3_{in_+}(k)$$

$$+ R_B\, R_G\, r1_{in}\, r1_{out}\, r2_{out}\, V3_{in_+}(k) + R_C\, R_G\, r2_{in}\, r1_{out}\, r2_{out}\, V3_{in_+}(k)$$

$$+ R_B\, r1_{in}\, r2_{in}\, r1_{out}\, r2_{out}\, V3_{in_+}(k) + R_C\, r1_{in}\, r2_{in}\, r1_{out}\, r2_{out}\, V3_{in_+}(k)$$

$$+ R_G\, r1_{in}\, r2_{in}\, r1_{out}\, r2_{out}\, V3_{in_+}(k) - A_2\, R_A\, R_B\, R_C\, R_D\, r2_{in}\, V1(k) + A_2\, R_A\, R_B\, R_C\, R_D\, r2_{in}\, V2(k)$$

$$+ A_2\, R_A\, R_C\, R_D\, r1_{in}\, r2_{in}\, V2(k) + A_2\, R_B\, R_C\, R_D\, r1_{in}\, r2_{in}\, V2(k) - A_2\, R_A\, R_B\, R_D\, r2_{in}\, r1_{out}\, V1(k)$$

$$+ A_2\, R_C\, R_D\, R_G\, r1_{in}\, r2_{in}\, V2(k) - A_2\, R_B\, R_C\, R_D\, r2_{in}\, r1_{out}\, V1(k) + A_2\, R_B\, R_C\, R_D\, r2_{in}\, r1_{out}\, V2(k)$$

$$+ A_1\, R_C\, R_D\, R_G\, r1_{in}\, r2_{out}\, V2(k) + A_2\, R_C\, R_D\, R_G\, r2_{in}\, r1_{out}\, V2(k)$$

$$+ A_1\, R_C\, R_D\, r1_{in}\, r2_{in}\, r2_{out}\, V1(k) + A_2\, R_B\, R_D\, r1_{in}\, r2_{in}\, r1_{out}\, V2(k)$$

$$+ A_2\, R_D\, R_G\, r1_{in}\, r2_{in}\, r1_{out}\, V2(k) + A_1\, R_B\, R_C\, R_G\, r1_{in}\, r2_{out}\, V3_{in_+}(k)$$

$$- A_2\, R_B\, R_D\, r1_{in}\, r2_{in}\, r1_{out}\, V3_{in_-}(k) + A_1\, R_C\, R_G\, r1_{in}\, r2_{in}\, r2_{out}\, V3_{in_+}(k)$$

$$+ A_1\, A_2\, R_C\, R_D\, R_G\, r1_{in}\, r2_{in}\, V2(k) \tag{372}$$

$$\beta_5 = R_A\, R_B\, R_C\, R_D\, R_G + R_A\, R_B\, R_C\, R_D\, r1_{in} + R_A\, R_B\, R_C\, R_D\, r2_{in} + R_A\, R_C\, R_D\, R_G\, r2_{in}$$

$$+ R_A\, R_C\, R_D\, r1_{in}\, r2_{in} + R_B\, R_C\, R_D\, r1_{in}\, r2_{in} + R_A\, R_B\, R_C\, R_G\, r2_{out} + R_A\, R_B\, R_D\, R_G\, r1_{out}$$

$$
\begin{aligned}
&+ R_A\,R_B\,R_C\,r_{1_{in}}\,r_{2_{out}} + R_A\,R_B\,R_C\,r_{2_{in}}\,r_{2_{out}} + R_B\,R_C\,R_D\,R_G\,r_{1_{out}} + R_A\,R_B\,R_D\,r_{1_{in}}\,r_{1_{out}} \\
&+ R_C\,R_D\,R_G\,r_{1_{in}}\,r_{2_{in}} + R_A\,R_C\,R_D\,r_{1_{in}}\,r_{2_{out}} + R_A\,R_C\,R_D\,r_{2_{in}}\,r_{2_{out}} + R_B\,R_C\,R_D\,r_{1_{in}}\,r_{1_{out}} \\
&+ R_A\,R_C\,R_G\,r_{2_{in}}\,r_{2_{out}} + R_A\,R_D\,R_G\,r_{2_{in}}\,r_{1_{out}} + R_B\,R_C\,R_G\,r_{1_{in}}\,r_{2_{out}} + R_B\,R_D\,R_G\,r_{1_{in}}\,r_{1_{out}} \\
&+ R_C\,R_D\,R_G\,r_{1_{in}}\,r_{2_{out}} + R_C\,R_D\,R_G\,r_{2_{in}}\,r_{1_{out}} + R_A\,R_D\,r_{1_{in}}\,r_{2_{in}}\,r_{1_{out}} + R_B\,R_C\,r_{1_{in}}\,r_{2_{in}}\,r_{2_{out}} \\
&+ R_A\,R_B\,R_G\,r_{1_{out}}\,r_{2_{out}} + R_C\,R_D\,r_{1_{in}}\,r_{2_{in}}\,r_{1_{out}} + R_C\,R_D\,r_{1_{in}}\,r_{2_{in}}\,r_{2_{out}} + R_A\,R_D\,R_G\,r_{1_{out}}\,r_{2_{out}} \\
&+ R_A\,R_B\,r_{1_{in}}\,r_{1_{out}}\,r_{2_{out}} + R_A\,R_B\,r_{2_{in}}\,r_{1_{out}}\,r_{2_{out}} + R_C\,R_G\,r_{1_{in}}\,r_{2_{in}}\,r_{2_{out}} + R_C\,R_D\,R_G\,r_{1_{out}}\,r_{2_{out}} \\
&+ R_A\,R_D\,r_{1_{in}}\,r_{1_{out}}\,r_{2_{out}} + R_B\,R_C\,r_{1_{in}}\,r_{1_{out}}\,r_{2_{out}} + R_A\,R_D\,r_{2_{in}}\,r_{1_{out}}\,r_{2_{out}} + R_B\,R_C\,r_{2_{in}}\,r_{1_{out}}\,r_{2_{out}} \\
&+ R_C\,R_D\,r_{2_{in}}\,r_{1_{out}}\,r_{2_{out}} + R_A\,R_G\,r_{2_{in}}\,r_{1_{out}}\,r_{2_{out}} + R_B\,R_G\,r_{1_{in}}\,r_{1_{out}}\,r_{2_{out}} + R_C\,R_G\,r_{2_{in}}\,r_{1_{out}}\,r_{2_{out}} \\
&+ R_D\,R_G\,r_{1_{in}}\,r_{1_{out}}\,r_{2_{out}} + R_B\,r_{1_{in}}\,r_{2_{in}}\,r_{1_{out}}\,r_{2_{out}} + R_C\,r_{1_{in}}\,r_{2_{in}}\,r_{1_{out}}\,r_{2_{out}} + R_D\,r_{1_{in}}\,r_{2_{in}}\,r_{1_{out}}\,r_{2_{out}} \\
&+ A_2\,R_A\,R_C\,R_D\,R_G\,r_{2_{in}} + A_1\,R_B\,R_C\,R_D\,R_G\,r_{1_{in}} + A_2\,R_A\,R_C\,R_D\,r_{1_{in}}\,r_{2_{in}} \\
&+ A_1\,R_C\,R_D\,R_G\,r_{1_{in}}\,r_{2_{in}} + A_2\,R_C\,R_D\,R_G\,r_{1_{in}}\,r_{2_{in}} + A_1\,R_B\,R_C\,R_G\,r_{1_{in}}\,r_{2_{out}} \\
&+ A_1\,R_C\,R_D\,R_G\,r_{1_{in}}\,r_{2_{out}} + A_2\,R_C\,R_D\,R_G\,r_{2_{in}}\,r_{1_{out}} + A_1\,R_B\,R_C\,r_{1_{in}}\,r_{2_{in}}\,r_{2_{out}} \\
&+ A_1\,R_C\,R_D\,r_{1_{in}}\,r_{2_{in}}\,r_{2_{out}} + A_2\,R_C\,R_D\,r_{1_{in}}\,r_{2_{in}}\,r_{1_{out}} + A_1\,R_C\,R_G\,r_{1_{in}}\,r_{2_{in}}\,r_{2_{out}} \\
&+ A_1\,A_2\,R_C\,R_D\,R_G\,r_{1_{in}}\,r_{2_{in}} \qquad (373)
\end{aligned}
$$

$$
\begin{aligned}
\alpha_6 = {} & R_A\,R_C\,R_F\,R_G\,R_L\,r_{2_{out}}\,r_{3_{out}}\,V_2(k) + R_B\,R_D\,R_F\,R_G\,R_L\,r_{1_{out}}\,r_{3_{out}}\,V_1(k) \\
&+ R_A\,R_C\,R_F\,r_{1_{in}}\,R_L\,r_{2_{out}}\,r_{3_{out}}\,V_2(k) + R_B\,R_D\,R_F\,r_{2_{in}}\,R_L\,r_{1_{out}}\,r_{3_{out}}\,V_1(k) \\
&+ R_B\,R_D\,R_G\,r_{3_{in}}\,R_L\,r_{1_{out}}\,r_{3_{out}}\,V_1(k) + R_B\,R_F\,R_G\,r_{3_{in}}\,R_L\,r_{1_{out}}\,r_{3_{out}}\,V_1(k) \\
&+ R_B\,R_D\,r_{1_{in}}\,r_{3_{in}}\,R_L\,r_{1_{out}}\,r_{3_{out}}\,V_2(k) + R_C\,R_F\,R_G\,r_{1_{in}}\,R_L\,r_{2_{out}}\,r_{3_{out}}\,V_2(k) \\
&+ R_B\,R_F\,r_{2_{in}}\,r_{3_{in}}\,R_L\,r_{1_{out}}\,r_{3_{out}}\,V_1(k) + R_B\,R_F\,r_{1_{in}}\,r_{3_{in}}\,R_L\,r_{1_{out}}\,r_{3_{out}}\,V_2(k) \\
&+ R_A\,R_F\,R_G\,R_L\,r_{1_{out}}\,r_{2_{out}}\,r_{3_{out}}\,V_2(k) + R_B\,R_F\,R_G\,R_L\,r_{1_{out}}\,r_{2_{out}}\,r_{3_{out}}\,V_1(k) \\
&+ R_A\,R_F\,r_{2_{in}}\,R_L\,r_{1_{out}}\,r_{2_{out}}\,r_{3_{out}}\,V_1(k) + R_C\,R_F\,R_G\,R_L\,r_{1_{out}}\,r_{2_{out}}\,r_{3_{out}}\,V_2(k) \\
&+ R_A\,R_F\,r_{1_{in}}\,R_L\,r_{1_{out}}\,r_{2_{out}}\,r_{3_{out}}\,V_2(k) + R_B\,R_F\,r_{2_{in}}\,R_L\,r_{1_{out}}\,r_{2_{out}}\,r_{3_{out}}\,V_1(k) \\
&+ R_C\,R_F\,r_{2_{in}}\,R_L\,r_{1_{out}}\,r_{2_{out}}\,r_{3_{out}}\,V_1(k) + R_B\,R_G\,r_{3_{in}}\,R_L\,r_{1_{out}}\,r_{2_{out}}\,r_{3_{out}}\,V_1(k) \\
&+ R_D\,R_F\,r_{2_{in}}\,R_L\,r_{1_{out}}\,r_{2_{out}}\,r_{3_{out}}\,V_1(k) + R_D\,R_F\,r_{1_{in}}\,R_L\,r_{1_{out}}\,r_{2_{out}}\,r_{3_{out}}\,V_2(k) \\
&+ R_B\,r_{2_{in}}\,r_{3_{in}}\,R_L\,r_{1_{out}}\,r_{2_{out}}\,r_{3_{out}}\,V_1(k) + R_B\,r_{1_{in}}\,r_{3_{in}}\,R_L\,r_{1_{out}}\,r_{2_{out}}\,r_{3_{out}}\,V_2(k) \\
&+ R_F\,R_G\,r_{3_{in}}\,R_L\,r_{1_{out}}\,r_{2_{out}}\,r_{3_{out}}\,V_1(k) + R_D\,r_{2_{in}}\,r_{3_{in}}\,R_L\,r_{1_{out}}\,r_{2_{out}}\,r_{3_{out}}\,V_1(k)
\end{aligned}
$$

$$+ R_D\, r_{1_{in}}\, r_{3_{in}}\, R_L\, r_{1_{out}}\, r_{2_{out}}\, r_{3_{out}}\, V_2(k) + R_F\, r_{2_{in}}\, r_{3_{in}}\, R_L\, r_{1_{out}}\, r_{2_{out}}\, r_{3_{out}}\, V_1(k)$$

$$+ R_G\, r_{2_{in}}\, r_{3_{in}}\, R_L\, r_{1_{out}}\, r_{2_{out}}\, r_{3_{out}}\, V_1(k) - A_2\, R_A\, R_B\, R_C\, R_F\, r_{2_{in}}\, R_L\, r_{3_{out}}\, V_1(k)$$

$$+ A_2\, R_A\, R_B\, R_C\, R_F\, r_{2_{in}}\, R_L\, r_{3_{out}}\, V_2(k) - A_1\, R_A\, R_B\, R_D\, R_F\, r_{1_{in}}\, R_L\, r_{3_{out}}\, V_2(k)$$

$$- A_1\, R_A\, R_B\, R_D\, r_{1_{in}}\, r_{3_{in}}\, R_L\, r_{3_{out}}\, V_2(k) + A_2\, R_A\, R_C\, R_F\, R_G\, r_{2_{in}}\, R_L\, r_{3_{out}}\, V_2(k)$$

$$+ A_3\, R_A\, R_C\, R_F\, R_G\, r_{3_{in}}\, R_L\, r_{2_{out}}\, V_2(k) + A_1\, R_A\, R_B\, R_F\, r_{1_{in}}\, r_{3_{in}}\, R_L\, r_{3_{out}}\, V_1(k)$$

$$- A_1\, R_A\, R_B\, R_F\, r_{1_{in}}\, r_{3_{in}}\, R_L\, r_{3_{out}}\, V_2(k) + A_3\, R_A\, R_C\, R_F\, r_{2_{in}}\, r_{3_{in}}\, R_L\, r_{2_{out}}\, V_1(k)$$

$$+ A_3\, R_A\, R_E\, R_F\, R_G\, r_{3_{in}}\, R_L\, r_{2_{out}}\, V_2(k) + A_1\, R_A\, R_D\, R_F\, r_{1_{in}}\, r_{2_{in}}\, R_L\, r_{3_{out}}\, V_1(k)$$

$$+ A_3\, R_A\, R_C\, R_F\, r_{1_{in}}\, r_{3_{in}}\, R_L\, r_{2_{out}}\, V_2(k) - A_3\, R_B\, R_D\, R_E\, r_{2_{in}}\, r_{3_{in}}\, R_L\, r_{1_{out}}\, V_1(k)$$

$$+ A_2\, R_B\, R_C\, R_F\, r_{1_{in}}\, r_{2_{in}}\, R_L\, r_{3_{out}}\, V_2(k) - A_3\, R_B\, R_D\, R_E\, r_{1_{in}}\, r_{3_{in}}\, R_L\, r_{1_{out}}\, V_2(k)$$

$$+ A_1\, R_B\, R_D\, R_G\, r_{1_{in}}\, r_{3_{in}}\, R_L\, r_{3_{out}}\, V_1(k) + A_3\, R_A\, R_E\, R_F\, r_{1_{in}}\, r_{3_{in}}\, R_L\, r_{2_{out}}\, V_2(k)$$

$$- A_3\, R_B\, R_E\, R_F\, r_{1_{in}}\, r_{3_{in}}\, R_L\, r_{1_{out}}\, V_2(k) + A_1\, R_A\, R_D\, r_{1_{in}}\, r_{2_{in}}\, r_{3_{in}}\, R_L\, r_{3_{out}}\, V_1(k)$$

$$+ A_1\, R_A\, R_B\, R_F\, r_{1_{in}}\, R_L\, r_{2_{out}}\, r_{3_{out}}\, V_1(k) - A_2\, R_A\, R_B\, R_F\, r_{2_{in}}\, R_L\, r_{1_{out}}\, r_{3_{out}}\, V_1(k)$$

$$- A_3\, R_D\, R_E\, R_G\, r_{2_{in}}\, r_{3_{in}}\, R_L\, r_{1_{out}}\, V_1(k) - A_1\, R_A\, R_B\, R_F\, r_{1_{in}}\, R_L\, r_{2_{out}}\, r_{3_{out}}\, V_2(k)$$

$$+ A_1\, R_A\, R_F\, r_{1_{in}}\, r_{2_{in}}\, r_{3_{in}}\, R_L\, r_{3_{out}}\, V_1(k) + A_1\, R_D\, R_F\, R_G\, r_{1_{in}}\, r_{2_{in}}\, R_L\, r_{3_{out}}\, V_1(k)$$

$$+ A_3\, R_C\, R_F\, R_G\, r_{1_{in}}\, r_{3_{in}}\, R_L\, r_{2_{out}}\, V_2(k) + A_1\, R_A\, R_D\, R_F\, r_{1_{in}}\, R_L\, r_{2_{out}}\, r_{3_{out}}\, V_1(k)$$

$$+ A_1\, R_B\, R_F\, r_{1_{in}}\, r_{2_{in}}\, r_{3_{in}}\, R_L\, r_{3_{out}}\, V_1(k) - A_3\, R_E\, R_F\, R_G\, r_{2_{in}}\, r_{3_{in}}\, R_L\, r_{1_{out}}\, V_1(k)$$

$$+ A_2\, R_B\, R_C\, R_F\, r_{2_{in}}\, R_L\, r_{1_{out}}\, r_{3_{out}}\, V_2(k) + A_1\, R_A\, R_B\, r_{1_{in}}\, r_{3_{in}}\, R_L\, r_{2_{out}}\, r_{3_{out}}\, V_1(k)$$

$$- A_1\, R_A\, R_B\, r_{1_{in}}\, r_{3_{in}}\, R_L\, r_{2_{out}}\, r_{3_{out}}\, V_2(k) - A_3\, R_B\, R_E\, R_G\, r_{3_{in}}\, R_L\, r_{1_{out}}\, r_{2_{out}}\, V_1(k)$$

$$+ A_1\, R_A\, R_D\, r_{1_{in}}\, r_{3_{in}}\, R_L\, r_{2_{out}}\, r_{3_{out}}\, V_1(k) + A_1\, R_B\, R_F\, R_G\, r_{1_{in}}\, R_L\, r_{2_{out}}\, r_{3_{out}}\, V_1(k)$$

$$+ A_3\, R_A\, R_F\, R_G\, r_{3_{in}}\, R_L\, r_{1_{out}}\, r_{2_{out}}\, V_2(k) - A_1\, R_A\, R_D\, r_{1_{in}}\, r_{3_{in}}\, R_L\, r_{2_{out}}\, r_{3_{out}}\, V_2(k)$$

$$+ A_1\, R_F\, R_G\, r_{1_{in}}\, r_{2_{in}}\, r_{3_{in}}\, R_L\, r_{3_{out}}\, V_1(k) + A_1\, R_A\, R_F\, r_{1_{in}}\, r_{2_{in}}\, R_L\, r_{2_{out}}\, r_{3_{out}}\, V_1(k)$$

$$+ A_3\, R_A\, R_F\, r_{2_{in}}\, r_{3_{in}}\, R_L\, r_{1_{out}}\, r_{2_{out}}\, V_1(k) - A_3\, R_B\, R_E\, r_{2_{in}}\, r_{3_{in}}\, R_L\, r_{1_{out}}\, r_{2_{out}}\, V_1(k)$$

$$+ A_1\, R_D\, R_F\, R_G\, r_{1_{in}}\, R_L\, r_{2_{out}}\, r_{3_{out}}\, V_1(k) + A_2\, R_C\, R_F\, R_G\, r_{2_{in}}\, R_L\, r_{1_{out}}\, r_{3_{out}}\, V_2(k)$$

$$+ A_3\, R_C\, R_F\, R_G\, r_{3_{in}}\, R_L\, r_{1_{out}}\, r_{2_{out}}\, V_2(k) + A_1\, R_B\, R_F\, r_{1_{in}}\, r_{2_{in}}\, R_L\, r_{2_{out}}\, r_{3_{out}}\, V_1(k)$$

$$+ A_2\, R_A\, R_F\, r_{1_{in}}\, r_{2_{in}}\, R_L\, r_{1_{out}}\, r_{3_{out}}\, V_2(k) + A_3\, R_A\, R_F\, r_{1_{in}}\, r_{3_{in}}\, R_L\, r_{1_{out}}\, r_{2_{out}}\, V_2(k)$$

$$- A_3\, R_E\, R_F\, R_G\, r_{3_{in}}\, R_L\, r_{1_{out}}\, r_{2_{out}}\, V_1(k) + A_1\, R_C\, R_F\, r_{1_{in}}\, r_{2_{in}}\, R_L\, r_{2_{out}}\, r_{3_{out}}\, V_1(k)$$

$$+ A_2\, R_B\, R_F\, r_{1_{in}}\, r_{2_{in}}\, R_L\, r_{1_{out}}\, r_{3_{out}}\, V_2(k) + A_3\, R_C\, R_F\, r_{2_{in}}\, r_{3_{in}}\, R_L\, r_{1_{out}}\, r_{2_{out}}\, V_1(k)$$

$$+ A_3\, R_E\, R_F\, R_G\, r_{3_{in}}\, R_L\, r_{1_{out}}\, r_{2_{out}}\, V_2(k) + A_1\, R_D\, R_F\, r_{1_{in}}\, r_{2_{in}}\, R_L\, r_{2_{out}}\, r_{3_{out}}\, V_1(k)$$

$$+ A_3\, R_C\, R_F\, r_{1_{in}}\, r_{3_{in}}\, R_L\, r_{1_{out}}\, r_{2_{out}}\, V_2(k) - A_3\, R_D\, R_E\, r_{1_{in}}\, r_{3_{in}}\, R_L\, r_{1_{out}}\, r_{2_{out}}\, V_2(k)$$

$$+ A_1\, R_D\, R_G\, r_{1_{in}}\, r_{3_{in}}\, R_L\, r_{2_{out}}\, r_{3_{out}}\, V_1(k) + A_2\, R_D\, R_F\, r_{1_{in}}\, r_{2_{in}}\, R_L\, r_{1_{out}}\, r_{3_{out}}\, V_2(k)$$

$$+ A_1\, R_B\, r_{1_{in}}\, r_{2_{in}}\, r_{3_{in}}\, R_L\, r_{2_{out}}\, r_{3_{out}}\, V_1(k) - A_3\, R_E\, R_G\, r_{2_{in}}\, r_{3_{in}}\, R_L\, r_{1_{out}}\, r_{2_{out}}\, V_1(k)$$

$$+ A_1\, R_F\, R_G\, r_{1_{in}}\, r_{3_{in}}\, R_L\, r_{2_{out}}\, r_{3_{out}}\, V_1(k) + A_2\, R_F\, R_G\, r_{2_{in}}\, r_{3_{in}}\, R_L\, r_{1_{out}}\, r_{3_{out}}\, V_1(k)$$

$$+ A_2\, R_F\, R_G\, r_{1_{in}}\, r_{2_{in}}\, R_L\, r_{1_{out}}\, r_{3_{out}}\, V_2(k) + A_3\, R_F\, R_G\, r_{1_{in}}\, r_{3_{in}}\, R_L\, r_{1_{out}}\, r_{2_{out}}\, V_2(k)$$

$$+ A_1\, R_F\, r_{1_{in}}\, r_{2_{in}}\, r_{3_{in}}\, R_L\, r_{2_{out}}\, r_{3_{out}}\, V_1(k) + A_1\, R_G\, r_{1_{in}}\, r_{2_{in}}\, r_{3_{in}}\, R_L\, r_{2_{out}}\, r_{3_{out}}\, V_1(k)$$

$$- A_1\, A_3\, R_A\, R_B\, R_D\, R_E\, r_{1_{in}}\, r_{3_{in}}\, R_L\, V_1(k) - A_2\, A_3\, R_A\, R_B\, R_C\, R_F\, r_{2_{in}}\, r_{3_{in}}\, R_L\, V_1(k)$$

$$+ A_2\, A_3\, R_A\, R_B\, R_C\, R_F\, r_{2_{in}}\, r_{3_{in}}\, R_L\, V_2(k) - A_1\, A_3\, R_A\, R_B\, R_E\, R_F\, r_{1_{in}}\, r_{3_{in}}\, R_L\, V_1(k)$$

$$+ A_1\, A_3\, R_A\, R_B\, R_E\, R_F\, r_{1_{in}}\, r_{3_{in}}\, R_L\, V_2(k) + A_2\, A_3\, R_A\, R_B\, R_E\, R_F\, r_{2_{in}}\, r_{3_{in}}\, R_L\, V_2(k)$$

$$+ A_2\, A_3\, R_A\, R_C\, R_F\, R_G\, r_{2_{in}}\, r_{3_{in}}\, R_L\, V_2(k) - A_1\, A_3\, R_A\, R_D\, R_E\, r_{1_{in}}\, r_{2_{in}}\, r_{3_{in}}\, R_L\, V_1(k)$$

$$+ A_2\, A_3\, R_A\, R_E\, R_F\, R_G\, r_{2_{in}}\, r_{3_{in}}\, R_L\, V_2(k) - A_1\, A_3\, R_B\, R_D\, R_E\, r_{1_{in}}\, r_{2_{in}}\, r_{3_{in}}\, R_L\, V_1(k)$$

$$- A_1\, A_3\, R_A\, R_E\, R_F\, r_{1_{in}}\, r_{2_{in}}\, r_{3_{in}}\, R_L\, V_1(k) + A_2\, A_3\, R_B\, R_C\, R_F\, r_{1_{in}}\, r_{2_{in}}\, r_{3_{in}}\, R_L\, V_2(k)$$

$$+ A_2\, A_3\, R_A\, R_E\, R_F\, r_{1_{in}}\, r_{2_{in}}\, r_{3_{in}}\, R_L\, V_2(k) + A_2\, A_3\, R_B\, R_E\, R_F\, r_{1_{in}}\, r_{2_{in}}\, r_{3_{in}}\, R_L\, V_2(k)$$

$$+ A_1\, A_3\, R_A\, R_B\, R_E\, r_{1_{in}}\, r_{3_{in}}\, R_L\, r_{2_{out}}\, V_2(k) - A_2\, A_3\, R_A\, R_B\, R_F\, r_{2_{in}}\, r_{3_{in}}\, R_L\, r_{1_{out}}\, V_1(k)$$

$$- A_1\, A_3\, R_A\, R_D\, R_E\, r_{1_{in}}\, r_{3_{in}}\, R_L\, r_{2_{out}}\, V_1(k) + A_2\, A_3\, R_A\, R_B\, R_F\, r_{2_{in}}\, r_{3_{in}}\, R_L\, r_{1_{out}}\, V_2(k)$$

$$+ A_1\, A_2\, R_A\, R_D\, R_F\, r_{1_{in}}\, r_{2_{in}}\, R_L\, r_{3_{out}}\, V_1(k) - A_1\, A_2\, R_B\, R_C\, R_F\, r_{1_{in}}\, r_{2_{in}}\, R_L\, r_{3_{out}}\, V_1(k)$$

$$- A_2\, A_3\, R_B\, R_C\, R_F\, r_{2_{in}}\, r_{3_{in}}\, R_L\, r_{1_{out}}\, V_1(k) - A_1\, A_3\, R_E\, R_F\, R_G\, r_{1_{in}}\, r_{2_{in}}\, r_{3_{in}}\, R_L\, V_1(k)$$

$$+ A_1\, A_2\, R_B\, R_C\, R_F\, r_{1_{in}}\, r_{2_{in}}\, R_L\, r_{3_{out}}\, V_2(k) - A_1\, A_3\, R_A\, R_E\, R_F\, r_{1_{in}}\, r_{3_{in}}\, R_L\, r_{2_{out}}\, V_1(k)$$

$$+ A_2\, A_3\, R_E\, R_F\, R_G\, r_{1_{in}}\, r_{2_{in}}\, r_{3_{in}}\, R_L\, V_2(k) + A_1\, A_3\, R_A\, R_E\, R_F\, r_{1_{in}}\, r_{3_{in}}\, R_L\, r_{2_{out}}\, V_2(k)$$

$$- A_1\, A_3\, R_B\, R_E\, R_G\, r_{1_{in}}\, r_{3_{in}}\, R_L\, r_{2_{out}}\, V_1(k) + A_2\, A_3\, R_B\, R_E\, R_F\, r_{2_{in}}\, r_{3_{in}}\, R_L\, r_{1_{out}}\, V_2(k)$$

$$+ A_2\, A_3\, R_A\, R_F\, R_G\, r_{2_{in}}\, r_{3_{in}}\, R_L\, r_{1_{out}}\, V_2(k) - A_1\, A_2\, R_A\, R_D\, r_{1_{in}}\, r_{2_{in}}\, r_{3_{in}}\, R_L\, r_{3_{out}}\, V_2(k)$$

$$- A_1\, A_3\, R_D\, R_E\, R_G\, r_{1_{in}}\, r_{3_{in}}\, R_L\, r_{2_{out}}\, V_1(k) - A_2\, A_3\, R_D\, R_E\, R_G\, r_{2_{in}}\, r_{3_{in}}\, R_L\, r_{1_{out}}\, V_1(k)$$

$$- A_1\, A_3\, R_B\, R_E\, r_{1_{in}}\, r_{2_{in}}\, r_{3_{in}}\, R_L\, r_{2_{out}}\, V_1(k) + A_1\, A_2\, R_C\, R_F\, R_G\, r_{1_{in}}\, r_{2_{in}}\, R_L\, r_{3_{out}}\, V_2(k)$$

$$+ A_1\, A_3\, R_C\, R_F\, R_G\, r_{1_{in}}\, r_{3_{in}}\, R_L\, r_{2_{out}}\, V_2(k) + A_2\, A_3\, R_C\, R_F\, R_G\, r_{2_{in}}\, r_{3_{in}}\, R_L\, r_{1_{out}}\, V_2(k)$$

$$+ A_2\,A_3\,R_A\,R_F\,r_{1_{in}}\,r_{2_{in}}\,r_{3_{in}}\,R_L\,r_{1_{out}}\,V_2(k) - A_1\,A_3\,R_E\,R_F\,R_G\,r_{1_{in}}\,r_{3_{in}}\,R_L\,r_{2_{out}}\,V_1(k)$$

$$+ A_1\,A_3\,R_C\,R_F\,r_{1_{in}}\,r_{2_{in}}\,r_{3_{in}}\,R_L\,r_{2_{out}}\,V_1(k) - A_1\,A_3\,R_D\,R_E\,r_{1_{in}}\,r_{2_{in}}\,r_{3_{in}}\,R_L\,r_{2_{out}}\,V_1(k)$$

$$+ A_1\,A_3\,R_E\,R_F\,R_G\,r_{1_{in}}\,r_{3_{in}}\,R_L\,r_{2_{out}}\,V_2(k) + A_2\,A_3\,R_E\,R_F\,R_G\,r_{2_{in}}\,r_{3_{in}}\,R_L\,r_{1_{out}}\,V_2(k)$$

$$- A_2\,A_3\,R_D\,R_E\,r_{1_{in}}\,r_{2_{in}}\,r_{3_{in}}\,R_L\,r_{1_{out}}\,V_2(k) + A_1\,A_2\,R_D\,R_G\,r_{1_{in}}\,r_{2_{in}}\,r_{3_{in}}\,R_L\,r_{3_{out}}\,V_1(k)$$

$$+ A_1\,A_2\,R_F\,R_G\,r_{1_{in}}\,r_{2_{in}}\,r_{3_{in}}\,R_L\,r_{3_{out}}\,V_1(k) + A_2\,A_3\,R_F\,R_G\,r_{1_{in}}\,r_{2_{in}}\,r_{3_{in}}\,R_L\,r_{1_{out}}\,V_2(k)$$

$$+ A_1\,A_2\,A_3\,R_A\,R_D\,R_E\,r_{1_{in}}\,r_{2_{in}}\,r_{3_{in}}\,R_L\,V_2(k) - A_1\,A_2\,A_3\,R_B\,R_C\,R_F\,r_{1_{in}}\,r_{2_{in}}\,r_{3_{in}}\,R_L\,V_1(k)$$

$$+ A_1\,A_2\,A_3\,R_B\,R_C\,R_F\,r_{1_{in}}\,r_{2_{in}}\,r_{3_{in}}\,R_L\,V_2(k) + A_1\,A_2\,A_3\,R_A\,R_E\,R_F\,r_{1_{in}}\,r_{2_{in}}\,r_{3_{in}}\,R_L\,V_2(k)$$

$$+ A_1\,A_2\,A_3\,R_B\,R_E\,R_F\,r_{1_{in}}\,r_{2_{in}}\,r_{3_{in}}\,R_L\,V_2(k) - A_1\,A_2\,A_3\,R_D\,R_E\,R_G\,r_{1_{in}}\,r_{2_{in}}\,r_{3_{in}}\,R_L\,V_1(k)$$

$$+ A_1\,A_2\,A_3\,R_E\,R_F\,R_G\,r_{1_{in}}\,r_{2_{in}}\,r_{3_{in}}\,R_L\,V_2(k) \tag{374}$$

$$\beta_6 = R_A\,R_B\,R_C\,R_D\,R_E\,R_G\,R_L + R_A\,R_B\,R_C\,R_D\,R_F\,R_G\,R_L + R_A\,R_B\,R_C\,R_E\,R_F\,R_G\,R_L$$

$$+ R_A\,R_B\,R_C\,R_D\,R_E\,r_{2_{in}}\,R_L + R_A\,R_B\,R_D\,R_E\,R_F\,R_G\,R_L + R_A\,R_B\,R_C\,R_D\,R_F\,r_{1_{in}}\,R_L$$

$$+ R_A\,R_B\,R_C\,R_D\,R_E\,R_G\,r_{3_{out}} + R_A\,R_B\,R_C\,R_E\,R_F\,r_{1_{in}}\,R_L + R_A\,R_B\,R_C\,R_E\,R_F\,r_{2_{in}}\,R_L$$

$$+ R_A\,R_B\,R_C\,R_D\,R_F\,R_G\,r_{3_{out}} + R_A\,R_B\,R_D\,R_E\,R_F\,r_{1_{in}}\,R_L + R_A\,R_B\,R_D\,R_E\,R_F\,r_{2_{in}}\,R_L$$

$$+ R_A\,R_B\,R_C\,R_D\,R_E\,r_{1_{in}}\,r_{3_{out}} + R_A\,R_B\,R_C\,R_D\,R_E\,r_{2_{in}}\,r_{3_{out}} + R_A\,R_B\,R_C\,R_F\,R_G\,r_{3_{in}}\,R_L$$

$$+ R_A\,R_B\,R_D\,R_E\,R_F\,R_G\,r_{3_{out}} + R_A\,R_B\,R_C\,R_D\,r_{1_{in}}\,r_{3_{in}}\,R_L + R_A\,R_B\,R_C\,R_D\,r_{2_{in}}\,r_{3_{in}}\,R_L$$

$$+ R_A\,R_B\,R_C\,R_D\,R_F\,r_{2_{in}}\,r_{3_{out}} + R_A\,R_C\,R_D\,R_E\,R_G\,r_{2_{in}}\,R_L + R_A\,R_B\,R_C\,R_E\,R_F\,r_{1_{in}}\,r_{3_{out}}$$

$$+ R_A\,R_B\,R_C\,R_D\,R_G\,r_{3_{in}}\,r_{3_{out}} + R_B\,R_C\,R_D\,R_E\,R_G\,r_{1_{in}}\,R_L + R_A\,R_C\,R_D\,R_F\,R_G\,r_{2_{in}}\,R_L$$

$$+ R_A\,R_B\,R_C\,R_F\,r_{1_{in}}\,r_{3_{in}}\,R_L + R_A\,R_B\,R_D\,R_E\,r_{1_{in}}\,r_{3_{in}}\,R_L + R_A\,R_B\,R_C\,R_F\,r_{2_{in}}\,r_{3_{in}}\,R_L$$

$$+ R_A\,R_B\,R_D\,R_E\,R_F\,r_{1_{in}}\,r_{3_{out}} + R_A\,R_B\,R_D\,R_E\,R_F\,r_{2_{in}}\,r_{3_{out}} + R_B\,R_C\,R_D\,R_F\,R_G\,r_{1_{in}}\,R_L$$

$$+ R_A\,R_C\,R_D\,R_E\,r_{1_{in}}\,r_{2_{in}}\,R_L + R_A\,R_B\,R_C\,R_F\,R_G\,r_{3_{in}}\,r_{3_{out}} + R_A\,R_B\,R_D\,R_E\,R_G\,r_{3_{in}}\,r_{3_{out}}$$

$$+ R_A\,R_B\,R_C\,R_D\,r_{2_{in}}\,r_{3_{in}}\,r_{3_{out}} + R_B\,R_C\,R_E\,R_F\,R_G\,r_{1_{in}}\,R_L + R_A\,R_D\,R_E\,R_F\,R_G\,r_{2_{in}}\,R_L$$

$$+ R_A\,R_C\,R_D\,R_F\,r_{1_{in}}\,r_{2_{in}}\,R_L + R_B\,R_C\,R_D\,R_E\,r_{1_{in}}\,r_{2_{in}}\,R_L + R_A\,R_B\,R_E\,R_F\,r_{1_{in}}\,r_{3_{in}}\,R_L$$

$$+ R_A\,R_C\,R_D\,R_E\,R_G\,r_{2_{in}}\,r_{3_{out}} + R_B\,R_D\,R_E\,R_F\,R_G\,r_{1_{in}}\,R_L + R_A\,R_B\,R_C\,R_E\,R_G\,R_L\,r_{2_{out}}$$

$$+ R_B\,R_C\,R_D\,R_F\,r_{1_{in}}\,r_{2_{in}}\,R_L + R_A\,R_C\,R_D\,R_G\,r_{2_{in}}\,r_{3_{in}}\,R_L + R_B\,R_C\,R_D\,R_E\,R_G\,r_{1_{in}}\,r_{3_{out}}$$

$$+ R_A\,R_B\,R_E\,R_F\,R_G\,r_{3_{in}}\,r_{3_{out}} + R_A\,R_B\,R_C\,R_F\,r_{1_{in}}\,r_{3_{in}}\,r_{3_{out}} + R_A\,R_B\,R_D\,R_E\,r_{1_{in}}\,r_{3_{in}}\,r_{3_{out}}$$

$$+ R_A\,R_B\,R_D\,R_E\,r_{2_{in}}\,r_{3_{in}}\,r_{3_{out}} + R_A\,R_B\,R_D\,R_E\,R_G\,R_L\,r_{1_{out}} + R_A\,R_B\,R_C\,R_F\,R_G\,R_L\,r_{2_{out}}$$

$$+ R_A R_D R_E R_F r_{1_{in}} r_{2_{in}} R_L + R_B R_C R_E R_F r_{1_{in}} r_{2_{in}} R_L + R_B R_C R_D R_G r_{1_{in}} r_{3_{in}} R_L$$

$$+ R_B R_C R_D R_F R_G r_{1_{in}} r_{3_{out}} + R_A R_B R_C R_D r_{2_{in}} R_L r_{3_{out}} + R_A R_C R_E R_F R_G r_{2_{in}} r_{3_{out}}$$

$$+ R_A R_B R_D R_F R_G R_L r_{1_{out}} + R_A R_C R_D R_E R_G R_L r_{2_{out}} + R_A R_B R_D R_F R_G R_L r_{3_{out}}$$

$$+ R_A R_C R_F R_G r_{2_{in}} r_{3_{in}} R_L + R_A R_D R_E R_G r_{2_{in}} r_{3_{in}} R_L + R_A R_B R_C R_E r_{1_{in}} R_L r_{2_{out}}$$

$$+ R_B R_C R_E R_F R_G r_{1_{in}} r_{3_{out}} + R_A R_D R_E R_F R_G r_{2_{in}} r_{3_{out}} + R_A R_C R_D r_{1_{in}} r_{2_{in}} r_{3_{in}} R_L$$

$$+ R_B R_C R_D R_E r_{1_{in}} r_{2_{in}} r_{3_{out}} + R_A R_B R_E R_F r_{1_{in}} r_{3_{in}} r_{3_{out}} + R_A R_B R_E R_F r_{2_{in}} r_{3_{in}} r_{3_{out}}$$

$$+ R_B R_C R_D R_E R_G R_L r_{1_{out}} + R_A R_B R_E R_F R_G R_L r_{2_{out}} + R_A R_C R_D R_F R_G R_L r_{2_{out}}$$

$$+ R_B R_D R_E R_G r_{1_{in}} r_{3_{in}} R_L + R_A R_B R_D R_E r_{1_{in}} R_L r_{1_{out}} + R_A R_B R_C R_F r_{1_{in}} R_L r_{2_{out}}$$

$$+ R_A R_B R_C R_F r_{1_{in}} R_L r_{3_{out}} + R_A R_B R_C R_F r_{2_{in}} R_L r_{2_{out}} + R_B R_D R_E R_F R_G r_{1_{in}} r_{3_{out}}$$

$$+ R_A R_B R_C R_E R_G r_{2_{out}} r_{3_{out}} + R_B R_C R_D r_{1_{in}} r_{2_{in}} r_{3_{in}} R_L + R_A R_C R_E R_F r_{1_{in}} r_{2_{in}} r_{3_{out}}$$

$$+ R_A R_C R_D R_G r_{2_{in}} r_{3_{in}} r_{3_{out}} + R_B R_C R_D R_F R_G R_L r_{1_{out}} + R_A R_C R_E R_F R_G R_L r_{2_{out}}$$

$$+ R_A R_E R_F R_G r_{2_{in}} r_{3_{in}} R_L + R_A R_B R_D R_F r_{1_{in}} R_L r_{1_{out}} + R_A R_B R_D R_F r_{2_{in}} R_L r_{1_{out}}$$

$$+ R_A R_B R_D R_F r_{1_{in}} R_L r_{3_{out}} + R_A R_C R_D R_E r_{2_{in}} R_L r_{2_{out}} + R_A R_B R_C R_G r_{3_{in}} R_L r_{2_{out}}$$

$$+ R_A R_B R_D R_E R_G r_{1_{out}} r_{3_{out}} + R_A R_B R_C R_F R_G r_{2_{out}} r_{3_{out}} + R_A R_C R_F r_{1_{in}} r_{2_{in}} r_{3_{in}} R_L$$

$$+ R_A R_D R_E R_F r_{1_{in}} r_{2_{in}} r_{3_{out}} + R_B R_C R_E R_F r_{1_{in}} r_{2_{in}} r_{3_{out}} + R_B R_C R_D R_G r_{1_{in}} r_{3_{in}} r_{3_{out}}$$

$$+ R_A R_D R_E R_F R_G R_L r_{2_{out}} + R_C R_D R_F R_G r_{1_{in}} r_{2_{in}} R_L + R_B R_E R_F R_G r_{1_{in}} r_{3_{in}} R_L$$

$$+ R_B R_C R_D R_E r_{1_{in}} R_L r_{1_{out}} + R_A R_B R_E R_F r_{1_{in}} R_L r_{2_{out}} + R_A R_B R_E R_F r_{2_{in}} R_L r_{1_{out}}$$

$$+ R_B R_C R_D R_E r_{2_{in}} R_L r_{1_{out}} + R_A R_B R_D R_G r_{3_{in}} R_L r_{1_{out}} + R_A R_B R_E R_F r_{2_{in}} R_L r_{2_{out}}$$

$$+ R_A R_B R_D R_G r_{3_{in}} R_L r_{3_{out}} + R_A R_B R_D R_F R_G r_{1_{out}} r_{3_{out}} + R_A R_C R_D R_E R_G r_{2_{out}} r_{3_{out}}$$

$$+ R_B R_D R_E r_{1_{in}} r_{2_{in}} r_{3_{in}} R_L + R_B R_D R_E R_F r_{1_{in}} r_{2_{in}} r_{3_{out}} + R_A R_C R_F R_G r_{2_{in}} r_{3_{in}} r_{3_{out}}$$

$$+ R_A R_B R_C R_E r_{1_{in}} r_{2_{out}} r_{3_{out}} + R_A R_B R_C R_E r_{2_{in}} r_{2_{out}} r_{3_{out}} + R_B R_D R_E R_F R_G R_L r_{1_{out}}$$

$$+ R_C R_E R_F R_G r_{1_{in}} r_{2_{in}} R_L + R_B R_C R_D R_F r_{1_{in}} R_L r_{1_{out}} + R_A R_C R_E R_F r_{1_{in}} R_L r_{2_{out}}$$

$$+ R_A R_C R_E R_F r_{2_{in}} R_L r_{2_{out}} + R_A R_B R_E R_G r_{3_{in}} R_L r_{2_{out}} + R_A R_C R_D R_G r_{2_{in}} R_L r_{3_{out}}$$

$$+ R_A R_B R_E R_F R_G r_{1_{out}} r_{3_{out}} + R_B R_C R_D R_E R_G r_{1_{out}} r_{3_{out}} + R_A R_B R_E R_F R_G r_{2_{out}} r_{3_{out}}$$

$$+ R_A R_E R_F r_{1_{in}} r_{2_{in}} r_{3_{in}} R_L + R_A R_B R_C r_{1_{in}} r_{3_{in}} R_L r_{2_{out}} + R_A R_B R_C r_{2_{in}} r_{3_{in}} R_L r_{2_{out}}$$

$$+ R_B R_D R_E R_G r_{1_{in}} r_{3_{in}} r_{3_{out}} + R_A R_B R_D R_E r_{1_{in}} r_{1_{out}} r_{3_{out}} + R_A R_B R_C R_F r_{1_{in}} r_{2_{out}} r_{3_{out}}$$

$$+ R_A\,R_B\,R_C\,R_F\,r_{2_{in}}\,r_{2_{out}}\,r_{3_{out}} + R_B\,R_C\,R_D\,r_{1_{in}}\,r_{2_{in}}\,r_{3_{in}}\,r_{3_{out}} + R_D\,R_E\,R_F\,R_G\,r_{1_{in}}\,r_{2_{in}}\,R_L$$

$$+ R_A\,R_D\,R_E\,R_F\,r_{1_{in}}\,R_L\,r_{2_{out}} + R_B\,R_C\,R_E\,R_F\,r_{2_{in}}\,R_L\,r_{1_{out}} + R_A\,R_B\,R_F\,R_G\,r_{3_{in}}\,R_L\,r_{1_{out}}$$

$$+ R_A\,R_D\,R_E\,R_F\,r_{2_{in}}\,R_L\,r_{2_{out}} + R_B\,R_C\,R_D\,R_G\,r_{1_{in}}\,R_L\,r_{3_{out}} + R_B\,R_C\,R_D\,R_G\,r_{3_{in}}\,R_L\,r_{1_{out}}$$

$$+ R_B\,R_C\,R_D\,R_F\,R_G\,r_{1_{out}}\,r_{3_{out}} + R_A\,R_C\,R_E\,R_F\,R_G\,r_{2_{out}}\,r_{3_{out}} + R_B\,R_E\,R_F\,r_{1_{in}}\,r_{2_{in}}\,r_{3_{in}}\,R_L$$

$$+ R_A\,R_B\,R_D\,r_{2_{in}}\,r_{3_{in}}\,R_L\,r_{1_{out}} + R_C\,R_D\,R_E\,R_G\,r_{1_{in}}\,r_{2_{in}}\,r_{3_{out}} + R_A\,R_B\,R_D\,r_{1_{in}}\,r_{3_{in}}\,R_L\,r_{3_{out}}$$

$$+ R_A\,R_E\,R_F\,R_G\,r_{2_{in}}\,r_{3_{in}}\,r_{3_{out}} + R_A\,R_B\,R_D\,R_F\,r_{1_{in}}\,r_{1_{out}}\,r_{3_{out}} + R_A\,R_B\,R_D\,R_F\,r_{2_{in}}\,r_{1_{out}}\,r_{3_{out}}$$

$$+ R_A\,R_C\,R_D\,R_E\,r_{2_{in}}\,r_{2_{out}}\,r_{3_{out}} + R_A\,R_B\,R_C\,R_G\,r_{3_{in}}\,r_{2_{out}}\,r_{3_{out}} + R_A\,R_C\,R_F\,r_{1_{in}}\,r_{2_{in}}\,r_{3_{in}}\,r_{3_{out}}$$

$$+ R_B\,R_D\,R_E\,R_F\,r_{1_{in}}\,R_L\,r_{1_{out}} + R_A\,R_D\,R_E\,R_G\,r_{2_{in}}\,R_L\,r_{1_{out}} + R_B\,R_C\,R_E\,R_G\,r_{1_{in}}\,R_L\,r_{2_{out}}$$

$$+ R_A\,R_C\,R_F\,R_G\,r_{2_{in}}\,R_L\,r_{2_{out}} + R_A\,R_C\,R_F\,R_G\,r_{2_{in}}\,R_L\,r_{3_{out}} + R_A\,R_C\,R_F\,R_G\,r_{3_{in}}\,R_L\,r_{2_{out}}$$

$$+ R_B\,R_C\,R_E\,R_F\,R_G\,r_{1_{out}}\,r_{3_{out}} + R_A\,R_D\,R_E\,R_F\,R_G\,r_{2_{out}}\,r_{3_{out}} + R_C\,R_D\,R_G\,r_{1_{in}}\,r_{2_{in}}\,r_{3_{in}}\,R_L$$

$$+ R_A\,R_C\,R_D\,r_{1_{in}}\,r_{2_{in}}\,R_L\,r_{3_{out}} + R_A\,R_C\,R_D\,r_{1_{in}}\,r_{3_{in}}\,R_L\,r_{2_{out}} + R_C\,R_D\,R_F\,R_G\,r_{1_{in}}\,r_{2_{in}}\,r_{3_{out}}$$

$$+ R_A\,R_C\,R_D\,r_{2_{in}}\,r_{3_{in}}\,R_L\,r_{2_{out}} + R_B\,R_E\,R_F\,R_G\,r_{1_{in}}\,r_{3_{in}}\,r_{3_{out}} + R_A\,R_B\,R_E\,R_F\,r_{1_{in}}\,r_{1_{out}}\,r_{3_{out}}$$

$$+ R_A\,R_B\,R_E\,R_F\,r_{1_{in}}\,r_{2_{out}}\,r_{3_{out}} + R_A\,R_B\,R_E\,R_F\,r_{2_{in}}\,r_{1_{out}}\,r_{3_{out}} + R_A\,R_C\,R_D\,R_F\,r_{1_{in}}\,r_{2_{out}}\,r_{3_{out}}$$

$$+ R_A\,R_B\,R_D\,R_G\,r_{3_{in}}\,r_{1_{out}}\,r_{3_{out}} + R_A\,R_B\,R_E\,R_F\,r_{2_{in}}\,r_{2_{out}}\,r_{3_{out}} + R_A\,R_C\,R_D\,R_F\,r_{2_{in}}\,r_{2_{out}}\,r_{3_{out}}$$

$$+ R_B\,R_D\,R_E\,r_{1_{in}}\,r_{2_{in}}\,r_{3_{in}}\,r_{3_{out}} + R_B\,R_D\,R_E\,R_G\,r_{1_{in}}\,R_L\,r_{1_{out}} + R_A\,R_D\,R_F\,R_G\,r_{2_{in}}\,R_L\,r_{1_{out}}$$

$$+ R_B\,R_C\,R_F\,R_G\,r_{1_{in}}\,R_L\,r_{3_{out}} + R_B\,R_C\,R_F\,R_G\,r_{3_{in}}\,R_L\,r_{1_{out}} + R_B\,R_D\,R_E\,R_G\,r_{3_{in}}\,R_L\,r_{1_{out}}$$

$$+ R_B\,R_D\,R_E\,R_F\,R_G\,r_{1_{out}}\,r_{3_{out}} + R_A\,R_B\,R_F\,r_{1_{in}}\,r_{3_{in}}\,R_L\,r_{1_{out}} + R_A\,R_C\,R_E\,r_{1_{in}}\,r_{2_{in}}\,R_L\,r_{2_{out}}$$

$$+ R_A\,R_B\,R_F\,r_{2_{in}}\,r_{3_{in}}\,R_L\,r_{1_{out}} + R_B\,R_C\,R_D\,r_{1_{in}}\,r_{2_{in}}\,R_L\,r_{3_{out}} + R_B\,R_C\,R_D\,r_{2_{in}}\,r_{3_{in}}\,R_L\,r_{1_{out}}$$

$$+ R_A\,R_B\,R_F\,r_{1_{in}}\,r_{3_{in}}\,R_L\,r_{3_{out}} + R_A\,R_B\,R_F\,r_{2_{in}}\,r_{3_{in}}\,R_L\,r_{3_{out}} + R_B\,R_C\,R_D\,R_F\,r_{1_{in}}\,r_{1_{out}}\,r_{3_{out}}$$

$$+ R_B\,R_C\,R_D\,R_F\,r_{2_{in}}\,r_{1_{out}}\,r_{3_{out}} + R_A\,R_C\,R_E\,R_F\,r_{2_{in}}\,r_{2_{out}}\,r_{3_{out}} + R_A\,R_B\,R_E\,R_G\,r_{3_{in}}\,r_{2_{out}}\,r_{3_{out}}$$

$$+ R_A\,R_E\,R_F\,r_{1_{in}}\,r_{2_{in}}\,r_{3_{in}}\,r_{3_{out}} + R_A\,R_B\,R_C\,r_{1_{in}}\,r_{3_{in}}\,r_{2_{out}}\,r_{3_{out}} + R_A\,R_B\,R_C\,r_{2_{in}}\,r_{3_{in}}\,r_{2_{out}}\,r_{3_{out}}$$

$$+ R_A\,R_E\,R_F\,R_G\,r_{2_{in}}\,R_L\,r_{1_{out}} + R_C\,R_D\,R_E\,R_G\,r_{1_{in}}\,R_L\,r_{2_{out}} + R_C\,R_D\,R_E\,R_G\,r_{2_{in}}\,R_L\,r_{1_{out}}$$

$$+ R_B\,R_D\,R_F\,R_G\,r_{1_{in}}\,R_L\,r_{3_{out}} + R_A\,R_E\,R_F\,R_G\,r_{3_{in}}\,R_L\,r_{2_{out}} + R_A\,R_B\,R_C\,R_G\,R_L\,r_{2_{out}}\,r_{3_{out}}$$

$$+ R_D\,R_E\,R_G\,r_{1_{in}}\,r_{2_{in}}\,r_{3_{in}}\,R_L + R_A\,R_D\,R_E\,r_{1_{in}}\,r_{2_{in}}\,R_L\,r_{1_{out}} + R_A\,R_C\,R_F\,r_{1_{in}}\,r_{2_{in}}\,R_L\,r_{2_{out}}$$

$$+ R_A\,R_C\,R_F\,r_{1_{in}}\,r_{2_{in}}\,R_L\,r_{3_{out}} + R_A\,R_C\,R_F\,r_{1_{in}}\,r_{3_{in}}\,R_L\,r_{2_{out}} + R_A\,R_D\,R_E\,r_{1_{in}}\,r_{3_{in}}\,R_L\,r_{2_{out}}$$

$$+ R_A\,R_C\,R_F\,r_{2_{in}}\,r_{3_{in}}\,R_L\,r_{2_{out}} + R_A\,R_D\,R_E\,r_{2_{in}}\,r_{3_{in}}\,R_L\,r_{2_{out}} + R_B\,R_C\,R_E\,R_F\,r_{1_{in}}\,r_{1_{out}}\,r_{3_{out}}$$

$$+ R_B\,R_C\,R_E\,R_F\,r_{2_{in}}\,r_{1_{out}}\,r_{3_{out}} + R_A\,R_B\,R_F\,R_G\,r_{3_{in}}\,r_{1_{out}}\,r_{3_{out}} + R_A\,R_C\,R_E\,R_G\,r_{2_{in}}\,r_{2_{out}}\,r_{3_{out}}$$

$$+ R_B\,R_C\,R_D\,R_G\,r_{3_{in}}\,r_{1_{out}}\,r_{3_{out}} + R_B\,R_E\,R_F\,r_{1_{in}}\,r_{2_{in}}\,r_{3_{in}}\,r_{3_{out}} + R_A\,R_B\,R_D\,r_{1_{in}}\,r_{3_{in}}\,r_{1_{out}}\,r_{3_{out}}$$

$$+ R_B\,R_E\,R_F\,R_G\,r_{1_{in}}\,R_L\,r_{1_{out}} + R_B\,R_E\,R_F\,R_G\,r_{1_{in}}\,R_L\,r_{2_{out}} + R_C\,R_D\,R_F\,R_G\,r_{1_{in}}\,R_L\,r_{2_{out}}$$

$$+ R_B\,R_E\,R_F\,R_G\,r_{3_{in}}\,R_L\,r_{1_{out}} + R_A\,R_B\,R_D\,R_G\,R_L\,r_{1_{out}}\,r_{3_{out}} + R_A\,R_D\,R_F\,r_{1_{in}}\,r_{2_{in}}\,R_L\,r_{1_{out}}$$

$$+ R_B\,R_C\,R_F\,r_{1_{in}}\,r_{2_{in}}\,R_L\,r_{2_{out}} + R_B\,R_C\,R_F\,r_{1_{in}}\,r_{3_{in}}\,R_L\,r_{1_{out}} + R_B\,R_D\,R_E\,r_{1_{in}}\,r_{3_{in}}\,R_L\,r_{1_{out}}$$

$$+ R_B\,R_C\,R_F\,r_{1_{in}}\,r_{2_{in}}\,R_L\,r_{3_{out}} + R_B\,R_C\,R_F\,r_{2_{in}}\,r_{3_{in}}\,R_L\,r_{1_{out}} + R_B\,R_D\,R_E\,r_{2_{in}}\,r_{3_{in}}\,R_L\,r_{1_{out}}$$

$$+ R_B\,R_D\,R_E\,R_F\,r_{1_{in}}\,r_{1_{out}}\,r_{3_{out}} + R_A\,R_D\,R_E\,R_G\,r_{2_{in}}\,r_{1_{out}}\,r_{3_{out}} + R_B\,R_C\,R_E\,R_G\,r_{1_{in}}\,r_{2_{out}}\,r_{3_{out}}$$

$$+ R_A\,R_C\,R_F\,R_G\,r_{2_{in}}\,r_{2_{out}}\,r_{3_{out}} + R_A\,R_C\,R_F\,R_G\,r_{3_{in}}\,r_{2_{out}}\,r_{3_{out}} + R_A\,R_D\,R_E\,R_G\,r_{3_{in}}\,r_{2_{out}}\,r_{3_{out}}$$

$$+ R_A\,R_B\,R_E\,r_{1_{in}}\,r_{3_{in}}\,r_{2_{out}}\,r_{3_{out}} + R_A\,R_C\,R_D\,r_{1_{in}}\,r_{3_{in}}\,r_{2_{out}}\,r_{3_{out}} + R_A\,R_B\,R_E\,r_{2_{in}}\,r_{3_{in}}\,r_{2_{out}}\,r_{3_{out}}$$

$$+ R_C\,R_E\,R_F\,R_G\,r_{1_{in}}\,R_L\,r_{2_{out}} + R_C\,R_E\,R_F\,R_G\,r_{2_{in}}\,R_L\,r_{1_{out}} + R_A\,R_B\,R_E\,R_G\,R_L\,r_{1_{out}}\,r_{2_{out}}$$

$$+ R_E\,R_F\,R_G\,r_{1_{in}}\,r_{2_{in}}\,r_{3_{in}}\,R_L + R_A\,R_E\,R_F\,r_{1_{in}}\,r_{2_{in}}\,R_L\,r_{1_{out}} + R_B\,R_D\,R_F\,r_{1_{in}}\,r_{2_{in}}\,R_L\,r_{1_{out}}$$

$$+ R_A\,R_E\,R_F\,r_{1_{in}}\,r_{2_{in}}\,R_L\,r_{2_{out}} + R_C\,R_D\,R_E\,r_{1_{in}}\,r_{2_{in}}\,R_L\,r_{2_{out}} + R_A\,R_D\,R_G\,r_{2_{in}}\,r_{3_{in}}\,R_L\,r_{1_{out}}$$

$$+ R_B\,R_C\,R_G\,r_{1_{in}}\,r_{3_{in}}\,R_L\,r_{2_{out}} + R_B\,R_D\,R_F\,r_{1_{in}}\,r_{2_{in}}\,R_L\,r_{3_{out}} + R_A\,R_E\,R_F\,r_{2_{in}}\,r_{3_{in}}\,R_L\,r_{2_{out}}$$

$$+ R_B\,R_D\,R_E\,R_G\,r_{1_{in}}\,r_{1_{out}}\,r_{3_{out}} + R_A\,R_B\,R_C\,r_{1_{in}}\,R_L\,r_{2_{out}}\,r_{3_{out}} + R_A\,R_D\,R_F\,R_G\,r_{2_{in}}\,r_{1_{out}}\,r_{3_{out}}$$

$$+ R_A\,R_B\,R_C\,r_{2_{in}}\,R_L\,r_{2_{out}}\,r_{3_{out}} + R_B\,R_C\,R_F\,R_G\,r_{3_{in}}\,r_{1_{out}}\,r_{3_{out}} + R_B\,R_D\,R_E\,R_G\,r_{3_{in}}\,r_{1_{out}}\,r_{3_{out}}$$

$$+ R_A\,R_C\,R_E\,r_{1_{in}}\,r_{2_{in}}\,r_{2_{out}}\,r_{3_{out}} + R_B\,R_C\,R_D\,r_{1_{in}}\,r_{3_{in}}\,r_{1_{out}}\,r_{3_{out}} + R_A\,R_B\,R_F\,r_{2_{in}}\,r_{3_{in}}\,r_{1_{out}}\,r_{3_{out}}$$

$$+ R_D\,R_E\,R_F\,R_G\,r_{1_{in}}\,R_L\,r_{2_{out}} + R_D\,R_E\,R_F\,R_G\,r_{2_{in}}\,R_L\,r_{1_{out}} + R_A\,R_B\,R_F\,R_G\,R_L\,r_{1_{out}}\,r_{2_{out}}$$

$$+ R_B\,R_C\,R_D\,R_G\,R_L\,r_{1_{out}}\,r_{3_{out}} + R_A\,R_B\,R_F\,R_G\,R_L\,r_{2_{out}}\,r_{3_{out}} + R_B\,R_E\,R_F\,r_{1_{in}}\,r_{2_{in}}\,R_L\,r_{1_{out}}$$

$$+ R_B\,R_D\,R_G\,r_{1_{in}}\,r_{3_{in}}\,R_L\,r_{1_{out}} + R_B\,R_E\,R_F\,r_{1_{in}}\,r_{2_{in}}\,R_L\,r_{2_{out}} + R_B\,R_E\,R_F\,r_{1_{in}}\,r_{3_{in}}\,R_L\,r_{1_{out}}$$

$$+ R_B\,R_E\,R_F\,r_{2_{in}}\,r_{3_{in}}\,R_L\,r_{1_{out}} + R_A\,R_E\,R_G\,r_{2_{in}}\,r_{3_{in}}\,R_L\,r_{2_{out}} + R_B\,R_D\,R_G\,r_{1_{in}}\,r_{3_{in}}\,R_L\,r_{3_{out}}$$

$$+ R_B\,R_D\,R_F\,R_G\,r_{1_{in}}\,r_{1_{out}}\,r_{3_{out}} + R_A\,R_B\,R_D\,r_{2_{in}}\,R_L\,r_{1_{out}}\,r_{3_{out}} + R_A\,R_E\,R_F\,R_G\,r_{2_{in}}\,r_{1_{out}}\,r_{3_{out}}$$

$$+ R_C\,R_D\,R_E\,R_G\,r_{2_{in}}\,r_{1_{out}}\,r_{3_{out}} + R_A\,R_E\,R_F\,R_G\,r_{2_{in}}\,r_{2_{out}}\,r_{3_{out}} + R_A\,R_E\,R_F\,R_G\,r_{3_{in}}\,r_{2_{out}}\,r_{3_{out}}$$

$$+ R_C\,R_F\,R_G\,r_{1_{in}}\,r_{2_{in}}\,r_{3_{in}}\,r_{3_{out}} + R_D\,R_E\,R_G\,r_{1_{in}}\,r_{2_{in}}\,r_{3_{in}}\,r_{3_{out}} + R_A\,R_D\,R_E\,r_{1_{in}}\,r_{2_{in}}\,r_{1_{out}}\,r_{3_{out}}$$

$$+ R_B\,R_C\,R_E\,r_{1_{in}}\,r_{2_{in}}\,r_{2_{out}}\,r_{3_{out}} + R_A\,R_C\,R_F\,r_{1_{in}}\,r_{3_{in}}\,r_{2_{out}}\,r_{3_{out}} + R_A\,R_D\,R_E\,r_{1_{in}}\,r_{3_{in}}\,r_{2_{out}}\,r_{3_{out}}$$

$$+ R_A\,R_D\,R_E\,r_{2_{in}}\,r_{3_{in}}\,r_{2_{out}}\,r_{3_{out}} + R_A\,R_D\,R_E\,R_G\,R_L\,r_{1_{out}}\,r_{2_{out}} + R_B\,R_C\,R_E\,R_G\,R_L\,r_{1_{out}}\,r_{2_{out}}$$

$$+ R_C\,R_E\,R_F\,r_{1_{in}}\,r_{2_{in}}\,R_L\,r_{1_{out}} + R_C\,R_E\,R_F\,r_{1_{in}}\,r_{2_{in}}\,R_L\,r_{2_{out}} + R_A\,R_F\,R_G\,r_{2_{in}}\,r_{3_{in}}\,R_L\,r_{1_{out}}$$

$$+ R_C\,R_D\,R_G\,r_{1_{in}}\,r_{2_{in}}\,R_L\,r_{3_{out}} + R_C\,R_D\,R_G\,r_{1_{in}}\,r_{3_{in}}\,R_L\,r_{2_{out}} + R_C\,R_D\,R_G\,r_{2_{in}}\,r_{3_{in}}\,R_L\,r_{1_{out}}$$

$$+ R_A\,R_B\,R_E\,r_{1_{in}}\,R_L\,r_{1_{out}}\,r_{2_{out}} + R_A\,R_B\,R_E\,r_{2_{in}}\,R_L\,r_{1_{out}}\,r_{2_{out}} + R_B\,R_E\,R_F\,R_G\,r_{1_{in}}\,r_{1_{out}}\,r_{3_{out}}$$

$$+ R_B\,R_E\,R_F\,R_G\,r_{1_{in}}\,r_{2_{out}}\,r_{3_{out}} + R_C\,R_D\,R_F\,R_G\,r_{1_{in}}\,r_{2_{out}}\,r_{3_{out}} + R_C\,R_D\,R_F\,R_G\,r_{2_{in}}\,r_{1_{out}}\,r_{3_{out}}$$

$$+ R_B\,R_E\,R_F\,R_G\,r_{3_{in}}\,r_{1_{out}}\,r_{3_{out}} + R_A\,R_D\,r_{1_{in}}\,r_{2_{in}}\,r_{3_{in}}\,R_L\,r_{1_{out}} + R_B\,R_C\,r_{1_{in}}\,r_{2_{in}}\,r_{3_{in}}\,R_L\,r_{2_{out}}$$

$$+ R_A\,R_D\,R_F\,r_{1_{in}}\,r_{2_{in}}\,r_{1_{out}}\,r_{3_{out}} + R_B\,R_D\,R_E\,r_{1_{in}}\,r_{2_{in}}\,r_{1_{out}}\,r_{3_{out}} + R_B\,R_C\,R_F\,r_{1_{in}}\,r_{2_{in}}\,r_{2_{out}}\,r_{3_{out}}$$

$$+ R_B\,R_D\,R_E\,r_{1_{in}}\,r_{3_{in}}\,r_{1_{out}}\,r_{3_{out}} + R_B\,R_C\,R_F\,r_{2_{in}}\,r_{3_{in}}\,r_{1_{out}}\,r_{3_{out}} + R_B\,R_D\,R_E\,r_{2_{in}}\,r_{3_{in}}\,r_{1_{out}}\,r_{3_{out}}$$

$$+ R_A\,R_D\,R_F\,R_G\,R_L\,r_{1_{out}}\,r_{2_{out}} + R_B\,R_C\,R_F\,R_G\,R_L\,r_{1_{out}}\,r_{2_{out}} + R_B\,R_C\,R_F\,R_G\,R_L\,r_{1_{out}}\,r_{3_{out}}$$

$$+ R_D\,R_E\,R_F\,r_{1_{in}}\,r_{2_{in}}\,R_L\,r_{1_{out}} + R_B\,R_F\,R_G\,r_{1_{in}}\,r_{3_{in}}\,R_L\,r_{1_{out}} + R_C\,R_E\,R_G\,r_{1_{in}}\,r_{2_{in}}\,R_L\,r_{2_{out}}$$

$$+ R_B\,R_F\,R_G\,r_{1_{in}}\,r_{3_{in}}\,R_L\,r_{3_{out}} + R_A\,R_B\,R_F\,r_{1_{in}}\,R_L\,r_{1_{out}}\,r_{2_{out}} + R_A\,R_B\,R_F\,r_{1_{in}}\,R_L\,r_{1_{out}}\,r_{3_{out}}$$

$$+ R_B\,R_C\,R_D\,r_{1_{in}}\,R_L\,r_{1_{out}}\,r_{3_{out}} + R_A\,R_B\,R_F\,r_{1_{in}}\,R_L\,r_{2_{out}}\,r_{3_{out}} + R_A\,R_B\,R_F\,r_{2_{in}}\,R_L\,r_{1_{out}}\,r_{3_{out}}$$

$$+ R_C\,R_E\,R_F\,R_G\,r_{1_{in}}\,r_{2_{out}}\,r_{3_{out}} + R_C\,R_E\,R_F\,R_G\,r_{2_{in}}\,r_{1_{out}}\,r_{3_{out}} + R_A\,R_B\,R_F\,r_{2_{in}}\,R_L\,r_{2_{out}}\,r_{3_{out}}$$

$$+ R_B\,R_D\,r_{1_{in}}\,r_{2_{in}}\,r_{3_{in}}\,R_L\,r_{1_{out}} + R_A\,R_E\,r_{1_{in}}\,r_{2_{in}}\,r_{3_{in}}\,R_L\,r_{2_{out}} + R_B\,R_D\,r_{1_{in}}\,r_{2_{in}}\,r_{3_{in}}\,R_L\,r_{3_{out}}$$

$$+ R_A\,R_E\,R_F\,r_{1_{in}}\,r_{2_{in}}\,r_{1_{out}}\,r_{3_{out}} + R_B\,R_D\,R_F\,r_{1_{in}}\,r_{2_{in}}\,r_{1_{out}}\,r_{3_{out}} + R_C\,R_D\,R_E\,r_{1_{in}}\,r_{2_{in}}\,r_{1_{out}}\,r_{3_{out}}$$

$$+ R_C\,R_D\,R_E\,r_{1_{in}}\,r_{2_{in}}\,r_{2_{out}}\,r_{3_{out}} + R_A\,R_D\,R_G\,r_{2_{in}}\,r_{3_{in}}\,r_{1_{out}}\,r_{3_{out}} + R_A\,R_E\,R_F\,r_{1_{in}}\,r_{3_{in}}\,r_{2_{out}}\,r_{3_{out}}$$

$$+ R_A\,R_E\,R_F\,r_{2_{in}}\,r_{3_{in}}\,r_{2_{out}}\,r_{3_{out}} + R_A\,R_E\,R_F\,R_G\,R_L\,r_{1_{out}}\,r_{2_{out}} + R_C\,R_D\,R_E\,R_G\,R_L\,r_{1_{out}}\,r_{2_{out}}$$

$$+ R_D\,R_E\,R_G\,r_{1_{in}}\,r_{2_{in}}\,R_L\,r_{1_{out}} + R_C\,R_F\,R_G\,r_{1_{in}}\,r_{2_{in}}\,R_L\,r_{2_{out}} + R_C\,R_F\,R_G\,r_{1_{in}}\,r_{2_{in}}\,R_L\,r_{3_{out}}$$

$$+ R_C\,R_F\,R_G\,r_{2_{in}}\,r_{3_{in}}\,R_L\,r_{1_{out}} + R_D\,R_E\,R_G\,r_{1_{in}}\,r_{3_{in}}\,R_L\,r_{2_{out}} + R_D\,R_E\,R_G\,r_{2_{in}}\,r_{3_{in}}\,R_L\,r_{1_{out}}$$

$$+ R_B\,R_C\,R_E\,r_{1_{in}}\,R_L\,r_{1_{out}}\,r_{2_{out}} + R_A\,R_D\,R_E\,r_{2_{in}}\,R_L\,r_{1_{out}}\,r_{2_{out}} + R_B\,R_C\,R_E\,r_{2_{in}}\,R_L\,r_{1_{out}}\,r_{2_{out}}$$

$$+ R_A\,R_C\,R_F\,r_{1_{in}}\,R_L\,r_{2_{out}}\,r_{3_{out}} + R_D\,R_E\,R_F\,R_G\,r_{1_{in}}\,r_{2_{out}}\,r_{3_{out}} + R_D\,R_E\,R_F\,R_G\,r_{2_{in}}\,r_{1_{out}}\,r_{3_{out}}$$

$$+ R_A\,R_B\,R_G\,r_{3_{in}}\,R_L\,r_{2_{out}}\,r_{3_{out}} + R_A\,R_B\,R_F\,R_G\,r_{1_{out}}\,r_{2_{out}}\,r_{3_{out}} + R_A\,R_F\,r_{1_{in}}\,r_{2_{in}}\,r_{3_{in}}\,R_L\,r_{1_{out}}$$

$$+ R_B\,R_E\,r_{1_{in}}\,r_{2_{in}}\,r_{3_{in}}\,R_L\,r_{2_{out}} + R_C\,R_D\,r_{1_{in}}\,r_{2_{in}}\,r_{3_{in}}\,R_L\,r_{2_{out}} + R_A\,R_F\,r_{1_{in}}\,r_{2_{in}}\,r_{3_{in}}\,R_L\,r_{3_{out}}$$

$$+ R_C\,R_D\,R_F\,r_{1_{in}}\,r_{2_{in}}\,r_{1_{out}}\,r_{3_{out}} + R_B\,R_D\,R_G\,r_{1_{in}}\,r_{3_{in}}\,r_{1_{out}}\,r_{3_{out}} + R_B\,R_E\,R_F\,r_{1_{in}}\,r_{2_{in}}\,r_{2_{out}}\,r_{3_{out}}$$

$$+ R_C\,R_D\,R_F\,r_{1_{in}}\,r_{2_{in}}\,r_{2_{out}}\,r_{3_{out}} + R_B\,R_E\,R_F\,r_{2_{in}}\,r_{3_{in}}\,r_{1_{out}}\,r_{3_{out}} + R_A\,R_E\,R_G\,r_{2_{in}}\,r_{3_{in}}\,r_{2_{out}}\,r_{3_{out}}$$

$$+ R_C\,R_D\,R_F\,R_G\,R_L\,r_{1_{out}}\,r_{2_{out}} + R_A\,R_C\,r_{1_{in}}\,r_{2_{in}}\,r_{3_{in}}\,r_{2_{out}}\,r_{3_{out}} + R_D\,R_F\,R_G\,r_{1_{in}}\,r_{2_{in}}\,R_L\,r_{1_{out}}$$

$$+ R_A\,R_D\,R_F\,r_{1_{in}}\,R_L\,r_{1_{out}}\,r_{2_{out}} + R_B\,R_C\,R_F\,r_{1_{in}}\,R_L\,r_{1_{out}}\,r_{2_{out}} + R_A\,R_D\,R_F\,r_{2_{in}}\,R_L\,r_{1_{out}}\,r_{2_{out}}$$

$$+ R_B\,R_C\,R_F\,r_{2_{in}}\,R_L\,r_{1_{out}}\,r_{2_{out}} + R_A\,R_D\,R_F\,r_{1_{in}}\,R_L\,r_{2_{out}}\,r_{3_{out}} + R_B\,R_C\,R_F\,r_{2_{in}}\,R_L\,r_{1_{out}}\,r_{3_{out}}$$

$$+ R_A\,R_D\,R_F\,r_{2_{in}}\,R_L\,r_{2_{out}}\,r_{3_{out}} + R_A\,R_D\,R_E\,R_G\,r_{1_{out}}\,r_{2_{out}}\,r_{3_{out}} + R_B\,R_C\,R_E\,R_G\,r_{1_{out}}\,r_{2_{out}}\,r_{3_{out}}$$

$$+ R_B\,R_F\,r_{1_{in}}\,r_{2_{in}}\,r_{3_{in}}\,R_L\,r_{3_{out}} + R_C\,R_E\,R_F\,r_{1_{in}}\,r_{2_{in}}\,r_{1_{out}}\,r_{3_{out}} + R_C\,R_E\,R_F\,r_{1_{in}}\,r_{2_{in}}\,r_{2_{out}}\,r_{3_{out}}$$

$$+ R_B\,R_E\,R_G\,r_{1_{in}}\,r_{3_{in}}\,r_{2_{out}}\,r_{3_{out}} + R_C\,R_D\,R_G\,r_{1_{in}}\,r_{3_{in}}\,r_{2_{out}}\,r_{3_{out}} + R_C\,R_D\,R_G\,r_{2_{in}}\,r_{3_{in}}\,r_{1_{out}}\,r_{3_{out}}$$

$$+ R_A\,R_B\,R_E\,r_{2_{in}}\,r_{1_{out}}\,r_{2_{out}}\,r_{3_{out}} + R_C\,R_E\,R_F\,R_G\,R_L\,r_{1_{out}}\,r_{2_{out}} + R_A\,R_D\,r_{1_{in}}\,r_{2_{in}}\,r_{3_{in}}\,r_{1_{out}}\,r_{3_{out}}$$

$$+ R_E\,R_F\,R_G\,r_{1_{in}}\,r_{2_{in}}\,R_L\,r_{1_{out}} + R_E\,R_F\,R_G\,r_{1_{in}}\,r_{2_{in}}\,R_L\,r_{2_{out}} + R_E\,R_F\,R_G\,r_{1_{in}}\,r_{3_{in}}\,R_L\,r_{2_{out}}$$

$$+ R_A\,R_E\,R_F\,r_{1_{in}}\,R_L\,r_{1_{out}}\,r_{2_{out}} + R_C\,R_D\,R_E\,r_{1_{in}}\,R_L\,r_{1_{out}}\,r_{2_{out}} + R_A\,R_E\,R_F\,r_{2_{in}}\,R_L\,r_{1_{out}}\,r_{2_{out}}$$

$$+ R_C\,R_D\,R_E\,r_{2_{in}}\,R_L\,r_{1_{out}}\,r_{2_{out}} + R_A\,R_D\,R_G\,r_{2_{in}}\,R_L\,r_{1_{out}}\,r_{3_{out}} + R_A\,R_D\,R_G\,r_{3_{in}}\,R_L\,r_{1_{out}}\,r_{2_{out}}$$

$$+ R_B\,R_C\,R_G\,r_{3_{in}}\,R_L\,r_{1_{out}}\,r_{2_{out}} + R_B\,R_D\,R_F\,r_{2_{in}}\,R_L\,r_{1_{out}}\,r_{3_{out}} + R_A\,R_D\,R_G\,r_{3_{in}}\,R_L\,r_{2_{out}}\,r_{3_{out}}$$

$$+ R_B\,R_C\,R_F\,R_G\,r_{1_{out}}\,r_{2_{out}}\,r_{3_{out}} + R_C\,R_F\,r_{1_{in}}\,r_{2_{in}}\,r_{3_{in}}\,R_L\,r_{1_{out}} + R_D\,R_E\,r_{1_{in}}\,r_{2_{in}}\,r_{3_{in}}\,R_L\,r_{1_{out}}$$

$$+ R_D\,R_E\,r_{1_{in}}\,r_{2_{in}}\,r_{3_{in}}\,R_L\,r_{2_{out}} + R_A\,R_B\,r_{1_{in}}\,r_{3_{in}}\,R_L\,r_{1_{out}}\,r_{2_{out}} + R_D\,R_E\,R_F\,r_{1_{in}}\,r_{2_{in}}\,r_{1_{out}}\,r_{3_{out}}$$

$$+ R_B\,R_F\,R_G\,r_{1_{in}}\,r_{3_{in}}\,r_{1_{out}}\,r_{3_{out}} + R_C\,R_E\,R_G\,r_{1_{in}}\,r_{2_{in}}\,r_{2_{out}}\,r_{3_{out}} + R_D\,R_E\,R_F\,r_{1_{in}}\,r_{2_{in}}\,r_{2_{out}}\,r_{3_{out}}$$

$$+ R_A\,R_B\,r_{2_{in}}\,r_{3_{in}}\,R_L\,r_{2_{out}}\,r_{3_{out}} + R_A\,R_B\,R_F\,r_{1_{in}}\,r_{1_{out}}\,r_{2_{out}}\,r_{3_{out}} + R_A\,R_B\,R_F\,r_{2_{in}}\,r_{1_{out}}\,r_{2_{out}}\,r_{3_{out}}$$

$$+ R_B\,R_D\,r_{1_{in}}\,r_{2_{in}}\,r_{3_{in}}\,r_{1_{out}}\,r_{3_{out}} + R_A\,R_E\,r_{1_{in}}\,r_{2_{in}}\,r_{3_{in}}\,r_{2_{out}}\,r_{3_{out}} + R_B\,R_E\,R_F\,r_{1_{in}}\,R_L\,r_{1_{out}}\,r_{2_{out}}$$

$$+ R_A\,R_E\,R_G\,r_{2_{in}}\,R_L\,r_{1_{out}}\,r_{2_{out}} + R_B\,R_D\,R_G\,r_{1_{in}}\,R_L\,r_{1_{out}}\,r_{3_{out}} + R_B\,R_E\,R_F\,r_{2_{in}}\,R_L\,r_{1_{out}}\,r_{2_{out}}$$

$$+ R_B\,R_D\,R_G\,r_{3_{in}}\,R_L\,r_{1_{out}}\,r_{3_{out}} + R_A\,R_E\,R_F\,R_G\,r_{1_{out}}\,r_{2_{out}}\,r_{3_{out}} + R_C\,R_D\,R_E\,R_G\,r_{1_{out}}\,r_{2_{out}}\,r_{3_{out}}$$

$$+ R_D\,R_E\,R_G\,r_{1_{in}}\,r_{2_{in}}\,r_{1_{out}}\,r_{3_{out}} + R_A\,R_C\,r_{1_{in}}\,r_{2_{in}}\,R_L\,r_{2_{out}}\,r_{3_{out}} + R_C\,R_F\,R_G\,r_{1_{in}}\,r_{2_{in}}\,r_{2_{out}}\,r_{3_{out}}$$

$$+ R_C\,R_F\,R_G\,r_{2_{in}}\,r_{3_{in}}\,r_{1_{out}}\,r_{3_{out}} + R_D\,R_E\,R_G\,r_{1_{in}}\,r_{3_{in}}\,r_{2_{out}}\,r_{3_{out}} + R_D\,R_E\,R_G\,r_{2_{in}}\,r_{3_{in}}\,r_{1_{out}}\,r_{3_{out}}$$

$$+ R_B\,R_C\,R_E\,r_{1_{in}}\,r_{1_{out}}\,r_{2_{out}}\,r_{3_{out}} + R_A\,R_D\,R_E\,r_{2_{in}}\,r_{1_{out}}\,r_{2_{out}}\,r_{3_{out}} + R_B\,R_C\,R_E\,r_{2_{in}}\,r_{1_{out}}\,r_{2_{out}}\,r_{3_{out}}$$

$$+ R_A\,R_F\,r_{1_{in}}\,r_{2_{in}}\,r_{3_{in}}\,r_{1_{out}}\,r_{3_{out}} + R_C\,R_D\,r_{1_{in}}\,r_{2_{in}}\,r_{3_{in}}\,r_{1_{out}}\,r_{3_{out}} + R_B\,R_E\,r_{1_{in}}\,r_{2_{in}}\,r_{3_{in}}\,r_{2_{out}}\,r_{3_{out}}$$

$$+ R_B\,R_E\,R_G\,r_{1_{in}}\,R_L\,r_{1_{out}}\,r_{2_{out}} + R_C\,R_E\,R_F\,r_{1_{in}}\,R_L\,r_{1_{out}}\,r_{2_{out}} + R_A\,R_F\,R_G\,r_{2_{in}}\,R_L\,r_{1_{out}}\,r_{2_{out}}$$

$$+ R_A\,R_F\,R_G\,r_{2_{in}}\,R_L\,r_{1_{out}}\,r_{3_{out}} + R_A\,R_F\,R_G\,r_{3_{in}}\,R_L\,r_{1_{out}}\,r_{2_{out}} + R_B\,R_E\,R_G\,r_{3_{in}}\,R_L\,r_{1_{out}}\,r_{2_{out}}$$

$$+ R_C\,R_D\,R_G\,r_{2_{in}}\,R_L\,r_{1_{out}}\,r_{3_{out}} + R_C\,R_D\,R_G\,r_{3_{in}}\,R_L\,r_{1_{out}}\,r_{2_{out}} + R_A\,R_F\,R_G\,r_{2_{in}}\,R_L\,r_{2_{out}}\,r_{3_{out}}$$

$$+ R_B\,R_E\,R_F\,R_G\,r_{1_{out}}\,r_{2_{out}}\,r_{3_{out}} + R_C\,R_D\,R_F\,R_G\,r_{1_{out}}\,r_{2_{out}}\,r_{3_{out}} + R_D\,R_G\,r_{1_{in}}\,r_{2_{in}}\,r_{3_{in}}\,R_L\,r_{1_{out}}$$

$$+ R_E\,R_F\,r_{1_{in}}\,r_{2_{in}}\,r_{3_{in}}\,R_L\,r_{2_{out}} + R_D\,R_G\,r_{1_{in}}\,r_{2_{in}}\,r_{3_{in}}\,R_L\,r_{3_{out}} + R_A\,R_D\,r_{1_{in}}\,r_{2_{in}}\,R_L\,r_{1_{out}}\,r_{3_{out}}$$

$$+ R_B\,R_C\,r_{1_{in}}\,r_{3_{in}}\,R_L\,r_{1_{out}}\,r_{2_{out}} + R_D\,R_F\,R_G\,r_{1_{in}}\,r_{2_{in}}\,r_{1_{out}}\,r_{3_{out}} + R_A\,R_D\,r_{2_{in}}\,r_{3_{in}}\,R_L\,r_{1_{out}}\,r_{2_{out}}$$

$$+ R_B\,R_C\,r_{2_{in}}\,r_{3_{in}}\,R_L\,r_{1_{out}}\,r_{2_{out}} + R_A\,R_D\,r_{1_{in}}\,r_{3_{in}}\,R_L\,r_{2_{out}}\,r_{3_{out}} + R_A\,R_D\,r_{2_{in}}\,r_{3_{in}}\,R_L\,r_{2_{out}}\,r_{3_{out}}$$

$$+ \mathrm{R_B\,R_C\,R_F\,r_{1_{in}}\,r_{1_{out}}\,r_{2_{out}}\,r_{3_{out}}} + \mathrm{R_A\,R_D\,R_F\,r_{2_{in}}\,r_{1_{out}}\,r_{2_{out}}\,r_{3_{out}}} + \mathrm{R_B\,R_C\,R_F\,r_{2_{in}}\,r_{1_{out}}\,r_{2_{out}}\,r_{3_{out}}}$$

$$+ \mathrm{R_B\,R_F\,R_G\,r_{1_{in}}\,R_L\,r_{1_{out}}\,r_{2_{out}}} + \mathrm{R_D\,R_E\,R_F\,r_{1_{in}}\,R_L\,r_{1_{out}}\,r_{2_{out}}} + \mathrm{R_B\,R_F\,R_G\,r_{1_{in}}\,R_L\,r_{1_{out}}\,r_{3_{out}}}$$

$$+ \mathrm{R_D\,R_E\,R_F\,r_{2_{in}}\,R_L\,r_{1_{out}}\,r_{2_{out}}} + \mathrm{R_B\,R_F\,R_G\,r_{1_{in}}\,R_L\,r_{2_{out}}\,r_{3_{out}}} + \mathrm{R_B\,R_F\,R_G\,r_{3_{in}}\,R_L\,r_{1_{out}}\,r_{3_{out}}}$$

$$+ \mathrm{R_E\,R_G\,r_{1_{in}}\,r_{2_{in}}\,r_{3_{in}}\,R_L\,r_{2_{out}}} + \mathrm{R_A\,R_E\,r_{1_{in}}\,r_{2_{in}}\,R_L\,r_{1_{out}}\,r_{2_{out}}} + \mathrm{R_B\,R_D\,r_{1_{in}}\,r_{2_{in}}\,R_L\,r_{1_{out}}\,r_{3_{out}}}$$

$$+ \mathrm{R_B\,R_D\,r_{1_{in}}\,r_{3_{in}}\,R_L\,r_{1_{out}}\,r_{3_{out}}} + \mathrm{R_E\,R_F\,R_G\,r_{1_{in}}\,r_{2_{in}}\,r_{2_{out}}\,r_{3_{out}}} + \mathrm{R_B\,R_D\,r_{2_{in}}\,r_{3_{in}}\,R_L\,r_{1_{out}}\,r_{3_{out}}}$$

$$+ \mathrm{R_E\,R_F\,R_G\,r_{2_{in}}\,r_{3_{in}}\,r_{1_{out}}\,r_{3_{out}}} + \mathrm{R_A\,R_E\,R_F\,r_{1_{in}}\,r_{1_{out}}\,r_{2_{out}}\,r_{3_{out}}} + \mathrm{R_C\,R_D\,R_E\,r_{1_{in}}\,r_{1_{out}}\,r_{2_{out}}\,r_{3_{out}}}$$

$$+ \mathrm{R_C\,R_D\,R_E\,r_{2_{in}}\,r_{1_{out}}\,r_{2_{out}}\,r_{3_{out}}} + \mathrm{R_A\,R_D\,R_G\,r_{3_{in}}\,r_{1_{out}}\,r_{2_{out}}\,r_{3_{out}}}$$

$$+ \mathrm{R_C\,R_F\,r_{1_{in}}\,r_{2_{in}}\,r_{3_{in}}\,r_{1_{out}}\,r_{3_{out}}} + \mathrm{R_D\,R_E\,r_{1_{in}}\,r_{2_{in}}\,r_{3_{in}}\,r_{1_{out}}\,r_{3_{out}}} + \mathrm{R_C\,R_F\,r_{1_{in}}\,r_{2_{in}}\,r_{3_{in}}\,r_{2_{out}}\,r_{3_{out}}}$$

$$+ \mathrm{R_A\,R_B\,r_{1_{in}}\,r_{3_{in}}\,r_{1_{out}}\,r_{2_{out}}\,r_{3_{out}}} + \mathrm{R_A\,R_B\,r_{2_{in}}\,r_{3_{in}}\,r_{1_{out}}\,r_{2_{out}}\,r_{3_{out}}} + \mathrm{R_D\,R_E\,R_G\,r_{1_{in}}\,R_L\,r_{1_{out}}\,r_{2_{out}}}$$

$$+ \mathrm{R_C\,R_F\,R_G\,r_{1_{in}}\,R_L\,r_{2_{out}}\,r_{3_{out}}} + \mathrm{R_C\,R_F\,R_G\,r_{2_{in}}\,R_L\,r_{1_{out}}\,r_{3_{out}}} + \mathrm{R_C\,R_F\,R_G\,r_{3_{in}}\,R_L\,r_{1_{out}}\,r_{2_{out}}}$$

$$+ \mathrm{R_A\,R_B\,R_G\,R_L\,r_{1_{out}}\,r_{2_{out}}\,r_{3_{out}}} + \mathrm{R_D\,R_E\,R_F\,R_G\,r_{1_{out}}\,r_{2_{out}}\,r_{3_{out}}} + \mathrm{R_F\,R_G\,r_{1_{in}}\,r_{2_{in}}\,r_{3_{in}}\,R_L\,r_{1_{out}}}$$

$$+ \mathrm{R_A\,R_F\,r_{1_{in}}\,r_{2_{in}}\,R_L\,r_{1_{out}}\,r_{2_{out}}} + \mathrm{R_B\,R_E\,r_{1_{in}}\,r_{2_{in}}\,R_L\,r_{1_{out}}\,r_{2_{out}}} + \mathrm{R_A\,R_F\,r_{1_{in}}\,r_{2_{in}}\,R_L\,r_{1_{out}}\,r_{3_{out}}}$$

$$+ \mathrm{R_B\,R_E\,r_{1_{in}}\,r_{3_{in}}\,R_L\,r_{1_{out}}\,r_{2_{out}}} + \mathrm{R_C\,R_D\,r_{1_{in}}\,r_{2_{in}}\,R_L\,r_{1_{out}}\,r_{3_{out}}} + \mathrm{R_C\,R_D\,r_{1_{in}}\,r_{3_{in}}\,R_L\,r_{1_{out}}\,r_{2_{out}}}$$

$$+ \mathrm{R_A\,R_F\,r_{2_{in}}\,r_{3_{in}}\,R_L\,r_{1_{out}}\,r_{2_{out}}} + \mathrm{R_B\,R_E\,r_{2_{in}}\,r_{3_{in}}\,R_L\,r_{1_{out}}\,r_{2_{out}}} + \mathrm{R_C\,R_D\,r_{1_{in}}\,r_{2_{in}}\,R_L\,r_{2_{out}}\,r_{3_{out}}}$$

$$+ \mathrm{R_A\,R_F\,r_{1_{in}}\,r_{3_{in}}\,R_L\,r_{2_{out}}\,r_{3_{out}}} + \mathrm{R_A\,R_F\,r_{2_{in}}\,r_{3_{in}}\,R_L\,r_{2_{out}}\,r_{3_{out}}} + \mathrm{R_B\,R_E\,R_F\,r_{1_{in}}\,r_{1_{out}}\,r_{2_{out}}\,r_{3_{out}}}$$

$$+ \mathrm{R_A\,R_E\,R_G\,r_{2_{in}}\,r_{1_{out}}\,r_{2_{out}}\,r_{3_{out}}} + \mathrm{R_B\,R_E\,R_F\,r_{2_{in}}\,r_{1_{out}}\,r_{2_{out}}\,r_{3_{out}}} + \mathrm{R_C\,R_D\,R_F\,r_{2_{in}}\,r_{1_{out}}\,r_{2_{out}}\,r_{3_{out}}}$$

$$+ \mathrm{R_D\,R_F\,R_G\,r_{1_{in}}\,R_L\,r_{1_{out}}\,r_{2_{out}}} + \mathrm{R_D\,R_F\,R_G\,r_{1_{in}}\,R_L\,r_{2_{out}}\,r_{3_{out}}} + \mathrm{R_D\,R_F\,R_G\,r_{2_{in}}\,R_L\,r_{1_{out}}\,r_{3_{out}}}$$

$$+ \mathrm{R_C\,R_E\,r_{1_{in}}\,r_{2_{in}}\,R_L\,r_{1_{out}}\,r_{2_{out}}} + \mathrm{R_B\,R_F\,r_{1_{in}}\,r_{2_{in}}\,R_L\,r_{1_{out}}\,r_{3_{out}}} + \mathrm{R_A\,R_G\,r_{2_{in}}\,r_{3_{in}}\,R_L\,r_{1_{out}}\,r_{2_{out}}}$$

$$+ \mathrm{R_B\,R_F\,r_{1_{in}}\,r_{3_{in}}\,R_L\,r_{1_{out}}\,r_{3_{out}}} + \mathrm{R_B\,R_F\,r_{2_{in}}\,r_{3_{in}}\,R_L\,r_{1_{out}}\,r_{3_{out}}} + \mathrm{R_A\,R_G\,r_{2_{in}}\,r_{3_{in}}\,R_L\,r_{2_{out}}\,r_{3_{out}}}$$

$$+ \mathrm{R_C\,R_E\,R_F\,r_{1_{in}}\,r_{1_{out}}\,r_{2_{out}}\,r_{3_{out}}} + \mathrm{R_A\,R_F\,R_G\,r_{2_{in}}\,r_{1_{out}}\,r_{2_{out}}\,r_{3_{out}}} + \mathrm{R_C\,R_E\,R_F\,r_{2_{in}}\,r_{1_{out}}\,r_{2_{out}}\,r_{3_{out}}}$$

$$+ \mathrm{R_B\,R_E\,R_G\,r_{3_{in}}\,r_{1_{out}}\,r_{2_{out}}\,r_{3_{out}}} + \mathrm{R_C\,R_D\,R_G\,r_{3_{in}}\,r_{1_{out}}\,r_{2_{out}}\,r_{3_{out}}} + \mathrm{R_D\,R_G\,r_{1_{in}}\,r_{2_{in}}\,r_{3_{in}}\,r_{1_{out}}\,r_{3_{out}}}$$

$$+ \mathrm{R_E\,R_F\,r_{1_{in}}\,r_{2_{in}}\,r_{3_{in}}\,r_{2_{out}}\,r_{3_{out}}} + \mathrm{R_A\,R_D\,r_{1_{in}}\,r_{3_{in}}\,r_{1_{out}}\,r_{2_{out}}\,r_{3_{out}}} + \mathrm{R_B\,R_C\,r_{1_{in}}\,r_{3_{in}}\,r_{1_{out}}\,r_{2_{out}}\,r_{3_{out}}}$$

$$+ \mathrm{R_B\,R_C\,r_{2_{in}}\,r_{3_{in}}\,r_{1_{out}}\,r_{2_{out}}\,r_{3_{out}}} + \mathrm{R_E\,R_F\,R_G\,r_{1_{in}}\,R_L\,r_{1_{out}}\,r_{2_{out}}} + \mathrm{R_E\,R_F\,R_G\,r_{2_{in}}\,R_L\,r_{1_{out}}\,r_{2_{out}}}$$

$$+ \mathrm{R_A\,R_D\,R_G\,R_L\,r_{1_{out}}\,r_{2_{out}}\,r_{3_{out}}} + \mathrm{R_B\,R_C\,R_G\,R_L\,r_{1_{out}}\,r_{2_{out}}\,r_{3_{out}}} + \mathrm{R_C\,R_F\,r_{1_{in}}\,r_{2_{in}}\,R_L\,r_{1_{out}}\,r_{2_{out}}}$$

$$+ \mathrm{R_B\,R_G\,r_{1_{in}}\,r_{3_{in}}\,R_L\,r_{1_{out}}\,r_{2_{out}}} + \mathrm{R_C\,R_F\,r_{1_{in}}\,r_{2_{in}}\,R_L\,r_{1_{out}}\,r_{3_{out}}} + \mathrm{R_C\,R_F\,r_{1_{in}}\,r_{3_{in}}\,R_L\,r_{1_{out}}\,r_{2_{out}}}$$

$$+ \mathrm{R_C\,R_F\,r_{1_{in}}\,r_{2_{in}}\,R_L\,r_{2_{out}}\,r_{3_{out}}} + \mathrm{R_C\,R_F\,r_{2_{in}}\,r_{3_{in}}\,R_L\,r_{1_{out}}\,r_{2_{out}}} + \mathrm{R_D\,R_E\,r_{2_{in}}\,r_{3_{in}}\,R_L\,r_{1_{out}}\,r_{2_{out}}}$$

$$+ \mathrm{R_A}\,\mathrm{R_B}\,\mathrm{r_{1_{in}}}\,\mathrm{R_L}\,\mathrm{r_{1_{out}}}\,\mathrm{r_{2_{out}}}\,\mathrm{r_{3_{out}}} + \mathrm{R_B}\,\mathrm{R_F}\,\mathrm{R_G}\,\mathrm{r_{1_{in}}}\,\mathrm{r_{1_{out}}}\,\mathrm{r_{2_{out}}}\,\mathrm{r_{3_{out}}} + \mathrm{R_D}\,\mathrm{R_E}\,\mathrm{R_F}\,\mathrm{r_{1_{in}}}\,\mathrm{r_{1_{out}}}\,\mathrm{r_{2_{out}}}\,\mathrm{r_{3_{out}}}$$

$$+ \mathrm{R_C}\,\mathrm{R_E}\,\mathrm{R_G}\,\mathrm{r_{2_{in}}}\,\mathrm{r_{1_{out}}}\,\mathrm{r_{2_{out}}}\,\mathrm{r_{3_{out}}} + \mathrm{R_D}\,\mathrm{R_E}\,\mathrm{R_F}\,\mathrm{r_{2_{in}}}\,\mathrm{r_{1_{out}}}\,\mathrm{r_{2_{out}}}\,\mathrm{r_{3_{out}}} + \mathrm{R_E}\,\mathrm{R_G}\,\mathrm{r_{1_{in}}}\,\mathrm{r_{2_{in}}}\,\mathrm{r_{3_{in}}}\,\mathrm{r_{2_{out}}}\,\mathrm{r_{3_{out}}}$$

$$+ \mathrm{R_D}\,\mathrm{R_F}\,\mathrm{r_{1_{in}}}\,\mathrm{r_{2_{in}}}\,\mathrm{R_L}\,\mathrm{r_{1_{out}}}\,\mathrm{r_{2_{out}}} + \mathrm{R_D}\,\mathrm{R_F}\,\mathrm{r_{1_{in}}}\,\mathrm{r_{2_{in}}}\,\mathrm{R_L}\,\mathrm{r_{1_{out}}}\,\mathrm{r_{3_{out}}} + \mathrm{R_C}\,\mathrm{R_G}\,\mathrm{r_{1_{in}}}\,\mathrm{r_{2_{in}}}\,\mathrm{R_L}\,\mathrm{r_{2_{out}}}\,\mathrm{r_{3_{out}}}$$

$$+ \mathrm{R_D}\,\mathrm{R_F}\,\mathrm{r_{1_{in}}}\,\mathrm{r_{2_{in}}}\,\mathrm{R_L}\,\mathrm{r_{2_{out}}}\,\mathrm{r_{3_{out}}} + \mathrm{R_D}\,\mathrm{R_E}\,\mathrm{R_G}\,\mathrm{r_{1_{in}}}\,\mathrm{r_{1_{out}}}\,\mathrm{r_{2_{out}}}\,\mathrm{r_{3_{out}}} + \mathrm{R_C}\,\mathrm{R_F}\,\mathrm{R_G}\,\mathrm{r_{2_{in}}}\,\mathrm{r_{1_{out}}}\,\mathrm{r_{2_{out}}}\,\mathrm{r_{3_{out}}}$$

$$+ \mathrm{R_D}\,\mathrm{R_E}\,\mathrm{R_G}\,\mathrm{r_{3_{in}}}\,\mathrm{r_{1_{out}}}\,\mathrm{r_{2_{out}}}\,\mathrm{r_{3_{out}}} + \mathrm{R_A}\,\mathrm{r_{1_{in}}}\,\mathrm{r_{2_{in}}}\,\mathrm{r_{3_{in}}}\,\mathrm{R_L}\,\mathrm{r_{1_{out}}}\,\mathrm{r_{2_{out}}} + \mathrm{R_F}\,\mathrm{R_G}\,\mathrm{r_{1_{in}}}\,\mathrm{r_{2_{in}}}\,\mathrm{r_{3_{in}}}\,\mathrm{r_{1_{out}}}\,\mathrm{r_{3_{out}}}$$

$$+ \mathrm{R_A}\,\mathrm{R_F}\,\mathrm{r_{1_{in}}}\,\mathrm{r_{2_{in}}}\,\mathrm{r_{1_{out}}}\,\mathrm{r_{2_{out}}}\,\mathrm{r_{3_{out}}} + \mathrm{R_B}\,\mathrm{R_E}\,\mathrm{r_{1_{in}}}\,\mathrm{r_{2_{in}}}\,\mathrm{r_{1_{out}}}\,\mathrm{r_{2_{out}}}\,\mathrm{r_{3_{out}}}$$

$$+ \mathrm{R_B}\,\mathrm{R_E}\,\mathrm{r_{1_{in}}}\,\mathrm{r_{3_{in}}}\,\mathrm{r_{1_{out}}}\,\mathrm{r_{2_{out}}}\,\mathrm{r_{3_{out}}} + \mathrm{R_C}\,\mathrm{R_D}\,\mathrm{r_{1_{in}}}\,\mathrm{r_{3_{in}}}\,\mathrm{r_{1_{out}}}\,\mathrm{r_{2_{out}}}\,\mathrm{r_{3_{out}}}$$

$$+ \mathrm{R_B}\,\mathrm{R_E}\,\mathrm{r_{2_{in}}}\,\mathrm{r_{3_{in}}}\,\mathrm{r_{1_{out}}}\,\mathrm{r_{2_{out}}}\,\mathrm{r_{3_{out}}} + \mathrm{R_C}\,\mathrm{R_D}\,\mathrm{r_{2_{in}}}\,\mathrm{r_{3_{in}}}\,\mathrm{r_{1_{out}}}\,\mathrm{r_{2_{out}}}\,\mathrm{r_{3_{out}}} + \mathrm{R_A}\,\mathrm{R_F}\,\mathrm{R_G}\,\mathrm{R_L}\,\mathrm{r_{1_{out}}}\,\mathrm{r_{2_{out}}}\,\mathrm{r_{3_{out}}}$$

$$+ \mathrm{R_D}\,\mathrm{R_G}\,\mathrm{r_{1_{in}}}\,\mathrm{r_{2_{in}}}\,\mathrm{R_L}\,\mathrm{r_{1_{out}}}\,\mathrm{r_{3_{out}}} + \mathrm{R_D}\,\mathrm{R_G}\,\mathrm{r_{1_{in}}}\,\mathrm{r_{3_{in}}}\,\mathrm{R_L}\,\mathrm{r_{1_{out}}}\,\mathrm{r_{2_{out}}} + \mathrm{R_E}\,\mathrm{R_F}\,\mathrm{r_{1_{in}}}\,\mathrm{r_{3_{in}}}\,\mathrm{R_L}\,\mathrm{r_{1_{out}}}\,\mathrm{r_{2_{out}}}$$

$$+ \mathrm{R_D}\,\mathrm{R_G}\,\mathrm{r_{1_{in}}}\,\mathrm{r_{3_{in}}}\,\mathrm{R_L}\,\mathrm{r_{2_{out}}}\,\mathrm{r_{3_{out}}} + \mathrm{R_D}\,\mathrm{R_G}\,\mathrm{r_{2_{in}}}\,\mathrm{r_{3_{in}}}\,\mathrm{R_L}\,\mathrm{r_{1_{out}}}\,\mathrm{r_{3_{out}}} + \mathrm{R_A}\,\mathrm{R_D}\,\mathrm{r_{1_{in}}}\,\mathrm{R_L}\,\mathrm{r_{1_{out}}}\,\mathrm{r_{2_{out}}}\,\mathrm{r_{3_{out}}}$$

$$+ \mathrm{R_D}\,\mathrm{R_F}\,\mathrm{R_G}\,\mathrm{r_{1_{in}}}\,\mathrm{r_{1_{out}}}\,\mathrm{r_{2_{out}}}\,\mathrm{r_{3_{out}}} + \mathrm{R_A}\,\mathrm{R_D}\,\mathrm{r_{2_{in}}}\,\mathrm{R_L}\,\mathrm{r_{1_{out}}}\,\mathrm{r_{2_{out}}}\,\mathrm{r_{3_{out}}} + \mathrm{R_B}\,\mathrm{R_C}\,\mathrm{r_{2_{in}}}\,\mathrm{R_L}\,\mathrm{r_{1_{out}}}\,\mathrm{r_{2_{out}}}\,\mathrm{r_{3_{out}}}$$

$$+ \mathrm{R_B}\,\mathrm{r_{1_{in}}}\,\mathrm{r_{2_{in}}}\,\mathrm{r_{3_{in}}}\,\mathrm{R_L}\,\mathrm{r_{2_{out}}}\,\mathrm{r_{3_{out}}} + \mathrm{R_B}\,\mathrm{R_F}\,\mathrm{r_{1_{in}}}\,\mathrm{r_{2_{in}}}\,\mathrm{r_{1_{out}}}\,\mathrm{r_{2_{out}}}\,\mathrm{r_{3_{out}}} + \mathrm{R_C}\,\mathrm{R_E}\,\mathrm{r_{1_{in}}}\,\mathrm{r_{2_{in}}}\,\mathrm{r_{1_{out}}}\,\mathrm{r_{2_{out}}}\,\mathrm{r_{3_{out}}}$$

$$+ \mathrm{R_B}\,\mathrm{R_F}\,\mathrm{R_G}\,\mathrm{R_L}\,\mathrm{r_{1_{out}}}\,\mathrm{r_{2_{out}}}\,\mathrm{r_{3_{out}}} + \mathrm{R_E}\,\mathrm{R_G}\,\mathrm{r_{1_{in}}}\,\mathrm{r_{2_{in}}}\,\mathrm{R_L}\,\mathrm{r_{1_{out}}}\,\mathrm{r_{2_{out}}} + \mathrm{R_E}\,\mathrm{R_G}\,\mathrm{r_{2_{in}}}\,\mathrm{r_{3_{in}}}\,\mathrm{R_L}\,\mathrm{r_{1_{out}}}\,\mathrm{r_{2_{out}}}$$

$$+ \mathrm{R_E}\,\mathrm{R_F}\,\mathrm{R_G}\,\mathrm{r_{2_{in}}}\,\mathrm{r_{1_{out}}}\,\mathrm{r_{2_{out}}}\,\mathrm{r_{3_{out}}} + \mathrm{R_E}\,\mathrm{R_F}\,\mathrm{R_G}\,\mathrm{r_{3_{in}}}\,\mathrm{r_{1_{out}}}\,\mathrm{r_{2_{out}}}\,\mathrm{r_{3_{out}}} + \mathrm{R_C}\,\mathrm{r_{1_{in}}}\,\mathrm{r_{2_{in}}}\,\mathrm{r_{3_{in}}}\,\mathrm{R_L}\,\mathrm{r_{1_{out}}}\,\mathrm{r_{2_{out}}}$$

$$+ \mathrm{R_D}\,\mathrm{R_E}\,\mathrm{r_{1_{in}}}\,\mathrm{r_{2_{in}}}\,\mathrm{r_{1_{out}}}\,\mathrm{r_{2_{out}}}\,\mathrm{r_{3_{out}}} + \mathrm{R_B}\,\mathrm{R_G}\,\mathrm{r_{1_{in}}}\,\mathrm{r_{3_{in}}}\,\mathrm{r_{1_{out}}}\,\mathrm{r_{2_{out}}}\,\mathrm{r_{3_{out}}}$$

$$+ \mathrm{R_D}\,\mathrm{R_E}\,\mathrm{r_{1_{in}}}\,\mathrm{r_{3_{in}}}\,\mathrm{r_{1_{out}}}\,\mathrm{r_{2_{out}}}\,\mathrm{r_{3_{out}}} + \mathrm{R_C}\,\mathrm{R_F}\,\mathrm{r_{2_{in}}}\,\mathrm{r_{3_{in}}}\,\mathrm{r_{1_{out}}}\,\mathrm{r_{2_{out}}}\,\mathrm{r_{3_{out}}}$$

$$+ \mathrm{R_C}\,\mathrm{R_F}\,\mathrm{R_G}\,\mathrm{R_L}\,\mathrm{r_{1_{out}}}\,\mathrm{r_{2_{out}}}\,\mathrm{r_{3_{out}}} + \mathrm{R_F}\,\mathrm{R_G}\,\mathrm{r_{1_{in}}}\,\mathrm{r_{2_{in}}}\,\mathrm{R_L}\,\mathrm{r_{1_{out}}}\,\mathrm{r_{2_{out}}} + \mathrm{R_F}\,\mathrm{R_G}\,\mathrm{r_{1_{in}}}\,\mathrm{r_{2_{in}}}\,\mathrm{R_L}\,\mathrm{r_{1_{out}}}\,\mathrm{r_{3_{out}}}$$

$$+ \mathrm{R_F}\,\mathrm{R_G}\,\mathrm{r_{1_{in}}}\,\mathrm{r_{2_{in}}}\,\mathrm{R_L}\,\mathrm{r_{2_{out}}}\,\mathrm{r_{3_{out}}} + \mathrm{R_F}\,\mathrm{R_G}\,\mathrm{r_{1_{in}}}\,\mathrm{r_{3_{in}}}\,\mathrm{R_L}\,\mathrm{r_{2_{out}}}\,\mathrm{r_{3_{out}}} + \mathrm{R_F}\,\mathrm{R_G}\,\mathrm{r_{2_{in}}}\,\mathrm{r_{3_{in}}}\,\mathrm{R_L}\,\mathrm{r_{1_{out}}}\,\mathrm{r_{3_{out}}}$$

$$+ \mathrm{R_C}\,\mathrm{R_D}\,\mathrm{r_{1_{in}}}\,\mathrm{R_L}\,\mathrm{r_{1_{out}}}\,\mathrm{r_{2_{out}}}\,\mathrm{r_{3_{out}}} + \mathrm{R_A}\,\mathrm{R_F}\,\mathrm{r_{2_{in}}}\,\mathrm{R_L}\,\mathrm{r_{1_{out}}}\,\mathrm{r_{2_{out}}}\,\mathrm{r_{3_{out}}} + \mathrm{R_C}\,\mathrm{R_D}\,\mathrm{r_{2_{in}}}\,\mathrm{R_L}\,\mathrm{r_{1_{out}}}\,\mathrm{r_{2_{out}}}\,\mathrm{r_{3_{out}}}$$

$$+ \mathrm{R_D}\,\mathrm{r_{1_{in}}}\,\mathrm{r_{2_{in}}}\,\mathrm{r_{3_{in}}}\,\mathrm{R_L}\,\mathrm{r_{1_{out}}}\,\mathrm{r_{3_{out}}} + \mathrm{R_D}\,\mathrm{r_{1_{in}}}\,\mathrm{r_{2_{in}}}\,\mathrm{r_{3_{in}}}\,\mathrm{R_L}\,\mathrm{r_{2_{out}}}\,\mathrm{r_{3_{out}}} + \mathrm{R_D}\,\mathrm{R_F}\,\mathrm{r_{1_{in}}}\,\mathrm{r_{2_{in}}}\,\mathrm{r_{1_{out}}}\,\mathrm{r_{2_{out}}}\,\mathrm{r_{3_{out}}}$$

$$+ \mathrm{R_D}\,\mathrm{R_F}\,\mathrm{R_G}\,\mathrm{R_L}\,\mathrm{r_{1_{out}}}\,\mathrm{r_{2_{out}}}\,\mathrm{r_{3_{out}}} + \mathrm{R_A}\,\mathrm{r_{1_{in}}}\,\mathrm{r_{2_{in}}}\,\mathrm{r_{3_{in}}}\,\mathrm{r_{1_{out}}}\,\mathrm{r_{2_{out}}}\,\mathrm{r_{3_{out}}} + \mathrm{R_B}\,\mathrm{R_F}\,\mathrm{r_{1_{in}}}\,\mathrm{R_L}\,\mathrm{r_{1_{out}}}\,\mathrm{r_{2_{out}}}\,\mathrm{r_{3_{out}}}$$

$$+ \mathrm{R_B}\,\mathrm{R_F}\,\mathrm{r_{2_{in}}}\,\mathrm{R_L}\,\mathrm{r_{1_{out}}}\,\mathrm{r_{2_{out}}}\,\mathrm{r_{3_{out}}} + \mathrm{R_E}\,\mathrm{r_{1_{in}}}\,\mathrm{r_{2_{in}}}\,\mathrm{r_{3_{in}}}\,\mathrm{R_L}\,\mathrm{r_{1_{out}}}\,\mathrm{r_{2_{out}}} + \mathrm{R_D}\,\mathrm{R_G}\,\mathrm{r_{1_{in}}}\,\mathrm{r_{3_{in}}}\,\mathrm{r_{1_{out}}}\,\mathrm{r_{2_{out}}}\,\mathrm{r_{3_{out}}}$$

$$+ \mathrm{R_E}\,\mathrm{R_F}\,\mathrm{r_{2_{in}}}\,\mathrm{r_{3_{in}}}\,\mathrm{r_{1_{out}}}\,\mathrm{r_{2_{out}}}\,\mathrm{r_{3_{out}}} + \mathrm{R_B}\,\mathrm{r_{1_{in}}}\,\mathrm{r_{2_{in}}}\,\mathrm{r_{3_{in}}}\,\mathrm{r_{1_{out}}}\,\mathrm{r_{2_{out}}}\,\mathrm{r_{3_{out}}}$$

$$+ \mathrm{R_C}\,\mathrm{R_F}\,\mathrm{r_{1_{in}}}\,\mathrm{R_L}\,\mathrm{r_{1_{out}}}\,\mathrm{r_{2_{out}}}\,\mathrm{r_{3_{out}}} + \mathrm{R_C}\,\mathrm{R_F}\,\mathrm{r_{2_{in}}}\,\mathrm{R_L}\,\mathrm{r_{1_{out}}}\,\mathrm{r_{2_{out}}}\,\mathrm{r_{3_{out}}} + \mathrm{R_B}\,\mathrm{R_G}\,\mathrm{r_{3_{in}}}\,\mathrm{R_L}\,\mathrm{r_{1_{out}}}\,\mathrm{r_{2_{out}}}\,\mathrm{r_{3_{out}}}$$

$$+ \mathrm{R_F}\,\mathrm{r_{1_{in}}}\,\mathrm{r_{2_{in}}}\,\mathrm{r_{3_{in}}}\,\mathrm{R_L}\,\mathrm{r_{1_{out}}}\,\mathrm{r_{3_{out}}} + \mathrm{R_F}\,\mathrm{r_{1_{in}}}\,\mathrm{r_{2_{in}}}\,\mathrm{r_{3_{in}}}\,\mathrm{R_L}\,\mathrm{r_{2_{out}}}\,\mathrm{r_{3_{out}}} + \mathrm{R_E}\,\mathrm{R_G}\,\mathrm{r_{1_{in}}}\,\mathrm{r_{2_{in}}}\,\mathrm{r_{1_{out}}}\,\mathrm{r_{2_{out}}}\,\mathrm{r_{3_{out}}}$$

$$+ \mathrm{R_C}\,\mathrm{r_{1_{in}}}\,\mathrm{r_{2_{in}}}\,\mathrm{r_{3_{in}}}\,\mathrm{r_{1_{out}}}\,\mathrm{r_{2_{out}}}\,\mathrm{r_{3_{out}}} + \mathrm{R_D}\,\mathrm{R_F}\,\mathrm{r_{1_{in}}}\,\mathrm{R_L}\,\mathrm{r_{1_{out}}}\,\mathrm{r_{2_{out}}}\,\mathrm{r_{3_{out}}}$$

$$+ R_D\, R_F\, r_{2_{in}}\, R_L\, r_{1_{out}}\, r_{2_{out}}\, r_{3_{out}} + R_G\, r_{1_{in}}\, r_{2_{in}}\, r_{3_{in}}\, R_L\, r_{1_{out}}\, r_{2_{out}} + R_G\, r_{1_{in}}\, r_{2_{in}}\, r_{3_{in}}\, R_L\, r_{2_{out}}\, r_{3_{out}}$$

$$+ R_F\, R_G\, r_{1_{in}}\, r_{2_{in}}\, r_{1_{out}}\, r_{2_{out}}\, r_{3_{out}} + R_F\, R_G\, r_{1_{in}}\, r_{3_{in}}\, r_{1_{out}}\, r_{2_{out}}\, r_{3_{out}}$$

$$+ R_D\, R_G\, r_{1_{in}}\, R_L\, r_{1_{out}}\, r_{2_{out}}\, r_{3_{out}} + R_D\, R_G\, r_{3_{in}}\, R_L\, r_{1_{out}}\, r_{2_{out}}\, r_{3_{out}} + R_B\, r_{1_{in}}\, r_{2_{in}}\, R_L\, r_{1_{out}}\, r_{2_{out}}\, r_{3_{out}}$$

$$+ R_B\, r_{2_{in}}\, r_{3_{in}}\, R_L\, r_{1_{out}}\, r_{2_{out}}\, r_{3_{out}} + R_E\, r_{1_{in}}\, r_{2_{in}}\, r_{3_{in}}\, r_{1_{out}}\, r_{2_{out}}\, r_{3_{out}}$$

$$+ R_F\, r_{1_{in}}\, r_{2_{in}}\, r_{3_{in}}\, r_{1_{out}}\, r_{2_{out}}\, r_{3_{out}} + R_F\, R_G\, r_{1_{in}}\, R_L\, r_{1_{out}}\, r_{2_{out}}\, r_{3_{out}} + R_F\, R_G\, r_{2_{in}}\, R_L\, r_{1_{out}}\, r_{2_{out}}\, r_{3_{out}}$$

$$+ R_D\, r_{1_{in}}\, r_{2_{in}}\, R_L\, r_{1_{out}}\, r_{2_{out}}\, r_{3_{out}} + R_D\, r_{1_{in}}\, r_{3_{in}}\, R_L\, r_{1_{out}}\, r_{2_{out}}\, r_{3_{out}}$$

$$+ R_G\, r_{1_{in}}\, r_{2_{in}}\, r_{3_{in}}\, r_{1_{out}}\, r_{2_{out}}\, r_{3_{out}} + R_F\, r_{1_{in}}\, r_{3_{in}}\, R_L\, r_{1_{out}}\, r_{2_{out}}\, r_{3_{out}}$$

$$+ R_G\, r_{1_{in}}\, r_{2_{in}}\, R_L\, r_{1_{out}}\, r_{2_{out}}\, r_{3_{out}} + R_G\, r_{2_{in}}\, r_{3_{in}}\, R_L\, r_{1_{out}}\, r_{2_{out}}\, r_{3_{out}}$$

$$+ A_3\, R_A\, R_B\, R_C\, R_D\, R_G\, r_{3_{in}}\, R_L + A_3\, R_A\, R_B\, R_C\, R_F\, R_G\, r_{3_{in}}\, R_L + A_3\, R_A\, R_B\, R_C\, R_D\, r_{1_{in}}\, r_{3_{in}}\, R_L$$

$$+ A_2\, R_A\, R_C\, R_D\, R_E\, R_G\, r_{2_{in}}\, R_L + A_1\, R_B\, R_C\, R_D\, R_E\, R_G\, r_{1_{in}}\, R_L + A_2\, R_A\, R_C\, R_D\, R_F\, R_G\, r_{2_{in}}\, R_L$$

$$+ A_3\, R_A\, R_B\, R_C\, R_F\, r_{2_{in}}\, r_{3_{in}}\, R_L + A_1\, R_B\, R_C\, R_D\, R_F\, R_G\, r_{1_{in}}\, R_L + A_2\, R_A\, R_C\, R_E\, R_F\, R_G\, r_{2_{in}}\, R_L$$

$$+ A_1\, R_B\, R_C\, R_E\, R_F\, R_G\, r_{1_{in}}\, R_L + A_2\, R_A\, R_D\, R_E\, R_F\, R_G\, r_{2_{in}}\, R_L + A_1\, R_B\, R_C\, R_D\, R_E\, r_{1_{in}}\, r_{2_{in}}\, R_L$$

$$+ A_2\, R_A\, R_C\, R_D\, R_E\, R_G\, r_{2_{in}}\, r_{3_{out}} + A_1\, R_B\, R_D\, R_E\, R_F\, R_G\, r_{1_{in}}\, R_L + A_1\, R_B\, R_C\, R_D\, R_F\, r_{1_{in}}\, r_{2_{in}}\, R_L$$

$$+ A_2\, R_A\, R_C\, R_D\, R_G\, r_{2_{in}}\, r_{3_{in}}\, R_L + A_3\, R_A\, R_C\, R_D\, R_G\, r_{2_{in}}\, r_{3_{in}}\, R_L$$

$$+ A_2\, R_A\, R_C\, R_D\, R_F\, R_G\, r_{2_{in}}\, r_{3_{out}} + A_1\, R_B\, R_C\, R_E\, R_F\, r_{1_{in}}\, r_{2_{in}}\, R_L + A_1\, R_B\, R_C\, R_D\, R_G\, r_{1_{in}}\, r_{3_{in}}\, R_L$$

$$+ A_3\, R_B\, R_C\, R_D\, R_G\, r_{1_{in}}\, r_{3_{in}}\, R_L + A_1\, R_B\, R_C\, R_D\, R_F\, R_G\, r_{1_{in}}\, r_{3_{out}}$$

$$+ A_2\, R_A\, R_C\, R_D\, R_E\, r_{1_{in}}\, r_{2_{in}}\, r_{3_{out}} + A_1\, R_B\, R_D\, R_E\, R_F\, r_{1_{in}}\, r_{2_{in}}\, R_L$$

$$+ A_2\, R_A\, R_D\, R_E\, R_G\, r_{2_{in}}\, r_{3_{in}}\, R_L + A_3\, R_A\, R_C\, R_F\, R_G\, r_{2_{in}}\, r_{3_{in}}\, R_L + A_1\, R_B\, R_C\, R_E\, R_F\, R_G\, r_{1_{in}}\, r_{3_{out}}$$

$$+ A_2\, R_A\, R_C\, R_D\, r_{1_{in}}\, r_{2_{in}}\, r_{3_{in}}\, R_L + A_3\, R_A\, R_C\, R_D\, r_{1_{in}}\, r_{2_{in}}\, r_{3_{in}}\, R_L$$

$$+ A_2\, R_A\, R_C\, R_D\, R_F\, r_{1_{in}}\, r_{2_{in}}\, r_{3_{out}} + A_1\, R_B\, R_C\, R_F\, R_G\, r_{1_{in}}\, r_{3_{in}}\, R_L$$

$$+ A_3\, R_B\, R_C\, R_F\, R_G\, r_{1_{in}}\, r_{3_{in}}\, R_L + A_1\, R_B\, R_D\, R_E\, R_F\, R_G\, r_{1_{in}}\, r_{3_{out}}$$

$$+ A_3\, R_B\, R_C\, R_D\, r_{1_{in}}\, r_{2_{in}}\, r_{3_{in}}\, R_L + A_1\, R_B\, R_C\, R_D\, R_F\, r_{1_{in}}\, r_{2_{in}}\, r_{3_{out}}$$

$$+ A_2\, R_A\, R_C\, R_D\, R_G\, r_{2_{in}}\, r_{3_{in}}\, r_{3_{out}} + A_1\, R_C\, R_D\, R_E\, R_G\, r_{1_{in}}\, r_{2_{in}}\, R_L$$

$$+ A_2\, R_A\, R_E\, R_F\, R_G\, r_{2_{in}}\, r_{3_{in}}\, R_L + A_3\, R_A\, R_B\, R_C\, R_G\, r_{3_{in}}\, R_L\, r_{2_{out}}$$

$$+ A_2\, R_A\, R_D\, R_E\, r_{1_{in}}\, r_{2_{in}}\, r_{3_{in}}\, R_L + A_3\, R_A\, R_C\, R_F\, r_{1_{in}}\, r_{2_{in}}\, r_{3_{in}}\, R_L$$

$$+ A_1\, R_B\, R_C\, R_D\, R_G\, r_{1_{in}}\, r_{3_{in}}\, r_{3_{out}} + A_2\, R_A\, R_D\, R_E\, R_F\, r_{1_{in}}\, r_{2_{in}}\, r_{3_{out}}$$

$$+ A_1\,R_B\,R_E\,R_F\,R_G\,r_{1_{in}}\,r_{3_{in}}\,R_L + A_2\,R_C\,R_D\,R_F\,R_G\,r_{1_{in}}\,r_{2_{in}}\,R_L + A_3\,R_A\,R_B\,R_D\,R_G\,r_{3_{in}}\,R_L\,r_{1_{out}}$$

$$+ A_1\,R_B\,R_D\,R_E\,r_{1_{in}}\,r_{2_{in}}\,r_{3_{in}}\,R_L + A_3\,R_B\,R_C\,R_F\,r_{1_{in}}\,r_{2_{in}}\,r_{3_{in}}\,R_L$$

$$+ A_2\,R_A\,R_C\,R_F\,R_G\,r_{2_{in}}\,r_{3_{in}}\,r_{3_{out}} + A_2\,R_A\,R_D\,R_E\,R_G\,r_{2_{in}}\,r_{3_{in}}\,r_{3_{out}}$$

$$+ A_1\,R_C\,R_E\,R_F\,R_G\,r_{1_{in}}\,r_{2_{in}}\,R_L + A_2\,R_C\,R_E\,R_F\,R_G\,r_{1_{in}}\,r_{2_{in}}\,R_L + A_2\,R_A\,R_C\,R_D\,R_G\,r_{2_{in}}\,R_L\,r_{3_{out}}$$

$$+ A_2\,R_A\,R_E\,R_F\,r_{1_{in}}\,r_{2_{in}}\,r_{3_{in}}\,R_L + A_1\,R_B\,R_C\,R_F\,R_G\,r_{1_{in}}\,r_{3_{in}}\,r_{3_{out}}$$

$$+ A_3\,R_A\,R_B\,R_C\,r_{1_{in}}\,r_{3_{in}}\,R_L\,r_{2_{out}} + A_3\,R_A\,R_B\,R_C\,r_{2_{in}}\,r_{3_{in}}\,R_L\,r_{2_{out}}$$

$$+ A_1\,R_D\,R_E\,R_F\,R_G\,r_{1_{in}}\,r_{2_{in}}\,R_L + A_2\,R_D\,R_E\,R_F\,R_G\,r_{1_{in}}\,r_{2_{in}}\,R_L + A_1\,R_B\,R_C\,R_D\,R_G\,r_{1_{in}}\,R_L\,r_{3_{out}}$$

$$+ A_3\,R_B\,R_C\,R_D\,R_G\,r_{3_{in}}\,R_L\,r_{1_{out}} + A_1\,R_B\,R_E\,R_F\,r_{1_{in}}\,r_{2_{in}}\,r_{3_{in}}\,R_L$$

$$+ A_2\,R_C\,R_D\,R_E\,R_G\,r_{1_{in}}\,r_{2_{in}}\,r_{3_{out}} + A_2\,R_A\,R_E\,R_F\,R_G\,r_{2_{in}}\,r_{3_{in}}\,r_{3_{out}}$$

$$+ A_3\,R_A\,R_B\,R_D\,r_{2_{in}}\,r_{3_{in}}\,R_L\,r_{1_{out}} + A_2\,R_A\,R_C\,R_F\,r_{1_{in}}\,r_{2_{in}}\,r_{3_{in}}\,r_{3_{out}}$$

$$+ A_1\,R_B\,R_C\,R_E\,R_G\,r_{1_{in}}\,R_L\,r_{2_{out}} + A_2\,R_A\,R_D\,R_E\,R_G\,r_{2_{in}}\,R_L\,r_{1_{out}}$$

$$+ A_3\,R_A\,R_C\,R_F\,R_G\,r_{3_{in}}\,R_L\,r_{2_{out}} + A_1\,R_C\,R_D\,R_G\,r_{1_{in}}\,r_{2_{in}}\,r_{3_{in}}\,R_L$$

$$+ A_3\,R_C\,R_D\,R_G\,r_{1_{in}}\,r_{2_{in}}\,r_{3_{in}}\,R_L + A_1\,R_C\,R_D\,R_F\,R_G\,r_{1_{in}}\,r_{2_{in}}\,r_{3_{out}}$$

$$+ A_2\,R_A\,R_C\,R_D\,r_{1_{in}}\,r_{2_{in}}\,R_L\,r_{3_{out}} + A_2\,R_C\,R_D\,R_F\,R_G\,r_{1_{in}}\,r_{2_{in}}\,r_{3_{out}}$$

$$+ A_3\,R_A\,R_C\,R_D\,r_{2_{in}}\,r_{3_{in}}\,R_L\,r_{2_{out}} + A_1\,R_B\,R_C\,R_F\,r_{1_{in}}\,r_{2_{in}}\,r_{3_{in}}\,r_{3_{out}}$$

$$+ A_1\,R_B\,R_C\,R_F\,R_G\,r_{1_{in}}\,R_L\,r_{2_{out}} + A_1\,R_B\,R_C\,R_F\,R_G\,r_{1_{in}}\,R_L\,r_{3_{out}}$$

$$+ A_2\,R_A\,R_D\,R_F\,R_G\,r_{2_{in}}\,R_L\,r_{3_{out}} + A_3\,R_B\,R_C\,R_F\,R_G\,r_{3_{in}}\,R_L\,r_{1_{out}}$$

$$+ A_1\,R_C\,R_E\,R_F\,R_G\,r_{1_{in}}\,r_{2_{in}}\,r_{3_{out}} + A_2\,R_C\,R_E\,R_F\,R_G\,r_{1_{in}}\,r_{2_{in}}\,r_{3_{out}}$$

$$+ A_3\,R_B\,R_C\,R_D\,r_{1_{in}}\,r_{3_{in}}\,R_L\,r_{1_{out}} + A_3\,R_A\,R_B\,R_F\,r_{2_{in}}\,r_{3_{in}}\,R_L\,r_{1_{out}}$$

$$+ A_2\,R_A\,R_E\,R_F\,r_{1_{in}}\,r_{2_{in}}\,r_{3_{in}}\,r_{3_{out}} + A_1\,R_C\,R_D\,R_E\,R_G\,r_{1_{in}}\,R_L\,r_{2_{out}}$$

$$+ A_2\,R_A\,R_E\,R_F\,R_G\,r_{2_{in}}\,R_L\,r_{1_{out}} + A_2\,R_C\,R_D\,R_E\,R_G\,r_{2_{in}}\,R_L\,r_{1_{out}}$$

$$+ A_1\,R_D\,R_E\,R_G\,r_{1_{in}}\,r_{2_{in}}\,r_{3_{in}}\,R_L + A_2\,R_C\,R_F\,R_G\,r_{1_{in}}\,r_{2_{in}}\,r_{3_{in}}\,R_L + A_2\,R_D\,R_E\,R_G\,r_{1_{in}}\,r_{2_{in}}\,r_{3_{in}}\,R_L$$

$$+ A_1\,R_B\,R_C\,R_E\,r_{1_{in}}\,r_{2_{in}}\,R_L\,r_{2_{out}} + A_1\,R_D\,R_E\,R_F\,R_G\,r_{1_{in}}\,r_{2_{in}}\,r_{3_{out}}$$

$$+ A_2\,R_A\,R_C\,R_F\,r_{1_{in}}\,r_{2_{in}}\,R_L\,r_{3_{out}} + A_2\,R_D\,R_E\,R_F\,R_G\,r_{1_{in}}\,r_{2_{in}}\,r_{3_{out}}$$

$$+ A_3\,R_A\,R_C\,R_F\,r_{2_{in}}\,r_{3_{in}}\,R_L\,r_{2_{out}} + A_1\,R_B\,R_E\,R_F\,r_{1_{in}}\,r_{2_{in}}\,r_{3_{in}}\,r_{3_{out}}$$

$$+ A_1\,R_C\,R_D\,R_F\,R_G\,r_{1_{in}}\,R_L\,r_{2_{out}} + A_2\,R_C\,R_D\,R_F\,R_G\,r_{2_{in}}\,R_L\,r_{1_{out}}$$

$$+ A_1\,R_B\,R_C\,R_F\,r_{1_{in}}\,r_{2_{in}}\,R_L\,r_{3_{out}} + A_2\,R_A\,R_D\,R_F\,r_{1_{in}}\,r_{2_{in}}\,R_L\,r_{1_{out}}$$

$$+ A_3\,R_B\,R_C\,R_F\,r_{1_{in}}\,r_{3_{in}}\,R_L\,r_{1_{out}} + A_3\,R_B\,R_C\,R_F\,r_{2_{in}}\,r_{3_{in}}\,R_L\,r_{1_{out}}$$

$$+ A_1\,R_B\,R_C\,R_E\,R_G\,r_{1_{in}}\,r_{2_{out}}\,r_{3_{out}} + A_2\,R_A\,R_D\,R_E\,R_G\,r_{2_{in}}\,r_{1_{out}}\,r_{3_{out}}$$

$$+ A_2\,R_C\,R_D\,R_G\,r_{1_{in}}\,r_{2_{in}}\,r_{3_{in}}\,r_{3_{out}} + A_1\,R_C\,R_E\,R_F\,R_G\,r_{1_{in}}\,R_L\,r_{2_{out}}$$

$$+ A_1\,R_E\,R_F\,R_G\,r_{1_{in}}\,r_{2_{in}}\,r_{3_{in}}\,R_L + A_2\,R_E\,R_F\,R_G\,r_{1_{in}}\,r_{2_{in}}\,r_{3_{in}}\,R_L$$

$$+ A_1\,R_C\,R_D\,R_E\,r_{1_{in}}\,r_{2_{in}}\,R_L\,r_{2_{out}} + A_1\,R_B\,R_C\,R_G\,r_{1_{in}}\,r_{3_{in}}\,R_L\,r_{2_{out}}$$

$$+ A_2\,R_A\,R_E\,R_F\,r_{1_{in}}\,r_{2_{in}}\,R_L\,r_{1_{out}} + A_2\,R_C\,R_D\,R_E\,r_{1_{in}}\,r_{2_{in}}\,R_L\,r_{1_{out}}$$

$$+ A_2\,R_A\,R_D\,R_G\,r_{2_{in}}\,r_{3_{in}}\,R_L\,r_{3_{out}} + A_3\,R_A\,R_D\,R_G\,r_{2_{in}}\,r_{3_{in}}\,R_L\,r_{1_{out}}$$

$$+ A_1\,R_B\,R_C\,R_F\,R_G\,r_{1_{in}}\,r_{2_{out}}\,r_{3_{out}} + A_2\,R_A\,R_D\,R_F\,R_G\,r_{2_{in}}\,r_{1_{out}}\,r_{3_{out}}$$

$$+ A_2\,R_D\,R_E\,R_F\,R_G\,r_{2_{in}}\,R_L\,r_{1_{out}} + A_1\,R_B\,R_E\,R_F\,r_{1_{in}}\,r_{2_{in}}\,R_L\,r_{2_{out}}$$

$$+ A_1\,R_B\,R_D\,R_G\,r_{1_{in}}\,r_{3_{in}}\,R_L\,r_{3_{out}} + A_2\,R_B\,R_E\,R_F\,r_{1_{in}}\,r_{2_{in}}\,R_L\,r_{1_{out}}$$

$$+ A_3\,R_B\,R_D\,R_G\,r_{1_{in}}\,r_{3_{in}}\,R_L\,r_{1_{out}} + A_1\,R_C\,R_D\,R_E\,R_G\,r_{1_{in}}\,r_{2_{out}}\,r_{3_{out}}$$

$$+ A_2\,R_C\,R_D\,R_E\,R_G\,r_{2_{in}}\,r_{1_{out}}\,r_{3_{out}} + A_1\,R_C\,R_F\,R_G\,r_{1_{in}}\,r_{2_{in}}\,r_{3_{in}}\,r_{3_{out}}$$

$$+ A_2\,R_C\,R_F\,R_G\,r_{1_{in}}\,r_{2_{in}}\,r_{3_{in}}\,r_{3_{out}} + A_2\,R_D\,R_E\,R_G\,r_{1_{in}}\,r_{2_{in}}\,r_{3_{in}}\,r_{3_{out}}$$

$$+ A_1\,R_B\,R_C\,R_E\,r_{1_{in}}\,r_{2_{in}}\,r_{2_{out}}\,r_{3_{out}} + A_2\,R_A\,R_D\,R_E\,r_{1_{in}}\,r_{2_{in}}\,r_{1_{out}}\,r_{3_{out}}$$

$$+ A_1\,R_B\,R_E\,R_G\,r_{1_{in}}\,r_{3_{in}}\,R_L\,r_{2_{out}} + A_1\,R_C\,R_D\,R_G\,r_{1_{in}}\,r_{2_{in}}\,R_L\,r_{3_{out}}$$

$$+ A_2\,R_C\,R_E\,R_F\,r_{1_{in}}\,r_{2_{in}}\,R_L\,r_{1_{out}} + A_2\,R_A\,R_F\,R_G\,r_{2_{in}}\,r_{3_{in}}\,R_L\,r_{1_{out}}$$

$$+ A_2\,R_C\,R_D\,R_G\,r_{2_{in}}\,r_{3_{in}}\,R_L\,r_{1_{out}} + A_2\,R_A\,R_F\,R_G\,r_{2_{in}}\,r_{3_{in}}\,R_L\,r_{3_{out}}$$

$$+ A_3\,R_C\,R_D\,R_G\,r_{1_{in}}\,r_{3_{in}}\,R_L\,r_{2_{out}} + A_3\,R_C\,R_D\,R_G\,r_{2_{in}}\,r_{3_{in}}\,R_L\,r_{1_{out}}$$

$$+ A_1\,R_C\,R_D\,R_F\,R_G\,r_{1_{in}}\,r_{2_{out}}\,r_{3_{out}} + A_2\,R_C\,R_D\,R_F\,R_G\,r_{2_{in}}\,r_{1_{out}}\,r_{3_{out}}$$

$$+ A_2\,R_A\,R_D\,r_{1_{in}}\,r_{2_{in}}\,r_{3_{in}}\,R_L\,r_{1_{out}} + A_2\,R_A\,R_D\,r_{1_{in}}\,r_{2_{in}}\,r_{3_{in}}\,R_L\,r_{3_{out}}$$

$$+ A_3\,R_B\,R_C\,r_{1_{in}}\,r_{2_{in}}\,r_{3_{in}}\,R_L\,r_{2_{out}} + A_1\,R_B\,R_C\,R_F\,r_{1_{in}}\,r_{2_{in}}\,r_{2_{out}}\,r_{3_{out}}$$

$$+ A_1\,R_C\,R_E\,R_G\,r_{1_{in}}\,r_{2_{in}}\,R_L\,r_{2_{out}} + A_1\,R_D\,R_E\,R_F\,r_{1_{in}}\,r_{2_{in}}\,R_L\,r_{2_{out}}$$

$$+ A_2\,R_D\,R_E\,R_F\,r_{1_{in}}\,r_{2_{in}}\,R_L\,r_{1_{out}} + A_3\,R_B\,R_F\,R_G\,r_{1_{in}}\,r_{3_{in}}\,R_L\,r_{1_{out}}$$

$$+ A_2\,R_C\,R_E\,R_F\,R_G\,r_{2_{in}}\,r_{1_{out}}\,r_{3_{out}} + A_1\,R_B\,R_D\,r_{1_{in}}\,r_{2_{in}}\,r_{3_{in}}\,R_L\,r_{3_{out}}$$

$$+ A_2\,R_E\,R_F\,R_G\,r_{1_{in}}\,r_{2_{in}}\,r_{3_{in}}\,r_{3_{out}} + A_3\,R_B\,R_D\,r_{1_{in}}\,r_{2_{in}}\,r_{3_{in}}\,R_L\,r_{1_{out}}$$

$$+ A_1\,R_C\,R_D\,R_E\,r_{1_{in}}\,r_{2_{in}}\,r_{2_{out}}\,r_{3_{out}} + A_1\,R_B\,R_C\,R_G\,r_{1_{in}}\,r_{3_{in}}\,r_{2_{out}}\,r_{3_{out}}$$

$$+ A_2\,R_C\,R_D\,R_E\,r_{1_{in}}\,r_{2_{in}}\,r_{1_{out}}\,r_{3_{out}} + A_2\,R_A\,R_D\,R_G\,r_{2_{in}}\,r_{3_{in}}\,r_{1_{out}}\,r_{3_{out}}$$

$$+ A_1\,R_C\,R_F\,R_G\,r_{1_{in}}\,r_{2_{in}}\,R_L\,r_{3_{out}} + A_1\,R_C\,R_F\,R_G\,r_{1_{in}}\,r_{3_{in}}\,R_L\,r_{2_{out}}$$

$$+ A_2\,R_D\,R_E\,R_G\,r_{1_{in}}\,r_{2_{in}}\,R_L\,r_{1_{out}} + A_2\,R_C\,R_F\,R_G\,r_{1_{in}}\,r_{2_{in}}\,R_L\,r_{3_{out}}$$

$$+ A_2\,R_D\,R_E\,R_G\,r_{2_{in}}\,r_{3_{in}}\,R_L\,r_{1_{out}} + A_3\,R_C\,R_F\,R_G\,r_{1_{in}}\,r_{3_{in}}\,R_L\,r_{2_{out}}$$

$$+ A_1\,R_D\,R_E\,R_F\,R_G\,r_{1_{in}}\,r_{2_{out}}\,r_{3_{out}} + A_2\,R_D\,R_E\,R_F\,R_G\,r_{2_{in}}\,r_{1_{out}}\,r_{3_{out}}$$

$$+ A_1\,R_B\,R_E\,r_{1_{in}}\,r_{2_{in}}\,r_{3_{in}}\,R_L\,r_{2_{out}} + A_1\,R_C\,R_D\,r_{1_{in}}\,r_{2_{in}}\,r_{3_{in}}\,R_L\,r_{2_{out}}$$

$$+ A_2\,R_C\,R_D\,r_{1_{in}}\,r_{2_{in}}\,r_{3_{in}}\,R_L\,r_{1_{out}} + A_2\,R_A\,R_F\,r_{1_{in}}\,r_{2_{in}}\,r_{3_{in}}\,R_L\,r_{3_{out}}$$

$$+ A_3\,R_C\,R_D\,r_{1_{in}}\,r_{2_{in}}\,r_{3_{in}}\,R_L\,r_{1_{out}} + A_3\,R_C\,R_D\,r_{1_{in}}\,r_{2_{in}}\,r_{3_{in}}\,R_L\,r_{2_{out}}$$

$$+ A_1\,R_C\,R_D\,R_F\,r_{1_{in}}\,r_{2_{in}}\,r_{2_{out}}\,r_{3_{out}} + A_2\,R_B\,R_E\,R_F\,r_{1_{in}}\,r_{2_{in}}\,r_{1_{out}}\,r_{3_{out}}$$

$$+ A_1\,R_D\,R_F\,R_G\,r_{1_{in}}\,r_{2_{in}}\,R_L\,r_{3_{out}} + A_2\,R_D\,R_F\,R_G\,r_{1_{in}}\,r_{2_{in}}\,R_L\,r_{1_{out}}$$

$$+ A_1\,R_B\,R_F\,r_{1_{in}}\,r_{2_{in}}\,r_{3_{in}}\,R_L\,r_{3_{out}} + A_3\,R_B\,R_F\,r_{1_{in}}\,r_{2_{in}}\,r_{3_{in}}\,R_L\,r_{1_{out}}$$

$$+ A_1\,R_B\,R_E\,R_G\,r_{1_{in}}\,r_{3_{in}}\,r_{2_{out}}\,r_{3_{out}} + A_1\,R_C\,R_D\,R_G\,r_{1_{in}}\,r_{3_{in}}\,r_{2_{out}}\,r_{3_{out}}$$

$$+ A_2\,R_A\,R_F\,R_G\,r_{2_{in}}\,r_{3_{in}}\,r_{1_{out}}\,r_{3_{out}} + A_2\,R_C\,R_D\,R_G\,r_{2_{in}}\,r_{3_{in}}\,r_{1_{out}}\,r_{3_{out}}$$

$$+ A_2\,R_A\,R_D\,r_{1_{in}}\,r_{2_{in}}\,r_{3_{in}}\,r_{1_{out}}\,r_{3_{out}} + A_1\,R_E\,R_F\,R_G\,r_{1_{in}}\,r_{2_{in}}\,R_L\,r_{2_{out}}$$

$$+ A_2\,R_E\,R_F\,R_G\,r_{1_{in}}\,r_{2_{in}}\,R_L\,r_{1_{out}} + A_2\,R_E\,R_F\,R_G\,r_{2_{in}}\,r_{3_{in}}\,R_L\,r_{1_{out}}$$

$$+ A_2\,R_A\,R_D\,R_G\,r_{2_{in}}\,R_L\,r_{1_{out}}\,r_{3_{out}} + A_3\,R_A\,R_D\,R_G\,r_{3_{in}}\,R_L\,r_{1_{out}}\,r_{2_{out}}$$

$$+ A_1\,R_C\,R_F\,r_{1_{in}}\,r_{2_{in}}\,r_{3_{in}}\,R_L\,r_{2_{out}} + A_1\,R_D\,R_E\,r_{1_{in}}\,r_{2_{in}}\,r_{3_{in}}\,R_L\,r_{2_{out}}$$

$$+ A_2\,R_D\,R_E\,r_{1_{in}}\,r_{2_{in}}\,r_{3_{in}}\,R_L\,r_{1_{out}} + A_3\,R_C\,R_F\,r_{1_{in}}\,r_{2_{in}}\,r_{3_{in}}\,R_L\,r_{1_{out}}$$

$$+ A_1\,R_C\,R_E\,R_G\,r_{1_{in}}\,r_{2_{in}}\,r_{2_{out}}\,r_{3_{out}} + A_1\,R_D\,R_E\,R_F\,r_{1_{in}}\,r_{2_{in}}\,r_{2_{out}}\,r_{3_{out}}$$

$$+ A_3\,R_A\,R_B\,r_{1_{in}}\,r_{3_{in}}\,R_L\,r_{1_{out}}\,r_{2_{out}} + A_3\,R_A\,R_B\,r_{2_{in}}\,r_{3_{in}}\,R_L\,r_{1_{out}}\,r_{2_{out}}$$

$$+ A_3\,R_C\,R_G\,r_{1_{in}}\,r_{2_{in}}\,r_{3_{in}}\,R_L\,r_{2_{out}} + A_1\,R_C\,R_F\,R_G\,r_{1_{in}}\,r_{2_{in}}\,r_{2_{out}}\,r_{3_{out}}$$

$$+ A_1\,R_D\,R_E\,R_G\,r_{1_{in}}\,r_{3_{in}}\,r_{2_{out}}\,r_{3_{out}} + A_2\,R_D\,R_E\,R_G\,r_{1_{in}}\,r_{2_{in}}\,r_{1_{out}}\,r_{3_{out}}$$

$$+ A_2\,R_D\,R_E\,R_G\,r_{2_{in}}\,r_{3_{in}}\,r_{1_{out}}\,r_{3_{out}} + A_1\,R_B\,R_E\,r_{1_{in}}\,r_{2_{in}}\,r_{3_{in}}\,r_{2_{out}}\,r_{3_{out}}$$

$$+ A_2\,R_A\,R_F\,r_{1_{in}}\,r_{2_{in}}\,r_{3_{in}}\,r_{1_{out}}\,r_{3_{out}} + A_2\,R_C\,R_D\,r_{1_{in}}\,r_{2_{in}}\,r_{3_{in}}\,r_{1_{out}}\,r_{3_{out}}$$

$$+ A_2\,R_A\,R_F\,R_G\,r_{2_{in}}\,R_L\,r_{1_{out}}\,r_{3_{out}} + A_2\,R_C\,R_D\,R_G\,r_{2_{in}}\,R_L\,r_{1_{out}}\,r_{3_{out}}$$

$$+ A_3\,R_C\,R_D\,R_G\,r_{3_{in}}\,R_L\,r_{1_{out}}\,r_{2_{out}} + A_1\,R_E\,R_F\,r_{1_{in}}\,r_{2_{in}}\,r_{3_{in}}\,R_L\,r_{2_{out}}$$

$$+ A_2\,R_D\,R_G\,r_{1_{in}}\,r_{2_{in}}\,r_{3_{in}}\,R_L\,r_{1_{out}} + A_2\,R_E\,R_F\,r_{1_{in}}\,r_{2_{in}}\,r_{3_{in}}\,R_L\,r_{1_{out}}$$

$$+ A_3\,R_D\,R_G\,r_{1_{in}}\,r_{2_{in}}\,r_{3_{in}}\,R_L\,r_{1_{out}} + A_1\,R_B\,R_C\,r_{1_{in}}\,r_{2_{in}}\,R_L\,r_{2_{out}}\,r_{3_{out}}$$

$$+ A_2\,R_D\,R_F\,R_G\,r_{1_{in}}\,r_{2_{in}}\,r_{1_{out}}\,r_{3_{out}} + A_3\,R_A\,R_D\,r_{1_{in}}\,r_{3_{in}}\,R_L\,r_{1_{out}}\,r_{2_{out}}$$

$$+ A_3\,R_A\,R_D\,r_{2_{in}}\,r_{3_{in}}\,R_L\,r_{1_{out}}\,r_{2_{out}} + A_3\,R_B\,R_C\,r_{2_{in}}\,r_{3_{in}}\,R_L\,r_{1_{out}}\,r_{2_{out}}$$

$$+ A_1\,R_E\,R_G\,r_{1_{in}}\,r_{2_{in}}\,r_{3_{in}}\,R_L\,r_{2_{out}} + A_1\,R_E\,R_F\,R_G\,r_{1_{in}}\,r_{2_{in}}\,r_{2_{out}}\,r_{3_{out}}$$

$$+ A_2\,R_E\,R_F\,R_G\,r_{1_{in}}\,r_{2_{in}}\,r_{1_{out}}\,r_{3_{out}} + A_2\,R_E\,R_F\,R_G\,r_{2_{in}}\,r_{3_{in}}\,r_{1_{out}}\,r_{3_{out}}$$

$$+ A_1\,R_D\,R_E\,r_{1_{in}}\,r_{2_{in}}\,r_{3_{in}}\,r_{2_{out}}\,r_{3_{out}} + A_2\,R_C\,R_F\,r_{1_{in}}\,r_{2_{in}}\,r_{3_{in}}\,r_{1_{out}}\,r_{3_{out}}$$

$$+ A_1\,R_C\,R_F\,R_G\,r_{1_{in}}\,R_L\,r_{2_{out}}\,r_{3_{out}} + A_2\,R_C\,R_F\,R_G\,r_{2_{in}}\,R_L\,r_{1_{out}}\,r_{3_{out}}$$

$$+ A_1\,R_F\,R_G\,r_{1_{in}}\,r_{2_{in}}\,r_{3_{in}}\,R_L\,r_{3_{out}} + A_2\,R_F\,R_G\,r_{1_{in}}\,r_{2_{in}}\,r_{3_{in}}\,R_L\,r_{1_{out}}$$

$$+ A_3\,R_F\,R_G\,r_{1_{in}}\,r_{2_{in}}\,r_{3_{in}}\,R_L\,r_{1_{out}} + A_1\,R_A\,R_F\,r_{1_{in}}\,r_{2_{in}}\,R_L\,r_{2_{out}}\,r_{3_{out}}$$

$$+ A_2\,R_A\,R_F\,r_{1_{in}}\,r_{2_{in}}\,R_L\,r_{1_{out}}\,r_{3_{out}} + A_2\,R_C\,R_D\,r_{1_{in}}\,r_{2_{in}}\,R_L\,r_{1_{out}}\,r_{3_{out}}$$

$$+ A_3\,R_C\,R_D\,r_{1_{in}}\,r_{3_{in}}\,R_L\,r_{1_{out}}\,r_{2_{out}} + A_3\,R_A\,R_F\,r_{2_{in}}\,r_{3_{in}}\,R_L\,r_{1_{out}}\,r_{2_{out}}$$

$$+ A_1\,R_C\,R_G\,r_{1_{in}}\,r_{2_{in}}\,r_{3_{in}}\,r_{2_{out}}\,r_{3_{out}} + A_1\,R_D\,R_F\,R_G\,r_{1_{in}}\,R_L\,r_{2_{out}}\,r_{3_{out}}$$

$$+ A_1\,R_B\,R_F\,r_{1_{in}}\,r_{2_{in}}\,R_L\,r_{2_{out}}\,r_{3_{out}} + A_2\,R_B\,R_F\,r_{1_{in}}\,r_{2_{in}}\,R_L\,r_{1_{out}}\,r_{3_{out}}$$

$$+ A_1\,R_E\,R_F\,r_{1_{in}}\,r_{2_{in}}\,r_{3_{in}}\,r_{2_{out}}\,r_{3_{out}} + A_2\,R_D\,R_G\,r_{1_{in}}\,r_{2_{in}}\,r_{3_{in}}\,r_{1_{out}}\,r_{3_{out}}$$

$$+ A_1\,R_C\,R_F\,r_{1_{in}}\,r_{2_{in}}\,R_L\,r_{2_{out}}\,r_{3_{out}} + A_1\,R_B\,R_G\,r_{1_{in}}\,r_{3_{in}}\,R_L\,r_{2_{out}}\,r_{3_{out}}$$

$$+ A_3\,R_B\,R_G\,r_{1_{in}}\,r_{3_{in}}\,R_L\,r_{1_{out}}\,r_{2_{out}} + A_3\,R_C\,R_F\,r_{1_{in}}\,r_{3_{in}}\,R_L\,r_{1_{out}}\,r_{2_{out}}$$

$$+ A_1\,R_E\,R_G\,r_{1_{in}}\,r_{2_{in}}\,r_{3_{in}}\,r_{2_{out}}\,r_{3_{out}} + A_1\,R_C\,R_G\,r_{1_{in}}\,r_{2_{in}}\,R_L\,r_{2_{out}}\,r_{3_{out}}$$

$$+ A_2\,R_D\,R_F\,r_{1_{in}}\,r_{2_{in}}\,R_L\,r_{1_{out}}\,r_{3_{out}} + A_3\,R_C\,R_G\,r_{2_{in}}\,r_{3_{in}}\,R_L\,r_{1_{out}}\,r_{2_{out}}$$

$$+ A_3\,R_A\,r_{1_{in}}\,r_{2_{in}}\,r_{3_{in}}\,R_L\,r_{1_{out}}\,r_{2_{out}} + A_1\,R_D\,R_G\,r_{1_{in}}\,r_{3_{in}}\,R_L\,r_{2_{out}}\,r_{3_{out}}$$

$$+ A_2\,R_D\,R_G\,r_{2_{in}}\,r_{3_{in}}\,R_L\,r_{1_{out}}\,r_{3_{out}} + A_3\,R_D\,R_G\,r_{1_{in}}\,r_{3_{in}}\,R_L\,r_{1_{out}}\,r_{2_{out}}$$

$$+ A_3\,R_B\,r_{1_{in}}\,r_{2_{in}}\,r_{3_{in}}\,R_L\,r_{1_{out}}\,r_{2_{out}} + A_3\,R_C\,r_{1_{in}}\,r_{2_{in}}\,r_{3_{in}}\,R_L\,r_{1_{out}}\,r_{2_{out}}$$

$$+ A_1\,R_F\,R_G\,r_{1_{in}}\,r_{3_{in}}\,R_L\,r_{2_{out}}\,r_{3_{out}} + A_2\,R_F\,R_G\,r_{1_{in}}\,r_{2_{in}}\,R_L\,r_{1_{out}}\,r_{3_{out}}$$

$$+ A_3\,R_F\,R_G\,r_{1_{in}}\,r_{3_{in}}\,R_L\,r_{1_{out}}\,r_{2_{out}} + A_1\,R_D\,r_{1_{in}}\,r_{2_{in}}\,r_{3_{in}}\,R_L\,r_{2_{out}}\,r_{3_{out}}$$

$$+ A_3\,R_D\,r_{1_{in}}\,r_{2_{in}}\,r_{3_{in}}\,R_L\,r_{1_{out}}\,r_{2_{out}} + A_1\,R_F\,r_{1_{in}}\,r_{2_{in}}\,r_{3_{in}}\,R_L\,r_{2_{out}}\,r_{3_{out}}$$

$$
\begin{aligned}
&+ A_1\, R_G\, r_{1_{in}}\, r_{2_{in}}\, r_{3_{in}}\, R_L\, r_{2_{out}}\, r_{3_{out}} + A_3\, R_G\, r_{1_{in}}\, r_{2_{in}}\, r_{3_{in}}\, R_L\, r_{1_{out}}\, r_{2_{out}} \\
&+ A_1\, A_3\, R_B\, R_C\, R_D\, R_G\, r_{1_{in}}\, r_{3_{in}}\, R_L + A_2\, A_3\, R_A\, R_C\, R_F\, R_G\, r_{2_{in}}\, r_{3_{in}}\, R_L \\
&+ A_1\, A_3\, R_B\, R_C\, R_F\, R_G\, r_{1_{in}}\, r_{3_{in}}\, R_L + A_1\, A_3\, R_B\, R_C\, R_D\, r_{1_{in}}\, r_{2_{in}}\, r_{3_{in}}\, R_L \\
&+ A_2\, A_3\, R_A\, R_C\, R_F\, r_{1_{in}}\, r_{2_{in}}\, r_{3_{in}}\, R_L + A_1\, A_2\, R_C\, R_D\, R_F\, R_G\, r_{1_{in}}\, r_{2_{in}}\, R_L \\
&+ A_1\, A_2\, R_C\, R_E\, R_F\, R_G\, r_{1_{in}}\, r_{2_{in}}\, R_L + A_1\, A_2\, R_D\, R_E\, R_F\, R_G\, r_{1_{in}}\, r_{2_{in}}\, R_L \\
&+ A_1\, A_2\, R_C\, R_D\, R_G\, r_{1_{in}}\, r_{2_{in}}\, r_{3_{in}}\, R_L + A_1\, A_3\, R_C\, R_D\, R_G\, r_{1_{in}}\, r_{2_{in}}\, r_{3_{in}}\, R_L \\
&+ A_1\, A_2\, R_C\, R_D\, R_F\, R_G\, r_{1_{in}}\, r_{2_{in}}\, r_{3_{out}} + A_1\, A_2\, R_C\, R_E\, R_F\, R_G\, r_{1_{in}}\, r_{2_{in}}\, r_{3_{out}} \\
&+ A_1\, A_2\, R_D\, R_E\, R_G\, r_{1_{in}}\, r_{2_{in}}\, r_{3_{in}}\, R_L + A_1\, A_3\, R_C\, R_F\, R_G\, r_{1_{in}}\, r_{2_{in}}\, r_{3_{in}}\, R_L \\
&+ A_1\, A_2\, R_D\, R_E\, R_F\, R_G\, r_{1_{in}}\, r_{2_{in}}\, r_{3_{out}} + A_1\, A_2\, R_C\, R_D\, R_G\, r_{1_{in}}\, r_{2_{in}}\, r_{3_{in}}\, r_{3_{out}} \\
&+ A_1\, A_3\, R_B\, R_C\, R_G\, r_{1_{in}}\, r_{3_{in}}\, R_L\, r_{2_{out}} + A_2\, A_3\, R_A\, R_D\, R_G\, r_{2_{in}}\, r_{3_{in}}\, R_L\, r_{1_{out}} \\
&+ A_1\, A_2\, R_D\, R_E\, R_G\, r_{1_{in}}\, r_{2_{in}}\, r_{3_{in}}\, r_{3_{out}} + A_1\, A_2\, R_C\, R_D\, R_G\, r_{1_{in}}\, r_{2_{in}}\, R_L\, r_{3_{out}} \\
&+ A_2\, A_3\, R_A\, R_F\, R_G\, r_{2_{in}}\, r_{3_{in}}\, R_L\, r_{1_{out}} + A_2\, A_3\, R_C\, R_D\, R_G\, r_{2_{in}}\, r_{3_{in}}\, R_L\, r_{1_{out}} \\
&+ A_2\, A_3\, R_A\, R_D\, r_{1_{in}}\, r_{2_{in}}\, r_{3_{in}}\, R_L\, r_{1_{out}} + A_1\, A_2\, R_E\, R_F\, R_G\, r_{1_{in}}\, r_{2_{in}}\, r_{3_{in}}\, r_{3_{out}} \\
&+ A_1\, A_3\, R_C\, R_F\, R_G\, r_{1_{in}}\, r_{3_{in}}\, R_L\, r_{2_{out}} + A_2\, A_3\, R_C\, R_F\, R_G\, r_{2_{in}}\, r_{3_{in}}\, R_L\, r_{1_{out}} \\
&+ A_2\, A_3\, R_A\, R_F\, r_{1_{in}}\, r_{2_{in}}\, r_{3_{in}}\, R_L\, r_{1_{out}} + A_2\, A_3\, R_C\, R_D\, r_{1_{in}}\, r_{2_{in}}\, r_{3_{in}}\, R_L\, r_{1_{out}} \\
&+ A_2\, A_3\, R_B\, R_F\, r_{1_{in}}\, r_{2_{in}}\, r_{3_{in}}\, R_L\, r_{1_{out}} + A_1\, A_3\, R_C\, R_F\, r_{1_{in}}\, r_{2_{in}}\, r_{3_{in}}\, R_L\, r_{2_{out}} \\
&+ A_1\, A_3\, R_C\, R_G\, r_{1_{in}}\, r_{2_{in}}\, r_{3_{in}}\, R_L\, r_{2_{out}} + A_1\, A_2\, R_D\, R_G\, r_{1_{in}}\, r_{2_{in}}\, r_{3_{in}}\, R_L\, r_{3_{out}} \\
&+ A_1\, A_2\, R_F\, R_G\, r_{1_{in}}\, r_{2_{in}}\, r_{3_{in}}\, R_L\, r_{3_{out}} + A_2\, A_3\, R_F\, R_G\, r_{1_{in}}\, r_{2_{in}}\, r_{3_{in}}\, R_L\, r_{1_{out}} \\
&+ A_1\, A_2\, A_3\, R_C\, R_F\, R_G\, r_{1_{in}}\, r_{2_{in}}\, r_{3_{in}}\, R_L
\end{aligned}
\tag{375}
$$

Likewise, the mathematical formulation of Figure: (160) — a task achieved through the utilization of Equation: (328), Equation: (333), Equation: (338), Equation: (343), Equation: (347), Equation: (351), and Equation: (356) — results in the simulation equations, as shown by Equation: (357), Equation: (358), Equation: (359), Equation: (360), Equation: (361), Equation: (362), and Equation: (363), and upon substituting the values, listed

Table 11: circuit parameters utilized within numerical simulation

Variable	Value	Units	Description
A_1	1000000	$\frac{V}{V}$	OP-AMP 1 Internal Gain
A_2	1000000	$\frac{V}{V}$	OP-AMP 2 Internal Gain
A_3	1000000	$\frac{V}{V}$	OP-AMP 3 Internal Gain
$r_{1_{\text{out}}}$	1	Ω	OP-AMP 1 Internal Output Resistance
$r_{2_{\text{out}}}$	1	Ω	OP-AMP 2 Internal Output Resistance
$r_{3_{\text{out}}}$	1	Ω	OP-AMP 3 Internal Output Resistance
$r_{1_{\text{in}}}$	100000000	Ω	OP-AMP 1 Internal Input Resistance
$r_{2_{\text{in}}}$	100000000	Ω	OP-AMP 2 Internal Input Resistance
$r_{3_{\text{in}}}$	100000000	Ω	OP-AMP 3 Internal Input Resistance
R_A	49900	Ω	Resistor A
R_B	49900	Ω	Resistor B
R_C	100000	Ω	Resistor C
R_D	100000	Ω	Resistor D
R_E	49900	Ω	Resistor E
R_F	49900	Ω	Resistor F
R_G	99800	Ω	Gain Resistor
R_L	10000	Ω	Output Loading Resistor
V_{dd}	10	V	Positive Power Supply
V_{ss}	-10	V	Negative Power Supply

within Table: (11), into these simulation equations and simulating for both the common and differential input signals, the following plots, Figure: (161) and Figure: (162), can be obtained. Similarly, upon visually inspecting the output voltage, as shown by plot (A) in

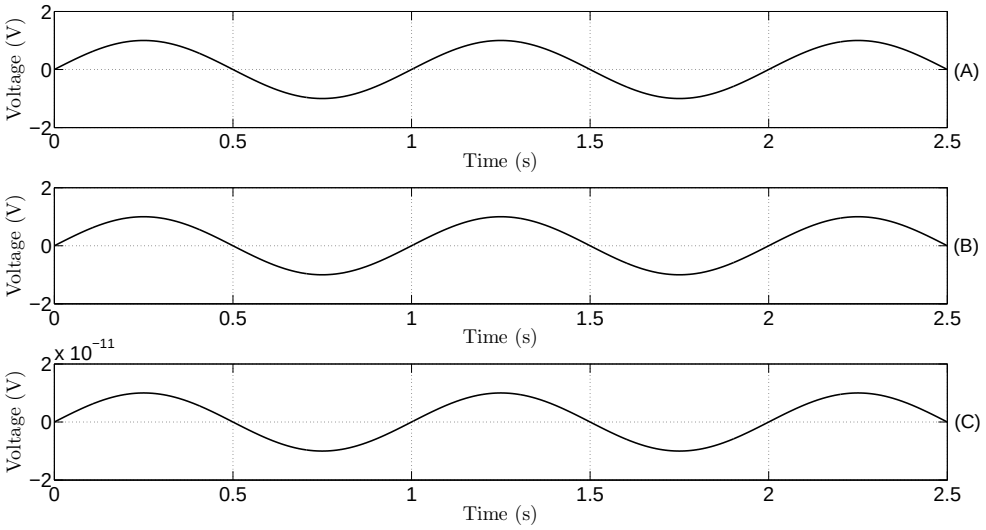

Figure 161: plot of (a) input signal one and (b) input signal two, versus (c) the resulting output signal of a instrumentational amplifier configuration during common mode operation

Figure: (161), when a common input signal is applied, as shown by plots (A) and (B) in Figure: (161), it becomes clear that the output signal produced is the pseudo-difference between the common input signal, and that the amplifier topology, in itself, is not inherently perfect at subtracting the common input signal, since the output voltage should have ideally been zero. Likewise, this observable error in the difference operation, once again created by the instrumentational amplifier topology, is commonly observed within commercial instrumentational amplifiers, so much so, that it is generally described by the term common mode rejection ratio (CMRR). Conversely, while the CMRR is fundamentally a ratio between the output and the common input signals, as formally defined by Equation: (376), — which happens to simplify to a voltage gain ratio — the conceptual idea behind the terms usage is the higher the CMRR is, the more accurate the electrical difference operation performed will be.

$$\text{CMRR} = 20 \log_{10} \left(\frac{A_{\text{Differential}}}{|A_{\text{Common}}|} \right) \tag{376}$$

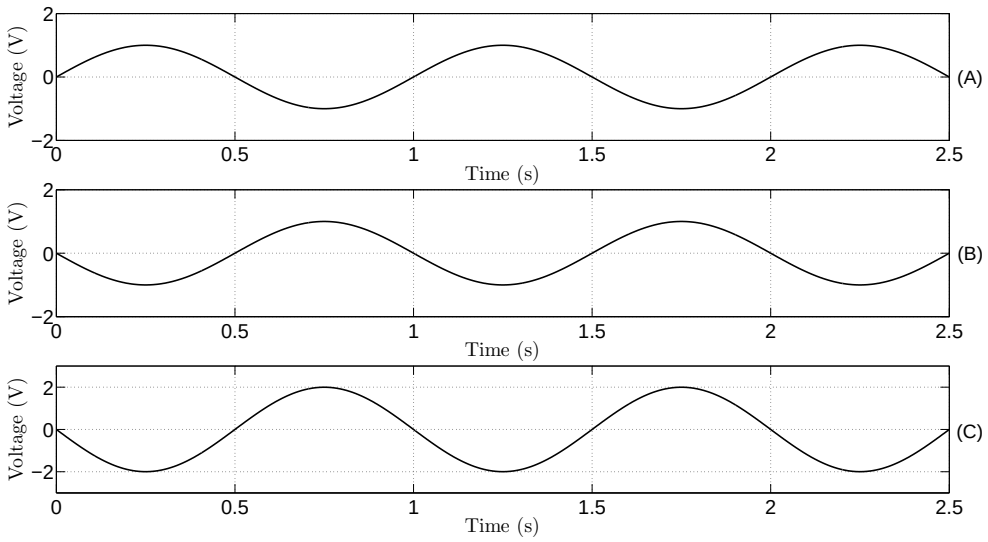

Figure 162: plot of (a) input signal one and (b) input signal two, versus (c) the resulting output signal of a instrumentational amplifier configuration during differential mode operation

Likewise, to expand upon the significance of having a high CMRR value, it is important to recognize that environmental noise, as previously discussed, can manifest itself equally across measuring apparatus interconnections — for example wires —, such that, when the instrumentational differential operation between the two interconnections is performed, a substantial reduction in the environmental noise encountered is observed, while — at the same time — a significant increase in the desired differential signal is also observed. To demonstrate such occurrences, consider for the moment the combinational input signals, as shown within Figure: (163), in which a common mode signal was added to the two differential inputs, as shown by plots (A) and (B) within Figure: (163), that is ultimately removed by the instrumentational differential operation, as shown by plot (C) within Figure: (163). Yet, while the pseudo-removal of the common mode signal is quite impressive — so much so that it might be proposed that this operation could compensate for any environmental effects encountered; however, it is important to recognize that this particular process is highly dependent upon the environmental effects encountered manifesting themselves equally and uniformly upon apparatus interconnections and such occurrences, to put

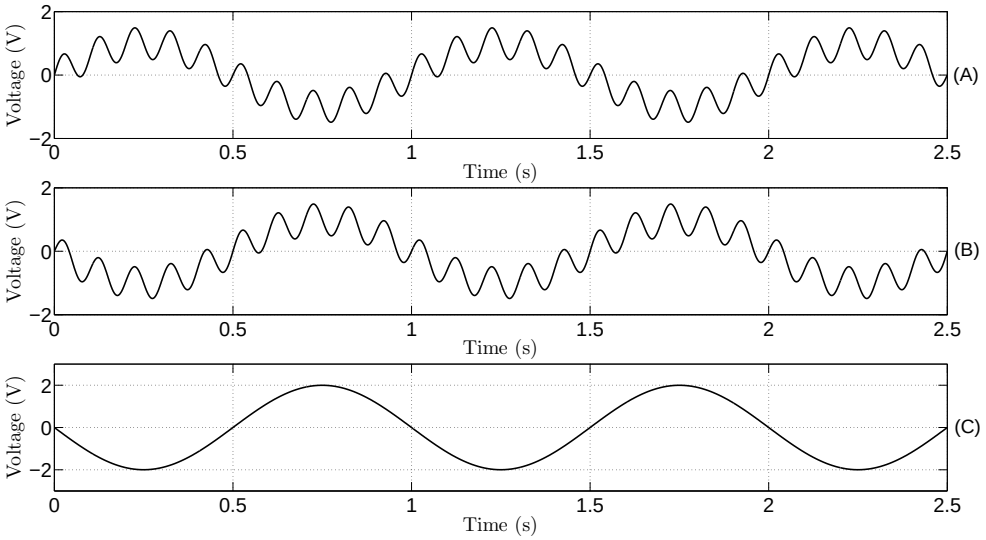

Figure 163: plot of (a) input signal one and (b) input signal two, versus (c) the resulting output signal of a instrumentational amplifier configuration during mixed mode operation

it mildly, are extremely rare. Regardless of such limitations, it is important to recognize that although the complete cancellation of environmental effects through the utilization of such techniques is unrealistic; however, some reduction can be usually achieved through the utilization of these techniques and, generally speaking, any reduction of such effects is — more often than not — considered to be a step in the right direction.

Nevertheless, while instrumentational amplifiers are frequently utilized, particularly within commercial acquisition apparatus, and a substantial amount of theoretical information regarding their design and implementation is available; however, it is important to recognize that some, if not all, of the acquisition attributes, previously discussed, are inherently embedded into these devices, such that, given the overall complexity of the devices ideal theoretical derivation, the inclusion of such attributes into the ideal theoretical model does tend to become extremely complex and generally will be only applicable to a particular device. Conversely, it is the existence of such attributes that ultimately rationalizes the practice of defining instrumentational operational boundaries, since operating within such boundaries significantly reduces the number of instrumentational effects that have to be considered, and typically allows for the simplistic lump sum approximation of such attributes within the operational boundaries.

Likewise, with this in mind, it would now seem prudent to shift the discussion away from individual acquisition instrumentational effects — of which some were not mentioned — towards examining such effects from a system perspective, or more precisely, from a commercial acquisition instrumentational perspective, that is strictly focused upon the acquisition instrumentation utilized, within this dissertation, to obtain laboratory measurements — as opposed to addressing individual acquisition distortions. Similarly, keeping such objectives in mind, the acquisition instrumentation utilized within this dissertation

was predominantly manufactured by Tektronix — although, on occasion, some experimentation with Agilent and Stanford Research Systems (SRS) devices was conducted —; however, most of the measurements taken, at least within this dissertation, were obtained using a Tektronix TPS2024, as shown by Figure: (164), and a Tektronix TDS2002.

Table 12: comparison between tektronix oscilloscopes utilized within laboratory experimentation [391, p.5] [392, p.5] [393, pp.151-168]

Boundary	Unit	TPS2024	TDS2002	Description
Sample Rate	$\frac{\text{Sample}}{GS}$	2	1	Nyquist Sample Rate
Bandwidth	MHz	200	70	Analog Bandwidth
Maximum Voltage	V	300	300	Maximum Input Voltage
Impedance Model	Z	1MΩ ‖ 20pF	1MΩ ‖ 20pF	Operational Model
Resistor Error	Ω	± 2 %	± 2 %	Resistor Deviation
Capacitor Error	pF	N/A	± 3 pf	Capacitor Deviation

Conversely, examination of the Tektronix technical documentation of the TPS2024 and TDS2002 provides information regarding the acquisition instrumentational boundaries, the most notable of which are depicted within Table: (12), and surmises the underlying ca-

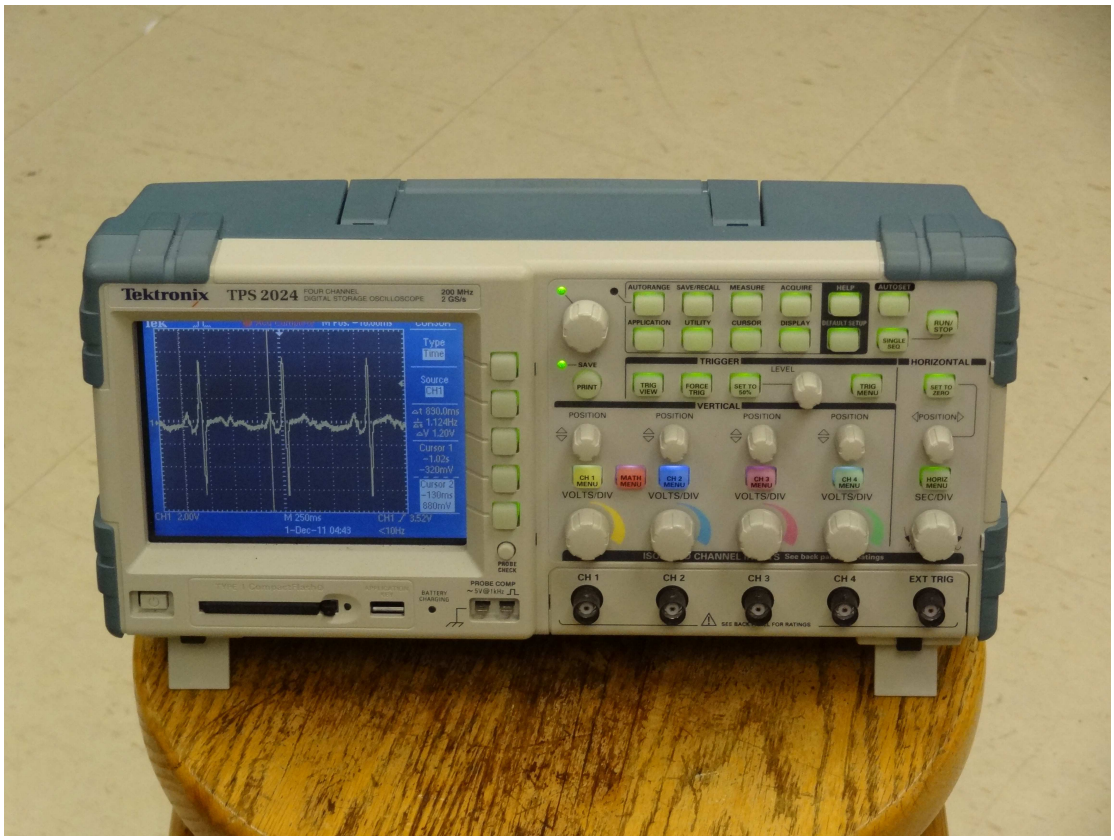

Figure 164: a picture of the tektronix tps2024 utilized to take laboratory measurements

pabilities of the acquisition apparatus. Likewise, for the sake of clarification, it should be mentioned that although some — less critical — measurements were taken using the Tektronix TDS2002, the primary acquisition device utilized was the Tektronix TPS2024, because of its superior acquisition characteristics — relative to the other commercial devices that were available in the laboratory — and its ability to operate on battery power — a notable requirement, previously discussed within the environmental effects section, for obtaining fully shielded measurements. Similarly, a preliminary examination of Table: (12) reveals a number of interesting attributes, one most notably being that the analog bandwidth is set significantly lower than the acquisition sample rate — which is to be expected given the information previously provided — while another notable attribute is that the operational lump sum impedance model is — approximately equivalent — to a one mega-ohm resister in parallel with a 20 picofarad capacitor. Likewise, another interesting attribute — deliberately not listed within Table: (12) — is the fact that the minimum acquisition voltage is a function of acquisition interconnection settings — such as oscilloscope probe multipliers— and internal device configurations.

Furthermore, it is interesting to note that some of the device specifications — a number of which were, once again, deliberately not listed within Table: (12) — are somewhat relative, one notable attribute being analog bandwidth, since acquisition interconnections and internal device gain settings appear to play a significant role in defining these attributes. Thus, because a dependency appears to exist between external connections and internal operational boundaries, it becomes apparent that the accurate acquisition of a signal not only requires a stringent adherence to the, previously mentioned, internal acquisition instrumentational boundaries, but also a significant amount of knowledge about the interconnections that will be attached to the acquisition instrumentation. Conversely, while such character-

istics might seem — at first — disheartening, it also appears that the equivalent internal impedance model provided — that is, once again, only valid within the specified operational boundaries — can be utilized in conjunction with external interconnection models to improve the accuracy of an acquired measurement and help create realistic operational boundaries for a specified laboratory acquisition apparatus.

Likewise, upon taking such attributes under advisement, it seems both natural and logical to adjust the scope of discussion further, and focus upon the process of modeling acquisition instrumentational interconnections since, such interconnections are, once again, primarily responsible for defining and limiting the capabilities of the acquisition apparatus utilized. Towards this end, such interconnections can typically be separated into the following categories: internal acquisition impedance at the boundary, internal generation impedance at the boundary — where applicable —, oscilloscope probes, wires, sensing loads, and the load being observed, while the subject of the load being observed — which is primarily referring to measuring a biomaterial — will be addressed in a later section within this chapter, it is important to recognize that the other categories listed are of significant importance when developing an accurate interconnections model that defines realistic operational characteristics of the acquisition apparatus being utilized. Conversely, as it might be expected, the process of realistically characterizing an acquisition apparatus usually begins by the development of a mathematical equivalent circuit model that, in this particular case, is primarily based upon basic electrical engineering modeling principles — although other approaches, like experimental curve fitting, do exist but are not typically utilized given the theoretical efficiency of the electrical engineering approach for this particular case. Likewise, because the electrical engineering approach allows for the isolated development and combination of electrical models, the categorized interconnections — that

were previously listed — can be modeled individually and then combined later into a single acquisition apparatus model.

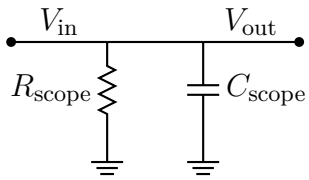

Figure 165: a simplistic equivalent circuit model of a oscilloscope operating within its specified acquisition boundaries

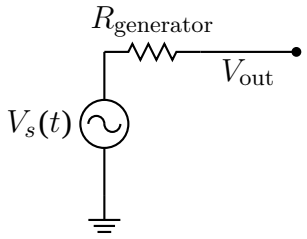

Figure 166: a simplistic equivalent circuit model of a function generator operating within its specified production boundaries

Thus, to begin addressing each of these attributes individually, it was previously mentioned that the internal impedance of the acquisition device utilized, so long as the device was operating within the specified operational boundaries, can be electrically modeled by a parallel RC circuit, as shown by Figure: (165). Although this particular model, at least upon reviewing the instrumentational attributes previously presented, does seem extremely simplistic; however, it is oftentimes beneficial to begin modeling a complicated process — like modeling an acquisition device — as simplistically as possible and then adding additional complexity to the model whenever discrepancies arise. Likewise, while the subject of signal production or generation has not, as of yet, been addressed — a shortcoming that will be remedied shortly — the most simplistic internal impedance model that is frequently utilized to electrically represent a signal generation device, is simply a voltage source and an in series resister, as shown by Figure: (166).

While both the acquisition and production devices have, as it might be expected, a number of unique and complex attributes that can be applied to increase their models overall accuracy; however, as it was previously mentioned, a simplistic modeling approach was selected, in part, because of the adherence to the internal operational boundaries previously specified, and, in part, to reduce the overall complexity of the apparatus model created. Nevertheless, despite the inherent simplicity of the model utilized to represent the complex internal instrumentational effects encountered while performing laboratory experiments — of which, the internal complexity of the signal generator will be discussed in more detail later within this section —; however, it is important to recognize that the utilization of simplistic models are generally only applicable, at least within this particular case, because of the deterministic nature of commercial instrumentation design — after all, such devices were designed to have simplistic internal characteristics when operating within a designated boundary —, and such assumptions are not generally applicable for modeling external interconnections since the notion of deterministic design — while present under certain circumstances — is not necessarily correct.

Conversely, setting such attributes aside for the moment, to begin discussing the commonly utilized and commercially available oscilloscope probe — a device that is designed to aid in the measurement of differential voltages — , as shown by Figure: (167), it is important to recognize that such devices are typically manufactured to minimize the amount of signal distortion that occurs between the external and internal instrumentational interconnection boundaries through matching the impedance of the oscilloscope probe with the specified operational internal oscilloscope impedance. Additionally, based upon this observation, it should come as no surprise that there is a strong dependency between the acquisition device and the acquisition probe, and such dependencies typically mandate —

at least when utilizing a commercial acquisition device — that a matching probe — typically manufactured by the same company that created the acquisition device — be utilized, and, more importantly, such selectivity generally implies that the model selected to describe such interconnections will likely be dependent upon the make and model of the probe selected. Nevertheless, despite the inherent uncertainty that arises from such dependencies, fundamentally — at least from a high-level system perspective — all oscilloscope probe models can be isolated into three basic structures: a head structure, an interconnection structure, and a termination structure, as shown by Figure: (168) [394, p.6].

Conversely, while the oscilloscope probe model can be broken down into three classifiable structures; however, as it was previously mentioned, the model of each of these structures — or at least the component values of these structures — can vary depending upon the make and model of the probe utilized. Likewise, because such ambiguity is a prevalent

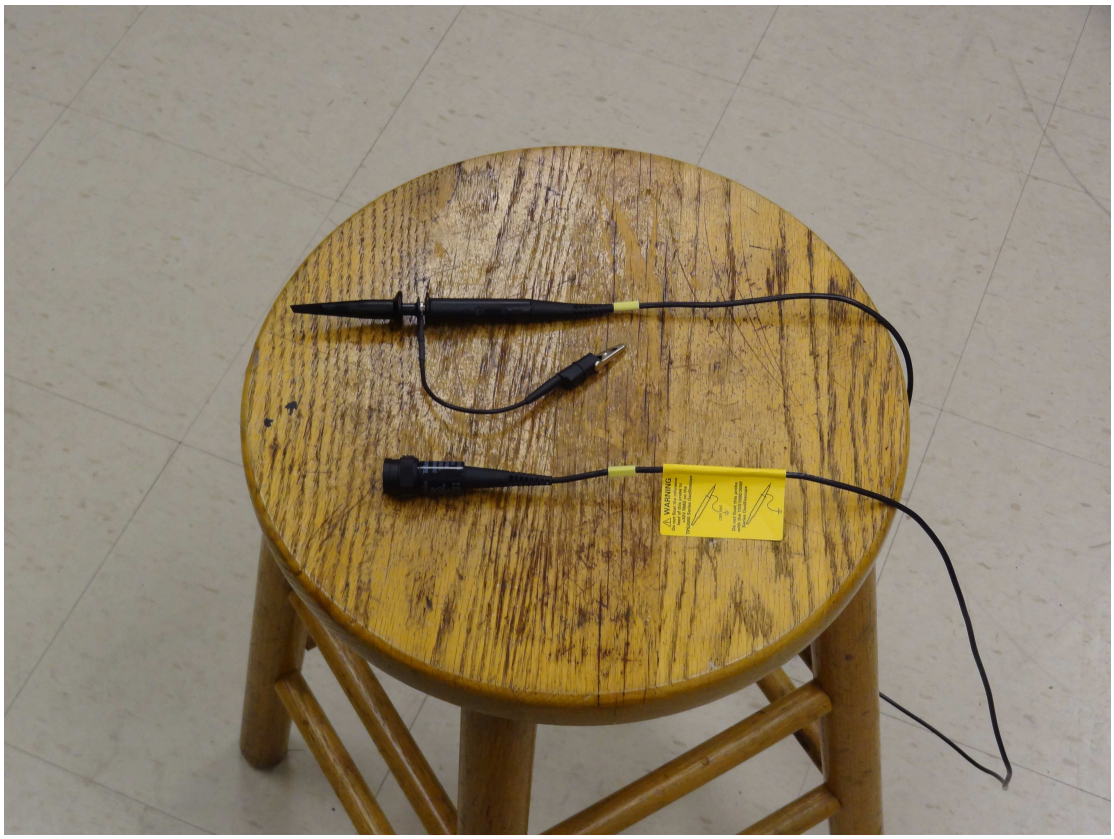

Figure 167: a picture of an oscilloscope probe utilized to acquire differential measurements within the laboratory

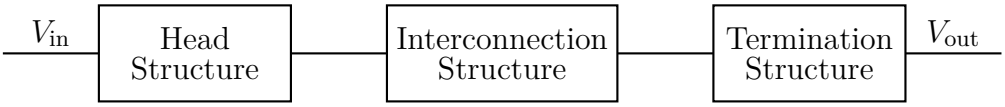

Figure 168: conceptual block diagram of a oscilloscope probe model

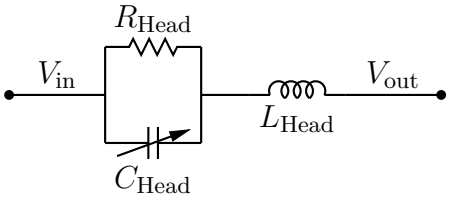

Figure 169: a equivalent circuit model of the oscilloscope probe head structure

attribute, it is prudent to begin modeling such structures as simplistically as possible while also incorporating any available structural information into these simplistic models. Towards this end — and with the aid of Tektronix oscilloscope probe documentation — it seems reasonable to approximate the probe head structure through the utilization of a parallel RC circuit topology — with some inductance added for structural reasons — , as shown by Figure: (169), the interconnection structure through the utilization of a simplistic transmission line structure, as shown by Figure: (170), and the termination structure through the utilization of a T- coil type termination structure, as shown by Figure: (171) [394, p.6]. While the combinational probe model created, as shown by Figure: (172), is — in the most general sense — far from being simplistic, since a less complex model, like the one shown within Figure: (173), could have been utilized to provide a relatively similar approximation; however, the model depicted within Figure: (172) symbolizes a balance

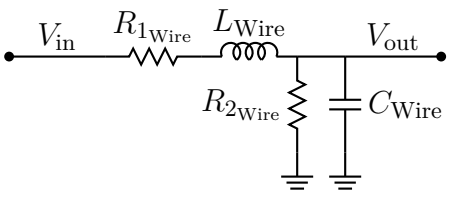

Figure 170: a equivalent circuit model of both a oscilloscope probe wire interconnection structure and a wire interconnection

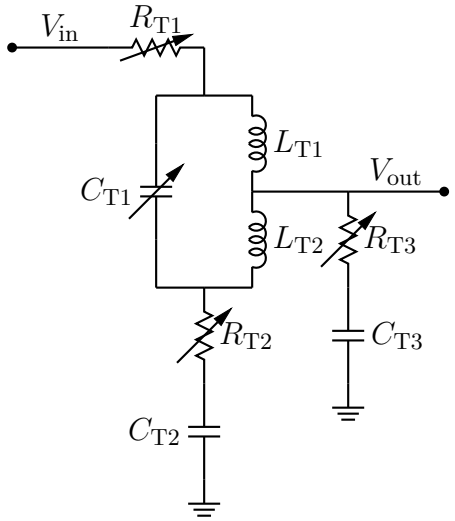

Figure 171: a equivalent circuit model of a oscilloscope probe t-type termination structure

between theoretical accuracy and simulation simplicity, since, after all, the removal of model parameters after the formulation of a simulation equation — so long as the model is not overly complex — tends to be easier than the introduction of additional model parameters — a process that would require the reformulation of such equations.

Likewise, despite the slight introduction of mathematical formulation and simulation into the discussion — an inclusion that can be attributed to the underlying desire to determine the operational parameters of the laboratory apparatus utilize to acquire bioelectrical signals —; however, now that a basic theoretical model of the oscilloscope probe has been provided, it would now seem appropriate to continue addressing the, previously listed, model categories by focusing upon wire interconnection modeling — a notion that was inadvertently described within the probe modeling discussion. Towards this end, it is worth mentioning that the majority of wire interconnections utilized within laboratory apparatus were frequently twisted together, as shown by Figure: (174), with the hopes of reducing electromagnetic interference, the occurrence of charge displacement, and to increase the likelihood of environmental effects manifesting themselves uniformly upon the wire — an

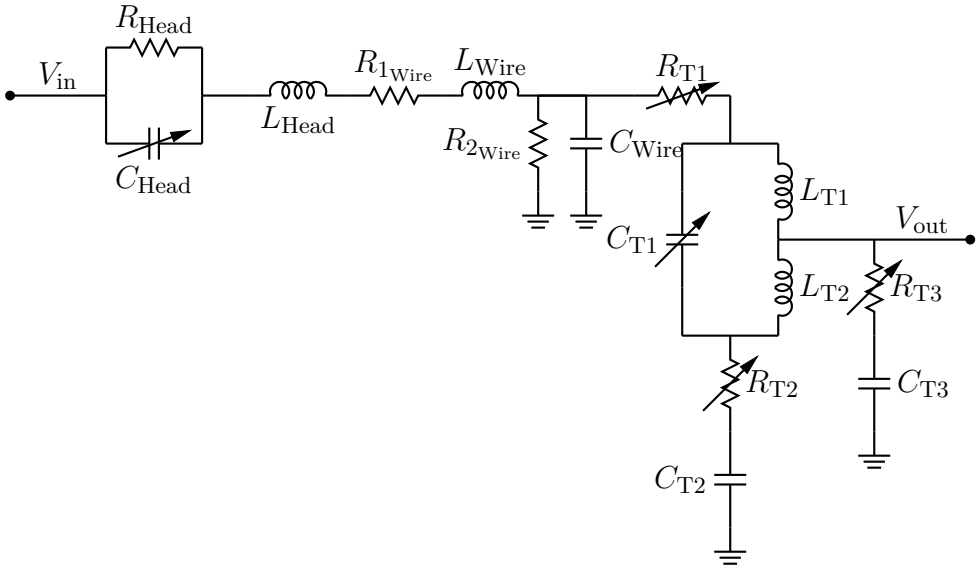

Figure 172: a equivalent circuit model of the complete oscilloscope probe structure

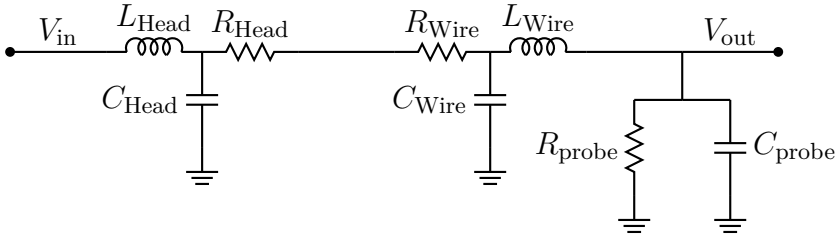

Figure 173: a simplified equivalent circuit model of the complete oscilloscope probe structure

attribute that, to some degree, will hopefully increase the effectiveness of common mode instrumentation amplifier removal — an amplifier topology that is commonly found within commercial acquisition instrumentation. Conversely, while a number of circuit topologies are available to represent an electrical wire — some more complicated than others, a fact depicted best by Figure: (175) —; however, based upon the twisted wire structure that was utilized and the operational boundaries being considered, it seems relatively reasonable — if not an excessive precaution — to utilize the simplistic transmission line structure, as shown by Figure: (170), to represent any distortions created by wire interconnections [395] [396] [397] [398, ch.4]. Lastly, because some laboratory measurements require knowledge regarding the amount of current flowing through a particular biomaterial and given

that the only acquisition method readily available — within the laboratory in which the measurements were taken — was the ability to measure a differential voltage through the utilization of a current sensing resistor — a circuit component that typically has a precise but extremely low resistance and is generally manufactured by winding wire —, and such — wirewound — devices typically have some inductance associated with their usage, an attribute depicted by Figure: (176), that should be considered prior to their inclusion into the apparatus model [399].

Likewise, now that a number of instrumentational modeling techniques have been discussed, it now seems appropriate to briefly address and rationalize the practice of avoiding the usage of Laplace analysis when attempting to mathematically formulate and examine any of the equivalent circuit models previously discussed. While the tendency to avoid this particular mathematical technique should not be construed as total exclusion — as

Figure 174: a picture of how interconnection wires were twisted when utilized to obtain a laboratory measurement

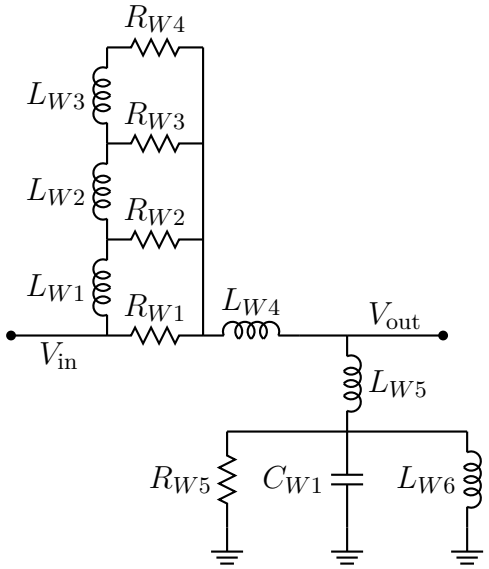

Figure 175: a equivalent circuit model of a wire with skin effect and inductive coupling included

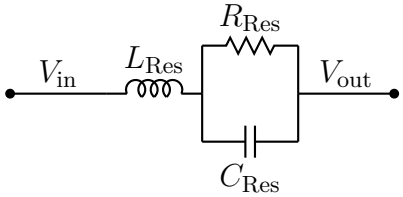

Figure 176: a equivalent circuit model of a non-ideal resistor with inductive leads

Laplace analysis was occasionally utilized —; however, the avoidance of this technique can be rationalized, at least within some academic circles, by the fact that measurements of nonlinear time varying (NLTV), linear time varying (LTV), or nonlinear time invariant (NLTI) phenomenon was possible, if not expected, and Laplace analysis, in stark contrast, is generally only utilized when working with linear time invariant (LTI) problems. Nevertheless, while such assumptions, regarding the usage of Laplace analysis, are frequently considered, although there are a number of publications that have demonstrated techniques to overcome this, so-called, LTI application barrier; yet, such techniques are, more often than not, very difficult for someone not actively associated with advanced mathematical methods to implement and generally requires the validation of theoretical derivations —

particularly surrounding accompanying mathematical operations like convolution — to ensure the applicability of such methods, and these innate difficulties tend to only further promote the avoidance of Laplace analysis, at least under such conditions, and promote the utilization of a time domain approach [400] [401] [402] [403] [404]. Yet, while the, previously mentioned, innate complexities associated with the utilization of Laplace analysis within non-LTI problems could be systematically demonstrated through the utilization of theoretical mathematical proofs by examining and assortment of classifiable systems with varying signal characteristics; however, while this approach is definitively valid, it seems more appropriate and understandable to rationalize this decision — once again, to avoid Laplace analysis — by demonstrating the problems that arise upon utilizing Laplace analysis to find a unknown impedance within a simplistic three component LTI circuit — a task that is very similar to some of the research objectives presented within this dissertation — as shown by [FIG:RES:INSLAPLCEDEMO1}.

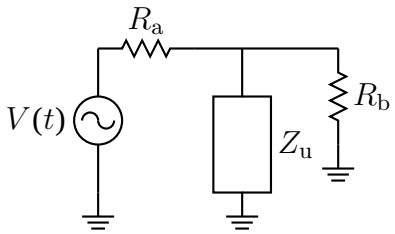

Figure 177: a simplistic three component circuit with a unknown impedance

$$I_{R_a}(s) = -\frac{\mathrm{V_{out}(s)} - \mathrm{V_x(s)}}{\mathrm{R_a}} \tag{377}$$

$$I_{Z_U}(s) = \frac{\mathrm{V_{out}(s)}}{\mathrm{Z_U}} \tag{378}$$

$$I_{R_b}(s) = \frac{\mathrm{V_{out}(s)}}{\mathrm{R_b}} \tag{379}$$

$$KCL_1 : \ 0 = I_{R_a}(s) - I_{Z_U}(s) - I_{R_b}(s) \tag{380}$$

$$KCL_1 : \ 0 \ = \ - \frac{\mathrm{V_{out}(s)}}{\mathrm{R_b}} - \frac{\mathrm{V_{out}(s)}}{\mathrm{Z_U}} - \frac{\mathrm{V_{out}(s)} - \mathrm{V_x(s)}}{\mathrm{R_a}} \tag{381}$$

Conversely, towards this end, the simplistic three component circuit, as shown by Figure: (177), can be expressed mathematically through the utilization of frequency domain KCL analysis — a technique that, in this particular case, might be considered excessive given the circuit analysis shortcuts available — as shown by Equation: (377) through Equation: (381). Likewise, for the moment, to simplify this example further, it will be briefly assumed that the unknown impedance is an ideal resistor — $(Z_U = R_c)$ —, as shown by Figure: (178), and, after which, Equation: (382) can be solved in terms of the unknown resistance.

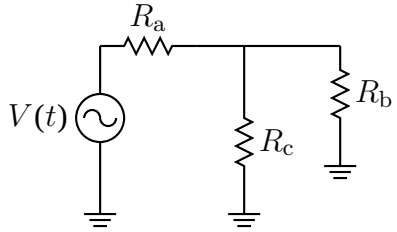

Figure 178: a simplistic three component circuit with a unknown resistance

$$R_c(s) = \ - \frac{\mathrm{V_{out}(s)}}{\frac{\mathrm{V_{out}(s)}}{\mathrm{R_b}} + \frac{\mathrm{V_{out}(s)} - \mathrm{V_x(s)}}{\mathrm{R_a}}} \tag{382}$$

Likewise, at this point, further mathematical manipulation becomes somewhat problematic — particularly when empirical measurements are involved— because Laplace analysis generally requires expressing input sources as mathematical equations within the frequency domain and, as it might be expected, obtaining such equations — particularly for empirical measurements — is typically considered to be a problematic process that, more often than not, allows for more than one possible mathematical representation depending upon the level of accuracy desired. To emphasize this point further, consider for the moment that the

component value of the resistor R_c is desired at a singular point in time; based upon such assumptions, it is possible to neglect all other input values at varying locations in time — despite this assumption being more than dubious and highly conditional — and represent the input signal — at that singular point in time — by a Dirac delta function that has been scaled by the input amplitude. Likewise, upon making this particular assumption, the input source becomes easily expressed within the frequency domain — since the Laplace transform of a Dirac Delta function is simply its scaled constant value — and additional mathematical manipulation, yields a solution to the unknown resistance for the specified point in time — in this particular case, assuming the simplistic circuit has the component values provided by Equation: (383) thru Equation: (388) — within the frequency domain, as shown by Equation: (389).

$$V_x(t) = 5\delta(t) \tag{383}$$

$$V_x(s) = 5 \tag{384}$$

$$V_{\text{out}}(t) = 2.5\delta(t) \tag{385}$$

$$V_{\text{out}}(s) = 2.5 \tag{386}$$

$$R_a = 5000 \tag{387}$$

$$R_b = 10000 \tag{388}$$

$$R_c = 10000 \tag{389}$$

Conversely, while such an approach does appear, at least at first, to be relatively simplistic and straightforward; however, this type of approach is severely limited by the exclusion of all input measurements — except for the, previously specified, temporal location — and, in all practicality, is seldom ever considered particularly useful or beneficial. Likewise,

with this being said, because — ordinarily — all measured input signals are of significant importance when attempting to model an unknown system, typically the input equation is expressed more completely — as in incorporating all measured points in time — within the frequency domain, and to depict this concept further, assuming for the moment the example provided utilized a DC input source, results in Equation: (383) thru Equation: (388) becoming Equation: (390) thru Equation: (395).

$$V_x(t) = 5 \tag{390}$$

$$V_x(s) = \frac{5}{s} \tag{391}$$

$$V_{\text{out}}(t) = 2.5 \tag{392}$$

$$V_{\text{out}}(s) = \frac{2.5}{s} \tag{393}$$

$$R_a = 5000 \tag{394}$$

$$R_b = 10000 \tag{395}$$

$$R_c = 10000 \tag{396}$$

While substitution of each singular input source — or Dirac Delta source — with a continuous time DC source, does inevitably yield a more complex frequency domain equation; however, the value of the unknown resistance, as shown by Equation: (396), does remain the same despite the introduction of additional complexity — an attribute that was expected given the overall simplicity of the circuit utilized. Nevertheless, while it is important to recognize that an assortment of time domain input signals could be applied to this particular problem, the frequency domain equivalent found, and — ultimately — the calculations utilized to solve the unknown resistance should — in theory — yield exactly the same result, yet upon introducing more complex frequency domain input equations, like a shifted sinu-

soidal signal, as shown by Equation: (397) thru Equation: (397), the resulting resistance equation, as shown by Equation: (403), becomes rather obscure.

$$V_x(t) = 5\ \cos(t) \tag{397}$$

$$V_x(s) = \frac{5\,s}{s^2+1} \tag{398}$$

$$V_{\text{out}}(t) = \frac{5\ \cos(t)}{2} \tag{399}$$

$$V_{\text{out}}(s) = \frac{5\,s}{2\ (s^2+1)} \tag{400}$$

$$R_a = 5000 \tag{401}$$

$$R_b = 10000 \tag{402}$$

$$R_c(s) = \frac{5\,s}{(2\,s^2+2)\ \left(\frac{5\,s}{10000\,s^2+10000} - \frac{5\,s}{20000\,s^2+20000}\right)} \tag{403}$$

While such obscurities, in this particular case, are relatively straightforward to overcome, since the limit of Equation: (403) can be taken from the left and right spectral boundaries, as shown by Equation: (404) and Equation: (406), and a convergence value found, as shown by Equation: (408), that is equal to the expected component value or, alternatively, Equation: (403) can be converted back into the time domain using the inverse Laplace operator, as shown by Equation: (409) — and intuitively correlated with the desired component value — as such correlation is necessary because, in this particular case, a Dirac Delta function is inherently embedded in to the time domain solution based upon the spectral continuity of the desired component; however, despite being able to directly isolate a component value within this particular case, it is important to recognize that the occurrence of such complexities, at least upon the utilization of simplistic trigonometric input functions, does tend to foreshadow the inherent problems associated with the utilization of this technique

to solve problems of this particular nature.

$$R_{c_{\text{left}}}(s) = \lim_{s \to 0} \frac{5\,s}{(2\,s^2+2)\,\left(\frac{5\,s}{10000\,s^2+10000} - \frac{5\,s}{20000\,s^2+20000}\right)} \tag{404}$$

$$R_{c_{\text{left}}}(s) = 10000 \tag{405}$$

$$R_{c_{\text{right}}}(s) = \lim_{s \to +\infty} \frac{5\,s}{(2\,s^2+2)\,\left(\frac{5\,s}{10000\,s^2+10000} - \frac{5\,s}{20000\,s^2+20000}\right)} \tag{406}$$

$$R_{c_{\text{right}}}(s) = 10000 \tag{407}$$

$$R_{c_{\text{left}}}(s) = R_{c_{\text{right}}}(s) = R_c(s) \tag{408}$$

$$R_c(t) = \mathcal{L}^{-1}\left(\frac{5\,s}{(2\,s^2+2)\,\left(\frac{5\,s}{10000\,s^2+10000} - \frac{5\,s}{20000\,s^2+20000}\right)}\right) = 10000\delta(t) \tag{409}$$

Conversely, to illustrate this point further, consider for the moment the previously provided DC input signal that has had an additional small amplitude periodic sinusoidal signal added — to loosely approximate the inclusion of a small amount of environmental effects, which is an expected innate characteristic that frequently manifests itself within empirical measurements — as shown by Equation: (410) thru Equation: (421).

$$V_x(t) = 5 + \frac{\cos(t)}{200} \tag{410}$$

$$V_x(s) = \frac{s}{200\,(s^2+1)} + \frac{5}{s} \tag{411}$$

$$V_{\text{out}}(t) = 2.5 + \frac{\cos(t)}{200} \tag{412}$$

$$V_{\text{out}}(s) = \frac{s}{200\,(s^2+1)} + \frac{5}{2\,s} \tag{413}$$

$$R_a = 5000 \tag{414}$$

$$R_b = 10000 \tag{415}$$

$$R_c(s) = -\frac{\frac{s}{200\,s^2+200} + \frac{5}{2\,s}}{\frac{s}{10000\left(200\,s^2+200\right)} - \frac{1}{4000\,s}} \tag{416}$$

$$R_c(t) = \mathcal{L}^{-1}\left(R_c(s)\right) \tag{417}$$

$$R_c(t) = \frac{5010000\,\delta(t)}{499} - \frac{200000\,\sqrt{5}\,\sqrt{499}\,\sin\left(\frac{10\,\sqrt{5}\,\sqrt{499}\,t}{499}\right)}{249001} \tag{418}$$

Likewise, upon solving for the unknown resistance — using the methods previously demonstrated, the resulting equation, as shown by Equation: (416), reveals a rather complicated solution that — upon being examined within the frequency domain using the, previously discussed, limit method — is found not to converge to a singular value, although the value obtained might be carelessly approximated as being equivalent or alternatively, averaged together, while the time domain analysis of Equation: (416) — obtained thru the utilization of the inverse Laplace transform —, as shown by Equation: (418), is not particularly easy to intuitively correlate to a passive component value. Additionally, while such complexities make the utilization of this technique, particularly with empirical measurements, a rather dubious proposition; further complications arise upon substitution of the unknown resistor with a reactive component — like a capacitor —, as shown by Figure: (179), since additional mathematical steps are required to relate the frequency domain representation of the reactive component, as shown by Equation: (419), to the unknown impedance, as shown by Equation: (420) thru Equation: (421).

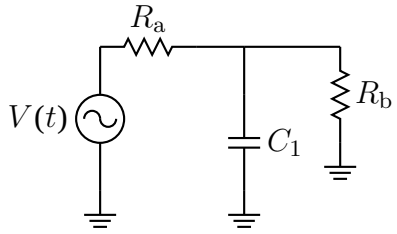

Figure 179: a simplistic three component circuit with a unknown capacitor

$$\mathrm{Z_U}(s) = \frac{1}{s\,\mathrm{C}_1} \tag{419}$$

$$KCL_1 : \; 0 \; = \; - \frac{\mathrm{V_{out}(s)}}{\mathrm{R_b}} - \frac{\mathrm{V_{out}(s)} - \mathrm{V_x(s)}}{\mathrm{R_a}} - \mathrm{C_1}\, s\, \mathrm{V_{out}(s)} \tag{420}$$

$$\mathrm{C_1}(s) = \; - \frac{\frac{\mathrm{V_{out}(s)}}{\mathrm{R_b}} + \frac{\mathrm{V_{out}(s)} - \mathrm{V_x(s)}}{\mathrm{R_a}}}{s\, \mathrm{V_{out}(s)}} \tag{421}$$

While the introduction of these — additional steps — might, at first, appear to be a relatively straightforward extension of the methods previously discussed, and although — under some circumstances — such conclusions can be legitimized; however, such conclusions are far from being the "*status quo ante*" [†1] and, in all actuality, the overall complexity of this particular method seems to increase harmoniously with the complexity of the unknown impedance topology selected [405]. Furthermore, the manifestation of such progressively increasing complexities — once again, owing its origin to the circuit topology selected — also results in a similar increase in the difficulty associated with isolating and correlating individual impedance parameters — within the circuit topology selected — to the total unknown impedance calculated. Thus, upon combining these topology difficulties with the difficulties associated with representing empirical input signals within the frequency domain, yields the inevitable conclusion that the results obtained — through the utilization of this particular method — will, more often than not, be extremely obscure, difficult to work with, and generally will have no intuitive connection to the physical system under examination.

Conversely, it is observations of this particular nature that have ultimately resulted in the tendency to avoid utilizing Laplace analysis within this dissertation — although this is not to say that this particular technique should be completely excluded or, for that matter, was completely shunned within this dissertation —; however, the adherence to such tendencies has resulted in some scrutiny being placed upon academic publications that

[†1] Latin phrase for: in the conditions as previously existed.

actively endorse the utilization of such techniques — for good reason given the problems associated with such techniques — when working with problems of a similar nature — like those publications found within the bioimpedance spectroscopy and chemical impedance spectroscopy research areas that attempt to utilize frequency domain analysis to correlate complicated processes with simplistic RC reactive structures.

Nevertheless, while the inclusion of such scrutiny might seem somewhat harsh — although no malcontent nor condescension was intended — it should be clarified that, while the attributes and observations, previously mentioned, have played a significant role in determining the mathematical techniques utilized within this dissertation, it is important to recognize that every technique has a "*pro*" †[1] or "*contra*" †[2] associated with its usage — including the assortment of numerical time domain techniques utilized within this dissertation — and the existence of such situational diversity makes the utilization of a particular mathematical technique analogous to the iconic notion of selecting the appropriate tool necessitated by the requirements of the current job, thus — in regard to those publications being scrutinized — the utilization of Laplace analysis under such circumstances can be completely justified provided that the situation permits its correct usage [267, p.1462,p.432].

Likewise, now that a basic overview of the problems associated with acquisition instrumentation has — for the most part — been addressed, it now seems appropriate to briefly examine the next category of instrumentational effects encountered: Processing and storage instrumentational effects. Towards this end, although there are — arguably — a plethora of controls and signal processing methodologies that would seem to be fundamentally applicable to such a discussion — some of which, like the Nyquist sampling criteria, bandwidth

†[1] Latin for: on behalf of.
†[2] Latin for: against.

limitations, and the concept of feedback stability have already been mentioned, at least to a sufficient depth —, such attributes, while being both important and applicable, are not necessarily the desired focal point of this particular discussion; however, regardless of such notions, attributes such as: truncation, rounding, storage limitations, and processing delays, have not — as of yet — been discussed and — because such attributes do frequently arise when working with acquisition instrumentation — further discussion regarding each of these topics is merited. Conversely, with this being said — given the previous discussion regarding the utilization of Laplace analysis — it seems prudent to begin — such a discussion — by addressing the effects of truncation and rounding, since such effects frequently arise when working with mathematical equations and numerical methods. Towards this end, while it is important to recognize that — traditionally — the ability to obtain a closed form expression for a given equation is the metaphoric, "*ars mathematica de anima*" [†1] ; however, the ability to do so is typically a luxury that neither time nor most system equations permits and, as a result, mathematical techniques like polynomial truncation and numerical approximation are frequently utilized [6].

Likewise, while a number of mathematical attributes and theorems tend to arise from the utilization of such techniques, the attribute of truncation, at least within this dissertation, does tend to give some pause since, in this particular case, the term truncation is utilized to convey both an order of accuracy and a region in which it is applicable [390] [107]. Yet, although such descriptive attributes — like numerical accuracy and its region of association — do accurately described the inherent implications that are attributed with the terms usage; however, some confusion tends to arise surrounding the terms manifestation, since — within computer science — the term is typically associated with a sudden loss of

[†1] Latin for: the mathematical art of the soul.

numerical information during typecasting, as shown by Equation: (422), while — within general mathematics — the term is typically associated with approximating or linearizing a complex mathematical expression by equating that expression with a more mathematically or computationally manageable one that is equivalent — or equal to — the original equation over a desired region.

$$\text{Int}\,(1.99999) \;\; = 1 \tag{422}$$

Conversely, while the terms associated with typecasting is rather prevalent — more so within some disciplines than within others — yet such occurrences, while being very problematic within digital signal processing — since such occurrences can create instabilities or introduce an intolerable amount of numerical errors — they are generally easy to correct — relative to the truncation of mathematical expressions — since, in the case of truncation due to numerical loss — the underlying mathematics have not been changed and the computational implementation — of such mathematical equations — which created this type of truncation can be easily corrected through memory management and careful data type selection. Still, although truncation from typecasting and computational overflows can typically be corrected relatively easily — although admittedly, some skill is required to identify and locate where this type of truncation is occurring within a computational implementation —; however, the occurrence of truncation from mathematical linearization or approximation is of greater interest, at least within the confines of this dissertation, since this type of truncation is typically utilized when attempting to model nonlinear equations using linear modeling techniques. While there are a number of mathematical ways that an equation can be linearized or approximated, yet to demonstrate such occurrences first-

hand, consider for the moment the Taylor or Maclaurin series polynomial approximation of a sinusoidal signal, as shown by Equation: (423) through Equation: (448), and graphically depicted over varying amounts of truncation — created by changing the number of polynomials utilized to approximate the original equation — by Figure: (180).

$$f_{\text{Taylor}}(a,x) = \sum_{n=0}^{\infty} \frac{\frac{d}{dx^n} f(a)}{n!} (x-a)^n \tag{423}$$

$$f_{\text{Taylor}}(a,x,O) = \sum_{n=0}^{O} \frac{\frac{d}{dx^n} f(a)}{n!} (x-a)^n \tag{424}$$

$$f(x) = \sin(x) \tag{425}$$

$$\frac{d}{dx} f(x) = \cos(x) \tag{426}$$

$$\frac{d}{dx^2} f(x) = -\sin(x) \tag{427}$$

$$\frac{d}{dx^3} f(x) = -\cos(x) \tag{428}$$

$$\frac{d}{dx^4} f(x) = \sin(x) \tag{429}$$

$$\frac{d}{dx^5} f(x) = \cos(x) \tag{430}$$

$$\frac{d}{dx^6} f(x) = -\sin(x) \tag{431}$$

$$\frac{d}{dx^7} f(x) = -\cos(x) \tag{432}$$

$$\frac{d}{dx^8} f(x) = \sin(x) \tag{433}$$

$$\frac{d}{dx^9} f(x) = \cos(x) \tag{434}$$

$$\frac{d}{dx^{10}} f(x) = -\sin(x) \tag{435}$$

$$\frac{d}{dx^{11}} f(x) = -\cos(x) \tag{436}$$

$$f_{\text{Taylor}}(0,x,0) = 0 \tag{437}$$

$$f_{\text{Taylor}}(0,x,1) = x \tag{438}$$

$$f_{\text{Taylor}}(0,x,2) = x \tag{439}$$

$$f_{\text{Taylor}}(0,x,3) = x - \frac{x^3}{6} \tag{440}$$

$$f_{\text{Taylor}}(0,x,4) = x - \frac{x^3}{6} \tag{441}$$

$$f_{\text{Taylor}}(0,x,5) = \frac{x^5}{120} - \frac{x^3}{6} + x \tag{442}$$

$$f_{\text{Taylor}}(0,x,6) = \frac{x^5}{120} - \frac{x^3}{6} + x \tag{443}$$

$$f_{\text{Taylor}}(0,x,7) = -\frac{x^7}{5040} + \frac{x^5}{120} - \frac{x^3}{6} + x \tag{444}$$

$$f_{\text{Taylor}}(0,x,8) = \frac{x^7}{5040} + \frac{x^5}{120} - \frac{x^3}{6} + x \tag{445}$$

$$f_{\text{Taylor}}(0,x,9) = \frac{1626697008263629\,x^9}{590295810358705651712} - \frac{x^7}{5040} + \frac{x^5}{120} - \frac{x^3}{6} + x \tag{446}$$

$$f_{\text{Taylor}}(0,x,10) = \frac{1626697008263629\,x^9}{590295810358705651712} - \frac{x^7}{5040} + \frac{x^5}{120} - \frac{x^3}{6} + x \tag{447}$$

$$f_{\text{Taylor}}(0,x,11) = -\frac{1892883791434041\,x^{11}}{75557863725914323419136} + \frac{1626697008263629\,x^9}{590295810358705651712} - \frac{x^7}{5040} + \frac{x^5}{120} - \frac{x^3}{6} + x \tag{448}$$

Likewise, upon visually inspecting Figure: (180), it becomes apparent that the truncation or approximation of a mathematical equation does, by in large, appear to result in a loss of accuracy; although, it also appears — at least within the confines of the Taylor or Maclaurin series polynomial approximation — that the amount of loss encountered is

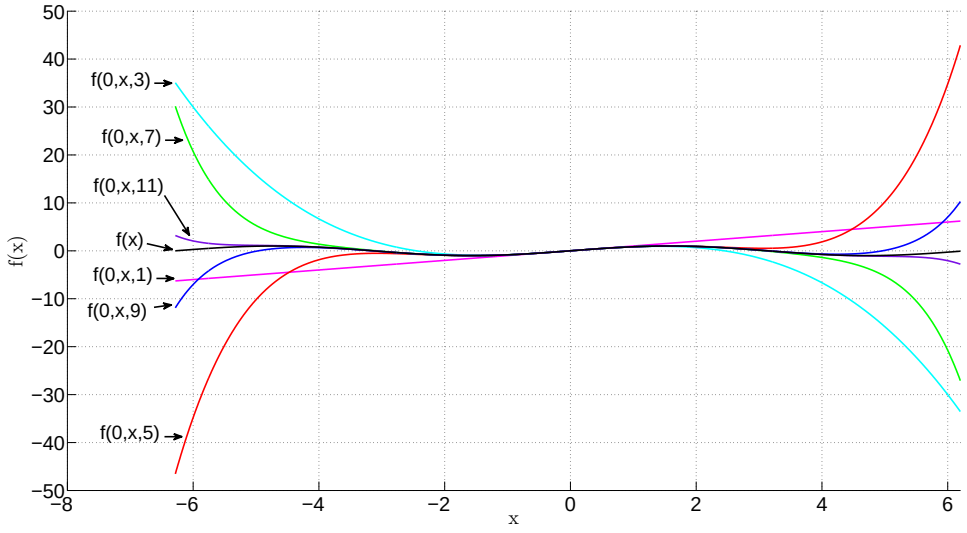

Figure 180: taylor series approximation of sin(x) as the number of polynomials increase

generally associated with the amount of information utilized when making such approximations and the desired location relative to the approximations region of acceptable accuracy. Conversely, while there are a number of technical and exclusionary nuances that are also associated with the utilization of such methods — most of which will not be addressed in any significant depth —, such examples do reasonably summarize the fundamental nature of truncation within a mathematical equation and the underlying types of problems associated with such occurrences. Similarly, while the effects of numerical truncation and equation truncation tend to represent the introduction of an accuracy limitation — either consciously or unconsciously made —; however, similar attributes can also be associated with the process of numerical rounding, as shown by Equation: (449) through Equation: (454), except — in the case of rounding — the implementation is generally consciously decided, conveys some type of intellectual significance — like increased computational efficiency or a correlation with experimental accuracy — , and generally minimizes the amount of error associated with its usage.

$$\text{Round by 0 Decimal}\left(1.12\right) = 1 \tag{449}$$

$$\text{Round by 0 Decimal}\left(1.87\right) = 2 \tag{450}$$

$$\text{Round by 1 Decimal}\left(1.12\right) = 1.1 \tag{451}$$

$$\text{Round by 1 Decimal}\left(1.87\right) = 1.9 \tag{452}$$

$$\text{Round by 2 Decimal}\left(1.12\right) = 1.12 \tag{453}$$

$$\text{Round by 2 Decimal}\left(1.87\right) = 1.87 \tag{454}$$

Furthermore, a similar association can also be made regarding the subject of storage limitations — given the number of characteristics that are similar to numerical truncation —

and — to a lesser extent — rounding, since — in the case of numerical truncation — the computational variable — in which the numerical information is stored — can no longer physically contain the desired information and thus, as a result, an error handling routine will be triggered that allows the variable to gracefully resolve such conditions — which is commonly called a variable overflow event —; while, in the case of rounding, casting between numerical storage types — such as conversion between a floating-point number to a integer — results in triggering a casting routine that is analogous to a biased implementation of rounding. Yet, although such descriptions tend to portray such computational operations as being highly sophisticated and conditional, it should be mentioned that — more often than not — such perceived sophistication is generally an inadvertent side effect of the hardware implementation and, as such, a number of convoluted nuances tend to arise — as opposed to a highly sophisticated conditional design that generally would not possess such nuances —; however, despite the existence of such asides, the fundamental concept to take away from such comparisons is the underlying implementational connections that exist between these concepts and laboratory instrumentation, since such connections arise frequently when acquiring laboratory measurements.

Thus, while there are a number of instances where truncation and rounding are mathematically oriented attributes that arise during the in-depth analysis of a design equation — particularly when it comes to system modeling —; however, in terms of their physical manifestation within laboratory instrumentation — upon direct entry into the signal generator stage —, a phenomenon similar to quantization error would be expected for rounding and numerical casting truncation — since such operations typically force numerical values into discrete discontinuous regions —, a phenomenon similar to the introduction of a windowed and spectrally lossy Delta function would be expected during a numerical overflow — given

the sudden change in the output signal between the upper and lower supply rail that originates from the highest storable value rolling back to the lowest storable value (Example: 0xFF to 0x00) —, and a sudden change in the output signal — relative to the original mode of operation — would be expected from equation truncation — provided that the operational boundary of the equation was exceeded.

Nevertheless, it is important to recognize that the acute manifestation of such occurrences generally requires a specific type of instrumentational configuration in order to observe — specifically, for the examples provided, a system with a signal generation stage that is directly connected to the source of the processing error, like a microprocessor connected to a digital to analog (D2A) converter —, yet it should not be forgotten that such sources of distortion can manifest themselves differently within complex systems — after all, a robotic controller that encountered such effects would, more often than not, exhibit such effects differently relative to the previous example, — and such occurrences can be extremely difficult, if not nearly impossible, to diagnose within such systems. Conversely, while such notions are beyond the intended scope of this discussion, a number of parallels also exist between these attributes and the problems that are associated with acquisition processing delays, since the improper introduction of processing delays can also yield unintended consequences — more so within complex systems like the, previously mentioned, robotic control system; although processing delays are more likely to be considered within instrumentational design since the concept of sampling delays is a fundamental topic within DSP and digital control system theory —, while the effects of truncation, rounding, and — to a lesser extent — storage limitations are, more often than not, unintended consequences that tend to arise from an inexperience with physical implementation.

Yet, while such complexities do exist within some research areas; however, within the

confines of laboratory instrumentation, the effects of processing delays are generally only problematic when attempting to acquire time sensitive information — like obtaining phase or simultaneous potential gradients — and, by in large, the only effective means to counteract such delays is by first obtaining an in-depth understanding of the sources of delays within the instrumentation utilized, second understanding how to utilize synchronization signals — typically called a trigger signal — to decrease the amount of delay between simultaneous instrumentation samples, and third ensuring that such delays are taken into account when attempting to mathematically model time dependent processes. Furthermore, the existence of such attributes — within acquisition instrumentation —, ultimately defines the types of experiments that can be performed as a function of the laboratory instrumentation available; although, a number of clever workarounds can be implemented to counteract some of these issues and will be discussed later within this chapter.

Accordingly, to summarize all of the processing concepts previously presented, it is important to recognize that equation truncation is, for the most part, an implementation attribute or, in more simplistic terms, the effects of equation truncation is generally of little concern to someone simply utilizing a commercial acquisition device to obtain a measurement within a laboratory, since the distortions created by such effects — for the most part — would have already been accounted for and acknowledged within the design specifications of the acquisition device — as generally such effects are inherently encapsulated within the assumed equivalent circuit model previously discussed — and — for events that occur after the initial acquisition and preliminary processing stage — the acquirer ultimately would have full control over the data obtained and the mathematical assumptions made when processing that data, thus making it reasonable to neglect such effects — although knowledge of such occurrences can aid a researcher in identifying possible problems with

implemented methodology.

Conversely, numerical truncation, rounding, and storage limitations — unlike equation truncation — can be more problematic because of the required transition between the acquisition stage and the processing stage that — in the case of the laboratory acquisition system example — generally necessitates both human interaction and the interaction between more than one computational architecture, since most commercial acquisition systems — like Tektronix oscilloscopes — requires the user to press a button to save a measurement to a CompactFlash card, remove the CompactFlash card and then inserted into a personal computer (PC) capable of reading this particular storage medium, and then requires the user to import the stored data into a processing program — like Excel or Matlab — for further analysis. Likewise, as it might be expected, any one of the steps — previously mentioned — could result in the introduction of a number of possible errors including numerical truncation, rounding errors, and data corruption — although the topic of data corruption is somewhat complex but best described as being the conversion of legitimate information into meaningless stochastic data. Yet, while the occurrence of such effects might seem somewhat out of place — especially since the introduction of human interaction would seem to segment such events into isolatable an individual processes —; however, upon replacing the human component with an automated interconnection — a task primarily accomplished through a remote interconnection system like a RS232 administration interface — such occurrences still remain applicable since, after all, the transition between computational architectures tends to increase the likelihood of encountering such effects and automation, in itself, also increases the likelihood of such effects occurring, if not inherently adds the possibility of creating new and undiscussed processing effects.

Thus, in short, there is no metaphoric one-size-fits-all solution to either identifying or

modeling the occurrence of processing effects given the proverbial black box nature of most processing effects encountered — especially if the effects are being analyzed from the outside looking in, as opposed to designing the system from the ground up. Conversely, while such observations might seem disheartening — since, after all, the desire to obtain a singular methodology that is applicable under any circumstance is a notion of significant importance within the sciences —, yet while such objectives are reasonably unrealistic — especially given the underlying flexibility associated with such effects — ; however, careful observation and adherence to a well-defined underlying methodological procedure can help to confine such ambiguity and allow a specific processing effect to be modeled to a much greater extent. Nevertheless, while such observations are not necessarily reassuring, it is important to recognize the fundamental link between the processes utilized and the underlying end objective of the model being created, since — in some cases — such process information is not particularly beneficial because the end objective is simply observation rather than application — as would be the case for modeling a unknown impedance for an academic publication —, while — in other cases — such information is of paramount importance because the end objective is, in fact, an application that requires an in-depth understanding of the process dynamics in order to implement correctly — as would be the case for a reactive muscle stimulator. Likewise, although there are a number of ways that such attributes could be discussed further, the only logical conclusion that remains prevalent, at least based upon the — previously presented — observations, is the notion that processing effects are strongly associated with their intended end application, and, as a result, because such attributes can only be accurately described within the confines of their intended application, it seems prudent to limit any further discussion — on this particular topic — within implementational dialogue that necessitates such discussion through a definitive

objective.

Accordingly, now that both the acquisition and processing stages have been discussed in substantial depth, it seems only natural to conclude such discussion — regarding instrumentational effects — by briefly examining the generation stage and any effects associated with its function. While, it will be conceded that there are a number of scenarios in which the processing and generation stage might appear to be seemingly inseparable from each other; however, the existence of such ambiguity tends to primarily arise from linguistic nuances within the application being examined and, to illustrate such nuances further, consider for the moment a signal that has been obtained by the acquisition stage and stored on a digital medium — like a secure digital (SD) memory card. Likewise, within this particular scenario, because the underlying objective was to simply acquire and store a laboratory signal, it can be argued that the process of storing the acquired signal — within the SD card — is, in itself, classifiable as being a signal generation effect — as opposed to being a processing effect —, since the data stored within the digital medium is, in some sense, a digitally encoded representation of the signal being measured and, thus — under some definitions of the term signal generation —, could be called a reproduction — albeit, such types of reproductions are conceptually different than the traditionally expected analog signal. Conversely, based upon such observations, it becomes apparent that the fundamental definition of the term, generation effect, appears to be rather subjective — at least depending upon the device examined and the desired objective — and, while such observations might appear seemingly counterintuitive — particularly within the electrical engineering discipline —; yet, it is also important to recognize that the, previously mentioned, concept of interdisciplinary common knowledge plays a significant role in creating this particular type of ambiguity, since the acceptable interdisciplinary concept of signal generation tends

to very from the, more rigid, perspective of analog representation towards more abstract representations like the, previously mentioned, notion of digital encoding and storage.

Nevertheless, while it is important to recognize places where interdisciplinary communication problems can arise — especially given that such attributes have already been discussed in significant detail within previous chapters — further discussion — at least on this particular attribute — does not seem merited; however, given that there is some inherent ambiguity associated with the usage of the term generation effect, it does seem rather prudent to formally define the term based upon the innate implications assumed upon its usage within this dissertation. Towards this end, to help clarify such concepts further, the term generation effect — at least within the confines of this dissertation — is generally utilized to describe the process of creating an end consumer analog output electrical signal — typically a voltage signal — and the usage of the term tends to also be synonymous with conveying the underlying imperfections that are associated with the process of creating such a signal. Conversely, to clarify a minor caveat here, it is important to recognize that, because the process of creating an electrical signal is generally accomplished through the utilization of two definitively distinct classifications of electrical circuitry — analog or digital circuitry —, it could be argued that every location — at least within a typical electrical circuit, whether it be predominantly analog or digital in nature — that is capable of creating an electrical signal is , by mere technicality, classifiable as a generation stage and thus, has a generation effect associated with its usage; however, with this being said, the underlying intent of the term, at least within the confines of this dissertation, was to describe the internal electrical circuitry from a metaphoric black box perspective of being outside a system looking in — as opposed to the all-encompassing designer perspective of having detail knowledge regarding every pertinent electrical component within

the system — and such implications tend to limit the terms association — at least within this dissertation — to simply describing the electrical circuitry that is connected to the external output terminal of the device being utilized. Thus, to simplify matters further, because any electrical device examined, along with the electrical effects encountered, — at least within this dissertation — was separated into three distinctively classifiable categories — acquisition, processing, and generation — it seems reasonable to assume that any overlapping effects encountered — at least within such classifications — that have already been accounted for within a prior categorization, should be, by in large, ignored to avoid the possibility of overcompensation. Therefore, with this being said, it seems only natural to exclude including the possibility of internal generation circuitry within this particular classification — as the inclusion of such circuitry is both redundant and goes against the desired black box philosophy of the signal generation stage —; furthermore, although it was never explicitly stated, it is worth mentioning that no device examined — at least within this dissertation — was forced — through methodological convention — to incorporate all three classifiable characteristics upon receiving the rigors of mathematical representation and, as a result, the possibility of stage exclusion does exist.

Conversely, based upon such observations and their common physical manifestation, the generation stage — at least within the confines of this dissertation — was predominantly considered to be an electrical circuit that is capable of taking a digital representation of a desired output signal and converting that digital representation into an analog equivalent voltage; although the occasional analog in, analog out amplifier was also considered within this context. Nevertheless, while such definitions might seem somewhat limited — especially given the terms usage within power production and the associated notion of mechanical to electrical energy conversion —, such limitations tend to be appropriate given

the inherent nature of bioelectrical research. Thus, towards this end, a surprising amount of overlap appears to exist between the effects encountered in the acquisition stage and the effects encountered in the generation stage — possibly because of the synonymous nature between the two operations — and, as a result, only a few clarifying attributes are needed to correlate the effects, previously discussed, to the effects frequently encountered within the generation stage. Likewise, to begin correlating such effects, it should be mentioned that the most common form of signal generation circuitry utilized — at least by the commercial devices utilized within this dissertation — was predominantly the application of a digital to analog (D2A) converter that, in essence, is very similar to the circuitry found within an analog to digital (A2D) converter, insofar as, both circuits generally have some type of quantization effect associated with their usage. While the electrical similarities between the physical implementations of such devices does tend to diverge significantly upon the introduction of more rigorous examination — since it would be inherently unwise to assume that the circuitry for both devices is the same — yet, in terms of implementation, A2D and D2A devices are designed to synonymously interchange an analog value (to or from) a quantized discrete value, are constrained by physical operational conditions — like supply voltage —, and, more often than not, are further limited by temporal restrictions — like sampling rates or processing delays. Thus, with this being said, it should come as no surprise that the generation stage, in a similar fashion as the acquisition stage, is significantly susceptible to quantization effects — which generally introduces unwonted spectral components —, is further limited by the supply rail — making it susceptible to clipping effects that can also introduce unwonted spectral components —, and is further restricted by the Nyquist rate — that generally restricts the devices spectral reproductive capabilities.

Furthermore, as it might be expected, the circuitry utilized to convert a digital signal

into an analog signal also possesses innate electrical characteristics — an attribute that is generally characterized by equivalent impedance modeling, like the, previously depicted, simplistic voltage source with an in series impedance —, and, more prevalently, generally utilizes a low pass filter to reduce some of the unwonted spectral components created — mostly from quantization effects — but, at the same time, such spectral reductive methods also tend to further limit the spectral reproductive capabilities of the generation device. Conversely, while generation effects can very to some extent, at least depending upon the method of D2A conversion selected — assuming a digital generation stage was utilized rather than an analog one, such as successive approximation or R2R voltage division, to provide some examples — the methodological approach utilized to represent such effects, and to some extent the amount of consideration that each effect is given, appears to remain rather consistent — at least upon comparison with the acquisition stage —; however, it is important to recognize that it is the end objective of the device being utilized that ultimately defines the amount of consideration that is taken into account when attempting to mathematically represent such effects.

For example, within the confines of this dissertation, the acquisition stage — at least for the laboratory bioimpedance acquisition apparatus utilized — is expected to measure an unknown voltage across an unknown bioimpedance, thus in order to accomplish this task, every significant instrumentational distortion that can occur between the point of measurement and the point of acquisition must be known in order to accurately determine the electrical response of the unknown bioimpedance within the processing stage. Likewise, while such observations are rather notable — though somewhat redundant given the previous discussion —, this particular application also requires the utilization of a generation stage — like a commercial signal generator — to produce the electrical stimulation — that is

ultimately acquired by the acquisition stage — needed to analyze the unknown impedance and such operational dependencies create some rather interesting modeling considerations that have to be taken into account. To elaborate further, one notable consideration is the ability of the signal generation stage to provide a consistent output voltage — a capability that is generally not found within most commercial generation devices, especially since the basic commercial signal generators available are reasonably approximated, within most applications, by a voltage source in series with a resistance — an attribute that innately implies that the output voltage produced will be strongly dependent upon the load impedance — or unknown bioimpedance in this particular case — connected.

While such observations might seem counterintuitive, mostly because the previous discussion — regarding instrumentational effects — focused heavily on integrated devices; however, given that the instrumentation utilized within this dissertation was seldom ever integrated into a singular system — like a commercial bioimpedance spectroscopy device — and given that the — arguably classifiable as being integrated — commercial generation devices utilized were not expected to possess a feedback regulated output, it becomes interesting to observe that the term generation stage, at least within the confines of this dissertation, seems to be innately unassociated — or at least, very loosely associated — with the electrical engineering concept of an ideal voltage source. Yet, such characteristics should not imply that the process of signal generation is either inherently unreliable or unpredictable since, after all, the signal produced — although usually being a function of load impedance — is generally considered to have a relatively linear relationship with the signal desired, thus, based upon such characteristics, it would be more reasonable to take such attributes in stride and focus upon understanding the innate specifications of the generation stage utilized since, such characteristics, ultimately determine the depen-

dency between the signal desired and the signal generated. With this being said, while such dependencies can be compensated for — to some extent — within the mathematical representation of the generation stage, such methods — at least within the confines of this dissertation and within the example provided — are somewhat problematic because of the nonlinear nature of the unknown bioimpedances being examined; however, while such attributes are definitively problematic, compensation — or at least, an effective workaround — for such occurrences can be achieved through the utilization of an acquisition device that is connected to the output of the generation stage in order to provide a point of mathematical reference for such variations.

Nevertheless, while such characteristics, within the generation stage, might appear somewhat disheartening, especially since such characteristics are typically innate within most commercial generation devices — with the rare exception being an ideal generation device that is capable of producing a desired output signal regardless of the connected load impedance — yet, the occurrence of such characteristics are, in many ways, analogous to the effects observed upon the introduction of a variable internal gain that was, previously observed, within the operational amplifier discussion, and as was the case within the variable gain discussion, the occurrence of, such innate characteristics, can only effectively be handled by considering such effects as just another conditional instrumentational oddity that must be taken under advisement prior to either performing an laboratory experiment or creating a mathematical model from experimentally obtained observations. Conversely, with this being said, because generation effects tend to be conditional and application dependent, thus it now seems prudent to shift the focus of discussion away from the rigors imposed by a broad examination of the term towards simply examining the particulars of the generation device utilized while performing laboratory experimentation and the effects

that are associated with that devices utilization. Towards this end, the majority of laboratory experiments performed — at least within this dissertation — utilized a Tektronix AFG3102 programmable function generator, as shown by Figure: (181), with operational characteristics that are defined within Table: (13).

Table 13: tektronix afg3102 signal generator specifications [406, pp.2-5]

Boundary	Unit	AFG3102
Bandwidth	MHz	100
DC Abs Max Output at 50Ω Load	V	±5
DC Abs Min Output at 50Ω Load	mV	±1
Output Impedance	Ω	50
Isolation Voltage	V_{pk}	42
Resolution Voltage	mV_{pk}	0.1
Digital Resolution	Bits	14
AC Abs Max Output at 50Ω Load	V_{pp}	±10
AC Abs Max Output at Open Load	V_{pp}	±20
AC Abs Min Output at 50Ω Load	mV_{pp}	±20
AC Abs Min Output at Open Load	mV_{pp}	±40

Likewise, upon examining the operational characteristics, listed within Table: (13), a

Figure 181: a picture of the tektronix afg3102 signal generator

number of attributes seem eerily reminiscent to those found within the, previously presented, acquisition instrumentation table and, based upon the previous discussion, the existence of such commonalities should not be surprising given the innate symmetry associated with the acquisition and generation stages. Thus, it should come as no surprise that the commercial signal generation device being utilized would have a well-defined — but limited — spectral reproductive range that is the accumulative result of the Nyquist rate, analog component limitations, and intentional low pass filtering — to compensate for digital quantization effects. Similarly, in the same manner that spectral limits were innately expected, the existence of a digital resolution parameter was also expected; although, the 14-bit resolution was somewhat unexpected given the overall commercial commonality of 8-bit and 12-bit D2A devices. Likewise, the characteristic output impedance of 50$\mathbf{\Omega}$ was definitively expected, especially given the frequent appearance and underlying engineering tradition that is associated with this value's utilization within a countless number of electrical applications, although — based upon the previous discussion — such simplicity is seldom ever physically valid beyond ideal circumstances and thus, such attributes, should be considered circumspect and rigorously reevaluated for legitimacy on a per application basis. Finally, while the existence of the — previously mentioned — parameters were definitively expected; however, the notable discrepancies between AC and DC minimal and maximal voltage specifications was, in fact, somewhat unexpected — at least within a singular D2A generation device — and the occurrence of such attributes does provide some insight into the complexity of the internal structure of the signal generation device being examined.

Since, for example, the inclusion of both an AC and DC parameter implies the existence of, at least, two internal generation stages — likely two D2A converters whose outputs are

added together prior to the external output — and the existence of such ambiguity is yet another reminder of some of the difficulties that are associated with black box system modeling. Nevertheless, while such operational characteristics are extremely important when defining and developing laboratory experiments — since, after all, such characteristics directly limit the types of experiments that can be performed —; however, such characteristics tend to become less important within the actual modeling process, primarily because of the acquisition techniques implemented to overcome the — previously mentioned — loading dependency, and, as a result, such characteristics are seldom ever included within the modeling process beyond the ideal source in series with the internal load impedance since, it is assumed that — so long as the device is utilized within its specified operational boundaries — that any generation effects that occur can — and will — be accounted for by the, previously mentioned, acquisition model. With this being said, while such observations might appear somewhat counterintuitive, especially upon examining the level of detail provided to describe acquisition effects, yet while there are scenarios, in which, such assumptions will begin to become invalid, — particularly when collecting and analyzing measurements that are outside of the equipment specifications — such assumptions — at least within this dissertation and through frequent laboratory experimentation — have been found to be both legitimate and acceptable for the laboratory experiments conducted. Accordingly, with this being said, it now seems prudent to conclude such discussion — regarding instrumentational effects — by simply surmising that the instrumentational effects presented within the acquisition, processing, and generation discussions does play a significant role in determining the types of experiments that can be performed and the amount of accuracy obtainable within a given research laboratory, the types of modeling techniques applicable within the experiments performed, and the overall flexibility and applicability of the model obtained.

6.2.4 Material Effects

The fundamental rationale behind the material effects section was to define and demonstrate information regarding the commonly identifiable sources of distortion within bioelectrical acquisitions that — while arguably could be categorizable as being instrumentational in origin, at least depending upon the categorizing criteria utilized, as shown by Figure: (182) and Figure: (183) — were classified by the term material effects — within this dissertation — because of there intrinsic association — in terms of manifestation — with the objective being examined. Likewise, while the amount of information presented within this section — particularly on the distortions created by the electrical conduction thru aqueous solutions of sodium chloride — was kept to a minimum — predominantly because such distortions were examined and discussed in greater detail within the experimentation and research results section — the fundamental rationalization behind this sections intended objective and unique contribution was to validate the necessity of further inquiry into this observed phenomena by demonstrating the inability of contemporary electrical theory to effectively predict such occurrences — primarily because of these materials intrinsic electrical nonlinearities — and to foreshadow the importance of distortion reduction thru the implementation of proper apparatus configuration — another attribute discussed within the experimentation and research results section thru the creation of a unique procedural testing methodology.

Thus, with this being said, material effects — while in some sections assumed implicitly understood, and in other sections deeply, though unintentionally, discussed, particularly within the environmental and instrumentation effects section — are best surmised as being the innate and observable manifestation of natural phenomena within the perceptible world,

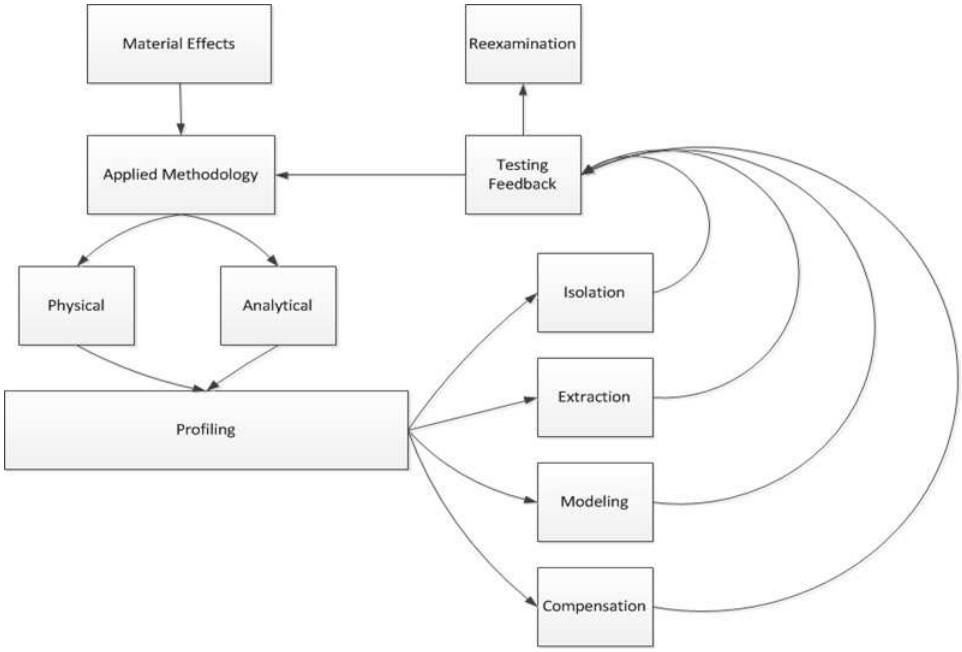

Figure 182: conceptual material effects flowchart

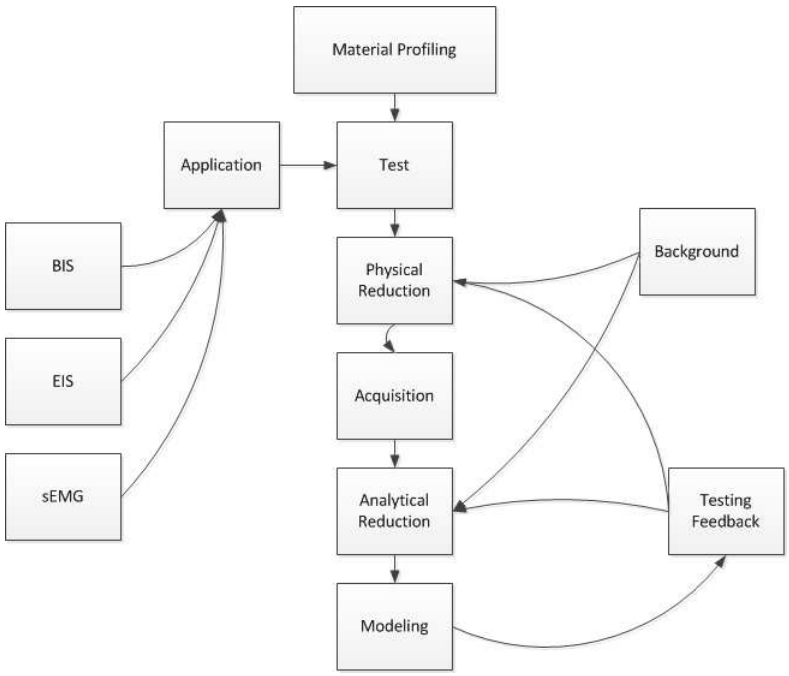

Figure 183: conceptual material effects profile flowchart

and while such descriptions might appear, at least at first, somewhat obscure; they are reasonably accurate, insofar as, they tend to convey the existence of an intrinsic complexity that is fundamentally inherent upon associating a natural phenomenon with a perceptible set of scientific characteristics. Likewise, to elaborate this point further, consider for the moment how materials are typically characterized — at least from the traditional perspec-

tive taken within the electrical engineering discipline — by their ability — or lack thereof — to conduct electricity. Conversely, while it is important to recognize that a number of other perceptible and classifiable attributes are also frequently utilized to characterize such materials, in addition to electrical conductivity, — like atomic structure or other supplementary chemical characteristics —; however, despite electrical conduction being inherently dependent upon a number of such attributes, the previously mentioned innate natural complexities — or more precisely, the observable peculiarities typically encountered — are generally more readily observed upon examining a materials innate electrical characteristics, as opposed to attempting to assess such characteristics through the examination of other partially observable mechanisms — such as analysis based on atomic parameters or other chemical effects.

Furthermore, because such sentiments tend to be a function of observational regularity, the existence of such complex anomalies — particularly those easily observed within the electrical engineering domain — might seem somewhat counterintuitive given that the materials most commonly encountered — within the electrical engineering domain — are generally simplistically classified as being either innately conductive or non-conductive — although such descriptions generally only articulate the most mundane, yet frequently assumed, scenarios —; nevertheless, despite the existence of this perceived assurance — within the electrical engineering discipline —, such simplistic assumptions will inevitably begin to break down upon examination of semi-conductive materials — like ion implanted, or doped, silicon — that is capable of conditionally changing its conductivity, and such assumptions are further invalidated upon examining electrical conductivity over an assortment of spectral frequencies, since even the most mundane materials began to conduct differently at different spectral frequencies. Therefore, while it is possible to associate such

variations in conductivity with an understood and classifiable disciplinary characteristic — a task generally avoided within the electrical engineering discipline —, it is worth mentioning that the existence of such connections are not necessarily as pertinent — to this particular dialog — as the observation that the classification of such material attributes as being either a simplistic conductor or insulator is a rather negligent assessment; since, after all, the existence of the, previously mentioned, conductive conditionality — or regions of bounded conductive variation — elegantly depicts how such simplistic assumptions can fail to describe scenarios that exist beyond common operational conditions and highlights the underlying innate complexities that are associated with this particular natural phenomenon, while, at the same time, also reiterating the, previously mentioned, importance of possessing an in-depth understanding of material operational boundaries.

Accordingly, with this being said, given that the central topic of discussion — within this dissertation — is primarily focused upon the modeling of material effects — particularly atypically conductive materials like biomaterials and simplistic aqueous solutions — an overly descriptive re-review of such attributes would seem to be redundant given the amount of time spent — within previous chapters — discussing traditional conductive and non-conductive materials and the pending discussion — within this chapter — regarding the conductivity of atypically conductivity materials. Therefore, with this being said, rather than re-examining these simplistic attributes, it seems more prudent to quickly surmise such attributes — to provide a point of comparison — and then begin introducing some of the more notable characteristics of atypically conductive materials experimentally observed — since such characteristics will be examined in more detail within this chapter. Thus, with this being said, since these simplistic electrical materials — like polychlorinated biphenyl (PCB), glass, copper and aluminum — are the underlying foundation upon which

the majority of electrical engineering applications are both built and theoretically understood — as PCB and glass are generally associated with electrical insulators, while copper and aluminum are generally associated with electrical conductors. Therefore, while these simplistic material classifications are readily understood — at least within easily assessable operational conditions — both of these simplistic classifications are — most importantly, though infrequently discussed — intrinsically associated with the concept of system linearity — or, more simplistically stated, are assumed to be adherent to the electrical engineering attributes of superposition and voltage versus current proportionality — the underlying foundations upon which Kirchhoff's voltage law (KVL) and Kirchhoff's current law (KCL) are assumed to be valid assumptions [207] [105].

Conversely, while these simplistic materials are fundamental to the creation of basic electronic devices, other more complex materials — like semiconductors — also play a substantial role within modern electronics but, more importantly, also possess qualities that — under certain circumstances — do not explicitly adhere to the electrical engineering concept of system linearity. Thus, to elaborate on this attribute further, consider for the moment the Lissajous diagrams of voltage versus current for an ideal resistor operating within traditional conduction boundaries — which can be modeled as a simplistic lossy conductor, governed by Equation: (455) — and an ideal Shockley diode, once again, operating within traditional conduction boundaries, — which is a complex semi-conductive device that can be conditionally modeled by Equation: (456) —, as shown by Figure: (184) and Figure: (185) [407, pp.392–400] [103, pp.161] [408, p.194].

$$I = \frac{V}{R} \tag{455}$$

$$I = I_S \left(\exp\left(\frac{V_D}{n\, V_t} \right) - 1 \right) \tag{456}$$

While Figure: (184) and Figure: (185) are somewhat disorienting to examine, primarily because Lissajous figures are infrequently utilize within electrical engineering analysis — or they are more frequently observed to depict voltage versus voltage comparisons —, the

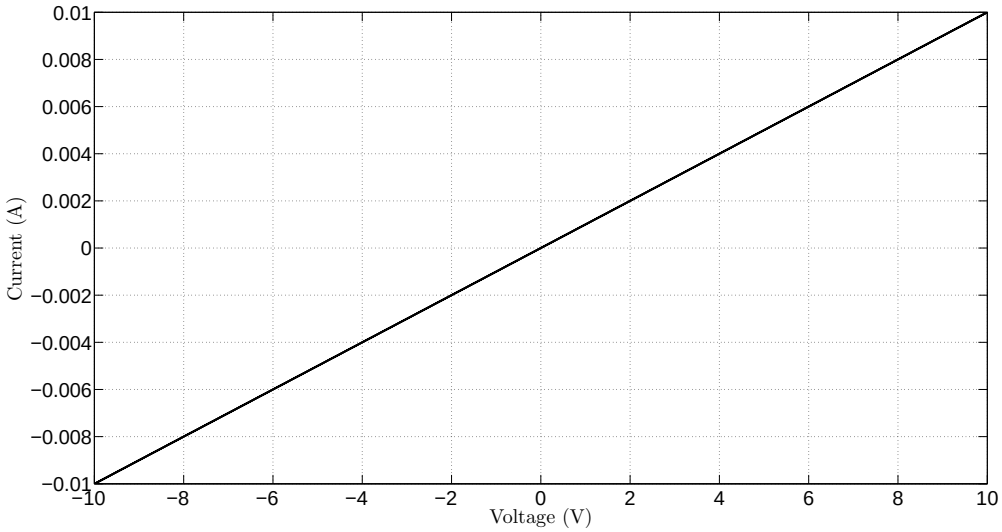

Figure 184: lissajous plot of a ideal resistor with v swept from -10 to 10 to -10 versus current with $r = 1000\Omega$

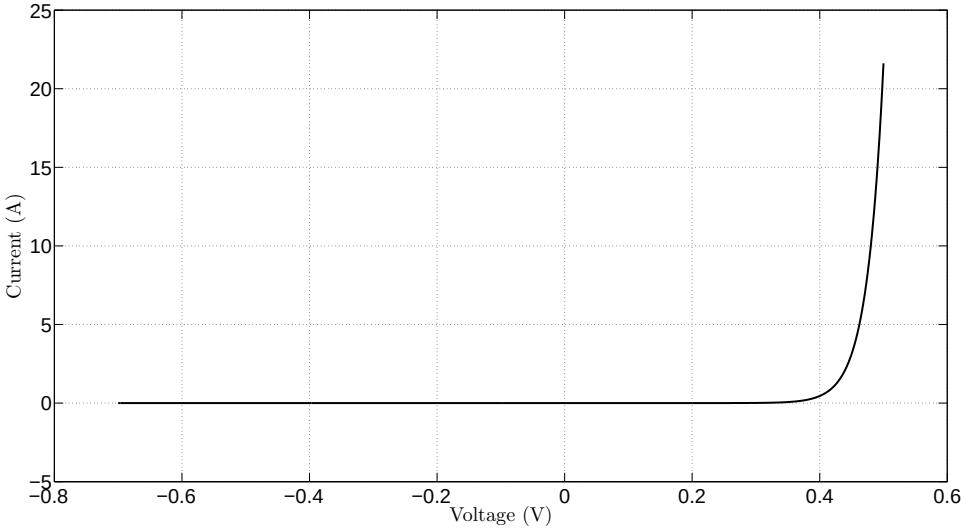

Figure 185: lissajous plot of a ideal shockley diode with v swept from $-.7$ to .5 to $-.7$ versus current with $i_s = 8.6 \times 10^{-8}$, $v_t = .02585$, and $n = 1$

critical attribute to take away from such figures is the observation that the current within Figure: (184) appears to change proportionally to changes in voltage, while the current within Figure: (185) appears to become disassociated to changes in voltage when the voltage enters a particular operational region — generally referred to as the Shockley diode reverse operational region, or junction cutoff region. Conversely, it is this observable disassociation between voltage and current, within Figure: (185), that ultimately invalidates the principles of superposition, thus making the Shockley diode a nonlinear device, while the strong proportional changes, within Figure: (184), makes the simplistic lossy conductor a linear device — an attribute that can be further validated through the partial application of the signals and systems linearity test, as shown by Equation: (457) thru Equation: (471) and Equation: (472) thru Equation: (488).

$$X_1 = -10\text{V} \tag{457}$$

$$X_2 = 10\text{V} \tag{458}$$

$$X_3 = X_1 + X_2 \tag{459}$$

$$X_3 = 0\text{V} \tag{460}$$

$$Y(X) = \frac{X}{R} \tag{461}$$

$$R = 1000\Omega \tag{462}$$

$$Y_1 = \frac{X_1}{1000} \tag{463}$$

$$Y_1 = -0.0100\text{A} \tag{464}$$

$$Y_2 = \frac{X_2}{1000} \tag{465}$$

$$Y_2 = 0.0100\text{A} \tag{466}$$

$$Y_{3a} = \frac{X_3}{1000} \tag{467}$$

$$Y_{3a} = 0\text{A} \tag{468}$$

$$Y_{3b} = Y_1 + Y_2 \tag{469}$$

$$Y_{3b} = 0\text{A} \tag{470}$$

$$Y_{3a} = Y_{3b} \tag{471}$$

$$X_1 = -.7\text{V} \tag{472}$$

$$X_2 = .5\text{V} \tag{473}$$

$$X_3 = X_1 + X_2 \tag{474}$$

$$X_3 = -0.2\text{V} \tag{475}$$

$$Y(X) = I_S \left(\exp\left(\frac{X}{n\, V_t} \right) - 1 \right) \tag{476}$$

$$I_S = 8.6 \times 10^{-8} \tag{477}$$

$$V_t = .02585 \tag{478}$$

$$n = 1 \tag{479}$$

$$Y_1 = 8.6 \times 10^{-8} \left(\exp\left(\frac{X_1}{.02585} \right) - 1 \right) \tag{480}$$

$$Y_1 = -8.6 \times 10^{-8}\text{A} \tag{481}$$

$$Y_2 = 8.6 \times 10^{-8} \left(\exp\left(\frac{X_2}{.02585} \right) - 1 \right) \tag{482}$$

$$Y_2 = 21.6162\text{A} \tag{483}$$

$$Y_{3a} = 8.6 \times 10^{-8} \left(\exp\left(\frac{X_3}{.02585} \right) - 1 \right) \tag{484}$$

$$Y_{3a} = -8.596 \times 10^{-8}\text{A} \tag{485}$$

$$Y_{3b} = Y_1 + Y_2 \tag{486}$$

$$Y_{3b} = 21.6162\text{A} \tag{487}$$

$$Y_{3a} \neq Y_{3b} \tag{488}$$

Nevertheless, despite these innate differences being interesting to graphically observe, the critical concept to take away from such observations is the notion that different materials are, not only capable of having variations in electrical conductivity — once again, based upon there innate atomic compositions —, but, more importantly, such characteristics can change as a result of complex internal material characteristics, and such characteristics — at least under certain circumstances — can be extremely difficult to mathematically model and predict, especially when trying to apply linear modeling techniques to these generally nonlinear problems. Conversely, to better quantify such descriptions, these attributes can be graphically conveyed upon examining an atypically conductive aqueous material — like normal saline or a similar aqueous NaCl solution — as shown by Figure: (186).

Likewise, while the electrical attributes depicted within Figure: (186) are definitively distinctive and — although, in this particular case, not rigorously validated through the utilization of mathematical derivation — appears to be — intuitively — highly nonlinear,

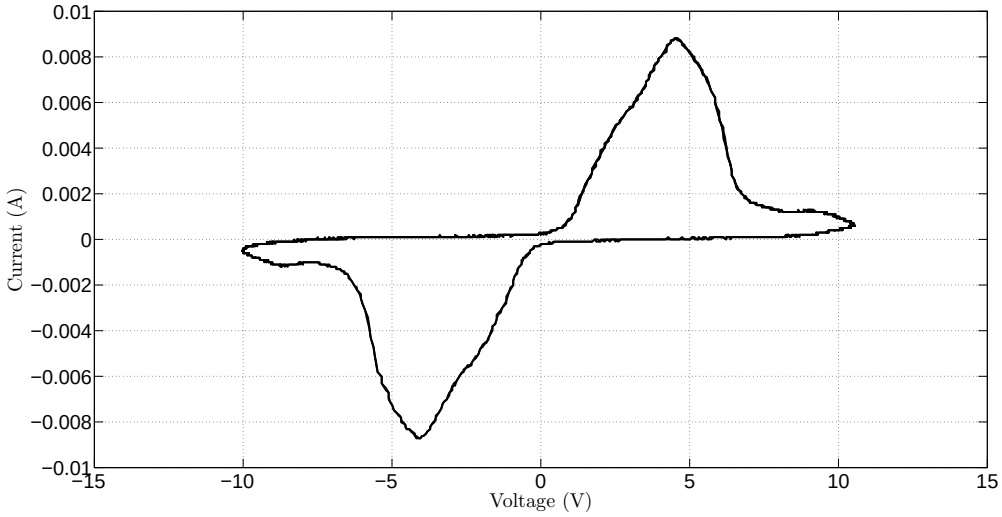

Figure 186: lissajous plot of a .7 molarity nacl (aqueous) solution with a 1hz at $10v_{pp}$ applied sinusoidal test signal

relative to a Lissajous plot of a simplistic linear phase shift between voltage versus current — as typically observed within a reactive electrical element, like a capacitor or inductor — as pseudo-demonstrated by Figure: (187).

Yet, regardless of such observations, while there are a substantial number of materials — each possessing its own unique set of electrical characteristics — that, depending upon the electrical operational conditions specified, can be classified as either being innately linear or nonlinear; however, while such notions are, in fact, very important when attempting to mathematically represent such materials; yet, the most important attribute — at least in terms of obtaining a high fidelity measurement —, is not necessarily an inherent understanding of system linearity — although such knowledge is generally required to effectively mathematically model such materials — but rather, the possession of a in-depth understanding about the physical conditions in which a measurement is to be obtained can be far more profound.

To elaborate on this issue further, consider for the moment the — previously mentioned — instrumentational effects discussed regarding apparatus interconnections and the accompanying effects encountered — like stray capacitance and inductance — that, in themselves,

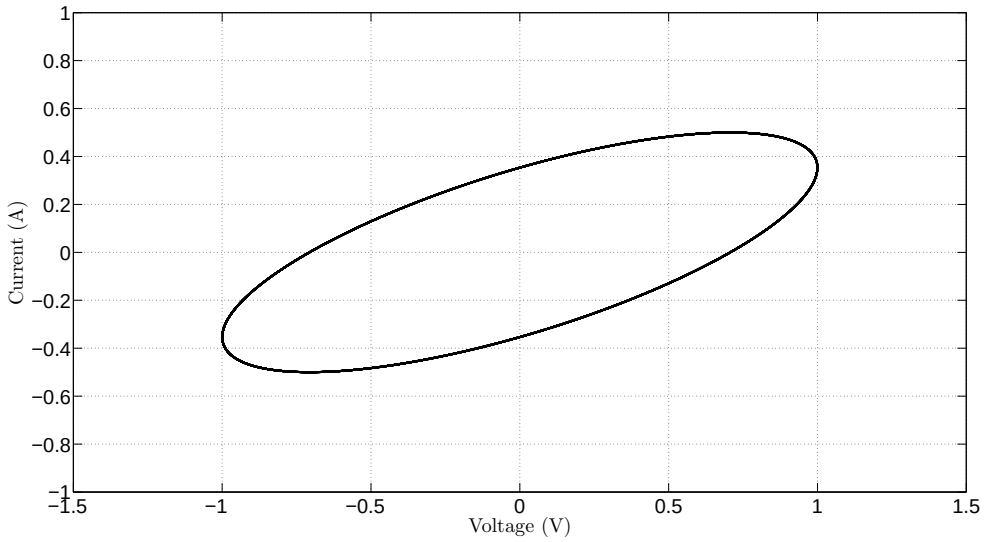

Figure 187: lissajous plot of $\sin(2\pi\, f\, t)$ versus $\frac{1}{2}\sin\left(2\pi\, f\, t + \frac{\pi}{4}\right)$

are fundamentally categorizable as being strictly the product of a material related attribute but, because of there frequent occurrence within the electrical engineering discipline, are generally surmised through the utilization of preexisting electrical engineering components and assumed topological circuit structures; typically without the benefit of any further investigative or intellectual thought. Likewise, while such attributes might seem particularly moot — especially given the amount of discussion previously provided on the subject, at least from a modeling perspective —, yet while the formulation of instrumentational models need no further consideration — at this point in time —, the underlying source of these effects — and of course the consequences that such effects can have upon acquisition fidelity — does merit both intellectual pause and further discussion. Conversely, based upon such discussion, it is important to recognize that one of the biggest banes to obtaining a high fidelity measurement lay not completely with the complexities associated with mathematically modeling an atypically conducted material — although the rigors of mathematical modeling can quickly exceed a researchers innate intellectual depth very quickly — but rather with the process of creating an appropriate acquisition apparatus that is capable of minimizing the amount of unassociated electrical phenomena measured — thus helping to reduce the overall complexity of the mathematical model required through the passive exclusion of extraneous effects.

While such mechanisms of increased fidelity were inadvertently discussed within the environmental effects section — primarily through the utilization of a RF shielded room — and other extraneous effects — like instrumentational effects — are generally an unavoidable necessity that cannot be removed nor easily reduced. Nevertheless, despite the presence of some extraneous sources of noise — that will naturally require some type of mathematical compensation within the model developed —, other sources of noise — ar-

guably deserving the instrumentational classification but presumed as being material effects — can be removed or significantly reduced through the intellectual possession of a proper theoretical understanding of the rigors associated with apparatus materials and configuration — a skill developed primarily through years of laboratory experience and an in-depth understanding of material effects. Likewise, because it would be impractical — if not impossible — to convey both intuition and experience within a single sub-chapter, or, for that matter, within the confines of a book — thus no disservice will be made through such attempts —; however, commonly observed material effects can be discussed to some significant depth — within the space allotted — along with some of their corresponding manifestations upon there haphazard utilization within laboratory apparatus. Thus, upon taking such notions under advisement, it seems reasonable to begin this particular discussion by first examining the intrinsic material effects that occur upon the utilization of dissimilar materials to create an electrical junction. While the traditional electrical engineering perspective tends to view such junctions as being either strictly conductive, lossy, or non-conductive; however, in reality, these localized points of interaction generally possess a substantial wealth of discontinuity — insofar as, possessing substantial variations in the underlying mechanisms that govern their observed conductivity — and such attributes generally manifest themselves in a number of different possible combinations.

For example, dissimilar metal junctions — while possessing a substantial amount of atomic similarities that allows the free flow of electrons between the two materials — can also introduce — depending upon the metals selected and the overall material purity — a slight potential gradient, primarily because of a notable difference in a materials response to external thermal or electromagnetic conditions — a popular , but extreme, example of thermal induced gradients is readily observed within a device called a thermopile [409] [184].

Yet, despite the existence of such occurrences, the development of a significant potential gradient from this particular type of junction — at least under the laboratory testing conditions utilized within this dissertation — would be an exceedingly rare an unlikely — or more precisely unnoticeable — occurrence; however, metal on metal junctions also tend to create discontinuities within electrical transmission structures — since metals are the predominant method utilized to transport electrical signals from point A to point B — thus, in turn, the introduction of structural discontinuities — within the electrical transmission structure utilized — generally increases the possibility of electromagnetic fringing occurring and allows for the development of convection currents within apparatus interconnections — an attribute that will be examined in more detail within this chapter [184].

While the latter manifestations are more prevalent than the former — although minor potential gradients are possible, but are generally, well below, the measuring capabilities of most acquisition instrumentation commercially available —; nevertheless, using such observations as a guide, an important first step — in obtaining a high fidelity measurement — is to minimize the number of material junctions utilized within an experimental apparatus, or when such minimization becomes impractical, to ensure that junctions are as uniform — in structure — and as similar in material composition as physically possible, in order to reduce the amount of distortion these particular effects can create. Furthermore, while material composition and the structural uniformity of interconnections can play a substantial role in determining the amount of distortions observed within metal on metal junctions, a similar thing can be said regarding the proper selection of geometrically appropriate signal transmission structures of such materials — referring to the wire structures utilized to transmit signals to a measuring apparatus — as such structures play a significant role in determining the amount of electromagnetic energy stored within the structure, referring

to inductance — and, to some extent, governing the overall magnitude of the, previously discussed, junction effects encountered.

Thus, in a manner similar to the minimization of metal on metal interconnections, great care should also be taken to; firstly, utilize a geometrically appropriate electrical transmission structure necessitated by the desired application — whether it be through the utilization of a commercially available solution, like coaxial cable, or a customized solution, like the previously shown twisting of transmission wires —, and secondly avoid common inductive structures — like coils — that increase passive electromagnetic energy storage. While there are always some inherent trade-offs associated with the utilization of such techniques — since the reduction of environmental effects through the utilization of geometric structures could, in turn , increase the amount of passive electromagnetic energy stored within the cable — thus environmental effects were substituted with material effects —; nevertheless, it is important to recognize that such attributes do, in fact, play a substantial role in determining the types of material effects encountered and such considerations must be taken under advisement during the development of experimental measuring apparatus.

Conversely, while metal interconnections are extremely common within the electrical engineering discipline, so much so, that a nearly countless number of studies have been conducted on this particular subject — and based upon such observations, it could be jestingly surmised, that the discipline of electrical engineering is nothing substantially more than the progressive study of the electrical properties of such interconnections —; however, setting such jests aside, other types of material interconnections are also equally prevalent — especially within the biomedical discipline —, the most notable being metal to nonmetal and nonmetal to nonmetal interconnections. While metal to nonconductive nonmetal junctions are reasonably well understood — as the electrical properties of capacitors have been

extensively modeled —, along with metal to semi-conductive junctions — as the advent of semiconductors is one of the notable events that transformed electrical engineering from a curious hobby into a everyday necessity —; however, while such material junctions are reasonably well understood — within the electrical engineering discipline — it is important to recognize that there are a substantial number of nonmetal materials that do not easily fall within such categories that have, for the most part, not undergone the rigors of electrical characterization — at least not beyond a brief inquiry for something substantially profound and practical —, and it is this inherent uncertainty amongst such material junctions, that seems to be a unspoken presence within the biomedical community — particularly within the bioelectrical research area — when it comes to examining biomaterials.

Likewise, with this being said, while it will not be proclaimed that the information presented — within this dissertation — will answer or address every attribute of this particular observation; however, a substantial amount of time will be spent — in the next section — examining the electrical properties of atypically conductive junctions — specifically aqueous sodium chloride solutions — in an attempt to determine, at the very least, the role that such junctions play in regard to the material distortions observed within bioelectrical signals. Furthermore, it is also worth mentioning that the types of distortions encountered — within these junctions — tends to be associated with the type of analysis performed since, for example, passive bioelectrical analysis — like EKG, EMG, or EEG — is likely to yield a more subtle distortion than active bioelectrical analysis — like bioimpedance spectroscopy (BIS) or electrochemical impedance spectroscopy (EIS) — since one technique is actively promoting the formation of a metal to atypically conductive nonmetal junction while the other technique — although possessing a metal to nonmetal junction — is not actively attempting to invoke electrical conduction within the nonmetal, but rather

is observing the passive electrical interactions that typically originate deep within the biomaterial being examined — which is, in itself, likely a nonmetal to nonmetal electrical interaction.

6.3 Experiments, Results, and Applications

Nevertheless, while the previously presented information — within the defining high fidelity subsection — is of substantial importance in obtaining a solid foundation to begin understanding both, sources of distortions, along with techniques to overcome these distortions; however, while such knowledge is inherently beneficial, often times the observation of such techniques in practice can be far more beneficial than simply a progressive theoretical monologue — like the one previously provided —, thus it now seems worthwhile to examine such theoretical principles in practice. Conversely, with this being said, it should be noted that a minor caveat exists within this particular section regarding the chronological order — or lack thereof — of the experiments presented, since — after numerous hours of intellectual inquiry — it was decided that the concepts presented — in their current order — are more understandable relative to there actual chronological order. Likewise, while this might sound like a minor nuance — after all clarity is a virtue —; however, it should be pointed out that a number of advanced acquisition techniques — some of which were previously discussed — were not implemented until after researching the subject for a number of years, and thus some minor peculiarities might exist as to why certain techniques were not implemented within some of the experimental results presented while other techniques were.

6.3.1 Managing Environmental Effects

The fundamental rationale behind the managing environmental effects section was to define both the testing conditions and apparatus utilized — within the research laboratory

— to obtain the biomaterial acquisitions collected within this dissertation. Likewise, this section provides unique information regarding the limitations of contemporary acquisition environments frequently utilized to reduce environmental distortions, along with provides a methodological approach — as shown by Figure: (45) — to obtain the highest acquisition fidelity possible, while reinforcing the importance of the — previously discussed — distortion reduction apparatus methodology and apparatus safety methodology developed. Furthermore, based upon the observations made upon the implementation of these methodological methods, it was observed that the environmental effects inherently encountered by laboratory acquisition devices were substantially reduced in environmental effect magnitude — from a 40mV peak environmental effect floor to a 20mV peak environmental effect floor under high impedance conditions — upon performing the laboratory acquisition within a partially shielded RF shielded room — implying the shielded room is still externally powered —, and a further reduction in environmental effect magnitude was obtained — from a 20mV peak environmental effect floor to a 10mV peak environmental effect floor — upon isolating the RF shielded room from the external power source — implying all laboratory instrumentation is operating off of battery power, but at the cost of limiting the types of experimentation that can be performed.

While a number of important attributes were presented within the defining high fidelity measurements subsection — although some attributes were discussed in more detail than others —, the attribute of environmental effects was, by and large, examined to a much greater extent — from a research perspective — than the other subjects presented within this section; however, with this being said, despite the amount of detail provided, a discussion regarding the physical implementation of such considerations was lacking and, based on such attributes, it would now seem to be a reasonable course of action to begin by first

examining the environmental conditions utilized — within this dissertation — for the successful acquisition of a high fidelity measurement and the techniques utilized to obtain such measurements. Conversely, as it was previously mentioned, it is possible to significantly reduce the occurrence of environmental effects through the proper utilization of physical shielding techniques — like the usage of a RF shielded room, as re-depicted by Figure: (70) — and such techniques are further visually validated upon examining the high impedance (High-Z) measurements taken of laboratory conditions encountered inside and outside of the physical shielding environment utilized — within this dissertation —, as re-depicted by Figure: (51), Figure: (72), and Figure: (73).

Likewise, while such figures help to validate that environmental effects can, in fact, be reduced through the utilization of physical shielding techniques; however, these figures fail to convey the amount of environmental reduction needed to obtain a high fidelity measurement — an attribute that was, as previously discussed, found to be inherently obscure. While examination of the observable peak to peak voltage values — within Figure: (51), Figure: (72), and Figure: (73) — does provide quantifiable numerical voltages to work with — $70mV_{pp}$, $50mV_{pp}$, and $20mV_{pp}$ respectively —, and it could be suggested that the lowest observed value —$20mV_{pp}$ in this particular case — be selected as the "de facto" [†1] standard, yet such assessments would seem to be inherently hasty, if not impractical, for a number of reasons [72, p.127]. Firstly, as it was previously discussed within the environmental effects section, such environmental conditions — re-depicted by Figure: (73) — were only obtained through the utilization of a RF shielded room that was operating under low-power conditions — as re-depicted by Figure: (70) — and such prerequisites makes the usage of this particular environmental noise value — as a high fidelity standard

[†1] Latin phrase for: being such in effect though not formally recognized.

— a metaphorically rather difficult pill to swallow, because of the substantial financial investment required to obtain such standards. Likewise, even if such financial burdens are overcome — in the case of this dissertation, a RF shielded room was readily available, compliments of the University of North Carolina at Charlotte —, the majority of commercial instrumentation available requires a connection to an external source of power — typically 120 Volts RMS at 60 Hz, within the United States — and commercially available battery-operated solutions — required for low-power operations within a RF shielded room — are both exceedingly rare and expensive, thus making low-power operations inherently impractical and problematic simply from a logistics perspective.

Conversely, assuming for the moment that the problem of low-power logistics are overcome — in the case of this dissertation, a battery-operated oscilloscope was available —, the level of shielding obtained can vary between shielding room manufacturers and the location in which the shielding room was placed. Secondly, while the problems — previously listed — are more than sufficient reasons to discourage the absolute usage of the, previously depicted, minimum value, as a environmental high fidelity standard, it is also worth pointing out that the environmental fidelity required — by a given bioelectrical application — is directly related to the strength of the signals being measured — as some applications require a higher environmental fidelity than others. For example, bioimpedance spectroscopy can be performed within a unshielded environment because the applied signal is usually substantially above — between $1V_{pp}$ to $20V_{pp}$ — the environmental effect level encountered — although there are a few exceptions to this statement as spectroscopy test signals can be defined at any value —; while electromyography (EMG), on the other hand, is extremely difficult to perform even within a shielded environment, primarily because this application is attempting to measure a extremely small signal — well below $10mV_{pp}$ —, and such mea-

surements generally require alternative methods of noise reduction in addition to physical shielding — typically achieved through the utilization of instrumentational amplifiers and digital signal processing (DSP) techniques.

Thus, with this being said, since the arbitrary proclamation of a particular environmental effect level — say below 20mV_{pp} — as a high fidelity environmental standard would seem somewhat absurd within this particular context, especially given the overall number of biomedical applications available and the varying amounts of environmental fidelity required by each of those applications. Nevertheless, while it could still be argued that the minimum environmental effect level obtained should be selected as the standard utilized, at least within the confines of this dissertation — as any reduction of such effects constitutes a improvement whether such reduction was necessitated or not —; yet, once again, the accompanying logistical issues that are associated with implementing such environmental standards must also be considered, and upon taking such considerations under advisement the following high fidelity environmental guidelines were implemented within the research being presented. Firstly, because a physical method of shielding was available — in this particular case, a RF shielding room —, all measurements acquired — within this dissertation — were taken within this shielding environment in order to reap the benefits of some reduction in environmental noise. Secondly, because low-power operations — within the RF shielded room utilized — is logistically problematic — primarily because the unavailability of a high fidelity battery-operated function generator —, such conditions were only utilized for obtaining passive measurements — like electrocardiography (EKG) and electromyography (EMG) measurements. Conversely, with this being said, because quantifiable values are generally more preferred than simply the mention of a arbitrary testing location, it should be noted that the environmental fidelity standards selected —

Figure 188: dr. mehdi miri demonstrating typical powered rf shielded room operations

within this dissertation — translates, more quantifiably, to $50mV_{pp}$ or lower for any active measurement acquired — like bioimpedance spectroscopy — and $20mV_{pp}$ or lower for any passive measurements acquired — like electrocardiography (EKG) and electromyography (EMG). Likewise, to clarify these quantifiable values further, it is worth mentioning that such high fidelity environmental standards do not incorporate the introduction of compensation techniques, like the utilization of instrumentational amplifiers or other environmental filtering techniques — whether they be digital, like finite impulse response (FIR) filtering or physical, like bandpass filtering — and are only intended to describe and restrict the physical environmental conditions in which a high fidelity measurement was taken.

Similarly, to describe the physical configurations and the procedural methodology utilized — to obtain high fidelity environmental conditions — the following actions were taken. Firstly, in the case of powered RF shielding conditions — once again, primarily utilized to obtain active measurements — the experimental apparatus being measured was simply placed within the RF shielded room and the entrance to the room was sealed in order to maximize the environmental shielding effects obtained, as depicted by Figure: (188). Secondly, while powered RF shielding conditions are — logistically — relatively straightforward to implement; however, the act of obtaining low-power RF shielding conditions — primarily utilized to obtain passive measurements — is far from being logistically trivial

Figure 189: (top left) a picture of the custom built ±12v battery box utilized to power electrical circuitry for low power rf shielded room operations, (top right) a picture of the electrical breaker utilize to isolate the rf shielded room from the power grid, (bottom left) a picture of the battery-operated lantern utilized to provide illumination for low power rf shielded room operations, (bottom right) a picture of the tektronix tps2024 oscilloscope battery utilized for low power rf shielded room operations

and requires both a significant amount of planning and procedural steps in order to obtain. To elaborate on this attribute further; first, all experimental apparatus and acquisition equipment utilized — once again, under low-power conditions — must, through necessity, be battery powered, as shown by Figure: (189) bottom right, Figure: (189) top left, and Figure: (190). Second, because all external electrical power to the RF shielded room must be disconnected prior to beginning low-power operations — a process accomplished through switching an electric circuit breaker, as shown by Figure: (189) top right —, it is important to recognize that no external lighting — within the RF shielded room — is available upon disconnecting the external electrical power, thus battery operated lighting, as shown by Figure: (189) bottom left, is needed for passive illumination in order to effec-

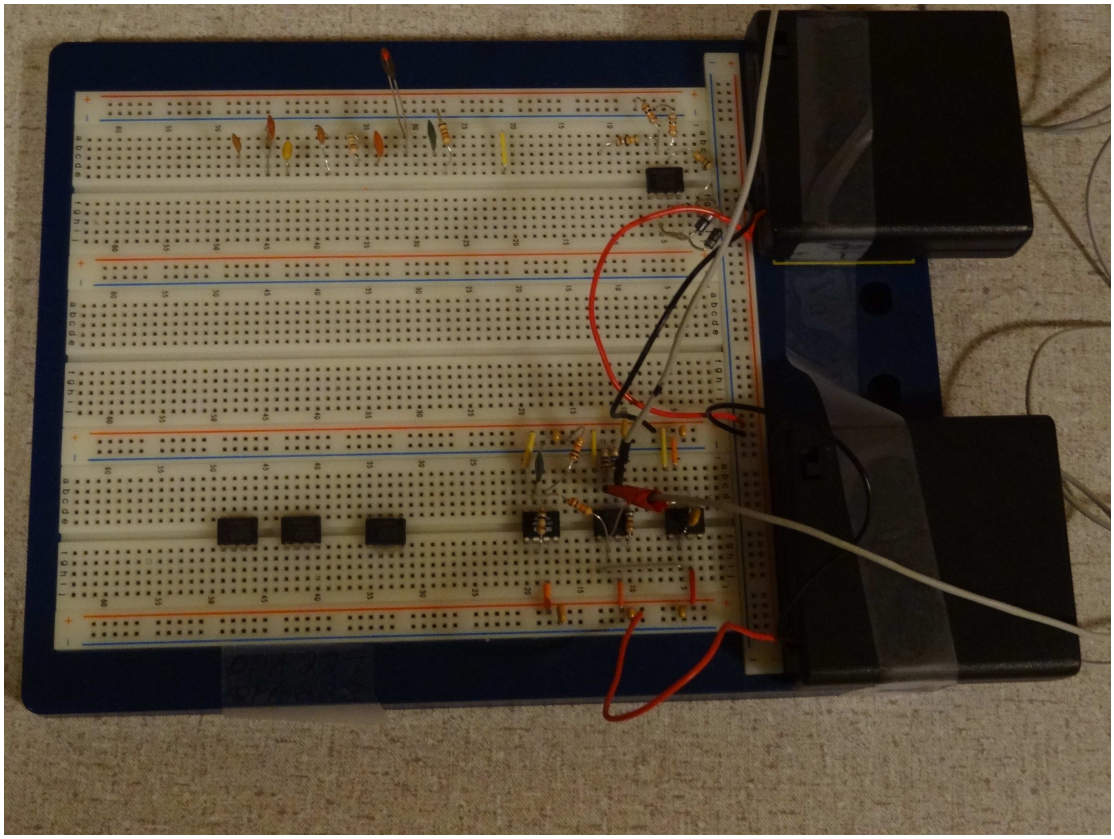

Figure 190: a picture of the custom built battery-powered instrumentational amplifier circuit designed to take ekg and emg measurements

tively operate laboratory apparatus under such conditions. Conversely, upon the successful implementation of conditions one and two, the shielded room is simply sealed and the desired low-power environmental measurements performed — a task that is reminiscent of the, previously discussed, powered RF shielded measurements.

Nevertheless, while such attributes might seem somewhat intuitive and simplistic — so much so, that their mention might seem needlessly extraneous —, yet it is important to recognize that such, seemingly needless, details can be very easily overlooked, and while it might be conceded that the possibility of a researcher forgetting to disconnect the power prior to performing a low-power RF shielded room test is unlikely — although recollection of personal experience seems to indicate that some complexities can arise regarding what breaker needs to be disconnected —; however, from a logistical standpoint, while the act of forgetting to disconnect the power might be very unlikely, it is, in fact, quite possible

that a researcher might forget to charge a battery, say for the battery-operated LED lamp or oscilloscope, and as a result, the experiment would need to be postpone until this, seemingly simplistic, yet mission-critical component was recharged. Conversely, with this being said, the introduction of this particular procedural problem tends to promote the invocation of additional logistical problems, mostly concerning the limitations imposed upon research experiments from the usage of battery power devices since, for example, batteries only provide a limited amount of power over a rigidly finite duration and such attributes, as a result, place operational limits upon experiments being performed under low-power conditions.

For example, experiments that require the extended observation of any given electrical phenomena — say over six hours in duration — under low-power shielded room conditions will inevitably become extremely impractical because of the physical limitations invoked upon the usage of battery power as a primary means of supporting acquisition instrumentation. Conversely, while such limitations can be overcome — to some extent — through the usage of a larger pseudo-metaphoric battery — pseudo-metaphoric in this particular case because the amount of power provided by a battery is not necessarily always dependent upon the physical size of the battery utilized —; however,such methods begin to become impractical and ultimately possess a distinctly definitive temporal upper limit — whether it be one day, one month, or one year —. Thus, while the concept of environmental fidelity and environmental effects is a inherently definable electrical concept — at least from a observable perspective —; nevertheless, when the term is applied to describe a real-world measuring capability, such attributes begin to have additional parameters inadvertently incorporate it into their meaning — in this particular case, the temporal limitations imposed by operating on battery-power must also be considered, within this dissertation anything

beyond two and a half hours for any low-power RF shielded room experiment becomes logistically problematic — and the introduction of such attributes must be considered when defining quantifiable high fidelity environmental standards.

Fortunately, despite the manifestation of such temporal limitations, the intended application of passively observing both electrocardiographic and electromyographic signals — a task that, for the sake of improved fidelity, requires a low-power RF shielded room — is a relatively quick process in terms of acquisition time — as experiments generally last less than 30 minutes —, thus making such temporal limitations of little concern, at least relative to the capabilities that were available within this dissertation. Yet, while such experiments can be conducted relatively quickly — a notable benefit because a human test subject is required —; however, other experiments — like the electrical characterization of a given material — can take a substantial amount of time — hours to days — and the temporal requirements of such experiments makes the utilization of low-power shielding conditions extremely impractical, hence further justifying the, previously presented, notion of utilizing partially shielded environmental conditions to perform such experiments.

6.3.2 Preliminary Data Management

The fundamental rationale behind the preliminary data management section was to define contemporary acquisition problems that frequently arise when attempting to obtain and retrieve bioelectrical acquisitions because of variations in the way that contemporary acquisition devices digitally store acquired information. Likewise, this section provides unique information regarding the development of a generalized methodological approach — as shown by Figure: (191), Figure: (192), Figure: (193), Figure: (194), and Figure: (195) — to both communicate — or automate — and extract information from a diverse assortment of acquisition devices — as more than one type of acquisition device is frequently utilized

when performing biomedical research. Similarly, based upon the observations made within the preliminary data management subsection and the methodological approach developed, it was also demonstrated that the management and processing of substantial amounts of laboratory acquisitions — an attribute that results from the automation of such acquisition devices — is an inherently complex task, especially if more than one acquisition device is being utilized concurrently — noting that within this dissertation a TPS2024 and two TDS2002 oscilloscopes were utilized concurrently —, that — to effectively utilize — requires the implementation of both a highly intuitive organizational system — in order to keep track of the experiments performed and what the acquisitions obtained physically represents —, and customized acquisition importation software — based upon the methodological approach developed —, in order to concatenate individual channel acquisitions — from multiple acquisition devices — into a easily accessible medium for further analysis. Conversely, while these attributes might appeared to be somewhat unassociated with fundamentally improving acquisition fidelity; however, it was later demonstrated within this section that if such issues are not actively addressed, the capability to analyze laboratory acquisitions is substantially reduced — an attribute that generally reduces fidelity —, while the likelihood of processing distortions increases, since a greater amount of human interaction would be required — in order to manually format the acquired data —, thus increasing the likelihood of human error occurring.

Although the acquired laboratory data, presented earlier within this chapter — primarily within the environmental sections —, provides some inside into the physical environmental effects encountered by laboratory apparatus — utilized within this dissertation —, and, at the same time, also provides a quantitative comparison between the physical reductive techniques implemented; however, with this being said, while this information is

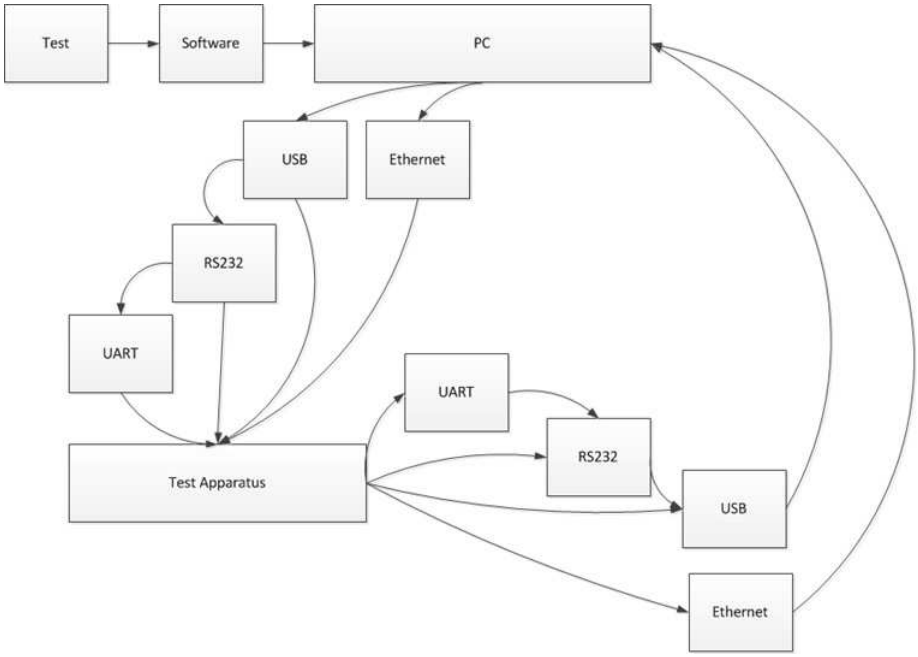

Figure 191: conceptual acquisition approach flowchart

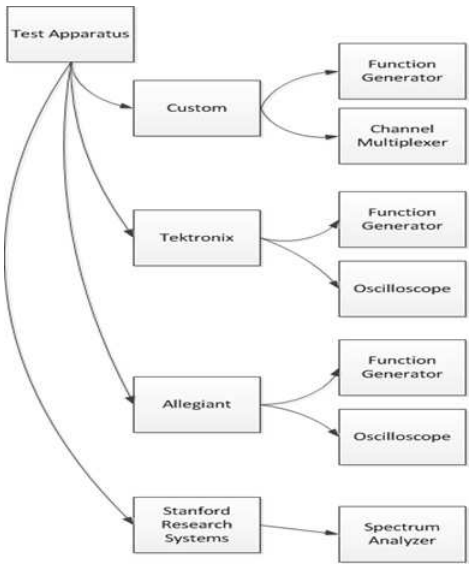

Figure 192: conceptual acquisition approach test apparatus flowchart

inherently important and beneficial, it should be noted that the underlying methodology utilized to acquire and process this information is — arguably — just as important and thus, merits further discussion. Conversely, while some discussion was provided on this particular issue — primarily from the perspective of distortions introduced by the utilization of such procedures —, yet such discussion feels lacking — at least in terms of describing the methodological processes utilized — and based upon such observations, it now seems appropriate to provide a methodological overview of the procedures utilized — within this

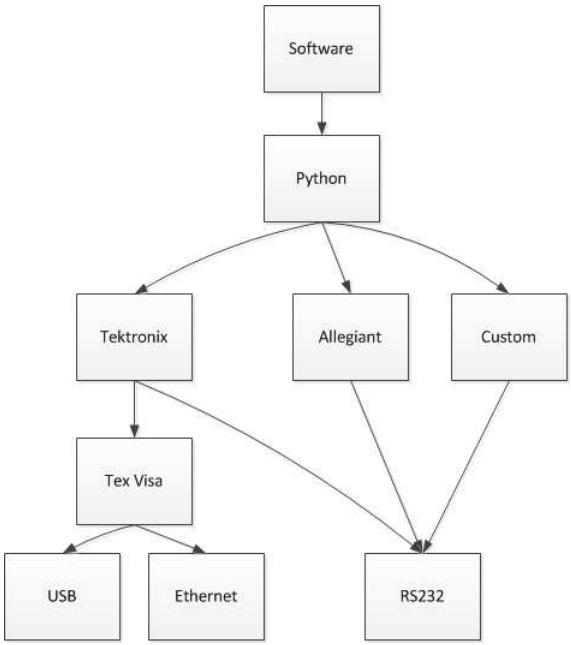

Figure 193: conceptual acquisition approach software flowchart

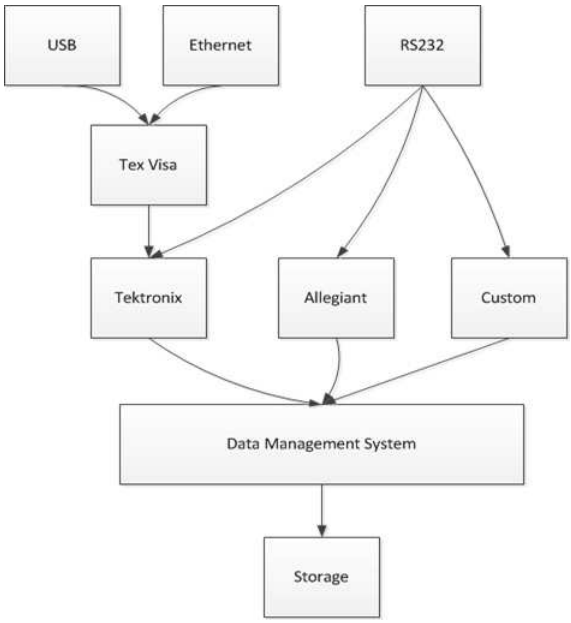

Figure 194: conceptual acquisition approach data management flowchart

dissertation — to acquire and process laboratory measurements.

Likewise, with such objectives being duly noted, it is important to recognize that their are a wide assortment of commercial acquisition devices available — although the information presented within this particular section is primarily focused upon the device commonly referred to as an oscilloscope — for purchase from a number of different manufacturers — some of the more notable being Agilent and Tektronix —, and while there is some standard-

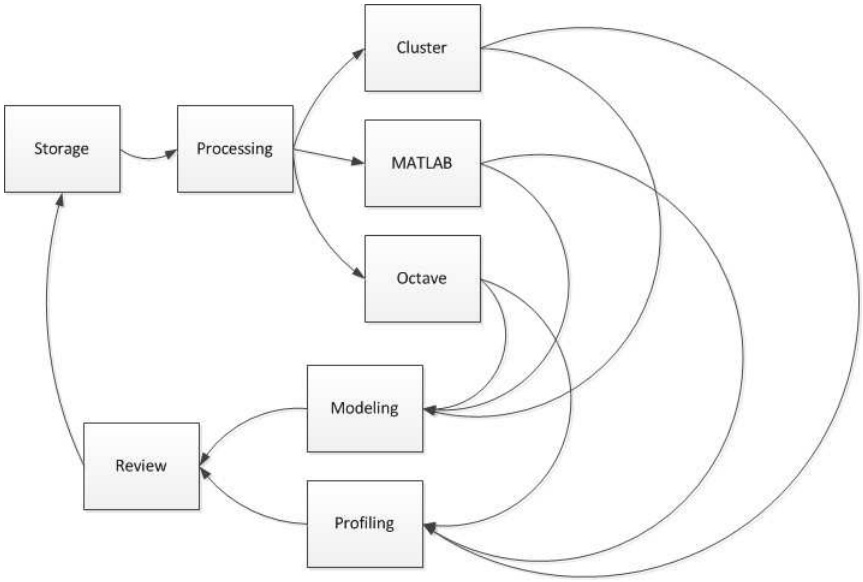

Figure 195: conceptual acquisition approach processing flowchart

ization amongst some of these manufacturers; however, every acquisition device tends to have its own individual peculiarities — primarily arising from the firmware utilized within the device, and variations in internal components; a notable example being the Tektronix TPS2024, the oscilloscope utilized within this dissertation to obtain electrical measurements, as this particular device had a tendency to lockup upon detecting an improper triggering signal — and such — quirky — characteristics can make the process of acquiring and analyzing a laboratory measurement a rather challenging task. Nevertheless, while the ability to select a particular acquisition device is generally beyond the scope of most researchers — as the underlying expectation is to work with what is available within the research laboratory, although there is always the occasional exception, especially if funding is available and the application necessitates it, — yet — at least upon restricting the scope of discussion to acquisition instrumentation sold by major commercial manufacturers — the process of acquiring and processing a laboratory measurement can be surmised in 4 steps, as shown by Figure: (196).

While the procedural steps depicted within Figure: (196) are fairly condensed and are not extremely descriptive since, after all, the methodology utilized to acquire an actual

laboratory measurement is fundamentally dependent upon the oscilloscope being utilized — thus, a abstract description was selected over a technical description in the interest of device compatibility —; however, despite the inherent lack of information, regarding the physical buttons to press in order to acquire a measurement using the TPS2024, the procedure outlined within Figure: (196) is overall a fairly accurate — tho, once again, deliberately abstracted — depiction of the physical steps required to obtain a electrical signal — at least using a common commercial oscilloscope — and process that acquired information. Conversely, to elaborate on Figure: (196) further, it should be noted that — once again, assuming the utilization of a contemporary commercial oscilloscope, all laboratory data acquisitions begin upon detection of a conditional event — like the press of a button — that triggers the process of migrating the acquired volatile measurements — volatile, in this particular case, because the measurements are only temporarily displayed on the oscilloscope screen — onto a nonvolatile storage medium — like a CompactFlash card — for later use. Likewise, after all necessary measurements are collected in this particular manner, the nonvolatile storage medium — in this particular case, the CompactFlash card — can be removed from the oscilloscope and physically inserted into a compliant extraction

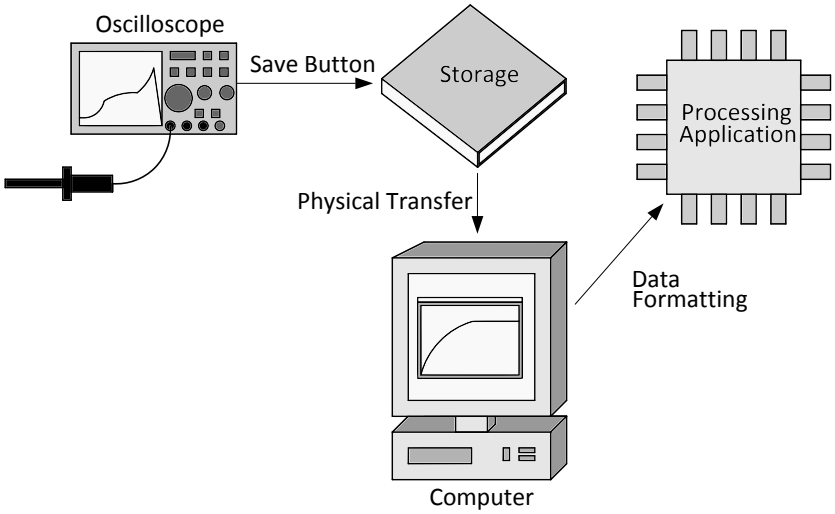

Figure 196: a figure depicting the conceptual process needed to acquire, transfer, and process a laboratory measurement

device — in this particular case, a CompactFlash card reader — that is connected to a personal computer, and the information stored — within the nonvolatile medium — can be copied to the personal computer for further computational analysis.

At this point, it might be tempting to presume that no further action is required to process the data transfered to the personal computer; however, because commonly utilized computational applications — like Matlab, Mathematica, Octave, and Sage — require the data collected to be in a particular format prior to performing any analytical action; thus, in the same way that linguistic translation might be required to facilitate communication between different languages, the acquired data generally must undergo a similar type of translation in order to convert the native storage format of the measuring apparatus to the native storage format of the processing application. Conversely, in terms of demonstrating

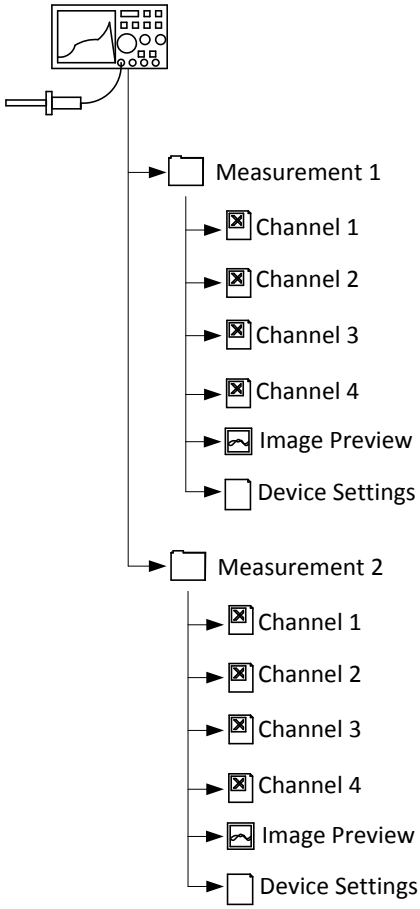

Figure 197: a figure depicting the native file storage structure of tektronix tps2024 oscilloscope

the physical manifestation of this particular attribute, consider for the moment the native storage format utilized by the Tektronix TPS2024, as shown by Figure: (197), in which each stored measurement is separated into individual folders, and each folder contains the acquired channel measurements — note, in the case of the Tektronix TPS2024, each measurement can simultaneously record up to four oscilloscope probe acquisitions —, a screen-shot of the image displayed by the oscilloscope monitor, and a configuration file containing information regarding the current settings utilized by the oscilloscope.

Furthermore, the information stored within each channel measurement taken is comma separated variable (CSV) delaminated and has additional channel parameters encoded within this file, as demonstrated by the following truncated CSV file:

```
Record Length,2.500000e+03,,  -0.250000000000,   2.00000,
Sample Interval,2.000000e-04,,  -0.249800000000,   2.00000,
Trigger Point,1.250000000000e+03,,  -0.249600000000,   1.92000,
,,,  -0.249400000000,   1.84000,
,,,  -0.249200000000,   1.76000,
,,,  -0.249000000000,   1.76000,
Source,CH1,,  -0.248800000000,   1.68000,
Vertical Units,V,,  -0.248600000000,   1.60000,
Vertical Scale,2.000000e+00,,  -0.248400000000,   1.52000,
Vertical Offset,0.000000e+00,,  -0.248200000000,   1.52000,
Horizontal Units,s,,  -0.248000000000,   1.44000,
Horizontal Scale,5.000000e-02,,  -0.247800000000,   1.36000,
Pt Fmt,Y,,  -0.247600000000,   1.28000,
Yzero,0.000000e+00,,  -0.247400000000,   1.20000,
Probe Atten,1.000000e+01,,  -0.247200000000,   1.20000,
Firmware Version,FV:v10.21,,  -0.247000000000,   1.12000,
,,,-00.246800000000,   1.04000,
,,,-00.246600000000,   0.96000,
,,,-00.246400000000,   0.88000,
,,,-00.246200000000,   0.88000,
,,,-00.246000000000,   0.80000,
,,,-00.245800000000,   0.72000,
,,,-00.245600000000,   0.64000,
,,,-00.245400000000,   0.56000,
,,,-00.245200000000,   0.56000
```

. While, in some applications — primarily referring to Matlab —, it is possible to allow

the application to attempt to translate the encoding scheme utilized — in this particular case, CSV delaminated — into something natively understandable, as demonstrated by the Matlab CSV file loading command shown within Appendix E script 8 ; however, because the Tektronix TPS2024 places non-numerical channel information within the encoded CSV channel file produced, attempting to run this particular command to extract the acquired data — in its current format — will result in the following error:

```
Error using ==> dlmread at 145

Mismatch between file and format string.

Trouble reading number from file (row 1, field 1) ==> Recor


Error in ==> csvread at 50

    m=dlmread(filename, ',', r, c);
```

. Although there are a number of possible solutions to this particular problem — within Matlab the code shown within Appendix E script 9 can be utilized to correct this error and successfully load the acquired data —, yet such solutions are not indicative of all analytical software and they do not address the inevitable issue of loading more than one channel simultaneously nor, for that matter, address the problem of loading more than one set of measurements simultaneously — keeping in mind, once again, that each measurement could have one to four CSV channel files associated with it.

Likewise, to address each of these problems in turn, the MATLAB code shown within Appendix E script 10, can be utilized to import a single oscilloscope measurement, while the MATLAB code shown within Appendix E script 11, can be utilized to import a set — as in series — of oscilloscope measurements. While the implementation of such techniques works reasonably well — although Matlab is notoriously slow at performing iterative file operations —, such techniques — as they are currently implemented — can be somewhat cumbersome to actively utilize — because of the odd data structure produced by these

functions — and such structures typically require additional reorganization to simplify accessibility depending upon the intended end objective — as illustrated by the MATLAB code shown within Appendix E script 12.

Furthermore, while such re-organizational techniques are relatively straightforward to implement, at least within Matlab, it is important to recognize that these functions, in general, are only applicable within Matlab, and while the underlying logic — within each function — can usually be translated into another software language — like octave — relatively easily; however, the necessity of such tasks imparts the underlying importance of both fully understanding the processing requirements of the intended application — or, in other words, determining if more than one processing application is required; like Matlab and Sage — and if so, can a common translational format be found to allow for the importation of the acquired measurements without having to re-implement the importation functions within each of the required applications. Although such questions might seem like an academical exercise — as oftentimes implementation trumps compatibility, even at the cost of re-implementation —; yet such attributes are worth considering, particularly within a interdisciplinary research environment — like the bioelectrical research area —, since it is somewhat unreasonable to assume that every related discipline — within the area — will utilize the same analytical tools.

Nevertheless, although such attributes might seem somewhat moot, particularly since Matlab was predominately utilized to perform the majority of all analytical analysis — at least, within this dissertation — primarily because of its overall acceptance within the academic community, yet such underlying problems did not go unnoticed and, based upon such notions, it appears that a possible solution can be found within intermediary programming languages — like Python or, to a lesser extent, Java — since, these languages are,

first and foremost, mostly platform-independent — as in, will execute written code similarly on Windows, OS X, and Linux —, fully implement the object-oriented programming paradigm, and are considered by the programming community as a common programming standard. Conversely, although the implementation of the, previously mentioned, data importation functions might sound eerily similar to simply substituting one processing application for another; however, in this particular case, while it is true that a loading class can be written within such languages — like Python — and such implementations would nearly be identical to the implementation previously provided – within Matlab —, yet after such information is loaded into memory, the capabilities available are significantly more profound, as such information could easily be passed into a conversion function that would restructure the data into something more palatable — like numerical CSV — by a particular processing application, piped directly into a processing application — the process of having the operating system move data from one application, like Python, to another application, like Matlab, within memory —, sent over a network to a remote processing application — like a computational Beowulf cluster —, or an assortment of other capabilities that would be normally unavailable within most analytical processing applications and all of these capabilities could be performed within the same — in this case Python — application at nearly the same time if necessitated by the research objective.

While, a number of these capabilities were explored — within this dissertation — and a number of these techniques will be presented within the coming sections; nevertheless, setting such notions aside for the moment, it is important to recognize that the effective utilization of data management is paramount to performing high fidelity measurements, since an inability to effectively extract and process measurements is just as crippling as any environmental, instrumentational, or material effect encountered. Thus, any invest-

ment into improving such capabilities can easily allow for the manifestation of processing techniques that were previously unavailable if such techniques were not introduced since, for example, the careful implementation of such capabilities, could easily allow for the processing of hundreds of laboratory measurements in the same amount of time it would have taken to process a single measurement by hand and the implementation of such techniques also generally reduces the likelihood of a human error being introduced. Yet, while such techniques are inevitably — just a tool within the metaphoric scientific researchers toolbox — and one can never assume that — more is always better—; however, regardless of such counterpoints, data management is — nevertheless — extremely important to effective high fidelity research, and in the same way that the proper selection of experiment location and apparatus configuration is important to reducing environmental and instrumentational effects respectively, the knowledge regarding the type of data produced and the requirements of the intended processing application is equally just as important.

6.3.3 DC Voltage and Environmental Effects

The fundamental rationale behind the DC voltage and environmental effects section was to develop a method of determining the overall ability of a bioelectrical acquisition device to accurately acquire DC signals and — more importantly — develop a method — as shown by Figure: (198) and Figure: (199) — of conveying this information — across an interdisciplinary platform — in order to allow for the equivalent comparison of biometric data across multiple acquisition platforms. Likewise, based upon the observations made — upon implementation of this method — it was also observed that — upon the application of a DC signal to a Tektronix oscilloscope — that the sensitivity of the acquisition device — or more precisely the devices overall susceptibility — to combine instrumentational and environmental (CIE) effects increases because of discrete changes in the internal gain of

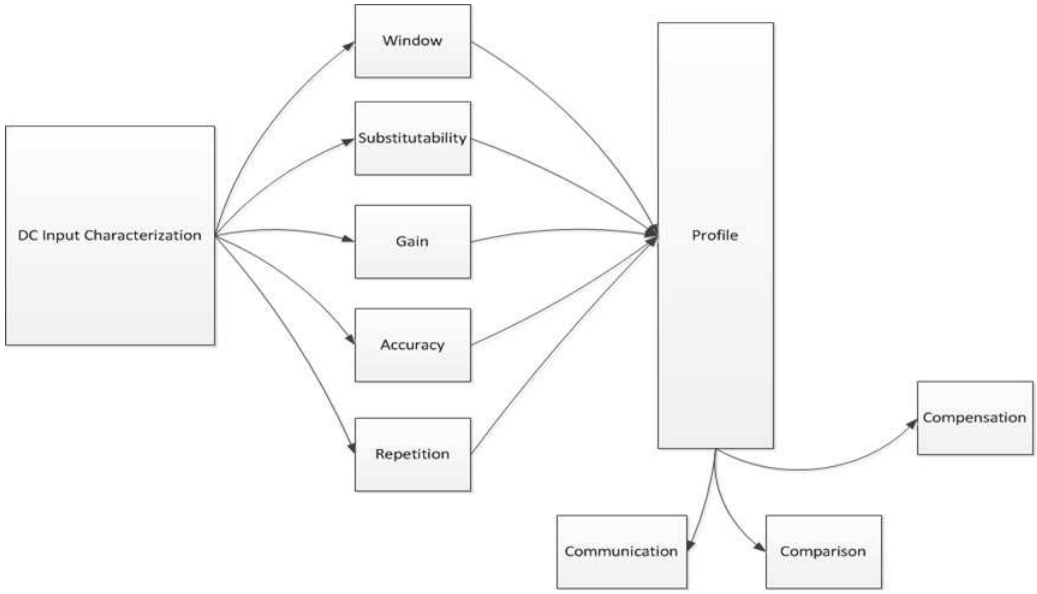

Figure 198: conceptual dc cie calibration approach flowchart

the instrumentational amplifier (IA) stage necessitated to prevent signal clipping, and such observations show that a direct comparison between different amplitude acquisitions, in itself, can introduce signal distortions because the CIE effects being compared have different CIE effect magnitudes. Similarly, such observations ultimately led to the observation that direct comparison should only be made between similar amplitude signals — or more precisely, that direct comparison should only be made between measurements acquired using a similar IA gain — and between signals that were acquired using a similar sample window — although this is generally less important relative to IA gain distortions when comparing DC acquisitions —, and that such observations are definitively applicable — if not more so — within commercial biomedical devices that attempt multi-voltage/multi-frequency spectroscopy since the acquisition methods utilized within these devices are very similar — though oftentimes less advanced — to the equipment utilized within this dissertation.

As it was previously mentioned, the manifestation of environmental effects upon laboratory acquisitions is an extremely important occurrence that must be fully understood in order to obtain a high fidelity measurement. Conversely, while an extensive discussion was provided regarding the environmental effects typically encountered during high impedance

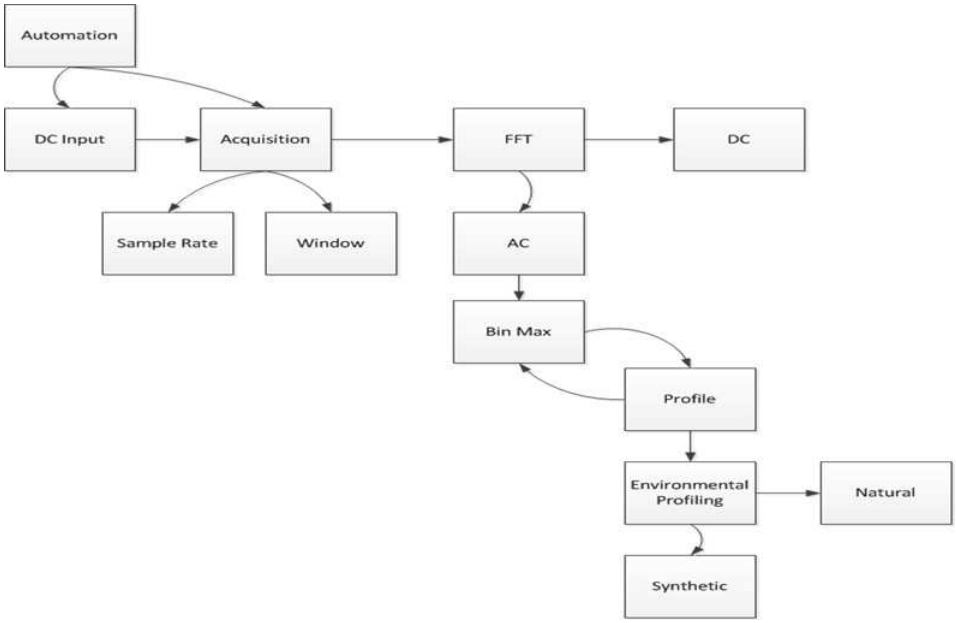

Figure 199: conceptual dc cie calibration process flowchart

(High-Z) laboratory acquisitions, a method of modeling such techniques presented, and the ability to reduce these effects through the utilization of physical shielding techniques discussed; however, such situations are far from being an ideal representation of those actually encountered during common laboratory acquisitions and further discussion on this subject

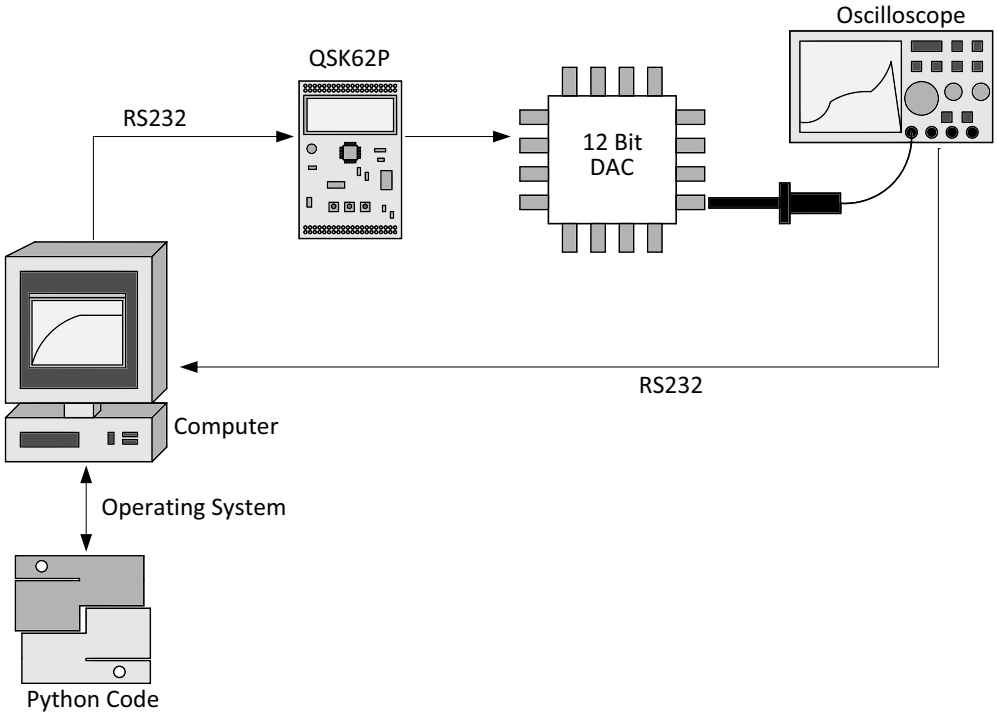

Figure 200: conceptual hardware diagram of the 12-bit dac testing apparatus utilized

is merited to address some of these scenarios.

Thus, to begin addressing such concerns, consider for the moment a simplistic laboratory apparatus, as conceptually depicted by Figure: (200), in which a Tektronix TPS2024 oscilloscope was connected to the output of a 12 bit digital to analog converter (DAC) within the, previously discussed, partially shielded environment. Conversely, the 12 bit DAC depicted within Figure: (200), was controlled remotely via a Renesas QSK62P development board connected to a RS232 communication interface; while the Tektronix TPS2024 oscilloscope utilized was controlled remotely and the acquisitions obtained transferred — again via a secondary RS232 interface. Furthermore, all controlling RS–232 communications were created and managed by a laboratory computer executing a Python script, and the methodological process utilized is graphically illustrated within Figure: (200).

While, the automation techniques utilized within the implementation of this experiment has, by and large, gone undiscussed — an attribute that will be rectified later within this chapter —; however, given the discussions current progression, it would seem that the incorporation of such logistical details, at least at this particular moment, would be more of a hindrance then helpful — although an inquisitive scholar may feel free to examine

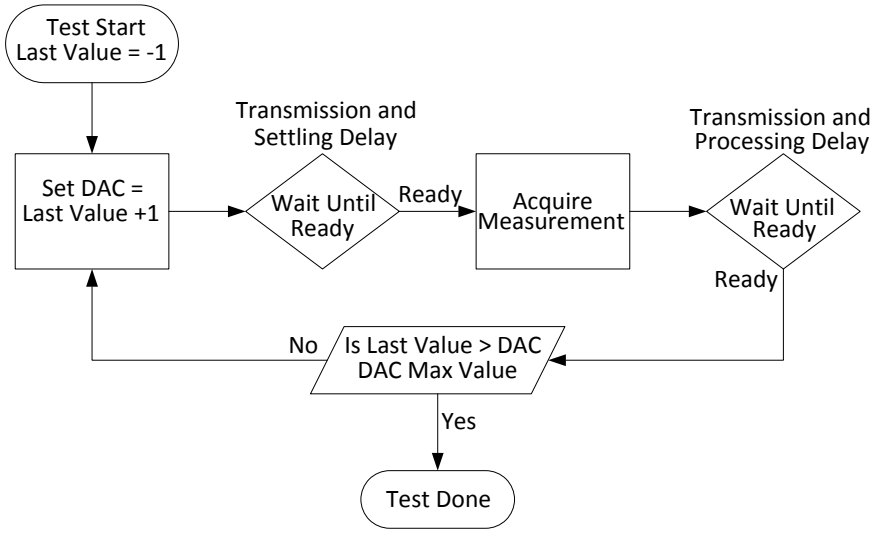

Figure 201: conceptual software diagram of the 12-bit dac testing apparatus utilized

the code utilized to perform this particular experiment within Appendix A — since, the critical attribute to focus on, within this section, is not the automated acquisition techniques utilized, but rather the information obtained from such observations. Likewise, with this being said, a minor caveat does exist here regarding the application of such sentiments since, as it was previously implied within the preliminary data management section, the utilization of a external programming language — like Python — inherently implies that the communication method selected to convey information between the external programming language and the processing application will likely be different than the, previously provided, Tektronix CSV format loading method. Conversely, as it might be expected, the automation techniques implemented utilized a straightforward numerical tab separated variable (TSV) format — a format identical to the numerical CSV format except the commas were substituted with tabs —, as demonstrated by the following truncated TSV file:

```
0.0 0.014
4e-09 0.016
8e-09 0.016
1.2e-08 0.016
1.6e-08 0.016
2e-08 0.014
2.4e-08 0.014
2.8e-08 0.014
3.2e-08 0.014
3.6e-08 0.012
4e-08 0.012
4.4e-08 0.012
4.8e-08 0.012
5.2e-08 0.012
5.6e-08 0.012
6e-08 0.012
6.4e-08 0.012
6.8e-08 0.012
7.2e-08 0.014
7.6e-08 0.014
8e-08 0.014
8.4e-08 0.014
```

```
8.8e-08 0.016
9.2e-08 0.014
9.6e-08 0.016
1e-07 0.016
1.04e-07 0.014
1.08e-07 0.014
```

, and each channel acquisition was tab delimited within the same file, while each test measurement was saved to a new TSV file within the same test folder — unlike the Tektronix storage format, in which every channel is saved to its own CSV file, while every measurement is placed within a new folder. Similarly, because an alternative storage method was utilized to save the test measurements obtained, a new importation function had to be written in order to load these measurements into Matlab as shown within Appendix E script 13, which loads a single acquisition into Matlab, and by the MATLAB code shown within Appendix E script 14, which loads a measurement set into Matlab.

Likewise, with the capability to both control and acquired the DC voltage produced by the 12 bit DAC in place, It was decided to examine the DC value produced from a incrementing — DAC value starts at 0 and ends at 4095 — and decrementing — DAC value starts at 4095 and ends at 0 — progression, with the assumption that a DAC value of 0 would yield 0 volts and a DAC value of 4095 would yield 2.5 volts respectively. Conversely, upon performing this test — a task that took roughly three and a half days at around 35 seconds per DAC measurement — the measurements were loaded into Matlab by the code shown within Appendix E script 15, and, in a manner similar to the analytical analysis performed within the environmental effects section, the FFT was applied to each of these measurements using the following MATLAB code shown within Appendix E script 16 — since the Matlab FFT operation, in itself, was designed for instrumentational flexibility rather than usability, thus requiring some extra steps in order to obtain graphically useful information.

At this point, it should be noted that a definitive difference exist between the measurements presented within this section and those that were presented within the environmental effects section; insofar as, the measurements presented with in the environmental effects section were acquired without the presence of a predominating input signal and such attributes, in turn, resulted in the oscilloscope — upon being unable to determine the existence of a obvious applied external signal — broadening its acquisition timebase to its maximum size — around 10 seconds — in an attempt to locate an externally applied signal. Conversely, this approach differs from the measurements taken within this section, insofar as, because a DC signal was applied as the external oscilloscope input, the oscilloscope — rather than searching for an external input — was primarily focused upon determining supplementary spectral content and, as a result, the acquisition timebase utilized by the oscilloscope was significantly smaller than the previous acquisition timebase utilized within the environmental effects section — for reasons that might seem somewhat obscure, but will be clarified in a moment — as shown by Figure: (202), Figure: (203), Figure: (204), and Figure: (205) — Note, the DC voltage shown within these figures was ordered by increasing value, thus no assumption should be made regarding the existence of a relationship between DAC value and sample window time, as such relationships are shown within Figure: (202), Figure: (203), Figure: (204), and Figure: (205).

Likewise, upon analyzing Figure: (202), Figure: (203), Figure: (204), and Figure: (205), it becomes definitively apparent that the sampling rate — equal to, in this case, the sample window time divided by 2500 — for each DC value measured, is not consistent across all DAC measurements — an attribute that can be further validated upon examining the Python test code in which the oscilloscopes auto scale feature was utilized before acquiring DAC voltages. While some pause might be merited for the allowance of such inconsisten-

cies, yet it is important to recognize that the Tektronix oscilloscope utilized had a finite 2500 discreet sample window regardless of the sampling rate selected and such attributes result in a trade-off between observable frequency versus frequency resolution. Conversely, because every laboratory measurement taken has this inherent trade-off associated with its acquisition — unless a very expensive continuous high frequency acquisition device was utilized, and such a device was neither available nor utilized — and in this particular case,

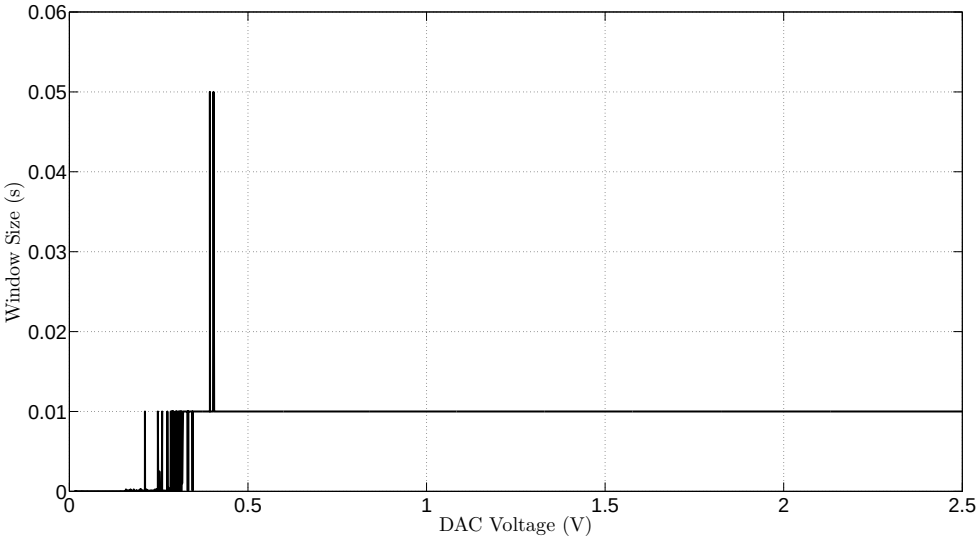

Figure 202: graphical comparison between dc voltage (test 1 dac 0 to 4095) and the sampling window automatically selected by the oscilloscope in linear scale

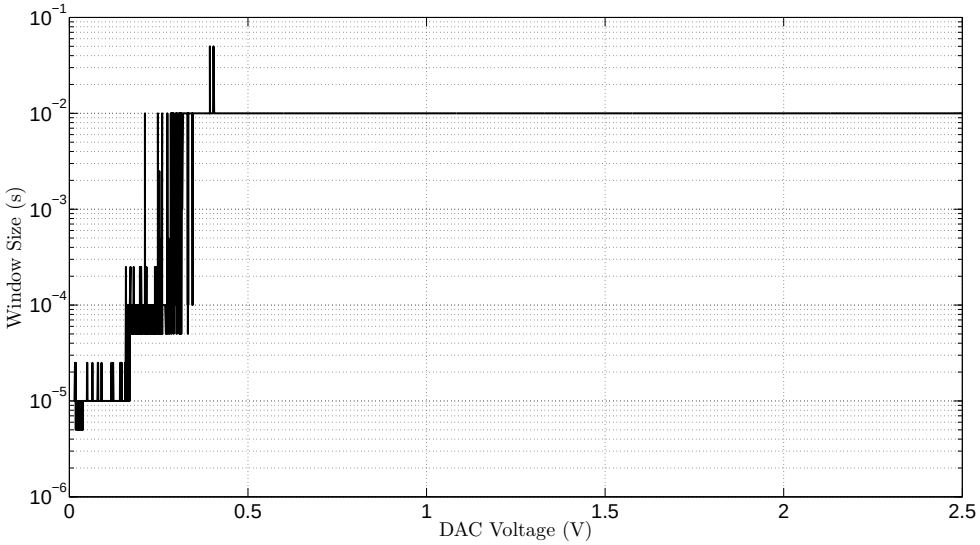

Figure 203: graphical comparison between dc voltage (test 1 dac 0 to 4095) and the sampling window automatically selected by the oscilloscope in semi-y logarithmic scale

the convenience of a consistent timebase was exchange for an improvement in frequency resolution over a limited yet flexible frequency window predominantly selected based upon the highest non-zero spectral power observed. Yet, setting such trade-offs aside for the moment, it appears — at least based upon Figure: (202), Figure: (203), Figure: (204), and Figure: (205) — that some type of underlying, but reasonably consistent, mechanism is present since the sample times utilized, by the oscilloscope, remains relatively consistent, at

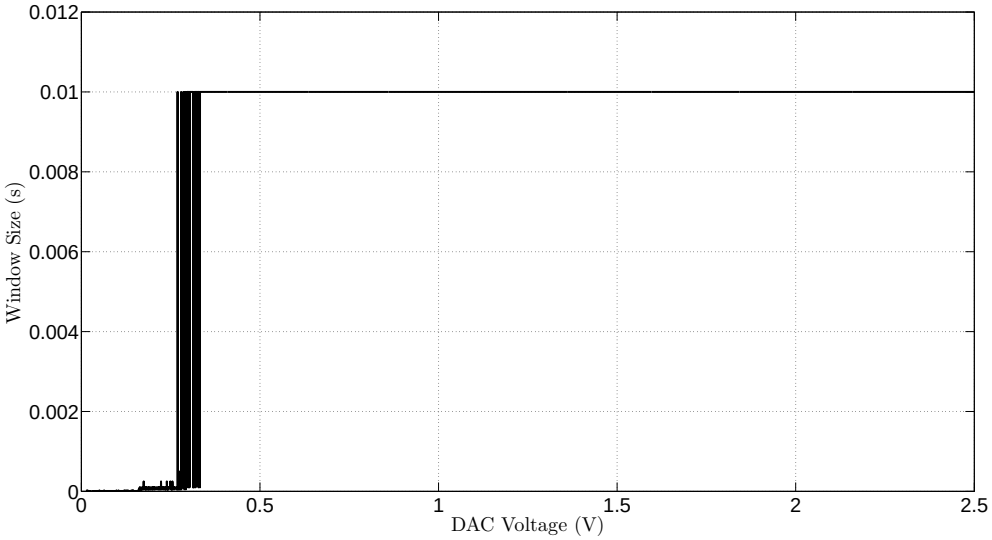

Figure 204: graphical comparison between dc voltage (test 2 dac 4095 to 0) and the sampling window automatically selected by the oscilloscope in linear scale

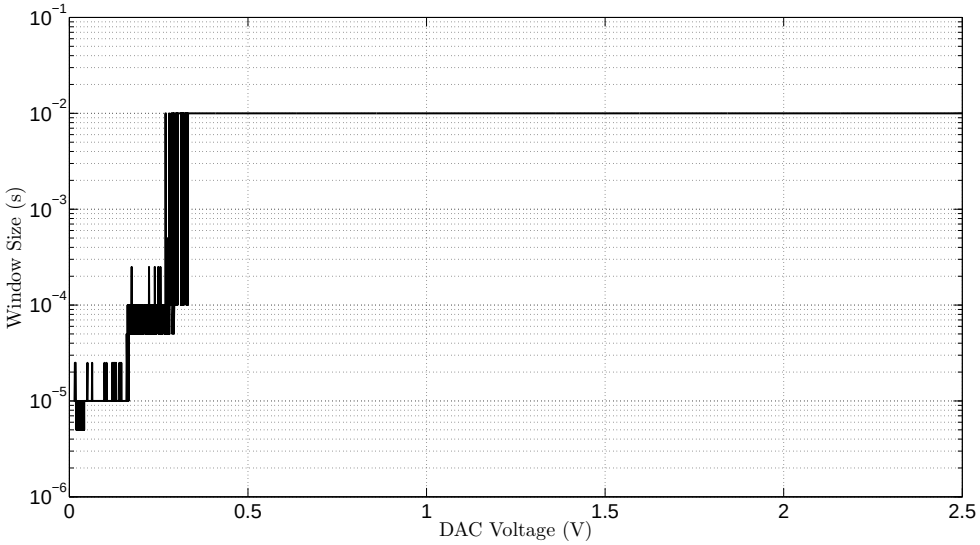

Figure 205: graphical comparison between dc voltage (test 2 dac 4095 to 0) and the sampling window automatically selected by the oscilloscope in semi-y logarithmic scale

least upon comparison with the forward path DC voltage — obtained by incremental DAC values from 0 to 4095 — and the reverse path DC voltage — obtained by decrementing DAC values from 4095 to 0 — that — within this dissertation — will be abbreviated by the terminology DAC test 1 and DAC test 2 respectively.

Likewise, while such observations might not seem very significant, at least at first, yet such observations are quite profound, at least upon considering the fact that the test took over three days to fully perform and the presence of such sampling consistency inherently implies that the overall environmental noise encountered, within the partially shielded environment, is relatively consistent from a power spectrum perspective. Furthermore, the existence of a nearly identical progressive change between the sample rate and the DC voltage also strongly indicates some type of correlation between DC voltage and the spectral frequencies encountered — although further information is inherently required to validate, or expand, such assessments. Conversely, upon taking such considerations under advisement, the next logical step to validate, or expand upon, such assessments — and, for that matter, refocus upon the original objective — would be to examine the DC values produced by the DAC and the corresponding frequency content introduced as a result of the intrinsic effects encountered within the partially shielded environment — presumably such effects are environmental, but they could also be classified — depending upon the definition utilized — as being instrumentational. Likewise, because the signal acquired is a combination of the DAC output voltage that has been correspondingly added with both synthetic and stochastic sources of noise, it seems reasonable to isolate the acquired signal into a static — or equal to 0Hz — and non-static — or greater than 0Hz — frequency components, a task best accomplished through the utilization of the FFT algorithm.

Conversely, while the static — or DC component — can be relatively easily presented —

since the magnitude obtained at 0Hz is the average DC value of the DAC —, as shown by Figure: (206) and Figure: (207); however, the two-dimensional representation of the non-static — or frequency enriched components — is a difficult parameter to graphically depict — primarily because each DAC measurement has 1250 individual FFT bins that must be condensed into a single data point either through summing, averaging, or peak detection — and upon being forced to work within the confines of such parameters, it seems that the most informative representation — especially given the variations in sampling window size — of such content would either be achieved through the summing of power spectral density — an overestimate of the spectral power encountered — or through the utilization of maximum magnitude peak detection — an overestimate of the magnitude coefficients of the presumably environmental effects encountered. Yet, before examining such attributes further, consider for the moment the graphical information presented within Figure: (206) and Figure: (207), along with the comparison between the two figures, as shown by Figure: (208).

Likewise, upon conducting a preliminary visual examination of Figure: (206) and Figure: (207), the information presented within these two figures seems visually reasonable

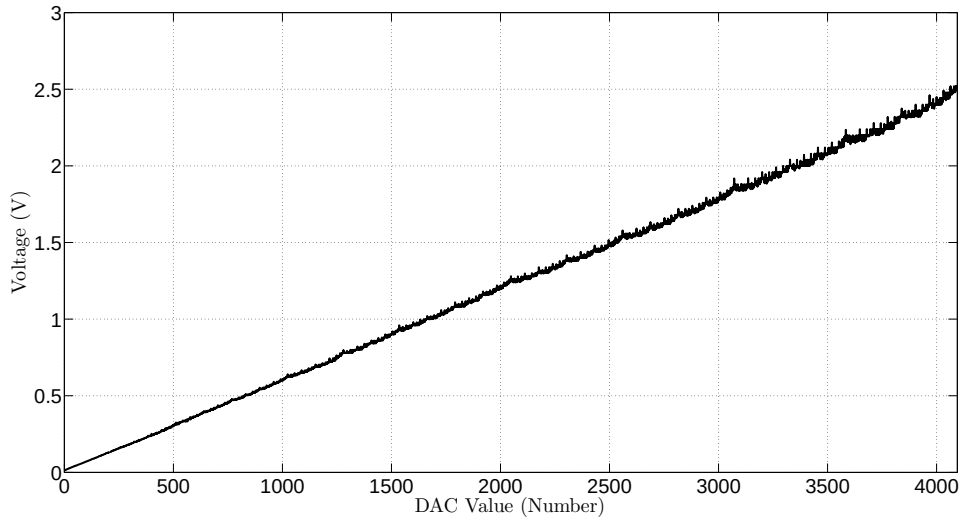

Figure 206: dac value versus the (fft bin 0) average dc magnitude (test 1 dac 0 to 4095)

after considering the progressive and consistent increase and decrease of the DAC value and the corresponding increase and decrease of the output voltage observed. Conversely, further examination of the DAC voltage — as shown by Figure: (206) and Figure: (207) — reveals a seemingly linear progression from near zero to around 2.5 volts respectively — excluding for the moment, the slight distortions encountered at DAC values above 1500 —, and the linear progression observed was expected giving the fundamental objective of the test and the device being examined. Similarly, while Figure: (206) and Figure: (207) were

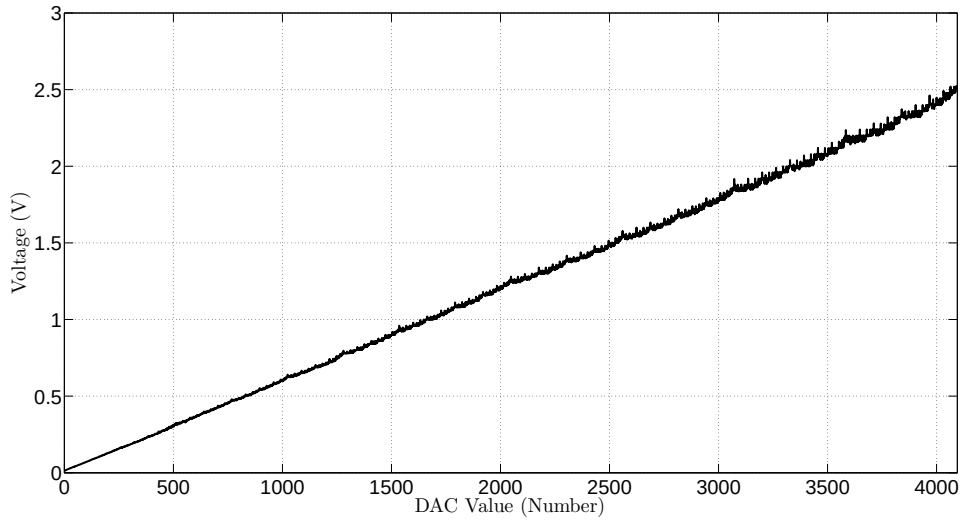

Figure 207: dac value versus the (fft bin 0) average dc magnitude (test 2 dac 4095 to 0)

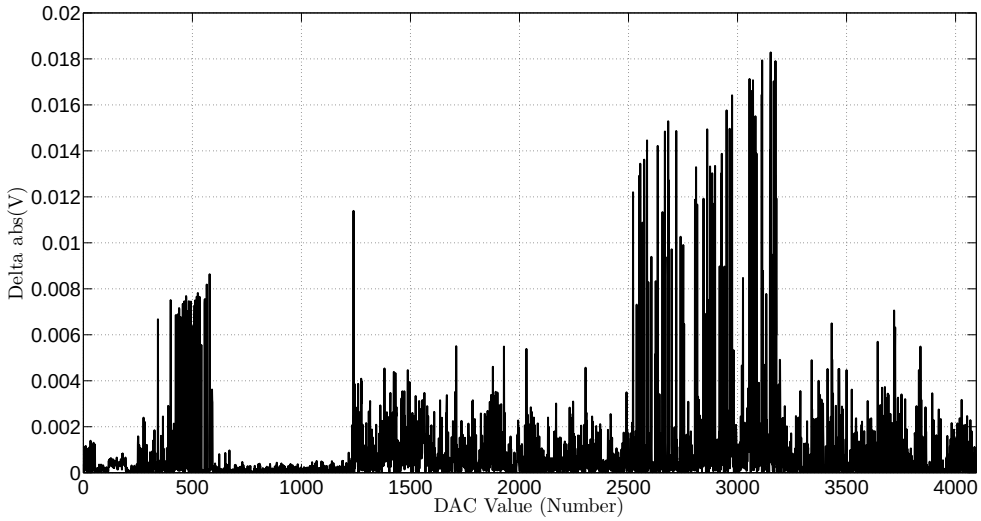

Figure 208: dac value versus the absolute value of the difference between the (fft bin 0) average dc magnitude of (test 1 dac 0 to 4095) and (test 2 dac 4095 to 0)

not graphically depicted in relation to there temporal DAC progression, primarily because the examination of such plots are not particularly beneficial beyond the revalidation of the DAC progression — although if a mental image is desired, the test started with a DAC value of zero and increased until it reached 4095 after which the DAC value was decreased until it reached zero, thus making a classical ramp shaped DAC DC output waveform —; nevertheless, the figure of the DAC value versus the DAC DC output voltage, provided within Figure: (206) and Figure: (207), can be tested for reciprocity — in this case, the process of checking if the forward DAC DC path is equivalent to the reverse DAC DC path — since both plots were presented using the same DAC value progression — implying that the second DAC test was mirrored across the y-axis and shifted upwards by the number of DAC values utilized in order to make the two temporal test progressions perfectly align — and upon taking the absolute value of the difference between the two figures — as shown by Figure: (208) — the deviation between the two DAC value progressions — or alternatively the reciprocity between the two paths — becomes visible.

Conversely, examination of Figure: (208) reveals a maximum deviation between the forward and reverse progression of 18mV — noting, once again, the previous utilization of the absolute value during the calculation —, a near match below 1mV between the DAC values 500 and 1000, a general expectation of at least a deviation of 4mV overall, and two heavily distorted regions between DAC values 100 to 600 and 2500 to 3250 with deviations of at least 8mV and 16mV respectively. Nevertheless, while such values are relatively reasonable — if not remarkable —, especially given the, previously provided, partially shielded high-Z environmental noise expectation of around 20mV peak, yet it is important to recognize that such observations were obtained through the utilization of acquisition environmental reductive techniques — like instrumentational amplifiers, sample averaging,

and bandwidth limiting — and more importantly, through the isolation of the DC bin after performing the FFT operation — which is analogous to the application of an extremely narrow Low Pass Filter (LPF). Furthermore, because the DAC under examination is being presented from a black box testing prospective — an attribute that was deliberate in nature in order to expand the applicability of the methods being discussed and allow for the discussion to focus strictly upon the environmental effects encountered —, although it should never be forgotten that it is possible that other external means of environmental effect compensation could exist within the device being examined given the ambiguity of the testing scenario — although, for the record, no such attributes were utilized within this particular scenario —.

Yet, while the consideration of such possibilities is reasonable given the circumstances provided; however, the information depicted within Figure: (206), Figure: (207), and Figure: (208) has not, as of yet, provided any definitive explanation for the previous observation of sample rate fluctuations beyond the conclusion that higher DC voltages seem to receive a slower sampling rate while lower DC voltages seem to receive a faster sampling rate. Likewise, with this being said, it becomes apparent that these answers cannot be completely found within the static analysis, thus an examination of the non-static frequency component must be conducted — a task that was previously avoided because of the problem of graphically condensing an extremely large data set into something visually manageable — and such analysis, once again, is inherently problematic because each of the 4096 measurements taken per test has 1249 frequency components — excluding negative spectral duplicates and the static DC component — and multiplication of the two values yields 5115904 unique frequency points that must be condensed into something graphically useful. Conversely, as it was previously mentioned, a number of processing

options are available — summing, averaging, and peak detecting — and each option has its own "pro" [†1] and "contra" [†2] associated with its usage along with an implication regarding its future graphical interpretation — summing and maximum peak detecting will provide an over estimate, while averaging and minimum detection will provide, given the flexible sampling rate utilized, an under estimate — [267, p.1462,p.432]. Yet, although such processing techniques are useful in condensing large amounts of information into a more manageable number of points, the issue of there applicability is still somewhat problematic — once again, primarily because of the flexible sampling rate utilized — since the spectral frequency bins produced by the FFT operation upon the time domain acquisition will not be consistent for all acquisitions, thus making it difficult to know which bins can be combined and condensed together through the utilization of the previously mentioned operations — like summing, averaging, or peak detecting —.

Likewise, upon careful consideration of the nature of this underlying problem, it was decided — given the discrete bins produced by the FFT operation — that something eerily similar to a tree sorting algorithm would be an effective approach to take an irregular FFT bin array and restructure that array into a common frequency array — that would naturally incorporate all expected FFT frequencies encountered throughout the DAC test — in order to allow the condensing operations to occur on equivalent frequency bins, as implemented by the MATLAB code shown within Appendix E script 17. Nevertheless, while such techniques do effectively reduce the overall number of discrete points available, the information still inherently remains in a three-dimensional form — DAC value, frequency, and magnitude — and further condensing is required in order to obtain a two-dimensional frequency versus magnitude or DAC value versus spectral power density plot. Conversely, upon taking such

[†1] Latin for: on behalf of.
[†2] Latin for: against.

observations under consideration, it seems a reasonable course of action to first, examine the three-dimensional information available — after the application of the first condensing method — prior to performing any additional condensing, as depicted by Figure: (209), Figure: (210), Figure: (211), and Figure: (212).

Likewise, upon conducting a preliminary visual examination of Figure: (206) and Figure: (207), the information presented within these two figures seems visually reasonable after considering the progressive and consistent increase and decrease of the DAC value and the corresponding increase and decrease of the output voltage observed. Conversely, further examination of the DAC voltage — as shown by Figure: (206) and Figure: (207) — reveals a seemingly linear progression from near zero to around 2.5 volts respectively — excluding for the moment, the slight distortions encountered at DAC values above 1500 —, and the linear progression observed was expected giving the fundamental objective of the test and the device being examined. Similarly, while Figure: (206) and Figure: (207) were not graphically depicted in relation to there temporal DAC progression, primarily because the examination of such plots are not particularly beneficial beyond the revalidation of the DAC progression — although if a mental visualization is required, the test started with a DAC value of zero and increased that value until it reached 4095 and then decremented that value back to zero, thus making a classical ramp shaped DAC DC output waveform —; nevertheless, the figure of the DAC value versus the DAC DC output voltage, provided within Figure: (206) and Figure: (207), can be tested for reciprocity — in this case, the process of checking if the forward DAC value DC path is equivalent to the reverse DAC value DC path — since both plots were presented using the same DAC value progression — implying that the second DAC test was mirrored across the y-axis and shifted upwards by the number of DAC values utilized in order to make the two temporal test progressions per-

fectly align — and upon taking the absolute value of the difference between the two figures — as shown by Figure: (208) — the deviation between the two DAC value progressions — or alternatively the reciprocity between the two paths — becomes visible.

Conversely, examination of Figure: (208) reveals a maximum deviation between the forward and reverse progression of 18mV — noting, once again, the previous utilization of the absolute value during the calculation —, a near match below 1mV between the DAC values 500 and 1000, a general expectation of at least a deviation of 4mV overall, and two bad zones between DAC values 100 to 600 and 2500 to 3250 with deviations of at least 8mV and 16mV respectively. Nevertheless, while such values are relatively reasonable — if not remarkable —, especially given the, previously provided, partially shielded high-Z environmental noise expectation of around 20mV peak, yet it is important to recognize that such observations were obtained through the utilization of acquisition environmental reductive techniques — like instrumentational amplifiers, sample averaging, and bandwidth limiting — and more importantly, through the isolation of the DC bin after performing the FFT operation — which is analogous to the application of an extremely narrow Low Pass Filter (LPF). Furthermore, because the DAC under examination is being presented from a black box testing prospective — an attribute that was deliberate in nature in order to expand the applicability of the methods being discussed and allow for the discussion to focus strictly upon the environmental effects encountered —, although it should never be forgotten that it is possible that other external means of environmental compensation could exist within the item being examined under such conditions — although no such attributes were present within this particular example —.

Yet, while the consideration that such possibilities is a reasonable course of action when attempting to rationalize such observations; however, the information provided within

Figure: (206), Figure: (207), and Figure: (208) has not, as of yet, provided any definitive explanation for the previous observation of sample rate fluctuation beyond the conclusion that higher DC values received a lower sampling rate while lower DC values received a faster sampling rate.

Likewise, a preliminary visual examination of Figure: (209), Figure: (210), Figure: (211), and Figure: (212) immediately reveals a significant region of inactivity — approxi-

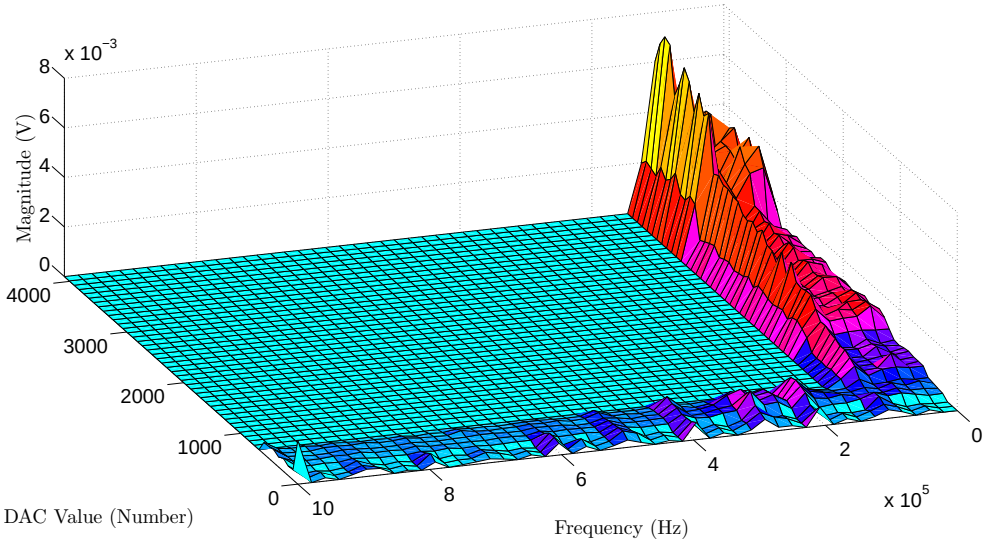

Figure 209: extended frequency plot of dac value versus frequency versus maximum magnitude for dac test 1 (incrementing dac values 0 to 4095)

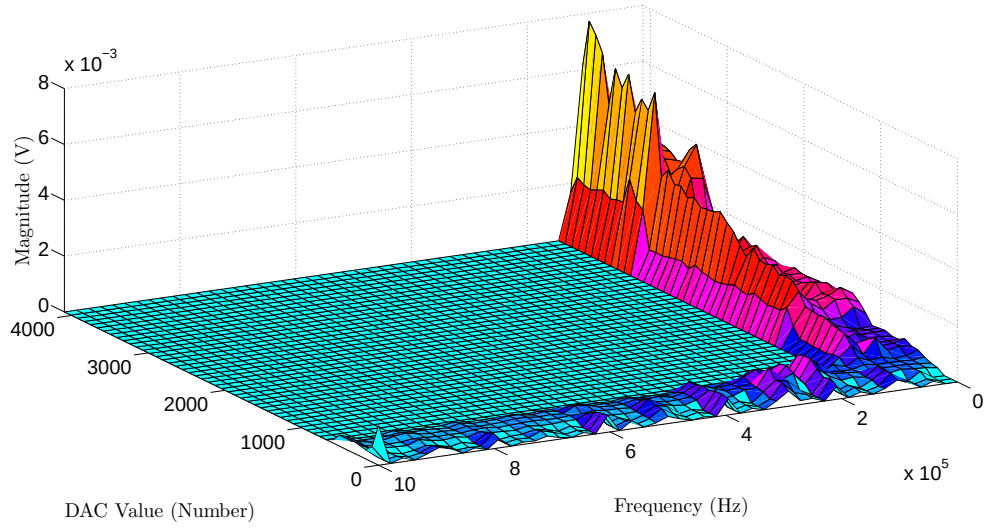

Figure 210: extended frequency plot of dac value versus frequency versus maximum magnitude for dac test 2 (decrementing dac values 4095 to 0)

mately between DAC values of 1000 to 4095 and 200kHz to 1MHz — and such observations are directly related to the progressive decrease in sample rate at higher DAC values that was previously observed, since lowering the sampling rate reduces the observable frequency range, thus no information was available to fill these bins at the specified DAC values. Similarly, preliminary visual examination of Figure: (209) and Figure: (210) reveals that lower DAC values — which directly corresponds to lowered DC output voltages — have a significantly lower combined instrumental and environmental (CIE) effect profile than the higher

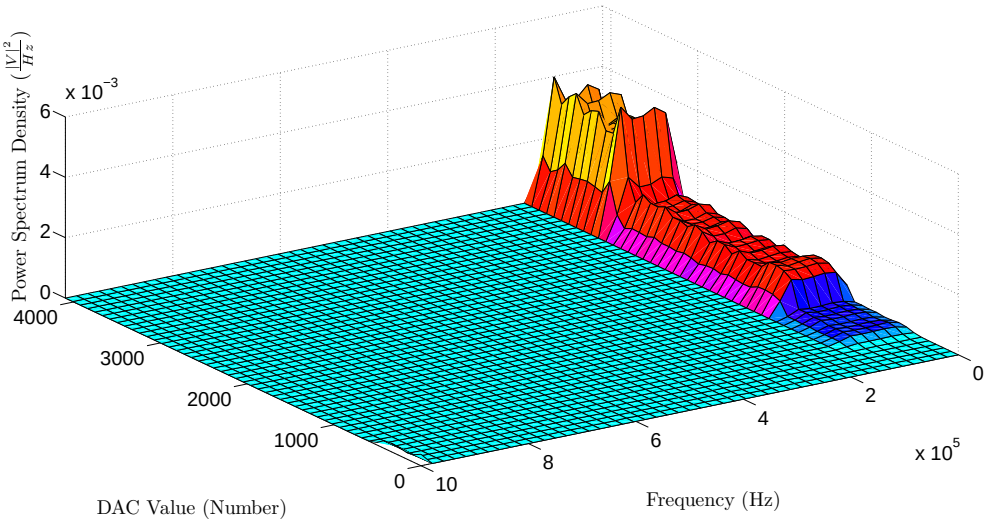

Figure 211: extended frequency plot of dac value versus frequency versus cumulative overestimation of power spectral density for dac test 1 (incrementing dac values 0 to 4095)

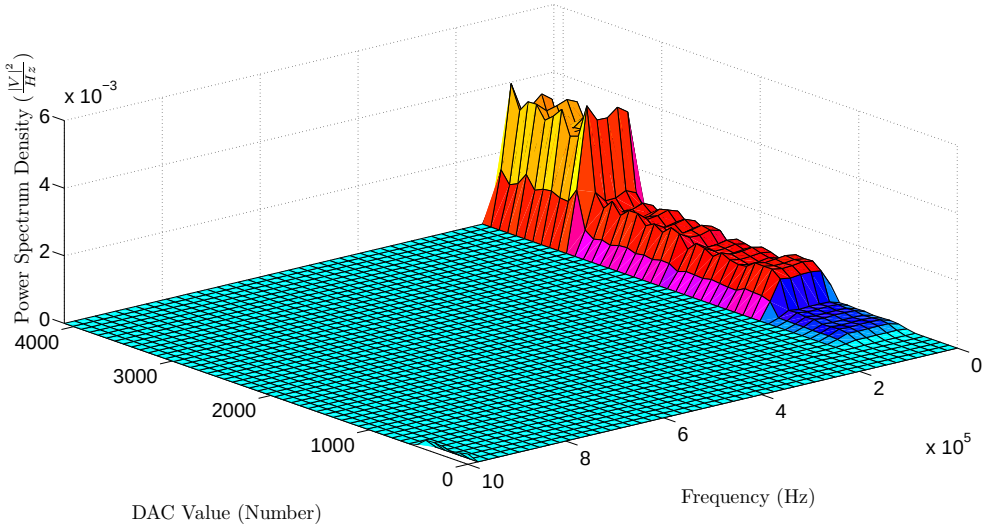

Figure 212: extended frequency plot of dac value versus frequency versus cumulative overestimation of power spectral density for dac test 2 (decrementing dac values 4095 to 0)

DAC values, while the majority of all CIE effects shown within these plots appear to be confined between the 0 to 200kHz frequency range — although admittedly such conclusions must be taken with a metaphoric grain of salt since higher frequencies were lumped together near the upper 200kHz band because of the slower sampling rate utilized within this region. Conversely, a preliminary visual examination of Figure: (211) and Figure: (212) reveals a similar summary — which is to be expected given that the power spectral density is calculated from the magnitude — although, it is worth mentioning that power spectral density provided within Figure: (211) and Figure: (212) is a overestimate of the actual spectral power density encountered since the sum was taken of every overlapping bin rather than an average because of the inconsistent rate of overlap — as one bin might be average five times while another bin might be averaged 20 times under such conditions—. Furthermore, upon visually comparing the first DAC test with the second DAC test, it seems reasonable to conclude that the CIE effects encountered remain relatively consistent over the three days in which the two tests were performed, since the two tests presented within Figure: (209), Figure: (210), Figure: (211), and Figure: (212) appear to be relatively similar in both shape and magnitude.

Yet, while the information presented within Figure: (209), Figure: (210), Figure: (211), and Figure: (212) are both impressive from a logistical perspective — as these plots represent over 5 million data points — and are extremely interesting — based upon the CIE effect information conveyed —; however, given that the majority of the samples taken only possessed spectral information up to 200kHz, it seems reasonable to narrow the frequency axis in order to increase the spectral resolution presented — although, any spectral information outside this new frequency window will be lumped into the last frequency bin presented on the axis based upon the algorithm implemented —, as shown by Figure: (213),

Figure: (214), Figure: (215), and Figure: (216).

Conversely, upon examining Figure: (213) and Figure: (214), it becomes apparent that the majority of all CIE effects encountered are, once again, located above DAC values greater than 1500 — in which the highest concentration of CIE effects are located between DAC values 3500 to 4095 — and the spectral frequencies in which CIE effects are most likely to exhibit there maximum value — while being predominantly uniform across the 0 to 100kHz frequency range — seems to metaphorically crescendo in magnitude around

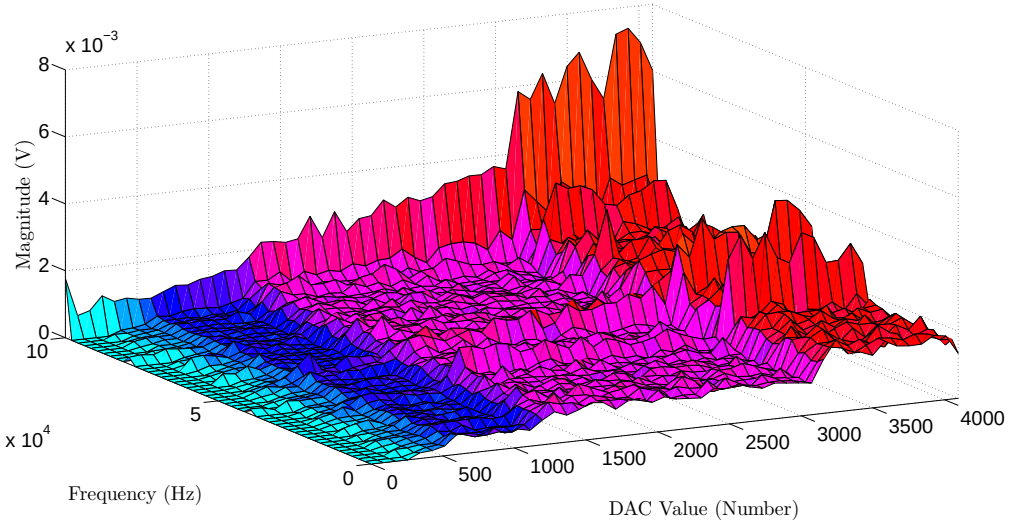

Figure 213: narrow frequency plot of dac value versus frequency versus maximum magnitude for dac test 1 (incrementing dac values 0 to 4095)

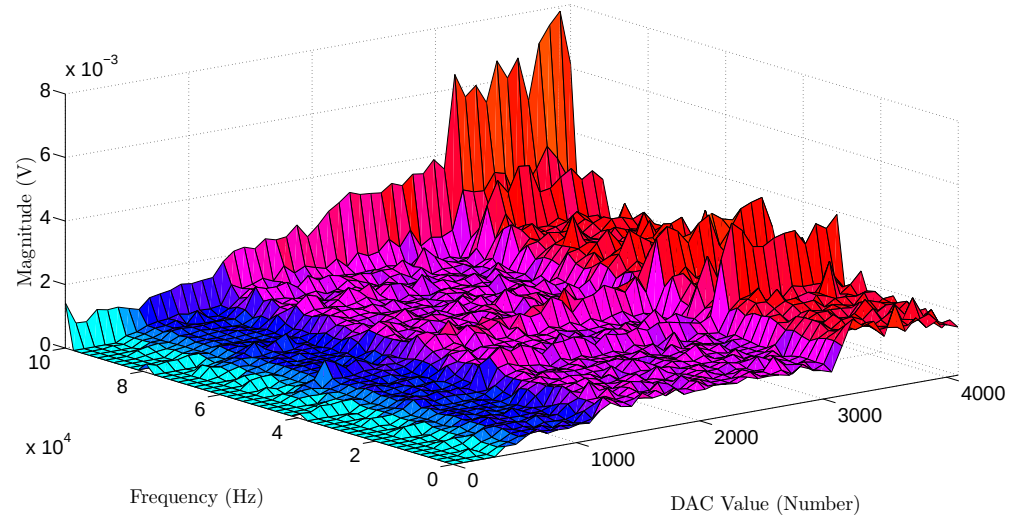

Figure 214: narrow frequency plot of dac value versus frequency versus maximum magnitude for dac test 2 (decrementing dac values 4095 to 0)

the 100kHz bin boundary — noting once again, that any frequency magnitude above this 100kHz bin boundary are placed into the 100KHz magnitude bin.

Likewise, while such observations are interesting and the visual comparison between the forward DAC test and the reverse DAC test seem reasonably consistent — which implies a relatively constant CIE effect existing within the testing environment —, a more comprehensive comparison seems merited — at least, for the sake of thoroughness — and upon combining the two tests together within a single series of plots — noting, once again,

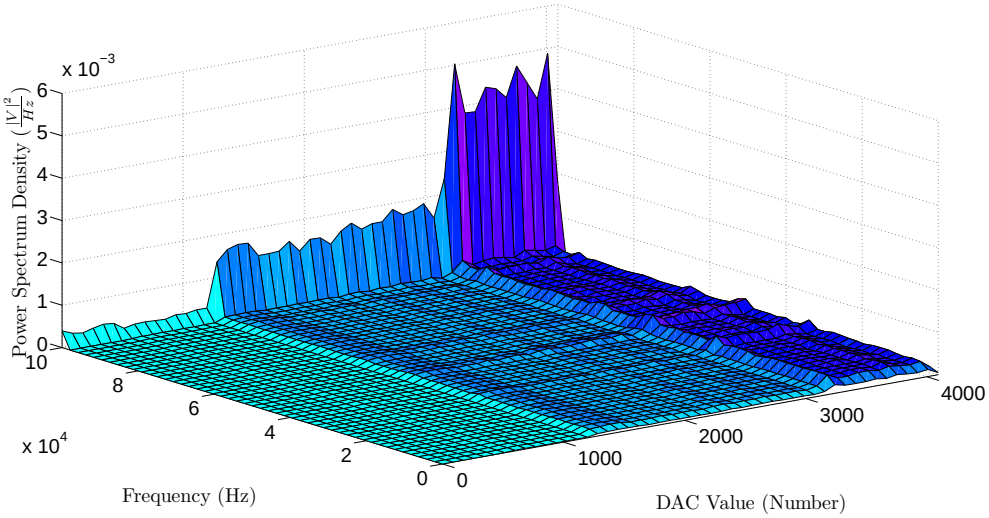

Figure 215: narrow frequency plot of dac value versus frequency versus cumulative overestimation of power spectral density for dac test 1 (incrementing dac values 0 to 4095)

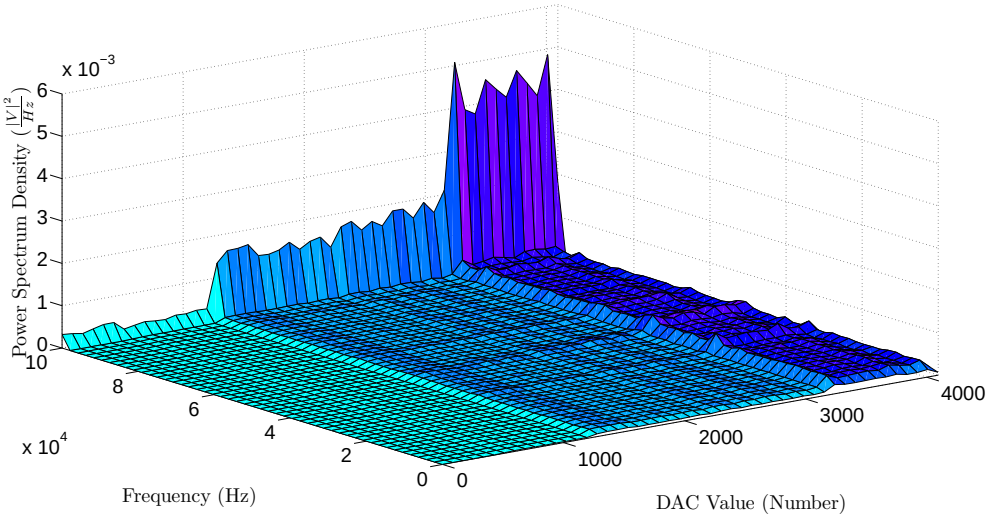

Figure 216: narrow frequency plot of dac value versus frequency versus cumulative overestimation of power spectral density for dac test 2 (decrementing dac values 4095 to 0)

that such plots would symbolize over 10 million data points —, as shown by Figure: (217), Figure: (218), Figure: (219), and Figure: (220), the visual information presented — within the, previously provided, two test comparisons — seems relatively similar to the combined test comparisons — excluding for the moment the z-axis value of the cumulative power spectral density plots, as shown by Figure: (218) and Figure: (220), since the presented power spectral density, within these plots, is the sum of the two, previously provided, power spectral density plots, thus the z-axis will visually appear to have been loosely increased

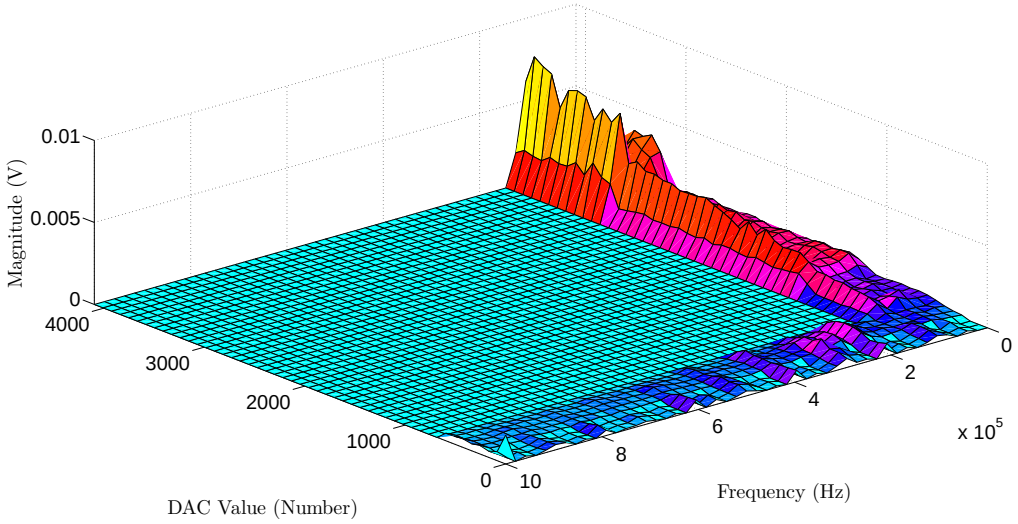

Figure 217: extended frequency plot of dac value versus frequency versus maximum magnitude for combined dac test 1 and 2

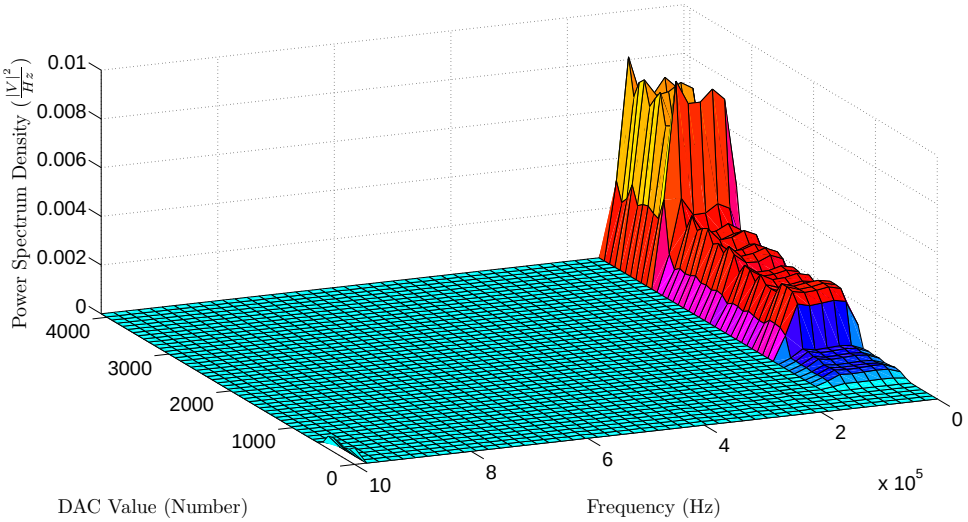

Figure 218: extended frequency plot of dac value versus frequency versus cumulative overestimation of power spectral density for combined dac test 1 and 2

by a factor of two. Similarly, as it was previously mentioned and now further validated, an in-depth visual examination of the extended frequency plots — as shown by Figure: (217) and Figure: (218) — reveals a overall consistent automatic sampling rate selection by the Tektronix TPS2024 oscilloscope — prior to signal acquisition — for both incrementing and decrementing DAC values — within the two test — and such consistency implies, not only a relatively consistent CIE effect exposure throughout the DAC test, but also a consistent internal acquisition mechanism within the oscilloscope utilized that seems to associate

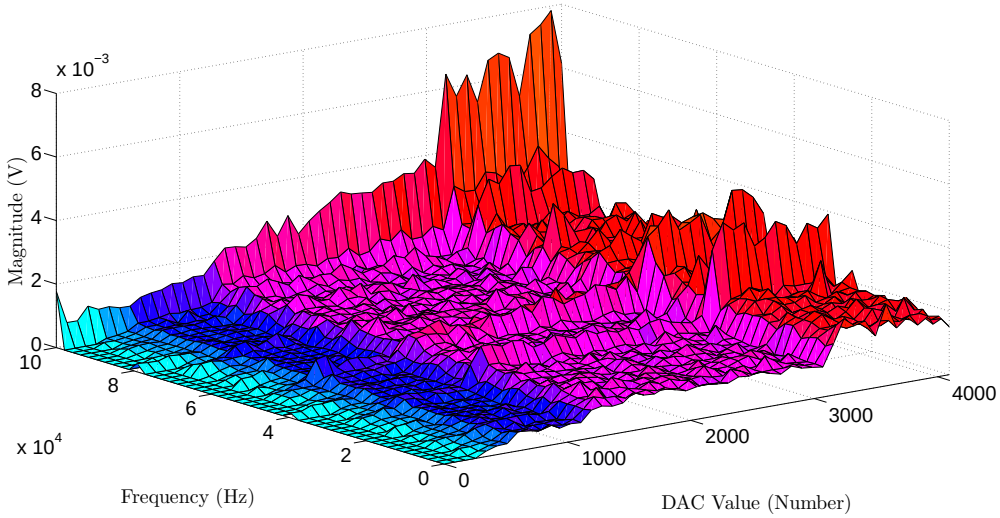

Figure 219: narrow frequency plot of dac value versus frequency versus maximum magnitude for combined dac test 1 and 2

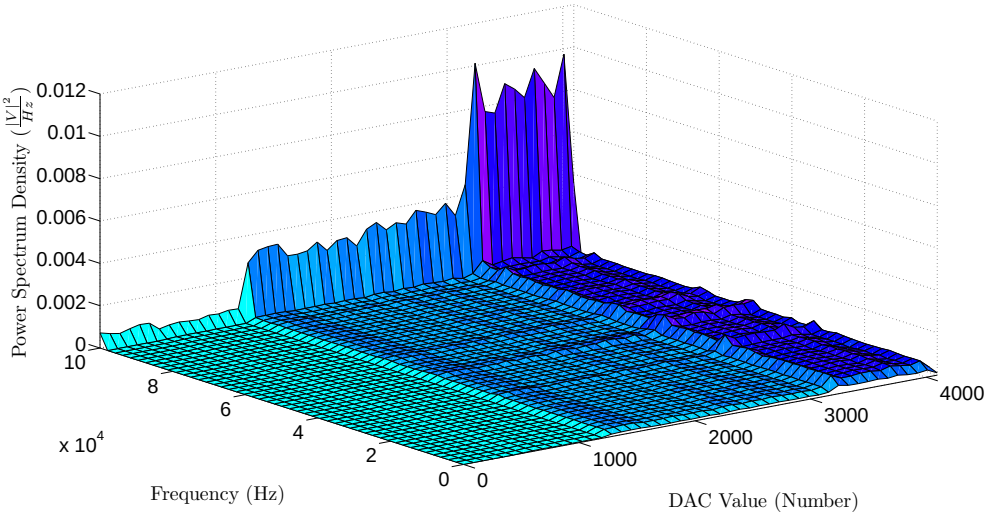

Figure 220: narrow frequency plot of dac value versus frequency versus cumulative overestimation of power spectral density for combined dac test 1 and 2

applied DC voltage with sample rate selection, or more precisely, seems to correlate the oscilloscopes susceptibility to CIE effects with the applied DC voltage.

Conversely, upon taking such observations under advisement and upon considering the fact that most oscilloscopes generally utilize an instrumentational amplifier input stage in order to achieve a high input impedance — an attribute that will hopefully prevent modification of the system being examined —, it becomes reasonable to conclude that this observed increase in susceptibility seems to arise from the fact that the internal gain of the instrumentational amplifier stage — within the oscilloscope — changes because of the increased DC voltage — otherwise the signal would likely be clipped by limitations imposed by the power supply rail — and the process of dynamically reducing this internal instrumentational amplifier gain — a process presumably performed by relays, since clicking noises are audibly heard prior to oscilloscope acquisition — seems to increase the oscilloscopes overall sensitivity to innate CIE effects. Likewise, the observed correlation between the DC voltage and the amount of CIE effects observed is quite concerning, particularly when significant fluctuations in external voltage is expected, especially since software CIE reductive techniques — like finite impulse response (FIR) filtering or the previously depicted process of magnitude masking — are generally dependent upon possessing some prior knowledge regarding how such effects will manifest themselves upon laboratory acquisitions; however, while the introduction of such knowledge might be disheartening to consider, yet such associations must inevitably be considered when attempting to obtain a high fidelity measurement and, given the information obtained from the three-dimensional plots, previously provided, it seems reasonable that a CIE reductive technique can be implemented to compensate for the variations observed from changes in hardware CIE rejection.

Nevertheless, while CIE reductive techniques are currently somewhat speculative — al-

though, some implementation of these techniques will be explored in greater detail within later sections of this chapter —, yet it is important to recognize that the primary objective of this particular section was not the reduction of such effects, but rather the identification of these effects, and clearly, at least based upon the observations graphically obtained, there is a strong association between acquired CIE effects and external DC voltage that, without prior examination, might have gone unnoticed. Likewise, while the three-dimensional plots provided do help to convey some significant insight regarding the CIE effects encountered, yet often times such plots can be difficult to interpret — primarily because a three-dimensional plot is particularly difficult to visually render on a two-dimensional plane —, thus it seems reasonable to consolidate the obtain measurements further — through the utilization of the bin algorithm previously discussed — and create a two-dimensional plot of these CIE effects for frequency versus magnitude — as shown by Figure: (221), Figure: (222), and Figure: (223) — and DAC value vs magnitude — as shown by Figure: (224).

Conversely, while the information conveyed within Figure: (221), Figure: (222), and Figure: (223) — as it might be expected — can easily be correlated with the information presented within the, previously provided, three-dimensional plots; however, it is important

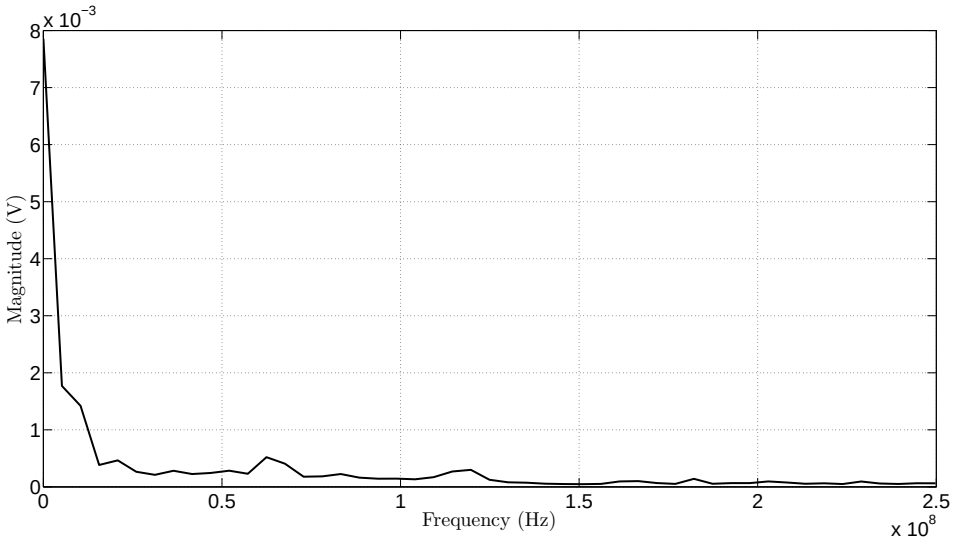

Figure 221: full frequency plot of frequency versus maximum magnitude for combined dac test 1 and 2

to recognize that the compression algorithm utilized, once again, places information outside of the specified boundaries into the first or last bin — depending on which boundary was exceeded — and, as a result, the information presented within Figure: (221) and Figure: (222) is somewhat misleading at the left and right boundaries because of this particular algorithmic nuance. Similarly, upon taking such nuances under consideration, it becomes apparent — at least upon comparing Figure: (221), Figure: (222), and Figure: (223) — that a substantial amount of CIE effects are occurring near the 100kHz frequency — al-

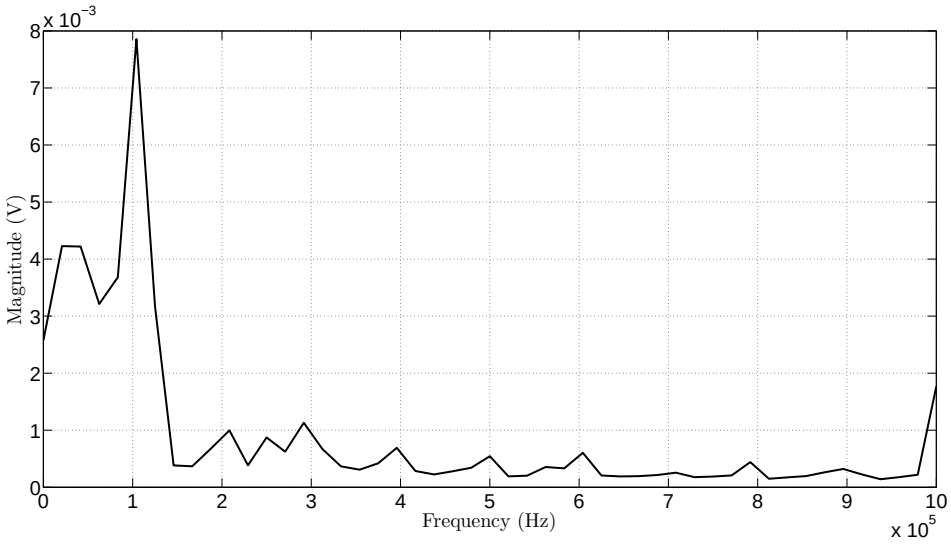

Figure 222: extended frequency plot of frequency versus maximum magnitude for combined dac test 1 and 2

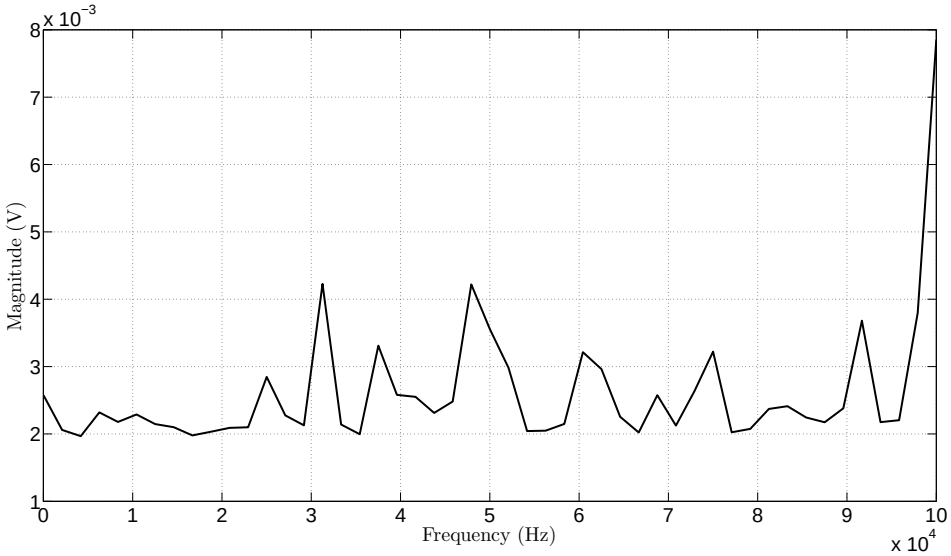

Figure 223: narrow frequency plot of frequency versus maximum magnitude for combined dac test 1 and 2

though this is likely a instrumentational effect rather than a environmental effect since 100kHz is a reasonable instrumentational digital clock source —, while frequencies well above the common synthetic harmonic frequencies — for example 60Hz, 120Hz, etc. — appear to manifest themselves consistently across the observable frequency spectrum. Likewise, examination of the DAC value versus the maximum spectral magnitude encountered 2-dimensional plot, as shown by Figure: (223), once again reveals that the amount of CIE effects encountered appears to increase in step with the externally applied DC voltage, and such observations, once again, supports the, previously provided, notion that the internal circuitry utilized by the oscilloscope is more susceptible to CIE effects at higher DC voltages than at lower DC voltages — although the, previously provided, rationale was admittedly derived from extensive knowledge of electrical instrumentation circuitry.

Yet, while such explanations are relatively reasonable, at least based upon the acquisitions obtained; however, some inherent discrepancy seems to exist between the high-Z environmental acquisitions, previously discussed, and the DC CIE measurements depicted here, and such observations, while being inherently profound, are rather easily explained upon considering the differences between the two measurements. Firstly, the initial high-Z

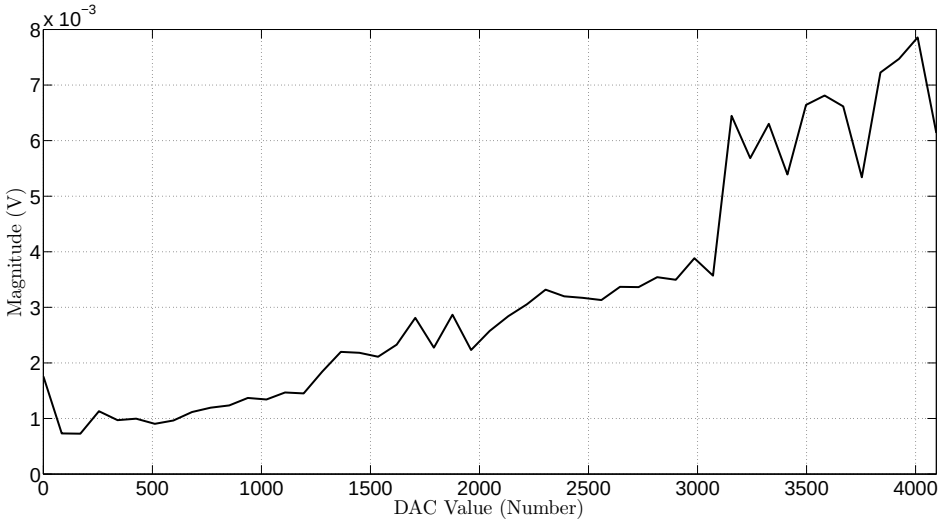

Figure 224: plot of dac value versus maximum magnitude for combined dac test 1 and 2

environmental measurements were acquired with the oscilloscope input stage operating under floating — or ungrounded — conditions, in which a charge imbalance can easily develop upon the acquisition cables and such imbalances seldom ever manifest themselves evenly thus, in turn, making the reductive capabilities of the instrumentational amplifier input stage — within the oscilloscope — less effective while, at the same time, increasing the overall magnitude of the environmental effects acquired. Secondly, because the sampling rate utilized when acquiring each of the two test cases was significantly different — the high-Z measurements had a uniformly sampled window size of around 10 seconds while the DC CIE measurements had a significantly smaller irregular window size — thus, the lower frequency effects observed within the high-Z measurements were inadvertently embedded within the DC component of the DC CIE measurements and examination of the DC plots — as shown by Figure: (206) and Figure: (207) — reveals this embedded spectral content and also helps to explain the fluctuations observed as the DAC changed values — at least beyond the preliminary assumption of pure DAC instrumentation error.

6.3.4 Extracting Embedded CIE Effects

The fundamental rationale behind the extracting embedded CIE effects section was to extend the method developed within the DC voltage and environmental effects section in order to develop a unique method of isolating embedded DC CIE effects — as shown by Figure: (225) — such that comparisons between dissimilar acquisitions can be made — between both a common acquisition device and two dissimilar acquisition devices. Conversely, based upon the observations obtained thru local experimentation , it was found that — under DC voltage input conditions — the automatic scaling feature of the oscilloscopes utilized was inherently based upon the CIE effect floor magnitude, and this attribute ultimately resulted in variations in sample window size occurring — if the sample rate was

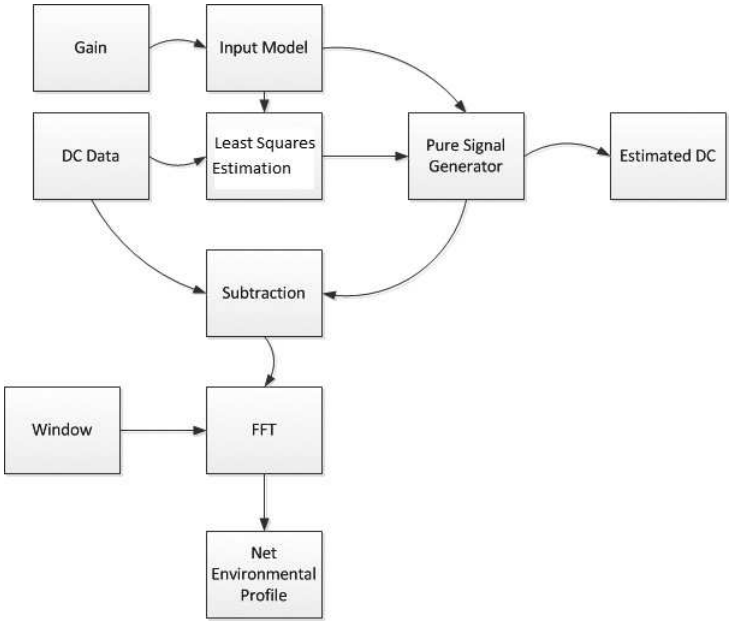

Figure 225: conceptual dc cie estimation approach flowchart

automatically selected by the oscilloscope — and such variations can distort any FFT frequency comparisons made, while — in the case of a incrementally increasing DC voltage — it was demonstrated that the signal obtained under such conditions — assuming that an acquisition was obtained for every change in DC voltage — can be more effectively modeled through the utilization of a piecewise estimation technique — like segmented least-squares — that inherently incorporates the observable changes in the CIE effect floor that results from changes in IA gain prior to attempting to isolate CIE effects from a desired signal.

Likewise, to help validate such conclusions further, consider for the moment the process of summing each individual sample window — for every DC DAC measurement previously obtained — in order to obtain the total window size of the DAC DC plot — as shown by Figure: (206) — and then segmenting this calculated total window size into uniformly spaced time segments that are based upon the number of acquisitions obtained — in this case, 4096 segments — as graphically shown by Figure: (226) and Figure: (227). Yet, although such techniques are innately dubious, especially since the forward DAC value test — 0 to 4095 — had a sample window timebase of 36.1486 seconds, while the reverse DAC

value test — 4095 to 0 — had a sample window timebase of 36.1323 seconds — as ideally these sample window should match in value —, and because such techniques neglect the intermediate time that occurred between oscilloscope acquisitions — an approximate 30 second window in which the DAC value changed and the oscilloscope reconfigured itself before taking the next acquisition —; however, despite the introduction of such dubious nuances — an unfortunate, but metaphorically necessary evil —, it is important to recognize that the underlying intent of this temporal unification process was to provide a consistent temporal axis that can be utilized to create some semblance of a frequency domain axis upon the utilization of the FFT operation — albeit the frequency axis created through the utilization of this technique should only truly be relied upon as a haphazard visual aid, although such assessments might be overly harsh.

Conversely, because the isolation and extraction of the embedded CIE effects from the underlying DAC signal produced by variations in DAC value was desired, such objectives — while sounding reasonably straightforward — are, in fact, somewhat difficult to achieve because of the spectral nature of the DAC output signal produced — in this particular case, the DAC output signal resembles a half ramp waveform. Similarly, to illustrate the

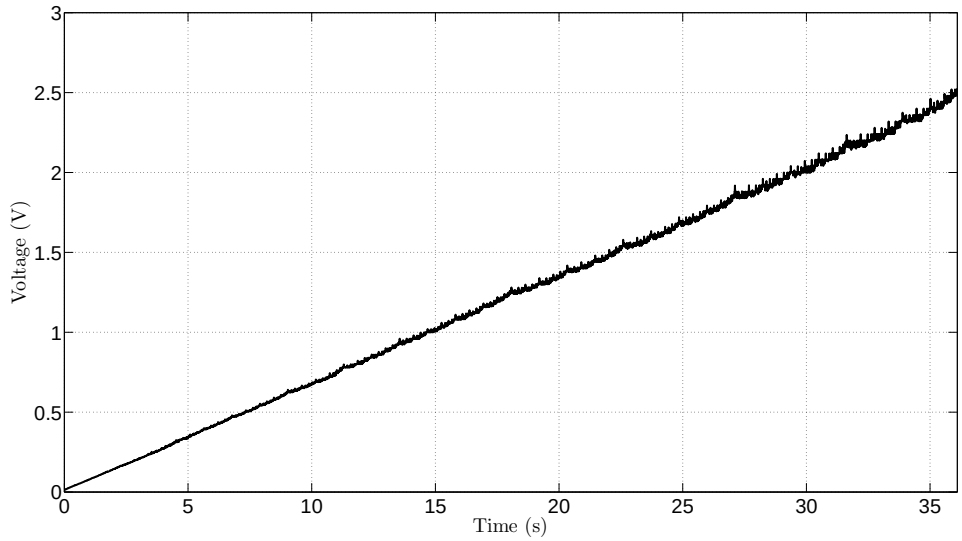

Figure 226: plot of dac test 1 (dac value 0 to 4095) estimated time versus dc voltage

importance — or rather complexity — of this particular attribute further, consider for the moment the spectral magnitude plot of a line, upon the application of the FFT operation — as mathematically described by Equation: (490), and plotted in the time domain by Figure: (228) —, as shown by Figure: (229), versus the spectral magnitude plot of Figure: (226), once again obtained through the utilization of the FFT operation, as shown by Figure: (230).

$$y(x) = C_0 + C_1 x \tag{489}$$

$$y(x) = 10 + 10x \tag{490}$$

Likewise, while the spectral magnitude shown within Figure: (229) might seem extremely disproportional to the spectral magnitude shown within Figure: (230) — and such attributes were expected, although it is worth mentioning that both signals could have been normalized in order to make the magnitude comparisons visually similar, but deliberately was not in order to convey the underlying isolation between frequency and magnitude —; however, the critical attribute to take away from such comparisons, — once again, ig-

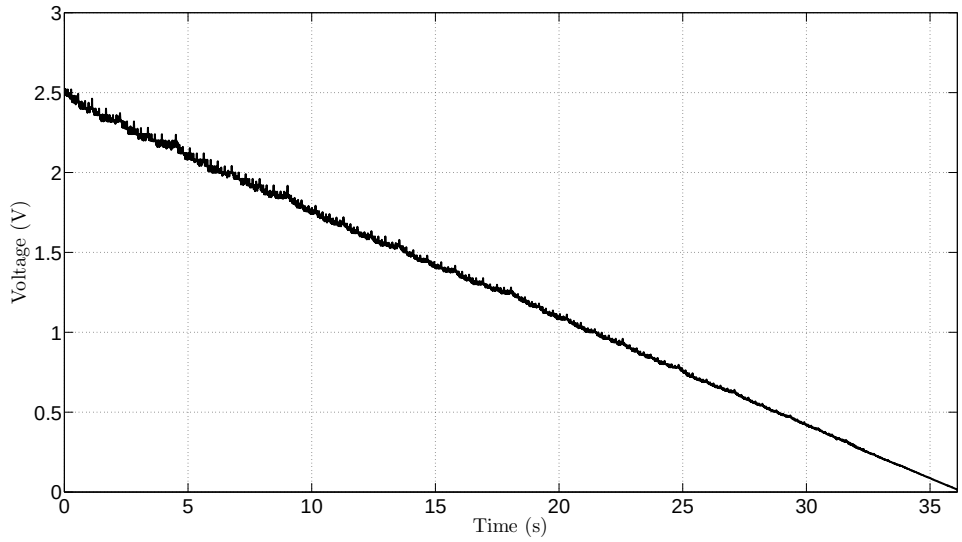

Figure 227: plot of dac test 2 (dac value 4095 to 0) estimated time versus dc voltage

noring for the moment, the observed disproportional magnitudes between Figure: (229) and Figure: (230) — is the overall spectral similarity between the two plots, as this attribute is particularly important because Figure: (229) represents the electrically coveted ideal noiseless measurement, while Figure: (230),on the other hand, represents a noisy real world measurement, and despite the intrinsic difference between the two time domain signals, both measurements — at least upon examining Figure: (229) and Figure: (230) — appear to visually manifest themselves in a eerily similar spectral manner.

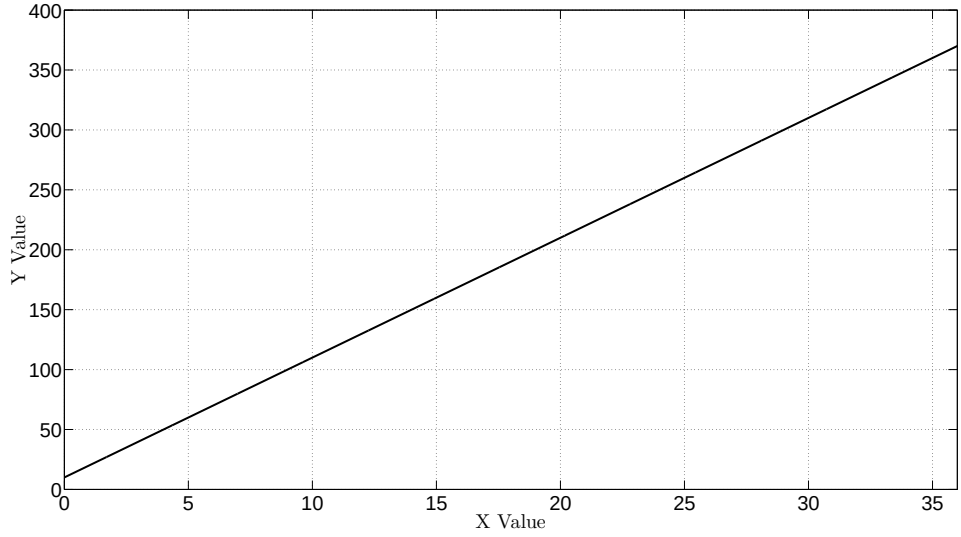

Figure 228: time domain plot of equation (490)

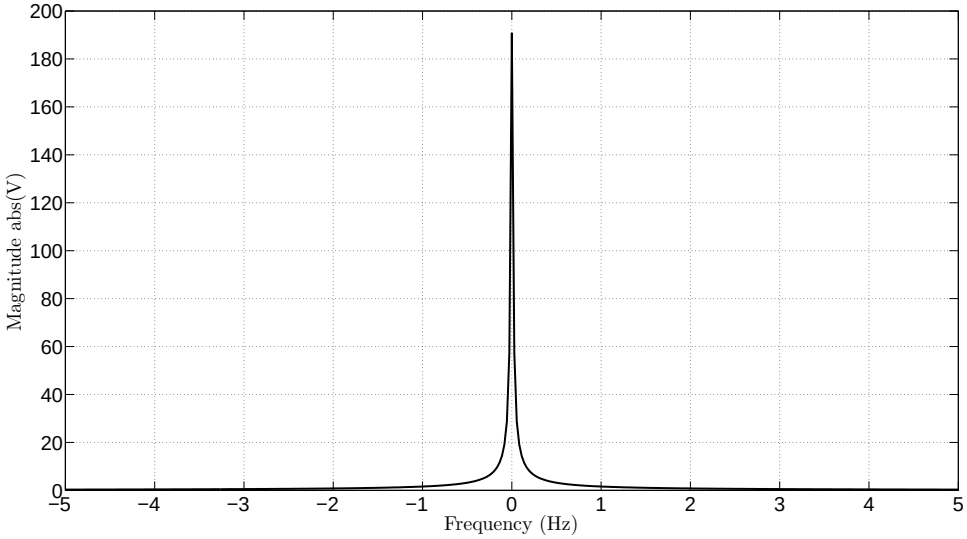

Figure 229: frequency domain plot of equation (490)

Conversely, it is the manifestation of the spectral similarities between the two signals — occurring primarily because of the shape of the waveform — that creates an interesting challenge when attempting to either extract or remove CIE effects for a number of reasons. Firstly, because CIE effects — as it was previously shown — are spectrally distributed across all observed frequencies, this innate characteristic, combined with the fact that the signal being observed is, in itself, spectrally large, inherently implies that any CIE effects that occur within the spectral boundary of the previously shown signal will be embedded within the spectral definition of the original signal. Secondly, because the original signal requires a large spectral definition — a term being utilized here to describe the number of cosine frequency terms needed, within the discreet Fourier transform DFT or FFT, to approximately re-create the original signal; although the term bandwidth could have been used here to convey a similar, though not necessarily as exact, meaning — the process of extracting or removing the observed CIE effects cannot be achieved through the utilization of bandpass or notch filtering techniques alone, since the original signal is strongly dependent upon the preservation of the full spectral definition and such techniques

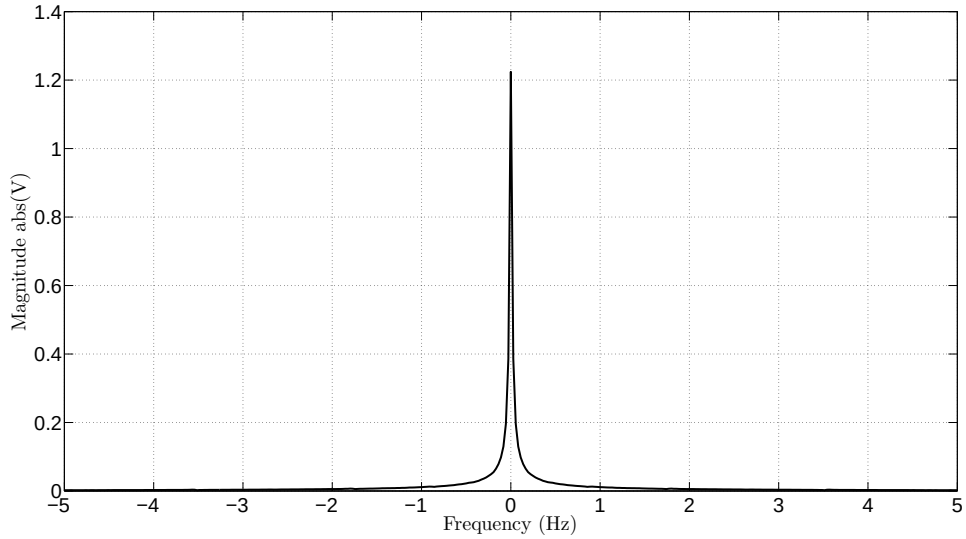

Figure 230: frequency plot of full fft frequency versus maximum magnitude for dac test 1 (dac values 0 to 4095)

inherently modified this dependency through the significant reduction of targeted spectral content.

Likewise, as it might be expected, the introduction of these two inadvertent rationales are, in essence, the fundamental bane of all high fidelity measurements, insofar as, there is little more that can be done — at least from a physical hardware perspective — to prevent the manifestation of these embedded CIE effects beyond the techniques previously discussed — although oversampling, simultaneous multi-spectral sampling, averaging, and control system theory implementations, like Kalman filtering, could possibly provide some added benefit here, although generally such techniques are implemented within a digital signal processor rather than within physical hardware. Conversely, the inevitable manifestation of this particular ingrained attribute does tend to bring about the concept of appropriate signal selection when attempting to obtain a high fidelity measurement — since, for example, a sinusoidal signal tends to utilize less spectral bandwidth than the ramp signal previously shown, thus, in some circumstances, a sinusoidal test signal might be preferred over, say a ramp signal, since the previously mentioned filtering techniques suddenly become more applicable when spectral dependencies are reduced —; however, as it was previously stated, because the term high fidelity is purely dependent upon the intended application, oftentimes such considerations are unrealistic — after all, one cannot simply entice a muscle within the body to emit a sinusoidal signal on a personal whelm, even if it is for the overall betterment of humanity —, thus alternative methods of CIE extraction and reduction must be utilized.

With this being said, while it is important to recognize that the underlying concept of CIE extraction and reduction is, by in large, a commonly investigated and reasonably well understood problem — particularly within the communication and control systems research

area — with a wide assortment of effective solutions available; however, it is also important to recognize that the vast majority of these solutions are, to some extent, exclusively designed for a particular application and, while such techniques can, in fact, typically be retrofitted and utilized within the biomedical research area, the inherent assumptions made surrounding there implementation — since such techniques typically require information regarding the spectral content of the observed signal and the CIE effects encountered — is seldom ever conveyed beyond the physical implementation. Conversely, to elaborate on this attribute further, a paramedic, nurse, or physician typically has no idea that, for example, an electrocardiographic (EKG) signal has been spectrally modified through the utilization of CIE compensation techniques, and while it is not always necessary that such information be conveyed beyond its original implementation —- so long as something beneficial is being conveyed, in this case, to medical personnel —, yet given the inherent tendency of biomaterials, CIE effects, and for that matter, electrical interconnections, to change over time, the implementation of such techniques frequently sacrifice real-time accuracy for perceived signal clarity — or in other words, a sudden spike on a EKG, while legitimately occurring within the body, might be inadvertently removed because its occurrence does not fit the presumed spectral profile of the CIE removal technique —, and such assumed perceptions can be problematic, particularly if a person's medical health is strictly dependent upon them.

Nevertheless, while such observations are definitively profound and, in many respects, are the foundation upon which a number of health and safety regulations are based; however, such attributes tend to extend well beyond the desired scope of this particular discussion — thus further discussion on this particular attribute will be avoided — while, at the same time, helping to martyr the importance of possessing an in-depth understanding

of the term high fidelity measurement, particularly within the biomedical research area. Therefore, while it will be conceded that a number of CIE reductive techniques are both available and applicable — and those unsatisfied with this conclusion should examined the techniques utilized within the signals and systems or control system theory research area —; however, to demonstrate the utilization of such techniques, one useful approach to this problem — particularly since this problem is relatively linear in nature — begins by attempting to isolate the desired spectral signal from the innately imposed CIE effects encountered through the utilization of least-squares estimation — a technique best surmised as being the process of minimizing the error between an assumed theoretical model and the acquired measurement, a technique also commonly referred to as curve fitting — as described mathematically by Equation: (494).

$$F = \begin{bmatrix} 1 & t \\ 1 & 2t \\ \vdots & \vdots \\ 1 & Nt \end{bmatrix} \tag{491}$$

$$Y = \begin{bmatrix} y(t) \\ y(2t) \\ \vdots \\ y(Nt) \end{bmatrix} \tag{492}$$

$$S = F^T F \tag{493}$$

$$C = (S)^{-1} F^T Y \tag{494}$$

Likewise, upon assuming that the equation of a line would best described the observed

DAC output voltage — as mathematically described by populating the fitting matrix (F) with a vertical column of value 1, to represent a constant term, and a progressively incrementing number that was equal to the time increment previously calculated, to represent an increasing singular variable — and inputting the acquired DAC DC Test 1 (DAC Value 0 to 4095) measurements into the (Y) matrix, the matrix coefficients (C) numerically calculated that best fit the assumed linear model with the measured data are shown by Equation: (496), in which Equation: (497) is the constant value and Equation: (498) is the slope of the line.

$$C = \begin{bmatrix} C_1 \\ \\ C_2 \end{bmatrix} \tag{495}$$

$$C = \begin{bmatrix} 0.0042 \\ \\ 0.0675 \end{bmatrix} \tag{496}$$

$$C_1 = 0.0042 \tag{497}$$

$$C_2 = 0.0675 \tag{498}$$

Conversely, upon substituting the coefficients obtained into the assumed linear model, as shown by Equation: (500), and comparing the model obtained to the acquired DAC DC Test 1 (DAC Value 0 to 4095) DC voltages, as shown by Figure: (231), reveals a reasonably accurate predictive model — although a slight deviation between the two does occur slightly before reaching the 2.5 voltage marker as a result of the increased amount of CIE effects encountered, and the occurrence of such deviations highlights a underlying and reoccurring theme that represents the biggest fundamental flaw when utilizing the least-squares estimation method as a analytical modeling technique — and to some extent,

such descriptions are also applicable to the vast majority of most contemporary modeling techniques —, since such techniques are fundamentally at the mercy of CIE effects, as the smallest unexpected CIE effect can significantly decrease the overall predictive accuracy of such techniques.

$$y(t) = C_1 + C_2 t \tag{499}$$

$$y(t) = 0.0042 + 0.0675t \tag{500}$$

Likewise, now that a estimate of the original TEST 1 DAC DC signal has been obtained, the original signal can be subtracted from the least-squares estimate in order to obtain an approximate representation of the CIE effects that were embedded within the original signal, as graphically shown by Figure: (232). Similarly, the FFT operation can be performed upon this estimated signal, as graphically shown by Figure: (233), and in a similar manner to the synthetic isolation routine, previously discussed within the environmental effects section, the significant CIE frequency components can be identified for further signal analysis — presumably within advance CIE reduction techniques —, as shown by Figure: (234) and

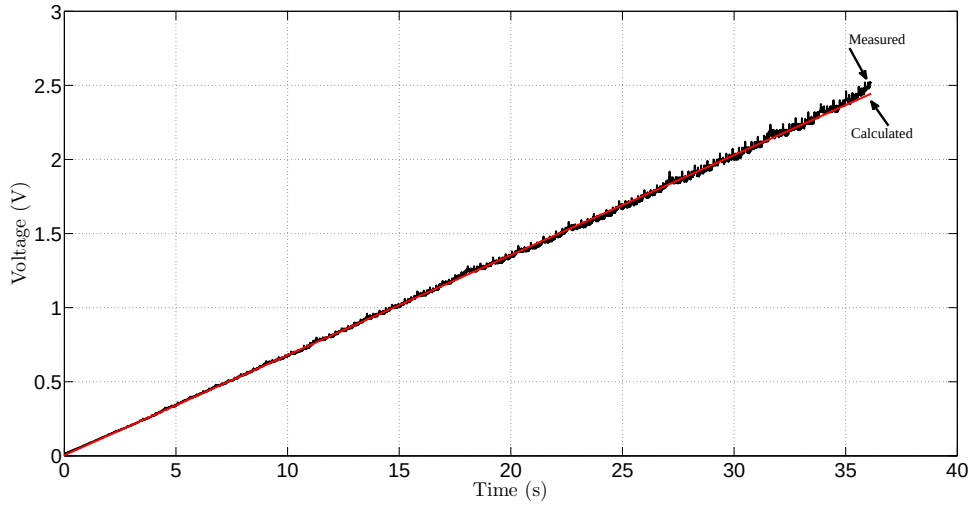

Figure 231: dac test 1 (dac values 0 to 4095) dc output voltage versus predicted least-squares estimated dc voltage

Figure: (235).

Conversely, further visual inspection of Figure: (232) reveals that a reasonably good numerical approximation was achieved through the utilization of the least-squares estimation technique, with the notable exception being the minor deviations observed beyond the 20 second mark — as the CIE variations observed seem to increase significantly beyond this point, although such variations are to be expected given that CIE effects were previously observed to increase at higher input voltages. Yet, while such estimates are reasonably accurate, at least upon examining the lower DC DAC voltages, the underlying problem that

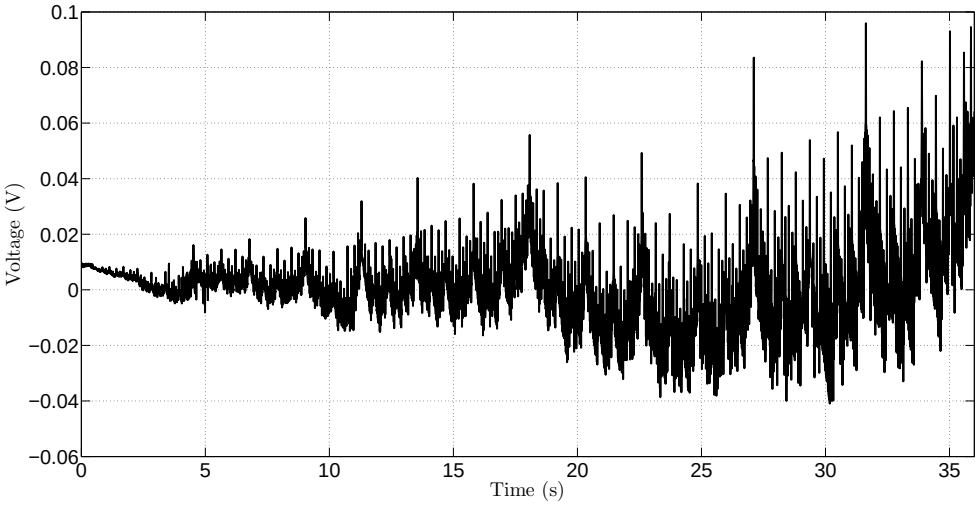

Figure 232: plot of dc dac test 1 (dac values 0 to 4095) estimated cie effects

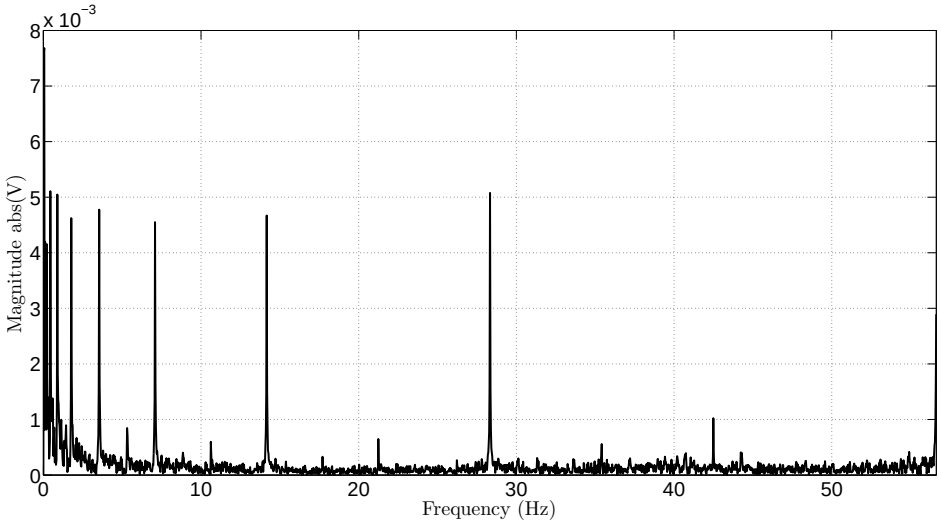

Figure 233: plot of fft dac test 1 (dac values 0 to 4095) estimated cie effects

arises from such assessments is the sudden change between internal oscilloscope acquisition gain that, in turn, inadvertently modifies the model from a simplistic linear system to, at the bare minimum, a piecewise linear system, because of the previously mentioned changes in instrumentational amplifier gain as the DC voltage being examined increased. Nevertheless, while such attributes should definitively be considered when attempting to obtain the highest fidelity model possible; however, given the overall accuracy of the current model and the end objective of this particular discussion, the linear model utilized here seems to be a reasonable starting point for further discussion — although the curious are advised

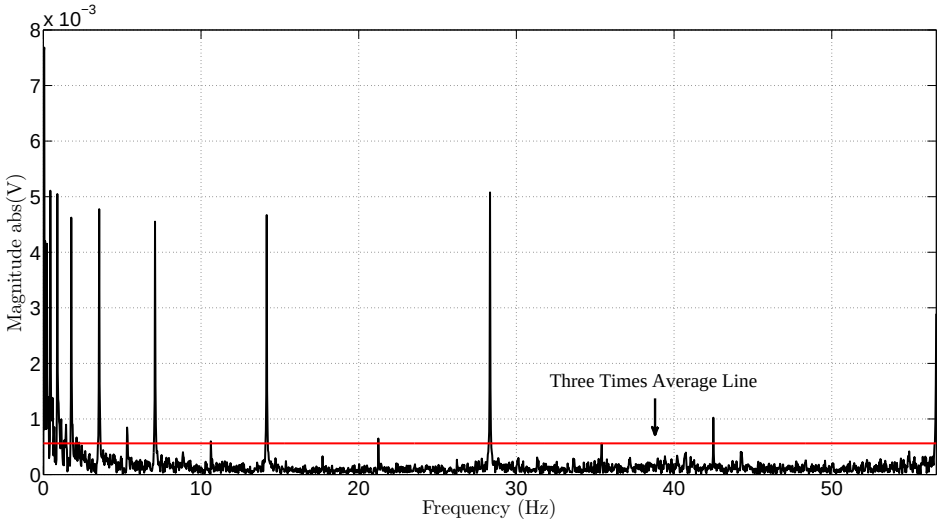

Figure 234: plot of three times average fft dac test 1 (dac values 0 to 4095) estimated cie effects

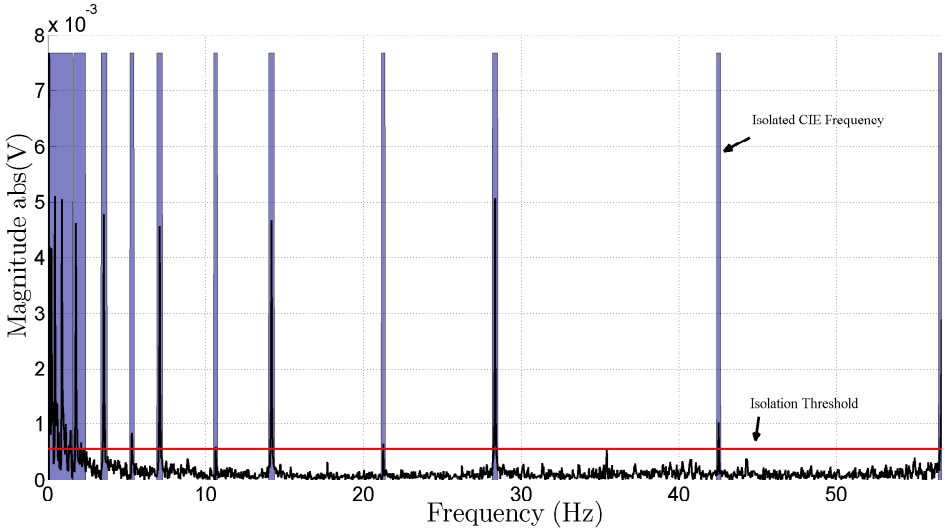

Figure 235: plot of estimated frequency domain cie reductive mask

to segment the acquired data into three segments, perform least-squares estimation of a line upon each segment, and create a piecewise function using the three linear functions estimated.

Likewise, performing the FFT operation on Figure: (232) yields Figure: (233) — although it is important to recognize that the frequency axis shown within Figure: (233) is, once again, somewhat dubious because of the, previously mentioned, method utilized to combined the measured segments into a visually perceived pseudo-continuous time signal — and, assuming for the moment that the frequency axis is reasonably accurate, it becomes apparent that the lower spectral content that existed below the first nonzero FFT bin was, in fact, superimposed within the acquired DC mean value obtained. Conversely, while — once again — the exact frequency of the superimposed CIE effects cannot be definitively known based upon the information currently available — additional acquisition with a larger sample window would be required to accurately obtain this information —; however, it is reasonable to conclude that a number of synthetic CIE sources are definitively present within Figure: (233) — like 60 Hz environmental effects and subsequent harmonics — and such attributes are clearly observed upon examining the placement of peak magnitude spikes — on the order of 5mV — relative to the approximate .25mV stochastic lower CIE effect acquisition floor.

Yet, while such attributes are inherently interesting and enlightening — although a more accurate frequency assessment would have ideally been preferred —; however, while the visualization of such effects is extremely beneficial, the profiling and removal of such effects is, by and large, considered to be of more interest, and, to build upon the previously mentioned concepts further, the average spectral magnitude can be found — by performing the mathematical mean operation upon the magnitude shown within Figure: (233) — and

multiplying the value obtained by three — a somewhat arbitrary choice that was visually selected because it seems to isolate the perceived stochastic CIE effects from the synthetic CIE effects —, as shown by Figure: (234). Likewise, this average value can then be utilized within the FFT masking algorithm, as shown by the MATLAB code within Appendix E script 18, and the mask obtained can then be utilized to either describe or isolate and remove the predominant synthetic CIE effects observed within Figure: (233) as graphically shown by Figure: (235).

Similarly, the masking information obtained within Figure: (235) — noting, once again, that the mask created, unlike the mask visually shown within Figure: (235), is actually derived from the full, non-shifted, non-normalized, magnitude information — can then be multiplied by the real and imaginary CIE frequency coefficients —- loosely illustrated by Figure: (232) — in order to create a highly selective FFT bin notch filter, and this value can be subtracted from the real and imaginary DC frequency coefficients — loosely depicted by Figure: (230) — and the inverse FFT operation taken in order to obtain a time domain plot of the DC effects encountered with a majority of the predominant synthetic CIE effects removed, as shown by Figure: (236).

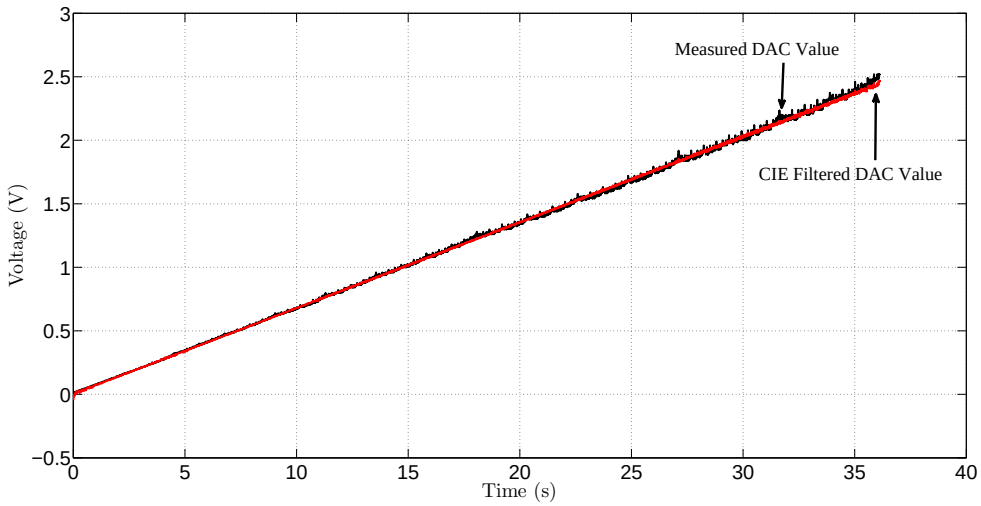

Figure 236: plot of cie effect reduced dc dac test 1 (dac values 0 to 4095)

Conversely, while — once again — it will be admitted that such techniques are far from being at the metaphoric bleeding edge of contemporary DSP CIE effect reductive techniques frequently utilized within communication systems; however, this particular technique does demonstrate a number of very interesting concepts that must be considered prior to attempting to implement a more popular CIE effect reductive method. Firstly, as a general rule, it should be assumed that the effectiveness of the reduction obtained is directly related to the accuracy of the model assumed, or within this particular example, because it was assumed that a equation of a line would ideally represent the actual DAC voltage measured; such assumptions — because they are not entirely correct given the piecewise nature of the system being measured — will, upon rigid filtering, — at best — provide results that are as accurate as the assumed model. Secondly, because rigid filtering — the process of subtracting the assumed complete CIE effect spectrum from the DC DAC spectrum — will yield the assumed model, a trade-off exist between allowing the CIE effects to remain superimposed upon the original signal but keeping the original signal as unaltered as possible or reducing the amount of superimposed CIE effects within the signal at the cost of modifying the original signal to become more like the assumed model.

Likewise, with this being said, because it was assumed that some error would arise within the least-squares estimate of the DC DAC voltage, it was reasonable to conclude that the utilization of a rigid filtering method would be extremely unwise, since the result would simply be — in this case — the previously found estimated linear equation. Conversely, using this knowledge as a guide, the isolation and removal of definitively strong — and presumably synthetic — CIE effects was selected because it seemed to be a metaphoric, middle-of-the-road, compromise, at least within this particular scenario, since definitively large CIE effects were removed while, at the same time, smaller — less intrusive — CIE

effects were preserved in an attempt to help maintain the overall shape of the original signal. Similarly, with this being said, upon conducting a further visual examination of Figure: (236), it becomes apparent that the larger CIE effects superimposed within the original signal has been significantly reduced; however, the filtered signal also appears to slightly deviate from the visual slope of the original signal — slightly after the 30 second marker — because of the inherent inaccuracies associated with the least-squares estimate, and while such deviations are, in this case, relatively minor, such deviations graphically represent the metaphoric internal struggle between obtaining presumed clarity versus acquired accuracy that is a inherently prevalent throughout high fidelity modeling.

Conversely, with this being said, it becomes apparent that the process of extracting embedded CIE effects is predominantly associated with the amount of information available — in this case no CIE profile information was available, thus the embedded CIE effects had to be extracted by making assumptions regarding the mathematical model of the original signal through the utilization of least-squares estimation —, and the accuracy of such information ultimately defines the level of fidelity obtained. Furthermore, while CIE effect reduction through the estimation of the original signal can be improved through

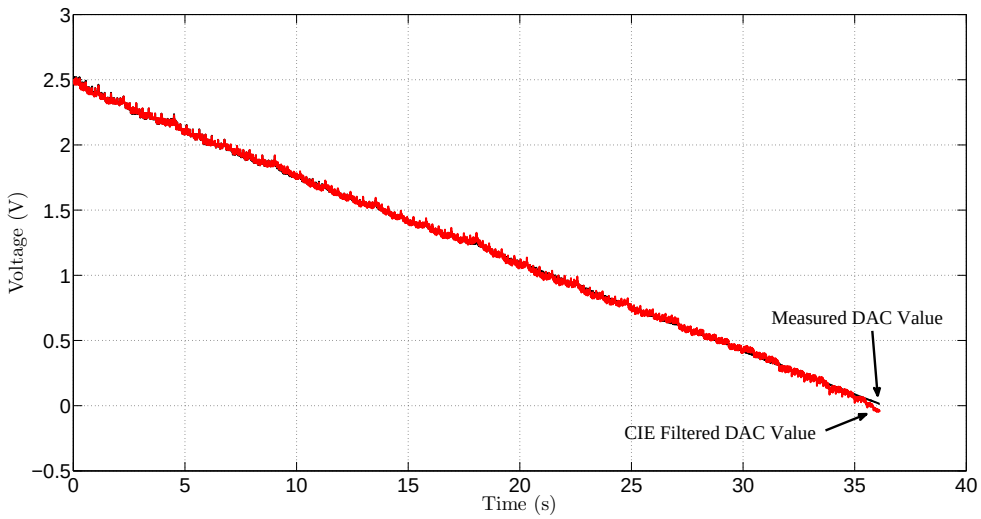

Figure 237: plot of cie effect reduced dc dac test 2 (dac values 0 to 4095) using cie effect one mask

iterative techniques — that are loosely based upon the methods shown above —; however, ultimately such reductive methods are no substitute for physical CIE reductive methods since analytical techniques can only increase a signals fidelity by a very limited amount before the process of substituting CIE effects for rounding or truncation effects occurs. Additionally, it is worth mentioning that while the techniques, previously shown, was only utilized on a singular DAC test measurement, the FFT bin mask,previously created, can — in fact — also be applied to other test acquisitions — although, in this particular case, the CIE FFT mask will need to be remapped to the new FFT test bin — a process achieved by the MATLAB code shown within Appendix E script 19 —, since the sample window size was different between the two test — as demonstrated by the CIE effect reduction preformed on DC DAC test 2 (4095 to 0) using the, previously calculated, CIE effect mask from DC DAC test 1, as shown by Figure: (237).

Nevertheless, upon visual examination of Figure: (237), it becomes apparent that such reductive techniques are, once again, highly dependent upon the accuracy of the models utilized and any embedded errors — within those models — will ultimately become embedded within the signal utilizing such reductive techniques — as was the case within Figure: (237), since the filtered signal visually appears to be more distorted than the original signal because the reductive mask utilized was insufficiently defined for this particular sample window despite the utilization of bin remapping. Consequently, the visualization of such attributes ultimately emphasizes the importance of proper and consistent window sampling size when implementing such reductive techniques, since the remapping of FFT bins is, in itself, a highly questionable practice — although a better approach to this particular problem might have been to synthesize the time domain equation using the FFT mask coefficients and then discretize this new continuous time domain signal into the appropriate

spectral window or, alternatively, attempt to pad the time domain measurement with zeros, prior to performing the FFT operation, in order to increase the FFT bin resolution and thus help reduce remapping error —; however, such techniques, if performed carefully and correctly, can yield results that are significantly better than those obtained within Figure: (237).

$$y(t) = 2.4432 - 0.067523t \tag{501}$$

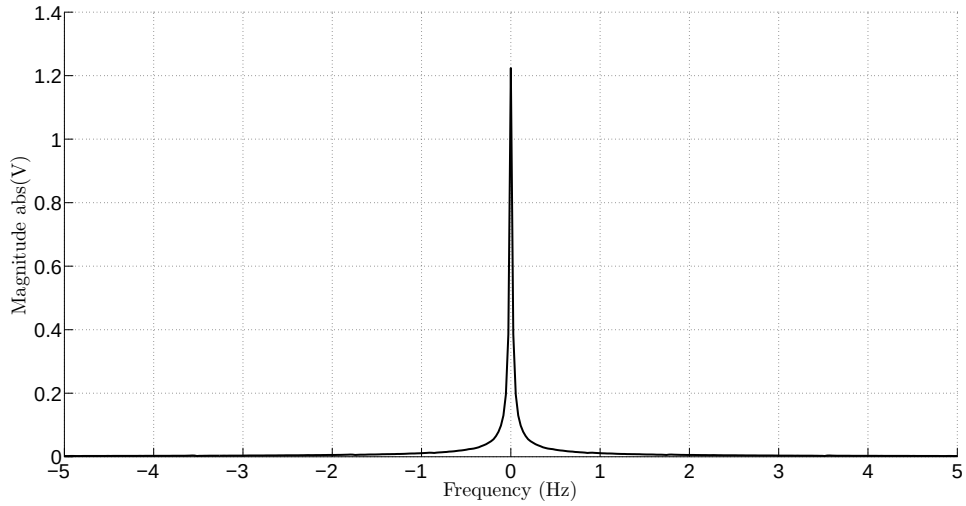

Figure 238: frequency plot of full fft frequency versus maximum magnitude for dac test 2 (dac values 4095 to 0)

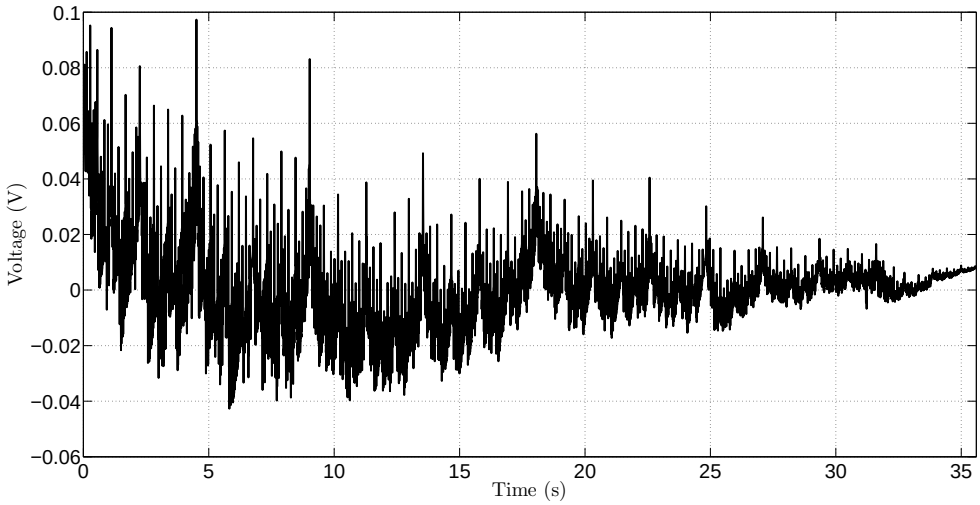

Figure 239: plot of dc dac test 2 (dac values 4095 to 0) estimated cie effects

Yet, with this being said, in an attempt to provide a thorough review of the DC DAC measurements taken, the second DAC test (4095 to 0) – as shown by Figure: (227) and Figure: (238) — can be linearly estimated using the, previously discussed, least-squares estimation technique — an attribute that yields Equation: (501) — and the embedded CIE effects can then be extracted from the original signal — as shown by Figure: (239) and Figure: (240) —, while the CIE effects embedded within the original signal can then be removed using the reductive mask obtained from the utilization of the, previously described, methods — as shown by Figure: (241). Conversely, a visual inspection of Figure: (227)

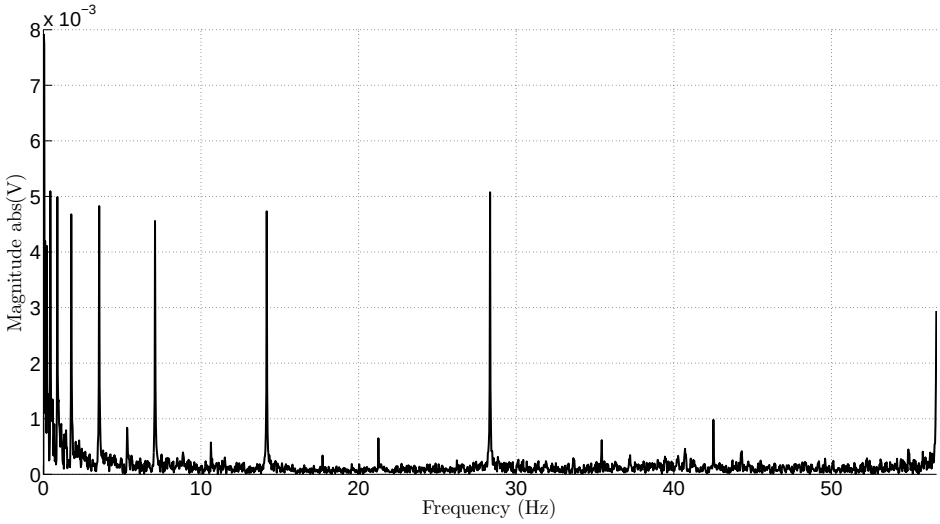

Figure 240: plot of fft dac test 2 (dac values 4095 to 0) estimated cie effects

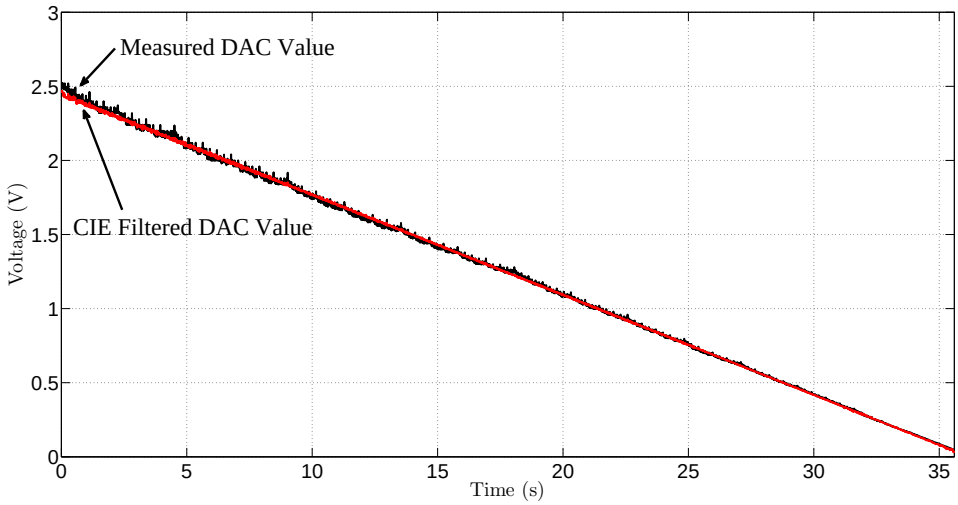

Figure 241: plot of cie effect reduced dc dac test 2 (dac values 4095 to 0)

and Figure: (238), despite the second test possessing a decreasing DAC DC output, reveals a nearly identical frequency domain plot, as observed within Figure: (230), — an attribute that is strongly associated with the frequency domain spectral transformation of a line —, and a visual comparison between Figure: (239) and Figure: (232) and Figure: (240) and Figure: (233) also yields a nearly identical CIE effect profile — although the time domain plot is visually reversed, because of the decreasing nature of the second signal, while the frequency domain is slightly shifted, because of the inconsistencies between the two sample windows. Likewise, the amount of CIE reduction obtained — within Figure: (241) — is comparable to the reduction obtained — within Figure: (236) —, and while such isolation and reductive techniques are far from being the "de facto" [†1] methodological approach, such methods are, in fact, a relatively reasonable first step towards obtaining a high fidelity bioelectrical signal acquisition, insofar as, such techniques set the metaphoric foundation upon which other methods are built, and such methods serve as a intrinsic reminder of the common simplistic pitfalls that can arise when attempting to implement a more complex reductive method [72, p.127].

6.3.5 CIE Effects and Spectral Leakage

The fundamental rationale behind the extracting embedded CIE effects and spectral leakage section was to reinforce the importance of the observations made within the DC voltage and environmental effects section and the extracting embedded CIE effects section regarding sample window selection and to uniquely convey the existence of a contemporary problem within the biomedical community surrounding the conveyance of spectral related information within academic publications — commonly conveyed thru the usage of Wessel diagrams, as shown by Figure: (242). Likewise, based upon the observations obtained, it

[†1] Latin phrase for: being such in effect though not formally recognized.

was determined that the FFT analysis of an acquired signal, if done improperly, can yield distorted results predominantly because of a processing distortion typically referred to as spectral leakage. Conversely, while the concept and theory behind the occurrence of spectral leakage is well understood — especially within the signals and systems research area —; however, it was determined that most commercial biomedical applications — particularly bioimpedance spectroscopy devices — either fail to compensate for this occurrence or utilize compensation techniques — like windowing — without providing information regarding the technique implemented, and because each compensation technique inherently modifies the spectrum obtained differently — typically spectral content accuracy is increased at the cost of magnitude accuracy —, thus any comparisons made between different commercial bioelectrical signal acquisition devices that utilize the Fourier transform within their analysis are highly susceptible to the introduction of distortions from unmatched preprocessing operations like windowing. Additionally, because the results obtained using these particular processing techniques are also dependent upon the sample window size selected — or the amount of signal captured — such attributes are seldom ever discussed beyond the presentation of a post-process Wessel diagram — or complex plane plot over frequency diagrams — and, once again, comparisons made using such information can inherently introduce distortions between acquisition comparisons because of inconsistencies in the preprocessing techniques utilized. Likewise, based upon such observations, a number of techniques were examined — with a focus upon methods to keep the acquired signal symmetric —, and based upon such examinations it was determined that periodic signals are best suited for BIS analysis, while passive measuring techniques that frequently encountered non-periodic waveforms are better off utilizing well documented windowing techniques, and in either case great care should be taken before attempting to compare one biomedical acquisition with

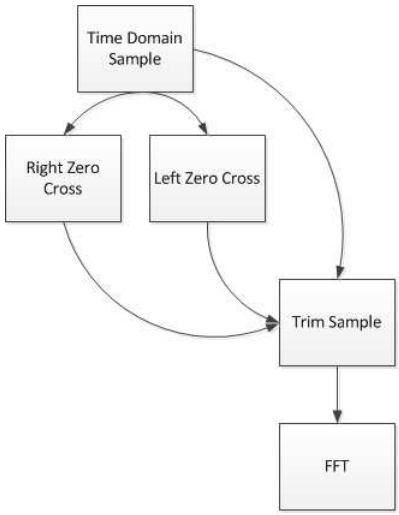

Figure 242: conceptual fft approach flowchart

another else distortions are likely to occur from discrepancies in the processing techniques utilized.

Nevertheless, while the CIE effect analysis of both DC and linear signals — although the linear line analysis performed, in this particular case, was actually an inadvertent byproduct of the extracted DC signal —; however, such presumed conditions are far from being an accurate representation of the types of signals frequently encountered within the bioelectrical research area, and based upon such assessments, it seems reasonable — at least, for the sake of thoroughness — that some examination of CIE effects encountered during non-DC acquisitions are investigated in order to determine if the CIE effects encountered when performing DC acquisitions are similar to the CIE effects encountered when performing non-DC acquisitions. Conversely, with this being said, there is an interesting and important problem that arises upon attempting to utilize the, previously discussed, spectral techniques, upon a non-DC signal — a problem frequently referred to as spectral leakage. Likewise, while the subject of spectral leakage is a commonly discussed subject — especially within the signals and systems research area and the digital signal processing research area — so much so, that based upon the amount of information available on this particular topic, only a brief overview of this particular problem will be provided within

this section; however, given that the majority of biomedical signals that were examined within this dissertation were inherently sinusoidal — primarily because active analysis was preferred over passive acquisition — consider for the moment the following simplistic sinusoidal signal with a arbitrarily selected magnitude of 10 volts and a frequency of 1 kHz, as shown by Figure: (243).

Similarly, upon performing the FFT operation on Figure: (243), the following spectral magnitude plot, as shown by Figure: (244), was obtained and, as it might be expected, the resulting plot has a singular point located at a magnitude of 10 volts with a frequency

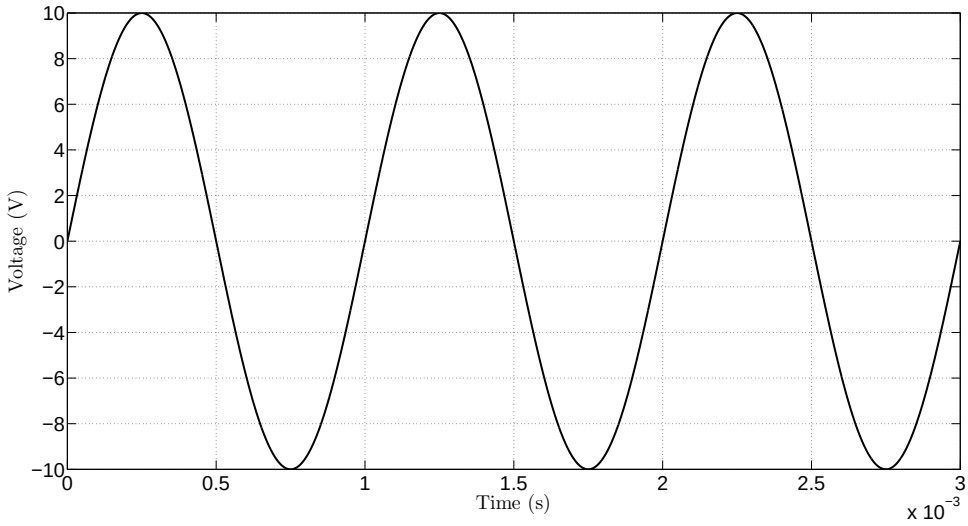

Figure 243: plot of $10\sin\left(2\pi\,1000\,t\right)$

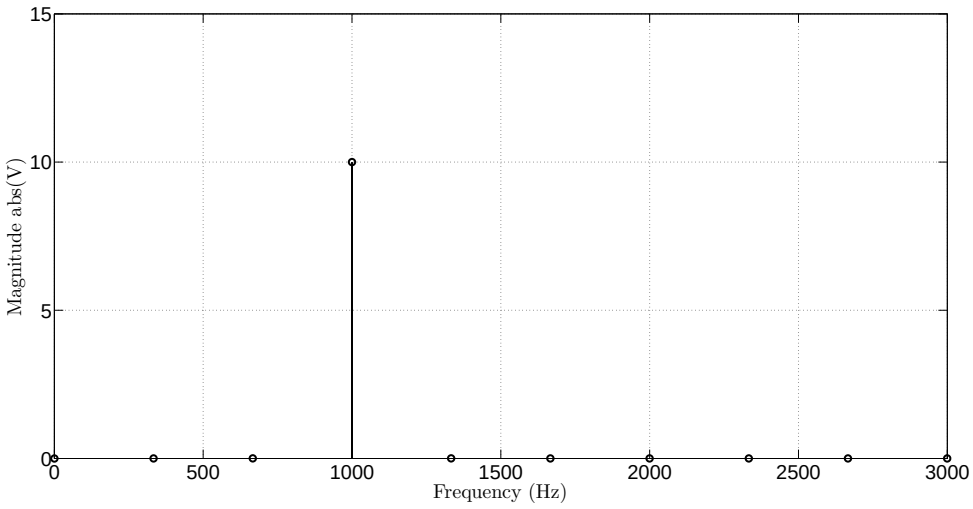

Figure 244: fft magnitude plot of $10\sin\left(2\pi\,1000\,t\right)$

of 1 kHz. Conversely, while the spectral information obtained within Figure: (244) was expected; however, the data utilized within the FFT operation, as shown by Figure: (243), is far from being an ideal representation of an laboratory acquisition, insofar as, — in this particular case — the process of obtaining a perfectly seamless periodic acquisition is something that is extremely difficult to achieve. Likewise, a more realistic real world acquisition of Figure: (243) might resemble Figure: (245), and upon performing the FFT operation on Figure: (245), the following spectral magnitude plot, as shown by Figure:

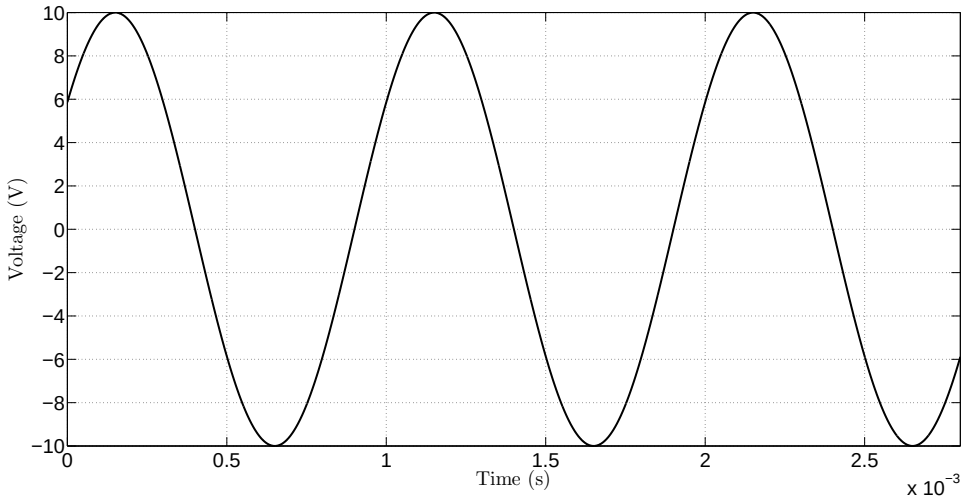

Figure 245: plot of a non-seamless capture of $10\sin\left(2\pi\,1000\,t\right)$

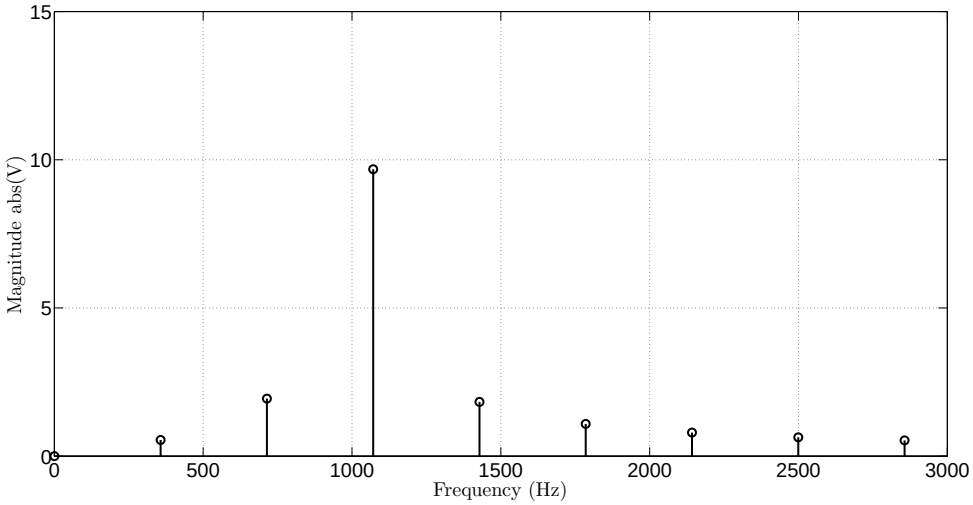

Figure 246: fft magnitude plot of a non-seamless capture of $10\sin\left(2\pi\,1000\,t\right)$

(246), is obtained.

Conversely, a visual comparison between Figure: (246) and Figure: (244) reveals the introduction of additional — and undesired — spectral components — within Figure: (246) — as a result of acquiring — in this particular case — a non-seamless periodic signal, and the introduction of these additional spectral components is — at least within the digital signal processing community — typically referred to as spectral leakage. Likewise, as it might be expected, the introduction of these unwanted spectral components can be extremely problematic, particularly if the modeling process being utilized is heavily dependent upon the spectral information obtained; thus, as a result of such observations, a number of possible solutions are available and are frequently implemented to reduce the effects of such distortions — although only two of these solutions will be addressed within this particular section. Similarly, the first commonly utilized technique to reduce the effects of spectral leakage is a technique usually referred to by the term windowing, and windowing is a process that is best described as multiplying a time domain signal by a scaling waveform — typically a box, triangular, Gaussian bell, or sinc shape normalized waveform—, with the intent of reducing spectral leakage through forcing the left and right amplitudes — of the original time domain signal — to smoothly transition towards a common value — that is analogous to turning a non-seamless waveform into a seamless waveform [390, p.80].

While the underlying mathematics behind windowing functions is rather complex; however, the most important concept to remember is that ultimately the windowing function selected does play a substantial role in determining the amount of spectral leakage that will manifest itself upon performing the DFT or FFT operation on a non-seamless waveform, yet to visually demonstrate the reductive capabilities of such techniques further, consider for the moment a windowing function typically classified as a Hanning window — easily

generated within Matlab by using the signals toolbox function "*hanning(n)*" —, as graphically shown by Figure: (247). Conversely, upon multiplying the handing window — as shown by Figure: (247) — with the non-seamless sinusoidal acquisition — shown within Figure: (245) — yields Figure: (248), and upon performing the FFT operation on Figure: (248) yields the spectral magnitude plot, as shown by Figure: (249) [390, p.81].

Likewise, while the initial visual comparison between Figure: (249) and Figure: (246) might bring about the conclusion that more harm than good was achieved through the utilization of the window function; however, such condemnation would be rather hasty

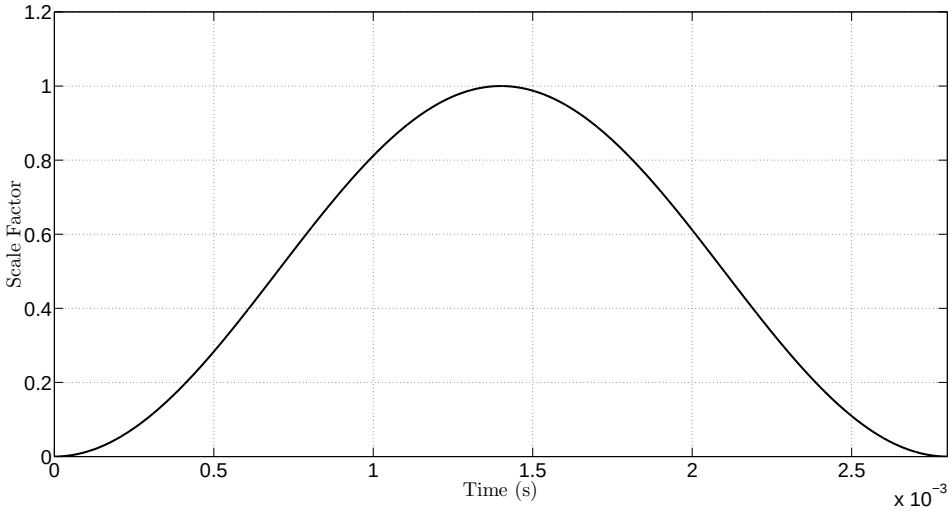

Figure 247: a 8402 point hanning window

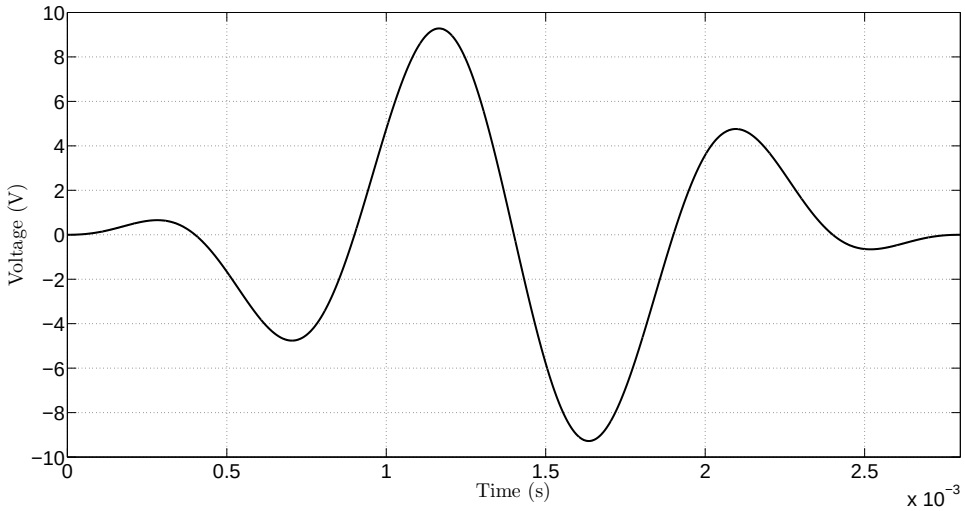

Figure 248: plot of a non-seamless capture of $10\sin\left(2\pi\,1000\,t\right)$ that was multiplied by the hanning window

considering that the function within Figure: (248) was — for all practical purposes — less than a full signal period, and upon increasing the number of periods that are allowed to fully occur within the Hanning window, the amount of leakage observed begins to reduce significantly — at 3 periods only 2 substantial points of leakage remains, at 10 periods only one substantial point of leakage remains, and at 20 periods no substantial points of leakage remains, as shown by Figure: (250). Yet, while the amount of spectral leakage

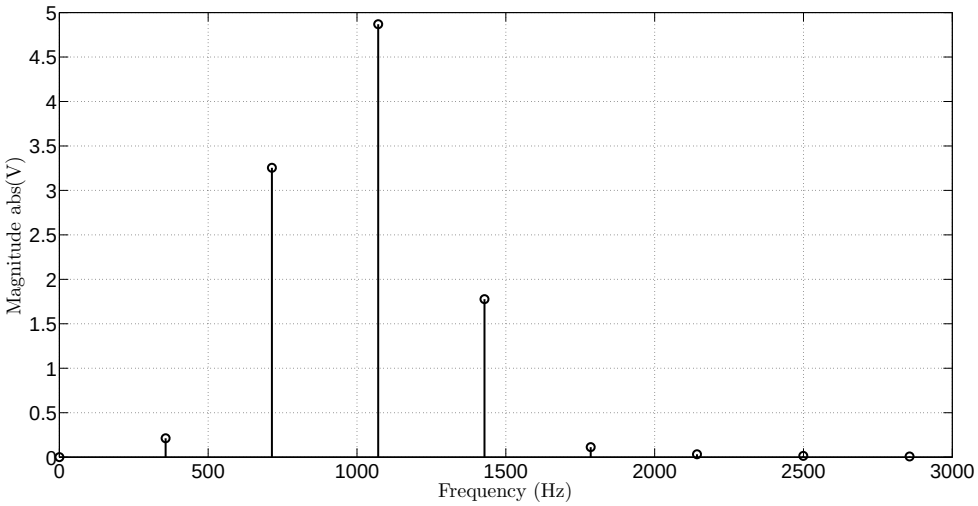

Figure 249: fft plot of a non-seamless capture of $10\sin(2\pi\,1000\,t)$ that was multiplied by the hanning window

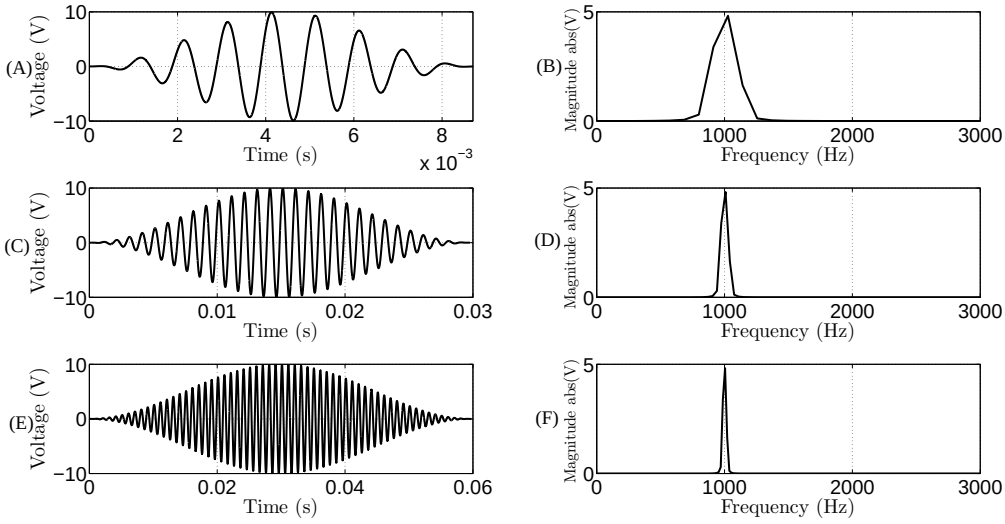

Figure 250: plots of a non-seamless captures of $10\sin(2\pi\,1000\,t)$ that was multiplied by the hanning window (a,c,e) and examined for spectral leakage within the fft domain (b,d,f) for varying periodic temporal window sizes (3x,10x,20x)

can, in fact, be reduced through the utilization of such techniques; however, in all cases the signal is substantially attenuated in magnitude — in this particular case by half — and this is a inherent and inadvertent trade-off that is associated with the utilization of a window function. Conversely, based upon such observations, it becomes apparent that the appropriate utilization of a windowing function is, in fact, truly a difficult decision to make, especially if most of the time domain information is substantially attenuated upon multiplication of the window function with the original signal — as was the case within Figure: (248). Furthermore, it is also conceivable that such techniques could be particularly problematic if a precise spectral magnitude for a given signal was required and, for example, the amount of magnitude reduction was inconsistent because the amount of information captured within the window changed substantially in between acquisitions — thus making the amount of window reduction obtained somewhat unpredictable.

Nevertheless, while there are a number of techniques and solutions to resolve such windowing problems, particularly within the signals and systems research area — and some of these solutions will be examined later within this chapter —; however, given that the next logical step in obtaining a high fidelity measurement is profiling the CIE effects encountered upon the acquisition of a non-DC signal — and given that the easiest non-DC waveform to work with is a sinusoidal signal —, it seems reasonable to assume that a number of non-seamless sinusoidal acquisitions will be acquired while attempting to obtain such a profile, thus it seems worthwhile to examine how to resolve spectral leakage given this particular set of circumstances. Conversely, because a non-seamless sinusoidal acquisition will either begin above or below the 0 voltage axis and end in a similar manner, thus rather than multiplying the signal by a windowing function that gradually forces the voltage towards a common value, it seems more reasonable, at least given the current testing circumstances,

to examine the acquisition from the left and right sides, at least until the zero crossing is found, and simply remove the segments of the signal that make the acquisition non-seamless — a task that is easily done using the MATLAB code shown within Appendix E script 20 and Appendix E script 21.

Likewise, while the implementation of this particular technique is relatively straightforward, a minor caveat does exist here, since this particular method is generally only

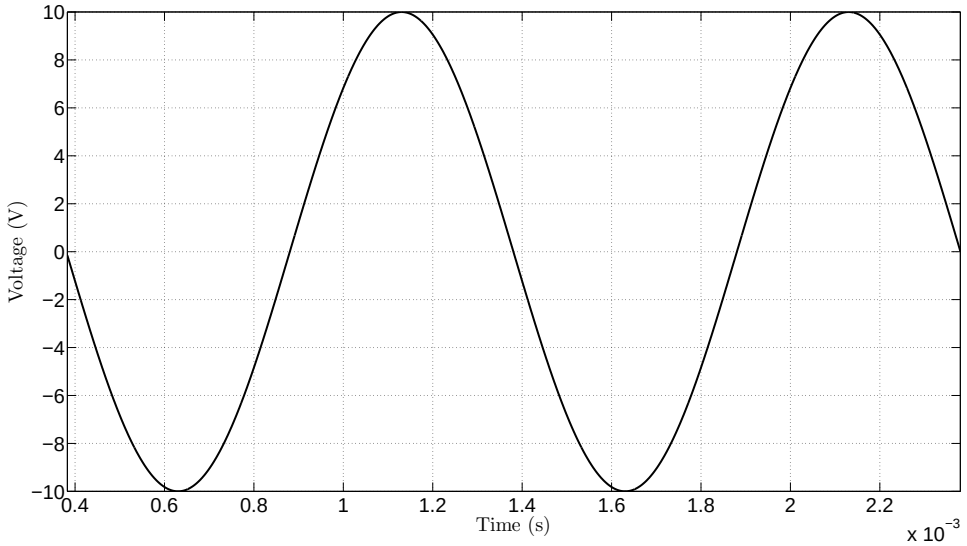

Figure 251: plot of a non-seamless capture of $10\sin(2\pi\,1000\,t)$ that was modified to become seamless

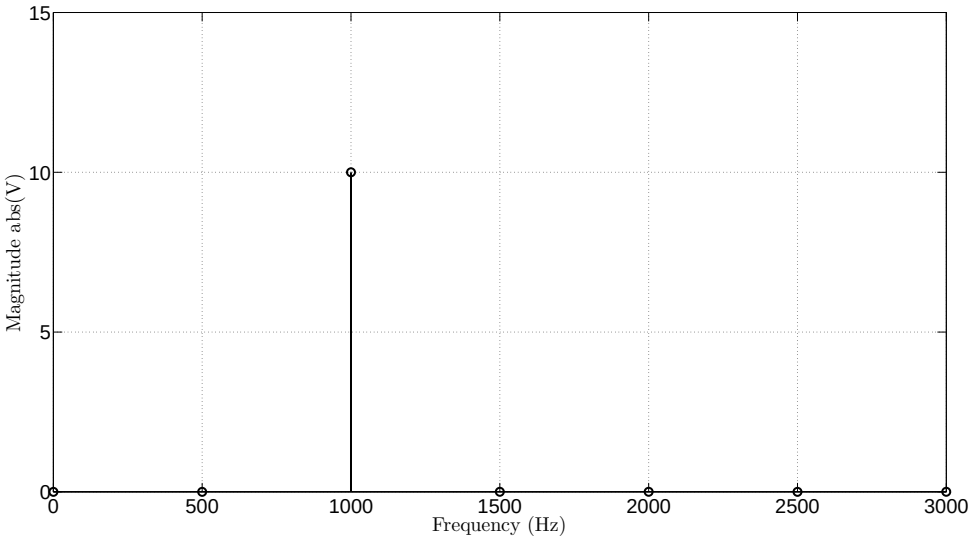

Figure 252: fft plot of a non-seamless capture of $10\sin(2\pi\,1000\,t)$ that was modified to become seamless

effective in reducing spectral leakage if the waveform being examined is both periodic and encompasses a complete signal period, and such requirements can be somewhat problematic particularly if the — previously provided — code produces a odd periodic symmetry — like a half sinusoidal oscillation. Thus, in lieu of such problems, one possible solution is to count the number of positive and negative oscillations, within the previously augmented signal — a task achieved by the MATLAB code shown within Appendix E script 22 — and compare the positive count of the signal with the negative count, and if the two comparisons do not match then the signal must be augmented again — either from the right or left boundary — and the oscillatory count performed again to ensure that symmetry has been achieved — if symmetry was not achieved then this process will repeat until symmetry has been achieved. Yet, while this particular augmentation method is generally effective; however, this technique is far from being ideal — since this method can, in turn, result in most of the acquired signal being removed prior to the signal processing stage —, and the occurrence of such attributes demonstrates the necessity of not only understanding the signal being acquired but the requirements of the processing methods being implemented.

Nevertheless, despite the existence of such caveats, upon applying these particular methods to the signal shown within Figure: (245), and then using the left and right boundary information obtained to trim the non-seamless sections of the signal, as shown by Figure: (245), prior to performing the FFT operation upon Figure: (251), yields a spectral magnitude plot, as shown by Figure: (252), that is nearly identical to the original periodic spectral magnitude plot, as shown by Figure: (244), and such observations, in turn, not only validate this particular method as a reasonable solution — at least for processing periodic sinusoidal signals —, but also demonstrates that this particular technique is, in fact, far superior to the — previously discussed — windowing techniques — at least given this

particular set of circumstances — since the spectral magnitude was not attenuated as a result of the utilization of the method nor was a substantially increased timebase required to reduce the amount of spectral leakage obtained.

Conversely, based upon such observations, it was decided that the periodic CIE effect characterization tests conducted would utilize this left and right boundary technique — over the windowing technique —, although the ability to use this particular method is, for the most part, strictly limited to single sinusoidal signal analysis since, for example, trying to apply this particular technique to multiple acquired signals individually would likely yield a inconsistent timebase — amongst the signals being processed — that would be inherently problematic to work with or, if a consistent time base was utilized — based upon this particular technique — for all measurements, the result obtained would likely produce one signal becoming seamless while the remaining acquired signals would still remain non-seamless — thus, under such circumstances, the previously mentioned windowing techniques, might be a more appropriate solution. Likewise, with this being said, while such concepts might appear to be — at least within some disciplines — a relatively straightforward topic; however, it is important to recognize that a vast number of biomedical disciplines are quite unfamiliar with the concept of spectral leakage and simply utilize the pre-processed spectral information provided by commercial biomedical acquisition devices and, as it might be imagined, consistency between these devices is not necessarily guaranteed, especially given the absurd number of possible spectral leakage compensation techniques available. Similarly, while there are a number of biomedical disciplines that are highly conscious of such attributes — particularly biomedical subsets that work heavily with medical signal processing — there is also an equal number of biomedical subsets that rely heavily upon the information obtained using commercial instrumentation — and notable examples have

been observed within the bioimpedance spectroscopy research area and within the electrochemical spectroscopy research area — that have unknowingly published compensated acquisitions without having ever acknowledged the intrinsic assumptions made by the commercial instrumentation utilized — at least, beyond the commercial make and model of the instrumentation — and, as it was previously discussed, attempting to compare such dissimilar acquisitions between researchers can potentially introduce — at least, depending upon the techniques implemented by the commercial device utilized — a substantial amount of error that, in turn, reduces the overall fidelity — if not the legitimacy — of the signals being compared.

6.3.6 AC Signals and the CIE Effects Measured

The fundamental rationale behind the AC signal and the CIE effects measured section was to develop a method of determining the overall ability of a bioelectrical acquisition device to accurately acquire AC signals and — more importantly — develop a method — as shown by Figure: (253), Figure: (254), and Figure: (255) — of conveying this information — across an interdisciplinary platform — in order to allow for the equivalent comparison of biometric data across multiple acquisition platforms. Conversely, the investigation and development of this methodology resulted in a number of interesting acquisition attributes being discovered that included every acquisition channel examined — including the four Tektronix TPS2024 channels and the collective four channels from the two Tektronix TDS2002 oscilloscopes — having a unique CIE effect profile for every applied frequency — noting that this profile was obtained and visualized by varying the input voltage and input frequency, acquiring the input voltage observed by the oscilloscope channel, performing the FFT operation on this acquired signal, removing the input frequency from the spectrum obtained via the FFT operation, and plotting the applied voltage, spectral frequency, and

magnitude for every test frequency examined.

Likewise, while some similarities were observed to exist between the CIE effect profiles obtained — particularly when a common oscilloscope probe was utilized or between oscilloscope channels on the same acquisition unit —, there was enough discrepancy between channels to merit some caution when attempting to directly compare one oscilloscope channel with another oscilloscope channel or attempting to apply a common filtering algorithm to all acquisitions taken. Additionally, while the majority of the magnitude of CIE effects encountered — with a maximum around 300mV in magnitude at 1MHz, although this value varies with applied frequency — were generally below the resolution of the acquisition rate — implying that low frequency CIE effects were lumped within the FFT 0Hz bin —; however, upon removing the 0Hz bin from the analysis, the next largest CIE effects encountered — with a maximum around 40mV in magnitude — was discovered to be the third, fifth, and seventh harmonic of the applied signal, followed by some disturbances in between the observed harmonics, with a surprising lack of 60Hz environmental effects — presumably because both the added physical shielding and the oscilloscope input stage are effectively reducing the overall magnitude of the synthetic effects encountered. Similarly, upon examining the presumed input voltage and the acquired input voltage for each oscilloscope channel, it was determined that some discrepancy exist between the presumed input voltage and the acquired input voltage — which is to be expected —; however, this discrepancy is not uniform across all oscilloscope channels and absolute variations between 100mV to 400mV are extremely common — noting that these variations are a function of frequency, and higher input frequencies seem to be more accurate than lower input frequencies — and this attribute is likely associated with the, previously mentioned, large magnitude of low frequency CIE effects encountered.

Conversely, a strong correlation appears to exist between the amount of CIE effects encountered and the applied AC voltage — which is to be expected given the, previously discussed, observations made within the DC CIE effects section. Likewise, upon examining the amount of time delay between channel acquisitions, it was noted that — on average — the first channel of the oscilloscope is seven sample rate steps — generally at lower input frequencies — out of sync from every other oscilloscope channel on the same oscilloscope unit —, and the time delay between channel 1 of the TPS2024 and the other two oscilloscope channels is around 20 to 40 sample rate steps — again, generally at lower input frequencies —, and such observations are extremely important because these acquisition delays, if they are not taken into account, will inevitably manifest themselves as a metaphoric phantom capacitor within an electrical model, and there seems to be a prominent assumption amongst instrumentational users that the acquisition between instrumentation channels is simultaneous, when in fact, it is not. Similarly, based upon such observations, it can be concluded that a vast majority of the fidelity obtained — particularly when performing a bioelectrical acquisition — is highly dependent upon possessing an in-depth understanding of the acquisition apparatus being utilized, because if the CIE profile of the device being utilized is not known, it becomes nearly impossible to separate a desired physical observation from a CIE effect, especially given how much CIE effects can vary depending upon the applied voltage and the applied frequency. Conversely, with this being said, given that the vast majority of publicize bioimpedance spectroscopy measurements do not adequately profile there acquisition apparatus for CIE effects prior to modeling, it is highly reasonable to assume — based upon the conservative numbers obtained — that the CIE errors introduced from this lack of profiling and implementation of compensation techniques — within the passive electrical component model that is typically developed from such experiments

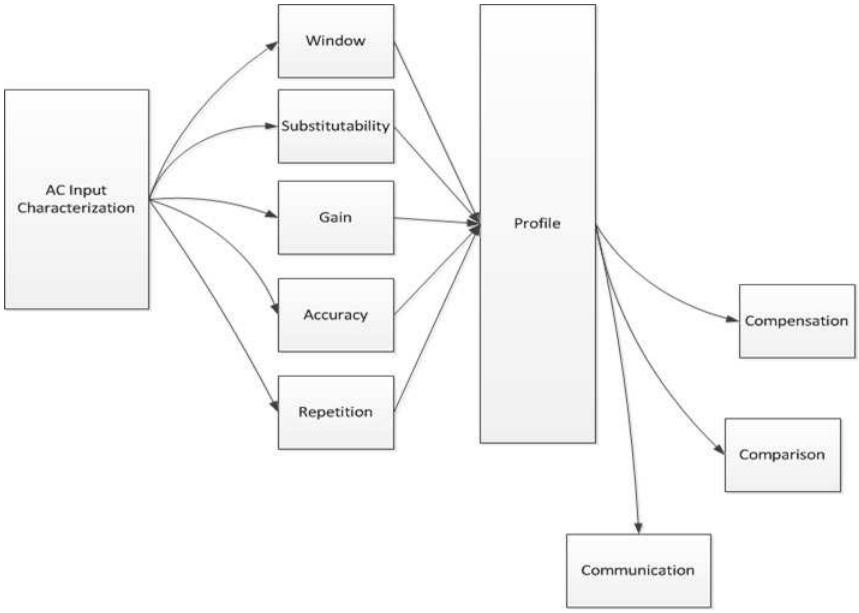

Figure 253: conceptual ac cie calibration flowchart

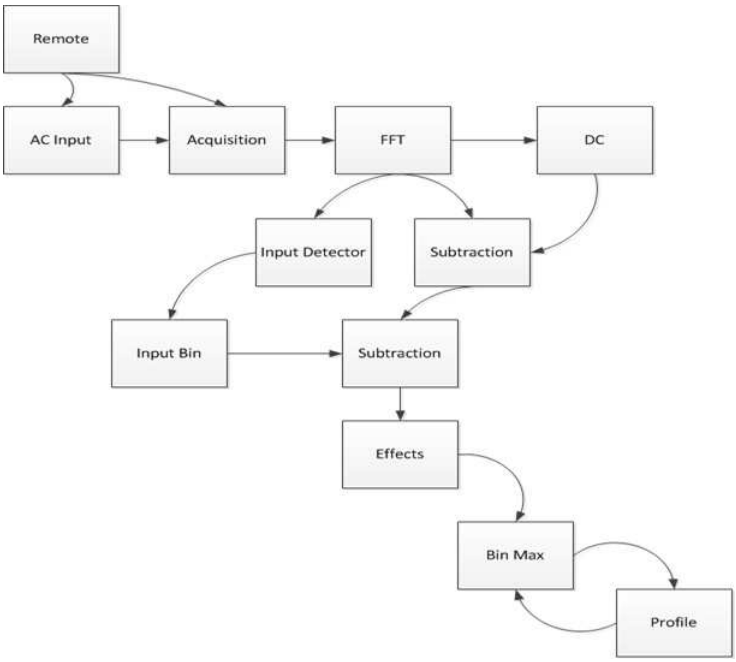

Figure 254: conceptual ac cie calibration process flowchart

— could have CIE effect errors in excess of 900mV, assuming that the instrumentation utilized has a similar CIE profile, and noting that such estimates are not incorporating the cumulative nature of spectral harmonic CIE effects.

Thus, with this being said, while the progressive examination of high-Z environmental effects, DC CIE effects, and the attribute of spectral leakage have been extremely beneficial in articulating the numerous attributes encountered that can reduce the overall fidelity of

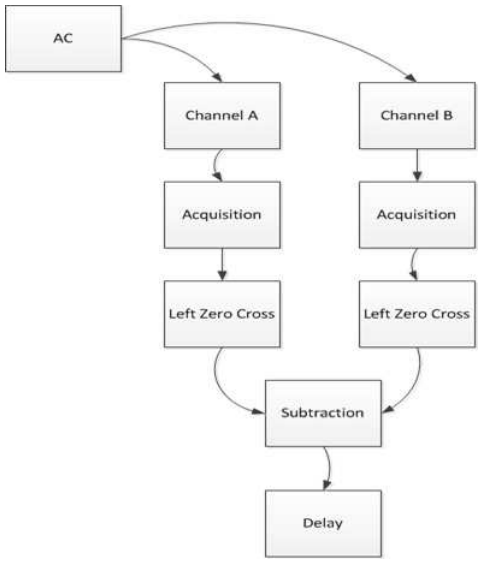

Figure 255: conceptual ac cie calibration time process flowchart

a bioelectrical signal; however, as it was previously mentioned, most of the bioelectrical signals encountered — at least within this dissertation — predominantly originate from the active application of a sinusoidal signal, in order to electrically characterize a given biomaterial over an assortment of electrical frequencies — a process generally referred to as bioimpedance spectroscopy —, and because the subject of CIE effects under sinusoidal AC conditions has not been — as of yet — examined, it seems prudent to now examined the types of CIE effects that are observed under these particular circumstances. Likewise, in order to begin this particular analysis, the following experimental apparatus, as shown by Figure: (256), was set up within the partially shielded environment and the signal produced by the Tektronix AFG3102 function generator was programmatically changed — through the utilization of the proprietary Tektronix Tekvisa USB communication protocol — within a custom created Python script — shown within Appendix B — in order to characterize the CIE effects measured in terms of both input frequency and input voltage.

Likewise, because some of the experiments performed — within this dissertation — required up to eight simultaneous acquisitions — or controlling three Tektronix oscilloscopes (one TPS2024 unit and two TDS2002 units) simultaneously — it was decided to perform

the AC CIE effect test on all eight acquisition channels in order to obtain both a baseline CIE effect measurement, and a individual oscilloscope channel measurement for future identification and possible removal of these encountered CIE effects. Similarly, it was also decided that the Tektronix AFG3102 function generator would produce a sinusoidal signal with frequencies that were spaced in a logarithmic scale between 1Hz to 1MHz — including 1Hz, 4.3Hz, 18Hz, 79Hz, 341Hz, 1.5kHz, 6.3kHz, 27kHz, 116kHz, 500kHz, and 1MHz — and that each frequency selected would also be examined over different peak amplitude voltages between 1mV to 10V that were also logarithmically spaced — including 1mV, 17mV, 28mV, 46mV, 77mV, 1.29V, 2.15V 3.6V, 6V, and 10V.

Conversely, upon analyzing the information obtained from this, previously mentioned, AC CIE test — a process that mostly utilized the techniques presented within the DC

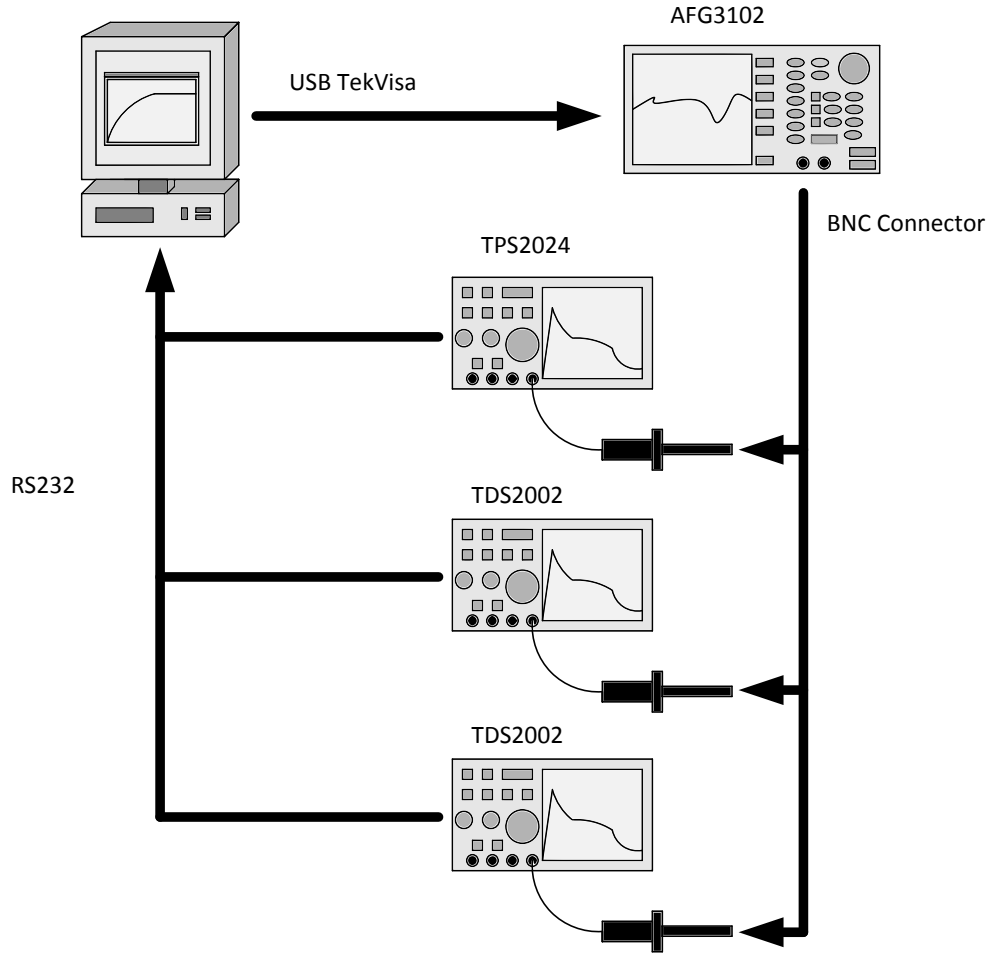

Figure 256: conceptual hardware diagram of the cie effect ac test apparatus utilized

CIE effects section — it was decided to, first graphically segment the spectral CIE results obtained into individual three-dimensional surface plots for every frequency and oscilloscope channel examined. Likewise, to elaborate further on the procedures that were utilized when creating these graphical plots, the acquired signals were first imported into Matlab — using the importation techniques previously discussed — and then augmented using the, previously discussed, left and right windowing techniques. Next, the test frequency was isolated and removed using a FFT mask filtering technique that was very similar to the, previously discussed, DC extraction method — although, in this particular case, the least-squares extraction method was not utilized because the sinusoidal test frequency was inherently known, thus the FFT bin with the maximum magnitude was assumed to be the test frequency and was removed, while the remaining bins were assumed to be the desired AC CIE effects. Lastly, the remaining spectral magnitudes — excluding the 0Hz FFT bin, that will be examined within a separate series of graphical plots because of its tendency to skew graphical scaling — were placed into a three-dimensional coordinate array — of test voltage, test frequency, and test magnitude — and interpolated into the three-dimensional surfaces that were graphically presented.

Conversely, upon examining the AC CIE effects observed for each of the oscilloscope channels at the test frequency of 1Hz, as shown by Figure: (257) and Figure: (258), it is interesting to note that the cheaper Tektronix TDS2002 seems to have a lower CIE effects peak — at approximately 20mV — than the more expensive battery-operated Tektronix TPS2024, which has a higher CIE effect peak — at approximately 40mV. Likewise, the spectral surface plots obtained seem to remain relatively consistent in shape between the individual oscilloscopes — with the exception of the third TPS2024 channel —, while the overall spectral content of the signals observed — excluding the observed peak values

— seems to be significantly less within the Tektronix TPS2024 when compared with the Tektronix TDS2002. Yet, while the comparison between the two oscilloscope models is somewhat interesting, the more profound observation — upon examining Figure: (257) and Figure: (258) — is the fact that the majority of the CIE effects observed appear to occur at the lower end of the frequency spectrum near the maximum signal voltage — an attribute that was predicted by the DC CIE effects analysis — and closer inspection reveals

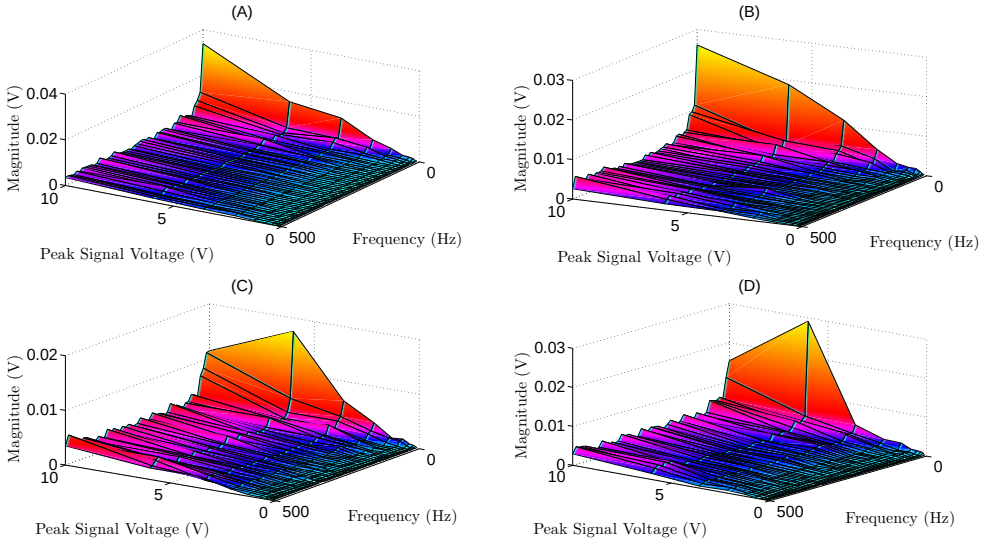

Figure 257: ac cie effects observed at 1hz for (a) tps2024 channel 1, (b) tps2024 channel 2, (c) tds2002 unit 1 channel 2, (d) tps2024 channel 3

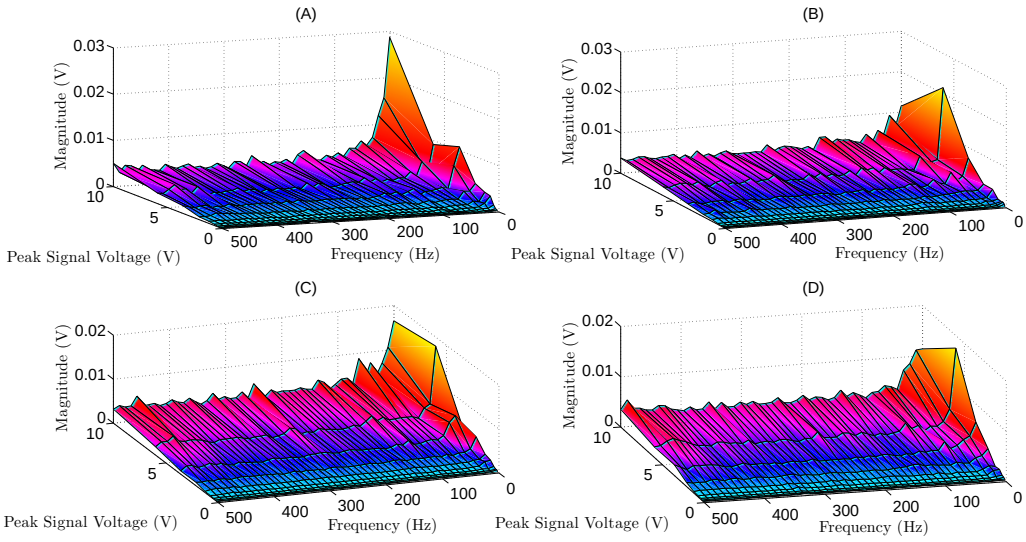

Figure 258: ac cie effects observed at 1hz for (a) tds2002 unit 1 channel 1, (b) tps2024 channel 4, (c) tds2002 unit 2 channel 1, (d) tds2002 unit 2 channel 2

that most of the CIE effects encountered are not the commonly expected 60 Hz power line radiation, which implies that the differential amplifier stage — within the oscilloscope — is effectively removing such effects and that the apparatus connected is effectively permitting the common mode manifestation of these effects — thus allowing for maximum reduction within the oscilloscopes differential amplifier stage.

Likewise, upon examining the AC CIE effects observed for each of the oscilloscope chan-

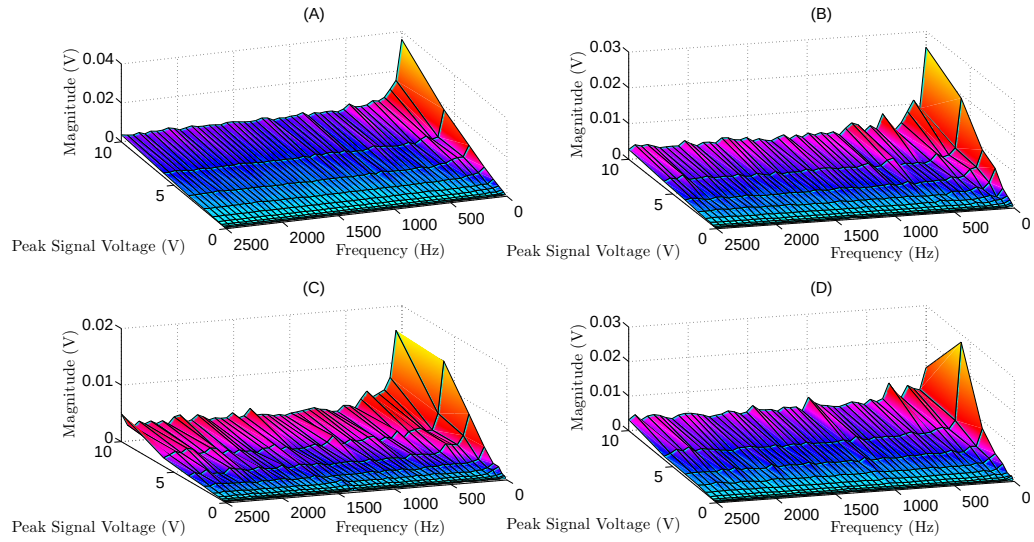

Figure 259: ac cie effects observed at 4.3hz for (a) tps2024 channel 1, (b) tps2024 channel 2, (c) tds2002 unit 1 channel 2, (d) tps2024 channel 3

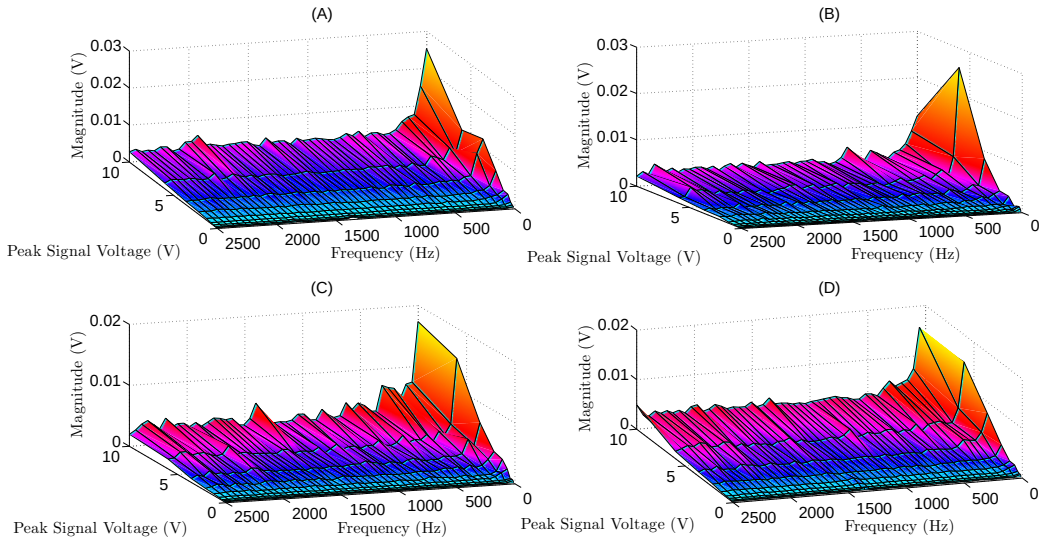

Figure 260: ac cie effects observed at 4.3hz for (a) tds2002 unit 1 channel 1, (b) tps2024 channel 4, (c) tds2002 unit 2 channel 1, (d) tds2002 unit 2 channel 2

nels at the test frequency of 4.3Hz, as shown by Figure: (259) and Figure: (260), a similar conclusion — to those obtained from examining Figure: (257) and Figure: (258) — can be made, since the observed CIE frequencies seem to be, once again, primarily located near the lower end of the frequency spectrum at the maximum applied signal voltage. Similarly, the Tektronix TPS2024 oscilloscope appears to still maintain its, previously observed, approximate 40mV CIE effect peak, while the two Tektronix TDS2002 oscilloscopes appear to remain within the, previously observed, 20mV CIE effect range — although a minor 5mV to 10mV increase in the CIE effects encountered were observed within some of the TDS2002 channels —, yet the CIE effect spectral distribution seems to remain consistent between the two oscilloscope models — the Tektronix TPS2024 having fewer spectral CIE effects than the Tektronix TDS2002.

Conversely, upon examining the AC CIE effects observed for each of the oscilloscope channels at the test frequency of 18Hz, as shown by Figure: (261) and Figure: (262), a similar conclusion — to those obtained from examining Figure: (259) and Figure: (260) — can be made, since the observed CIE frequencies seem to be, once again, primarily located near

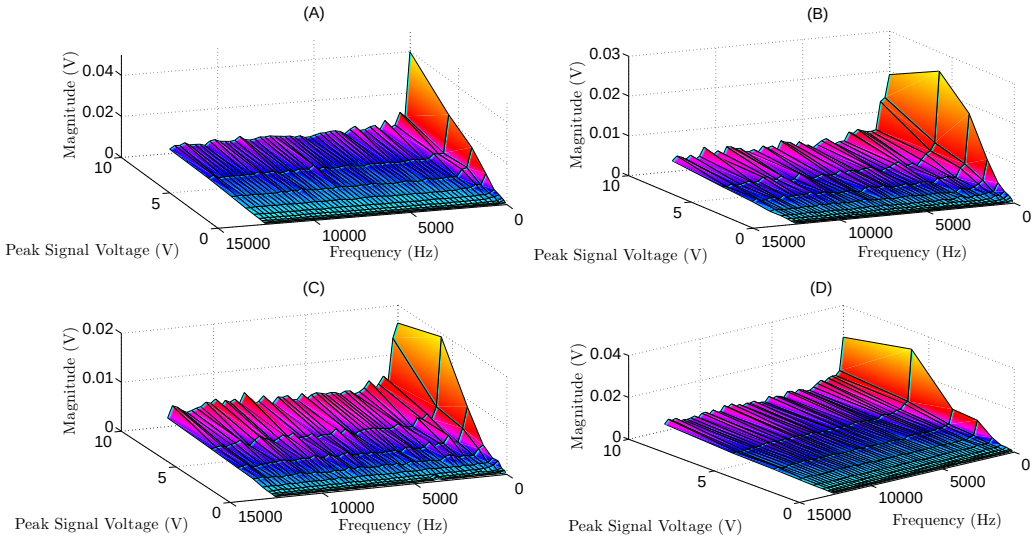

Figure 261: ac cie effects observed at 18hz for (a) tps2024 channel 1, (b) tps2024 channel 2, (c) tds2002 unit 1 channel 2, (d) tps2024 channel 3

the lower end of the frequency spectrum at the maximum applied signal voltage, although an interesting increase in CIE effects was noted at the 6V peak magnitude low frequency region. Similarly, the Tektronix TPS2024 oscilloscope appears to still maintain its, previously observed, approximate 40mV CIE effect peak — although some slight reduction was noticed within some channels —, while the two Tektronix TDS2002 oscilloscopes appear to remain within the, previously observed, 20mV to 30mV CIE effect range , yet the CIE effect spectral distribution seems to remain consistent between the two oscilloscope models — the Tektronix TPS2024 having fewer spectral CIE effects than the Tektronix TDS2002.

Likewise, upon examining the AC CIE effects observed for each of the oscilloscope channels at the test frequency of 79Hz, as shown by Figure: (263) and Figure: (264), a similar conclusion, once again, — to those obtained from examining Figure: (261) and Figure: (262) — can be made, since the observed CIE frequencies seem to be primarily located near the lower end of the frequency spectrum at the maximum applied signal voltage, although that, previously observed, interesting increase in CIE effects near the 6V peak magnitude low frequency region seems to have decreased substantially. Similarly, the Tek-

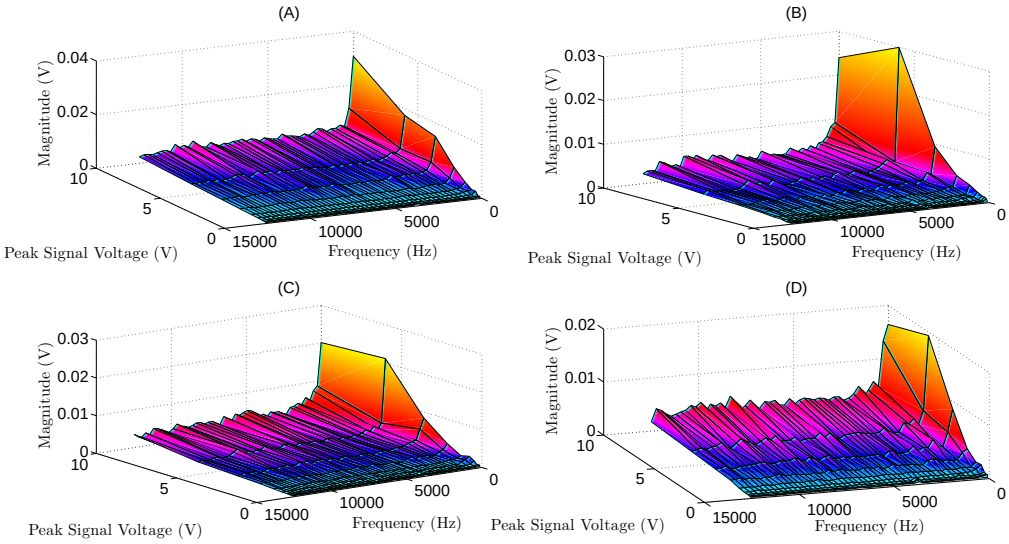

Figure 262: ac cie effects observed at 18hz for (a) tds2002 unit 1 channel 1, (b) tps2024 channel 4, (c) tds2002 unit 2 channel 1, (d) tds2002 unit 2 channel 2

tronix TPS2024 oscilloscope appears to still maintain its, previously observed, approximate 40mV CIE effect peak — although a slight increase of around 5mV to 10 mV was observed —, while the two Tektronix TDS2002 oscilloscopes appear to remain within the, previously observed, 20mV to 30mV CIE effect range , yet the CIE effect spectral distribution seems to remain consistent between the two oscilloscope models — the Tektronix TPS2024 having fewer spectral CIE effects than the Tektronix TDS2002 — although more noticeable

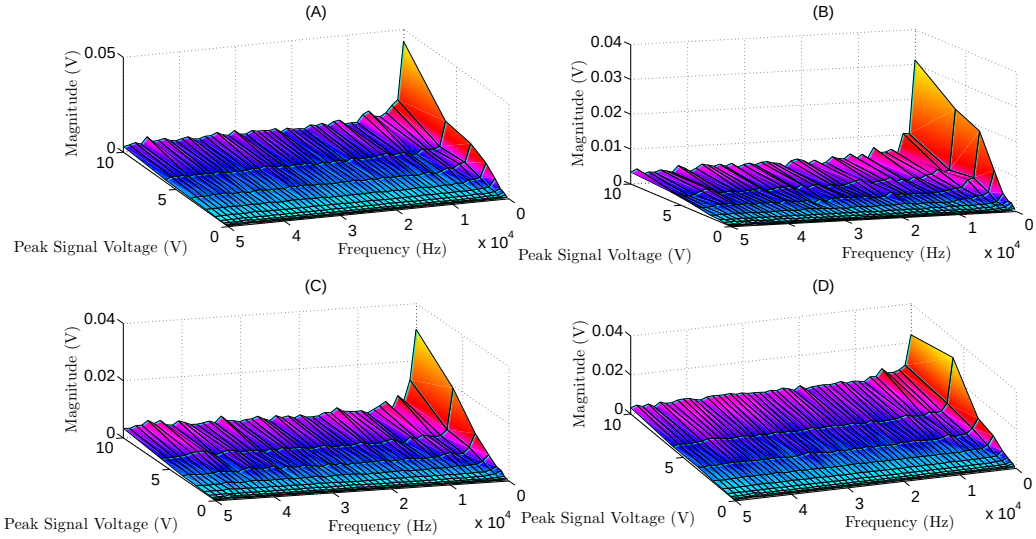

Figure 263: ac cie effects observed at 79hz for (a) tps2024 channel 1, (b) tps2024 channel 2, (c) tds2002 unit 1 channel 2, (d) tps2024 channel 3

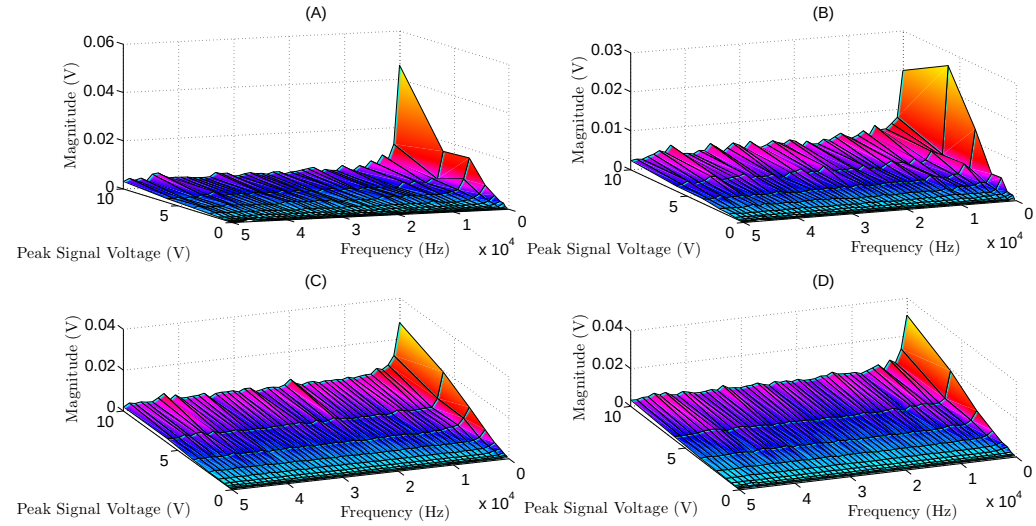

Figure 264: ac cie effects observed at 79hz for (a) tds2002 unit 1 channel 1, (b) tps2024 channel 4, (c) tds2002 unit 2 channel 1, (d) tds2002 unit 2 channel 2

sidebands effects are beginning to appear near the lower peak frequency bands.

Conversely, upon examining the AC CIE effects observed for each of the oscilloscope channels at the test frequency of 341Hz, as shown by Figure: (265) and Figure: (266), a similar conclusion, once again, — to those obtained from examining Figure: (263) and Figure: (264) — can be made, since the observed CIE frequencies seem to be primarily located near the lower end of the frequency spectrum at the maximum applied signal volt-

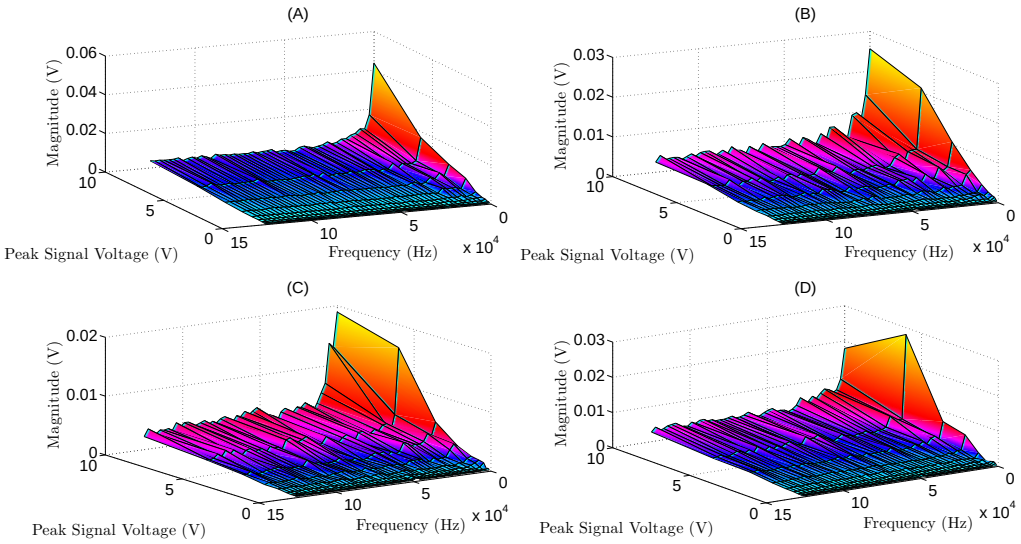

Figure 265: ac cie effects observed at 341hz for (a) tps2024 channel 1, (b) tps2024 channel 2, (c) tds2002 unit 1 channel 2, (d) tps2024 channel 3

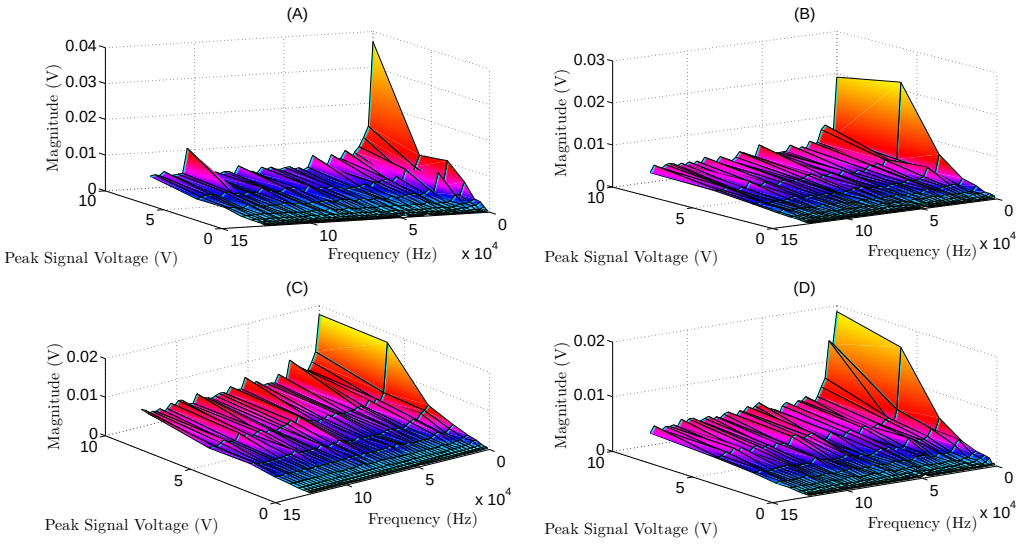

Figure 266: ac cie effects observed at 341hz for (a) tds2002 unit 1 channel 1, (b) tps2024 channel 4, (c) tds2002 unit 2 channel 1, (d) tds2002 unit 2 channel 2

age. Similarly, the Tektronix TPS2024 oscilloscope appears to still maintain its, previously observed, approximate 40mV to 50mV CIE effect peak — although a slight increase in the CIE effect bandwidth appears to have occurred for voltages above 6V —, while the two Tektronix TDS2002 oscilloscopes appear to remain within the, previously observed, 20mV to 30mV CIE effect range, yet the CIE effect spectral distribution seems to remain consistent between the two oscilloscope models — the Tektronix TPS2024 having fewer spectral CIE effects than the Tektronix TDS2002 — although a peculiar high frequency spectral magnitude spike is observed within TDS2002 unit 1 on channel number 1.

Likewise, upon examining the AC CIE effects observed for each of the oscilloscope channels at the test frequency of 1.5kHz, as shown by Figure: (267) and Figure: (268), a similar conclusion, once again, — to those obtained from examining Figure: (265) and Figure: (266) — can be made, since the observed CIE frequencies seem to be primarily located near the lower end of the frequency spectrum at the maximum applied signal voltage. Similarly, the Tektronix TPS2024 oscilloscope appears to still maintain its, previously observed, approximate 40mV to 50mV CIE effect peak, while the two Tektronix TDS2002

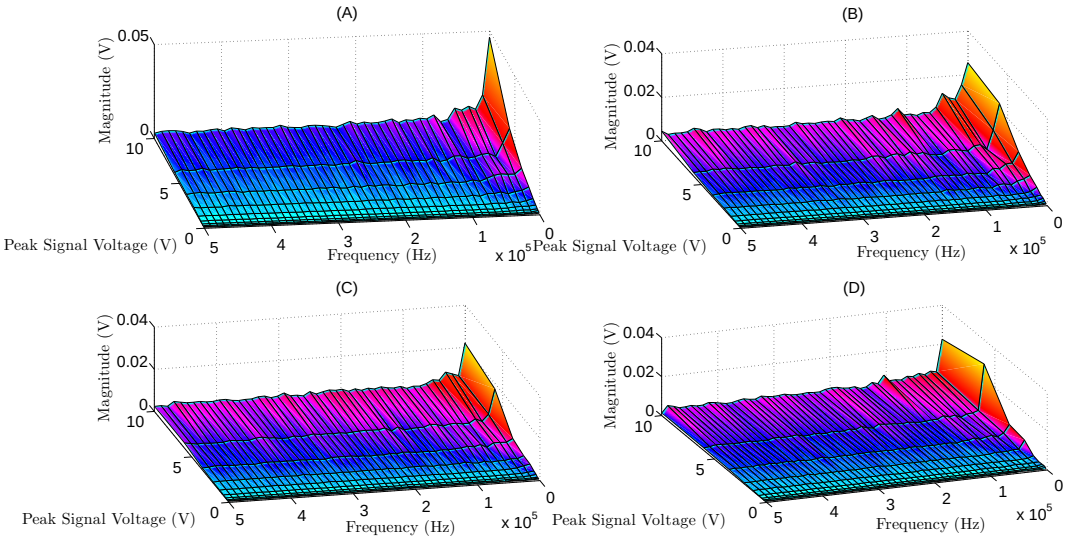

Figure 267: ac cie effects observed at 1.5khz for (a) tps2024 channel 1, (b) tps2024 channel 2, (c) tds2002 unit 1 channel 2, (d) tps2024 channel 3

oscilloscopes appear to remain within the, previously observed, 20mV to 30mV CIE effect range — although a slight increase of 5mV to 10mV was observed within some of the channels —, yet the CIE effect spectral distribution seems to remain consistent between the two oscilloscope models — the Tektronix TPS2024 having fewer spectral CIE effects than the Tektronix TDS2002 — although the, previously observed, peculiar high frequency spectral magnitude spike observed within TDS2002 unit 1 on channel number 1 appears to have

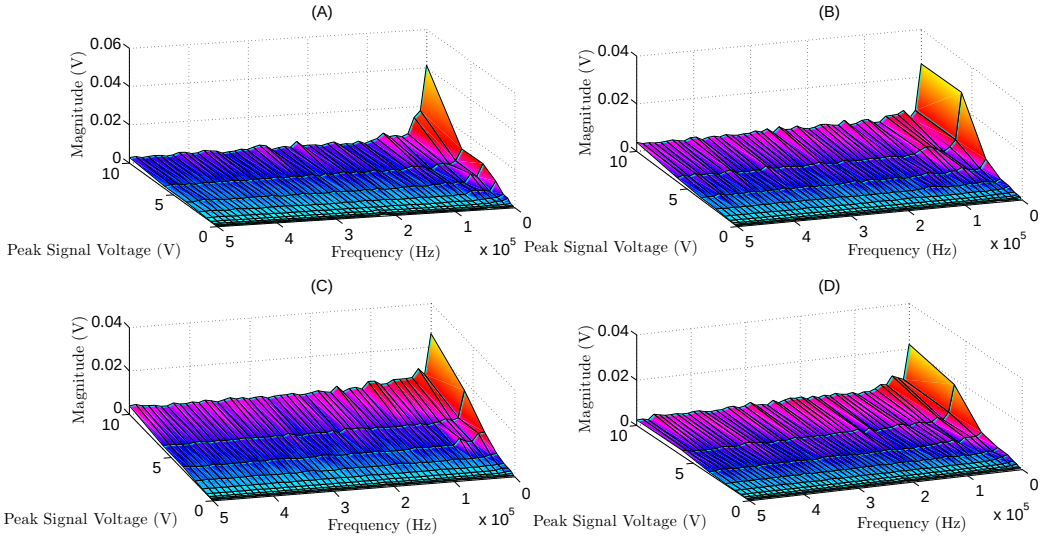

Figure 268: ac cie effects observed at 1.5khz for (a) tds2002 unit 1 channel 1, (b) tps2024 channel 4, (c) tds2002 unit 2 channel 1, (d) tds2002 unit 2 channel 2

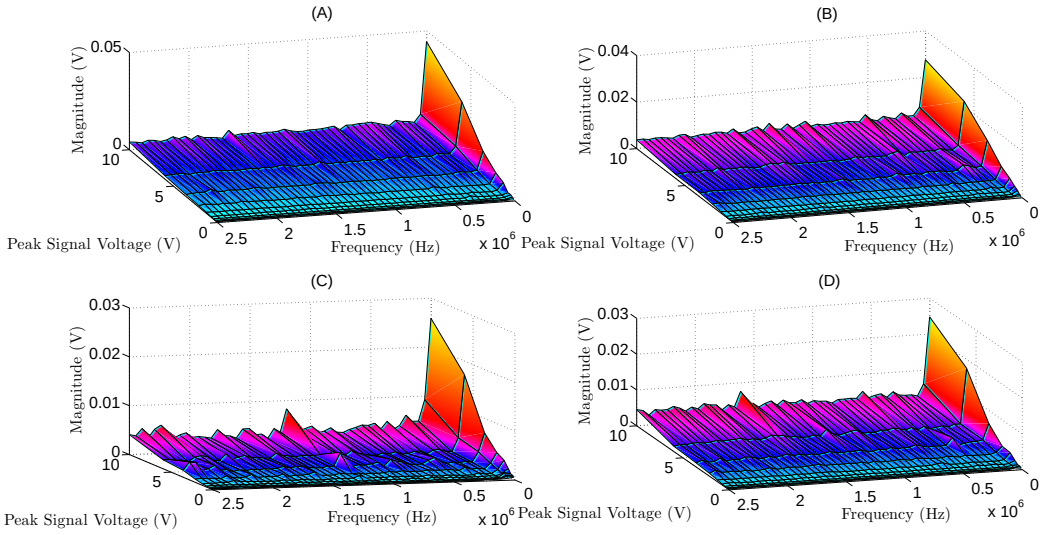

Figure 269: ac cie effects observed at 6.3khz for (a) tps2024 channel 1, (b) tps2024 channel 2, (c) tds2002 unit 1 channel 2, (d) tps2024 channel 3

disappeared.

Conversely, upon examining the AC CIE effects observed for each of the oscilloscope channels at the test frequency of 6.5kHz, as shown by Figure: (269) and Figure: (270), a similar conclusion, once again, — to those obtained from examining Figure: (267) and Figure: (268) — can be made, since the observed CIE frequencies seem to be primarily located near the lower end of the frequency spectrum at the maximum applied signal voltage. Similarly, the Tektronix TPS2024 oscilloscope appears to still maintain its, previously observed, approximate 40mV to 50mV CIE effect peak, while the two Tektronix TDS2002 oscilloscopes appear to remain within the, previously observed, 40mV to 50mV CIE effect range, yet the CIE effect spectral distribution seems to remain consistent between the two oscilloscope models — the Tektronix TPS2024 having fewer spectral CIE effects than the Tektronix TDS2002 — although a number of higher frequency magnitude spikes were observed within both the TPS2024 and TDS2002 oscilloscopes.

Likewise, upon examining the AC CIE effects observed for each of the oscilloscope channels at the test frequency of 27kHz, as shown by Figure: (271) and Figure: (272),

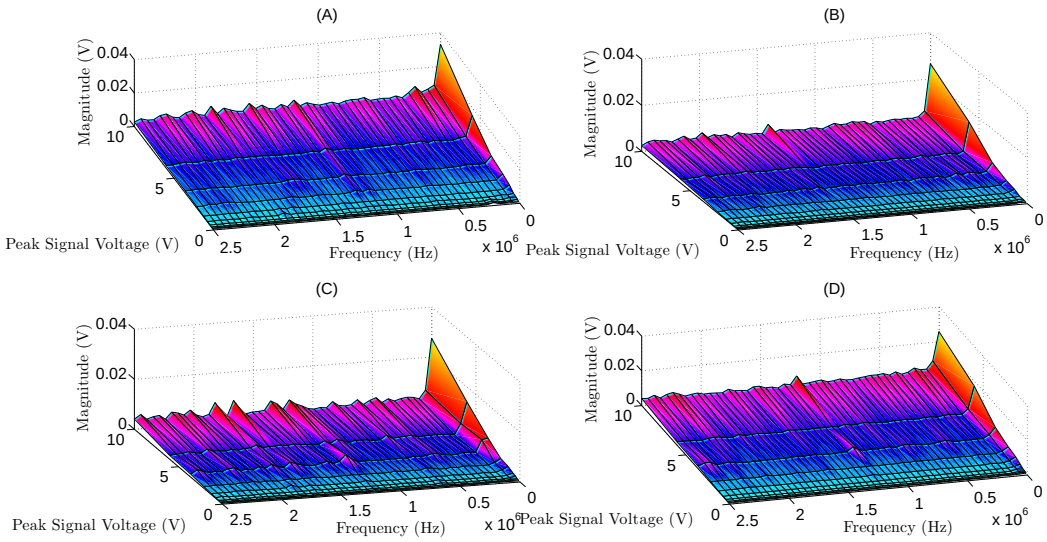

Figure 270: ac cie effects observed at 6.khz for (a) tds2002 unit 1 channel 1, (b) tps2024 channel 4, (c) tds2002 unit 2 channel 1, (d) tds2002 unit 2 channel 2

a similar conclusion, once again, — to those obtained from examining Figure: (269) and Figure: (270) — can be made, since the observed CIE frequencies seem to be primarily located near the lower end of the frequency spectrum at the maximum applied signal voltage. Similarly, the Tektronix TPS2024 oscilloscope appears to still maintain its, previously observed, approximate 40mV to 50mV CIE effect peak, while the two Tektronix TDS2002 oscilloscopes appear to remain within the, previously observed, 40mV to 50mV CIE effect

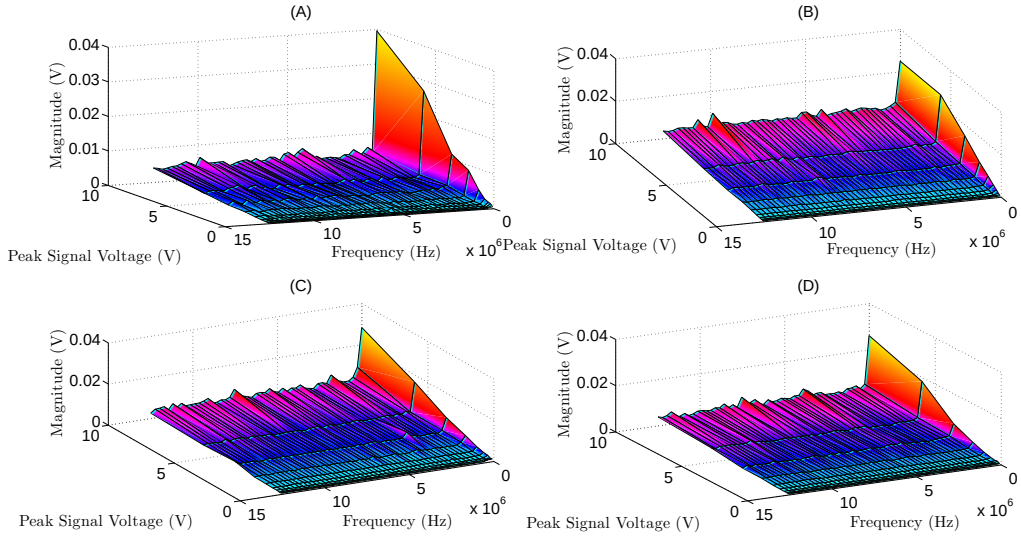

Figure 271: ac cie effects observed at 27khz for (a) tps2024 channel 1, (b) tps2024 channel 2, (c) tds2002 unit 1 channel 2, (d) tps2024 channel 3

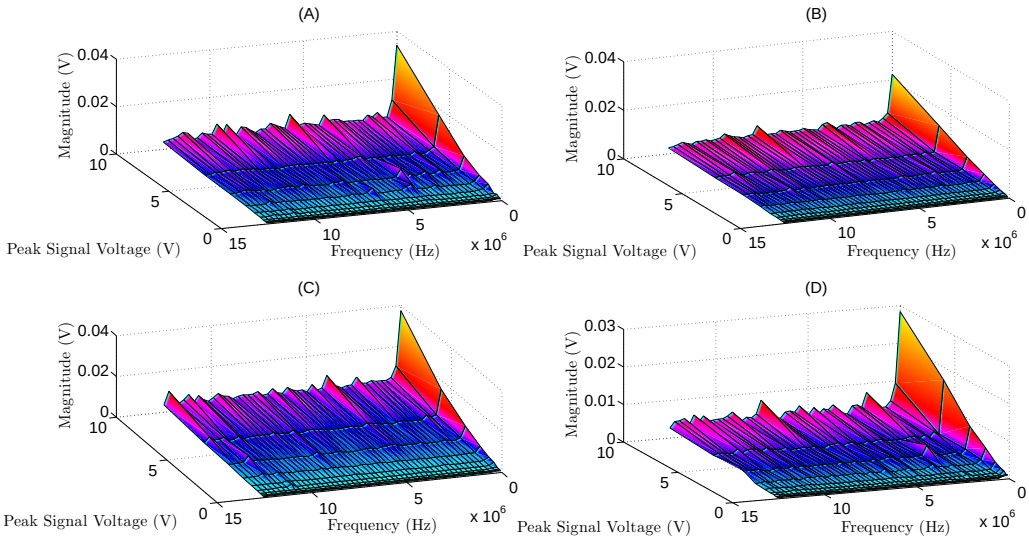

Figure 272: ac cie effects observed at 27khz for (a) tds2002 unit 1 channel 1, (b) tps2024 channel 4, (c) tds2002 unit 2 channel 1, (d) tds2002 unit 2 channel 2

range, yet the CIE effect spectral distribution seems to remain consistent between the two oscilloscope models — the Tektronix TPS2024 having fewer spectral CIE effects than the Tektronix TDS2002 — although a number of higher frequency magnitude spikes were, once again, observed within both the TPS2024 and TDS2002 oscilloscopes.

Conversely, upon examining the AC CIE effects observed for each of the oscilloscope channels at the test frequency of 116kHz, as shown by Figure: (273) and Figure: (274),

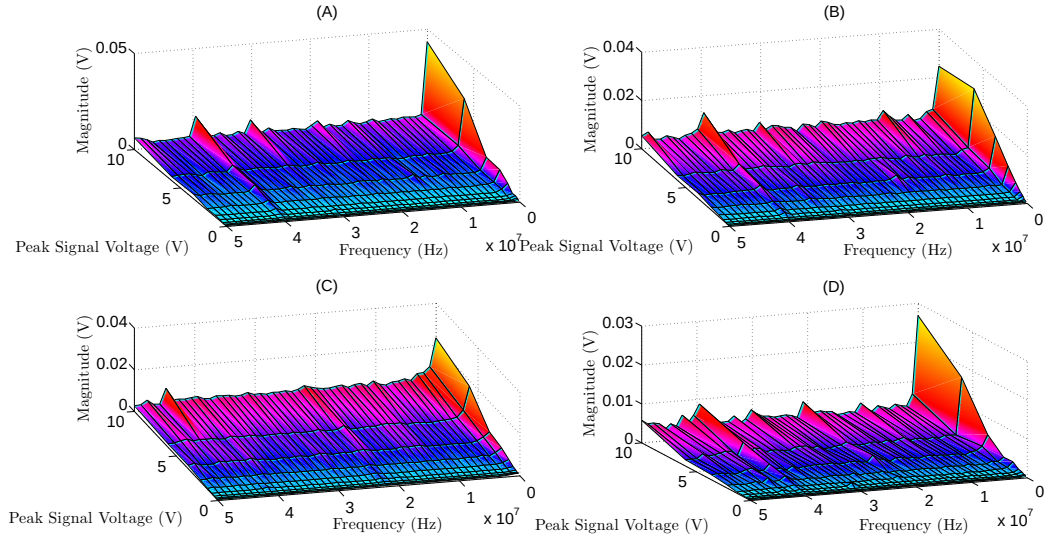

Figure 273: ac cie effects observed at 116khz for (a) tps2024 channel 1, (b) tps2024 channel 2, (c) tds2002 unit 1 channel 2, (d) tps2024 channel 3

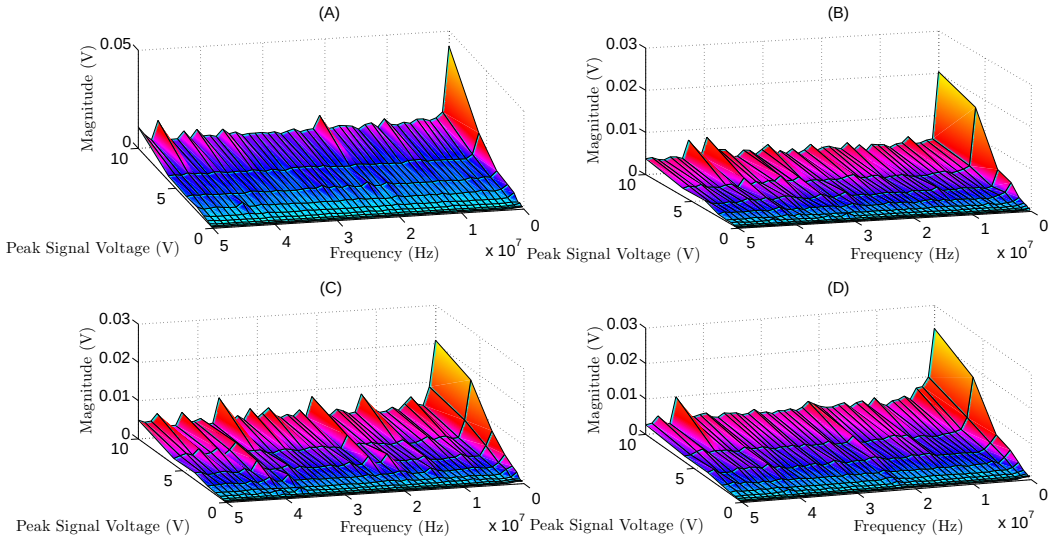

Figure 274: ac cie effects observed at 116khz for (a) tds2002 unit 1 channel 1, (b) tps2024 channel 4, (c) tds2002 unit 2 channel 1, (d) tds2002 unit 2 channel 2

a similar conclusion, once again, — to those obtained from examining Figure: (271) and Figure: (272) — can be made, since the observed CIE frequencies seem to be primarily located near the lower end of the frequency spectrum at the maximum applied signal voltage. Similarly, the Tektronix TPS2024 oscilloscope appears to still maintain its, previously observed, approximate 40mV to 50mV CIE effect peak — although a slight reductions was observed —, while the two Tektronix TDS2002 oscilloscopes appear to remain within the, previously observed, 40mV to 50mV CIE effect range — although a slight reductions was observed here as well —, yet the CIE effect spectral distribution seems to remain consistent between the two oscilloscope models — the Tektronix TPS2024 having fewer spectral CIE effects than the Tektronix TDS2002 — although a number of higher frequency magnitude spikes were, yet again, observed within both the TPS2024 and TDS2002 oscilloscopes.

Likewise, upon examining the AC CIE effects observed for each of the oscilloscope channels at the test frequency of 500kHz, as shown by Figure: (275) and Figure: (276), a similar conclusion, once again, — to those obtained from examining Figure: (273) and Figure: (274) — can be made, since the observed CIE frequencies seem to be primarily

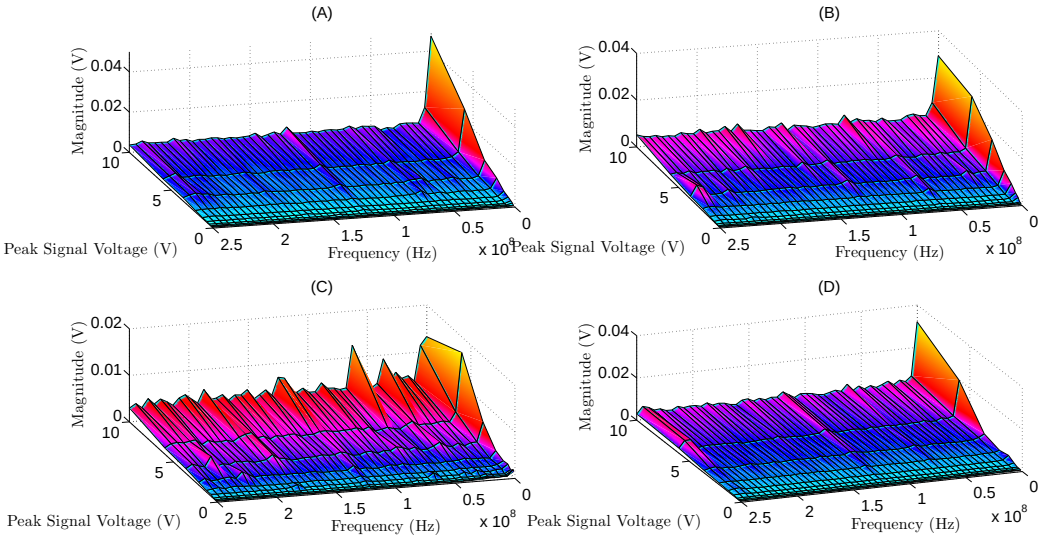

Figure 275: ac cie effects observed at 500khz for (a) tps2024 channel 1, (b) tps2024 channel 2, (c) tds2002 unit 1 channel 2, (d) tps2024 channel 3

located near the lower end of the frequency spectrum at the maximum applied signal voltage. Similarly, the Tektronix TPS2024 oscilloscope appears to still maintain its, previously observed, approximate 40mV to 50mV CIE effect peak, while the two Tektronix TDS2002 oscilloscopes appear to remain within the, previously observed, 40mV to 50mV CIE effect range — although the spectral bandwidth of the TDS2002 unit 2 on channel 2 seems to be abnormally wide given the previous observations —, yet the CIE effect spectral distribution seems to remain consistent between the two oscilloscope models — the Tektronix TPS2024 having fewer spectral CIE effects than the Tektronix TDS2002 — although a number of higher frequency magnitude spikes were, once again, observed within both the TPS2024 and TDS2002 oscilloscopes.

Likewise, upon examining the AC CIE effects observed for each of the oscilloscope channels at the test frequency of 1MHz, as shown by Figure: (277) and Figure: (278), a similar conclusion, once again, — to those obtained from examining Figure: (275) and Figure: (276) — can be made, since the observed CIE frequencies seem to be primarily located near the lower end of the frequency spectrum at the maximum applied signal volt-

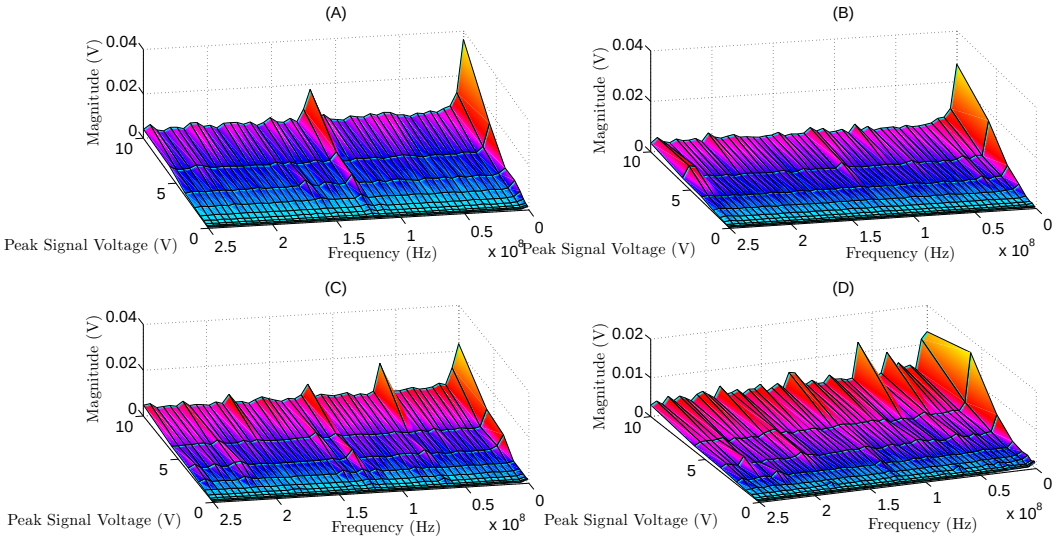

Figure 276: ac cie effects observed at 500khz for (a) tds2002 unit 1 channel 1, (b) tps2024 channel 4, (c) tds2002 unit 2 channel 1, (d) tds2002 unit 2 channel 2

age. Similarly, the Tektronix TPS2024 oscilloscope appears to still maintain its, previously observed, approximate 40mV to 50mV CIE effect peak — although a substantial reduction appears to have occurred within some of the channels —, while the two Tektronix TDS2002 oscilloscopes appear to remain within the, previously observed, 40mV to 50mV CIE effect range — although the spectral bandwidth seems to have reduced significantly when compared with the previous measurement —, yet the CIE effect spectral distribution

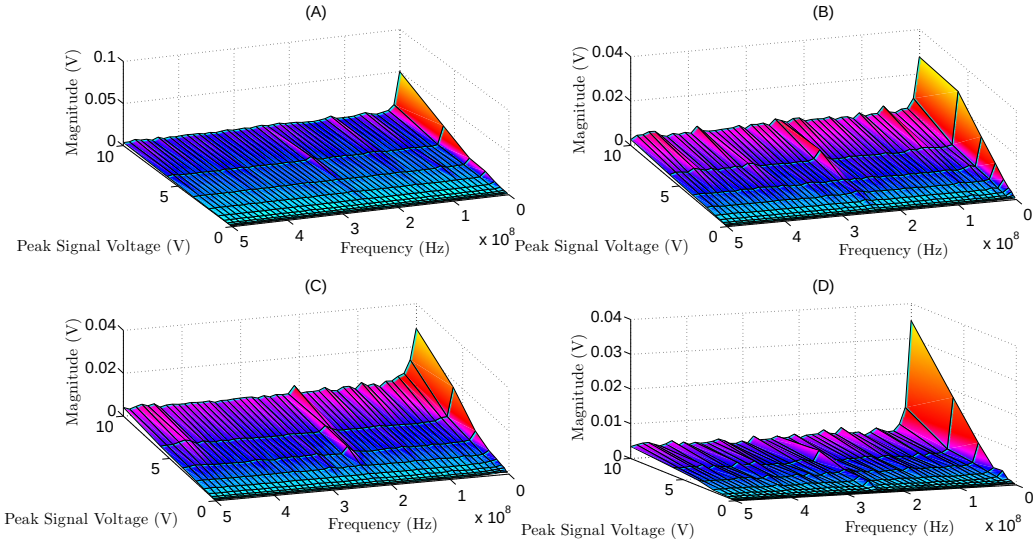

Figure 277: ac cie effects observed at 1mhz for (a) tps2024 channel 1, (b) tps2024 channel 2, (c) tds2002 unit 1 channel 2, (d) tps2024 channel 3

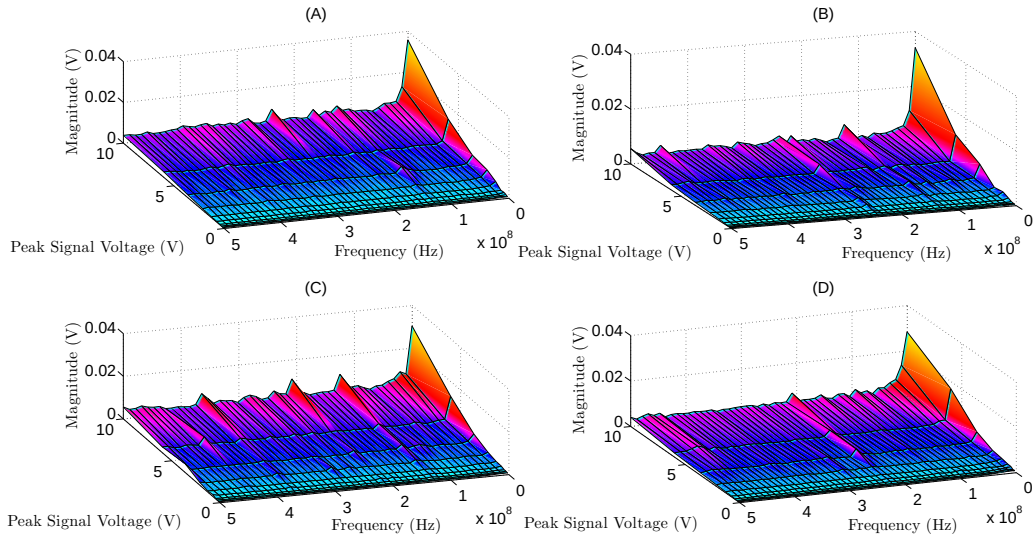

Figure 278: ac cie effects observed at 1mhz for (a) tds2002 unit 1 channel 1, (b) tps2024 channel 4, (c) tds2002 unit 2 channel 1, (d) tds2002 unit 2 channel 2

seems to remain consistent between the two oscilloscope models — the Tektronix TPS2024 having fewer spectral CIE effects than the Tektronix TDS2002 — although a number of higher frequency magnitude spikes were, once again, observed within both the TPS2024 and TDS2002 oscilloscopes.

While the discussion regarding Figure: (257) through Figure: (278) was, unfortunately, somewhat redundant — although such attributes are rather positive, since system consistency is generally beneficial when attempting to identify or reduce such effects —; however, the underlying observation obtained from visually examining Figure: (257) through Figure: (278) is the fact that, once again, the vast majority of all CIE effects encountered seem to be associated with the signals peak amplitude — since the oscilloscope instrumentational amplifier stage must adjust its internal gain to prevent clipping and this process seems to make the oscilloscope more susceptible to CIE effects. Likewise, such observations also revealed a relatively unintuitive lack of synthetic 60 Hz environmental effects, and while a significant amount of environmental reduction was obtained because the acquisition is occurring within a partially shielded environment — obtained from the utilization of a externally powered RF shielded room —; however, it is frequently assumed — a notion that appears to be rather incorrect, at least within a partially shielded environment — that the majority of the CIE distortions observed are the result of synthetic 60 Hz environmental effects when, in fact, the vast majority of CIE effects encountered seems to be harmonic — particularly third harmonic — in origin. Conversely, while the apparent lack of 60 Hz environmental effects measured might be somewhat surprising, yet given the frequent occurrence of such effects, in retrospect, the lack of such effects is not overly surprising given that most commercial acquisition devices deliberately utilized a multitude of environmental reduction techniques in order to reduce these effects — including notch filtering, bandwidth

limiting, internal shielding, and instrumentational amplifiers.

Nevertheless, while such observations are indeed profound, such observations are far from being completely quantitative, thus based upon the information obtained — noting, once again, that the surface plots Figure: (257) through Figure: (278) had the 0 Hz FFT bin removed in order to make the higher order CIE effects more observable — it appears reasonable to assume that the CIE effects encountered will the around 10mV for input signals that are less than 2.5V peak, 10mV to 30mV for input signals that are between 2.5V peak and 6V peak, and 30mV to 60mV for input signals that are above 6V peak.

Likewise, because it is somewhat difficult to mentally overlay the information provided within Figure: (257) through Figure: (278) into a single plot, upon combining the maximum magnitude peaks detected — within each of the figures — into a series of plots that correspond with the acquired input channel — as shown by Figure: (279), Figure: (280), Figure: (281), Figure: (282), Figure: (283), Figure: (284), Figure: (285), and Figure: (286) — a similar summarization — as the one previously provided — can be obtained. Conversely, upon combining the spectral magnitude information presented within Figure: (257)

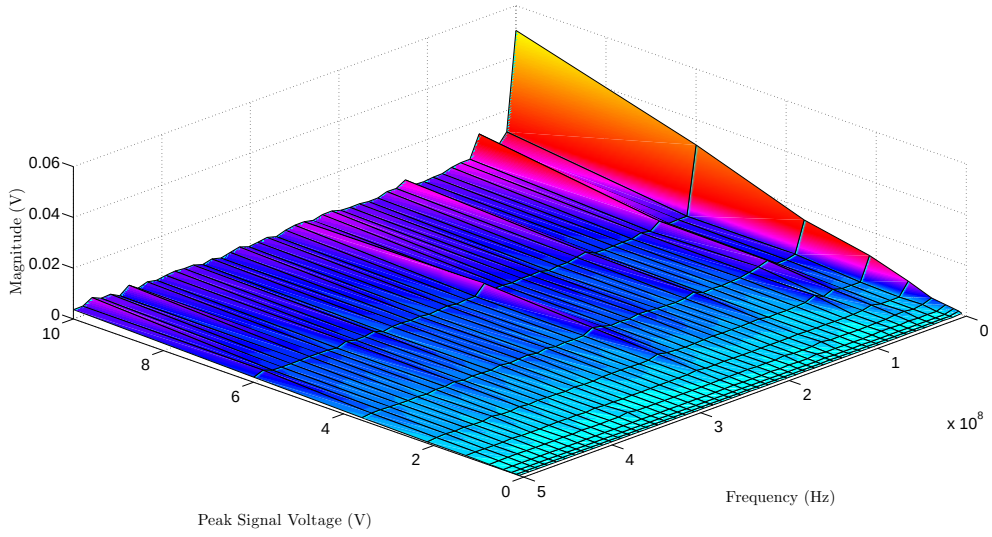

Figure 279: maximum magnitude ac cie effects plot for all test frequencies for tps2024 channel 1

through Figure: (278) into Figure: (279), Figure: (280), Figure: (281), Figure: (282), Figure: (283), Figure: (284), Figure: (285), and Figure: (286), and visually inspecting Figure: (279) reveals — once again — that the maximum CIE effects encountered by channel one of the TPS2024 unit occurred during the 10V peak test near the third harmonic frequency of the applied signal — given the interpolated scale of the plot this frequency occurred within the first graphical bin — with a magnitude of 60mV, while a number of presumably higher

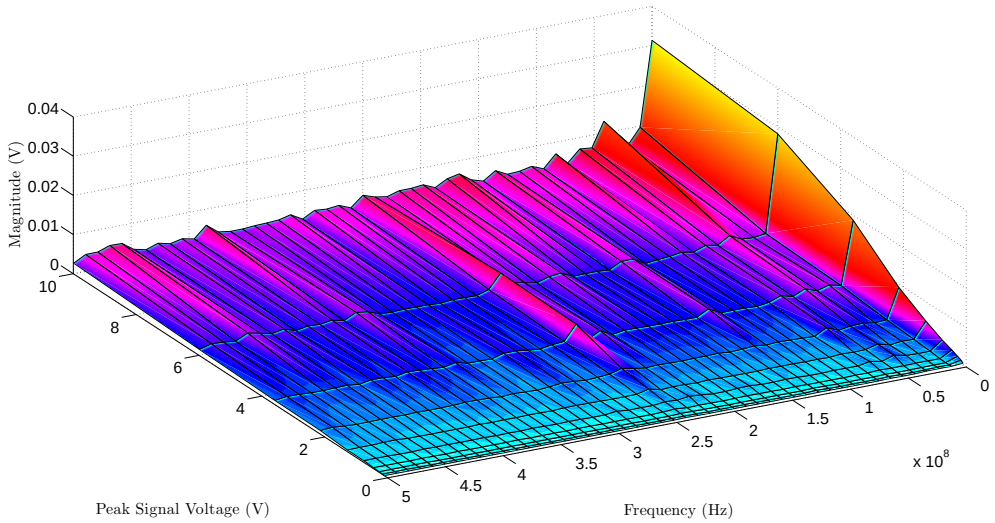

Figure 280: maximum magnitude ac cie effects plot for all test frequencies for tps2024 channel 2

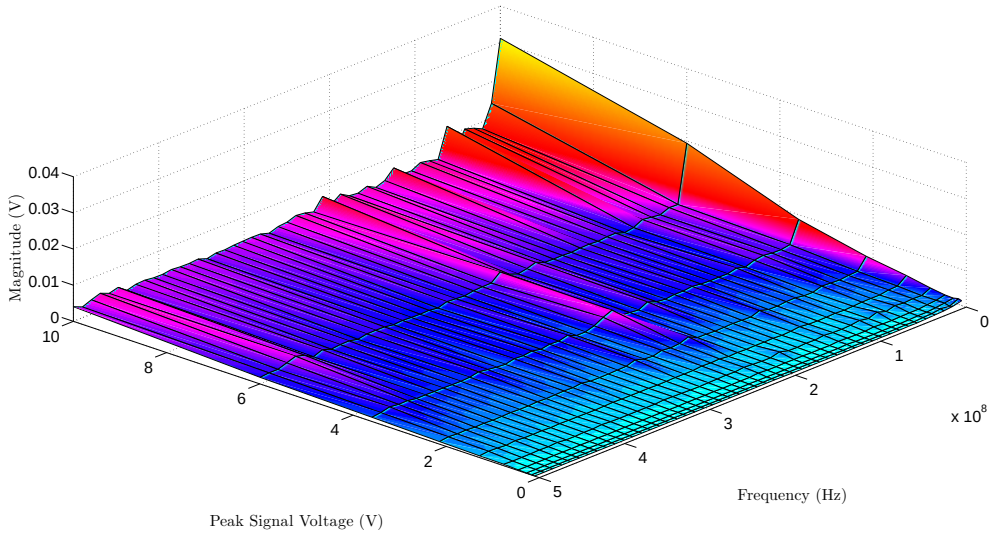

Figure 281: maximum magnitude ac cie effects plot for all test frequencies for tds2002 unit 1 channel 2

order harmonics appear to manifest themselves across the observed frequency spectrum with a magnitude somewhere between 5mV to 10mV. Similarly, a visual inspection of the second channel of the TPS2024 unit, as shown by Figure: (280), reveals a slightly lower magnitude of CIE effects — with a third harmonic of 30mV — than those encountered within Figure: (279) — primarily because the oscilloscope probe utilized by channel one of the TPS2024 unit was not specifically designed for this particular oscilloscope while the

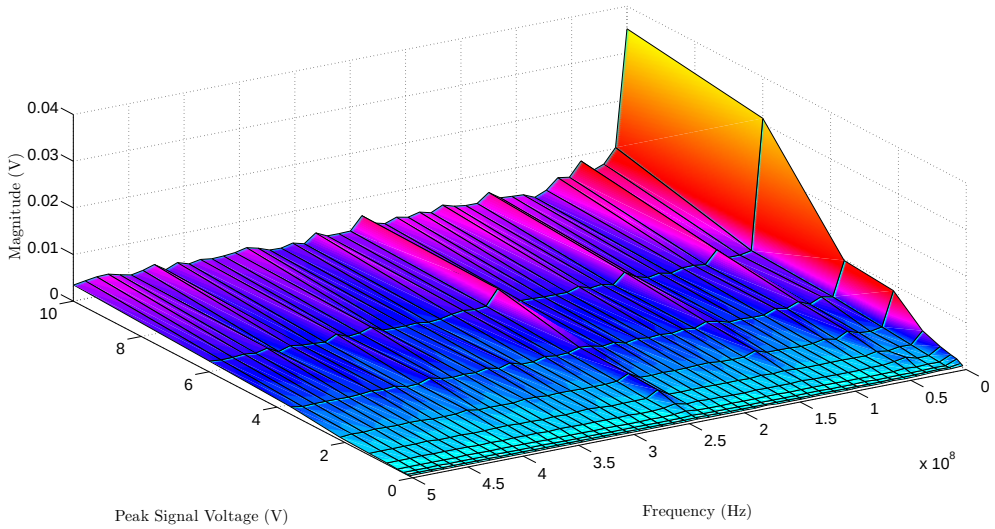

Figure 282: maximum magnitude ac cie effects plot for all test frequencies for tps2024 channel 3

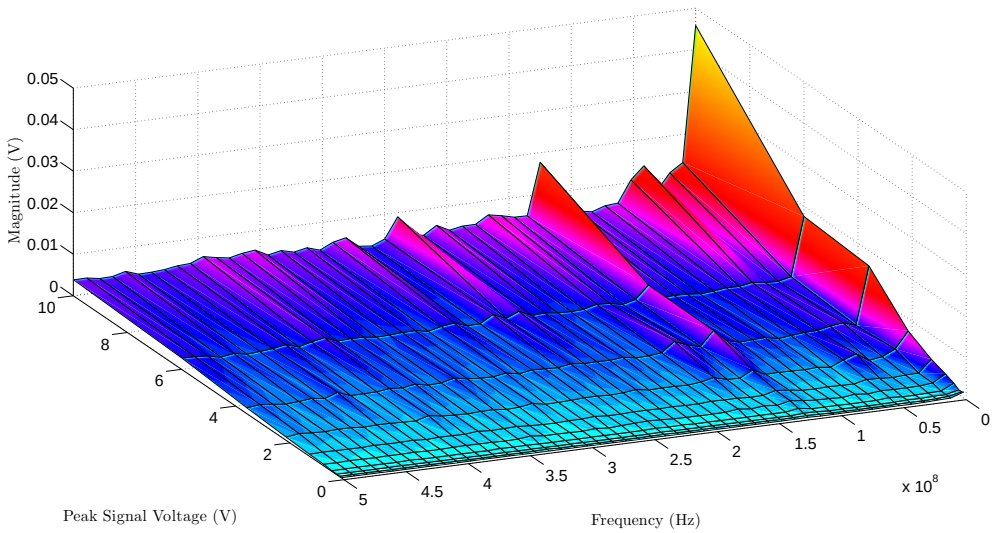

Figure 283: maximum magnitude ac cie effects plot for all test frequencies for tds2002 unit 1 channel 1

probe utilized to obtain the channel 2 measurement was — and a average higher frequency spectral magnitude floor that is substantially below 10mV.

Likewise, a visual inspection of the third channel of the TPS2024 unit, as shown by Figure: (282), reveals a graphical surface that is very similar to the surface obtained upon examining channel one of the TPS2024 unit — as shown by Figure: (279) — although the information obtained appears to be scaled since the peak magnitude is 40mV within this

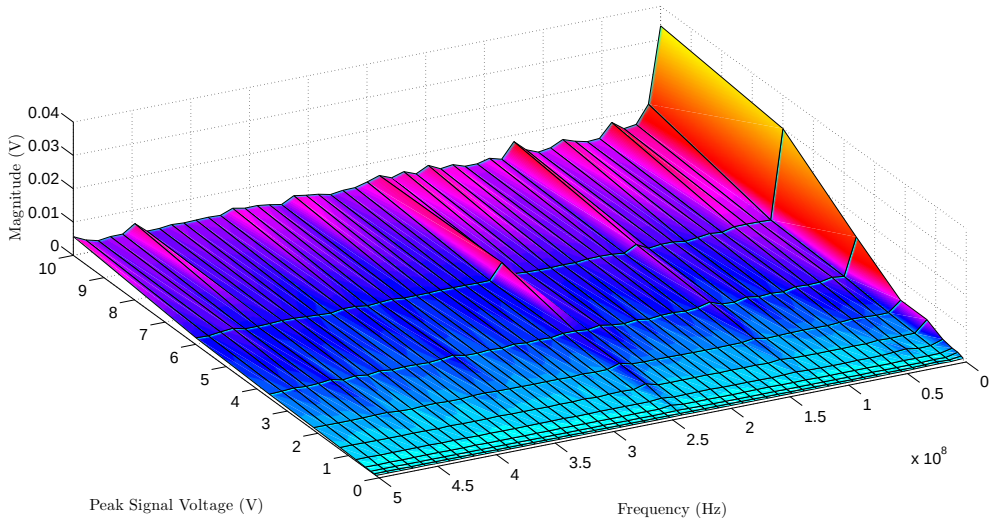

Figure 284: maximum magnitude ac cie effects plot for all test frequencies for tps2024 channel 4

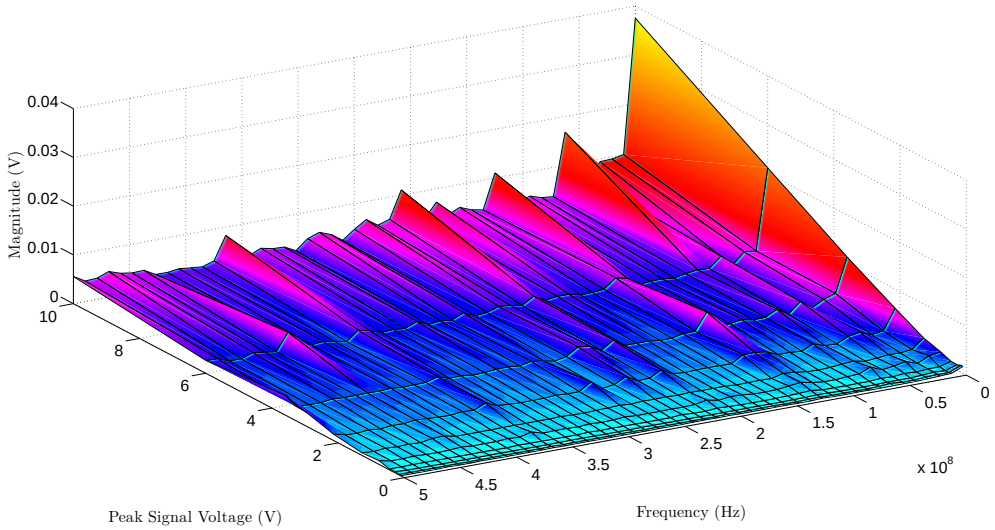

Figure 285: maximum magnitude ac cie effects plot for all test frequencies for tds2002 unit 2 channel 1

surface rather than the, previously observed, 60mV peak magnitude, while, at the same time, the spectral floor observed — within both plots — seem to be similar since higher order harmonics appear to be dominant relative to the background effect floor observed within Figure: (280). Conversely, a visual inspection of the forth channel of the TPS2024 unit, as shown by Figure: (284), reveals a graphical plot nearly identical to the third channel of the TPS2024 unit — as shown by Figure: (282) —, and the similar shape of the surface obtained within channel 1 — neglecting for the moment the incorrect scaling from the oscilloscope probe used —, channel 3, and channel 4 seem to indicate that these plots symbolize the average CIE effects that will be acquired, while channel 2 symbolizes the best case scenario given its significantly lower spectral magnitude values.

Similarly, a visual inspection of the first channel of the TDS2002 unit 1, as shown by Figure: (283), reveals a plot that is very similar to channel one of the TPS2024 unit — as shown by Figure: (279) — with the exception of having a slightly lower maximum third harmonic magnitude of 45mV, and a slightly larger higher order harmonic magnitude, which seems to indicate that the oscilloscope probe — since the same type of probe was utilized on

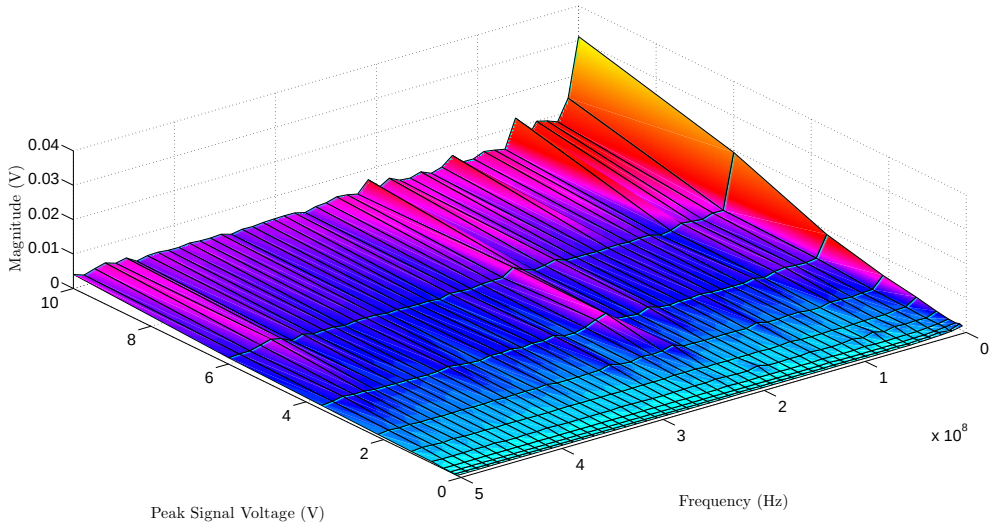

Figure 286: maximum magnitude ac cie effects plot for all test frequencies for tds2002 unit 2 channel 2

this particular channel and on the first channel of the TPS2024 unit — plays a significant role in determining the amount of CIE effects acquired, along with the possibility that the bandwidth limiting feature is slightly different between the two oscilloscope models. Likewise, a visual inspection of the second channel of the TDS2002 unit 1, as shown by Figure: (281), reveals a similar plot as the one obtained within — Figure: (283) —, although the presumed third harmonic magnitude is slightly lower — located at 30mV rather than 45mV —, while a number of seemingly non-harmonic higher order spectral content appears to become more prevalent — particularly near the lower frequency region. Conversely, a visual inspection of the first channel of the TDS2002 unit 2, as shown by Figure: (285), reveals a plot that is extremely similar to Figure: (281), with the exception that the higher order spectral harmonics appear to be substantially higher — on the order of 20mV rather than 10mV. Likewise, a visual inspection of the second channel of the TDS2002 unit 2, as shown by Figure: (286), reveals a plot that is also extremely similar to Figure: (281), with the exception that the higher order spectral harmonics appear to be substantially lower — on the order of 5mV rather than 10mV —. Conversely, in a manner similar to the common similarities found upon analyzing the four oscilloscope channels within the TPS2024 unit, a similar association can also be made between the two TDS2002 units, since the CIE effects observed appear to be reasonably consistent for each measurement obtained — although an element of metaphoric potluck does appear to exist here, particularly when it comes to higher order spectral frequencies — ; however, once again, the manifestation of CIE effects appears to be substantially worse at higher input voltages — for reasons that have already been discussed — and such attributes should be considered prior to performing any type of high fidelity characterization since, based upon the information obtained, the spectral content of the applied signal will ultimately determine the predominating type of CIE ef-

fects encountered — especially since the harmonic frequencies of the applied signal appears to be a major source of the CIE effects encountered, at least within the partially shielded environment — and the classical perception of increasing the magnitude of the characterization voltage in order to increase the signal-to-noise ratio (SNR) is somewhat misleading, especially upon considering how the magnitude of the CIE effects observed increased as the input voltage increased — although such observations are generally only predominant when the signal being measured is inherently small but, under such circumstances, requires a large external stimulus prior to acquisition, as would be the case for noninvasive muscle stimulation and measurement.

Likewise, while the individual characterization of the CIE effects encountered for each of the oscilloscope channels utilized can be extremely beneficial; yet, often times a summarized perspective is preferred — particularly within general discussion and within preliminary calculations —, thus based upon such observations, upon combining all of the observed CIE effects maximum magnitude values — as shown by Figure: (279), Figure: (280), Figure: (281), Figure: (282), Figure: (283), Figure: (284), Figure: (285), and Figure: (286) — into

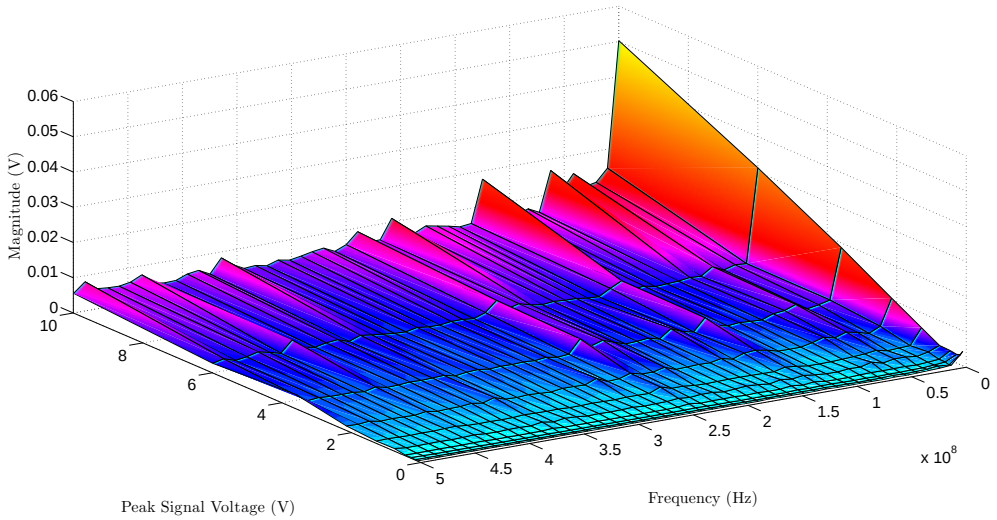

Figure 287: the maximum magnitude ac cie effects plot for all test frequencies, oscilloscope channels, and oscilloscope units utilized

a single plot, as shown by Figure: (287), a similar series of conclusions can be obtained without the hassle of having to perform an individual examination of every oscilloscope channel utilized — these conclusions being that the maximum observed CIE effects encountered are generally odd harmonic in nature, will be larger at higher amplitudes, and will never be substantially above 50mV within the test framework provided. Nevertheless, while the in-depth analysis of the FFT bins above 0Hz has been enlightening; however, it now seems prudent to examine the FFT 0Hz bin for each of the, previously presented, oscilloscope channels, a task that can be achieved in eight surface plots — because the number of dimensions has been reduced from 4 (input frequency, input voltage, FFT spectral frequency above 0Hz, and FFT spectral magnitude above 0Hz) to 3 (input frequency, input voltage, FFT 0Hz spectral magnitude) dimensions —, as shown by Figure: (288), Figure: (289), Figure: (290), Figure: (291), Figure: (292), Figure: (293), Figure: (294), and Figure: (295), since these particular plots was separated from the nonzero Hertz FFT bin because there higher magnitude tends to negatively effect the surface plots scaling — thus making the, previously discussed harmonic CIE effects difficult to graphically observe —, primarily because — as it was previously observed within the embedded DC CIE effects section — this particular FFT bin tends to incorporate, not only the physical DC component embedded within the acquired signal, but also partial segments of lower frequency spectral components that are substantially below the first nonzero FFT bin — once again, defined by the sample rate utilized.

Conversely, with this being said, upon visually examining Figure: (288) — which graphically depicts the magnitude of the 0Hz FFT bin obtained from the first channel of the Tektronix TPS2024 oscilloscope utilized —, it can be concluded, once again, that the perceived DC CIE effects encountered — perceived, in this particular case, because of the, previously

discussed, knowledge that other factors beyond an externally applied DC voltage determines this particular value — are strongly associated with the magnitude of the applied input signal, which, in itself, strengthens the previous assertion that CIE effects become progressively worse as the input voltage increases because of the variation in physical acquisition configuration within the oscilloscopes instrumentational amplifier stage. Likewise, in terms of CIE effect DC magnitude, it is visually apparent — at least based upon Figure: (288) — that input voltages above 6V will be subjected to DC CIE effects that are around 200mV to 300mV and are, seemingly, frequency independent — if the variation of 100mV across the spectral band is considered to be inconsequential above the 200mV threshold — , although it appears that the lower test frequencies utilized were more susceptible to such DC CIE effects than the higher frequencies utilized — although this is primarily because acquisition sampling can effectively function as a limited digital hi-pass filter (HPF) depending upon circumstances.

Similarly, upon visually examining Figure: (289) — which graphically depicts the magnitude of the 0Hz FFT bin obtained from the second channel of the Tektronix TPS2024 oscilloscope utilized —, a similar graphical shape — as shown within Figure: (288) — is

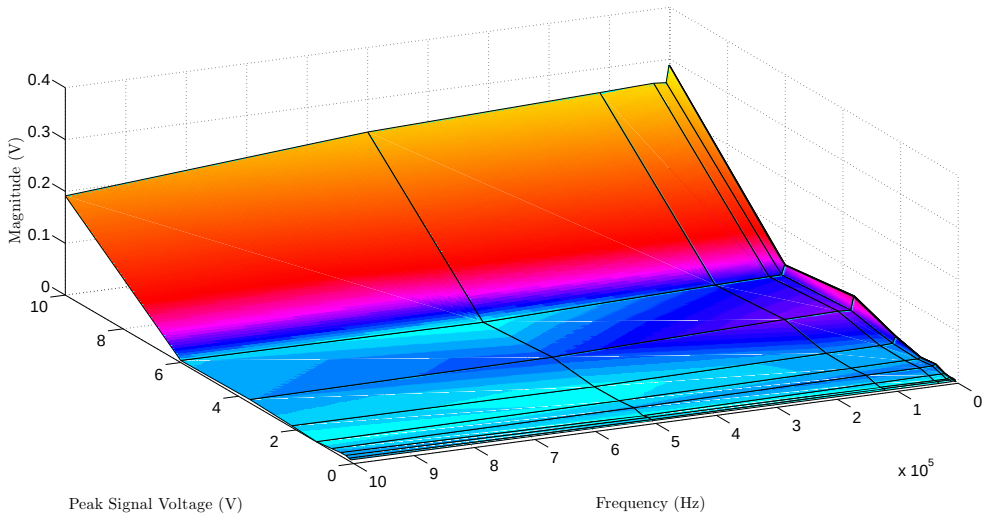

Figure 288: fft 0hz bin cie effects plot for all test frequencies for the tps2024 channel 1

obtained, although the magnitude of the 10V DC CIE effects encountered appear to have substantially reduced in magnitude — from 200mV or 300mV to around 100 mV — which, as it was previously discussed, is probably because the oscilloscope probe utilized on the first Tektronix TPS2024 channel was not inherently designed for this particular oscilloscope — which promotes the importance of proper equipment selection when attempting to acquire a high fidelity measurement — and the overall DC effects encountered are, for the most part, typically within the 50 mV range — as was the case within Figure: (288)

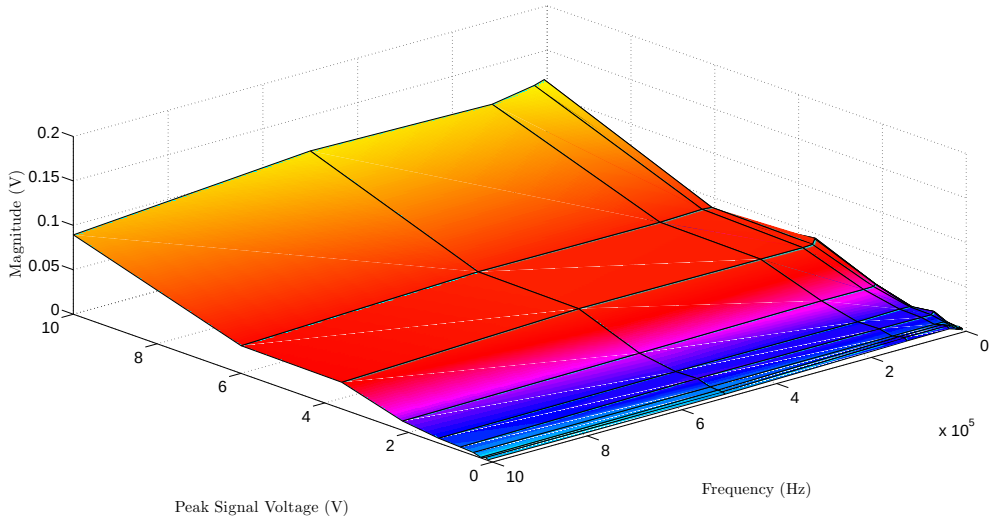

Figure 289: fft 0hz bin cie effects plot for all test frequencies for the tps2024 channel 2

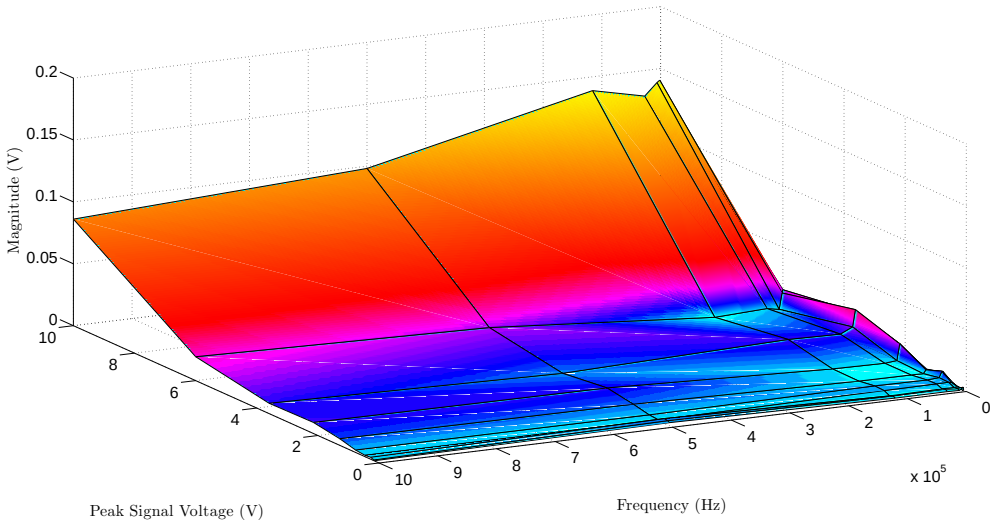

Figure 290: fft 0hz bin cie effects plot for all test frequencies for the tps2024 channel 3

— so long as the input voltage is kept below 6V.

Likewise, upon visually examining Figure: (290) — which graphically depicts the magnitude of the 0Hz FFT bin obtained from the third channel of the Tektronix TPS2024 oscilloscope utilized —, a similar surface plot is obtained — as shown within Figure: (288) and Figure: (289) — that, once again, visually indicates that the input voltage is ultimately the primary factor in determining the magnitude of the DC CIE effects encountered — at least within a partially shielded environment —, and once again it appears that the maximum DC CIE effects encountered — at least for this particular oscilloscope channel — will be between 80mV to 145mV —, although a minor low frequency spike above the visual average is observed when the input signal is at 4V, while the average DC CIE effects observed seem to have visually reduced from 50 mV to around 15 mV.

Conversely, upon visually examining Figure: (291) — which graphically depicts the magnitude of the 0Hz FFT bin obtained from the forth channel of the Tektronix TPS2024 oscilloscope utilized —, a similar surface plot is obtained — as shown within Figure: (289), although the higher frequency DC CIE effect magnitude for the 10V input signal seems to have substantially decreased — from around 95mV to 50mV —, while the remaining DC

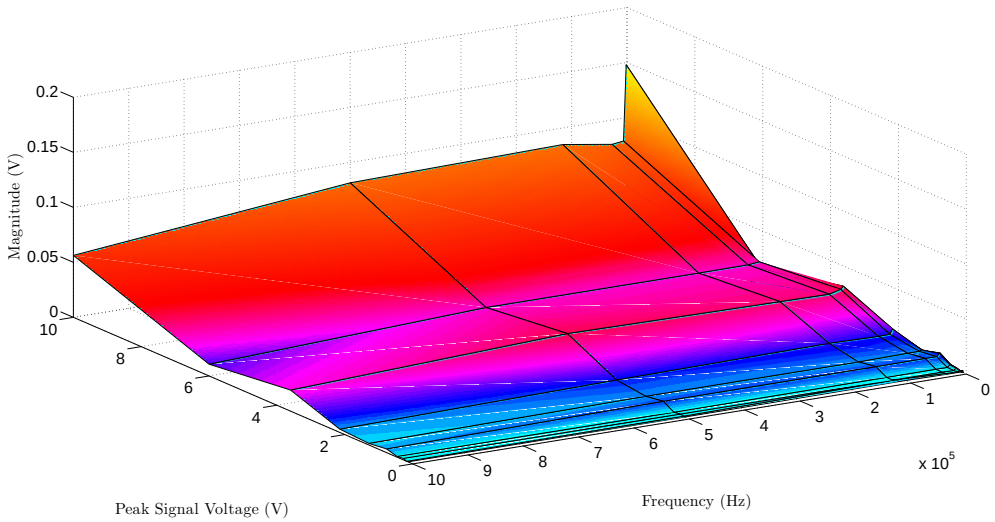

Figure 291: fft 0hz bin cie effects plot for all test frequencies for the tps2024 channel 4

magnitudes appear to remain seemingly consistent relative to the, previously shown, DC CIE effects magnitude surface plot.

Likewise, upon visually examining Figure: (292) — which graphically depicts the magnitude of the 0Hz FFT bin obtained from the first channel of the first Tektronix TDS2002 oscilloscope utilized —, a similar shaped surface plot is obtained — as shown within Figure: (291) — with the notable exception of the 10V DC CIE effect magnitudes being substantially higher — on the order of 100mV to 300mV —, an attribute that is reminiscent to the Tektronix TPS2024 channel 1 plot — as shown by Figure: (288). Furthermore, because the oscilloscope probes utilized by the two Tektronix TDS2002 oscilloscopes and the first channel of the Tektronix TPS2024 oscilloscope were someone similar, it becomes reasonable to begin suspecting that this particular attribute is, in part, somewhat dependent upon the oscilloscope probe utilized — particularly since the Tektronix TPS2024 channel 2 through 4 probes produced reasonably similar results and have the same make and model oscilloscope probe, while the Tektronix TPS2024 channel 1 and Tektronix TDS2002 unit 1 channel 1

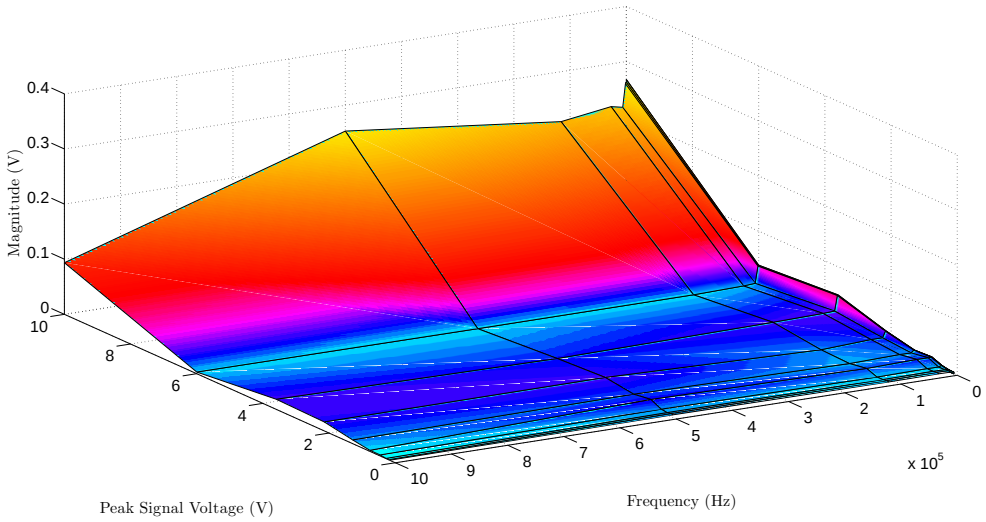

Figure 292: fft 0hz bin cie effects plot for all test frequencies for the tds2002 unit 1 channel 1

also produce similar DC CIE effects.

Similarly, upon visually examining Figure: (293) — which graphically depicts the magnitude of the 0Hz FFT bin obtained from the second channel of the first Tektronix TDS2002 oscilloscope utilized —, a similar shaped surface plot is obtained — as shown within Figure: (292) — with the notable exception of the 10V DC CIE effect magnitude being substantially lower — going from between 100mV to 300mV to between 50mV to 125mV — than the previous measurement. Likewise, such observations, while casting some doubt upon the, previously proposed, oscilloscope probe dependency — although a connection likely exist between the CIE effects measured and he oscilloscope probe model, but is likely dependent upon additional parameters —, does actively demonstrate that considerable differences between oscilloscope acquisition channels can exist and such occurrences substantially strengthened the importance of both properly calibrating and empirically understanding the laboratory instrumentation utilized prior to attempting to acquire any high fidelity measurement.

Conversely, upon visually examining Figure: (294) — which graphically depicts the magnitude of the 0Hz FFT bin obtained from the first channel of the second Tektronix

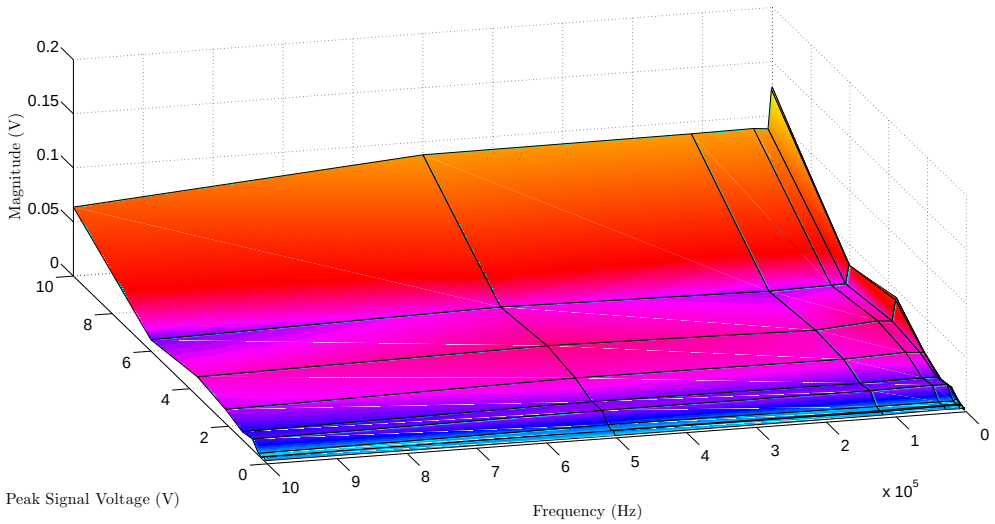

Figure 293: fft 0hz bin cie effects plot for all test frequencies for the tds2002 unit 1 channel 2

TDS2002 oscilloscope utilized —, a similar shaped surface plot is obtained — as shown within Figure: (293) — with the notable exception of the 10V DC CIE effect being slightly lower — going from between 50mV to 125mV to between 35mV to 120mV — than the previous measurement, while a substantial low frequency magnitude spike is observed between the 2V and 6V region.

Likewise, upon visually examining Figure: (295) — which graphically depicts the magnitude of the 0Hz FFT bin obtained from the second channel of the second Tektronix

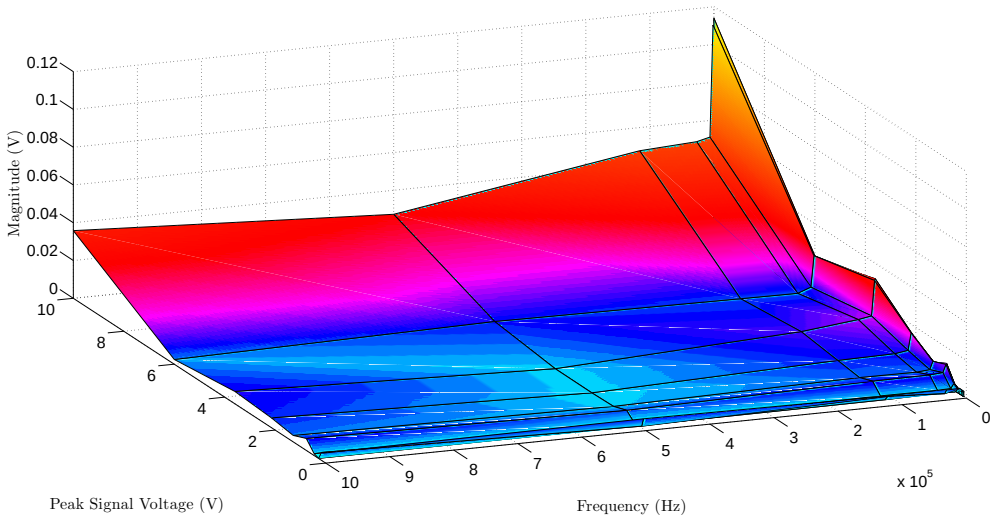

Figure 294: fft 0hz bin cie effects plot for all test frequencies for the tds2002 unit 2 channel 1

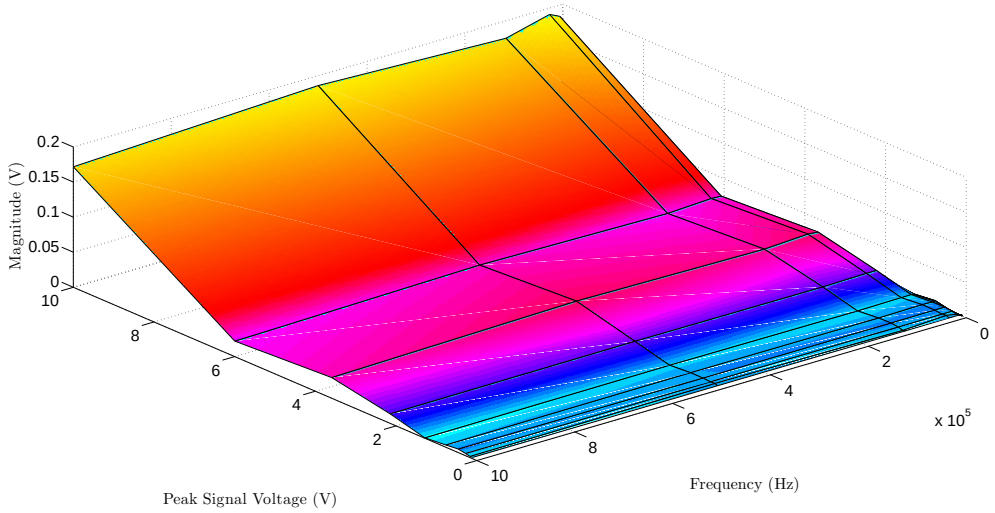

Figure 295: fft 0hz bin cie effects plot for all test frequencies for the tds2002 unit 2 channel 2

TDS2002 oscilloscope utilized —, a similar shaped surface plot is obtained — as shown within Figure: (294) — with the notable exception of the 10V DC CIE effect magnitude being substantially higher — going from between 35mV to 120mV to between 150mV to 160mV — than the previous measurement, while the, previously observed, spike in low frequency magnitude — between the 2V and 6V region — is no longer present — an attribute that might imply a minor susceptibility to CIE effects in this particular region exist within the previous oscilloscope channel being examined. Conversely, as it was previously mentioned, while the individual characterization of the DC CIE effects encountered for each of the oscilloscope channels utilized can be extremely beneficial — particularly within channel signal processing algorithms —; yet, often times a summarized perspective is preferred — particularly within general discussion and within preliminary calculations —, thus based upon such observations, upon combining all of the observed DC CIE effects maximum magnitude values — as shown by Figure: (288), Figure: (289), Figure: (290), Figure: (291), Figure: (292), Figure: (293), Figure: (294), and Figure: (295) — into a single plot, as shown by Figure: (296), a similar series of conclusions can be obtained without the hassle of having to perform an individual examination of every oscilloscope channel utilized — these conclusions being that the maximum observed DC CIE effects encountered are generally larger at higher amplitudes, and will never be substantially above 200mV to 300mv within the test framework provided.

Likewise, upon comparing the CIE effects observed within the DC test to those observed within the, previously depicted, AC test, it now seems apparent that the DC CIE effects observed are, in retrospect, relatively similar — especially upon considering the fact that the DC test only examined voltages up to a maximum of 2.5V, and the AC test examined voltages up to a maximum of 10V —, while the nonzero FFT bin CIE effects

observed were — definitively — higher within the AC test relative to the DC test — predominantly because of the harmonic frequencies that were invoked upon the application of a periodic waveform. Nevertheless, while such agreement between the two tests is, to put it mildly, a particularly metaphoric good sign — especially since the introduction of additional Tektronix oscilloscopes, within the AC test, appeared to possess similar CIE effect characteristics —; however, while the acquisition of such information is, overall, rather profound — especially when attempting to both manage and compensate for the laboratory CIE effects encountered during the acquisition process —, yet despite successfully demonstrating the ability to obtain consistent CIE effect characterization, such results are still somewhat lacking in thoroughness, especially since the subject of signal magnitude accuracy has not, as of yet, been addressed.

Conversely, upon taking such observations under advisement, extracting the signal magnitude is a relatively straightforward process — especially since the CIE effect processing method , previously described and depicted, was obtained by removing the signal within the frequency domain —, and upon surface plotting the magnitudes obtained — as shown

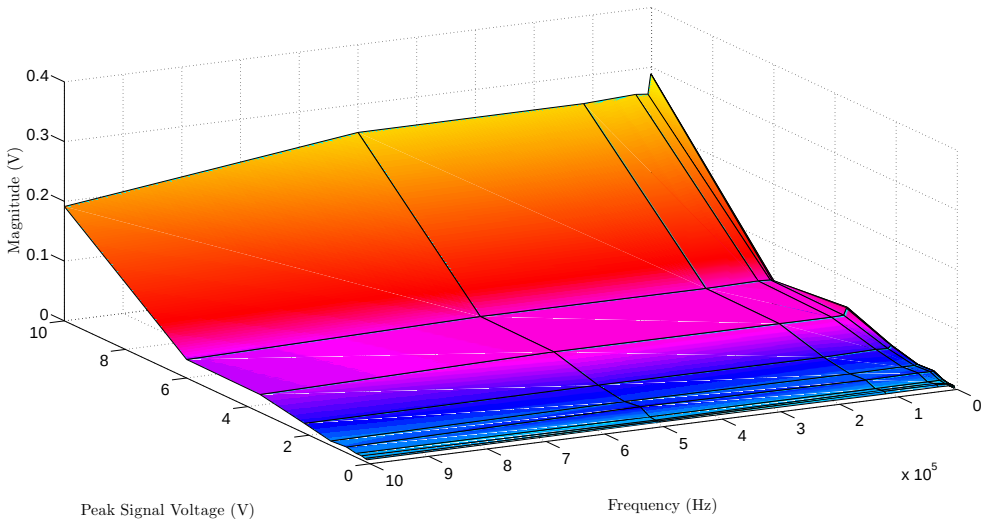

Figure 296: the maximum magnitude dc cie effects plot for all test frequencies, oscilloscope channels, and oscilloscope units utilized

by Figure: (297) and Figure: (298) — it becomes apparent that the measured input signal is reasonably consistent with the — test specified — ideal input signal, since the surface plot created — for all oscilloscope channels — is simply a linear plane with a specified slope. Yet, although the magnitude plots — shown by Figure: (297) and Figure: (298) — appears to be visually consistent with the desired input signal; however, a better assessment of the

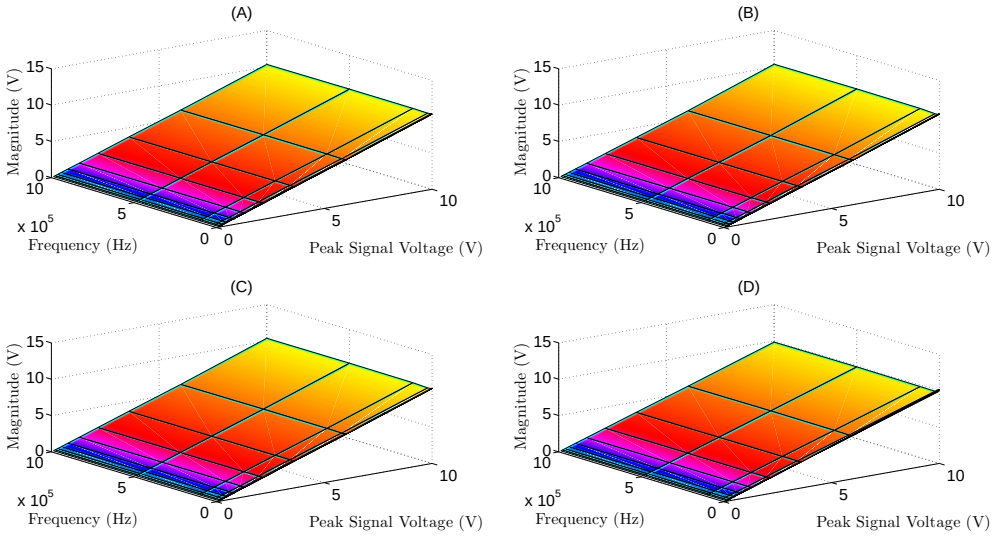

Figure 297: a plot of the peak magnitude of the input signal measured for (a) tektronix tps2024 channel 1, (b) tektronix tps2024 channel 2, (c) tektronix tps2024 channel 3, (d) tektronix tps2024 channel 4

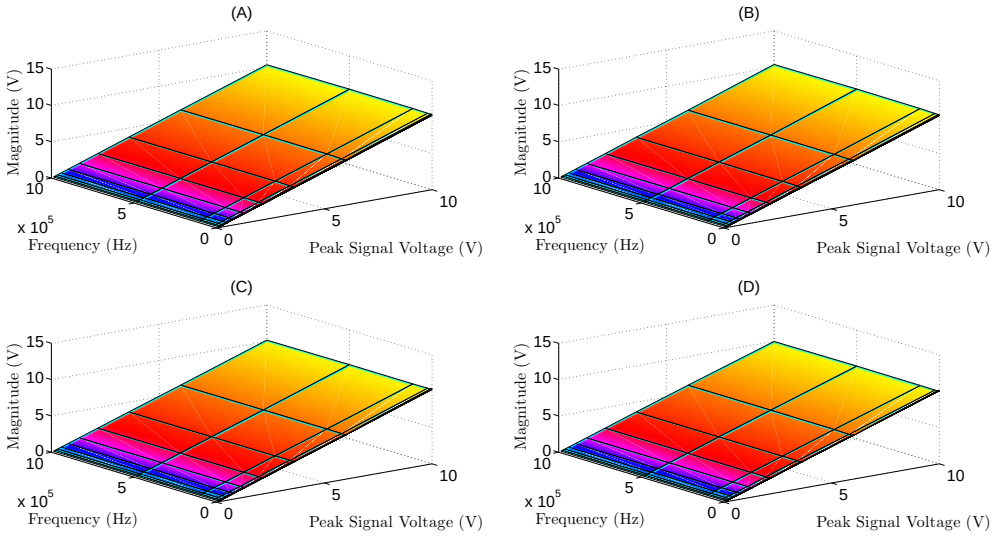

Figure 298: a plot of the peak magnitude of the input signal measured for (a) tektronix tds2002 unit 1 channel 1, (b) tektronix tds2002 unit 1 channel 2, (c) tektronix tds2002 unit 2 channel 1, (d) tektronix tds2002 unit 2 channel 2

accuracy obtained can be mathematically calculated by subtracting the ideal magnitude — that was defined within the Python code located in appendix B — from the measured magnitude and plotting the surface obtained after performing this particular mathematical operation — as shown by Figure: (299), Figure: (300), Figure: (301), Figure: (302), Figure: (303), Figure: (304), Figure: (305), and Figure: (306).

Likewise, upon visually inspecting the difference obtained after subtracting the ideal input voltages from the measured input voltages for channel 1 of the Tektronix TPS2024 oscilloscope — as shown by Figure: (299) —, it becomes obviously apparent that some discrepancy exists between the ideal input voltage and the measured input voltage — although such discrepancies only really become substantial when the input voltage becomes large —, and that the acquired signal — at least within this particular oscilloscope channel acquisition — appears to be slightly higher in magnitude — by around 400mV — than the desired ideal signal. Conversely, the rationale behind such observations is, once again, extremely difficult to definitively define — at least without an intensive iterative study of a multitude of instrumentational properties —; however, if some type of rationalization to

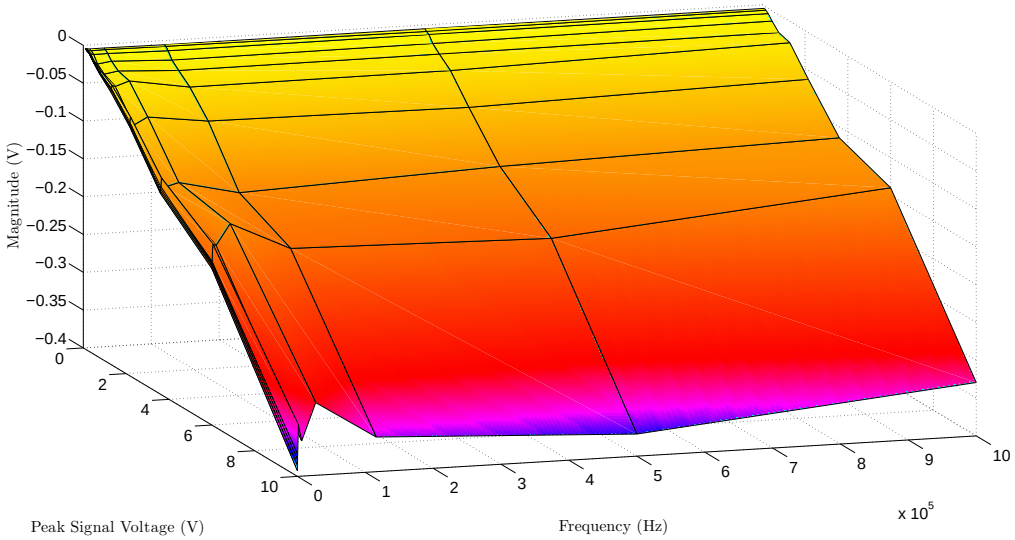

Figure 299: plot of the difference between the ideal maximum signal magnitude and the measured maximum signal magnitude for all test frequencies and voltages for channel 1 of the tektronix tps2024 oscilloscope

explain such occurrences is required , it is conceivable that the function generator is producing a input signal that slightly higher in magnitude, the oscilloscope channel input stage could be calibrated incorrectly, or the digital processing performed upon the signal could be introducing a slight error in the magnitude analysis. Yet, in all cases, the attribute that remains consistent within each of the presented scenarios is the fact that, such observations are definitively classifiable as being observable CIE effects, and, in turn, can be identified and compensated for using the techniques previously described.

Similarly, upon visually inspecting the difference obtained after subtracting the ideal input voltages from the measured input voltages for channel 2 of the Tektronix TPS2024 oscilloscope — as shown by Figure: (300) —, it appears that some consistency exist between the surface plot obtained from the first Tektronix TPS2024 oscilloscope channel — as shown by Figure: (299) — and the second Tektronix TPS2024 oscilloscope channel — as shown by Figure: (300) —, insofar as, the maximum magnitude of the second channel is 400 mV above the desired input signal; however, it also appears that a slight surface trough that was located at the 1kHz frequency — within Figure: (299) — is not within Figure: (300),

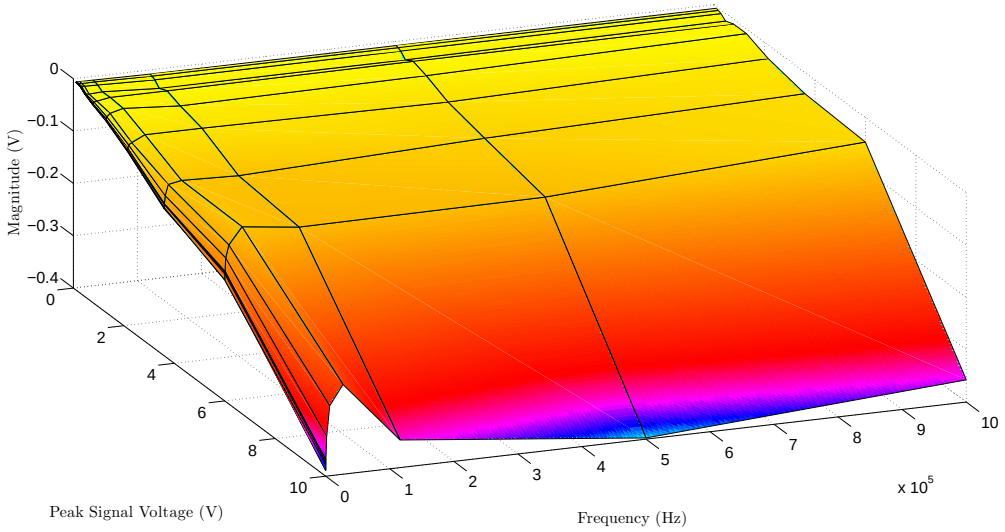

Figure 300: plot of the difference between the ideal maximum signal magnitude and the measured maximum signal magnitude for all test frequencies and voltages for channel 2 of the tektronix tps2024 oscilloscope

and such observations are rather interesting to consider.

Likewise, upon visually inspecting the difference obtained after subtracting the ideal input voltages from the measured input voltages for channel 3 of the Tektronix TPS2024 oscilloscope — as shown by Figure: (301) —, it appears that this particular surface plot significantly resembles the surface plot obtained within Figure: (300), and that, once again, the maximum deviation between the ideal signal magnitude versus the measured signal magnitude is around 400mV — or, more precisely, the measured signal was, at its worst point of deviation, 400mV larger than the ideal signal.

Conversely, upon visually inspecting the difference obtained after subtracting the ideal input voltages from the measured input voltages for channel 4 of the Tektronix TPS2024 oscilloscope — as shown by Figure: (302) —, it appears that some substantial changes have occurred — at least upon comparing Figure: (302) with Figure: (301) — since the maximum point of deviation is now located at 200mV above the original signal, while, at the same time, the first visual example of a measured 100mV undershoot becomes prevalent at the — now aptly named — 1 kHz trough. While the rationale behind this particular

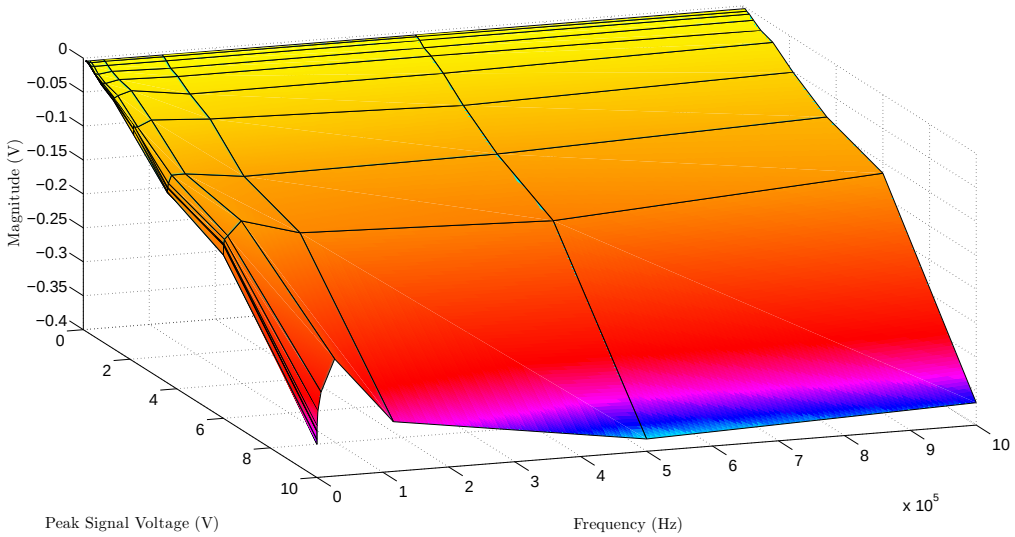

Figure 301: plot of the difference between the ideal maximum signal magnitude and the measured maximum signal magnitude for all test frequencies and voltages for channel 3 of the tektronix tps2024 oscilloscope

occurrence is, definitively somewhat speculative, although given the physical structure of the probe to oscilloscope interface, it seems conceivable that this particular junction could be responsible for sudden variations in input magnitude because of changes in input impedance; however, despite such observations, the results obtained within Figure: (302) do appear substantially better than those obtained within Figure: (299), Figure: (300), and Figure: (301), at least in terms of the amount of deviation observed upon performing a 10V signal acquisition across the visually defined frequency spectrum.

Likewise, upon visually inspecting the difference obtained after subtracting the ideal input voltages from the measured input voltages for channel 1 of the unit 1 Tektronix TDS2002 oscilloscope — as shown by Figure: (303) —, a similar surface plot to Figure: (299), Figure: (300), and Figure: (301) was obtained; yet, in this particular case, the maximum observed deviation has increased to the input signal being 500mV above the ideal input signal, and based upon the fact that the oscilloscope utilized — within Figure: (303)— has changed, such deviations were expected.

Conversely, upon visually inspecting the difference obtained after subtracting the ideal

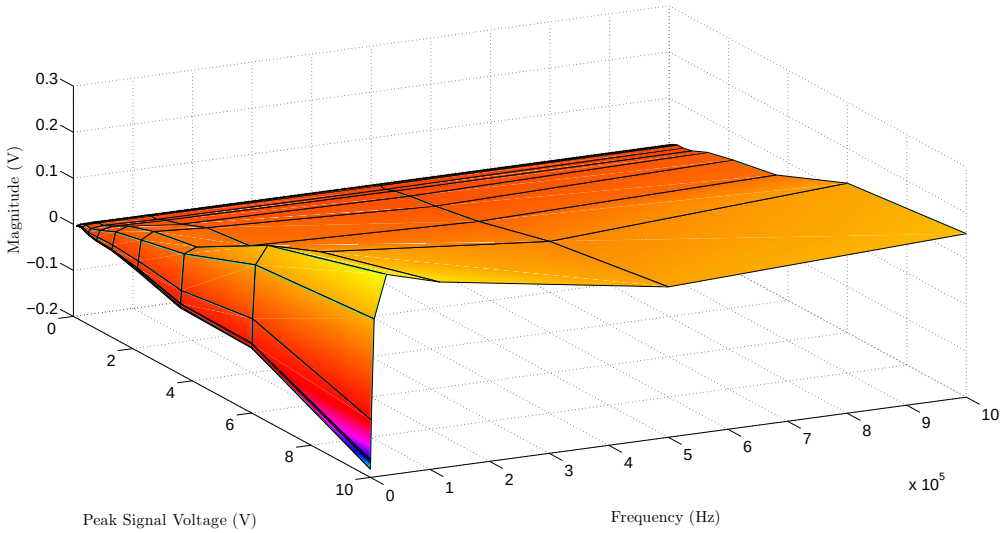

Figure 302: plot of the difference between the ideal maximum signal magnitude and the measured maximum signal magnitude for all test frequencies and voltages for channel 4 of the tektronix tps2024 oscilloscope

input voltages from the measured input voltages for channel 2 of the unit 1 Tektronix TDS2002 oscilloscope — as shown by Figure: (304) —, a similar surface plot to Figure: (303) was obtained, and the maximum observed deviation appears to have remained relatively consistent at 500mV above the ideal input signal. While such observations are somewhat expected — especially after comparison with a secondary channel on the same

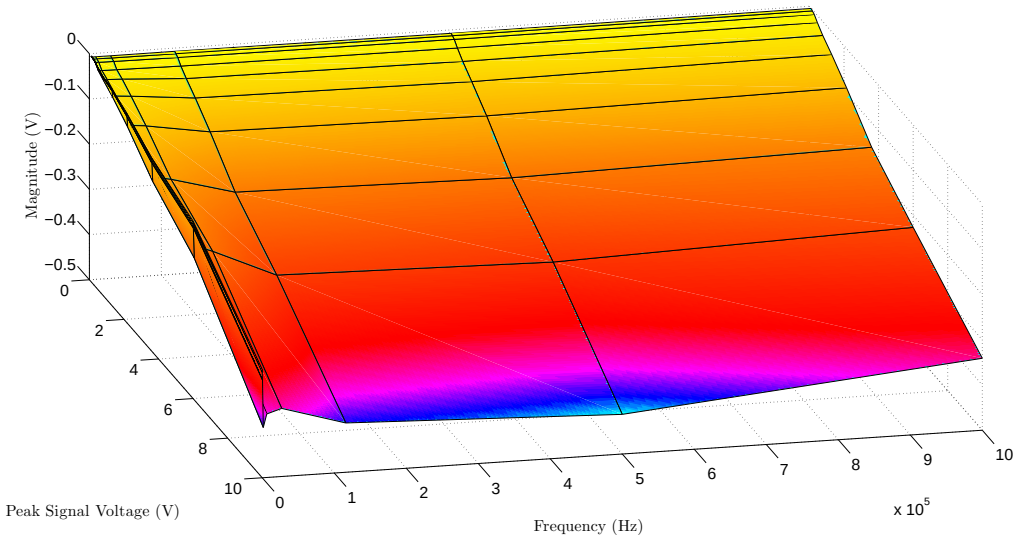

Figure 303: plot of the difference between the ideal maximum signal magnitude and the measured maximum signal magnitude for all test frequencies and voltages for channel 1 of the unit 1 tektronix tds2002 oscilloscope

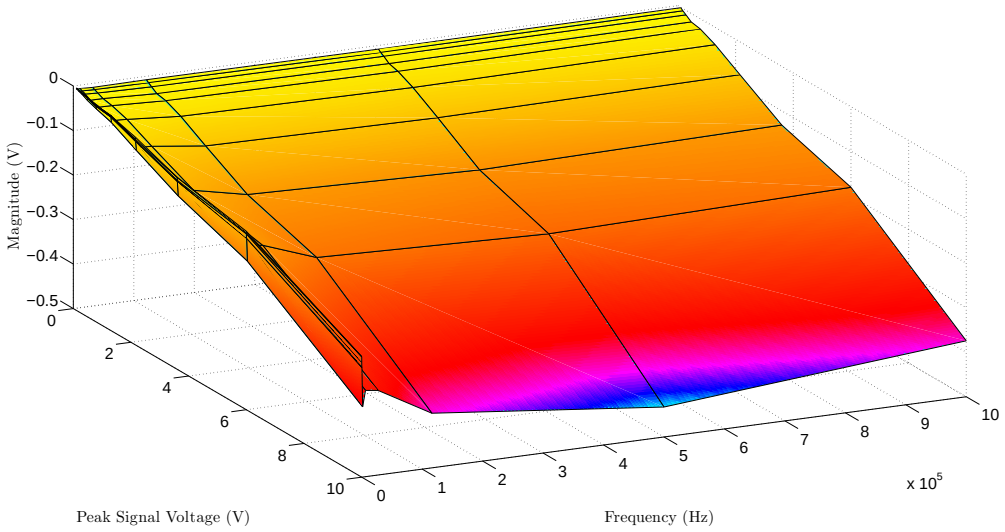

Figure 304: plot of the difference between the ideal maximum signal magnitude and the measured maximum signal magnitude for all test frequencies and voltages for channel 2 of the unit 1 tektronix tds2002 oscilloscope

oscilloscope —, yet, as it has been previously observed, such assumptions should be proven rather than assumed, and it is definitively a metaphoric good sign that this particular oscilloscope unit is acquiring signals relatively consistently between its two acquisition channels in terms of the acquired signal magnitudes measured.

Likewise, upon visually inspecting the difference obtained after subtracting the ideal input voltages from the measured input voltages for channel 1 of the unit 2 Tektronix TDS2002 oscilloscope — as shown by Figure: (305) —, a similar surface plot to Figure: (299) and Figure: (300) was obtained — this attribute inherently implies that the maximum deviation of the magnitude of the signal measured was 400 mV higher than the ideal signal —, although the, previously discussed, 1 kHz trough is not as prevalent within Figure: (305), and while such observations are somewhat moot under the circumstances, yet the substantial lack of this 1 kHz trough seems to indicate a probe to scope attribute more so than a internal function generation problem — since the former would be unique to the oscilloscope channel, while the latter would be consistent across all oscilloscope

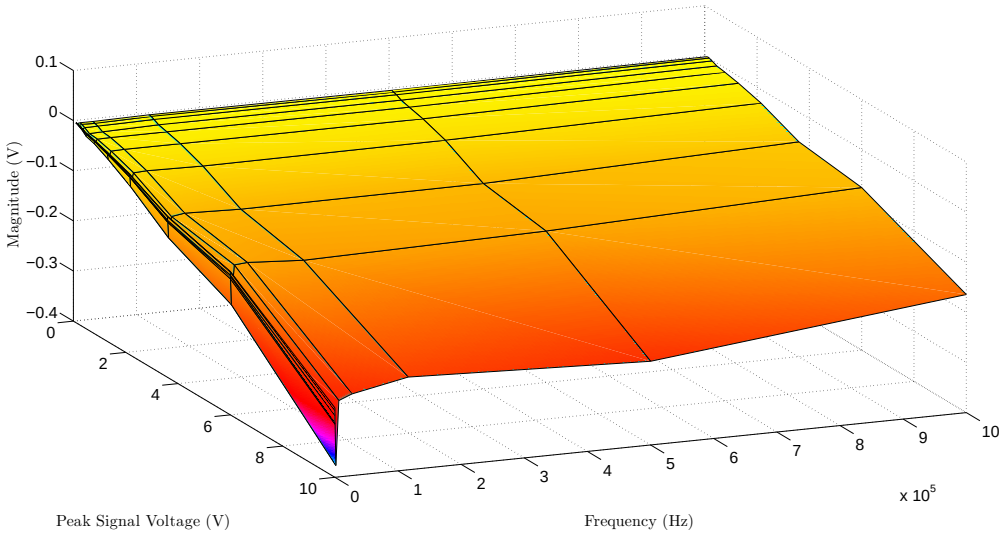

Figure 305: plot of the difference between the ideal maximum signal magnitude and the measured maximum signal magnitude for all test frequencies and voltages for channel 1 of the unit 2 tektronix tds2002 oscilloscope

measurements.

Conversely, upon visually inspecting the difference obtained after subtracting the ideal input voltages from the measured input voltages for channel 2 of the unit 2 Tektronix TDS2002 oscilloscope — as shown by Figure: (306) —, a similar surface plot to Figure: (305) was obtained, and the maximum observed deviation appears to have remained relatively consistent at 400mV above the ideal input signal. While such observations are, again, somewhat expected — especially after comparison with a secondary channel on the same oscilloscope —, yet, while this might be redundant, as it has been already previously observed, such assumptions should be, once again, proven rather than assumed, and — based upon the observed consistency — it is definitively a metaphoric good sign that this particular oscilloscope unit is acquiring signals relatively consistently between its two acquisition channels in terms of the acquired signal magnitudes measured.

Nevertheless, upon visually analyzing Figure: (299), Figure: (300), Figure: (301), Figure: (302), Figure: (303), Figure: (304), Figure: (305), and Figure: (306), it becomes apparent that the measurements obtained become substantially less accurate when the

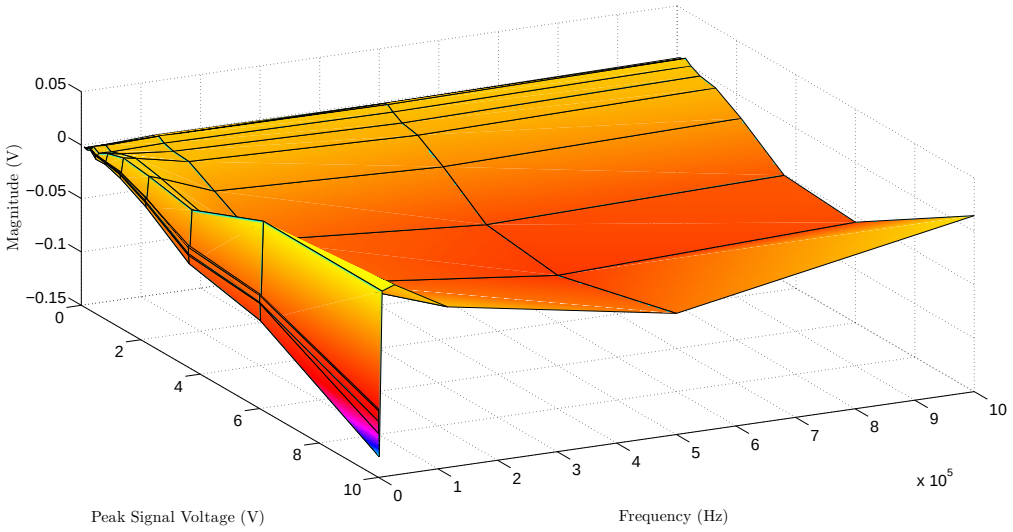

Figure 306: plot of the difference between the ideal maximum signal magnitude and the measured maximum signal magnitude for all test frequencies and voltages for channel 2 of the unit 2 tektronix tds2002 oscilloscope

input signal magnitude is significantly above 6V peak — with the worst case scenario occurring when the input signal magnitude is set to 10V peak — and that these observed deviations — despite being substantially sizable at higher voltages — are relatively consistent across the frequency spectrum being examined. Conversely, with this being said, such observations inherently imply that the highest amount of CIE effects possibly encountered would be approximately 960mV, a figure that incorporates 60mV in AC CIE effects — although this value is somewhat underestimated because spectral magnitudes could add cumulatively if the cosine term was in phase —, 300mV DC CIE effects, and a 600mV signal deviation that was previously discussed, and while observing nearly 1V of CIE effects would be rather appalling; however, this particular visual manifestation of CIE effects would be extremely unlikely since all CIE effects encountered would have to manifest themselves such that they are both subtractive and synchronous — a highly unlikely possibility — and — for the sake of argument — even if these effects did somehow become synchronized , there overall additive and subtractive nature would make it somewhat difficult to immediately visually identify, since, for example, the input signal could be 600mV higher than the desired signal, while the oscilloscope passively attenuates — through CIE effects — 300mV, thus making the observed deviation only 300mV rather then 900mV.

Likewise, while it could be argued — if it has not already been argued — that the observable measurements obtained — after performing a acquisition — is what ultimately matters in terms of determining the amount of CIE effects encountered, yet a blatant disregard for the cumulative nature of such effects is not advised since, once again, such effects can be extremely difficult to predict — particularly in terms of additive or reductive manifestation —, and if the acquisition device being utilized is entering a multitude of different environmental conditions — a notable example being the portable EKG which paramedics

frequently utilize in the field —, such environmental variations could significantly change the observable CIE effects encountered — even if the CIE effect profile was reasonably well known — and — assuming for the moment, that the DSP algorithm implemented, within such a device, made static assumptions regarding the amount of CIE effects observed, rather than utilize assumptions based upon the actual CIE effect profile — could potentially produce incorrect results when the device was moved. Conversely, while the CIE effect profile presented is predominantly focused upon actively acquired measuring techniques — like bioimpedance spectroscopy (BIS) — such profiling techniques are also valid for passive acquisition as well — although additional amplification stages are generally required when performing passive acquisitions and these additional amplification stages would naturally require, the previously discussed, CIE effect profiling.

Conversely, while such musings are definitively important, another interesting observation is obtained upon briefly analyzing the percentile relationship between the input signal and the CIE effects encountered — in this particular case the DC CIE effects were utilized since they were larger in magnitude — relative to the input signal for each of the instrumentational acquisition zones — an attribute that will loosely segment the applied test voltages into three distinct operational regions, the first region being the lower zone (voltages around and below 2V), the second region being the middle zone (voltages somewhere between 2V and 6V), and the last region being the high zone (voltages well above 6V). Likewise, upon calculating the CIE effect percentage within each zone — a task easily achieved by taking the measured CIE effects, dividing that voltage by the input voltage, and then multiplying the result obtained by 100 — as depicted within Table: (14) —, it appears that — in terms of CIE effect manifestation — the lower zone , by far, possesses the highest ratio of CIE effects to input signal encountered, although the high zone is ap-

proaching a similar percentile. Yet, as it was previously mentioned, such percentages are based upon the attribute that the input signal will be defined by the operational region — previously mentioned —, and this is not always the case, especially since it is possible to force the oscilloscope to operate within a particular magnitude region, while — at the same time — varying the input signal magnitude — an attribute that will either greatly increase or decrease the percentile values obtained depending upon whether the signal was increased or decreased in magnitude.

Table 14: percentile relationship between the input signal and the measured DC CIE effects

Zone	Input Voltage	DC CIE Effect Voltage	Percent
Lower	0.1	0.003485	3.49
Lower	2.15	0.02249	1.05
Middle	3.6	0.05136	1.43
Middle	6	0.03819	0.64
High	10	0.289	2.89

Nevertheless, although the information, previously discussed, is extremely important in terms of obtaining a high fidelity acquisition — especially the process of creating an accurate AC and DC CIE effect profile —; however, another — oftentimes unconsidered — type of CIE effect also exists, and this undiscussed CIE effect occurs when the instrumentation — being utilized — is unable to acquire a measurement synchronously — an attribute that will be referred to as temporal CIE effects. While the fundamental concept of temporal CIE effects is — at least within the electrical engineering discipline — nothing definitively new — although if further proof is required, a preliminary investigation into the concept of signal aliasing, Nyquist sampling, and communication latency, would provide more than adequate evidence —; however, such associations are generally only considered within the design phase of a application — like, for example, the development of a communication system — , yet when it comes to the utilization of a commercial acquisition device, there seems to be

a metaphoric unspoken tendency to let such concepts fall to the metaphoric wayside. While such descriptions are admittedly somewhat ambiguous — after all it is rather difficult to definitively know what every end consumer mentally considers prior to using a commercial acquisition device —; nevertheless, it is easily conceivable that a consumer could potentially assume that, because all of the acquisition channels are within the same device, that the acquisitions obtained would be synchronized, and such assumptions — as it will soon be shown — are not necessarily correct.

Conversely, with this being said, given that the nature of this particular problem primarily involves identifying a temporal shift between two acquired signals that are — notably — unrelated to a material effect — or in other words, the signal is assumed to manifest itself in temporal synchronicity at the input of every acquisition channel —, the acquisition delay between the two signals can be mathematically calculated — a process that is fundamentally analogous to visually determining the phase shift between two signals. Likewise, while there are a number of techniques available to calculate the time delay or phase angle between two signals; however, because there is typically a substantial amount of CIE effects inherently embedded within most acquired signals — an attribute that makes most automatic phase analysis techniques, like FFT or finding the crosscorrelation maximum typically inaccurate —, it was decided that the Matlab zero crossing method previously developed — within the CIE effect and spectral leakage subsection — could be utilized to obtain the temporal delay between two signals, as shown by the MATLAB code shown within Appendix E script 23, and then applied to the — previously observed — oscilloscope channels, such that the index shift — or discreet phase shift — could be visually examined.

Similarly, upon application of this particular technique to the Tektronix TPS2024 channel 1 input signal and the Tektronix TPS2024 channel 1 input signal, as shown by Figure:

(307) — admittedly this particular comparison is not overly beneficial, but it does demonstrate that the method utilized is functioning correctly —, it becomes apparent that there is no visible discrete time delay present, at least upon performing the phase comparison between the two signals, and this result was inherently expected given that the signals being compared were exactly the same — thus this plot serves as the visual representation of what a ideal acquisition device would look like across all input channels.

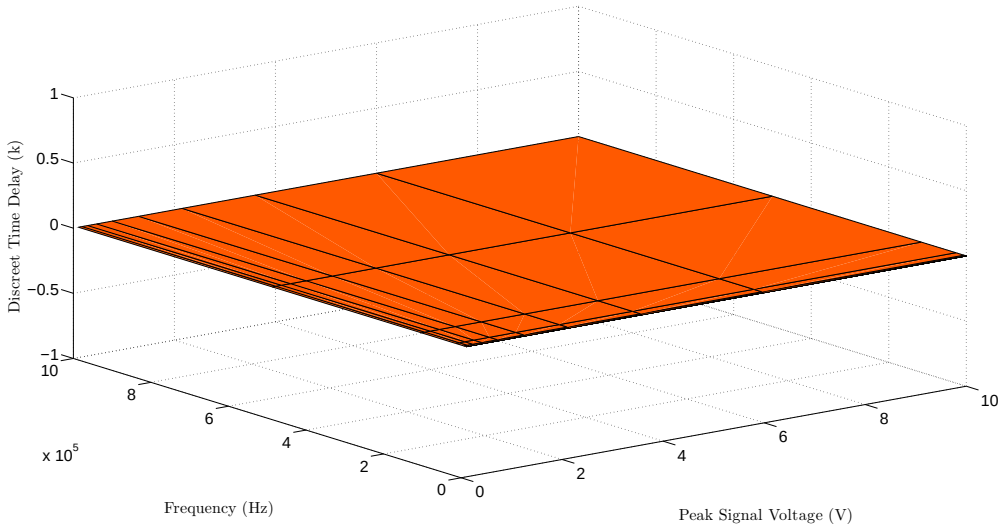

Figure 307: plot of the discreet temporal delay between the tektronix tps2024 channel 1 versus the tektronix tps2024 channel 1

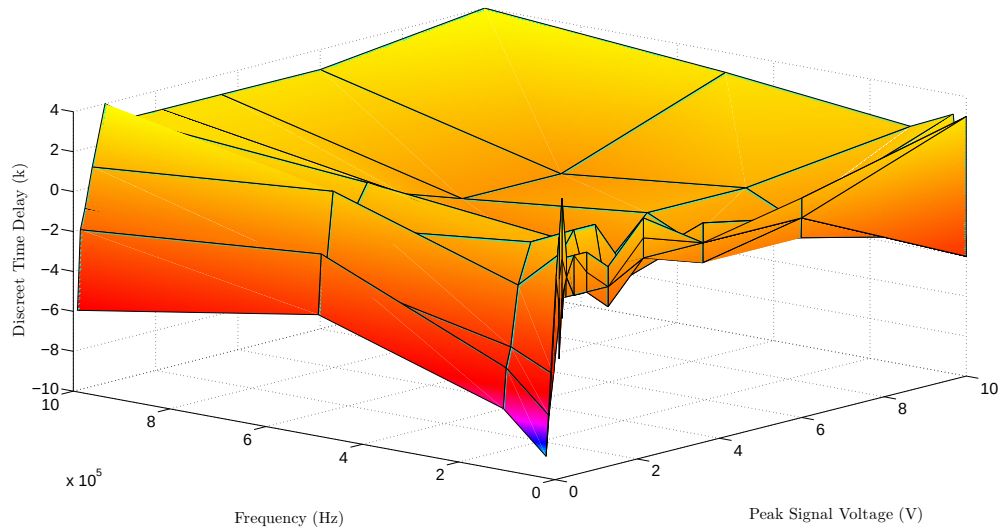

Figure 308: plot of the discreet temporal delay between the tektronix tps2024 channel 1 versus the tektronix tps2024 channel 2

Conversely, while the ideal scenario — shown within Figure: (307) — does provide a good mental image of what a synchronous acquisition device would visually look like; however, upon application of this particular technique to the Tektronix TPS2024 channel 1 input signal and the Tektronix TPS2024 channel 2 input signal — noting the prior layman assumption that local acquisition channels should resemble Figure: (307) —, as shown by Figure: (308), it becomes apparent that discreet sample delays, not only exist between local acquisition channels, but also very in amount depending upon the input voltage and sample frequency being applied. Likewise, based upon the information visually presented within Figure: (308), it appears that a maximum offset of 4 to 6 samples — of the oscilloscopes 2500 samples — should be expected, and while such offsets are — in truth — somewhat minor depending upon the sample rate being utilized, yet such inherent delays are generally unexpected, particularly amongst local acquisition channels.

Similarly, upon application of this particular technique to the Tektronix TPS2024 channel 1 input signal and the Tektronix TPS2024 channel 3 input signal, as shown by Figure: (309), a somewhat similar sample delay is observed — as was shown within Figure: (308)

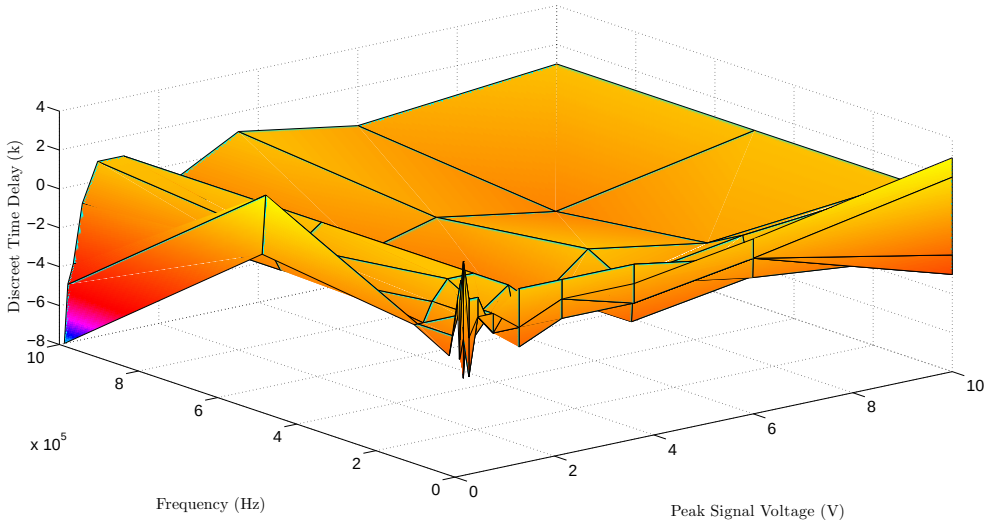

Figure 309: plot of the discreet temporal delay between the tektronix tps2024 channel 1 versus the tektronix tps2024 channel 3

— with the notable exception being a slight increase in the overall maximum sample delay observed — from 6 to 8 samples. While, some similarities does exist between Figure: (308) and Figure: (309), it visually appears that Figure: (309) is far more inconsistent across the voltage and frequency spectrum than Figure: (308), and such observations are particularly disheartening — especially for someone who held the belief that local acquisition channels sampled synchronously.

Conversely, upon application of this particular technique to the Tektronix TPS2024 channel 1 input signal and the Tektronix TPS2024 channel 4 input signal, as shown by Figure: (310), a somewhat similar sample delay is observed — as was shown within Figure: (309) —, which is a metaphoric good sign, since some acquisition similarity implies that a somewhat generic technique can be implemented to compensate for such delays; however, based upon the information presented within Figure: (308), Figure: (308), Figure: (309), and Figure: (310), it seems that a maximum 4 to 6 bin sample delay should be expected between oscilloscope channel acquisitions depending upon the voltage and frequency being measured.

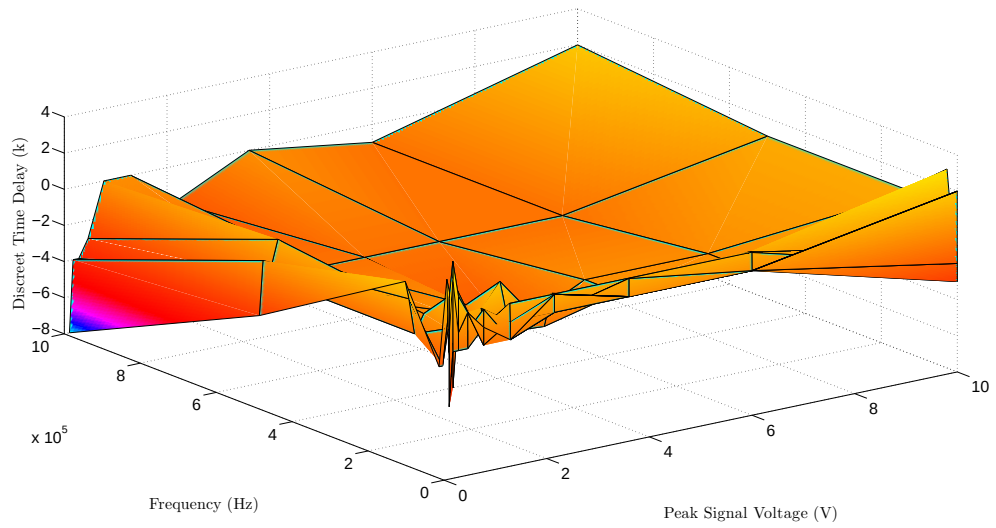

Figure 310: plot of the discreet temporal delay between the tektronix tps2024 channel 1 versus the tektronix tps2024 channel 4

Likewise, upon application of this particular technique to the Tektronix TDS2002 unit 1 channel 1 input signal and the Tektronix unit 1 TDS2002 channel 2 input signal, as shown by Figure: (311), a slight increase in the sample delay — from a maximum offset of 6 to a maximum offset of 10 — is observed — which is to be expected given that a different oscilloscope unit is being examined —; however, the overall delay seems to remain relatively consistent over the assortment of voltages and frequencies applied, at least relative to the Tektronix TPS2024 — although this attribute might be because the Tektronix TPS2024 utilizes isolated grounding for each channel, while the TDS2002 utilizes a common ground for all its input channels.

Conversely, upon application of this particular technique to the Tektronix TDS2002 unit 2 channel 1 input signal and the Tektronix unit 2 TDS2002 channel 2 input signal, as shown by Figure: (312), a similar maximum offset sample delay — of 10 — is observed; however, a substantial amount of offset variation over input voltage and frequency is observed — relative to the information obtained within Figure: (311) —, and while some variation is expected, especially since a different oscilloscope unit is being examined, yet

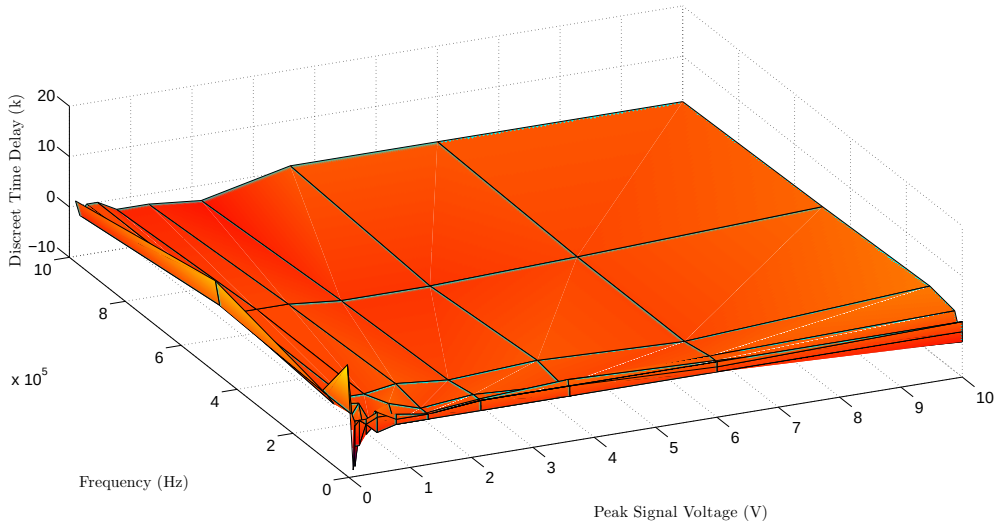

Figure 311: plot of the discreet temporal delay between the tektronix tds2002 unit 1 channel 1 versus the tektronix tds2002 unit 1 channel 2

the observation of such inconsistencies, particularly between similar oscilloscope models, is inherently problematic and such observations tend to strengthen the importance of properly assessing the acquisition instrumentation being utilized prior to attempting to perform a high fidelity signal acquisition. Nevertheless, while the discreet temporal delay observed between oscilloscope channels within the same acquisition unit is a rather profound — if not unexpected — discovery; however, a more substantial problem arises upon attempting to simultaneously synchronize multiple oscilloscope units — a task that is generally necessitated within complex bioimpedance spectroscopy experiments —, and while there is a underlying notion — amongst some researchers — that synchronization can be obtained through the utilization of triggering techniques, yet a similar examination of such methods — as it will soon be shown — seems to conclude otherwise.

Likewise, with this being said, because there is a number of possible comparisons that can be performed between the oscilloscope configurations currently demonstrated, it seems reasonably convenient to select the first channel of the TPS2024 oscilloscope as a fixed point of comparison — an attribute that was previously done within the individual TPS2024

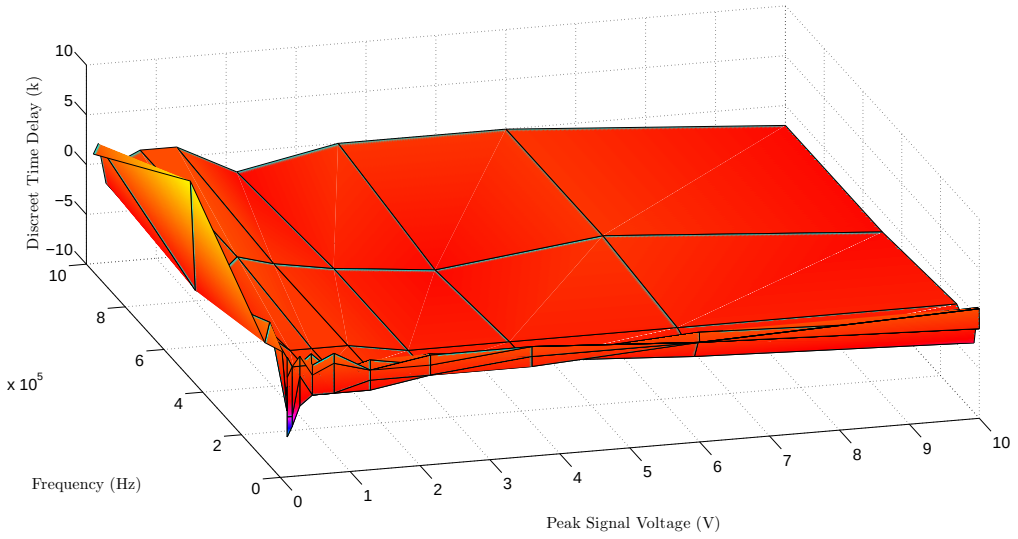

Figure 312: plot of the discreet temporal delay between the tektronix tds2002 unit 2 channel 1 versus the tektronix tds2002 unit 2 channel 2

temporal channel analysis —, since any other correlations can be derived through the utilization of simplistic algebra based upon the information already obtained. Conversely, upon application of this particular technique to the Tektronix TPS2024 channel 1 input signal and the Tektronix unit 1 TDS2002 channel 1 input signal, as shown by Figure: (313), a substantial delay — with a maximum offset of around 40 — is observed between the acquisition obtained within the TPS2024 and the TDS2002 oscilloscopes even after synchronous triggering techniques were implemented.

Likewise, upon application of this particular technique to the Tektronix TPS2024 channel 1 input signal and the Tektronix unit 1 TDS2002 channel 2 input signal, as shown by Figure: (314), a similar delay — with a maximum offset of around 40 — is observed between the acquisition obtained within the TPS2024 and the TDS2002 oscilloscopes, and while this delay is somewhat substantial; however, at least it remains relatively consistent between the two oscilloscope units — an attribute that makes compensation easier.

Conversely, upon application of this particular technique to the Tektronix TPS2024 channel 1 input signal and the Tektronix unit 2 TDS2002 channel 1 input signal, as shown

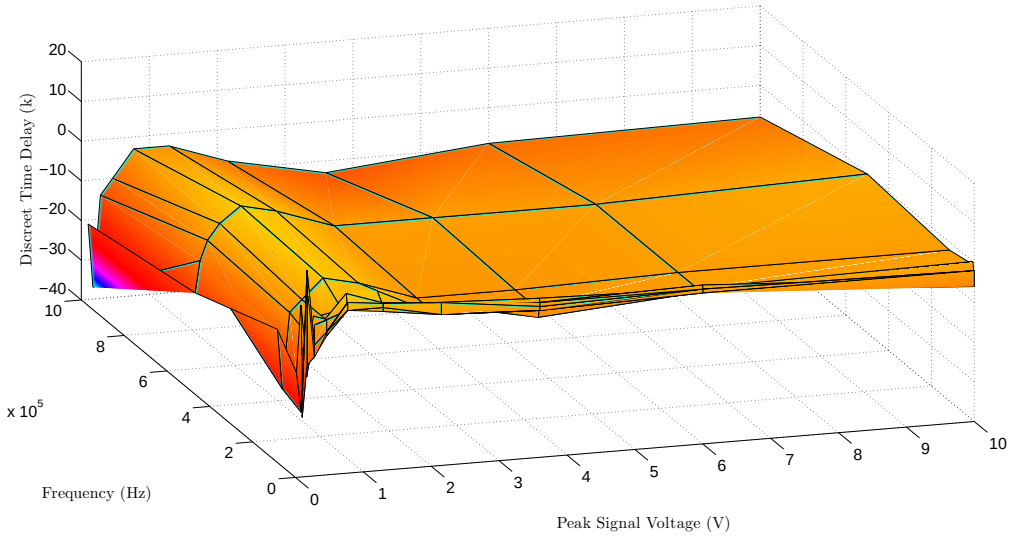

Figure 313: plot of the discreet temporal delay between the tektronix tps2024 channel 1 versus the tektronix tds2002 unit 1 channel 1

by Figure: (315), a similar — but slightly smaller — delay — with a maximum offset of around 30 — is observed between the acquisition obtained within the TPS2024 and the TDS2002 oscilloscopes, and while this delay is still substantial; however, at least it is remotely related to the delay observed within the prior TDS2002 acquisition unit.

Likewise, upon application of this particular technique to the Tektronix TPS2024 channel 1 input signal and the Tektronix unit 2 TDS2002 channel 2 input signal, as shown by

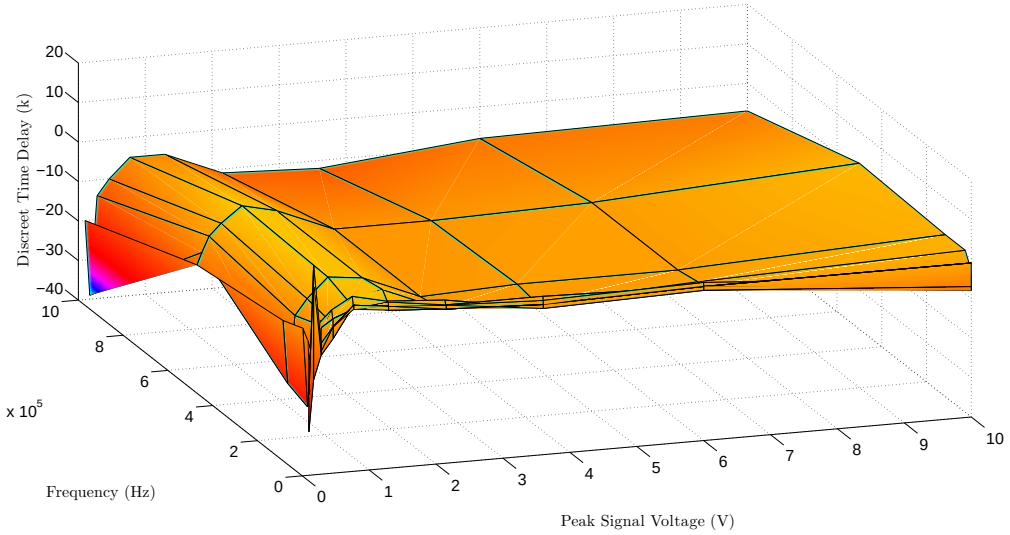

Figure 314: plot of the discreet temporal delay between the tektronix tps2024 channel 1 versus the tektronix tds2002 unit 1 channel 2

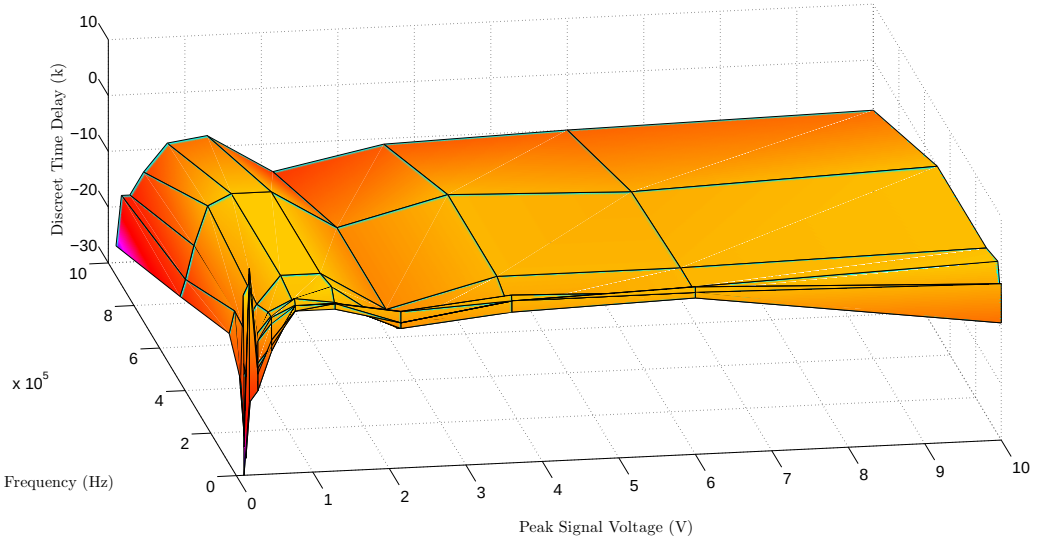

Figure 315: plot of the discreet temporal delay between the tektronix tps2024 channel 1 versus the tektronix tds2002 unit 2 channel 1

Figure: (316), a similar — but slightly larger — delay — with a maximum offset of around 40 — is observed, and observations of this nature are somewhat problematic to work with, primarily because such observations seemingly incorporate local acquisition delays within the remote acquisition delay, and the occurrence of such inconsistencies typically implies that each acquisition channel will need to be individually compensated for in order to remove the introduction of temporal CIE effects. Nevertheless, while the visual analysis of the, previously depicted, temporal surfaces can provide a substantial amount of intuitive information into the nature of the acquisition delays encountered; however, it is oftentimes more beneficial to observe the numerical average and peak values for such circumstances — as provided within Table: (15) —, since such values can be utilized to estimate the acquisition delays encountered when attempting to develop temporal CIE effect compensation methods.

Conversely, upon visually examining Table: (15), it becomes apparent that there is a substantial difference between the average and maximum temporal delays encountered — an attribute that is to be expected —, and based upon such observations it would

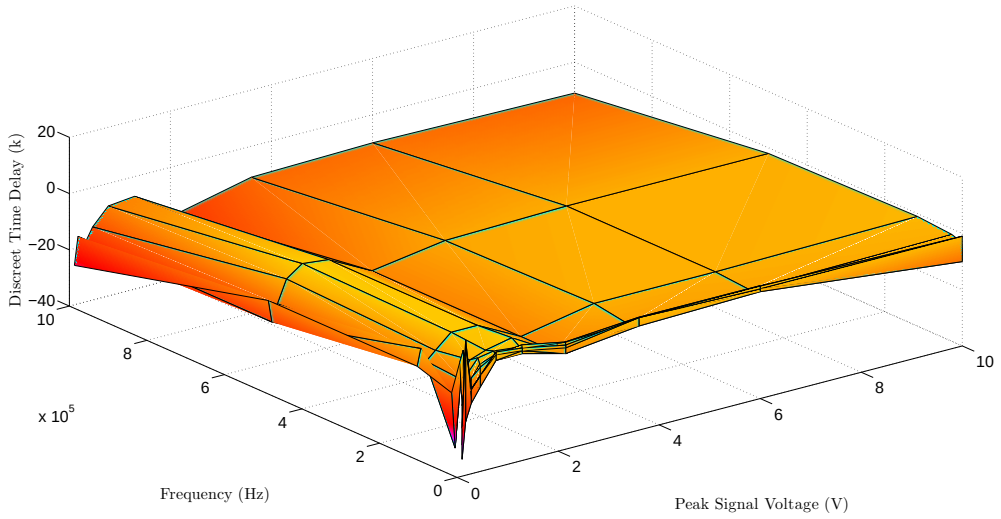

Figure 316: plot of the discreet temporal delay between the tektronix tps2024 channel 1 versus the tektronix tds2002 unit 2 channel 2

Table 15: temporal sample delay observed between oscilloscope channel acquisitions

Unit A	Channel A	Unit B	Channel B	Mean	|Mean|	Max -	Max +
TPS2024	1	TPS2024	1	0	0	0	0
TPS2024	1	TPS2024	2	-0.2909	1.5636	-9	4
TPS2024	1	TPS2024	3	-0.3909	1.1	-8	3
TPS2024	1	TPS2024	4	-0.1273	1.0909	-8	4
TDS2002 1	1	TDS2002 1	2	-0.0364	1.2364	-9	11
TDS2002 2	1	TDS2002 2	2	-0.2909	1.1091	-6	9
TPS2024	1	TDS2002 1	1	-3.9818	5.3636	-37	12
TPS2024	1	TDS2002 1	2	-4.0182	5.4182	-39	13
TPS2024	1	TDS2002 2	1	-5.4364	6.0182	-30	7
TPS2024	1	TDS2002 2	2	-5.7273	6.2545	-34	8

appear that the absolute average delay encountered is somewhere between 1 and 6 discrete sample units — depending upon the comparison being made — which overall is not overly disruptive, although the larger delays observed — particularly the 34 discrete sample units delay — could be somewhat problematic, particularly when utilizing a analytical technique — like least-squares estimation or a nonlinear solver —, since such delays would be directly translated into a energy storage component — either a inductor or capacitor — that would be incorrectly added within the model created in order to compensate for these, previously depicted, temporal CIE effects. Likewise, with this being said, while the profiling and compensation of discrete temporal CIE effects is a extremely important part of the high fidelity acquisition process, it is worth mentioning that it could also be propose that such descriptions should also include the examination of any passive energy storage element inherently embedded within the acquisition hardware. While the physical logic behind such an approaches cannot be directly faulted; however, because such effects are extremely dependent upon the test apparatus being utilized, it seems more appropriate to address such concerns when examining the apparatus model rather than within the, previously presented temporal CIE effects analysis discussion, and while this particular approach is, for the most part, a matter of personal preference, this is the approach that was taken within this dissertation.

6.3.7 Test Boundaries and Electromagnetics

The fundamental rationale behind the test boundaries and electromagnetics section was to develop a simplistic method of determining the effective operational range of bioimpedance spectroscopy devices before the effects of electromagnetic distortions — like signal reflection — predominated the acquired results. Likewise, based upon the results obtained it was concluded that — given the high impedance nature of biomaterials — that bioimpedance spectroscopy — or active electrode impedance analysis — should avoid utilizing input frequencies above 1MHz in order to prevent the occurrence of electromagnetic effects — typically described as electromagnetic standing wave phenomenon — from developing upon the acquisition instrumentation interconnections that, in turn, not only substantially disrupts the electrical potential measured at the oscilloscope input, but modifies the phase information obtained and generally, invalidates the biomaterial acquisition as a whole unless highly specialized broadband impedance transformers are utilized to effectively transition from a 50 ohm electrical interconnection to the high input impedance of a biomaterial — although such techniques are not recommended unless necessitated by the intended end application.

Conversely, while the information presented within the previous sections — primarily referring to AC and DC CIE effect modeling — is definitively an important attribute that must be considered when attempting to obtain a high fidelity bioelectrical acquisition; however, while such attributes are inherently substantial, careful examination of the, previously provided, sections will yield a curious observation concerning the CIE effects testing boundaries selected since such attributes were not directly addressed. Likewise, with this being said, while the voltage boundaries utilized — within the AC and DC CIE effects

tests — are reasonably straightforward to justify, especially since the Tektronix AFG3102 function generator has a maximum output voltage of 10V peak under high-Z conditions and the — unspecified MAX530 — digital to analog converter circuit — utilized within the DC CIE effects test — was configured for a maximum output of around 2.5V; however, while the voltage boundary selected is readily explainable, the frequency boundary selected is not as metaphorically transparent, especially since the Tektronix TPS2024 and Tektronix TDS2002 oscilloscopes are capable of acquiring signals far above the 1 MHz boundary selected within the AC CIE effects test.

Nevertheless, although the acquisition hardware — previously mentioned — is physically capable of acquiring a higher frequency signal and, for that matter, the AFG3102 function generator is also capable of producing signals above 1 MHz; yet there is some inherent wisdom in the anonymous quote "*Just because you can, doesn't mean you should*", and such sentiments are further vindicated upon visually examining the electrical attributes that occur as a result of high frequency electromagnetic phenomenon. While the underlying theoretical mechanisms that govern electromagnetic propagation and electromagnetic radiation (EMR) are generally considered to be theoretically complex, but are seemingly well understood — although this notion will be questioned to some extent within the next section —; however, such occurrences are the underlying rationalization behind the self-imposed CIE effect testing boundaries selected — as it will soon be visually demonstrated. Conversely, with this being said, upon configuring a testing apparatus, in which a — un-

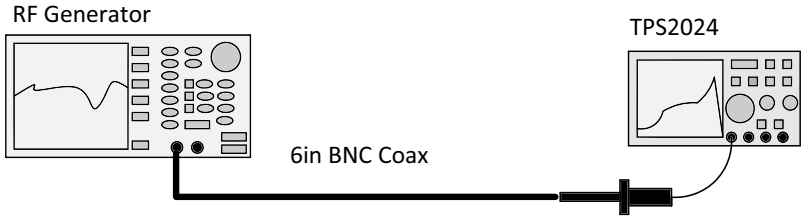

Figure 317: conceptual diagram of a high-frequency function generator connected to channel 1 of the tektronix tps2024 oscilloscope through a six-inch bnc coaxial cable

specified — commercially calibrated RF generator was connected to the first channel of the Tektronix TPS2024 oscilloscope through a 6 inch length of BNC coaxial cable — a commercial RF generator was utilized, in this particular case, in order to create a baseline reference since the Tektronix AFG3102 is not strictly considered to be a RF generator —, as shown by Figure: (317), and acquisitions taken of both the observed magnitude and phase for frequencies ranging from 1.2MHz to 100MHz, as shown by Figure: (318) and Figure: (319), it becomes apparent that some interesting effects are occurring slightly after the 10MHz applied RF input frequency.

Likewise, while the phase information presented within Figure: (319) is somewhat dubious — because of its acquisition through the utilization of the FFT operation —, although the changes observed — relative to the original measurement — are reasonably accurate. Yet, upon visually examining the information obtained within Figure: (318), it becomes apparent that substantial changes in magnitude are definitively observed at frequencies above 10MHz — relative to the 800 mV lower frequency magnitude selected — and such changes — as it has already been discussed within the CIE effects section — are extremely

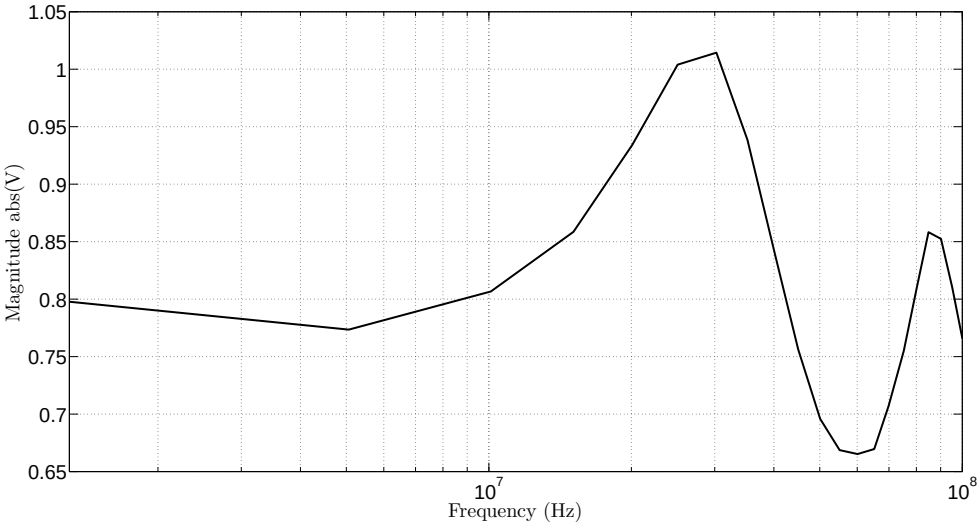

Figure 318: magnitude plot of a 6in coax cable connecting the tps2024 oscilloscope channel 1 to a rf signal generator

problematic in terms of acquiring a high fidelity measurement — as such variations distort the desired signals magnitude and phase —, and such effects are predominantly occurring because of a impedance mismatch between the RF signal generator, the transmission cable, and the oscilloscope channel input that, in turn, has resulted in the creation of a electromagnetic standing wave that changes in magnitude at the oscilloscope input as the frequency is increased.

Conversely, upon substituting the 6 inch BNC coaxial cable with a 12 inch BNC coaxial

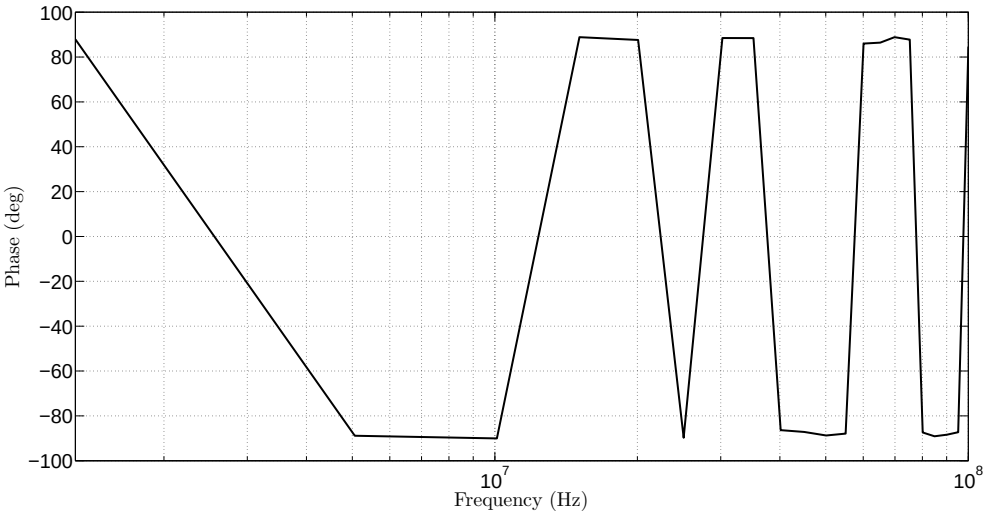

Figure 319: phase plot of a 6in coax cable connecting the tps2024 oscilloscope channel 1 to a rf signal generator

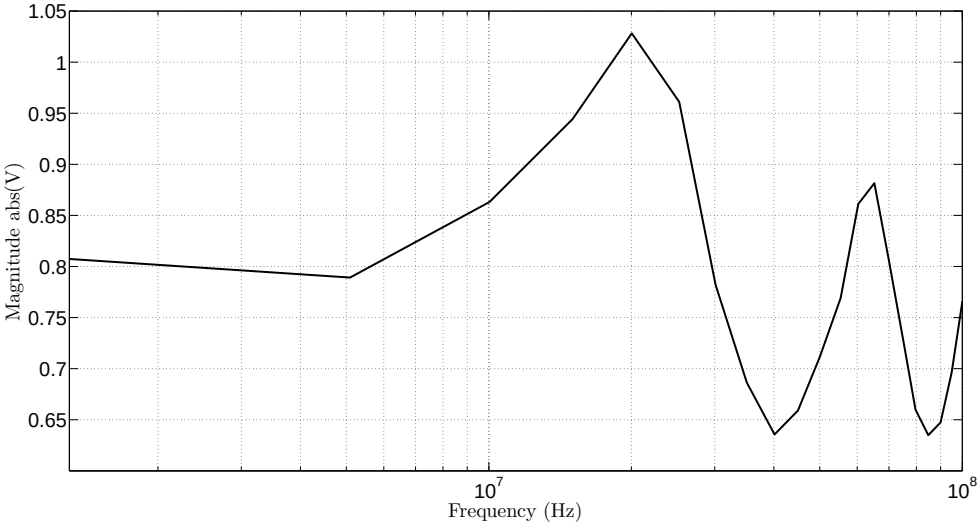

Figure 320: magnitude plot of a 12in coax cable connecting the tps2024 oscilloscope channel 1 to a rf signal generator

cable, as shown by Figure: (320) and Figure: (321), it becomes somewhat evident that the changes in magnitude observed — or rather, the point in which the electromagnetic standing wave begins to occur is shifted to the left — which implies a downward frequency shift — and such observations are expected since the occurrence of such effects are dependent upon the length of the transmission structure utilized — since the longer a transmission structure is, the lower the frequency of occurrence is. Likewise, it is the occurrence of these electromagnetic effects — once again, predominantly metaphorically governed by both frequency selection and interconnection length — are ultimately the rationale behind why the operational frequency boundaries selected were implemented, especially since having to compensate for the occurrence of a high frequency electromagnetic phenomenon is something that should be avoided — if possible — in order to help alleviate some of the CIE compensation complexities encountered — as the identification and removal of the, previously discussed, CIE effects is already an inherently complex task without having to incorporate additional electromagnetic theory into such compensation techniques.

Nevertheless, while such observations are paramount in discerning the rationale behind

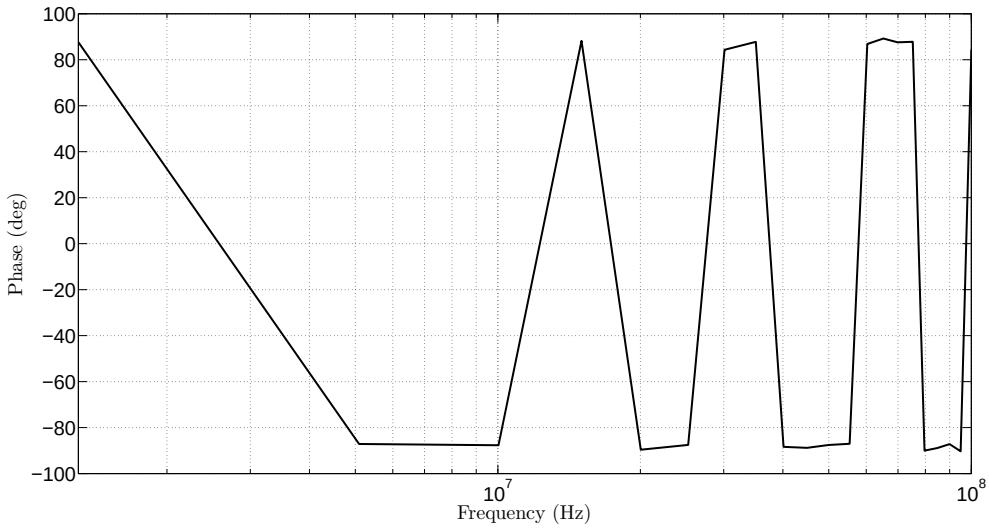

Figure 321: phase plot of a 12in coax cable connecting the tps2024 oscilloscope channel 1 to a rf signal generator

the CIE test frequency boundary selected; however, an internal desire for thoroughness mandates that the test, previously discussed, be examined through the utilization of the Tektronix AFG3102 function generator — rather than the commercial RF generator that notably used (either a TNC or N) to BNC adapter — and upon preforming the same test with the 6 inch BNC coaxial cable — using the Tektronix AFG3102 function generator —, as shown by Figure: (322) and Figure: (323), it becomes apparent that a similar standing wave phenomenon is observed slightly before the 10MHz frequency — as was the case

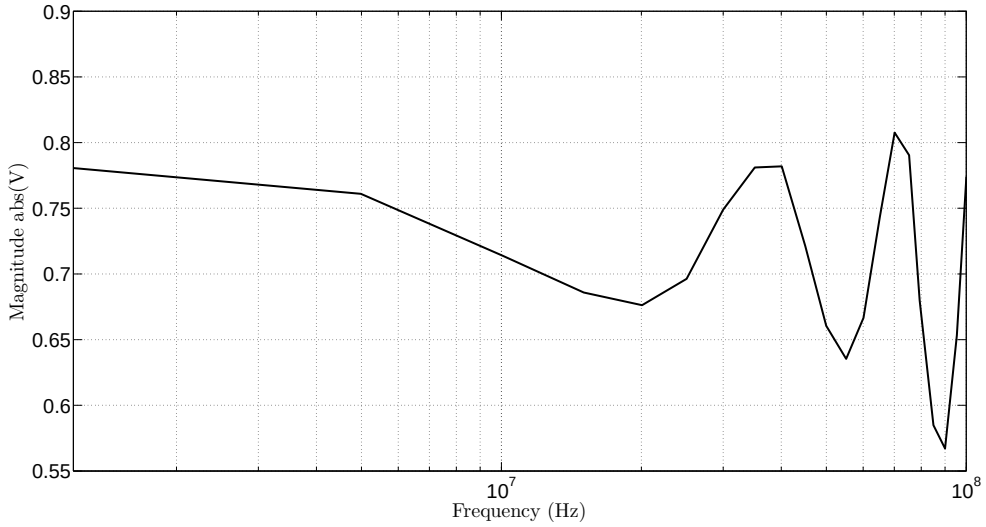

Figure 322: magnitude plot of a 6in coax cable connecting the tps2024 oscilloscope channel 1 to a afg3102 signal generator

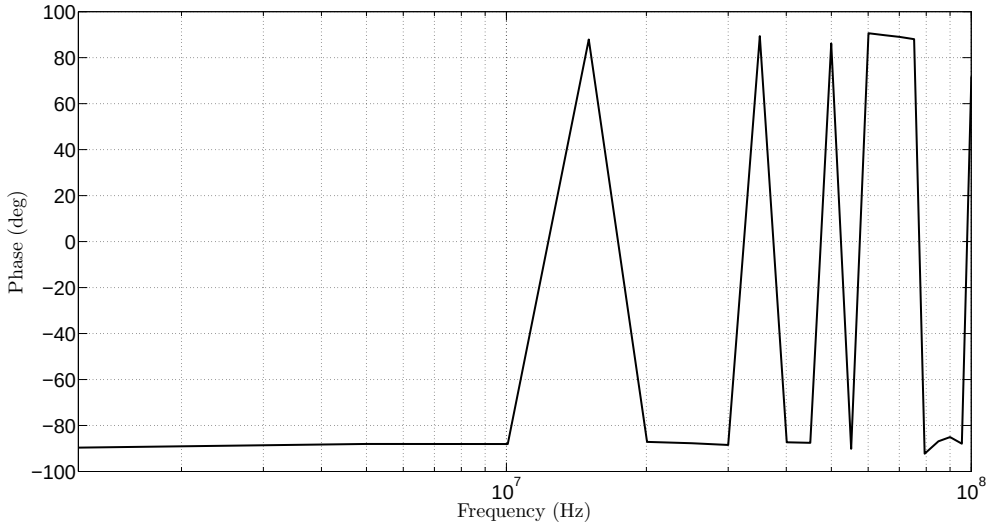

Figure 323: phase plot of a 6in coax cable connecting the tps2024 oscilloscope channel 1 to a afg3102 signal generator

within the previous RF experiments.

Conversely, upon substituting the 6 inch BNC coaxial cable with the 12 inch BNC coaxial cable, as shown by Figure: (324) and Figure: (325), a similar shifting of the, previously discussed, standing wave is observed and the occurrence of such effects are, once again, predominantly visible upon exceeding frequencies slightly before 10MHz. Similarly, as it was previously mentioned within the commercial RF function generator test, it is important to recognize that values before the 1.2MHz starting point remained consistent

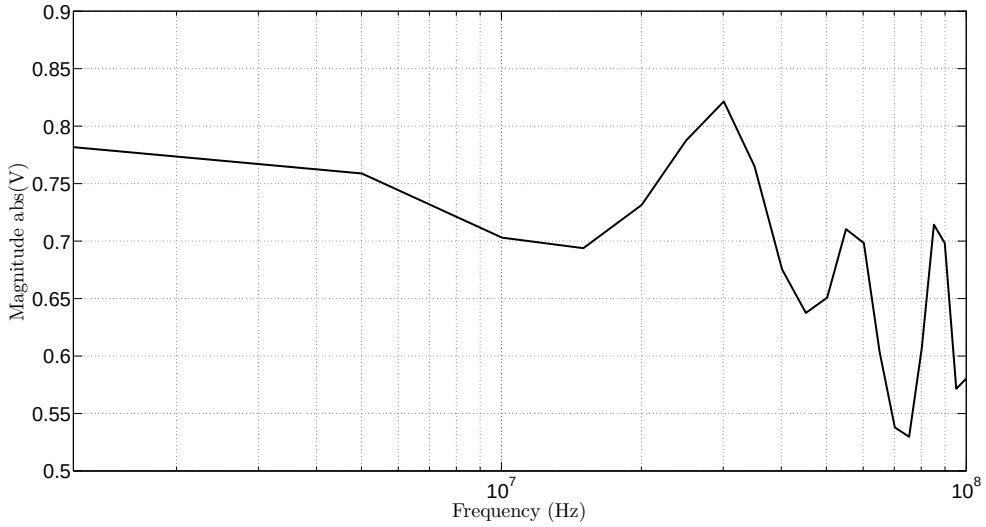

Figure 324: magnitude plot of a 12in coax cable connecting the tps2024 oscilloscope channel 1 to a afg3102 signal generator

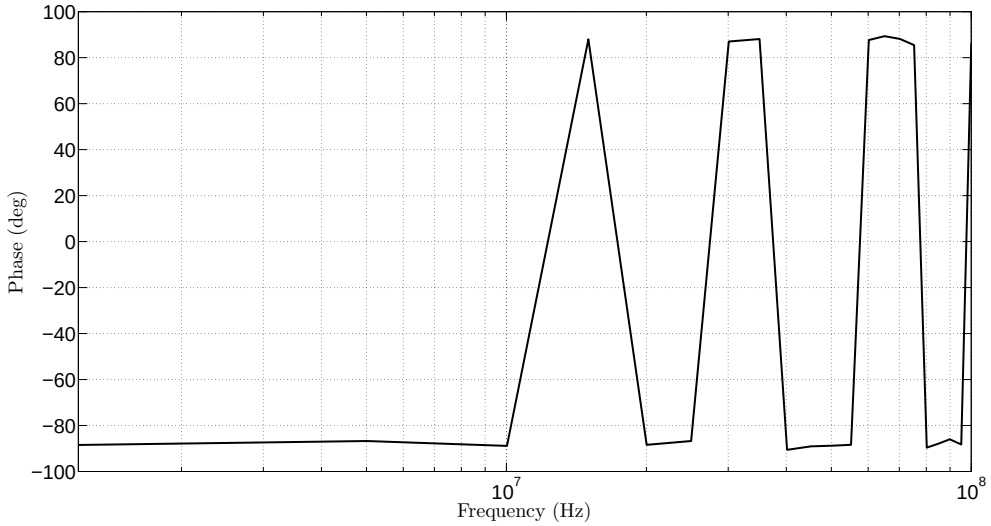

Figure 325: phase plot of a 12in coax cable connecting the tps2024 oscilloscope channel 1 to a afg3102 signal generator

— around 800 mV — and the phase angle observed also remains reasonably consistent until this starting point — although the phase obtained from the utilization of the FFT operation does require offset adjustment prior to any analytical comparison. Likewise, based upon such observations, and given the fact that 1 foot of cable is typically too short for most instrumentational acquisitions — arguably 3 to 6 feet would be a more realistic assumption, especially if a connection to a human is required —, and based upon the fact that the transmission structure implemented is not — necessarily — inherently designed for RF operation — a notable example being EKG probe leads that are simply a singular length of wire connected to an electrode pad — it seems rather appropriate to restrict any experiments conducted to frequencies below 1MHz, particularly since the characteristic impedance of the transmission structure, along with its length, can substantially modify — typically lowering — the frequency in which a standing wave will occur — especially since, based upon such observations, the apparatus configurations utilized was likely operating near the region, in which, such effects could manifest themselves.

6.3.8 Unbalanced Transmission Line Theory

The fundamental rationale behind the unbalanced transmission line theory section was to present the unique discoveries made regarding the creation of a generalized transmission line theory that is valid for modeling unbalanced transmission lines — unlike the classical transmission line theory that is not applicable to many of today's common transmission structures such as striplines, microstrips, and instrumentation probes because they are unbalanced. Likewise, the unbalanced transmission line theory developed expands the classical theory into a new fundamental theory that is applicable to all two-conductor transmission lines and develops a theory for the generation of the nonlinear convection current — the mysterious common-mode current — and includes its radiation parameters

in the transmission line equations. Conversely, the theory developed — for the generation of this convection current — enabled the creation of a transmission line model that can be used in the analysis and understanding of the nonlinear behaviors of unbalanced transmission lines observed in the field, and this model has been verified via computer simulations and laboratory tests. Likewise, it is worth noting that the spatial distribution of the convection current in an unbalanced transmission line is more controllable than the radiating current in a conventional antenna, and the theory presented within this section can be expanded to help design traveling wave narrow-beam antenna systems — which is objective of future research.

Likewise, based upon such observations, another curious attribute that was observed — as the direct result of experimenting with frequencies above 1MHz — was the curious observation of a sudden change in oscilloscope measurements upon the movement of a human hand close to the apparatus interconnections — a task that was inadvertently required, prior to the development of automation acquisition software, in order to save laboratory observations [410]. Conversely, while the havoc and aggravation this particular phenomena created was paramount, and a number of solutions were eventually implemented to workaround this particular occurrence — such solutions included twisting wires, limiting the maximum test frequency to 1MHz, and the development of automatic data collection methods —; however, while such solutions were effective in overcoming the problem, they were far from being intellectually gratifying and, as a result, some time was spent attempting to identify the underlying mechanism behind this particular phenomena [410].

Similarly, with this being said, given that such problems seem to be predominately associated with the acquisition of laboratory measurements under RF conditions, a preliminary investigation into the radiated emissions from transmission lines was conducted and

— based upon this investigation — it was discovered that some of the earliest information on the subject dates back to the circa 1900's and seems to attribute such — emissions — with the formation of "*common-mode currents*" within the transmission line structure; however, while such information seems to be commonly known within the subject of electromagnetics, yet the underlying mechanism that created these "*common-mode currents*" is, in fact, not completely understood [411] [412] [410]. Conversely, while the effects created by transmission line radiation — referring to the propagation characteristics — are generally observed within a laboratory as a signal distortion over a set of specific frequency ranges — an attribute that was thoroughly presented within the previous section of this chapter. Likewise, further investigation reveals — as it was previously proposed —, that this particular phenomenon — referring to transmission line radiation — is also responsible for the observed sudden changes in propagation characteristics when objects, such as human hands, are moved around the transmission line, and such effects are typically attributed to — or rather described by — the equivalent transfer admittance of the cable [413] [414] [410].

Likewise, while the association of such effects to equivalent transfer admittance has produced some beneficial models surrounding coaxial equivalent transfer admittance — although sometimes this admittance is ignored —; however, based upon the phenomena observed within the laboratory, it seems prevalent to investigate this phenomena further, predominantly thru examining unbalanced transmission lines and the underlying mechanisms that results in both electromagnetic radiation and the nonlinear propagational characteristics observed [415] [410]. Conversely, further investigation into the nonlinear propagational characteristics of unbalanced transmission lines reveals that the radiation observed from unbalanced transmission structures is of great interest to the scientific community, and

after a* "*period of extensive research" into this particular subject, a understanding beyond the contemporary published theory was obtained, insofar as, first, what is referred to as* "common-mode current"* within contemporary literature is, in fact, a convection current that arises within transmission lines with a unequal conductor resistance. Second, that the flow of conduction currents, within such transmission lines, gives rise to unbalanced charge distributions and the flow of convection currents. Third, that the time-variation of these convection currents results in electromagnetic radiation occurring along the transmission line. Forth, that convection currents can alter the propagational characteristics of the transmission line in a complex way — as in cause a number of nonlinearities to occur that are simply not modeled by the classical transmission line theory within contemporary literature — noting — once again — that the theory developed is applicable to the evaluation and design of all two-conductor transmission lines and that none of the generalizations of the classical theory found within the examined literature can correctly model the radiation or the flow of nonlinear convection currents; although a paper by Chandia and Flores ([416]) does model the quantum mechanical effects of discrete electrical charges in mesoscopic scale, but does not consider the flow of bulk convection currents or radiation

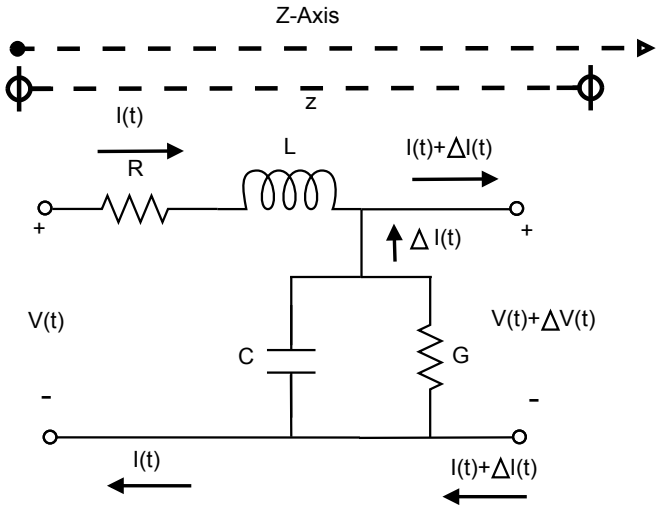

Figure 326: classical incremental transmission line model

[417] [418] [419] [420] [421] [422] [423] [410].

Likewise, with this being said, because the classical transmission line theory has been developed based on the assumption that an incremental length (ℓ) of transmission line can be modeled by the equivalent circuit — as shown by Figure: (326) —, the transmission line equations that are based on this model are given by Equation: (502) and Equation: (503)

$$\frac{\partial v\left(t,z\right)}{\partial z} = -R\, i\left(t,z\right) - L\frac{\partial i\left(t,z\right)}{\partial t} \tag{502}$$

$$\frac{\partial i\left(t,z\right)}{\partial z} = -G\, v\left(t,z\right) - C\frac{\partial v\left(t,z\right)}{\partial t} \tag{503}$$

, where $v\left(t,z\right)$ is the differential voltage between the two lines and $i\left(t,z\right)$ is the conduction current in the two transmission lines at time (t) and location (z). Similarly, the combined resistances and inductances of both transmission lines per unit length (PUL) are modeled by (R) and (L), while the PUL capacitance — between the two transmission lines — is modeled by (C), and the PUL conductance (G), is representing the losses in the dielectric that is separating the two conductors [410].

$$\frac{\partial v_1\left(t,z\right)}{\partial z} = -R_1\, i\left(t,z\right) - L_1\frac{\partial i\left(t,z\right)}{\partial t} - L_{12}\frac{\partial i(t,z)}{\partial t} \tag{504}$$

$$\frac{\partial v_2\left(t,z\right)}{\partial z} = R_2\, i\left(t,z\right) + L_2\frac{\partial i\left(t,z\right)}{\partial t} + L_{21}\frac{\partial i(t,z)}{\partial t} \tag{505}$$

$$\frac{\partial i\left(t,z\right)}{\partial z} = -G\left(v_1\left(t,z\right) - v_2\left(t,z\right)\right) - C\frac{\partial\left(v_1\left(t,z\right) - v_2\left(t,z\right)\right)}{\partial t} \tag{506}$$

Conversely, as it might be expected, this model assumes that the transmission line is balanced and that the resistances and inductances of the two conductors can be lumped

together, and upon examining these assumptions by rewriting Equation: (502) and Equation: (503) in terms of signals and parameters for each line, as shown by Figure: (327),— where $v_1(t, z)$ and $v_2(t, z)$ are the scalar voltages of the two conductors with respect to some common reference, R_1 and R_2 are the two PUL conductor resistances, and $i(t, z)$ is assumed to be the same in each conductor for a given time and location as required by the classical theory — noting that, all the four inductive terms in Equation: (504), Equation: (505), and Equation: (506) are derived from Faraday's Law of Induction, that the inductances L_1 and L_2 account for the PUL voltages induced in each conductor by its own current, that the inductances L_{12} and L_{21} account for the PUL voltages induced in each conductor by the current in the other, and that the magnetic flux linking the transmission line circuit, due to the current in one of the conductors, induces an equal PUL voltage in both conductors — a fact that requires the equality of L_1 with L_{21} and the equality of L_2 with L_{12}.

Likewise, The magnetic flux linking the transmission line circuit due to the current $i(t, z)$ in one of the conductors is equal to the magnetic flux linking the circuit due to the same current $i(t, z)$ in the other conductor; therefore, $L_1 = L_2$ and based upon such observations

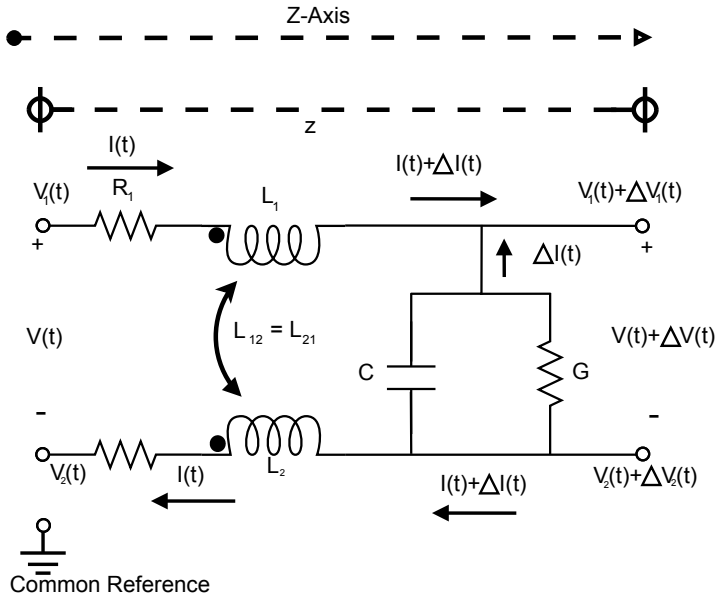

Figure 327: unbalanced incremental transmission line model

it can be firmly concluded that all four inductances in Equation: (504), Equation: (505), and Equation: (506) are equal and each inductance equals one-fourth of the total PLU inductance of the transmission line L, that the inductive voltage gradients on the right hand sides of Equation: (504) and Equation: (505) are magnetically induced and are equal along the two conductors, and that the resistive voltage gradients $-R_1\, i(t,z)$ and $R_2\, i(t,z)$ are due to nonzero charge gradients along the transmission line conductors.

Conversely, when $R_1 \neq R_2$, the charge distributions associated with the two resistively induced voltage gradients cannot totally balance each other via the shunt admittance and this results in an unbalanced charge distribution along the conductor with the higher resistance. Likewise, when $R_1 > R_2$, the voltage gradient that is balanced along the two conductors is $\pm\left(R_2\, i\,(t,z) + 0.5L\frac{\partial i(t,z)}{\partial t}\right)$, where the unbalanced component is obtained by adding Equation: (504) to Equation: (505) and letting $\frac{\partial v_u(t,z)}{\partial z} \triangleq \frac{\partial v_1(t,z)}{\partial z} + \frac{\partial v_2(t,z)}{\partial z}$, and this component is given by the classical theory as Equation: (507), while the unbalanced voltage gradient that develops will be along the conductor with the higher resistance — in this case conductor 1 [410].

$$\frac{\partial v_u\,(t,z)}{\partial z} = (R_2 - R_1)\; i\,(t,z) \tag{507}$$

Likewise, the unbalanced charge distribution associated with the unbalanced voltage gradient does not contribute to the balanced charges on the shunt capacitance. Thus, the voltage across the transmission lines capacitance is not the same as the transmission line's differential voltage $v_1(t,z) - v_2(t,z)$. This is a significant discovery and shows that the last term in Equation: (506) is invalid, and that the classical transmission line theory is not applicable to unbalanced transmission lines. Conversely, the unbalanced charges are

free to interact with charges in the surrounding matter and with unbalanced charges at neighboring locations along the higher resistance conductor — in this case conductor 1 —, and when the ratio of the transmission lines length (ℓ) to the wavelength (λ) is much smaller than unity, this interaction is mainly via stray capacitances with the surrounding matter [410]. Otherwise, unbalanced charge distributions of both polarities being develop — in this case along conductor 1 — and interact; giving rise to the convection current observed. Likewise, the importance of this unbalanced convection current is that it leads to the creation of transverse electromagnetic radiation since — within any two-conductor transmission line — the balanced line charge density — in $\frac{C}{m}$ — is given by Equation: (508), where $v(t, z)$ is the voltage across the transmission line capacitance c , while — within an unbalanced transmission line with $R_1 > R_2$ — the line charge density is $\rho_2(t, z) = -\rho_b(t, z)$ for the conductor with the higher resistance and is given by Equation: (509), where ρ_u is the unbalanced line charge density — once again, in $\frac{C}{m}$. Similarly, the unbalanced charge distribution that is induced by the conduction current — as shown by Equation: (507) — travels along the conductor as a transverse wave with a phase velocity equal to that of the conduction current, and this wave motion does not result in convection of charges along the conductor; however, consider the distribution of unbalanced charges along the higher resistance conductor — conductor 1 — at time t , as shown by Figure: (329), noting how the heights of the charge columns represent the magnitude and u_p denotes the phase velocity of the traveling wave $\rho_u(t, z)$, while the convection velocities of the m^{th} and the n^{th} unbalanced electrons are denoted by u_m and u_n [410].

$$\rho_b(t, z) = c\, v(t, z) \tag{508}$$

$$\rho_1(t,z) = \rho_b(t,z) + \rho_u(t,z) \tag{509}$$

Conversely, the life cycle of an unbalanced charge begins and ends when it is induced and then picked up by the flow of the conduction current, and assuming that $i(t,z)$ and $\rho_u(t,z)$ waves are traveling in the $+z$ direction then it can also be assumed that the leading edge of each charged packet will be located on the right — as shown by Figure: (329). Likewise, since — within a metallic conductor — the electrons are mobile, while positively charged holes are stationary, thus, within Figure: (329), the subscript t denotes the trailing edge of a unbalanced electron packet, subscript l denotes the leading edge of a unbalanced electron packet, subscript m denotes the minima of the $\rho_u(t,z)$ wave, and subscript p denotes the maxima of the $\rho_u(t,z)$ wave. Similarly, the locations z_{lB} and z_{rB} denote the transmission lines left and right boundaries respectively, and as the conduction current wave travels in the $+z$ direction, it picks up unbalanced electrons between z_t and z_m locations and deposits them between z_m and z_l locations, thus moving the unbalanced electron wave along with it [410]. Conversely, when an unbalanced electron is induced within the leading half of a negative packet, it experiences an acceleration in the $+z$ direction, according to Coulomb's law — as shown by Equation: (510), where a_n is the acceleration of the nth electron, e is the charge of an electron, m_e is the mass of an electron, ϵ is the effective permittivity of the medium, and d_n is the distance between the n^{th} electron and its counterpart hole

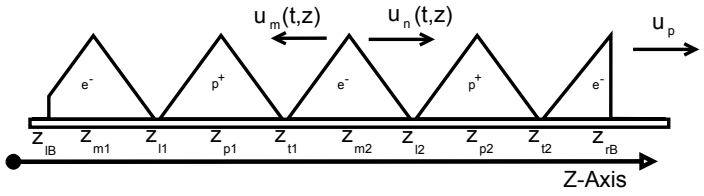

Figure 328: a traveling unbalanced charge distribution along an unbalanced transmission line

within the leading positive packet — and, this acceleration gives rise to electron velocities and the observed convection current [410].

$$a_n = \frac{e^2}{4\pi\epsilon\, m_e d_n^2} \tag{510}$$

Likewise, as the distance between the n^{th} electron and the leading positive packet increases with velocity $u_p - u_n$, the n^{th} electron pairs with the closest positive hole — that has not yet been paired with a electron —, and the location of the n^{th} electron shifts away from the leading edge of the negatively charged packet, while the location of its — complementary hole — shifts away symmetrically from the trailing edge of the positively charged packet. Similarly, the distance d_n increases with velocity $2\,(u_p - u_n)$, and this distance varies from a minimum value — which is on the order of the inter-atomic distance of the conductor's material — to the maximum value of $\frac{\lambda}{2}$, and beyond the distance of $\frac{\lambda}{2}$ the electron becomes closer to the lagging positive packet, thus the electron begins to decelerate, stop, and then re-accelerate in the opposite direction — until the electron is now in the trailing half of the convection packet and the distance d_n begins to decrease at the rate of $2\,(u_p + u_n)$ [410].

Conversely, the variation in the convection velocities of the unbalanced electrons leads to electromagnetic radiation, and radiation forces oppose the Coulomb forces on the convection electrons and the acceleration in Equation: (510) is impeded, while the unbalanced charges are part of the conduction process and the flow of convection current distorts the conduction current, such that, the unbalanced electrons induced between z_m and z_l locations experience different accelerations and attain convection velocities that depend on the locations where they are induced [410]. Likewise, with this being said, upon denoting t_0

as the time and z as the location within the leading half of the negative packet where the group n of the unbalanced electrons are induced then $d_n = 2\left(z_l(t) - z\right)$ — noting that when $u_p \gg u_n$ the distance d_n increases at the rate of about $2u_p$ and can be defined by $d_n = 2\left(z_l(t_0) + u_p\ (t - t_0) - z\right)$ —, thus the unimpeded velocity of this group of electrons for $t_0 < t < t_{\frac{\lambda}{4}}$ can be determined from integration of Equation: (510) — as shown by Equation: (511) — where $\xi \triangleq \frac{e^2}{16\pi\epsilon\, m_e\, u_p}$ and $t_{\frac{\lambda}{4}} = t_0 + \frac{1}{u_p}\left(\frac{\lambda}{4} + z - z_l(t_0)\right)$ is the time beyond which the group n electrons experience accelerations in the opposite direction [410].

$$u_n(t,z) = \int_{t_0}^{t} \frac{e^2\, dt}{16\pi\epsilon\, m_e \left[z_l(t_0) + (t - t_0)\, u_p - z\right]^2} = \xi\left[\frac{1}{z_l(t_0) - z} - \frac{1}{z_l(t) - z}\right] \tag{511}$$

Similarly, within the leading half of a negatively charged packet, the unbalanced electrons induced are at the leading edge of the packet — within the inter-atomic distance from the trailing edge of the leading positive packet — attain the maximum possible velocity because they experience the strongest amount of Coulombic forces, and this maximum velocity — which is in the $+z$ direction — does not depend on t_0 , thus can be approximated by Equation: (512), where d_a is the inter-atomic distance in the conductor material, $t_{max} = \frac{1}{u_p}\left(\frac{\lambda}{4} - 2d_a\right)$, and $\frac{\lambda}{4} - 2d_a$ is the length of the region within the leading half of the negative packet where unbalanced electrons experience Coulomb acceleration — noting that u_{max} becomes negligible for wavelengths in the order of d_a [410].

$$u_{max} = \int_{0}^{t_{max}} \frac{e^2\, dt}{16\pi\epsilon\, m_e \left(d_a + u_p t\right)^2} = \xi\left[\frac{1}{d_a} - \frac{1}{d_a + u_p t_{max}}\right] \tag{512}$$

Likewise, to confirm the assumption that $u_p \gg u_n$, it can be shown that upon evalu-

ating Equation: (512) for copper — which has a $d_a \approx 256pm$, $\epsilon = \epsilon_0$, and $u_p = 2 \times 10^8 \frac{m}{s}$ — that for frequencies less than 10^{16} Hz, Equation: (512) evaluates to $u_{max} \approx 1230 \frac{m}{s}$. Similarly, the convection current $i_c(t, z)$ can be defined — using the average velocity of the unbalanced electrons $u_a(t, z)$ by Equation: (513) —, and the unbalanced electrons that contribute to the average velocity at (t, z) are those that are induced at z between the time t_n and t , where t_n is the time when the leading edge of the unbalanced electron wave is at $(z + d_a)$. Conversely, with this being said, the average velocity of the unbalanced electrons at any location within the leading half of a negative packet can be determined from the weighted average of $u_n(t, z)$ over the range $(z + d_a) \leq z_l(t_0) \leq z_l(t)$ with $t_n \leq t_0 \leq t$ — as shown by Equation: (514) — where the variable of integration is the location of the leading edge of the unbalanced electron wave at the time t_0 when each group of electrons with density $\rho_u(t_0, z)$ is induced at time t_0 and location z [410].

$$i_c(t, z) = \begin{cases} \rho(t, z)\, u_a(t, z); & \rho_u < 0 \end{cases} \tag{513}$$

$$u_a(t, z) = \frac{\int_{z+d_a}^{z_l(t)} u_n(t, z) \rho_u(t_0, z)\, dz_l(t_0)}{\int_{z+d_a}^{z_l(t)} \rho_u(t_0, z)\, dz_l(t_0)} \tag{514}$$

Similarly, in order to evaluate Equation: (514), a simplifying assumption can be made, insofar as, the charge densities of the newly induced electrons at location z over the time $t_n \leq t_0 \leq t$ are the same and independent from $z_l(t_0)$, and this assumption estimates the spatial distribution of $\rho_u(t, z)$ within a triangular waveform in the evaluation of Equation: (514), and results in the cancellation of $\rho_u(t_0, z)$ from the numerator and the denominator

of Equation: (514) which then, using Equation: (511), reduces to Equation: (516) where $2d_a \leq z_l(t) - z \leq \frac{\lambda}{4}$. Likewise, Equation: (516) is valid for any location within the leading half — except at locations d_a from the leading edge of the $\rho_u(t,z)$ wave since the unbalanced electrons will always have zero velocity here —, thus to determine the convection current using Equation: (513), the average velocity of the unbalanced electrons will need to be determined at any location within the trailing half of a negatively charged packet [410].

$$u_a(t,z) = \frac{\xi}{z_l(t) - z - d_a} \int_{z+d_a}^{z_l(t)} \left[\frac{1}{z_l(t_0) - z} - \frac{1}{z_1(t) - z} \right] dz_l(t_0) \tag{515}$$

$$= \frac{\xi}{z_l(t) - z - d_a} \ln\left(\frac{z_l(t) - z}{d_a} \right) - \frac{\xi}{z_l(t) - z} \tag{516}$$

Conversely, since all unbalanced electrons are induced within the leading half, as the $\rho_u(t,z)$ wave travels in the $+z$ direction it will become part of the trailing half with an initial velocity in the $+z$ direction while experiencing accelerations in the $-z$ direction. Similarly, the average velocity of the unbalanced electrons at any location within the trailing half of a negative packet — as shown by Equation: (517), where $z_t(t)$ is the trailing edge of the unbalanced electron packet and $d_a \leq z - z_t(t) \leq \frac{\lambda}{4}$, noting that locations d_a from the trailing edge of the $\rho_u(t,z)$ is where the unbalanced electrons attain there highest velocity in $-z$ direction — such that Equation: (513), Equation: (516), and Equation: (517) can be used to determine the convection current at the interior locations along the line, while — near the boundaries — the unbalanced electrons may have no counterpart holes and may not experience any acceleration. For example, at the left boundary in Figure: (329), the unbalanced electrons between z_{lB} and z_{m1} have no counterpart holes thus do not experience acceleration in the $-z$ direction, yet these electrons maintain the initial

velocities they attain in the $+z$ direction when they are at the peak of the negatively charged packet nearest the left boundary, and because the boundary conditions are time-varying this effect can, at times, apply to regions near the boundaries rather than simply a single location [410].

$$u_a(t,z) = \xi \left[\frac{4}{\lambda - 4\,d_a} \ln\left(\frac{\lambda}{4d_a}\right) - \frac{1}{z - z_t(t)} \right] \tag{517}$$

Likewise, the conduction current at any location along a conductor is defined as the time-rate of the longitudinal flow of conduction electrons at that location, and for the same conduction current to flow in both conductors of an unbalanced transmission line, a greater line charge density develops along the conductor with higher resistance; thus, the algebraic sum of the charge densities along the two conductors is the unbalanced charge density that exists along the conductor with higher resistance. Conversely, as it was previously discussed, this unbalanced charge distribution gives rise to the convection current, and the convection current is internal to the transmission line and is discontinuous at boundaries with lump parameter loads and sources, while the boundary conditions for the conduction current are forced by the external source voltage and load impedance and the convection flow of the unbalanced electrons leads to electromagnetic radiation and to impeding radiation forces that must be accounted for.

Similarly, with this being said, it is customary to use series radiation resistance R_r and inductance L_r to model the radiation forces, and in order to account for the radiation forces directly; consider for the moment the two-conductor unbalanced transmission line — as shown by Figure: (329) —, in which it is assumed that the transmission line conductors

are of length l or ℓ and are in parallel with the z-axis.

Likewise, within Figure: (329), $i(t,z)$ represents the conduction current, $i_c(t,z)$ represents the convection current, and $v(t,z)$ represents the scalar potential across the transmission line's capacitance, and assuming that — Conductor 1 — has a higher resistance than — Conductor 2 —, an unbalanced charge distribution, $\rho_u(t,z)$, will develop along Conductor 1 — similar to Figure: (329). Conversely, this unbalanced charge distribution can be related to the longitudinal component of its electric field via the point form of Gauss' law — as shown by Equation: (520) —, where D_u is the z-component of the electric flux density D resulting from ρ_u , $\nabla\cdot$ is the divergence operator, E_u is the z-component of the electric field intensity resulting from the unbalanced charge distribution, ϵ is the effective permittivity of the medium, and S is the cross-sectional area of the conductor.

$$\nabla \cdot D(t,z) = \frac{\partial D_u}{\partial z} \tag{518}$$

$$= \epsilon \frac{\partial E_u}{\partial z} \tag{519}$$

$$= \frac{1}{S}\rho_u(t,z) \tag{520}$$

Similarly, Equation: (520) relates the unbalanced charge distribution to its own electric field intensity, and this electric field intensity is related to the unbalanced voltage gradient

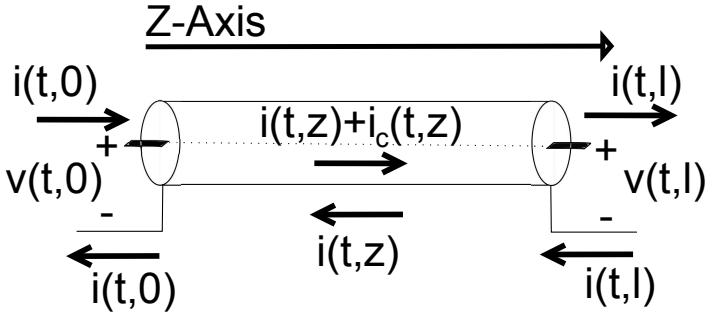

Figure 329: an unbalanced transmission line with $r_1 > r_2$

via $E_u = -\nabla v_u$ or as shown by Equation: (521) — noting that E_u represents the electric field of the unbalanced charges and that the time-derivative of the vector magnetic potential — the $\frac{\partial A}{\partial t}$ term is zero —, thus plugging Equation: (521) in to Equation: (520), solving for $\rho_u(t, z)$ and using Equation: (507), yields Equation: (523) — where $C_v \triangleq \epsilon\, S$ is the volume capacitance in $F\, m$.

$$E_u(t, z) = -\frac{\partial v_u(t, z)}{\partial z} \tag{521}$$

$$\rho_u(t, z) = -C_v \frac{\partial^2 v_u}{\partial z^2} \tag{522}$$

$$= C_v \left(R_1 - R_2\right) \frac{\partial i(t, z)}{\partial z} \tag{523}$$

Likewise, upon solving for the convection current by combining Equation: (513), Equation: (516), Equation: (517), and Equation: (523) — as shown by Equation: (524) — is the so-called common-mode current and it is the source of electromagnetic radiation.

$$i_c(t, z) = \begin{cases} \left[\frac{\xi}{z_l(t)-z-d_a} \ln\left(\frac{z_l(t)-z}{d_a}\right) - \frac{\xi}{z_l(t)-z}\right] \left[C_v \left(R_1 - R_2\right) \frac{\partial i(t,z)}{\partial z}\right]; & \rho_u(t, z) < 0 \text{ and } 2d_a \leq z_l(t) - z \leq \frac{\lambda}{4} \\ \left[\frac{4\xi}{\lambda-4d_a} \ln\left(\frac{\lambda}{4d_a}\right) - \frac{\xi}{z-z_t(t)}\right] \left[C_v \left(R_1 - R_2\right) \frac{\partial i(t,z)}{\partial z}\right]; & \rho_u(t, z) < 0 \text{ and } d_a \leq z - z_t(t) \leq \frac{\lambda}{4} \\ 0; & \rho_u(t, z) \geq 0 \end{cases} \tag{524}$$

Conversely, time-variation of the unbalanced electrons' convection velocities given by Equation: (516) and Equation: (517) results in radiation forces that impede the Coulomb accelerations defined by Equation: (510), and the magnitude of the radiation force on a

convection electron is proportional to the electron's acceleration. Similarly, as the potential energy of the unbalanced charge distribution is converted to the kinetic energy in the motion of the unbalanced electrons, additional potential energy is spent to overcome the opposing radiation forces, the convection electrons attain velocities that are lower than those defined by Equation: (516) and Equation: (517), which are valid only in the absence of radiation, and thus radiation forces can be taken into account by redefining the acceleration in Equation: (510) — as shown by Equation: (525) — where m_r is the proportionality constant in modeling the radiation force as $m_r\, a_n$.

$$a_n = \frac{e^2}{4\pi\epsilon\,(m_e + m_r)\,d_n^2} \tag{525}$$

Likewise, with this definition, all previous equations remain valid with the constant ξ being redefined — as shown by Equation: (526).

$$\xi \triangleq \frac{e^2}{16\pi\epsilon\,(m_e + m_r)\,u_p} \tag{526}$$

Conversely, The convection flow of the unbalanced electrons distorts the conduction current wave shape — referring to Figure: (329) —, and the traveling conduction current wave induces unbalanced electrons within the leading halves of the negative packets between locations z_m and z_l . Likewise, these electrons gain convection velocities and rejoin the conduction electrons in the trailing halves between z_t and z_m locations — or more precisely, when the unbalanced electrons join the conduction current, they have initial velocities that give rise to additional conduction current, distorting its wave shape. Thus, to model the

contribution of the convection flow of the unbalanced electrons to the conduction current, the time-rate at which these electrons interact with the conduction electrons should be determined — noting that Equation: (513) yields Equation: (527), where the first term in Equation: (527) is the time-rate of conversion of the convection current to conduction current and is responsible for the distortion of the conduction current [410].

$$\frac{\partial i_c(t,z)}{\partial t} = u_a(t,z)\frac{\partial \rho_u(t,z)}{\partial t} + \rho_u(t,z)\frac{\partial u_a(t,z)}{\partial t} \tag{527}$$

Likewise, within the trailing-half of the unbalanced electron packet, where $\frac{\partial \rho_u}{\partial t} > 0$, this conversion rate is positive, while within the leading-half, where $\frac{\partial \rho_u}{\partial t} < 0$, the conversion rate is negative. Conversely, this term needs to be included in the unbalanced transmission line equation for the conduction current, and the second term in Equation: (527) is due to time-variation of the convection velocity and, along with the first term, is responsible for electromagnetic radiation, while the convection current $i_c(t,z)$ is used to determine the patterns of radiation from unbalanced transmission lines.

Upon substituting Equation: (523) in the first term in Equation: (527) and include this term in the conduction current equation to obtain the unbalanced transmission line equations, as shown by Equation: (528), Equation: (529), Equation: (530), and Equation: (531) — noting that the boundary conditions for $u_a(t,z)$ are, as it was previously explained, nonstandard .

$$\frac{\partial i(t,z)}{\partial t} + C_v\,(R_1 - R_2)\,u_a(t,z)\frac{\partial^2 i(t,z)}{\partial t\,\partial z} = \begin{cases} -\frac{1}{L}\left[R\,i(t,z) + \frac{\partial v(t,z)}{\partial z}\right] 0; & \frac{\partial \rho_u}{\partial t} \geq 0 \end{cases} \tag{528}$$

$$\frac{\partial i(t,z)}{\partial t} - C_v\,(R_1 - R_2)\,u_a(t,z)\frac{\partial^2 i(t,z)}{\partial t\,\partial z} = \begin{cases} -\frac{1}{L}\left[R\,i(t,z) + \frac{\partial v(t,z)}{\partial z}\right] 0; & \frac{\partial \rho_u}{\partial t} \leq 0 \end{cases} \tag{529}$$

$$\frac{\partial v(t,z)}{\partial t} = -\frac{1}{C}\left[G\,v(t,z) + \frac{\partial i(t,z)}{\partial z}\right] \tag{530}$$

$$u_a(t,z) = \begin{cases} \frac{\xi}{z_l(t)-z-d_a}\ln\left(\frac{z_l(t)-z}{d_a}\right) - \frac{\xi}{z_l(t)-z}; & \rho_u(t,z) < 0 \text{ and } 2d_a \leq z_l(t) - z \leq \frac{\lambda}{4} \\ \xi\left[\frac{4}{\lambda-4d_a}\ln\left(\frac{\lambda}{4d_a}\right) - \frac{1}{z-z_t(t)}\right]; & \rho_u(t,z) < 0 \text{ and } d_a \leq z - z_t(t) \leq \frac{\lambda}{4} \\ 0; & \rho_u(t,z) \leq 0 \end{cases} \tag{531}$$

Likewise, — once again referring to Figure: (329) —, it should be noted that when the trailing-half of a negative packet is at the load boundary – the right boundary within Figure: (329) —, the second equation in Equation: (531) applies, while when the leading-half of a negative packet is at the source boundary, the first equation in Equation: (531) applies; however, the velocity equations for the trailing-half electrons near the source boundary and for the leading-half electrons near the load boundary are different from Equation: (531), and the boundary conditions are determined using integral equations similar to Equation: (516) but with integration limits applicable to the boundaries. Conversely, for the source boundary at $z = 0$, the boundary condition for the conduction current and the differential voltage is defined by Equation: (532), and for the convection velocity of the unbalanced electrons near the source boundary, the boundary condition is defined either by Equation: (531) or, for the trailing-half electrons, by Equation: (533) — where in Equation: (532) $v_s(t)$ is the source voltage and R_s is the source internal resistance, while in Equation: (533) z_{t1} and z_{m1} are as defined in Figure: (329).

$$v(t,0) = v_s(t) - R_s i(t,0) \tag{532}$$

$$u_a(t,z) = \begin{cases} \xi\left[\frac{2}{z} - \frac{1}{z - z_{t1}(t)} + \frac{4}{\lambda - 4d_a}\ln\left(\frac{\lambda}{4d_a}\right) - \frac{4}{\lambda}\right]; & \rho_u(t,z) < 0,\ 2d_a \leq z \leq 2z_{t1}(t) \text{ and } d_a \leq z_{t1}(t) \leq \frac{\lambda}{4} \\ \xi\left[\frac{4}{\lambda - 4d_a}\ln\left(\frac{\lambda}{4d_a}\right) - \frac{4}{\lambda}\right]; & \rho_u(t,z) < 0 \text{ and } z < z_{m1}(t) < \frac{\lambda}{4} \text{ or } 2z_{t1}(t) < z < z_{m1}(t) \end{cases} \tag{533}$$

Likewise, for regions near the source boundary not defined in Equation: (533), equations in Equation: (531) apply, while — at load boundary $z = l$ — the boundary condition for the conduction current and the differential voltage is described by Equation: (534) where R_L is the load resistance. Similarly, for the convection velocity of the unbalanced electrons near the load boundary, the boundary condition is defined either by Equation: (531) or, for the leading-half electrons, by Equation: (535) — where $z_{mk}(t)$ is the negative peak of [\rho_{u}(t,z)] closest to the load boundary.

$$v(t,\ell) = R_l i(t,\ell) \tag{534}$$

$$u_a(t,z) = \left\{ \frac{\xi}{z_{mk}(t) - z + \frac{\lambda}{4} - d_a}\left[\ln\left(\frac{\ell - z}{2d_a}\right) - 1 + \frac{2d_a}{\ell - z}\right]; \quad \rho_u(t,z) < 0 \text{ and } z_{mk}(t) \leq z \leq \ell - 2d_a \right. \tag{535}$$

Conversely, Equation: (528), Equation: (529), Equation: (530), Equation: (531), Equation: (532), Equation: (533), Equation: (534), and Equation: (535) can be used to model

any two-conductor unbalanced transmission line, and for balanced lines, where $R_1 = R_2$ and $\rho_u = i_c = 0$, the unbalanced equations reduce to the two classical equations in Equation: (502) and Equation: (503) with the same frequency-domain definitions for the propagation constant and the characteristic impedance. Also, in transmission lines with low degree of unbalancedness where R_1 and R_2 are not equal but are close, one may neglect radiation and use the classical model; however, to determine the convection current and to analyze the emitted radiation, the nonlinear system of equations in Equation: (528) through Equation: (535) will need to be solved in time-domain, and the Finite-Difference Time-Domain (FDTD) method can be used to solve these equations for an unbalanced transmission line.

Likewise, to validate the presented theory and to develop a trust in the model, laboratory tests were conducted, and Figure: (330) shows the experimental set up where the balanced and unbalanced transmission lines $T2$ were tested — where the transmission line $T1$ represents the coaxial leads of the function generator used with signal $v_s(t)$ and internal resistance R_s , while L_{ss} and L_{sr} represent the inductances of the coaxial signal and the reference terminations that connects to the sending end of $T2$, while the load resistance — at the receiving end of $T2$ — is represented by R_L , the circuitry to the right of R_L models the probe and the channel input impedance of the TDS2024 oscilloscope used, and the probes coax — represented by $T3$ — is in itself, an unbalance transmission line with its center conductor being a highly resistive Nichrome wire which is commonly used in high

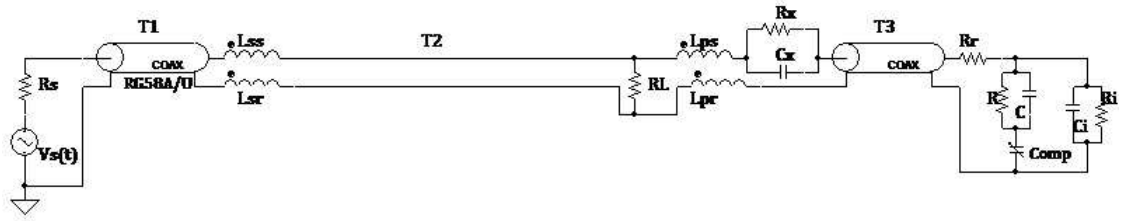

Figure 330: experimental set up for the validation of the unbalanced transmission line theory

end oscilloscopes to damp out ringing.

Conversely, as the convection current along an unbalanced $T2$ it cannot be measured directly and the objective of our experiments was to capture the distortion of the conduction current created by the convection current, thus to ensure that any distortion observed in the conduction current is only the result of the flow of convection electrons, it was first verified that no distortion were observed when the transmission line T2 is balanced, and this verification is important particularly because the probe coax is a potential source of radiation and distortion. Likewise, the arrangement shown in Figure: (330) was set up inside a shielded room where all tests were conducted, and the shielded room was used to minimize interference and possible distortions from external sources. Similarly, balanced tests were conducted with two identical conductors used to construct T2 as a transmission line with parallel conductors, and in one test, T2 was constructed from two identical solid bare copper wires, while in the second test, T2 was constructed from two identical solid Nickel-Titanium (Nitinol) wires [410].

Likewise, the unbalanced test was conducted with one copper wire and one Nitinol wire to construct T2 as an unbalanced transmission line, and to minimize the interaction of T2 with its surrounding matter, the sending and receiving ends of T2 were mounted on the two sides of a U-shape all wood structure with a 1.8m base, while the two parallel lines of T2 were stretched in air at the height of 1.35m, providing more than 1m clearance all around. Similarly, A 50 ohm source with a matched coax, a resistive load of 10 ohms, and a scope probe setting of x10 was used in all experiments preformed — noting that a low resistance load was used to maximize the conduction current and to eliminate scope probe distortions that can occur with high impedance loads. Conversely, the transmission line data for T2 used in the three experiments are given in Table: (16), Table: (17), and

Table: (18) respectively, and the parameter values shown are the measured values with the theoretical values for parallel two-wire transmission lines shown in parentheses — noting that dielectric losses are assumed to be negligible [410].

Table 16: experiment 1: balanced copper lines

Parameter	Conductor 1	Conductor 2
Conductor Material	Solid Copper	Solid Copper
Conductor dia (mm)	0.644	0.644
R1 ($\frac{\Omega}{m}$)	0.069 (0.053)	—
R2 ($\frac{\Omega}{m}$)	—	0.069 (0.053)
L ($\frac{\mu H}{m}$)	0.711 (0.72)	0.711 (0.72)
C ($\frac{pF}{m}$)	16.3 (15.5)	16.3 (15.5)
Line Length (m)	1.81	1.81
Line Separation (mm)	2	2

Table 17: experiment 2: balanced nitinol lines

Parameter	Conductor 1	Conductor 2
Conductor Material	Solid Nitinol	Solid Nitinol
Conductor dia (mm)	0.202	0.202
R1 ($\frac{\Omega}{m}$)	29.4 (27.8)	—
R2 ($\frac{\Omega}{m}$)	—	29.4 (27.8)
L ($\frac{\mu H}{m}$)	1.1 (1.19)	1.1 (1.19)
C ($\frac{pF}{m}$)	10.5 (9.3)	10.5 (9.3)
Line Length (m)	1.81	1.81
Line Separation (mm)	2	2

Table 18: experiment 3: unbalanced copper and nitinol lines

Parameter	Conductor 1	Conductor 2
Conductor Material	Solid Nitinol	Solid Copper
Conductor dia (mm)	0.202	0.644
R1 ($\frac{\Omega}{m}$)	29.4 (27.8)	—
R2 ($\frac{\Omega}{m}$)	—	0.069 (0.053)
L ($\frac{\mu H}{m}$)	0.957	0.957
C ($\frac{pF}{m}$)	13.6	13.6
Line Length (m)	1.81	1.81
Line Separation (mm)	2	2

Likewise, in all three experiments, the source voltage was sinusoidal and its frequency was varied from 1 MHz to 100 MHz, and the conduction current was observed via the load voltage on the oscilloscope. Similarly, in Experiment 1, where the line's total resistance

was in milli-Ohms, the source voltage amplitude was 5 V whereas in Experiments 2 and 3, the amplitude was 10 V, while in Experiments 1 and 2, no distortion of the conduction current was observed at any frequency, and in Experiment 3, distortions of the conduction current was observed at specific frequencies — noting that [FIGLRES:UDB:FIG6] shows the typical distortion of the load voltage waveforms observed in the lab.

Similarly,the FDTD solution of the unbalanced transmission line model described by Equation: (528) through Equation: (535) is shown by Figure: (536) through Figure: (542) — where, $b_1 = \frac{C_v(R_1-R_2)}{\Delta z}$ where $\frac{\partial \rho_u}{\partial t} < 0$, $b_1 = -\frac{C_v(R_1-R_2)}{\Delta z}$ where $\frac{\partial \rho_u}{\partial t} > 0$, $b_2 = 1 - \frac{R\Delta t}{L}$, $b_3 = \frac{\Delta t}{L\Delta z}$, $b_4 = 1 - \frac{G\Delta t}{C}$, $b_5 = \frac{\Delta t}{C\Delta z}$, a mesh size of $\Delta z \times \Delta t$ has been assumed, and all initial conditions not specified are zero.

$$i(t+\Delta t,z) = \frac{1}{1-b_1 u_a(t,z)} \left[[b_1 u_a(t,z) + b_2] \; i(t,z) + b_1 u_a(t,z) \left[i(t+\Delta t, z-\Delta z) - i(t, z-\Delta z) \right] + b_3 \left[v(t,z) - v(t,z+\Delta z) \right] \right] \tag{536}$$

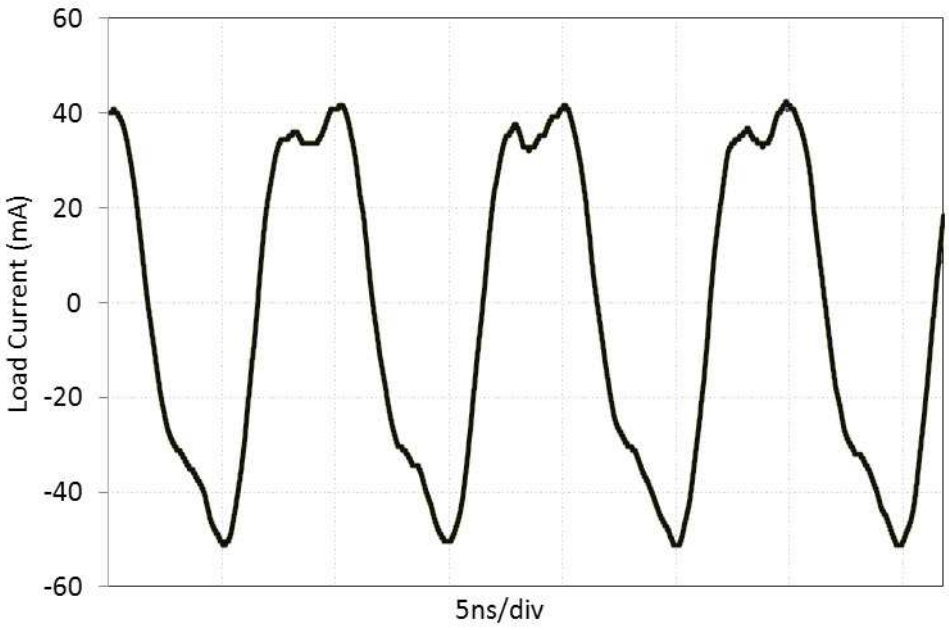

Figure 331: copper and nitinol transmission line's load current distortion observed in the lab

$$v(t+\Delta t, z) = b_4 v(t,z) + b_5 \left[i(t, z-\Delta z) - i(t,z) \right] \tag{537}$$

$$v(t+\Delta t, 0) = v_s(t+\Delta t) - R_s\, i(t+\Delta t, 0) \tag{538}$$

$$i(t+\Delta t, \ell) = \frac{1}{R_L} v(t+\Delta t, 0) \tag{539}$$

$$v(0,0) = 0.5 v_s(0) \tag{540}$$

$$i(0,0) = \frac{0.5}{R_s} v_s(0) \tag{541}$$

$$\rho_u(t,z) = \frac{C_v \left(R_1 - R_2 \right)}{\Delta z} \left[i(t,z) - i(t, z-\Delta z) \right] \tag{542}$$

Likewise, At every grid point (t, z) , $\rho_u(t, z)$ is used to determine the distances $z_l(t) - z$ and $z - z_t(t)$ which are then used to calculate $u_a(t, z)$, and for the interior grid points, $u_a(t, z)$ is determined from Equation: (531), for the source boundary points, it is determined from Equation: (533) , and for the load boundary points, it is determined from Equation: (535). Conversely, these FDTD equations are solved for the unbalanced transmission line described in Table: (16), Table: (17), and Table: (18) using the parameters shown, while Figure: (332) shows the simulated spatial distributions of the convection current, the conduction current, and the unbalanced charge distribution along the copper-Nitinol transmission line, while the conduction current solution of the classical transmission line equations is shown for comparison and only the conduction currents are plotted to scale [410].

Similarly, Figure: (333) shows the simulated steady state conduction current at the load for this unbalanced transmission line, and the simulated load current shows distortions similar to those measured in the lab — as shown by Figure: (331) —, while the distortions are mainly near the peaks of the conduction current waveform because these

locations correspond to the +/- unbalanced charge packets' boundary locations where the convection current is highest as seen in Figure: (332), and the asymmetrical distortions of the conduction current are caused by the flow of the asymmetrical convection current.

Likewise, the traveling wave nature of the convection current results in radiation patterns that are intrinsically bipolarized and time-variant, and assuming an unbalanced transmission line of length l along the z-axis, the retarded vector magnetic potential A has only a z-component given by Equation: (543) — where i_c is the convection current given by Equation: (524), z' denotes the source location along the z-axis, μ_0 is the permeability of free space, $t - \frac{R}{c}$ is the retarded time, R is the magnitude of the position vector locating the field point relative to the source point, and c is the speed of light in free space. Conversely, In spherical coordinates (r, θ, φ) , A has A_r and A_θ components but only the A_θ component contributes to the far field radiation, while the magnetic component of the radiation in the far field is defined by Equation: (546) — where $\nabla\times$ is the curl operator, a_φ is the

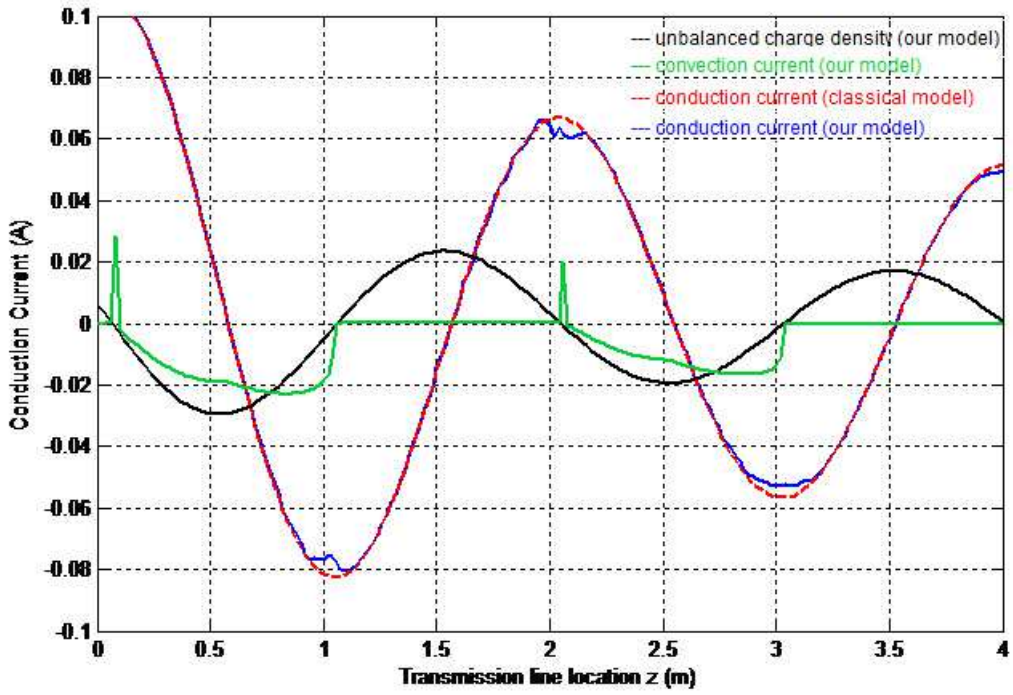

Figure 332: conduction current, convection current and unbalanced charge density along the copper/nitinol line

unit vector in the φ direction, and A_z is given by Equation: (543), Whereas the radiating current in a conventional antenna is a standing wave, i_c in Equation: (543) is a traveling wave [410].

$$A_z = \frac{\mu_0}{4\pi}\left[\int_0^{\ell} \frac{i_c(t - \frac{R}{C}, z)}{R} dz'\right] \tag{543}$$

$$H = H_\varphi \, a_\varphi \tag{544}$$

$$= \frac{1}{\mu_0} \nabla \times A \tag{545}$$

$$= \frac{-\sin(\theta)}{\mu_0} \frac{\partial A_z}{\partial r} a_\varphi \tag{546}$$

Likewise, expression of the nonlinear convection current as a traveling wave using the

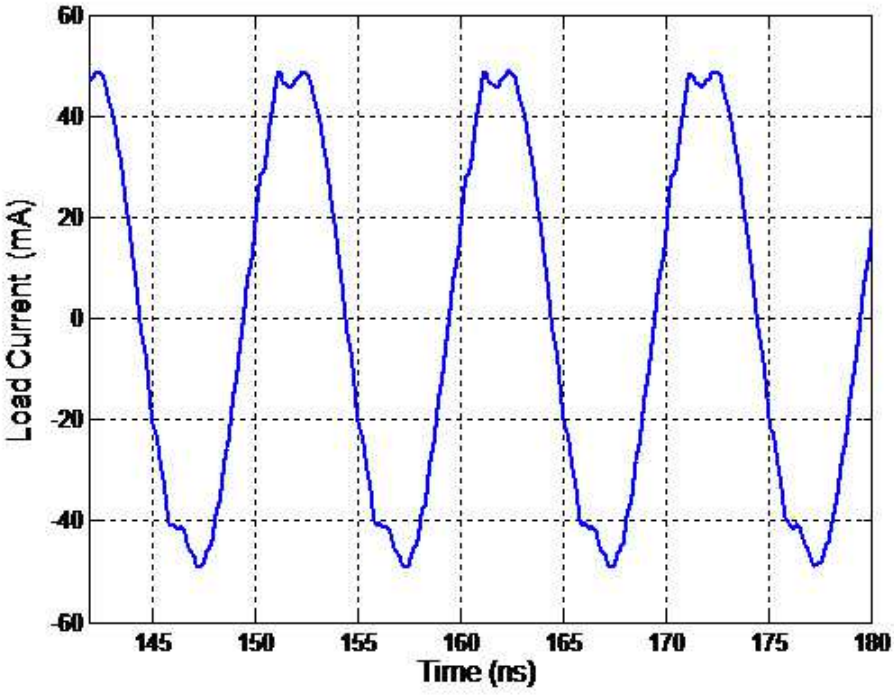

Figure 333: copper and nitinol transmission line's load current from model simulation

Discrete Fourier Transform (DFT) approximation for its spatial distribution given by Equation: (547) — where a_k and b_k are the DFT coefficients, $\lambda_c = \frac{\lambda}{2}$, λ is the conduction current's wavelength, ω is the source frequency, and 2ω is the fundamental frequency of i_c used in its DFT approximation.

$$i_c(t, z') = \sum_{k=1}^{N-1} \left[a_k \cos\left(\frac{2\pi\, z'}{\lambda_c} - 2\omega\, t \right) + b_k \sin\, k \left(\frac{2\pi\, z'}{\lambda_c} - 2\omega\, t \right) \right] \tag{547}$$

Conversely, to obtain the corresponding radiation pattern, plug Equation: (547) in Equation: (543) and Equation: (543) in (Equation: (546), making the common assumptions that $R = r$ in the denominator and $R = r - z' \cos(\theta)$ in the numerator, the magnetic component of the far field radiation becomes Equation: (548) — where the phase constants $\beta = \frac{2\pi}{\lambda}$ and $\beta_s = \frac{2\pi}{\lambda_s}$ with $\lambda_s = \frac{c}{f}$ being the radiation wavelength in space, noting that the integration limits in Equation: (543) have been replaced by z_1' and z_2' that define the regions of nonzero convection current along the transmission line [410].

$$\begin{aligned} H_\varphi(r, \theta, t) \approx \frac{-\beta_s \sin(\theta)}{4\pi\, r\, (\beta - \beta_s \cos(\theta))} \sum_{k=1}^{N-1} a_k \cos\left[2k \left((\beta - \beta_s \cos(\theta))\, z' + \beta_s r - \omega\, t \right) \right] \\ + b_k \sin\left(2k \left((\beta - \beta_s)\, z' + \beta_s r - \omega\, t \right) \right)_{z=z_1'}^{z_s'} \end{aligned} \tag{548}$$

Likewise, Figure: (334), Figure: (335), and Figure: (336), show the snapshots of the convection current distribution at times $t_1 < t_2 < t_3$ as it travels along the copper/Nitinol transmission line of one wavelength long, while also shown in these figures are the DFT approximations (with N=50) that are used to evaluate Equation: (548); as the DFT approximations are indistinguishable from the actual convection currents. Conversely, with the

source frequency of 100MHz and the conduction current's phase velocity of $u_p = 2 \times 10^8 \frac{m}{s}$, if the wavelength is $\lambda = 2m$ then to determine the radiation patterns for these current distributions, simply let $t_1 = 0$, find $t_2 = \frac{.5}{u_p} = 2.5ns$ and $t_3 = \frac{1}{u_p} = 5ns$, and evaluate Equation: (548) with $z_1' = 0$ and $z_2' = 1$ — as shown by Figure: (337) —, $z_1' = 0.5$ and $z_2' = 1.5$ — as shown by Figure: (338)—, and $z_1' = 1$ and $z_2' = 2$ — as shown by Figure: (339). Conversely, The normalized E-plane radiation patterns shown in Figure: (337), Figure: (338), and Figure: (339) are evaluated with $r = 100m$ and are plotted for $0 \leq \theta \leq \pi$

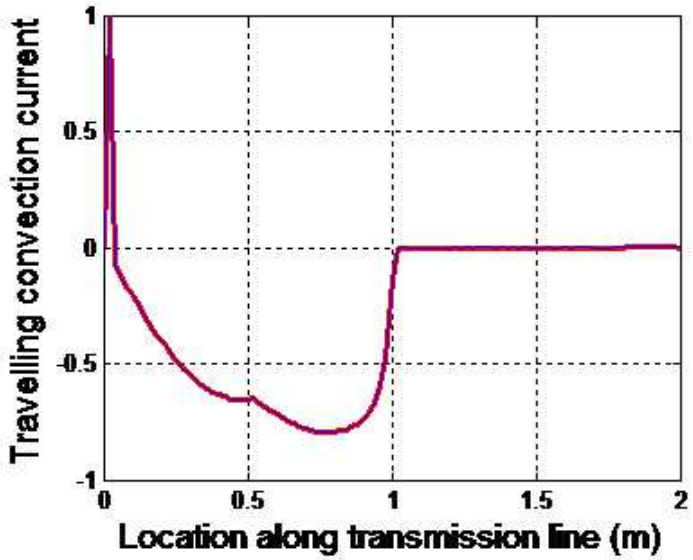

Figure 334: convection current and its dft approximation

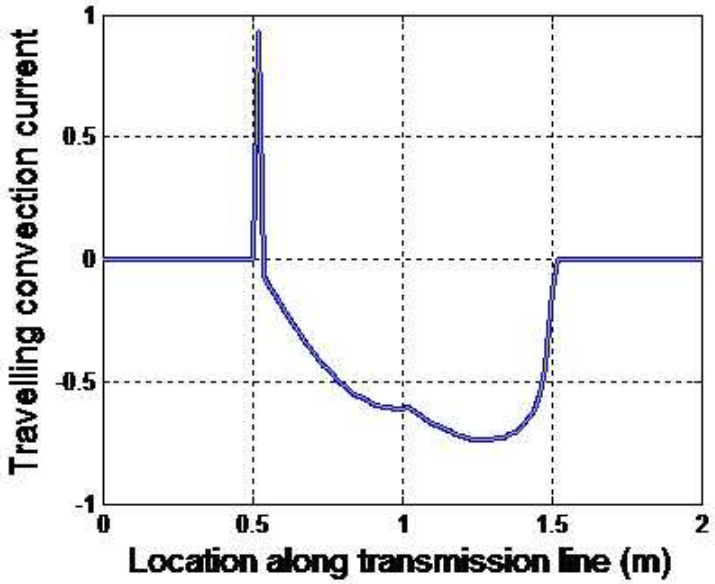

Figure 335: convection current and its dft approximation

[410].

Likewise, for about a century, transmission line radiation has been attributed to the mysterious "common-mode current" without knowing its nature or the process that gives rise to its generation, and it has now been shown that transmission line radiation is due to the time-variation of the convection currents that develop along unbalanced lines. Conversely, the developed theory — for the generation of this convection current — enabled the development of a transmission line model that can be used in the analysis and understanding of the nonlinear behaviors of unbalanced transmission lines observed in the field,

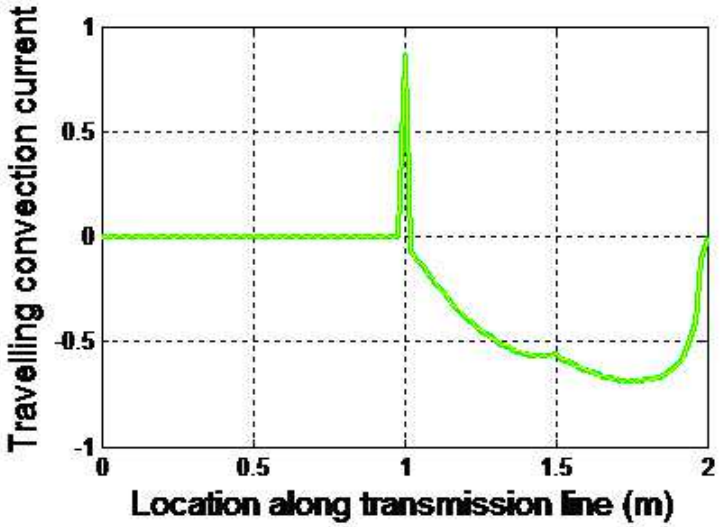

Figure 336: convection current and its dft approximation

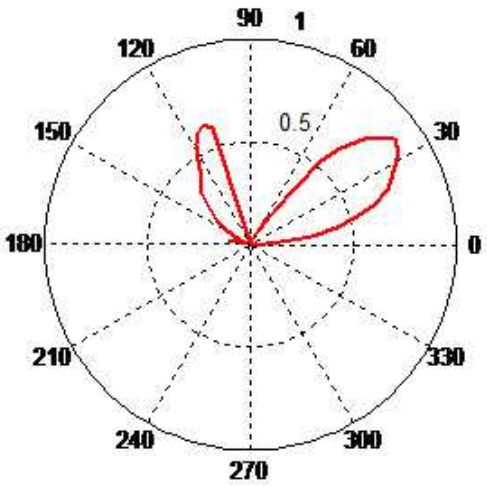

Figure 337: radiation pattern for the current in figure: (334)

and this model has been verified via computer simulations and laboratory tests. Likewise, it is worth noting that the spatial distribution of the convection current in an unbalanced transmission line is more controllable than the radiating current in a conventional antenna, and the theory presented here can be expanded to help design traveling wave narrow-beam antenna systems and this work is currently under active investigation.

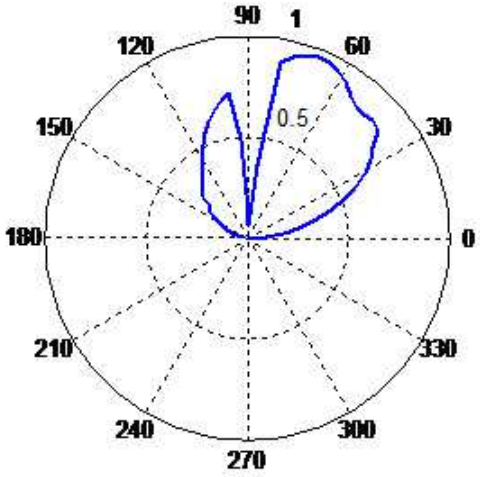

Figure 338: radiation pattern for the current in figure: (335)

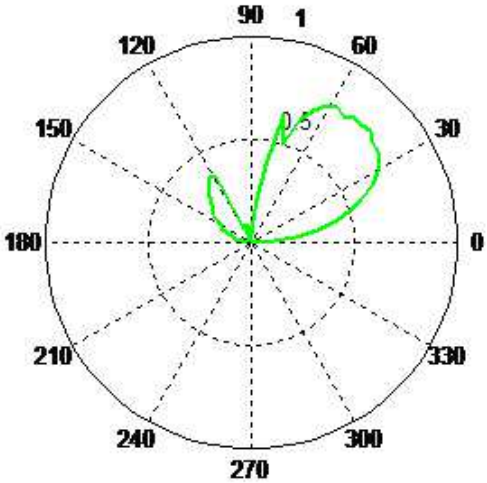

Figure 339: radiation pattern for the current in figure: (336)

6.3.9 Modeling a BIS Apparatus

The fundamental rationale behind the modeling a BIS apparatus section was to present the inherent problems with contemporary instrumentational modeling approaches — particularly step input impedance characterization techniques utilized within the bioimpedance spectroscopy research area — thru the in depth examination of such methods. Likewise, during the process of performing such assessments, a number of unique modeling methodologies were developed — as shown by Figure: (340) — in order to electrically represent laboratory instrumentation using an assumed electrical topology — generally in an automatic fashion. Conversely, based upon the observations obtained, it was determined that the usage of a step input function — while from a mathematical perspective being a perfectly logical method of determining the total frequency response of a linear system — is generally a bad technique to utilize when characterizing a real acquisition system because the step response is not tolerated very well by the input of the acquisition device — an attribute that is somewhat expected because of the reactive components within the acquisition circuitry —, and while it could be argued that such techniques could — in theory — aid in modeling the internal parameters of the acquisition device in addition to the apparatus interconnections; however, based upon the tendency of CIE effects to vary with frequency — and given that CIE effects are not guaranteed to be linear — it is extremely likely that the model developed will substantially change upon attempting to apply another type of input waveform, and, to make matters worse, without being able to observe the applied input signal without distortions occurring on the input acquired, it becomes extremely problematic to compensate for, the previously mentioned, CIE effects — like acquisition delay and harmonic distortions —, thus this type of multispectral characteri-

zation technique should be avoided unless it can be definitively determined that the CIE effects are linear and the acquisition delay that occurs is known to be consistent under such conditions.

Likewise, based upon this previous observation, it was also determined that single spectrum characterization — or electrical profiling through the usage of a sinusoidal signal —, despite being more data intensive to work with, is generally more acquisition friendly — in terms of permitting the isolation of CIE effects —, and that a number of electrical equivalent circuit modeling techniques — previously discussed within the instrumentational effects subsection — are available to electrically represent the distortions created by the acquisition apparatus. Similarly, while a number of equivalent circuit modeling techniques are available — a notable method being least-squares estimation —; however, as it was previously observed within the development of the non-linear/non-ideal instrumentational amplifier model, some of these modeling methods require the mathematical derivation of their equivalent circuit model, and because such derivations are rather lengthy — as it might be expected —, this attribute can be extremely problematic when the physical structure is not definitively known — predominantly because a substantial amount of time is required to re-derive the mathematical equations when the electrical topology changes — and further complications can arise since equation-based modeling methods — like least-squares estimation — are notorious for producing nonphysical results — like negative resistors, capacitors, and inductors — that goes against the underlying philosophy of using equivalent circuit modeling techniques. Conversely, based upon such observations, it was also determined that such numerical techniques — while being inherently powerful and useful — should ideally not be utilized until a reasonable circuit topology is obtained — predominantly to avoid the time-consuming task of reformulating equivalent circuit equations —,

thus, with this being said, it was decided that equivalent circuit modeling techniques that numerically formulate these equations — via graph theory like Berkeley spice — should be utilized in conjunction with educated guesses regarding both circuit topology and parameter values. Likewise, based upon such assessments, a number of modeling methods were developed — noting that the brute force parametric spice solver named Violet was observed to be effective but slow if bad parameter estimates were provided, while the non-linear Nth order Newtonian solver developed that utilized a spice calculated numerically approximated Jacobian was observed to be faster but was metaphorically hit or miss depending upon the amount of data available and the estimations made — the less observable a system was the harder it was to generally model.

Furthermore, while implementation of such numerically-based techniques were shown to be effective in obtaining an equivalent circuit model of the apparatus being examined; however, the model obtained generally differed from the proposed instrumentational model — shown within the instrumentational effects subsection — primarily because a more intuitive equivalent circuit topology is preferred when implementing these particular modeling techniques over a more complex but physically realistic circuit topology — since estimating LPF or HPF topology parameters is generally easier than estimating a complex combination of reactive topologies —, although a transformation back into the proposed physical structure can be obtained with some effort —, and faster parametric solving techniques — like a particle swarm parametric solver — could be beneficial in improving the overall effectiveness of the violet method, while expansion of the Newtonian solver to better incorporate time domain changes might increase the overall success rate of this particular solution.

Conversely, now that a number of attributes have been discussed — regarding the nu-

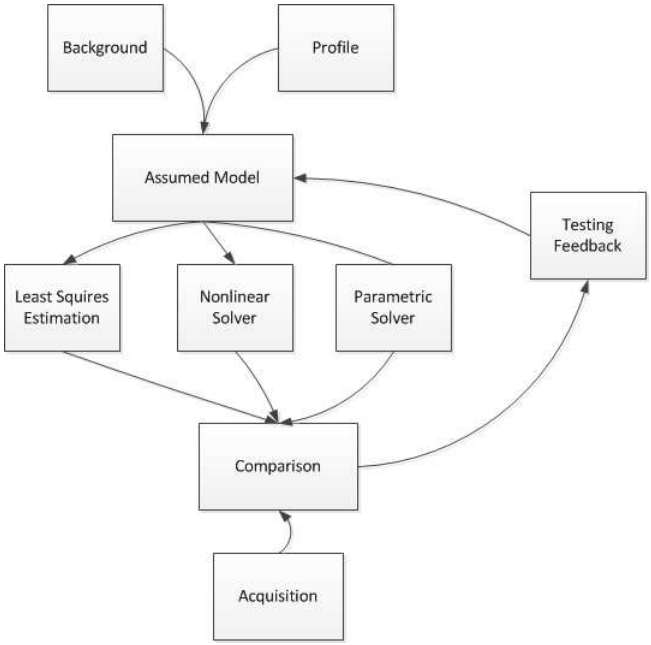

Figure 340: conceptual modeling process flowchart

merous ways, in which, a bioelectrical acquisition can become distorted —, it now seems appropriate to, metaphorically switch gears, and began examining how the CIE effects encountered and the reduction methods discussed, can play a substantial role in obtaining a high fidelity bioelectrical measurement within a laboratory environment. Likewise, with this being said, to begin such a discussion, consider for the moment the, previously mentioned, research related problem of attempting to model a bioimpedance spectroscopy (BIS) laboratory apparatus, as conceptually depicted by Figure: (341), in which a Tektronix TPS2024 oscilloscope and a Tektronix AFG3102 function generator can be used in conjunction with two "*DRE ECG Grabber/Squeeze Style electrode patient connectors*" with a in series — wire-wound — 110 ohm current sensing resister attached to either side of the electrical circuit created — noting the minor caveat that some of the experiments had the first in series wire-wound 110 ohm current sensing resistor removed — in order to minimize some of the CIE effects encountered —, and other experiments had the 110 ohm resistance substituted with a 10k ohm current sensing resistor — in order to overcome loading effects

[424].

Similarly, while the implementation of such a device might, at first, appear to be a metaphoric — far cry — from resembling the neatly packaged commercial BIS devices observed within the medical community; however, in terms of functionality and acquisition fidelity, a case can be made that the device portrayed within Figure: (341) is actually a far superior alternative to the commercially available BIS devices currently being utilized — especially upon considering the, previously discussed, types of acquisition CIE effects that tend to metaphorically run rampant if such effects are not carefully handled — , along with the fact that the apparatus, shown within Figure: (341), was only utilized within a partially shielded environment and thus has the benefit of additional physical CIE effect reduction that is typically unavailable within commercially sold acquisition apparatus [112]. Likewise, while such proposals are rather intriguing — although it is important to remember that the underlying theme of this dissertation is not simply the a isolated and highly localized improvement of a BIS analyzer, but rather the development of a solid informational foundation upon which to build future, "*higher fidelity*", biomedical devices —, yet the vindication of such assertions can best be presented by examining the modeling processes required to obtain a bioimpedance measurement using this particular type of apparatus. Thus to elaborate further, because the electronics — within a BIS

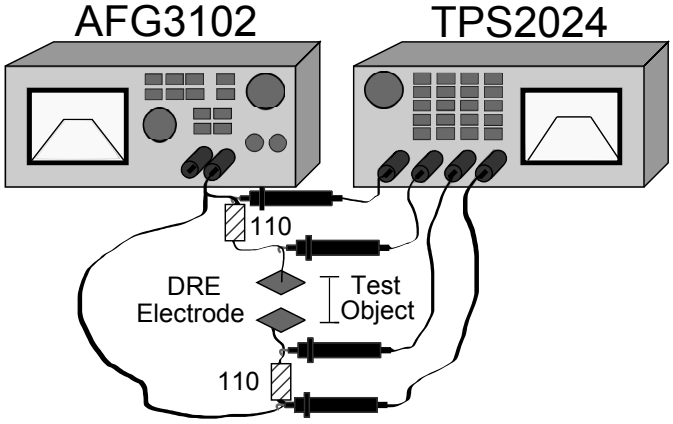

Figure 341: conceptual bioimpedance spectroscopy apparatus utilized

analyzer — can be fundamentally separated into three categorizable stages, a generation stage that produces a predefined signal that will stimulate the biomaterial being examined, a acquisition stage that acquires the test signal after it stimulated, and a processing stage that determines the amount of attenuation between the applied and acquired signals.

Conversely, because a BIS analyzer can be separated into three categorizable stages, it becomes apparent — upon reviewing the concepts presented within the instrumentational effects subsection — that most of the underlying theory surrounding the effects incurred within these stages has, for the most part, already been substantially discussed — so much so, that further discussion on this particular topic temps to invoke redundancy — ; however, with this being said, in terms of applying the, previously presented, theory to physically model a BIS analyzer, the following methodological progression seems to be both a rational and reasonable preliminarily approach. First, the identified electronic stages can be electrically modeled and combined into a proposed equivalent apparatus model or mathematical equation. Second, experiments can be performed and measurements taken in order to determine both the validity of the model created and some insight into the value of the internal parameters of the device. Third, CIE profiling information can be generated from the data collected in order to determine the distortions that are associated with the devices usage. Forth, the CIE profile created can be utilized — if so desired by the researcher — to reduce or account for the CIE effects encountered and thus, create a "*higher fidelity*" measurement.

Likewise, based upon such observations, the physical implementation of the first step yields the following 3 stage proposed equivalent apparatus model, as shown by Figure: (342); however, at this point in the process — or for that matter at any point in the process — it would be highly unadvised to make any lasting assumptions regarding the physical

structure of the circuit model created since, a multitude of possible circuit structures can produce similar analytical results and — given the unknown circumstances surrounding the inner workings of the device being examined — each of these structures — so long as they do not violate the fundamental principles of physical hardware implementation and provide accurate predictions — are legitimate possibilities that cannot be discounted — since, for example, Figure: (342) could equally be represented by Figure: (343), or Figure: (344), and while some of these models are, in fact, either expansions or reductions, none of these options can be precluded.

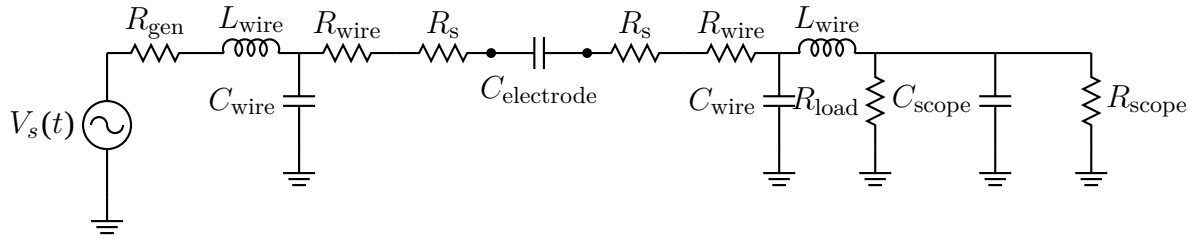

Figure 342: a proposed bioimpedance spectroscopy equivalent circuit model

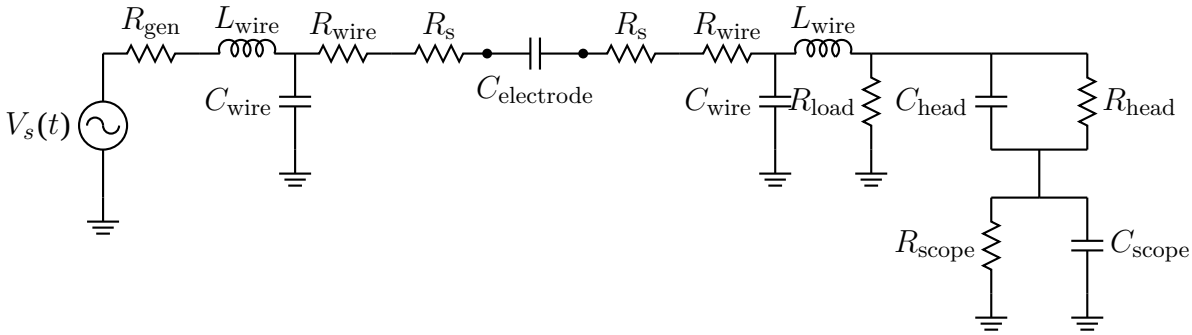

Figure 343: a proposed bioimpedance spectroscopy equivalent circuit model

Similarly, it is also important to recognize that the proposed equivalent model developed does not necessarily have to conform to the — previously presented — traditional electrical engineering equivalent circuit diagram approach and could, in fact, be described in a strictly mathematical fashion from a controls system identification perspective — although such methods are typically frowned upon given these particular circumstances, since intuitive

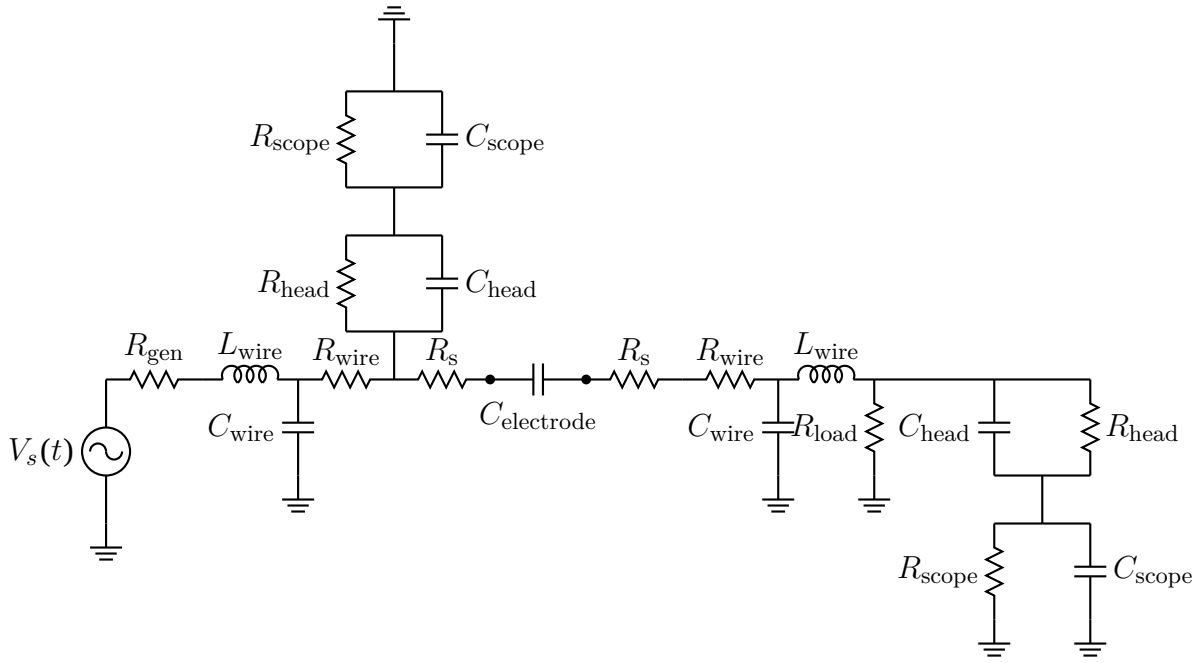

Figure 344: a proposed bioimpedance spectroscopy equivalent circuit model

electrical structural information would be inherently lost; however, while the equivalent circuit approach is the preferred method to most electrical modeling problems, yet there are certain circumstances where this approach, in itself, is not very physically intuitive — especially when it comes to ionic modeling [207] [184]. Nevertheless, setting such issues aside for the moment, at this point it might be tempting to begin deriving the underlying mathematical equations that describe Figure: (342) — a task that can be achieved using a number of circuit analysis techniques, although the recommended method, in this particular case, is the numerical time domain approach, implying that derivatives are numerically approximated, using the, previously demonstrated, progressive KVL and KCl equations shown within the instrumentational effects section —; however, substantial caution is advised here since some circuit analysis techniques are ill-suited — particularly classical AC analysis techniques — for formulating such equations — an attribute that will be explained shortly — and it is advised that the derivation of such equations be postponed until after observing the results obtained from laboratory experimentation.

Conversely, upon implementing step two of the proposed process, a task that was achieved by utilizing the conceptual configuration — as shown by Figure: (341) — in which the DRG electrode connectors were connected — via DS26 electrodes — electrically but were separated by a piece of scotch tape — in order to create a loading capacitance between the electrical structure — and secured to a flat surface with a fixed wire separation of 2.5in, while a applied single sided variable width 10V peak square wave was applied and observed at the transient — rising and falling — segments of the signal at the signal input and across the 10k current sensing resistor [425]. Likewise, upon the application of a approximate 5ns in width 10V peak square wave to the — previously described — apparatus, a plot — as shown by Figure: (345) — was obtained, and based upon the information observed, within Figure: (345), the following observations, can be made. First, while the utilization of a square wave pulse — as a, previously discussed, pseudo-delta input — is a theoretically sound method of determining the frequency response of a electrical system across the desired spectrum of interest — assuming the sample rate corresponds with the pulse width —; however, such methods — particularly within this testing apparatus — appear to be rather problematic because — upon examining the input signal within Fig-

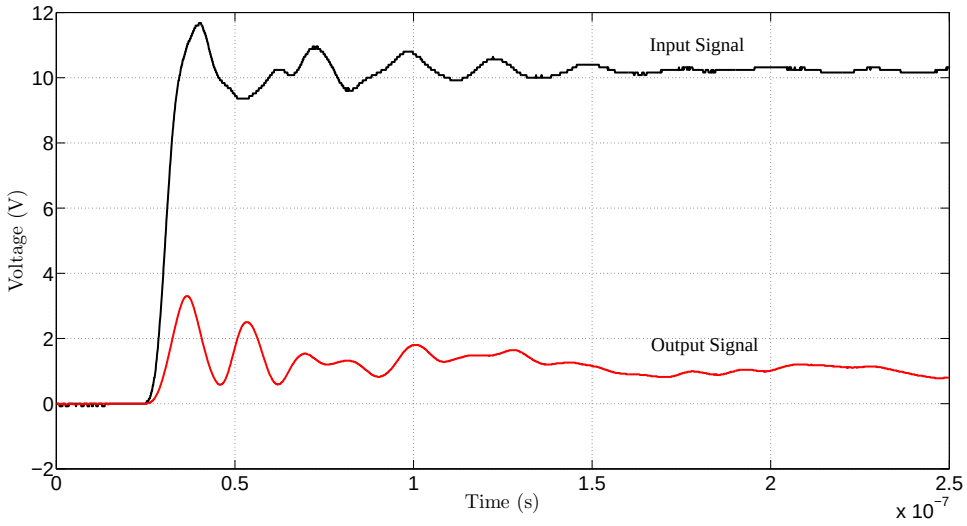

Figure 345: plot of input versus output of a applied 5ns 10v peak square wave to a bis acquisition apparatus

ure: (345) — the acquisition of the expected ramp waveform is substantially distorted — primarily because of the internal circuitry of the Tektronix TPS2024 acquisition device. Second, because the acquired input signal has been substantially distorted — most likely because of the internal circuitry of the Tektronix TPS2024 acquisition device — it is extremely difficult to determine the overall validity of the applied signal, and this attribute is extremely problematic because the mathematical formulation of Figure: (342) through the utilization of Laplace analytical techniques ultimately requires the frequency domain representation of the input signal and, in this particular case, while the input signal could be assumed as being a ramp function; however, such assumptions are speculative — at best — especially given the observations obtained within Figure: (345).

Conversely, with this being said, given the overall amount of distortions observed within the input signal obtained, it is, first and foremost, highly recommended that any acquisition characterization performed utilize periodic examination — like the previously shown sinusoidal CIE effect characterization — rather than simultaneous multi spectral techniques — like pseudo-delta analysis — in order to reduce the amount of distortions embedded within the input signal, and while such techniques cannot alleviate the inevitable input distortions encountered — as previously discussed within the CIE effects section —; however, such methods are easier to compensate for — given the CIE effects characterization performed — than the cumulative distortions that occurred because of simultaneous spectral examination — which could, depending upon the width of the pulse utilized, also incorporate transmission line distortions as well. Likewise, upon examining this particular problem further — rather than performing a new series of profiling test using a sinusoidal input —, and returning once again to the subject of obtaining a mathematical derivation of Figure: (342), it is, once again, highly recommended that the, previously discussed, numer-

ical formulation approach be applied here, primarily because of the ability to utilize any time domain input signal with relative ease when simulating such equations — although, so long as it is assumed that the input signal will be simplistic, which is admittedly a highly circumspect assumption, Laplace modeling techniques can be reluctantly applied here.

Yet, while the appropriate selection of a mathematical derivation technique will, upon successful implementation, yield a mathematical representation of the equivalent circuit model; however, upon recalling the overall complexity of the — previously derived — instrumentational amplifier equation, it is worth mentioning that such equations — given the overall complexity and structural volatility of the system being modeled — are rarely intuitively beneficial from a designers perspective — insofar as, the results obtained will likely be a multi page mathematical expression that is, truly, only meaningful to a computational solver —, so much so, that the utilization of these derivational techniques are not, based on the observations obtained throughout the research conducted, recommended, since analytical circuit software — like Berkeley spice — can produce equivalent analytical results — with less chance of a mistake within the mathematical derivation — than a explicit, by hand, mathematical formulation of the same equations [426].

Conversely, with this being said, because the assumed electrical structure — within Figure: (342) — could require some future modification — an attribute that would require the re-derivation of mathematical equations — it was decided, at least based upon such observations, that rather than attempting to implement the, previously discussed, numerical equation formulation technique, that Berkeley spice would be utilized to mathematically simulate this particular electrical structure. While it is important to recognize that Berkeley spice, in itself, utilizes a combination of classical matrix graph theory synthesis techniques in order to formulate the KCL in KVL equations — necessitated by the

problem — and an assortment of other matrix solving algorithms — possibly Gaussian, Newtonian, Runge-Kutta (RK), and finite solver — depending upon the circuit elements being electrically modeled, thus, in many respects, the utilization of spice is inherently analogous to deriving the mathematical expressions by hand; however, such techniques — including a by hand formulation of the equivalent circuit model —, in themselves, are only the simulated results of a particular electrical circuit with a well defined set of parameters, and the utilization of such techniques will not, in itself, match an acquired laboratory measurement to the equivalent electrical parameters necessitated to duplicate such observations [427] [428] [429] [426].

Likewise, based upon such assessments, a number of additional analytical techniques must be utilized in order to determine the component parameters — within the equivalent circuit model — that will approximate the acquired electrical signal — as outlined in step three of the modeling process — and the most primitive modeling method available, under such circumstances, is a trial and error approach based upon human intuition, which typically begins with a initial guess of the model parameters, followed by a recursive process of simulating, examining, and modifying the model parameters until a equivalent fit is obtained. Conversely, as it might be expected, this particular technique is typically extremely time-consuming and does not necessarily provide the best equivalent representational model — although, human intuition, when properly developed, can be extremely powerful in determining circuit parameters that are the most accurate real-world representation of the actual physical system being examined.

Alternatively, given the inherent problems associated with this particular technique, one possible automated method was developed and named "*Variations of Input to Output for Lengthy Engineering Testing*" (Violet) — the source code is available within Appendix C

—, which was designed to perform a full parametric analysis on multiple circuit components and then save the results obtain for further processing within Matlab. Conversely, given the highly independent nature of this particular analytical technique — insofar as, each simulation is not dependent upon another simulation — Violet was inherently designed to incorporate simultaneous simulations through the utilization of a multi threaded execution of Berkeley spice.

Conversely, in terms of implementation, the conceptual execution of the Violet application, as shown by Figure: (346), first begins by loading a modified Berkeley spice netlist file

```
Example.cir Example VIOLET Netlist
VS 1 0   PULSE 0 20 0 20u 20u 30u 50u
R1 2 1 [10:10:100]
R2 0 2 [10:10:100]
.TRAN  20ns 142.78us 100us 20ns
.PRINT TRAN V(2)
.PROBE
.END
```

— which depicts the parametric variation of two Resistors R_1 and R_2 over a range between 10Ω to 100Ω in increments of 10Ω — and,

```
Example.cir Example VIOLET Netlist With Prefixes
VS 1 0   PULSE 0 20 0 20u 20u 30u 50u
R1 2 1 [1k:500:100k]
C1 0 2 [1p:1p:100p]
.TRAN  20ns 142.78us 100us 20ns
.PRINT TRAN V(2)
.PROBE
.END
```

— which depicts the parametric variation of a Resistor R_1 and a capacitor C_1, over a range between $1k\Omega$ to $100k\Omega$ in increments of $500k\Omega$, and $1pf$ to $100pf$ in increments of $1pf$ respectively — into memory, in which the additional Violet parametric prefix, as shown by Equation: (549) — where (A) represents the starting value, (B) represents the incrementing

step size, and (C) represents the ending value — is processed, and any associated scientific units, as shown by Table: (19), are identified and processed, after which every possible parametric netlist simulation file is generated for further execution within Berkeley spice.

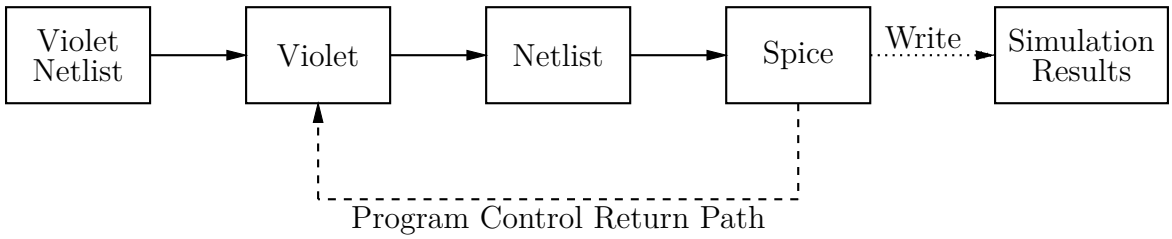

Figure 346: conceptual violet to spice interface

$$[A : B : C] \tag{549}$$

Table 19: violet netlist prefixes

Prefix	Numeric Representation
G	1×10^{9}
M	1×10^{6}
K	1×10^{3}
k	1×10^{3}
	1×10^{0}
m	1×10^{-3}
u	1×10^{-6}
n	1×10^{-9}
p	1×10^{-12}

Likewise, after all of the simulation files have been generated, Violet enters a threaded Berkeley spice execution stage, as conceptually illustrated by Figure: (347), in which , as depicted within Figure: (348), simulations are loaded into a thread manager, process by Berkeley spice when a CPU is available to simulate the produced netlist, the results of the simulations saved, and the thread pool notified that the simulation is done and that the CPU is ready to execute another spice simulation.

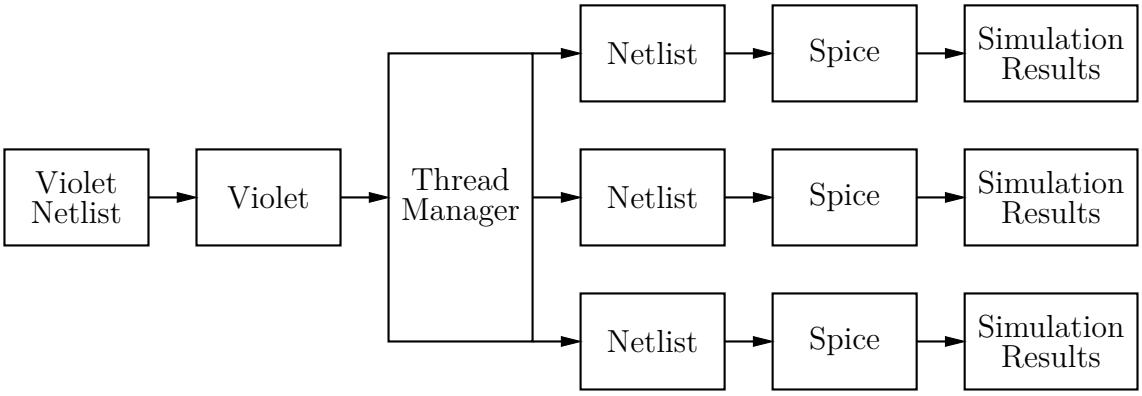

Figure 347: conceptual violet to spice interface with threading

Table 20: other violet arguments

Argument	Description
-t Number	Specifies the maximum number of threads that can simultaneously run in the thread pool, the default is defined by Microsoft at 25. Increasing or decreasing this number incorrectly could increase processing time depending upon the type of hardware the system has.
-i File Name	Alternative way to set the VIOLET netlist file
-o Output Path	Alternative way to set the VIOLET output folder location
-p	Deletes all Simulation files from the output folder before starting the simulation

Conversely, in order to provide some additional configurability to the execution of the Violet application, the following command line arguments were added, as shown by Table: (20), in order to allow the user to specify the input file, output folder location, removal of any prior simulation attempts, and the maximum number of threads to be simultaneously executed — while the minimum number of parameters required to utilize Violet is as follows

```
DRIVE\PATH>VIOLET.exe "\VIOLET_NETLIST.cir" \OUTPUT_FOLDER"
```

. Nevertheless, while the Violet application — in theory — is capable of eventually finding a set of circuit parameters — assuming the equivalent circuit model selected was correct — that is capable of matching the acquisitions obtained to a spice simulation; however, depending upon the number of parameters utilized within the assumed equivalent circuit

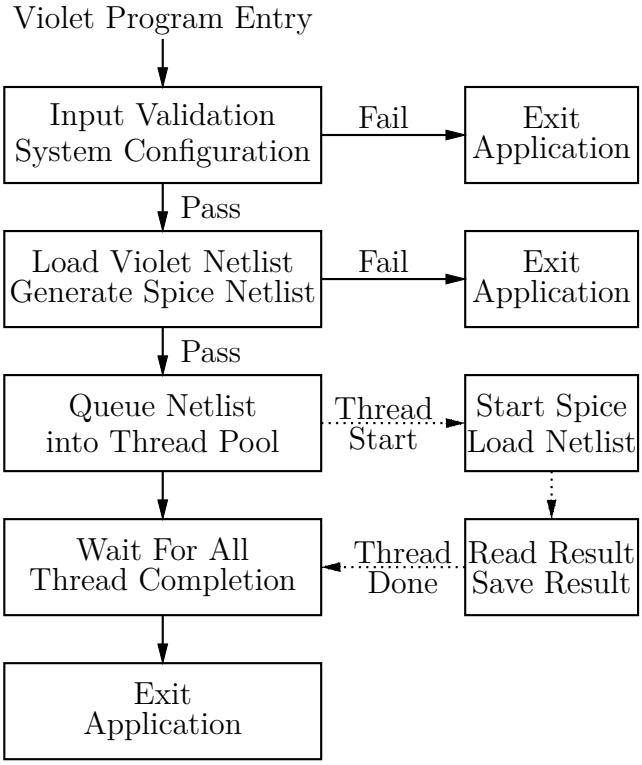

Figure 348: violet conceptual application architecture

model and the knowledge available surrounding the value of these parameters, the number of simulations required by Violet can quickly become unmanageable — even for a modern computer —, and the information produced by Violet, in itself, requires additional post processing — within a program like Matlab — in order to determine the minimum error obtained from all the simulations performed. Likewise, while such attributes are to be expected given the underlying brute force nature of the Violet method; another, more functional, alternative involves creating a interface between spice and Matlab, as shown within Appendix D, in which spice is executed within Matlab via the "System()" command — within the SpiceRunSimulation function — thru the usage of the following sequence of commands, as shown by the MATLAB code shown within Appendix E script 24, — noting that the results obtained are extracted using a python script, shown within Appendix C. While this method might seem eerily similar to Violet — with the notable difference between this particular spice communication interface and Violet being, the ability to obtain and

process a spice simulation in a synchronous fashion at the cost of losing threadability — ; however, the main advantage of this method over Violet, is the ability to incorporate human intuition into the modeling process, beyond an initial guess — as opposed to the simplistic application of bruit force —, and methods of this nature typically mix short burst of the, previously discussed human intuitive guesses, within a parametric type simulation. Conversely, to demonstrate the functionality of this particular modeling technique, after a short period of iterative parametric simulation combined with frequent human adjustments, an equivalent circuit model for Figure: (341), as shown by Figure: (349), was created and simulated, and the results obtained are shown within Figure: (350), Figure: (351), Figure: (352), Figure: (353), and Figure: (354) over an assortment of input pulses — noting that the input oscilloscope probe was removed from the circuit in a attempt to reduce the, previously observed, pulse input distortions.

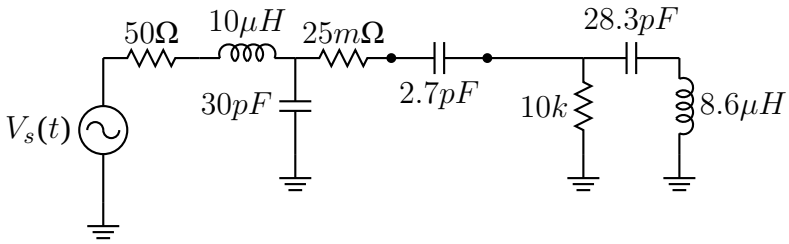

Figure 349: a proposed bioimpedance spectroscopy equivalent circuit model

Likewise, upon visually examining Figure: (350), Figure: (351), Figure: (352), Figure: (353), and Figure: (354), it becomes apparent that the parameters selected — within Figure: (349) — are far from being an ideal match; however, with this being said, it is important to recognize that the simulated results obtained —- within Figure: (350), Figure: (351), Figure: (352), Figure: (353), and Figure: (354) — do, in fact, reasonably approximate the acquired measurements — thus demonstrating that this particular modeling method, if given enough time, can yield very reasonable approximations — yet the

manifestation of such results brings up a number of peculiar questions. First, given that the model utilized within Figure: (349) is very loosely related to the more electrically realistic models — shown within Figure: (342), Figure: (343), and Figure: (344) —, at what point does the structural knowledge — regarding the underlying electrical system — override a accurate but structurally unrelated model? Second, given the problem of distortions that manifested upon the input channel — as a result of using a pulse function —, can

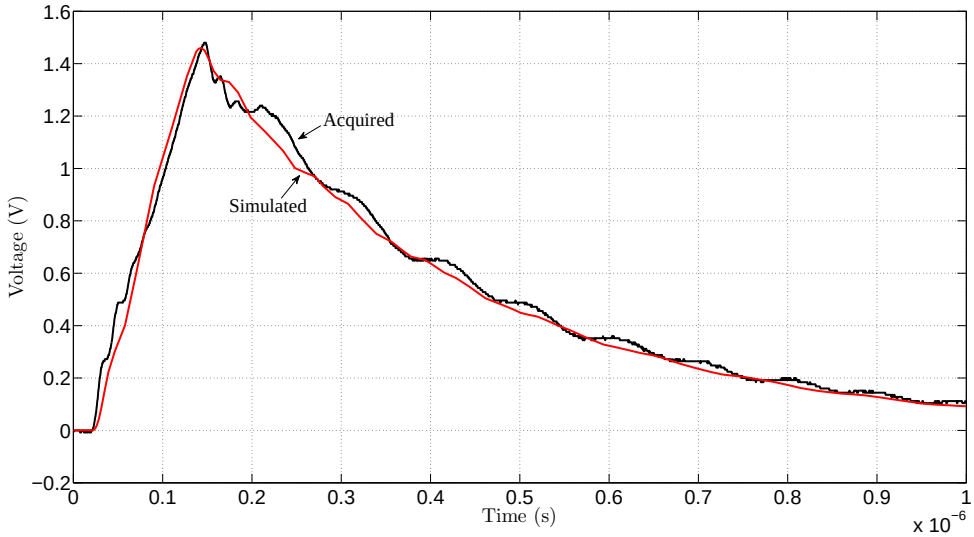

Figure 350: plot of acquired versus spice simulated model for a 10v peak 120ns width pulse

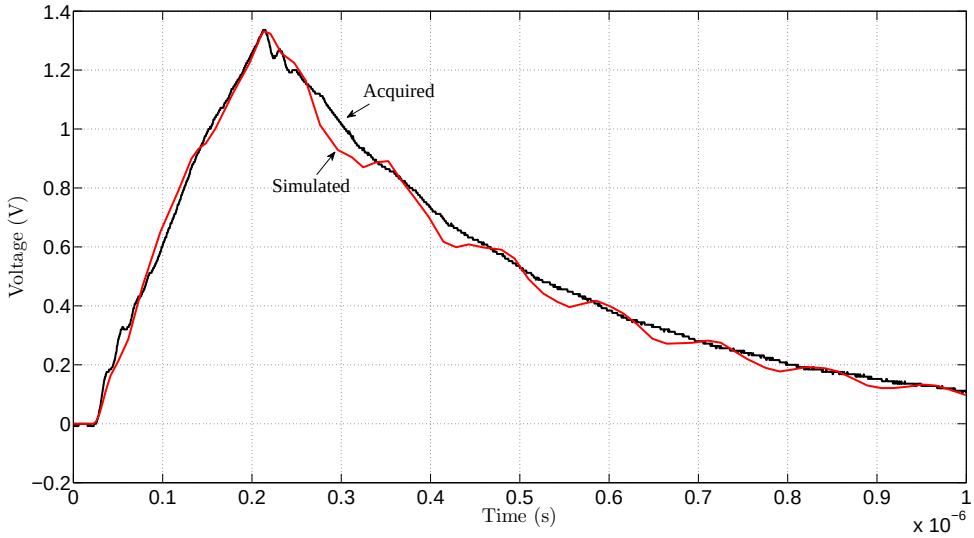

Figure 351: plot of acquired versus spice simulated model for a 10v peak 187ns width pulse

the results obtained — even with the first oscilloscope input disconnected — actually be trusted? Third, at what point can a simulated model be deemed not only a good match, but a high-fidelity match?

Conversely, while such questions are somewhat subjective — especially since the end objective of the model being developed will ultimately determine the practices utilized —; however, within the confines of this dissertation, the first question does tend to invoke an

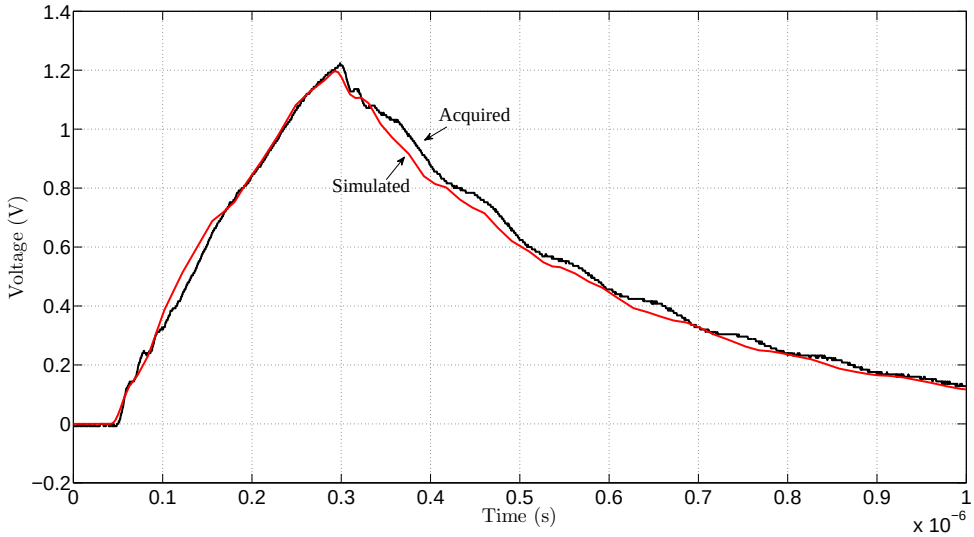

Figure 352: plot of acquired versus spice simulated model for a 10v peak 250ns width pulse

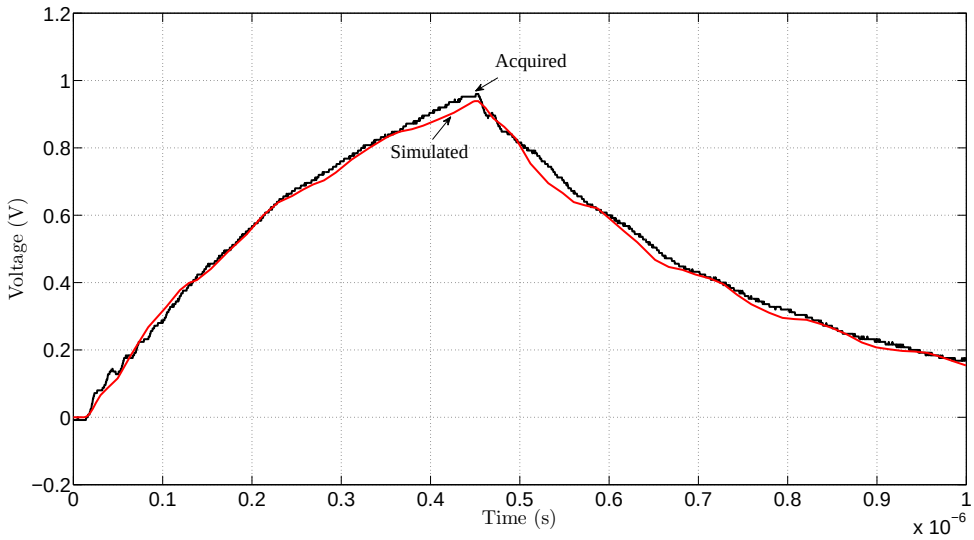

Figure 353: plot of acquired versus spice simulated model for a 10v peak 437ns width pulse

interesting philosophical conundrum — primarily because the subject of acceptable perception is being examined — and based upon such attributes, it seems appropriate to assign the answer of maybe to this question, insofar as, it truly depends upon the end objective of the application since, in the case of building upon an existing electrical system, the answer would be no — since internal electrical information is generally necessary —, while, in the case of obtaining a black box response without any regard to the electrical superstructure, the answer would be yes — since the internal electrical structure is not required. Alternatively, the answer to the second question — at least within this dissertation — is a relatively straightforward, no — the results obtain cannot be trusted because the input signal was distorted from the very beginning of the test — however, looking beyond this particular attribute for the moment, just because the acquisitions obtain cannot be completely trusted does not inherently imply that the model created is not a accurate representation of the oscilloscopes current acquisition state — noting that the extension of a model derived under such conditions will likely be inherently incorrect upon comparison with a periodic acquisition. Likewise, in a manner similar to the first question, the third question also tends to

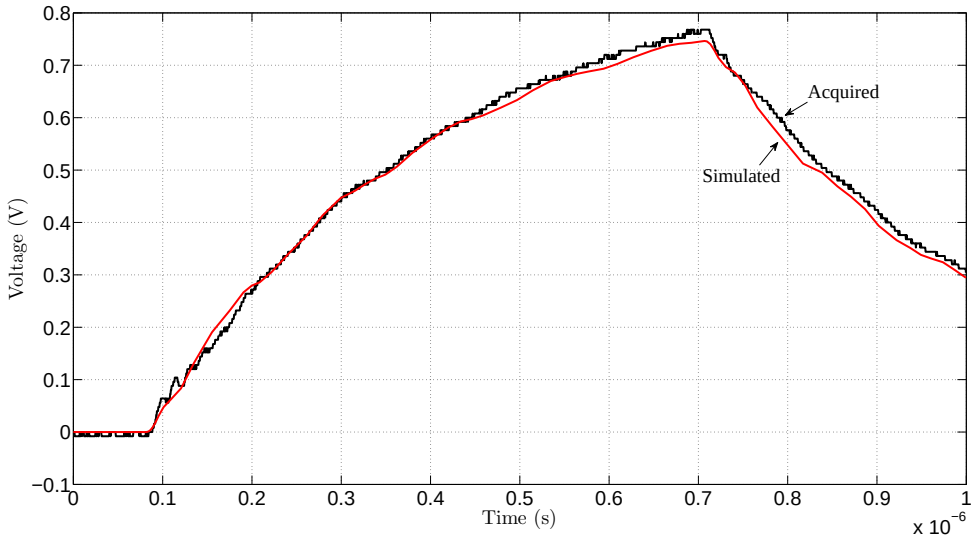

Figure 354: plot of acquired versus spice simulated model for a 10v peak 625ns width pulse

invoke an interesting philosophical conundrum, insofar as, the inherent ambiguity of the term high-fidelity makes such assessments difficult and application dependent, yet given the circumstances in which Figure: (350), Figure: (351), Figure: (352), Figure: (353), and Figure: (354) were obtained, and assuming that only predictions for pulse input conditions were required between the input pulse range of 120ns to 625ns, then the model — shown within Figure: (349) — could be deemed at the very least, to be a reasonably high fidelity model; however, if predictions above or below 120ns and 625ns are required, or another type of input signal is required, then such assessments cannot be made, thus the model obtained is not truly a high fidelity model.

Nevertheless, which such conclusions might be somewhat flexible — as they are unfortunately inherently ambiguous —; however, based upon the results obtain within Figure: (350), Figure: (351), Figure: (352), Figure: (353), and Figure: (354), it will be admitted that, while the simulations produced are reasonably accurate, a better fitting solution is always welcome — particular in terms of a better match on the ringing effects produced. Yet, despite such observations, it is important to remember that — such results — are not — in themselves — overly important when compared to the underlying objective of developing a high-fidelity modeling foundation — after all no singular model can accurately describe every BIS acquisition device in existence, and clearly great success has been made in identifying the need to avoid step inputs — and while the methods provided — to approximate a BIS system — is of substantial importance; however, the greater victory — in this particular case — is the development of the underlying high-fidelity modeling foundation regarding the sources of distortions encountered.

Conversely, with this being said, while the methods described above are oftentimes effective; however, more mathematical solutions to such problems also exist — like the

least squares estimation method and the nonlinear Newtonian method, to name a few — ; however, the implementation of such solutions does inevitably require the mathematical derivation of the equivalent circuit model of the system being examined — an attribute that can be rather challenging, particularly if the model of the system needs to be changed —, thus, while these equation based methods will not be discussed further within this section — primarily because of the length of the equations produced, the overall susceptibility of such methods to combined instrumentational, environmental, and material (CIEM) effects, and the overall amount of CIE effects observed on the input signal — a computational alternative — the nonlinear Newtonian solver — will be briefly provided as a possible automated solution [427] [429]. Likewise, the nonlinear Newtonian solver method can — best — be described as an iterative method, in which the Jacobian matrix of a known set of system equations is calculated, inverted, and multiplied by the set of system equations, and the result obtain is then subtracted from the current location within the system — as shown by Equation: (553) — and the new location obtained is subtracted from the last location, the matrix norm taken, and if the change between the two is less than a defined threshold the equation is assumed to be solved [427] [429].

$$X = \begin{bmatrix} X_1 & X_2 & \dots & X_N \end{bmatrix} \tag{550}$$

$$F(X) = \begin{bmatrix} F_1(X) \\ F_2(X) \\ \vdots \\ F_N(X) \end{bmatrix} \tag{551}$$

$$J(X) = \begin{bmatrix} \frac{\partial F_1(X)}{\partial X_1} & \frac{\partial F_1(X)}{\partial X_2} & \cdots & \frac{\partial F_1(X)}{\partial X_N} \\ \frac{\partial F_2(X)}{\partial X_1} & \frac{\partial F_2(X)}{\partial X_2} & \ddots & \frac{\partial F_2(X)}{\partial X_N} \\ \vdots & \ddots & \ddots & \vdots \\ \frac{\partial F_N(X)}{\partial X_1} & \frac{\partial F_N(X)}{\partial X_2} & \cdots & \frac{\partial F_N(X)}{\partial X_N} \end{bmatrix} \tag{552}$$

$$X_{\text{next}} = X_{\text{last}} - J^{-1}(X)F(X) \tag{553}$$

Similarly, while the method — shown within Equation: (553) — is correct; however, it is generally considered to be very computationally intensive — because of the inverse matrix operation — thus, when this method is typically implemented, the last location is subtracted from Equation: (553), the Jacobian is multiplied by Equation: (553), the new location minus the last location term, is substituted with the variable y, the y term is solved, and the solved y term is then added to the last location in order to estimate the next location — after which the norm of the difference can be taken and checked for system convergence — as shown by Equation: (558) and Equation: (559) [427] [429].

$$X_{\text{next}} = X_{\text{last}} - J^{-1}(X)F(X) \tag{554}$$

$$X_{\text{next}} - X_{\text{last}} = -J^{-1}(X)F(X) \tag{555}$$

$$J(X)\left(X_{\text{next}} - X_{\text{last}}\right) = -F(X) \tag{556}$$

$$Y = X_{\text{next}} - X_{\text{last}} \tag{557}$$

$$J(X)Y = -F(X) \tag{558}$$

$$X_{\text{next}} = X_{\text{last}} + Y \tag{559}$$

Likewise, because no mathematical derivation of system equations is desired — and the

calculation of both the system equations, $F(X)$, and the Jacobian, $J(X)$, typically requires that the mathematical derivation be performed —, it was discovered that the partial derivative — within the Jacobian — can be numerically estimated, as shown by Figure: (560), if some information about the system equations is known, and in this particular case, it was found that spice can be utilized to obtain this information for a given circuit model — which inherently implies that the mathematical derivation of the circuit model is not required since, $F_N(X)$ for any $X_N + h_N$ can be calculated within spice and both the $F(X)$ and $J(X)$ matrix suddenly become known [427].

$$\frac{\partial F_N(X)}{\partial X_N} = \frac{F_N\left(\begin{bmatrix} X_1 & X_2 & \dots & X_N + h_N \end{bmatrix}\right) - F_N\left(\begin{bmatrix} X_1 & X_2 & \dots & X_N \end{bmatrix}\right)}{h_N} \tag{560}$$

Conversely, while such attributes are a metaphorically good sign that this particular approach might be functional; however, the problem of program implementation arises because a Nth dimensional solving capability is necessitated by the algorithm — a attribute that typically requires the utilization of a Nth dimensional nested for loop — and such attributes become problematic because, first, nested for loops, after a certain depth, become particularly difficult to manage — especially when the code exceeds multiple pages, second, nested for loop array indexing, along with the computational simulation — via spice — of the system equations is highly inefficient since either more simulations are being performed then necessitated by the problem or a Nth dimensional amount of programming logic must be added to prevent un-necessitated calculations — noting that the Jacobian estimation stage is somewhat similar to a partial differential equation solver in memory structure.

Likewise, the manifestation of these implementational problems resulted in the substi-

tution of a Nth dimensional nested for loop with a two dimensional representation that only permitted the computation of the required elements, and this two-dimensional array access method is eerily reminiscent to a identity matrix added by a ones matrix — because Matlab indexes start at one rather than zero — with an additional ones vector augmented after the last row in order for the evaluation of the system equations at the original location. While this particular formulation might sound somewhat obscure, the derivation of this particular method arises as a result of attempting to access a Nth dimensional grid of two points for each dimension — in which one point represents the X_N while the other point represents the $X_N + h_N$ — and the matrix obtained was examined for a minimizing access pattern — relative to the required indexes needed to perform the desired mathematical operations — and the modified identity matrix was observed to minimize the access required with the exclusion of the original location that had to be augmented to the end of the access matrix manually.

Nevertheless, while the implementation of such methods might, at first, seem somewhat obscure, the physical implementation, as shown by the MATLAB code shown within Appendix E script 25, is relatively straightforward, at least upon examining the algorithms implementation, and upon further review of the implementation provided, it is interesting to note that — this particular method — only requires $N + 1$ executions of spice per iteration in order to fully estimate both the Jacobian and system equations necessitated by the nonlinear Newtonian solver. Conversely, while the overall integration of spice into the nonlinear Newtonian solver is an extremely interesting concept, the results of such methods are rather temperamental — as is generally the case with any iterative solver. For example, within the demonstrational case provided, the unknown resister values needed to produce the desired output voltages — within a simplistic voltage divider — are found within 5

iterations of the, previously shown, method — noting that such solutions are not necessarily unique —; however, more complex problems — particularly problems with phase shifts — can become particularly problematic for this technique for a number of reasons: first, because spice typically returns a time-based vector of voltages and the Jacobian approximation requires a singular point of comparison, some type of conversion is required to convert the time based vector into a singular quantity — or the method must be modified to incorporate time into the calculation —, and — in this particular example — the solution selected summed the difference between the simulated and desired signals; however, such solutions are not necessarily the best approach given the periodic nature of the signal being examined and the tendency of such estimates to not directly represent the type of error that has occurred — like phase error versus magnitude error. Second, because this method is relying upon the accuracy of the Jacobian and, within this particular method, the Jacobian is being approximated — an attribute that inherently implies error — the step size utilized within the partial derivative approximation must be appropriately selected — an attribute that can be somewhat problematic to figure out since solver instability generally only occurs after a number of iterations have occurred — otherwise the method will not converge. Third, the initial location — or component parameters — utilized must be appropriately selected — an attribute that can be intuitively difficult —, since the improper selection of initial conditions — under certain circumstances — can make the solver either not converge or increase the number of iterations required. Fourth, even when all these conditions are considered, significant differences in component sizes — for example mega versus pica — can, under certain circumstances, be numerically problematic and result in errors developing within the Jacobian, which in turn leads to solver instability, and such cases typically require scaling techniques to overcome. Fifth, this method is highly dependent upon the

amount of information provided — an example being how many voltages were observed — and the ratio of observable values to unknown parameters ultimately determines how successful the results obtained by this method will be. Sixth, convergence of a circuit topology to a particular set of parameters can only be obtained if there is, in fact, an actual solution based upon the assumed circuit topology — or, to provide an example, a purely resistive topology cannot accurately represent a system that contains reactive components.

Nevertheless, while the utilization of this particular method does have a number of problems associated with its usage, similar things can be said regarding the mathematically derived version of such techniques, and while this particular method is far from being an ideal solution to every modeling scenario; however, such techniques can be utilized successfully assuming the, previously mentioned, conditions are resolved. Likewise, while this particular technique can be applied to the, previously discussed, BIS modeling apparatus problem and some successful results obtained — although the problems, listed above, are definitively predominant within the implementation of this technique to this particular problem, and such attributes make it less practical when compared to the, previously presented, modeling techniques —; however, given the, previously discussed, attributes surrounding this particular problem, it was decided that the simplistic demonstration — provided above — of this technique was more beneficial than focusing predominately upon the problems that arise because of the apparatus configuration utilized — as additional points of acquisition would have been extremely beneficial within this method, but also extremely problematic because of the distortions produced from the step signal utilized —, yet it is hoped that the simplistic and successful demonstration provided will merit some consideration when designing a test apparatus, since the appropriate selection of testing parameters can increase the successfulness of such techniques. Therefore, with this being

said, not only is the apparatus design important to the reduction of CIE effects encountered, but also to the successfulness of the modeling method implemented, and such observations are of substantial importance given the innate dependency between the apparatus and the signal fidelity obtained.

6.3.10 Modeling the FDI Region with BIS

The fundamental rationale behind the modeling the FDI region with BIS section was to examine the electrical characteristics of the FDI region of the human hand and to develop both a preliminary electrical model of FDI material and a unique method of electrically representing this particular region. Likewise, based upon the observations obtained, it was determined that the selection of the FDI region of the human hand — as a focal point of biomaterial modeling efforts — was an ideal place to begin experimenting with biomaterial characterization because of this particular regions tendency to avoid producing substantial manifestations of atypical nonlinearities — an attribute that was discovered to typically results when ionic conduction is occurring and is generally avoided, within this particular region, because of the concentration of dense FDI muscle mass that tends to contain less of these nonlinear materials — which allows for the development and refinement of characterization techniques that predominantly focus upon examining more traditional dielectric modeling methods, and its overall ease of accessibility.

Conversely, while a number of electrical equivalent circuit modeling techniques are available to represent the electrical characteristics of this particular region — some of which were noted within prior sections —; however, based upon laboratory experience and academic review it was determined that dielectric modeling methods — like the Dow method — or relaxation modeling methods — like Debye and Cole and Cole — are a highly effective starting point when attempting to electrically characterize these particular regions —

so long as the materials nonlinearity are not overly substantial. Furthermore, despite the overall successfulness of utilizing the dielectric modeling methods — like the Dow method — to electrically represent a relatively linear biomaterial; however, it was also discovered that these models are highly susceptible to CIE effects — implying that a comparison between similarly synthesized models developed from different acquisition instrumentations — implying different CIE effect profiles — would inherently reduce the overall fidelity of such models, and the existence of such effects — along with the natural electrical variations observed within a living biomaterial — makes the correlation of electrical attributes to a singular physical parameter — like fat content or water retention — extremely difficult, especially since reasonable correlations cannot be directly made if comparisons between similar models — particularly within publicized acquisitions — cannot be fully trusted to have accounted for such CIE effects, and the existence of this attribute tends to imply that some type of CIE effect standardization — like the methods previously proposed — needs to occur — particularly within the BIS research area — before any substantial headway in physical correlation can be made. Likewise, in a manner similar to the — previously discussed — CIE effect profiling standardization problem, the modeling technique utilized to electrically represent such materials — prior to comparison — needs to also be standardized — possibly utilizing the modeling methods developed —, along with the locations in which the measurements were taken, in order to increase the overall fidelity of the comparisons being made, and again such attributes require a communal effort within the BIS research area before any headway on this issue can be made.

Conversely, now that some preliminary modeling information has been provided regarding the laboratory BIS acquisition device developed — as shown by Figure: (341) — it seems prudent to extend these modeling techniques further by examining the

electrical characteristics — using the BIS testing apparatus shown within Figure: (341) — of an actual biomaterial. Likewise, while — as it was previously discussed within the background theory chapter — there are a number of different types of biomaterials available for study — although the noninvasive active examination of living tissues is by far the most interesting, but most volatile —, and based upon such assessments — along with a number of human safety considerations that should be considered before performing any BIS examination —, the FDI region of the human hand — as shown by Figure: (355) — was selected as a ideal testing location, given its overall electrical safety — implying that a BIS test in this location has a very low chance of inducing cardiac ventricular fibrillation — and a reduced chance of sudden electrical changes occurring within the material — or reduced material volatility [120] [343] [292] [16] [97] [326].

Similarly, before any BIS acquisitions of the FDI region were taken — once again, within the partially shielded environment — the upper 110 ohm resistor — within Figure: (341) — was removed and the lower 110 ohm resistor — within Figure: (341)— was replaced with a 50 ohm current sensing resistor. Likewise, two DS26 electrodes were attached to the DRG electrode grippers and saline based conductive gel was applied — to improve the

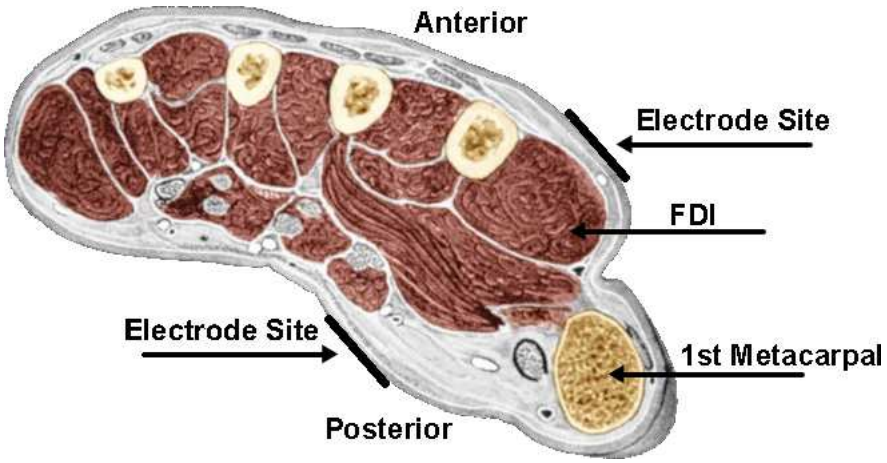

Figure 355: conceptual dre electrode attachment for a bis first dorsal interosseous (fdi) material test; fdi image complements of biovere

conductivity of the interface created between the electrode and biomaterial being examined —, after which the electrodes were attached to the FDI region as shown by Figure: (355) — noting that the FDI region is located approximately .8in back from the middle of the outer skin that exists between the thumb and the pointing finger, and that the distance between the anterior and posterior electrodes — shown within Figure: (355) — was measured to be approximately 23 millimeters apart upon electrode contact with the FDI region [430] [424] [424]. Likewise, upon electrode attachment to a human subject — in this particular case Dr. Mehdi Miri volunteered — the subject was seated into a specially design CIE effect reductive wooden chair — which ironically resembles a jail house electric chair, as shown by Figure: (356) — in order to reduce the chance of grounding effects — since the sub floor of the RF shielding room is made of copper, thus permitting the possibility of a electrical path being created between the test subject, the copper sub floor, and the function generator being utilized via the shielding room power distribution grid —, and the test subject was then secured to the wooden chair — via nylon straps — in order to prevent sudden movements that could loosen electrodes or create sudden changes in the previously discussed, unbalanced transmission line effects encountered.

Conversely, before a BIS frequency sweep was performed upon the FDI region of the human hand, a quick DC signal test was done — in which the DRG grippers were briefly decoupled from the attached electrodes, the connection between the two shorted, and a $5V$ DC voltage was applied and measured in order to determine the amount of wire resistance within the configuration being utilized, as shown by Table: (21). Likewise, upon reviewing the results obtain within Table: (21), it was determined that there is no substantial resistance between the electrode to patient interconnection, thus any resistance observed while performing the BIS analysis is not part of the electrode patient interconnection —

although the existence of wire inductance was not precluded from such assessments.

Table 21: measuring bis apparatus interconnection resistance at dc

Input Voltage (V)	R_{sense} Voltage (V)	R_{sense} Current (mA)
4.96	4.96	99.2

Similarly, upon reconnecting the DRG grippers to the electrodes already attached to the FDI region — and insuring that a proper electrical connection was made — a BIS test was performed that utilized a 10V peak sinusoidal sequence of input frequencies — including 100Hz, 500Hz, 1kHz, 5kHz, 10kHz, 50kHz, 100kHz, 500kHz, and 1MHz — and these input signals were then applied to the FDI region of the human hand and then measured at both the input site and at the current sensing resistor — shown within Figure: (341). Likewise, after each test was performed, the — previously discussed — FFT test signal isolation method was implemented to extract both the input and output frequency, magnitude, and phase information respectively — as this information, particularly the input signal, was utilized within the spice simulator, since the spice simulator — as it was quickly discovered — does not tolerate the inclusion of CIEM effects very well — and the magnitude of both the input and the output signal obtained were plotted verses frequency, as shown by Figure:

Figure 356: wooden chair designed to preform fdi experiments

(357) and Figure: (358).

Conversely, as it was — previously observed — within the modeling BIS apparatus subsection, the appropriate selection of the input signal is paramount in determining the amount of CIE effects encountered; likewise, a similar series of conclusions can be obtained — upon examining Figure: (357) — concerning the proper selection of test loading conditions, since — in this particular case —- the function generator — at high frequencies — is so substantially loaded — implying that more current is being drawn from the function generator than it can handle at a given voltage — that the output voltage produced —

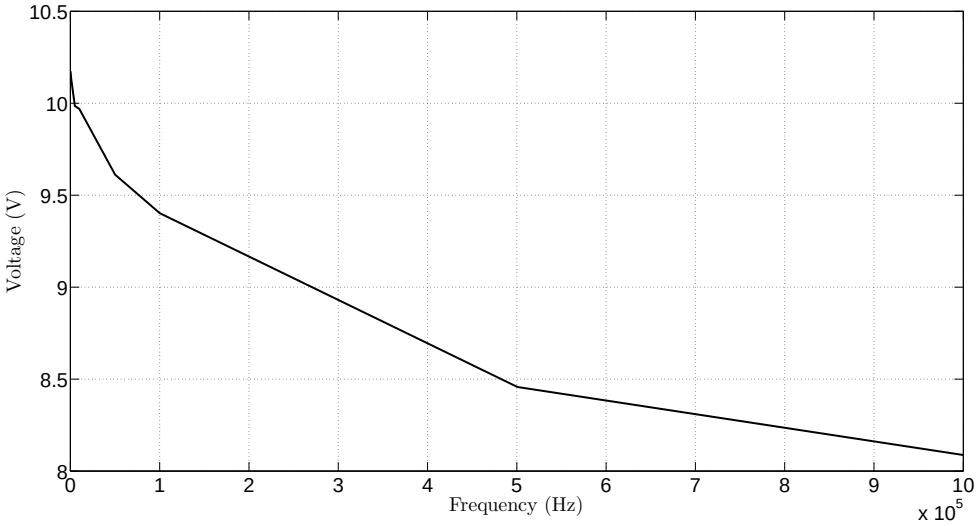

Figure 357: function generator input voltage measured during the fdi test

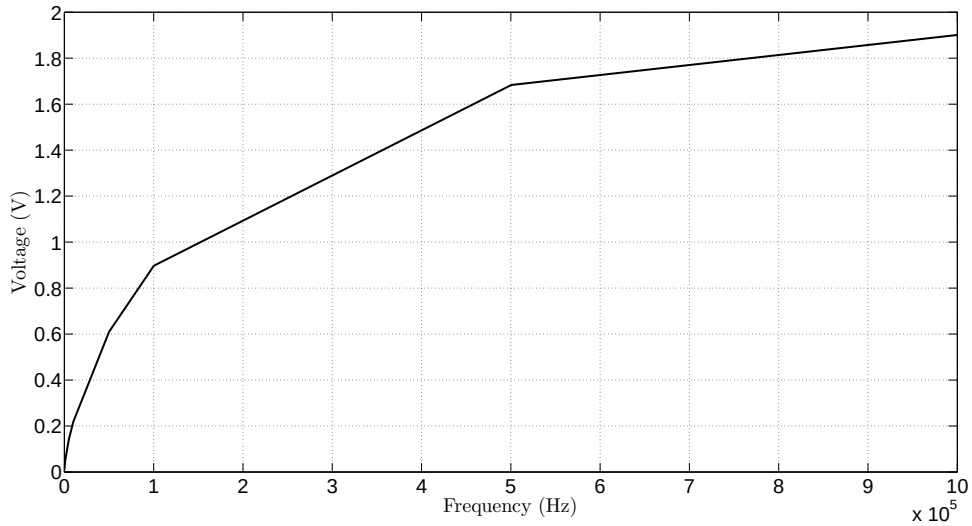

Figure 358: voltage measured across the current sensing resistor during the fdi test

by the function generator — is significantly reduced — an attribute that primarily results from the internal 50 ohm loading impedance, of the function generator, being placed in series with a even lower external loading impedance that, in tern, creates a voltage divider and results in the input signal having a substantially lower magnitude. Similarly, based upon such input signal observations, the following questions tend to arise: First, given that the input remains sinusoidal during this particular loading condition and is known via measurement, are such occurrences truly concerning? Second, what alternatives can be implemented to prevent this particular type of distortion?

Likewise, the answer to the first question is — as it might be expected — somewhat debatable and is highly dependent upon the end application since, for example, if no dependencies exist between the input voltage and the materials being examined then the reduction in input voltage might not be of significant concern — a common scenario of this particular case being the testing of a simplistic linear voltage divider, since the amount of division obtained is ideally independent from the input voltage and the amount of division observed should remain constant —; however, in terms of characterizing a unknown biomaterial, such assumptions cannot be made since, the conductivity of the material being examined might change with the input voltage. Furthermore, because it has already been shown that the amount of CIE effects encountered — within a laboratory acquisition — is associated with the voltage magnitude measured, thus even if the electrical properties of a material being examined were not dependent upon the applied input voltage, the amount of CIE effects encountered will not remain consistent between measurements and this attribute is very problematic in terms of obtaining a high fidelity measurement, since CIE effect consistency is rather important when attempting to automatically remove such effects. Conversely, the answer to the second question — unlike the first question — is

relatively straightforward to answer, since either the current sensing resistor of the BIS application can be increased — although this can modify the observations obtained through current reduction while lowering the amount of output signal obtained —, the test voltage utilized for all measurements decreased — again possibly modifying observed material characteristics —, or a function generator with a higher current output capacity utilized — all though this is not recommended since high current and high voltage are dangerous to a human body.

Nevertheless, while such observations are definitively paramount to obtaining a high fidelity acquisition; however, given the inherent nature of this dissertation to identify the sources of inaccuracies within bioelectrical measurements, it seems rather appropriate to utilize the inconsistent input acquisitions obtained and attempt to model such observations, especially since such attributes seem to be somewhat predominant within contemporary BIS devices and publicize measurements [367] [112]. Conversely, with this being said, it is important to recognize that the electrical properties of a biomaterial does not necessarily physically conform to the traditional electrical equivalent circuit models frequently utilized within the electrical engineering discipline — resistor, inductor, and capacitor —, or at the very least, if some association does exist — with existing ideal electrical components —, it is highly unique relative to the traditional electrical engineering theory commonly utilized — an example being a non-uniformly distributed and variable dielectric based capacitor, or a non-ideal and variable resistor [97] [129] [135]. Likewise, while it could be argued that the utilization of numerical analytical techniques — like least-squares estimation — to create a black box electrical component that is governed by a curve fitted equation, is just as physically intuitive as an equivalent circuit model; yet, given the tendency of most academic BIS publications to utilize an electrically equivalent circuit component model,

such approaches will be the predominant focus within this particular discussion.

Similarly, based upon such specifications, while it is true that some academic BIS publications do attempt to create a structurally equivalent circuit model — similar to the modeling methods discussed within the BIS apparatus subsection — that is based upon the perceived conduction through the material and the materials properties — bone and skin possibly being represented as a dielectric, while blood and living tissue possibly being represented by a combinational resistance and capacitance topology —; however, while such techniques are not inherently incorrect — in fact, it could be argued that this method is more structurally accurate —, yet — based upon the previous discussion regarding parameter estimation techniques —, such methods are inherently problematic because of the unobservable internal structure of the material being examined and the tendency of such techniques — particularly the non-linear Newtonian solver — to become non-convergent or, if convergence is found, the unobservable nature of the topology decreases the overall likelihood that the component values obtained are unique — thus implying that the structure obtain is not necessarily the physical manifestation of the electrical structure of the biomaterial being examined. Conversely, based upon such assessments, and given the difficulties in obtaining both convergence and a accurate physical structure using such modeling techniques, more procedural-based methods are frequently employed to problems of this particular nature and include — but are not limited to — the following: The Dielectric Relaxation modeling methods that notably include the Debye relaxation model and The Cole & Cole relaxation model — as shown by Figure: (359) and Figure: (360), The Dow poll placement method — as shown by Figure: (361) —, and the combinational pole placement method — as shown by Figure: (362) — [338] [97] [129] [135] [336] [337] [339] [340].

Likewise, upon reviewing each of these modeling techniques, a combinational approach

was selected and upon iteratively examining each of the output frequencies in order to observe the amount of attenuation each frequency received — relative to the input signal, since variation in the input voltage was observed —, and selecting the appropriate RC structure — or pole configuration — required to obtain the necessary amount of attenua-

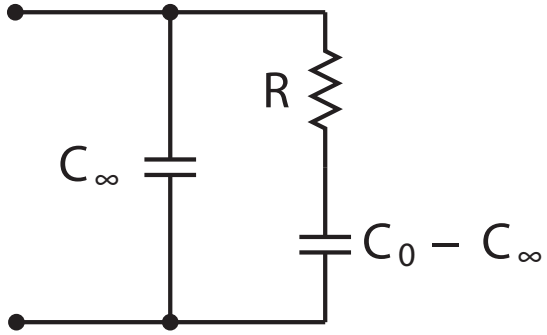

Figure 359: conceptual equipment circuit model of a debye dielectric relaxation process

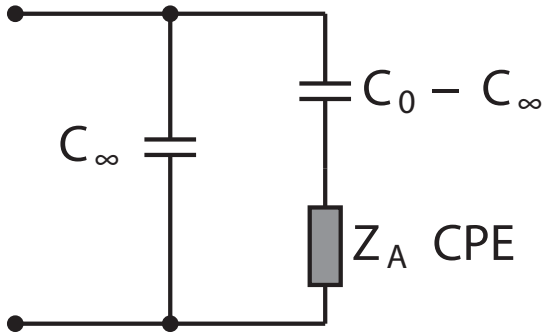

Figure 360: conceptual equivalent circuit model of a cole and cole dielectric relaxation process

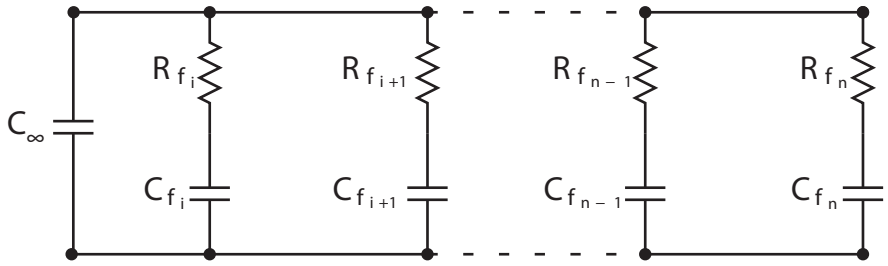

Figure 361: conceptual equivalent circuit model of a dow dielectric modeling method

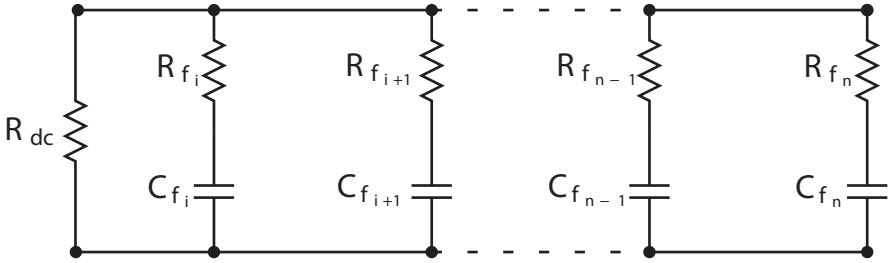

Figure 362: conceptual equivalent circuit model of a combinational dielectric modeling method

tion, an equivalent model of the FDI region of the human hand was obtained through the utilization of this particular modeling technique — as shown by Figure: (363) —, simulated within spice , and compared for accuracy relative to the observed output signals — as shown by Figure: (364), Figure: (365), Figure: (366), Figure: (367), Figure: (368), Figure: (369), Figure: (370), Figure: (371), and Figure: (372) respectively.

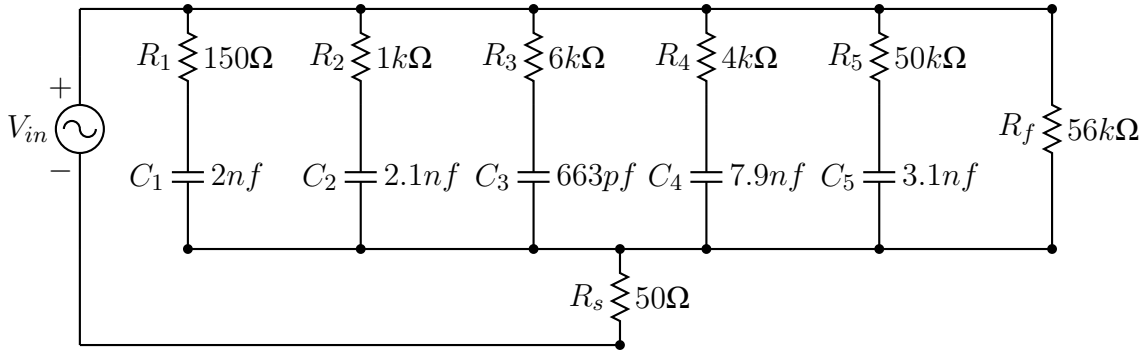

Figure 363: a proposed bioimpedance spectroscopy equivalent circuit model of the fdi region of the human hand using the combinational dielectric modeling method

Conversely, upon reviewing the results obtained within Figure: (364), Figure: (365), Figure: (366), Figure: (367), Figure: (368), Figure: (369), Figure: (370), Figure: (371), and Figure: (372), it becomes apparent that some discrepancy between the simulated

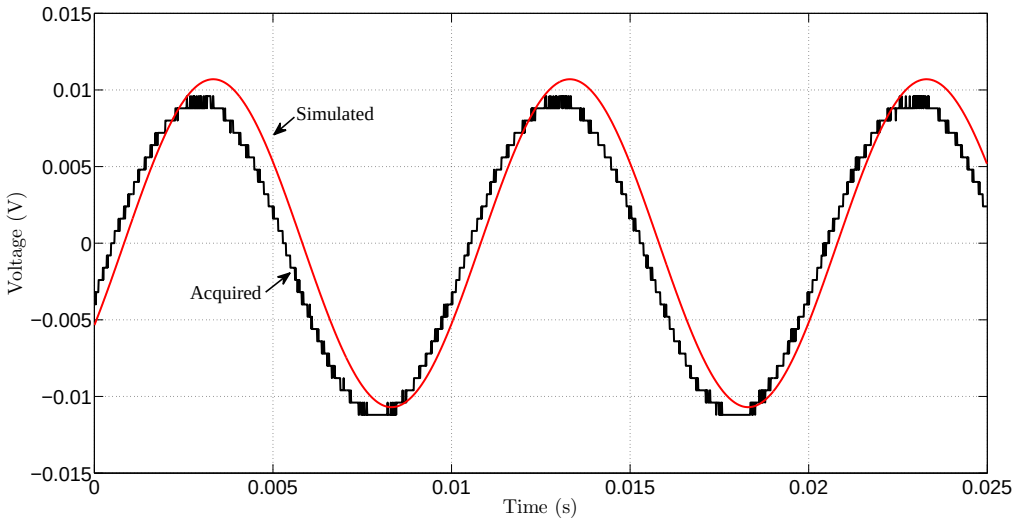

Figure 364: plot of the voltage across the current sensing resistor acquired during the fdi bis examination at a input frequency of 100hz versus the spice simulated voltage obtained from the proposed electrical model

model — as shown by Figure: (363) — and the acquired signal does exist; however, the existence of such discrepancies — especially given the dynamic nature of the input voltage observed, the amount of CIE effects known to exist within the acquisition apparatus, the nonmetallic conductive nature of the material being examined, and the ability to increase the accuracy of Figure: (363) through the modification or addition of RC pole locations — are not substantial enough to discredit the model — shown within Figure: (363) — as being

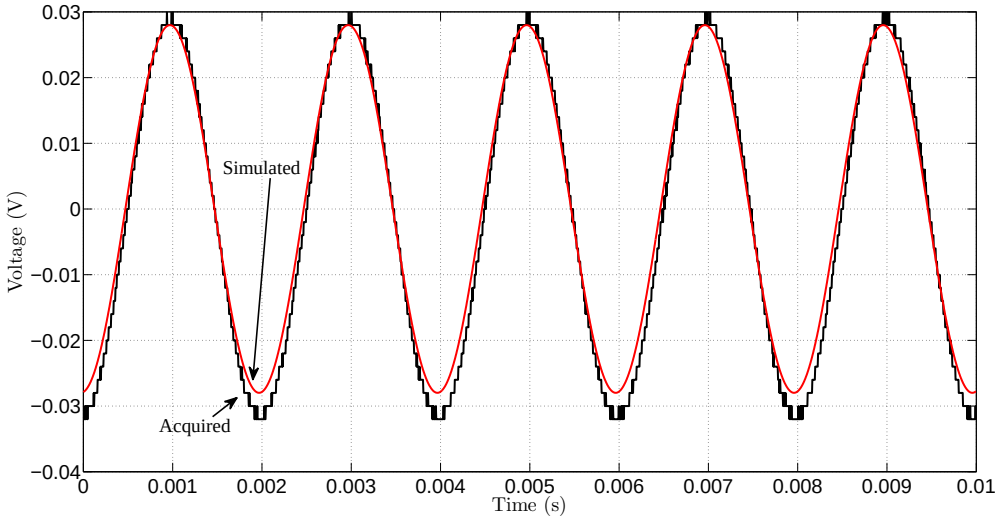

Figure 365: plot of the voltage across the current sensing resistor acquired during the fdi bis examination at a input frequency of 500hz versus the spice simulated voltage obtained from the proposed electrical model

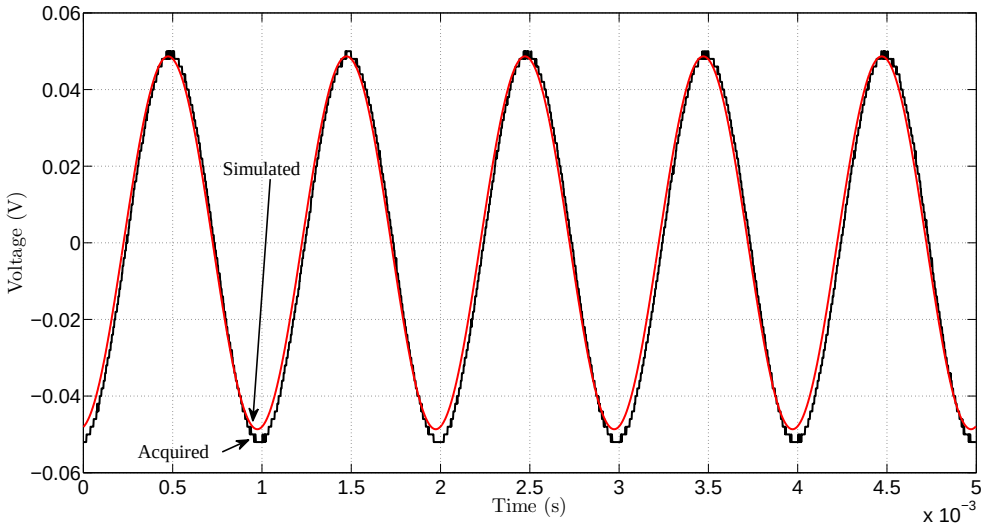

Figure 366: plot of the voltage across the current sensing resistor acquired during the fdi bis examination at a input frequency of 1khz versus the spice simulated voltage obtained from the proposed electrical model

a reasonably accurate approximation of the FDI region being examined, especially upon examining the intrinsic circumstances associated with this particular modeling method, and while improvements could be made — using the considerations previously discussed — such improvements are not inherently necessary, in this particular case, upon considering the desired objective was simply the examination of the effectiveness of this particular modeling technique rather than the physical component parameters obtained.

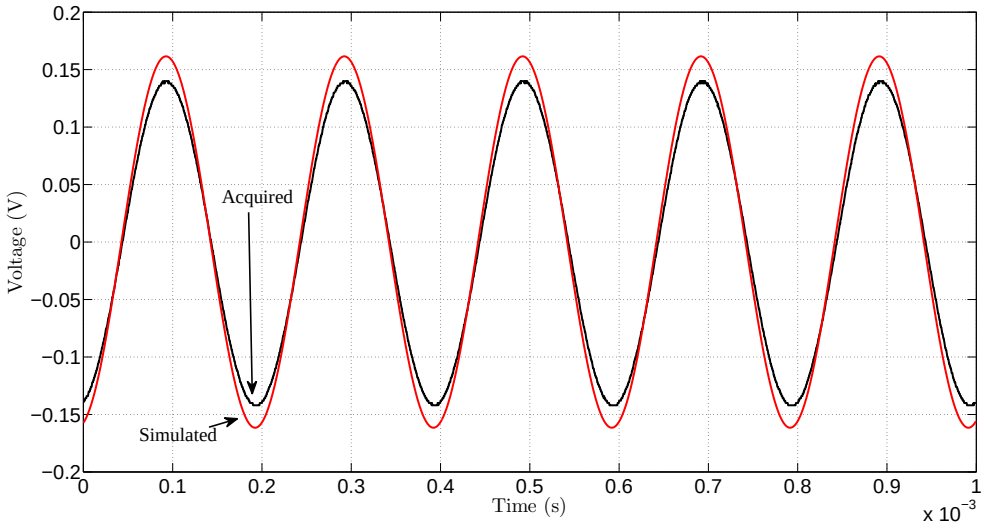

Figure 367: plot of the voltage across the current sensing resistor acquired during the fdi bis examination at a input frequency of 5khz versus the spice simulated voltage obtained from the proposed electrical model

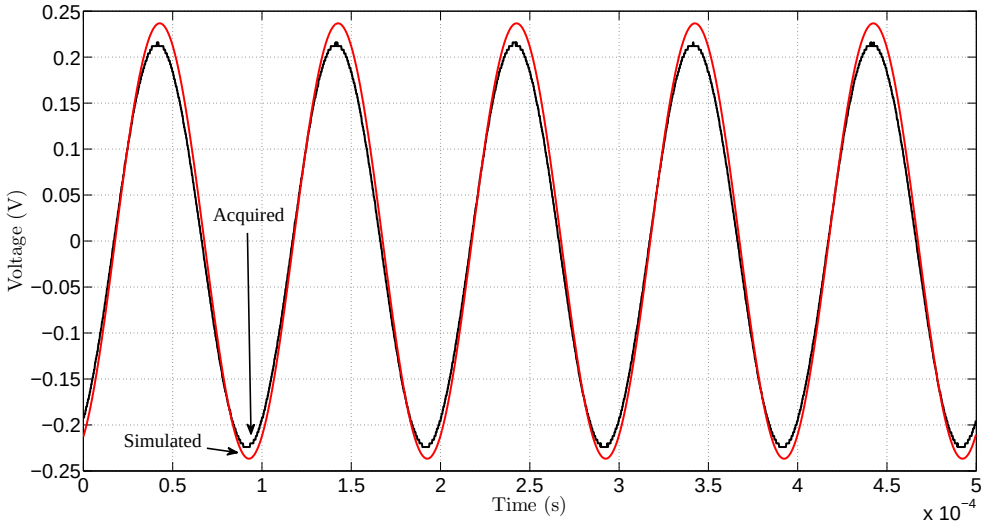

Figure 368: plot of the voltage across the current sensing resistor acquired during the fdi bis examination at a input frequency of 10khz versus the spice simulated voltage obtained from the proposed electrical model

Nevertheless, while this particular method does provide a reasonable procedural alternative — relative to the previously discussed structural modeling method — to the synthesis of a electrical model describing the electrical conductivity of a unknown biomaterial — in this particular case, the FDI region of the human hand —; however, some questions surrounding the legitimacy of such techniques — in terms of obtaining a physical description of the electrical characteristics of the material being examined — does arise, and while such

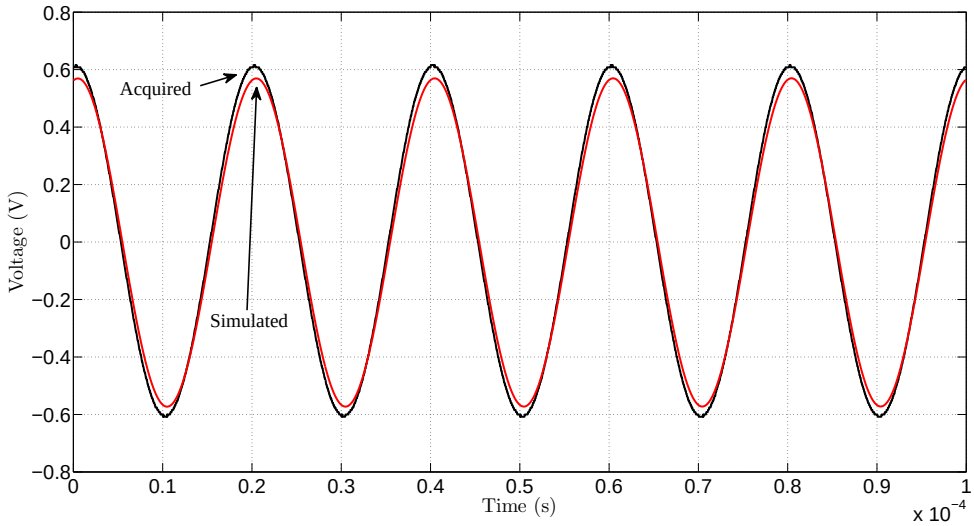

Figure 369: plot of the voltage across the current sensing resistor acquired during the fdi bis examination at a input frequency of 50khz versus the spice simulated voltage obtained from the proposed electrical model

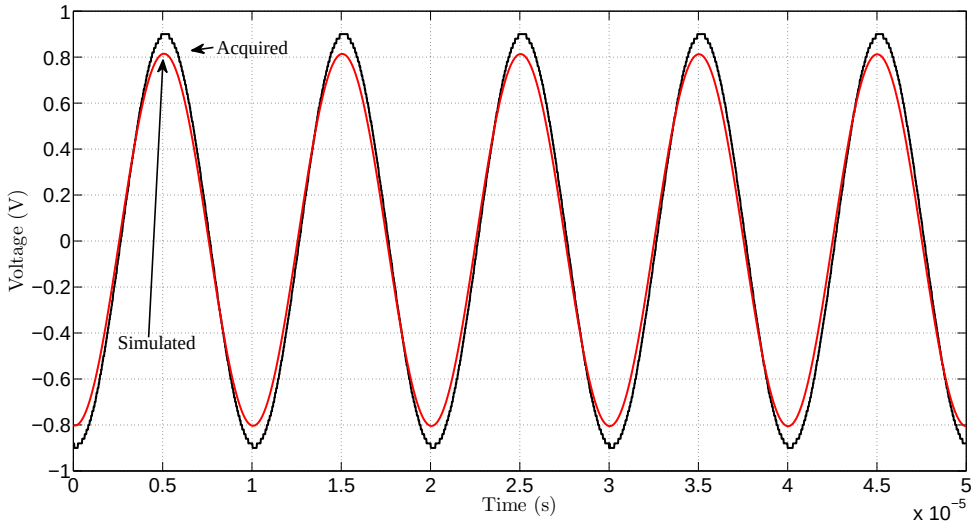

Figure 370: plot of the voltage across the current sensing resistor acquired during the fdi bis examination at a input frequency of 100khz versus the spice simulated voltage obtained from the proposed electrical model

intrigue is definitively merited, especially given the overall multitude of possible equivalent models obtainable — either through structural assumptions or through synthetic derivation —, it appears that the only reasonable answers, to such questions, is:0 First, the physical internal conductive properties of the biomaterial being examined cannot, in itself — at least upon being limited to the information obtained through the utilization of noninvasive characterization techniques —, allow for the identification of the actual physical electrical

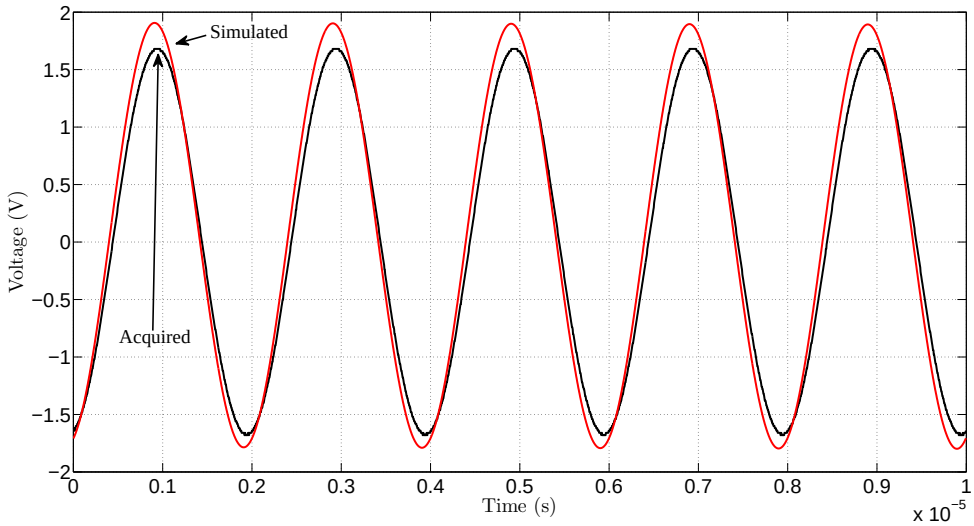

Figure 371: plot of the voltage across the current sensing resistor acquired during the fdi bis examination at a input frequency of 500khz versus the spice simulated voltage obtained from the proposed electrical model

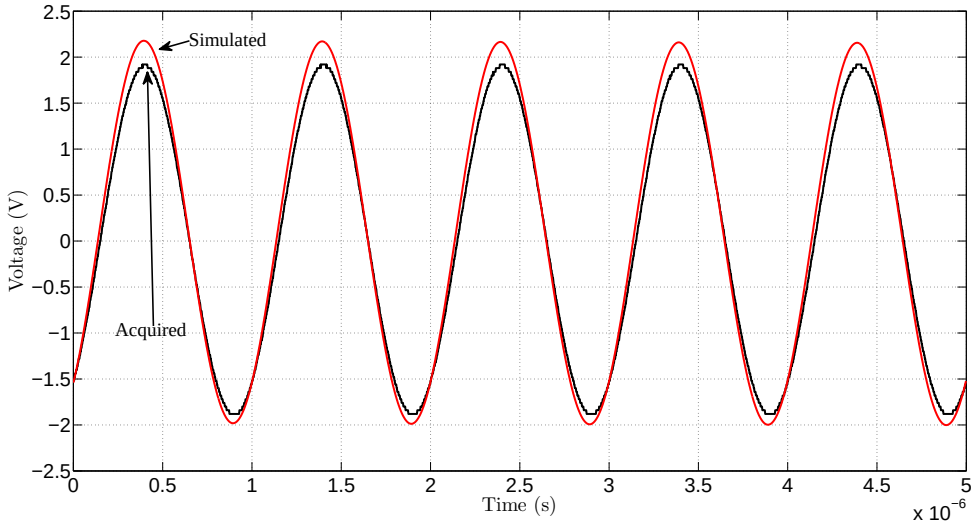

Figure 372: plot of the voltage across the current sensing resistor acquired during the fdi bis examination at a input frequency of 1mhz versus the spice simulated voltage obtained from the proposed electrical model

structure to be known or be reasonably well estimated. Second, while the actual physical structure cannot be directly known using strictly noninvasive analysis techniques; however, so long as the modeling method utilized to examine such characteristics remains consistent, the results obtained should be reasonably comparable and generally will allow for the correlation of the model obtained to a physical attribute — water content or muscle mass [350] [97].

Conversely, while the, previously mentioned, input distortions are naturally present within Figure: (364), Figure: (365), Figure: (366), Figure: (367), Figure: (368), Figure: (369), Figure: (370), Figure: (371), and Figure: (372), and the inherent lack of the, previously discussed, BIS apparatus model parameters — like wire inductance or oscilloscope capacitance — or, for that matter, the overall lack of acquisition CIE effects, inherently implies that such distortions were also incorporated within the synthesized FDI impedance model shown within Figure: (363), and while such inclusions — within Figure: (363) — could have been removed through the utilization of the, previously presented, techniques; however the inclusion of such distortions — within Figure: (363) — was done so deliberately in order to address another type of distortion that is frequently — but unknowingly — encountered, comparison distortion.

Likewise, while the term — comparison distortion — might seem, at first, somewhat abstract; however, the conceptual idea behind the usage of this particular term is based upon the underlying observation that the information — presented within Figure: (364), Figure: (365), Figure: (366), Figure: (367), Figure: (368), Figure: (369), Figure: (370), Figure: (371), and Figure: (372) — and within Figure: (363), first, does not visually demonstrate — at least upon casual observation — the existence of any underlying distortions which are known to exist — implying that such distortions — when they occur — will predominantly

manifest themselves in a non-intuitive and highly non-visible manner within the model developed, and second, assuming that equivalent modeling methodologies were utilized when making material comparisons — which, in itself, is a dubious assumption —, inherently implies that the comparisons made amongst academic researchers — particularly if those researchers are using a variety of different commercial BIS acquisition devices, in which each device would have its own unique CIE profile — could be inadvertently incorporating, such distortions, within any model developed.

Conversely, with this being said, while such attributes can be overcome and accurate comparisons made, assuming that the , previously discussed, distortions are reasonably well understood and accounted for prior to publication — which is the underlying objective of this dissertation —; however, giving the interdisciplinary nature of the disciplines involved, combating this particular type of distortion is not something that is easily achieved without the wide acknowledgment of such distortions, and while such occurrences might someday occur, until then any comparisons made amongst academic researchers — particularly publicized biomaterial results — should be reviewed with some degree of circumspect. Likewise, while such conclusions might seem somewhat pragmatic — if not overly critical —, and the intent of such observations was not to propose that such comparisons are, in themselves, inherently flawed; but rather, that such occurrences should be taken under advisement in order to obtain the highest fidelity possible.

Nevertheless, while such attributes are definitively important in obtaining the highest fidelity possible, and the modeling techniques — previously discussed — are an effective means to represent the electrical properties of a biomaterial for further comparison — assuming that the sources of distortions encountered are either isolated and compensated for, or are heavily documented — ; however, the results observed within Figure: (364),

Figure: (365), Figure: (366), Figure: (367), Figure: (368), Figure: (369), Figure: (370), Figure: (371), and Figure: (372), are far from being typical amongst other regions of the body — an attribute observed within Figure: (373) — since the results obtained, in this particular case, did not possess a substantial amount of observable material distortions that typically arise in atypically conductive materials — like saline.

Conversely, because material effects are a known and observable quantity — especially within bioimpedance spectroscopy —, to demonstrate such characteristics further through the utilization of an alternative BIS testing location — primarily because the FDI region was initially selected because of its tendency to avoid creating substantial atypically conductive anomalies, an attribute that is no longer desired —, and upon utilizing BIS to characterize the region of the body between the anterior wrist and the midpoint of the anterior forearm — as shown by Figure: (373) —, a number of peculiar distortions are observed upon the sinusoidal signal obtained across the current sensing resistor and these distortions, although not overly substantial in this particular case, demonstrate the types

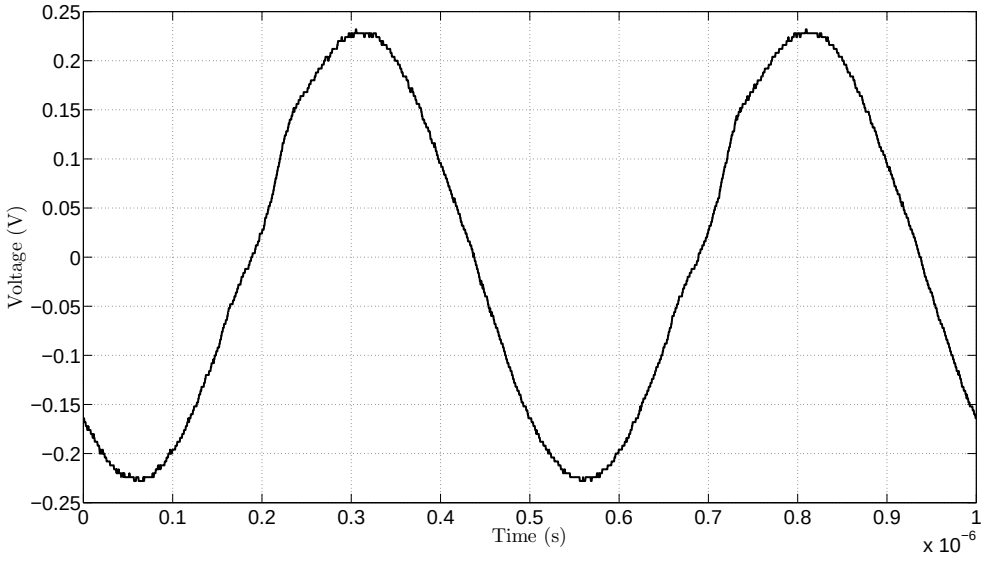

Figure 373: plot of the voltage across the current sensing resistor acquired during the wrist to forearm bis examination at a input frequency of 2mhz versus the spice simulated voltage obtained from the proposed electrical model

of anomalies that generally will manifest themselves upon the active characterization of a living biomaterial or atypically conductive material. Likewise, while it is worth mentioning that the, previously discussed, modeling techniques can be utilized, within this particular scenario, to approximate some of the atypically conductive effects encountered — although proper RC selection, within the Dow or cumulative method, might become rather problematic — especially if a zero is required rather than a pole —, thus, when such effects are encountered, oftentimes the, previously discussed, structural modeling approach is preferred; however, such techniques only attempt to approximate the observed material effects using only ideal circuit components, which may or may not be an appropriate or physically intuitive solution to this particular problem.

6.3.11 BIS and Electrode Corrosion

The fundamental rationale behind the BIS and electrode corrosion section was to provide a preliminary examination of effects that electrical corrosion has on BIS measurements under DC testing conditions. Likewise, based upon the observations obtained within this section, it was determined that the material of the electrode utilized to examine a biomaterial is extremely important in obtaining the highest fidelity possible, since — it was observed — that electrical corrosion can substantially change the overall conductivity of the electrode being utilized, thus electrode materials of platinum, gold, titanium, and to some extent silver should be utilized whenever possible in order to reduce the likelihood of these corrosive effects occurring, and that corrosion is more likely to occur when the test signal applied is a DC voltage or has a DC offset — like an asymmetric periodic waveform —, which implies that these signals should be avoided, particularly when utilizing active material characterization techniques — like BIS or EIS. Furthermore, the discovery of such assessments helped to further refine the unique high fidelity modeling methodology

developed, particularly when DC operational conditions were required.

Likewise, while it must be inevitably accepted that an assortment of atypically conductive materials exist and each material generally will have its own unique electrical modeling approach — noting that the research area of electro-chemistry, and the subset research area of electrochemical spectroscopy (ESI), predominantly investigates such attributes, although some of the observations, previously discussed, would be directly applicable and beneficial to these particular research subsets —; however, because living human biomaterials are predominantly infused with aqueous ionic solutions — aqueous saline would be a likely atypically conductive substance frequently encountered, although aqueous potassium compounds are also a likely possibility —, thus, based upon such observations, the next reasonable course of action would seem to be the examination of the types of material effects encountered upon attempting to analyze, in this particular case aqueous sodium chloride, using bioimpedance spectroscopy [184] [188] [208] [16].

Conversely, while it was tempting to simply connect the, previously presented, BIS acquisition device to a set of electrodes placed within an aqueous saline solution; however, it was decided to first examine how metal electrodes behaved electrically within this particular medium at extended DC voltages — as such potentials can inadvertently be created by the improper application of a test signal, either through the accidental selection of a DC offset or by the usage of a asymmetric waveform —, since the underlying, previously discussed, concept of oxidation reduction or corrosion was known, in order to determine if such attributes would play a substantial role in extended time BIS analysis or extended time bio-signal analysis — an attribute that would frequently arise within a hospital environment when a EKG is utilized to monitor the heart rate of patients over an extended period of time. Likewise, with this being said, it was decided to utilize an

experimental apparatus that consisted of a Agilent E3612A DC power supply that had one terminal attached to a approximately 3in by .5 by .1in brass electrode submerged in a approximately 2in by 2in by 2in container of normal saline at one end of the container, with another approximately 3in by .5 by .06in brass electrode submerged at the other end of the container that was connected to a 110 ohm current sensing resistor that was then connected to the other terminal of the Agilent E3612A DC power supply. Similarly, both submerged electrodes were monitored using the Tektronix TPS2024 oscilloscope — allowing the observation of the voltage across the saline container —, the DC voltage was set to 10V, and the, previously discussed, automatic acquisition code written in Python was utilized to acquire channel samples from the TPS2024 oscilloscope approximately every 5 minutes over a span of approximately two days — as shown by Figure: (374) and Figure: (375).

Conversely, a preliminary observation of Figure: (374) reveals the classical manifestation of the, previously discussed, DC CIE effects, and it is interesting to note how such effects seem to become more predominant as the temporal length of a acquisition test is

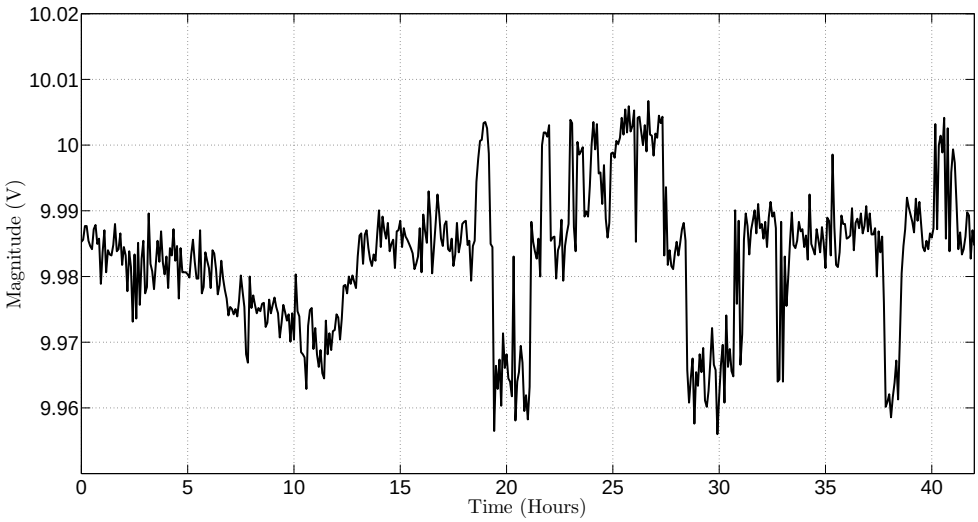

Figure 374: plot of the applied electrode voltage created by the agilent e3612a dc power supply over an extended period of time

substantially extended, and while a number of compensation techniques have already been discussed on this particular attribute — thus no further discussion on the subject will be provided —; however, the manifestation of such effects tends to articulate the importance of both understanding why these effects occur and when compensation measures should be put into effect in order to obtain the highest fidelity acquisition possible — particularly within EIS analysis. Likewise, while the identification of DC CIE effects is inherently im-

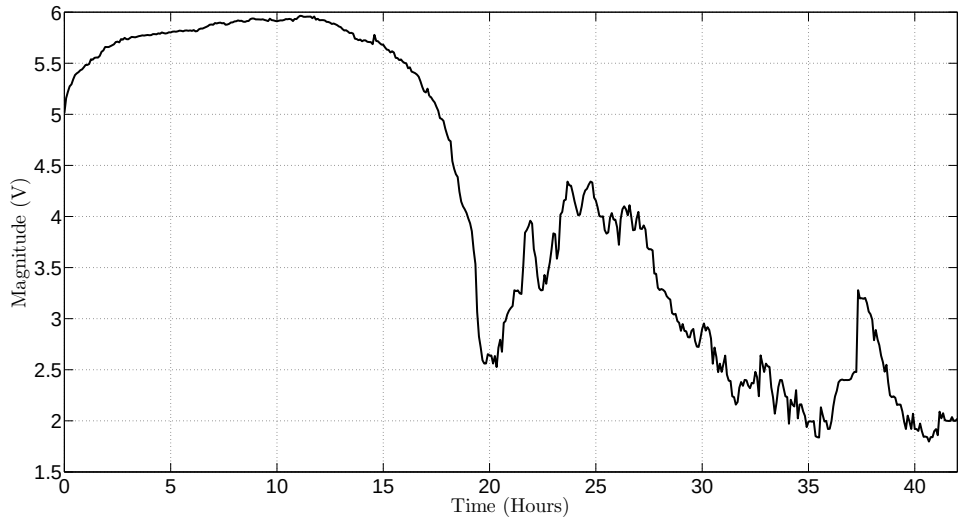

Figure 375: plot of the output voltage obtained by measuring the 110 ohm current sensing resistor over an extended period of time

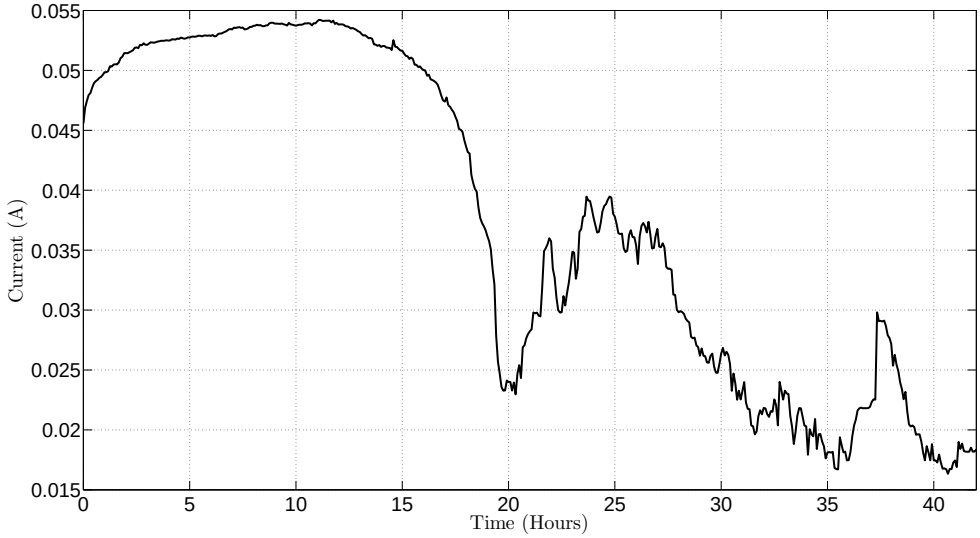

Figure 376: plot of the current measured through the 110 ohm current sensing resistor over an extended period of time

portant, a more interesting observation is obtained upon examining Figure: (375), since the progressive change in output voltage implies a change in the electrical conductivity between the two electrodes that is presumed to be the result of electrode corrosion. Similarly, upon calculating the amount of current moving through the 110 ohm current sensing resistor — as shown by Figure: (376) — it is interesting to observe that the chamber current remains relatively consistent — at around 55mA — until about 15 hours into the experiment, at which point in time the conductivity of the chamber decreases substantially — to 25mA — over a span of five hours, after which it increases again for five hours — to 40mA —, then decreases for 10 hours — to 20mA —, increases again for 2 and a half hours — to 30mA — , and finally begins to taper off to a value around 18mA. Likewise, a similar observation can also be made upon examining Figure: (377) — primarily because of the inverse association between chamber current and the chamber resistance, within this particular circuit —, and it is interesting to observe that the chamber resistance remains relatively consistent — at around 100 ohms — until about 15 hours into the experiment, at which point in time the resistance of the chamber increases substantially — to 325 ohms — over a span of five hours, after which it decreases again for five hours — to 150 ohms —, then increases for 10

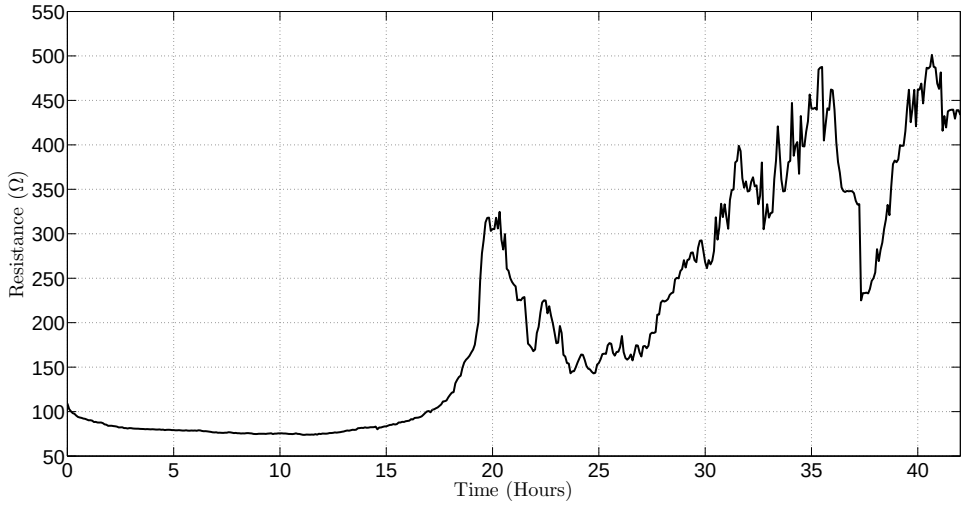

Figure 377: plot of the calculated resistance across the saline solution over an extended period of time

hours — to 475 ohms —, decreases again for 2 and a half hours — to 225 ohms — , and finally begins to taper off to a value around 425 ohms.

While it will be proposed that the observed oscillatory pattern of the chamber resistance seems eerily similar to a passive circuit energy storage element — insofar as implying some type of differential equation is governing this particular process —, such observations — while both interesting and fundamentally demonstrating that these, previously discussed, acquisition techniques can be applied to the subject of EIS — were, nevertheless, predominantly intended to illustrate that electrode corrosion can be a substantial distorting factor within both BIS and passive electrode acquisitions [184] [188] [208] [16]. Likewise, based upon such observations, while the appropriate selection of a chemically nonreactive electrode is paramount in reducing the amount of corrosion effects encountered, it is also important to recognize that the application of a static DC voltage as a test signal is an inherently problematic attribute — because static voltages tend to create chemical gradients within the aqueous material being examined —, and while the attribute of corrosion might be resolved with proper electrode selection — along with some limits being placed upon the applied DC potential —, yet even if a non corrosive electrode is selected, it is very likely that a time increasing resistance will still be observed under such testing conditions, primarily because the application of a DC voltage will create a chemical gradient within the test chamber — because of the steady flow of ions from one side of the chamber to the other — and since electrical conduction — within a saline solution — is achieved thru the movement of ions, if no ions are available for transport — because of a existing chemical gradient — no current will flow across the chamber [184] [188] [208] [16]. Thus, based upon such observations, it is strongly recommended that any type of DC or asymmetric AC waveform biomaterial tests are avoided — wherever possible —, since the results obtained

from such tests are typically plagued with both corrosion and gradient distortions — or, if the avoidance of such tests is not possible, such tests should be limited to short time analysis only — hopefully using non corrosive electrodes like gold, platinum, or titanium — in order to obtain the highest signal fidelity possible under the inherently problematic testing conditions.

6.3.12 BIS, Aqueous Sodium Chloride, and Electrodes

The fundamental rationale behind the BIS, aqueous sodium chloride, and electrodes section was to provide a preliminary examination of the effects that aqueous sodium chloride has upon BIS electrodes when exposed to AC BIS testing conditions in order to determine the viability of commonly found electrode materials — stainless steel versus brass — within a BIS application and the types of distortions that will occur as a result of these materials exposure to such operational conditions. Likewise, based upon the observations obtained it was determined that, while some corrosion did inherently occur — as the materials tested did visually change in appearance, though not as substantially as they did within the prior DC corrosion test — such effects typically did not substantially impact the electrical results obtained over short time durations and that the corrosion effects encountered predominantly appeared to electrically manifest themselves similarly across both materials tested. Conversely, while a slight increase in electrical conductivity was noted within the stainless steel electrode versus the brass electrode test, such effects were not found to be overly profound — relative to the results obtained within the DC corrosion test. Nevertheless, while it was inherently discovered that great care must be taken when selecting a BIS electrode material for electrochemical operation; however, based upon the results obtained within this section it was determined that, so long as the material was not overly electrochemically reactive within the testing environment and the testing duration was kept

short, an electrochemically reactive material could be successfully utilized without the introduction of significant electrical distortions. Likewise, based upon such observations — including those obtained within the DC electrical corrosion test —, it was determined that the prudent course of action — within the high fidelity acquisition methodology developed — was to ensure the usage of an electrode that is noncorrosive — or at the minimum the usage of an electrode that only slowly corrodes — within the medium being examined — during the required testing duration in order to minimize the corrosive distortions encountered. Conversely, while the results obtained — upon examining the tested materials — did appear substantially undistorted by corrosive effects — although it is likely that the distortions observed were subtle, like a slight increase in capacitance because of the formation of an oxide layer upon the electrode surface rather than a substantial change in the concentration of the solution being tested — some slight differences in frequency response were noted, and such observations imply that corrosive effects — even minor ones — can introduce a bandwidth limitation into the system being examined and this attribute had to also be considered within the high fidelity acquisition methodology developed.

Conversely, while the examination of extended time DC corrosion is, in itself, an interesting subject — particularly within the electrochemical spectroscopy (EIS) research area —; however, once again, such testing conditions tend to extend well beyond the metaphoric desired focal point of discussion within this dissertation, primarily because — as it was previously shown within the FDI modeling section — there is generally not a substantial amount of in series resistance within such models, which implies that the living biomaterials being noninvasively examined are not easily electrically stimulated by the application of a DC voltage — an attribute further endorsed by the electrical engineering concept of a DC blocking capacitance, although the utilization of an invasive examination technique would

likely change this particular material attribute. Likewise, because DC analysis — as it has been previously shown — tends to introduce unwanted material distortions, and based upon the fact that the types of tests being examined — within this dissertation — seem not to benefit from such analysis, it was decided that — in the interest of obtaining the highest fidelity possible — that further DC analysis techniques would be avoided. Similarly, while such testing restrictions ultimately help to increase the overall fidelity obtained since, after all, such restrictions prevent the utilization of a sinusoidal signal that has been added to a DC offset along with the usage of asymmetrical waveforms — within BIS analysis — that could potentially corrode electrodes and unknowingly skew ionic concentrations within the material being examined; however, a number of questions still remain regarding the effects of electrode materials upon AC analysis — after all corrosion could still occur at AC — and such questions — like DC corrosion — merit further, though brief, examination.

Conversely, with this being said, because the liquid chamber — utilized within the previous DC corrosion test — was rather large, and based upon the amount of corrosive byproduct observed, within this particular test, it was decided that a smaller, less expensive, test chamber — approximately 1in by 1.5in by .5in — that could be easily replaced for every test performed would be utilized — in this particular case an ice cube tray was selected. Likewise, because the, previously performed, DC test predominantly focused upon normal saline solutions, it was decided to expand the sodium chloride solution utilized to incorporate water, $0.10\%\frac{w}{v}$, $0.20\%\frac{w}{v}$, $0.30\%\frac{w}{v}$, $0.40\%\frac{w}{v}$, $0.50\%\frac{w}{v}$, $0.60\%\frac{w}{v}$, $0.70\%\frac{w}{v}$, $0.80\%\frac{w}{v}$, $0.90\%\frac{w}{v}$ (normal saline), and $1.00\%\frac{w}{v}$ solutions respectively. Similarly, because the subject of electrode material was important, it was also decided that two different types of electrodes would be examined — brass and stainless steel — and each electrode was sized — approximately 1in by 1in by .06in — to fit the testing chamber utilized — an attribute

that allows the electrode to fit snugly at either end of the testing chamber. Conversely, this particular experiment utilize the, previously discussed, BIS single resistor testing apparatus — with a single 110 ohm resistor before the ground connection — and a 5V sinusoidal signal was selected — although, as it has been previously shown, this input signal can vary substantially depending upon the amount of current drawn through the material — and a number of sinusoidal frequencies — including 10 100Hz, 1kHz, 10kHz, 20kHz, 30kHz, 40kHz, 50kHz, 60kHz, 70kHz, 80kHz, 90kHz, 100kHz, 125kHz, 150kHz, 175kHz, 200kHz, 250kHz, 300kHz, 600kHz, 900kHz, 1MHz, 2MHz, 4MHz, 6MHz, 10MHz — were selected to provide a reasonable range of spectral information to graphically observed.

Likewise, upon performing the analysis for the testing conditions outlined above — noting that each change in concentration and electrode material utilized a new test chamber in order to prevent contamination — for the brass electrode, the following information — as shown by Figure: (378), Figure: (379), Figure: (380), Figure: (381), Figure: (382), and Figure: (383) — was obtained.

Similarly, a visual examination of the BIS input voltage — as shown by Figure: (378)

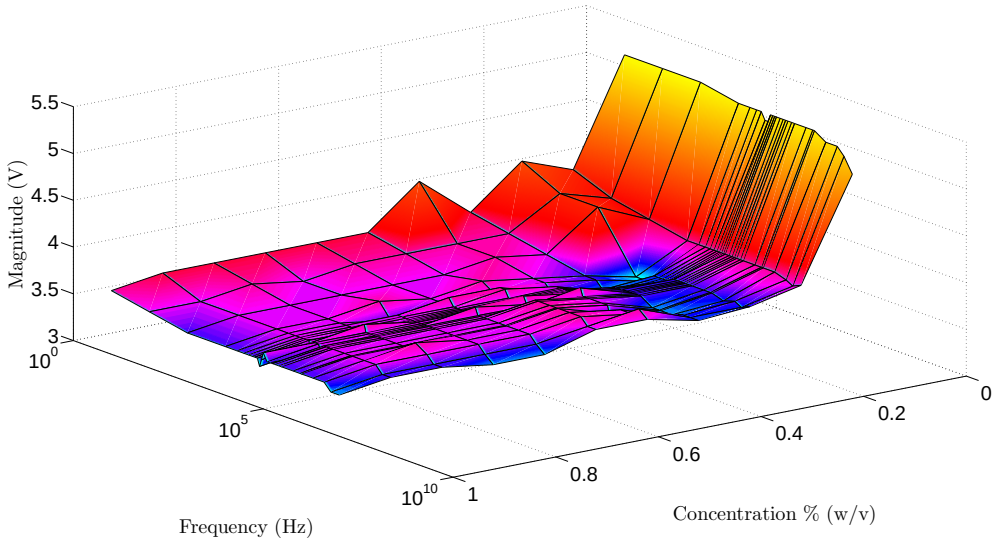

Figure 378: 3d plot of the input voltage on a brass electrode versus concentration and frequency

— reveals that — as it was expected — some observable attenuation has occurred — as a result of the loading requirements placed upon the function generator utilized —; and that the input attenuation observed seems to be in step with the concentration being examined — implying that a increase in the solution concentration will result in a increase in the AC electrical conduction observed — which seems to make intuitive sense given that more aqueous sodium chloride ions are available for charge transportation. Conversely, a visual

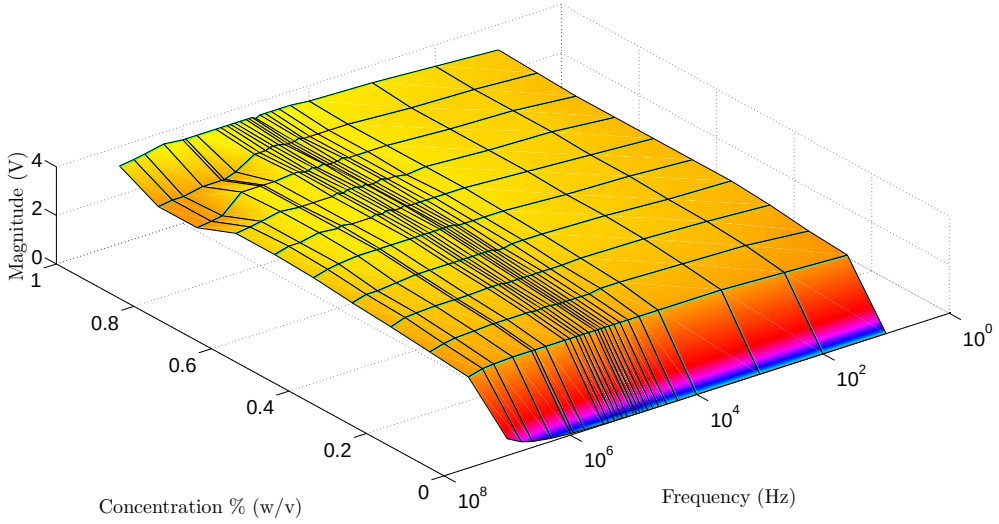

Figure 379: 3d plot of the voltage at the current sensing resistor for a brass electrode versus concentration and frequency

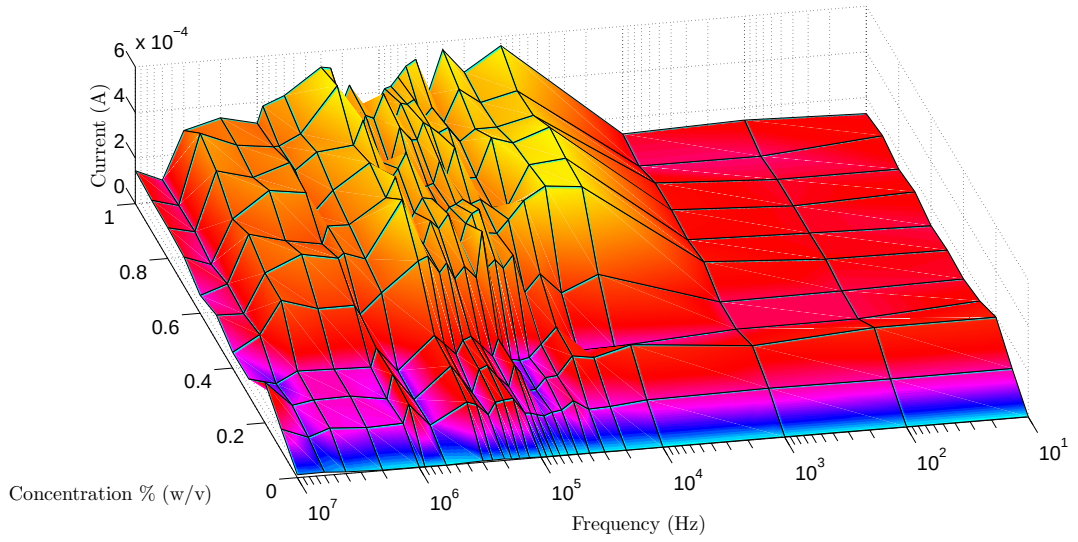

Figure 380: 3d plot of the current measured through the current sensing resister for a brass electrode versus concentration and frequency

examination of the voltage across the current sensing resistor — as shown by Figure: (379) — seems to reveal an expected increase in electrical conduction between the concentration of water to $0.10\%\frac{w}{v}$ region; however, the voltage seems to remain relatively consistent for concentrations at, and above, $0.10\%\frac{w}{v}$ for across all frequencies, with the minor exception of some reduction being observed for frequencies above 10MHz — an attribute that is likely attributed to the, previously discussed, distortions created by RF phenomena. Likewise,

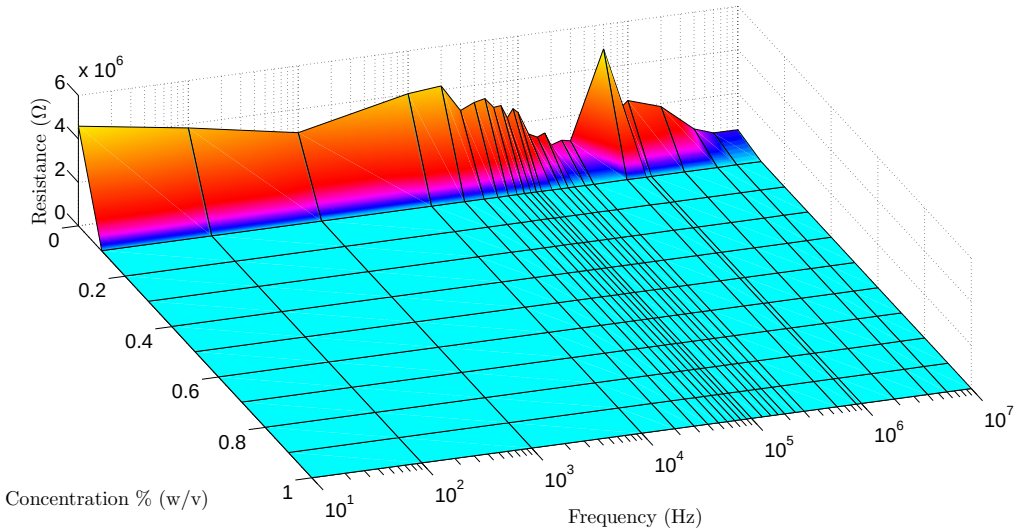

Figure 381: 3d plot of the resistance across the test chamber for a brass electrode versus concentration and frequency

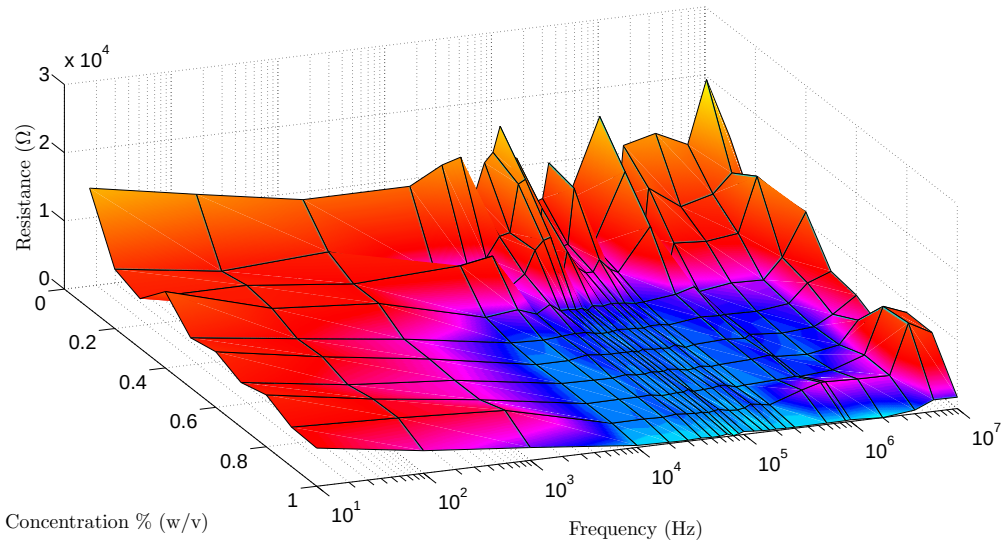

Figure 382: partial 3d plot of the resistance across the test chamber for a brass electrode versus concentration and frequency

a visual examination of the current through the current sensing resistor — as shown by Figure: (380) — naturally seems to convey a similar meaning as Figure: (379), with the exception of doing so at a higher resolution, and — based upon such observations — it would appear that a slight increase in electrical conduction is observed at concentrations above $0.40\%\frac{w}{v}$ and above 1kHz respectively.

Similarly, a visual examination of the calculated resistance across the test chamber — as shown by Figure: (381) — seems to indicate that the electrical conduction of a AC signal through distilled water across a multitude of frequencies is rather insignificant — although this result was expected —; however, upon excluding the water concentration from Figure: (381) — as shown by Figure: (382) — a more visually decipherable figure is obtained, and it appears — upon examining Figure: (382) — that some interesting changes in resistance are occurring over both concentration and frequency — the most notable occurrences occurring within the region above concentrations of $0.40\%\frac{w}{v}$ and between 100kHz and 1MHz. Likewise, a visual examination of the calculated phase shift across the test chamber — as shown by Figure: (383) — seems to indicate some progressive fluctuations in chamber

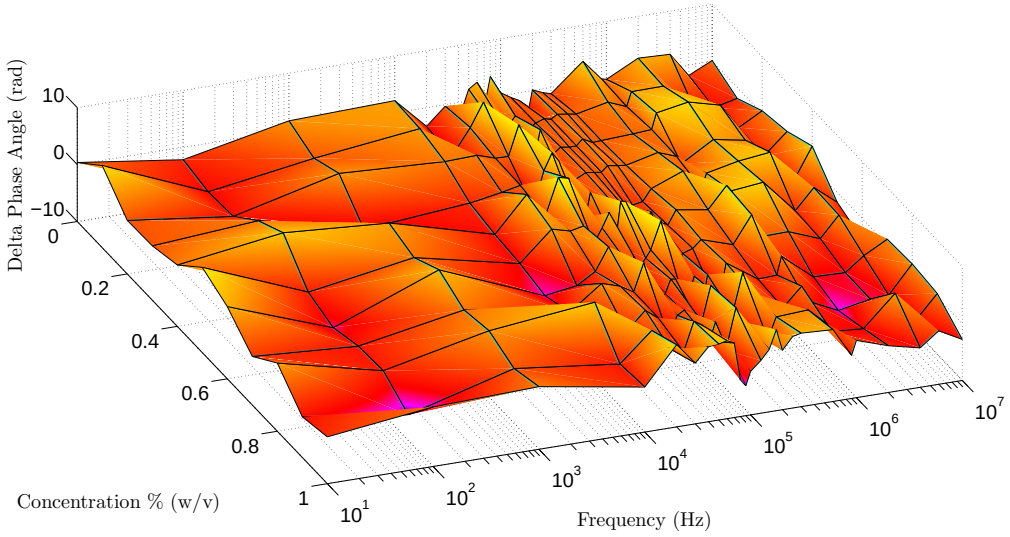

Figure 383: 3d plot of the difference between input and output instantaneous phase across the test chamber for a brass electrode versus concentration and frequency

phase shift — although such attributes are somewhat circumspect given the difficulties in obtaining phase information on noisy signals and were provided predominately for reference than for in-depth analysis.

Likewise, upon the completion of the brass electrode analysis, the stainless steel electrode analysis was performed using the testing procedures outlined above — noting, once again, that each change in concentration and electrode material utilized a new test chamber in order to prevent contamination — for the stainless steel electrode, the following information — as shown by Figure: (384), Figure: (385), Figure: (386), Figure: (387), Figure: (388), and Figure: (389) — was obtained.

Similarly, a visual examination of the BIS input voltage — as shown by Figure: (384) — reveals that, once again, — as it was expected — some observable attenuation has occurred — as a result of the loading requirements placed upon the function generator utilized —; and that the input attenuation observed seems to be in step with the concentration being examined — implying that a increase in the solution concentration will result in a increase in the AC electrical conduction observed — which seems to make intuitive sense given that

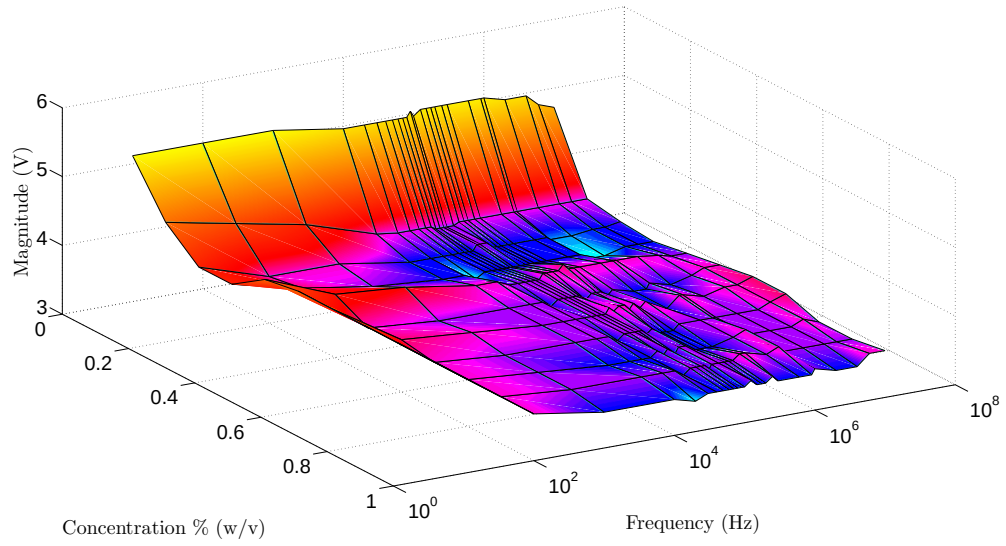

Figure 384: 3d plot of the input voltage on a stainless steel electrode versus concentration and frequency

more aqueous sodium chloride ions are available for charge transportation. Conversely, a visual examination of the voltage across the current sensing resistor — as shown by Figure: (385) —, once again, seems to reveal an expected increase in electrical conduction between the concentration of water to $0.10\%\frac{w}{v}$ region; however, the voltage seems to remain relatively consistent for concentrations at, and above, $0.10\%\frac{w}{v}$ for across all frequencies, with the minor exception of some reduction being observed for frequencies above 10MHz

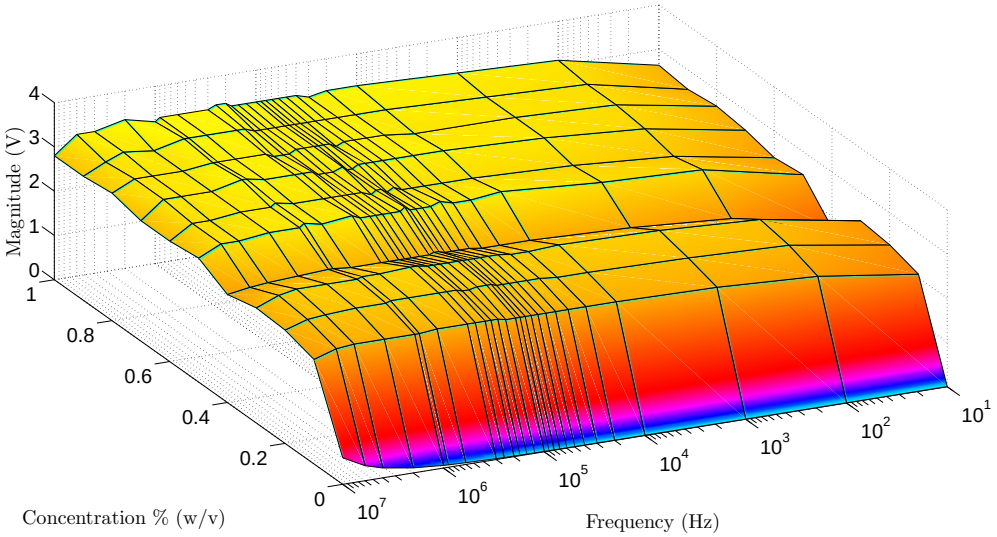

Figure 385: 3d plot of the voltage at the current sensing resistor for a stainless steel electrode versus concentration and frequency

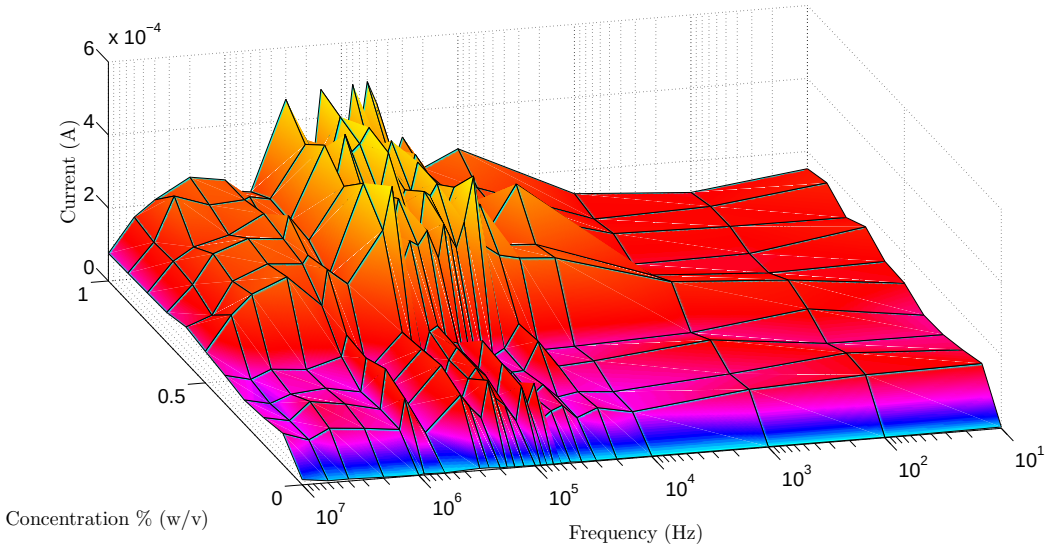

Figure 386: 3d plot of the current measured through the current sensing resister for a stainless steel electrode versus concentration and frequency

— an attribute that is likely attributed to the, previously discussed, distortions created by RF phenomena. Likewise, once again, a visual examination of the current through the current sensing resistor — as shown by Figure: (386) — naturally seems to convey a similar meaning as Figure: (385), with the exception of doing so at a higher resolution, and — based upon such observations — it would appear that a slight increase in electrical conduction is observed at concentrations above $0.40\%\frac{w}{v}$ and above 1kHz respectively. Similarly, a visual

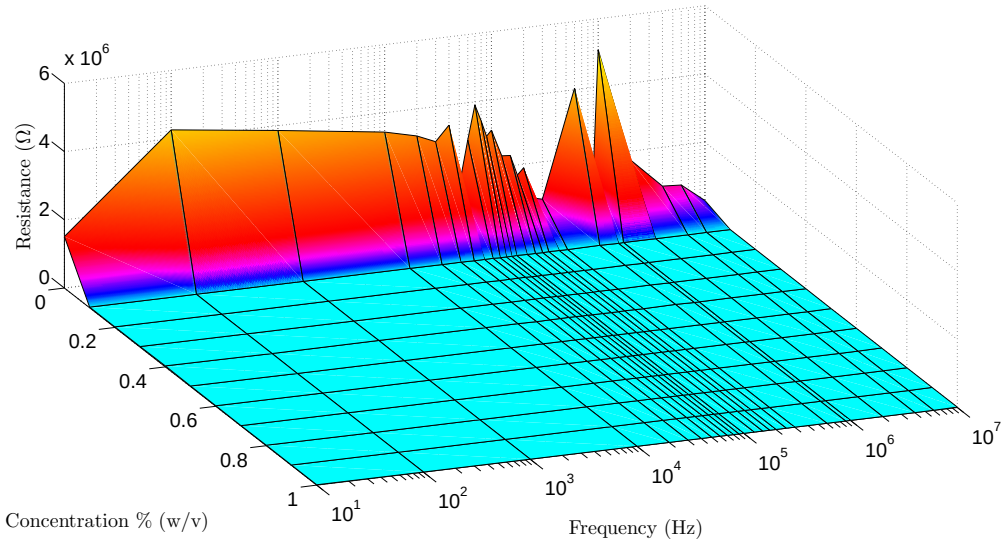

Figure 387: 3d plot of the resistance across the test chamber for a stainless steel electrode versus concentration and frequency

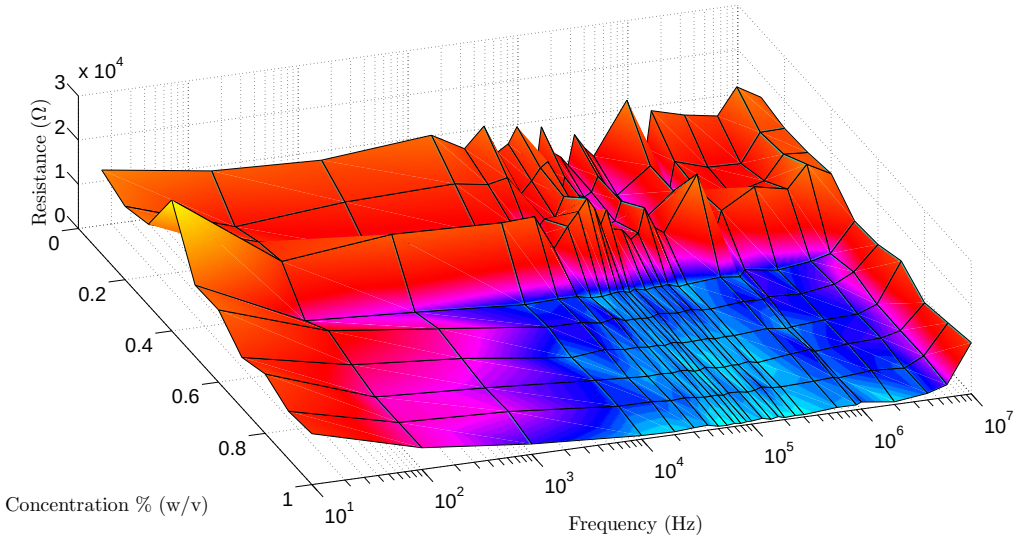

Figure 388: partial 3d plot of the resistance across the test chamber for a stainless steel electrode versus concentration and frequency

examination of the calculated resistance across the test chamber — as shown by Figure: (387) —, once again, seems to indicate that the electrical conduction of a AC signal through distilled water across a multitude of frequencies is rather insignificant — although this result was expected —; however, upon excluding the water concentration from Figure: (387) — as shown by Figure: (388) — a more visually decipherable figure is obtained, and it appears — upon examining Figure: (388) — that some interesting changes in resistance are occurring over both concentration and frequency — the most notable occurrences occurring within the region above concentrations of $0.40\%\frac{w}{v}$ and between 10kHz and slightly above 1MHz — which implies that the stainless steel electrode seems to conduct better within this region than the brass electrode did. Likewise, a visual examination of the calculated phase shift across the test chamber — as shown by Figure: (383) — seems to indicate some progressive fluctuations in chamber phase shift — although such attributes are somewhat circumspect given the difficulties in obtaining phase information on noisy signals and were provided predominately for reference than for in-depth analysis.

Conversely, upon comparing the results obtained for each electrode material examined

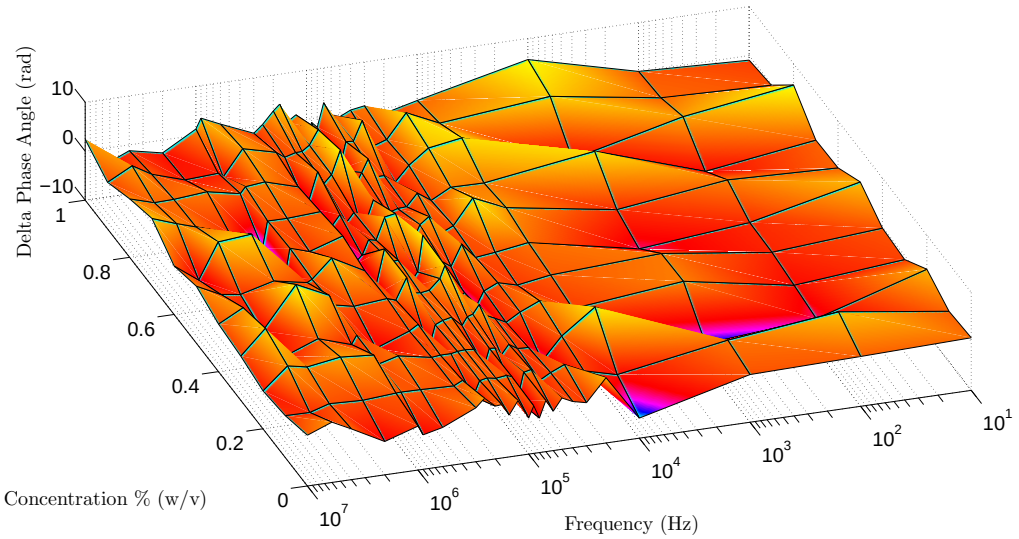

Figure 389: 3d plot of the difference between input and output instantaneous phase across the test chamber for a stainless steel electrode versus concentration and frequency

— those materials, once again, being brass and stainless steel —, the following conclusions can be made: First, while some corrosion is inherently occurring within these materials — as the electrodes observed did visually change in appearance after performing each test — it appears that such effects are either not substantially affecting the results obtained — at least over the time slot required to perform the test — or that the corrosion process that occurred manifested itself similarly within both materials. Second, while a slight increase in electrical conductivity was noted within the stainless steel electrode versus the brass electrode, such effects were not overly profound, and while extreme caution should be utilized when selecting a BIS electrode, it could be argued that — so long as the material is not overly reactive with the testing environment — that either electrodes would produce similar results — although it might also be equally argued that the corrosive effects encountered were simply similar, within both electrodes, and thus were embedded within the measurements acquired equally, although this seems highly unlikely given that the corrosive byproducts would likely be different within each test case [184] [188].

Nevertheless, based upon such observations — including those obtained within the DC electrical corrosion test —, it seems prudent to select an electrode that is noncorrosive — or at the minimum, only slowly corrodes — within the testing medium being examined — an attribute that reinforces the need to fully understand every nuance of the test being performed — in order to obtain the highest fidelity possible, and while the results obtained — as previously shown — appeared to have not been substantially distorted by corrosive effects — although it is likely that the distortions observed were visually subtle, like a slight increase in capacitance because of the formation of an oxide layer upon the electrode surface rather than a substantial change in the concentration of the solution being tested — some slight differences in frequency response were noted, and such observations imply

that corrosion might metaphorically bandwidth limit the conduction region of a material being examined. Likewise, while it might be tempting to begin the process of attempting to model such observations; however, it seems that the subject of electrical potential within the solution should be examined prior to attempting to develop such mathematical models — along with selecting a noncorrosive electrode — since, as it currently stands, the mechanism of voltage drop within the medium being examined is still relatively unknown and unobserved — an attribute that cannot be investigated noninvasively within a living biomaterial, which, given the nature of this particular test, can be examined within this particular testing scenario and possibly provide some beneficial insight into the required electrical structure needed to model a living biomaterial.

6.3.13 AC Signals and Liquid Gradients

The fundamental rationale behind the AC signals and liquid gradients section was to develop a low cost method of examining potential gradients within a conductive aqueous solution in order to determine the viability of noninvasive FDI muscle stimulation using both differential voltage modulation and impedance modulation, and to examine the electrical properties of normal saline within a bulk injection environment. Likewise, based upon the observations obtained, it was determined that the shape of the gradient created appears to remain relatively consistent, with the notable exceptions being a slight flattening — or reduction in resistance between electrode locations — within the bulk of the medium, and a unique drop in potential below the observed value of the current sinking electrodes — at frequencies above 6kHz — , seems to imply the existence of a collection of negative charges — within this region — that might be somewhat analogous to the development of a standing wave — within a transmission line —, insofar as, such collected negative charges could be the result of a substantial buildup of positive charges near the current sinking

electrodes. Likewise, because the shape of the gradient did not change with frequency — beyond the formation of the minor discrepancy observed near the current sinking electrodes —, it seems reasonable to assume that the underlying process responsible for the creation of these gradients — presumably an exclusion zone (EZ) phenomenon — is not inherently dependent upon electrical frequency. Similarly, the overall resistance across the liquid seems to decrease as a function of frequency, which seems to imply that the charge transport mechanism across the liquid is, in fact, a function of frequency. Conversely, while such observations were deliberately more empirical than mathematical, predominantly because the intended objective of these experiments was intuitive observation rather than predictive modeling; however, given the nature of the gradients observed, it was determined that differential voltage injection — the process of using two function generators in such a configuration that the common ground is not exposed to the test apparatus — or impedance modulation — the act of programmatically varying the current sensing resistor — could be utilized to modify the shape of the gradient created and force particular regions, within the gradient, to be a particular potential value — although, some physical restrictions do apply. Likewise, similar stimulation methods — when applied to the FDI muscle — did yield painful FDI stimulus and based upon such observations it was determined that such attributes should be researched further, since such stimulation methods appears to be both unique and beneficial to the advancement of precision noninvasive muscle stimulation.

Conversely, because the observation of the electrical potential created across a liquid medium was desired — predominantly because it would hopefully provide some insight into the internal transmission structure of the medium being examined prior to electrical modeling —, such research objectives were inherently problematic — at least from a logistical perspective —, insofar as, only eight channels were available — across three oscilloscopes

— for data acquisition, and of those eight channels a minimum of three would be required to ensure synchronization between the three oscilloscopes utilized. Likewise, based upon such logistical observations, in turn, leaves five channels available for data acquisition, and because a minimum of one channel is required for measuring the current across the current sensing resistor, the number of channels decreases to four — two from the TPS2024 oscilloscope, and two from the two TDS2002 oscilloscopes respectively —, and because the oscilloscopes are different this inherently increases the potential for the, previously discussed, CIE distortions to occur, along with the fact that four channels of acquired information does not inherently provide a reasonably good depiction of any potential gradient created — especially since electrodes would need to be manually disconnected and reconnected, which could change the system being examined, in order to expand information about the potential gradient created.

Similarly, while the ideal solution — to such problems — would be the development of a multichannel — on the order of 50 Channel — simultaneous acquisition device; however, because such devices are very expensive to either commercially purchase or develop, while the alternative of manually changing electrode locations was inherently so problematic it merited no further consideration; thus, based upon such observations, a compromise was developed — by the code name of Medusa — that utilized a single TPS2024 oscilloscope — in order to alleviate some of the acquisition CIE effects encountered — and a 40 to 1 remote-controlled analog channel multiplexer in order to permit the automated acquisition of electrical potentials at 40 unique locations within a liquid solution — as shown by Figure: (390) and Figure: (391).

Conversely, while the implementation — of this particular acquisition device — inherently introduces an added time delay between potential location acquisitions — since only

one channel was being utilized to obtain a potential measurement at a singular location per oscilloscope acquisition —; however, given the steady-state application of the intended sinusoidal signal to be applied, it was hoped that any effects that might result from such delays would be substantially reduced because of the formation of a quiescent potential gradient within the medium being examined — an assumption that seems to be reasonably

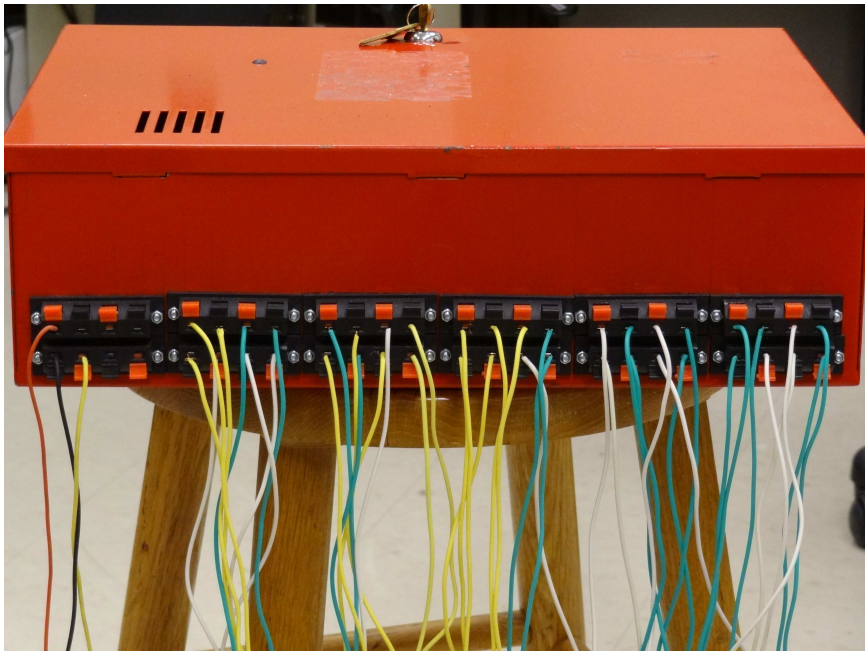

Figure 390: a picture of medusa, the custom-designed 40 to 1 remote-controlled analog channel multiplexer

Figure 391: a picture of the internal workings of medusa, the custom-designed 40 to 1 remote-controlled analog channel multiplexer

correct after examining the results obtained from a number of experiments conducted with this particular device. Likewise, while the external interface of Medusa — as shown by Figure: (390) — might appear, at first, somewhat hectic; however, the overall connection mapping utilized is relatively straightforward, as the upper and lower left most terminal blocks — noting that each terminal block contains two red and two black tabs — is the circuitry plus and minus power and oscilloscope probe connection points — or visually red wire, black wire, yellow wire respectively — , while the remaining 10 upper and lower terminal blocks are the 40 Multiplex channels that begin counting upwards from left to right — the lower left terminal starts at 0 and goes to 19 while the upper left terminal starts at 20 and goes to 40 — respectively. Similarly, while the external connection structure of Medusa is — admittedly — somewhat complex, this initial complexity significantly wanes upon examining the internal circuitry utilized to control Medusa — as shown by Figure: (391) — since control wires are running all over the place in a haphazard fashion. Likewise, while it will be admitted that such wiring practices are inherently impractical — both from a servicing and CIE effects perspective —; however, given the materials available and the amount of space within the box such attributes were somewhat unavoidable. Nevertheless, while the wiring practices implemented might be questionable, the device itself utilized a Renesas SKP QSk62P development board that toggled the required relays upon receiving a simplistic binary encoded RS–232 command — in a manner similar to the DAC code available within appendix A.

Conversely, with a solution to the channel acquisition problem found, the next problem that had to be addressed was the selection of a electrode material that would not easily corrode when electrically stimulated within a normal saline solution that was also not cost prohibitive — like gold or platinum —, and upon doing some background research on the

subject, it was decided that a grade 2 titanium electrode — while not entirely electrically noncorrosive within a sodium chloride solution, ,although experimentation seems to indicate that corrosion will only significantly occur at DC voltages —, seem to perform reasonably well under sinusoidal test conditions and was thus selected as the electrode material utilized is the within this particular experiment. Likewise, because attempting to place and connect approximately 40 electrodes within a small liquid region — like a 1in by 1.5in by .5in container — is inherently problematic, it was decided to expand the test chamber size substantially — as shown by Figure: (392) — in which the electrode apparatus was placed within the middle of a — approximately 1ft by 6in by 6in — tupperware container — that could hold approximately a gallon of normal saline solution. Similarly, the electrode apparatus utilized was approximately 6in by 4in by 4in in total size and contained 42, .20in in diameter titanium electrodes, that were vertically spaced by 19mm increments and horizontally spaced by 14 mm increments respectively.

At this point, now that the testing apparatus and acquisition problems have been addressed, it was decided that the, previously utilized, BIS acquisition system would be used

Figure 392: a picture of experimental apparatus utilize to create bis liquid gradients

in conjunction with Medusa given the sinusoidal nature of the test to be performed. Likewise, the — previously discussed — BIS acquisition python control script was slightly modified to communicate with Medusa, in order to cycle through each of the electrode locations prior to moving to the next sinusoidal test frequency — once again noting that the upper current sensing resistor was removed and the lower current sensing resistor was replaced with a 1K ohm resistance, in an attempt to reduce the amount of loading placed upon the function generator. Conversely, the upper electrodes — or the electrodes located near the upper end of the longer side of the liquid tank — were connected to the function generator, while the lower electrodes — or the electrodes located near the lower end of the longer side of the liquid tank — were connected to the current sensing resistor — implying that the seven upper electrodes were connected to the function generator, while the seven lower electrodes were connected to the current sensing resistor, thus leaving the remaining 28 electrodes to be connected to the Medusa unit, which in turn, would be multiplexed to a selected channel of the Tektronix TPS2024 oscilloscope.

Likewise, while the electrode configuration selected might seem, at first, somewhat strange; however, the objective of connecting the upper and lower horizontal electrodes to similar potentials was to approximate the existence of a solid electrode across the top and bottom section of the apparatus being utilized, since the diameters of the apparatus electrodes were relatively small — predominantly because large titanium electrodes are somewhat cost prohibitive, and would reduce the overall flexibility of the testing apparatus. Conversely, with this being said, based upon the, previously discussed, experiments a input voltage of 10 V peak was selected — in order to maximize the chances of a gradient being created across a liquid medium this large — and a number of sinusoidal frequencies — including 100Hz, 200Hz, 400Hz, 600Hz, 800Hz, 1kHz, 2kHz, 4kHz, 6kHz, 8kHz, 10kHz,

20kHz, 40kHz, 60kHz, 80kHz, and 100kHz — were applied at the input, while the potential gradient was measured with the aid of Medusa, and the results obtained were plotted in three dimensions — length, width, voltage —, as shown by Figure: (393), Figure: (394), Figure: (395), Figure: (396), Figure: (397), Figure: (398), Figure: (399), Figure: (400), Figure: (401), Figure: (402), Figure: (403), Figure: (404), Figure: (405), Figure: (406), Figure: (407), and Figure: (408), in order to visualize the created potential gradient within the normal saline solution being examined — noting that each frequency analysis took approximately 40 minutes to perform.

Similarly, upon visually examining the gradient created after the application of a 10V sinusoidal signal at a frequency of 100Hz was applied with a calculated steady-state AC current of 900nA and a chamber resistance of 10.3k ohms respectively — as shown by Figure: (393) —, it becomes apparent that, first and foremost, a potential gradient across the liquid does, in fact, exist — an attribute that was inherently speculated but not necessarily known. Likewise, further examination of Figure: (393) seems to reveal that the majority of the applied input voltage is attenuated at the metal liquid interface current sourcing

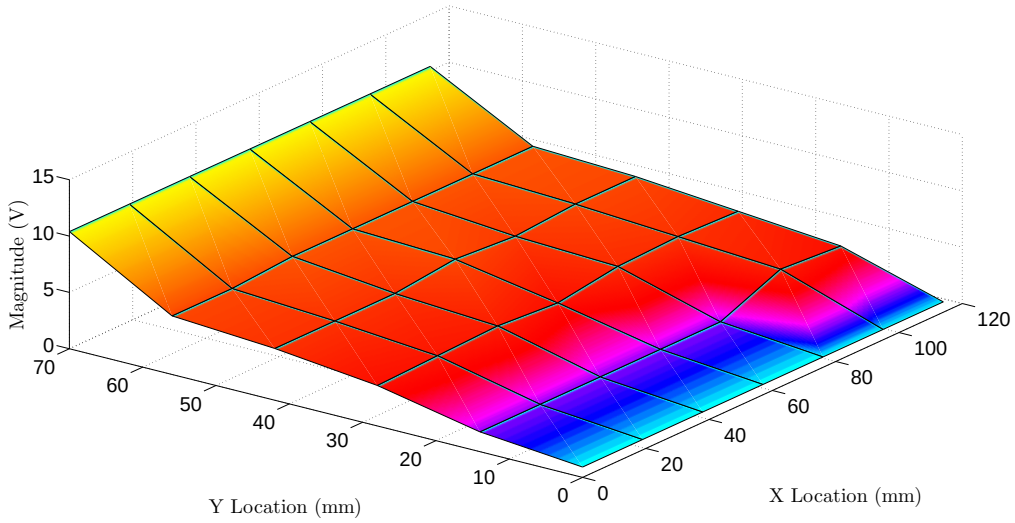

Figure 393: potential gradient observed within a normal saline solution using titanium electrodes and a sinusoidal input frequency of 100hz

electrodes — an observation that seems reasonable — and that the gradient created — within the liquid itself — appears to remain relatively consistent — although an approximate 3V decay across the liquid medium is noted — until another substantial drop occurs near the current sinking electrodes. Conversely, while the visual presence of a relatively constant liquid potential might seem somewhat strange; however, there is some theoretical precedents that could associate such observations with the formation of a exclusion zone

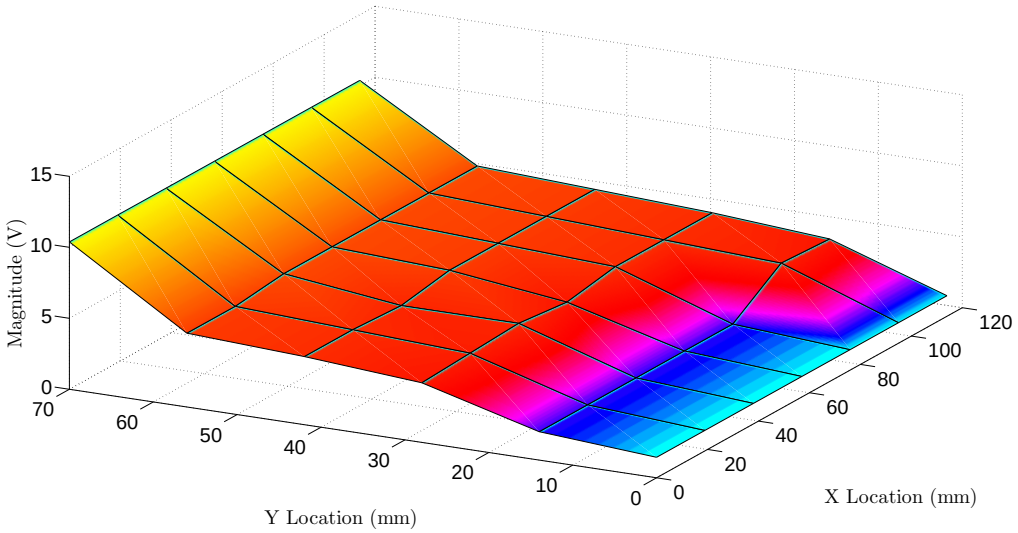

Figure 394: potential gradient observed within a normal saline solution using titanium electrodes and a sinusoidal input frequency of 200hz

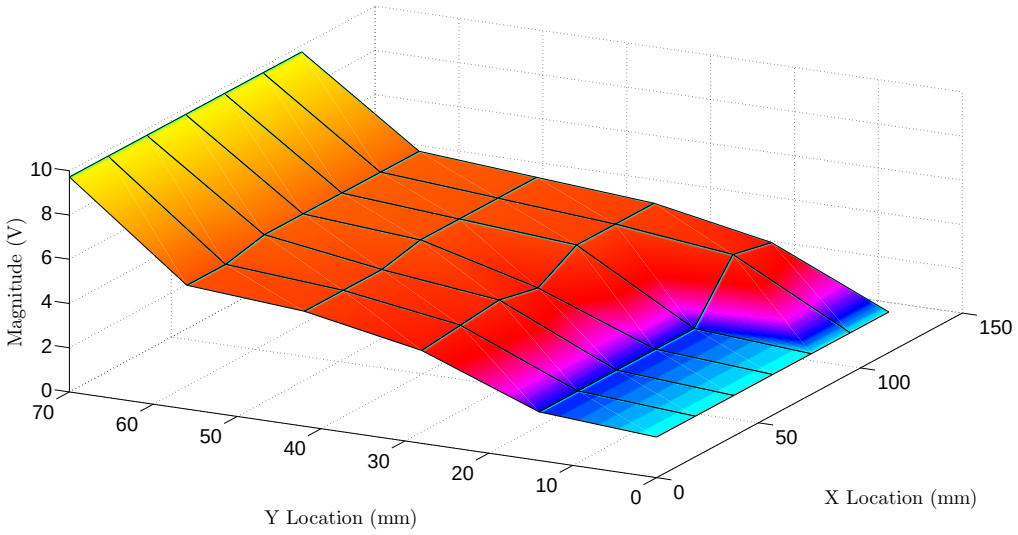

Figure 395: potential gradient observed within a normal saline solution using titanium electrodes and a sinusoidal input frequency of 400hz

(EZ) between the aqueous solution and the metal electrode that seems to be the result of a forth — honeycomb structure H_3O_2 phase of water — although the addition of both large external potentials and extraneous ions have not been fully incorporated into these particular theoretical precedents [431] [432] [433] [434]. Nevertheless, based upon the results obtained, it becomes apparent that most of the signal attenuation is predominantly occurring at the input signal interface — or presumed it EZ region — with a effective

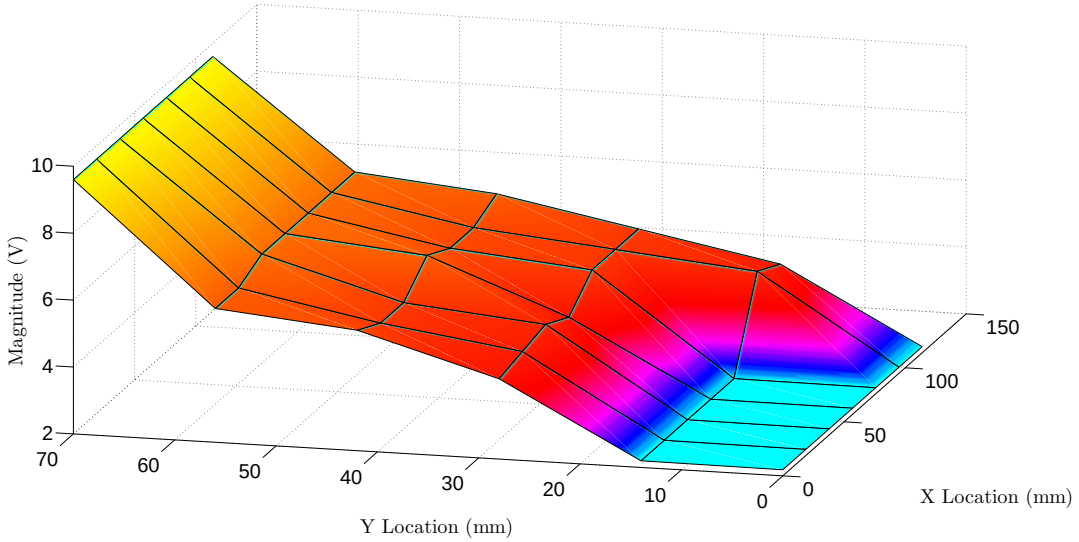

Figure 396: potential gradient observed within a normal saline solution using titanium electrodes and a sinusoidal input frequency of 600hz

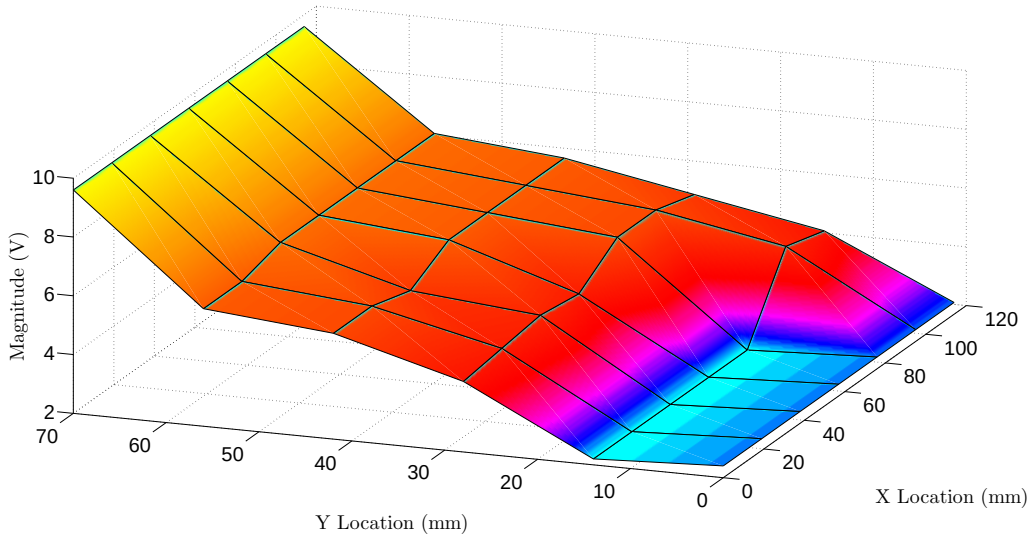

Figure 397: potential gradient observed within a normal saline solution using titanium electrodes and a sinusoidal input frequency of 800hz

resistance of approximately 5K ohms, while the remaining potential drops seem to occur in approximately 1k ohm increments per electrode separation unit utilized, until reaching the electrodes prior to the sourcing electrodes, at which point a substantial increase in resistance is noted — at approximately 3K ohms — and a final 1k ohm transition between the liquid and sinking electrodes is observed — noting that the potential drop observed is symmetric in location for both positive and negative cycles of the applied sinusoidal

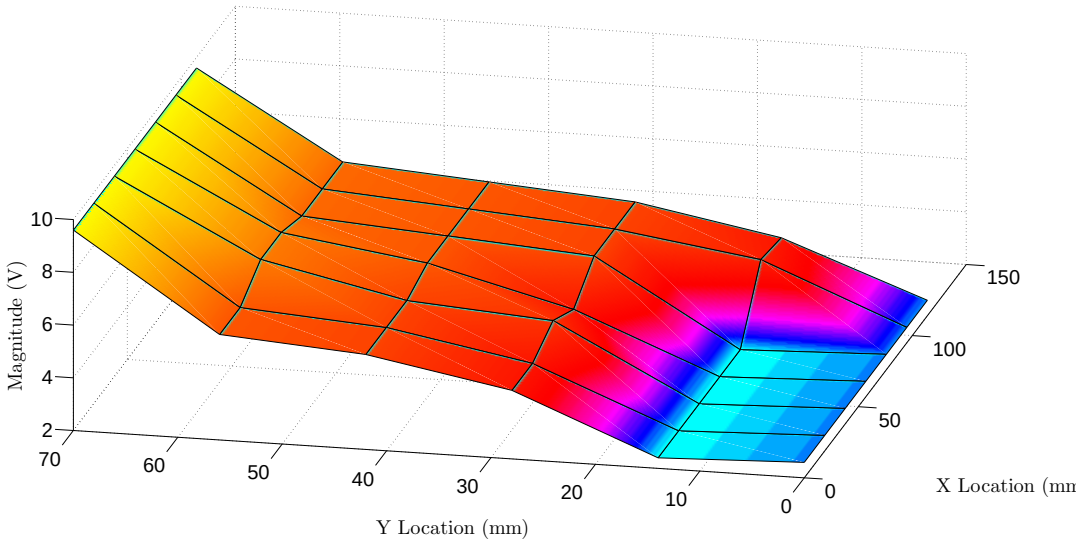

Figure 398: potential gradient observed within a normal saline solution using titanium electrodes and a sinusoidal input frequency of 1khz

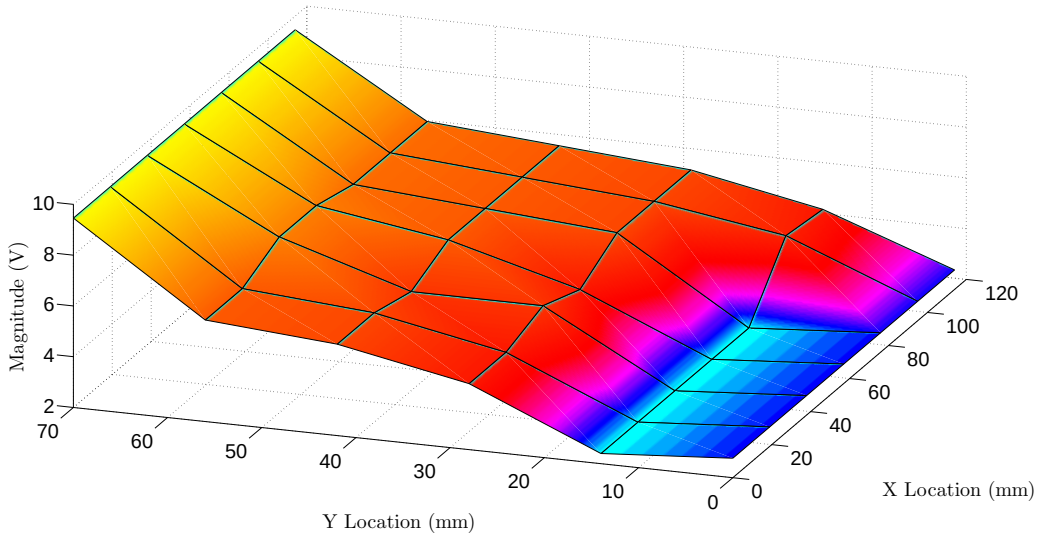

Figure 399: potential gradient observed within a normal saline solution using titanium electrodes and a sinusoidal input frequency of 2khz

signal. Likewise, while gradient information obtained — within Figure: (393) — appears to coincide, to some extent, with the proposed EZ theory, insofar as, some type of physical change in material conductivity is causing the observed potential drops; however, the curious asymmetry — between the source electrode and the sink electrode — seem to indicate that the region surrounding the sinking electrode differs from the sourcing electrode — although a minor, more symmetric, discrepancy seems to exist near the 10mm by 80mm

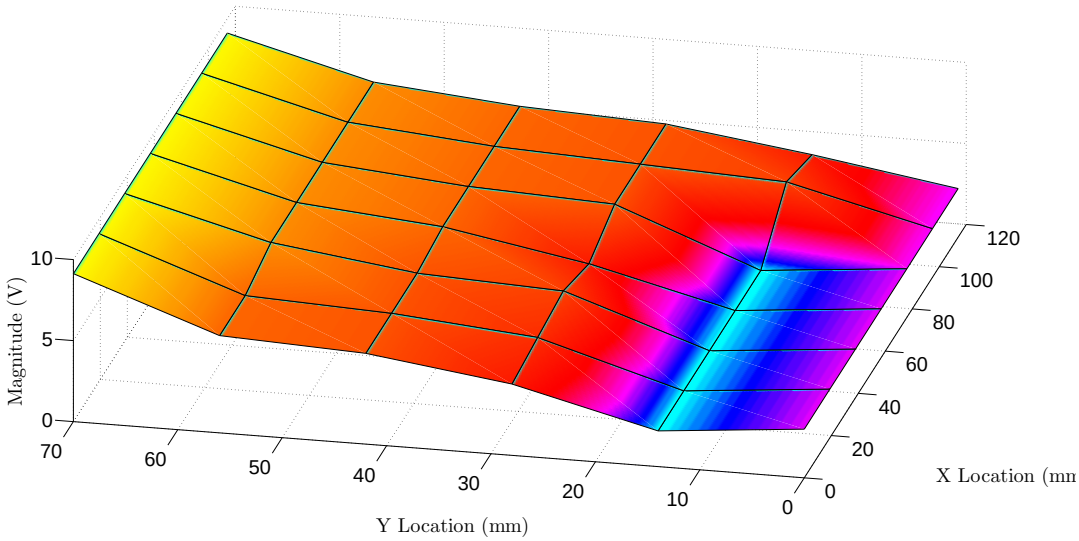

Figure 400: potential gradient observed within a normal saline solution using titanium electrodes and a sinusoidal input frequency of 4khz

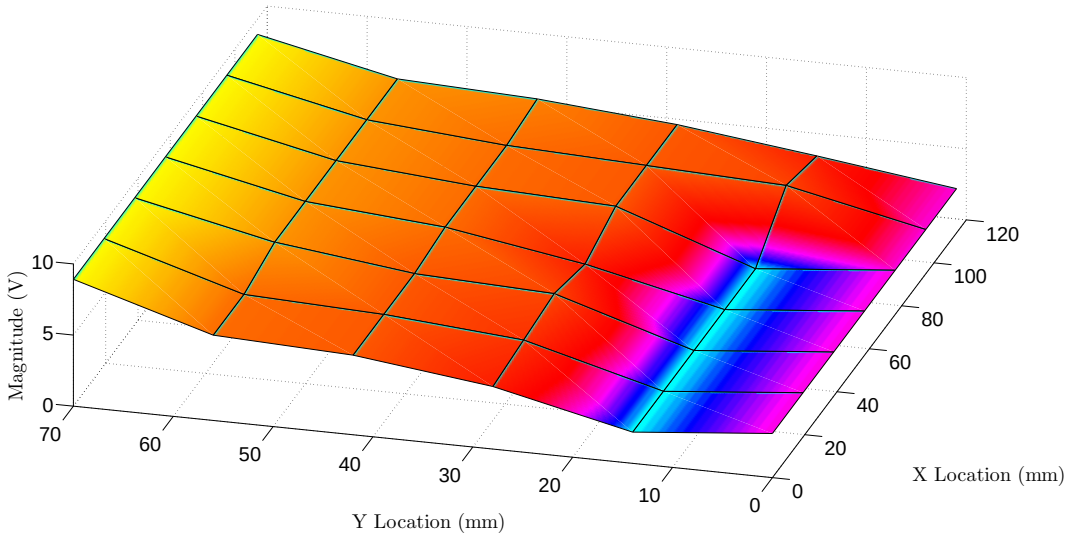

Figure 401: potential gradient observed within a normal saline solution using titanium electrodes and a sinusoidal input frequency of 6khz

electrode location, which in itself is somewhat curious and might be explained by something analogous to electromagnetic fringing or an inaccuracy in electrode placement.

Similarly, a visual examination of Figure: (394), in which a 10V sinusoidal signal at a frequency of 200Hz was applied with a calculated steady-state AC current of 1.44mA and a chamber resistance of 6.1k ohms respectively, seems to visually reveal a similar plot as Figure: (393), with the notable difference being that the electrical conductivity — of the

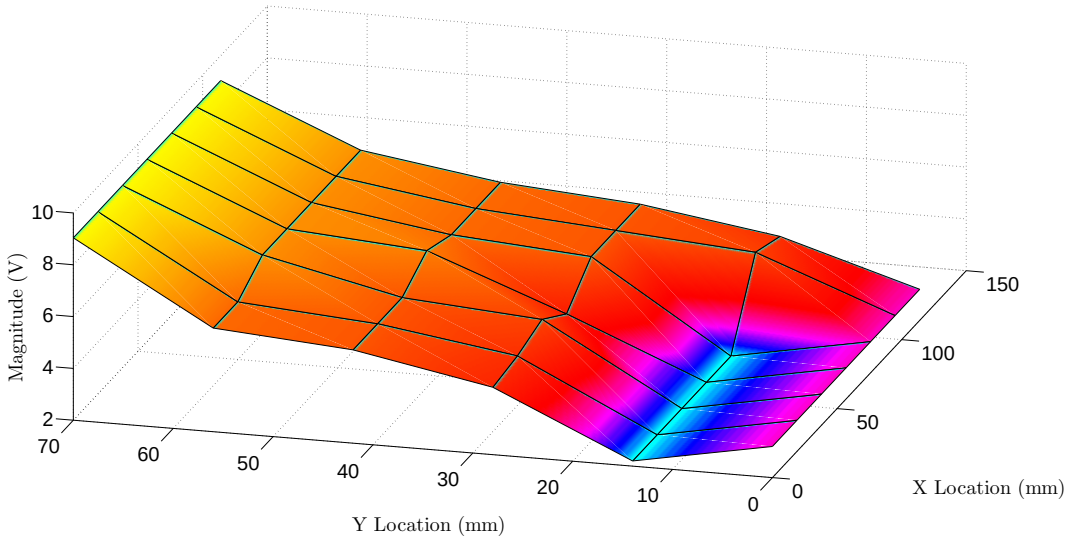

Figure 402: potential gradient observed within a normal saline solution using titanium electrodes and a sinusoidal input frequency of 8khz

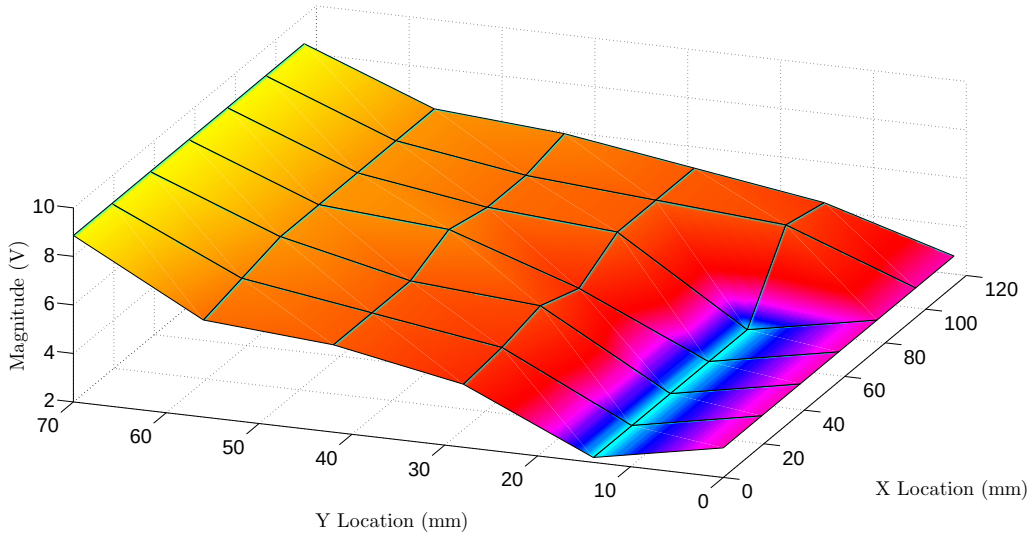

Figure 403: potential gradient observed within a normal saline solution using titanium electrodes and a sinusoidal input frequency of 10khz

solution — has increased somewhat substantially as the frequency was increased. Likewise, a visual examination of Figure: (395), in which a 10V sinusoidal signal at a frequency of 400Hz was applied with a calculated steady-state AC current of 1.83mA and a chamber resistance of 4.2k ohms respectively, seems to visually reveal a similar plot as Figure: (394), with the notable difference being that the electrical conductivity — of the solution — has slightly increased as the frequency was increased while the gradient created remains similar

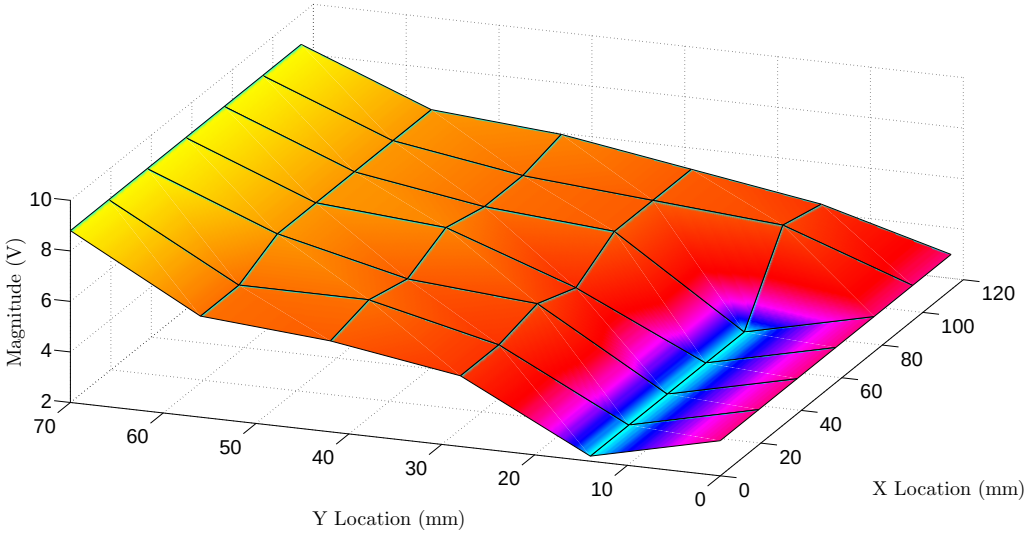

Figure 404: potential gradient observed within a normal saline solution using titanium electrodes and a sinusoidal input frequency of 20khz

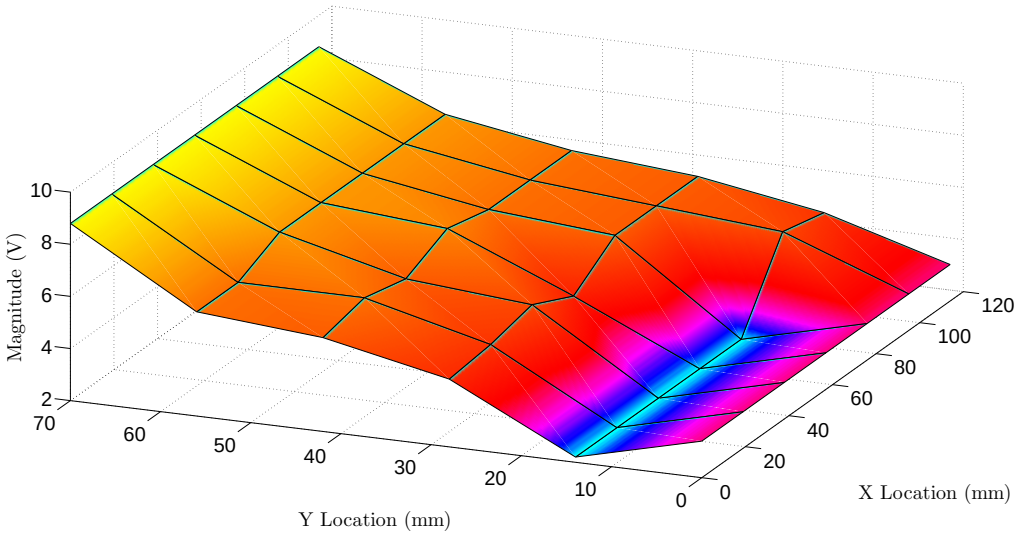

Figure 405: potential gradient observed within a normal saline solution using titanium electrodes and a sinusoidal input frequency of 40khz

in shape. Conversely, a visual examination of Figure: (396), in which a 10V sinusoidal signal at a frequency of 600Hz was applied with a calculated steady-state AC current of 2.18mA and a chamber resistance of 3.4k ohms respectively, seems to visually reveal a similar plot as Figure: (395), with the notable difference being that the electrical conductivity — of the solution — has slightly increased as the frequency was increased while the gradient created still remains similar in shape.

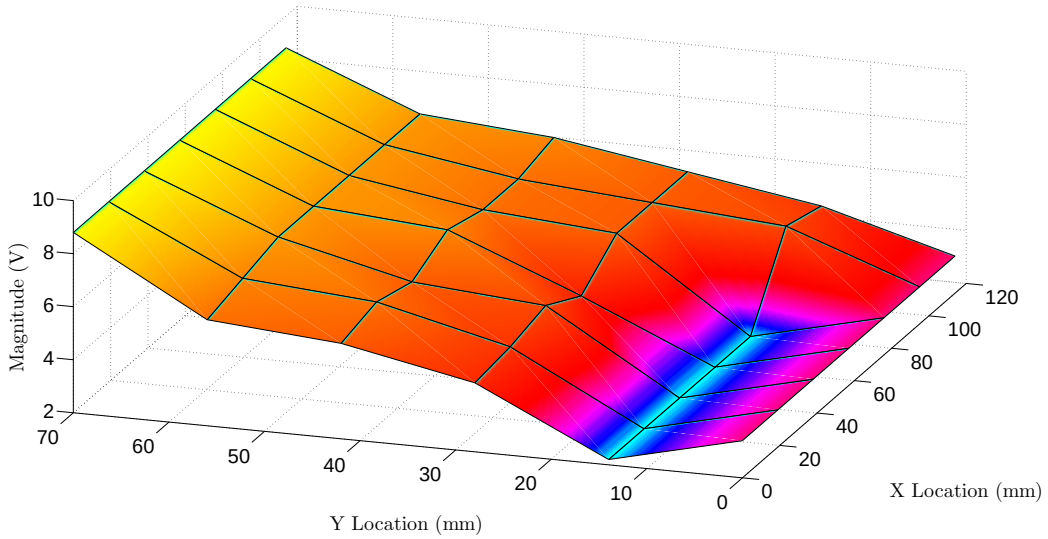

Figure 406: potential gradient observed within a normal saline solution using titanium electrodes and a sinusoidal input frequency of 60khz

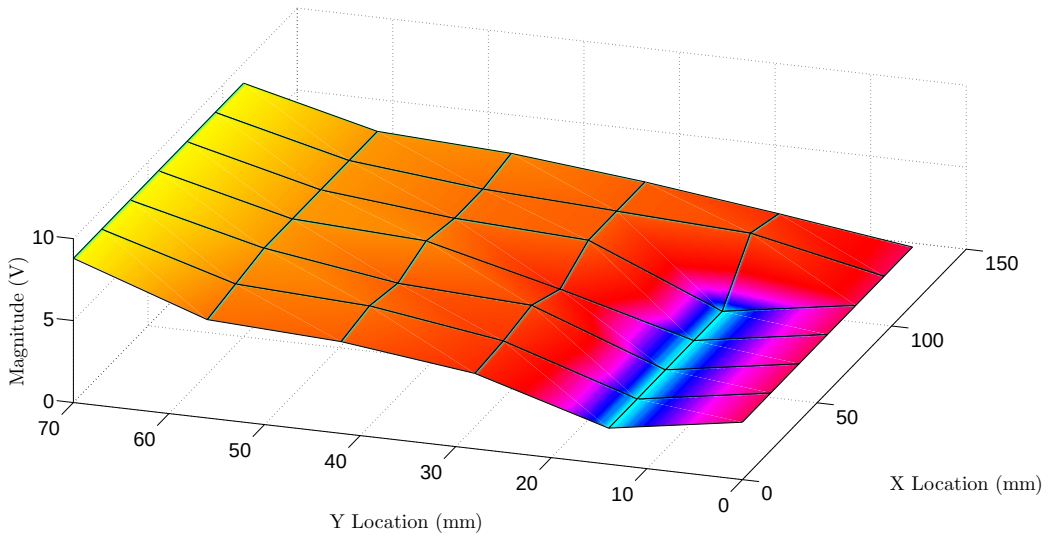

Figure 407: potential gradient observed within a normal saline solution using titanium electrodes and a sinusoidal input frequency of 80khz

Likewise, a visual examination of Figure: (397), in which a 10V sinusoidal signal at a frequency of 800Hz was applied with a calculated steady-state AC current of 2.4mA and a chamber resistance of 3k ohms respectively, seems to visually reveal a similar plot as Figure: (396), with the notable difference being that the electrical conductivity — of the solution — has vary slightly increased as the frequency was increased while the gradient created, again, remains similar in shape. Similarly, a visual examination of Figure: (398), in which a 10V sinusoidal signal at a frequency of 1kHz was applied with a calculated steady-state AC current of 2.5mA and a chamber resistance of 2.7k ohms respectively, seems to visually reveal a similar plot as Figure: (397), with the notable difference being that the electrical conductivity — of the solution — has, again, slightly increased as the frequency was increased while the gradient created still remains similar in shape. Likewise, a visual examination of Figure: (399), in which a 10V sinusoidal signal at a frequency of 2kHz was applied with a calculated steady-state AC current of 2.7mA and a chamber resistance of 2.4k ohms respectively, seems to visually reveal a similar plot as Figure: (398), with the notable difference being that the electrical conductivity — of the solution —, once again,

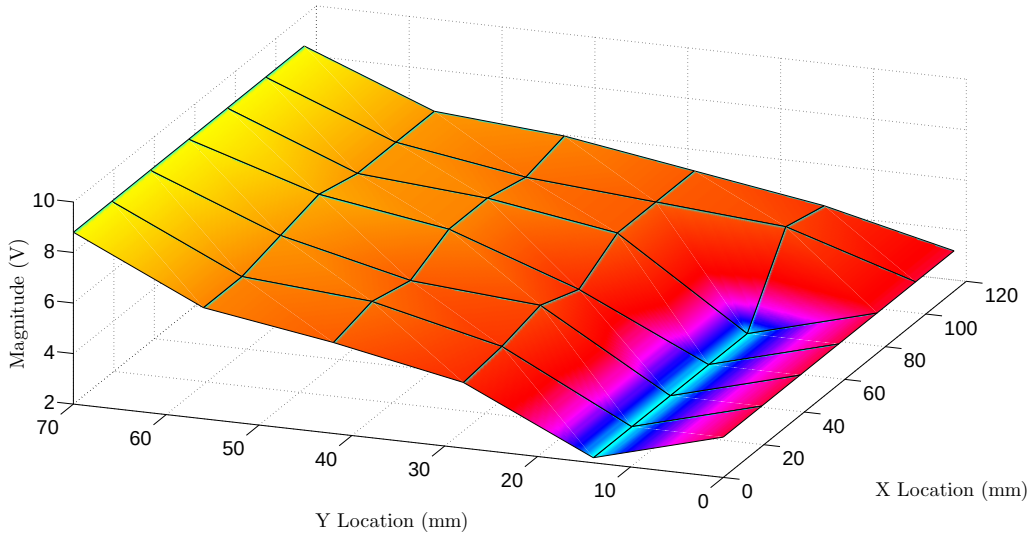

Figure 408: potential gradient observed within a normal saline solution using titanium electrodes and a sinusoidal input frequency of 100khz to

has slightly increased as the frequency was increased while the gradient created still remains similar in shape.

Conversely, a visual examination of Figure: (400), in which a 10V sinusoidal signal at a frequency of 4kHz was applied with a calculated steady-state AC current of 3mA and a chamber resistance of 2k ohms respectively, seems to visually reveal a similar plot as Figure: (399), with the notable difference being that the electrical conductivity — of the solution — has slightly increased as the frequency was increased while the gradient created still remains similar in shape. Likewise, a visual examination of Figure: (401), in which a 10V sinusoidal signal at a frequency of 6kHz was applied with a calculated steady-state AC current of 3.1mA and a chamber resistance of 1.872k ohms respectively, seems to visually reveal a similar plot as Figure: (400), with the notable difference being that the electrical conductivity — of the solution — has slightly increased as the input frequency was increased and an observable potential oddity appears to exist at the 10mm by 0mm thru 10mm by 80mm location, in which the electrode potential — at this particular location — appears to drop below the sinking electrode potential. Conversely, a visual examination of Figure: (402), in which a 10V sinusoidal signal at a frequency of 8kHz was applied with a calculated steady-state AC current of 3.2mA and a chamber resistance of 1.825k ohms respectively, seems to visually reveal a similar plot as Figure: (401), with the notable difference being that the electrical conductivity — of the solution — has slightly increased as the frequency was increased while the gradient created still remains similar in shape.

Similarly, a visual examination of Figure: (403), in which a 10V sinusoidal signal at a frequency of 10kHz was applied with a calculated steady-state AC current of 3.22mA and a chamber resistance of 1.751k ohms respectively, seems to visually reveal a similar plot as Figure: (402), with the notable difference being that the electrical conductivity — of

the solution — has slightly increased as the frequency was increased while the gradient created still remains similar in shape. Likewise, a visual examination of Figure: (404), in which a 10V sinusoidal signal at a frequency of 20kHz was applied with a calculated steady-state AC current of 3.39mA and a chamber resistance of 1.595k ohms respectively, seems to visually reveal a similar plot as Figure: (403), with the notable difference being that the electrical conductivity — of the solution — has slightly increased as the frequency was increased while the gradient created still remains similar in shape. Conversely, a visual examination of Figure: (405), in which a 10V sinusoidal signal at a frequency of 40kHz was applied with a calculated steady-state AC current of 3.4mA and a chamber resistance of 1.588k ohms respectively, seems to visually reveal a similar plot as Figure: (404), with the notable difference being that the electrical conductivity — of the solution — has slightly increased as the frequency was increased while the gradient created still remains similar in shape.

Likewise, a visual examination of Figure: (406), in which a 10V sinusoidal signal at a frequency of 60kHz was applied with a calculated steady-state AC current of 3.4mA and a chamber resistance of 1.588k ohms respectively, seems to visually reveal a similar plot as Figure: (404), with the notable difference being that the electrical conductivity — of the solution — has slightly increased as the frequency was increased while the gradient created still remains similar in shape. Conversely, a visual examination of Figure: (407), in which a 10V sinusoidal signal at a frequency of 80kHz was applied with a calculated steady-state AC current of 3.5mA and a chamber resistance of 1.510k ohms respectively, seems to visually reveal a similar plot as Figure: (406), with the notable difference being that the electrical conductivity — of the solution — has slightly increased as the frequency was increased while the gradient created still remains similar in shape. Finally, a visual

examination of Figure: (408), in which a 10V sinusoidal signal at a frequency of 100kHz was applied with a calculated steady-state AC current of 3.595mA and a chamber resistance of 1.447k ohms respectively, seems to visually reveal a similar plot as Figure: (407), with the notable difference being that the electrical conductivity — of the solution — has slightly increased as the frequency was increased while the gradient created still remains similar in shape.

Conversely, while the information presented within Figure: (393), Figure: (394), Figure: (395), Figure: (396), Figure: (397), Figure: (398), Figure: (399), Figure: (400), Figure: (401), Figure: (402), Figure: (403), Figure: (404), Figure: (405), Figure: (406), Figure: (407), and Figure: (408), was somewhat redundant; however, the following remarks can be made: first, the shape of the gradient created appears to remain relatively consistent, with the notable exceptions being a slight flattening — or reduction in resistance between electrode locations — within the bulk of the medium, and a unique drop in potential below the observed value of the current sinking electrodes — at frequencies above 6kHz — , seems to imply the existence of a congregation of negative charges — within this region — that might be somewhat metaphorically analogous to the development of a standing wave — within a transmission line —, insofar as, such congregated negative charges could be the result of a substantial buildup of positive charges near the current sinking electrodes. Second, because the shape of the gradient did not change with frequency — beyond the formation of the minor discrepancy observed near the current sinking electrodes —, it seems reasonable to assume that the underlying process responsible for the creation of these gradients — presumably a EZ phenomenon — is not inherently dependent upon electrical frequency. Third, the overall resistance across the liquid seems to decrease as a function of frequency, which seems to imply that the charge transport mechanism across

the liquid is, in fact, a function of frequency.

Nevertheless, while such observations were deliberately more empirical than mathematical, predominantly because the intended objective of these experiments was intuitive observation rather than predictive modeling; however, given the nature of the gradients observed, it seems likely that differential voltage injection — the process of using two function generators in such a configuration that the common ground is not exposed to the test apparatus — or impedance modulation — the act of programmatically varying the current sensing resistor — could be utilized to modify the shape of the gradient created and possibly force particular regions, within the gradient, to be a particular potential value — although, undoubtedly some physical restrictions would apply. Likewise, while no substantial investigation was conducted on this particular attribute — although a few minor experiments on the FDI muscle using impedance modulation did yield painful stimulus — it is the opinion of this dissertation that such attributes should be researched further, as such phenomenon is likely to be extremely beneficial to the development of precision noninvasive muscle stimulation.

6.3.14 BIS and Aqueous NaCl

The fundamental rationale behind the BIS and Aqueous NaCl section was to develop both a method of modeling in series and bulk electrochemical phenomena, to develop operational guidelines to avoid the introduction of electrical nonlinearities when working with these materials, to examine the possible usages of the electrical nonlinearities observed within these materials, and to examine the effects chemical concentration has upon the electrical properties of these materials. Likewise, based upon the observations obtained, it was determined that the aqueous NaCl solutions examined were definitively nonlinear within certain operational regions — a notion supported by observing that a sinusoidal input is

being transformed into a pulse looking shape across the sinking electrode current sensing resistor at frequencies below 100Hz and voltages above 2.5V. Conversely, upon examining all of the information obtained, it was also determined that the distortion being observed are relatively consistent in shape over frequency — although the magnitude appears to change with concentration —, and it was theorized that exclusion zone (EZ) phenomenon is playing a substantial role in defining the electrical effects observed, although the verification of this particular theory was not possible given the limitations of the laboratory utilized, since a chemical lab with a high resolution microscope and access to nanoparticles would be required to determine if a EZ effect was occurring or a pH changing solvent required to check for the development of ionic concentrations; however, based upon the observed current spikes, it was determined that the electrical current does begin to briefly flow across the test chamber upon exceeding a threshold voltage — around 2V at 1Hz— and then suddenly stops — implying the creation of a charge gradient — and this process repeats during the negative half of the input wave cycle. Likewise, it was determined that when the aqueous NaCl began to conduct current in a nonlinear fashion, the electrical potential within the liquid also began to operate in a nonlinear fashion, and that if the input voltage was subtracted from the potential within the solution — while conducting current under nonlinear conditions — that a potential clipping effect — similar to a diode —- was the result, and that upon plotting the difference between the input and the values obtained, after performing this mathematical operation, yields the conclusion that linear regions were generally substantially lower in subtracted magnitude — since linear regions were sinusoidal — than non-linear regions, thus, upon creating a three-dimensional topological plot of input frequency versus input voltage, an effective visual means of determining what BIS operational regions were linear and nonlinear was developed — an attribute that

can improve BIS fidelity through the avoidance of material nonlinearities. Additionally, it was also determined that the usage of nonlinear least squares RRCR circuit modeling techniques can provide a reasonably good approximation electrical circuit approximation of this highly nonlinear electrical phenomenon; however, while such methods do work reasonably well, so long as some system information is known thru experimentation, yet such methods tend to bend the unspoken rules of static circuit equations — because variable components are required —, and such attributes are simply unavoidable given the nature of the problem being examined, especially since it is obvious that a unknown chemical process — like EZ regions — are governing the conductivity of this particular system, and based upon such observations, it was highly presumptuous to assume that the dynamics — of this particular system — easily conform to the simplicity of a basic electrical circuit model. Thus, while this method will work for modeling this particular system within this particular paradigm; however, more native chemical modeling methods are also worth exploring here, since simplicity is not something easily obtained for such problems using current electrical engineering modeling theory, and there is nothing really gained by its utilization within such problems beyond being able to interface with an existing electrical framework — which is the only true advantage gained under such circumstances.

Likewise, given that the information regarding the distortions created by electrode corrosion at both AC and DC operational conditions and the underlying potential gradients created within aqueous sodium chloride solutions has been discussed, it now seems prevalent to perform a more in-depth inquiry surrounding the types of time domain distortions encountered within such mediums since, based upon the observations made within Figure: (373), such time domain distortions seem to be predominantly the result of the passage of electrical current through an aqueous medium — presumably normal saline —, and the

ability to either avoid or compensate for such distortions would go a long way in improving the accuracy of BIS analysis — if not other passive bioelectrical acquisition techniques like EKG and EMG. Conversely, with this being said, because the testing apparatus utilized within the BIS, liquids, and electrode materials section was rather large, utilized a open chamber — which allowed interaction with the ambient atmosphere —, had electrodes that were inherently electrically corrosive, and predominantly focused upon one operational voltage; it was decided that a new testing apparatus — as shown by Figure: (409) — would be utilized — in which, the chamber was smaller, atmospherically sealed, utilized corrosive resistant titanium electrodes, and a varying input voltage — in order to better characterize different concentrations of aqueous sodium chloride.

Similarly, in a manner similar to the tests performed within the acquisition of AC CIE effects, three Tektronix oscilloscopes — one TPS2024 and two TDS2002 — were utilized to acquire eight independent electrical signals — although one channel from each oscilloscope was connected to the same input signal in order to account for the, previously mentioned,

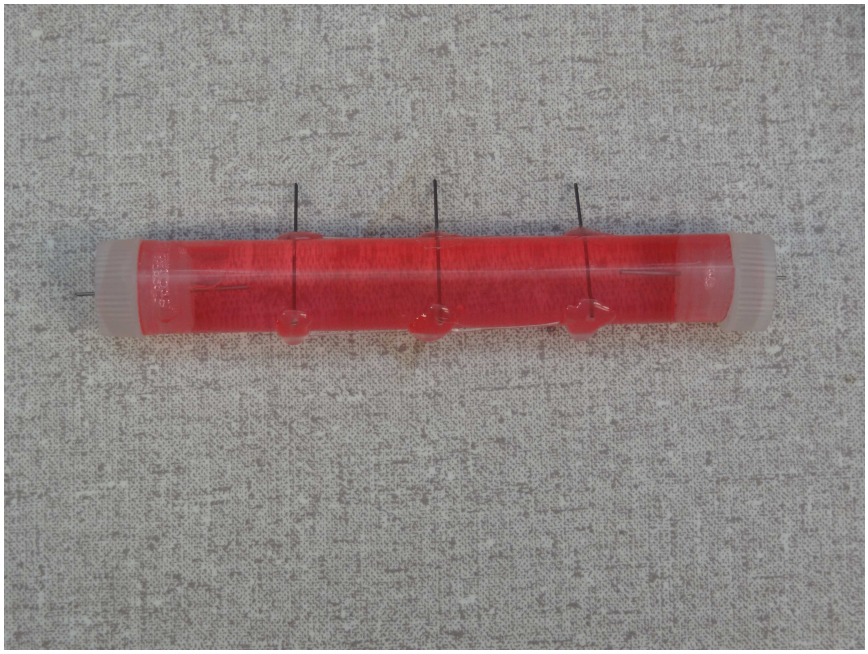

Figure 409: a picture of the testing apparatus developed to electrically characterize aqueous sodium chloride

attributes of acquisition delay and oscilloscope acquisition differences —, while two channels of the TPS2024 oscilloscope were connected to two in series 110 ohm current sensing resistors that were connected to either end of the testing apparatus electrodes — with one end being connected to the sourcing side of the Tektronix AFG3102 function generator, while the other end being connected to the sinking side of the Tektronix AFG3102 function generator. Likewise, the remaining three oscilloscope channels — one per oscilloscope unit — were connected to the three potential observational electrodes located along the top of the test chamber, while a Python application — nearly identical to the one previously presented within Appendix B — was utilized to vary both frequency and voltage of the input signal produced by the Tektronix AFG3102 — incorporating voltages of 1mV, 17mV, 28mV, 46mV, 77mV, 1.29V, 2.15V 3.6V, 6V, and 10V respectively, and frequencies of 1Hz, 4.3Hz, 18Hz, 79Hz, 341Hz, 1.5kHz, 6.3kHz, 27kHz, 116kHz, 500kHz, and 1MHz respectively. Similarly, a total of 11 test chambers were created and field with varying concentrations of aqueous sodium chloride — including water, $0.10\%\frac{w}{v}$, $0.20\%\frac{w}{v}$, $0.30\%\frac{w}{v}$, $0.40\%\frac{w}{v}$, $0.50\%\frac{w}{v}$, $0.60\%\frac{w}{v}$, $0.70\%\frac{w}{v}$, $0.80\%\frac{w}{v}$, $0.90\%\frac{w}{v}$ (normal saline), and $1.00\%\frac{w}{v}$ solutions respectively —, the experiments outlined above performed were upon each of these test chambers, and the results obtained were converted into surface plots for further analysis.

Conversely, because the amount of information obtained from this particular automated acquisition process is rather overwhelming, it was decided that the data collected — for each of the observed oscilloscope channels, with the exclusion of the applied signal input, since the AC CIE section does a fair job of depicting this particular attribute — would best be conveyed thru the utilization of a surface plot in order to help with the facilitation of further discussion on this particular subject.

Likewise, upon visually examining the voltage of the sourcing electrode site — or the

location after the first 110 ohm current sensing resistor —, as shown by Figure: (410), Figure: (411), and Figure: (412), it becomes apparent — based upon the linear slope of the plots obtained — that first, hardly any current is flowing through the distilled water concentration test — although this is expected given the non-conductive nature of water — and second, it also appears that as the concentration of aqueous sodium chloride increases that the amount of current appears to also increase — particularly at higher frequencies at or above 10^4 Hz — until the current appears to reach a reasonably consistent

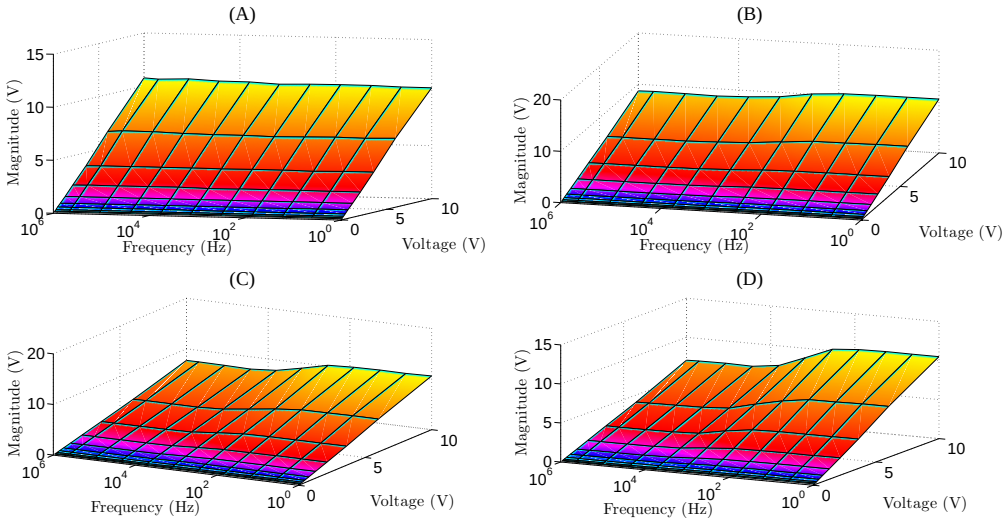

Figure 410: surface plot of input voltage versus frequency versus sourcing site electrical voltage for (a) water, (b) $0.10\%\frac{w}{v}$, (c) $0.20\%\frac{w}{v}$, and (d) $0.30\%\frac{w}{v}$

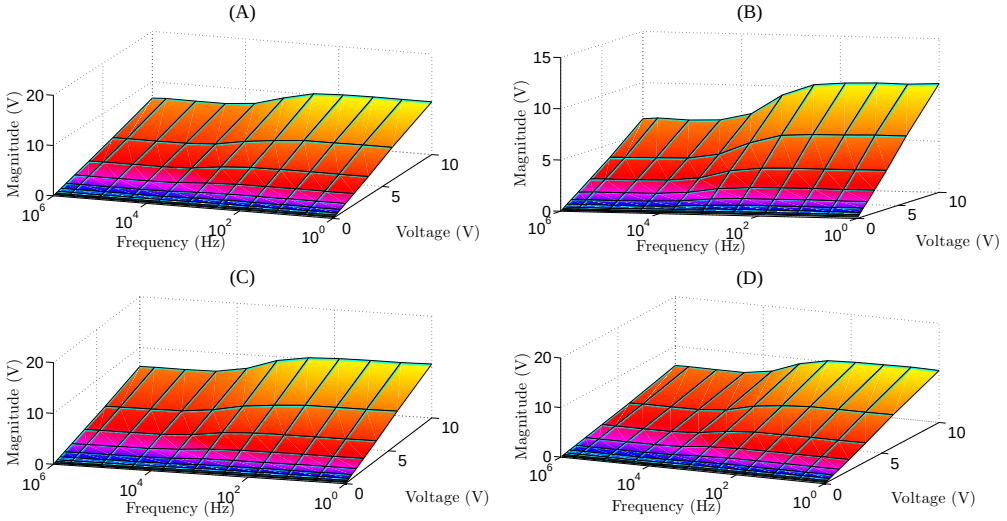

Figure 411: surface plot of input voltage versus frequency versus sourcing site electrical voltage for (a) $0.40\%\frac{w}{v}$, (b) $0.50\%\frac{w}{v}$, (c) $0.60\%\frac{w}{v}$, and (d) $0.70\%\frac{w}{v}$

visual surface plot for concentrations at or above $0.40\frac{w}{v}$ in concentration. While, such observations are somewhat moot, it does appear that there is a slight increase in electrical conductivity within the aqueous sodium chloride test, as the frequency increases — an attribute determined by the increased voltage drop across the current sensing resistor over the frequency axis — that seems to correspond with the traditional notions of how a electrical dielectric typically will respond over frequency.

Conversely, upon visually examining the voltage of the sinking electrode site — or the

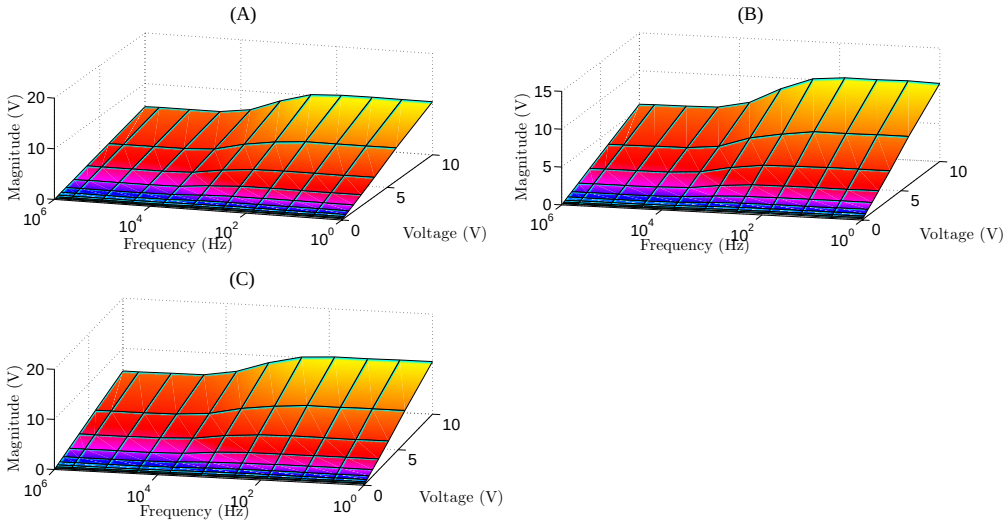

Figure 412: surface plot of input voltage versus frequency versus sourcing site electrical voltage for (a) $0.80\%\frac{w}{v}$, (b) $0.90\%\frac{w}{v}$, (c) $1.00\%\frac{w}{v}$

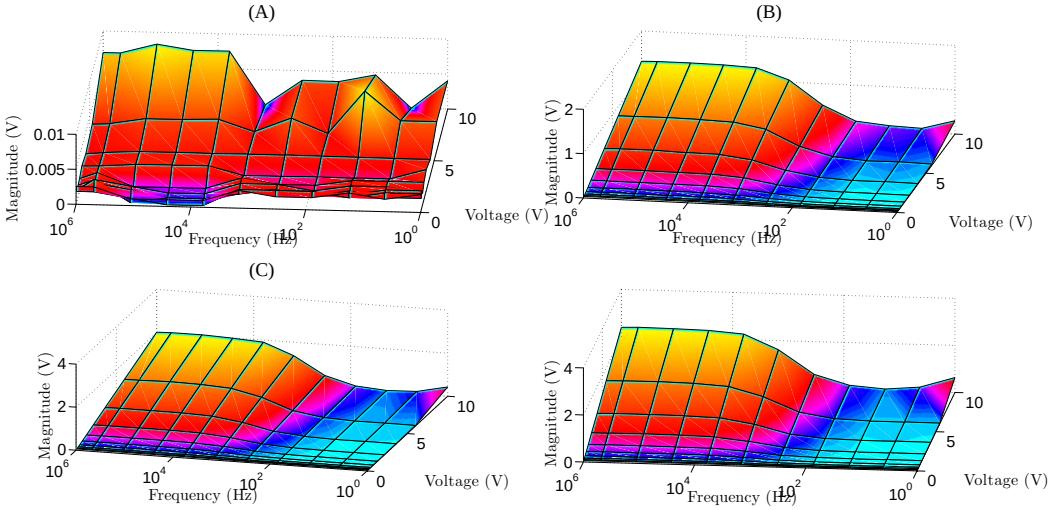

Figure 413: surface plot of input voltage versus frequency versus sinking site electrical voltage for (a) water, (b) $0.10\%\frac{w}{v}$, (c) $0.20\%\frac{w}{v}$, and (d) $0.30\%\frac{w}{v}$

electrode located before the second 110 ohm current sensing resistor —, as shown by Figure: (413), Figure: (414), and Figure: (415), it becomes apparent that first, the amount of current permitted to flow through the distilled water testing apparatus is, once again, very minimal — as distilled water is not very electrically conductive even over an assortment of electrical frequencies —, and second, upon visually examining the remaining subplots, it becomes apparent that aqueous sodium chloride is conductive and that the amount of conduction obtained will vary depending upon the frequency, voltage, and concentration being

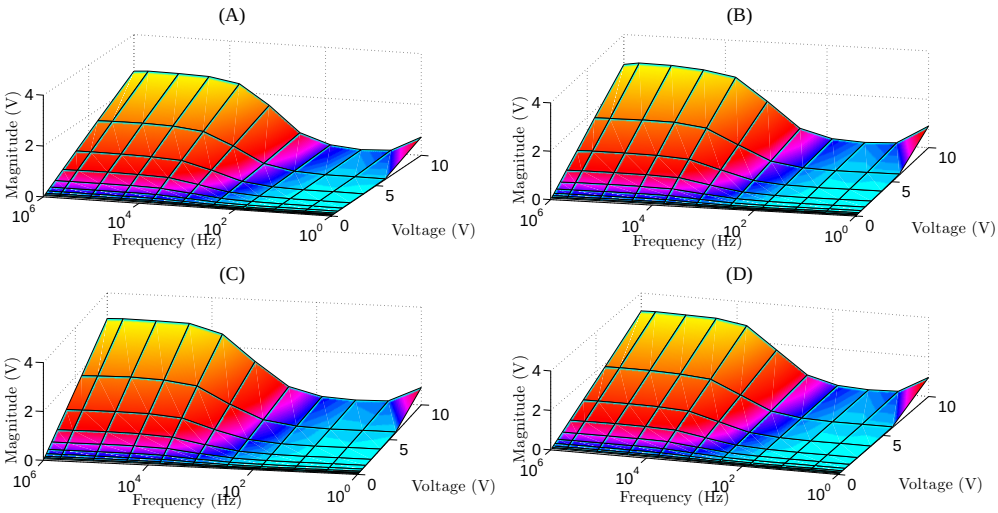

Figure 414: surface plot of input voltage versus frequency versus sinking site electrical voltage for (a) $0.40\%\frac{w}{v}$, (b) $0.50\%\frac{w}{v}$, (c) $0.60\%\frac{w}{v}$, and (d) $0.70\%\frac{w}{v}$

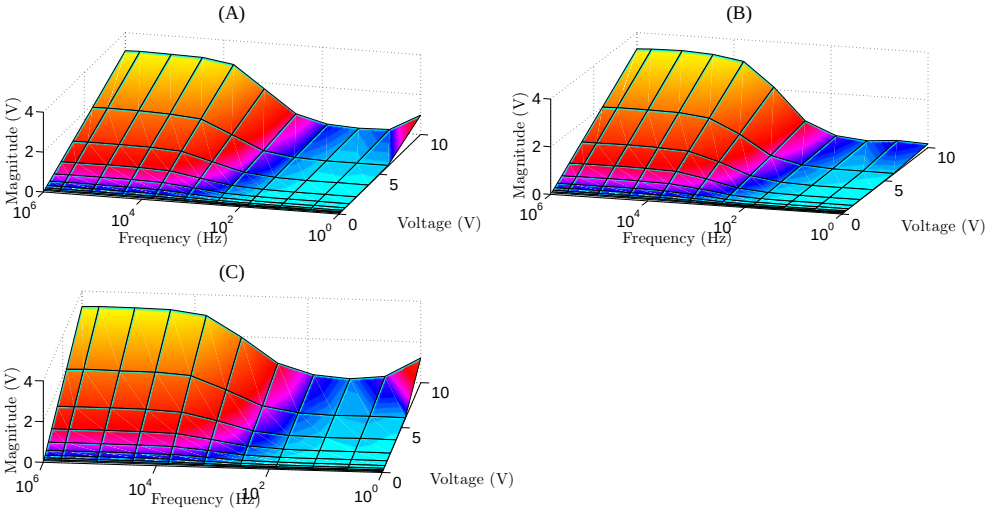

Figure 415: surface plot of input voltage versus frequency versus sinking site electrical voltage for (a) $0.80\%\frac{w}{v}$, (b) $0.90\%\frac{w}{v}$, (c) $1.00\%\frac{w}{v}$

examined — noting that concentrations above $0.40\frac{w}{v}$ yield progressively smaller increases in conductivity for every increase in concentrations above this point.

Likewise, upon visually examining the voltage of the left liquid potential monitoring electrode, as shown by Figure: (416), Figure: (417), and Figure: (418), it appears that first, water, as it might be expected, looks like a open circuit at lower frequencies and a short circuit at higher frequencies, and Second, while aqueous sodium chloride appears to create a internal potential gradient — implying electrical conduction — across all frequencies

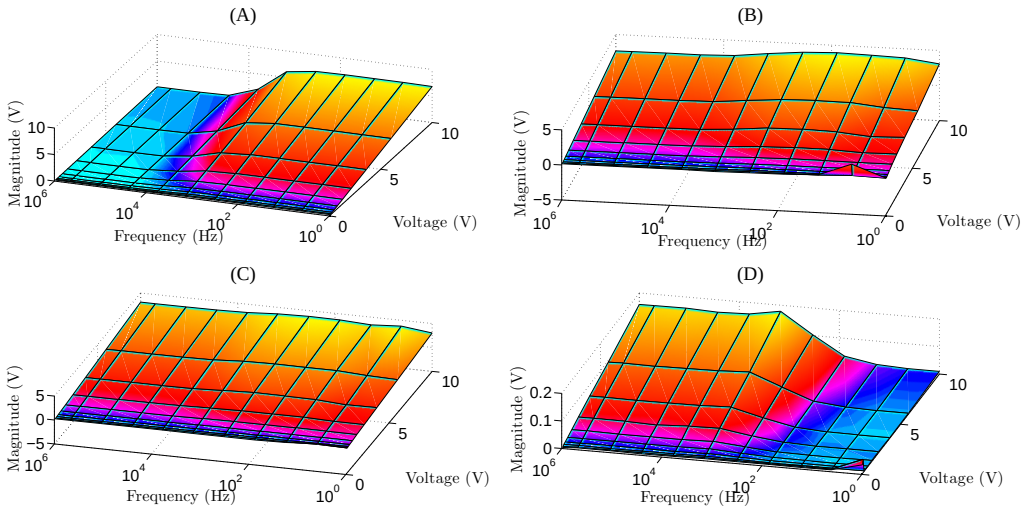

Figure 416: surface plot of input voltage versus frequency versus left potential electrode voltage for (a) water, (b) $0.10\%\frac{w}{v}$, (c) $0.20\%\frac{w}{v}$, and (d) $0.30\%\frac{w}{v}$

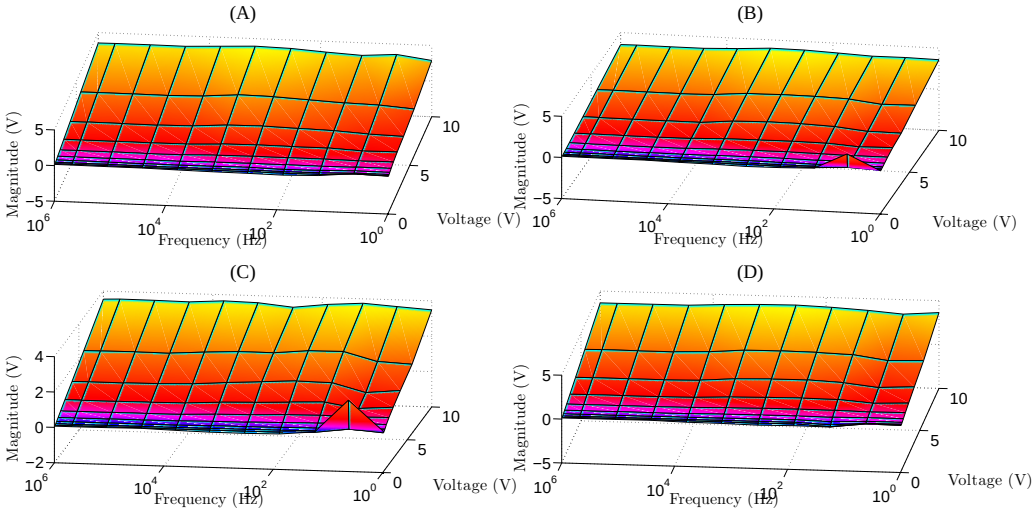

Figure 417: surface plot of input voltage versus frequency versus left potential electrode voltage for (a) $0.40\%\frac{w}{v}$, (b) $0.50\%\frac{w}{v}$, (c) $0.60\%\frac{w}{v}$, and (d) $0.70\%\frac{w}{v}$

that corresponds with the applied voltage — noting that the $0.30\frac{w}{v}$ plot appears to be incorrect, because of a bad connection on the oscilloscope channel probe, an attribute that reinforces the underlying need of being able to intuitively deduce if a measurement obtained is reasonable or not.

Conversely, upon visually examining the voltage of the middle liquid potential monitoring electrode, as shown by Figure: (419), Figure: (420), and Figure: (421), it appears that first, water, as it might be expected, looks like a open circuit at lower frequencies and

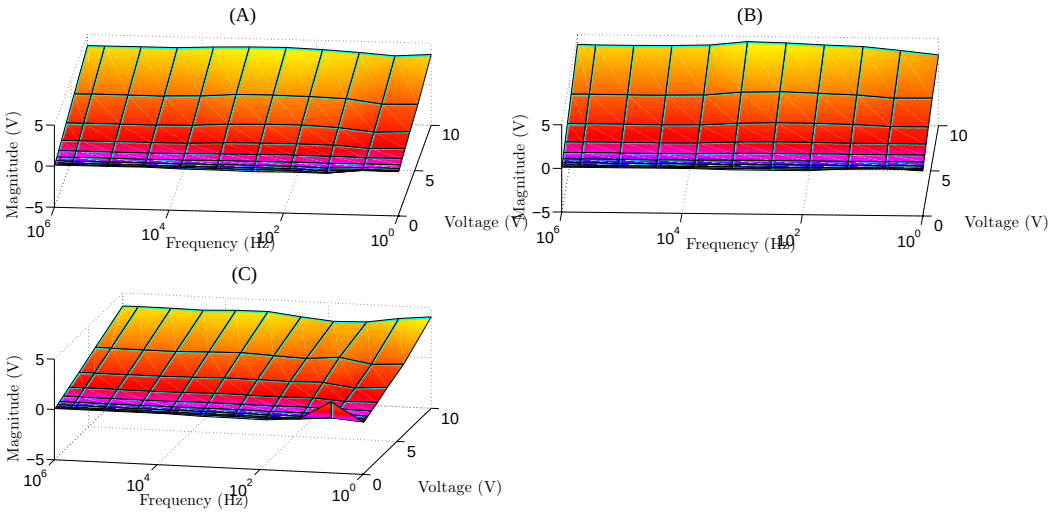

Figure 418: surface plot of input voltage versus frequency versus left potential electrode voltage for (a) $0.80\%\frac{w}{v}$, (b) $0.90\%\frac{w}{v}$, (c) $1.00\%\frac{w}{v}$

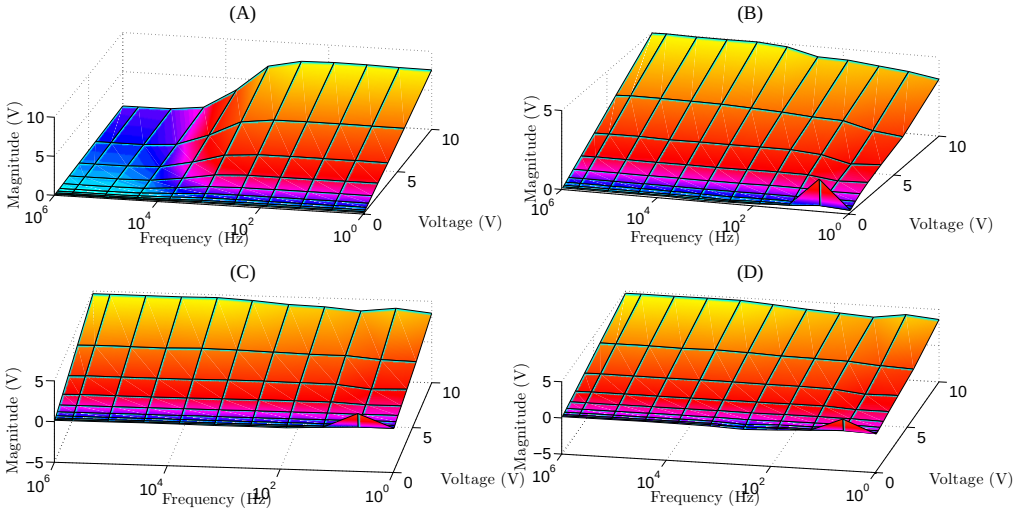

Figure 419: surface plot of input voltage versus frequency versus middle potential electrode voltage for (a) water, (b) $0.10\%\frac{w}{v}$, (c) $0.20\%\frac{w}{v}$, and (d) $0.30\%\frac{w}{v}$

a short circuit at higher frequencies, and second, while aqueous sodium chloride appears to create a internal potential gradient — implying electrical conduction — across all frequencies that corresponds with the applied voltage — noting that concentrations at and above the $0.70\frac{w}{v}$ plot appears to have a lower middle electrode gradient within the lower frequency region then they do at higher frequencies.

Similarly, upon visually examining the voltage of the right liquid potential monitoring electrode, as shown by Figure: (432), Figure: (433), and Figure: (434), it appears that first,

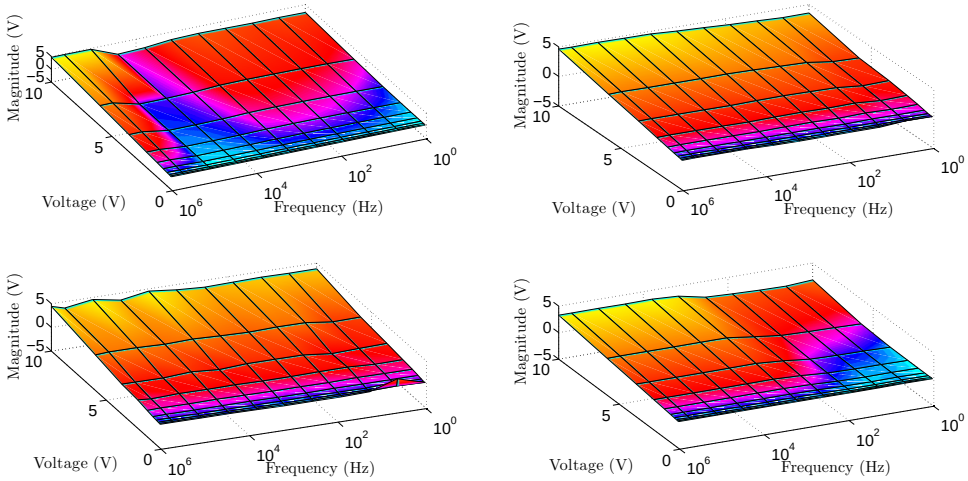

Figure 420: surface plot of input voltage versus frequency versus middle potential electrode voltage for (a) $0.40\%\frac{w}{v}$, (b) $0.50\%\frac{w}{v}$, (c) $0.60\%\frac{w}{v}$, and (d) $0.70\%\frac{w}{v}$

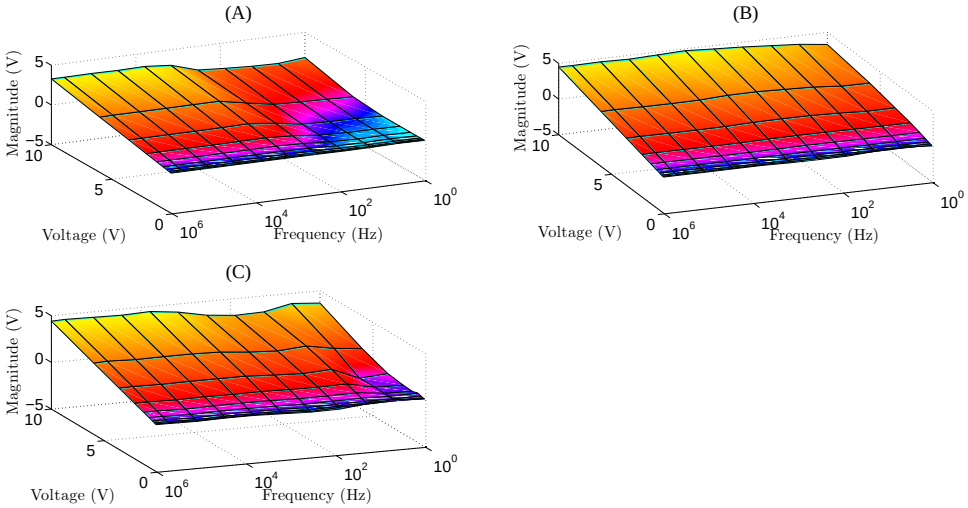

Figure 421: surface plot of input voltage versus frequency versus middle potential electrode voltage for (a) $0.80\%\frac{w}{v}$, (b) $0.90\%\frac{w}{v}$, (c) $1.00\%\frac{w}{v}$

water, as it might be expected, looks like a open circuit at lower frequencies and a short circuit at higher frequencies, and second, while aqueous sodium chloride appears to create a internal potential gradient — implying electrical conduction — across all frequencies that corresponds with the applied voltage — noting that concentrations at $1.00\frac{w}{v}$ plot appears to have a lower middle electrode gradient at the midband test frequency region — although all potential gradients are relatively similar upon considering the, previously mentioned AC CIE effects.

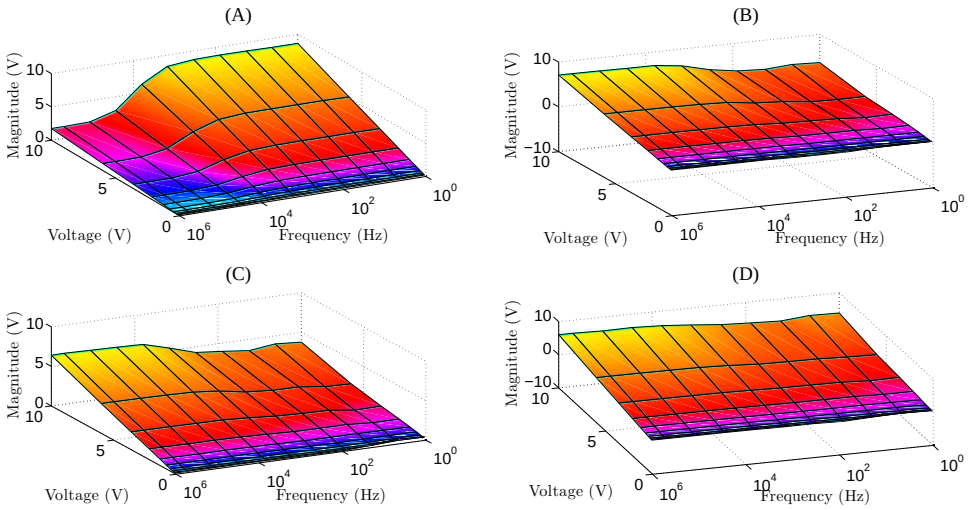

Figure 422: surface plot of input voltage versus frequency versus right potential electrode voltage for (a) water, (b) $0.10\%\frac{w}{v}$, (c) $0.20\%\frac{w}{v}$, and (d) $0.30\%\frac{w}{v}$

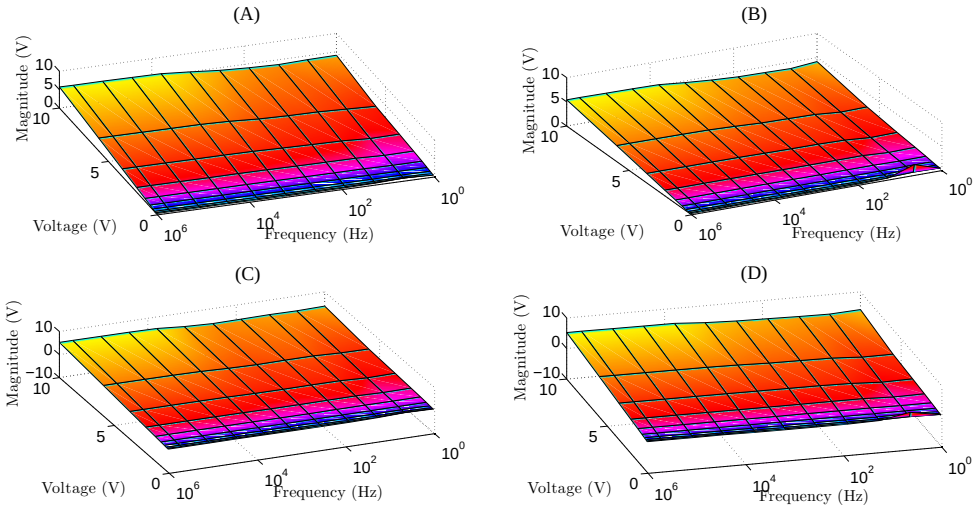

Figure 423: surface plot of input voltage versus frequency versus right potential electrode voltage for (a) $0.40\%\frac{w}{v}$, (b) $0.50\%\frac{w}{v}$, (c) $0.60\%\frac{w}{v}$, and (d) $0.70\%\frac{w}{v}$

Nevertheless, while such surface visualizations are interesting, they are not overly informative regarding the nonlinearities that are encountered within these liquids at lower frequencies, and while it should be noted that the electrical potential observed — at least upon considering AC CIE effects — at each of the gradient monitoring electrodes utilized is the same across the test chamber; however, the current observed thru the chamber at lower frequencies — from 1Hz to 75Hz — over variations in aqueous sodium chloride concentration is very interesting, as shown by Figure: (425), Figure: (426), Figure: (427), Figure: (428), Figure: (429) Figure: (430), and Figure: (431).

Likewise, upon visually examining Figure: (425), it becomes apparent that the liquids being examined are definitively nonlinear — a notion supported by noticing that a sinusoidal input is being transformed into a pulse looking shape across the sinking current sensing resistor. Conversely, upon examining all of the subplots, within Figure: (425), it appears that the distortion that is occurring is relatively consistent in shape over frequency — although the magnitude appears to change with concentration —, with the exception of subplot (H) that appears to have another phenomena occurring in addition to the pulse shaping mechanism. While the identification of the exact process that is occurring within

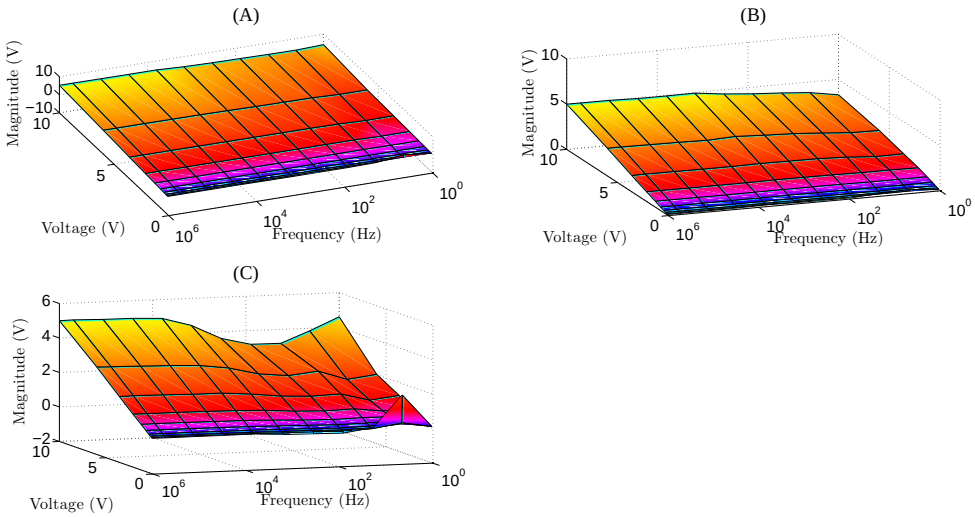

Figure 424: surface plot of input voltage versus frequency versus right potential electrode voltage for (a) $0.80\%\frac{w}{v}$, (b) $0.90\%\frac{w}{v}$, (c) $1.00\%\frac{w}{v}$

Figure: (425) was not possible given the limitations of the laboratory utilized — as a chemical lab with a high resolution microscope and access to nanoparticles would be required to determine if the effect occurring is the result of EZ formation or a pH changing solvent required to check for some type of ionic related effect; however, based upon the observed positional spikes — within Figure: (425) — it is known that electrical current is briefly flowing across the chamber — likely thru the shifting of ions —, stops and reverses upon the negative wave cycle, while the odd pulses — within subplot (H) — seem to imply the existence of a double charge reorientation — from a higher energy state to a lower energy state — that might be analogous to a resonance condition within the solution [184] [188] [431] [432] [433] [434].

Conversely, upon visually examining Figure: (426), it becomes apparent that the liquids being examined are also nonlinear — a notion supported by noticing that a sinusoidal input is being transformed into a pulse and ramp looking shapes across the sinking current sensing resistor. Likewise, upon examining all of the subplots, within Figure: (426), it appears that

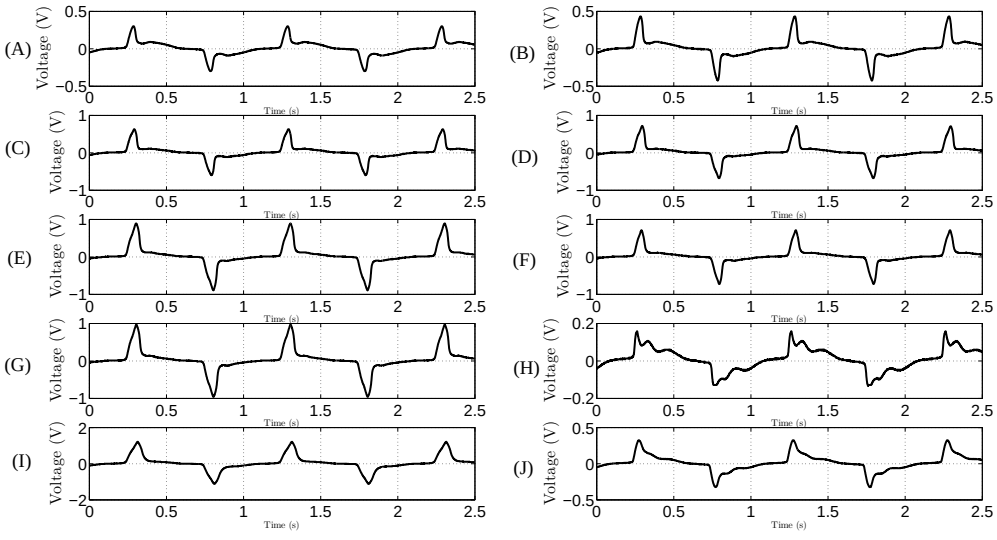

Figure 425: plots of sinking electrode using an input of 10v peak, frequency of 1hz for concentrations of (a) $0.10\%\frac{w}{v}$, (b) $0.20\%\frac{w}{v}$, (c) $0.30\%\frac{w}{v}$, (d) $0.40\%\frac{w}{v}$, (e) $0.50\%\frac{w}{v}$, (f) $0.60\%\frac{w}{v}$, (g) $0.70\%\frac{w}{v}$, (h) $0.80\%\frac{w}{v}$, (i) $0.90\%\frac{w}{v}$, and (j) $1\%\frac{w}{v}$

the distortion that is occurring is relatively consistent in shape over frequency — although, unlike Figure: (425) the magnitude appears to remain similar over concentration —, with the exception of subplot (E) that appears to have another phenomena occurring in addition to the pulse shaping mechanism — likely the same analogous resonance condition, that is

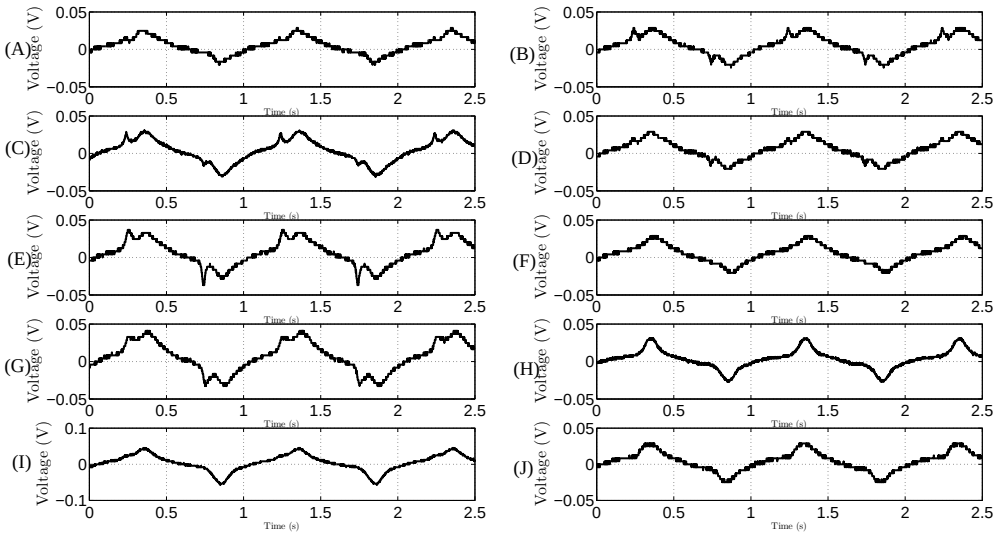

Figure 426: plots of sinking electrode using an input of 6v peak, frequency of 1hz for concentrations of (a) $0.10\%\frac{w}{v}$, (b) $0.20\%\frac{w}{v}$, (c) $0.30\%\frac{w}{v}$, (d) $0.40\%\frac{w}{v}$, (e) $0.50\%\frac{w}{v}$, (f) $0.60\%\frac{w}{v}$, (g) $0.70\%\frac{w}{v}$, (h) $0.80\%\frac{w}{v}$, (i) $0.90\%\frac{w}{v}$, and (j) $1\%\frac{w}{v}$

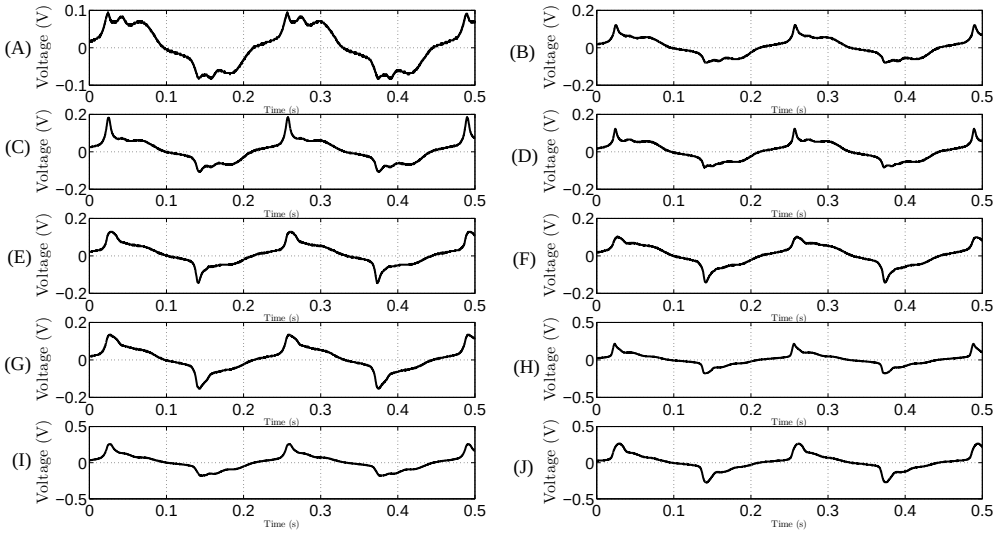

Figure 427: plots of sinking electrode using an input of 10v peak, frequency of 4.3hz for concentrations of (a) $0.10\%\frac{w}{v}$, (b) $0.20\%\frac{w}{v}$, (c) $0.30\%\frac{w}{v}$, (d) $0.40\%\frac{w}{v}$, (e) $0.50\%\frac{w}{v}$, (f) $0.60\%\frac{w}{v}$, (g) $0.70\%\frac{w}{v}$, (h) $0.80\%\frac{w}{v}$, (i) $0.90\%\frac{w}{v}$, and (j) $1\%\frac{w}{v}$

dependent upon the applied voltage.

Similarly, upon visually examining Figure: (427), it becomes apparent that the liquids being examined are also nonlinear — a notion supported by noticing that a sinusoidal input is being transformed into a pulse and ramp looking shapes across the sinking current sensing resistor. Likewise, upon examining all of the subplots, within Figure: (427), it appears that the distortion that is occurring is relatively consistent in shape over frequency — noting that the magnitude appears to remain similar over concentration —, with the exception of subplot (A) that appears to have another phenomena occurring in addition to the pulse shaping mechanism — likely the same analogous resonance condition, that is also dependent upon the applied frequency.

Conversely, upon visually examining Figure: (428), it becomes apparent that the liquids being examined are now somewhat linear — a notion supported by noticing that a sinusoidal input is being transformed into a ramp looking shape across the sinking current sensing resistor that is frequently observed within capacitive circuits. Likewise, upon examining

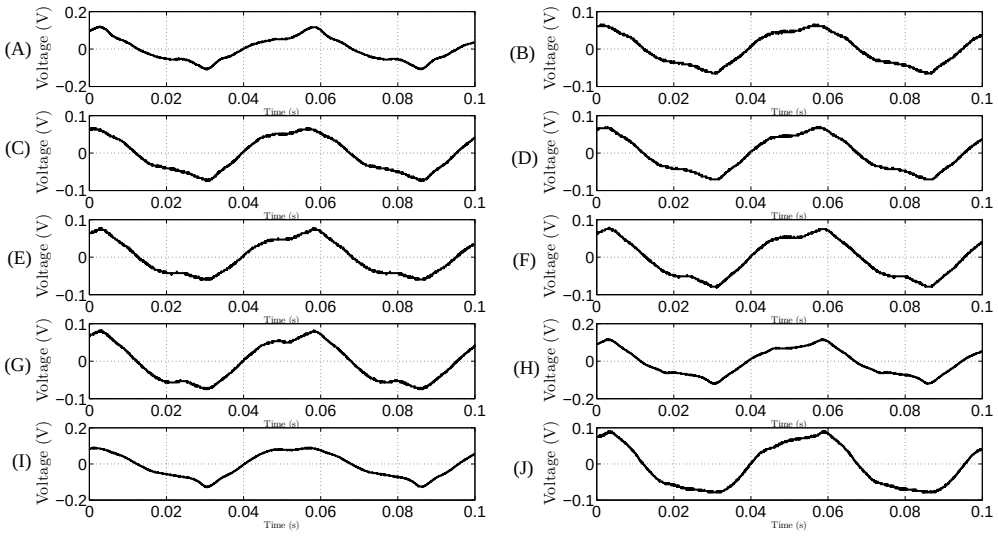

Figure 428: plots of sinking electrode using an input of 10v peak, frequency of 18hz for concentrations of (a) $0.10\%\frac{w}{v}$, (b) $0.20\%\frac{w}{v}$, (c) $0.30\%\frac{w}{v}$, (d) $0.40\%\frac{w}{v}$, (e) $0.50\%\frac{w}{v}$, (f) $0.60\%\frac{w}{v}$, (g) $0.70\%\frac{w}{v}$, (h) $0.80\%\frac{w}{v}$, (i) $0.90\%\frac{w}{v}$, and (j) $1\%\frac{w}{v}$

all of the subplots, within Figure: (428), it appears that the distortion that is occurring is relatively consistent in shape over frequency — noting that the magnitude appears to remain similar over concentration.

Likewise, upon visually examining Figure: (429), it becomes apparent that the liquids being examined are now mostly linear — a notion supported by noticing that a sinusoidal input is being transformed into a sinusoidal output across the sinking current sensing resistor that is frequently observed within capacitive circuits. Likewise, upon examining all of the subplots, within Figure: (429), it appears that the distortion that is occurring is relatively consistent in shape over frequency — noting that the magnitude appears to remain similar over concentration.

Conversely, upon visually examining Figure: (430), it is interesting to note that the potential gradient that develops within the test chamber appears to function like a inverted diode — insofar as, it clips the positive waveform of the applied signal —, and the underlying reason behind this occurrence is both unexpected and unknown, although given that the EZ

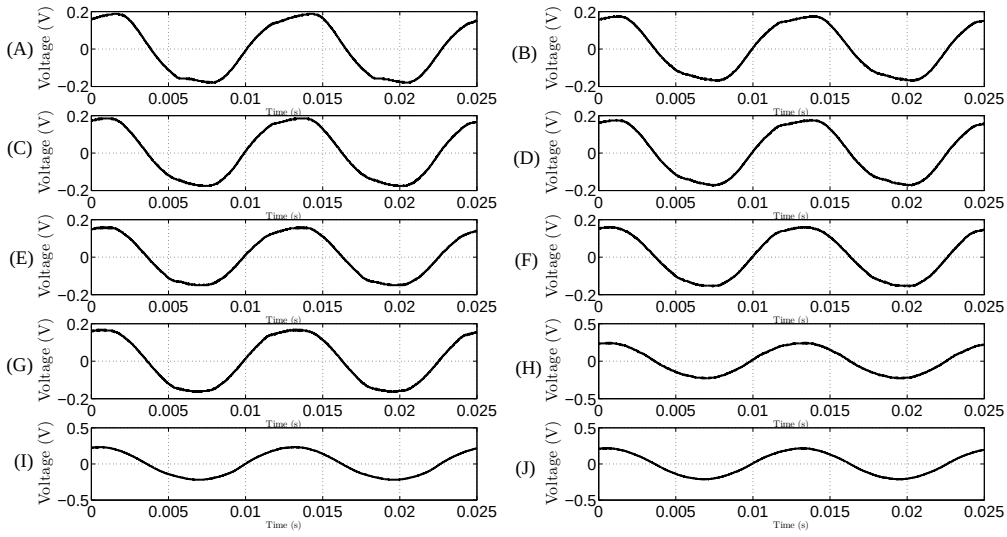

Figure 429: plots of sinking electrode using an input of 10v peak, frequency of 79hz for concentrations of (a) $0.10\%\frac{w}{v}$, (b) $0.20\%\frac{w}{v}$, (c) $0.30\%\frac{w}{v}$, (d) $0.40\%\frac{w}{v}$, (e) $0.50\%\frac{w}{v}$, (f) $0.60\%\frac{w}{v}$, (g) $0.70\%\frac{w}{v}$, (h) $0.80\%\frac{w}{v}$, (i) $0.90\%\frac{w}{v}$, and (j) $1\%\frac{w}{v}$

region is negatively charged there is a chance that the EZ region is somehow screening the buildup of electrical gradients within the medium — noting that all potential electrodes within the apparatus have this same wave shape —, although the fact that there is a substantial reduction in potential magnitude, within subplot (D), could be connecting this

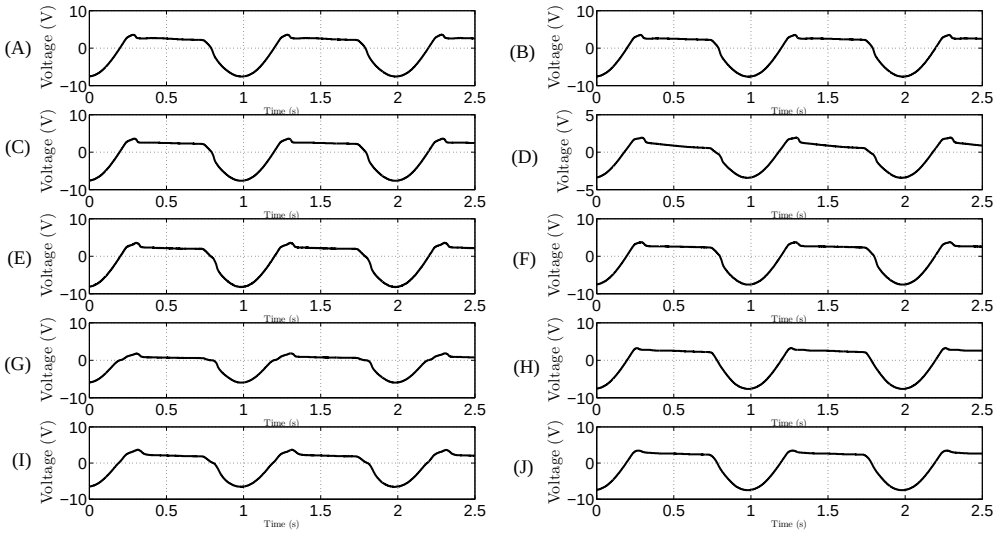

Figure 430: plots of middle electrode potential for an input of 10v peak, frequency of 1hz for concentrations of (a) $0.10\%\frac{w}{v}$, (b) $0.20\%\frac{w}{v}$, (c) $0.30\%\frac{w}{v}$, (d) $0.40\%\frac{w}{v}$, (e) $0.50\%\frac{w}{v}$, (f) $0.60\%\frac{w}{v}$, (g) $0.70\%\frac{w}{v}$, (h) $0.80\%\frac{w}{v}$, (i) $0.90\%\frac{w}{v}$, and (j) $1\%\frac{w}{v}$

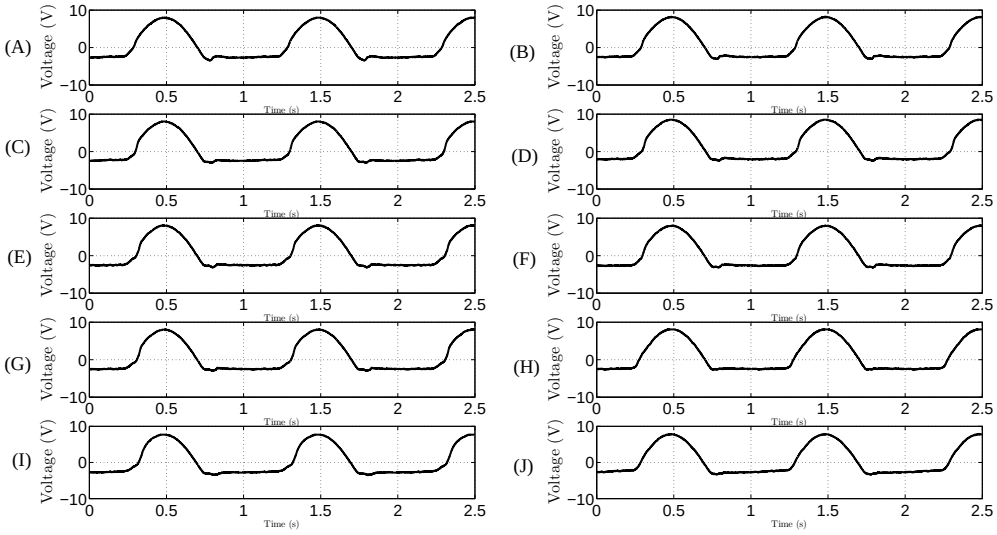

Figure 431: plots of sourcing electrode minus middle electrode potential for an input of 10v peak, frequency of 1hz for concentrations of (a) $0.10\%\frac{w}{v}$, (b) $0.20\%\frac{w}{v}$, (c) $0.30\%\frac{w}{v}$, (d) $0.40\%\frac{w}{v}$, (e) $0.50\%\frac{w}{v}$, (f) $0.60\%\frac{w}{v}$, (g) $0.70\%\frac{w}{v}$, (h) $0.80\%\frac{w}{v}$, (i) $0.90\%\frac{w}{v}$, and (j) $1\%\frac{w}{v}$

screening mechanism with ionic concentrations [184] [188] [431] [432] [433] [434].

Similarly, upon visually examining Figure: (431), it is interesting to note that the difference between the sourcing electrode potential and the potential gradient that develops within the test chamber appears to behave like a diode — insofar as, it clips the negative waveform of the applied signal —, and while the underlying reason behind this occurrence is both unexpected and unknown; however, this attribute allows for the development of a plot to determine the nonlinear regions of operation within a aqueous solution of sodium chloride, since when the liquid is linear the waveform is sinusoidal — thus when subtracted from the sourcing electrode the result will be a small voltage —; likewise, when the liquid is nonlinear the diode effect becomes dominant and the subtraction operation yields half of the sourcing electrode magnitude, and since this waveform is — generally — larger than the nonlinear waveform, the linear region is identified within a surface plot of this function by a flat floor while the nonlinear region is identified by the hills on the surface plot — as shown by Figure: (432), Figure: (433), and Figure: (434).

Conversely, with this being said, while Figure: (432), Figure: (433), and Figure: (434)

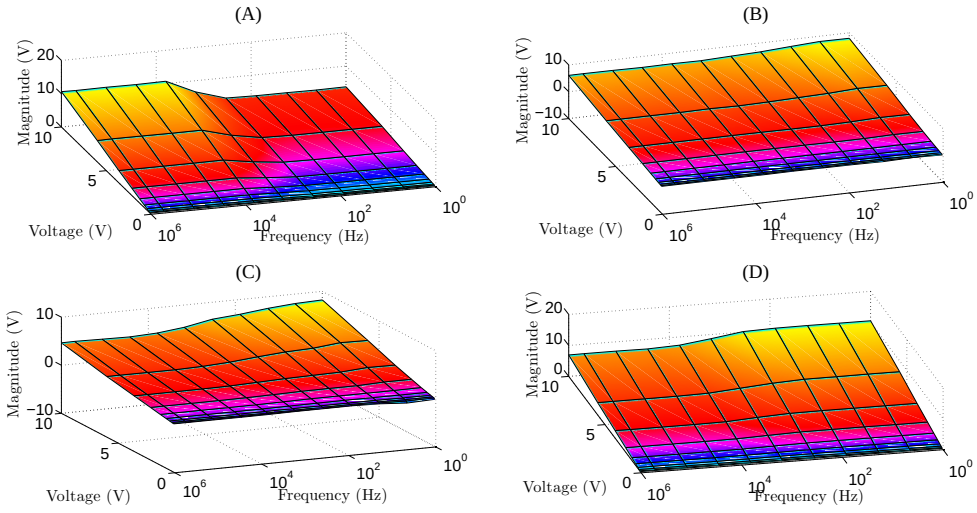

Figure 432: surface plot of input voltage versus frequency versus sourcing site electrical minus left potential electrode voltage for (a) water, (b) $0.10\%\frac{w}{v}$, (c) $0.20\%\frac{w}{v}$, and (d) $0.30\%\frac{w}{v}$

do graphically provide some indication as to what frequencies, voltages and concentrations will produce nonlinear results; however, to provide a general rule of thumb, typically any frequency under 100Hz runs the risk of encountering nonlinear effects — especially frequencies above 3V in magnitude within this region. Likewise, while the avoidance of this particular region is highly advised for classical BIS analysis; however, if operation within this region is desired, there are analytical methods that can be utilized to model the occurrence of these effects — although, it should be noted that these methods are predominately

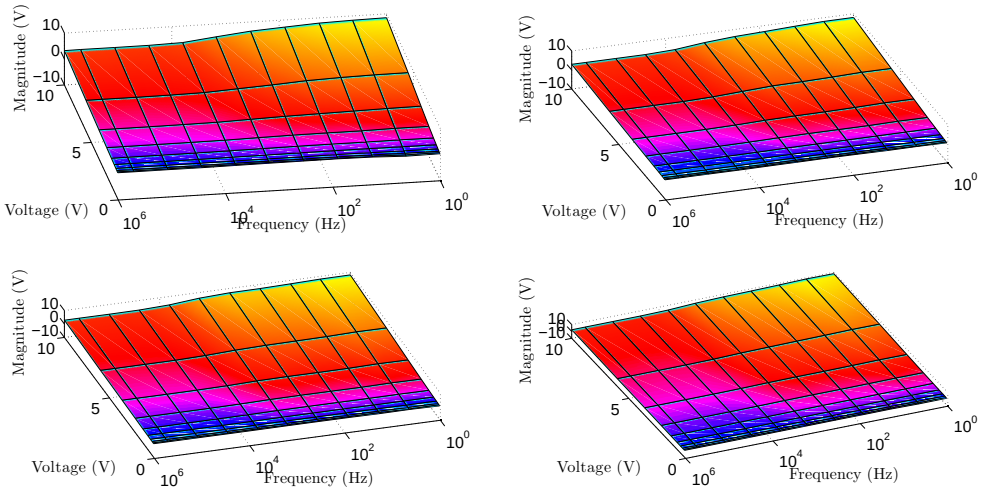

Figure 433: surface plot of input voltage versus frequency versus sourcing site electrical minus left potential electrode voltage for (a) $0.40\%\frac{w}{v}$, (b) $0.50\%\frac{w}{v}$, (c) $0.60\%\frac{w}{v}$, and (d) $0.70\%\frac{w}{v}$

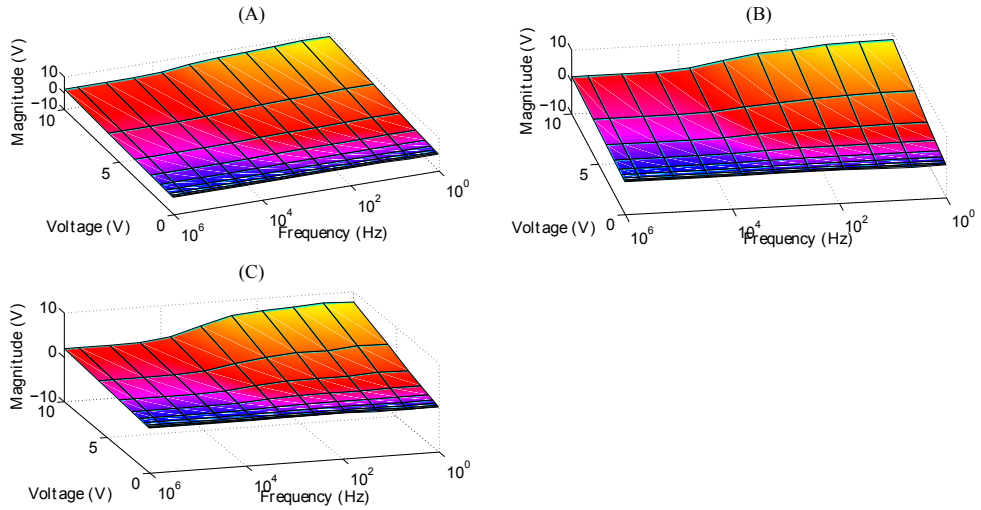

Figure 434: surface plot of input voltage versus frequency versus sourcing site electrical minus left potential electrode for (a) $0.80\%\frac{w}{v}$, (b) $0.90\%\frac{w}{v}$, (c) $1.00\%\frac{w}{v}$

based upon the classical circuit modeling approach, and it is very likely that a better conceptual modeling method exist that is based upon the underlying chemical mechanisms that is creating these distortions — like the EZ region —, which is a research topic that would likely require a full interdisciplinary research team to completely develop.

Nevertheless, to provide an example of one possible modeling method that can be utilized, consider the following parallel RC circuit topology — as shown by Figure: (435) — noting that Figure: (435) is somewhat analogous to the, previously discussed, synthesized Dow structure.

Likewise, upon utilizing KVL and KCL to create a mathematical equation of Figure: (435), as shown by Equation: (561) through Equation: (568), it can be shown that Equation: (569) and that Equation: (570) — thru the utilization of KVL — can be carefully grouped such that these equations can be easily translated into matrix form — as shown by Equation: (571) through Equation: (580) —, where X is the state vector, U is the input vector, Y is the output vector, A is the State matrix, B is the input matrix, C is the output matrix, D is the feed-forward matrix.

$$V_A(t) = R_A I_{R_A}(t) \tag{561}$$

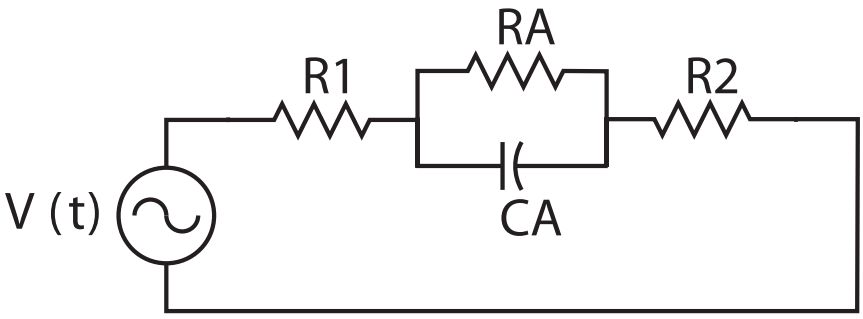

Figure 435: a picture of a simplistic r-rc-r model for a aqueous sodium chloride of a particular concentration

$$V_A(t) = \frac{1}{C_A}\int_{t_0}^{t} I_c(\tau)\,d\tau + V_A(t_0) \tag{562}$$

$$KVL: V_{in}(t) = I(t)R_1 + V_A + I(t)R_2 \tag{563}$$

$$KCL: I(t) = I_{R_A}(t) + I_{C_A}(t) \tag{564}$$

$$V_{in}(t) = \left[I_{R_A}(t) + I_{C_A}(t)\right]R_1 + V_A(t) + \left[I_{R_A}(t) + I_{C_A}(t)\right]R_2 \tag{565}$$

$$I_{C_A}(t) = C_A\frac{d}{dt}\left\{V_A(t)\right\} \tag{566}$$

$$I_{C_A}(t) = C_A V_A'(t) \tag{567}$$

$$V_{in}(t) = \left[I_{R_A}(t) + C_A V_A'(t)\right]R_1 + V_A(t) + \left[I_{R_A}(t) + C_A V_A'(t)\right]R_2 \tag{568}$$

$$V_A'(t) = \frac{V_{in}(t) - V_A(t)\left[\frac{R_1}{R_A} + 1 + \frac{R_2}{R_A}\right]}{C_A R_1 + C_A R_2} \tag{569}$$

$$I_{R_A}(t) = I_{R_B}(t) = \frac{-1}{R_1 + R_2}V_A(t) + \frac{1}{R_1 + R_2}V_{in}(t) \tag{570}$$

$$X' = V_A'(t) \tag{571}$$

$$A = \frac{-1}{C_A R_1 + C_A R_2} - \frac{R_1}{C_A R_A R_1 + C_A R_A R_2} - \frac{R_2}{C_A R_A R_1 + C_A R_A R_2} \tag{572}$$

$$X = V_A(t) \tag{573}$$

$$B = \frac{1}{C_A R_1 + C_A R_2} \tag{574}$$

$$U = V_{in}(t) \tag{575}$$

$$Y = I_A(t) \tag{576}$$

$$C = \frac{-1}{R_1 + R_2} \tag{577}$$

$$X = V_A(t) \tag{578}$$

$$D = \frac{1}{R_1 + R_2} \tag{579}$$

$$U = V_{in}(t) \tag{580}$$

$$\tag{581}$$

Conversely, with this being said, upon converting Equation: (571) through Equation: (580) into matrix form — using the notation defined by Equation: (582) and Equation: (583) — It can be shown that the closed form solution of a differential equation within state space form can be found by Equation: (584), and if assumptions are made and the system is discretized then Equation: (585) becomes true, where $A^{\star} = e^{A}\,T$, and, $B^{\star} = A^{-1}\left(A^{\star} - I\right)\,B$, such that the RRCR model developed can be solved using a segmented — or nonlinear — least squares estimation technique — as shown by Equation: (586), Equation: (587), Equation: (588), and Equation: (589) — to determine the model parameters based upon acquired laboratory measurements — where, $A^{\star} = Co_1$, $B^{\star} = Co_2$, $A = \left(\frac{1}{h}\right)\log\left(A^{\star}\right)$, $B = \left(A^{\star} - 1\right)^{-1}\,A\,B^{\star}$, $C_A(k) = \frac{1}{b\,(R_1+R_2)}$, $R_A(k) = \frac{-(R_1+R_2)}{A\,C_A\,(R_1+R_2)-1}$, and k is the least squares estimate for a given segment.

$$X' = AX + BU \tag{582}$$

$$Y = CX + DU \tag{583}$$

$$X(t) = e^{A(t-t_0)}X(t_0) + \int_{t_0}^{t} e^{A(t-\tau)}B(\tau)U(\tau)d\tau \tag{584}$$

$$X(k+1) = A^{*}X(k) + B^{*}U(k+1) \tag{585}$$

$$C_o = \left[F^T F\right]^{-1} F^T Y \tag{586}$$

$$Y = \begin{bmatrix} X(k+1) \\ X(k+2) \\ \vdots \\ X(k+n) \end{bmatrix} \tag{587}$$

$$F = \left[\begin{array}{c|c} X(k) & U(k) \\ X(k+1) & U(k+1) \\ \vdots & \vdots \\ X(k+n-1) & U(k+n-1) \end{array}\right] \tag{588}$$

$$C_o = \begin{bmatrix} A^* \\ B^* \end{bmatrix} \tag{589}$$

Likewise, to demonstrate this method further, upon application of this particular method to the, previously depicted, aqueous sodium chloride data at a molarity of $.90\frac{w}{v}$ — or normal saline — at 10Hz at 10V peak , results in the following resistor and capacitor

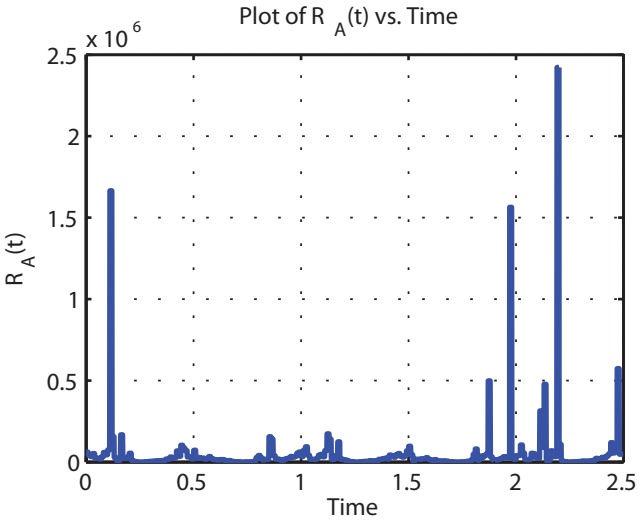

Figure 436: plot of nonlinear least squares estimate of r_a for normal saline

values — as shown by Figure: (436) and Figure: (439) respectively.

Conversely, upon numerically simulating the R-RC-R circuit equations derived above, while letting the value of R_A equal to Figure: (436) and C_A equal to Figure: (439) yields both the voltage and current across the test chamber — as shown by Figure: (438) and Figure: (439) respectively.

Likewise, upon visually examining both Figure: (438) and Figure: (439), it becomes apparent that a reasonably good approximation was obtained for this highly nonlinear system, especially given that no advanced signal preprocessing was performed prior to ap-

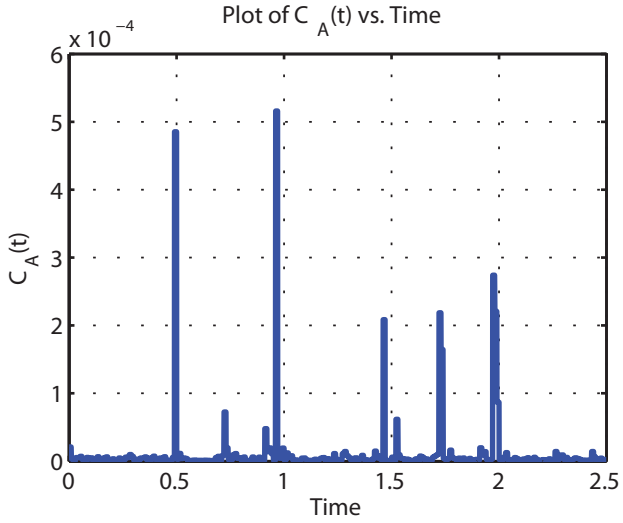

Figure 437: plot of nonlinear least squares estimate of c_a for normal saline

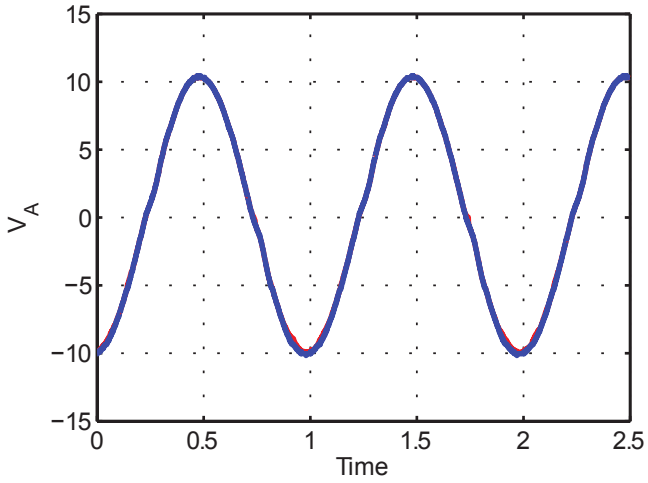

Figure 438: plot of simulated voltage across the test chamber for normal saline using a nonlinear least squares estimation method

plying the nonlinear least square method, and a better fit could have been obtained had some of the, previously discussed, preprocessing techniques been applied here — but a baseline demonstration was desired for this particular example to illustrate the methods effectiveness within a CIE effect environment. Nevertheless, while such methods do work, however the segmentation utilized by the nonlinear least square method was defined very small — on the order of 5 in this particular case — to overcome the lack of CIE compensation, thus a more general solution can be obtained by increasing the segmentation size — a size of 100 acquisitions works well for CIE effect reduced signals — and observing the time varying R_A and C_A estimations, selecting a periodic segment from these estimations, and ether fitting a function to the estimations or creating a lookup table based upon the estimates obtained.

Nevertheless, while such modeling methods can provide reasonable results — so long as some system information is known thru experimentation —, yet such methods tend to bend the unspoken rules of static circuit equations, and such attributes are simply unavoidable given the nature of the problem being examined, especially since it is obvious that a unknown chemical process — like EZ regions — are governing the conductivity of this

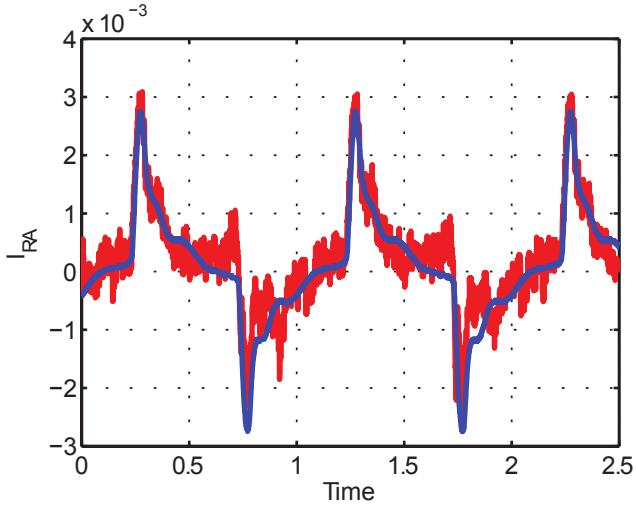

Figure 439: plot of simulated current through the test chamber for normal saline using a nonlinear least squares estimation method

particular system, and based upon such observations, it is highly presumptuous to assume that the dynamics — of this particular system — will easily conform to the simplicity of a basic electrical circuit model. Thus while this method will work for modeling this particular system within this particular paradigm; however, more native chemical modeling methods are also worth exploring here, since simplicity is not something easily obtained for such problems using current electrical engineering modeling theory, and there is nothing really gained by its utilization within such problems beyond being able to interface with an existing electrical framework — which is the only true advantage gained under such circumstances.

6.3.15 A High Fidelity EMG

The fundamental rationale behind the high fidelity EMG section was to apply the high fidelity methodology developed to a contemporary biomedical application and examine the results obtained in order to determine the overall effectiveness of the methodology developed. Likewise, based upon the observations obtained, it was determined that environmental effects encountered can be substantially reduced upon introducing physical shielding techniques like a partially shielded or a fully shielded RF shielding environment. Conversely, given that noninvasively acquired EMG signals have an extremely small amplitude — on the order of 100 μ V — attempting to acquire such measurements directly using an oscilloscope is generally not practical — especially given the tendency of instrumentational effects to be substantially higher — in terms of the CIE effects encountered — at lower voltage settings, then they are at mid-voltage settings. Therefore, an external instrumentational amplifier configuration is required to pre-amplify the EMG signal prior to acquisition. Similarly, because improper wire interconnections can inevitably create distortions, some reduction can be obtained through twisting wire interconnections

together, in order to reduce any remaining background electromagnetic radiation — within the shielding room — through the acquisition attribute of common mode rejection found within a differential amplifier. Likewise, because the physical movement of the test subject can create distortions — both from muscles producing action potentials, electrodes shifting location, and from unbalanced transmission line effects — the usage of a wooden test chair helped to reduce not only grounding effects but also help prevent undesired subject movement. Conversely, it was determined that the EMG results obtained, upon effectively implementing the, previously discussed, precautionary CEIM effect reductive procedures, yields incredibly high fidelity results, especially upon considering that the peak feature size was less than 200nV, while sub features below 50nV were clearly visible without the utilization of any substantial digital signal processing techniques. Furthermore, while there are some minor signal distortions observable below 20nv, predominantly CIE effects, such distortions can be reduced further through the utilization of the, previously discussed, CIE characterization techniques should additional signal fidelity be required — noting that such techniques tend to substitute physical fidelity with perceivable fidelity, which may or may not truly be an actual increase in fidelity depending upon the reductive techniques implemented since, for example, a signal can be smoothed through the usage of averages, but the usage of such techniques only generally yields a smoother plot, which is not an actual increase in signal acquisition fidelity.

Likewise, as it has been previously discussed, a substantial number of attributes can reduce the overall fidelity of a bioelectrical signal acquisition; however, because the discussion presented, thus far, has predominantly focused upon the distortions encountered during the active electrical characterization of materials using BIS, it now seems appropriate to metaphorically switch gears and focus upon passive biomedical acquisition techniques —

specifically the implementation of high fidelity EMG measuring techniques. Likewise, while it should be pointed out that the reduction techniques, previously presented, must be taken under advisement — with the possible exclusion of aqueous NaCl theory depending upon the end objective of the acquisitions taken —, prior to performing any passive biomedical acquisitions — assuming that the highest possible fidelity is desired. Similarly upon using the — previously presented — fidelity improving concepts as a guide, a high fidelity EMG acquisition device was created in order to demonstrate the active implementation of the, previously mentioned, combined environmental, instrumentational, and material (CEIM) effect reductive techniques.

Conversely, to outline the high fidelity EMG acquisition methodology implemented, First, as it was previously discussed, environmental effects can be substantially reduced upon introducing physical shielding techniques, and with this being said, it was decided that low-power RF shielded room conditions would be utilized since no function generation elements would be required to perform this particular acquisition; along with the fact that, all of the laboratory equipment needed — to perform this particular experiment — was capable of battery-powered operation. Second, given that noninvasively acquired EMG signals have a extremely small amplitude — on the order of 100 μ V — attempting to acquire such measurements directly using an oscilloscope is generally not practical — especially given the tendency of instrumentational effects to be substantially higher — in terms of the noise encountered — at lower voltage settings, then they are at mid-voltage settings [97]. Therefore, an external instrumentational amplifier configuration — developed and refined through a number of years of experimentation —, as shown by Figure: (440), and Figure: (189) top left, was utilized to pre-amplify the EMG signal prior to acquisition by the TPS2024 oscilloscope [1] [2]. Third, because improper wire

interconnections can inevitably create distortions, it was decided that wire interconnections would be twisted together, in order to reduce any remaining background electromagnetic radiation — within the shielding room — through the, previously discussed, attribute of common mode rejection found within a differential amplifier. Forth, because the physical movement of the test subject can create distortions — either from muscles producing action potentials, electrodes shifting location, and from unbalanced transmission line effects — the, previously discussed, wooden test chair — as shown by Figure: (356) — was utilized to both reduce grounding effects and prevent undesired subject movement [2] [97].

Likewise, upon the implementation of these, previously discussed, high fidelity acquisition procedures, two DRG electrode grippers were connected to two DS26 electrodes, and the negative input electrode — V_{in-} within Figure: (440) — was placed on the left-hand FDI muscle, while the positive input electrode — V_{in+} within Figure: (440) — was placed on the center of the back left-hand at the wrist, and the signal output — V_{out} — was

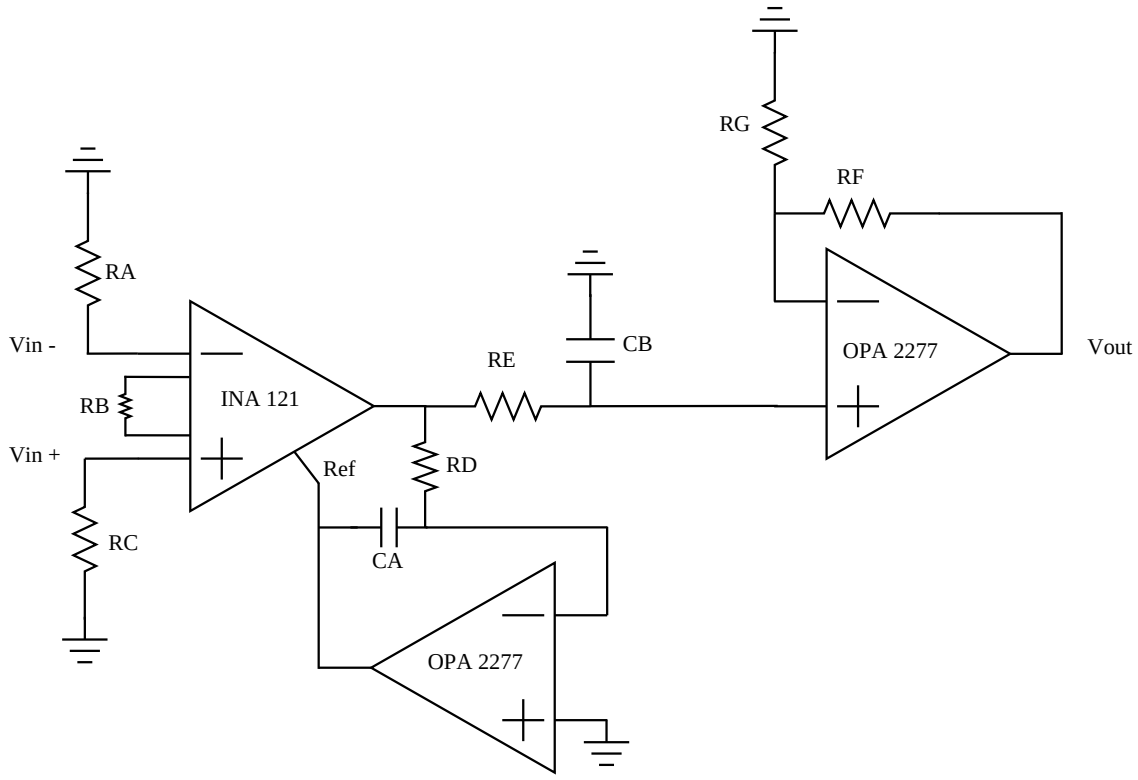

Figure 440: a low noise high gain instrumentational amplifier utilized to obtain emg measurements

connected to the first channel of the TPS2024 oscilloscope. Conversely, a third grounding electrode was connected to the left knee cap in order to create a pseudo-common ground between the amplifier and the bulk body mass — which helps prevent the unwanted amplification of biological signals, like the signals produced by cardiac contractions. Similarly, because EMG signals are extremely small, a amplifier gain of approximately 16238 $\frac{V}{V}$ was selected — with an approximate 90 $\frac{V}{V}$ gain at the instrumentational stage R_B and a 181 $\frac{V}{V}$ gain at the non-inverting amplifier stage R_G and R_F . Likewise, a active high pass filter with a cutoff frequency of 1.59Hz was utilized within Figure: (440), along with a passive low pass filter with a cutoff frequency of 7.234kHz — noting that all component values utilized within Figure: (440) are listed within Table: (22).

Table 22: components utilized by the high fidelity EMG amplifier

Component	Value	Unit	Description
RA	1	MΩ	MOSFET input grounding path 1
RB	470	Ω	IA Gain
RC	1	MΩ	MOSFET input grounding path 2
RD	1	MΩ	Active HPF Parameter
RE	1	kΩ	Passive LPF Parameter
CA	100	nf	Active HPF Parameter
CB	22	nf	Passive LPF Parameter
RF	100	kΩ	non-inverting gain Parameter
RG	1	kΩ	non-inverting gain Parameter

Conversely, prior to performing the EMG measurements, the test subject — in this particular case Dr. Mehdi Miri volunteered — was strapped into the wooden test chair, the electrodes were attached as described, and the left index finger was stimulated via movement, as shown by Figure: (441) — noting that the acquired values measured were divided by 16238 in order to approximate the actual potential measured. Likewise, upon examining Figure: (441), it becomes apparent that the EMG FDI muscle acquisition obtained was of substantially high-quality — especially upon being compared with other publicized EMG measurements taken that did not implement the, previously discussed, CEIM effect

reduction techniques —, and while the equipment utilized to perform this experiment was — overall — deliberately kept to an economical minimum — excluding the utilization of a RF shielded room — the results obtained, upon effectively implementing the, previously discussed, precautionary CEIM effect reductive procedures, yields incredibly high fidelity results, especially upon considering that the peak feature size was less than 200nV, while sub features below 50nV were clearly visible without the utilization of any substantial digital signal processing techniques [97] [155] [154] [157] [135]. Furthermore, while there are some minor signal distortions observable below 20nv, predominantly CIE effects, such distortions can be reduced further through the utilization of the, previously discussed, CIE characterization techniques should additional signal fidelity be required — noting that such techniques tend to substitute physical fidelity with perceivable fidelity, which may or may not truly be a actual increase in fidelity depending upon the reductive techniques implemented since, for example, a signal can be smoothed through the usage of averages, but the usage of such techniques only generally yields a smoother plot, which is not an actual increase in signal acquisition fidelity.

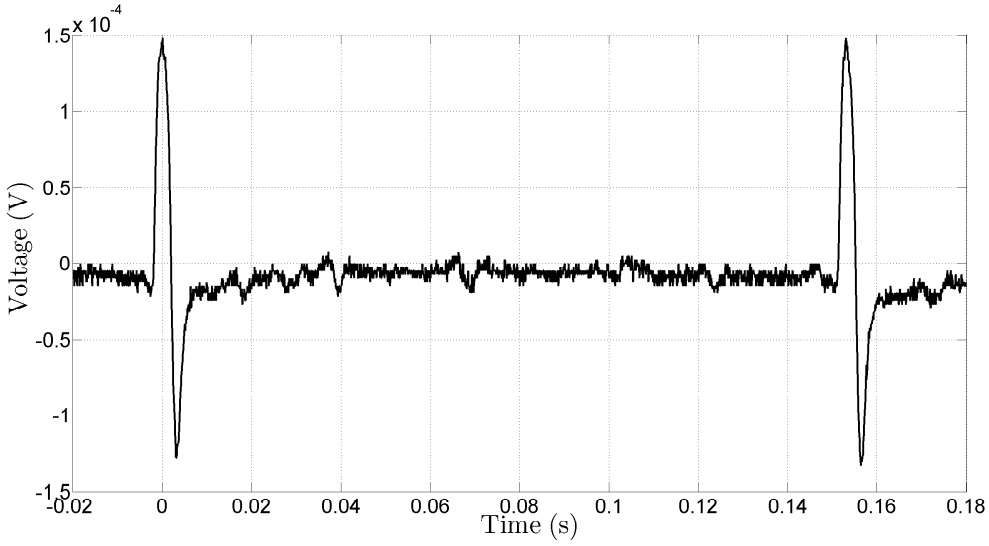

Figure 441: a high fidelity raw surface electromyography from an fdi muscle contraction measured in our lab.

6.3.16 Signal Propagation Within a Saline Body

The fundamental rationale behind the signal propagation within a saline body section was to apply the high fidelity methodology developed to a PVC approximation of a human torso filled with an aqueous solution in order to examine the role an aqueous solution plays in the propagation of common bioelectrical signals — like an EKG signal. Likewise, based upon the observations obtained, it was determined that the applied 10V peak at 1Hz sinusoidal signal was, in fact, capable of transversing the PVC pseudo-torso structure without obtaining a unrecoverable amount of attenuation from propagating through the saline medium. Conversely, it also was determined that the applied 10V peak sinusoidal signal was barely able to allow the signal to be successfully received by the instrumentational amplifier — implying that a PVC pseudo-torso filled with normal saline is not inherently the best structure to represent the underlying propagational medium of the human body, since such voltages are not generally found within the human body —, and while this particular model might be an over estimate of the amount of saline medium encountered; however, the observed distortions to the input signal — predominantly arising from the, previously discussed, tendency of lower frequencies to only invoke potential gradients above particular thresholds — does appear visually reminiscent to the waveforms observed, and such observations does merit some pause since there is a strong likelihood that some type of intrinsic correlation exists between the noninvasively observed bioelectrical signals and those visually depicted within this particular experiment. Nevertheless, while this particular experiment was far from being an ideal human body model — particularly given the required magnitude necessitated for differential acquisition at the hands —; however, although matching results are generally preferred within scientific research, it is

worth mentioning that such observations are important, insofar as, they clearly show that other propagational methods — like dielectric propagation and biological signal repeaters — are a predominant factor in the propagation of a signal within the human body, and, while aqueous attenuation does definitively play a role within signal transmission within the body, such attributes — in themselves — are not the only mechanism that must be considered. Likewise, while this particular experiment was not pursued further, the next logical step would be to feel the test apparatus with a porous medium — like a sponge — and then saturate — but not excessively — the porous medium with a saline solution in order to determine if a better approximation is obtained given the overall semi-porous structure of the human body. Similarly, based upon the observations obtained within the lessons in experimentation subsection, it was concluded that apparatus design is extremely important in obtaining the highest fidelity measurement possible. Likewise, prototyping and experimentation can go a long ways in determining what apparatus building techniques are successful and what apparatus building techniques are not since successful.

Likewise, given the overall success in obtaining a high fidelity EMG FDI muscle acquisition, it was decided — at least upon also considering the observations obtained from the aqueous saline experiments — that some further inquiry was merited regarding the underlying electrical transmission structure of the body — particularly cardiac contractions. While this particular subject is, by all accounts, a singular doctoral research topic in itself — thus only a preliminary inquiry will be provided here —; yet, the underlying mechanism behind how an electrical signal — say a cardiac contraction — can propagate from the center of the human body outward through an attached extremity — as it is possible to detect a heartbeat from the FDI region — is an extremely profound and fascinating observation. Conversely, based upon such interest, an experiment was devised in which a

pseudo-human torso replica — as shown by Figure: (442) — made entirely of PVC pipe — with five titanium electrode locations — was constructed, filled with a normal saline solution, and a electrical signal applied to the region that simulates the location of the heart, while the, previously mentioned, EMG acquisition apparatus was utilized to obtain a differential measurement across the electrodes that approximated the location where human hands would ideally exist, and this was done primarily to obtain some conceptual semblance between the pseudo-human torso and a real human torso using the highest possible acquisition equipment available.

While, it will be admitted that a PVC torso replica filled with a normal saline solution is inherently far from being a realistic substitute for an actual human torso; however, it must be remembered that scientific experiments typically begin with the metaphoric glass elephant in a vacuum model and add additional parameters from there, and — based upon such notions — it is important to recognize that this particular experiment is attempting to determine: First, is a signal that is produced in the approximate region of the heart

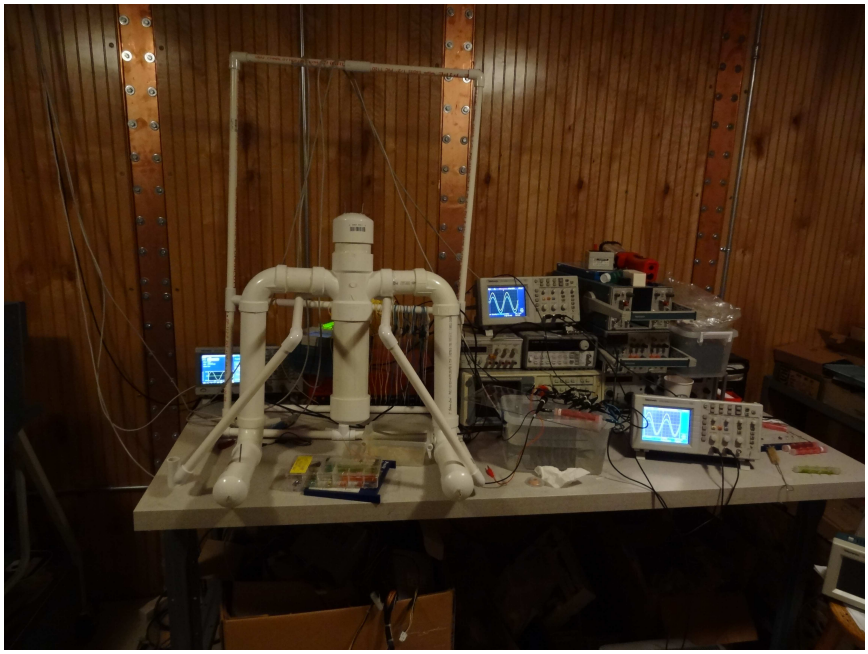

Figure 442: pvc replica of the human torso with five electrode locations for normal saline signal testing

within an aqueous medium — like normal saline — actually capable of transversing the torso structure without encountering a unrecoverable amount of attenuation. Second, if a signal is capable of transversing this particular distance, how much voltage is required and does that voltage exceed the amount of potential produced by an actual human organ — like the heart — within the body. Third, based upon the results of the first two questions, what types of distortions are encountered upon transversing this distance and are they remotely similar to observable bioelectrical signals.

Conversely, with this being said, a 10V peak sinusoidal signal with a frequency of approximately 1Hz was applied to a 110 ohm current sensing resistor — via the Tektronix AFG3102 function generator — that was then connected to the left terminal of the ionic testing apparatus, while the right terminal of the ionic testing apparatus was connected to another 110 ohm current sensing resistor that, in turn, was connected to the function generator ground. Likewise, the — previously shown — high fidelity EMG differential amplifier circuit developed was then utilized to aid in the acquisition of the applied signal, and one differential input of the acquisition circuit was attached to the lower left-hand electrode of the ionic testing apparatus, while the other differential input was attached to the right-hand electrode of the ionic testing apparatus, and the corresponding output of the differential amplifier was connected to the Tektronix TPS2024 oscilloscope for acquisition. Similarly, because the Tektronix AFG3102 function generator was required to create a input signal, the test conducted was performed under partially shielded conditions — rather than fully shielded low-power operational conditions — and the results obtained from the differential amplifier are shown within Figure: (443).

Conversely, upon visually inspecting Figure: (443), the following conclusions can be made: First, it appears — based upon Figure: (443) — that the applied 10V peak at

1Hz sinusoidal signal was, in fact, capable of transversing the PVC pseudo-torso structure without obtaining a unrecoverable amount of attenuation from propagating through the saline medium. Second, it also appears — based upon Figure: (443) — that the applied 10V peak sinusoidal signal was barely able to allow the signal to be successfully received by the instrumentational amplifier — implying that a PVC pseudo-torso filled with normal saline is not inherently the best structure to represent the underlying propagational medium of the human body, since such voltages are not generally found within the human body. Third, while this particular model might be a over estimate of the amount of saline medium encountered; however, the observed distortions to the input signal — predominantly arising from the, previously discussed, tendency of lower frequencies to only invoke potential gradients above particular thresholds — does appear visually reminiscent to the waveforms observed within Figure: (441), and such observations does merit some pause since there is a strong likelihood that some type of intrinsic correlation exists between the noninvasively observed bioelectrical signals and those visually depicted within this particular experiment.

Nevertheless, while this particular experiment was far from being an ideal human body model — particularly given the required magnitude necessitated for differential acquisition

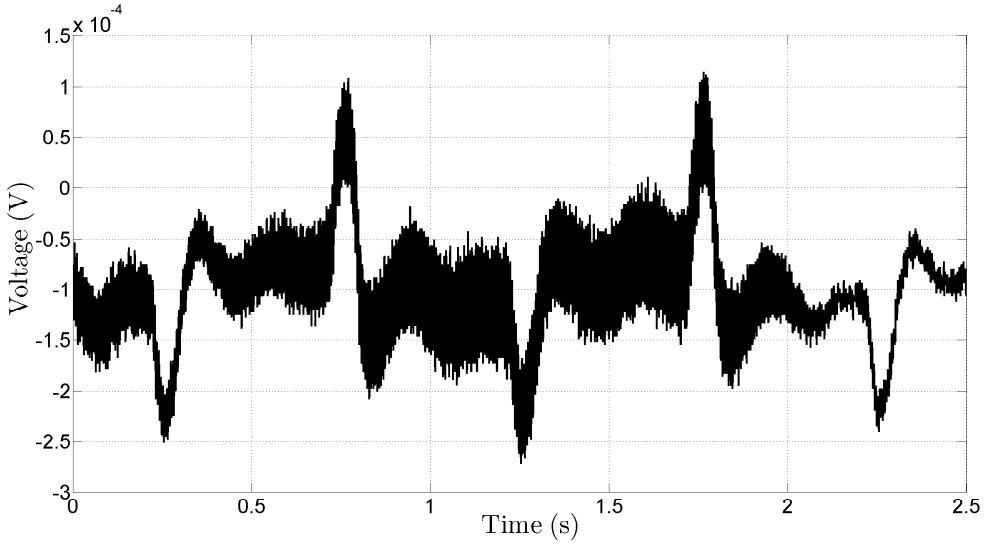

Figure 443: plot of the observed differential voltage across the ionic testing apparatus hands

at the hands —; however, although matching results are generally preferred within scientific research, it is worth mentioning that such observations are important, insofar as, they clearly show that other propagational methods — like dielectric propagation and biological signal repeaters — are a predominant factor in the propagation of a signal within the human body, and, while aqueous attenuation does definitively play a role within signal transmission within the body, such attributes — in themselves — are not the only mechanism that must be considered. Likewise, while this particular experiment was not pursued further within this dissertation, the next logical step would be to feel the test apparatus with a porous medium — like a sponge — and then saturate — but not excessively — the porous medium with a saline solution in order to determine if a better approximation is obtained given the overall semi-porous structure of the human body.

6.3.17 Lessons in Experimentation

The fundamental rationale behind the lessons in experimentation section was to provide a recollection of the development process — both successes and failures — in the creation of the physical laboratory apparatus developed. Conversely, based upon the observations obtained, it was determined that the successful development and implementation of acquisition automation can go a long ways in increasing the overall fidelity obtained — either through allowing CIE characterization to occur and reducing human error. Likewise, the substantial amount of information obtained through automated acquisition can become problematic if not carefully managed, and sometime should be spent in developing organizational procedures.

Conversely, now that a number of interesting attributes about high fidelity signal acquisition has been discussed, it seems prudent to begin the process of wrapping up this particular discussion by taking a brief moment to address some of the lessons learned

through the development of the experimental apparatus utilized within this dissertation — noting that some of the apparatuses developed were successful while others were not. Likewise, one of the first lessons learned — particularly when it comes to creating a liquid containing apparatus — is the proper utilization of a watertight sealant — like silicon gel or PVC glue — , especially since these liquid containers will be working in close proximity with expensive electrical acquisition instrumentation and mistakes could be both costly and potentially deadly. Similarly, based upon such observations and given the precision required when creating aqueous sodium chloride solutions, it is highly recommended that a laboratory liquid workspace — as shown by Figure: (444) — is utilized when mixing solutions and filling testing chambers, since such a station creates an isolation barrier between expensive acquisition electronics, while also providing a convenient place to store all stock solutions necessitated by the experiments being performed.

Likewise, while silicone sealant and a liquid workspace can go a long ways in reducing the chance of a laboratory liquid accident, another important attribute to consider when designing a liquid apparatus is the minimization of points of leakage — like filling locations

Figure 444: a picture of the laboratory liquid workspace utilized

and electrode sites — since, for example, one of the original aqueous test chambers developed — as shown by Figure: (445) — had a bad tendency of slightly leaking despite the amount of sealant utilized — as the attachment of electrical interconnections eventually broke the sealant and the reapplication of sealant generally put the apparatus out of service for a couple of days which was highly inconvenient.

Conversely, while such attributes are manageable; however, the shape of the testing apparatus should be considered — at least from a public perspective — before manufacturing, since — in the case of Figure: (445) — it is highly possible that the general public could easily mistake this particular testing apparatus with some type of harmful device — like a bomb — and create some substantial legal troubles as a result — although, in the case of Figure: (445), movement and storage of the device was carefully orchestrated to prevent such occurrences. Likewise, as it was previously mentioned, the proper selection of a noncorrosive electrode material is extremely important when creating a custom liquid apparatus, especially since improperly selected electrode materials can corrode upon contact with the liquid solution — an attribute best demonstrated by the first prototype gradient

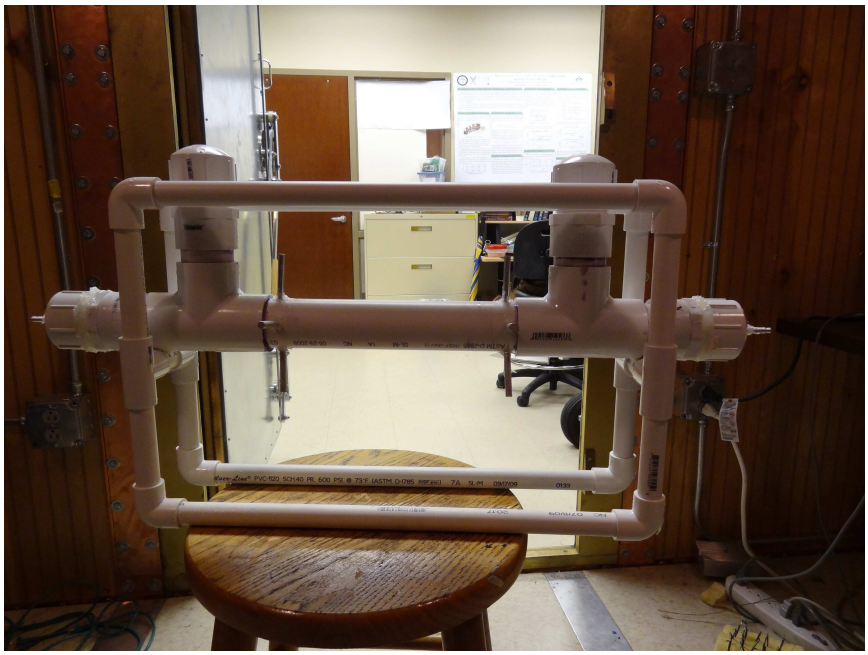

Figure 445: a picture of a prototype liquid testing chamber

apparatus developed, as shown by Figure: (446).

Similarly, while proper material selection is extremely important, often times the commercial availability of an appropriate material in the desired shape or structure at an affordable cost is seldom , if ever, obtained outright; thus, often times the custom assembly of raw materials is required in order to reach the intended objective — as shown by Figure: (447), in which a custom aluminum screen was created from raw aluminum parts to fit a liquid container in order to perform dielectric testing on distilled water.

Nevertheless, while such fabrication considerations are extremely important in obtaining an effective testing apparatus, it is also important to recognize that the development of a effective testing apparatus is a iterative process that is seldom ever achieved on the first try — particularly when working with raw materials and conceptual theoretical ideas. Conversely, to illustrate this point further, consider for the moment a conceptual notion that a possible electrically induced hydraulic effect might exist, which in turn led to the development of a testing apparatus — as shown by Figure: (448) — that ultimately yielded

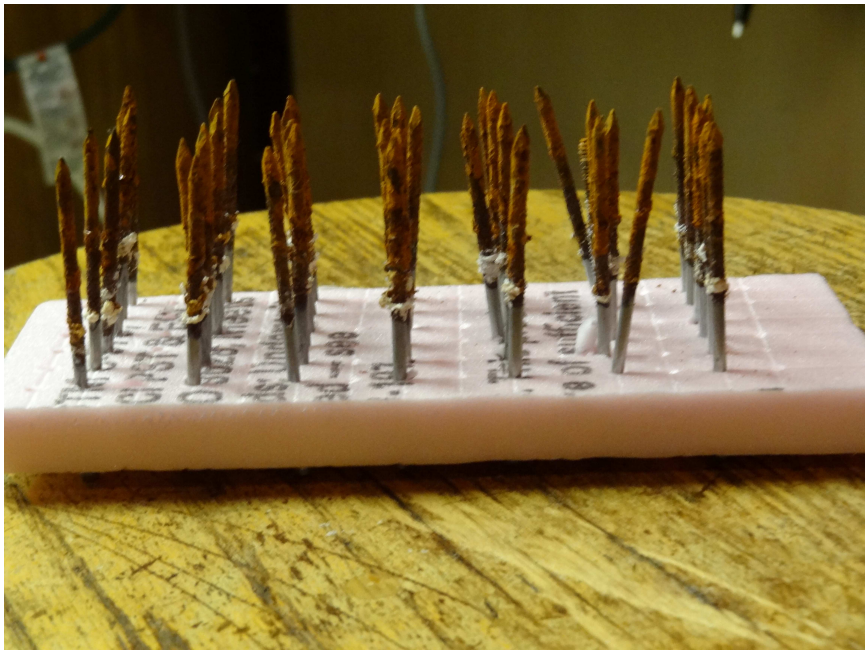

Figure 446: a picture of a prototype gradients measuring apparatus

results that were either classifiable as inconclusive or dissuasive.

Likewise, while such experiments generally will go undocumented within published research results — possibly to avoid embarrassment —; however, it is important to recognize that these types of experiments — along with the apparatus utilized — are simply the inevitable consequence of working with a foreign — and generally unknown — research topic, and the development of such experiments — at least if implemented in a scientifi-

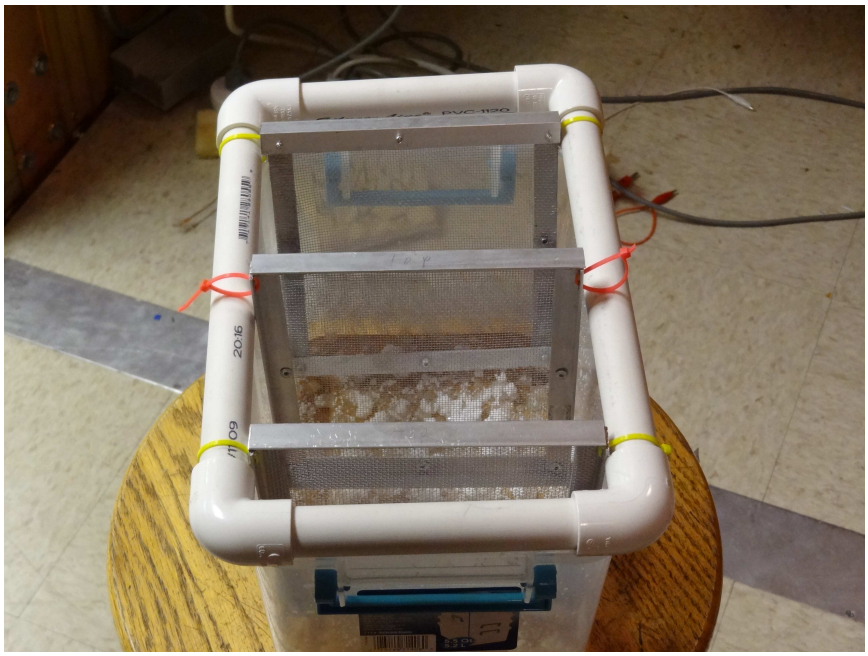

Figure 447: a picture of a custom fabricated aluminum screen testing apparatus

Figure 448: a picture of a custom fabricated prototype electric hydraulic device

cally appropriate way using cost-effective construction techniques — can aid in obtaining an intuitive understanding of the desired subject being investigated.

6.3.18 Lessons in Computing

The fundamental rationale behind the lessons in computing section was to provide a recollection of the development process — both successes and failures — in the creation of the computerized laboratory apparatus developed. Likewise, based upon the observations obtained, it was determined that Beowulf computational clusters — while having some inherent uses — are not necessarily ideal for processing large volumes of laboratory acquisitions — at least not without careful design of a fast data transferal systems —, and these computational clusters can be somewhat difficult to manage if similar computers are not being utilized within the cluster. Additionally, computationally intensive simulation models — like those found within Electrohydrodynamics —, while being a very promising research area, are not effectively implemented within a low end computational cluster — like the budget Beowulf clusters — and should be avoided unless the resources available it can handle their computational intensity.

Conversely, as it might have been observed — particularly within the experiments, results, and applications sub chapter — that a substantial number of computationally aided experimental operations and processing techniques were utilized — arguably, more so, than the underlying traditional approach —, and while opinions on this particular method of handling such problems can vary — either favorably or unfavorably —; however, the utilization of such computer oriented methods does have a number of profound benefits — notably the capability of acquiring a substantial amount of laboratory acquisitions without the aid of human interaction —, and the results obtained from the computer implementation selected — in a manner similar to the lessons learned within the experimentation subsection

— ultimately had a number of little lessons associated with its implementation.

Likewise, as it has already been discussed in substantial detail within the preliminary data management subsection and the DC voltage and the environmental effects measured subsection, the remote communication with the Tektronix TPS2024 and the TDS2002 oscilloscopes utilized a serial RS–232 communication protocol that — in the most traditional sense — was designed to directly connect to a — slowly becoming obsolete — personal computer serial port that could be accessed through the computers operating system using a variety of programming languages — in this particular case Python was selected because of its portability across operating systems — as Linux, and Windows were supported —, overall processing speed relative to its interpreted nature, and overall ease-of-use. Similarly, while such attributes are relatively straightforward from a conceptual perspective — with the fundamental implementation being connect cables, open communication port, control device —; however, such attributes begin to become somewhat logistically, problematic upon the introduction of multiple acquisition devices for number of reasons: First, most older personal computers only have one to two RS–232 serial ports — noting that most contemporary computers are removing this port entirely —, second, even similar manufactured oscilloscopes — like the Tektronix TPS2024 and the TDS2002 — can have interesting and unique communication quirks — notably the improper selection of the TPS2024 trigger would lock up the device and hang any automatic experiments, third, typically interactions with all utilized acquisition devices must — ideally — occur simultaneously, lastly, data transfer from the oscilloscope back to the computer must be accurate and reasonably fast — in order to minimize the amount of time needed to perform an experiment and to prevent such delays from introducing additional distortions within the experiment being conducted.

Conversely, upon addressing each of these logistical problems, it was determined that: first, USB could be utilized to replace serial connections using RS–232 to USB converters, and that — given the slow communication rate of RS–232 — that there was more than enough bandwidth to have more than one RS–232 device on the same USB connection — a task achieved using a USB hub, second, that Python — along with a lot of trial and error — could be utilized to develop a cross instrumentational control class in order to create a common interface that would resolve any device specific communication quirks — thus separating the device quirks from the commands used to control the device, third, while the concept of simultaneous communication — particularly using one USB communication port — is inherently flawed; however, because USB is faster than RS–232, it is possible — through the usage of threading — to synthesize and send controlling commands in parallel — and while they will not arrive at the unit simultaneously — as the commands will be queued and sent synchronously —, the time delay between there execution by the oscilloscope should be relatively similar given the slower communication expectation — by the oscilloscope — of a RS–232 clock rate, lastly, while the RS–232 data rate selected ultimately determines the communication speed from the oscilloscope, some improvements in transfer rate — within the data rate selected — can be obtained by the utilization of a binary communication format over a ASCII based format.

Likewise, another logistical attribute that had to be addressed, was the fact that the Tektronix AFG3102 function generator did not utilize the RS–232 communication protocol — as it supported USB and ethernet communication via the tekvisa communication protocol —, thus another communication class was required to facilitate communications with this particular device in addition to the, previously mentioned, oscilloscope communication class. Nevertheless, once these particular logistical problems were resolved, all the labo-

ratory equipment utilized was controlled via a singular computer — as shown by Figure: (449) — that was located outside of the RF shielded room — as a USB wire was connected to the instrumentation through a access port within the wall of the RF shielded room.

Conversely, because of the successful implementation of this automatic acquisition system, a smaller GUI based control application — as shown by Figure: (450) — was developed in Python and donated to the ECE laboratory department in order allow ECE students to download measurements from there Tektronix TDS2002 oscilloscope — to a computer — without having to buy a CompactFlash card to do so, thus saving the sophomore ECE students an estimated 2000 dollars yearly — assuming 5 sophomore labs with 14 students per lab and a average cost of 30 dollars per CompactFlash card and reader —, and the ECE department an unknown amount of money in Tektronix TDS2002 CompactFlash card module repairs — as damage typically results from improper installation of a CompactFlash card into a Tektronix TDS2002 oscilloscope.

Likewise, while the implementation of a automatic laboratory acquisition system was extremely important; another interesting attribute that arose as a result of the system —

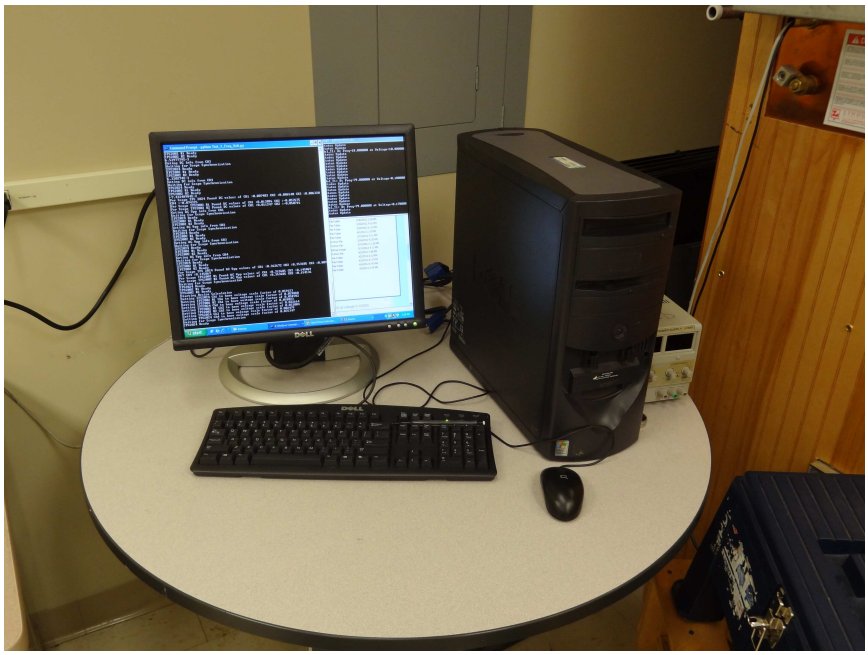

Figure 449: a picture of the computer utilized to perform automatic simulations

the attribute being a substantial amount of data —, and given the inherent limitations of Matlab to efficiently perform parallel operations — an attribute that newer versions of Matlab are attempting to resolve — the problem of processing the massive amounts of data obtained — while fortunately not overly substantial — was investigated and a number of possible solutions developed — the most notable being the creation of a small Beowulf cluster that consisted of a hodgepodge of old computers, as shown by Figure: (451).

Conversely, while the oddities associated with the development of a Beowulf cluster will not be substantially addressed — within this dissertation —; however, it will be mentioned that the hodgepodge nature of the computers utilized — some computers used Linux while others used Solaris — made coordination amongst the computers inherently problematic

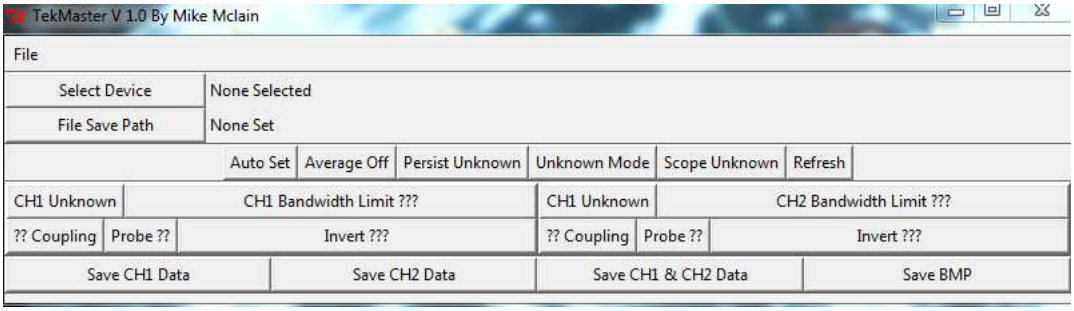

Figure 450: a picture of the laboratory gui application developed to download oscilloscope measurements

Figure 451: a picture of the beowulf cluster created

— typically when attempting to utilize open source cluster controlling software — that ultimately led to the development of a network based Python control system. Likewise, while the overall successfulness of the cluster develop was somewhat questionable — since in some cases, the network limitations imposed by a cheap 10Mbit network interface — ultimately made some operations faster to perform on a higher end personal computer then through the usage of the cluster, and the utilization of precompiled C++ Matlab functions also decrease the overall benefit obtained in some cases as well.

Nevertheless, the implementation of this — particular cluster — was beneficial in obtaining some insight into the infrastructure required to effectively perform automated acquisition and processing, and while the results obtained are far from superior — especially given the limited amount of funding to develop this particular piece of infrastructure —; however, the amount of experience obtained from the attempt made the experiment worthwhile, and help to define the research capabilities that could be utilized. Likewise, during this period of experimentation with cluster computing, some brief preliminary attempts were also made at electrostatically modeling the ionic systems observed — as shown by

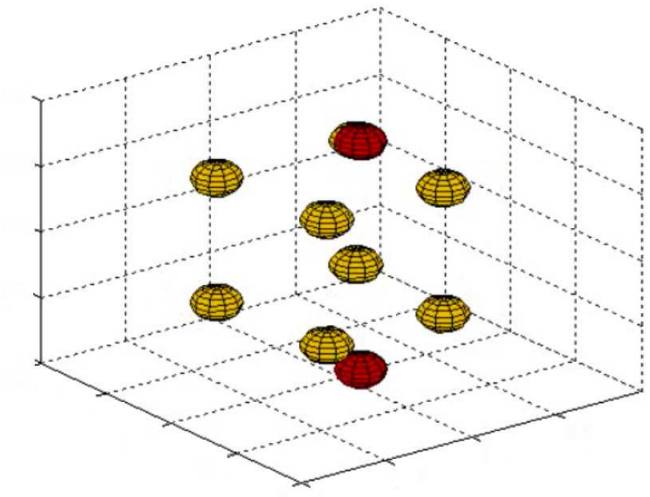

Figure 452: a picture of attempting to model the movement of ions using quasi-electrostatic forces

Figure: (452), Figure: (453), and Figure: (454) — and ultimately it was determined that such modeling techniques require computational resources beyond those that were available within the research laboratory utilized, thus such approaches were eventually substituted with more macroscopic modeling methods previously presented.

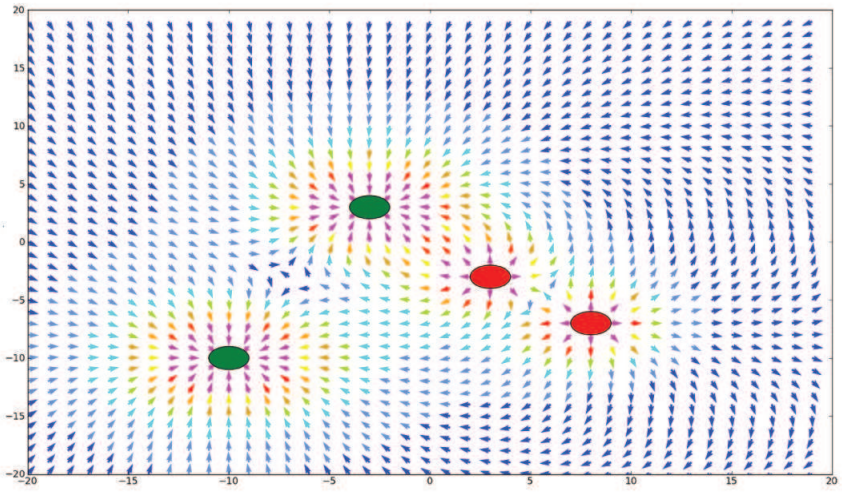

Figure 453: a picture of attempting to model the movement of ions using quasi-electrostatic forces

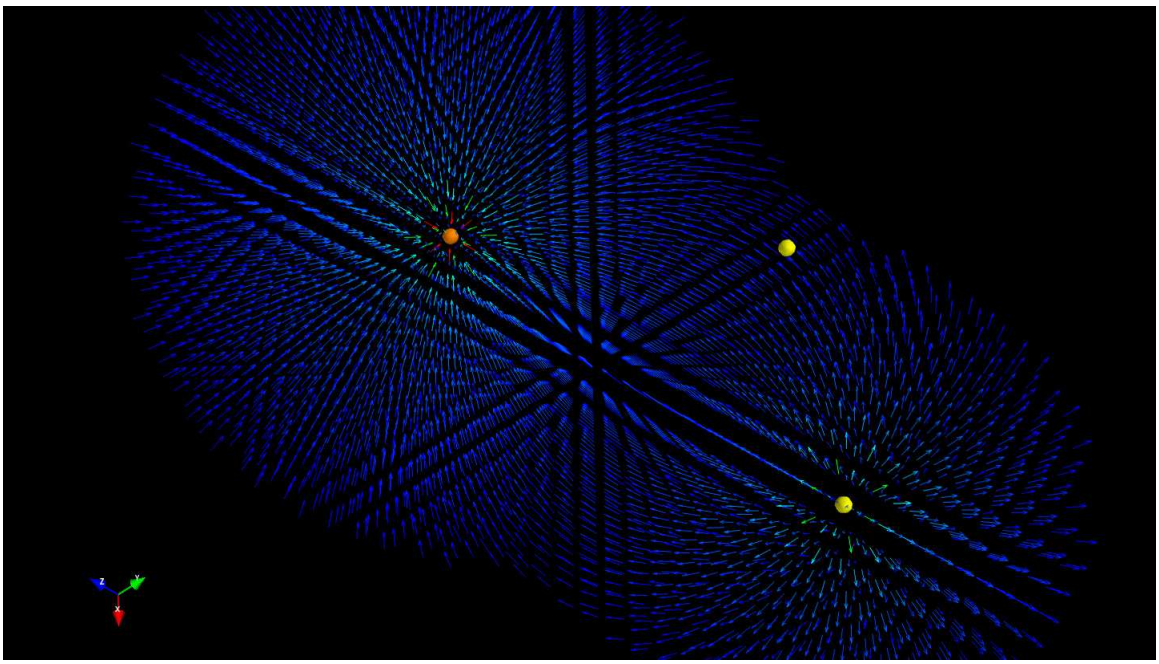

Figure 454: a picture of attempting to model the movement of ions using quasi-electrostatic forces

CHAPTER 7: CONCLUSION

In conclusion, while it has been shown that the successful acquisition of a high fidelity bioelectrical signal is an inevitably complicated task that requires not only a highly diverse interdisciplinary academic background, but also a substantial amount of knowledge regarding acquisition instrumentation and signal processing techniques; however, regardless of such intrinsic difficulties, the following specific conclusions can be made. Likewise, based upon the information presented — within this dissertation — it can be concluded that a high-fidelity surface electromyogram (sEMG) was successfully obtained — as previously shown within Figure: (441) — and upon comparison of our acquired laboratory sEMG to a contemporary "*state of the art*" sEMG — like the one shown within Figure: (455) — it can be concluded that the techniques attempting to improve signal fidelity thru post-acquisition filtering alone — the results of which are shown within Figure: (455) — tends to add additional distortion and attenuation to the acquired sEMG signal rather than actually improve the sEMG acquisitions overall fidelity [5]. Nevertheless, with this being said, such filtering techniques, while generally yielding smoother and arguably better visually appearing results, are observed — upon comparison with Figure: (441) — to have substantially less fidelity than the raw sEMG acquisitions obtained using the — previously discussed — CEIM effect reductive techniques, so much so, that within Figure: (455) it can be noted that a substantial amount of electrical detail was lost upon the application of the applied post acquisition filtering techniques [5]. Likewise, while the results obtained were a substantial improvement to the contemporary acquisition of a sEMG signal, such CEIM

effect reductive techniques are also applicable to almost all electrical acquisition systems and this attribute is a topic of further research, particularly when it comes to researching improvements to EEG and EKG electrical acquisition systems [5].

Additionally, while the sEMG fidelity obtained — relative to other contemporary techniques — was found to be a substantial improvement; however, another specific — and profound — conclusion obtained was the discovery of a generalized transmission line theory that is valid for unbalanced transmission lines — unlike the classical theory — that enables the modeling of electromagnetic radiation for unbalanced transmission lines. Likewise, within this developed generalized transmission line theory, it was determined that the type of transmission line radiation that has frequently been attributed to the metaphorically mysterious "*common-mode current*" without knowing its nature or the process that gives rise to its generation, was in fact, due to the time-variation of the convection currents that develop along unbalanced transmission lines. Conversely, the theory developed — for the generation of this convection current — enabled the creation of a transmission line model that can be used in the analysis and understanding of the nonlinear behaviors of unbalanced transmission lines observed in the field, and this model has been verified via computer simulations and laboratory tests. Likewise, it is worth noting that the spatial

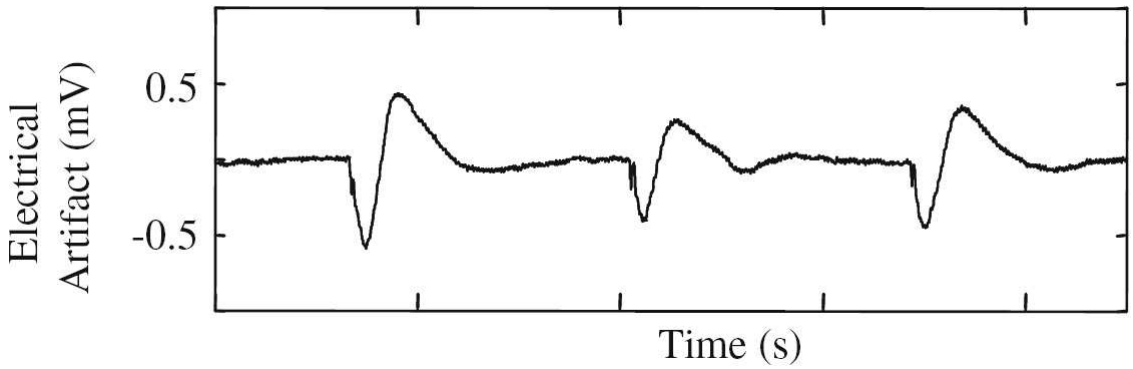

Figure 455: samples of the movement artifact detected by the semg sensor and the accelerometer sensor. data is for the first dorsal interosseous (fdi) was filtered with a 2-pole butterworth filter [5]

distribution of the convection current in an unbalanced transmission line is more controllable than the radiating current in a conventional antenna, and the theory presented within this section can be expanded to help design traveling wave narrow-beam antenna systems and this work is a topic of further research.

Conversely, while the specific conclusions provided are indeed profound, such conclusions were built from lesser prolific conclusions that — in themselves — might not appear overly substantial; however, upon careful implementation and investigation, are found to set the stage for the, previously presented, specific conclusions and — based upon such assessments — merit some notable remarks. To begin, based upon the observations made, within the philosophical foundation section, it can be concluded that the interactions between theoretically diverse disciplines — who are either collaborating or working in parallel to reach a common biomedical research objective — in itself, inherently increases the likelihood that misunderstandings or misrepresentations can occur. Likewise, such occurrences, as it was previously discussed, can be extremely detrimental to the forward progression of biomedical research topics since, for example, a misunderstanding or misrepresentation of a concept deemed to be simplistic within one discipline — by another discipline — tends to create a metaphorically caustic environment of mistrust that — if left unchecked — can result in one discipline inherently discrediting another disciplines research without fully evaluating the conclusions made — a noted example of this was found within a EIS journal that used a operational amplifier as a metaphor that, upon review within the electrical engineering discipline, was literally interpreted to be incorrect.

Similarly, such observations ultimately led to a discussion regarding the formation of academic research cultures — an attribute that arose because scientific disciplines with similar theoretical backgrounds and frequent positive interactions have a tendency to col-

laborate with each other — and the creation of these academic cultures — while, in some cases, increasing the efficiency of some research topics — generally degraded interdisciplinary research efforts through the introduction of the innate tendency to avoid the position of cultural unfamiliarity. Conversely, some discussion was provided depicting how microscopic interdisciplinary attributes — like the ones previously mentioned — are ultimately govern and are governed by macroscopic social interactions — like the contemporary social perspective of the research being performed within a given country — since contemporary societies perception of biomedical research — arising predominantly from political, cultural, and ethical beliefs — ultimately defines the research methodology utilized, the funding available, and the social acceptability of the subject being examined. Likewise, such attributes were found to ultimately play a role in defining academic culture that, in turn, is built upon interdisciplinary interactions, which was necessitated by social expectations — thus creating a complex and interconnected cycle of abstract interactions that is highly unique to the biomedical research area that must be somewhat understood in order to effectively perform research within this particular area.

Conversely, the observations made within the historical heritage and fundamental background theory sections, upon comparison with the concepts obtained from the philosophical foundation sections, seems to rationalize why the, previously observed, philosophical nuances exists within this particular research area — as it was proposed, within this dissertation, that questions asked by early Greek philosophers, surrounding the definition of life and its purpose, probably evolved into the complex social/scientific/interdisciplinary interactions frequently encountered today —, while, at the same time, physically demonstrating the amount of diverse — implying interdisciplinary — scientific theory required to make an inquiry into the fundamental electrical nature of a biomaterial, like the FDI

region of the human hand or a aqueous sodium chloride solution; although it was noted that some interdisciplinary concepts — so long as they were conceptually understood — did not necessarily have to conform to a particular interdisciplinary methodological implementation beyond the discipline of origin, in this case, the methodology frequently utilized within electrical engineering research.

Nevertheless, while such prolific conclusions might seem inherently abstract, at least from a traditional electrical engineering perspective — an attribute that, in itself, inherently provide some validity to the notion of academic cultures and the formation of conceptual biases —; however, such observations are only a minor segment of a larger number of prolific conclusions — once again, regarding how to obtain a high fidelity bioelectrical measurement —, and the observations made within the experimentation and research results section, while admittedly being numerous, are what ultimately defines the metaphoric foundation necessitated to obtain the highest bioelectrical acquisition fidelity possible and have the most profound implications, in which the following prolific conclusions can be made. Since, as it was previously discussed , within the defining the term high fidelity subsection, that the term — high fidelity — at least based upon its historical origins, is, in itself, an abstract and application dependent term that has no standardized specific and measurable quantitative association innate with its usage, and based upon such conclusions it was decided that the terms usage, within this dissertation, would be used to predominantly describe a progressive improvement to a contemporary topic — in this case an overall improvement in bioelectrical signal acquisition techniques — and, based upon the conclusions obtained from the philosophical foundations section, the terms usage was further refined — once again, in order to prevent interdisciplinary miscommunications — to focus predominantly upon improving bioelectrical signal acquisitions through the under-

standing and compensation of environmental, instrumentational, and material effects that are inherently ingrained within such acquisitions.

Likewise, based upon such refinements, the concept of environmental effects — a term used to describe the occurrence of electrical phenomenon unrelated to either the material being examined or the instrumentation being utilized, like 60Hz power line radiation, lightning strikes, and stochastic background disturbances — was examined in terms of their effect upon an acquisition device — in this case a Tektronix TPS2024 oscilloscope — and it was concluded that such effects can be categorized as being either natural in origin — implying a stochastic occurrence that can be modeled through the utilization of a Gaussian process within statistical analysis, like random number generation — or synthetic in origin — implying a periodic process that can be modeled through the usage of the isolation of particular FFT coefficients —, while also demonstrating how such effects can be reduced — thus improving acquisition fidelity — through the implementation of physical shielding techniques like acquiring measurements within a RF shielded room. Conversely, from the previous discussion, the concept of instrumentational effects — a term used to describe the internal problems associated with the usage of a non-ideal laboratory apparatus, with a predominant focus being on the electrical circuitry necessary to either create a signal, acquire a signal, or process a signal — was found to play a substantial role in determining the overall level of fidelity obtained within a bioelectrical acquisition — predominantly because the distortions arising from the interactions between the electrical circuitry utilized to create such devices and the biomaterials being examined ultimately defined the amount of fidelity obtained — and such conclusions ultimately led to the development of a number of methods to account for such effects, noting that such methods included: non-ideal/non-linear instrumentational amplifier equivalent modeling techniques, oscilloscope

and oscilloscope probe equivalent modeling techniques with a discussion on ADC effects and sampling rate, function generator equivalent modeling techniques with a discussion on DAC effects, and wire interconnection modeling techniques.

Likewise, based upon the development of such techniques, it was demonstrated — within the experimentation and research results section — how these, previously discussed, techniques are either reduced within the design of experimental laboratory apparatus or compensated for within the equivalent circuit model developed, and, in both cases, such techniques were shown to improve the overall fidelity of the laboratory acquisition taken. Similarly, again from the previous discussion, the concept of material effects — a term used to describe the distortions that occur between sudden changes in electrical mediums, either through wire interconnections or wire to biomaterial interconnections — was examined and, based upon this examination, it was shown that the minimization of wire interconnections, usage of common materials between required electrical interconnections, and the uniformity of the electrical transmission and interconnection structure utilized can, metaphorically go a long ways, in increasing the overall fidelity of a bioelectrical acquisition and can help aid in the isolation of a particular electrical attribute — like the distortions that occur within aqueous sodium chloride — observed within the analysis of a desired biomaterial.

Conversely, with this being said, these lesser prolific conclusions — regarding the techniques previously utilized to improve the overall fidelity of a bioelectrical signal acquisition — as it was previously shown, ultimately resulted in a number of experiments being conducted in order to either further validate such conclusions, or to show that a practical biomedical implementation of these, previously presented, fidelity increasing concepts could be effectively utilized, and based upon these lesser prolific conclusions a number of experimental conclusions were made. Likewise, based upon the observations made within

the managing environmental effects subsection, it was concluded that the environmental effects inherently encountered by laboratory acquisition devices can be substantially reduced in environmental effect magnitude — from a 40mV peak environmental effect floor to a 20mV peak environmental effect floor under high impedance conditions — upon performing the laboratory acquisition within a partially shielded RF shielded room — implying the shielded room is still externally powered —, and a further reduction in environmental effect magnitude can be obtained — from a 20mV peak environmental effect floor to a 10mV peak environmental effect floor — upon isolating the RF shielded room from the external power source — implying all laboratory instrumentation is operating off of battery power.

Similarly, based upon the observations made within the preliminary data management subsection, it was also concluded that the management and processing of substantial amounts of laboratory acquisitions is an inherently important but complex task, especially if there is more than one acquisition device being utilized — noting that within this dissertation a TPS2024 and two TDS2002 oscilloscopes were utilized —, that — to effectively utilize — requires the implementation of both a highly intuitive organizational system — in order to keep track of the experiment performed and what the acquisitions obtained physically represents —, and customized acquisition importation software, in order to concatenate individual channel acquisitions — from multiple acquisition devices — into a easily accessible medium for further analysis. Conversely, while these attributes originally appeared to be unimportant to improving acquisition fidelity; however, it was later concluded within this section that if such issues are not actively addressed, the capability to analyze laboratory acquisitions is substantially reduced — an attribute that generally reduces fidelity —, while the likelihood of processing distortions increases, since a greater amount of human interaction would be required — in order to manually format the acquired data —, thus

increasing the likelihood of a human error occurring.

Likewise, based upon the observations made within the DC voltage and environmental effects subsection and the extracting embedded CIE effects subsection, it was also concluded that — upon the application of a DC signal to a Tektronix oscilloscope — that the sensitivity of the acquisition device — or more precisely the devices overall susceptibility — to combine instrumentational and environmental (CIE) effects increases because of discrete changes in the internal gain of the instrumentational amplifier (IA) stage necessitated to prevent signal clipping, and such observations show that a direct comparison between different amplitude acquisitions, in itself, can introduce signal distortions because the CIE effects being compared have different CIE effect magnitudes. Conversely, based upon this discovery, it was also found that — under DC voltage input conditions — the automatic scaling feature of the oscilloscope was inherently based upon the CIE effect floor magnitude, and this attribute ultimately resulted in variations in sample window size occurring — if the sample rate was automatically selected by the oscilloscope — and such variations can distort any FFT frequency comparisons made, while — in the case of a incrementally increasing DC voltage — it was demonstrated that the signal obtained under such conditions — assuming that an acquisition was obtained for every change in DC voltage — can be more effectively modeled through the utilization of a piecewise estimation technique — like segmented least-squares — that inherently incorporates the observable changes in the CIE effect floor that results from changes in IA gain prior to attempting to isolate CIE effects from a desired signal. Similarly, such observations ultimately led to the conclusion that comparison should only be made between similar amplitude signals — or more precisely, that comparison should only be made between measurements acquired using a similar IA gain — and between signals that were acquired using a similar sample window — although

this is generally less important relative to IA gain distortions when comparing DC acquisitions —, and that such observations are definitively applicable — if not more so — within commercial biomedical devices that attempt multi-voltage/multi-frequency spectroscopy.

Likewise, based upon the observations made within the CIE effects and spectral leakage subsection, it was determined that the FFT analysis of a acquired signal, if done improperly, can yield distorted results predominantly because of a processing distortion typically referred to as spectral leakage. Conversely, while the concept and theory behind the occurrence of spectral leakage is well understood — especially within the signals and systems research area —; however, the important conclusion that arises from this particular discussion was the discovery that most commercial biomedical applications — particularly bioimpedance spectroscopy devices — either fail to compensate for this occurrence or utilize compensation techniques — like windowing — without providing information regarding the technique implemented, and because each compensation technique inherently modifies the spectrum obtained differently — typically spectral content accuracy is increased at the cost of magnitude accuracy —, thus any comparisons made between different commercial bioelectrical signal acquisition devices that utilize the Fourier transform within their analysis are highly susceptible to the introduction of distortions from unmatched preprocessing operations like windowing. Additionally, because the results obtained using these particular processing techniques are also dependent upon the sample window size selected — or the amount of signal captured — such attributes are seldom ever discussed beyond the presentation of a post-process Wessel diagram — or complex plane plot over frequency diagrams — and, once again, comparisons made using such information can inherently introduce distortions between acquisition comparisons because of inconsistencies in the preprocessing techniques utilized. Likewise, based upon such observations, a number of techniques were

examined — with a focus upon methods to keep the acquired signal symmetric —, and such examinations ultimately led to the conclusion that periodic signals are best suited for BIS analysis, while passive measuring techniques that frequently encountered non-periodic waveforms are better off utilizing well documented windowing techniques, and in either case great care should be taken before attempting to compare one biomedical acquisition with another else distortions are likely to occur from discrepancies in the processing techniques utilized.

Conversely, based upon the observations made within the AC signals and the CIE effect measured subsection, a number of interesting acquisition attributes were discovered that included: Firstly, every acquisition channel examined — including the four Tektronix TPS2024 channels and the collective four channels from the two Tektronix TDS2002 oscilloscopes — had a unique CIE effect profile for every applied frequency — noting that this profile was obtained and visualized by varying the input voltage and input frequency, acquiring the input voltage observed by the oscilloscope channel, performing the FFT operation on this acquired signal, removing the input frequency from the spectrum obtained via the FFT operation, and plotting the applied voltage, spectral frequency, and magnitude for every test frequency examined. Likewise, while some similarities were observed to exist between the CIE effect profiles obtained — particularly when a common oscilloscope probe was utilized or between oscilloscope channels on the same acquisition unit —, there was enough discrepancy between channels to merit some caution when attempting to directly compare one oscilloscope channel with another oscilloscope channel or attempting to apply a common filtering algorithm to all acquisitions taken. Additionally, while the majority of the magnitude of CIE effects encountered — with a maximum around 300mV in magnitude at 1MHz, although this value varies with applied frequency — were generally below the

resolution of the acquisition rate — implying that low frequency CIE effects were lumped within the FFT 0Hz bin —; however, upon removing the 0Hz bin from the analysis, the next largest CIE effects encountered — with a maximum around 40mV in magnitude — was discovered to be the third, fifth, and seventh harmonic of the applied signal, followed by some disturbances in between the observed harmonics, with a surprising lack of 60Hz environmental effects — presumably because both the added physical shielding and the oscilloscope input stage are effectively reducing the overall magnitude of the synthetic effects encountered. Similarly, upon examining the presumed input voltage and the acquired input voltage for each oscilloscope channel, it was determined that some discrepancy exist between the presumed input voltage and the acquired input voltage — which is to be expected —; however, this discrepancy is not uniform across all oscilloscope channels and absolute variations between 100mV to 400mV are extremely common — noting that these variations are a function of frequency, and higher input frequencies seem to be more accurate than lower input frequencies — and this attribute is likely associated with the, previously mentioned, large magnitude of low frequency CIE effects encountered. Conversely, a strong correlation appears to exist between the amount of CIE effects encountered and the applied AC voltage — which is to be expected given the, previously discussed, observations made within the DC CIE effects section.

Likewise, upon examining the amount of time delay between channel acquisitions, it was noted that — on average — the first channel of the oscilloscope is seven sample rate steps — generally at lower input frequencies — out of sync from every other oscilloscope channel on the same oscilloscope unit —, and the time delay between channel 1 of the TPS2024 and the other two oscilloscope channels is around 20 to 40 sample rate steps — again, generally at lower input frequencies —, and such observations are extremely important

because these acquisition delays, if they are not taken into account, will inevitably manifest themselves as a metaphoric phantom capacitor within an electrical model, and there seems to be a prominent assumption amongst instrumentational users that the acquisition between instrumentation channels is simultaneous, when in fact, it is not. Similarly, based upon such observations, it can be concluded that a vast majority of the fidelity obtained — particularly when performing a bioelectrical acquisition — is highly dependent upon possessing an in-depth understanding of the acquisition apparatus being utilized, because if the CIE profile of the device being utilized is not known, it becomes nearly impossible to separate a desired physical observation from a CIE effect, especially given how much CIE effects can vary depending upon the applied voltage and the applied frequency. Conversely, with this being said, given that the vast majority of publicize bioimpedance spectroscopy measurements do not adequately profile there acquisition apparatus for CIE effects prior to modeling, it is highly reasonable to assume — based upon the conservative numbers obtained — that the CIE errors introduced from this lack of profiling and implementation of compensation techniques — within the passive electrical component model that is typically developed from such experiments — could have CIE effect errors in excess of 900mV, noting that such estimates are not incorporating the cumulative nature of spectral harmonic CIE effects.

Additionally, based upon the observations obtained within the test boundaries and electromagnetics subsection, it can be concluded that — given the high impedance nature of biomaterials — that bioimpedance spectroscopy — or active electrode impedance analysis — should avoid utilizing input frequencies above 1MHz in order to prevent the occurrence of electromagnetic effects — typically described as electromagnetic standing wave phenomenon — from developing upon the acquisition instrumentation interconnections that, in turn, not only substantially disrupts the electrical potential measured at the oscilloscope

input, but modifies the phase information obtained and generally, invalidates the biomaterial acquisition as a whole unless highly specialized broadband impedance transformers are utilized to effectively transition from a 50 ohm electrical interconnection to the high input impedance of a biomaterial — although such techniques are not recommended unless necessitated by the intended end application.

Furthermore, based upon the observations obtained within the modeling a BIS apparatus subsection, it was concluded that the usage of a step input function — while from a mathematical perspective being a perfectly logical method of determining the total frequency response of a linear system — is generally a bad technique to utilize when characterizing a real acquisition system because the step response is not tolerated very well by the input of the acquisition device — an attribute that is somewhat expected because of the reactive components within the acquisition circuitry —, and while it could be argued that such techniques could — in theory — aid in modeling the internal parameters of the acquisition device in addition to the apparatus interconnections; however, based upon the tendency of CIE effects to vary with frequency — and given that CIE effects are not guaranteed to be linear — it is extremely likely that the model developed will substantially change upon attempting to apply another type of input waveform, and, to make matters worse, without being able to observe the applied input signal without distortions occurring on the input acquired, it becomes extremely problematic to compensate for, the previously mentioned, CIE effects — like acquisition delay and harmonic distortions —, thus this type of multispectral characterization technique should be avoided unless it can be definitively determined that the CIE effects are linear and the acquisition delay that occurs is known to be consistent under such conditions.

Likewise, based upon the previous observation, it was concluded that single spectrum

characterization — or electrical profiling through the usage of a sinusoidal signal —, despite being more data intensive to work with, is generally more acquisition friendly — in terms of permitting the isolation of CIE effects —, and that a number of electrical equivalent circuit modeling techniques — previously discussed within the instrumentational effects subsection — are available to electrically represent the distortions created by the acquisition apparatus. Similarly, while a number of equivalent circuit modeling techniques are available — a notable method being least-squares estimation —; however, as it was previously observed within the development of the non-linear/non-ideal instrumentational amplifier model, some of these modeling methods require the mathematical derivation of their equivalent circuit model, and because such derivations are rather lengthy — as it might be expected —, this attribute can be extremely problematic when the physical structure is not definitively known — predominantly because a substantial amount of time is required to re-derive the mathematical equations when the electrical topology changes — and further complications can arise since equation-based modeling methods — like least-squares estimation — are notorious for producing nonphysical results — like negative resistors, capacitors, and inductors — that goes against the underlying philosophy of using equivalent circuit modeling techniques. Conversely, based upon such observations, it was concluded that such numerical techniques — while being inherently powerful and useful — should ideally not be utilized until a reasonable circuit topology is obtained — predominantly to avoid the time-consuming task of reformulating equivalent circuit equations —, thus, with this being said, it was decided that equivalent circuit modeling techniques that numerically formulate these equations — via graph theory like Berkeley spice — should be utilized in conjunction with educated guesses regarding both circuit topology and parameter values. Likewise, based upon such assessments, a number of numerical techniques were demon-

strated — noting that the brute force parametric spice solver named Violet was observed to be effective but slow if bad parameter estimates were provided, while the non-linear Newtonian solver that utilized a spice calculated numerically approximated Jacobian was observed to be metaphorically hit or miss depending upon the amount of data available and the estimations made.

Additionally, while the implementation of such numerically-based techniques were shown to be effective in obtaining a equivalent circuit model of the apparatus being examined; however, the model obtained generally differed from the proposed instrumentational model — shown within the instrumentational effects subsection — primarily because a more intuitive equivalent circuit topology is preferred when implementing these particular modeling techniques over a more complex but physically realistic circuit topology — since estimating LPF or HPF topology parameters is generally easier than estimating a complex combination of reactive topologies —, although a transformation back into the proposed physical structure can be obtained with some effort —, and faster parametric solving techniques — like a particle swarm parametric solver — could be beneficial in improving the overall effectiveness of the violet method, while expansion of the Newtonian solver to better incorporate time domain changes might increase the overall success rate of this particular solution.

Nevertheless, based upon the observations obtained within the modeling the FDI region with BIS subsection, it was concluded that the selection of the FDI region of the human hand is a ideal place to begin experimenting with biomaterial characterization because of this particular regions tendency to avoid producing substantial manifestations of atypical nonlinearities — an attribute that typically results when ionic conduction is occurring and is generally avoided, within this particular region, because of the concentration of dense

FDI muscle mass that tends to contain less of these nonlinear materials — which allows for the development and refinement of characterization techniques that predominantly focus upon examining more traditional dielectric modeling methods, and its overall ease of accessibility. Likewise, while a number of electrical equivalent circuit modeling techniques are available to represent the electrical characteristics of this particular region — some of which were just previously noted —; however, laboratory experience and academic review has found that dielectric modeling methods — like the Dow method — or relaxation modeling methods — like Debye and Cole and Cole — are highly effective in electrically characterizing these particular regions — so long as the materials nonlinearity are not overly substantial. Conversely, despite the overall successfulness of utilizing the dielectric modeling methods — like the Dow method — to electrically represent a relatively linear biomaterial; however, it was also discovered that these models are highly susceptible to CIE effects — implying that a comparison between similarly synthesized models developed from different acquisition instrumentations — implying different CIE effect profiles — would inherently reduce the overall fidelity of such models, and the existence of such effects — along with the natural electrical variations observed within a living biomaterial — makes the correlation of electrical attributes to a physical parameter extremely difficult, especially since reasonable correlations cannot be directly made if comparisons between similar models — particularly within publicized acquisitions — cannot be fully trusted to have accounted for such CIE effects, and the existence of this attribute tends to imply that some type of CIE effect standardization needs to occur — particularly within the BIS research area — before any substantial headway in physical correlation can be made. Furthermore, in a manner similar to the — previously discussed — CIE effect profiling standardization problem, the modeling technique utilized to electrically represent such materials — prior to comparison

— needs to also be standardized, along with the locations in which the measurements were taken, in order to increase the overall fidelity of the comparisons being made, and again such attributes require a communal effort within the BIS research area before any headway on this issue can be made.

Likewise, based upon the observations obtained within the BIS and electrical corrosion subsection, it was concluded that the material of the electrode utilized to examine a biomaterial is extremely important in obtaining the highest fidelity possible, since — it was observed — that electrical corrosion can substantially change the overall conductivity of the electrode being utilized, thus electrode materials of platinum, gold, titanium, and to some extent silver should be utilized whenever possible in order to reduce the likelihood of these corrosive effects occurring, and that corrosion is more likely to occur when the test signal applied is a DC voltage or has a DC offset — like an asymmetric periodic waveform —, which implies that these signals should be avoided, particularly when utilizing active material characterization — like BIS or EIS.

Conversely, based upon the observations obtained within the BIS, aqueous sodium chloride, and electrodes subsection, it was concluded that: while some corrosion did inherently occur during these AC material test — as the electrodes observed did visually change in appearance after performing each test but not as substantially as they did within the DC test — it appears that such effects are either not substantially impacting the electrical results obtained — at least over short time durations — or that the corrosion process that occurred manifested itself similarly within both materials, secondly, while a slight increase in electrical conductivity was noted within the stainless steel electrode versus the brass electrode, such effects were not overly profound, and while extreme caution should be utilized when selecting a BIS electrode, it could be argued that — so long as the material is

not overly reactive with the testing environment — that either electrode materials would produce similar results — although it might also be equally argued that the corrosive effects encountered were simply similar, within both electrodes, and thus were embedded within the measurements acquired equally, although this seems highly unlikely given that the corrosive byproducts would likely be different for every test case and thus electrically different. Likewise, based upon such observations — including those obtained within the DC electrical corrosion test —, it seems prudent to select an electrode that is noncorrosive — or at the minimum, only slowly corrodes — within the testing medium being examined — an attribute that reinforces the need to fully understand every nuance of the test being performed — in order to obtain the highest fidelity possible, and while the results obtained did appeared to have not been substantially distorted by corrosive effects — although it is likely that the distortions observed were visually subtle, like a slight increase in capacitance because of the formation of an oxide layer upon the electrode surface rather than a substantial change in the concentration of the solution being tested — some slight differences in frequency response were noted, and such observations imply that corrosion might metaphorically bandwidth limit the conduction region of a material being examined.

Additionally, based upon the observations obtained within the BIS and liquid gradients subsection, it was concluded that the shape of the gradient created appears to remain relatively consistent, with the notable exceptions being a slight flattening — or reduction in resistance between electrode locations — within the bulk of the medium, and a unique drop in potential below the observed value of the current sinking electrodes — at frequencies above 6kHz — , which seems to imply the existence of a congregation of negative charges — within this region — that might be somewhat metaphorically analogous to the development of a standing wave — within a transmission line —, insofar as, such congregated negative

charges could be the result of a substantial buildup of positive charges near the current sinking electrodes. Likewise, because the shape of the gradient did not change with frequency — beyond the formation of the minor discrepancy observed near the current sinking electrodes —, it seems reasonable to assume that the underlying process responsible for the creation of these gradients — presumably a exclusion zone (EZ) phenomenon — is not inherently dependent upon electrical frequency. Thirdly, the overall resistance across the liquid seems to decrease as a function of frequency, which seems to imply that the charge transport mechanism across the liquid is, in fact, a function of frequency. Conversely, while such observations were deliberately more empirical than mathematical, predominantly because the intended objective of these experiments was intuitive observation rather than predictive modeling; however, given the nature of the gradients observed, it seems likely that differential voltage injection — the process of using two function generators in such a configuration that the common ground is not exposed to the test apparatus — or impedance modulation — the act of programmatically varying the current sensing resistor — could be utilized to modify the shape of the gradient created and possibly force particular regions, within the gradient, to be a particular potential value — although, undoubtedly some physical restrictions would apply. Likewise, while no substantial investigation was conducted on this particular attribute — although a few minor experiments on the FDI muscle using impedance modulation did yield painful stimulus — it can be concluded that such attributes should be researched further, as such phenomenon is likely to be extremely beneficial to the development of precision noninvasive muscle stimulation.

Likewise, based upon the observations obtained within the BIS and Aqueous NaCl subsection, it was concluded that the aqueous NaCl solutions being examined are definitively nonlinear within certain operational regions — a notion supported by observing that a si-

nusoidal input is being transformed into a pulse looking shape across the sinking electrode current sensing resistor at frequencies below 100Hz and voltages above 2.5V. Conversely, upon examining all of the plots obtained, it appears that the distortion being observed are relatively consistent in shape over frequency — although the magnitude appears to change with concentration —, and it can be proposed that exclusion zone (EZ) phenomenon is playing a substantial role in defining the electrical effects observed, although the verification of this particular theory was not possible given the limitations of the laboratory utilized since a chemical lab with a high resolution microscope and access to nanoparticles would be required to determine if a EZ effect was occurring or a pH changing solvent required to check for the development of ionic concentrations; however, based upon the observed current spikes, it can be definitively concluded that the electrical current will begin to briefly flow across the test chamber upon exceeding a threshold voltage — around 2V at 1Hz— and then suddenly stop — implying the creation of a charge gradient — and this process repeats during the negative half of the input wave cycle. Likewise, it was observed that when the aqueous NaCl began to conduct current in a nonlinear fashion, the electrical potential within the liquid also began to operate in a nonlinear fashion, and that if the input voltage was subtracted from the potential within the solution — while conducting current under nonlinear conditions — that a potential clipping effect — similar to a diode —- would be the result, and that upon plotting the difference between the input and the values obtained, after performing this mathematical operation, yields the conclusion that linear regions were generally substantially lower in subtracted magnitude — since linear regions were sinusoidal — than non-linear regions, thus, upon creating a three-dimensional topological plot of input frequency versus input voltage, an effective visual means of determining what BIS operational regions were linear and nonlinear was developed — an

attribute that can improve BIS fidelity through the avoidance of material nonlinearities.

Additionally, it can also be concluded that the usage of nonlinear least squares RRCR circuit modeling techniques can provide a reasonably good approximation electrical circuit approximation of this highly nonlinear electrical phenomenon; however, while such methods do work reasonably well, so long as some system information is known thru experimentation, yet such methods tend to bend the unspoken rules of static circuit equations, and such attributes are simply unavoidable given the nature of the problem being examined, especially since it is obvious that a unknown chemical process — like EZ regions — are governing the conductivity of this particular system, and based upon such observations, it is highly presumptuous to assume that the dynamics — of this particular system — will easily conform to the simplicity of a basic electrical circuit model. Thus, while this method will work for modeling this particular system within this particular paradigm; however, more native chemical modeling methods are also worth exploring here, since simplicity is not something easily obtained for such problems using current electrical engineering modeling theory, and there is nothing really gained by its utilization within such problems beyond being able to interface with an existing electrical framework — which is the only true advantage gained under such circumstances.

Nevertheless, based upon the observations obtained within the acquisition of a high fidelity EMG subsection, it was concluded that environmental effects can be substantially reduced upon introducing physical shielding techniques like a partially shielded or a fully shielded RF shielding environment. Likewise, given that noninvasively acquired EMG signals have a extremely small amplitude — on the order of 100 μ V — attempting to acquire such measurements directly using an oscilloscope is generally not practical — especially given the tendency of instrumentational effects to be substantially higher — in terms of the

CIE effects encountered — at lower voltage settings, then they are at mid-voltage settings. Therefore, an external instrumentational amplifier configuration is required to pre-amplify the EMG signal prior to acquisition. Conversely, because improper wire interconnections can inevitably create distortions, some reduction can be obtained through twisting wire interconnections together, in order to reduce any remaining background electromagnetic radiation — within the shielding room — through the acquisition attribute of common mode rejection found within a differential amplifier. Similarly, because the physical movement of the test subject can create distortions — either from muscles producing action potentials, electrodes shifting location, and from unbalanced transmission line effects — the usage of a wooden test chair seem to help to reduce not only grounding effects but also help prevent undesired subject movement.

Conversely, it was concluded that the EMG results obtained, upon effectively implementing the, previously discussed, precautionary CEIM effect reductive procedures, yields incredibly high fidelity results, especially upon considering that the peak feature size was less than 200nV, while sub features below 50nV were clearly visible without the utilization of any substantial digital signal processing techniques. Furthermore, while there are some minor signal distortions observable below 20nv, predominantly CIE effects, such distortions can be reduced further through the utilization of the, previously discussed, CIE characterization techniques should additional signal fidelity be required — noting that such techniques tend to substitute physical fidelity with perceivable fidelity, which may or may not truly be a actual increase in fidelity depending upon the reductive techniques implemented since, for example, a signal can be smoothed through the usage of averages, but the usage of such techniques only generally yields a smoother plot, which is not an actual increase in signal acquisition fidelity.

Likewise, based upon the observations obtained within the signal propagation within a saline body subsection, it was concluded that the applied 10V peak at 1Hz sinusoidal signal was, in fact, capable of transversing the PVC pseudo-torso structure without obtaining a unrecoverable amount of attenuation from propagating through the saline medium. Conversely, it also appears that the applied 10V peak sinusoidal signal was barely able to allow the signal to be successfully received by the instrumentational amplifier — implying that a PVC pseudo-torso filled with normal saline is not inherently the best structure to represent the underlying propagational medium of the human body, since such voltages are not generally found within the human body —, and while this particular model might be a over estimate of the amount of saline medium encountered; however, the observed distortions to the input signal — predominantly arising from the, previously discussed, tendency of lower frequencies to only invoke potential gradients above particular thresholds — does appear visually reminiscent to the waveforms observed, and such observations does merit some pause since there is a strong likelihood that some type of intrinsic correlation exists between the noninvasively observed bioelectrical signals and those visually depicted within this particular experiment.

Nevertheless, while this particular experiment was far from being an ideal human body model — particularly given the required magnitude necessitated for differential acquisition at the hands —; however, although matching results are generally preferred within scientific research, it is worth mentioning that such observations are important, insofar as, they clearly show that other propagational methods — like dielectric propagation and biological signal repeaters — are a predominant factor in the propagation of a signal within the human body, and, while aqueous attenuation does definitively play a role within signal transmission within the body, such attributes — in themselves — are not the only mechanism that must

be considered. Likewise, while this particular experiment was not pursued further, the next logical step would be to feel the test apparatus with a porous medium — like a sponge — and then saturate — but not excessively — the porous medium with a saline solution in order to determine if a better approximation is obtained given the overall semi-porous structure of the human body. Similarly, based upon the observations obtained within the lessons in experimentation subsection, it was concluded that apparatus design is extremely important in obtaining the highest fidelity measurement possible. Likewise, prototyping and experimentation can go a long ways in determining what apparatus building techniques are successful and what apparatus building techniques are not since successful.

Conversely, based upon the observations obtained within the lessons in computing subsection, it was concluded that the successful development and implementation of acquisition automation can go a long ways in increasing the overall fidelity obtained — either through allowing CIE characterization to occur and reducing human error. Likewise, the substantial amount of information obtained through automated acquisition can become problematic if not carefully managed, and sometime should be spent in developing organizational procedures. Similarly, Beowulf computational clusters — while having some inherent uses — are not necessarily ideal for processing large volumes of laboratory acquisitions — at least not without careful design of a fast data transferal systems —, and these computational clusters can be somewhat difficult to manage if similar computers are not being utilized within the cluster. Additionally, computationally intensive simulation models — like those found within electrohydrodynamics —, while being a very promising research area, are not effectively implemented within a low end computational cluster — like the budget Beowulf clusters — and should be avoided unless the resources available it can handle their computational intensity.

Finally, based upon all the conclusions provided above, a number of future research topics — in addition to those already mentioned — were identified and these possible future research topics included the progressive development of a standardized CIEM categorization methodology that can hopefully become accepted within the biomedical research area in order to account for the — previously discussed — CIEM distortions encountered, the investigation of differential bioimpedance spectroscopy and impedance modulation as a method of controlling potentials within a bulk liquid and possibly stimulate muscles selectively, and the determination of whether the development of an exclusion zone within water plays a role in the underlying conduction mechanism observed within aqueous NaCL solutions. Conversely, further investigation is also merited into the examination of possible usages of the liquid diode effect encountered, and into improving the numerical Jacobian spice modeling method developed.

REFERENCES

[1] M. A. Mclain, "Bioimpedance modeling of the fdi region of the human hand via noninvasive electrical characterization," Master's thesis, The University of North Carolina at Charlotte, 2009.

[2] V. Sankaran, "Locating skeletal muscle motor units from surface electromyogram measurements," Master's thesis, The University of North Carolina at Charlotte, 2007.

[3] F. Tenore, A. Ramos, A. Fahmy, S. Acharya, R. Etienne-Cummings, and N. V. Thakor, "Towards the control of individual fingers of a prosthetic hand using surface emg signals," in *Proceedings of the 29th Annual International Conference of the IEEE EMBS Cite Internationale*, 2007.

[4] A. S. a, M. Y. b, and H. R. Ozcalik, "Classification of emg signals using wavelet neural network," *Journal of Neuroscience Methods*, vol. 156, pp. 360–367, 2006.

[5] C. J. DeLuca, L. D. Gilmore, M. Kuznetsov, and S. H. Roy, "Filtering the surface emg signal: Movement artifact and baseline noise contamination," *Journal of Biomechanics*, vol. 43, pp. 1573–1579, 2010.

[6] W. Robertson, *A Dictionary of Latin Phrases.* A. J. Valfy, 1829.

[7] C. G. Morris and A. A. Maisto, *Psychology An Introduction.* Pearson Education Inc., 12 ed., 2005.

[8] J. Tyndall, *Fragments of Science Volume 1.* D. Appleton and Company, 1915.

[9] G. Berkeley, *A Treatise Concerning the principles of human knowledge.* J. B. Lippincott & CO., 1878.

[10] D. Hume, *A Treatise of Human Nature.* Oxford at the Clarendon Press, 1878.

[11] R. L. Ackoff, S. K. Gupta, and J. S. Minas, *Scientific Method optimizing applied research decisions.* John Wiley & Sons, Inc., 1967.

[12] D. C. Lindberg, *Science in the Middle Ages.* The University of Chicago Press, Ltd., 1978.

[13] S. Gaukroger, *Francis Bacon and the Transformation of Early-Modern Philosophy.* Cambridge university press, 2004.

[14] L. du Nouy, *The Road to Reason.* Longman, Green And Co., 1948.

[15] E. A. Burtt, *The Metaphysical Foundations of Modern Physical Science.* Kegan Paul, Trench, Trunbner and Co., LTD, 1925.

[16] S. Grimnes and O. G. Martinsen, *Bioimpedance and Bioelectricity Basics.* Academic Press, 2000.

[17] K. Maiese, *Neurovascular Medicine: Pursuing Cellular Longevity for Healthy Aging.* Oxford University Press, 2009.

[18] A. Serafini, *The Epic History of Biology*. Perseus Books Group, 1993.

[19] R. A. Carson and C. R. Burns, eds., *Philosophy of Medicine and Bioethics: A Twenty-Year Retrospective and Critical Appraisal*. Kluwer Academic Publishers, 1997.

[20] W. Welsch and W. Singer, *Interdisciplinary Anthropology: Continuing Evolution of Man*. Springer, 2011.

[21] K. Futatsugi, A. Nakagawa, and T. Tamai, eds., *CAFE: An Industrial-Strength Algebraic Formal Method*. Elsevier, 2000.

[22] G. A. Miller, "The magical number seven, plus or minus two some limits on our capacity for processing information," *Psychological Re*, vol. 101, no. 2, pp. 343–352, 1956.

[23] F. H. Martini, W. C. Ober, C. W. Garrison, K. Welch, and R. T. Hutchings, *Fundamentals of Anatomy and Physiology*. Pearson Benjamin Cummings, 2006.

[24] D. J. Sartoris, ed., *Principles of Shoulder Imaging*. McGRAW-HILL Book Company, Inc, 1995.

[25] A. C. Guyton, *Textbook of Medical Physiology*. W. B. Saunders Company, 1971.

[26] H. Gray, *Gray's Anatomy*. Barnes & Noble, 1995.

[27] C. R. Mann and G. R. Twiss, *Physics*. Robert O. Law Company, 1910.

[28] G. Dicker, *Kant's Theory of Knowledge: An Analytical Introduction*. Oxford University Press, 2004.

[29] M. Heidegger and M. Heim, *The Metaphysical Foundations of Logic*. Indiana University Press, 1992.

[30] F. Kreith, ed., *The CRC Handbook of Mechanical Engineering*. CRC Press, 2005.

[31] F. Gifford, ed., *Philosophy of Medicine*. Elsevier, 2011.

[32] S. Salinari, A. Bertuzzi, G. Mingrone, E. Capristo, A. Pietrobelli, P. Campioni, A. V. Greco, and S. B. Heymsfield, "New bioimpedance model accurately predicts lower limb muscle volume: validation by magnetic resonance imaging," *American Journal of Physics - Endocrinology and Metabolism*, vol. 282, pp. E960–E966, 1994.

[33] K. R. Foster and H. C. Lukaski, "Whole-body impedance – what does it measure?," *American Society for Clinical Nutrition*, vol. 64(suppl), pp. 388S–96S, 1996.

[34] S. W. Smye, C. J. Evans, M. P. Robinson, and B. D. Sleeman, "Modelling the electrical properties of tissue as a porous medium," *Physics in Medicine and Biology*, vol. 52, p. 7007Ű7022, 2007.

[35] P. Davies, *Physics and Philosophy: The Revolution in Modern Science*. Penguin Books, 1990.

[36] M. E. Valentinuzzi, *Understanding the Human Machine: A primer for Bioengineering*. World Scientific publishing, 2004.

[37] T. Jue, ed., *Biomedical Applications of Biophysics*. Humana Press, 2010.

[38] R. Fazel-Rezai, ed., *Biomedical Engineering: Frontiers and Challenges*. InTech, 2011.

[39] R. A. Wallace, G. P. Sanders, and R. J. Ferl, *Biology The Science of Life*. Harper Collins College Publishers, fourth ed., 1996.

[40] J. P. Harrison, *Sources, Evils and Correctives of Professional Discontent: An Introductory Lecture*. Franklin Printing House, 1845.

[41] J. Frenkel, *Wave Mechanics Elementary Theory*. Dover Publications, Inc, 1950.

[42] M. Gonen, *Analyzing Receiver Operating Characteristic Curves with SAS*. SAS Institute Inc., 2007.

[43] J. Tyndall, *Fragments of Science Volume 2*. D. Appleton and Company, 1896.

[44] A. E. Heath, "The principle of parsimony and ethical neutrality," *The Monist*, vol. 29, no. 3, pp. 448–450, 1919.

[45] G. Buescher, *The Eucharistic Teaching of William Ockham*. The Franciscan Institute, 1950.

[46] I. Asimov, *A Short History of Chemistry*. Dover Publications, Inc, 1965.

[47] J. A. Smith, *De Anima from The Works of Aristotle Translated into English VOL. III*. Oxford University Press, 1963.

[48] S. Finger and M. Piccolino, *The shocking history of electric fishes : from ancient epochs to the birth of modern neurophysiology*. Oxford University Press, 2011.

[49] A. D'Abro, *The Evolution of Scientific Thought: From Newton to Einstine*. Dover Publications, Inc, 1950.

[50] B. Powell, *History of natural philosophy : from the earliest p eriods to the present time*. Longman Brown, Green and Longmans Paternoster Bow, 1834.

[51] A. Castiglioni, *A History of Medicine*. Jason Aronson Inc., 1975.

[52] J. P. Kleinz, *The Theory of Knowledge of Hugh of Saint Victor*. PhD thesis, The Catholic University of America Press, 1944.

[53] C. Singer, *From Magic to Science Essays on the Scientific Twilight*. Dover Publications, Inc, 1958.

[54] A. J. Toynbee, *A Study of History*. Oxford University Press, 1956.

[55] S. H. Miles, *The Hippocratic Oath and The Ethics of Medicine*. Oxford University Press, 2004.

[56] R. Kugelmann, *Psychology and Catholicism: Contested Boundaries*. Cambridge University Press, 2011.

[57] E. Levinas, *Totality and Infinity: An Essay on Exteriority*. Martinus Nijhoff Publishers, 1979.

[58] H. J. Humphrey, "Medical professionalism: Introduction," *Perspectives in Biology and Medicine*, vol. 51, no. 4, pp. 491–494, 2008.

[59] J. Tyndall, *Lessons in Electricity at the Royal Institution*. D. Appleton and Company, 1898.

[60] C. Zittel, G. Engel, R. Nanni, and N. C. Karafyllis, eds., *Philosophies of Technology: Francis Bacon and his Contemporaries*. Koninklijke Brill, 2008.

[61] K. Sterelny and P. E. Griffiths, *Sex and Death: An Introduction to Philosophy of Biology*. The University of Chicago Press, Ltd., 1999.

[62] H. H. Hock, ed., *The Languages and Linguistics of Europe: A Comprehensive Guide*. Walter de Gruyter GmbH and Co., 2011.

[63] M. Chaichian, O. Rojas, and A. Tureanu, *From the Cosmos to Quarks: Basic Concepts in Physics*. Springer, 2012.

[64] E. A. M. Neal H. Hooker, ed., *Interdisciplinary Food Safety Research*. CRC Press, 2001.

[65] T. Becher and P. R. Trowler, *Academic Tribes and Territories: Intellectual enquiry and the culture of disciplines*. Open University Press, 2001.

[66] A. Fawcett, K. Garcia, and R. Parker, *Translation: Theory and Practice in Dialogue*. Continuum International Publishing Group, 2010.

[67] B. H. Sellers, *On The Mathematics of Modelling Metamodelling, Ontologies and Modelling Languages*. Springer, 2007.

[68] H. M. Leicester, *The Historical Background of Chemistry*. Dover Publications, Inc, 1971.

[69] R. Biehler, R. W. Scholz, R. Staber, and B. Winkelmann, eds., *Didactics of Mathematics as a Scientific Discipline*. Kluwer Academic Publishers, 2002.

[70] J. Bronowski, *Science and Human Values*. The Copp Clark Publishing Co., 1956.

[71] D. Berlinski, *Infinite Ascent: A Short History of Mathematics*. Modern Library, 2005.

[72] I. Merriam-Webster, *Merrian Webster's Dictionary of Law*. Merriam Webseter, Incorporated, 1996.

[73] A. Nait-ali, ed., *Advanced Biosignal Processing*. Springer, 2009.

[74] S. Yamamoto, ed., *Producing qualified graduates and assuring education quality in the knowledge-base society: roles and issues of graduate education*. Research Institute for Higher Education Hiroshima University, 2010.

[75] H. M. Chittenden and A. T. Richardson, *Life, Letters and Travels of Father Pierre-Jean De Smet, S. J. 1801-1873*. Francis P. Harper, 1905.

[76] Pfeffer, V. H. Arrhenius, and Raoult, *The Modern Theory Of Solution*. Harper & Brothers Publishers, 1899.

[77] N. Jacobson, *Pride and Solace: The Functions and Limits of Political Theory*. University of California Press, 1978.

[78] M. Newmark, *Dictionary of Foreign Words And Phrases*. Philosophical Library Inc., 1950.

[79] R. L. Perlman, "Evolutionary biology: A basic science for medicine in the 21st century," *Perspectives in Biology and Medicine*, vol. 54, no. 1, pp. 75–88, 2011.

[80] E. Treharne, *Living Through Conquest: The politics of Early English 1020 to 1220*. Oxford University Press, 2012.

[81] D. R. Dudley, *A History of Cynicism: From Diogenes to the 6th Century A.D.* Methuen and Co. LTD., 1937.

[82] F. von Gottfried Wilhelm Leibniz, *Theodicy: Essays on the goodness of God, The Freedom of Man and the Origin of Evil*. BiblioBazaar, 2007.

[83] Voltaire, *Candide*. Boni and Liveright inc, 1918.

[84] J. Burnet, *Greek Philosophy Part 1 Thales to Plato*. Macmillan And Co., 1928.

[85] T. C. Ryan, *Finite and Infinite*. Philadelphia and london J. B. Lippincott Company, 1905.

[86] S. Schwartzman and E. Balbachevsky, "The academic profession in a diverse institutional environment: converging or diverging values and beliefs?," *RIHE International Seminar Reports*, vol. 13, pp. 145– 164, 2009.

[87] R. Hirasawa, "Mission-oriented knowledge system in graduate schools: how can we ingrain it and assure the quality?," *RIHE International Seminar Reports*, vol. 14, pp. 17–27, 2010.

[88] M.-L. Kearney, "Challenges for tertiary education governance and management in the knowledge economy," *RIHE International Seminar Reports*, vol. 18, pp. 1–12, 2012.

[89] F. Huang, "What kinds of governance and management arrangements should be made in universities in the future?," *RIHE International Seminar Reports*, vol. 18, pp. 73–76, 2012.

[90] F. Brentano, R. M. Chisholm, and E. H. Schneewind, *The Origin of Our Knowledge of Right and Wrong*. Humanities Press, 1969.

[91] J. Martin, *Francis Bacon, The State, and The Reform of Natural Philosophy*. Cambridge University Press, 1992.

[92] R. A. Spears, *McGraw-Hill's Dictionary of American Idioms: The Most Practical Reference to the Idiomatic and Verbal Expressions of Contemporary American English*. Mcgraw-Hill, 2005.

[93] E. F. Edinger, *The Psyche in Antiquity Book One: Early Greek Philosophy From Thales to Plotinus*. Inner City Books, 1999.

[94] N. Machiavelli and W. K. Marriott, *The Prince*. Project Gutenberg, 2004.

[95] N. Teich, *Regerian Perspectives: Collaborative Rhetoric for Oral and Written Communication*. Ablex Publishing Corporation, 1992.

[96] R. B. Axelrod and C. R. Cooper, *The St. Martin's Guide to Writing*. Bedford and St. Martin's, 2001.

[97] S. Grimnes and O. G. Martinsen, *Bioimpedance and Bioelectricity Basics*. Academic Press, 2 ed., 2008.

[98] C. S. S. R. Kumar, J. Hormes, and C. Leuschner, eds., *Nanofabrication Towards Biomedical Applications: Techniques, Tools, Applications, And Impact*. Wiley-VCH, 2005.

[99] M. Shelley, *Frankenstein*. Broadview Press Ltd., 1955.

[100] C. E. Pullar, ed., *The Physiology of Bioelectricity in Development, Tissue Regeneration, and Cancer*. CRC Press, 2011.

[101] P. Wang and Q. Liu, *Biomedical Sensors and Measurement*. Springer, 2011.

[102] X. Zhang, H. Ju, and J. Wang, eds., *Electrochemical Sensors, Biosensors and Their Biomedical Applications*. Academic Press, 2008.

[103] F. Ren and S. J. Pearton, eds., *Semiconductor Device-Based Sensors for GAS, Chemical, And Biomedical Applications*. CRC Press, 2011.

[104] K. Williston, ed., *Digital Signal Processing: World Class Designs*. Elsevier, 2009.

[105] D. E. Johnson, J. R. Johnson, J. L. Hilburn, and P. D. Scott, *Electric Circuit Analysis*. Prentice Hall, Inc., 1997.

[106] J. D. Irwin and C.-H. Wu, *Basic Engineering Circuit Analysis*. John Wiley and Sons, Inc, 1999.

[107] C. L. Phillips and J. M. Parr, *Signals, Systems, And Transformation*. Prentice Hall, Inc., 1999.

[108] C. N. Herrick, *Instruments And Measurements For Electronics*. McGRAW-HILL Book Company, Inc, 1972.

[109] D. L. Wise, *Biomaterials and bioengineering handbook*. Marcel Dekker, 2000.

[110] J. L. Semmlow, *Circuits, Signals, And Systems For Bioengineers*. Elsevier, 2005.

[111] J. Behari, *Biophysical Bone Behavior*. John Wiley and Sons, Inc, 2009.

[112] M. P. Bolton, L. Ward, A. Khan, I. Campbell, P. Nightingale, O. Dewit, and M. Elia, "Sources of error in bioimpedance spectroscopy," *Physiological Measurement*, vol. 19, pp. 235–245, December 1998.

[113] H. Scharfetter, P. Hartinger, H. Hinghofer-Szalkay, and H. Hutten, "A model of artefacts produced by stray capacitance during whole body or segmental bioimpedance spectroscopy," *Physiological Measurement*, vol. 19, pp. 247–261, May 1998.

[114] L. B. Houtkooper, T. G. Lohman, S. B. Going, and W. H. Howell, "Why bioelectrical impedance analysis should be used for estimating adiposity," *American Journal of Clinical Nutrition*, vol. 64(suppl), pp. 436S–448S, 1996.

[115] R. E. Kohler, *From Medical Chemistry to Biochemistry: The Making of a Biomedical Discipline*. Cambridge University Press, 2008.

[116] J. Keljik, *Electricity 3: Power Generation and Delivery*. Delmar, 2009.

[117] A. J. Pansini and K. D. Smalling, *Guide to Electric Power Generation*. CRC Press, 2005.

[118] P. Kiameh, *Power Generation Handbook: Selection, Applications, Operation, And Maintenance*. McGRAW-HILL Professional, 2002.

[119] C. F. Dalziel, "Electric shock hazard," *IEEE Spectrum*, vol. 9, pp. 41–50, February 1972.

[120] L. P. Ferris, B. G. King, P. W. Spence, and H. B. Williams, "Effect of electric shock on the heart," *Transactions of the American Institute of Electrical Engineers*, vol. 55, pp. 498–515, May 1936.

[121] A. C. Koumbourlis, "Electrical injuries," *Critical Care Medicine*, vol. 30, no. 11, pp. S424–S430, 2002.

[122] A. Ghahary and J. G. Webster, "Electrical safety for an electrical impedance tomograph," *Proceedings of the Annual International Conference of the IEEE Engineering in Engineering in Medicine and Biology Society, 1989. Images of the Twenty-First Century.*, vol. 2, pp. 461–462, November 1989.

[123] F. J. Weibell, "Electrical safety in the hospital," *Annals of Biomedical Engineering*, vol. 2, pp. 126–148, 1974.

[124] J. E. Bridges, "Electrical safety standards," *Annals of the New York Academy of Sciences*, vol. 720, pp. 246–271, 2006.

[125] G. Luttgens and N. Wilson, *Electrostatic Hazards*. Butterworth-Heinemann, 1997.

[126] M. A. G. Mitolo, *Electrical Safety of Low-Voltage Systems*. McGRAW-HILL Book Company, Inc, 2009.

[127] B. He, *Bioelectric Engineering: Modeling and imaging of Bioelectrical Activity*. Kluwer Academic Publishers, 2004.

[128] I. M. Artemieva, *The Lithosphere: An Interdisciplinary Approach*. Cambridge University Press, 2011.

[129] J. Malmivuo and R. Plonsey, *Bioelectromagnetism Principles and Applications of Bioelectric and Biomagnetic Fields*. Oxford University Press, 1995.

[130] B. Pejcic and R. D. Marco, "Impedance spectroscopy: Over 35 years of electrochemical sensor optimization," *Electrochimica Acta*, vol. 51, pp. 6217–6229, April 2006.

[131] E. Masi, M. Ciszak, G. Stefano, L. Renna, E. Azzarello, C. Pandolfi, S. Mugnai, F. Baluška, and F. T. Arecchi, "Spatiotemporal dyanmics of the electrical network activity in the root apex," *Proceedings of the National Academy of Sciences of the United States of America*, vol. 106, pp. 4048–4053, 2009.

[132] T. L. Brown, H. E. LeMay, B. E. Bursten, and J. R. Burdge, *Chemistry The Central Science*. Pearson Education, Inc., 2003.

[133] W. H. Hayt and J. A. Buck, *Engineering Electromagnetics*. McGraw-Hill, 2006.

[134] E. Barsoukov and J. R. Macdonald, eds., *Impedance Spectroscopy: Theory, Experiment, and Applications*. John Wiley & Sons, Inc., 2005.

[135] R. Plonsey and R. C. Barr, *Bioelectricity A Quantitative Approach*. Plenum Press, 1988.

[136] J. D. Irwin, *Basic Engineering Circuit Analysis*. John Wiley and Sons, Inc, 2002.

[137] G. S. Kino, *Acoustic Waves: Devices, Imaging, And Analog Signal Processing*. Prentice Hall, 2000.

[138] L. Clendening, *Source Book of Medical History*. Dover Publications, Inc, 1942.

[139] S. McCarter, *Oxford English For Careers Medicine 2*. Oxford University Press, 2010.

[140] R. L. Rogers, A. Mattu, M. Winters, and J. Martinez, eds., *Practical Teaching in Emergency Medicine*. John Wiley and Sons, Inc, 2009.

[141] C. M. Townsend, R. D. Beauchamp, B. M. Evers, and K. L. Mattox, *Sabiston Textbook of Surgery: The biological basis of Modern Surgical Practice*. Elsevier, 2012.

[142] A. P. Kelly and S. C. Taylor, *Dermatology for Skin of Color*. McGRAW-HILL Medical, 2009.

[143] D. J. Gawkrodger, *An Illustrated Colour Text: Dermatology*. Churchhill Livingstone, 1997.

[144] R. Smith, *Netter's Obstetrics and Gynecology*. Elsevier, 2008.

[145] D. K. Edmonds, ed., *Dewhurst's Textbook of Obstetrics and Gynaecology for Postgraduates*. Blackwell Science Ltd, 1999.

[146] E. J. Topol, ed., *Textbook of Interventional Cardiology*. Saunders Elsevier, 2008.

[147] G. N. Levine, *Cardiology Secrets*. Mosby Elsevier, 2010.

[148] J. R. Bender, K. S. Russell, L. E. Rosenfeld, and S. Chaudry, *Oxford American Handbook of Cardiology*. Oxford University Press, 2011.

[149] R. I. Simon and L. H. Gold, eds., *Textbook of Forensic Psychiatry*. American Psychiatric Publishing, 2010.

[150] G. P. Whyte, M. Harries, and C. Williams, eds., *ABC of Sports and Exercise Medicine*. Blackwell Publishing, 2005.

[151] J. E. Herrera and G. Cooper, eds., *Essential Sports Medicine*. Humana Press, 2008.

[152] W. G. Bradley, R. B. Daroff, G. M. Fenichel, and J. Jankovic, eds., *Neurology in Clinical Practice*. Butterworth-Heinemann, 2004.

[153] P. N. Bennett and M. J. Brown, *Clinical Pharmacology*. Churchhill Livingstone, 2003.

[154] A. Gacek and W. Pedrycz, eds., *ECG Signal Processing, Classification and Interpretation*. Springer, 2012.

[155] A. Mattu and W. Brady, *ECGs For the Emergency Physician 2*. Blackwell Publishing, 2008.

[156] J. R. Hampton, *The ECG in Practice*. Churchhill Livingstone, 2003.

[157] S. Sanei and J. A. Chambers, *EEG Signal Processing*. John Wiley and Sons, Inc, 2007.

[158] B. Katirji, *Electromyography in Clinical Practice*. Modern Library, 2007.

[159] P. L. Lutz, *The Rise of Experimental Biology: An Illustrated History*. Humana Press, 2002.

[160] B. J. Hunt, "Practice vs. theory : The british electrical debate, 1888-1891," *Isis*, vol. 74, pp. 341–355, Sep 1983.

[161] I. Yavetz, "Oliver heaviside and the significance of the british electrical debate," *Annals of Science*, vol. 50, pp. 135–173, 1993.

[162] C. Rosenberg, "Science in american society : A generation of historical debate," *Isis*, vol. 74, pp. 356–365, Sep 1983.

[163] M. Burmeister and L. Ulanovsky, *Pulsed-Field Gel Electrophoresis*. Humana Press, 1992.

[164] J. M. Bujnicki, ed., *Practical Bioinformatics*. Springer, 2008.

[165] J. Moore and G. Zouridakis, eds., *Biomedical Technology and Devices Handbook*. CRC Press, 2004.

[166] L. L. Whyte, *Critique Of Physics*. Kegan Paul, Trench, Trunbner and Co., LTD, 1931.

[167] D. Halliday, R. Resnick, and J. Walker, *Fundamentals of Physics*. John Wiley and Sons, Inc, 2001.

[168] A. C. Melissinos, *Experiments in Modern Physics*. Academic Press, 1966.

[169] H. S. Lipson, *Crystals and X-rays*. Wykeham Publications (London) LTD, 1970.

[170] M. Conversi, ed., *Evolution of Particle Physics*. Academic Press, 1970.

[171] R. T. Beyer, ed., *Foundations of Nuclear Physics*. Dover Publications, Inc, 1949.

[172] A. M. Munn, *From Nought to Relativity: creating the physical world model*. George Allen and Unwin Ltd, 1974.

[173] C. P. Snow, *The Two Cultures*. Cambridge University Press, 1993.

[174] R. R. Wright and H. R. Skutt, *Electronics: Circuits and Devices*. The Ronald Press Company, 1965.

[175] M. Akay, ed., *Whiley Encyclopedia of Biomedical Engineering*. John Wiley and Sons, 2006.

[176] M. A. Annacchino, *New Product Development: From Initial Idea to Product Management*. Amsterdam Butterworth-Heinemann, 2003.

[177] A. Marston, *The History of Engineering*. A. Marston, 1912.

[178] E. A. Guillemin, *The Mathematics of Circuit Analysis: Extensions to the Mathematical Training of Electrical Engineers*. John Wiley and Sons, 1951.

[179] D. B. Marghitu, *Mechanical Engineer's Handbook*. Academic Press, 2001.

[180] R. Bansal, *Fundamentals of Engineering Electromagnetics*. CRC Press, 2006.

[181] G. B. Marin, ed., *Advances in Chemical Engineering: Volume 32*. Academic Press, 2007.

[182] B. G. Liptak, ed., *Process Measurement and Analysis - Volume 1*. CRC Press, 1995.

[183] J. Nielsen, J. Villadsen, and G. Liden, *Bioreaction Engineering Principles*. Kluwer Academic Publishers, 2003.

[184] J. S. Newman, *Electrochemical Systems*. Prentice Hall, Inc., 1973.

[185] J. W. Hill and R. H. Petrucci, *General Chemistry: An Integrated Approach*. Prentice Hall, 1999.

[186] S. S. Zumdahl, *Chemistry*. D. C. Heath and Company, 1993.

[187] T. H. Levere, *Transforming Matter: A History of Chemistry from Alchemy to the Buckyball*. The Johns Hopkins University Press, 2001.

[188] M. E. Orazem and B. Tribollet, *Electrochemical Impedance Spectroscopy*. John Wiley & Sons, Inc., first ed., 2008.

[189] G. W. Castellan, *Physical Chemistry*. Addison-Wesley Publishing Company, Inc., 1971.

[190] W. Pauli and M. H. Fischer, *Physical Chemistry in the Service of Medicine*. John Wiley and Son, 1907.

[191] D. Kondepudi and I. Prigogine, *Modern Thermodynamics: From Heat Engines to Dissipative Structures*. John Wiley and Sons, 1998.

[192] R. K. Hobbie and B. J. Roth, *Intermediate Physics for Medicine and Biology*. Springer, 2007.

[193] E. Tyrkiel and P. Dearnley, *A Guide to Surface Engineering Terminology*. The Institute of Materials, 1995.

[194] J. Stillwell, *Mathematics and its History*. Springer, 1989.

[195] R. Cooke, *The History of Mathematics: A Brief Course*. Wiley- Interscience, 2005.

[196] C. Tenopir and D. W. King, *Communication Patterns of Engineers*. John Wiley and Sons, 2004.

[197] S. Brightman and K. Livgren, "Dust in the wind." Eden CD, Nemo Studios under license to Angel Records, November 1998.

[198] C. Hess and E. Ostrom, eds., *Understanding Knowledge as a Commons: From Theory to Practice*. Massachusetts Institute of Technology, 2007.

[199] F. Cajori, *A History of Mathematical Notations*. Dover Publications, Inc, 1993.

[200] S. J. Derry, C. D. Schunn, and M. A. Gernsbacher, eds., *Interdisciplinary Collaboration: An Emerging Cognitive Science*. Lawrence Erlbaum Associates, 2005.

[201] T. O'Connor and D. Robb, eds., *Philosophy of Mind: Contemporary Readings*. Routledge, 2003.

[202] M. E. Orazem and B. Tribollet, "An integrated approach to electrochemical impedance spectroscopy," *Electrochimica Acta*, vol. 53, pp. 7360–7366, December 2008.

[203] A. S. Sedra and K. C. Smith, *Micro-Electronics Circuits*. HRW Series in Electrical and Computer Engineering, CBS College Publishing, first ed., 1982.

[204] B. C. Kuo, *Automatic Control Systems*. Prentice Hall, sixth ed., 1991.

[205] J. R. Macdonald, "Impedance spectroscopy: Old problems and new developments," *Electrochimica Acta*, vol. 35, pp. 1483–1492, April 1990.

[206] R. Comer and E. Gould, *Psychology Around Us*. John Wiley and Sons, 2011.

[207] F. F. Kuo, *Network Analysis & Synthesis*. John Wiley & Sons, Inc., 1966.

[208] D. A. Saville, "Electrohydrodynamics: The taylor-melcher leaky dielectric model," *Annual Review of Fluid Mechanics*, vol. 29, pp. 27–64, 1997.

[209] H. Morgan and N. G. Green, *AC Electrokinetics: colloids and nanoparticles*. Research Studies Press, 2003.

[210] T. Becher and S. Parry, "The endurance of the disciplines," in *Governing Knowledge*, pp. 133–144, Springer, 2005.

[211] J. L. Zalabardo, *Introduction to the Theory of Logic*. Westview Press, 2000.

[212] J. Heil, *Philosophy of Mind: a Contemporary Introduction*. Routledge, 2013.

[213] A. Arimoto, "Changing academic profession in the world from 1992 to 2007," *RIHE International Seminar Reports*, vol. 13, pp. 1–37, 2009.

[214] J. Pearl, "Causal inference in the health sciences: A conceptual introduction," *Health Services and Outcomes Research Methodology*, vol. 2, pp. 189–220, 2001.

[215] C. A. Russell and D. C. Goodman, eds., *Science and the Rise of Technology Since 1800*. John Wright and Sons, 1972.

[216] B. P. . W. F. Trotter, *Pensees*. Christian Classics Ethereal Library, 1660.

[217] A. S. Collot, *Collots French-English and English-French Dictionary*. William R. Jenkins Co., 1910.

[218] M. L. Jones, "Writing and sentiment: Blaise pascal, the vacuum, and the pensees," *Studies in History & Philosophy of Science*, vol. 32, pp. 139–181, 2001.

[219] E. Gilby, "Reflexivity in the pensees. pascal's discourse on discourse," *French studies*, vol. 3, pp. 315–326, 2001.

[220] S. Bold, "Borges, inventor of the pensees; or la busca de pascal," *Romance Quarterly*, vol. 52, pp. 115–134, 2005.

[221] K. Hart and B. E. Wall, *The experience of God : a postmodern response*. Fordham University Press, 2005.

[222] E. El-Khawas, "Emerging academic identities: A new research and policy agenda," in *From Governance to Identity*, pp. 31–44, Springer, 2009.

[223] R. R. Parse, "Building a research culture," *Nursing Science Quarterly*, vol. 3, p. 197, 2007.

[224] A. L. Avins and H. Goldberg, "Creating a culture of research," *Contemporary Clinical Trials*, vol. 28, pp. 557–562, 2007.

[225] W. R. Jzmroz, R. Kruzelecky, and E. I. Haddad, *Applied Microphotonics*. CRC Press, 2006.

[226] M. Onabajo and J. Silva-Martinez, *Analog Circuit Design for Process Variation-Resilient Systems-on-a-Chip*. Springer, 2012.

[227] S. M. Hofer and D. F. Alwin, eds., *Handbook of Cognitive Aging: Interdisciplinary Perspectives*. Sage Publications, 2008.

[228] B. A. Nadel, *Building security : handbook for architectural planning and design*. McGRAW-HILL Book Company, Inc, 2004.

[229] K. H. Rubin, W. M. Bukowski, and B. Laursen, eds., *Handbook of Peer Interactions, RelatRelation, and Groups*. The Guilford Press, 2009.

[230] D. Evans, *Social Media Marketing: An Hour a Day*. Wiley Publishing, 2008.

[231] R. Rorty, *Philosophy and Social Hope*. Penguin Books, 1999.

[232] E. R. Dorsey, J. de Roulet, J. P. Thompson, J. I. Reminick, A. Thai, Z. White-Stellato, C. A. Beck, B. P. George, and H. Moses, "Funding of us biomedical research, 2003-2008," *The Journal of the American Medical Association*, vol. 303, pp. 137–143, 2010.

[233] S. V. McCrary, C. B. Anderson, J. Jakovljevic, T. Khan, L. B. McCullough, N. P. Wray, and B. A. Brody, "A national survey of policies on disclosure of conflicts of interest in biomedical research," *The New England Journal of Medicine*, vol. 343, pp. 1621–1626, 2000.

[234] J. E. Bekelman, Y. Li, and C. P. Gross, "Scope and impact of financial conflicts of interest in biomedical research," *The Journal of the American Medical Association*, vol. 289, no. 4, pp. 454–465, 2003.

[235] M. A. Heller and R. S. Eisenberg, "Can patents deter innovation? the anticommons in biomedical research," *Science*, vol. 280, pp. 698–701, 1998.

[236] D. Korn, "Conflicts of interest in biomedical research," *The Journal of the American Medical Association*, vol. 284, no. 17, pp. 2234–2237, 2000.

[237] E. A. Zerhouni, "Nih in the post-doubling era realities and strategies," *Science*, vol. 17, pp. 1088–1090, 2006.

[238] H. G. Mandel and E. S. Vesell, "From progress to regression: biomedical research funding," *The Journal of Clinical Investigation*, vol. 114, p. 7, 2004.

[239] M. Albert, S. Laberge, B. D. Hodges, G. Regehr, and L. Lingard, "Biomedical scientistsŠ perception of the social sciences in health research," *Social Science and Medicine*, vol. 66, pp. 2520 – 2531, 2008.

[240] J. M. Grimshaw, M. P. Eccles, J. Greener, G. Maclennan, T. Ibbotson, J. P. Kahan, and F. Sullivan, "Is the involvement of opinion leaders in the implementation of research findings a feasible strategy," *Implementation Science*, vol. 1, no. 3, 2006.

[241] M. D. Woods and C. Tarrant, "Why do people cooperate with medical research? findings from three studies," *Social Science and Medicine*, vol. 68, pp. 2215 – 2222, 2009.

[242] B. A. Israel, A. J. Schulz, E. A. Parker, and A. B. Becker, "Review of community-based research: Assessing partnership approaches to improve public health," *Annual Review of Public Health*, vol. 19, pp. 173–202, 1998.

[243] S. Gilbody, P. Wilson, and I. Watt, "Benefits and harms of direct to consumer advertising: a systematic review.," *Quality and Safety In Health Care*, vol. 14, pp. 246–250, 2005.

[244] A. Giordan, "Health education, recent and future trends," *Memorias do Instituto*, vol. 95, pp. 53–58, 2000.

[245] N. Risch, E. Burchard, E. Ziv, and H. Tang, "Categorization of humans in biomedical research: genes, race and disease," *Genome Biology*, vol. 3, no. 7, pp. 1–12, 2002.

[246] K. M. Murphy and R. H. Topel, "Diminishing returns?: The costs and benefits of improving health," *Perspectives in Biology and Medicine*, vol. 46, no. 3, pp. S108–S128, 2003.

[247] D. W. Shapiro, N. S. Wenger, and M. F. Shapiro, "The contributions of authors to multiauthored biomedical research papers," *JAMA-Journal of the American Medical Association-International Edition*, vol. 271, no. 6, pp. 438–442, 1994.

[248] V. Yank and D. Rennie, "Disclosure of researcher contributions: a study of original research articles in the lancet," *Annals of Internal Medicine*, vol. 130, no. 8, pp. 661–670, 1999.

[249] J. S. Wislar, A. Flanagin, P. B. Fontanarosa, and C. D. DeAngelis, "Honorary and ghost authorship in high impact biomedical journals: a cross sectional survey," *BMJ: British Medical Journal*, vol. 343, 2011.

[250] Y. Iwasa, F. Michor, and M. A. Nowak, "Evolutionary dynamics of escape from biomedical intervention," *Proceedings of the Royal Society of London. Series B: Biological Sciences*, vol. 270, no. 1533, pp. 2573–2578, 2003.

[251] J. E. Hirsch, "An index to quantify an individual's scientific research output," *Proceedings of the National academy of Sciences of the United States of America*, vol. 102, no. 46, pp. 16569–16572, 2005.

[252] B. Wynne, "Misunderstood misunderstanding: social identities and public uptake of science," *Public understanding of science*, vol. 1, no. 3, pp. 281–304, 1992.

[253] J. R. Ravetz, "Usable knowledge, usable ignorance incomplete science with policy implications," *Science Communication*, vol. 9, no. 1, pp. 87–116, 1987.

[254] A. Irwin and B. Wynne, *Misunderstanding science?: the public reconstruction of science and technology.* Cambridge University Press, 1996.

[255] M. Smithson, "Ignorance and science dilemmas, perspectives, and prospects," *Science Communication*, vol. 15, no. 2, pp. 133–156, 1993.

[256] M. Smithson, *Ignorance and uncertainty: Emerging paradigms.* Springer-Verlag Publishing, 1989.

[257] H. Sabelli, *BIOS A Study of Creation.* World Scientific publishing, 2005.

[258] J. Ziman, "Public understanding of science," *Science, Technology, and Human Values*, vol. 16, no. 1, pp. 99–105, 1991.

[259] L. Sevgi, "Speaking with numbers: Scientific literacy and public understanding of science," *Turkish Journal of Electrical Engineering and Computer Sciences*, vol. 14, pp. 33 – 40, 2006.

[260] J. D. Miller, "Theory and measurement in the public understanding of science: A rejoinder to bauer and schoon," *Public understanding of science*, vol. 2, no. 3, pp. 235–243, 1993.

[261] J. G. Webster, ed., *Encyclopedia of Medical Devices and Instrumentation.* Wiley-Interscience, 2006.

[262] J. S. Suri, D. L. Wilson, and S. Laxminarayan, *Handbook of Biomedical Image Analysis: Volume II Segmentation MModel Part B.* Kluwer Academic Publishers, 2005.

[263] N. Oldham, "Overview of bioelectrical impedance analyzers," *American Journal of Clinical Nutrition*, vol. 64, pp. 405S–412S, 1996.

[264] A. Arora and alfonso Gambardella, "The impact of nsf support for basic research in economics," *Economics Working Paper Archive at WUSTL*, 1998.

[265] Z. Huang, H. Chen, X. Li, and M. C. Roco, "Connecting nsf funding to patent innovation in nanotechnology (2001Ű2004)," *Journal of Nanoparticle Research*, vol. 8, no. 6, pp. 859–879, 2006.

[266] A. G. Heffner, "Funded research, multiple authorship, and subauthorship collaboration in four disciplines," *Scientometrics*, vol. 3, pp. 5–12, 1981.

[267] J. M. Wyllie, ed., *Oxford Latin Dictionary*. Oxford University Press, 1968.

[268] A. C. Clarke, *Profiles of the future : an enquiry into the limits of the possible*. Gollancz, 1962.

[269] A. H. N. Cillessen, D. Schwartz, and L. Mayeux, eds., *Popularity in the Peer System*. The Guilford Press, 2011.

[270] B. Dibner, *Luigi Galvani*. Burndy Library, 1972.

[271] M. Pera, *The Ambiguous Frog*. Princeton University Press, 1992.

[272] N. military tribunal, "The nuremberg code," *Trials of war criminals before the Nuremberg military tribunals under control council law*, vol. 10, pp. 181–182, 1949.

[273] M. Nyiszli, *Auschwitz: A Doctor's Eyewitness Account*. Arcade Publishing, 1960.

[274] P. R. Benson, "The social control of human biomedical research: an overview and review of the literature," *Social Science and Medicine*, vol. 29, no. 1, pp. 1–12, 1989.

[275] A. Corones, "Philosophy of science and its malcontents," *Social Studies of Science*, vol. 24, pp. 139–142, 1994.

[276] W. Hield, "The study of change in social science," *The British Journal of Sociology*, vol. 5, pp. 1–11, 1954.

[277] T. M. Porter, *Trust in Numbers The Pursuit of Objectivity in Science and Public LIfe*. Princeton University Press, 1995.

[278] M. M. Sohlberg and C. A. Mateer, *Congnitive Rehabilitation An Integrative Neuropsychological Approach*. The Guilford Press, 2001.

[279] C. A. M. Fennell, *The Stanford Dictionary of Anglicised Words and Phrases*. Cambridge University Press, 1892.

[280] W. W. Briggs, ed., *Dictionary of Literary Biography Volume 176: Ancient Greek Authors*. Gale Research, 1997.

[281] D. L. ërtius and C. D. Yonge, *The Lives and Opinions of Eminent Philosophers*. London, H. G. Bohn, 1853.

[282] G. Petrou, "Translation studies and the history of science: The greek textbooks of the 18th century," *Science and Education*, vol. 15, no. 7-8, pp. 823–840, 2006.

[283] D. W. Thompson, *Historia Animalium from The Works of Aristotle Translated into English VOL. IV.* Oxford University Press, 1962.

[284] G. M. A. Grube, *Plato's Meno.* Hackett Publishing Company, 1976.

[285] P. Kellaway, *The part played by electric fish in the early history of bioelectricity and electrotherapy.* Baltimore, 1946.

[286] C. H. Wu, "Electric fish and the discovery of animal electricity," *American Scientist*, vol. 72, pp. 598–607, 1984.

[287] C. E. Dinsmore, ed., *A History of Regeneration Research.* Cambridge University Press, 1991.

[288] J. P. Allen, *Middle Egyptian An Introduction to the Language and Culture of Hieroglyphs.* Cambridge University Press, 2000.

[289] M. V. L. Bennett, "Comparative physiology: Electric organs," *Annual Review of Physiology*, vol. 32, no. 1, pp. 471–528, 1970.

[290] L. R. Squire, ed., *Encyclopedia of Neuroscience.* Oxford University Press, 2009.

[291] N. Sperelakis, ed., *Cell Physiology Sourcebook : A Molecular Approach.* Academic Press, 2001.

[292] R. T. Cox, C. W. Coates, and M. V. Brown, "Electrical characteristics of electric tissue," *Annals of the New York Academy of Sciences*, vol. 47, no. 4, pp. 487–500, 1946.

[293] C. W. Coates and R. T. Cox, "Observations on the electric discharge of torpedo occidentalis," *Zoologica*, vol. 27, pp. 25–28, 1942.

[294] H. Grundfest, "The mechanisms of discharge of the electric organs in relation to general and comparative electrophysiology," *Progress in Biophysics and Biophysical Chemistry*, vol. 7, pp. 1–86, 1957.

[295] F. Gotch and G. J. Burch, "The electromotive properties of malapterurus electricus," *Philosophical Transactions of the Royal Society of London*, vol. 187, pp. 347–407, 1896.

[296] W. Feldberg and A. Fessard, "The cholinergic nature of the nerves to the electric organ of the torpedo (torpedo marmorata)," *Journal of Physiology*, vol. 101, pp. 200–216, 1942.

[297] A. Roth, "Central neurons involved in the electroreception of the catfish kryptopterus," *Journal of Applied Physiology*, vol. 100, pp. 135–146, 1975.

[298] R. C. Peters and R. J. A. Buwalda, "Frequency response of the electroreceptors ("small pit organs") of the catfish, ictalurus nebulosus les," *Journal of Applied Physiology*, vol. 79, pp. 29–38, 1972.

[299] R. C. Peters and J. Meek, "Catfish and electric fields," *Cellular and Molecular Life Sciences*, vol. 29, no. 3, pp. 299–300, 1973.

[300] C. C. Bell, J. Bradbury, and C. J. Russell, "The electric organ of a mormyrid as a current and voltage source," *Journal of Comparative Physiology*, vol. 110, pp. 65–88, 1976.

[301] M. V. L. Bennett, M. Wurzel, and H. Grundfest, "The electrophysiology of electric organs of marine electric fishes," *The Journal of General Physiology*, vol. 44, no. 4, pp. 757–804, 1961.

[302] A. Janetzko, H. Zimmermann, and W. Volknandt, "The electromotor system of the electric catfish (malapterurus electricus): A fine-structural analysis," *Cell and Tissue Research*, vol. 247, pp. 613–624, 1987.

[303] M. N. Leeming, C. Ray, and W. S. Howland, "Low-voltage, direct-current burns," *The Journal of the American Medical Association*, vol. 214, no. 9, pp. 1681–1684, 1970.

[304] R. M. Zaner, ed., *Death: Beyond Whole-Brain Criteria*. Kluwer Academic Publishers, 1988.

[305] E. J. Kenney, *Lucretius*. Oxford at the Clarendon Press, 1977.

[306] H. A. J. Munro and G. Long, *Great Books of the Western World: V12 Lucretius Epictetus Marcus Aurelius*. Encyclopædia Britannica, inc., 1952.

[307] R. E. McGrew, *Encyclopedia of Medical History*. McGRAW-HILL Book Company, Inc, 1985.

[308] M. B. Pugh, ed., *Stedman's medical dictionary*. Lippincott Williams & Wilkins, 27 ed., 2000.

[309] M. Dugopolski, *Fundamentals of Pre Calculus*. Pearson Education, Inc, 2003.

[310] M. N. O. Sadiku, *Elements of Electromagnetics*. Oxford University Press, 2001.

[311] A. T. Craven, *Electricity and Magnetism for Electrical Engineers*. Addison-Wesley Publishing Company, Inc, 1962.

[312] C. H. Edwards and D. E. Penney, *Differential Equations and Boundary Value Problems Computing and Modeling*. Pearson Education, Inc, 2001.

[313] F. A. Bettelheim, W. H. Brown, and J. March, *Introduction to General, Organic, And Biochemistry*. Thomson Learning, Inc, 2004.

[314] D. R. Lide, ed., *CRC Handbook of Chemistry and Physics*. CRC Press, 1998.

[315] F. White, *Mass Spectrometry in Science and Technology*. John Wiley & Sons, 1968.

[316] D. Neamen, *An Introduction to Semiconductor Devices*. McGraw-Hill, 2006.

[317] N. Kumar, *Comprehensive Physics For Class XII*. Laxmi Publications, 2008.

[318] Faraday, Hittorf, and F. Kohlrausch, *The Fundamental Laws of Electrolytic Conduction*. Harper & Brothers Publishers, 1899.

[319] A. D. Smith, S. P. Datta, G. H. Smith, P. N. Campbell, R. Bentley, H. A. Bender, A. J. Harris, T. W. Goodwin, H. A. McKenzie, J. H. Parish, and C. Stanford, eds., *Oxford Dictionary of Biochemistry and Molecular Biology*. Oxford University Press, 2000.

[320] H. A. Laitinen and W. E. Harris, *Chemical Analysis*. McGraw Hill, 1975.

[321] M. J. Moran and H. N. Shapiro, *Fundamentals of Engineering Thermodynamics*. John Wiley and Sons, Inc Sons, 2004.

[322] E. S. Lewis, "A biography of distinguished scientist gilbert newton lewis," *Journal of Chemical Education*, vol. 76, p. 1487, 1999.

[323] M. G. Kim, "Wilhelm ostwald (1853-1932)," *International Journal for Philosophy of Chemistry*, vol. 12, pp. 141–148, 2006.

[324] M. J. Sienko and R. A. Plane, *Chemistry*. McGraw Hill, 1966.

[325] H. C. Longuet-Higgins and M. E. Fisher, "Lars onsager," *National Academy of Sciences of the United States of America Biographical Memoirs*, vol. 60, pp. 183–184, 1991.

[326] Biovere, "Anatomica 3d software (www.biovere.com)." CD, 2005.

[327] O. F. Schanne and E. R. P.-Ceretti, *Impedance Measurements in Biological Cells*. John Wiley and Sons, Inc, 1978.

[328] S. Z. Yanovski, V. S. Hubbard, H. C. Lukaski, and S. B. Heymsfield, "Introduction," *American Society for Clinical Nutrition*, vol. 64, p. 387S, 1996.

[329] H. C. Burger and J. B. Milaan, "Measurements of the specific resistance of the human body to direct current," *acta medica scandinavica*, vol. 114, pp. 584–607, December 1943.

[330] H. P. Schwan and C. F. Kay, "Specific resistance of body tissues," *Circulation Research*, vol. 4, pp. 664–670, November 1956.

[331] H. C. Burger and R. V. Dongen, "Specific electric resistance of body tissues," *Physics in Medicine and Biology*, vol. 5, pp. 431–447, April 1961.

[332] B. la G. Liptá k, *Instrument Engineers' Handbook, Fourth Edition, Volume One*. CRC Press, 2003.

[333] R. Holm, *Electric Contacts Theory and Application*. Springer, fourth ed., 2000.

[334] C. P. Smyth, *Dielectric Behavior and Structure*. McGRAW-HILL Book Company, Inc, 1955.

[335] R. Gabler, *Electrical Interactions in Molecular Biophysics*. Academic Press, 1978.

[336] P. Debye, *Polar Molecules*. The Chemical Catalog Company, Inc., 1929.

[337] K. S. Cole, "Electric impedance of suspensions of sphears," *The Journal of General Physiology*, vol. 12, no. 1, pp. 29–36, 1928.

[338] K. Kundert, "Modeling dielectric absorption in capacitors." Online, 2008.

[339] K. S. Cole and R. H. Cole, "Dispersion and absorption in dielectrics i. alternating currents characteristics.," *The Journal of Chemical Physics*, vol. 9, pp. 341–351, April 1941.

[340] K. S. Cole and R. H. Cole, "Dispersion and absorption in dielectrics ii. direct current characteristics," *The Journal of Chemical Physics*, vol. 10, pp. 98–105, 1942.

[341] C. Grieve and M. Henneberg, "How solid is the theoretical basis for bioelectrical impedance analysis?," *American Journal of Clinical Nutrition*, vol. 61, pp. 1306–1308, June 1995.

[342] S. H. Liu, "Fractal model for the ac response of a rough interface," *Physical Review Letters*, vol. 55, pp. 529–532, July 1984.

[343] J. C. Lawler, M. J. Davis, and E. C. Griffith, "Electrical characteristics of the skin," *The Journal Of Investigative Dermatology*, vol. 34, pp. 301–308, May 1960.

[344] T. Lewis and Y. Zotterman, "Vascular reactions of the skin to injury. part viii. the resistance of the human skin to constant currents, in relation to injury and vascular response," *The Journal of Physiology*, vol. 62, pp. 280–288, January 1927.

[345] R. T. Tregear, *Physical Functions of Skin.* Academic Press, 1966.

[346] T. J. C. Faes, H. A. van der Meij, J. de Munck, and R. M. Heethaar, "The electric resistivity of human tissues (100hz-10 mhz): a meta-analysis of review studies," *Physiological Measurement*, vol. 20, pp. R1–R10, May 1999.

[347] *Trials of War Criminals before the Nuremberg Military Tribunals under Control Council Law*, vol. 2, 1949. pp.181-182.

[348] "World medical association declaration of helsinki: Recommendations guiding medical doctors in biomedical research involving human subjects," October 1996.

[349] M. F. Smiechowski, V. F. Lvovich, S. Srikanthan, and R. L. Silverstein, "Non-linear impedance characterization of blood cells-derived microparticle biomarkers suspensions," *Electrochimica Acta*, vol. 56, pp. 7763–7771, April 2011.

[350] N. I. of Health Technology Assessment Conference Statement, "Bioelectrical impedance analysis in body composition measurement. national institutes of health technology assessment conference statement," *The American Journal of Clinical Nutrition*, vol. 64(suppl), pp. 524S–532S, 1994.

[351] S. B. Heymsfield, Z. Wang, M. Visser, D. Gallagher, and R. N. Pierson, "Techniques used in the measurement of body composition: an overview with emphasis on bioelectrical impedance analysis," *The American Journal of Clinical Nutrition*, vol. 64(suppl), pp. 478S–484S, 1996.

[352] S. Kun, B. Ristic, R. A. Peura, and R. M. Dunn, "Real-time extraction of tissue impedance model parameters for electrical impedance spectrometer," *Medical and Biological Engineering and Computing*, vol. 37, pp. 428–432, 1999.

[353] A. D. Lorenzo, A. Andreoli, J. Matthie, and P. Withers, "Predicting body cell mass with bioimpedance by using theoretical methods: a technological review," *Journal of Applied Physiology*, vol. 82, pp. 1542–1558, May 1997.

[354] R. F. Kushner and D. A. Schoeller, "Estimation of total body water by bioelectrical impedance analysis," *The American Journal of Clinical Nutrition*, vol. 44, pp. 417–424, 1986.

[355] P. Deurenberg, "Limitations of the bioelectrical impedance method for the assessment of body fat in severe obesity," *The American Journal of Clinical Nutrition*, vol. 64(suppl), pp. 449S–452S, 1996.

[356] O. L. Svendsen, J. Haarbo, B. L. Heitmann, A. Gotfredsen, and C. Christiansen, "Measurement of body fat in elderly subjects by dual-energy x-ray absorptiometry, bioelectrical impedance, and anthropometry," *The American Journal of Clinical Nutrition*, vol. 53, pp. 1117–1123, 1991.

[357] M. Horlick, S. M. Arpadi, J. Bethel, J. Wang, J. Moye, P. Cuff, R. N. Pierson, and D. Kotler, "Bioelectrical impedance analysis models for prediction of total body water and fat-free mass in healthy and hiv-infected children and adolescents," *The American Journal of Clinical Nutrition*, vol. 76, pp. 991–999, 2002.

[358] E. Mok, L. Béghin, P. Gachon, C. Daubrosse, J.-E. Fontan, J.-M. Cuisset, F. dé ric Gottrand, and R. gis Hankard, "Estimating body composition in children with duchenne muscular dystrophy: comparison of bioelectrical impedance analysis and skinfold-thickness," *The American Journal of Clinical Nutrition*, vol. 83, pp. 65–69, 2006.

[359] D. P. Kotler, S. Burastero, J. Wang, and R. N. Pierson, "Prediction of body cell mass, fat-free mass, and total body water with bioelectrical impedance analysis: effects of race, sex, and disease," *The American Journal of Clinical Nutrition*, vol. 64(suppl), pp. 489S–497S, 1996.

[360] D. Gupta, C. A. Lammersfeld, J. L. Burrows, S. L. Dahlk, P. G. Vashi, J. F. Grutsch, S. Hoffman, and C. G. Lis, "Bioelectrical impedance phase angle in clinical practice: implications for prognosis in advanced colorectal cancer," *The American Journal of Clinical Nutrition*, vol. 80, pp. 1634–1638, 2004.

[361] R. N. Baumgartner, R. Ross, and S. B. Heymsfield, "Does adipose tissue influence bioelectric impedance in obese men and women?," *Journal of Applied Physiology*, vol. 84, no. 1, pp. 257–262, 1998.

[362] A. A. Turner, A. Lozano-Nieto, and M. Bouffard, "Comparison of segmental and global bioimpedance spectroscopy errors using generalizability theory," *Physiological Measurement*, vol. 23, pp. 43–57, 2002.

[363] A. Gartner, B. Maire, F. Delpeuch, P. Sarda, R. P. Dupuy, and D. Rieu, "Importance of electrode position in bioelectrical impedance analysis," *The American Journal of Clinical Nutrition*, vol. 56, pp. 1067–1068, 1992.

[364] L. C. Ward and B. H. Cornish, "Bioelectrical impedance analysis at the characteristic frequency," *The International Journal of Applied and Basic Nutritional Sciences*, vol. 23, p. 96, 2007.

[365] F. Zhu, S. Sarkar, C. Kaitwatcharachai, R. Greenwood, C. Ronco, and N. W. Levin, "Methods and reproducibility of measurement of resistivity in the calf using regional bioimpedance analysis," *Blood Purification*, vol. 21, pp. 29–31, 2003.

[366] M. Miyatani, H. Kanehisa, Y. Masuo, M. Ito, and T. Fukunaga, "Validity of estimating limb muscle volume by bioelectrical impedance," *Journal of Applied Physiology*, vol. 91, pp. 386–394, 2001.

[367] F. Zhu, E. F. Leonard, and N. W. Levin, "Body composition modeling in the calf using an equivalent circuit model of multi-frequency bioimpedance analysis," *Physiological Measurement*, vol. 26, pp. S133–S143, 2005.

[368] F. Zhu and N. W. Levin, "An electrical resistivity model of segmental body composition using bioimpedance analysis," *Proceedings of the 25th Annual International Conference of the IEEE Engineering in Medicine and Biology Society*, vol. 3, pp. 2679–2682, 2003.

[369] S. S. Guo, W. C. Chumlea, and D. Cockram, "Use of statistical methods to estimate body composition," *The American Journal of Clinical Nutrition*, vol. 64, pp. 428S–435S, 1996.

[370] F. Ciucci, T. Carraro, W. C. Chueh, and W. Lai, "Reducing error and measurement time in impedance spectroscopy using model based optimal experimental design," *Electrochimica Acta*, vol. 56, pp. 5416–5434, 2011.

[371] C. L. Barnhart, ed., *The American College Dictionary.* Random House, 1964.

[372] M. Scanziani and M. H. usser, "Electrophysiology in the age of light," *Nature Insight Review*, vol. 461, pp. 930–939, 2009.

[373] P. B. Gove, ed., *Webster's Seventh New Collegiate Disctionary.* G. & C. Merriam Company, 1961.

[374] E. Mckena, ed., *Concise Oxford American Dictionary.* Oxford University Press, 2006.

[375] C.-C. Huang, C.-C. Huang, J.-F. Chung, L.-D. Van, and C.-T. Lin, "Front-end amplifier of low-noise and tunable bw / gain for portable biomedical signal acquisition," *Circuits and Systems, 2008. ISCAS 2008. IEEE International Symposium on*, vol. 1, pp. 2717 – 2720, 2008.

[376] R. P. Patterson, "Fundamentals of impedance cardiography," *IEEE Engineering in Medicine and Biology Magazine*, vol. 8, p. 3538, March 1989.

[377] S. Franco, *Design with operational amplifers and analog integrated circuits.* Mcgraw Hill, third ed., 2002.

[378] C. F. Dalziel and R. W. Lee, "Leathal electric currents," *IEEE Spectrum*, vol. 6, pp. 44–50, February 1969.

[379] E. A. Pfeiffer, "Electrical stimulation of sensory nerves with skin electrodes for research, diagnosis, communication and behavioral conditioning: A survey," *Medical and Biological Engineering and Computing*, vol. 6, no. 6, pp. 637–651, 1968.

[380] J. A. Meyer, "Werner forssmann and catheterization of the heart, 1929," *The Annals of Thoracic Surgery*, vol. 49, pp. 497–499, 1990.

[381] I. Chatterjee, D. Wu, and O. P. Gandhi, "Human body impedance and threshold current for perception and pain for contact hazard analysis in the vlf-mf band," *IEEE Transactions on Biomedical Engineering*, vol. BME-33, pp. 486–494, May 1986.

[382] K. H. Billings, *Switchmode Power Supply Handbook*. Mcgraw Hill, second ed., 2005.

[383] L. G. Gomella and S. A. Haist, *Clinician's Pocket Reference*. Mcgraw Hill, 2002.

[384] R. E. Marshak, *Meson Physics*. Dover Publications, Inc, 1952.

[385] A. Malvino and D. J. Bates, *Electronic Principles*. Mcgraw Hill, 2007.

[386] H. A. Hartley, *Audio design handbook*. Gernsback Library, 1958.

[387] J. L. Semmlow, *Biosignal and Biomedical Image Processing*. Marcel Dekker Inc, 2004.

[388] D. L. Powers, *Boundary Value Problems and Partial Differential Equations*. Elsevier, 2006.

[389] J. D. Enderle, D. C. Farden, and D. J. Krause, *Intermediate Probability Theory for Biomedical Engineers*. Morgan and Claypool Publishers, 2006.

[390] R. G. Lyons, *Understanding Digital Signal Processing*. Addison Wesley Logman, Inc, 1997.

[391] Tektronix, *Digital Storage Oscilloscope: TPS2012, TPS2014, TPS2024 - TPS2012, TPS2014, and TPS2024 Data Sheet*. Tektronix, tek.com.

[392] Tektronix, *Digital Storage Oscilloscopes: TDS2000C Series Datasheet*. Tektronix, tek.com.

[393] Tektronix, *TDS2000C and TDS1000C-EDU Series: Digital Storage Oscilloscopes User Manual*. Tektronix, tek.com, 2002.

[394] J. Weber, *Oscilloscope Probe Circuits*. Tektronix, Inc, 1969.

[395] C.-S. Yen, Z. Fazarinc, and R. L. Wheeler, "Time-domain skin-effect model for transient analysis of lossy transmission lines," *Proceedings of the IEEE*, vol. 70, no. 7, pp. 750–757, 1982.

[396] H. A. Wheeler, "Formulas for the skin effect," *Proceedings of the IRE*, vol. 30, no. 9, pp. 412 – 424, 1942.

[397] S. Kim and D. P. Neikirk, "Compact equivalent circuit model for the skin effect," *Microwave Symposium Digest*, vol. 3, pp. 1815 – 1818, 1996.

[398] J. M. Rabaey, A. P. Chandrakasan, and B. Nikolic, *Digital integrated circuits : a design perspective*. Pearson Education, 2003.

[399] Y. Fan, "Non-ideal behavior of components lecture notes." cee.cqu.edu.cn, June 2013.

[400] T. H. Donnelly, "Some capabilities and limitations of the laplace transform method for the direct estimation of continuous molecular weight distributions from equilibrium ultracen trifugation," *Annals of the New York Academy of Sciences*, vol. 164, pp. 147–155, 1969.

[401] S. B. Karmakar, "Laplace transform solution of nonlinear differential equations," *Indian Journal of Pure and Applied Mathematics*, vol. 11, no. 4, pp. 407–412, 1980.

[402] S. Can and A. Unal, "Transfer functions for nonlinear systems via fourier-borel transforms," *US Army Aviation Systems Command Aviation Research and Technology Activity Technical Report*, vol. 87-A-6, p. Memorandum 100034, 1988.

[403] K. S. Kundert and A. S. Vincentelli, "Simulation of nonlinear circuits in the frequency domain," *IEEE Transactions on Computer-Aided Design of Integrated Circuits and Systems*, vol. 5, no. 4, pp. 521–535, 1986.

[404] T. Wang, H. Liu, Y. Wang, and N. Wong, "Weakly nonlinear circuit analysis based on fast multidimensional inverse laplace transform," in *Design Automation Conference (ASP-DAC), 2012 17th Asia and South Pacific*, IEEE, 2012.

[405] S. Adebola, *Soma's Dictionary of Latin Quotations, Maxims and Phrases: A compendium of Latin Thought and Rhetoric Instruments for the Speaker, Author and Legal Practitioner Who Must Stand out and Excel*. Trafford On Demand, 2010.

[406] Tektronix, *Arbitrary/Function Generators AFG 3011, 3021B, 3022B, 3101, 3102, 3251, 3252 Datasheet*. Tektronix, tek.com.

[407] L. Foucault, C. M. Gariel, and J. A. Lissajous, *Recueil des travaux scientifiques*. Gauthier-Villars, 1878.

[408] G. C. Jain, *Properties of Electrical Engineering Materials*. Harper and Row, 1967.

[409] M. Nelkson, *Heat*. Blackie London and Glasgow, 1978.

[410] M. Miri and M. McLain, "Electromagnetic radiation from unbalanced transmission lines," *Progress In Electromagnetics Research B*, vol. 43, pp. 129–150, 2012.

[411] C. Manneback, "Radiation from transmission lines," *Transactions of the American Institute of Electrical Engineers*, vol. 42, pp. 289–301, 1923.

[412] D. Moongilan, "Radiation characteristics of short unterminated transmission lines," in *IEEE International Symposium on Electromagnetic Compatibility*, 2009.

[413] H. Morishita, H. Furuuchi, and K. Fujimoto, "Performance of balance-fed antenna system for handsets in the vicinity of a human head or hand," in *IEE Proceedings Microwaves, Antennas and Propagation*, vol. 149, pp. 85–91, IET, 2002.

[414] H. Haase and J. Nitsch, "High frequency model for the transfer impedance based on a generalized transmission-line theory," in *IEEE International Symposium on Electromagnetic Compatibility*, vol. 2, pp. 1242–1247, IEEE, 2001.

[415] F. Broyde, E. Clavelier, D. Givord, and P. Vallet, "Discussion of the relevance of transfer admittance and some through elastance measurement results," *IEEE Transactions on electromagnetic compatiblity*, vol. 35, pp. 417–422, 1993.

[416] K. Chandia and J. Flores, "Mesoscopic dual transmission line with discrete charge," *Journal of Electromagnetic Waves and Applications*, vol. 8-9, pp. 1021–1028, 2009.

[417] H. Haase, T. Steinmetz, and J. Nitsch, "New propagation models for electromagnetic waves along uniform and nonuniform cables," *IEEE Transactions on Electromagnetic Compatibility*, vol. 46, pp. 345–352, 2004.

[418] M. Tang and J. Mao, "Transient analysis of lossy nonuniform transmission lines using a time-step integration method," *Progress In Electromagnetics Research*, vol. 69, pp. 257–266, 2007.

[419] M. Khalaj-Amirhosseini, "Analysis of coupled or single nonuniform transmission lines using step-by-step numerical integration," *Progress In Electromagnetics Research*, vol. 58, pp. 187–198, 2006.

[420] A. K. Bhattacharyya, L. Shafai, and G. Garg, "Microstrip antenna – a generalized transmission line," *Progress In Electromagnetics Research*, vol. 4, pp. 45–84, 1991.

[421] A. Maffucci, G. Miano, and F. Villone, "An enhanced transmission line model for conducting wires," *IEEE Transactions on Electromagnetic Compatibility*, vol. 46, pp. 512–528, 2004.

[422] D. Wendt and J. Ter Haseborg, "Consideration and representation of radiation losses in the transmission line theory," in *Antennas and Propagation Society International Symposium*, vol. 3, pp. 1948–1951, IEEE, 1994.

[423] Y. Kami and R. Sato, "Analysis of radiation characteristics of a finite-length transmission line using a circuit-concept approach," *IEEE Transactions on Electromagnetic Compatibility*, vol. 30, no. 2, pp. 114–121, 1988.

[424] D. Inc., "5-lead ecg leadwire set - grabber/squeeze style." orsupply.com, 2008.

[425] I. Bio-Medical Instruments, "Ds26 disposable semg sensors data sheet." bio-medical.com, 2009.

[426] T. Quarles, D. Pederson, R. Newton, A. Sangiovanni-Vincentelli, C. Wayne, and J. M. Rabaey, "The spice home page." bwrcs.eecs.berkeley.edu/Classes/IcBook/SPICE, November 2009.

[427] L. V. Fausett, *Applied Numerical Analysis Using Matlab*. Pearson Prentice Hall, 2008.

[428] S.-P. Chan, *Introductory Topological Analysis of Electrical Networks*. Hold,Rinehart, and Winston, Inc, 1969.

[429] E. Kreyszig, *Advanced Engineering Mathematics*. Joh, 1993.

[430] I. Bio-Medical Instruments, "Cg04 saline base signa gel - 2oz tube data sheet." bio-medical.com, 2009.

[431] A. Klimov and G. H. Pollack, "Visualization of charge-carrier propagation in water," *Langmuir*, vol. 23, no. 23, pp. 11890–11895, 2007.

[432] J.-m. Zheng, A. Wexler, and G. H. Pollack, "Effect of buffers on aqueous solute-exclusion zones around ion-exchange resins," *Journal of colloid and interface science*, vol. 332, pp. 511–514, 2009.

[433] K. Ovchinnikova and G. H. Pollack, "Can water store charge?," *Langmuir*, vol. 25, pp. 542–547, 2008.

[434] X. A. Figueroa and G. H. Pollack, "Exclusion-zone formation from discontinuous nafion surfaces," *Journal of Design and Nature and Ecodynamics*, vol. 6, pp. 286–296, 2011.

APPENDIX A: ENVIRONMENTAL DIGITAL TO ANALOG TEST CODE

The code presented within this appendix was utilized to perform a laboratory experiment in which, a 12 bit DAC was remotely controlled, via RS–232 protocol, by a Python application and the output voltage observed — via a oscilloscope — was acquired and transferred back to the Python application — via RS–232 protocol.

The following C code was written within the Renesas High Performance Embedded Workshop (HEW) integrated developer environment (IDE), compiled within this environment, and downloaded into the QSK62p flash memory via the universal serial bus (USB) Joint Test Action Group (JTAG) HEW programming interface. The function of this code was to receive a RS–232 command containing a 12 bit value and change the external 12 bit DAC — connected to the QSK29P — value to this new remotely received value. Note, this code was originally written by Mike Mclain to control a Vibrating Sample Magnetometer (VSM) machine for Dr. Ryan Adams and was later modified to perform DAC analysis, hence the reference to a VSM machine within the code.

```
//*************************************************************
// File Name: ADC.h
// Project: 12-Bit DAC DC Experiment
// Description: This File is the ADC.c Preprocessor file
// Author: Mike Mclain
// Note the QSK62P is a product of the Renesas Electronics
// company and all board support variables and documentation
// is provided compliments of Renesas Electronics
//*************************************************************
// Predefine functions
void setup_ADC();

//*************************************************************
// File Name: ADC.c
// Project: 12-Bit DAC DC Experiment
// Description: This File Configures the QSK62P ADC
// Author: Mike Mclain
// Note the QSK62P is a product of the Renesas Electronics
// company and all board support variables and documentation
// is provided compliments of Renesas Electronics
//*************************************************************

//*************************************************************
// Include Preprocessor Headers
//*************************************************************
#include "ADC.h"     // Define the ADC functions
#include "qsk_bsp.h"  // Board Support Package

//*************************************************************
// Setup the ADC for Sampling
//*************************************************************
void setup_ADC()
```

```
{
  adcon0 = 0x98;
  /*
  10011000;    ** Repeat sweep mode 0, soft trigger, fAD/2
  ||||||||_____Analog input select bit 0
  |||||||______Analog input select bit 1
  ||||||_______Analog input select bit 2
  |||||________A/D operation mode select bit 0
  ||||_________A/D operation mode select bit 1
  |||__________Trigger select bit
  ||___________A/D conversion start flag
  |____________Frequency select bit 0 */

  adcon1 = 0x39;
  /*
  00111001;    ** Scan AN0-AN3, 10-bit mode,
  ||||||||         fAD/2, Vref connected
  ||||||||_____A/D sweep pin select bit 0
  |||||||______A/D sweep pin select bit 1
  ||||||_______A/D operation mode select bit 1
  |||||________8/10 bit mode select bit
  ||||_________Frequency select bit 1
  |||__________Vref connect bit
  ||___________External op-amp connection mode bit 0
  |____________External op-amp connection mode bit 1 */

  adcon2 = 0x01;
  /*
  00000001;    ** Sample and hold enabled, fAD/2
  ||||||||_____AD conversion method select bit
  |||||||______AD input group select bit 0
  ||||||_______AD input group select bit 1
  |||||________Reserved
  ||||_________Frequency select bit 2
  |||__________Reserved
  ||___________Reserved
  |____________Reserved */

  // Start a ADC conversion Now
    adst = 1;
}

//*************************************************************
// File Name: DAC.c
// Project: 12-Bit DAC DC Experiment
// Description: This File Configures the QSK62P DAC
// Author: Mike Mclain
// Note the QSK62P is a product of the Renesas Electronics
```

```
// company and all board support variables and documentation
// is provided compliments of Renesas Electronics
//*************************************************************

//*************************************************************
// Include Preprocessor Headers
//*************************************************************
#include "DAC.h"     // Define the DAC functions
#include "qsk_bsp.h"  // Board Support Package
#include "suport.h"    // Define Custom User names
             // for common extern pins

//*************************************************************
// Define Global Variables
//*************************************************************
// This is the current ADC output value
int VSM_DAC_VALUE=0;
int VSM_TARGET_VALUE=0;
char VSM_POLARITY=POSITIVE;
char VSM_TARGET_POLARITY=POSITIVE;

//*************************************************************
// Define Functions
//*************************************************************

//*************************************************************
// Active the onboard DAC within the QSK62P
//*************************************************************
void Setup_QSK_DAC()
{
  da1e=1;
}

//*************************************************************
// set the onboard DAC to a given value
//*************************************************************
void Set_QSK_DAC(char value)
{
  da1=value;
}

//*************************************************************
// Setup the external DAC
//*************************************************************
void DAC_SETUP()
{
  // setup the port for output
  prc1=1;            // allow write to the
```

```
                    // direction latch
  DAC_PORT_IO_LATCH=0xFF;    // Allow output from pins
   prc1=0;              // lock writeing to the
                    // direction latch

   // flush ADC PORT zero
   DAC_PORT=0x00;

   // PRC1 should auto reset to zero after next
   // instruction so we need todo this everytime, i
   // allways set it back to zero for kicks after im done
   prc1=1;              // allow write to the
                    // direction latch
   DAC_COMMAND_IO_LATCH=0xFF;  // not useing ports 5 6 7
                    // but all just in case
   prc1=0;              // lock writeing to the
                    // direction latch

   // flush ADC COMMAND PORT TO ZERO
   // logic low for commands so set the low
   // nibble+1bit high
   DAC_COMMAND=0x1F;
   // LATCH IS TRANSPARENT
}

//*************************************************************
// Write a byte to the external DAC pins
// Note this just puts it on the pins it does not set the
// external ADC latch
//*************************************************************
void DAC_WRITE_BYTE(int value)
{
   // mask off the upper byte
   DAC_PORT=value & 0x00FF;
}

//*************************************************************
// Write a nibble to the external DAC pins
// Note this just puts it on the pins it does not set the
// external ADC latch
//*************************************************************
void DAC_WRITE_NIBBLE(int value)
{
   // mask and set value
   DAC_PORT=(value & 0x0F00)>>8;
}

//*************************************************************
```

```
// Set the external DAC Value
//*************************************************************
void DAC_SET_VALUE(int value)
{

  // STEP 1
  DAC_A0=1;
  DAC_A1=1;
  // write the byte to the port
  DAC_WRITE_NIBBLE(value);
  // relese CS protection
  DAC_CS=DAC_YES;
  // set write on
  DAC_WR=DAC_YES;

  // STEP 2
  DAC_CS=DAC_NO;
  DAC_WR=DAC_NO;

  // STEP 3
  // set both A0 and A1 to Zero
  DAC_A0=0;
  DAC_A1=0;
  // write the byte to the port
  DAC_WRITE_BYTE(value);
  // relese CS protection
  DAC_CS=DAC_YES;
  // set write on
  DAC_WR=DAC_YES;

  // STEP 4
  DAC_CS=DAC_NO;
  DAC_WR=DAC_NO;
}

//*************************************************************
// File Name: DAC.h
// Project: 12-Bit DAC DC Experiment
// Description: This File is the DAC.c Preprocessor file
// Author: Mike Mclain
// Note the QSK62P is a product of the Renesas Electronics
// company and all board support variables and documentation
// is provided compliments of Renesas Electronics
//*************************************************************

//*************************************************************
// Macros allow us to make external pin locations into
// something human readable so use them!
```

```
//*********************************************************

// define the ADC ports
#define DAC_PORT p2
#define DAC_PORT_IO_LATCH pd2

// define the ADC command lines
#define DAC_COMMAND_IO_LATCH pd1
#define DAC_COMMAND pd1

// define each port if needed
#define DAC_0 p2_0
#define DAC_1 p2_1
#define DAC_2 p2_2
#define DAC_3 p2_3
#define DAC_4 p2_4
#define DAC_5 p2_5
#define DAC_6 p2_6
#define DAC_7 p2_7
#define DAC_8 p2_0
#define DAC_9 p2_1
#define DAC_10 p2_2
#define DAC_11 p2_3

// Bool Macro
#define DAC_YES 0
#define DAC_NO  1

// ADC Pins
#define DAC_CS  p1_3
#define DAC_WR  p1_2
// This pin was not connect so this ability is offline
// #define ADC_CLR  p1_5
#define DAC_LDAC p1_4
#define DAC_A0  p1_0
#define DAC_A1  p1_1

// Like #define , but auto numbering
// DAC Events
enum DAC_ENUM
{
  DAC_EWRITE_NIBBLE=0,
  DAC_EPAUSE,
  DAC_EWRITE_BYTE,
  DAC_EPAUSE2,
  DAC_SET,
  DAC_EEND
};
```

```
//*************************************************************
// Predefine functions
//*************************************************************

void DAC_SETUP();
void DAC_SET_VALUE(int value);
void DAC_WRITE_BYTE(int value);
void DAC_WRITE_NIBBLE(int value);
void Setup_QSK_DAC();
void Set_QSK_DAC(char value);

//*************************************************************
// File Name: suport.c
// Project: 12-Bit DAC DC Experiment
// Description: common supporting functions
// Author: Mike Mclain
// Note the QSK62P is a product of the Renesas Electronics
// company and all board support variables and documentation
// is provided compliments of Renesas Electronics
//*************************************************************

//*************************************************************
// Include Preprocessor Headers
//*************************************************************
#include "qsk_bsp.h" // Board Support Package
#include "suport.h"  // Define the support functions
#include "Task.h" //  define round robin task
#include "RoundRobin.h" // define the round robin task manager

//*************************************************************
// Define Global Variables
//*************************************************************
char ISERROR=0; // Has an error occurred?

//*************************************************************
// Setup our IO pins
//*************************************************************
void SetupPins()
{
  // setup local and remote leds as output
  LOCAL_DDR=OUTPUT;
  REMOTE_DDR=OUTPUT;

  // setup our local and remote input
  SW_LOCAL_REMOTE_DDR=INPUT;
  pu00=1;
```

```
  // turn both LEDS off
  LOCAL=OFF;
  REMOTE=OFF;

  // setup the POLARITY
  SW_POLARITY_DDR=INPUT;
  pu01=1;

  // setup the POLARITY feedback

  FB_POLARITY_NEG_DDR=INPUT;
  FB_POLARITY_POS_DDR=INPUT;

  // setup the POLARITY output switch
  POLARITY_NEG_DDR=OUTPUT;
  POLARITY_POS_DDR=OUTPUT;

  pu03=1;

  // setup the chiller
  CHILLER_DDR=INPUT;

}

//*************************************************************
// see if a error has occurred and if so preform the
// desired action
//*************************************************************
void Error_Alert()
{
  extern char MODE;
  if(ISERROR==0)
  {
    ISERROR=1;
    MODE=MODE_REMOTE;
     KillTask(LOCAL_REMOTE_CHECK_TASK);
     addTask(LOCAL_REMOTE_BLINK, 1000,
       LOCAL_REMOTE_BLINK_TASK);
  }
}

//*************************************************************
// if we had a error and it was resoled abort the
// error state
//*************************************************************
void Error_Alert_Abort()
{
  if(ISERROR==1)
```

```
  {
    KillTask(LOCAL_REMOTE_BLINK_TASK);
    addTask(CHECK_LOCAL_REMOTE_STATE, 10,
      LOCAL_REMOTE_CHECK_TASK);
    LOCAL=OFF;
    REMOTE=OFF;
    ISERROR=0;
  }
  else
  {
    return;
  }
}

//************************************************************
// used by the VSM to change polarity +
//************************************************************
void Polarity_Positive()
{
  addTask(POLARITY_POS_BONK, 3000, POLARITY_BONK_TASK);
}

//************************************************************
// used by the VSM to change polarity -
//************************************************************
void Polarity_Negative()
{
  addTask(POLARITY_NEG_BONK, 3000, POLARITY_BONK_TASK);
}

//************************************************************
// A modified Renesas Electronics function to
// convert a decimal into a string
//************************************************************
char * IntToAsciiDec(char * dest_string,int min_digits
  ,unsigned int value)
{
  const unsigned long base10[] = {1,10,100,1000
    ,10000,100000};

  unsigned int tmp;
  unsigned int i, total_digits = 0;
  char buff[5];

  for(i=0;i<5;i++) {
    tmp = (int)( value % base10[i+1] );
    value -= tmp;
```

```
    buff[i] = (char)( tmp / base10[i] );
    buff[i] += '0';

    if(buff[i] != '0')
      total_digits = i+1;
  }

  if( total_digits <  min_digits)
    total_digits = min_digits;

  i = total_digits;

  while(i) {
    *dest_string++ = buff[i-1];
    i--;
  }

  *dest_string = 0;

  return dest_string;
}

//************************************************************
// File Name: suport.h
// Project: 12-Bit DAC DC Experiment
// Description: This File is the support Preprocessor file
// Author: Mike Mclain
// Note the QSK62P is a product of the Renesas Electronics
// company and all board support variables and documentation
// is provided compliments of Renesas Electronics
//************************************************************

//************************************************************
// Macros allow us to make external pin locations into
// something human readable so use them!
//************************************************************

// Define the local and remote LED pins
#define LOCAL_DDR pd3_0
#define REMOTE_DDR pd3_1
#define LOCAL p3_0
#define REMOTE p3_1

// Define if a pin is a input or output pin
#define OUTPUT 1
#define INPUT 0
```

```
// Define flags for the current mode of the system
#define MODE_NONE 0
#define MODE_LOCAL 1
#define MODE_REMOTE 2
#define MODE_ERROR 3

// Define the input switch for the local and
// remote button
#define SW_LOCAL_REMOTE_DDR pd0_2
#define SW_LOCAL_REMOTE p0_2

// Define flags for if a output or input is On or Off
#define OFF 0
#define ON 1

// Define flags to check for local or remote mode
#define IS_LOCAL ON
#define IS_REMOTE OFF

// Define the Polarity direction pin for switch
#define SW_POLARITY_DDR pd0_4
#define SW_POLARITY p0_4

// Polarity Feedback Information
#define FB_POLARITY_NEG_DDR pd0_7
#define FB_POLARITY_NEG p0_7
#define FB_POLARITY_POS_DDR pd0_6
#define FB_POLARITY_POS p0_6

// Polarity Output Toggle
#define POLARITY_NEG_DDR pd1_7
#define POLARITY_NEG p1_7
#define POLARITY_POS_DDR pd1_6
#define POLARITY_POS p1_6

// Polarity Types
#define POSITIVE 1
#define NEGATIVE 0

// setup our ADC names
#define COARSE ad3
#define FINE ad2

#define DACTIME 5

// setup our CHILLER input
#define CHILLER_DDR pd0_0
#define CHILLER p0_0
```

```
//*************************************************************
// Predefine functions
//*************************************************************
void SetupPins();
void Polarity_Positive();
void Polarity_Negative();
void Error_Alert();
void Error_Alert_Abort();

char * IntToAsciiDec(char * dest_string,int min_digits,
  unsigned int value);

//*************************************************************
// File Name: Task.c
// Project: 12-Bit DAC DC Experiment
// Description: Define all round robin task
// Author: Mike Mclain
// Note the QSK62P is a product of the Renesas Electronics
// company and all board support variables and documentation
// is provided compliments of Renesas Electronics
//*************************************************************

//*************************************************************
// Include Preprocessor Headers
//*************************************************************
#include "qsk_bsp.h" // Board Support Package
#include "DAC.h"  // Define the DAC functions
#include "RoundRobin.h" // define the round robin
          // task manager
#include "Task.h" // define round robin tasks
#include "suport.h" // Define the support functions
#include "uart.h" // Define RS232 Support
#include "ADC.h"    // Define the ADC functions
#include "queue.h" // define RS232 queue suport

//*************************************************************
// Define Global Variables
//*************************************************************
char RESTARTDACFLAG=0;

//*************************************************************
// Used to blink the Remote LEDS
//*************************************************************
void REMOTE_BLINK(void)
{
  REMOTE ^= LED_OFF;
}
```

```
//*************************************************************
// Used to blink the Local LEDS
//*************************************************************
void LOCAL_BLINK(void)
{
  LOCAL ^= LED_OFF;
}

//*************************************************************
// Used to blink the Remote and Local LEDS
//*************************************************************
void LOCAL_REMOTE_BLINK(void)
{
  LOCAL ^= LED_OFF;
  REMOTE ^= LED_OFF;
}

//*************************************************************
// Used to check the polarity
//*************************************************************
void CHECK_POLARITY_INPUT(void)
{
  static char lastinput=OFF;
  static int count=0;
  // Local Mode Only
  extern char MODE;
  if(MODE!=MODE_LOCAL)
  {
    return;
  }

  if(lastinput!=SW_POLARITY || count>0)
  {
    lastinput=SW_POLARITY;
    if(lastinput==ON)
    {
      if(count>100)
      {
        extern char VSM_TARGET_POLARITY;
        if(VSM_TARGET_POLARITY==POSITIVE)
        {
          VSM_TARGET_POLARITY=NEGATIVE;
          //TX_XMIT_String("Polarity set
          // to negative\n");
        }
        else
        {
```

```
            VSM_TARGET_POLARITY=POSITIVE;
            //TX_XMIT_String("Polarity set
            // to positive\n");
          }
          count=0;
        }
        else
        {
          count++;
        }
      }
      else
      {
        count=0;
      }
    }
}

//************************************************************
// Used to get the COARSE and FINE values if needed
//************************************************************
void ADC_READ_EVENT(void)
{
  // Local Mode Only
  int BUF1=0;
  int BUF2=0;
  extern char MODE;
  extern unsigned int coarse_value;
  extern unsigned int fine_value;
  extern int VSM_TARGET_VALUE;

  if(MODE!=MODE_LOCAL)
  {
    return;
  }
  // read the ADC values
  coarse_value=COARSE& 0x03ff;
  fine_value=FINE& 0x03ff;

  // do some math for COARSE and FINE
  BUF1 = (coarse_value &0x03F0)<<2;
  BUF2 = fine_value>>4;

  VSM_TARGET_VALUE=BUF1|BUF2;
  Set_QSK_DAC(VSM_TARGET_VALUE>>4);
}

//************************************************************
```

```
// Used to check the Local Remote switch state
//*************************************************************
void CHECK_LOCAL_REMOTE_STATE(void)
{
  extern char MODE;
  char NewMode=MODE_NONE;
  if(SW_LOCAL_REMOTE==IS_LOCAL)
  {
    NewMode=MODE_LOCAL;
  }
  else
  {
    NewMode=MODE_REMOTE;
  }

  if(NewMode!=MODE)
  {
    LOCAL=OFF;
    REMOTE=OFF;
    MODE=NewMode;
    if(MODE==MODE_LOCAL)
    {
      LOCAL=ON;
    }
    else
    {
      REMOTE=ON;
    }
  }
}
//*************************************************************
// get the ADC to where it should be going
//*************************************************************
void DAC_BRAIN(void)
{
  extern char VSM_TARGET_POLARITY;
  extern char VSM_POLARITY;
  extern int VSM_DAC_VALUE;
  extern int VSM_TARGET_VALUE;
  extern char ISERROR;

  // our current POLARITY can allways be found
  // via feedback
  // Debug Remove
  /*
  if(FB_POLARITY_NEG==ON && FB_POLARITY_POS==OFF
  && CHILLER==ON)
  {
```

```
   VSM_POLARITY=NEGATIVE;
   Error_Alert_Abort();
}
else if(FB_POLARITY_POS==ON && FB_POLARITY_NEG==OFF
&& CHILLER==ON)
{
   VSM_POLARITY=POSITIVE;
   Error_Alert_Abort();
}
else
{
   // this is a crazy case where feedback is offline
   // or something is up so throw a error
   Error_Alert();
}

// in the event of some type of error we should
   // allways reduce back to zero
if(ISERROR==1)
{
   // move the DAC slowly to zero
   if(VSM_DAC_VALUE>0)
   {
      VSM_DAC_VALUE--;
      // set the dac
      DAC_SET_VALUE(VSM_DAC_VALUE);
   }
   // exit loop
   return;
}
*/
VSM_POLARITY=POSITIVE;
if (VSM_DAC_VALUE!=VSM_TARGET_VALUE)
{
  DAC_SET_VALUE(VSM_TARGET_VALUE);
}
return;
// see if we have a polarity mismatch
if(VSM_TARGET_POLARITY!=VSM_POLARITY)
{
   // see if its safe to change the polarity
   if(VSM_DAC_VALUE==0)
   {
      // if so then see if it should go positive
      if(VSM_TARGET_POLARITY==POSITIVE)
      {
         // we dont want the dac to change while
         // polarity is changeing
```

```
        // so stop our DAC task for the change
        RESTARTDACFLAG=1;
        KillTask(DAC_UPDATE_TASK);
        Polarity_Positive();
        return;
      }
      else
      {
        // we dont want the dac to change while
        // polarity is changeing
        // so stop our DAC task for the change
        RESTARTDACFLAG=1;
        KillTask(DAC_UPDATE_TASK);
        // else it should go negative
        Polarity_Negative();
        return;
      }
    }
    else
    {
      // else we need to back our value down
      // slowly before switching
      if(VSM_DAC_VALUE>0)
      {
        VSM_DAC_VALUE--;
        // set the dac
        DAC_SET_VALUE(VSM_DAC_VALUE);
      }
      return;
    }
  }
  else
  {
    // polarity matchs so check values now
    if(VSM_DAC_VALUE>VSM_TARGET_VALUE)
    {
      VSM_DAC_VALUE--;
      // set the dac
      DAC_SET_VALUE(VSM_DAC_VALUE);
      return;
    }
    else if (VSM_DAC_VALUE<VSM_TARGET_VALUE)
    {
      VSM_DAC_VALUE++;
      // set the dac
      DAC_SET_VALUE(VSM_DAC_VALUE);
      return;
    }
```

```
    else
    {
      // im at my target value;
      return;
    }
  }

}

//*************************************************************
// make a 1 sec pulse for high pos
//*************************************************************
void POLARITY_POS_BONK(void)
{
  static char count=0;
  if(count==0)
  {
    POLARITY_POS=ON;
    count++;
  }
  else
  {
    POLARITY_POS=OFF;
    count=0;
    KillTask(POLARITY_BONK_TASK);

    if(RESTARTDACFLAG==1)
    {
      RESTARTDACFLAG=0;
      addTask(DAC_BRAIN, DACTIME,
      DAC_UPDATE_TASK);
    }
  }
}

//*************************************************************
// make a 1 sec pulse for low pos
//*************************************************************
void POLARITY_NEG_BONK(void)
{
  static char count=0;
  if(count==0)
  {
    POLARITY_NEG=ON;
    count++;
  }
  else
  {
```

```
    POLARITY_NEG=OFF;
    count=0;
    KillTask(POLARITY_BONK_TASK);

    if(RESTARTDACFLAG==1)
    {
      RESTARTDACFLAG=0;
      addTask(DAC_BRAIN, DACTIME,
      DAC_UPDATE_TASK);
    }
  }
}

//************************************************************
// Handle RS232 Communication Receive
//************************************************************
void UART_RX_EVENT(void)
{
  extern int RX_Ready;
  extern Queue RX_Q;
  extern char ISERROR;
  extern int VSM_TARGET_VALUE;
  extern int VSM_DAC_VALUE;
  extern char VSM_TARGET_POLARITY;
  extern char VSM_POLARITY;
  extern char MODE;
  char val=0;
  char val3=0;
  unsigned int val1;
  unsigned int val2;
  // this is for remote only
  if(MODE!=MODE_REMOTE || ISERROR==1)
  {
    return;
  }

  // if someone pumps trash into the buffer and
  // overflows it then dump all data
  if(Queue_Full(&RX_Q)==1 && RX_Ready==0)
  {
    REMOTE ^= LED_OFF;
    while(RX_Q.Size>0)
    {
      Dequeue(&RX_Q);
    }
    RX_Ready=0;
    REMOTE ^= LED_OFF;
    return;
```

```
}
if(RX_Q.Size==0)
{
  RX_Ready=0;
  return;
}

if(RX_Ready>0)
{
 REMOTE ^= LED_OFF;
  while(RX_Ready>0)
  {
    if(RX_Q.Size<4)
    {
      // this means there is trash in the
      // buffer so purge it and abort
      while(RX_Q.Size>0)
      {
        val=Dequeue(&RX_Q);
        if(val=='\n')
        {
          RX_Ready--;
          break;
        }
      }
     REMOTE ^= LED_OFF;
      return;
    }
    // get the current value
    val=Dequeue(&RX_Q);
    if(val=='+' || val=='-')
    {
      val3=val;
      if(RX_Q.Size==3)
      {
        val=Dequeue(&RX_Q);
        val1=val;
        val1=val1<<8;
        val=Dequeue(&RX_Q);
        val2=val1|val;
        // this is /n so we dont care
        // about it
        val=Dequeue(&RX_Q);
       RX_Ready--;

        if(val3=='+')
        {
          VSM_TARGET_POLARITY=POSITIVE;
```

```
            }
            else
            {
              VSM_TARGET_POLARITY=NEGATIVE;
            }
            if(val2<=4095)
            {
              VSM_TARGET_VALUE=val2;
            }
            else
            {
              VSM_TARGET_VALUE=4095;
            }
          }
          else
          {
            // bad packet
            while(RX_Q.Size>0)
            {
              val=Dequeue(&RX_Q);
              if(val=='\n')
              {
                RX_Ready--;
                break;
              }
            }
          }
        }
        else
        {
          // bad packet
          while(RX_Q.Size>0)
          {
            val=Dequeue(&RX_Q);
            if(val=='\n')
            {
              RX_Ready--;
              break;
            }
          }
        }
      }
      REMOTE ^= LED_OFF;
    }

}

//*************************************************************
```

```
// Handle RS232 Communication transmit
//*************************************************************
void UART_TX_EVENT(void)
{
  extern char MODE;
  extern int VSM_TARGET_VALUE;
  extern int VSM_DAC_VALUE;
  extern char VSM_TARGET_POLARITY;
  extern char VSM_POLARITY;
  extern Queue TX_Q;
  char out;
  extern char ISERROR;

  // this is for remote only
  if(MODE!=MODE_REMOTE|| ISERROR==1)
  {
    return;
  }

  // XMIT our state
  if(VSM_POLARITY==POSITIVE)
  {
    Enqueue(&TX_Q, '+');
  }
  else
  {
    Enqueue(&TX_Q, '-');
  }

  // high byte first
  out=VSM_DAC_VALUE>>8;
  Enqueue(&TX_Q, out);
  // low byte next
  out=VSM_DAC_VALUE;
  Enqueue(&TX_Q, out);
  // end string
  Enqueue(&TX_Q, '\n');
  TX_XMIT();
}

//*************************************************************
// File Name: Task.h
// Project: 12-Bit DAC DC Experiment
// Description: round robin task Preprocessor file
// Author: Mike Mclain
// Note the QSK62P is a product of the Renesas Electronics
// company and all board support variables and documentation
// is provided compliments of Renesas Electronics
```

```
//************************************************************

//************************************************************
// Macros allow us to make external pin locations into
// something human readable so use them!
//************************************************************

// enums are auto numbering so you only need to
// set one value the rest get last num+1
// zero is the first to run
enum
{
  DAC_UPDATE_TASK,
  POLARITY_BONK_TASK,
  LOCAL_REMOTE_CHECK_TASK,
  POLARITY_BUTTON_CHECK_TASK,
  ADC_READ_TASK,
  LOCAL_REMOTE_BLINK_TASK,
  UART_RX_TASK,
  UART_TX_TASK,
  MAX_TASKS // This denotes the end of all tasks
};


//************************************************************
// Predefine functions
//************************************************************
// LED BLINK TASK
// this will blink the local and remote lights off and on
void LOCAL_REMOTE_BLINK(void);
// this will blink the remote lights off and on
void REMOTE_BLINK(void);
// this will blink the local lights off and on
void LOCAL_BLINK(void);
// Polarity output task
void POLARITY_POS_BONK(void);
void POLARITY_NEG_BONK(void);
// INPUT CHECK TASK
void CHECK_LOCAL_REMOTE_STATE(void);
void CHECK_POLARITY_INPUT(void);
void ADC_READ_EVENT(void);
// DAC Master Ticker Task
void DAC_BRAIN(void);
// UART TASK
void UART_RX_EVENT(void);
void UART_TX_EVENT(void);

//************************************************************
```

```
// File Name: RoundRobin.c
// Project: 12-Bit DAC DC Experiment
// Description: round robin task manager
// Author: Original Code by UNCC ECGR 4101-5101
//         Embedded Systems Lab Creator
// this originates from Dr. James Conrad Notes
// Modifications by Mike Mclain
// Note the QSK62P is a product of the Renesas Electronics
// company and all board support variables and documentation
// is provided compliments of Renesas Electronics
//*************************************************************

//*************************************************************
// Include Preprocessor Headers
//*************************************************************
#include "qsk_bsp.h" // Board Support Package
#include "Task.h" // define round robin tasks
#include "RoundRobin.h" // define round robin


#if USE_ROUND_ROBIN_SCH
//*************************************************************
// Define Global Variables
//*************************************************************

// Warning C is not object oriented  and this is more
// of a memory macro than a object
typedef struct
{
  int initialTimerValue;
  int timer;
  int run;
  int enabled;
  void (* task)(void);
} task_t;

task_t GBL_task_list[MAX_TASKS];
int    GBL_run_scheduler=0;

//*************************************************************
// Warning This is a ISR!!!!
// Make sure to load the vector table with this ISR
//*************************************************************
#pragma INTERRUPT tick_timer_intr
void tick_timer_intr(void)
{
  static char i;
  for (i=0 ; i<MAX_TASKS ; i++)
```

```
  { // If scheduled task
    if (GBL_task_list[i].task != NULL)
    {
      if (GBL_task_list[i].enabled == 1)
      {
        if (GBL_task_list[i].timer)
        {
          if (--GBL_task_list[i].timer == 0)
          {
            GBL_task_list[i].run = 1;
            GBL_task_list[i].timer =
            GBL_task_list[i].initialTimerValue;
          }
        }
      }
    }
  }
}

#endif

//*************************************************************
// this is the master Task Manager
// its always running
//*************************************************************
void Run_RR_Scheduler(void)
{
  int i;
  GBL_run_scheduler = 1;
  while (1)
  {               // Loop forever & Check each task
    for (i=0 ; i<MAX_TASKS ; i++)
    {
          // If this is a scheduled task
      if (GBL_task_list[i].task != NULL)
      {
        if (GBL_task_list[i].enabled == 1)
        {
          if (GBL_task_list[i].run == 1)
          {
            GBL_task_list[i].task();
            // Run the task
            GBL_task_list[i].run=0;
            // Reset task timer
            break;
          }
        }
      }
```

```
    }
  }
}

//************************************************************
// Initialize all tasks
//************************************************************
void init_Task_Timers(void)
{
  int i;
  for (i=0 ; i<MAX_TASKS ; i++)
  {
    GBL_task_list[i].initialTimerValue = 0;
    GBL_task_list[i].run = 0;
    GBL_task_list[i].timer = 0;
    GBL_task_list[i].enabled = 0;
    GBL_task_list[i].task = NULL;
  }
}

//************************************************************
// add a task
//************************************************************
int addTask(void (*task)(void), int time, int priority)
{
  unsigned int t_time;
  /* Check for valid priority */
  if (priority >= MAX_TASKS || priority < 0)
  {
    return 0;
  }
  // Check to see if we are overwriting
  // an already scheduled task
  if (GBL_task_list[priority].task != NULL)
  {
    return 0;
  }
  /* Schedule the task */
  GBL_task_list[priority].task = task;
  GBL_task_list[priority].run  = 0;
  GBL_task_list[priority].timer = time;
  GBL_task_list[priority].enabled = 1;
  GBL_task_list[priority].initialTimerValue = time;
  return 1;
}

//************************************************************
// Remove the Task
```

```
//*********************************************************
void removeTask(void (* task)(void))
{
  int i;
  for (i=0 ; i<MAX_TASKS ; i++)
  {
    if (GBL_task_list[i].task == task)
    {
      GBL_task_list[i].task = NULL;
      GBL_task_list[i].timer = 0;
      GBL_task_list[i].initialTimerValue = 0;
      GBL_task_list[i].run =0;
      GBL_task_list[i].enabled = 0;
      return;
    }
  }
}

//*********************************************************
// Stop a task from running
//*********************************************************
void KillTask(int task_number)
{
  GBL_task_list[task_number].task = NULL;
  GBL_task_list[task_number].timer = 0;
  GBL_task_list[task_number].initialTimerValue = 0;
  GBL_task_list[task_number].run =0;
  GBL_task_list[task_number].enabled = 0;
}

//*********************************************************
// see if a task is enabled
//*********************************************************
char Get_Task_Stat(int task_number)
{
  return GBL_task_list[task_number].enabled;
}

//*********************************************************
// Enable a task
//*********************************************************
void Enable_Task(int task_number)
{
  GBL_task_list[task_number].run=1;
  GBL_task_list[task_number].enabled = 1;
}

//*********************************************************
```

```
// Disable a task
//*************************************************************
void Disable_Task(int task_number)
{
  GBL_task_list[task_number].enabled = 0;
}

//*************************************************************
// Reschedule a task
//*************************************************************
void Reschedule_Task(int task_number, int new_timer_val)
{
  GBL_task_list[task_number].initialTimerValue = new_timer_val;
  GBL_task_list[task_number].timer = new_timer_val;
}

//*************************************************************
// Setup Round Robin
//*************************************************************
void RR_init()
{
  init_Task_Timers();    // Initialize all tasks
  tb0 = 12000;        // 1 ms timer tick
  DISABLE_IRQ
  tb0ic = 1;         // Timer B0 overflow
  ENABLE_IRQ
  tb0s = 1;       // start timer B0
}

//*************************************************************
// File Name: RoundRobin.h
// Project: 12-Bit DAC DC Experiment
// Description: round robin task manager Preprocessor file
// Author: Original Code by UNCC ECGR 4101-5101
//         Embedded Systems Lab Creator
// this originates from Dr. James Conrad Notes
// Modifications by Mike Mclain
// Note the QSK62P is a product of the Renesas Electronics
// company and all board support variables and documentation
// is provided compliments of Renesas Electronics
//*************************************************************

//*************************************************************
// Macros allow us to make external pin locations into
// something human readable so use them!
//*************************************************************
#define NULL 0x00 // yep this is null, nill, nada!
```

```
// this is defined within Task.h enum now!
//# MAX_TASKS 10
// Set to 1 if using Round Robin Task Scheduler
#define USE_ROUND_ROBIN_SCH 1


//*************************************************************
// Predefine functions
//*************************************************************
void RR_init();
void Reschedule_Task(int task_number, int new_timer_val);
void Disable_Task(int task_number);
void Enable_Task(int task_number);
void removeTask(void (* task)(void));
int addTask(void (*task)(void), int time, int priority);
void init_Task_Timers(void);
void Run_RR_Scheduler(void);
void RR_init();
void tick_timer_intr(void);
char Get_Task_Stat(int task_number);
void KillTask(int task_number);

//*************************************************************
// File Name: queue.c
// Project: 12-Bit DAC DC Experiment
// Description: RS232 UART Data Queue Class
// Author: Original Code by UNCC ECGR 4101-5101
//         Embedded Systems Lab Creator
// this originates from Dr. James Conrad Notes
// Modifications by Mike Mclain
// Note the QSK62P is a product of the Renesas Electronics
// company and all board support variables and documentation
// is provided compliments of Renesas Electronics
//*************************************************************

#include "queue.h" // define the queue

//*************************************************************
// Initialize queue
//*************************************************************
void Queue_Init(Queue * q)
 {
  unsigned int i;
  q->MaxSize=UART_QUEUE_SIZE;
  for (i=0; i<q->MaxSize; i++)
  {
    q->Data[i] = 0;
  }
```

```
  q->Head = 0;
  q->Tail = 0;
  q->Size = 0;
}

//*************************************************************
// see if the queue is empty
//*************************************************************
int Queue_Empty(Queue * q)
{
  return q->Size == 0;
}

//*************************************************************
// see if the queue is full
//*************************************************************
int Queue_Full(Queue * q)
 {
  return q->Size == q->MaxSize;
}

//*************************************************************
// add data to the queue
//*************************************************************
int Enqueue(Queue * q, unsigned char d)
{
  if (!Queue_Full(q))
  {
    q->Data[q->Tail++] = d;
    q->Tail %= q->MaxSize;
    q->Size++;
    return 1;
  }
  else
  {
    return 0;
  }
}

//*************************************************************
// remove data from the queue
//*************************************************************
unsigned char Dequeue(Queue * q)
 {
  unsigned char t=0;
  if (!Queue_Empty(q))
  {
    t = q->Data[q->Head];
```

```
    q->Data[q->Head++] = 0;
    q->Head %= q->MaxSize;
    q->Size--;
  }
  return t;
}

 //*************************************************************
 // compare string from the Queue
 //*************************************************************
char Queue_strcmp(Queue * q, _far char * string)
{
  char at=0;
  char len=0;

  // if the queue is empty or if the queue size is
  // smaller than string length there is no way the
  // queue can contain the string
  if(Queue_Empty(q)||q->Size<strlen(string))
  {
    // return that it was not found
    return 0;
  }
  // at is = to string head
  at=q->Head;
  while(len<strlen(string))
  {
    // see if the string members match
    if(q->Data[at]!=string[len])
    {
      // if thay dont return failed
      return 0;
    }
    // move to the next point
    at++;
    len++;
    // the queue can roll so check for roll over
    at %= q->MaxSize;
  }
  // if we get here we matched the string!
  // remove the string from the queue
  for(len=0;len<strlen(string);len++)
  {
    Dequeue(q);
  }
  // return that we found it!
  return 1;
}
```

```
//*************************************************************
// clean up a Q after Q strcmp fails
//*************************************************************
void Queue_Clean(Queue *q)
{
  while(!Queue_Empty(q))
  {
    if(Dequeue(q)=='\n')
    {
      return;
    }
  }
}
//*************************************************************
// Copy a Queue into a buffer
//*************************************************************
void Queue_Copy_TO(Queue *q,char * buffer,
  unsigned char find)
{
  unsigned char object=0;
  while(!Queue_Empty(q))
  {
    object=Dequeue(q);
    if(object!=find)
    {
      *buffer=object;
    }
    else
    {
      *buffer=0;
      return;
    }
    buffer++;
  }
}

//*************************************************************
// File Name: queue.h
// Project: 12-Bit DAC DC Experiment
// Description: RS232 UART Data Queue Class Preprocessor file
// Author: Original Code by UNCC ECGR 4101-5101
//         Embedded Systems Lab Creator
// this originates from Dr. James Conrad Notes
// Modifications by Mike Mclain
// Note the QSK62P is a product of the Renesas Electronics
// company and all board support variables and documentation
// is provided compliments of Renesas Electronics
```

```
//*************************************************************

#include "uart.h" // include uart suport


// Warning C is not object oriented and this is more
// of a memory macro than a object
// Edited for dyanmic memory
// Setup a Data QUEUE
typedef struct
 {
  unsigned char Data[UART_QUEUE_SIZE];
  unsigned int Head; // points to oldest data element
  unsigned int Tail; // points to next free space
  unsigned int Size; // quantity of elements in queue
  unsigned int MaxSize;
} Queue;


//*************************************************************
// Predefine functions
//*************************************************************
void Queue_Init(Queue * q);
int Queue_Empty(Queue * q) ;
int Queue_Full(Queue * q);
int Enqueue(Queue * q, unsigned char d) ;
unsigned char Dequeue(Queue * q);
char Queue_strcmp(Queue * q, _far char * string);
void Queue_Clean(Queue *q);
void Queue_Copy_TO(Queue *q,char * buffer, unsigned char find);

//*************************************************************
// File Name: main.c
// Project: 12-Bit DAC DC Experiment
// Description: Main Application
// Author: Mike Mclain
// Note the QSK62P is a product of the Renesas Electronics
// company and all board support variables and documentation
// is provided compliments of Renesas Electronics
//*************************************************************

#include "qsk_bsp.h"  // include file for basic
            // board IO support
#include "RoundRobin.h" // include file for a simplistic
            // task manager from
            // Dr. Conrads Class
#include "Task.h"   // include file for Round Robin
            // task manager Task
```

```
#include "DAC.h"     // include file for extern
                     // DAC interface
#include "suport.h"    // include file for custom
                     // IO support
#include "queue.h"     // include file for data queue
#include "uart.h"    // include file for UART suport
#include "ADC.h"     // include file for ADC suport

//*************************************************************
// Predefine functions
//*************************************************************
void mcu_init(void);


//*************************************************************
// Define Global Variables
//*************************************************************
// This is the current local remote mode
char MODE=MODE_NONE;
unsigned int coarse_value=0;
unsigned int fine_value=0;

// setup our TX and RX Buffers
Queue TX_Q;
Queue RX_Q;

//*************************************************************
// this is the code starting point
//*************************************************************
void main(void)
{
  extern int VSM_DAC_VALUE;
  // setup the MUC clock speed
  mcu_init();

  // setup the round robin
  RR_init();

  // setup the ADC
  DAC_SETUP();

  // setup our IO pins
  SetupPins();

  // setup our TX and RX UART Queue
  Queue_Init(&TX_Q);
  Queue_Init(&RX_Q);
```

```
    // setup the uart
    uart_init();

    // setup the ADC
    setup_ADC();
    DAC_SET_VALUE(0x0000);

    // setup the QSK DAC
    Setup_QSK_DAC();


    // add our core task here


    //VSM_DAC_VALUE=0xFFFF;
    //addTask(DAC_WRITE_DELAY, 10, DAC_WRITE_DELAY_TASK);
    //Disable_Task(ADC_WRITE_DELAY_ORDER);

    addTask(CHECK_LOCAL_REMOTE_STATE, 10,
      LOCAL_REMOTE_CHECK_TASK);
    //addTask(CHECK_POLARITY_INPUT, 10,
      POLARITY_BUTTON_CHECK_TASK);
    addTask(ADC_READ_EVENT, 10, ADC_READ_TASK);
    addTask(DAC_BRAIN, DACTIME, DAC_UPDATE_TASK);

    addTask(UART_TX_EVENT, 1000, UART_TX_TASK);
    addTask(UART_RX_EVENT, 500, UART_RX_TASK);
    Run_RR_Scheduler();
    // nothing below this will run unless
    // Run_RR_Scheduler is removed
    // then RR wont work!
    // not needed RR enters a endless loop!
    while(1)
    {
      // nothing will run here unless
      // USE_ROUND_ROBIN_SCH in
      // RoundRobin.h is set to 0
      // then Round Robin is off
    }
}
```

The following Python code was written within a standard text editor and was utilized to communicate DAC commands to the QSK62P over a RS–232 serial connection, while, at the same time, also communicating with a Tektronix TPS2024 oscilloscope in order to acquire and save the voltage produced by the DAC.

```
#*************************************************************
# File Name: DCTest1.py
# Project: 12-Bit DAC DC Experiment
```

```
# Description: Main Python Application
# Author: Mike Mclain
#*************************************************************

# include Tektronix Communication Class
import tektronix
# include Agilent Communication Class
import agilent
# include Tektronix visa Communication Class
import visa
# include system time
import time
# include os commands
import os
# include system commands
import sys
# include base rs232 support
import serial
# include data packing suport
from struct import *

#*************************************************************
# Setup RS232 connection to QSK62p
#*************************************************************
redbox=serial.Serial(port="\\.\COM2",baudrate=19200,
  parity=serial.PARITY_NONE,
  stopbits=serial.STOPBITS_ONE,
  bytesize=serial.EIGHTBITS)
redbox.close()
redbox.open()
redbox.isOpen()

# Define the DAC Test Values
#Test 1 is from 0 to 4095 (range is not end inclusive)
# Test 2 is from 4095 to 0 (range is not end inclusive)

testvals=range(0,4096)
testvals2=range(4095,-1,-1)
for lx in testvals2:
  testvals.append(lx)

# Set RS343 communication with TPS2024 oscilloscope
Scope=tektronix.Tektronix('\\.\COM9',19200)
Scope.Startup()


print Scope.GetId()
```

```
#*********************************************************
# Make a test Folder
folder=".\DCTEST"
os.makedirs(folder)
os.chdir(folder)
Scope.SetScopeRunState(1)

testat=-1
for lp in range(1):
  # make a new folder to hold the freq sweep
  folder=".\Test"+str(lp+1)
  os.makedirs(folder)
  os.chdir(folder)
  # Define our Test


  for lx in testvals:
    testat=testat+1
    print "Run %s At Test %s" % (str(testat),str(lx))
    output=str(pack('H', lx))
    print ord(output[0])
    print ord(output[1])
    for lx in range(5):
      redbox.write('+')
      redbox.write(output[1])
      redbox.write(output[0])
      redbox.write('\n')
      time.sleep(1)
    time.sleep(5)

    Scope.ScopeAutoSet()
    # Back the time base off to get more wave info
    #Scope.TimeScaleINC()
    #Scope.VoltageScaleDEC(1)
    #Scope.VoltageScaleDEC(2)
    #Scope.VoltageScaleDEC(3)
    Scope.ScopeSetAverage(16)
    Scope.ScopeUseAverage()
    if Scope.ScopeGetSelect(1)==0:
      Scope.ScopeSetSelect(1,1)
      Scope.VoltageScaleSet(1,0)
    Scope.ScopeCHPosition(1,0)

    # Test and see if the scope
    # is ready for more action
    Scope.ScopeBlock()
    Scope.BusyBlock()
    Scope.SetScopeRunState(0)
```

```
#*************************************************************
    while 1:
      try:
        # Define the Save Info prefix
        Datasave="F"+str(testat)
        filecheck=Datasave+"CH"+str(1)+".dat"
        # Save CH1 Data
        #data=Scope.GetCH(1,Datasave)
        Scope.GetBinCH(1,Datasave)
        if os.path.isfile(filecheck):
          print "Data Read %s Done" % filecheck
          break
        else:
          print "File Not Found Scope"
          print "Locked Up Again Doing"
          print "a 10 Sec Purge"
          Scope.readbutpurge(10)
      except:
          print "File Not Found Scope"
          print "Locked Up Again Doing"
          print "a 10 Sec Purge"
          Scope.readbutpurge(10)

    Scope.SetScopeRunState(1)

  os.chdir("..")

Scope.Shutdown()
redbox.close()

#*************************************************************
# File Name: tektronix.py
# Project: 12-Bit DAC DC Experiment
# Description: This is the Tektronix RS232
#   communication Class pyserial is needed
# for this to work
# Author: Mike Mclain
#*************************************************************
# This is the Tektronix RS232 communication Class
# pyserial is needed for this to work

# VoltageScaleINC(Ch#)  Increment a channels voltage scale
# VoltageScaleDEC(Ch#)  Decrement a channels voltage scale
# ScopeBlock()       Make the scope block all
#              operations until current
#              command
#              is finished
# BusyBlock()      Make the python code block until
```

```
                #the scope is no longer busy
# Shutdown()        Shutdown the RS232
# Startup()         Setup the RS232
# GetInfo()         Get information about the device
# ScopeLock()       Lock the Scopes Buttons
# ScopeUnLock()       Unlock the Scopes Buttons
# GetTPS2024(filepath)  Save channels 1 2 3 4 data
#               to a file path
# GetTDS2002(filepath)  Save channels 1 2 data to a
#               file path
# GetCH(CH#,filepath) Save channel CH# to a file path
# Delay(length)       Pause for X Seconds same
#             as time.sleep()
# ScopeAutoSet()      Performs the auto set operation
#             on the scope
# TimeScaleINC()      Increment the time scale
# TimeScaleDEC()      Decrement the time scale
# ScopeSetMeasurementSource(Mes#,CH#)
#             Set the measurement source to a
#               given CH#
# ScopeCHPosition(CH#,value)
#             Set the Zero voltage position
#               to a given offset
# ScopePrintScreen(filepath)
#             Take a bmp snapshot of the scope
#*************************************************************
import os
import re
import time
import sys
# Needed For Threading
from threading import Thread
# Needed For Rs232
import serial
import struct
from struct import *

#*************************************************************
class Tektronix(Thread):
  def __init__ (self,port,speed):
    Thread.__init__(self)
    self.port=port
    self.speed=speed
    self.voltagescalefactor = [
      "2.0E-2", "5.0E-2", "1.0E-1", "2.0E-1",
      "5.0E-1", "1.0E0", "2.0E0", "5.0E0",
      "1.0E1", "2.0E1", "5.0E1" ]
    self.timescalefactor = [
```

```
      "5.0E1","2.5E1","1.0E1","5.0E0","2.5E0",
      "1.0E0","5.0E-1","2.5E-1","1.0E-1","5.0E-2",
      "2.5E-2","1.0E-2","5.0E-3","2.5E-3","1.0E-3",
      "5.0E-4","2.5E-4","1.0E-4","5.0E-5","2.5E-5",
      "1.0E-5","5.0E-6","2.5E-6","1.0E-6","5.0E-7",
      "2.5E-7","1.0E-7","5.0E-8","2.5E-8","1.0E-8",
      "5.0E-9","2.5E-9"]
      self.fail=""
    def run(self):
      print "RUN"

#*************************************************************
    def Startup(self):
      self.rs232=serial.Serial(port=self.port,
        baudrate=self.speed,
        parity=serial.PARITY_NONE,
        stopbits=serial.STOPBITS_ONE,
        bytesize=serial.EIGHTBITS)
      self.rs232.close()
      self.rs232.open()
      self.rs232.isOpen()

#*************************************************************
    def GetScopeRunState(self):
      self.write('ACQuire:STATE?')
      value=self.readlb()
      self.BusyBlock()
      return value

#*************************************************************
    def SetScopeRunState(self,value):
      if value==1:
        self.write('ACQuire:STATE␣RUN')
      else:
        self.write('ACQuire:STATE␣STOP')
      self.BusyBlock()
#*************************************************************

    def ScopeSetAverage(self,number):
      self.write('ACQuire:NUMAVg␣'+str(number))
      self.BusyBlock()
#*************************************************************

    def ScopeSetSelect(self,ch,state):
      if state==1:
        self.write("SELect:CH%s␣ON"%(str(ch)))
      else:
        self.write("SELect:CH%s␣OFF"%(str(ch)))
```

```
    self.BusyBlock()
#****************************************************************

  def ScopeGetSelect(self,ch):
    self.write("SELect:CH%s?"%(str(ch)))
    data=self.readlb()
    self.BusyBlock()
    data=data.replace('\n','')
    data=data.replace('\r','')
    if int(data)==0:
      return 0
    elif int(data)==1:
      return 1
#****************************************************************

  def ScopeSetMeasurement(self,id,ch):
    self.write("MEASUrement:MEAS%s:SOUrce CH%s"
      %(str(id),str(ch)))
    self.BusyBlock()
#****************************************************************

  def ScopeUseAverage(self):
    self.write("ACQuire:MODe AVERage")
    self.BusyBlock()
#****************************************************************

  def ScopePrintScreen(self,prefix):
    self.write('HARDCopy:BUTTON PRINTS')
    self.write('HARDCopy:FORMat BMP')
    self.write('HARDCopy:LAYout PORTRait')
    self.write('HARDCopy:PORT RS232')

    self.BusyBlock()
    self.write('HARDCopy STARt')

    data=self.readlb()

    if data=="":
      return
    self.writefile(prefix+"Screen.bmp",data)
#****************************************************************

  def ScopeCHPosition(self,ch,number):
    output='CH'+str(ch)+':POSition '+str(number)
    self.write(output)
    self.BusyBlock()
#****************************************************************
```

```
  def ScopeSetMeasurementSource(self,number,ch):
    output=('MEASUrement:MEAS'+str(number)
      +':SOUrce␣CH'+str(ch))
    self.write(output)
    self.BusyBlock()
#*************************************************************

  def ScopeAutoSet(self):
    self.write('AUTOSet␣EXECute')
    self.ScopeBlock()
    self.BusyBlock()
#*************************************************************

  def Delay(self,length):
    time.sleep(length)
#*************************************************************

  def TimeScaleINC(self):
    self.write('HORizontal:MAIn:SCAle?')
    value=self.read()
    value=value.strip()
    if value=="":
      return ""
    for lp in range(len(self.timescalefactor)):
      if self.timescalefactor[lp]==value:
        if(lp-1>-1):
          value=self.timescalefactor[lp-1]
          break

    self.BusyBlock()
    output='HORizontal:MAIn:SCAle␣'+value
    self.rs232.write(output+'\r\n')
#*************************************************************

  def TimeScaleDEC(self):
    self.write('HORizontal:MAIn:SCAle?')
    value=self.read()
    value=value.strip()
    if value=="":
      return ""
    for lp in range(len(self.timescalefactor)):
      if self.timescalefactor[lp]==value:
        if(lp+1<len(self.timescalefactor)):
          value=self.timescalefactor[lp+1]
          break

    self.BusyBlock()
    output='HORizontal:MAIn:SCAle␣'+value
```

```
    self.rs232.write(output+'\r\n')
#*************************************************************

  def VoltageScaleINC(self,number):
    output='CH'+str(number)+':SCAle?'
    self.rs232.write(output+'\r\n')
    value=self.read()
    value=value.strip()
    if value=="":
      return ""
    for lp in range(len(self.voltagescalefactor)):
      if self.voltagescalefactor[lp]==value:
        if(lp+1<len(self.voltagescalefactor)):
          value=self.voltagescalefactor[lp+1]
          break

    self.BusyBlock()
    output='CH'+str(number)+':SCAle '+value
    self.rs232.write(output+'\r\n')
#*************************************************************

  def VoltageScaleSet(self,number,id):
    if id>=0 and id<=len(self.voltagescalefactor):
      value=self.voltagescalefactor[id]
      output='CH'+str(number)+':SCAle '+value
      self.rs232.write(output+'\r\n')
#*************************************************************

  def VoltageScaleDEC(self,number):
    output='CH'+str(number)+':SCAle?'
    self.rs232.write(output+'\r\n')
    value=self.read()
    value=value.strip()
    if value=="":
      return ""
    for lp in range(len(self.voltagescalefactor)):
      if self.voltagescalefactor[lp]==value:
        if(lp-1>-1):
          value=self.voltagescalefactor[lp-1]
          break

    self.BusyBlock()
    output='CH'+str(number)+':SCAle '+value
    self.rs232.write(output+'\r\n')
#*************************************************************

  def ScopeBlock(self):
    self.rs232.write('*WAI\r\n')
```

```
#*************************************************************

  def BusyBlock(self):
    while 1:
      self.rs232.write('BUSY?\r\n')
      value=self.readb()
      if value=="":
        continue
      if value.strip()!="1":
        break
#*************************************************************

  def Shutdown(self):
    self.rs232.close()
#*************************************************************

  def GetId(self):
    self.rs232.write('ID?\r\n')
    data= self.read()
    return data
#*************************************************************

  def GetInfo(self):
    self.rs232.write('ID?\r\n')
    data= self.read()
    if data=="":
      return ""
    dataA = data.split(',')
    dataB = dataA[0].split('/')
    return dataB[1]
#*************************************************************

  def ScopeLock(self):
    self.rs232.write('LOCk ALL\r\n')
#*************************************************************

  def ScopeUnLock(self):
    self.rs232.write('UNLock ALL\r\n')
#*************************************************************

  def GetTPS2024(self,prefix):
    self.ScopeLock()
    self.GetCH(1,prefix)
    self.GetCH(2,prefix)
    self.GetCH(3,prefix)
    self.GetCH(4,prefix)
    self.ScopeUnLock()
#*************************************************************
```

```
  def GetTDS2002(self,prefix):
    self.ScopeLock()
    self.GetCH(1,prefix)
    self.GetCH(2,prefix)
    self.ScopeUnLock()
#**************************************************************

  def GetDataWidth(self):
    self.rs232.write('DATa:WIDth?\r\n')
    return self.read()
#**************************************************************

  def SetDataWidth(self,width):
    self.write('DATa:WIDth %s'%str(width))
#**************************************************************

  def SetDataEncoding(self,code):
    self.write('DATa:ENCdg %s'%code)
#**************************************************************

  def GetBinCH(self,number,prefix):
    self.rs232.write('DATa:SOUrce CH'
      +str(number)+'\r\n')
    self.SetDataWidth(1)
    self.SetDataEncoding('RIBinary')

    # Get the units
    self.rs232.write('WFMPre:WFId?\r\n')
    units=self.read()
    if units=="":
      return
    unitsA= units.split(',')
    voltsS=unitsA[2]
    voltsA=voltsS.split()
    voltsV=voltsA[0]
    timeS=unitsA[3]
    timeA=timeS.split()
    timeV=timeA[0]

    voltsVf=float(timeV)
    timeVf=float(timeV)

    self.rs232.write('WFMPre:YOFf?\r\n')
    yoff=self.read()
    if yoff=="":
      return
    yoffF=float(yoff)
```

```
self.rs232.write('WFMPre:YMUlt?\r\n')
Ymult=self.read()
if Ymult=="":
  return
YmultF=float(Ymult)

self.rs232.write('WFMPre:YZEro?\r\n')
YZero=self.read()
if YZero=="":
  return
YZeroF=float(YZero)

self.rs232.write('WFMPre:XINcr?\r\n')
Xinc=self.read()
if Xinc=="":
  return
XincF=float(Xinc)

self.rs232.write('CURVe?\r\n')
data=self.readlb()
if data=="":
  return


self.SetDataWidth(1)
self.SetDataEncoding('ASCIi')
self.rs232.write('CURVe?\r\n')
data2=self.readlb()
if data2=="":
  return
#dataA=data2.split(',')
#print len(dataA)
#print len(data)

#debug=''
#for lp in range(0,len(dataA),1):
#    debug+=str(ord(data[lp]))+" "
# +dataA[lp]+"\r\n"
#
#self.writefile(prefix+"CH"+str(number)
# +".dat",debug)
#return

out=''
index=0
for lp in range(6,len(data)-2,1):
  pointsF=float(unpack('b',
```

```
            pack('c',data[lp]))[0])
          value=((pointsF-yoffF)*YmultF)+YZeroF
          out+=str(index*XincF)+"\t"+str(value)+"\r\n"
          index=index+1
        self.fail="File Write"
        print prefix+"CH"+str(number)+".dat"
        self.writefile(prefix+"CH"+str(number)+".dat",out)
        return out
#*************************************************************

    def GetCH(self,number,prefix):
        out=''

        # Set the Scope up
        self.rs232.write('DATa:SOUrce CH'
          +str(number)+'\r\n')
        #self.rs232.write('DATa:WIDth 1\r\n')
        self.SetDataWidth(1)
        self.SetDataEncoding('ASCIi')
        #self.rs232.write('DATa:ENCdg ASCIi\r\n')

        # Get the units
        self.rs232.write('WFMPre:WFId?\r\n')
        units=self.read()
        if units=="":
          return
        unitsA= units.split(',')
        voltsS=unitsA[2]
        voltsA=voltsS.split()
        voltsV=voltsA[0]
        timeS=unitsA[3]
        timeA=timeS.split()
        timeV=timeA[0]

        voltsVf=float(timeV)
        timeVf=float(timeV)

        self.rs232.write('WFMPre:YOFf?\r\n')
        yoff=self.read()
        if yoff=="":
          return
        yoffF=float(yoff)

        self.rs232.write('WFMPre:YMUlt?\r\n')
        Ymult=self.read()
        if Ymult=="":
          return
        YmultF=float(Ymult)
```

```
        self.rs232.write('WFMPre:YZEro?\r\n')
        YZero=self.read()
        if YZero=="":
          return
        YZeroF=float(YZero)

        self.rs232.write('WFMPre:XINcr?\r\n')
        Xinc=self.read()
        if Xinc=="":
          return
        XincF=float(Xinc)

        self.rs232.write('CURVe?\r\n')
        data=self.readlb()
        if data=="":
          return

        dataA=data.split(',')
        index=0
        for points in dataA:
          self.fail=points
          pointsF=float(points)
          value=((pointsF-yoffF)*YmultF)+YZeroF
          out+=str(index*XincF)+"\t"+str(value)+"\r\n"
          index=index+1
        self.fail="File Write"
        self.writefile(prefix+"CH"
          +str(number)+".dat",out)
        return out
    #*************************************************************

    def DebugGetCH(self,number,prefix):
        out=''

        # Set the Scope up
        self.rs232.write('DATa:SOUrce CH'
          +str(number)+'\r\n')
        self.rs232.write('DATa:WIDth 1\r\n')
        self.rs232.write('DATa:ENCdg ASCIi\r\n')

        # Get the units
        self.rs232.write('WFMPre:WFId?\r\n')
        units=self.read()
        print units
        if units=="":
          return
        unitsA= units.split(',')
```

```
voltsS=unitsA[2]
voltsA=voltsS.split()
voltsV=voltsA[0]
timeS=unitsA[3]
timeA=timeS.split()
timeV=timeA[0]

voltsVf=float(timeV)
timeVf=float(timeV)

self.rs232.write('WFMPre:YOFf?\r\n')
yoff=self.read()
print yoff
if yoff=="":
  return
yoffF=float(yoff)

self.rs232.write('WFMPre:YMUlt?\r\n')
Ymult=self.read()
print Ymult
if Ymult=="":
  return
YmultF=float(Ymult)

self.rs232.write('WFMPre:YZEro?\r\n')
YZero=self.read()
print YZero
if YZero=="":
  return
YZeroF=float(YZero)

self.rs232.write('WFMPre:XINcr?\r\n')
Xinc=self.read()
print Xinc
if Xinc=="":
  return
XincF=float(Xinc)

self.rs232.write('CURVe?\r\n')
data=self.read()
print data
return
if data=="":
  return

dataA=data.split(',')
index=0
out=""
```

```
    for points in dataA:
      if points=="" or points==None:
        continue
      self.fail=points
      pointsF=float(points)
      value=((pointsF-yoffF)*YmultF)+YZeroF
      out+=str(index*XincF)+"\t"+str(value)+"\r\n"
      index=index+1
    self.fail="File Write"
    print prefix+"CH"+str(number)+".dat"
    self.writefile(prefix+"CH"
      +str(number)+".dat",out)
    return out
#**************************************************************

  def writefile(self,name,data):
    file = open(name,"wb")
    file.write(data)
    file.close()
#**************************************************************

  def write(self,data):
    self.rs232.write(data+'\r\n')
#**************************************************************

  def readbutpurge(self,intime):
    out=''
    done=0
    count=0
    while done==0:
      if count>intime:
        break
      while self.rs232.inWaiting() > 0:
        out += self.rs232.read(
          self.rs232.inWaiting())
      time.sleep(1)
      count=count+1
#**************************************************************

  def readb(self): # no timeout read
    out=''
    done=0
    while done==0:
      while self.rs232.inWaiting() > 0:
        done=1
        out += self.rs232.read(
          self.rs232.inWaiting())
        time.sleep(.1)
```

```
    return out
#*****************************************************

  def readlb(self): # no timeout read long blocking
    out=''
    done=0
    while done==0:
      while self.rs232.inWaiting() > 0:
        done=1
        out += self.rs232.read(
          self.rs232.inWaiting())
        time.sleep(1)
    return out
#*****************************************************

  def read(self):
    out=''
    done=0
    # if you dont have any data
    if self.rs232.inWaiting()<=0:
      # wait 1 second
      time.sleep(1)
      # check again
      if self.rs232.inWaiting()<=0:
        # if still no data abort
        return "";
    while done==0:
      while self.rs232.inWaiting() > 0:
        done=1
        out += self.rs232.read(
          self.rs232.inWaiting())
        time.sleep(.1)
    return out
#*****************************************************

#*****************************************************
# File Name: agilent.py
# Project: 12-Bit DAC DC Experiment
# Description: This is the Agilent RS232
#   communication Class pyserial is needed
# for this to work
# Author: Mike Mclain
#*****************************************************
# This is the Agilent RS232 communication Class
# pyserial is needed for this to work
# Shutdown()  Shutdown the RS232
# Startup()   Setup the RS232
# GetId()   Get the Id of the Agilent Device
```

```
# ApplyWave(type,freq,freq unit,amp,
# amp unit,offset,offset unit)
#       Set the function generator waveform
# Delay(length) Pause for X Seconds same as time.sleep()
#*************************************************************

import os
import re
import time
import sys
# Needed For Threading
from threading import Thread
# Needed For Rs232
import serial
#*************************************************************
class Agilent(Thread):
  def __init__ (self,port,speed):
    Thread.__init__(self)
    self.port=port
    self.speed=speed
#*************************************************************

  def run(self):
    print "RUN"
#*************************************************************

  def Startup(self):
    self.rs232=serial.Serial(port=self.port,
      baudrate=self.speed,
      parity=serial.PARITY_NONE,
      stopbits=serial.STOPBITS_TWO,
      bytesize=serial.EIGHTBITS)
    self.rs232.close()
    self.rs232.open()
    self.rs232.isOpen()
#*************************************************************

  def ApplyWave(self,type,freq,funit,amp,
    aunit,offset,ounit):
    output= 'APPL:'+type+' '+str(freq)+' '
    +funit+',0,'+str(amp)+' '+aunit+',0,'
    +str(offset)+' '+ounit
    self.write(output)
#*************************************************************

  def GetId(self):
    self.write('*IDN?')
    print self.read()
```

```
#*****************************************************************

  def Delay(self,length):
    time.sleep(length)
#*****************************************************************

  def Shutdown(self):
    self.rs232.close()
#*****************************************************************

  def writefile(self,name,data):
    file = open(name,"wb")
    file.write(data)
    file.close()
#*****************************************************************

  def write(self,data):
    self.rs232.write(data+'\r\n')
#*****************************************************************

  def readb(self): # no timeout read
    out=''
    done=0
    while done==0:
      while self.rs232.inWaiting() > 0:
        done=1
        out += self.rs232.read(
          self.rs232.inWaiting())
        time.sleep(.1)
    return out
#*****************************************************************
  def readlb(self): # no timeout read long blocking
    out=''
    done=0
    while done==0:
      while self.rs232.inWaiting() > 0:
        done=1
        out += self.rs232.read(
          self.rs232.inWaiting())
        time.sleep(1)
    return out
#*****************************************************************

  def read(self):
    out=''
    done=0
    # if you dont have any data
    if self.rs232.inWaiting()<=0:
```

```
        # wait 1 second
        time.sleep(1)
        # check again
        if self.rs232.inWaiting()<=0:
          # if still no data abort
          return "";
      while done==0:
        while self.rs232.inWaiting() > 0:
          done=1
          out += self.rs232.read(
            self.rs232.inWaiting())
          time.sleep(.1)
      return out
#**************************************************************
```

APPENDIX B: AC CIE EFFECTS TEST CODE

The code presented within this appendix was utilized to perform a laboratory experiment in which, a Tektronix AFG3102 function generator was remotely controlled, via the Tekvisa USB protocol, by a Python application and the output voltage observed — via three Tektronix oscilloscopes (one TPS2024 and two TDS2002) — was acquired and transferred back to the Python application — via RS–232 protocol.

The following Python code was written within a standard text editor and was utilized to convey function generator commands over the Tekvisa USB communication interface, while, at the same time, also conveying oscilloscope commands over the RS–232 communication interface in order to create and acquire the required test signals.

```
#*********************************************************
# File Name: CIETeset.py
# Project: AC CIE Experiment
# Description: Main Python Application
# Author: Mike Mclain
#*********************************************************
# Voltage and Frequency Automatic Sampling System V 2.0
import sys
import os
import time
pathname = os.path.dirname(sys.argv[0])
fullpath=os.path.abspath(pathname)
sys.path.append('%s/Class' % fullpath)
import Tektronix
import rs232
import threading


#*********************************************************
# A Threaded Class to Talk TPS2024 to the Scope
#*********************************************************
class Scope_TPS2024_Get(threading.Thread):
  def __init__(self,Scope_TPS2024):
    self.Scope_TPS2024=Scope_TPS2024
    self.result=[]
    threading.Thread.__init__(self)
  def run(self):
    print "Waiting for TPS2024 Scope Synchronization"
    self.Scope_TPS2024.Wait()
    self.Scope_TPS2024.Wait_While_Busy()
    for channel in [
      Tektronix.Scope.Scope_Data_Source_CH1,
      Tektronix.Scope.Scope_Data_Source_CH2,
      Tektronix.Scope.Scope_Data_Source_CH3,
      Tektronix.Scope.Scope_Data_Source_CH4]:
      print ("""TPS2024:Geting
```

```
        Waveform from %s""" % channel
      Data=self.Scope_TPS2024.Get_Waveform(channel)
      self.result.append(Data)
      print "TPS2024:Got Waveform from %s" % channel

#************************************************************
# Threaded Class to talk to TPS2002 Scope
#************************************************************
class Scope_TPS2002_Get(threading.Thread):
  def __init__(self,Scope_TPS2002,id):
    self.id=id
    self.Scope_TPS2002=Scope_TPS2002
    self.result=[]
    threading.Thread.__init__(self)
  def run(self):
    print """Waiting for TPS2002 #%d Scope
    Synchronization""" % self.id
    self.Scope_TPS2002.Wait()
    self.Scope_TPS2002.Wait_While_Busy()
    for channel in [
      Tektronix.Scope.Scope_Data_Source_CH1,
      Tektronix.Scope.Scope_Data_Source_CH2]:
      print """TPS2002_%d:Geting Waveform
      from %s""" % (self.id,channel)
      Data=self.Scope_TPS2002.Get_Waveform(channel)
      self.result.append(Data)
      print """TPS2002_%d:Got Waveform
        from %s""" % (self.id,channel)

#************************************************************
# Wait for Scopes to Sync
#************************************************************
def Scope_Wait(Scope_TPS2024,Scope_TPS2002_1,
  Scope_TPS2002_2):
  print "Waiting for Scope Synchronization"
  # Ensure our scopes self synchronize
  Scope_TPS2024.Wait()
  Scope_TPS2002_1.Wait()
  Scope_TPS2002_2.Wait()
  # Wait untill all scopes are ready
  Scope_TPS2024.Wait_While_Busy()
  print "TPS2024 Ready"
  Scope_TPS2002_1.Wait_While_Busy()
  print "TPS2002 #1 Ready"
  Scope_TPS2002_2.Wait_While_Busy()
  print "TPS2002 #2 Ready"

#************************************************************
```

```
# print the run time
#*************************************************************
def Run_Time(atime):
  Current_Time = time.time()
  Current_Seconds=Current_Time-atime
  # Show Info in H:M:S
  Current_Hours=int(Current_Seconds/3600)
  Current_Seconds=Current_Seconds-3600*Current_Hours
  Current_Minutes=int(Current_Seconds / 60)
  Current_Seconds=Current_Seconds-60*Current_Minutes

  return " %d:%d:%f" %(Current_Hours,
    Current_Minutes,float(Current_Seconds))

#*************************************************************
# Make a Log File
#*************************************************************
def Status(name,file_path,message):
  try:
    print "Write to status"
    if os.path.exists(file_path)==1:
      Status_File = open(file_path,"a")
    else:
      Status_File = open(file_path,"w")
    Status_File.write("%s: %s\r\n" % (name,message))
    Status_File.close()
  except:
    print "Status Write Error"

#*************************************************************
# Program Will Start Here
#*************************************************************


# Setup Save Location
Save_Data_Input = raw_input(
  "Enter New Folder Name to Save Data: ")
Save_Data_Path="./%s" % Save_Data_Input
Status_Path="%s/status.txt"%(Save_Data_Path)

Index_Reload=False
Index_Last_Index=0
Index_Last_Freq=0
Index_Last_Volt=0

#*************************************************************
if os.path.exists(Save_Data_Path)==1:
  print "Folder %s Already Exists" % Save_Data_Path
```

```
  print "Trying to Recover from last index"
  Output_Index_Name="%s/index.txt"%(Save_Data_Path)
  if os.path.exists(Output_Index_Name)==1:
    Output_Index_File = open(Output_Index_Name,"r")
    Index_File_Data=Output_Index_File.read()
    Output_Index_File.close()

    print "Finding last Good Index"
    Index_Segments=Index_File_Data.split('\n')
    Index_Segments_Number=len(Index_Segments)
    print "Found %d Keys" % Index_Segments_Number
    # -2 becuase the extra \n\r adds
    # a extra element that is bad
    Index_last_core=Index_Segments_Number-2
    if Index_Segments_Number-2>=0:
      Index_Last=Index_Segments[
        Index_Segments_Number-2]
      Index_Last_s=Index_Last.replace('\r',"")
      Index_Last_s=Index_Last_s.strip()
      Index_Last_a=Index_Last_s.split('\t')
      print "Found %d Subkeys" % len(Index_Last_a)
      Index_Last_Index=int(Index_Last_a[0])
      Index_Last_Freq=float(Index_Last_a[1])
      Index_Last_Volt=float(Index_Last_a[2])
      print """Restart from index %d at
        Freq=%f Volt=%f"""%(Index_Last_Index,
          Index_Last_Freq,Index_Last_Volt)
      Status(Save_Data_Input,Status_Path,
      "Restart from index %d at Freq=%f Volt=%f"%(
        Index_Last_Index,Index_Last_Freq,
        Index_Last_Volt))
    else:
      print "Error in Index File TOC"
      Status(Save_Data_Input,Status_Path,
        "Error Reload Failed")
      exit()
    Index_Reload=True

  else:
    Status(Save_Data_Input,Status_Path,
      "Error No Index Found")
    print "No index found Closing Application"
    exit()
else:
  print "Makeing Folder %s" % Save_Data_Path
  os.makedirs(Save_Data_Path)
```

```
Status(Save_Data_Input,Status_Path,"Starting Test")

# setup start time
App_Start_Time = time.time()
#*******************************************************
# Setup our Data acquisition System
#*******************************************************
Generator_AFG3000=Tektronix.Generator(
  "USB::0x0699::0x0343::C020495::INSTR")
Scope_TPS2024=Tektronix.Scope(
  rs232.com_defines.Get_Port(5),19200,"\r\n","TDS2024")
Scope_TPS2002_1=Tektronix.Scope(
  rs232.com_defines.Get_Port(4),19200,"\r\n","TPS2002 1")
Scope_TPS2002_2=Tektronix.Scope(
  rs232.com_defines.Get_Port(6),19200,"\r\n","TPS2002 2")

# Open all Scopes
Scope_TPS2024.Open()
Scope_TPS2002_1.Open()
Scope_TPS2002_2.Open()

# Open Generator
Generator_AFG3000.Open()

print "Found IDs"
print "1",Scope_TPS2024.Get_ID()
print "2",Scope_TPS2002_1.Get_ID()
print "3",Scope_TPS2002_2.Get_ID()

#*******************************************************
# Setup Generator
#*******************************************************
Generator_AFG3000.Generator_Reset()
Generator_AFG3000.Generator_Function(
  Tektronix.Generator.Generator_Channel_1,"SIN")
Generator_AFG3000.Generator_Voltage(
  Tektronix.Generator.Generator_Channel_1,1)
Generator_AFG3000.Generator_Frequency(
  Tektronix.Generator.Generator_Channel_1,1000)
Generator_AFG3000.Generator_Output(
  Tektronix.Generator.Generator_Channel_1,
  Tektronix.Generator.Generator_Output_Off)
Generator_AFG3000.Generator_Output(
  Tektronix.Generator.Generator_Channel_2,
  Tektronix.Generator.Generator_Output_Off)

print "Reset Scope"
# Setup Scope
```

```
Scope_TPS2024.Reset()
Scope_TPS2002_1.Reset()
Scope_TPS2002_2.Reset()

#*********************************************************
print "Stoping all data acquisition"
Scope_TPS2024.Set_Acquire_Mode(
  Tektronix.Scope.Scope_Acquire_State_Stop)
Scope_TPS2002_1.Set_Acquire_Mode(
  Tektronix.Scope.Scope_Acquire_State_Stop)
Scope_TPS2002_2.Set_Acquire_Mode(
  Tektronix.Scope.Scope_Acquire_State_Stop)
#*********************************************************
Scope_Wait(Scope_TPS2024,Scope_TPS2002_1,Scope_TPS2002_2)

print "Setup Scope"
#*********************************************************
# Setup Channels
#*********************************************************
for channel in [Tektronix.Scope.Scope_Channel_1,
  Tektronix.Scope.Scope_Channel_2,
  Tektronix.Scope.Scope_Channel_3,
  Tektronix.Scope.Scope_Channel_4]:

  # Set Channel On
  Scope_TPS2024.Set_Channel_State(
    channel,Tektronix.Scope.Scope_Channel_On)
  if channel<=Tektronix.Scope.Scope_Channel_2:
    Scope_TPS2002_1.Set_Channel_State(
      channel,Tektronix.Scope.Scope_Channel_On)
    Scope_TPS2002_2.Set_Channel_State(
      channel,Tektronix.Scope.Scope_Channel_On)

  # Set Bandwidth Limit On (20Mhz)
  Scope_TPS2024.Set_Channel_Bandwidth(
    channel,Tektronix.Scope.Scope_On)
  if channel<=Tektronix.Scope.Scope_Channel_2:
    Scope_TPS2002_1.Set_Channel_Bandwidth(
      channel,Tektronix.Scope.Scope_On)
    Scope_TPS2002_2.Set_Channel_Bandwidth(
      channel,Tektronix.Scope.Scope_On)
#*********************************************************
# Set DC Coupling
#*********************************************************
  Scope_TPS2024.Set_Channel_Coupling(
    channel,Tektronix.Scope.Scope_Coupling_DC)
  if channel<=Tektronix.Scope.Scope_Channel_2:
    Scope_TPS2002_1.Set_Channel_Coupling(
```

```
        channel,Tektronix.Scope.Scope_Coupling_DC)
      Scope_TPS2002_2.Set_Channel_Coupling(
        channel,Tektronix.Scope.Scope_Coupling_DC)

    # Set Invert off
    Scope_TPS2024.Set_Channel_Invert(
      channel,Tektronix.Scope.Scope_Off)
    if channel<=Tektronix.Scope.Scope_Channel_2:
      Scope_TPS2002_1.Set_Channel_Invert(
        channel,Tektronix.Scope.Scope_Off)
      Scope_TPS2002_2.Set_Channel_Invert(
        channel,Tektronix.Scope.Scope_Off)
#*********************************************************
# Set Position to zero
#*********************************************************
    Scope_TPS2024.Set_Channel_Position(channel,0)
    if channel<=Tektronix.Scope.Scope_Channel_2:
      Scope_TPS2002_1.Set_Channel_Position(channel,0)
      Scope_TPS2002_2.Set_Channel_Position(channel,0)

    # Set Probe to 10x
    Scope_TPS2024.Set_Channel_Probe(channel,
      Tektronix.Scope.Scope_Probe_10)
    if channel<=Tektronix.Scope.Scope_Channel_2:
      Scope_TPS2002_1.Set_Channel_Probe(channel,
        Tektronix.Scope.Scope_Probe_10)
      Scope_TPS2002_2.Set_Channel_Probe(channel,
        Tektronix.Scope.Scope_Probe_10)

Scope_Wait(Scope_TPS2024,Scope_TPS2002_1,Scope_TPS2002_2)

print "␣Generator␣Online␣to␣Help␣Trigger"
Generator_AFG3000.Generator_Output(
  Tektronix.Generator.Generator_Channel_1,
  Tektronix.Generator.Generator_Output_On)

print "Setup␣Trigger"
#*********************************************************
# Setup Scope Trigger Type to Edge
#*********************************************************
Scope_TPS2024.Set_Trigger_Type(
  Tektronix.Scope.Scope_Trigger_Type_Edge)
Scope_TPS2002_1.Set_Trigger_Type(
  Tektronix.Scope.Scope_Trigger_Type_Edge)
Scope_TPS2002_2.Set_Trigger_Type(
  Tektronix.Scope.Scope_Trigger_Type_Edge)

# Setup Scope Trigger Edge Coupling to DC
```

```
Scope_TPS2024.Set_Trigger_Coupling(
  Tektronix.Scope.Scope_Trigger_Edge_DC)
Scope_TPS2002_1.Set_Trigger_Coupling(
  Tektronix.Scope.Scope_Trigger_Edge_DC)
Scope_TPS2002_2.Set_Trigger_Coupling(
  Tektronix.Scope.Scope_Trigger_Edge_DC)

# Setup Scope Trigger Edge Slope to Rise
Scope_TPS2024.Set_Trigger_Slope(
  Tektronix.Scope.Scope_Trigger_Edge_Rise)
Scope_TPS2002_1.Set_Trigger_Slope(
  Tektronix.Scope.Scope_Trigger_Edge_Rise)
Scope_TPS2002_2.Set_Trigger_Slope(
  Tektronix.Scope.Scope_Trigger_Edge_Rise)

# Setup Scope Trigger Source to EXT
Scope_TPS2024.Set_Trigger_Source(
  Tektronix.Scope.Scope_Trigger_Source_CH1)
Scope_TPS2002_1.Set_Trigger_Source(
  Tektronix.Scope.Scope_Trigger_Source_CH1)
Scope_TPS2002_2.Set_Trigger_Source(
  Tektronix.Scope.Scope_Trigger_Source_CH1)

#*********************************************************
# Setup Scope Trigger Mode to Auto
#*********************************************************
Scope_TPS2024.Set_Trigger_Mode(
  Tektronix.Scope.Scope_Trigger_Mode_Auto)
Scope_TPS2002_1.Set_Trigger_Mode(
  Tektronix.Scope.Scope_Trigger_Mode_Auto)
Scope_TPS2002_2.Set_Trigger_Mode(
  Tektronix.Scope.Scope_Trigger_Mode_Auto)

Scope_Wait(Scope_TPS2024,Scope_TPS2002_1,Scope_TPS2002_2)

# Setup Scope Acquire runstop mode to Sequence
Scope_TPS2024.Set_Acquire_Stop_After(
  Tektronix.Scope.Scope_Acquire_Stop_Mode_Sequence)
Scope_TPS2002_1.Set_Acquire_Stop_After(
  Tektronix.Scope.Scope_Acquire_Stop_Mode_Sequence)
Scope_TPS2002_2.Set_Acquire_Stop_After(
  Tektronix.Scope.Scope_Acquire_Stop_Mode_Sequence)

# Setup Acquire Mode average
Scope_TPS2024.Set_Acquire_Mode(
  Tektronix.Scope.Scope_Acquire_Mode_Average)
Scope_TPS2002_1.Set_Acquire_Mode(
  Tektronix.Scope.Scope_Acquire_Mode_Average)
```

```
Scope_TPS2002_2.Set_Acquire_Mode(
   Tektronix.Scope.Scope_Acquire_Mode_Average)
#*************************************************************
# Setup Acquire Mode average number to 16
#*************************************************************
Scope_TPS2024.Set_Acquire_Number_Acquisitions(
   Tektronix.Scope.Scope_Acquire_Acquisitions_16)
Scope_TPS2002_1.Set_Acquire_Number_Acquisitions(
   Tektronix.Scope.Scope_Acquire_Acquisitions_16)
Scope_TPS2002_2.Set_Acquire_Number_Acquisitions(
   Tektronix.Scope.Scope_Acquire_Acquisitions_16)

Scope_Wait(Scope_TPS2024,Scope_TPS2002_1,Scope_TPS2002_2)


print "␣Generator␣Now␣Offline"
Generator_AFG3000.Generator_Output(
   Tektronix.Generator.Generator_Channel_1,
   Tektronix.Generator.Generator_Output_On)

# Setup a Generator Test array
Test_CH1_Frequency_Hz=[]
Test_CH1_Voltages_Vpk=[]

#*************************************************************
# Experment Code Starts here
#*************************************************************
print "Starting␣Test␣Demo␣1"

#*************************************************************
# Experment Mapping
# Scope_TPS2024
   # Ch1 Vin A
   # Ch2 After R1
   # Ch3 Before R2
   # Ch4 A2

# Scope_TDS2002_1
   # Ch1 Vin B
   # Ch2 A1

# Scope_TDS2002_2
   # Ch1 Vin C
   # Ch2 A3
#*************************************************************
Test_Mode=2
Test_Stabilizing_Time=10
Test_Number_of_Periods=3.0
```

```
Scope_Number_of_Time_Division=11.0
#Scope_Voltage_Overshoot_Factor=0.28
Scope_Voltage_Overshoot_Factor=0.45
Scope_Voltage_Overshoot_Find_Factor=5
Scope_Number_of_Voltage_Division=9.0

#*************************************************************
if Test_Mode==1:
  Test_CH1_Frequency_Hz=[1.0]
  Test_CH1_Voltages_Vpk=[.1]
elif Test_Mode==2:
  Test_CH1_Frequency_Hz=[1.0,4.3,18.0,79.0,
    341.0,1500.0,6300.0,27000.0,116000.0,
      500000.0,1000000.0]
  Test_CH1_Voltages_Vpk=[.1,.17,.28,.46,.77,
    1.29,2.15,3.6,6.0,10.0]


#*************************************************************
print "Makeing Output Index File"
Output_Index_Name="%s/index.txt"%(Save_Data_Path)
Output_Index_Counter=0
if Index_Reload==False:
  Output_Index_File = open(Output_Index_Name,"w")
  Output_Index_File.write(
    "Index\tFrequency\tVoltage\r\n")
  Output_Index_File.close()
else:
  print "Starting Restart"
  Output_Index_Counter=Index_Last_Index+1
  print """Save File index
    now at %d""" % Output_Index_Counter

print "Setup Took %s" % Run_Time(App_Start_Time)
Status(Save_Data_Input,Status_Path,
  "Setup Took %s"% Run_Time(App_Start_Time))



F_Can_Run=False
V_Can_Run=False
#*************************************************************
#*************************************************************
for Frequency in Test_CH1_Frequency_Hz:
  Rev_Start_Time = time.time()

  if Index_Reload==True:
    if Frequency==Index_Last_Freq:
```

```
        print "Found Reload Point at  %f" % Frequency
        F_Can_Run=True
    else:
      F_Can_Run=True
      V_Can_Run=True

    if F_Can_Run==True and V_Can_Run==True:
      print """Generator Frequency
        Now at %f Hz""" % Frequency
      Generator_AFG3000.Generator_Frequency(
      Tektronix.Generator.Generator_Channel_1,Frequency)
#************************************************************
      # Calculate Time Scale
#************************************************************
      Peroid=1.0/Frequency
      Time_Scale_Factor=((Peroid*Test_Number_of_Periods)
        /Scope_Number_of_Time_Division)

      print """Setting all Scopes to have
        time scale factor of %f""" % Time_Scale_Factor
      Scope_TPS2024.Set_Horizontal_Scale(
        Time_Scale_Factor)
      Scope_TPS2002_1.Set_Horizontal_Scale(
        Time_Scale_Factor)
      Scope_TPS2002_2.Set_Horizontal_Scale(
        Time_Scale_Factor)
#************************************************************
    for Voltage in Test_CH1_Voltages_Vpk:
      Set_Start_Time = time.time()

      if Index_Reload==True:
        if F_Can_Run==True:
          if Voltage==Index_Last_Volt:
            print """Found Reload Voltage
              Point at %f""" % Voltage
            V_Can_Run=True
            # it is a good idea to load the
            #function generator at this point
            print """Generator Frequency
              Now at %f Hz""" % Frequency
            Generator_AFG3000.Generator_Frequency(
            Tektronix.Generator.Generator_Channel_1,
            Frequency)
#************************************************************
            # Calculate Time Scale
            Peroid=1.0/Frequency
            Time_Scale_Factor=(
            (Peroid*Test_Number_of_Periods)
```

```
            /Scope_Number_of_Time_Division)

                print """Setting all Scopes to have
            time scale factor of %f""" % Time_Scale_Factor
                Scope_TPS2024.Set_Horizontal_Scale(
                Time_Scale_Factor)
                Scope_TPS2002_1.Set_Horizontal_Scale(
                Time_Scale_Factor)
                Scope_TPS2002_2.Set_Horizontal_Scale(
                Time_Scale_Factor)
#***********************************************************
                # Force movement to next point
                continue
        else:
            V_Can_Run=True
#***********************************************************
        if V_Can_Run==True:
            Status(Save_Data_Input,Status_Path,
            "At␣Freq=%f␣at␣Voltage=%f"% (Frequency,Voltage))

            print """Generator Voltage Now at
            %f Vp or %f Vpp""" % (Voltage,2*Voltage)
            # Note this is currently set to
            # Vp becuase of non high z matching
            Generator_AFG3000.Generator_Voltage(
            Tektronix.Generator.Generator_Channel_1,
            Voltage)
            print "Generator␣is␣now␣On"
            Generator_AFG3000.Generator_Output(
            Tektronix.Generator.Generator_Channel_1,
            Tektronix.Generator.Generator_Output_On)
            print """Delay of %f for
        System Stabilization""" % (Test_Stabilizing_Time)
            time.sleep(Test_Stabilizing_Time)
#***********************************************************
            # Calculate Default Voltage Scale Factor
            Max_Voltage_Scale=((Voltage*2)+(Voltage*2)
                *Scope_Voltage_Overshoot_Find_Factor)
            /Scope_Number_of_Voltage_Division

            Scope_Wait(Scope_TPS2024,Scope_TPS2002_1,
              Scope_TPS2002_2)

            print """Setting all Scope channels to
            have voltage scale factor
            of %f""" % Max_Voltage_Scale
#***********************************************************
            for channel in [Tektronix.Scope.Scope_Channel_1,
```

```
        Tektronix.Scope.Scope_Channel_2,
        Tektronix.Scope.Scope_Channel_3,
        Tektronix.Scope.Scope_Channel_4]:
          Scope_TPS2024.Set_Channel_Scale(
          channel,Max_Voltage_Scale)
          if channel<=Tektronix.Scope.Scope_Channel_2:
            Scope_TPS2002_1.Set_Channel_Scale(
            channel,Max_Voltage_Scale)
            Scope_TPS2002_2.Set_Channel_Scale(
            channel,Max_Voltage_Scale)

        Scope_Wait(Scope_TPS2024,Scope_TPS2002_1,
        Scope_TPS2002_2)

        # Take a Scope Sample now
        Scope_TPS2024.Set_Acquire_State(
        Tektronix.Scope.Scope_Acquire_State_On)
        Scope_TPS2002_1.Set_Acquire_State(
        Tektronix.Scope.Scope_Acquire_State_On)
        Scope_TPS2002_2.Set_Acquire_State(
        Tektronix.Scope.Scope_Acquire_State_On)

        Scope_Wait(Scope_TPS2024,Scope_TPS2002_1,
        Scope_TPS2002_2)
#*********************************************************
        # Get info about DC Offsets
        Scope_TPS2024.Set_Immediate_Measurement_Type(
        Tektronix.Scope.Scope_Measurement_Type_Mean)
        Scope_TPS2002_1.Set_Immediate_Measurement_Type(
        Tektronix.Scope.Scope_Measurement_Type_Mean)
        Scope_TPS2002_2.Set_Immediate_Measurement_Type(
        Tektronix.Scope.Scope_Measurement_Type_Mean)

        # define array and index
        Scope_TPS2024_Index=0
        Scope_TPS2002_1_Index=1
        Scope_TPS2002_2_Index=2
        Scope_String=["TPS␣2024","TPS2002␣#1",
        "TPS2002␣#2"]

        # define info for DC offset
        DC_Offsets=[[],[],[]]

        Scope_Wait(Scope_TPS2024,Scope_TPS2002_1,
        Scope_TPS2002_2)

#*********************************************************
        print "Beginning␣customized␣auto␣fit"
```

```
        for channel in [
        Tektronix.Scope.Scope_Data_Source_CH1,
        Tektronix.Scope.Scope_Data_Source_CH2,
        Tektronix.Scope.Scope_Data_Source_CH3,
        Tektronix.Scope.Scope_Data_Source_CH4]:
          print "Geting␣DC␣info␣from␣%s" % channel
          Scope_TPS2024
            .Set_Immediate_Measurement_Source(
            channel)
          if not (
          channel==
          Tektronix.Scope.Scope_Data_Source_CH3
          and not
          channel==
          Tektronix.Scope.Scope_Data_Source_CH4):
            Scope_TPS2002_1.
            Set_Immediate_Measurement_Source(
            channel)
            Scope_TPS2002_2.
            Set_Immediate_Measurement_Source(
            channel)
#*********************************************************
          Scope_Wait(Scope_TPS2024,
          Scope_TPS2002_1,Scope_TPS2002_2)

          temp=
          Scope_TPS2024.
          Get_Immediate_Measurement_Value()
          print temp

          Scope_TPS2024_DC=float(temp)
          DC_Offsets[Scope_TPS2024_Index].append(
          Scope_TPS2024_DC)

          if (
          not channel==
          Tektronix.Scope.Scope_Data_Source_CH3
          and not
          channel==
          Tektronix.Scope.Scope_Data_Source_CH4):
            Scope_TPS2002_1_DC = float(
  Scope_TPS2002_1.Get_Immediate_Measurement_Value())
            Scope_TPS2002_2_DC = float(
  Scope_TPS2002_2.Get_Immediate_Measurement_Value())
            DC_Offsets[
            Scope_TPS2002_1_Index].append(
            Scope_TPS2002_1_DC)
            DC_Offsets[
```

```
            Scope_TPS2002_2_Index].append(
  Scope_TPS2002_2_DC)
#************************************************************
        for scope_index,DC_Vals in enumerate(
        DC_Offsets):
          newstr_a=[]
          for Ch_index,DC_Val in enumerate(DC_Vals):
            newstr_a.append("CH%d :%f "%(
            Ch_index+1,DC_Val))
          newstr=''.join(newstr_a)
          print """For Scope %s Found
DC values of %s""" %(Scope_String[scope_index],newstr)


#************************************************************
        # obtain AC Vpp info
        Scope_TPS2024.Set_Immediate_Measurement_Type(
Tektronix.Scope.Scope_Measurement_Type_Peak_To_Peak)
        Scope_TPS2002_1.Set_Immediate_Measurement_Type(
Tektronix.Scope.Scope_Measurement_Type_Peak_To_Peak)
        Scope_TPS2002_2.Set_Immediate_Measurement_Type(
Tektronix.Scope.Scope_Measurement_Type_Peak_To_Peak)

        # define info for Vpp
        AC_Vpp=[[],[],[]]
#************************************************************
        for channel in [
Tektronix.Scope.Scope_Data_Source_CH1,
Tektronix.Scope.Scope_Data_Source_CH2,
Tektronix.Scope.Scope_Data_Source_CH3,
Tektronix.Scope.Scope_Data_Source_CH4]:
          print """Geting AC Vpp info
from %s""" % channel
          Scope_TPS2024.
Set_Immediate_Measurement_Source(channel)
          if (not channel==
Tektronix.Scope.Scope_Data_Source_CH3 and not
channel==Tektronix.Scope.Scope_Data_Source_CH4):
            Scope_TPS2002_1
.Set_Immediate_Measurement_Source(channel)
            Scope_TPS2002_2
.Set_Immediate_Measurement_Source(channel)

          Scope_Wait(
Scope_TPS2024,Scope_TPS2002_1,Scope_TPS2002_2)
#************************************************************
          Scope_TPS2024_AC=float(
Scope_TPS2024.Get_Immediate_Measurement_Value())
```

```
            AC_Vpp[Scope_TPS2024_Index].append(
            Scope_TPS2024_AC)

            if (not
channel==Tektronix.Scope.Scope_Data_Source_CH3 and not
channel==Tektronix.Scope.Scope_Data_Source_CH4):
                Scope_TPS2002_1_AC = float(
Scope_TPS2002_1.Get_Immediate_Measurement_Value())
                Scope_TPS2002_2_AC = float(
Scope_TPS2002_2.Get_Immediate_Measurement_Value())
                AC_Vpp[Scope_TPS2002_1_Index].append(
Scope_TPS2002_1_AC)
                AC_Vpp[Scope_TPS2002_2_Index].append(
Scope_TPS2002_2_AC)
#*************************************************************
        for scope_index,AC_Vals in enumerate(AC_Vpp):
            newstr_a=[]
            for Ch_index,AC_Val in enumerate(AC_Vals):
                newstr_a.append("CH%d␣:%f␣"%(
Ch_index+1,AC_Val))
            newstr=''.join(newstr_a)
            print """For Scope %s Found
AC Vpp values of %s""" %(Scope_String[scope_index],newstr)

        Scope_Wait(Scope_TPS2024,Scope_TPS2002_1,
        Scope_TPS2002_2)
#*************************************************************
        print "Starting␣Resize␣Calculation"

        TPS2024_DC_Array=DC_Offsets[
        Scope_TPS2024_Index]
        TPS2002_1_DC_Array=DC_Offsets[
        Scope_TPS2002_1_Index]
        TPS2002_2_DC_Array=DC_Offsets[
        Scope_TPS2002_2_Index]

        TPS2024_AC_Array=AC_Vpp[
        Scope_TPS2024_Index]
        TPS2002_1_AC_Array=AC_Vpp[
        Scope_TPS2002_1_Index]
        TPS2002_2_AC_Array=AC_Vpp[
        Scope_TPS2002_2_Index]
#*************************************************************
        # resize all channels based upon result
        for channel in [
Tektronix.Scope.Scope_Channel_1,
Tektronix.Scope.Scope_Channel_2,
Tektronix.Scope.Scope_Channel_3,
```

```
Tektronix.Scope.Scope_Channel_4]:
        Channel_To_Array=channel-1

        Current_TPS2024_DC=TPS2024_DC_Array[
        Channel_To_Array]
        Current_TPS2024_AC=TPS2024_AC_Array[
        Channel_To_Array]

        TPS2024_Resize=(Current_TPS2024_AC
        +abs(Current_TPS2024_DC))
        TPS2024_New_Scale=((TPS2024_Resize+
TPS2024_Resize*Scope_Voltage_Overshoot_Factor)
/Scope_Number_of_Voltage_Division)
        print """Setting TPS2024 Ch%d to have
voltage scale factor of %f""" % (channel,TPS2024_New_Scale)
#*********************************************************
        Scope_TPS2024.Set_Channel_Scale(
channel,TPS2024_New_Scale)

        if channel<=Tektronix.Scope.Scope_Channel_2:
          Current_TPS2002_1_DC=TPS2002_1_DC_Array[
          Channel_To_Array]
          Current_TPS2002_1_AC=TPS2002_1_AC_Array[
          Channel_To_Array]
          Current_TPS2002_2_DC=TPS2002_2_DC_Array[
          Channel_To_Array]
          Current_TPS2002_2_AC=TPS2002_2_AC_Array[
          Channel_To_Array]
#*********************************************************
          TPS2002_1_Resize=(Current_TPS2002_1_AC
          +abs(Current_TPS2002_1_DC))
          TPS2002_1_New_Scale=((
TPS2002_1_Resize+TPS2002_1_Resize
*Scope_Voltage_Overshoot_Factor)
/Scope_Number_of_Voltage_Division)

          TPS2002_2_Resize=(Current_TPS2002_2_AC+
          abs(Current_TPS2002_2_DC))
          TPS2002_2_New_Scale=((TPS2002_2_Resize+
TPS2002_2_Resize*Scope_Voltage_Overshoot_Factor)
/Scope_Number_of_Voltage_Division)
#*********************************************************
          print """Setting TPS2002 #1 Ch%d to have
voltage scale factor of %f""" % (channel,TPS2002_1_New_Scale)
          print """Setting TPS2002 #2 Ch%d to have
voltage scale factor of %f""" % (channel,TPS2002_2_New_Scale)
          Scope_TPS2002_1.Set_Channel_Scale(
channel,TPS2002_1_New_Scale)
```

```
            Scope_TPS2002_2.Set_Channel_Scale(
channel,TPS2002_2_New_Scale)
#*********************************************************

        Scope_Wait(Scope_TPS2024,Scope_TPS2002_1,
        Scope_TPS2002_2)

        print "Resizing Now"

        # Take a Scope Sample now
        Scope_TPS2024.Set_Acquire_State(
        Tektronix.Scope.Scope_Acquire_State_On)
        Scope_TPS2002_1.Set_Acquire_State(
        Tektronix.Scope.Scope_Acquire_State_On)
        Scope_TPS2002_2.Set_Acquire_State(
        Tektronix.Scope.Scope_Acquire_State_On)
#*********************************************************
        Scope_Wait(Scope_TPS2024,
        Scope_TPS2002_1,Scope_TPS2002_2)
        print "Resize done"

        print "Geting Scope Waveforms"
        TPS2024_Waveget=Scope_TPS2024_Get(
        Scope_TPS2024)
        TPS2002_1_Waveget=Scope_TPS2002_Get(
        Scope_TPS2002_1,1)
        TPS2002_2_Waveget=Scope_TPS2002_Get(
        Scope_TPS2002_2,2)

        TPS2024_Waveget.start()
        TPS2002_1_Waveget.start()
        TPS2002_2_Waveget.start()

        print "Waiting on TPS2024"
        TPS2024_Waveget.join()
        print "Waiting on TPS2002 #1"
        TPS2002_1_Waveget.join()
        print "Waiting on TPS2002 #2"
        TPS2002_2_Waveget.join()
        print "Waveform Get Done"
#*********************************************************
        print "Formating Data"

        # This is channel Data [time,value]
        Vin_A_Ch=TPS2024_Waveget.result[0]
        Vin_B_Ch=TPS2002_1_Waveget.result[0]
        Vin_C_Ch=TPS2002_2_Waveget.result[0]
        V_R1_Ch=TPS2024_Waveget.result[1]
```

```
        V_R2_Ch=TPS2024_Waveget.result[2]
        V_A1_Ch=TPS2002_1_Waveget.result[1]
        V_A2_Ch=TPS2024_Waveget.result[3]
        V_A3_Ch=TPS2002_2_Waveget.result[1]

        Vin_A_time=Vin_A_Ch[0]
        Vin_A=Vin_A_Ch[1]

        Vin_B_time=Vin_B_Ch[0]
        Vin_B=Vin_B_Ch[1]

        Vin_C_time=Vin_C_Ch[0]
        Vin_C=Vin_C_Ch[1]

        V_R1_time=V_R1_Ch[0]
        V_R1=V_R1_Ch[1]

        V_R2_time=V_R2_Ch[0]
        V_R2=V_R2_Ch[1]

        V_A1_time=V_A1_Ch[0]
        V_A1=V_A1_Ch[1]

        V_A2_time=V_A2_Ch[0]
        V_A2=V_A2_Ch[1]

        V_A3_time=V_A3_Ch[0]
        V_A3=V_A3_Ch[1]
#*************************************************************
        Data_To_Write_a=[]
        for index,Vx in enumerate(Vin_A):
#                "ii   tt   AA   BB   CC   R1   R2   A1   A2   A3
          Data_To_Write_a.append(
"%d\t%f\t%f\t%f\t%f\t%f\t%f\t%f\t%f\t%f\r\n"%(
index,Vin_A_time[index],Vin_A[index],Vin_B[index],
Vin_C[index],V_R1[index],V_R2[index],V_A1[index],
V_A2[index],V_A3[index]))
#*************************************************************
        Save_File_As="%s/%.10d.txt"%(
        Save_Data_Path,Output_Index_Counter)
        print "Saveing File as %s" % Save_File_As
        Output_File = open(Save_File_As,"wb")
        Output_File.write(''.join(Data_To_Write_a))
        Output_File.close()
        print "Adding Index"
        Output_Index_File = open(
        Output_Index_Name,"a")
        Output_Index_File.write(
```

```
"%d\t%f\t%f\r\n"%(Output_Index_Counter,Frequency,Voltage))
        Output_Index_File.close()
#*************************************************************
        Output_Index_Counter=Output_Index_Counter+1
        print "Set Took %s" % Run_Time(Set_Start_Time)
#Status(Save_Data_Input,Status_Path,
# "Freq=%f at Voltage=%f Done at %s"% (Frequency,
#Voltage,Run_Time(Set_Start_Time)))
   print "Rev Took %s" % Run_Time(Rev_Start_Time)
#*************************************************************
print "Shutdown Generator"
Generator_AFG3000.Generator_Output(
Tektronix.Generator.Generator_Channel_1,
Tektronix.Generator.Generator_Output_Off)
Generator_AFG3000.Generator_Output(
Tektronix.Generator.Generator_Channel_2,
Tektronix.Generator.Generator_Output_Off)

print "Test is Now Done!"
print "Test Took %s" % Run_Time(App_Start_Time)
Status(Save_Data_Input,Status_Path,
"Done after %s"% (Run_Time(App_Start_Time)))
#*************************************************************
# Experment Code Stops Here
#*************************************************************

#Shutdown Scopes
Scope_TPS2024.Close()
Scope_TPS2002_1.Close()
Scope_TPS2002_2.Close()

# Shutdown Generator
Generator_AFG3000.Close()

#*************************************************************
# File Name: rs232.py
# Project: rs232 class for basic rs232 communication
# Description: Python RS232 Class
# Author: Mike Mclain
#*************************************************************

import serial
import time
#*************************************************************
# Baby class to hold configuration information
#*************************************************************
class com_defines():
   Default_Port_Prefix="COM"
```

```
  @staticmethod
  def Get_Port(number):
    return "%s%d" % (
    com_defines.Default_Port_Prefix,number)

  @staticmethod
  def Get_Port_With_Path(number):
    return "\\.\%s" % com_defines.Get_Port(number)


#*****************************************************************
# rs232 communication class
#*****************************************************************
class rs232():

  def __init__ (self,port=None,baudrate=9600,
  name="",parity=serial.PARITY_NONE,
  stopbits=serial.STOPBITS_ONE,
  bytesize=serial.EIGHTBITS,timeout=None):
    if port==None:
      return
    self.port=port
    self.baudrate=baudrate
    self.parity=parity
    self.stopbits=stopbits
    self.bytesize=bytesize
    self.timeout=timeout
    self.rs232=None
    self.name=name
    self.debug=False

#*****************************************************************
  def Open(self):
    try:
      self.rs232=serial.Serial(
      port=self.port,baudrate=self.baudrate,
      parity=self.parity,stopbits=self.stopbits,
      bytesize=self.bytesize,timeout=self.timeout)
      self.rs232.close()
      self.rs232.open()
      return True
    except serial.SerialException:
      self.rs232=None
      return False
#*****************************************************************
  def Close(self):
    if self.rs232==None:
      return True
```

```
    else:
      try:
        self.rs232.close()
        self.rs232=None
        return True
      except:
        return False
#*************************************************************
  def Read(self,number=1):
    if self.rs232==None:
      return None
    else:
      return self.rs232.read(size=number)
#*************************************************************
  def ReadLine(self,eom='\n'):
    local_eom=eom
    if len(eom)>1:
      local_eom=eom[len(eom)-1]
    message=[]
    while True:
      value=self.Read()
      message.append(value)
      if value==None or value=="":
        if self.debug==True:
          print "%s Timeout" % self.name
        return None
      if value==local_eom:
        break
    output=''.join(message)
    for item in eom:
      output=output.replace(item,"")
    if self.debug==True:
      print "%s Read |%s|" % (self.name,output)
    return output
#*************************************************************
  def ReadBulk(self,delay=.5,numberoftrys=3):
    if self.rs232==None:
      return None

    message=[]
    Fail=0
    while True:
      if Fail>numberoftrys:
        break
      value=self.rs232.inWaiting()
      if value>0:
        Fail=0
        data=self.Read(self.rs232.inWaiting())
```

```
            if value==None:
              return None
            message.append(data)
          else:
            Fail=Fail+1
            time.sleep(delay)
        if message==[]:
          return None

        return ''.join(message)
    #*************************************************************
      def Query(self,message,eom='\n',retry=True):
        if self.rs232==None:
          return None
        while True:
          self.Write(message,eom)
          retval=self.ReadLine(eom)
          if not retval==None:
            break
          else:
            if retry==False:
              return None
            if retry==True and self.debug==True:
              print (
              "%s Query Timeout Will Try Again"
             % (self.name)
              )
        return retval
    #*************************************************************
      def Write(self,message,eom='\n',delay=.25):
        if self.rs232==None:
          return False
        else:
          output="%s%s"%(message,eom)
          if self.debug==True:
            print "%s Write: |%s|" % (
            self.name,message)
          self.rs232.write(output)
          if not delay==None:
            time.sleep(delay)
          return True

    #*************************************************************
      def Port_Scan(self,until=20):
        Port_Array = []
        for i in range(until):
          try:
            target=rs232_defines.Get_Port(i)
```

```
            rs232_test = serial.Serial(target)
            Port_Array.append(target)
            # explicit close 'cause of
            # delayed GC in java
            rs232_test.close()
          except serial.SerialException:
            pass

      return Port_Array

#*****************************************************
# File Name: Tektronix2.py
# Project: Tektronix's Device Contorl Class REV 2
# Description: Contorl Scopes and Generators with this
# Author: Mike Mclain
#*****************************************************
import rs232
import serial
import time
import struct
from struct import *
import visa

#*****************************************************
# Contorl a Tex Generator with this class via Visa
#*****************************************************
class Generator():
  Generator_Channel_1=1
  Generator_Channel_2=2
  Generator_Output_On="ON"
  Generator_Output_Off="OFF"
#*****************************************************
  def __init__ (self,visa_id):
    self.visa_id=visa_id
    self.device=None
    self.ready=False
#*****************************************************
  def Open(self):
    # Visa is sloppy so do a catch
    # to try and get it to boot
    try:
      self.device = visa.instrument(self.visa_id)
      self.ready=True
    except:
      try:
        self.device = visa.instrument(
        self.visa_id)
        self.ready=True
```

```
        except:
          self.ready=False
          self.device =None
      return self.ready
#************************************************************
    def Close(self):
      pass
#************************************************************
    def Generator_Reset(self):
      if self.ready==False:
        return
      self.device.write("*RST")
#************************************************************
    def Generator_Function(self,source,function):
      if self.ready==False:
        return
      self.device.write("SOURce%d:FUNCTION %s" % (
      source,function))
#************************************************************
    def Generator_Voltage(self,source,voltage):
      if self.ready==False:
        return
      self.device.write(
      "SOURce%d:VOLTAGE:AMPLITUDE %e" % (source, voltage))
#************************************************************
    def Generator_Output(self,source,value):
      if self.ready==False:
        return
      self.device.write(
      "OUTPut%d:STATe %s" % (source, value))
#************************************************************
    def Generator_Frequency(self,source,value):
      if self.ready==False:
        return
      self.device.write(
      "SOURce%d:FREQUENCY %e Hz" % (source, value))
#************************************************************

#************************************************************
# Contorl a Scope with this Via RS232
#************************************************************
class Scope():
  Scope_Acquire_Stop_Mode_Run_Stop="RUNSTop"
  Scope_Acquire_Stop_Mode_Sequence="SEQuence"
  Scope_Acquire_State_On="ON"
  Scope_Acquire_State_Off="OFF"
  Scope_Acquire_State_Run="RUN"
  Scope_Acquire_State_Stop="STOP"
```

```
    Scope_Acquire_Mode_Sample="SAMple"
    Scope_Acquire_Mode_Peak_Detect="PEAKdetect"
    Scope_Acquire_Mode_Average="AVErage"
    Scope_Acquire_Acquisitions_4=4
    Scope_Acquire_Acquisitions_16=16
    Scope_Acquire_Acquisitions_64=64
    Scope_Acquire_Acquisitions_128=128
    Scope_On="ON"
    Scope_Off="OFF"
    Scope_Channel_On="ON"
    Scope_Channel_Off="OFF"
    Scope_Channel_1=1
    Scope_Channel_2=2
    Scope_Channel_3=3
    Scope_Channel_4=4
    Scope_Measurement_1=1
    Scope_Measurement_2=2
    Scope_Measurement_3=3
    Scope_Measurement_4=4
    Scope_Measurement_5=4
    Scope_Measurement_Type_Frequency="FREQuency"
    Scope_Measurement_Type_Mean="MEAN"
    Scope_Measurement_Type_Period="PERIod"
    Scope_Measurement_Type_Peak_To_Peak="PK2pk"
    Scope_Measurement_Type_RMS="CRMs"
    Scope_Measurement_Type_Minimum="MINImum"
    Scope_Measurement_Type_Maximum="MAXImum"
    Scope_Measurement_Type_Rise="RISe"
    Scope_Measurement_Type_Fall="FALL"
    Scope_Measurement_Type_Positive_Pulse_Width="PWIdth"
    Scope_Measurement_Type_Negative_Pulse_Width="NWIdth"
    Scope_Measurement_Type_None="NONe"
#*****************************************************
    Scope_Horizontal_Scale = ["5.0E1","2.5E1","1.0E1",
    "5.0E0","2.5E0","1.0E0","5.0E-1","2.5E-1","1.0E-1",
    "5.0E-2","2.5E-2","1.0E-2","5.0E-3","2.5E-3",
    "1.0E-3","5.0E-4","2.5E-4","1.0E-4","5.0E-5",
    "2.5E-5","1.0E-5","5.0E-6","2.5E-6","1.0E-6",
    "5.0E-7","2.5E-7","1.0E-7","5.0E-8","2.5E-8",
    "1.0E-8","5.0E-9","2.5E-9"]
    Scope_Channel_Scale = ["2.0E-2", "5.0E-2", "1.0E-1",
    "2.0E-1", "5.0E-1", "1.0E0", "2.0E0", "5.0E0",
    "1.0E1", "2.0E1", "5.0E1" ]
    Scope_Data_Width_1=1
    Scope_Data_Width_2=1
    Scope_Data_Encoding_Ascii="ASCIi"
    Scope_Data_Encoding_Ribinary="RIBinary"
    Scope_Data_Encoding_Rpbinary="RPBinary"
```

```
    Scope_Data_Encoding_Sribinary="SRIbinary"
    Scope_Data_Encoding_Srpbinary="SRPbinary"
    Scope_Data_Source_CH1="CH1"
    Scope_Data_Source_CH2="CH2"
    Scope_Data_Source_CH3="CH3"
    Scope_Data_Source_CH4="CH4"
    Scope_Data_Source_Math="Math"
    Scope_Data_Source_REFA="REFA"
    Scope_Data_Source_REFB="REFB"
    Scope_Coupling_AC="AC"
    Scope_Coupling_DC="DC"
    Scope_Coupling_GND="GND"
    Scope_Probe_1=1
    Scope_Probe_10=10
    Scope_Probe_20=20
    Scope_Probe_50=50
    Scope_Probe_100=100
    Scope_Probe_500=500
    Scope_Probe_1000=1000
    Scope_Trigger_Edge_AC="AC"
    Scope_Trigger_Edge_DC="DC"
    Scope_Trigger_Edge_HFREJ="HFRej"
    Scope_Trigger_Edge_LFREJ="LFRej"
    Scope_Trigger_Edge_Fall="FALL"
    Scope_Trigger_Edge_Rise="Rise"
    Scope_Trigger_Source_CH1="CH1"
    Scope_Trigger_Source_CH2="CH2"
    Scope_Trigger_Source_CH3="CH3"
    Scope_Trigger_Source_CH4="CH4"
    Scope_Trigger_Source_Ext="EXT"
    Scope_Trigger_Source_Ext_5="EXT5"
    Scope_Trigger_Source_Ext_10="EXT10"
    Scope_Trigger_Source_Line="LINE"
    Scope_Trigger_Mode_Auto="AUTO"
    Scope_Trigger_Mode_Normal="NORMal"
    Scope_Trigger_Type_Edge="EDGE"
    Scope_Trigger_Type_Video="VIDeo"
    Scope_Trigger_Type_Pulse="PULse"
#*************************************************************

#*************************************************************
    def __init__ (self,port,baudrate,eom='\n',name="Scope",
    parity=serial.PARITY_NONE,stopbits=serial.STOPBITS_ONE,
    bytesize=serial.EIGHTBITS,timeout=60):
        self.device=rs232.rs232(port,baudrate,name,
        \parity,stopbits,bytesize,timeout)
        self.eom=eom
        self.ready=False
```

```
#**************************************************************
  def Open(self):
    self.ready=self.device.Open()
    return self.ready
#**************************************************************
  def Close(self):
    if not self.ready==False:
      self.device.Close()
#**************************************************************
  def Get_ID(self):
    if self.ready==False:
      return None
    return self.device.Query("ID?",self.eom)
#**************************************************************
  def Get_Measurement_Value(self,id):
    if self.ready==False:
      return None
    return self.device.Query(
    'MEASUrement:MEAS%d:VALue?'%(id),self.eom)
#**************************************************************
  def Get_Immediate_Measurement_Value(self):
    if self.ready==False:
      return None
    return self.device.Query(
    'MEASUrement:IMMed:VALue?',self.eom)
#**************************************************************
  def Get_Measurement_Source(self,id):
    if self.ready==False:
      return None
    return self.device.Query(
    'MEASUrement:MEAS%d:SOUrce?'%(id),self.eom)
#**************************************************************
  def Set_Measurement_Source(self,id,state):
    if self.ready==False:
      return None
    self.device.Write(
    'MEASUrement:MEAS%d:SOUrce␣%s'% (id,state),self.eom)
#**************************************************************
  def Get_Immediate_Measurement_Source(self):
    if self.ready==False:
      return None
    return self.device.Query(
    'MEASUrement:IMMed:SOUrce1?',self.eom)
#**************************************************************
  def Set_Immediate_Measurement_Source(self,state):
    if self.ready==False:
      return None
    self.device.Write(
```

```
    'MEASUrement:IMMed:SOUrce1 %s' % (state), self.eom)
#**************************************************************
  def Get_Measurement_Type(self,id):
    if self.ready==False:
      return None
    return self.device.Query(
    'MEASUrement:MEAS%d:TYPe?'%(id), self.eom)
#**************************************************************
  def Set_Measurement_Type(self,id,state):
    if self.ready==False:
      return None
    self.device.Write(
    'MEASUrement:MEAS%d:TYPe %s' % (id,state), self.eom)
#**************************************************************
  def Get_Immediate_Measurement_Type(self):
    if self.ready==False:
      return None
    return self.device.Query(
    'MEASUrement:IMMed:TYPe?', self.eom)
#**************************************************************
  def Set_Immediate_Measurement_Type(self,state):
    if self.ready==False:
      return None
    self.device.Write(
    'MEASUrement:IMMed:TYPe %s' % (state), self.eom)
#**************************************************************
  def Get_Channel_Bandwidth(self,channel):
    if self.ready==False:
      return None
    return self.device.Query(
    'CH%d:BANdwidth?'%(channel), self.eom)
#**************************************************************
  def Set_Channel_Bandwidth(self,channel,state):
    if self.ready==False:
      return None
    self.device.Write(
    'CH%d:BANdwidth %s' % (channel,state), self.eom)
#**************************************************************
  def Get_Channel_Coupling(self,channel):
    if self.ready==False:
      return None
    return self.device.Query(
    'CH%d:COUPling?'%(channel), self.eom)
#**************************************************************
  def Set_Channel_Coupling(self,channel,state):
    if self.ready==False:
      return None
    self.device.Write(
```

```
      'CH%d:COUPling %s' % (channel,state),self.eom)
#**************************************************************
  def Get_Channel_Invert(self,channel):
    if self.ready==False:
      return None
    return self.device.Query(
    'CH%d:INVert?'%(channel),self.eom)
#**************************************************************
  def Set_Channel_Invert(self,channel,state):
    if self.ready==False:
      return None
    self.device.Write(
    'CH%d:Invert %s' % (channel,state),self.eom)
#**************************************************************
  def Get_Channel_Probe(self,channel):
    if self.ready==False:
      return None
    return self.device.Query(
    'CH%d:PRObe?'%(channel),self.eom)
#**************************************************************
  def Set_Channel_Probe(self,channel,state):
    if self.ready==False:
      return None
    self.device.Write(
    'CH%d:PRObe %d' % (channel,state),self.eom)
#**************************************************************
  def Get_Acquire_State(self):
    if self.ready==False:
      return None
    return self.device.Query(
    'ACQuire:STATE?',self.eom)
#**************************************************************
  def Set_Acquire_State(self,state):
    if self.ready==False:
      return None
    self.device.Write(
    'ACQuire:STATE %s' % state,self.eom)
#**************************************************************
  def Get_Acquire_Stop_After(self):
    if self.ready==False:
      return None
    return self.device.Query(
    'ACQuire:STOPAfter?',self.eom)
#**************************************************************
  def Set_Acquire_Stop_After(self,state):
    if self.ready==False:
      return None
    self.device.Write(
```

```
    'ACQuire:STOPAfter %s' % state, self.eom)
#**************************************************************
  def Get_Acquire_Mode(self):
    if self.ready==False:
      return None
    return self.device.Query('ACQuire:MODe?', self.eom)
#**************************************************************
  def Set_Acquire_Mode(self,mode):
    if self.ready==False:
      return None
    self.device.Write(
    'ACQuire:MODe %s' % mode, self.eom)
#**************************************************************
  def Get_Acquire_Number_Acquisitions(self):
    if self.ready==False:
      return None
    return self.device.Query(
    'ACQuire:NUMAVg?', self.eom)
#**************************************************************
  def Set_Acquire_Number_Acquisitions(self,number):
    if self.ready==False:
      return None
    self.device.Write(
    'ACQuire:NUMAVg %d' % number, self.eom)
#**************************************************************
  def Get_Trigger_Coupling(self):
    if self.ready==False:
      return None
    return self.device.Query(
    'TRIGger:MAIn:EDGE:COUPling?', self.eom)
#**************************************************************
  def Set_Trigger_Coupling(self,state):
    if self.ready==False:
      return None
    self.device.Write(
    'TRIGger:MAIn:EDGE:COUPling %s'%(state), self.eom)
#**************************************************************
  def Get_Trigger_Slope(self):
    if self.ready==False:
      return None
    return self.device.Query(
    'TRIGger:MAIn:EDGE:SLOpe?', self.eom)
#**************************************************************
  def Set_Trigger_Slope(self,state):
    if self.ready==False:
      return None
    self.device.Write(
    'TRIGger:MAIn:EDGE:SLOpe %s'%(state), self.eom)
```

```
#**************************************************************
  def Get_Trigger_Source(self):
    if self.ready==False:
      return None
    return self.device.Query(
    'TRIGger:MAIn:EDGE:SOUrce?',self.eom)
#**************************************************************
  def Set_Trigger_Source(self,state):
    if self.ready==False:
      return None
    self.device.Write(
    'TRIGger:MAIn:EDGE:SOUrce %s'%(state),self.eom)
#**************************************************************
  def Get_Trigger_Mode(self):
    if self.ready==False:
      return None
    return self.device.Query(
    'TRIGger:MAIn:MODe?',self.eom)
#**************************************************************
  def Set_Trigger_Mode(self,state):
    if self.ready==False:
      return None
    self.device.Write(
    'TRIGger:MAIn:MODe %s'%(state),self.eom)
#**************************************************************
  def Get_Trigger_Type(self):
    if self.ready==False:
      return None
    return self.device.Query(
    'TRIGger:MAIn:TYPe?',self.eom)
#**************************************************************
  def Set_Trigger_Type(self,state):
    if self.ready==False:
      return None
    self.device.Write(
    'TRIGger:MAIn:TYPe %s'%(state),self.eom)
#**************************************************************
  def Get_Channel_State(self,number):
    if self.ready==False:
      return None
    return self.device.Query(
    'SELect:CH%d?'%number,self.eom)
#**************************************************************
  def Set_Channel_State(self,number,state):
    if self.ready==False:
      return None
    self.device.Write(
    'SELect:CH%d %s'%(number,state),self.eom)
```

```
#**************************************************************
  def Get_Channel_Position(self,number):
    if self.ready==False:
      return None
    return self.device.Query(
    'CH%d:POSition?'%number,self.eom)
#**************************************************************
  def Set_Channel_Position(self,number,location):
    if self.ready==False:
      return None
    self.device.Write(
    'CH%d:POSition %.4e'%(number,location),self.eom)
#**************************************************************
  def Get_Channel_Scale(self,number):
    if self.ready==False:
      return None
    return self.device.Query(
    'CH%d:SCAle?'%number,self.eom)
#**************************************************************
  def Set_Channel_Scale(self,number,value):
    if self.ready==False:
      return None
    self.device.Write(
    'CH%d:SCAle %.4e'%(number,float(value)),self.eom)
#**************************************************************
  def Get_Horizontal_Scale(self):
    if self.ready==False:
      return None
    return self.device.Query(
    'HORizontal:MAIn:SCAle?',self.eom)
#**************************************************************
  def Set_Horizontal_Scale(self,value):
    if self.ready==False:
      return None

    self.device.Write(
    'HORizontal:MAIn:SCAle %.4e'%(
    float(value)),self.eom)
#**************************************************************
  def Horizontal_Scale_Increment(self):
    Current_Scale=self.Get_Horizontal_Scale()
    Current_Scale=Current_Scale.strip()
    if Current_Scale=="" or Current_Scale== None:
      return

    for index,item in enumerate(
    Scope.Scope_Horizontal_Scale):
      if float(item)==float(Current_Scale):
```

```
            if index-1>=0:
              self.Set_Horizontal_Scale(
              Scope.Scope_Horizontal_Scale[index-1])
              self.Wait()
              self.Wait_While_Busy()
              break
#*************************************************************
  def Horizontal_Scale_Decrement(self):
    Current_Scale=self.Get_Horizontal_Scale()
    Current_Scale=Current_Scale.strip()
    if Current_Scale=="" or Current_Scale== None:
      return

    for index,item in enumerate(
    Scope.Scope_Horizontal_Scale):
      if float(item)==float(Current_Scale):
        if index+1<len(
        Scope.Scope_Horizontal_Scale):
          self.Set_Horizontal_Scale(
          Scope.Scope_Horizontal_Scale[index+1])
          self.Wait()
          self.Wait_While_Busy()
          break
#*************************************************************
  def Channel_Scale_Increment(self,number):
    Current_Scale=self.Get_Channel_Scale(number)
    Current_Scale=Current_Scale.strip()
    if Current_Scale=="" or Current_Scale== None:
      return

    for index,item in enumerate(
    Scope.Scope_Channel_Scale):
      if float(item)==float(Current_Scale):
        if index+1<len(Scope.Scope_Channel_Scale):
          self.Set_Channel_Scale(
        number,Scope.Scope_Channel_Scale[index+1])
          self.Wait()
          self.Wait_While_Busy()
          break
#*************************************************************
  def Channel_Scale_Decrement(self,number):
    Current_Scale=self.Get_Channel_Scale(number)
    Current_Scale=Current_Scale.strip()
    if Current_Scale=="" or Current_Scale== None:
      return

    for index,item in enumerate(
    Scope.Scope_Channel_Scale):
```

```
        if float(item)==float(Current_Scale):
          if index-1>=0:
            self.Set_Channel_Scale(
          number,Scope.Scope_Channel_Scale[index-1])
            self.Wait()
            self.Wait_While_Busy()
            break
#***************************************************************
  def Get_Data_Width(self):
    if self.ready==False:
      return None
    return self.device.Query(
    'DATa:WIDth?',self.eom)
#***************************************************************
  def Set_Data_Width(self,value):
    if self.ready==False:
      return None
    self.device.Write(
    'DATa:WIDth %d'%(value),self.eom)
#***************************************************************
  def Get_Data_Encoding(self):
    if self.ready==False:
      return None
    return self.device.Query(
    'DATa:ENCdg?',self.eom)
#***************************************************************
  def Set_Data_Encoding(self,value):
    if self.ready==False:
      return None
    self.device.Write(
    'DATa:ENCdg %s'%(value),self.eom)
#***************************************************************
  def Get_Data_Source(self):
    if self.ready==False:
      return None
    return self.device.Query(
    'DATa:SOUrce?',self.eom)
#***************************************************************
  def Set_Data_Source(self,value):
    if self.ready==False:
      return None
    self.device.Write(
    'DATa:SOUrce %s'%(value),self.eom)
#***************************************************************
  def Get_Waveform_Header(self):
    if self.ready==False:
      return None
    return self.device.Query(
```

```
      'WFMPre:WFId?',self.eom)
#*************************************************************
  def Set_Measurement_Source(self,measurement,channel):
    if self.ready==False:
      return None
    self.device.Write(
'MEASUrement:MEAS%d:SOUrce CH%d'%(
measurement,channel),self.eom)
#*************************************************************
  def Get_Waveform(self,number):
    self.Wait()
    self.Wait_While_Busy()

    self.Set_Data_Source(number)
    self.Set_Data_Width(Scope.Scope_Data_Width_1)
    self.Set_Data_Encoding(
    Scope.Scope_Data_Encoding_Ribinary)


    Header=self.Get_Waveform_Header()
    if Header==None or Header== "":
      return None

    Split_Header=Header.split(',')
    Raw_Voltage=Split_Header[2].strip()
    Split_Raw_Voltage=Raw_Voltage.split(' ')
    String_Voltage=Split_Raw_Voltage[0].strip()
    Raw_Time=Split_Header[3].strip()
    Split_Raw_Time=Raw_Time.split(' ')
    String_Time=Split_Raw_Time[0].strip()

    Float_Voltage=float(String_Voltage)
    Float_Time=float(String_Time)
#*************************************************************
    String_Y_Offset=self.device.Query(
    'WFMPre:YOFf?',self.eom)
    if String_Y_Offset==None or String_Y_Offset=="":
      return None

    String_Multiplier=self.device.Query(
    'WFMPre:YMULt?',self.eom)
    if String_Multiplier==None or String_Multiplier=="":
      return None

    String_Y_Zero=self.device.Query(
    'WFMPre:YZEro?',self.eom)
    if String_Y_Zero==None or String_Y_Zero=="":
      return None
```

```
      String_X_Axis=self.device.Query(
      'WFMPre:XINcr?',self.eom)
      if String_X_Axis==None or String_X_Axis=="":
        return None

      Float_Y_Offset=float(String_Y_Offset)
      Float_Multiplier=float(String_Multiplier)
      Float_Y_Zero=float(String_Y_Zero)
      Float_X_Axis=float(String_X_Axis)

      self.Wait()
      self.Wait_While_Busy()

      self.device.Write('CURVe?',self.eom)
      Data=self.device.ReadBulk(.5,10)
#*************************************************************
      timearray=[]
      valuearray=[]
      index=0
      for lp in range(6,len(Data)-2,1):
        Unpacked_Point=float(
        unpack('b',pack('c',Data[lp]))[0])
        value=(
    (Unpacked_Point-Float_Y_Offset)
    *Float_Multiplier)+Float_Y_Zero
        time_at=index*Float_X_Axis
        timearray.append(time_at)
        valuearray.append(value)
        #output.append(str(index*Float_X_Axis))
        #output.append("\t")
        #output.append(str(value))
        #output.append("\r\n")
        index=index+1
      #return ''.join(output)
      return [timearray,valuearray]
#*************************************************************
    def Autoset(self):
      self.device.Write('AUTOSet␣EXECute',self.eom)
      self.Wait()
      self.Wait_While_Busy()
#*************************************************************
    def Reset(self):
      if self.ready==False:
        return
      self.device.Write("*RST")
#*************************************************************
    def Lock(self):
```

```
    if self.ready==False:
      return None
    self.device.Write('LOCk ALL',self.eom)
#*************************************************************
  def Unlock(self):
    if self.ready==False:
      return None
    self.device.Write('UNLock ALL',self.eom)
#*************************************************************
  def Get_Busy(self):
    if self.ready==False:
      return None
    return self.device.Query("BUSY?",self.eom)
#*************************************************************
  def Wait(self):
    if self.ready==False:
      return None
    # For the time null this
    #self.device.Write('*WAI',self.eom)
#*************************************************************
  def Wait_While_Busy(self,delay=2):
    if self.ready==False:
      return None
    while True:
      value=self.Get_Busy()
      if value==None:
        return None
      if value=="0":
        break
      time.sleep(delay)
    return True
#*************************************************************
  def Print_Screen(self):
    if self.ready==False:
      return None
    self.device.Write(
    'HARDCopy:BUTTON PRINTS',self.eom)
    self.device.Write('HARDCopy:FORMat BMP',self.eom)
    self.device.Write(
    'HARDCopy:LAYout PORTRait',self.eom)
    self.device.Write('HARDCopy:PORT RS232',self.eom)
    self.Wait()
    self.Wait_While_Busy()
    self.device.Write('HARDCopy STARt',self.eom)
    Image=self.device.ReadBulk(.5,10)
    return Image
#*************************************************************
```

APPENDIX C: VIOLET SOURCE CODE

The source code presented below is the C# source code for the application called VIOLET, and is segmented into three separate C# classes. The first class is the console interface — used to control the application —, the second class is the actual VIOLET simulator — used to send commands to Berkeley Spice —, and the third class is a simplistic data storage and data casting class to help pass information between the console and the simulator.

```
ïż£//*********************************************************
// Variations of Input to Output for Lengthy Engineering
// Testing (VIOLET)
// V 1.0 By Mike Mclain
// Created Monday October 12, 2009
//*********************************************************
// The propose of this program is to give Simulation
// Program with Integrated
// Circuit Emphasis (SPICE) the ability to perform
// custom complex parametric
// analysis in a threaded environment.
//*********************************************************
// This program is designed to interface with
//  SPICE 3F5 from EECS Department
// of the University of California at Berkeley
// that can be obtained from
// http://embedded.eecs.berkeley.edu/
// pubs/downloads/spice/index.htm
// which is Copyright (c) 1985-1991
// The Regents of the University of
// California. All rights reserved.
// under the BSD Copyright.
//*********************************************************
// This part of the program interfaces
//  with the user via a console
// application, the main function of this application
// is to collect command
// line arguments and feed this information
// into a class object
//*********************************************************
using System;
using System.Collections.Generic;
using System.Text;

namespace violet
{
class Program
{
// application entry point
static void Main(string[] args)
```

```
{
// get the program start time
DateTime VioletStartTime = DateTime.Now;
// make a new instance of Violet
VIOLET Software = new VIOLET();
//*********************************************************
// Because this is a console
//application we can accept arguments
// so process these arguments
for(int lp=0;lp<args.Length;lp++)
{
// get the argument
string arg = args[lp];
// use a switch statement to allow
// for additional configurations
switch (arg)
{
//*********************************************************
// See how many threads the application should create
case "-t":
#region Set Thread Number
// Check to see if there is another
// parameter in existence
if (lp + 1 < args.Length)
{
// create a temporary variable to hold data
int temp_max_threads = 0;
// Get the Next Parameter
lp++;
arg = args[lp];
// check for non numeric value
//*********************************************************
if (int.TryParse(arg, out temp_max_threads) == false)
{
Console.WriteLine(
"Error: Non Numeric Value Entered for Number of Threads");
// Exit Program
return;
}
//*********************************************************
// try to apply the parameter to the application
if (Software.Set_Max_Threads(temp_max_threads) == false)
{
Console.WriteLine(
"Error: Invalid Number Used Threads Must be > 0");
// Exit Program
return;
}
```

```
else
{
//*********************************************************
Console.WriteLine(
"Max Threads Set To {0}",
Software.Get_Max_Threads().ToString());
}
}
else
{
// if not alert the user
Console.WriteLine(
"Error: Additional Parameter Missing -t");
// Exit Program
return;
}
#endregion
break;
case "-i":
#region Set Input File
//*********************************************************
// Check to see if there is another parameter in existence
if (lp + 1 < args.Length)
{
// Get the Next Parameter
lp++;
arg = args[lp];
// see if the input file is defined
if (Software.Get_Input_File() != "")
{
Console.WriteLine(
"Warning: Input file already defined as \"{0}\"",
Software.Get_Input_File());
continue;
}
// try seting the value
//*********************************************************
if (Software.Set_Input_File(arg)==false)
{
Console.WriteLine(
"Warning: Input file not found \"{0}\"", arg);
// Exit Program
continue;
}
Console.WriteLine(
"Input File Set To \"{0}\"", Software.Get_Input_File());
}
else
```

```
{
// if not alert the user
Console.WriteLine(
"Error: Additional Parameter Missing for -i");
// Exit Program
return;
}
#endregion
break;
case "-o":
#region Set Output File
//*********************************************************
// Check to see if there is another parameter in existence
if (lp + 1 < args.Length)
{
// Get the Next Parameter
lp++;
arg = args[lp];
// see if the input file is defined
if (Software.Get_Output_Folder() != "")
{
Console.WriteLine(
"Warning: Output Folder already defined as \"{0}\""
, Software.Get_Output_Folder());
continue;
}
// try seting the value
if (Software.Set_Output_Folder(arg) == false)
{
Console.WriteLine(
"Warning: Output Folder cannot be created as \"{0}\"",
 arg);
// Exit Program
//*********************************************************
continue;
}
Console.WriteLine(
"Output File Set To \"{0}\"",
 Software.Get_Output_Folder());
}
else
{
// if not alert the user
//*********************************************************
Console.WriteLine(
"Error: Additional Parameter Missing for -o");
// Exit Program
return;
```

```
}
#endregion
break;
case "-p":
#region Set Output Folder Purge
Software.Set_Output_Folder_Purge(true);
Console.WriteLine("Output Folder Purge is Active");
#endregion
break;
default:
#region Generic Actions
//*********************************************************
// allow generic inputs to be accepted based on order
if (Software.Get_Input_File() == "")
{
if (Software.Set_Input_File(arg) == false)
{
Console.WriteLine(
"Warning: Input file not found \"{0}\"",arg);
continue;
}
Console.WriteLine(
"Input File Set To \"{0}\"",Software.Get_Input_File());
}
else if (Software.Get_Output_Folder() == "")
{
if (Software.Set_Output_Folder(arg) == false)
{
Console.WriteLine(
"Warning: Output Folder cannot be created as \"{0}\"",
 arg);
continue;
}
Console.WriteLine("Output File Set To \"{0}\"",
Software.Get_Output_Folder());
}
else
{
//*********************************************************
Console.WriteLine(
"Warning: \"{0}\" is a unknown parameter and was ignored",
arg);
}
#endregion
break;
}
}
//*********************************************************
```

```
// now do software startup check
// check input
if (Software.Get_Input_File() == "")
{
Console.WriteLine("Error: No Input File Defined");
return;
}
// check output
if (Software.Get_Output_Folder() == "")
{
Console.WriteLine("Error: No Output Folder Defined");
return;
}
// do purge if needed
if (Software.Get_Output_Folder_Purge() == true)
{
Console.WriteLine("Starting output folder purge");
Software.Purge();
Console.WriteLine("Purge complete");
}
// run our software
Software.Run();
//*********************************************************
// get the stop time
DateTime VioletStopTime = DateTime.Now;
// get the run time
TimeSpan VioletRunTime = VioletStopTime - VioletStartTime;
// write out the total run time
Console.WriteLine(
"Violet Took {0} Seconds To Run",VioletRunTime);
}
}
}

ïż£//*********************************************************
// Variations of Input to Output for Lengthy Engineering
// Testing (VIOLET)
// V 1.0 By Mike Mclain
// Created Monday October 12, 2009
//*********************************************************
// The propose of this program is to give Simulation
// Program with Integrated
// Circuit Emphasis (SPICE) the ability to perform
// custom complex parametric
// analysis in a threaded environment.
//*********************************************************
// This program is designed to interface with
//  SPICE 3F5 from EECS Department
```

```
// of the University of California at Berkeley
// that can be obtained from
// http://embedded.eecs.berkeley.edu/
// pubs/downloads/spice/index.htm
// which is Copyright (c) 1985-1991
// The Regents of the University of
// California. All rights reserved.
// under the BSD Copyright.
//*********************************************************
// This is the master class that actually does
// the Variations of Input to
// Output for Lengthy Engineering Testing
//*********************************************************
using System;
using System.Collections.Generic;
using System.Text;
using System.IO;
using System.Text.RegularExpressions;
using System.Diagnostics;
using System.Runtime.InteropServices;
using System.Threading;

namespace violet
{
class VIOLET
{
#region Internal class variables are defined here
//*********************************************************
// Define the number of threads the
// application should create
// during analysis
private int max_threads = 25;
// define the location that all the
//  simulation results will be saved to
private string output_folder = "";
// define the input file that will be processed
private string input_file = "";
//*********************************************************
// define if the output folder should
// be purged of all files
private bool output_folder_purge = false;
// holds our spice model
private string model = "";
// holds what number of sim were on
private int count = 0;
// define the sweeping objects
List<pram> sweep_prams = new List<pram>();
// define reset events for threads
```

```
ManualResetEvent[] CirEvents;
//*********************************************************
// a struct to pass data around in the system.
struct ThreadDataPass
{
public string filepath;
public int cireventID;
}
#endregion
#region  External Class Functions For initialization
// This function sets the number of threads
//*********************************************************
public bool Set_Max_Threads(int number)
{
if (number > 0)
{
max_threads = number;
return true;
}
else
{
return false;
}
}
// this function gets the number of threads
//*********************************************************
public int Get_Max_Threads()
{
return max_threads;
}
// this function gets the output folder
public string Get_Output_Folder()
{
return output_folder;
}
// this function gets the input file
public string Get_Input_File()
{
return input_file;
}
// this function sets the input file
public bool Set_Input_File(string file)
{
// check and see if the file exists
if (File.Exists(file) == true)
{
input_file = file;
return true;
```

```
}
else
{
return false;
}
}
// this function sets the output folder
public bool Set_Output_Folder(string folder)
{
// check and see if the folder exist
if (Directory.Exists(folder) == true)
{
output_folder = folder;
return true;
}
else
{
try
{
//*********************************************************
// the folder dont exist try and make it
DirectoryInfo item = Directory.CreateDirectory(folder);
// see if it was made
if (item.Exists == true)
{
output_folder = folder;
return true;
}
else
{
return false;
}
}
catch
{
// this is a bad file
//*********************************************************
return false;
}
}
}
// this function sets the purge flag
public bool Set_Output_Folder_Purge(bool value)
{
output_folder_purge = value;
return true;
}
// this function gets the purge flag
```

```
public bool Get_Output_Folder_Purge()
{
return output_folder_purge;
}
#endregion
//*********************************************************
// a string extractor for single case occurance
public static string Get_String(
string value, string start, string end)
{
string[] hash = Regex.Split(value, start);
if (hash.Length < 2)
{
return "";
}
string[] hash2 = Regex.Split(hash[1], end);
if (hash2.Length < 2)
{
return "";
}
return hash2[0];
}
// do the purge if needed
public bool Purge()
{
if (output_folder_purge == true)
{
//*********************************************************
DirectoryInfo folder = new DirectoryInfo(output_folder);
FileInfo[] files = folder.GetFiles("*.txt");
foreach (FileInfo file in files)
{
file.Delete();
}
return true;
}
else
{
return false;
}
}
// run violet
//*********************************************************
public void Run()
{
// ensure that this is reset on run
List<pram> sweep_prams = new List<pram>();
// check for a real file
```

```
if (input_file == "")
{
return;
}
// check for a real output folder
if (output_folder == "")
{
return;
}
// reset the model before building a new one
model = "";
// open the file and look for parms
StreamReader file = new StreamReader(input_file);
// string to hold the line
string line = "";
// this is the line number
int linenum=0;
// value to caculate total syms to run
double totalsyms = 1;
while ((line = file.ReadLine()) != null)
{
// rase the line number up by 1
linenum++;
// try and extract a pram
string parm = Get_String(line, "\\[", "\\]");
if (parm != "")
{
// parms have the format of [ Start : Step : Stop]
string[] data = parm.Split(':');
if (data.Length < 3)
{
//*******************************************************
// if you dont have 3 strings then you have bad syntax
Console.WriteLine(
"Error On Intput File {0} Line \"{1}\"",
Get_Input_File(), linenum);
return;
}
else
{
// make a new simulation
pram newitem = new pram();
// take spice data and turn it to double
newitem.Set(data[0], data[1], data[2]);
// this is used to find number of simulations
totalsyms *= newitem.numbersteps;
// add the simulation
sweep_prams.Add(newitem);
```

```
//*********************************************************
// remove the pram and sub a injection code
line=line.Replace("[" + parm + "]",
 "{" + (sweep_prams.Count-1).ToString().Trim() + "}");
// update our master file
model += line + "\r\n";
}
}
else
{
// no pram found then just append file
model += line + "\r\n";
}
}
// close the input file
file.Close();
// Report Total Syms
//*********************************************************
Console.WriteLine(
"Software will simulate {0} times", totalsyms.ToString());
// Run our number of simulations
Console.WriteLine(
"Generating Required Net lists To Output Folder");
BuildPrams(ref sweep_prams,0);
Console.WriteLine(
"Net List Creation Done Preparing"+
" to Start Threaded Simulation");
// Now start working some magic
// link our output folder
//*********************************************************
DirectoryInfo folder = new DirectoryInfo(output_folder);
if (folder.Exists == false)
{
Directory.CreateDirectory(output_folder);
folder = new DirectoryInfo(output_folder);
}
//*********************************************************
// get all the cir files we made
FileInfo[] files = folder.GetFiles("*.cir");
// allocate our threadpool to our max threads allowed
ThreadPool.SetMaxThreads(max_threads, max_threads);
// setup events for our pool
CirEvents = new ManualResetEvent[files.Length];
// setup counter for the events
int fcount=0;
// loop each file
foreach (FileInfo mycir in files)
{
```

```
// set the event
//*********************************************************
CirEvents[fcount]= new ManualResetEvent(false);
// make the thread
ThreadDataPass myprams = new ThreadDataPass();
myprams.filepath=output_folder+"//"+mycir.Name;
myprams.cireventID=fcount;
ThreadPool.QueueUserWorkItem(
new WaitCallback(RunSimulation), myprams);
fcount++;
}
// wait till all events are done
//*********************************************************
BigThreadPoolWait(CirEvents);
}
private void BigThreadPoolWait(WaitHandle[] myevents)
{
foreach (WaitHandle cir in myevents)
{
if (cir == null)
{
continue;
}
cir.WaitOne();
}
}
// wait callback for threading
//*********************************************************
private void RunSimulation(object locpram)
{
ThreadDataPass myprams = (ThreadDataPass)locpram;
RunSimulation(myprams.filepath, myprams.cireventID);
}
// this runs a spice simulation
public void RunSimulation(string filepath, int cirID)
{
Console.WriteLine("Starting Simulation {0}", cirID);
// get info about the file
FileInfo myfile = new FileInfo(filepath);
// see if the file exist
if (myfile.Exists== false)
{
return;
}
//*********************************************************
// start a new spice process
Process spiceprocess = new Process();
// this is cspice that is being used
```

```
ProcessStartInfo spiceprocessinfo =
 new ProcessStartInfo("cspice.exe", filepath);
// we want output back from spice
spiceprocessinfo.RedirectStandardOutput = true;
// we want to hide the window
spiceprocessinfo.WindowStyle = ProcessWindowStyle.Hidden;
// no becuase we want output back
spiceprocessinfo.UseShellExecute = false;
// no becuase we dont care about writeing to it
spiceprocessinfo.RedirectStandardInput = false;
// define our setings
spiceprocess.StartInfo = spiceprocessinfo;
// enforce no window
spiceprocess.StartInfo.CreateNoWindow = true;
// start the process
spiceprocess.Start();
//*********************************************************
// make a new file to hold the result in a .txt format
string outputsim=myfile.Name.Replace(
myfile.Extension, ".txt");
// make a new spice result file
TextWriter mysimfile = new StreamWriter(
output_folder + "\\"+outputsim);
// write the output of cspice to our file
mysimfile.Write(
spiceprocess.StandardOutput.ReadToEnd());
// close our file
mysimfile.Close();
// remove the sim file
myfile.Delete();
Console.WriteLine("Simulation␣{0}␣Done!", cirID);
// let the system know where done
CirEvents[cirID].Set();
}
//*********************************************************
private void BuildPrams(ref List<pram> prams,int index)
{
if (index == 0)
{
count = 0;
}
if (index >= prams.Count)
{
count++;
string output = count.ToString()+")\t";
string simmodel=model;
for (int lp = 0; lp < prams.Count; lp++)
{
```

```
//*********************************************************
simmodel = simmodel.Replace("{" + lp.ToString().Trim() + "}",
 pram.Spice_From_Numb(prams[lp].at));
}
if (count % 50 == 0)
{
//*********************************************************
Console.WriteLine(
"Update: Spice Simulation File Write At \"{0}\"", count);
}
//*********************************************************
TextWriter mysimfile = new StreamWriter(
output_folder + "\\SIM" +
count.ToString("000000000000")+".cir");
mysimfile.Write(simmodel);
mysimfile.Close();
return;
}
//*********************************************************
while (prams[index].at <= prams[index].stop)
{
BuildPrams(ref prams,index + 1);
prams[index].Next();
}
if (index != 0)
{
prams[index].Reset();
}
}
}
}

iż£//*********************************************************
// Variations of Input to Output for Lengthy Engineering
// Testing (VIOLET)
// V 1.0 By Mike Mclain
// Created Monday October 12, 2009
//*********************************************************
// The propose of this program is to give Simulation
// Program with Integrated
// Circuit Emphasis (SPICE) the ability to perform
// custom complex parametric
// analysis in a threaded environment.
//*********************************************************
// This program is designed to interface with
//  SPICE 3F5 from EECS Department
// of the University of California at Berkeley
// that can be obtained from
```

```
// http://embedded.eecs.berkeley.edu/
// pubs/downloads/spice/index.htm
// which is Copyright (c) 1985-1991
// The Regents of the University of
// California. All rights reserved.
// under the BSD Copyright.
//*********************************************************
// parameter data type
//*********************************************************

using System;
using System.Collections.Generic;
using System.Text;
using System.Text.RegularExpressions;

namespace violet
{
class pram
{
// the starting number
public double start=0;
// the stoping number
public double stop = 0;
// the step size
public double stepsize = 0;
// how many steps it will take
public double numbersteps = 0;
// what step is the software at
public double at = 0;
// have we passed our mark
public bool passflag = false;
// set the data from spice values
//*********************************************************
public void Set(string spicestart,
string spicestep, string spicestop)
{
start = Numb_From_Spice(spicestart);
stepsize = Numb_From_Spice(spicestep);
stop = Numb_From_Spice(spicestop);
// if there steping down then switch the values
if (start > stop)
{
double temp = start;
stop = start;
start = temp;
}
// set the starting step
Reset();
```

```
// its allways +1
numbersteps = ((stop - start) / stepsize)+1;
}
// go to our next step
public bool Next()
{
at += stepsize;
if (at > stop)
{
// do some casting to check for overstepsize
int inumbersteps = (int)numbersteps;
double dnumbersteps = inumbersteps;
// if its not even steps jump to max
if (passflag == false && inumbersteps != numbersteps)
{
at = stop;
passflag = true;
return false;
}
else
{
return true;
}
}
return false;
}
//*********************************************************
// reset back to our starting step
public void Reset()
{
passflag = false;
at = start;
}
public static string Get_Prefix(string spice)
{
string prefix = Regex.Replace(spice, "\\d", "");
prefix = prefix.Replace("-", "");
prefix = prefix.Replace(".", "");
prefix = prefix.Trim();
return prefix;
}
// cast a number back to a spice value
public static string Spice_From_Numb(double value)
{
double val = value;
if (value >= 1E9)
{
val /= 1E9;
```

```
return val.ToString() + "G";
}
else if (value >= 1E6)
{
val /= 1E6;
return val.ToString() + "MEG";
}
else if (value >= 1E3)
{
val /= 1E3;
return val.ToString() + "k";
}
else if (value >= 1)
{
return val.ToString();
}
else if (value >= 1E-3)
{
val *= 1E3;
return val.ToString() + "m";
}
else if (value >= 1E-6)
{
val *= 1E6;
return val.ToString() + "u";
}
else if (value >= 1E-9)
{
val *= 1E9;
return val.ToString() + "n";
}
else if (value >= 1E-12)
{
val *= 1E12;
return val.ToString() + "p";
}
// else return as a string
return val.ToString();
}
// cast spice values to numbers
//*******************************************************
public static double Numb_From_Spice(string spice)
{
string prefix = Get_Prefix(spice);
string number = spice;
if (prefix != "")
{
number = spice.Replace(prefix, "");
```

```
}
double numb = 0;
if (double.TryParse(number, out numb) == false)
{
return numb;
}
switch (prefix)
{
case "G":
numb *= 1E9;
break;
case "M":
numb *= 1E6;
break;
case "k":
case "K":
numb *= 1E3;
break;
case "m":
numb *= 1E-3;
break;
case "u":
numb *= 1E-6;
break;
case "n":
numb *= 1E-9;
break;
case "p":
numb *= 1E-12;
break;
}
return numb;
}
}
}
```

The source code presented below is the Python Berkeley Spice processing code utilized to extract and reformat the information obtain from a Berkeley spice simulation into a form that can be quickly imported into Matlab for further processing.

```
#*********************************************************
# File Name: SpiceFormat.py
# Project: Spice data extractor
# Author: Mike Mclain
# Because Matlab is very slow at extracting file IO python
# is used to quickly extract the information
# created by spice
#*********************************************************
import sys
```

```
import os
import getopt

input = ""
output = ""
try:
  opts, args = getopt.getopt(sys.argv[1:],"hi:o:",
  ["ifile=","ofile="])
except getopt.GetoptError:
  print "SpiceFormat.py␣-i␣<inputfile>␣-o␣<outputfile>"
  exit(2)

#*********************************************************
for opt, arg in opts:
  if opt == '-h':
    print ("SpiceFormat.py␣-i␣"+
    "<inputfile>␣-o␣<outputfile>")
    exit()
  elif opt in ("-i", "--ifile"):
    input = arg
  elif opt in ("-o", "--ofile"):
    output = arg

if input=="":
  print "null␣input"
  exit()

if output=="":
  print "null␣output"
  exit()


#*********************************************************
f = open(input)
lines = f.readlines()
f.close()

FileData=[]
Mode=0
SimName=""
CurrentData=[]
for index,line in enumerate(lines):

  line=line.replace("\n","")
  line=line.replace("\r","")
  line=line.strip()
```

```
    if Mode==0:
      # Simulation Name Seperator
      if line[0:8]=="Circuit:":
        SimName= line[8:].strip()
        Mode=Mode+1
    elif Mode==1:
      # File Header
      if line[0:4]=="----":
        Mode=Mode+1
    elif Mode==2:
      # Sim Header
      items=line.split()
      CurrentData.append(items)
      Mode=Mode+1
    elif Mode==3:
      # Skip the Bottom Segment
      if line[0:4]=="----":
        Mode=Mode+1
    elif Mode==4:
      if line=="":
        Mode=Mode+1
      else:
        items=line.split()
        CurrentData.append(items)
    elif Mode==5:
      # see if this is a new augment
      if line==SimName:
        FileData.append(CurrentData)
        CurrentData=[]
        Mode=1
      elif line[0:7]=="elapsed":
        FileData.append(CurrentData)
        break
      else:
        Mode=3
#************************************************************
Output=[]
for elem in FileData:
  for index,seg in enumerate(elem):
    if len(Output)<=index:
      Output.append("")
    for subseg in seg:
      print subseg
      if Output[index]=="":
        Output[index]=subseg
      else:
        Output[index]=Output[index]+"\t"+subseg
```

```
#*************************************************************
f = open(output, 'w')
f.write("\n".join(Output))
f.close()
```

APPENDIX D: MATLAB SPICE INTERFACE SOURCE CODE

The source code presented below is the Matlab source code for the Matlab Berkeley spice interface.

```
%************************************************************************
%* This function runs a copy of spice and extracts the results          *
%* obtain using python                                                  *
%************************************************************************
function [ Header, SimData] = SpiceRunSimulation(
netlist,simulationinfo,outputinfo)

Spice_Application='cspice.exe';
Spice_Simulation_File='Spice_Matlab_Sim.cir';


fid = fopen(Spice_Simulation_File,'w');
fprintf(fid,'%s\r\n','Spice_Matlab_Sim.cir - Mikes Matlab Spice');


[a,b]=size(netlist);
for lp=1:1:a
    line=netlist{lp};
    fprintf(fid,'%s\r\n',line);
end

[a,b]=size(simulationinfo);
for lp=1:1:a
    line=simulationinfo{lp};
    fprintf(fid,'%s\r\n',line);
end

[a,b]=size(outputinfo);
for lp=1:1:a
    line=outputinfo{lp};
    fprintf(fid,'%s\r\n',line);
end
fprintf(fid,'%s\r\n','.END');

fclose(fid);

[status,cmdout] =system('del Spice_Matlab_Sim_Stream.txt');


[status,cmdout] =system([Spice_Application ' '
 Spice_Simulation_File ' >> Spice_Matlab_Sim_Stream.txt']);

fid = fopen('Spice_Matlab_Sim.txt','w');
fprintf(fid,'%s',cmdout);
fclose(fid);

%************************************************************************
[status,cmdout] =system(['python SpiceFormat.py -i'
'Spice_Matlab_Sim_Stream.txt -o Spice_Matlab_Sim_Format.txt > plog.txt']);
fid = fopen('Spice_Matlab_Sim_Format.txt');
fline = fgetl(fid);
Header = strread(fline,'%s','delimiter','\t');
Header=Header';
fline = fgetl(fid);
SimData=[];
while ischar(fline)
    % Segment the line into a array based upon the comma delimiter
    tempdata=strread(fline,'%f','delimiter','\t');
    SimData=[SimData;tempdata'];
    fline = fgetl(fid);
end
fclose(fid);
end
```

```
%************************************************************************
%* This is a netlist macro and returns a capacitor netlist string       *
%************************************************************************
function [ output_args ] = SpiceCapacitor( Name, Node1, Node2, Value,...
 Unit)
    if nargin < 5
        [SValue,Unit]=SpiceUnits(Value);
    else
        SValue=num2str(Value);
    end
    output_args=['C' Name ' ' num2str(Node2) ' ' num2str(Node1) ' ' ...
        SValue Unit];
end
```

```
%************************************************************************
%* This is a netlist macro and returns a resistor netlist string         *
%************************************************************************
function [ output_args ] = SpiceResistor( Name, Node1, Node2, Value, ...
 Unit)
    if nargin < 5
        [SValue,Unit]=SpiceUnits(Value);
    else
        SValue=num2str(Value);
    end
    output_args=['R' Name ' ' num2str(Node2) ' ' num2str(Node1) ' ' ...
        SValue Unit];
end
```

```
%************************************************************************
%* This is a netlist macro and returns a inductor netlist string         *
%************************************************************************
function [ output_args ] = SpiceInductor( Name, Node1, Node2, Value, ...
 Unit)
    if nargin < 5
        [SValue,Unit]=SpiceUnits(Value);
    else
        SValue=num2str(Value);
    end
    output_args=['L' Name ' ' num2str(Node2) ' ' num2str(Node1) ' ' ...
        SValue Unit];
end
```

```
%************************************************************************
%* This is a netlist macro and returns a piecewise input signal netlist  *
%* string                                                                *
%************************************************************************
function [ output_args ] = SpiceCustomVoltageSource( Name, Node1, ...
Node2, Time,Value)
    output_args=['V' Name ' ' num2str(Node2) ' ' num2str(Node1) ' ' ...
        'PWL('];

    [a,b]=size(Time);
    for lp=1:1:b
        output_args=[output_args  num2str(Time(lp)) ' ' ...
            num2str(Value(lp)) ' '];
    end
    output_args=[output_args ')'];
end
```

```
%************************************************************************
%* Converts a spice simulation time index into a Tektronix time index    *
%************************************************************************
function [RSig] = SpiceRemap(Otime,Stime,Ssig)

[a,b]=size(Otime);
RSig=zeros(a,b);

for lp=1:1:b
    targettime=Otime(lp);
    index=FindEquivalentBin(targettime,Stime);
    RSig(lp)=Ssig(index);
end
end
```

```
%************************************************************************
%* This is a netlist macro and returns a TRAN simulation string          *
%************************************************************************
function [ output_args ] = SpiceTransient( Starttime, StarttimeU, ...
    Stoptime,StoptimeU, Stepsize, StepsizeU, timeMax,timeMaxU)
    if nargin < 7
        timeMax='';
        timeMaxU='';
    else
        timeMax=num2str(timeMax);
    end
    output_args=['.TRAN ' num2str(Stepsize) StepsizeU ' ' ...
        num2str(Stoptime) StoptimeU ' ' num2str(Starttime) StarttimeU  ...
```

```
        ' ' timeMax timeMaxU];
end
```

```
%************************************************************************
%* obtain the array index of a spice simulation                         *
%************************************************************************
function index  = SpiceGetHeaderIndex(find,header )
index=0;
fval=lower(find);
[a,b]=size(header);
for lp=1:1:b
    hstr=lower(header(lp));
    if strcmp(hstr,fval)
        index= lp;
        return
    end
end
end
```

```
%************************************************************************
%* Converts a a 1EX value into a spice unit (M,k, ,m,u,n,p)             *
%************************************************************************
function [ nval,unit ] = SpiceUnits( value )

nval='';
unit='';

neg='';
if sign(value)==-1
    neg='-';
end

if value==0
    nval=num2str(0);
    unit='';
    return
end
value=abs(value);

if value>=1E6
    real=floor(value/1E6);
    left=floor((value-real*10^6));
    nval=[num2str(real,'%g') '.' num2str(left,'%g')] ;
    unit='M';
elseif value>=1E3
    real=floor(value/1E3);
    left=floor(value-real*10^3);
    nval=[num2str(real,'%g') '.' num2str(left,'%g')] ;
    unit='k';
elseif value>=1E0
    real=floor(value/1E0);
    left=floor((value-real*10^0)*1E3);
    nval=[num2str(real,'%g') '.' num2str(left,'%g')] ;
    unit='';
elseif value>=1E-3
    real=floor(value/1E-3);
    left=floor((value-real*10^-3)*1E6);
    nval=[num2str(real,'%g') '.' num2str(left,'%g')] ;
    unit='m';
elseif value>=1E-6
    real=floor(value/1E-6);
    left=floor((value-real*10^-6)*1E9);
    nval=[num2str(real,'%g') '.' num2str(left,'%g')] ;
    unit='u';
elseif value>=1E-9
    real=floor(value/1E-9);
    left=floor((value-real*10^-9)*1E12);
    nval=[num2str(real,'%g') '.' num2str(left,'%g')] ;
    unit='n';
elseif value>=1E-12
    real=floor(value/1E-12);
    left=floor((value-real*10^-12)*1E15);
    nval=[num2str(real,'%g') '.' num2str(left,'%g')] ;
    unit='p';
else
    real=floor(value/1E-12);
    left=floor((value-real*10^-12)*1E18);
    nval=['.' num2str(left,'%05g')] ;
    unit='p';
end
nval=[neg nval];
end
```

APPENDIX E: MATLAB SCRIPTS

Matlab Script 1:

```
%**************************************************************************
%* Preliminary Matlab Program Configuration                               *
%**************************************************************************
% Get Fourier Coefficients
Fourier_Coefficients=fft(Input_Signal);
% Scale by Sample Size
Scaled_Fourier_Coefficients=Fourier_Coefficients./length(Input_Signal);
% Exclude the Redundant Half of the Spectrum
Half_Fourier_Coefficients=Fourier_Coefficients(1:floor(length(Fourier_Coefficients)/2));
Scaled_Half_Fourier_Coefficients=Scaled_Fourier_Coefficients(1:floor(length(Fourier_Coefficients)/2));
% Obtain Magnitude Value and Double for Removed Half of Spectrum
Amplitude_Coefficients=2.*abs(Scaled_Half_Fourier_Coefficients);
```

Matlab Script 2:

```
%**************************************************************************
%* Matlab Code to Identify Synthetic Environmental Effects Array Indices *
%**************************************************************************
% Calculate Synthetic Signal Floor
Synthetic_Floor=mean(Amplitude_Coefficients)*3;
% Determine Synthetic Signal Locations
Extraction_Array_Indices=[];
for i=1:length(Amplitude_Coefficients)
    if Amplitude_Coefficients(i)>Synthetic_Floor
       Extraction_Array_Indices(end+1)=i;
    end
end
% Obtain Length of Extraction Array Indices
n=length(Extraction_Array_Indices)
```

Matlab Script 3:

```
%**************************************************************************
%* Simulate Synthetic Environmental Effects                               *
%**************************************************************************
% Calculate Sample Frequency
Sample_Frequency=1/(Input_Signal_Time(2)-Input_Signal_Time(1));
% Calculate Positive Frequency Spectrum
Half_Frequency=(Sample_Frequency/length(Fourier_Coefficients))*(0:floor(length(Fourier_Coefficients)/2)-1);
% Obtain Phase Value
Phase_Coefficients= angle(Half_Fourier_Coefficients);

% Simulate Synthetic Environmental Effects
Simulated_Environmental_Effects=zeros(1,length(Input_Signal));
for i=1:length(Extraction_Array_Indices)
    k=Extraction_Array_Indices(i);
    K_Frequency_Simulation=Amplitude_Coefficients(k)*cos(2*pi*Half_Frequency(k)*Input_Signal_Time+Phase_Coefficients(k));
    Simulated_Environmental_Effects=Simulated_Environmental_Effects+ K_Frequency_Simulation;
end
```

Matlab Script 4:

```
%**************************************************************************
%*Create a Coefficient Mask to Filter out Synthetic Environmental Effects*
%**************************************************************************
Half_Coefficient_Filter_Mask=ones(1,length(Amplitude_Coefficients));
% Left and Right Size of Filter Upon Encountering Coefficient
Filter_Size=3;
for i=1:length(Amplitude_Coefficients)
    % Is value above Synthetic Floor?
    if Amplitude_Coefficients(i)>Synthetic_Floor
       Half_Coefficient_Filter_Mask(i)=0;
       % increase the mask area by the Filter Size on the Left
       if(i-Filter_Size-1>0)
           for j=i-Filter_Size-1:i
              Half_Coefficient_Filter_Mask(j)=0;
           end
       else
           for j=1:i
              Half_Coefficient_Filter_Mask(j)=0;
           end
       end

       % increase the mask area by the Filter Size on the Right
       if(i+Filter_Size+1>length(Amplitude_Coefficients))
           for j=i:length(amps)
              Half_Coefficient_Filter_Mask(j)=0;
           end
       else
           for j=i:i+Filter_Size+1
              Half_Coefficient_Filter_Mask(j)=0;
           end
       end
```

```
    end
end
% Because the original signal was doubled sided, we need to reverse the mask
Reversed_Half_Coefficient_Filter_Mask=fliplr(Half_Coefficient_Filter_Mask);
% Then concatenate the two sides the make the full mask
Coefficient_Filter_Mask=[Half_Coefficient_Filter_Mask Reversed_Half_Coefficient_Filter_Mask];
% Some operations might require the Inverse mask
Inverse_Coefficient_Filter_Mask=~Coefficient_Filter_Mask;
```

Matlab Script 5:

```
%************************************************************************
%* Filter Out Synthetic Effects                                         *
%************************************************************************
% Obtain Natural Magnitude Coefficient
Filtered_Real_Coefficient=abs(Fourier_Coefficients).*Coefficient_Filter_Mask;
% Obtain an estimate of the average Natural Noise Floor
Average_Natural_Noise=mean(Filtered_Real_Coefficient);
% Filter the Coefficients and replace the zero values with the Average Natural Noise
Filtered_Coefficients=Fourier_Coefficients.*Coefficient_Filter_Mask+Inverse_Coefficient_Filter_Mask*Average_Natural_Noise;
% Convert the Coefficients back into the time domain
Natural_Signal=real(ifft(Filtered));
```

Matlab Script 6:

```
%************************************************************************
%* Gaussian Estimation of Natural Effects                               *
%************************************************************************
[mean,variance ,mean_range,variance_range] = normfit(Natural_Signal);
```

Matlab Script 7:

```
%************************************************************************
%* Simulate Natural Effects                                             *
%************************************************************************
Simulated_Natural_Effects=normrnd(mean,variance,1,length(Natural_Signal));
```

Matlab Script 8:

```
%************************************************************************
%*Command to load numeric CSV file in Matlab*
%************************************************************************
Data= csvread('File.CSV')
```

Matlab Script 9:

```
%************************************************************************
%*This function will load a Tektronix encoded CSV File                 *
%************************************************************************
function [ output,header] = LoadTexCSV(filename)

% Open the File
fileID = fopen(filename);

% Create a storage elements to hold channel information
output=[];
% Create a storage element to hold scope information
header={};

% Get the first line
csvline = fgetl(fileID);

% a storage element to keep track of the current line within the file
linenumber=1;

% a constant value that determines when to stop processing header
% information
constant_header_stops_after=16;
% define constant delimiter locations
constant_line_index_header_name=1;
constant_line_index_header_value=2;
constant_line_index_time=4;
constant_line_index_value=5;

% if the line has a character process the line
while ischar(csvline)
    % Segment the line into a array based upon the comma delimiter
    data=strread(csvline,'%s','delimiter',',');

    % see if we are working within the header
    if linenumber <= constant_header_stops_after
        % buffer the header item
        parameter=data(constant_line_index_header_name);
```

```
        % check and see if the header is good
        if strcmp(parameter,'')-=1
            % Attempt to Convert value to a number
            value=str2double(data(constant_line_index_header_value));
            % check and see if the conversion worked
            if isnan(value)
                % if the conversion did not work, revert back to a string
                value=data(constant_line_index_header_value);
            end

            % see if this is the first time executing
            if linenumber==1
                % if it is then overwrite header
                header=[{parameter value}];
            else
                % else augment header
                header=[header; {parameter value}];
            end
        end
    end

    % Take the good extracted Data and turn it into a numerical value
    time=str2double(data(constant_line_index_time));
    value=str2double(data(constant_line_index_value));

    % see if this is the first time executing
    if linenumber==1
        % if it is then overwrite output
        output=[time value];
    else
        % else augment output
        output=[output; time value];
    end

    % Get the next line
    csvline = fgetl(fileID);

    % increment the line number
    linenumber=linenumber+1;
end

% Close the File
fclose(fileID);
end
```

Matlab Script 10:

```
%**************************************************************************
%* This function will load a Tektronix Measurement Folder                 *
%*                                                                        *
%* This function requires LoadTexCSV                                      *
%**************************************************************************
function [ output, header ] = LoadTexMes( folder )

% Create a directory search string limited to CSV files
SearchString=[folder '/*.csv'];

% Get a list of all channel measurements
Channels=dir(SearchString);

% obtain a count of channel files
[filecount,NA]=size(Channels);

% Create a storage elements to hold channel information
output=[];

% Create a storage element to hold scope information
header={};

% a loop to open each channel file
for index=1:1:filecount
    % create a path string to open the csv file
    % related to the current directory
    OpenString= [folder '/' Channels(index).name];

    % extract the channel information
    [data,info]=LoadTexCSV(OpenString);

    % see if this is the first time executing
    if index==1
         % if it is then overwrite output and the header
        output=data;
        header=info;
    else
        % else augment the output and the header
        output=[output data];
        header={header info};
    end
end
```

Matlab Script 11:

```
%************************************************************************
%* This function will load a set of Tektronix Measurement Folders       *
%*                                                                      *
%* This function requires LoadTexCSV                                    *
%* This function requires LoadTexMes                                    *
%************************************************************************
function [ set ] = LoadTexSet( folder )

% obtain a list of all folder sub elmements
Measurments=dir(folder);

% Generate a logical vector of sub folders that excludes files
SubFolderVector = [Measurments(:).isdir];

% Obtain a list of all sub folders
SubFolders={Measurments(SubFolderVector).name};

% remove the generic current (.) and previous folder (..) prefixes
% that get attached
SubFolders(ismember(SubFolders,{'.','..'})) = [];

% obtain a count of Measurement folders
[NA,foldercount]=size(SubFolders);

% Create a storage element to hold set information
set={};

% a loop to open each measurement file
for index=1:1:foldercount
    % create a path string to open the measurement
    % related to the current directory
    FileString = ['./' folder '/' SubFolders{index}];

    % Load the Measurement
    [output,header]=LoadTexMes(FileString);

    % see if this is the first time executing
    if index==1
        % if it is then overwrite set
        set=[{output header}];
    else
        % else augment the set
        set=[set;{output header}];
    end
end
end
```

Matlab Script 12:

```
%************************************************************************
%* This function converts a Tektronix Measurement Set into a            *
%* a convenient to use data cell                                        *
%*                                                                      *
%************************************************************************
function [ output ] = ConvertSetToCell( set )

% First obtain the size of the incoming measurement set
[Measurement_Count,NA]=size(set)

% define the output cell
output={};

% a loop and get each measurement
for index=1:1:Measurement_Count

    % create an array to hold our current measurement
    Current_Measurement=[];

    % get the channel values from the measurement
    channels=set{index,1};

     % assume all channels have the same sample time and get the first
     % channel time
    time=set{index,1}(:,1);

    % assume current measurements always start with time
    Current_Measurement=[time];

    % assume all channels have the same sample time
    [NA,Channels_Count]=size(channels);

    %loop thru each channel and skip each time segment
    for lp=2:2:Channels_Count
        % obtain the channel data
        CurrentChannel=set{index,1}(:,lp);
        % save the channel data into a new array
        Current_Measurement=[Current_Measurement CurrentChannel];
    end

    % see if this is the first time executing
    if index==1
        % if it is then overwrite output
        output={Current_Measurement};
    else
```

```
        % else augment the output
        output=[output; {Current_Measurement}];
    end
end
```

Matlab Script 13:

```
%**************************************************************************
%* This function loads a simplistic csv encoded 1 channel numerical      *
%* oscilloscope measurement                                               *
%**************************************************************************
function [ time,value ] = LoadSimplisticDatChannel( filename )
csvdata = dlmread(filename);
time=csvdata(:,1);
value=csvdata(:,2);
end
```

Matlab Script 14:

```
%**************************************************************************
%* this function will load a set of simplistic CSV measurements          *
%*                                                                        *
%* This function requires LoadSimplisticDatChannel                        *
%**************************************************************************
function [ set ] = LoadSimplisticDatSet( folder )

set={};

% Create a directory search string limited to CSV files
SearchString=[folder '/*.dat'];

% Get a list of all channel measurements
Channels=dir(SearchString);

% obtain a count of channel files
[filecount,NA]=size(Channels);

for index=1:1:filecount
    % create a path string to open the csv file
    % related to the current directory
    OpenString= [folder '/' Channels(index).name];

    % extract the channel information
    [time,data]=LoadSimplisticDatChannel(OpenString);

    % see if this is the first time executing
    if index==1
        set={time,data};
    else
        set=[set;{time,data}];
    end
end


end
```

Matlab Script 15:

```
%**************************************************************************
%* This Script first determines if the DAC tests are loaded into memory  *
%* and if not loads the test into memory                                  *
%**************************************************************************
if exist('DAC_Test1','var')==0
    DAC_Test1= LoadSimplisticDatSet('../../Data/DAC Test/Test_0_to_4095');
end

if exist('DAC_Test2','var')==0
    DAC_Test2= LoadSimplisticDatSet('../../Data/DAC Test/Test_4095_to_0');
end
```

Matlab Script 16:

```
%**************************************************************************
%* because there are a number of steps required to produce fft plots     *
%* using the Matlab fft command this function is a wrapper                *
%* function to make this process easier                                   *
%*                                                                        *
%* Demo call                                                              *
%* [f,X,fn,Xn,m,p,hf,Xnorm,hm,hp,hpsd,hpsd10]=EasyFFT(t,y);               *
%**************************************************************************
function [F, X, Fnn, Xnn, M, P, HF, HXorm, HM, HP, ...
    HPSD,HPSD10] = EasyFFT( time,value )

% first obtain some information about the size of the time array
```

```
[A,B]=size(time);

% if the row is larger than the columns
if A>B
    % transpose
    time=time';
end

% now obtain some information about the size of the data array
[A,B]=size(value);
 % if the row is larger than the columns
if A>B
    % transpose
    value=value';
end

% obtain some information about the number of samples
[NA,samples]=size(time);

% find the sample rate
sample_rate=time(2)-time(1);

total_time=sample_rate*samples;

sample_frequency=1/sample_rate;
frequency_increment=1/total_time;


% now calculate the spectral window
spectral_window=samples*frequency_increment;

% Note Matlabs FFT implementation is notoriously confusing, at
% least relative to the implementations described within most
% academic text. Conversely, after a lot of experimentation,
% reading the Matlab manual, reading the Matlab newsgroup, a
% a helpful post by Greg Heath of the Matlab newsgroup, and a
% helpful post by Elige Grant of the Matlab newsgroup
% the following conclusions were made

% First, the Matlab FFT was designed to be used with a uniformly
% sampled time domain function that is defined over a
% non-negative time interval

% Second, the result of FFT, as it might be expected, is defined
% over a nonnegative frequency interval as a result

% Third, the function fftshift was designed to transform a nonnegative
% frequency interval into a normal positive and negative frequency
% interval

% Forth the function ifftshift was designed to convert a
% positive and negative frequency interval back into a nonnegative
% frequency interval

% Fifth, the functions fftshift and ifftshift function differently
% for even and odd sequences. For even sequences they return the same
% result when preformed upon the same sequence, for odd sequences they
% return different results but when utilized consecutively they can
% recovery the original sequence

% Thus when implementing FFT within Matlab not only does spectral
% interval matter but the number of sequence terms

% Conversely, as a result, a lot of Matlab FFT implementations will cast
% odd sequences into an even sequence to avoid fftshift and ifftshift
% issues and also into padded N bit values in order to receive processing
% improvements from radix simplification.
% but such methods modify the resulting fft and, should a ifft
% be required, will yield a result that is not the same as
% the original signal.

% Also note that the fft function is not normalized but ifft is
% normalized, so this is a bit of a problem since to use ifft you
% need to leave fft unnormalized but to calculate useful information
% like magnitude or PSD normalization is required

% also note that half spectral representations require a multiplication
% of 2 to incorporate the negative half of the frequency spectrum

% calculate the nonnegative window frequency
nonnegative_frequency= ...
    0:frequency_increment:spectral_window-frequency_increment;

% calculate the normal window frequency
% casting is required for odd intervals
half_window_Size_cast_down=ceil((samples+1)/2);
half_window_Size_cast_up=floor((samples+1)/2);
lower_spectral_window=(half_window_Size_cast_down-1)*frequency_increment;
upper_spectral_window=(half_window_Size_cast_up-1)*frequency_increment;

frequency=-lower_spectral_window:frequency_increment:upper_spectral_window;

% at this point preform the FFT
nonnegative_frequency_value=fft(value);
frequency_value=fftshift(nonnegative_frequency_value);

% output assignments
X=frequency_value;
Xnn=nonnegative_frequency_value;
```

```
F=frequency;
Fnn=nonnegative_frequency;



% normalization can be achieved by either using FFT/samples
% or FFT*sample_rate
% But some discussion on this issue indicate that FFT*sample_rate is
% the correct methodic in order to make Parseval's theorem hold true
% yet FFT/ samples seems to yield the correct results with raw data
% This needs some further investigation and its possible that the
% sample_rate used is not the sample_rate needed to make this
% conversion work....
normalized_nonnegative_frequency_value= ...
    nonnegative_frequency_value/samples ;
normalized_frequency_value=frequency_value/samples;

% Note angle is a terrible problem with fft, it can be corrupted by
% discretization noise, modified by the window, and is all around bad
% to work with if attempting to obtain a meaningful plot, since such
% attributes are inherent, only the instantaneous phase will be
% provided --- as this information can be utilized to generate a
% cos chain to synthesis a signal and such information might be
% usefull for known fft bins.
% in some cases the unwrap() function can be utilized to
% obtain a more meaningful plot but all requests should be
% considered questionable

instantaneous_phase_in_rads=angle(normalized_frequency_value);

% this is not needed atm but I left it here just in case
% nonnegative_instantaneous_phase_in_rads= ...
%    angle(normalized_nonnegative_frequency_value);

% the spectral magnitude comes in a number of different flavors full
% and half, if half spectrum is utilized then the signal must be
% doubled with the exclusion of the DC component to because of the
% repeating spectrum

magnitude=abs(normalized_frequency_value);

% output assignments
M=magnitude;
P=instantaneous_phase_in_rads;

half_frequency=frequency(frequency>=0);
half_normalized_frequency_value=normalized_frequency_value(frequency>=0);

half_magnitude=abs(half_normalized_frequency_value);
half_magnitude(2:end)=half_magnitude(2:end)*2;

half_instantaneous_phase_in_rads= ...
    instantaneous_phase_in_rads(frequency>=0);

% there are a number of ways to calculate power spectrum
% density, but magnitude square seems to be the most common
% a possible alternative is doubling half spectrum minus DC then
% PSD = X.*conj(X)/N.

half_power_spectrum_density=half_magnitude.^2;
half_power_spectrum_density_log_10=10*log10(half_power_spectrum_density);

% output assignments
HF=half_frequency;
HXorm=half_normalized_frequency_value;
HM=half_magnitude;
HP=half_instantaneous_phase_in_rads;
HPSD=half_power_spectrum_density;
HPSD10=half_power_spectrum_density_log_10;
end
```

Matlab Script 17:

```
%************************************************************************
%* This function is analogous to a tree sort                            *
%* It is intended to convert a given test value into its equivalent     *
%* location within a new array                                          *
%* This is useful if you have two fft operations that were sampled at   *
%*                                                                      *
%* different rates and you would like to compare the first test with    *
%* the second test.                                                     *
%*                                                                      *
%* Note, in the case above you are truncating spectral information by   *
%* performing this conversion                                           *
%************************************************************************


function [ index ] = FindEquivalentBin( test,bin)

[NA,Binsize]=size(bin);

% first look for the above and below cases
if test <= bin(1)
    index=1;
    return;
end
```

```
if test >= bin(end)
    index=Binsize;
    return;
end

[a,b] = min(abs(bin-test));
index=b;
end
```

Matlab Script 18:

```
%************************************************************************
%* This function Creates a FFT Mask to Isolate Frequencies              *
%* above a given value                                                  *
%************************************************************************
function [ Mask ] = MakeFFTMask(amps,amps_mean,zonesize)
     % Get the size of the input data
     [a,b]=size(amps);
     % start with a pass all mask
     Mask=ones(a,b);
     % process every fft bin
     for i=1:b
          % if the bin is > than given value
          if amps(i)>amps_mean
               % remove the bin from the mask
               Mask(i)=0;
               % because of spectral leakage the bins near this signal
               % might need to be removed
               % Remove Left Side by Zone size
               if(i-zonesize-1>0)
                    % Ensure we do not exceed the negative array index
                    for j=i-zonesize-1:i
                         Mask(j)=0;
                    end
               else
                    for j=1:i
                         Mask(j)=0;
                    end
               end
               % remove the Right Side by Zone Size
               if(i+zonesize+1>b)
               % Ensure we do not exceed the negative array index
                    for j=i:length(amps)
                         Mask(j)=0;
                    end
               else
                    for j=i:i+zonesize+1
                         Mask(j)=0;
                    end
               end
          end
     end
end
```

Matlab Script 19:

```
%************************************************************************
%* This function attempts to simplistically remap a FFT mask from       *
%* one frequency  bin  mapping to another frequency bin mapping.        *
%*                                                                      *
%* Note, this function does not handle bin size differences very        *
% *well so used with extreme caution                                    *
%************************************************************************
function [ Mask ] = RemapFilter(newfbin,oldfbin,oldmask )

[a,b]=size(oldfbin);
[c,d]=size(newfbin);
% created new mask
Mask=zeros(c,d);
% loop through each element in the old bin
for lp=1:1:b
     % extract old bin data for convenience
    freq=oldfbin(lp);
    cmask=oldmask(lp);
     % find index using the equivalent then functioned previously
     % created
    rindex=FindEquivalentBin(freq,newfbin);
     % remap the mask
    if Mask(rindex)==0
        Mask(rindex)=cmask;
    else
        Mask(rindex)=Mask(rindex)+cmask;
    end
end
end
```

Matlab Script 20:

```
%************************************************************************
%* Search a signal from the left and find the index in which the signal  *
%* crosses a given value                                                *
%************************************************************************
function [ index ] = LeftCrossing( input,value )
% Get the size of the signal
[a,b]=size(input);

% start by assuming that we above the crossing
Mode=0;

% see if we have crossed before we started
if input(1)==value
% This is very unlikely
    index=1;
    return
end

% now see if we are actually below the crossing
if input(1)<value
    % we are below the crossing
    Mode=1;
end

% Loop thru every point in the signal from the left to the right
for lp=1:1:b

% if we are above the value
    if Mode==0
% see if we crossed
        if input(lp)<value
            index=lp
            return
        end
    else
% if we are below the value see if we crossed
        if input(lp)>value
            index=lp
            return
        end
    end
end

% Nothing was found so assume first index on left as a fallback
index=1;
```

Matlab Script 21:

```
%************************************************************************
%* Search a signal from the right and find the index in which the signal *
%* crosses a given value                                                *
%************************************************************************
function [ index ] = RightCrossing( input,value )
% Get the size of the signal
[a,b]=size(input);

% start by assuming that we above the crossing
Mode=0;

% see if we have crossed before we started
if input(b)==value
% This is very unlikely
    index=b;
    return
end

% now see if we are actually below the crossing
if input(b)<value
    % we are below the crossing
    Mode=1;
end

% Loop thru every point in the signal from the right to the left
for lp=b:-1:1
    % if we are above the value
    if Mode==0
% see if we crossed
        if input(lp)<value
            index=lp
            return
        end
    else
% if we are below the value see if we crossed
        if input(lp)>value
            index=lp
            return
        end
    end
end

% Nothing was found so assume first index on right as a fallback
index=b;
```

Matlab Script 22:

```
%************************************************************************
%* count the number of minimum and maximum periods of a signal          *
%************************************************************************
function [ above,below ] = CountSegments( input)

% get the size of the input
[a,b]=size(input);

% set our counter to 0
above=0;
below=0;

% obtain the minimum and maximum signal value
valuemin=min(input);
valuemax=max(input);

% enter a progressive loop
lp=1;
while lp<=b
%  see if we found a minimum
       if input(lp)<valuemin*.9;
% if so increment the below counter
          below=below+1;
% loop until we are out of the minimum
          while input(lp)< valuemin*.8
               lp=lp+1;
               if lp>b
                   continue;
               end
          end
% see if we have found the maximum
       elseif input(lp)>valuemax*.9;
% if so increment the above counter
          above=above+1;
% loop until we are out of the maximum
          while input(lp)> valuemax*.8
               lp=lp+1;
               if lp>b
                   continue;
               end
          end
       end
    lp=lp+1;
end

end
```

Matlab Script 23:

```
%************************************************************************
%* this function determines the index delay between two input signals    *
%* this function returns the signed index and the augmented input        *
%* signals including augmented values of time                            *
%************************************************************************
function [Delta,TO1,YO1,TO2,YO2] = UnShift( T1,Y1,T2,Y2 )

% begin our analysis by determining the zero crossing, from the left,
% of each signal
A=LeftCrossing(Y1,0);
B=LeftCrossing(Y2,0);

% the difference between the two is the Index shift amount
% note this could be plus or minus one off depending upon the signal
Delta=B-A;

% if the delta value is positive
if Delta>0
% the second signal needs to be augmented in
% order to obtain phase alignment
    YO2=Y2(Delta:end);
    [a,b]=size(YO2);
% and the remaining signals need to be trimmed
% by the augmented amount in order to plot correctly
% with the augmented signal
    YO1=Y1(1:b);
    TO1=T1(1:b);
    TO2=T2(1:b);
elseif Delta<0
% if the delta value is negative
% the reverse is true
% and the process repeats as above
    aDelta=abs(Delta);
    YO1=Y1(aDelta:end);
    [a,b]=size(YO1);
    YO2=Y2(1:b);
    TO1=T1(1:b);
    TO2=T2(1:b);
```

```
else
% if no index shift has occurred
% return the input arrays
    YO1=Y1;
    YO2=Y2;
    TO1=T1;
    TO2=T2;
end
end
```

Matlab Script 24:

```
%************************************************************************
%* Demonstrating the usage of spice within Matlab                       *
%************************************************************************

% setup simulation input
StopTime=10;
StepSize=StopTime/2500;
t=0:StepSize:StopTime-StepSize;
% define the input
input=sin(t);

% Make a Spice Netlist char array
Netlist= ...
{
     SpiceCustomVoltageSource('s',0,1,t,input)
     SpiceResistor('1',2,1,100)
     SpiceResistor('2',2,0,100)
};
% Define the Simulation
Simulation = ...
{
%    '.TRAN  20ns 142.78us 0us'
    SpiceTransient(0,'S',StopTime,'S',StepSize,'S')
};
% Define the output
Output= ...
{
    '.PRINT TRAN V(1) V(2)'
    '.PROBE'
};

% run spice and get the data
[header,data]=SpiceRunSimulation(Netlist,Simulation,Output);


% extract the information
Index=data(:,SpiceGetHeaderIndex('index',header))';
time=data(:,SpiceGetHeaderIndex('time',header))';
SV1=data(:,SpiceGetHeaderIndex('v(1)',header))';
SV2=data(:,SpiceGetHeaderIndex('v(2)',header))';

% Remap the infomration into our test time
V1=SpiceRemap(t,time,SV1);
V2=SpiceRemap(t,time,SV2);
```

Matlab Script 25:

```
%************************************************************************
%* Demonstrates the usage of the nonlinear newton method to solve       *
%* circuit parameters within pspice.                                    *
%************************************************************************
% Define the Input signal
StopTime=20;
StepSize=StopTime/2500;
t=0:StepSize:StopTime;
Inputs={
    sin(t);
    sin(t);
    sin(t);
    };
% Define the systems ideal outputs
Outputs={
    .8*input;
    .5*input;
    .25*input;
    };

% defined the number of unknown parameters
N=4;
% defined the initial estimate of the unknown parameters
at=[500 500 500 500];
% define the step size of the jacobian partial derivatives
Step=[.25 .25 .25 .25];

Step=[10 10 10 10];

% this will convert a Matlab array index into a numerical offset
index2num=ones(1,N);
```

```
% defined Newtonian solver  parameters
intter=1
serror=.001;
kmax=1000;


LastInput=[];
Lastcurrent=[];
%************************************************************************
% enter a processing loop until the specified maximum is reached
while intter<=kmax

    % every function to be solved gets its own state matrix
    CurrentM={};

     % the necessary calculations required to approximate the jacobian
     % is amusingly defined by this equations that consists of a ordered
     % array sequence of progressive numbers that correspond to our
     % previously defined parameters an example being [ indexA, indexB]
     % while this approach might seem kind of odd, this technique allows
     % for  parameters to be defined in N dimensional terms, otherwise a
     % series of nested for loops would have been required...
     % although, oddly enough, i was able to simplify the number of
     % calculations required using this technique
     % thus, the calculation is as follows,
     % the elements necessary to numerically calculate jacobian,
 % assuming a  n-dimensional array is saved in the following
 % order (for a 2 by 2 dimensions the following storage
 % elements would exist)
     % 0 0
     % 1 0
     % 0 1
     % 1 1
     % in which
     % 0 0 is simulated at the current location
     % 1 0 is simulated at the x location plus the step size while y
     % remains the same
     % 0 1 s simulated at the t location pplus the step size while X
     % remains the same
     % naturally this process repeats for every parameter
 % within the array
     % after determining what partial derivatives the jacobian required
     % and their location within this array a identity matrix provides
     % the array augmentation to estimate  the jacobian
     % but because Matlab indexes start at one rather than zero
     % a one's array must be added to the identity matrix to make the
     % calculation index correct
     JIndex=eye(N)+ones(N,N);
%************************************************************************
     % Likewise because the jacobian requires the starting location
 % and the
     % technique above does not incorporate this location within
 % the index
     % is produced the starting point must be and manually added to the
     % index array
     JIndex=[JIndex;ones(1,N)];

     % at this point we are ready to evaluate the spice function
     % at at each simulation will point defined within the
 % jacobian index
     [a,b]=size(JIndex);
     for lp=1:1:a
         % oabtain our array index
         Cindex=JIndex(lp,:);
         % create a augmentation mask to determine our step direction
         augment=Cindex-index2num;
         % modifier the parameter location within the jacobian
 % estimator
         Current=at+Step.*augment;
         % perform our spice simulation

        [OA,OB]=size(Outputs);
        for loa=1:1:OA
        input=Inputs{loa};
%************************************************************************
        if ArrayCompare(input,LastInput)~=1 || ...
ArrayCompare(Current,Lastcurrent)~=1
            disp([intter lp loa])
            Netlist= ...
            {
                 SpiceCustomVoltageSource('s',0,1,t,input)
                 SpiceResistor('1',1,2,Current(1))
                 SpiceResistor('2',2,3,Current(2))
                 SpiceResistor('3',3,4,Current(3))
                 SpiceResistor('4',4,0,Current(4))
            };
            Simulation = ...
            {
            %    '.TRAN  20ns 142.78us 0us'
                SpiceTransient(0,'s',StopTime,'s',StepSize,'s')
            };
            Output= ...
            {
                '.PRINT TRAN V(1) V(2) V(3) V(4)'
                '.PROBE'
            };
            %disp('Starting Spice Sim')
            [header,data]=SpiceRunSimulation(Netlist,Simulation,...
Output);
            %disp('Spice Sim Done')
```

```
            SIndex=data(:,SpiceGetHeaderIndex('index',header))';
            Stime=data(:,SpiceGetHeaderIndex('time',header))';
            SV1=data(:,SpiceGetHeaderIndex('v(1)',header))';
            SV2=data(:,SpiceGetHeaderIndex('v(2)',header))';
            SV3=data(:,SpiceGetHeaderIndex('v(3)',header))';
            SV4=data(:,SpiceGetHeaderIndex('v(4)',header))';

            % Remap the spice value into the test array format
            RSV2=SpiceRemap(t,Stime,SV2);
            RSV3=SpiceRemap(t,Stime,SV3);
            RSV4=SpiceRemap(t,Stime,SV4);

            SVA={ RSV2;  RSV3; RSV4};
            LastInput=input;
            Lastcurrent=Current;
        end

%************************************************************************
        % obtain our function value
        % note if we are solving for output voltage we need to modify this
        % result slightly to obtain a single value
        % sum the error, no error is zero!
%************************************************************************
            output=Outputs{loa};
            foundvalue=sum(SVA{loa}-output);
            CurrentM{loa}(Cindex(1),Cindex(2),Cindex(3),...
Cindex(4))=foundvalue;
        end
     end

     % now estimate our jacobian
    [OA,OB]=size(Outputs);
    J=[]
    CF=[];
    for loa=1:1:OA
        JR1=(CurrentM{loa}(2,1,1,1)-CurrentM{loa}(1,1,1,1))/Step(1);
        JR2=(CurrentM{loa}(1,2,1,1)-CurrentM{loa}(1,1,1,1))/Step(2);
        JR3=(CurrentM{loa}(1,1,2,1)-CurrentM{loa}(1,1,1,1))/Step(3);
        JR4=(CurrentM{loa}(1,1,1,2)-CurrentM{loa}(1,1,1,1))/Step(4);
        J=[J; JR1 JR2 JR3 JR4];
        CF=[CF; CurrentM{loa}(1,1,1,1)];
    end


    y= -J\CF;

    newat=at+y';
%************************************************************************
% diff can be replaced with sum(delta) or other checks in some cases
%************************************************************************
    diff=norm(newat-at);
    disp([intter newat diff]);
    if diff<serror
        break;
    else
        at=newat;
    end
    intter=intter+1;
end
```